

Central and Eastern United States Seismic Source Characterization for Nuclear Facilities

Volume 5: Appendices C to F



U.S. Nuclear Regulatory Commission
Office of Nuclear Regulatory Research
Washington DC 20555
NUREG-2115



U.S. Department of Energy
1000 Independence Avenue SW
Washington, DC 20585
Report # DOE/NE-0140



Electric Power Research Institute
3420 Hillview Avenue
Palo Alto, CA 94304
Report # 1021097

AVAILABILITY OF REFERENCE MATERIALS IN NRC PUBLICATIONS

NRC Reference Material

As of November 1999, you may electronically access NUREG-series publications and other NRC records at NRC's Public Electronic Reading Room at <http://www.nrc.gov/reading-rm.html>.

Publicly released records include, to name a few, NUREG-series publications; *Federal Register* notices; applicant, licensee, and vendor documents and correspondence; NRC correspondence and internal memoranda; bulletins and information notices; inspection and investigative reports; licensee event reports; and Commission papers and their attachments.

NRC publications in the NUREG series, NRC regulations, and *Title 10, Energy*, in the Code of *Federal Regulations* may also be purchased from one of these two sources.

1. The Superintendent of Documents
U.S. Government Printing Office
Mail Stop SSOP
Washington, DC 20402-0001
Internet: bookstore.gpo.gov
Telephone: 202-512-1800
Fax: 202-512-2250
2. The National Technical Information Service
Springfield, VA 22161-0002
www.ntis.gov
1-800-553-6847 or, locally, 703-605-6000

A single copy of each NRC draft report for comment is available free, to the extent of supply, upon written request as follows:

Address: U.S. Nuclear Regulatory Commission
Office of Administration
Publications Branch
Washington, DC 20555-0001

E-mail: DISTRIBUTION.SERVICES@NRC.GOV

Facsimile: 301-415-2289

Some publications in the NUREG series that are posted at NRC's Web site address <http://www.nrc.gov/reading-rm/doc-collections/nuregs> are updated periodically and may differ from the last printed version. Although references to material found on a Web site bear the date the material was accessed, the material available on the date cited may subsequently be removed from the site.

Non-NRC Reference Material

Documents available from public and special technical libraries include all open literature items, such as books, journal articles, and transactions, *Federal Register* notices, Federal and State legislation, and congressional reports. Such documents as theses, dissertations, foreign reports and translations, and non-NRC conference proceedings may be purchased from their sponsoring organization.

Copies of industry codes and standards used in a substantive manner in the NRC regulatory process are maintained at—

The NRC Technical Library
Two White Flint North
11545 Rockville Pike
Rockville, MD 20852-2738

These standards are available in the library for reference use by the public. Codes and standards are usually copyrighted and may be purchased from the originating organization or, if they are American National Standards, from—

American National Standards Institute
11 West 42nd Street
New York, NY 10036-8002
www.ansi.org
212-642-4900

Legally binding regulatory requirements are stated only in laws; NRC regulations; licenses, including technical specifications; or orders, not in NUREG-series publications. The views expressed in contractor-prepared publications in this series are not necessarily those of the NRC.

The NUREG series comprises (1) technical and administrative reports and books prepared by the staff (NUREG-XXXX) or agency contractors (NUREG/CR-XXXX), (2) proceedings of conferences (NUREG/CP-XXXX), (3) reports resulting from international agreements (NUREG/IA-XXXX), (4) brochures (NUREG/BR-XXXX), and (5) compilations of legal decisions and orders of the Commission and Atomic and Safety Licensing Boards and of Directors' decisions under Section 2.206 of NRC's regulations (NUREG-0750).

Central and Eastern United States Seismic Source Characterization for Nuclear Facilities

Cosponsors

U.S. Department of Energy

1000 Independence Avenue SW
Washington, DC 20585

R. H. Lagdon, Jr.
Chief of Nuclear Safety
Office of the Under Secretary for Nuclear Security, S-5

M.E. Shields
Project Manager
Office of Nuclear Energy, NE-72

Electric Power Research Institute

3420 Hillview Avenue
Palo Alto, CA 94304

J. F. Hamel
Program Manager
Advanced Nuclear Technology

U.S. Nuclear Regulatory Commission

Office of Nuclear Regulatory Research
Washington DC 20555

R.G. Roche-Rivera
NRC Project Manager

*This document was **not** developed under a 10CFR50
Appendix B program.*

DISCLAIMER OF WARRANTIES AND LIMITATION OF LIABILITIES

EPRI DISCLAIMER

THIS DOCUMENT WAS PREPARED AS AN ACCOUNT OF WORK SPONSORED OR COSPONSORED BY THE ELECTRIC POWER RESEARCH INSTITUTE, INC. (EPRI). NEITHER EPRI, ANY MEMBER OF EPRI, ANY COSPONSOR BELOW, NOR ANY PERSON ACTING ON BEHALF OF ANY OF THEM:

(A) MAKES ANY WARRANTY OR REPRESENTATION WHATSOEVER, EXPRESS OR IMPLIED, (I) WITH RESPECT TO THE USE OF ANY INFORMATION, APPARATUS, METHOD, PROCESS, OR SIMILAR ITEM DISCLOSED IN THIS DOCUMENT, INCLUDING MERCHANTABILITY AND FITNESS FOR A PARTICULAR PURPOSE, OR (II) THAT SUCH USE DOES NOT INFRINGE ON OR INTERFERE WITH PRIVATELY OWNED RIGHTS, INCLUDING ANY PARTY'S INTELLECTUAL PROPERTY, OR (III) THAT THIS DOCUMENT IS SUITABLE TO ANY PARTICULAR USER'S CIRCUMSTANCE; OR

(B) ASSUMES RESPONSIBILITY FOR ANY DAMAGES OR OTHER LIABILITY WHATSOEVER (INCLUDING ANY CONSEQUENTIAL DAMAGES, EVEN IF EPRI OR ANY EPRI REPRESENTATIVE HAS BEEN ADVISED OF THE POSSIBILITY OF SUCH DAMAGES) RESULTING FROM YOUR SELECTION OR USE OF THIS DOCUMENT OR ANY INFORMATION, APPARATUS, METHOD, PROCESS, OR SIMILAR ITEM DISCLOSED IN THIS DOCUMENT.

DOE DISCLAIMER

THIS REPORT WAS PREPARED AS AN ACCOUNT OF WORK SPONSORED BY AN AGENCY OF THE UNITED STATES GOVERNMENT. NEITHER THE UNITED STATES GOVERNMENT NOR ANY AGENCY THEREOF, NOR ANY OF THEIR EMPLOYEES, MAKES ANY WARRANTY, EXPRESS OR IMPLIED, OR ASSUMES ANY LEGAL LIABILITY OR RESPONSIBILITY FOR THE ACCURACY, COMPLETENESS, OR USEFULNESS OF ANY INFORMATION, APPARATUS, PRODUCT, OR PROCESS DISCLOSED, OR REPRESENTS THAT ITS USE WOULD NOT INFRINGE PRIVATELY OWNED RIGHTS. REFERENCE HEREIN TO ANY SPECIFIC COMMERCIAL PRODUCT, PROCESS, OR SERVICE BY TRADE NAME, TRADEMARK, MANUFACTURER, OR OTHERWISE DOES NOT NECESSARILY CONSTITUTE OR IMPLY ITS ENDORSEMENT, RECOMMENDATION, OR FAVORING BY THE UNITED STATES GOVERNMENT OR ANY AGENCY THEREOF. THE VIEWS AND OPINIONS OF AUTHORS EXPRESSED HEREIN DO NOT NECESSARILY STATE OR REFLECT THOSE OF THE UNITED STATES GOVERNMENT OR ANY AGENCY THEREOF.

NRC DISCLAIMER

THIS REPORT WAS PREPARED AS AN ACCOUNT OF WORK SPONSORED BY AN AGENCY OF THE U.S. GOVERNMENT. NEITHER THE U.S. GOVERNMENT NOR ANY AGENCY THEREOF, NOR ANY EMPLOYEE, MAKES ANY WARRANTY, EXPRESSED OR IMPLIED, OR ASSUMES ANY LEGAL LIABILITY OR RESPONSIBILITY FOR ANY THIRD PARTY'S USE, OR THE RESULTS OF SUCH USE, OF ANY INFORMATION, APPARATUS, PRODUCT, OR PROCESS DISCLOSED IN THIS PUBLICATION, OR REPRESENTS THAT ITS USE BY SUCH THIRD PARTY WOULD NOT INFRINGE PRIVATELY OWNED RIGHTS. THE STATEMENTS, FINDINGS, CONCLUSIONS AND RECOMMENDATIONS ARE THOSE OF THE AUTHOR(S) AND DO NOT NECESSARILY REFLECT THE VIEW OF THE US NUCLEAR REGULATORY COMMISSION.

SPONSORS' ACKNOWLEDGMENTS

The project sponsors would like to acknowledge the following individuals for directing the project:

Coppersmith Consulting, Inc.
2121 N. California Blvd., #290
Walnut Creek, CA 94596

Technical Integration (TI) Lead
K.J. Coppersmith

Savannah River Nuclear Solutions, LLC
Savannah River Site
Building 730-4B, Room 313
Aiken, SC 29808

CEUS SSC Project Manager
L.A. Salomone

This document describes research sponsored by the Electric Power Research Institute (EPRI), U.S. Department of Energy (U.S. DOE) under Award Number DE-FG07-08ID14908, and the U.S. Nuclear Regulatory Commission (U.S. NRC) under Award Number NCR-04-09-144.

This publication is a corporate document that should be cited in the literature in the following manner:

Technical Report: Central and Eastern United States Seismic Source Characterization for Nuclear Facilities. EPRI, Palo Alto, CA, U.S. DOE, and U.S. NRC: 2012.

AUTHORS

This document was prepared by the following investigators:

Technical Integration Lead	Kevin J. Coppersmith
Project Manager	Lawrence A. Salomone
Technical Integration Team	Chris W. Fuller Laura L. Glaser Kathryn L. Hanson Ross D. Hartleb William R. Lettis Scott C. Lindvall Stephen M. McDuffie Robin K. McGuire Gerry L. Stirewalt Gabriel R. Toro Robert R. Youngs
Database Manager	David L. Slayter
Technical Support	Serkan B. Bozkurt Randolph J. Cumbest Valentina Montaldo Falero Roseanne C. Perman Allison M. Shumway Frank H. Syms Martitia (Tish) P. Tuttle, Paleoliquefaction Data Resource

**This document has been
reproduced from the best available copy.**

ABSTRACT

This report describes a new seismic source characterization (SSC) model for the Central and Eastern United States (CEUS). It will replace the *Seismic Hazard Methodology for the Central and Eastern United States*, EPRI Report NP-4726 (July 1986) and the *Seismic Hazard Characterization of 69 Nuclear Plant Sites East of the Rocky Mountains*, Lawrence Livermore National Laboratory Model, (Bernreuter et al., 1989). The objective of the CEUS SSC Project is to develop a new seismic source model for the CEUS using a Senior Seismic Hazard Analysis Committee (SSHAC) Level 3 assessment process. The goal of the SSHAC process is to represent the center, body, and range of technically defensible interpretations of the available data, models, and methods. Input to a probabilistic seismic hazard analysis (PSHA) consists of both seismic source characterization and ground motion characterization. These two components are used to calculate probabilistic hazard results (or seismic hazard curves) at a particular site. This report provides a new seismic source model.

Results and Findings

The product of this report is a regional CEUS SSC model. This model includes consideration of an updated database, full assessment and incorporation of uncertainties, and the range of diverse technical interpretations from the larger technical community. The SSC model will be widely applicable to the entire CEUS, so this project uses a ground motion model that includes generic variations to allow for a range of representative site conditions (deep soil, shallow soil, hard rock). Hazard and sensitivity calculations were conducted at seven test sites representative of different CEUS hazard environments.

Challenges and Objectives

The regional CEUS SSC model will be of value to readers who are involved in PSHA work, and who wish to use an updated SSC model. This model is based on a comprehensive and traceable process, in accordance with SSHAC guidelines in NUREG/CR-6372, *Recommendations for Probabilistic Seismic Hazard Analysis: Guidance on Uncertainty and Use of Experts*. The model will be used to assess the present-day composite distribution for seismic sources along with their characterization in the CEUS and uncertainty. In addition, this model is in a form suitable for use in PSHA evaluations for regulatory activities, such as Early Site Permit (ESPs) and Combined Operating License Applications (COLAs).

Applications, Values, and Use

Development of a regional CEUS seismic source model will provide value to those who (1) have submitted an ESP or COLA for Nuclear Regulatory Commission (NRC) review before 2011; (2) will submit an ESP or COLA for NRC review after 2011; (3) must respond to safety issues resulting from NRC Generic Issue 199 (GI-199) for existing plants and (4) will prepare PSHAs to meet design and periodic review requirements for current and future nuclear facilities. This work replaces a previous study performed approximately 25 years ago. Since that study was

completed, substantial work has been done to improve the understanding of seismic sources and their characterization in the CEUS. Thus, a new regional SSC model provides a consistent, stable basis for computing PSHA for a future time span. Use of a new SSC model reduces the risk of delays in new plant licensing due to more conservative interpretations in the existing and future literature.

Perspective

The purpose of this study, jointly sponsored by EPRI, the U.S. Department of Energy (DOE), and the NRC was to develop a new CEUS SSC model. The team assembled to accomplish this purpose was composed of distinguished subject matter experts from industry, government, and academia. The resulting model is unique, and because this project has solicited input from the present-day larger technical community, it is not likely that there will be a need for significant revision for a number of years. See also Sponsors' Perspective for more details.

Approach

The goal of this project was to implement the CEUS SSC work plan for developing a regional CEUS SSC model. The work plan, formulated by the project manager and a technical integration team, consists of a series of tasks designed to meet the project objectives. This report was reviewed by a participatory peer review panel (PPRP), sponsor reviewers, the NRC, the U.S. Geological Survey, and other stakeholders. Comments from the PPRP and other reviewers were considered when preparing the report. The SSC model was completed at the end of 2011.

Keywords

Probabilistic seismic hazard analysis (PSHA)
Seismic source characterization (SSC)
Seismic source characterization model
Central and Eastern United States (CEUS)

CONTENTS

Abstract.....	ix
Contents.....	xi
List of Figures	xxv
List of Tables.....	lxxvii
Executive Summary	lxxxv
Participatory Peer Review Panel Final Report Dated October 24, 2011	xcv
Project Acknowledgements.....	ciii
Sponsor's Perspective	cv
Abbreviations	cix
1 INTRODUCTION	1-1
1.1 Background and History	1-1
1.1.1 EPRI-SOG and LLNL Projects	1-2
1.1.2 Development of the SSHAC Process	1-2
1.1.3 Implementation of the SSHAC Methodology	1-3
1.1.4 Regional SSC Model for Nuclear Facilities.....	1-3
1.1.5 Differences from USGS National Seismic Hazard Mapping Project.....	1-4
1.2 Purpose of the CEUS SSC Project	1-5
1.2.1 Implementation of SSHAC Level 3 Process	1-6
1.2.2 Goals: Stability and Longevity	1-8
1.2.3 Interface with Ground Motion Models	1-8
1.3 Study Region.....	1-10
1.4 Products of Project.....	1-10
1.4.1 Seismic Source Model for Study Region	1-10
1.4.2 Hazard Input Document.....	1-12
1.4.3 Documentation of Technical Bases for All Assessments	1-12
1.4.4 Other Key Products	1-13
1.4.4.1 Data Evaluation and Data Summary Tables.....	1-13

1.4.4.2 Database of Geologic, Geophysical, and Seismological Data.....	1-13
1.4.4.3 Earthquake Catalog with Uniform Moment Magnitudes.....	1-13
1.4.4.4 Updated Paleoseismicity Data and Guidance.....	1-14
1.4.4.5 Recommendations for Future Applications of SSC Model.....	1-14
2 SSHAC LEVEL 3 ASSESSMENT PROCESS AND IMPLEMENTATION	2-1
2.1 Goals and Activities of a SSHAC Assessment Process.....	2-2
2.1.1 Evaluation	2-4
2.1.2 Integration	2-4
2.2 Roles of CEUS SSC Project Participants.....	2-5
2.3 CEUS SSC Project Organization	2-7
2.4 Key Tasks and Activities	2-9
2.4.1 Database Development	2-9
2.4.2 Identification of Significant Issues	2-10
2.4.3 Workshop #1—Key Issues and Available Data	2-10
2.4.4 Workshop #2—Alternative Interpretations	2-12
2.4.5 Working Meetings.....	2-13
2.4.6 SSC Sensitivity Model Development	2-14
2.4.7 Workshop #3—Feedback	2-15
2.4.8 SSC Preliminary Model Development	2-16
2.4.9 Finalization and Review of SSC Draft and Final Model.....	2-17
2.4.10 Documentation	2-19
2.4.10.1 Development of the Hazard Input Document.....	2-19
2.4.10.2 Development of Earlier Draft Report.....	2-19
2.4.10.3 Draft Report Review.....	2-19
2.4.10.4 Final Report Development	2-20
2.5 Participatory Peer Review Panel.....	2-20
2.5.1 Roles and Responsibilities	2-20
2.5.2 Reviews and Feedback	2-20
2.5.3 Fulfillment of SSHAC-Prescribed Scope of Review of Both Technical and Process Issues	2-21
2.6 Consistency of CEUS SSC Assessment Process with SSHAC Guidelines	2-22
3 EARTHQUAKE CATALOG.....	3-1
3.1 Goals for the Earthquake Catalog Development.....	3-1
3.1.1 Completeness.....	3-1

3.1.2 Uniformity of Catalog Processing	3-2
3.1.3 Catalog Review	3-3
3.2 Catalog Compilation	3-4
3.2.1 Continental-Scale Catalogs	3-5
3.2.2 Regional Catalogs	3-7
3.2.3 Catalogs from Special Studies	3-7
3.2.4 Focal Depth Data.....	3-8
3.2.5 Nontectonic Events.....	3-9
3.2.6 Identification of Unique Earthquake Entries	3-9
3.3 Development of a Uniform Moment Magnitude Earthquake Catalog	3-11
3.3.1 Approach for Uniform Magnitude and Unbiased Recurrence Estimation	3-11
3.3.2 Estimation of $E[M]$ for the CEUS SSC Project Catalog	3-19
3.3.2.1 Effect of Magnitude Rounding on Statistical Tests	3-19
3.3.2.2 Moment Magnitude Data.....	3-20
3.3.2.3 Estimation of $E[M]$ from Body-Wave Magnitudes	3-22
3.3.2.4 Estimation of $E[M]$ from M_L Magnitudes.....	3-28
3.3.2.5 Estimation of $E[M]$ from M_S Magnitudes	3-29
3.3.2.6 Estimation of $E[M]$ from M_C and M_D Magnitudes.....	3-30
3.3.2.7 Estimation of $E[M]$ from the Logarithm of Felt Area	3-32
3.3.2.8 Estimation of $E[M]$ from the Maximum Intensity, I_0	3-32
3.3.2.9 Uniform Moment Magnitude Catalog of $E[M]$ and N^* Values.....	3-36
3.4 Identification of Independent Earthquakes	3-37
3.5 Catalog Completeness	3-39
4 CONCEPTUAL SEISMIC SOURCE CHARACTERIZATION FRAMEWORK.....	4-1
4.1 Needs for a Conceptual SSC Framework	4-2
4.1.1 Logic Tree Approach to Representing Alternatives and Assessing Uncertainties.....	4-2
4.1.1.1 Examples of Logic Trees	4-3
4.1.1.2 Assigning Weights to Logic Tree Branches	4-3
4.1.2 Data Identification and Evaluation	4-5
4.1.2.1 “Generic” Data Identification to Address Indicators of a Seismic Source	4-5
4.1.2.2 Data Evaluation for Particular Seismic Sources: Data Evaluation and Data Summary Tables	4-7
4.1.3 Methodology for Identifying Seismic Sources.....	4-9

4.1.3.1 Hazard-Informed Approach	4-11
4.1.3.2 Conclusions Regarding the Hazard Significance of Various SSC Issues	4-13
4.1.3.3 Criteria for Defining Seismic Sources	4-14
4.2 Master Logic Tree	4-18
4.2.1 Description of Logic Tree Elements	4-18
4.2.2 RLME Source Logic Tree	4-20
4.2.3 Mmax Zones Logic Tree	4-22
4.2.4 Seismotectonic Zones Branch	4-24
5 SSC MODEL: OVERVIEW AND METHODOLOGY	5-1
5.1 Overview of Spatial and Temporal Models	5-1
5.1.1 Spatial Model Considerations	5-1
5.1.2 Considerations Regarding Temporal Models	5-3
5.1.3 Perspective on CEUS SSC Models	5-4
5.2 Maximum Earthquake Magnitude Assessment	5-5
5.2.1 Approaches to Mmax Estimation in the CEUS	5-6
5.2.1.1 Bayesian Mmax Approach	5-8
5.2.1.2 Kijko Approach to Mmax Assessment	5-17
5.2.1.3 Weights for the Alternative Mmax Approaches	5-20
5.2.1.4 Example Mmax Distributions	5-20
5.2.2 Other Mmax Issues	5-21
5.3 Earthquake Recurrence Assessment	5-22
5.3.1 Smoothing to Represent Spatial Stationarity	5-22
5.3.2 Smoothing Approach	5-23
5.3.2.1 Development of Penalized-Likelihood Approach and Formulation	5-23
5.3.2.2 Application of the Model and Specification of Model Parameters	5-36
5.3.2.3 Exploration of Model Results in Parameter Space	5-40
5.3.2.4 Consideration of Constant b-Value Kernel Approaches	5-42
5.3.2.5 Comparison to EPRI-SOG Approach	5-45
5.3.2.6 Assessment of the Lombardi Study	5-46
5.3.3 Estimation of Recurrence for RLME Sources	5-47
5.3.3.1 Estimation of Occurrence Rates for the Poisson Model	5-48
5.3.3.2 Estimation of Occurrence Rates for a Renewal Model	5-51
5.3.3.3 Incorporating Uncertainty in the Input	5-52
5.3.3.4 RLME Magnitude Distribution	5-53

5.4 Assessment of Future Earthquake Characteristics	5-54
5.4.1 Tectonic Stress Regime	5-55
5.4.2 Sense of Slip/Style of Faulting.....	5-55
5.4.3 Strike and Dip of Ruptures	5-55
5.4.4 Seismogenic Crustal Thickness	5-56
5.4.5 Fault Rupture Area	5-57
5.4.6 Rupture Length-to-Width Aspect Ratio.....	5-57
5.4.7 Relationship of Rupture to Source Zone Boundaries	5-58
5.5 Predicted Seismic Moment Rate	5-58
6 SSC MODEL: RLME SOURCES AND MMAX ZONES BRANCH.....	6-1
6.1 RLME Sources	6-1
6.1.1 Charlevoix.....	6-3
6.1.1.1 Evidence for Temporal Clustering.....	6-4
6.1.1.2 Localizing Tectonic Features	6-4
6.1.1.3 Geometry and Style of Faulting	6-5
6.1.1.4 RLME Magnitude	6-7
6.1.1.5 RLME Recurrence	6-8
6.1.2 Charleston	6-10
6.1.2.1 Evidence for Temporal Clustering.....	6-11
6.1.2.2 Localizing Feature	6-12
6.1.2.3 Geometry and Style of Faulting	6-12
6.1.2.4 RLME Magnitude	6-15
6.1.2.5 RLME Recurrence	6-17
6.1.3 Cheraw Fault	6-22
6.1.3.1 Evidence for Temporal Clustering.....	6-23
6.1.3.2 Geometry and Style of Faulting	6-24
6.1.3.3 RLME Magnitude	6-25
6.1.3.4 RLME Recurrence	6-26
6.1.4 Meers Fault.....	6-28
6.1.4.1 Evidence for Temporal Clustering.....	6-29
6.1.4.2 Localizing Feature	6-29
6.1.4.3 Geometry and Style of Faulting	6-30
6.1.4.4 RLME Magnitude	6-31
6.1.4.5 RLME Recurrence	6-34

6.1.5 Reelfoot Rift–New Madrid Fault System	6-35
6.1.5.1 Evidence for Temporal Clustering.....	6-40
6.1.5.2 Geometry and Style of Faulting	6-42
6.1.5.3 RLME Magnitude	6-44
6.1.5.4 RLME Recurrence	6-47
6.1.6 Reelfoot Rift—Eastern Rift Margin Fault	6-50
6.1.6.1 Evidence for Temporal Clustering.....	6-53
6.1.6.2 Geometry and Style of Faulting	6-53
6.1.6.3 RLME Magnitude	6-54
6.1.6.4 RLME Recurrence	6-56
6.1.7 Reelfoot Rift—Marianna	6-57
6.1.7.1 Evidence for Temporal Clustering.....	6-58
6.1.7.2 Geometry and Style of Faulting	6-59
6.1.7.3 RLME Magnitude	6-60
6.1.7.4 RLME Recurrence	6-61
6.1.8 Reelfoot Rift—Commerce Fault Zone	6-62
6.1.8.1 Evidence for Temporal Clustering.....	6-63
6.1.8.2 Geometry and Style of Faulting	6-64
6.1.8.3 RLME Magnitude	6-65
6.1.8.4 RLME Recurrence	6-66
6.1.9 Wabash Valley	6-68
6.1.9.1 Evidence for Temporal Clustering.....	6-69
6.1.9.2 Geometry and Style of Faulting	6-69
6.1.9.3 RLME Magnitude	6-72
6.1.9.4 RLME Recurrence	6-73
6.2 Mmax Distributed Seismicity Source Zones.....	6-74
6.2.1 Definition of Mmax Zones	6-74
6.2.2 Criteria for Defining the MESE/NMESE Boundary	6-75
6.3 Maximum Magnitude Distributions for Mmax Distributed Seismicity Sources.....	6-76
6.3.1 Maximum Observed Earthquake Magnitude	6-76
6.3.2 Mmax Distributions	6-77
6.4 Recurrence Parameters	6-78
6.4.1 Rate and b-Value Maps for Single Zone and Two Zones.....	6-78
6.4.2 Comparison of Recurrence Parameters to Catalog.....	6-79

7 SSC MODEL: SEISMOTECTONIC ZONES BRANCH	7-1
7.1 Approaches and Data Used to Define Seismotectonic Zones	7-1
7.2 RLME Sources in the Seismotectonic Zones Branch.....	7-4
7.3 Seismotectonic Source Zones.....	7-4
7.3.1 St. Lawrence Rift Zone (SLR)	7-4
7.3.1.1 Background.....	7-5
7.3.1.2 Basis for Defining Seismotectonic Zone	7-11
7.3.1.3 Basis for Zone Geometry	7-12
7.3.1.4 Basis for Zone Mmax	7-12
7.3.1.5 Future Earthquake Characteristics	7-13
7.3.2 Great Meteor Hotspot Zone (GMH)	7-15
7.3.2.1 Background.....	7-16
7.3.2.2 Basis for Defining Seismotectonic Zone	7-18
7.3.2.3 Basis for Zone Geometry	7-19
7.3.2.4 Basis for Zone Mmax	7-19
7.3.2.5 Future Earthquake Characteristics	7-20
7.3.3 Northern Appalachian Zone (NAP)	7-21
7.3.3.1 Background.....	7-21
7.3.3.2 Basis for Defining Seismotectonic Zone	7-23
7.3.3.3 Basis for Zone Geometry	7-24
7.3.3.4 Basis for Zone Mmax	7-24
7.3.3.5 Future Earthquake Characteristics	7-25
7.3.4 Paleozoic Extended Crust (PEZ).....	7-25
7.3.4.1 Background.....	7-26
7.3.4.2 Basis for Defining Seismotectonic Zone	7-32
7.3.4.3 Basis for Zone Geometry	7-33
7.3.4.4 Basis for Zone Mmax	7-34
7.3.4.5 Future Earthquake Characteristics	7-36
7.3.5 Illinois Basin Extended Basement Zone (IBEB)	7-37
7.3.5.1 Background.....	7-38
7.3.5.2 Basis for Defining Seismotectonic Zone	7-38
7.3.5.3 Basis for Zone Geometry	7-40
7.3.5.4 Basis for Zone Mmax	7-41
7.3.5.5 Future Earthquake Characteristics	7-41
7.3.6 Reelfoot Rift Zone (RR)	7-42

7.3.6.1 Background.....	7-42
7.3.6.2 Basis for Defining Seismotectonic Zone	7-46
7.3.6.3 Basis for Zone Geometry	7-46
7.3.6.4 Basis for Zone Mmax	7-47
7.3.6.5 Future Earthquake Characteristics	7-48
7.3.7 Extended Continental Crust–Atlantic Margin Zone (ECC-AM)	7-48
7.3.7.1 Background.....	7-49
7.3.7.2 Basis for Defining Seismotectonic Zone	7-53
7.3.7.3 Basis for Geometry	7-54
7.3.7.4 Basis for Mmax	7-54
7.3.7.5 Future Earthquake Characteristics	7-55
7.3.8 Atlantic Highly Extended Crust Zone (AHEx).....	7-55
7.3.8.1 Basis for Defining Seismotectonic Zone	7-56
7.3.8.2 Basis for Geometry	7-57
7.3.8.3 Basis for Mmax	7-57
7.3.8.4 Future Earthquake Characteristics	7-57
7.3.9 Extended Continental Crust–Gulf Coast Zone (ECC-GC).....	7-58
7.3.9.1 Basis for Defining Seismotectonic Zone	7-58
7.3.9.2 Basis for Zone Geometry	7-59
7.3.9.3 Basis for Zone Mmax	7-62
7.3.9.4 Future Earthquake Characteristics	7-63
7.3.9.5 Possible Paleoliquefaction Features in Arkansas, Louisiana, and Mississippi	7-64
7.3.10 Gulf Coast Highly Extended Crust Zone (GHEx).....	7-65
7.3.10.1 Basis for Defining Seismotectonic Zone	7-66
7.3.10.2 Basis for Zone Geometry	7-66
7.3.10.3 Basis for Zone Mmax	7-66
7.3.10.4 Future Earthquake Characteristics	7-67
7.3.11 Oklahoma Aulacogen Zone (OKA).....	7-68
7.3.11.1 Basis for Defining Seismotectonic Zone	7-69
7.3.11.2 Basis for Zone Geometry	7-69
7.3.11.3 Basis for Zone Mmax	7-70
7.3.11.4 Future Earthquake Characteristics	7-70
7.3.12 Midcontinent-Craton Zone (MidC)	7-70
7.3.12.1 Background.....	7-71

7.3.12.2 Basis for Defining Seismotectonic Zone	7-76
7.3.12.3 Basis for Zone Geometry	7-77
7.3.12.4 Basis for Zone Mmax	7-77
7.3.12.5 Future Earthquake Characteristics	7-77
7.4 Maximum Magnitude Distributions for Seismotectonic Distributed Seismicity Sources	7-78
7.4.1 Maximum Observed Earthquake Magnitude	7-78
7.4.2 Mmax Distributions	7-79
7.5 Recurrence Parameters	7-80
7.5.1 Rate and b-Value Maps for Single Zone and Two Zones	7-80
7.5.2 Comparison of Recurrence Parameters to Catalog	7-80
8 DEMONSTRATION HAZARD CALCULATIONS	8-1
8.1 Background on Demonstration Hazard Calculations	8-1
8.2 Demonstration Hazard Calculations	8-2
8.2.1 Central Illinois Site	8-4
8.2.2 Chattanooga Site	8-5
8.2.3 Houston Site	8-6
8.2.4 Jackson Site	8-7
8.2.5 Manchester Site	8-9
8.2.6 Savannah Site	8-9
8.2.7 Topeka Site	8-10
9 USE OF THE CEUS SSC MODEL IN PSHA	9-1
9.1 Overview	9-1
9.2 Hazard Input Document (HID)	9-2
9.3 Implementation Instructions	9-2
9.3.1 Simplifications to Seismic Sources	9-2
9.3.1.1 Charleston RLME	9-3
9.3.1.2 Charlevoix RLME	9-3
9.3.1.3 Cheraw RLME	9-4
9.3.1.4 Commerce Fault Zone RLME	9-5
9.3.1.5 Eastern Rift Margin North RLME	9-5
9.3.1.6 Eastern Rift Margin South RLME	9-5
9.3.1.7 Marianna RLME	9-6
9.3.1.8 Meers RLME	9-6

9.3.1.9 New Madrid Fault System RLME	9-7
9.3.1.10 Wabash Valley RLME	9-7
9.3.1.11 Background Sources.....	9-8
9.3.2 Accessing the SSC Model and Components from the Website	9-8
9.3.3 Accessing Project Databases	9-9
9.3.4 Use of SSC Model with Site-Specific Refinements	9-10
9.4 Hazard Significance	9-10
9.4.1 Data Available to Evaluate the Precision of Seismic Hazard Estimates.....	9-10
9.4.2 Observed Imprecision in Seismic Hazard Estimates	9-11
9.4.2.1 Area Seismic Sources.....	9-11
9.4.2.2 RLME Seismic Sources	9-12
9.4.2.3 Ground Motion Equations	9-15
9.4.2.4 Site Response	9-19
9.4.3 Conclusions on the Precision in Seismic Hazard Estimates	9-19
10 REFERENCES	10-1
11 GLOSSARY OF KEY TERMS	11-1
A DESCRIPTION OF THE CEUS SSC PROJECT DATABASE	A-1
A.1 Data Sources	A-2
A.2 Project Database Design and Management	A-3
A.3 Workflow and Data Assessment	A-3
A.3.1 Workflow	A-3
A.3.2 Digital Data.....	A-4
A.3.3 Nondigital Data	A-4
A.4 Use of Project Database in Model Development	A-5
A.5 Metadata	A-5
A.6 Database Delivery Format	A-6
B EARTHQUAKE CATALOG DATABASE	B-1
B.1 CEUS SSC Uniform Moment Magnitude Earthquake Catalog	B-1
B.2 Moment Magnitude Data.....	B-2
B.3 Approximate Moment Magnitude Data	B-3
B.4 CEUS SSC Project Data.....	B-3

C DATA EVALUATION TABLES.....	C-1
Introduction	C-2
D DATA SUMMARY TABLES	D-1
Introduction	D-2
E CEUS PALEOLIQUEFACTION DATABASE, UNCERTAINTIES ASSOCIATED WITH PALEOLIQUEFACTION DATA, AND GUIDANCE FOR SEISMIC SOURCE CHARACTERIZATION.....	E-i
E.1 Development of the Paleoliquefaction Database	E-1
E.1.1 Database Structure	E-1
E.1.2 Regional Data Sets	E-4
E.2 Uncertainties Associated with Paleoliquefaction Data	E-24
E.2.1 Collection of Paleoliquefaction Data	E-24
E.2.2 Uncertainties Related to Interpretation of Paleoliquefaction Data.....	E-35
E.2.3 Recommendations for Future Research	E-43
E.3 Guidance for the Use of Paleoliquefaction Data in Seismic Source Characterization.....	E-44
E.4 Glossary.....	E-46
E.5 References	E-49
E.5.1 References Cited in Paleoliquefaction Database	E-49
E.5.2 References Cited in Appendix E	E-54
F WORKSHOP SUMMARIES	F-1
WORKSHOP 1: KEY ISSUES AND AVAILABLE DATA	
DAY 1–TUESDAY, JULY 22, 2008	F-1
DAY 2–WEDNESDAY, JULY 23, 2008	F-10
REFERENCES.....	F-17
WORKSHOP 2: ALTERNATIVE INTERPRETATIONS	
DAY 1–WEDNESDAY, FEBRUARY 18, 2009	F18
DAY 2–THURSDAY, FEBRUARY 19, 2009.....	F-24
DAY 3–FRIDAY, FEBRUARY 20, 2009	F-29
REFERENCES	F-34
WORKSHOP 3: FEEDBACK	
DAY 1–TUESDAY, AUGUST 25, 2009	F-42
DAY 2–WEDNESDAY, AUGUST 26, 2009.....	F-49

G BIOGRAPHIES OF PROJECT TEAM.....	G-1
EPRI MANAGEMENT	G-2
PROJECT MANAGER	G-2
TI TEAM	G-3
TECHNICAL SUPPORT.....	G-7
DATABASE MANAGER	G-9
PARTICIPATORY PEER REVIEW PANEL.....	G-9
SPONSOR REVIEWERS.....	G-14
 H CEUS SSC MODEL HAZARD INPUT DOCUMENT (HID).....	H-1
H.1 Introduction	H-1
H.2 Seismic Source Model Structure and Master Logic Tree	H-1
H.3 Mmax Zones Distributed Seismicity Sources	H-2
H.3.1 Division of Study Region	H-2
H.3.2 Location of Boundary of Mesozoic Extension	H-2
H.3.3 Magnitude Interval Weights for Fitting Earthquake Occurrence Parameters	H-2
H.3.4 Mmax Zones	H-2
H.3.5 Seismogenic Crustal Thickness	H-2
H.3.6 Future Earthquake Rupture Characteristics	H-3
H.3.7 Assessment of Seismicity Rates	H-3
H.3.8 Degree of Smoothing Applied in Defining Spatial Smoothing of Seismicity Rates	H-3
H.3.9 Uncertainty in Earthquake Recurrence Rates.....	H-3
H.3.10 Uncertainty in Maximum Magnitude.....	H-4
H.4 Seismotectonic Zones	H-4
H.4.1 Alternative Zonation Models	H-4
H.4.2 Magnitude Interval Weights for Fitting Earthquake Occurrence Parameters	H-4
H.4.3 Seismotectonic Zones.....	H-5
H.4.4 Seismogenic Crustal Thickness.....	H-5
H.4.5 Future Earthquake Rupture Characteristics	H-5
H.4.6 Assessment of Seismicity Rates	H-5
H.4.7 Degree of Smoothing Applied in Defining Spatial Smoothing of Seismicity Rates	H-5
H.4.8 Uncertainty in Earthquake Recurrence Rates	H-5
H.4.9 Uncertainty in Maximum Magnitude	H-6
H.5 RLME Sources	H-6

H.5.1 Charlevoix RLME Seismic Source Model	H-6
H.5.2 Charleston RLME Seismic Source Model	H-7
H.5.3 Cheraw RLME Seismic Source Model	H-9
H.5.4 Meers RLME Seismic Source Model	H-11
H.5.5 New Madrid Fault System RLME Seismic Source Model	H-12
H.5.6 Eastern Rift Margin Fault RLME Seismic Source Model	H-14
H.5.7 Marianna Zone RLME Seismic Source Model	H-15
H.5.8 Commerce Fault RLME Seismic Source Model	H-16
H.5.9 Wabash Valley RLME Seismic Source Model	H-18
/ PPRP REVIEW COMMENTS	I-1
CORRESPONDENCE—CONTENTS	I-3
Participatory Peer Review Panel (PPRP) Letters	I-3
Technical Integration (TI) Team and Project Manager (PM) Response to PPRP Letters	I-4
J MAGNITUDE-RECURRENCE MAPS FOR ALL REALIZATIONS AND ALL SOURCE-ZONE CONFIGURATIONS	J-1
K SCR DATABASE USED TO DEVELOP MMAX PRIOR DISTRIBUTIONS	K-1
K.1 SCR Earthquake Catalog	K-1
K.2 SCR Crustal Domains	K-3
L QUALITY ASSURANCE	L-1
L.1 BACKGROUND	L-1
L.2 CEUS SSC PROJECT	L-2
L.2.1 Introduction	L-2
L.3 BEST BUSINESS PRACTICES	L-3
L.3.1 General	L-3
L.4 CEUS SSC EARTHQUAKE CATALOG DEVELOPMENT	L-3
L.4.1 External Review of Earthquake Catalog	L-3
L.4.2 Simulation Testing	L-4
L.4.3 Checks for Consistency in Magnitude Conversion from Intensity	L-4
L.4.4 Use of Verified Computer Programs	L-4
L.5 RECURRENCE ANALYSIS AND SPATIAL SMOOTHING	L-4
L.5.1 Introduction	L-4
L.5.2 Recurrence Comparisons at the Source-Zone Level	L-5

L.5.3 Recurrence Comparisons for Portions of a Source Zone	L-5
L.5.4 Examination of Recurrence Maps	L-5
L.5.5 Test with a Synthetic Catalog Homogeneous Seismicity	L-5
L.5.6 Test for the Adequacy of Eight Maps to Represent Epistemic Uncertainty	L-6
L.6 HAZARD CALCULATION SOFTWARE	L-6
L.6.1 Introduction.....	L-6
L.6.2 Test for the Treatment of Variable b.....	L-6
L.6.3 Test for the Treatment of Dipping Ruptures Within a Source Zone.....	L-6
L.6.4 Tests for Treatment of Epistemic Uncertainty from Sources that Make Small Contribution to Hazard.....	L-6

LIST OF FIGURES

Figure 1.3-1 Map showing the study area and test sites for the CEUS SSC Project.....	1-15
Figure 2.3-1 CEUS SSC Project organization	2-33
Figure 2.3-2 Lines of communication among the participants of the CEUS SSC Project	2-34
Figure 2.4-1 Essential activities associated with a SSHAC Level 3 or 4 project (Coppersmith et al., 2010).....	2-35
Figure 3.2-1 Areal coverage of the primary earthquake catalog sources. Top: GSC catalog (Halchuk, 2009); bottom: USGS seismic hazard mapping catalog (Petersen et al., 2008). Red line denotes boundary of study region. Blue line denotes portion of each catalog used for development of project catalog.....	3-57
Figure 3.2-2 Histogram of M_L magnitudes from the GSC SHEEF catalog for the time period 1600-1899 and the region east of longitude -105° and south of latitude 53°	3-58
Figure 3.2-3 Histogram of M_L magnitudes from the GSC SHEEF catalog for the time period 1900-1929 and the region east of longitude -105° and south of latitude 53°	3-59
Figure 3.2-4 Histogram of M_L magnitudes from the GSC SHEEF catalog for the time period 1930-1979 and the region east of longitude -105° and south of latitude 53°	3-60
Figure 3.2-5 Histogram of M_L magnitudes from the GSC SHEEF catalog for the time period 1980-2007 and the region east of longitude -105° and south of latitude 53°	3-61
Figure 3.2-6 Histogram of M_L magnitudes from the revised catalog with GSC as the source for the time period 1928-1979	3-62
Figure 3.2-7 Map of the CEUS SSC Project catalog showing earthquakes of uniform moment magnitude $E[M]$ 2.9 and larger. Colored symbols denote earthquakes not contained in the USGS seismic hazard mapping catalog.	3-63
Figure 3.3-1 Illustration of equivalence of the M^* and γ^2 corrections to remove bias in earthquake recurrence relationships estimated from magnitudes with uncertainty	3-64
Figure 3.3-2 Approximate moment magnitudes from Atkinson (2004b) compared to values of M given in Table B-2 in Appendix B for earthquakes in common	3-65
Figure 3.3-3 Approximate moment magnitudes from Boatwright (1994) compared to values of M given in Table B-2 in Appendix B for earthquakes in common	3-66
Figure 3.3-4 Approximate moment magnitudes from Moulis (2002) compared to values of M given in Table B-2 in Appendix B for earthquakes in common.....	3-67
Figure 3.3-5 Difference between M_N reported by the GSC and M_N or $m_{Lg(f)}$ reported by the Weston Observatory catalog as a function of time.....	3-68
Figure 3.3-6 Spatial distribution of earthquakes with body-wave (m_b , m_{bLg} , M_N) and M magnitudes in the CEUS SSC Project catalog for the Midcontinent region. Color codes indicate the source of the body-wave magnitudes.....	3-69
Figure 3.3-7 m_b - M data for the earthquakes shown on Figure 3.3-6. Red curve shows the preferred offset fit $M = m_b - 0.28$	3-70

Figure 3.3-8 Residuals from offset fit shown on Figure 3.3-7 plotted against earthquake year	3-71
Figure 3.3-9 Spatial distribution of earthquakes with body wave (m_b , m_{bLg} , M_N) and M magnitudes in the CEUS SSC Project catalog for the northeastern portion of the study region. Color codes indicate the source of the body-wave magnitudes.	3-72
Figure 3.3-10 m_b - M data for the earthquakes shown on Figure 3.3-9. Red curve shows the preferred offset fit $M = m_b - 0.42$	3-73
Figure 3.3-11 Residuals from offset fit shown on Figure 3.3-10 plotted against earthquake year	3-74
Figure 3.3-12 Residuals for GSC data from offset fit shown on Figure 3.3-10 plotted against earthquake year.....	3-75
Figure 3.3-13 Residuals for WES data from offset fit shown on Figure 3.3-10 plotted against earthquake year.....	3-76
Figure 3.3-14 Residuals for data from sources other than GSC or WES from offset fit shown on Figure 3.3-10 plotted against earthquake year	3-77
Figure 3.3-15 Difference between body-wave magnitudes reported by LDO and those by other sources as a function of year	3-78
Figure 3.3-16 Spatial distribution of earthquakes with reported GSC body-wave magnitudes. Red and blue symbols indicate earthquakes with both m_b and M magnitudes for $m_b \geq 3.5$. Dashed line indicates the portion of the study region considered the “Northeast” for purposes of magnitude scaling.....	3-79
Figure 3.3-17 M - m_b as a function of time for m_b data from the GSC shown on Figure 3.3-16	3-80
Figure 3.3-18 Plot of magnitude differences $m_{bLg} - m(3 \text{ Hz})$ for the OKO catalog.....	3-81
Figure 3.3-19 Final m_b - M data set. Vertical dashed lines indicate the magnitude range used to develop the scaling relationship. Diagonal line indicates a one-to-one correlation.	3-82
Figure 3.3-20 Spatial distribution of earthquakes in the CEUS SSC Project catalog with instrumental M_L magnitudes.....	3-83
Figure 3.3-21 Spatial distribution of earthquakes in the CEUS SSC Project catalog with instrumental M_L magnitudes and M magnitudes	3-84
Figure 3.3-22 M_L - M data from the CEUS SSC Project catalog and robust regression fit to the data	3-85
Figure 3.3-23 Relationship between M_N and M_L for the GSC data	3-86
Figure 3.3-24 Data from the northeastern portion of the study region with M_L and M_C or M_D magnitude from catalog sources other than the GSC	3-87
Figure 3.3-25 Data from the northeastern portion of the study region with M_L and M magnitudes from sources other than the GSC.....	3-88
Figure 3.3-26 Spatial distribution of earthquakes in the CEUS SSC Project catalog with $M_S \geq 3$ magnitudes	3-89
Figure 3.3-27 M_S - M data from the CEUS SSC Project catalog and quadratic polynomial fit to the data	3-90
Figure 3.3-28 Spatial distribution of earthquakes in the CEUS SSC Project catalog with $M_C \geq 2.5$ magnitudes	3-91

Figure 3.3-29 Spatial distribution of earthquakes in the CEUS SSC Project catalog with $M_C \geq 2.5$ and M magnitudes	3-92
Figure 3.3-30 Spatial distribution of earthquakes in the CEUS SSC Project catalog with $M_D \geq 3$ magnitudes	3-93
Figure 3.3-31 Spatial distribution of earthquakes in the CEUS SSC Project catalog with both M_D and M magnitudes	3-94
Figure 3.3-32 M_C - M data from the CEUS SSC Project catalog and linear regression fit to the data	3-95
Figure 3.3-33 Spatial distribution of earthquakes with reported M_C and M_D magnitudes	3-96
Figure 3.3-34 Comparison of M_C and M_D magnitudes for the LDO and WES catalogs	3-97
Figure 3.3-35 Comparison of M_C with M_D for at least one of the two magnitude types reported in the OKO catalog	3-98
Figure 3.3-36 Comparison of M_C with M_D for at least one of the two magnitude types reported in the CERI catalog	3-99
Figure 3.3-37 Comparison of M_C with M_D for at least one of the two magnitude types reported in the SCSN catalog	3-100
Figure 3.3-38 Comparison of M_C with M_D for at least one of the two magnitude types reported in other catalogs for earthquakes in the Midcontinent portion of the study region	3-101
Figure 3.3-39 Relationship between M and M_C , M_D , or M_L for the Midcontinent portion of the study region	3-102
Figure 3.3-40 Comparison of M_C and M_D magnitudes with M_L magnitudes for the region between longitudes 105°W and 100°W	3-103
Figure 3.3-41 Comparison of m_b magnitudes with M_L magnitudes for the region between longitudes 105°W and 100°W	3-104
Figure 3.3-42 Comparison of m_b magnitudes with M_C and M_D magnitudes for the region between longitudes 105°W and 100°W	3-105
Figure 3.3-43 Spatial distribution of earthquake with $\ln(\text{FA})$ in the CEUS SSC Project catalog	3-106
Figure 3.3-44 Catalog $\ln(\text{FA})$ - M data and fitted model	3-107
Figure 3.3-45 Spatial distribution of earthquakes in the CEUS SSC Project catalog with reported values of I_0	3-108
Figure 3.3-46 I_0 and M data for earthquakes in the CEUS SSC Project catalog. Curves show locally weighted least-squares fit (Loess) to the data and the relationship published by Johnston (1996b).	3-109
Figure 3.3-47 I_0 and m_b data from the NCEER91 catalog. Plotted are the relationships between I_0 and m_b developed by EPRI (1988) (EPRI-SOG) and Sibol et al. (1987)	3-110
Figure 3.3-48 Categorical model fits of I_0 as a function and M for earthquakes in the CEUS SSC Project catalog	3-111
Figure 3.3-49 Results from proportional odds logistic model showing the probability of individual intensity classes as a function of M	3-112
Figure 3.3-50 Comparison of I_0 and m_b data from the CEUS SSC Project catalog for those earthquakes with reported values of M (M set) and the full catalog (full set). Locally weighted least-squares fits to the two data sets are shown along with the	

relationship use to develop the EPRI (1988) catalog and the Sibol et al. (1987) relationship used in the NCEER91 catalog.....	3-113
Figure 3.3-51 Linear fits to the data from Figure 3.3-50 for $I_0 \geq V$	3-114
Figure 3.3-52 Comparison of I_0 and m_b data from the project, with m_b adjusted for the difference in m_b to M scaling	3-115
Figure 3.3-53 Linear fits to the data from Figure 3.3-52 for $I_0 \geq V$	3-116
Figure 3.3-54 Composite I_0 –M data set used for assessment of I_0 scaling relationship	3-117
Figure 3.3-55 Linear and inverse sigmoid models fit to the project data for $I_0 > IV$	3-118
Figure 3.4-1 Illustration of process used to identify clusters of earthquakes (from EPRI, 1988, Vol. 1): (a) local and extended time and distance windows, (b) buffer window, and (c) contracted window	3-119
Figure 3.4-2 Identification of secondary (dependent) earthquakes inside the cluster region through Poisson thinning (from EPRI, 1988, Vol. 1).....	3-120
Figure 3.4-3 Comparison of dependent event time and distance windows with results for individual clusters in the project catalog.....	3-121
Figure 3.5-1 Earthquake catalog and catalog completeness regions used in EPRI-SOG (EPRI, 1988)	3-122
Figure 3.5-2 CEUS SSC Project earthquake catalog and modified catalog completeness regions	3-123
Figure 3.5-3 Plot of year versus location for the CEUS SSC Project earthquake catalog. Red lines indicate the boundaries of the catalog completeness time periods.....	3-124
Figure 3.5-4 (1 of 7) “Stepp” plots of earthquake recurrence rate as a function of time for the individual catalog completeness regions shown on Figure 3.5-2	3-125
Figure 3.5-4 (2 of 7) “Stepp” plots of earthquake recurrence rate as a function of time for the individual catalog completeness regions shown on Figure 3.5-2	3-126
Figure 3.5-4 (3 of 7) “Stepp” plots of earthquake recurrence rate as a function of time for the individual catalog completeness regions shown on Figure 3.5-2	3-127
Figure 3.5-4 (4 of 7) “Stepp” plots of earthquake recurrence rate as a function of time for the individual catalog completeness regions shown on Figure 3.5-2	3-128
Figure 3.5-4 (5 of 7) “Stepp” plots of earthquake recurrence rate as a function of time for the individual catalog completeness regions shown on Figure 3.5-2	3-129
Figure 3.5-4 (6 of 7) “Stepp” plots of earthquake recurrence rate as a function of time for the individual catalog completeness regions shown on Figure 3.5-2	3-130
Figure 3.5-4 (7 of 7) “Stepp” plots of earthquake recurrence rate as a function of time for the individual catalog completeness regions shown on Figure 3.5-2	3-131
Figure 4.1.1-1 Example logic tree from the PEGASOS project (NAGRA, 2004) showing the assessment of alternative conceptual models on the logic tree. Each node of the logic tree represents an assessment that is uncertain. Alternative branches represent the alternative models or parameter values, and the weights associated with each branch reflect the TI Team’s relative degree of belief that each branch is the correct model or parameter value.	4-40
Figure 4.1.1-2 Example logic tree from the PVHA-U (SNL, 2008) project showing the treatment of alternative conceptual models in the logic tree	4-41

Figure 4.2.1-1 Master logic tree showing the Mmax zones and seismotectonic zones alternative conceptual models for assessing the spatial and temporal characteristics of future earthquake sources in the CEUS.....	4-42
Figure 4.2.2-1 Example of a logic tree for RLME sources. Shown is the tree for the Marianna RLME source.	4-43
Figure 4.2.2-2 Map showing RLME sources, some with alternative source geometries (discussed in Section 6.1).	4-44
Figure 4.2.3-1 Logic tree for the Mmax zones branch of the master logic tree.....	4-45
Figure 4.2.3-2 Subdivision used in the Mmax zones branch of the master logic tree. Either the region is considered one zone for purposes of Mmax or the region is divided into two zones as shown: a Mesozoic-and-younger extension (MESE) zone and a non-Mesozoic-and-younger zone (NMESE). In this figure the “narrow” MESE zone is shown	4-46
Figure 4.2.3-3 Subdivision used in the Mmax zones branch of the master logic tree. Either the region is considered one zone for purposes of Mmax or the region is divided into two zones as shown: a Mesozoic-and-younger extension (MESE) zone and a non-Mesozoic-and-younger zone (NMESE). In this figure the “wide” MESE zone is shown	4-47
Figure 4.2.4-1(a) Logic tree for the seismotectonic zones branch of the master logic tree	4-48
Figure 4.2.4-1(b) Logic tree for the seismotectonic zones branch of the master logic tree	4-49
Figure 4.2.4-2 Seismotectonic zones shown in the case where the Rough Creek Graben is not part of the Reelfoot Rift (RR), and the Paleozoic Extended Zone is narrow (PEZ-N)	4-50
Figure 4.2.4-3 Seismotectonic zones shown in the case where the Rough Creek Graben is part of the Reelfoot Rift (RR-RCG), and the Paleozoic Extended Zone is narrow (PEZ-N)	4-51
Figure 4.2.4-4 Seismotectonic zones shown in the case where the Rough Creek Graben is not part of the Reelfoot Rift (RR), and the Paleozoic Extended Crust is wide (PEZ-W)	4-52
Figure 4.2.4-5 Seismotectonic zones shown in the case where the Rough Creek Graben is part of the Reelfoot Rift (RR-RCG), and the Paleozoic Extended Crust is wide (PEZ-W)	4-53
Figure 5.2.1-1 Diagrammatic illustration of the Bayesian Mmax approach showing (a) the prior distribution, (b) the likelihood function, and (c) the posterior distribution. The posterior distribution is represented by a discrete distribution (d) for implementation in hazard analysis.	5-72
Figure 5.2.1-2 Diagrammatic illustration of the Bayesian Mmax approach showing (a) the prior distribution, (b) the likelihood function, and (c) the posterior distribution. The posterior distribution is represented by a discrete distribution (d) for implementation in hazard analysis.	5-73
Figure 5.2.1-3 Median values of $m_{\max-obs}$ as a function of maximum magnitude, m^u , and sample size N , the number of earthquakes $\geq M$ 4.5.....	5-74
Figure 5.2.1-4 Histograms of $m_{\max-obs}$ for extended and non-extended superdomains	5-75

Figure 5.2.1-5 Histograms of $m_{\max-obs}$ for Mesozoic-and-younger extended (MESE) superdomains and for older extended and non-extended (NMESE) superdomains	5-76
Figure 5.2.1-6 Histograms of $m_{\max-obs}$ for Mesozoic-and-younger extended (MESE) superdomains and for older extended and non-extended (NMESE) superdomains using age of most recent extension for the age classification	5-77
Figure 5.2.1-7 Histograms of $m_{\max-obs}$ for Mesozoic-and-younger extended (MESE) superdomains and for older extended and non-extended (NMESE) superdomains using final sets indicated by asterisks in Tables 5.2.1-1 and 5.2.1-2	5-78
Figure 5.2.1-8 Histograms of $m_{\max-obs}$ for combined (COMB) superdomains using final sets indicated by asterisks in Table 5.2.1-3	5-79
Figure 5.2.1-9 Bias adjustments from $m_{\max-obs}$ to m^u for the three sets of superdomain analysis results presented in Table 5.2.1-4.....	5-80
Figure 5.2.1-10 Results of simulations of estimates of Mmax using the Bayesian approach for earthquake catalogs ranging in size from 1 to 1,000 earthquakes. True Mmax is set at the mean of the prior distribution.....	5-81
Figure 5.2.1-11 Comparison of the Kijko (2004) estimates of m^u for given values of $m_{\max-obs}$ and N , the number of earthquakes of magnitude ≥ 4.5 . Also shown is the median value of $m_{\max-obs}$ for given m^u obtained using Equation 5.2.1-2.....	5-82
Figure 5.2.1-12 Behavior of the cumulative probability function for m^u (Equation 5.2.1-9) for the K-S-B estimator and a value of $m_{\max-obs}$ equal to 6.....	5-83
Figure 5.2.1-13 Example Mmax distribution assessed for the Mesozoic-and-younger extended Mmax zone for the case where the zone is “narrow” (MESE-N). Distributions are shown for the Kijko approach and for the Bayesian approach using either the Mesozoic-and-younger extended prior distribution or the composite prior distribution. The final composite Mmax distribution, which incorporates the relative weights, is shown by the red probability distribution.	5-84
Figure 5.2.1-14 Example Mmax distribution assessed for the Northern Appalachian seismotectonic zone (NAP). Distributions are shown for the Kijko approach and for the Bayesian approach using either the Mesozoic-and-younger extended prior distribution or the composite prior distribution. Note that the Kijko results are shown in this example for illustration, even though they have zero weight. The final composite Mmax distribution, which incorporates the relative weights, is shown by the red probability distribution.	5-85
Figure 5.3.2-1 Likelihood function for rate per unit area in a Poisson process, for multiple values of the earthquake count N : (a) arithmetic scale, and (b) logarithmic scale used to illustrate decreasing COV as N increases	5-86
Figure 5.3.2-2 Likelihood function for b -value of an exponential magnitude distribution, for multiple values of the earthquake count N . The value of b is normalized by the maximum-likelihood estimate, which is derived from Equation 5.3.2-5.....	5-87
Figure 5.3.2-3 Histogram of magnitudes in the earthquake catalog used in this section. The minimum magnitude shown (M 2.9) is the lowest magnitude used in these recurrence calculations.	5-88

Figure 5.3.2-4 Objectively determined values of the penalty function for $\ln(\text{rate})$ for Case A magnitude weights. Source zones are sorted from smallest to largest. See list of abbreviations for full source-zone names.	5-89
Figure 5.3.2-5 Objectively determined values of the penalty function for β for Case A magnitude weights	5-90
Figure 5.3.2-6 Objectively determined values of the penalty function for $\ln(\text{rate})$ for Case B magnitude weights	5-91
Figure 5.3.2-7 Objectively determined values of the penalty function for β for Case B magnitude weights. Source zones are sorted from smallest to largest.	5-92
Figure 5.3.2-8 Objectively determined values of the penalty function for $\ln(\text{rate})$ for Case E magnitude weights	5-93
Figure 5.3.2-9 Objectively determined values of the penalty function for β for Case E magnitude weights. Source zones are sorted from smallest to largest.	5-94
Figure 5.3.2-10 Mean map of rate and b -value for ECC-AM calculated using Case A magnitude weights	5-95
Figure 5.3.2-11 Mean map of rate and b -value for ECC-GC calculated using Case A magnitude weights	5-96
Figure 5.3.2-12 Mean map of rate and b -value for ECC-AM calculated using Case B magnitude weights	5-97
Figure 5.3.2-13 Mean map of rate and b -value for ECC-GC calculated using Case B magnitude weights	5-98
Figure 5.3.2-14 Mean map of rate and b -value for ECC-AM calculated using Case E magnitude weights	5-99
Figure 5.3.2-15 Mean map of rate and b -value for ECC-GC calculated using Case E magnitude weights	5-100
Figure 5.3.2-16 Sensitivity of seismic hazard at Manchester site to the strength of the prior on b	5-101
Figure 5.3.2-17 Sensitivity of seismic hazard at Topeka site to the strength of the prior on b	5-102
Figure 5.3.2-18 Sensitivity of seismic hazard at Manchester site to the choice of magnitude weights	5-103
Figure 5.3.2-19 Sensitivity of seismic hazard at Topeka site to the choice of magnitude weights	5-104
Figure 5.3.2-20 Sensitivity of seismic hazard from source NAP at Manchester site to the eight alternative recurrence maps for Case B magnitude weights	5-105
Figure 5.3.2-21 Sensitivity of seismic hazard from source MID-C–A at Topeka site to the eight alternative recurrence maps for Case B magnitude weights	5-106
Figure 5.3.2-22 Mean recurrence-parameter map for the study region under the highest weighted source-zone configuration in the master logic tree. See Sections 6.3 and 7.5 for all mean maps.	5-107
Figure 5.3.2-23 Map of the uncertainty in the estimated recurrence parameters, expressed as the coefficient of variation of the rate (left) and the standard deviation of the b -value (right) for the study region, under the highest weighted source-zone configuration in the master logic tree. See Appendix J for all maps of uncertainty.	5-108

Figure 5.3.2-24 First of eight equally likely realizations of the recurrence-parameter map for the study region under the highest weighted source-zone configuration in the master logic tree. See Appendix J for maps of all realizations for all source-zone configurations.....	5-109
Figure 5.3.2-25 Eighth of eight equally likely realizations of the recurrence-parameter map for the study region under the highest weighted source-zone configuration in the master logic tree. See Appendix J for maps of all realizations for all source-zone configurations.....	5-110
Figure 5.3.2-26 Map of geographic areas considered in the exploration of model results.....	5-111
Figure 5.3.2-27 Comparison of model-predicted earthquake counts for the USGS Eastern Tennessee area using Case A magnitude weights. The error bars represent the 16%–84% uncertainty associated with the data, computed using the Weichert (1980) procedure.	5-112
Figure 5.3.2-28 Comparison of model-predicted earthquake counts for the USGS Eastern Tennessee area using Case B magnitude weights.....	5-113
Figure 5.3.2-29 Comparison of model-predicted earthquake counts for the USGS Eastern Tennessee area using Case E magnitude weights.....	5-114
Figure 5.3.2-30 Comparison of model-predicted earthquake counts for the central New England area using Case A magnitude weights	5-115
Figure 5.3.2-31 Comparison of model-predicted earthquake counts for the central New England area using Case B magnitude weights	5-116
Figure 5.3.2-32 Comparison of model-predicted earthquake counts for the central New England area using Case E magnitude weights	5-117
Figure 5.3.2-33 Comparison of model-predicted earthquake counts for the Nemaha Ridge area using Case A magnitude weights	5-118
Figure 5.3.2-34 Comparison of model-predicted earthquake counts for the Nemaha Ridge area using Case B magnitude weights	5-119
Figure 5.3.2-35 Comparison of model-predicted earthquake counts for the Nemaha Ridge area using Case E magnitude weights	5-120
Figure 5.3.2-36 Comparison of model-predicted earthquake counts for the Miami, FL, area using Case A magnitude weights.....	5-121
Figure 5.3.2-37 Comparison of model-predicted earthquake counts for the Miami, FL, area using Case B magnitude weights.....	5-122
Figure 5.3.2-38 Comparison of model-predicted earthquake counts for the Miami, FL, area using Case E magnitude weights.....	5-123
Figure 5.3.2-39 Comparison of model-predicted earthquake counts for the St. Paul, MN, area using Case A magnitude weights.....	5-124
Figure 5.3.2-40 Comparison of model-predicted earthquake counts for the St. Paul, MN, area using Case B magnitude weights.....	5-125
Figure 5.3.2-41 Comparison of model-predicted earthquake counts for the St. Paul, MN, area using Case E magnitude weights.....	5-126
Figure 5.3.2-42 Recurrence parameters for the ECC-AM, MID-C–A, and NAP seismotectonic source zones and Case A magnitude weights computed using an objective adaptive kernel approach.....	5-127

Figure 5.3.3-1 Likelihood distribution for rate parameter λ derived using Equation 5.3.3-1 for $N = 2$ and $T = 2,000$ years. Top: normalized probability density function for λ . Bottom: resulting cumulative distribution function. Dashed lines show the cumulative probability levels for the Miller and Rice (1983) discrete approximation of a continuous probability distribution.	5-128
Figure 5.3.3-2 Uncertainty distributions for the age of Charleston RLMEs	5-129
Figure 5.4.4-1 Spatial distribution of earthquakes in the CEUS SSC Project catalog. Solid lines indicate the boundaries of the seismotectonic source zones (narrow interpretation)	5-130
Figure 5.4.4-2 Spatial distribution of earthquakes in the CEUS SSC Project catalog with good quality depth determinations used for assessing crustal thickness. Solid lines indicate the boundaries of the seismotectonic source zones (narrow interpretation).....	5-131
Figure 5.4.4-3 Distribution of better-quality focal depths in Mmax source zones.....	5-132
Figure 5.4.4-4 (1 of 3) Distribution of better-quality focal depths in seismotectonic source zones.....	5-133
Figure 5.4.4-4 (2 of 3) Distribution of better-quality focal depths in seismotectonic source zones.....	5-134
Figure 5.4.4-4 (3 of 3) Distribution of better-quality focal depths in seismotectonic source zones.....	5-135
Figure 6.1-1 Map showing the RLME sources characterized in the CEUS SSC model. Detailed alternatives to the source geometries are shown on figures associated with each RLME discussion.....	6-111
Figure 6.1-2a Map showing the RLME sources and seismicity from the CEUS SSC earthquake catalog. Some of the RLMEs occur in regions of elevated seismicity, but others do not.	6-112
Figure 6.1-2b Close-up of the Wabash Valley and New Madrid/Reelfoot Rift RLME sources and seismicity from the CEUS SSC earthquake catalog. Some of the RLMEs occur in regions of elevated seismicity, but others do not.	6-113
Figure 6.1.1-1 Logic tree for the Charlevoix RLME source	6-114
Figure 6.1.1-2 Seismicity and tectonic features of the Charlevoix RLME	6-115
Figure 6.1.1-3 Magnetic and gravity anomaly maps of the Charlevoix RLME	6-116
Figure 6.1.2-1a Logic tree for the Charleston RLME source	6-117
Figure 6.1.2-1b Logic tree for the Charleston RLME source	6-118
Figure 6.1.2-2 Charleston RLME source zones with (a) total magnetic anomaly and (b) residual isostatic gravity data	6-119
Figure 6.1.2-3 Postulated faults and tectonic features in the Charleston region	6-120
Figure 6.1.2-4 Postulated faults and tectonic features in the local Charleston area	6-121
Figure 6.1.2-5a Postulated faults and tectonic features in the Charleston region with Charleston RLME source zones	6-122
Figure 6.1.2-5b Postulated faults and tectonic features in the local Charleston area with Charleston RLME source zones	6-123
Figure 6.1.2-6 Schematic diagram showing contemporary, maximum, and minimum constraining age sample locations	6-124

Figure 6.1.2-7 Charleston space-time diagram of earthquakes interpreted from paleoliquefaction, contemporary-ages-only scenario	6-125
Figure 6.1.2-8 Charleston space-time diagram of earthquakes interpreted from paleoliquefaction, all-ages scenario	6-126
Figure 6.1.2-9 Distribution of liquefaction from earthquake A, contemporary-ages-only scenario	6-127
Figure 6.1.2-10 Distribution of liquefaction from earthquake B, contemporary-ages-only scenario	6-128
Figure 6.1.2-11 Distribution of liquefaction from earthquake C, contemporary-ages-only scenario	6-129
Figure 6.1.2-12 Distribution of liquefaction from earthquake D, contemporary-ages-only scenario	6-130
Figure 6.1.2-13 Distribution of liquefaction from earthquake E, contemporary-ages-only scenario	6-131
Figure 6.1.2-14 Distribution of liquefaction from earthquake A, all-ages scenario	6-132
Figure 6.1.2-15 Distribution of liquefaction from earthquake B, all-ages scenario	6-133
Figure 6.1.2-16 Distribution of liquefaction from earthquake C, all-ages scenario	6-134
Figure 6.1.2-17 Distribution of liquefaction from earthquake D, all-ages scenario	6-135
Figure 6.1.2-18 Distribution of liquefaction from earthquake E, all-ages scenario.....	6-136
Figure 6.1.2-19 Uncertainty distributions for the age of Charleston RLMEs	6-137
Figure 6.1.3-1 Logic tree for the Cheraw fault RLME source.....	6-138
Figure 6.1.3-2 Map (c) and hillshade relief images (a, b, and d) showing location of mapped Cheraw fault, possible northeast extension, and paleoseismic locality	6-139
Figure 6.1.3-3 Cheraw RLME source relative to (a) total magnetic anomaly and (b) residual isostatic gravity data	6-140
Figure 6.1.4-1 Meers fault location	6-141
Figure 6.1.4-2 Logic tree for the Meers fault source	6-142
Figure 6.1.5-1 Logic tree for the NMFS RLME source	6-143
Figure 6.1.5-2 Map showing seismicity and major subsurface structural features in the New Madrid region	6-144
Figure 6.1.5-3 Map showing geomorphic and near-surface tectonic features in the New Madrid region and locations of NMFS RLME fault sources	6-145
Figure 6.1.5-4 Rupture segments (a) and models (b) for the New Madrid faults from Johnston and Schweig (1996) and (c) the NMFS RLME fault sources	6-146
Figure 6.1.5-5 Map of NMSZ showing estimated ages and measured sizes of liquefaction features	6-147
Figure 6.1.5-6 Earthquake chronology for NMSZ from dating and correlation of liquefaction features at sites (listed at top) along N-S transect across region.....	6-148
Figure 6.1.5-7 Probability distributions for the age of the AD 900 and AD 1450 NMFS RLMEs	6-149
Figure 6.1.5-8 Liquefaction fields for the 1811-1812, AD 1450, and AD 900 earthquakes as interpreted from spatial distribution and stratigraphy of sand blows.....	6-150

Figure 6.1.6-1a Logic tree for the Reelfoot Rift–Eastern Rift Margin South RLME source. Two options for the southern extent of the ERM-S are considered: ERM-SCC includes the Crittenden County fault zone, and ERM-SRP includes the postulated zone of deformation based on fault picks identified in a high-resolution seismic profile along the Mississippi River.	6-151
Figure 6.1.6-1b Logic tree for the Reelfoot Rift–Eastern Rift Margin North RLME source.....	6-152
Figure 6.1.6-2 Map showing structural features and paleoseismic investigation sites along the eastern margin of the Reelfoot rift. The inset map shows the locations of inferred basement faults that border and cross the Reelfoot rift (Csontos et al., 2008) and the inferred Joiner Ridge–Meeman-Shelby fault (JR-MSF; Odum et al., 2010).	6-153
Figure 6.1.6-3 Maps showing surficial geology and locations of subsurface investigations at (a) Meeman-Shelby Forest State Park locality and (b) Union City site (MSF and UC on Figure 6.1.6-2). Modified from Cox et al. (2006) and Odum et al. (2010).	6-154
Figure 6.1.6-4 Figure showing the timing of events along the eastern Reelfoot rift margin. Modified from Cox (2009).	6-155
Figure 6.1.7-1 Logic tree for the Reelfoot rift–Marianna RLME source	6-156
Figure 6.1.7-2 Map showing tectonic features and locations of paleoliquefaction sites in the vicinity of Marianna, Arkansas	6-157
Figure 6.1.7-3 Map showing liquefaction features near Daytona Beach lineament southwest of Marianna, Arkansas	6-158
Figure 6.1.8-1 Logic tree for the Commerce Fault Zone RLME source	6-159
Figure 6.1.8-2 Map showing tectonic features, seismicity, and paleoseismic localities along the Commerce Fault Zone RLME source	6-160
Figure 6.1.8-3 Location of the Commerce geophysical lineament and Commerce Fault Zone RLME source relative to the (a) regional magnetic anomaly map and (b) regional gravity anomaly map	6-161
Figure 6.1.8-4 Space-time diagram showing constraints on the location and timing of late Pleistocene and Holocene paleoearthquakes that may be associated with the Commerce Fault Zone RLME source.....	6-162
Figure 6.1.9-1 Logic tree for the Wabash Valley RLME source.....	6-163
Figure 6.1.9-2 Map showing seismicity, subsurface structural features, paleoearthquake energy centers, and postulated neotectonic deformation in the Wabash Valley region of southern Illinois and southern Indiana	6-164
Figure 6.1.9-3 Wabash Valley RLME source relative to (a) magnetic anomaly, and (b) residual isostatic gravity data	6-165
Figure 6.2-1 Map showing the two Mmax zones for the “narrow” interpretation of the Mesozoic-and-younger extended zone	6-166
Figure 6.2-2 Map showing the two Mmax zones for the “wide” interpretation of the Mesozoic-and-younger extended zone	6-167
Figure 6.3.1-1 Distributions for $m_{\text{max-obs}}$ for the Mmax distributed seismicity source zones ..	6-168
Figure 6.3.2-1 Mmax distributions for the study region treated as a single Mmax zone	6-169
Figure 6.3.2-2 Mmax distributions for the MESE-N Mmax zone	6-170

Figure 6.3.2-3 Mmax distributions for the MESE-W Mmax zone	6-171
Figure 6.3.2-4 Mmax distributions for the NMESE-N Mmax zone	6-172
Figure 6.3.2-5 Mmax distributions for the NMESE-W Mmax zone	6-173
Figure 6.4.1-1 Mean map of rate and b-value for the study region under the source-zone configuration, with no separation of Mesozoic extended and non-extended; Case A magnitude weights	6-174
Figure 6.4.1-2 Mean map of rate and b-value for the study region under the source-zone configuration, with no separation of Mesozoic extended and non-extended; Case B magnitude weights	6-175
Figure 6.4.1-3 Mean map of rate and b-value for the study region under the source-zone configuration, with no separation of Mesozoic extended and non-extended; Case E magnitude weights	6-176
Figure 6.4.1-4 Mean map of rate and b-value for the study region under the source-zone configuration, with separation of Mesozoic extended and non-extended, narrow geometry for MESE; Case A magnitude weights	6-177
Figure 6.4.1-5 Mean map of rate and b-value for the study region under the source-zone configuration, with separation of Mesozoic extended and non-extended, narrow geometry for MESE; Case B magnitude weights	6-178
Figure 6.4.1-6 Mean map of rate and b-value for the study region under the source-zone configuration, with separation of Mesozoic extended and non-extended, narrow geometry for MESE; Case E magnitude weights	6-179
Figure 6.4.1-7 Mean map of rate and b-value for the study region under the source-zone configuration, with separation of Mesozoic extended and non-extended, wide geometry for MESE; Case A magnitude weights	6-180
Figure 6.4.1-8 Mean map of rate and b-value for the study region under the source-zone configuration, with separation of Mesozoic extended and non-extended, wide geometry for MESE; Case B magnitude weights	6-181
Figure 6.4.1-9 Mean map of rate and b-value for the study region under the source-zone configuration, with separation of Mesozoic extended and non-extended, wide geometry for MESE; Case E magnitude weights	6-182
Figure 6.4.2-1 Comparison of model-predicted earthquake counts for study region using Case A magnitude weights. The error bars represent the 16%–84% uncertainty associated with the data, computed using the Weichert (1980) procedure.....	6-183
Figure 6.4.2-2 Comparison of model-predicted earthquake counts for study region using Case B magnitude weights. The error bars represent the 16%–84% uncertainty associated with the data, computed using the Weichert (1980) procedure.....	6-184
Figure 6.4.2-3 Comparison of model-predicted earthquake counts for study region using Case E magnitude weights. The error bars represent the 16%–84% uncertainty associated with the data, computed using the Weichert (1980) procedure.....	6-185
Figure 6.4.2-4 Comparison of model-predicted earthquake counts for MESE-N using Case A magnitude weights. The error bars represent the 16%–84% uncertainty associated with the data, computed using the Weichert (1980) procedure.....	6-186
Figure 6.4.2-5 Comparison of model-predicted earthquake counts for MESE-N using Case B magnitude weights. The error bars represent the 16%–84% uncertainty associated with the data, computed using the Weichert (1980) procedure.....	6-187

Figure 6.4.2-6 Comparison of model-predicted earthquake counts for MESE-N using Case E magnitude weights. The error bars represent the 16%–84% uncertainty associated with the data, computed using the Weichert (1980) procedure.....	6-188
Figure 6.4.2-7 Comparison of model-predicted earthquake counts for MESE-W using Case A magnitude weights. The error bars represent the 16%–84% uncertainty associated with the data, computed using the Weichert (1980) procedure.....	6-189
Figure 6.4.2-8 Comparison of model-predicted earthquake counts for MESE-W using Case B magnitude weights. The error bars represent the 16%–84% uncertainty associated with the data, computed using the Weichert (1980) procedure.....	6-190
Figure 6.4.2-9 Comparison of model-predicted earthquake counts for MESE-W using Case E magnitude weights. The error bars represent the 16%–84% uncertainty associated with the data, computed using the Weichert (1980) procedure.....	6-191
Figure 6.4.2-10 Comparison of model-predicted earthquake counts for NMESE-N using Case A magnitude weights. The error bars represent the 16%–84% uncertainty associated with the data, computed using the Weichert (1980) procedure.....	6-192
Figure 6.4.2-11 Comparison of model-predicted earthquake counts for NMESE-N using Case B magnitude weights. The error bars represent the 16%–84% uncertainty associated with the data, computed using the Weichert (1980) procedure.....	6-193
Figure 6.4.2-12 Comparison of model-predicted earthquake counts for NMESE-N using Case E magnitude weights. The error bars represent the 16%–84% uncertainty associated with the data, computed using the Weichert (1980) procedure.....	6-194
Figure 6.4.2-13 Comparison of model-predicted earthquake counts for NMESE-W using Case A magnitude weights. The error bars represent the 16%–84% uncertainty associated with the data, computed using the Weichert (1980) procedure.....	6-195
Figure 6.4.2-14 Comparison of model-predicted earthquake counts for NMESE-W using Case B magnitude weights. The error bars represent the 16%–84% uncertainty associated with the data, computed using the Weichert (1980) procedure.....	6-196
Figure 6.4.2-15 Comparison of model-predicted earthquake counts for NMESE-W using Case E magnitude weights. The error bars represent the 16%–84% uncertainty associated with the data, computed using the Weichert (1980) procedure.....	6-197
Figure 7.1-1 Seismotectonic zones shown in the case where the Rough Creek graben is not part of the Reelfoot rift (RR) and the Paleozoic Extended Crust is narrow (PEZ-N)	7-83
Figure 7.1-2 Seismotectonic zones shown in the case where the Rough Creek graben is part of the Reelfoot rift (RR_RCG) and the Paleozoic Extended Crust is narrow (PEZ-N)	7-84
Figure 7.1-3 Seismotectonic zones shown in the case where the Rough Creek graben is not part of the Reelfoot rift (RR) and the Paleozoic Extended Crust is wide (PEZ-W).....	7-85
Figure 7.1-4 Seismotectonic zones shown in the case where the Rough Creek graben is part of the Reelfoot rift (RR_RCG) and the Paleozoic Extended Crust is wide (PEZ-W).....	7-86
Figure 7.1-5 Example of comparing seismotectonic zones with magnetic map developed as part of the CEUS SSC Project.....	7-87
Figure 7.1-6 Example of comparing seismotectonic zones with isostatic gravity map developed as part of the CEUS SSC Project	7-88

Figure 7.1-7 Map of seismicity based on the earthquake catalog developed for the CEUS SSC Project.....	7-89
Figure 7.1-8 Map showing example comparison of seismotectonic zones with seismicity. Note the non-uniform spatial distribution of seismicity within the zones. Spatial smoothing of <i>a</i> - and <i>b</i> -values accounts for these spatial variations.....	7-90
Figure 7.3-1 Logic tree for the seismotectonic zones branch of the master logic tree.....	7-91
Figure 7.3.1-1 Significant earthquakes and paleoseismology of the SLR seismotectonic zone	7-92
Figure 7.3.1-2 Tectonic features of the SLR seismotectonic zone	7-93
Figure 7.3.1-3 Magnetic and gravity anomaly maps of the SLR seismotectonic zone	7-94
Figure 7.3.2-1 Significant earthquakes and paleoseismic study area in the region of the GMH seismotectonic zone	7-95
Figure 7.3.2-2 Igneous rocks attributed to the GMH seismotectonic zone	7-96
Figure 7.3.2-3 Relocated hypocentral depths and crustal depth of the GMH seismotectonic zone.....	7-97
Figure 7.3.2-4 Magnetic and gravity anomaly maps of the GMH seismotectonic zone	7-98
Figure 7.3.3-1 Seismicity of the NAP seismotectonic zone	7-99
Figure 7.3.3-2 Magnetic and gravity anomaly maps of the NAP seismotectonic zone	7-100
Figure 7.3.4-1 Seismicity and tectonic features of the PEZ seismotectonic zone.....	7-101
Figure 7.3.4-2 Magnetic and gravity anomaly maps of the PEZ seismotectonic zone	7-102
Figure 7.3.5-1 Map showing seismicity, subsurface Paleozoic and basement structures, and postulated energy centers for prehistoric earthquakes	7-103
Figure 7.3.5-2 Map showing alternative boundaries for Precambrian (proto-Illinois basin) rift basins.....	7-104
Figure 7.3.5-3 Maps showing the IBEB source zone boundaries, seismicity, and prehistoric earthquake centers relative to (a) regional magnetic anomalies and (b) regional gravity anomalies	7-105
Figure 7.3.6-1 Map of seismicity and geomorphic features and faults showing evidence for Quaternary neotectonic deformation and reactivation. Inset map shows basement structures associated with the Reelfoot rift.	7-106
Figure 7.3.6-2 Maps showing geophysical anomalies in the Reelfoot rift region	7-107
Figure 7.3.7-1 Mesozoic basins within the ECC-AM zone	7-108
Figure 7.3.7-2 Seismicity within the ECC-AM and AHEX zones.....	7-109
Figure 7.3.7-3 Magnetic and gravity data for ECC-AM and AHEX zones.....	7-110
Figure 7.3.7-4 Estimated locations of the 1755 M 6.1 Cape Ann earthquake	7-111
Figure 7.3.8-1 Correlation of interpreted transitional crust with the East Coast magnetic anomaly.....	7-112
Figure 7.3.9-1 The ECC-GC seismotectonic zone.....	7-113
Figure 7.3.10-1 The GHEX seismotectonic zone.....	7-114
Figure 7.3.11-1 The OKA seismotectonic zone and regional gravity and magnetic data	7-115
Figure 7.3.12-1 Simplified tectonic map showing the distribution of principal basement faults, rifts, and sutures in the Midcontinent.....	7-116

Figure 7.3.12-2 Maps showing major basement structural features relative to (a) regional magnetic anomalies and (b) regional gravity anomalies	7-117
Figure 7.3.12-3 Seismic zones and maximum observed earthquakes in the MidC zone	7-118
Figure 7.3.12-4 Alternative MidC source zone configurations	7-119
Figure 7.4.1-1 (1 of 3) Distributions for $m_{\text{max-obs}}$ for the seismotectonic distributed seismicity source zones	7-120
Figure 7.4.1-1 (2 of 3) Distributions for $m_{\text{max-obs}}$ for the seismotectonic distributed seismicity source zones	7-121
Figure 7.4.1-1 (3 of 3) Distributions for $m_{\text{max-obs}}$ for the seismotectonic distributed seismicity source zones	7-122
Figure 7.4.2-1 Mmax distributions for the AHEX seismotectonic zone	7-123
Figure 7.4.2-2 Mmax distributions for the ECC_AM seismotectonic zone	7-124
Figure 7.4.2-3 Mmax distributions for the ECC_GC seismotectonic zone	7-125
Figure 7.4.2-4 Mmax distributions for the GHEX seismotectonic zone	7-126
Figure 7.4.2-5 Mmax distributions for the GMH seismotectonic zone	7-127
Figure 7.4.2-6 Mmax distributions for the IBEB seismotectonic zone	7-128
Figure 7.4.2-7 Mmax distributions for the MidC-A seismotectonic zone	7-129
Figure 7.4.2-8 Mmax distributions for the MidC-B seismotectonic zone	7-130
Figure 7.4.2-9 Mmax distributions for the MidC-C seismotectonic zone	7-131
Figure 7.4.2-10 Mmax distributions for the MidC-D seismotectonic zone	7-132
Figure 7.4.2-11 Mmax distributions for the NAP seismotectonic zone	7-133
Figure 7.4.2-12 Mmax distributions for the OKA seismotectonic zone	7-134
Figure 7.4.2-13 Mmax distributions for the PEZ_N seismotectonic zone	7-135
Figure 7.4.2-14 Mmax distributions for the PEZ_W seismotectonic zone	7-136
Figure 7.4.2-15 Mmax distributions for the RR seismotectonic zone	7-137
Figure 7.4.2-16 Mmax distributions for the RR_RCG seismotectonic zone	7-138
Figure 7.4.2-17 Mmax distributions for the SLR seismotectonic zone	7-139
Figure 7.5.1-1 Mean map of rate and b -value for the study region under the source-zone configuration with narrow interpretation of PEZ, Rough Creek graben associated with Midcontinent; Case A magnitude weights	7-140
Figure 7.5.1-2 Mean map of rate and b -value for the study region under the source-zone configuration with narrow interpretation of PEZ, Rough Creek graben associated with Midcontinent; Case B magnitude weights	7-141
Figure 7.5.1-3 Mean map of rate and b -value for the study region under the source-zone configuration with narrow interpretation of PEZ, Rough Creek graben associated with Midcontinent; Case E magnitude weights	7-142
Figure 7.5.1-4 Mean map of rate and b -value for the study region under the source-zone configuration with narrow interpretation of PEZ, Rough Creek graben associated with Reelfoot rift; Case A magnitude weights	7-143

Figure 7.5.1-5 Mean map of rate and b -value for the study region under the source-zone configuration with narrow interpretation of PEZ, Rough Creek graben associated with Reelfoot rift; Case B magnitude weights.....	7-144
Figure 7.5.1-6 Mean map of rate and b -value for the study region under the source-zone configuration with narrow interpretation of PEZ, Rough Creek graben associated with Reelfoot rift; Case E magnitude weights.....	7-145
Figure 7.5.1-7 Mean map of rate and b -value for the study region under the source-zone configuration with wide interpretation of PEZ, Rough Creek graben associated with Midcontinent; Case A magnitude weights	7-146
Figure 7.5.1-8 Mean map of rate and b -value for the study region under the source-zone configuration with wide interpretation of PEZ, Rough Creek graben associated with Midcontinent; Case B magnitude weights	7-147
Figure 7.5.1-9 Mean map of rate and b -value for the study region under the source-zone configuration with wide interpretation of PEZ, Rough Creek graben associated with Midcontinent; Case E magnitude weights	7-148
Figure 7.5.1-10 Mean map of rate and b -value for the study region under the source-zone configuration with wide interpretation of PEZ, Rough Creek graben associated with Reelfoot rift; Case A magnitude weights.....	7-149
Figure 7.5.1-11 Mean map of rate and b -value for the study region under the source-zone configuration with wide interpretation of PEZ, Rough Creek graben associated with Reelfoot rift; Case B magnitude weights.....	7-150
Figure 7.5.1-12 Mean map of rate and b -value for the study region under the source-zone configuration with wide interpretation of PEZ, Rough Creek graben associated with Reelfoot rift; Case E magnitude weights.....	7-151
Figure 7.5.2-1 Comparison of model-predicted earthquake counts for AHEx using Case A magnitude weights. No earthquake counts are shown because this source zone contains no seismicity.	7-152
Figure 7.5.2-2 Comparison of model-predicted earthquake counts for AHEx using Case B magnitude weights. No earthquake counts are shown because this source zone contains no seismicity.. . . .	7-153
Figure 7.5.2-3 Comparison of model-predicted earthquake counts for AHEx using Case E magnitude weights. No earthquake counts are shown because this source zone contains no seismicity.	7-154
Figure 7.5.2-4 Comparison of model-predicted earthquake counts for ECC_AM using Case A magnitude weights. The error bars represent the 16%–84% uncertainty associated with the data, computed using the Weichert (1980) procedure.	7-155
Figure 7.5.2-5 Comparison of model-predicted earthquake counts for ECC_AM using Case B magnitude weights. Error bars as in Figure 7.5.2-4.	7-156
Figure 7.5.2-6 Comparison of model-predicted earthquake counts for ECC_AM using Case E magnitude weights. Error bars as in Figure 7.5.2-4.	7-157
Figure 7.5.2-7 Comparison of model-predicted earthquake counts for ECC_GC using Case A magnitude weights. Error bars as in Figure 7.5.2-4.	7-158
Figure 7.5.2-8 Comparison of model-predicted earthquake counts for ECC_GC using Case B magnitude weights. Error bars as in Figure 7.5.2-4.	7-159
Figure 7.5.2-9 Comparison of model-predicted earthquake counts for ECC_GC using Case E magnitude weights. Error bars as in Figure 7.5.2-4.	7-160

Figure 7.5.2-10 Comparison of model-predicted earthquake counts for GHEX using Case A magnitude weights. Error bars as in Figure 7.5.2-4.	7-161
Figure 7.5.2-11 Comparison of model-predicted earthquake counts for GHEX using Case B magnitude weights. Error bars as in Figure 7.5.2-4.	7-162
Figure 7.5.2-12 Comparison of model-predicted earthquake counts for GHEX using Case E magnitude weights. Error bars as in Figure 7.5.2-4.	7-163
Figure 7.5.2-13 Comparison of model-predicted earthquake counts for GMH using Case A magnitude weights. Error bars as in Figure 7.5.2-4.	7-164
Figure 7.5.2-14 Comparison of model-predicted earthquake counts for GMH using Case B magnitude weights. Error bars as in Figure 7.5.2-4.	7-165
Figure 7.5.2-15 Comparison of model-predicted earthquake counts for GMH using Case E magnitude weights. Error bars as in Figure 7.5.2-4.	7-166
Figure 7.5.2-16 Comparison of model-predicted earthquake counts for IBEB using Case A magnitude weights. Error bars as in Figure 7.5.2-4.	7-167
Figure 7.5.2-17 Comparison of model-predicted earthquake counts for IBEB using Case B magnitude weights. Error bars as in Figure 7.5.2-4.	7-168
Figure 7.5.2-18 Comparison of model-predicted earthquake counts for IBEB using Case E magnitude weights. Error bars as in Figure 7.5.2-4.	7-169
Figure 7.5.2-19 Comparison of model-predicted earthquake counts for MidC-A using Case A magnitude weights. Error bars as in Figure 7.5.2-4.	7-170
Figure 7.5.2-20 Comparison of model-predicted earthquake counts for MidC-A using Case B magnitude weights. Error bars as in Figure 7.5.2-4.	7-171
Figure 7.5.2-21 Comparison of model-predicted earthquake counts for MidC-A using Case E magnitude weights. Error bars as in Figure 7.5.2-4.	7-172
Figure 7.5.2-22 Comparison of model-predicted earthquake counts for MidC-B using Case A magnitude weights. Error bars as in Figure 7.5.2-4.	7-173
Figure 7.5.2-23 Comparison of model-predicted earthquake counts for MidC-B using Case B magnitude weights. Error bars as in Figure 7.5.2-4.	7-174
Figure 7.5.2-24 Comparison of model-predicted earthquake counts for MidC-B using Case E magnitude weights. Error bars as in Figure 7.5.2-4.	7-175
Figure 7.5.2-25 Comparison of model-predicted earthquake counts for MidC-C using Case A magnitude weights. Error bars as in Figure 7.5.2-4.	7-176
Figure 7.5.2-26 Comparison of model-predicted earthquake counts for MidC-C using Case B magnitude weights. Error bars as in Figure 7.5.2-4.	7-177
Figure 7.5.2-27 Comparison of model-predicted earthquake counts for MidC-C using Case E magnitude weights. Error bars as in Figure 7.5.2-4.	7-178
Figure 7.5.2-28 Comparison of model-predicted earthquake counts for MidC-D using Case A magnitude weights. Error bars as in Figure 7.5.2-4.	7-179
Figure 7.5.2-29 Comparison of model-predicted earthquake counts for MidC-D using Case B magnitude weights. Error bars as in Figure 7.5.2-4.	7-180
Figure 7.5.2-30 Comparison of model-predicted earthquake counts for MidC-D using Case E magnitude weights. Error bars as in Figure 7.5.2-4.	7-181
Figure 7.5.2-31 Comparison of model-predicted earthquake counts for NAP using Case A magnitude weights. Error bars as in Figure 7.5.2-4.	7-182

Figure 7.5.2-32 Comparison of model-predicted earthquake counts for NAP using Case B magnitude weights. Error bars as in Figure 7.5.2-4.	7-183
Figure 7.5.2-33 Comparison of model-predicted earthquake counts for NAP using Case E magnitude weights. Error bars as in Figure 7.5.2-4.	7-184
Figure 7.5.2-34 Comparison of model-predicted earthquake counts for OKA using Case A magnitude weights. Error bars as in Figure 7.5.2-4.	7-185
Figure 7.5.2-35 Comparison of model-predicted earthquake counts for OKA using Case B magnitude weights. Error bars as in Figure 7.5.2-4.	7-186
Figure 7.5.2-36 Comparison of model-predicted earthquake counts for OKA using Case E magnitude weights. Error bars as in Figure 7.5.2-4.	7-187
Figure 7.5.2-37 Comparison of model-predicted earthquake counts for PEZ_N using Case A magnitude weights. Error bars as in Figure 7.5.2-4.	7-188
Figure 7.5.2-38 Comparison of model-predicted earthquake counts for PEZ_N using Case B magnitude weights. Error bars as in Figure 7.5.2-4.	7-189
Figure 7.5.2-39 Comparison of model-predicted earthquake counts for PEZ_N using Case E magnitude weights. Error bars as in Figure 7.5.2-4.	7-190
Figure 7.5.2-40 Comparison of model-predicted earthquake counts for PEZ_W using Case A magnitude weights. Error bars as in Figure 7.5.2-4.	7-191
Figure 7.5.2-41 Comparison of model-predicted earthquake counts for PEZ_W using Case B magnitude weights. Error bars as in Figure 7.5.2-4.	7-192
Figure 7.5.2-42 Comparison of model-predicted earthquake counts for PEZ_W using Case E magnitude weights. Error bars as in Figure 7.5.2-4.	7-193
Figure 7.5.2-43 Comparison of model-predicted earthquake counts for RR using Case A magnitude weights. Error bars as in Figure 7.5.2-4.	7-194
Figure 7.5.2-44 Comparison of model-predicted earthquake counts for RR using Case B magnitude weights. Error bars as in Figure 7.5.2-4.	7-195
Figure 7.5.2-45 Comparison of model-predicted earthquake counts for RR using Case E magnitude weights. Error bars as in Figure 7.5.2-4.	7-196
Figure 7.5.2-46 Comparison of model-predicted earthquake counts for RR_RCG using Case A magnitude weights. Error bars as in Figure 7.5.2-4.	7-197
Figure 7.5.2-47 Comparison of model-predicted earthquake counts for RR_RCG using Case B magnitude weights. Error bars as in Figure 7.5.2-4.	7-198
Figure 7.5.2-48 Comparison of model-predicted earthquake counts for RR_RCG using Case E magnitude weights. Error bars as in Figure 7.5.2-4.	7-199
Figure 7.5.2-49 Comparison of model-predicted earthquake counts for SLR using Case A magnitude weights. Error bars as in Figure 7.5.2-4.	7-200
Figure 7.5.2-50 Comparison of model-predicted earthquake counts for SLR using Case B magnitude weights. Error bars as in Figure 7.5.2-4.	7-201
Figure 7.5.2-51 Comparison of model-predicted earthquake counts for SLR using Case E magnitude weights. Error bars as in Figure 7.5.2-4.	7-202
Figure 8.1-1 Map showing the study area and seven test sites for the CEUS SSC Project	8-28
Figure 8.1-2 Mean VS profile for shallow soil site	8-29
Figure 8.1-3 Mean VS profile for deep soil site	8-30

Figure 8.1-4 Mean amplification factors for shallow soil site.....	8-31
Figure 8.1-5 Mean amplification factors for deep soil site.....	8-32
Figure 8.2-1a Central Illinois 10 Hz rock hazard: mean and fractile total hazard.....	8-33
Figure 8.2-1b Central Illinois 1 Hz rock hazard: mean and fractile total hazard.....	8-34
Figure 8.2-1c Central Illinois PGA rock hazard: mean and fractile total hazard.....	8-35
Figure 8.2-1d Central Illinois 10 Hz rock hazard: total and contribution by RLME and background	8-36
Figure 8.2-1e Central Illinois 1 Hz rock hazard: total and contribution by RLME and background	8-37
Figure 8.2-1f Central Illinois PGA rock hazard: total and contribution by RLME and background	8-38
Figure 8.2-1g Central Illinois 10 Hz rock hazard: contribution by background source	8-39
Figure 8.2-1h Central Illinois 1 Hz rock hazard: contribution by background source	8-40
Figure 8.2-1i Central Illinois PGA rock hazard: contribution by background source	8-41
Figure 8.2-1j Central Illinois 10 Hz rock hazard: comparison of three source models	8-42
Figure 8.2-1k Central Illinois 1 Hz rock hazard: comparison of three source models	8-43
Figure 8.2-1l Central Illinois PGA rock hazard: comparison of three source models.....	8-44
Figure 8.2-1m Central Illinois 10 Hz shallow soil hazard: total and total and contribution by RLME and background.....	8-45
Figure 8.2-1n Central Illinois 1 Hz shallow soil hazard: total and contribution by RLME and background	8-46
Figure 8.2-1o Central Illinois PGA shallow soil hazard: total and contribution by RLME and background	8-47
Figure 8.2-1p Central Illinois 10 Hz deep soil hazard: total and contribution by RLME and background	8-48
Figure 8.2-1q Central Illinois 1 Hz deep soil hazard: total and contribution by RLME and background	8-49
Figure 8.2-1r Central Illinois PGA deep soil hazard: total and contribution by RLME and background	8-50
Figure 8.2-1s Central Illinois 10 Hz hazard: comparison of three site conditions	8-51
Figure 8.2-1t Central Illinois 1 Hz hazard: comparison of three site conditions	8-52
Figure 8.2-1u Central Illinois PGA hazard: comparison of three site conditions.....	8-53
Figure 8.2-1v Central Illinois 10 Hz rock hazard: sensitivity to seismotectonic vs. Mmax zones.....	8-54
Figure 8.2-1w Central Illinois 1 Hz rock hazard: sensitivity to seismotectonic vs. Mmax zones.....	8-55
Figure 8.2-1x Central Illinois 10 Hz rock hazard: sensitivity to Mmax for source IBEB.....	8-56
Figure 8.2-1y Central Illinois 1 Hz rock hazard: sensitivity to Mmax for source IBEB.....	8-57
Figure 8.2-1z Central Illinois 10 Hz rock hazard: sensitivity to smoothing options	8-58
Figure 8.2-1aa Central Illinois 1 Hz rock hazard: sensitivity to smoothing options	8-59
Figure 8.2-1bb Central Illinois 10 Hz rock hazard: sensitivity to eight realizations for source IBEB, Case A	8-60

Figure 8.2-1cc Central Illinois 10 Hz rock hazard: sensitivity to eight realizations for source IBEB, Case B	8-61
Figure 8.2-1dd Central Illinois 10 Hz rock hazard: sensitivity to eight realizations for source IBEB, Case E	8-62
Figure 8.2-1ee Central Illinois 1 Hz rock hazard: sensitivity to eight realizations for source IBEB, Case A	8-63
Figure 8.2-1ff Central Illinois 1 Hz rock hazard: sensitivity to eight realizations for source IBEB, Case B	8-64
Figure 8.2-1gg Central Illinois 1 Hz rock hazard: sensitivity to eight realizations for source IBEB, Case E	8-65
Figure 8.2-2a Chattanooga 10 Hz rock hazard: mean and fractile total hazard	8-66
Figure 8.2-2b Chattanooga 1 Hz rock hazard: mean and fractile total hazard.....	8-67
Figure 8.2-2c Chattanooga PGA rock hazard: mean and fractile total hazard	8-68
Figure 8.2-2d Chattanooga 10 Hz rock hazard: total and contribution by RLME and background	8-69
Figure 8.2-2e Chattanooga 1 Hz rock hazard: total and contribution by RLME and background	8-70
Figure 8.2-2f Chattanooga PGA rock hazard: total and contribution by RLME and background	8-71
Figure 8.2-2g Chattanooga 10 Hz rock hazard: contribution by background source	8-72
Figure 8.2-2h Chattanooga 1 Hz rock hazard: contribution by background source	8-73
Figure 8.2-2i Chattanooga PGA rock hazard: contribution by background source	8-74
Figure 8.2-2j Chattanooga 10 Hz rock hazard: comparison of three source models	8-75
Figure 8.2-2k Chattanooga 1 Hz rock hazard: comparison of three source models	8-76
Figure 8.2-2l Chattanooga PGA rock hazard: comparison of three source models.....	8-77
Figure 8.2-2m Chattanooga 10 Hz shallow soil hazard: total and contribution by RLME and background	8-78
Figure 8.2-2n Chattanooga 1 Hz shallow soil hazard: total and contribution by RLME and background	8-79
Figure 8.2-2o Chattanooga PGA shallow soil hazard: total and contribution by RLME and background	8-80
Figure 8.2-2p Chattanooga 10 Hz deep soil hazard: total and contribution by RLME and background	8-81
Figure 8.2-2q Chattanooga 1 Hz deep soil hazard: total and contribution by RLME and background	8-82
Figure 8.2-2r Chattanooga PGA deep soil hazard: total and contribution by RLME and background	8-83
Figure 8.2-2s Chattanooga 10 Hz hazard: comparison of three site conditions	8-84
Figure 8.2-2t Chattanooga 1 Hz hazard: comparison of three site conditions	8-85
Figure 8.2-2u Chattanooga PGA hazard: comparison of three site conditions	8-86
Figure 8.2-2v Chattanooga 10 Hz rock hazard: sensitivity to seismotectonic vs. Mmax zones.....	8-87

Figure 8.2-2w Chattanooga 1 Hz rock hazard: sensitivity to seismotectonic vs. Mmax zones.....	8-88
Figure 8.2-2x Chattanooga 10 Hz rock hazard: sensitivity to Mmax for source PEZ-N.....	8-89
Figure 8.2-2y Chattanooga 1 Hz rock hazard: sensitivity to Mmax for source PEZ-N.....	8-90
Figure 8.2-2z Chattanooga 10 Hz rock hazard: sensitivity to smoothing options	8-91
Figure 8.2-2aa Chattanooga 1 Hz rock hazard: sensitivity to smoothing options	8-92
Figure 8.2-2bb Chattanooga 10 Hz rock hazard: sensitivity to eight realizations for source PEZ-N, Case A.....	8-93
Figure 8.2-2cc Chattanooga 10 Hz rock hazard: sensitivity to eight realizations for source PEZ-N, Case B.....	8-94
Figure 8.2-2dd Chattanooga 10 Hz rock hazard: sensitivity to eight realizations for source PEZ-N, Case E.....	8-95
Figure 8.2-2ee Chattanooga 1 Hz rock hazard: sensitivity to eight realizations for source PEZ-N, Case A.....	8-96
Figure 8.2-2ff Chattanooga 1 Hz rock hazard: sensitivity to eight realizations for source PEZ-N, Case B.....	8-97
Figure 8.2-2gg Chattanooga 1 Hz rock hazard: sensitivity to eight realizations for source PEZ-N, Case E.....	8-98
Figure 8.2-3a Houston 10 Hz rock hazard: mean and fractile total hazard.....	8-99
Figure 8.2-3b Houston 1 Hz rock hazard: mean and fractile total hazard.....	8-100
Figure 8.2-3c Houston PGA rock hazard: mean and fractile total hazard.....	8-101
Figure 8.2-3d Houston 10 Hz rock hazard: total and contribution by RLME and background	8-102
Figure 8.2-3e Houston 1 Hz rock hazard: total and contribution by RLME and background	8-103
Figure 8.2-3f Houston PGA rock hazard: total and contribution by RLME and background ..	8-104
Figure 8.2-3g Houston 10 Hz rock hazard: contribution by background source	8-105
Figure 8.2-3h Houston 1 Hz rock hazard: contribution by background source	8-106
Figure 8.2-3i Houston PGA rock hazard: contribution by background source	8-107
Figure 8.2-3j Houston 10 Hz rock hazard: comparison of three source models	8-108
Figure 8.2-3k Houston is 1 Hz rock hazard: comparison of three source models.....	8-109
Figure 8.2-3l Houston PGA rock hazard: comparison of three source models.....	8-110
Figure 8.2-3m Houston 10 Hz shallow soil hazard: total and contribution by RLME and background	8-111
Figure 8.2-3n Houston 1 Hz shallow soil hazard: total and contribution by RLME and background	8-112
Figure 8.2-3o Houston PGA shallow soil hazard: total and contribution by RLME and background	8-113
Figure 8.2-3p Houston 10 Hz deep soil hazard: total and contribution by RLME and background	8-114
Figure 8.2-3q Houston 1 Hz deep soil hazard: total and contribution by RLME and background	8-115

Figure 8.2-3r Houston PGA deep soil hazard: total and contribution by RLME and background	8-116
Figure 8.2-3s Houston 10 Hz hazard: comparison of three site conditions.....	8-117
Figure 8.2-3t Houston 1 Hz hazard: comparison of three site conditions	8-118
Figure 8.2-3u Houston PGA hazard: comparison of three site conditions	8-119
Figure 8.2-3v Houston 10 Hz rock hazard: sensitivity to seismotectonic vs. Mmax zones	8-120
Figure 8.2-3w Houston 1 Hz rock hazard: sensitivity to seismotectonic vs. Mmax zones	8-121
Figure 8.2-3x Houston 10 Hz rock hazard: sensitivity to Mmax for source GHEX.....	8-122
Figure 8.2-3y Houston 1 Hz rock hazard: sensitivity to Mmax for source GHEX.....	8-123
Figure 8.2-3z Houston 10 Hz rock hazard: sensitivity to smoothing options.....	8-124
Figure 8.2-3aa Houston 1 Hz rock hazard: sensitivity to smoothing options	8-125
Figure 8.2-3bb Houston 10 Hz rock hazard: sensitivity to eight realizations for source GHEX, Case A	8-126
Figure 8.2-3cc Houston 10 Hz rock hazard: sensitivity to eight realizations for source GHEX, Case B	8-127
Figure 8.2-3dd Houston 10 Hz rock hazard: sensitivity to eight realizations for source GHEX, Case E	8-128
Figure 8.2-3ee Houston 1 Hz rock hazard: sensitivity to eight realizations for source GHEX, Case A	8-129
Figure 8.2-3ff Houston 1 Hz rock hazard: sensitivity to eight realizations for source GHEX, Case B	8-130
Figure 8.2-3gg Houston 1 Hz rock hazard: sensitivity to eight realizations for source GHEX, Case E	8-131
Figure 8.2-4a Jackson 10 Hz rock hazard: mean and fractile total hazard	8-132
Figure 8.2-4b Jackson 1 Hz rock hazard: mean and fractile total hazard	8-133
Figure 8.2-4c Jackson PGA rock hazard: mean and fractile total hazard	8-134
Figure 8.2-4d Jackson 10 Hz rock hazard: total and contribution by RLME and background	8-135
Figure 8.2-4e Jackson 1 Hz rock hazard: total and contribution by RLME and background	8-136
Figure 8.2-4f Jackson PGA rock hazard: total and contribution by RLME and background ..	8-137
Figure 8.2-4g Jackson 10 Hz rock hazard: contribution by background source	8-138
Figure 8.2-4h Jackson 1 Hz rock hazard: contribution by background source	8-139
Figure 8.2-4i Jackson PGA rock hazard: contribution by background source	8-140
Figure 8.2-4j Jackson 10 Hz rock hazard: comparison of three source models	8-141
Figure 8.2-4k Jackson is 1 Hz rock hazard: comparison of three source models.....	8-142
Figure 8.2-4l Jackson PGA rock hazard: comparison of three source models	8-143
Figure 8.2-4m Jackson 10 Hz shallow soil hazard: total and contribution by RLME and background	8-144
Figure 8.2-4n Jackson 1 Hz shallow soil hazard: total and contribution by RLME and background	8-145

Figure 8.2-4o Jackson PGA shallow soil hazard: total and contribution by RLME and background	8-146
Figure 8.2-4p Jackson 10 Hz deep soil hazard: total and contribution by RLME and background	8-147
Figure 8.2-4q Jackson 1 Hz deep soil hazard: total and contribution by RLME and background	8-148
Figure 8.2-4r Jackson PGA deep soil hazard: total and contribution by RLME and background	8-149
Figure 8.2-4s Jackson 10 Hz hazard: comparison of three site conditions	8-150
Figure 8.2-4t Jackson 1 Hz hazard: comparison of three site conditions	8-151
Figure 8.2-4u Jackson PGA hazard: comparison of three site conditions	8-152
Figure 8.2-4v Jackson 10 Hz rock hazard: sensitivity to seismotectonic vs. Mmax zones	8-153
Figure 8.2-4w Jackson 1 Hz rock hazard: sensitivity to seismotectonic vs. Mmax zones	8-154
Figure 8.2-4x Jackson 10 Hz rock hazard: sensitivity to Mmax for source ECC-GC	8-155
Figure 8.2-4y Jackson 1 Hz rock hazard: sensitivity to Mmax for source ECC-GC	8-156
Figure 8.2-4z Jackson 10 Hz rock hazard: sensitivity to smoothing options	8-157
Figure 8.2-4aa Jackson 1 Hz rock hazard: sensitivity to smoothing options	8-158
Figure 8.2-4bb Jackson 10 Hz rock hazard: sensitivity to eight realizations for source ECC-GC, Case A	8-159
Figure 8.2-4cc Jackson 10 Hz rock hazard: sensitivity to eight realizations for source ECC-GC, Case B	8-160
Figure 8.2-4dd Jackson 10 Hz rock hazard: sensitivity to eight realizations for source ECC-GC, Case E	8-161
Figure 8.2-4ee Jackson 1 Hz rock hazard: sensitivity to eight realizations for source ECC-GC, Case A	8-162
Figure 8.2-4ff Jackson 1 Hz rock hazard: sensitivity to eight realizations for source ECC-GC, Case B	8-163
Figure 8.2-4gg Jackson 1 Hz rock hazard: sensitivity to eight realizations for source ECC-GC, Case E	8-164
Figure 8.2-5a Manchester 10 Hz rock hazard: mean and fractile total hazard	8-165
Figure 8.2-5b Manchester 1 Hz rock hazard: mean and fractile total hazard	8-166
Figure 8.2-5c Manchester PGA rock hazard: mean and fractile total hazard	8-167
Figure 8.2-5d Manchester 10 Hz rock hazard: total and contribution by RLME and background	8-168
Figure 8.2-5e Manchester 1 Hz rock hazard: total and contribution by RLME and background	8-169
Figure 8.2-5f Manchester PGA rock hazard: total and contribution by RLME and background	8-170
Figure 8.2-5g Manchester 10 Hz rock hazard: contribution by background source	8-171
Figure 8.2-5h Manchester 1 Hz rock hazard: contribution by background source	8-172
Figure 8.2-5i Manchester PGA rock hazard: contribution by background source	8-173
Figure 8.2-5j Manchester 10 Hz rock hazard: comparison of three source models	8-174

Figure 8.2-5k Manchester 1 Hz rock hazard: comparison of three source models	8-175
Figure 8.2-5l Manchester PGA rock hazard: comparison of three source models.....	8-176
Figure 8.2-5m Manchester 10 Hz shallow soil hazard: total and contribution by RLME and background	8-177
Figure 8.2-5n Manchester 1 Hz shallow soil hazard: total and contribution by RLME and background	8-178
Figure 8.2-5o Manchester PGA shallow soil hazard: total and contribution by RLME and background	8-179
Figure 8.2-5p Manchester 10 Hz deep soil hazard: total and contribution by RLME and background	8-180
Figure 8.2-5q Manchester 1 Hz deep soil hazard: total and contribution by RLME and background	8-181
Figure 8.2-5r Manchester PGA deep soil hazard: total and contribution by RLME and background	8-182
Figure 8.2-5s Manchester 10 Hz hazard: comparison of three site conditions	8-183
Figure 8.2-5t Manchester 1 Hz hazard: comparison of three site conditions	8-184
Figure 8.2-5u Manchester PGA hazard: comparison of three site conditions.....	8-185
Figure 8.2-5v Manchester 10 Hz rock hazard: sensitivity to seismotectonic vs. Mmax zones.....	8-186
Figure 8.2-5w Manchester 1 Hz rock hazard: sensitivity to seismotectonic vs. Mmax zones.....	8-187
Figure 8.2-5x Manchester 10 Hz rock hazard: sensitivity to Mmax for source NAP	8-188
Figure 8.2-5y Manchester 1 Hz rock hazard: sensitivity to Mmax for source NAP	8-189
Figure 8.2-5z Manchester 10 Hz rock hazard: sensitivity to smoothing options	8-190
Figure 8.2-5aa Manchester 1 Hz rock hazard: sensitivity to smoothing options.....	8-191
Figure 8.2-5bb Manchester 10 Hz rock hazard: sensitivity to eight realizations for source NAP, Case A.....	8-192
Figure 8.2-5cc Manchester 10 Hz rock hazard: sensitivity to eight realizations for source NAP, Case B	8-193
Figure 8.2-5dd Manchester 10 Hz rock hazard: sensitivity to eight realizations for source NAP, Case E	8-194
Figure 8.2-5ee Manchester 1 Hz rock hazard: sensitivity to eight realizations for source NAP, Case A	8-195
Figure 8.2-5ff Manchester 1 Hz rock hazard: sensitivity to eight realizations for source NAP, Case B	8-196
Figure 8.2-5gg Manchester 1 Hz rock hazard: sensitivity to eight realizations for source NAP, Case E	8-197
Figure 8.2-6a Savannah 10 Hz rock hazard: mean and fractile total hazard	8-198
Figure 8.2-6b Savannah 1 Hz rock hazard: mean and fractile total hazard	8-199
Figure 8.2-6c Savannah PGA rock hazard: mean and fractile total hazard	8-200
Figure 8.2-6d Savannah 10 Hz rock hazard: total and contribution by RLME and background	8-201

Figure 8.2-6e Savannah 1 Hz rock hazard: total and contribution by RLME and background	8-202
Figure 8.2-6f Savannah PGA rock hazard: total and contribution by RLME and background	8-203
Figure 8.2-6g Savannah 10 Hz rock hazard: contribution by background source	8-204
Figure 8.2-6h Savannah 1 Hz rock hazard: contribution by background source	8-205
Figure 8.2-6i Savannah PGA rock hazard: contribution by background source	8-206
Figure 8.2-6j Savannah 10 Hz rock hazard: comparison of three source models	8-207
Figure 8.2-6k Savannah 1 Hz rock hazard: comparison of three source models.....	8-208
Figure 8.2-6l Savannah PGA rock hazard: comparison of three source models	8-209
Figure 8.2-6m Savannah 10 Hz shallow soil hazard: total and contribution by RLME and background	8-210
Figure 8.2-6n Savannah 1 Hz shallow soil hazard: total and contribution by RLME and background	8-211
Figure 8.2-6o Savannah PGA shallow soil hazard: total and contribution by RLME and background	8-212
Figure 8.2-6p Savannah 10 Hz deep soil hazard: total and contribution by RLME and background	8-213
Figure 8.2-6q Savannah 1 Hz deep soil hazard: total and contribution by RLME and background	8-214
Figure 8.2-6r Savannah PGA deep soil hazard: total and contribution by RLME and background	8-215
Figure 8.2-6s Savannah 10 Hz hazard: comparison of three site conditions.....	8-216
Figure 8.2-6t Savannah 1 Hz hazard: comparison of three site conditions.....	8-217
Figure 8.2-6u Savannah PGA hazard: comparison of three site conditions	8-218
Figure 8.2-6v Savannah 10 Hz rock hazard: sensitivity to seismotectonic vs. Mmax zones.....	8-219
Figure 8.2-6w Savannah 1 Hz rock hazard: sensitivity to seismotectonic vs. Mmax zones ..	8-220
Figure 8.2-6x Savannah 10 Hz rock hazard: sensitivity to Mmax for source ECC-AM	8-221
Figure 8.2-6y Savannah 1 Hz rock hazard: sensitivity to Mmax for source ECC-AM	8-222
Figure 8.2-6z Savannah 10 Hz rock hazard: sensitivity to smoothing options.....	8-223
Figure 8.2-6aa Savannah 1 Hz rock hazard: sensitivity to smoothing options	8-224
Figure 8.2-6bb Savannah 10 Hz rock hazard: sensitivity to eight realizations for source ECC-AM, Case A	8-225
Figure 8.2-6cc Savannah 10 Hz rock hazard: sensitivity to eight realizations for source ECC-AM, Case B	8-226
Figure 8.2-6dd Savannah 10 Hz rock hazard: sensitivity to eight realizations for source ECC-AM, Case E	8-227
Figure 8.2-6ee Savannah 1 Hz rock hazard: sensitivity to eight realizations for source ECC-AM, Case A	8-228
Figure 8.2-6ff Savannah 1 Hz rock hazard: sensitivity to eight realizations for source ECC-AM, Case B	8-229

Figure 8.2-6gg Savannah 1 Hz rock hazard: sensitivity to eight realizations for source ECC-AM, Case E	8-230
Figure 8.2-7a Topeka 10 Hz rock hazard: mean and fractile total hazard	8-231
Figure 8.2-7b Topeka 1 Hz rock hazard: mean and fractile total hazard	8-232
Figure 8.2-7c Topeka PGA rock hazard: mean and fractile total hazard	8-233
Figure 8.2-7d Topeka 10 Hz rock hazard: total and contribution by RLME and background	8-234
Figure 8.2-7e Topeka 1 Hz rock hazard: total and contribution by RLME and background...	8-235
Figure 8.2-7f Topeka PGA rock hazard: total and contribution by RLME and background ...	8-236
Figure 8.2-7g Topeka 10 Hz rock hazard: contribution by background source.....	8-237
Figure 8.2-7h Topeka 1 Hz rock hazard: contribution by background source.....	8-238
Figure 8.2-7i Topeka PGA rock hazard: contribution by background source	8-239
Figure 8.2-7j Topeka 10 Hz rock hazard: comparison of three source models.....	8-240
Figure 8.2-7k Topeka is 1 Hz rock hazard: comparison of three source models	8-241
Figure 8.2-7l Topeka PGA rock hazard: comparison of three source models	8-242
Figure 8.2-7m Topeka 10 Hz shallow soil hazard: total and contribution by RLME and background	8-243
Figure 8.2-7n Topeka 1 Hz shallow soil hazard: total and contribution by RLME and background	8-244
Figure 8.2-7o Topeka PGA shallow soil hazard: total and contribution by RLME and background	8-245
Figure 8.2-7p Topeka 10 Hz deep soil hazard: total and contribution by RLME and background	8-246
Figure 8.2-7q Topeka 1 Hz deep soil hazard: total and contribution by RLME and background	8-247
Figure 8.2-7r Topeka PGA deep soil hazard: total and contribution by RLME and background	8-248
Figure 8.2-7s Topeka 10 Hz hazard: comparison of three site conditions	8-249
Figure 8.2-7t Topeka 1 Hz hazard: comparison of three site conditions.....	8-250
Figure 8.2-7u Topeka PGA hazard: comparison of three site conditions	8-251
Figure 8.2-7v Topeka 10 Hz rock hazard: sensitivity to seismotectonic vs. Mmax zones	8-252
Figure 8.2-7w Topeka 1 Hz rock hazard: sensitivity to seismotectonic vs. Mmax zones.....	8-253
Figure 8.2-7x Topeka 10 Hz rock hazard: sensitivity to Mmax for source MidC-A	8-254
Figure 8.2-7y Topeka 1 Hz rock hazard: sensitivity to Mmax for source MidC-A	8-255
Figure 8.2-7z Topeka 10 Hz rock hazard: sensitivity to smoothing options.....	8-256
Figure 8.2-7aa Topeka 1 Hz rock hazard: sensitivity to smoothing options.....	8-257
Figure 8.2-7bb Topeka 10 Hz rock hazard: sensitivity to eight realizations for source MidC-A, Case A	8-258
Figure 8.2-7cc Topeka 10 Hz rock hazard: sensitivity to eight realizations for source MidC-A, Case B	8-259

Figure 8.2-7dd Topeka 10 Hz rock hazard: sensitivity to eight realizations for source MidC-A, Case E	8-260
Figure 8.2-7ee Topeka 1 Hz rock hazard: sensitivity to eight realizations for source MidC-A, Case A	8-261
Figure 8.2-7ff Topeka 1 Hz rock hazard: sensitivity to eight realizations for source MidC- A, Case B	8-262
Figure 8.2-7gg Topeka 1 Hz rock hazard: sensitivity to eight realizations for source MidC-A, Case E	8-263
Figure 9.3-1 1 Hz sensitivity to rupture orientation at Savannah for the Charleston regional source.....	9-24
Figure 9.3-2 10 Hz sensitivity to rupture orientation at Savannah for the Charleston regional source.....	9-25
Figure 9.3-3 1 Hz sensitivity to seismogenic thickness at Manchester for the Charlevoix area source	9-26
Figure 9.3-4 10 Hz sensitivity to seismogenic thickness at Manchester for the Charlevoix area source	9-27
Figure 9.3-5 1 Hz sensitivity to rupture orientation (dip) at Manchester for the Charlevoix area source	9-28
Figure 9.3-6 10 Hz sensitivity to rupture orientation (dip) at Manchester for the Charlevoix area source	9-29
Figure 9.3-7 1 Hz sensitivity to seismogenic thickness at Topeka for the Cheraw fault source	9-30
Figure 9.3-8 10 Hz sensitivity to seismogenic thickness at Topeka for the Cheraw fault source	9-31
Figure 9.3-9 1 Hz sensitivity to rupture orientation (dip) at Topeka for the Cheraw fault source	9-32
Figure 9.3-10 10 Hz sensitivity to rupture orientation at Topeka for the Cheraw fault source	9-33
Figure 9.3-11 1 Hz sensitivity to seismogenic thickness at Jackson for the Commerce area source	9-34
Figure 9.3-12 10 Hz sensitivity to seismogenic thickness at Jackson for the Commerce area source	9-35
Figure 9.3-13 1 Hz sensitivity to seismogenic thickness at Jackson for the ERM-N area source	9-36
Figure 9.3-14 10 Hz sensitivity to seismogenic thickness at Jackson for the ERM-N area source	9-37
Figure 9.3-15 1 Hz sensitivity to seismogenic thickness at Jackson for the ERM-S area source	9-38
Figure 9.3-16 10 Hz sensitivity to seismogenic thickness at Jackson for the ERM-S area source	9-39
Figure 9.3-17 1 Hz sensitivity to seismogenic thickness at Jackson for the Marianna area source	9-40
Figure 9.3-18 10 Hz sensitivity to seismogenic thickness at Jackson for the Marianna area source	9-41

Figure 9.3-19 1 Hz sensitivity to seismogenic thickness at Topeka for the Meers fault and OKA area sources.....	9-42
Figure 9.3-20 1 Hz sensitivity to seismogenic thickness at Houston for the Meers fault and OKA area sources.....	9-43
Figure 9.3-21 10 Hz sensitivity to seismogenic thickness at Topeka for the Meers fault and OKA area sources.....	9-44
Figure 9.3-22 10 Hz sensitivity to seismogenic thickness at Houston for the Meers fault and OKA area sources.....	9-45
Figure 9.3-23 1 Hz sensitivity to rupture orientation at Houston for the OKA area source	9-46
Figure 9.3-24 10 Hz sensitivity to rupture orientation at Houston for the OKA area source	9-47
Figure 9.3-25 1 Hz sensitivity to rupture orientation (dip) at Topeka for the OKA area source	9-48
Figure 9.3-26 1 Hz sensitivity to rupture orientation (dip) at Houston for the OKA area source	9-49
Figure 9.3-27 10 Hz sensitivity to rupture orientation (dip) at Topeka for the OKA area source	9-50
Figure 9.3-28 10 Hz sensitivity to rupture orientation (dip) at Houston for the OKA area source	9-51
Figure 9.3-29 1 Hz sensitivity to rupture orientation (dip) at Topeka for the Meers fault source	9-52
Figure 9.3-30 1 Hz sensitivity to rupture orientation (dip) at Houston for the Meers fault source	9-53
Figure 9.3-31 10 Hz sensitivity to rupture orientation (dip) at Topeka for the Meers fault source	9-54
Figure 9.3-32 10 Hz sensitivity to rupture orientation (dip) at Houston for the Meers fault source	9-55
Figure 9.3-33 1 Hz sensitivity to seismogenic thickness at Jackson for the NMFS fault sources.....	9-56
Figure 9.3-34 10 Hz sensitivity to seismogenic thickness at Jackson for the NMFS fault sources.....	9-57
Figure 9.3-35 1 Hz sensitivity to seismogenic thickness at Central Illinois for the Wabash Valley area source	9-58
Figure 9.3-36 10 Hz sensitivity to seismogenic thickness at Central Illinois for the Wabash Valley area source	9-59
Figure 9.3-37 1 Hz sensitivity to rupture orientation (dip) at Central Illinois for the Wabash Valley area source	9-60
Figure 9.3-38 10 Hz sensitivity to rupture orientation (dip) at Central Illinois for the Wabash Valley area source	9-61
Figure 9.3-39 1 Hz sensitivity to fault ruptures vs. point source for the Central Illinois site from the Mid C–A background source.....	9-62
Figure 9.3-40 10 Hz sensitivity to fault ruptures vs. point source for the Central Illinois site from the Mid C–A background source	9-63
Figure 9.4-1 COV_{MH} from EPRI (1989) team sources vs. ground motion amplitude for seven test sites: PGA (top), 10 Hz SA (middle), and 1 Hz SA (bottom).....	9-64

Figure 9.4-2 COV_{MH} from EPRI (1989) team sources vs. seismic hazard (i.e., annual frequency of exceedance) for seven test sites: PGA (top), 10 Hz SA (middle), and 1 9-Hz SA (bottom)	9-65
Figure 9.4-3 COV_{MH} from seismic source experts (PEGASOS project) vs. amplitude (top) and annual frequency (bottom)	9-66
Figure 9.4-4 COV_K and COV_{MH} from Charleston alternatives for PGA, plotted vs. PGA amplitude (top) and hazard (bottom). COV_{MH} is the total COV of mean hazard; see Table 9.4-2 for other labels for curves.	9-67
Figure 9.4-5 COV_K and COV_{MH} from Charleston alternatives for 10 Hz, plotted vs. 10 Hz amplitude (top) and hazard (bottom). COV_{MH} is the total COV of mean hazard; see Table 9.4-2 for other labels for curves.	9-68
Figure 9.4-6 COV_K and COV_{MH} from Charleston alternatives for 1 Hz, plotted vs. 1 Hz amplitude (top) and hazard (bottom). COV_{MH} is the total COV of mean hazard; see Table 9.4-2 for other labels for curves.	9-69
Figure 9.4-7 COV_K and COV_{MH} of total hazard from New Madrid for 1 Hz, plotted vs. 1 Hz amplitude (top) and hazard (bottom). COV_{MH} is the total COV; see the text for other labels for curves.	9-70
Figure 9.4-8 PGA hazard curves for Manchester test site	9-71
Figure 9.4-9 COV_{MH} of PGA hazard at Manchester site from ground motion equation vs. PGA	9-72
Figure 9.4-10 COV of PGA hazard at Manchester site from ground motion equation vs. hazard	9-73
Figure 9.4-11 COV of 10 Hz hazard at Manchester site from ground motion equations vs. hazard.....	9-74
Figure 9.4-12 COV of 1 Hz hazard at Manchester site from ground motion equations vs. hazard	9-75
Figure 9.4-13 1 Hz spectral acceleration hazard curves for Manchester test site	9-76
Figure 9.4-14 COV_{MH} of PGA hazard at Chattanooga from ground motion equation vs. hazard	9-77
Figure 9.4-15 COV_{MH} of 10 Hz hazard at Chattanooga from ground motion equation vs. hazard	9-78
Figure 9.4-16 COV_{MH} of 1 Hz hazard at Chattanooga site from ground motion equation vs. hazard.....	9-79
Figure 9.4-17 PGA hazard curves for Savannah test site.....	9-80
Figure 9.4-18 COV_{MH} of PGA hazard at Savannah site from ground motion equations vs. hazard	9-81
Figure 9.4-19 COV_{MH} of 10 Hz hazard at Savannah site from ground motion equations vs. hazard.....	9-82
Figure 9.4-20 COV_{MH} of 1 Hz hazard at Savannah site from ground motion equations vs. hazard	9-83
Figure 9.4-21 PGA hazard curves for Columbia site	9-84
Figure 9.4-22 COV_{MH} of PGA hazard at Columbia from ground motion equations vs. hazard	9-85

Figure 9.4-23 COV_{MH} of 10 Hz hazard at Columbia from ground motion equations vs. hazard	9-86
Figure 9.4-24 COV_{MH} of 1 Hz hazard at Columbia from ground motion equations vs. hazard	9-87
Figure 9.4-25 COV_{MH} of PGA hazard at Chattanooga (New Madrid only) vs. hazard	9-88
Figure 9.4-26 COV_{MH} of 10 Hz hazard at Chattanooga (New Madrid only) vs. hazard.....	9-89
Figure 9.4-27 COV_{MH} of 1 Hz hazard at Chattanooga (New Madrid only) vs. hazard.....	9-90
Figure 9.4-28 COV_{MH} for PGA and 1 Hz SA vs. ground motion amplitude resulting from alternative ground motion experts, PEGASOS project.....	9-91
Figure 9.4-29 COV_{MH} for PGA and 1 Hz SA vs. mean hazard from alternative ground motion experts, PEGASOS project	9-92
Figure 9.4-30 COV_{HAZ} from ground motion equations vs. mean hazard for Chattanooga	9-93
Figure 9.4-31 COV_{MH} from ground motion equations vs. mean hazard for Central Illinois	9-94
Figure 9.4-32 COV_{MH} from soil experts vs. PGA and 1 Hz SA, PEGASOS project	9-95
Figure 9.4-33 COV_{MH} from soil experts vs. mean hazard for PGA and 1 Hz SA, PEGASOS project.....	9-96
Figure 9.4-34 COV_{MH} resulting from site response models vs. mean hazard for four sites, 1 Hz (top) and 10 Hz (bottom).....	9-97
Figure 11-1 Geologic time scale (Walker and Geissman, 2009)	11-10
Figure A-1 GEBCO elevation data for the CEUS study area (BODC, 2009).	A-22
Figure A-2 CEUS SSC independent earthquake catalog	A-24
Figure A-3 Bedrock geology and extended crust after Kanter (1994).....	A-26
Figure A-4 Crustal provinces after Rohs and Van Schmus (2007)	A-28
Figure A-5 Geologic map of North America	A-31
Figure A-6 Locations of geologic cross sections in the CEUS	A-33
Figure A-7 Precambrian crustal boundary after Van Schmus et al. (1996)	A-35
Figure A-8a Precambrian geology and features after Reed (1993)	A-37
Figure A-8b Explanation of Precambrian geology and features after Reed (1993)	A-38
Figure A-9 Precambrian provinces after Van Schmus et al. (2007).....	A-40
Figure A-10 Precambrian units after Whitmeyer and Karlstrom (2007)	A-42
Figure A-11 Surficial materials in the conterminous United States after Soller et al. (2009).....	A-44
Figure A-12 Basement and sediment thickness in the USGS Crustal Database for North America. Symbol size represents overlying sediment thickness (km); symbol color represents basement thickness (km).	A-46
Figure A-13 Top of basement P-wave seismic velocity in the USGS Crustal Database for North America	A-47
Figure A-14 Sediment thickness for North America and neighboring regions	A-49
Figure A-15 Physiographic divisions of the conterminous United States after Fenneman and Johnson (1946)	A-51
Figure A-16 CEUS SSC free-air gravity anomaly grid. Shaded relief with 315-degree azimuth and 30-degree inclination applied.....	A-54

Figure A-17 CEUS SSC free-air gravity anomaly grid. Shaded relief with 180-degree azimuth and 30-degree inclination applied.....	A-55
Figure A-18 CEUS SSC complete Bouguer gravity anomaly grid with free-air gravity anomaly in marine areas. Shaded relief with 315-degree azimuth and 30-degree inclination applied.....	A-56
Figure A-19 CEUS SSC complete Bouguer gravity anomaly grid with free-air gravity anomaly in marine areas. Shaded relief with 180-degree azimuth and 30-degree inclination applied.....	A-57
Figure A-20 CEUS SSC residual isostatic gravity anomaly grid. Shaded relief with 315-degree azimuth and 30-degree inclination applied.	A-58
Figure A-21 CEUS SSC residual isostatic gravity anomaly grid Shaded relief with 180-degree azimuth and 30-degree inclination applied.	A-59
Figure A-22 CEUS SSC regional isostatic gravity anomaly grid.....	A-60
Figure A-23 CEUS SSC first vertical derivative of residual isostatic gravity anomaly grid.....	A-61
Figure A-24 CEUS SSC first vertical derivative of Bouguer gravity anomaly grid with free-air anomaly in marine areas	A-62
Figure A-25 CEUS SSC complete Bouguer (with marine free-air) gravity anomaly grid low pass filtered at 240 km.....	A-63
Figure A-26 CEUS SSC complete Bouguer (with marine free-air) gravity anomaly grid high pass filtered at 240 km. Shaded relief with 315-degree azimuth and 30-degree inclination applied.....	A-64
Figure A-27 CEUS SSC complete Bouguer (with marine free-air) gravity anomaly grid high pass filtered at 240 km. Shaded relief with 180-degree azimuth and 30-degree inclination applied.....	A-65
Figure A-28 CEUS SSC complete Bouguer (with marine free-air) gravity anomaly grid high pass filtered at 120 km. Shaded relief with 315-degree azimuth and 30-degree inclination applied.....	A-66
Figure A-29 CEUS SSC complete Bouguer (with marine free-air) gravity anomaly grid high pass filtered at 120 km. Shaded relief with 180-degree azimuth and 30-degree inclination applied.....	A-67
Figure A-30 CEUS SSC complete Bouguer (with marine free-air) gravity anomaly grid upward continued to 40 km	A-68
Figure A-31 CEUS SSC complete Bouguer (with marine free-air) gravity anomaly grid minus the complete Bouguer (with marine free-air) gravity anomaly upward continued to 40 km. Shaded relief with 315-degree azimuth and 30-degree inclination applied.....	A-69
Figure A-32 CEUS SSC complete Bouguer (with marine free-air) gravity anomaly grid minus the complete Bouguer (with marine free-air) gravity anomaly upward continued to 40 km. Shaded relief with 180-degree azimuth and 30-degree inclination applied.....	A-70
Figure A-33 CEUS SSC complete Bouguer (with marine free-air) gravity anomaly grid upward continued to 100 km	A-71
Figure A-34 CEUS SSC complete Bouguer (with marine free-air) gravity anomaly grid minus the complete Bouguer (with marine free-air) gravity anomaly anomaly	

upward continued to 100 km. Shaded relief with 315-degree azimuth and 30-degree inclination applied.....	A-72
Figure A-35 CEUS SSC complete Bouguer (with marine free-air) gravity anomaly grid minus the complete Bouguer (with marine free-air) gravity anomaly upward continued to 100 km. Shaded relief with 180-degree azimuth and 30-degree inclination applied.....	A-73
Figure A-36 CEUS SSC horizontal derivative of residual isostatic gravity anomaly grid	A-74
Figure A-37 CEUS SSC horizontal derivative of first vertical derivative of residual isostatic gravity anomaly grid	A-75
Figure A-38 Corrected heat flow values from the SMU Geothermal Laboratory Regional Heat Flow Database (2008)	A-77
Figure A-39 CEUS SSC total intensity magnetic anomaly grid (Ravat et al., 2009). Shaded relief with 315-degree azimuth and 30-degree inclination applied.....	A-80
Figure A-40 CEUS SSC total intensity magnetic anomaly grid (Ravat et al., 2009). Shaded relief with 180-degree azimuth and 30-degree inclination applied.....	A-81
Figure A-41 CEUS SSC differentially reduced to pole magnetic anomaly grid (Ravat, 2009). Shaded relief with 315-degree azimuth and 30-degree inclination applied.....	A-82
Figure A-42 CEUS SSC differentially reduced to pole magnetic anomaly grid (Ravat, 2009). Shaded relief with 180-degree azimuth and 30-degree inclination applied.....	A-83
Figure A-43 CEUS SSC tilt derivative of differentially reduced to pole magnetic anomaly grid (degrees) (Ravat, 2009)	A-84
Figure A-44 CEUS SSC horizontal derivative of tilt derivative of differentially reduced to pole magnetic anomaly grid (radians) (Ravat, 2009)	A-85
Figure A-45 CEUS SSC tilt derivative of differentially reduced to pole magnetic anomaly grid (Ravat, 2009)	A-86
Figure A-46 CEUS SSC amplitude of analytic signal magnetic anomaly grid (Ravat, 2009)	A-87
Figure A-47 CEUS SSC paleoliquefaction database	A-89
Figure A-48 CEUS SSC compilation of seismic reflection and seismic refraction lines.....	A-91
Figure A-49 USGS National Seismic Hazard Maps (Petersen et al., 2008)	A-93
Figure A-50 USGS NSHM ground motion hazard at spectral acceleration of 1 hz with 2% probability of exceedance in 50 years (Petersen et al., 2008)	A-94
Figure A-51 USGS NSHM ground motion hazard at spectral acceleration of 1 hz with 5% probability of exceedance in 50 years (Petersen et al., 2008)	A-95
Figure A-52 USGS NSHM ground motion hazard at spectral acceleration of 1 hz with 10% probability of exceedance in 50 years (Petersen et al., 2008)	A-96
Figure A-53 USGS NSHM ground motion hazard at spectral acceleration of 3 hz with 2% probability of exceedance in 50 years (Petersen et al., 2008)	A-97
Figure A-54 USGS NSHM ground motion hazard at spectral acceleration of 3 hz with 5% probability of exceedance in 50 years (Petersen et al., 2008)	A-98
Figure A-55 USGS NSHM ground motion hazard at spectral acceleration of 3 hz with 10% probability of exceedance in 50 years (Petersen et al., 2008)	A-99
Figure A-56 USGS NSHM ground motion hazard at spectral acceleration of 5 hz with 2% probability of exceedance in 50 years (Petersen et al., 2008)	A-100

Figure A-57 USGS NSHM ground motion hazard at spectral acceleration of 5 hz with 5% probability of exceedance in 50 years (Petersen et al., 2008)	A-101
Figure A-58 USGS NSHM ground motion hazard at spectral acceleration of 5 hz with 10% probability of exceedance in 50 years (Petersen et al., 2008)	A-102
Figure A-59 USGS NSHM peak ground acceleration with 2% probability of exceedance in 50 years (Petersen et al., 2008)	A-103
Figure A-60 USGS NSHM peak ground acceleration with 5% probability of exceedance in 50 years (Petersen et al., 2008)	A-104
Figure A-61 USGS NSHM peak ground acceleration with 10% probability of exceedance in 50 years (Petersen et al., 2008)	A-105
Figure A-62 Deformation of the North American Plate interior using GPS station data (Calais et al., 2006)	A-107
Figure A-63 Stress measurement update for the CEUS (Hurd, 2010).....	A-110
Figure A-64 CEUS SSC Project study area boundary	A-112
Figure A-65 USGS Quaternary fault and fold database (USGS, 2006)	A-114
Figure A-66 Quaternary features compilation for the CEUS (Crone and Wheeler, 2000; Wheeler, 2005; USGS, 2010)	A-116
Figure A-67 CEUS Mesozoic rift basins after Benson (1992).....	A-118
Figure A-68 CEUS Mesozoic rift basins after Dennis et al. (2004)	A-120
Figure A-69 CEUS Mesozoic rift basins after Schlische (1993).....	A-122
Figure A-70 CEUS Mesozoic rift basins after Withjack et al. (1998).....	A-124
Figure A-71 RLME zones for the CEUS	A-126
Figure A-72 Mesozoic and non-Mesozoic zones for the CEUS, wide interpretation.....	A-128
Figure A-73 Mesozoic and non-Mesozoic zones for the CEUS, narrow interpretation	A-129
Figure A-74 CEUS seismotectonic zones model A.....	A-130
Figure A-75 CEUS seismotectonic zones model B.....	A-131
Figure A-76 CEUS seismotectonic zones model C	A-132
Figure A-77 CEUS seismotectonic zones model D	A-133
Figure E-1 Map of CEUS showing locations of regional data sets included in the CEUS SSC Project paleoliquefaction database, including New Madrid seismic zone and surrounding region; Marianna, Arkansas, area; St. Louis region; Wabash Valley seismic zone and surrounding region; Arkansas-Louisiana-Mississippi region; Charleston seismic zone; Atlantic Coastal region and the Central Virginia seismic zone; Newburyport, Massachusetts, and surrounding region; and Charlevoix seismic zone and surrounding region.	E-68
Figure E-2 Diagram illustrating size parameters of liquefaction features, including sand blow thickness, width, and length; dike width; and sill thickness, as well as some of the diagnostic characteristics of these features.	E-69
Figure E-3 Diagram illustrating sampling strategy for dating of liquefaction features as well as age data, such as ¹⁴ C maximum and ¹⁴ C minimum, used to calculate preferred age estimates and related uncertainties of liquefaction features.....	E-70
Figure E-4 GIS map of New Madrid seismic zone and surrounding region showing portions of rivers searched for earthquake-induced liquefaction features by M.	

Tuttle, R. Van Arsdale, and J. Vaughn and collaborators (see explanation); information contributed for this report. Map projection is USA Contiguous Albers Equal Area Conic, North America Datum 1983.....	E-71
Figure E-5 GIS map of New Madrid seismic zone and surrounding region showing locations of liquefaction features for which there are and are not radiocarbon data. Map projection is USA Contiguous Albers Equal Area Conic, North America Datum 1983.	E-72
Figure E-6 GIS map of New Madrid seismic zone and surrounding region showing locations of liquefaction features that are thought to be historical or prehistoric in age or whose ages are poorly constrained. Map projection is USA Contiguous Albers Equal Area Conic, North America Datum 1983.	E-73
Figure E-7 GIS map of New Madrid seismic zone and surrounding region showing preferred age estimates of liquefaction features; features whose ages are poorly constrained are excluded. Map projection is USA Contiguous Albers Equal Area Conic, North America Datum 1983.	E-74
Figure E-8 GIS map of New Madrid seismic zone and surrounding region showing measured thicknesses of sand blows. Map projection is USA Contiguous Albers Equal Area Conic, North America Datum 1983.....	E-75
Figure E-9 GIS map of New Madrid seismic zone and surrounding region showing preferred age estimates and measured thicknesses of sand blows. Map projection is USA Contiguous Albers Equal Area Conic, North America Datum 1983.	E-76
Figure E-10 GIS map of New Madrid seismic zone and surrounding region showing measured widths of sand dikes. Map projection is USA Contiguous Albers Equal Area Conic, North America Datum 1983.....	E-77
Figure E-11 GIS map of New Madrid seismic zone and surrounding region showing preferred age estimates and measured widths of sand dikes. Map projection is USA Contiguous Albers Equal Area Conic, North America Datum 1983.	E-78
Figure E-12 GIS map of New Madrid seismic zone and surrounding region illustrating preferred age estimates and measured thicknesses of sand blows as well as preferred age estimates and measured widths of sand dikes for sites where sand blows do not occur. Map projection is USA Contiguous Albers Equal Area Conic, North America Datum 1983.....	E-79
Figure E-13 GIS map of Marianna, Arkansas, area showing seismicity and locations of paleoliquefaction features relative to mapped traces of Eastern Reelfoot rift margin fault, White River fault zone, Big Creek fault zone, Marianna escarpment, and Daytona Beach lineament. Map projection is USA Contiguous Albers Equal Area Conic, North America Datum 1983.	E-80
Figure E-14 (A) Trench log and (B) ground-penetrating radar profile, showing vertical sections of sand blows and sand dikes at Daytona Beach SE2 site along the Daytona Beach lineament southwest of Marianna, Arkansas. Vertical scale of GPR profile is exaggerated (modified from Al-Shukri et al., 2009).	E-81
Figure E-15 GIS map of Marianna, Arkansas, area showing locations of liquefaction features for which there are and are not radiocarbon data. Map projection is USA Contiguous Albers Equal Area Conic, North America Datum 1983.	E-82
Figure E-16 GIS map of Marianna, Arkansas, area showing locations of liquefaction features that are thought to be historical or prehistoric in age or whose ages are poorly constrained. To date, no liquefaction features thought to have formed during	

1811-1812 earthquakes have been found in area. Map projection is USA Contiguous Albers Equal Area Conic, North America Datum 1983.	E-83
Figure E-17 GIS map of Marianna, Arkansas, area showing preferred age estimates of liquefaction features; features whose ages are poorly constrained are excluded. Map projection is USA Contiguous Albers Equal Area Conic, North America Datum 1983.	E-84
Figure E-18 GIS map of Marianna, Arkansas, area showing measured thicknesses of sand blows. Map projection is USA Contiguous Albers Equal Area Conic, North America Datum 1983.	E-85
Figure E-19 GIS map of Marianna, Arkansas, area showing preferred age estimates and measured thicknesses of sand blows. Map projection is USA Contiguous Albers Equal Area Conic, North America Datum 1983.....	E-86
Figure E-20 GIS map of Marianna, Arkansas, area showing measured widths of sand dikes. Map projection is USA Contiguous Albers Equal Area Conic, North America Datum 1983.....	E-87
Figure E-21 GIS map of Marianna, Arkansas, area showing preferred age estimates and measured widths of sand dikes. Map projection is USA Contiguous Albers Equal Area Conic, North America Datum 1983.....	E-88
Figure E-22 GIS map of St. Louis, Missouri, region showing seismicity and portions of rivers searched for earthquake-induced liquefaction features by Tuttle and collaborators; information contributed for this report. Map projection is USA Contiguous Albers Equal Area Conic, North America Datum 1983.	E-89
Figure E-23 GIS map of St. Louis, Missouri, region showing locations of liquefaction features, including several soft-sediment deformation structures, for which there are and are not radiocarbon data. Map projection is USA Contiguous Albers Equal Area Conic, North America Datum 1983.	E-90
Figure E-24 GIS map of St. Louis, Missouri, region showing locations of liquefaction features that are thought to be historical or prehistoric in age or whose ages are poorly constrained. Map projection is USA Contiguous Albers Equal Area Conic, North America Datum 1983.....	E-91
Figure E-25 GIS map of St. Louis, Missouri, region showing preferred age estimates of liquefaction features; features whose ages are poorly constrained, including several that are prehistoric in age, are not shown. Map projection is USA Contiguous Albers Equal Area Conic, North America Datum 1983.....	E-92
Figure E-26 GIS map of St. Louis, Missouri, region showing measured thicknesses of sand blows at similar scale as used in Figure E-8 of sand blows in New Madrid seismic zone. Note that few sand blows have been found in St. Louis region. Map projection is USA Contiguous Albers Equal Area Conic, North America Datum 1983.	E-93
Figure E-27 GIS map of St. Louis, Missouri, region showing preferred age estimates and measured thicknesses of sand blows. Map projection is USA Contiguous Albers Equal Area Conic, North America Datum 1983.....	E-94
Figure E-28 GIS map of St. Louis, Missouri, region showing measured widths of sand dikes at similar scale as that used in Figure E-10 for sand dikes in New Madrid seismic zone. Map projection is USA Contiguous Albers Equal Area Conic, North America Datum 1983.	E-95

Figure E-29 GIS map of St. Louis, Missouri, region showing measured widths of sand dikes at similar scale as that used in Figures E-42 and E-48 for sand dikes in the Newburyport and Charlevoix regions, respectively. Map projection is USA Contiguous Albers Equal Area Conic, North America Datum 1983.	E-96
Figure E-30 GIS map of St. Louis, Missouri, region showing preferred age estimates and measured widths of sand dikes. Map projection is USA Contiguous Albers Equal Area Conic, North America Datum 1983.	E-97
Figure E-31 GIS map of Wabash Valley seismic zone and surrounding region showing portions of rivers searched for earthquake-induced liquefaction features (digitized from McNulty and Obermeier, 1999). Map projection is USA Contiguous Albers Equal Area Conic, North America Datum 1983.	E-98
Figure E-32 GIS map of Wabash Valley seismic zone and surrounding region showing measured widths of sand dikes at similar scale as that used in Figures E-10 and E-11 for sand dikes in New Madrid seismic zone. Map projection is USA Contiguous Albers Equal Area Conic, North America Datum 1983.	E-99
Figure E-33 GIS map of Wabash Valley region of Indiana and Illinois showing preferred age estimates and paleoearthquake interpretation. Map projection is USA Contiguous Albers Equal Area Conic, North America Datum 1983.	E-100
Figure E-34 GIS map of Arkansas-Louisiana-Mississippi (ALM) region showing paleoliquefaction study locations. Map projection is USA Contiguous Albers Equal Area Conic, North America Datum 1983.	E-101
Figure E-35 GIS map of Charleston, South Carolina, region showing locations of paleoliquefaction features for which there are and are not radiocarbon dates. Map projection is USA Contiguous Albers Equal Area Conic, North America Datum 1983.	E-102
Figure E-36 GIS map of Charleston, South Carolina, region showing locations of historical and prehistoric liquefaction features. Map projection is USA Contiguous Albers Equal Area Conic, North America Datum 1983.	E-103
Figure E-37 Map of Atlantic coast region showing areas searched for paleoliquefaction features by Gelinis et al. (1998) and Amick, Gelinis, et al. (1990). Rectangles indicate 7.5-minute quadrangles in which sites were investigated for presence of paleoliquefaction features. The number of sites investigated is shown within that quadrangle, if known. Orange and yellow indicate quadrangles in which paleoliquefaction features were recognized.	E-104
Figure E-38 Map of Central Virginia seismic zone region showing portions of rivers searched for earthquake-induced liquefaction features by Obermeier and McNulty (1998).	E-105
Figure E-39 GIS map of Newburyport, Massachusetts, and surrounding region showing seismicity and portions of rivers searched for earthquake-induced liquefaction features (Gelinis et al., 1998; Tuttle, 2007, 2009). Solid black line crossing map represents Massachusetts–New Hampshire border. Map projection is USA Contiguous Albers Equal Area Conic, North America Datum 1983.	E-106
Figure E-40 GIS map of Newburyport, Massachusetts, and surrounding region showing locations of liquefaction features for which there are and are not radiocarbon dates. Map projection is USA Contiguous Albers Equal Area Conic, North America Datum 1983.	E-107

Figure E-41 GIS map of Newburyport, Massachusetts, and surrounding region showing locations of liquefaction features that are thought to be historical or prehistoric in age or whose ages are poorly constrained. Map projection is USA Contiguous Albers Equal Area Conic, North America Datum 1983.	E-108
Figure E-42 GIS map of Newburyport, Massachusetts, and surrounding region showing measured widths of sand dikes. Map projection is USA Contiguous Albers Equal Area Conic, North America Datum 1983.	E-109
Figure E-43 GIS map of Newburyport, Massachusetts, and surrounding region showing preferred age estimates and measured widths of sand dikes. Map projection is USA Contiguous Albers Equal Area Conic, North America Datum 1983.	E-110
Figure E-44 Map of Charlevoix seismic zone and adjacent St. Lawrence Lowlands showing mapped faults and portions of rivers along which reconnaissance and searches for earthquake-induced liquefaction features were performed. Charlevoix seismic zone is defined by concentration of earthquakes and locations of historical earthquakes northeast of Quebec City. Devonian impact structure in vicinity of Charlevoix seismic zone is outlined by black dashed line. Taconic thrust faults are indicated by solid black lines with sawteeth on upper plate; lapetan rift faults are shown by solid black lines with hachure marks on downthrown side (modified from Tuttle and Atkinson, 2010).	E-111
Figure E-45 GIS map of Charlevoix seismic zone and surrounding region showing locations of liquefaction features, including several soft-sediment deformation structures, for which there are and are not radiocarbon data. Note the location of 1988 M 5.9 Saguenay earthquake northwest of the Charlevoix seismic zone. Map projection is USA Contiguous Albers Equal Area Conic, North America Datum 1983.	E-112
Figure E-46 GIS map of Charlevoix seismic zone and surrounding region showing locations of liquefaction features that are modern, historical, or prehistoric in age, or whose ages are poorly constrained. Map projection is USA Contiguous Albers Equal Area Conic, North America Datum 1983.	E-113
Figure E-47 GIS map of Charlevoix seismic zone and surrounding region showing preferred age estimates of liquefaction features; features whose ages are poorly constrained are excluded. Map projection is USA Contiguous Albers Equal Area Conic, North America Datum 1983.	E-114
Figure E-48 GIS map of Charlevoix seismic zone and surrounding region showing measured widths of sand dikes. Map projection is USA Contiguous Albers Equal Area Conic, North America Datum 1983.	E-115
Figure E-49 GIS map of Charlevoix seismic zone and surrounding region showing preferred age estimates and measured widths of sand dikes. Map projection is USA Contiguous Albers Equal Area Conic, North America Datum 1983.	E-116
Figure E-50 Photograph of moderate-sized sand blow (12 m long, 7 m wide, and 14 cm thick) that formed about 40 km from epicenter of 2001 M 7.7 Bhuj, India, earthquake (from Tuttle, Hengesh, et al., 2002), combined with schematic vertical section illustrating structural and stratigraphic relations of sand blow, sand dike, and source layer (modified from Sims and Garvin, 1995).	E-117
Figure E-51 Tree trunks buried and killed by sand blows, vented during 1811-1812 New Madrid earthquakes (from Fuller, 1912).	E-118

Figure E-52 Large sand-blow crater that formed during 2002 M 7.7 Bhuj, India, earthquake. Backpack for scale. Photograph: M. Tuttle (2001).	E-119
Figure E-53 Sand-blow crater that formed during 1886 Charleston, South Carolina, earthquake. Photograph: J.K. Hillers (from USGS Photograph Library).	E-120
Figure E-54 Photograph of sand blow and related sand dikes exposed in trench wall and floor in New Madrid seismic zone. Buried soil horizon is displaced downward approximately 1 m across two dikes. Clasts of soil horizon occur within dikes and overlying sand blow. Degree of soil development above and within sand blow suggests that it is at least several hundred years old and formed prior to 1811-1812 New Madrid earthquakes. Organic sample (location marked by red flag) from crater fill will provide close minimum age constraint for formation of sand blow. For scale, each colored intervals on shovel handle represents 10 cm. Photograph: M. Tuttle.....	E-121
Figure E-55 Sand dikes, ranging up to 35 cm wide, originate in pebbly sand layer and intrude overlying diamicton, These features were exposed in cutbank along Cahokia Creek about 25 km northeast of downtown St. Louis (from Tuttle, 2000).	E-122
Figure E-56 Photograph of small diapirs of medium sand intruding base of overlying deposit of interbedded clayey silt and very fine sand, and clasts of clayey silt in underlying medium sand, observed along Ouelle River in Charlevoix seismic zone. Sand diapirs and clasts probably formed during basal erosion and foundering of clayey silt due to liquefaction of the underlying sandy deposit. Red portion of shovel handle represents 10 cm (modified from Tuttle and Atkinson, 2010).	E-123
Figures E-57 (A) Load cast formed in laminated sediments of Van Norman Lake during 1952 Kern County, California, earthquake. Photograph: J. Sims (from Sims, 1975). (B) Load cast, pseudonodules, and related folds formed in laminated sediment exposed along Malbaie River in Charlevoix seismic zone. Sand dikes crosscutting these same laminated sediments occur at a nearby site. For scale, each painted interval of the shovel handle represents 10 cm (modified from Tuttle and Atkinson, 2010).	E-124
Figure E-58 Log of sand blow and uppermost portions of related sand dikes exposed in trench wall at Dodd site in New Madrid seismic zone. Sand dikes were also observed in opposite wall and trench floor. Sand blow buries pre-event A horizon, and a subsequent A horizon has developed in top of sand blow. Radiocarbon dating of samples collected above and below sand blow brackets its age between 490 and 660 yr BP. Artifact assemblage indicates that sand blow formed during late Mississippian (300–550 yr BP or AD 1400–1670) (modified from Tuttle, Collier, et al., 1999).	E-125
Figures E-59 (A) Photograph of earthquake-induced liquefaction features found in association with cultural horizon and pit exposed in trench wall near Blytheville, Arkansas, in New Madrid seismic zone. Photograph: M. Tuttle. (B) Trench log of features shown in (A). Sand dike formed in thick Native American occupation horizon containing artifacts of early Mississippian cultural period (950–1,150 yr BP). Cultural pit dug into top of sand dike contains artifacts and charcoal used to constrain minimum age of liquefaction features (modified from Tuttle and Schweig, 1995).	E-126
Figure E-60 In situ tree trunks such as this one buried and killed by sand blow in New Madrid seismic zone offer opportunity to date paleoearthquakes to the year and season of occurrence. Photograph: M. Tuttle.	E-127

Figure E-61 Portion of dendrocalibration curve illustrating conversion of radiocarbon age to calibrated date in calendar years. In example, 2-sigma radiocarbon age of 2,280–2,520 BP is converted to calibrated date of 770–380 BC (from Tuttle, 1999).	E-128
Figure E-62 Empirical relation developed between A horizon thickness of sand blows and years of soil development in New Madrid region. Horizontal bars reflect uncertainties in age estimates of liquefaction features; diamonds mark midpoints of possible age ranges (from Tuttle et al., 2000).	E-129
Figure E-63 Diagram illustrating earthquake chronology for New Madrid seismic zone for past 5,500 years based on dating and correlation of liquefaction features at sites (listed at top) across region from north to south. Vertical bars represent age estimates of individual sand blows, and horizontal bars represent event times of 138 yr BP (AD 1811-1812); 500 yr BP \pm 150 yr; 1,050 yr BP \pm 100 yr; and 4,300 yr BP \pm 200 yr (modified from Tuttle, Schweig, et al., 2002; Tuttle et al., 2005).	E-130
Figure E-64 Diagram illustrating earthquake chronology for New Madrid seismic zone for past 2,000 years, similar to upper portion of diagram shown in Figure E-63. As in Figure E-63, vertical bars represent age estimates of individual sand blows, and horizontal bars represent event times. Analysis performed during CEUS SSC Project derived two possible uncertainty ranges for timing of paleoearthquakes, illustrated by the darker and lighter portions of the colored horizontal bars, respectively: 503 yr BP \pm 8 yr or 465 yr BP \pm 65 yr, and 1,110 yr BP \pm 40 yr or 1055 \pm 95 yr (modified from Tuttle, Schweig, et al., 2002).	E-131
Figure E-65 Maps showing spatial distributions and sizes of sand blows and sand dikes attributed to 500 and 1,050 yr BP events. Locations and sizes of liquefaction features that formed during AD 1811-1812 (138 yr BP) New Madrid earthquake sequence shown for comparison (modified from Tuttle, Schweig, et al., 2002).	E-132
Figure E-66 Liquefaction fields for 138 yr BP (AD 1811-1812); 500 yr BP (AD 1450); and 1,050 yr BP (AD 900) events as interpreted from spatial distribution and stratigraphy of sand blows (modified from Tuttle, Schweig, et al., 2002). Ellipses define areas where similar-age sand blows have been mapped. Overlapping ellipses indicate areas where sand blows are composed of multiple units that formed during sequence of earthquakes. Dashed ellipse outlines area where historical sand blows are composed of four depositional units. Magnitudes of earthquakes in 500 yr BP and 1,050 yr BP are inferred from comparison with 1811-1812 liquefaction fields. Magnitude estimates of December (D), January (J), and February (F) main shocks and large aftershocks taken from several sources; rupture scenario from Johnston and Schweig (1996; modified from Tuttle, Schweig, et al., 2002).	E-133
Figure E-67 Empirical relation between earthquake magnitude and epicentral distance to farthest known sand blows induced by instrumentally recorded earthquakes (modified from Castilla and Audemard, 2007).	E-134
Figure E-68 Distances to farthest known liquefaction features indicate that 500 and 1,050 yr BP New Madrid events were at least of M 6.7 and 6.9, respectively, when plotted on Ambraseys (1988) relation between earthquake magnitude and epicentral distance to farthest surface expression of liquefaction. Similarity in size distribution of historical and prehistoric sand blows, however, suggests that paleoearthquakes were comparable in magnitude to 1811-1812 events or M \sim 7.6 (modified from Tuttle, 2001).	E-135
Figure H-1-1 Region covered by the CEUS SSC model.	H-44

Figure H-2-1 Master logic tree for the CEUS SSC model.....	H-45
Figure H-3-1 Logic tree for the Mmax zones branch of the master logic tree	H-46
Figure H-3-2 Mesozoic extended (MESE-W) and non-extended (NMESE-W) Mmax zones for the “wide” interpretation.....	H-47
Figure H-3-3 Mesozoic extended (MESE-N) and non-extended (NMESE-N) Mmax zones for the “narrow” interpretation.....	H-48
Figure H-4-1(a) Logic tree for the seismotectonic zones branch of the master logic tree.....	H-49
Figure H-4-1(b) Logic tree for the seismotectonic zones branch of the master logic tree.....	H-50
Figure H-4-2 Seismotectonic zones shown in the case where the Rough Creek Graben is not part of the Reelfoot Rift (RR) and the Paleozoic Extended zone is narrow (PEZ-N)	H-51
Figure H-4-3 Seismotectonic zones shown in the case where the Rough Creek Graben is part of the Reelfoot Rift (RR-RCG) and the Paleozoic Extended zone is narrow (PEZ-N)	H-52
Figure H-4-4 Seismotectonic zones shown in the case where the Rough Creek Graben is not part of the Reelfoot Rift (RR) and the Paleozoic Extended zone is wide (PEZ- W).....	H-53
Figure H-4-5 Seismotectonic zones shown in the case where the Rough Creek Graben is part of the Reelfoot Rift (RR-RCG) and the Paleozoic Extended zone is wide (PEZ-W)	H-54
Figure H-5-1 Logic tree for the RLME source branch of the master logic tree.....	H-55
Figure H-5-2 Location of RLME sources in the CEUS SSC model.....	H-56
Figure H-5.1-1 Logic tree for Charlevoix RLME source	H-57
Figure H-5.1-2 Charlevoix RLME source geometry	H-58
Figure H-5.2-1(a) Logic tree for Charleston RLME source	H-59
Figure H-5.2-1(b) Logic tree for Charleston RLME source	H-60
Figure H-5.2-2 Charleston RLME alternative source geometries	H-61
Figure H-5.3-1 Logic tree for Cheraw RLME source.....	H-62
Figure H-5.3-2 Cheraw RLME source geometry.....	H-63
Figure H-5.4-1 Logic tree for Meers RLME source	H-64
Figure H-5.4-2 Meers RLME source geometries	H-65
Figure H-5.5-1 Logic tree for NMFS RLME source	H-66
Figure H-5.5-2 New Madrid South (NMS) fault alternative RMLE source geometries: Blytheville Arch-Bootheel Lineament (BA-BL) and Blytheville Arch-Blytheville fault zone (BA-BFZ)	H-67
Figure H-5.5-3 New Madrid North (NMN) fault alternative RMLE source geometries: New Madrid North (NMN_S) and New Madrid North plus extension (NMN_L)	H-68
Figure H-5.5-4 Reelfoot Thrust (RFT) fault alternative RMLE source geometries: Reelfoot thrust (RFT_S) and Reelfoot thrust plus extensions (RFT_L).....	H-69
Figure H-5.6-1 Logic tree for ERM-S RLME source	H-70
Figure H-5.6-2 Logic tree for ERM-N RLME source	H-71
Figure H-5.6-3 ERM-S RLME source geometries.....	H-72

Figure H-5.6-4 ERM-N RLME source geometry	H-73
Figure H-5.7-1 Logic tree for Marianna RLME source	H-74
Figure H-5.7-2 Marianna RLME source geometry	H-75
Figure H-5.8-1 Logic tree for Commerce Fault Zone RLME source	H-76
Figure H-5.8-2 Commerce RLME source geometry	H-77
Figure H-5.9-1 Logic tree for Wabash Valley RLME source	H-78
Figure H-5.9-2 Wabash Valley RLME source geometry	H-79
Figure J-1 Map of the rate and b -value for the study region under the Mmax zonation, with no separation of Mesozoic extended and non-extended; Case A magnitude weights: Realization 1	J-2
Figure J-2 Map of the rate and b -value for the study region under the Mmax zonation, with no separation of Mesozoic extended and non-extended; Case A magnitude weights: Realization 2	J-3
Figure J-3 Map of the rate and b -value for the study region under the Mmax zonation, with no separation of Mesozoic extended and non-extended; Case A magnitude weights: Realization 3	J-4
Figure J-4 Map of the rate and b -value for the study region under the Mmax zonation, with no separation of Mesozoic extended and non-extended; Case A magnitude weights: Realization 4	J-5
Figure J-5 Map of the rate and b -value for the study region under the Mmax zonation, with no separation of Mesozoic extended and non-extended; Case A magnitude weights: Realization 5	J-6
Figure J-6 Map of the rate and b -value for the study region under the Mmax zonation, with no separation of Mesozoic extended and non-extended; Case A magnitude weights: Realization 6	J-7
Figure J-7 Map of the rate and b -value for the study region under the Mmax zonation, with no separation of Mesozoic extended and non-extended; Case A magnitude weights: Realization 7	J-8
Figure J-8 Map of the rate and b -value for the study region under the Mmax zonation, with no separation of Mesozoic extended and non-extended; Case A magnitude weights: Realization 8	J-9
Figure J-9 Map of the coefficient of variation of the rate and the standard deviation of the b -value for the study region under the Mmax zonation, with no separation of Mesozoic extended and non-extended; Case A magnitude weights.....	J-10
Figure J-10 Map of the rate and b -value for the study region under the Mmax zonation, with no separation of Mesozoic extended and non-extended; Case B magnitude weights: Realization 1	J-11
Figure J-11 Map of the rate and b -value for the study region under the Mmax zonation, with no separation of Mesozoic extended and non-extended; Case B magnitude weights: Realization 2	J-12
Figure J-12 Map of the rate and b -value for the study region under the Mmax zonation, with no separation of Mesozoic extended and non-extended; Case B magnitude weights: Realization 3	J-13

Figure J-13 Map of the rate and b -value for the study region under the Mmax zonation, with no separation of Mesozoic extended and non-extended; Case B magnitude weights: Realization 4	J-14
Figure J-14 Map of the rate and b -value for the study region under the Mmax zonation, with no separation of Mesozoic extended and non-extended; Case B magnitude weights: Realization 5	J-15
Figure J-15 Map of the rate and b -value for the study region under the Mmax zonation, with no separation of Mesozoic extended and non-extended; Case B magnitude weights: Realization 6	J-16
Figure J-16 Map of the rate and b -value for the study region under the Mmax zonation, with no separation of Mesozoic extended and non-extended; Case B magnitude weights: Realization 7	J-17
Figure J-17 Map of the rate and b -value for the study region under the Mmax zonation, with no separation of Mesozoic extended and non-extended; Case B magnitude weights: Realization 8	J-18
Figure J-18 Map of the coefficient of variation of the rate and the standard deviation of the b -value for the study region under the Mmax zonation, with no separation of Mesozoic extended and non-extended; Case B magnitude weights.....	J-19
Figure J-19 Map of the rate and b -value for the study region under the Mmax zonation, with no separation of Mesozoic extended and non-extended; Case E magnitude weights: Realization 1	J-20
Figure J-20 Map of the rate and b -value for the study region under the Mmax zonation, with no separation of Mesozoic extended and non-extended; Case E magnitude weights: Realization 2	J-21
Figure J-21 Map of the rate and b -value for the study region under the Mmax zonation, with no separation of Mesozoic extended and non-extended; Case E magnitude weights: Realization 3	J-22
Figure J-22 Map of the rate and b -value for the study region under the Mmax zonation, with no separation of Mesozoic extended and non-extended; Case E magnitude weights: Realization 4	J-23
Figure J-23 Map of the rate and b -value for the study region under the Mmax zonation, with no separation of Mesozoic extended and non-extended; Case E magnitude weights: Realization 5	J-24
Figure J-24 Map of the rate and b -value for the study region under the Mmax zonation, with no separation of Mesozoic extended and non-extended; Case E magnitude weights: Realization 6	J-25
Figure J-25 Map of the rate and b -value for the study region under the Mmax zonation, with no separation of Mesozoic extended and non-extended; Case E magnitude weights: Realization 7	J-26
Figure J-26 Map of the rate and b -value for the study region under the Mmax zonation, with no separation of Mesozoic extended and non-extended; Case E magnitude weights: Realization 8	J-27
Figure J-27 Map of the coefficient of variation of the rate and the standard deviation of the b -value for the study region under the Mmax zonation, with no separation of Mesozoic extended and non-extended; Case E magnitude weights.....	J-28

Figure J-28 Map of the rate and b -value for the study region under the Mmax zonation, with separation of Mesozoic extended and non-extended; Case A magnitude weights: Realization 1	J-29
Figure J-29 Map of the rate and b -value for the study region under the Mmax zonation, with separation of Mesozoic extended and non-extended; Case A magnitude weights: Realization 2	J-30
Figure J-30 Map of the rate and b -value for the study region under the Mmax zonation, with separation of Mesozoic extended and non-extended; Case A magnitude weights: Realization 3	J-31
Figure J-31 Map of the rate and b -value for the study region under the Mmax zonation, with separation of Mesozoic extended and non-extended; Case A magnitude weights: Realization 4	J-32
Figure J-32 Map of the rate and b -value for the study region under the Mmax zonation, with separation of Mesozoic extended and non-extended; Case A magnitude weights: Realization 5	J-33
Figure J-33 Map of the rate and b -value for the study region under the Mmax zonation, with separation of Mesozoic extended and non-extended; Case A magnitude weights: Realization 6	J-34
Figure J-34 Map of the rate and b -value for the study region under the Mmax zonation, with separation of Mesozoic extended and non-extended; Case A magnitude weights: Realization 7	J-35
Figure J-35 Map of the rate and b -value for the study region under the Mmax zonation, with separation of Mesozoic extended and non-extended; Case A magnitude weights: Realization 8	J-36
Figure J-36 Map of the coefficient of variation of the rate and the standard deviation of the b -value for the study region under the Mmax zonation, with separation of Mesozoic extended and non-extended; Case A magnitude weights.....	J-37
Figure J-37 Map of the rate and b -value for the study region under the Mmax zonation, with separation of Mesozoic extended and non-extended; Case B magnitude weights: Realization 1	J-38
Figure J-38 Map of the rate and b -value for the study region under the Mmax zonation, with separation of Mesozoic extended and non-extended; Case B magnitude weights: Realization 2	J-39
Figure J-39 Map of the rate and b -value for the study region under the Mmax zonation, with separation of Mesozoic extended and non-extended; Case B magnitude weights: Realization 3	J-40
Figure J-40 Map of the rate and b -value for the study region under the Mmax zonation, with separation of Mesozoic extended and non-extended; Case B magnitude weights: Realization 4	J-41
Figure J-41 Map of the rate and b -value for the study region under the Mmax zonation, with separation of Mesozoic extended and non-extended; Case B magnitude weights: Realization 5	J-42
Figure J-42 Map of the rate and b -value for the study region under the Mmax zonation, with separation of Mesozoic extended and non-extended; Case B magnitude weights: Realization 6	J-43

Figure J-43 Map of the rate and b -value for the study region under the Mmax zonation, with separation of Mesozoic extended and non-extended; Case B magnitude weights: Realization 7	J-44
Figure J-44 Map of the rate and b -value for the study region under the Mmax zonation, with separation of Mesozoic extended and non-extended; Case B magnitude weights: Realization 8	J-45
Figure J-45 Map of the coefficient of variation of the rate and the standard deviation of the b -value for the study region under the Mmax zonation, with separation of Mesozoic extended and non-extended; Case B magnitude weights.....	J-46
Figure J-46 Map of the rate and b -value for the study region under the Mmax zonation, with separation of Mesozoic extended and non-extended; Case E magnitude weights: Realization 1	J-47
Figure J-47 Map of the rate and b -value for the study region under the Mmax zonation, with separation of Mesozoic extended and non-extended; Case E magnitude weights: Realization 2	J-48
Figure J-48 Map of the rate and b -value for the study region under the Mmax zonation, with separation of Mesozoic extended and non-extended; Case E magnitude weights: Realization 3	J-49
Figure J-49 Map of the rate and b -value for the study region under the Mmax zonation, with separation of Mesozoic extended and non-extended; Case E magnitude weights: Realization 4	J-50
Figure J-50 Map of the rate and b -value for the study region under the Mmax zonation, with separation of Mesozoic extended and non-extended; Case E magnitude weights: Realization 5	J-51
Figure J-51 Map of the rate and b -value for the study region under the Mmax zonation, with separation of Mesozoic extended and non-extended; Case E magnitude weights: Realization 6	J-52
Figure J-52 Map of the rate and b -value for the study region under the Mmax zonation, with separation of Mesozoic extended and non-extended; Case E magnitude weights: Realization 7	J-53
Figure J-53 Map of the rate and b -value for the study region under the Mmax zonation, with separation of Mesozoic extended and non-extended; Case E magnitude weights: Realization 8	J-54
Figure J-54 Map of the coefficient of variation of the rate and the standard deviation of the b -value for the study region under the Mmax zonation, with separation of Mesozoic extended and non-extended; Case E magnitude weights.....	J-55
Figure J-55 Map of the rate and b -value for the study region under the Mmax zonation, with separation of Mesozoic extended and non-extended; Case A magnitude weights: Realization 1	J-56
Figure J-56 Map of the rate and b -value for the study region under the Mmax zonation, with separation of Mesozoic extended and non-extended; Case A magnitude weights: Realization 2	J-57
Figure J-57 Map of the rate and b -value for the study region under the Mmax zonation, with separation of Mesozoic extended and non-extended; Case A magnitude weights: Realization 3	J-58

Figure J-58 Map of the rate and b -value for the study region under the Mmax zonation, with separation of Mesozoic extended and non-extended; Case A magnitude weights: Realization 4	J-59
Figure J-59 Map of the rate and b -value for the study region under the Mmax zonation, with separation of Mesozoic extended and non-extended; Case A magnitude weights: Realization 5	J-60
Figure J-60 Map of the rate and b -value for the study region under the Mmax zonation, with separation of Mesozoic extended and non-extended; Case A magnitude weights: Realization 6	J-61
Figure J-61 Map of the rate and b -value for the study region under the Mmax zonation, with separation of Mesozoic extended and non-extended; Case A magnitude weights: Realization 7	J-62
Figure J-62 Map of the rate and b -value for the study region under the Mmax zonation, with separation of Mesozoic extended and non-extended; Case A magnitude weights: Realization 8	J-63
Figure J-63 Map of the coefficient of variation of the rate and the standard deviation of the b -value for the study region under the Mmax zonation, with separation of Mesozoic extended and non-extended; Case A magnitude weights.....	J-64
Figure J-64 Map of the rate and b -value for the study region under the Mmax zonation, with separation of Mesozoic extended and non-extended; Case B magnitude weights: Realization 1	J-65
Figure J-65 Map of the rate and b -value for the study region under the Mmax zonation, with separation of Mesozoic extended and non-extended; Case B magnitude weights: Realization 2	J-66
Figure J-66 Map of the rate and b -value for the study region under the Mmax zonation, with separation of Mesozoic extended and non-extended; Case B magnitude weights: Realization 3	J-67
Figure J-67 Map of the rate and b -value for the study region under the Mmax zonation, with separation of Mesozoic extended and non-extended; Case B magnitude weights: Realization 4	J-68
Figure J-68 Map of the rate and b -value for the study region under the Mmax zonation, with separation of Mesozoic extended and non-extended; Case B magnitude weights: Realization 5	J-69
Figure J-69 Map of the rate and b -value for the study region under the Mmax zonation, with separation of Mesozoic extended and non-extended; Case B magnitude weights: Realization 6	J-70
Figure J-70 Map of the rate and b -value for the study region under the Mmax zonation, with separation of Mesozoic extended and non-extended; Case B magnitude weights: Realization 7	J-71
Figure J-71 Map of the rate and b -value for the study region under the Mmax zonation, with separation of Mesozoic extended and non-extended; Case B magnitude weights: Realization 8	J-72
Figure J-72 Map of the coefficient of variation of the rate and the standard deviation of the b -value for the study region under the Mmax zonation, with separation of Mesozoic extended and non-extended; Case B magnitude weights.....	J-73

Figure J-73 Map of the rate and b -value for the study region under the Mmax zonation, with separation of Mesozoic extended and non-extended; Case E magnitude weights: Realization 1	J-74
Figure J-74 Map of the rate and b -value for the study region under the Mmax zonation, with separation of Mesozoic extended and non-extended; Case E magnitude weights: Realization 2	J-75
Figure J-75 Map of the rate and b -value for the study region under the Mmax zonation, with separation of Mesozoic extended and non-extended; Case E magnitude weights: Realization 3	J-76
Figure J-76 Map of the rate and b -value for the study region under the Mmax zonation, with separation of Mesozoic extended and non-extended; Case E magnitude weights: Realization 4	J-77
Figure J-77 Map of the rate and b -value for the study region under the Mmax zonation, with separation of Mesozoic extended and non-extended; Case E magnitude weights: Realization 5	J-78
Figure J-78 Map of the rate and b -value for the study region under the Mmax zonation, with separation of Mesozoic extended and non-extended; Case E magnitude weights: Realization 6	J-79
Figure J-79 Map of the rate and b -value for the study region under the Mmax zonation, with separation of Mesozoic extended and non-extended; Case E magnitude weights: Realization 7	J-80
Figure J-80 Map of the rate and b -value for the study region under the Mmax zonation, with separation of Mesozoic extended and non-extended; Case E magnitude weights: Realization 8	J-81
Figure J-81 Map of the coefficient of variation of the rate and the standard deviation of the b -value for the study region under the Mmax zonation, with separation of Mesozoic extended and non-extended; Case E magnitude weights.....	J-82
Figure J-82 Map of the rate and b -value for the study region under the seismotectonic zonation, with narrow interpretation of PEZ; Case A magnitude weights: Realization 1	J-83
Figure J-83 Map of the rate and b -value for the study region under the seismotectonic zonation, with narrow interpretation of PEZ; Case A magnitude weights: Realization 2	J-84
Figure J-84 Map of the rate and b -value for the study region under the seismotectonic zonation, with narrow interpretation of PEZ; Case A magnitude weights: Realization 3	J-85
Figure J-85 Map of the rate and b -value for the study region under the seismotectonic zonation, with narrow interpretation of PEZ; Case A magnitude weights: Realization 4	J-86
Figure J-86 Map of the rate and b -value for the study region under the seismotectonic zonation, with narrow interpretation of PEZ; Case A magnitude weights: Realization 5	J-87
Figure J-87 Map of the rate and b -value for the study region under the seismotectonic zonation, with narrow interpretation of PEZ; Case A magnitude weights: Realization 6	J-88

Figure J-88 Map of the rate and b -value for the study region under the seismotectonic zonation, with narrow interpretation of PEZ; Case A magnitude weights: Realization 7	J-89
Figure J-89 Map of the rate and b -value for the study region under the seismotectonic zonation, with narrow interpretation of PEZ; Case A magnitude weights: Realization 8	J-90
Figure J-90 Map of the coefficient of variation of the rate and the standard deviation of the b -value for the study region under the seismotectonic zonation, with narrow interpretation of PEZ; Case A magnitude weights	J-91
Figure J-91 Map of the rate and b -value for the study region under the seismotectonic zonation, with narrow interpretation of PEZ; Case B magnitude weights: Realization 1	J-92
Figure J-92 Map of the rate and b -value for the study region under the seismotectonic zonation, with narrow interpretation of PEZ; Case B magnitude weights: Realization 2	J-93
Figure J-93 Map of the rate and b -value for the study region under the seismotectonic zonation, with narrow interpretation of PEZ; Case B magnitude weights: Realization 3	J-94
Figure J-94 Map of the rate and b -value for the study region under the seismotectonic zonation, with narrow interpretation of PEZ; Case B magnitude weights: Realization 4	J-95
Figure J-95 Map of the rate and b -value for the study region under the seismotectonic zonation, with narrow interpretation of PEZ; Case B magnitude weights: Realization 5	J-96
Figure J-96 Map of the rate and b -value for the study region under the seismotectonic zonation, with narrow interpretation of PEZ; Case B magnitude weights: Realization 6	J-97
Figure J-97 Map of the rate and b -value for the study region under the seismotectonic zonation, with narrow interpretation of PEZ; Case B magnitude weights: Realization 7	J-98
Figure J-98 Map of the rate and b -value for the study region under the seismotectonic zonation, with narrow interpretation of PEZ; Case B magnitude weights: Realization 8	J-99
Figure J-99 Map of the coefficient of variation of the rate and the standard deviation of the b -value for the study region under the seismotectonic zonation, with narrow interpretation of PEZ; Case B magnitude weights	J-100
Figure J-100 Map of the rate and b -value for the study region under the seismotectonic zonation, with narrow interpretation of PEZ; Case E magnitude weights: Realization 1	J-101
Figure J-101 Map of the rate and b -value for the study region under the seismotectonic zonation, with narrow interpretation of PEZ; Case E magnitude weights: Realization 2	J-102
Figure J-102 Map of the rate and b -value for the study region under the seismotectonic zonation, with narrow interpretation of PEZ; Case E magnitude weights: Realization 3	J-103

Figure J-103 Map of the rate and b -value for the study region under the seismotectonic zonation, with narrow interpretation of PEZ; Case E magnitude weights: Realization	
4	J-104
Figure J-104 Map of the rate and b -value for the study region under the seismotectonic zonation, with narrow interpretation of PEZ; Case E magnitude weights: Realization	
5	J-105
Figure J-105 Map of the rate and b -value for the study region under the seismotectonic zonation, with narrow interpretation of PEZ; Case E magnitude weights: Realization	
6	J-106
Figure J-106 Map of the rate and b -value for the study region under the seismotectonic zonation, with narrow interpretation of PEZ; Case E magnitude weights: Realization	
7	J-107
Figure J-107 Map of the rate and b -value for the study region under the seismotectonic zonation, with narrow interpretation of PEZ; Case E magnitude weights: Realization	
8	J-108
Figure J-108 Map of the coefficient of variation of the rate and the standard deviation of the b -value for the study region under the seismotectonic zonation, with narrow interpretation of PEZ; Case E magnitude weights	J-109
Figure J-109 Map of the rate and b -value for the study region under the seismotectonic zonation, with narrow interpretation of PEZ; Case A magnitude weights: Realization	
1	J-110
Figure J-110 Map of the rate and b -value for the study region under the seismotectonic zonation, with narrow interpretation of PEZ; Case A magnitude weights: Realization	
2	J-111
Figure J-111 Map of the rate and b -value for the study region under the seismotectonic zonation, with narrow interpretation of PEZ; Case A magnitude weights: Realization	
3	J-112
Figure J-112 Map of the rate and b -value for the study region under the seismotectonic zonation, with narrow interpretation of PEZ; Case A magnitude weights: Realization	
4	J-113
Figure J-113 Map of the rate and b -value for the study region under the seismotectonic zonation, with narrow interpretation of PEZ; Case A magnitude weights: Realization	
5	J-114
Figure J-114 Map of the rate and b -value for the study region under the seismotectonic zonation, with narrow interpretation of PEZ; Case A magnitude weights: Realization	
6	J-115
Figure J-115 Map of the rate and b -value for the study region under the seismotectonic zonation, with narrow interpretation of PEZ; Case A magnitude weights: Realization	
7	J-116
Figure J-116 Map of the rate and b -value for the study region under the seismotectonic zonation, with narrow interpretation of PEZ; Case A magnitude weights: Realization	
8	J-117
Figure J-117 Map of the coefficient of variation of the rate and the standard deviation of the b -value for the study region under the seismotectonic zonation, with narrow interpretation of PEZ; Case A magnitude weights	J-118

Figure J-118 Map of the rate and b -value for the study region under the seismotectonic zonation, with narrow interpretation of PEZ; Case B magnitude weights: Realization 1	J-119
Figure J-119 Map of the rate and b -value for the study region under the seismotectonic zonation, with narrow interpretation of PEZ; Case B magnitude weights: Realization 2	J-120
Figure J-120 Map of the rate and b -value for the study region under the seismotectonic zonation, with narrow interpretation of PEZ; Case B magnitude weights: Realization 3	J-121
Figure J-121 Map of the rate and b -value for the study region under the seismotectonic zonation, with narrow interpretation of PEZ; Case B magnitude weights: Realization 4	J-122
Figure J-122 Map of the rate and b -value for the study region under the seismotectonic zonation, with narrow interpretation of PEZ; Case B magnitude weights: Realization 5	J-123
Figure J-123 Map of the rate and b -value for the study region under the seismotectonic zonation, with narrow interpretation of PEZ; Case B magnitude weights: Realization 6	J-124
Figure J-124 Map of the rate and b -value for the study region under the seismotectonic zonation, with narrow interpretation of PEZ; Case B magnitude weights: Realization 7	J-125
Figure J-125 Map of the rate and b -value for the study region under the seismotectonic zonation, with narrow interpretation of PEZ; Case B magnitude weights: Realization 8	J-126
Figure J-126 Map of the coefficient of variation of the rate and the standard deviation of the b -value for the study region under the seismotectonic zonation, with narrow interpretation of PEZ; Case B magnitude weights	J-127
Figure J-127 Map of the rate and b -value for the study region under the seismotectonic zonation, with narrow interpretation of PEZ; Case E magnitude weights: Realization 1	J-128
Figure J-128 Map of the rate and b -value for the study region under the seismotectonic zonation, with narrow interpretation of PEZ; Case E magnitude weights: Realization 2	J-129
Figure J-129 Map of the rate and b -value for the study region under the seismotectonic zonation, with narrow interpretation of PEZ; Case E magnitude weights: Realization 3	J-130
Figure J-130 Map of the rate and b -value for the study region under the seismotectonic zonation, with narrow interpretation of PEZ; Case E magnitude weights: Realization 4	J-131
Figure J-131 Map of the rate and b -value for the study region under the seismotectonic zonation, with narrow interpretation of PEZ; Case E magnitude weights: Realization 5	J-132
Figure J-132 Map of the rate and b -value for the study region under the seismotectonic zonation, with narrow interpretation of PEZ; Case E magnitude weights: Realization 6	J-133

Figure J-133 Map of the rate and b -value for the study region under the seismotectonic zonation, with narrow interpretation of PEZ; Case E magnitude weights: Realization 7	J-134
Figure J-134 Map of the rate and b -value for the study region under the seismotectonic zonation, with narrow interpretation of PEZ; Case E magnitude weights: Realization 8	J-135
Figure J-135 Map of the coefficient of variation of the rate and the standard deviation of the b -value for the study region under the seismotectonic zonation, with narrow interpretation of PEZ; Case E magnitude weights	J-136
Figure J-136 Map of the rate and b -value for the study region under the seismotectonic zonation, with wide interpretation of PEZ; Case A magnitude weights: Realization 1 ...	J-137
Figure J-137 Map of the rate and b -value for the study region under the seismotectonic zonation, with wide interpretation of PEZ; Case A magnitude weights: Realization 2 ...	J-138
Figure J-138 Map of the rate and b -value for the study region under the seismotectonic zonation, with wide interpretation of PEZ; Case A magnitude weights: Realization 3 ...	J-139
Figure J-139 Map of the rate and b -value for the study region under the seismotectonic zonation, with wide interpretation of PEZ; Case A magnitude weights: Realization 4 ...	J-140
Figure J-140 Map of the rate and b -value for the study region under the seismotectonic zonation, with wide interpretation of PEZ; Case A magnitude weights: Realization 5 ...	J-141
Figure J-141 Map of the rate and b -value for the study region under the seismotectonic zonation, with wide interpretation of PEZ; Case A magnitude weights: Realization 6 ...	J-142
Figure J-142 Map of the rate and b -value for the study region under the seismotectonic zonation, with wide interpretation of PEZ; Case A magnitude weights: Realization 7 ...	J-143
Figure J-143 Map of the rate and b -value for the study region under the seismotectonic zonation, with wide interpretation of PEZ; Case A magnitude weights: Realization 8 ...	J-144
Figure J-144 Map of the coefficient of variation of the rate and the standard deviation of the b -value for the study region under the seismotectonic zonation, with wide interpretation of PEZ; Case A magnitude weights	J-145
Figure J-145 Map of the rate and b -value for the study region under the seismotectonic zonation, with wide interpretation of PEZ; Case B magnitude weights: Realization 1 ...	J-146
Figure J-146 Map of the rate and b -value for the study region under the seismotectonic zonation, with wide interpretation of PEZ; Case B magnitude weights: Realization 2 ...	J-147
Figure J-147 Map of the rate and b -value for the study region under the seismotectonic zonation, with wide interpretation of PEZ; Case B magnitude weights: Realization 3 ...	J-148
Figure J-148 Map of the rate and b -value for the study region under the seismotectonic zonation, with wide interpretation of PEZ; Case B magnitude weights: Realization 4 ...	J-149
Figure J-149 Map of the rate and b -value for the study region under the seismotectonic zonation, with wide interpretation of PEZ; Case B magnitude weights: Realization 5 ...	J-150
Figure J-150 Map of the rate and b -value for the study region under the seismotectonic zonation, with wide interpretation of PEZ; Case B magnitude weights: Realization 6 ...	J-151
Figure J-151 Map of the rate and b -value for the study region under the seismotectonic zonation, with wide interpretation of PEZ; Case B magnitude weights: Realization 7 ...	J-152
Figure J-152 Map of the rate and b -value for the study region under the seismotectonic zonation, with wide interpretation of PEZ; Case B magnitude weights: Realization 8 ...	J-153

Figure J-153 Map of the coefficient of variation of the rate and the standard deviation of the b -value for the study region under the seismotectonic zonation, with wide interpretation of PEZ; Case B magnitude weights	J-154
Figure J-154 Map of the rate and b -value for the study region under the seismotectonic zonation, with wide interpretation of PEZ; Case E magnitude weights: Realization 1 ...	J-155
Figure J-155 Map of the rate and b -value for the study region under the seismotectonic zonation, with wide interpretation of PEZ; Case E magnitude weights: Realization 2 ...	J-156
Figure J-156 Map of the rate and b -value for the study region under the seismotectonic zonation, with wide interpretation of PEZ; Case E magnitude weights: Realization 3 ...	J-157
Figure J-157 Map of the rate and b -value for the study region under the seismotectonic zonation, with wide interpretation of PEZ; Case E magnitude weights: Realization 4 ...	J-158
Figure J-158 Map of the rate and b -value for the study region under the seismotectonic zonation, with wide interpretation of PEZ; Case E magnitude weights: Realization 5 ...	J-159
Figure J-159 Map of the rate and b -value for the study region under the seismotectonic zonation, with wide interpretation of PEZ; Case E magnitude weights: Realization 6 ...	J-160
Figure J-160 Map of the rate and b -value for the study region under the seismotectonic zonation, with wide interpretation of PEZ; Case E magnitude weights: Realization 7 ...	J-161
Figure J-161 Map of the rate and b -value for the study region under the seismotectonic zonation, with wide interpretation of PEZ; Case E magnitude weights: Realization 8 ...	J-162
Figure J-162 Map of the coefficient of variation of the rate and the standard deviation of the b -value for the study region under the seismotectonic zonation, with wide interpretation of PEZ; Case E magnitude weights	J-163
Figure J-163 Map of the rate and b -value for the study region under the seismotectonic zonation, with wide interpretation of PEZ; Case A magnitude weights: Realization 1 ...	J-164
Figure J-164 Map of the rate and b -value for the study region under the seismotectonic zonation, with wide interpretation of PEZ; Case A magnitude weights: Realization 2 ...	J-165
Figure J-165 Map of the rate and b -value for the study region under the seismotectonic zonation, with wide interpretation of PEZ; Case A magnitude weights: Realization 3 ...	J-166
Figure J-166 Map of the rate and b -value for the study region under the seismotectonic zonation, with wide interpretation of PEZ; Case A magnitude weights: Realization 4 ...	J-167
Figure J-167 Map of the rate and b -value for the study region under the seismotectonic zonation, with wide interpretation of PEZ; Case A magnitude weights: Realization 5 ...	J-168
Figure J-168 Map of the rate and b -value for the study region under the seismotectonic zonation, with wide interpretation of PEZ; Case A magnitude weights: Realization 6 ...	J-169
Figure J-169 Map of the rate and b -value for the study region under the seismotectonic zonation, with wide interpretation of PEZ; Case A magnitude weights: Realization 7 ...	J-170
Figure J-170 Map of the rate and b -value for the study region under the seismotectonic zonation, with wide interpretation of PEZ; Case A magnitude weights: Realization 8 ...	J-171
Figure J-171 Map of the coefficient of variation of the rate and the standard deviation of the b -value for the study region under the seismotectonic zonation, with wide interpretation of PEZ; Case A magnitude weights	J-172
Figure J-172 Map of the rate and b -value for the study region under the seismotectonic zonation, with wide interpretation of PEZ; Case B magnitude weights: Realization 1 ...	J-173

Figure J-173 Map of the rate and b -value for the study region under the seismotectonic zonation, with wide interpretation of PEZ; Case B magnitude weights: Realization 2 ...	J-174
Figure J-174 Map of the rate and b -value for the study region under the seismotectonic zonation, with wide interpretation of PEZ; Case B magnitude weights: Realization 3 ...	J-175
Figure J-175 Map of the rate and b -value for the study region under the seismotectonic zonation, with wide interpretation of PEZ; Case B magnitude weights: Realization 4 ...	J-176
Figure J-176 Map of the rate and b -value for the study region under the seismotectonic zonation, with wide interpretation of PEZ; Case B magnitude weights: Realization 5 ...	J-177
Figure J-177 Map of the rate and b -value for the study region under the seismotectonic zonation, with wide interpretation of PEZ; Case B magnitude weights: Realization 6 ...	J-178
Figure J-178 Map of the rate and b -value for the study region under the seismotectonic zonation, with wide interpretation of PEZ; Case B magnitude weights: Realization 7 ...	J-179
Figure J-179 Map of the rate and b -value for the study region under the seismotectonic zonation, with wide interpretation of PEZ; Case B magnitude weights: Realization 8 ...	J-180
Figure J-180 Map of the coefficient of variation of the rate and the standard deviation of the b -value for the study region under the seismotectonic zonation, with wide interpretation of PEZ; Case B magnitude weights	J-181
Figure J-181 Map of the rate and b -value for the study region under the seismotectonic zonation, with wide interpretation of PEZ; Case E magnitude weights: Realization 1 ...	J-182
Figure J-182 Map of the rate and b -value for the study region under the seismotectonic zonation, with wide interpretation of PEZ; Case E magnitude weights: Realization 2 ...	J-183
Figure J-183 Map of the rate and b -value for the study region under the seismotectonic zonation, with wide interpretation of PEZ; Case E magnitude weights: Realization 3 ...	J-184
Figure J-184 Map of the rate and b -value for the study region under the seismotectonic zonation, with wide interpretation of PEZ; Case E magnitude weights: Realization 4 ...	J-185
Figure J-185 Map of the rate and b -value for the study region under the seismotectonic zonation, with wide interpretation of PEZ; Case E magnitude weights: Realization 5 ...	J-186
Figure J-186 Map of the rate and b -value for the study region under the seismotectonic zonation, with wide interpretation of PEZ; Case E magnitude weights: Realization 6 ...	J-187
Figure J-187 Map of the rate and b -value for the study region under the seismotectonic zonation, with wide interpretation of PEZ; Case E magnitude weights: Realization 7 ...	J-188
Figure J-188 Map of the rate and b -value for the study region under the seismotectonic zonation, with wide interpretation of PEZ; Case E magnitude weights: Realization 8 ...	J-189
Figure J-189 Map of the coefficient of variation of the rate and the standard deviation of the b -value for the study region under the seismotectonic zonation, with wide interpretation of PEZ; Case E magnitude weights	J-190
Figure K-1 Comparison of relationships between number of reporting stations and moment magnitude presented in Johnston et al. (1994) and Johnston (1996b).	K-41
Figure K-2 Comparison of relationships between isoseismal areas and moment magnitude presented in Johnston et al. (1994) and Johnston (1996b).	K-42

LIST OF TABLES

Table 2.2-1 Technical Meetings Conducted as Part of the CEUS SSC Project.....	2-29
Table 2.2-2 Contributors to the CEUS SSC Project.....	2-30
Table 3.2-1 Summary of Earthquakes Added–USGS Earthquake Catalog by Time Period.....	3-44
Table 3.2-2 Summary of Earthquakes Added–USGS Earthquake Catalog by Source.....	3-45
Table 3.3-1 Conversion Relationships Used–Develop Uniform Moment Magnitudes E[M].....	3-46
Table 3.4-1 Comparison of CEUS SSC Catalog Declustering Results Obtained Using the EPRI (1988) Approach with the Gardner Knopoff (1974) Approach	3-47
Table 3.5-1 Probability of Detection and Equivalent Periods of Completeness for the CEUS for Magnitude Weighting Case A	3-48
Table 3.5-2 Probability of Detection and Equivalent Periods of Completeness for the CEUS for Magnitude Weighting Case B	3-51
Table 3.5-3 Probability of Detection and Equivalent Periods of Completeness for the CEUS for Magnitude Weighting Case E	3-54
Table 4.1.2-1 Sample table indicating particular types of data that can be considered in the identification and characterization of seismic sources (Table 2, ANSI/ANS-2.27- 2008).....	4-26
Table 4.1.2-2 Sample table identifying the types of data that can be considered for characterizing different types of seismic sources, and an evaluation of the relative usefulness or credibility of the various data types (Budnitz et al., 1997).....	4-27
Table 4.1.2-3 Table showing the “generic” (not source-specific) evaluation of data to address indicators of a unique seismic source. The table indicates the TI Team’s assessment of the types of data that can be used to address the indicators and their relative usefulness.	4-28
Table 4.1.2-4 Example of Data Evaluation Table for the Illinois Basin–Extended Basement Zone (IBEB)	4-34
Table 4.1.2-5 Example of Data Summary Table for the Extended Continental Crust– Atlantic Margin (ECC-AM) and Atlantic Highly Extended Crust (AHEx) Zones	4-35
Table 4.1.3-1 Criteria Used to Define the Seismotectonic Zones and Mmax Zones	4-37
Table 4.2.2-1 RLME Sources.....	4-38
Table 4.2.4-1 Seismotectonic Zones	4-39
Table 5.2.1-1 Mesozoic-and-Younger Extended Superdomains (MESE).....	5-60
Table 5.2.1-2 Older Extended and Non-Extended Superdomains (NMESE)	5-61
Table 5.2.1-3 Composite SCR Superdomains (COMP).....	5-62
Table 5.2.1-4 Results of Analyses of Updated SCR Superdomains	5-63

Table 5.2.1-5 Source Zones, $P(m^u > 8\frac{1}{4})$ Values, and Weights on Kijko (2004) K-S-B Estimates	5-64
Table 5.2.1-6 Mmax Distributions for the Two Example Seismic Sources.....	5-65
Table 5.3.2-1 Alternative Cases Considered for the Magnitude-Dependent Weights.....	5-65
Table 5.3.3-1 Miller and Rice (1983) Discrete 5-Point Approximation to a Continuous Probability Distribution and the Modified Form Used in This Study	5-65
Table 5.4-1 Assessment of Default Characteristics of Future Earthquakes in the CEUS.....	5-66
Table 5.4-2 Characteristics of Future Earthquakes for Individual Seismic Sources	5-68
Table 5.4-3 Estimates of D_{90} for Individual Seismic Source Zones.....	5-71
Table 6.1-1 Summary of Data Used to Assess RLME Recurrence Frequencies.....	6-80
Table 6.1.1-1 Charlevoix RLME Recurrence Frequency	6-83
Table 6.1.2-1 Summary of Interpreted Charleston Earthquake Ages and Sizes from “Contemporary Ages Only” Scenario	6-84
Table 6.1.2-2 Summary of Interpreted Charleston Earthquake Ages and Sizes from “All Ages” Scenario.....	6-84
Table 6.1.2-3 Charleston Liquefaction Feature Ages Used to Assess Ages of Prehistoric Earthquakes	6-85
Table 6.1.2-4 Charleston RLME Recurrence Frequency for Poisson Model	6-86
Table 6.1.2-5 Charleston RLME Recurrence Frequency for Renewal Model	6-87
Table 6.1.3-1 Range of Cheraw Fault Estimated Magnitudes (M).....	6-88
Table 6.1.3-2 Cheraw RLME In-Cluster Recurrence Frequency	6-89
Table 6.1.3-3 Cheraw RLME In-Cluster Slip Rates	6-89
Table 6.1.3-4 Cheraw RLME Out-of-Cluster Recurrence Frequency	6-90
Table 6.1.3-5 Cheraw RLME Out-of-Cluster Slip Rates	6-90
Table 6.1.4-1 Range of Estimated Meers Fault Earthquake Magnitudes (M).....	6-91
Table 6.1.4-2 Meers RLME In-Cluster Recurrence Frequency.....	6-91
Table 6.1.4-3 Meers RLME Out-of-Cluster Recurrence Frequency.....	6-91
Table 6.1.5-1 Preferred Ages for Paleoearthquakes in the New Madrid Region ¹	6-92
Table 6.1.5-2 Magnitude Comparisons for New Madrid 1811-1812 Earthquake Sequence	6-93
Table 6.1.5-3 Liquefaction Constraints on Age of AD 1450 NMFS RLME.....	6-94
Table 6.1.5-4 Liquefaction Constraints on Age of AD 900 NMFS RLME.....	6-95
Table 6.1.5-5 NMFS In-Cluster RLME Recurrence Frequency—Poisson Model	6-96
Table 6.1.5-6 NMFS In-Cluster RLME Recurrence Frequency—Renewal Model	6-96
Table 6.1.5-7 NMFS Out-of-Cluster RLME Recurrence Frequency—Poisson Model	6-96
Table 6.1.6-1 Range of ERM-S Estimated Magnitudes (M).....	6-97
Table 6.1.6-2 Range of ERM-N Estimated Magnitudes (M)	6-98
Table 6.1.6-3 ERM-S RLME Recurrence Frequency.....	6-98
Table 6.1.6-4 ERM-N RLME Recurrence Frequency	6-99
Table 6.1.7-1 Marianna RLME Recurrence Frequency	6-99

Table 6.1.8-1 Range of Commerce Fault Zone RLME Estimated Magnitudes (M).....	6-100
Table 6.1.8-2 Commerce Fault Zone RLME Recurrence Frequency.....	6-101
Table 6.1.9-1 Liquefaction Evidence for Prehistoric Earthquakes in the Southern Illinois Basin	6-102
Table 6.1.9-2 Wabash RLME Recurrence Frequency	6-109
Table 6.2-1 Alternative Mmax Zonation Models	6-109
Table 6.3.2-1 Maximum Magnitude Distributions for Mmax Distributed Seismicity Sources	6-110
Table 7.1-1 Data Summary and Data Evaluation Tables for Seismotectonic Zones in Appendices C and D	7-81
Table 7.4.2-1 Maximum Magnitude Distributions for Seismotectonic Distributed Seismicity Sources.....	7-82
Table 8.1-1 Description of Seven Test Sites.....	8-13
Table 8.2.1-1 Mean and Select Fractiles for Rock Hazard at Central Illinois: Digital Data for Figures 8.2-1a through 8.2-1c.....	8-14
Table 8.2.2-1 Mean and Select Fractiles for Rock Hazard at Chattanooga: Digital Data for Figures 8.2-2a through 8.2-2c.....	8-16
Table 8.2.3-1 Mean and Select Fractiles for Rock Hazard at Houston: Digital Data for Figures 8.2-3a through 8.2-3c.....	8-18
Table 8.2.4-1 Mean and Select Fractiles for Rock Hazard at Jackson: Digital Data for Figures 8.2-4a through 8.2-4c.....	8-20
Table 8.2.5-1 Mean and Select Fractiles for Rock Hazard at Manchester: Digital Data for Figures 8.2-5a through 8.2-5c.....	8-22
Table 8.2.6-1 Mean and Select Fractiles for Rock Hazard at Savannah: Digital Data for Figures 8.2-6a through 8.2-6c.....	8-24
Table 8.2.7-1 Mean and Select Fractiles for Rock Hazard at Topeka: Digital Data for Figures 8.2-7a through 8.2-7c.....	8-26
Table 9.4-1 Available Information for Determining the Precision of Mean Hazard	9-21
Table 9.4-2 Summary of an Example Logic Tree Representing Uncertainties for the Charleston Seismic Zone	9-21
Table 9.4-3 Basic Weights Given in EPRI (2004) for Ground Motion Equations	9-22
Table 9.4-4 Ground Motion Equations and Weights Used in USGS 2008 National Hazard Map for CEUS	9-23
Table 9.4-5 Minimum COV _{MH} Values Observed in Seismic Hazard	9-23
Table A-1 CEUS SSC GIS Database	A-7
Table B-1 Earthquake Catalog.....	B-6
Table B-2 Moment Magnitude Data	B-312
Table B-3 Approximate Moment Magnitude Data	B-324
Table C-5.4 Data Evaluation Future Earthquake Characteristics	C-3
Table C-6.1.1 Data Evaluation Charlevoix RLME	C-9
Table C-6.1.2 Data Evaluation Charleston RLME	C-14
Table C-6.1.3 Data Evaluation Cheraw Fault RLME	C-30

Table C-6.1.4 Data Evaluation Oklahoma Aulacogen RLME	C-36
Table C-6.1.5 Data Evaluation Reelfoot Rift–New Madrid Fault System RLMEs	C-42
Table C-6.1.6 Data Evaluation Reelfoot Rift–Eastern Margin Fault(s) RLMEs.....	C-51
Table C-6.1.7 Data Evaluation Reelfoot Rift–Marianna RLME	C-62
Table C-6.1.8 Data Evaluation Reelfoot Rift–Commerce Fault Zone RLME	C-67
Table C-6.1.9 Data Evaluation Wabash Valley RLME	C-75
Table C-7.3.1 Data Evaluation St. Lawrence Rift Zone	C-83
Table C-7.3.2 Data Evaluation Great Meteor Hotspot Zone	C-92
Table C-7.3.3 Data Evaluation Northern Appalachian Zone.....	C-99
Table C-7.3.4 Data Evaluation Paleozoic Extended Crust Zone	C-105
Table C-7.3.5 Data Evaluation Illinois Basin-Extended Basement Zone	C-112
Table C-7.3.6 Data Evaluation Reelfoot Rift Zone	C-124
Tables C-7.3.7/7.3.8 Data Evaluation Extended Continental Crust—Atlantic.....	C-131
Tables C-7.3.9/7.3.10 Data Evaluation Extended Continental Crust—Gulf Coast	C-138
Table C-7.3.12 Data Evaluation Midcontinent-Craton Zone	C-146
Table D-5.4 Data Summary Future Earthquake Characteristics.....	D-3
Table D-6.1.1 Data Summary Charlevoix RLME	D-10
Table D-6.1.2 Data Summary Charleston RLME	D-17
Table D-6.1.3 Data Summary Cheraw Fault RLME	D-35
Table D-6.1.4 Data Summary Oklahoma Aulacogen RLME	D-38
Table D-6.1.5 Data Summary Reelfoot Rift–New Madrid Seismic Zone (NMSZ) Region.....	D-44
Table D-6.1.9 Data Summary Wabash Valley RLME	D-92
Table D-7.3.1 Data Summary St. Lawrence Rift Zone (SLR)	D-121
Table D-7.3.2 Data Summary Great Meteor Hotspot Zone (GMH).....	D-141
Table D-7.3.3 Data Summary Northern Appalachian Zone (NAP)	D-151
Table D-7.3.4 Data Summary Paleozoic Extended Crust Zone.....	D-163
Table D-7.3.7 Data Summary Extended Continental Crust Zone—Atlantic Margin (ECC-AM).....	D-191
Table D-7.3.9 Data Summary Extended Continental Crust Zone—Gulf Coast (ECC-GC).....	D-225
Table D-7.3.12 Data Summary Midcontinent-Craton Zone (MidC)	D-240
Table E-1.2-1. Summary of Information on Liquefaction Features in Regional Data Sets.....	E-5
Table E-1.2-2 Summary of Type and Prevalence of Paleoliquefaction Features	E-7
Table E-2.1.3. Summary of Dating Techniques Used in Paleoliquefaction Studies.....	E-30
Table E-2.2. Uncertainties Related to Interpretation of Paleoearthquake Parameters	E-36
Table 1: Key Questions and Topics That Workshop 2 Presenters Were Asked to Address	F-35
Table H-3-1 Weighted Alternative Seismogenic Crustal Thickness Values for Mmax Zones	H-20
Table H-3-2 Aleatory Distributions for Characterization of Future Earthquake Ruptures for Mmax Zones	H-20

Table H-3-3 Maximum Magnitude Distributions for Mmax Distributed Seismicity Sources	H-20
Table H-4-1 Seismotectonic Source Zones	H-21
Table H-4-2 Weighted Alternative Seismogenic Crustal Thickness Values for Seismotectonic Zones	H-21
Table H-4-3 Aleatory Distributions for Characterization of Future Earthquake Ruptures for Seismotectonic Zones.....	H-22
Table H-4-4 Maximum Magnitude Distributions for Seismotectonic Distributed Seismicity Sources	H-24
Table H-5.1-1 Charlevoix RLME Magnitude Distribution	H-25
Table H-5.1-2 Annual Frequencies for Charlevoix RLME Events Data Set 1: 1870 and 1663	H-25
Table H-5.1-3 Annual Frequencies for Charlevoix RLME Events Data Set 2: 3 Earthquakes in 6–7 kyr BP.....	H-25
Table H-5.1-4 Annual Frequencies for Charlevoix RLME Events Data Set 3: 4 Earthquakes in 9.5–10.2 kyr BP.....	H-26
Table H-5.2-1 Charleston RLME Magnitude Distribution	H-26
Table H-5.2-2 Annual Frequencies for Charleston RLME Events Poisson Model, 2,000- Year Time Period Earthquakes 1886, A, B, and C.....	H-26
Table H-5.2-3 Annual Frequencies for Charleston RLME Events Poisson Model, 5,500- Year Time Period Earthquakes 1886, A, B, and C.....	H-27
Table H-5.2-4 Annual Frequencies for Charleston RLME Events Poisson Model, 5,500- Year Time Period Earthquakes 1886, A, B, C, and D	H-27
Table H-5.2-5 Annual Frequencies for Charleston RLME Events Poisson Model, 5,500- Year Time Period Earthquakes 1886, A, B, C, and E	H-27
Table H-5.2-6 Annual Frequencies for Charleston RLME Events Poisson Model, 5,500- Year Time Period Earthquakes 1886, A, B, C, D, and E.....	H-28
Table H-5.2-7 Annual Frequencies for Charleston RLME Events BPT Renewal Model, α = 0.3, 2,000-Year Time Period Earthquakes 1886, A, B, and C	H-28
Table H-5.2-8 Annual Frequencies for Charleston RLME Events BPT Renewal Model, α = 0.5, 2,000-Year Time Period Earthquakes 1886, A, B, and C	H-28
Table H-5.2-9 Annual Frequencies for Charleston RLME Events BPT Renewal Model, α = 0.7, 2,000-Year Time Period Earthquakes 1886, A, B, and C	H-29
Table H-5.2-10 Annual Frequencies for Charleston RLME Events BPT Renewal Model, α = 0.3, 5,500-Year Time Period Earthquakes 1886, A, B, and C	H-29
Table H-5.2-11 Annual Frequencies for Charleston RLME Events BPT Renewal Model, α = 0.5, 5,500-Year Time Period Earthquakes 1886, A, B, and C	H-29
Table H-5.2-12 Annual Frequencies for Charleston RLME Events BPT Renewal Model, α = 0.7, 5,500-Year Time Period Earthquakes 1886, A, B, and C	H-30
Table H-5.2-13 Annual Frequencies for Charleston RLME Events BPT Renewal Model, α = 0.3, 5,500-Year Time Period Earthquakes 1886, A, B, C, and D.....	H-30
Table H-5.2-14 Annual Frequencies for Charleston RLME Events BPT Renewal Model, α = 0.5, 5,500-Year Time Period Earthquakes 1886, A, B, C, and D.....	H-30

Table H-5.2-15 Annual Frequencies for Charleston RLME Events BPT Renewal Model, α = 0.7, 5,500-Year Time Period Earthquakes 1886, A, B, C, and D	H-31
Table H-5.2-16 Annual Frequencies for Charleston RLME Events BPT Renewal Model, α = 0.3, 5,500-Year Time Period Earthquakes 1886, A, B, C, and E	H-31
Table H-5.2-17 Annual Frequencies for Charleston RLME Events BPT Renewal Model, α = 0.5, 5,500-Year Time Period Earthquakes 1886, A, B, C, and E	H-31
Table H-5.2-18 Annual Frequencies for Charleston RLME Events BPT Renewal Model, α = 0.7, 5,500-Year Time Period Earthquakes 1886, A, B, C, and E	H-32
Table H-5.2-19 Annual Frequencies for Charleston RLME Events BPT Renewal Model, α = 0.3, 5,500-Year Time Period Earthquakes 1886, A, B, C, D, and E	H-32
Table H-5.2-20 Annual Frequencies for Charleston RLME Events BPT Renewal Model, α = 0.5, 5,500-Year Time Period Earthquakes 1886, A, B, C, D, and E	H-32
Table H-5.2-21 Annual Frequencies for Charleston RLME Events BPT Renewal Model, α = 0.7, 5,500-Year Time Period Earthquakes 1886, A, B, C, D, and E	H-33
Table H-5.3-1 Cheraw RLME Magnitude Distribution	H-33
Table H-5.3-2 Annual Frequencies for Cheraw RLME Events In-Cluster Case, Data Set: 2 Earthquakes in 20–25 kyr	H-33
Table H-5.3-3 Annual Frequencies for Cheraw RLME Events In-Cluster Case, Data Set: 3 Earthquakes in 20–25 kyr	H-34
Table H-5.3-4 Slip Rates for Cheraw Fault In-Cluster Case, Data Set: 3.2–4.1 m in 20–25 kyr	H-34
Table H-5.3-5 Annual Frequencies for Cheraw RLME Events Out-of-Cluster Case, Time Between Clusters	H-34
Table H-5.3-6 Slip Rates for Cheraw Fault Out-of-Cluster Case, Data Set: 7–8 m in 0.4–2.0 myr	H-35
Table H-5.4-1 Meers RLME Magnitude Distribution	H-35
Table H-5.4-2 Annual Frequencies for Meers RLME Events In-Cluster Case	H-35
Table H-5.4-3 Annual Frequencies for Meers RLME Events Out-of-Cluster Case	H-36
Table H-5.5-1 NMFS RLME Magnitude Distribution	H-36
Table H-5.5-2 Annual Frequencies for NMFS RLME Events In-Cluster Case, Poisson Model	H-36
Table H-5.5-3 Annual Frequencies for NMFS RLME Events In-Cluster Case, BPT Model, α = 0.3	H-37
Table H-5.5-4 Annual Frequencies for NMFS RLME Events In-Cluster Case, BPT Model, α = 0.5	H-37
Table H-5.5-5 Annual Frequencies for NMFS RLME Events In-Cluster Case, BPT Model, α = 0.7	H-37
Table H-5.5-6 Annual Frequencies for NMFS RLME Events Out-of-Cluster Case, Poisson Model	H-38
Table H-5.6-1 ERM-S RLME Magnitude Distribution	H-38
Table H-5.6-2 ERM-N RLME Magnitude Distribution	H-38
Table H-5.6-3 Annual Frequencies for ERM-S RLME Events Data Set: 2 Earthquakes in 17.7–21.7 kyr	H-39

Table H-5.6-4 Annual Frequencies for ERM-S RLME Events Data Set: 3 Earthquakes in 17.7–21.7 kyr	H-39
Table H-5.6-5 Annual Frequencies for ERM-S RLME Events Data Set: 4 Earthquakes in 17.7–21.7 kyr	H-39
Table H-5.6-6 Annual Frequencies for ERM-N RLME Events Data Set: 1 Earthquake in 12–35 kyr	H-40
Table H-5.6-7 Annual Frequencies for ERM-N RLME Events Data Set: 2 Earthquakes in 12–35 kyr	H-40
Table H-5.7-1 Marianna RLME Magnitude Distribution	H-40
Table H-5.7-2 Annual Frequencies for Marianna RLME Events Data Set: 3 Earthquakes in 9.6–10.2 kyr.....	H-41
Table H-5.7-3 Annual Frequencies for Marianna RLME Events Data Set: 4 Earthquakes in 9.6–10.2 kyr.....	H-41
Table H-5.8-1 Commerce RLME Magnitude Distribution.....	H-41
Table H-5.8-2 Annual Frequencies for Commerce RLME Events Data Set: 2 Earthquakes in 18.9–23.6 kyr	H-42
Table H-5.8-3 Annual Frequencies for Commerce RLME Events Data Set: 3 Earthquakes in 18.9–23.6 kyr	H-42
Table H-5.9-1 Wabash RLME Magnitude Distribution	H-42
Table H-5.9-2 Annual Frequencies for Wabash RLME Events Data Set: 2 Earthquakes in 11–13 kyr.....	H-43
PPRP Comment Response Table	(Appendix I)
Table K-1 SCR Earthquake Catalog	K-5
Table K-2 SCR Domains Updated from Johnston et al. (1994)	K-34

EXECUTIVE SUMMARY

The Central and Eastern United States Seismic Source Characterization for Nuclear Facilities (CEUS SSC) Project was conducted over the period from April 2008 to December 2011 to provide a regional seismic source model for use in probabilistic seismic hazard analyses (PSHAs) for nuclear facilities. The study replaces previous regional seismic source models conducted for this purpose, including the Electric Power Research Institute–Seismicity Owners Group (EPRI-SOG) model (EPRI, 1988, 1989) and the Lawrence Livermore National Laboratory model (Bernreuter et al., 1989). Unlike the previous studies, the CEUS SSC Project was sponsored by multiple stakeholders—namely, the EPRI Advanced Nuclear Technology Program, the Office of Nuclear Energy and the Office of the Chief of Nuclear Safety of the U.S. Department of Energy (DOE), and the Office of Nuclear Regulatory Research of the Nuclear Regulatory Commission (NRC). The study was conducted using Senior Seismic Hazard Analysis Committee (SSHAC) Study Level 3 methodology to provide high levels of confidence that the data, models, and methods of the larger technical community have been considered and the center, body, and range of technically defensible interpretations have been included.

The regional seismic source characterization (SSC) model defined by this study can be used for site-specific PSHAs, provided that appropriate site-specific assessments are conducted as required by current regulations and regulatory guidance for the nuclear facility of interest. This model has been designed to be compatible with current and anticipated ground-motion characterization (GMC) models. The current recommended ground-motion models for use at nuclear facilities are those developed by EPRI (2004, 2006a, 2006b). The ongoing Next Generation Attenuation–East (NGA-East) project being supported by the NRC, DOE, and EPRI will provide ground-motion models that are appropriate for use with the CEUS SSC model. The methodology for a SSHAC Level 3 project as applied to the CEUS SSC Project is explained in the SSHAC report (Budnitz et al., 1997), which was written to discuss the evolution of expert assessment methodologies conducted during the previous three decades for purposes of probabilistic risk analyses. The methodological guidance provided in the SSHAC report was intended to build on the lessons learned from those previous studies and, specifically, to arrive at processes that would make it possible to avoid the issues encountered by the previous studies (NRC, 2011).

The SSHAC assessment process, which differs only slightly for Level 3 and 4 studies, is a technical process accepted in the NRC’s seismic regulatory guidance (Regulatory Guide 1.208) for ensuring that uncertainties in data and scientific knowledge have been properly represented in seismic design ground motions consistent with the requirements of the seismic regulation 10 CFR Part 100.23 (“Geologic and Seismic Siting Criteria”). Therefore, the goal of the SSHAC assessment process is the proper and complete representation of knowledge and uncertainties in the SSC and GMC inputs to the PSHA (or similar hazard analysis). As discussed extensively in

the SSHAC report (Budnitz et al., 1997) and affirmed in NRC (2011), a SSHAC assessment process consists of two important sequential activities, *evaluation* and *integration*. For a Level 3 assessment, these activities are conducted by the Technical Integration (TI) Team under the leadership of the TI Lead. As described in NRC (2011),

The fundamental goal of a SSHAC process is to carry out properly and document completely the activities of evaluation and integration, defined as:

Evaluation: The consideration of the complete set of data, models, and methods proposed by the larger technical community that are relevant to the hazard analysis.

Integration: Representing the center, body, and range of technically defensible interpretations in light of the evaluation process (i.e., informed by the assessment of existing data, models, and methods).

Each of the assessment and model-building activities of the CEUS SSC Project is associated with the evaluation and integration steps in a SSHAC Level 3 process. Consistent with the requirements of a SSHAC process, the specific roles and responsibilities of all project participants were defined in the Project Plan, and adherence to those roles was the responsibility of the TI Lead and the Project Manager. The technical assessments are made by the TI Team, who carry the principal responsibility of evaluation and integration, under the technical leadership of the TI Lead. The Database Manager and other technical support individuals assist in the development of work products. Resource and proponent experts participate by presenting their data, models, and interpretations at workshops and through technical interchange with the TI Team throughout the project. The Participatory Peer Review Panel (PPRP) is responsible for a continuous review of both the SSHAC process being followed and the technical assessments being made. The project management structure is headed by the Project Manager, who serves as the liason with the sponsors and the PPRP and manages the activities of all participants. The SSHAC Level 3 assessment process and implementation is discussed in depth in Chapter 2 of this report.

Each of the methodology steps in the SSHAC guidelines (Budnitz, 1997) was addressed adequately during the CEUS SSC Project. Furthermore, the project developed a number of enhancements to the process steps for conducting a SSHAC Study Level 3 project. For example, the SSHAC guidelines call for process steps that include developing a preliminary assessment model, calculating hazard using that model in order to identify the key issues, and finalizing the model in light of the feedback provided from the hazard calculations and sensitivity analyses. Because of the regional nature of the project and the multitude of assessments required, four rounds of model-building and three rounds of feedback were conducted. These activities ensured that all significant issues and uncertainties were identified and that the appropriate effort was devoted to the issues of most significance to the hazard results. A comparison of the activities conducted during the CEUS SSC Project with those recommended in the SSHAC guidelines themselves (Section 2.6) led to the conclusion that the current standards of practice have been met for a SSHAC Study Level 3 process—both those that are documented in the SSHAC report and those that resulted from precedents set by projects conducted since the SSHAC report was issued.

The catalog of past earthquakes that have occurred in a region is an important source of information for the quantification of future seismic hazards. This is particularly true in stable continental regions (SCRs) such as the CEUS where the causative mechanisms and structures for the occurrence of damaging earthquakes are generally poorly understood, and the rates of crustal deformation are low such that surface and near-surface indications of stresses in the crust and the buildup and release of crustal strains are difficult to quantify. Because the earthquake catalog is used in the characterization of the occurrence of future earthquakes in the CEUS, developing an updated earthquake catalog for the study region was an important focus of the CEUS SSC Project. The specific goals for earthquake catalog development and methods used to attain those goals are given in Chapter 3.

The earthquake catalog development consists of four main steps: catalog compilation, assessment of a uniform size measure to apply to each earthquake, identification of dependent earthquakes (catalog declustering), and assessment of the completeness of the catalog as a function of location, time, and earthquake size. An important part of the catalog development process was review by seismologists with extensive knowledge and experience in catalog compilation. The result is an earthquake catalog covering the entire study region for the period from 1568 through the end of 2008. Earthquake size is defined in terms of the moment magnitude scale (Hanks and Kanamori, 1979), consistent with the magnitude scale used in modern ground-motion prediction equations (GMPEs) for CEUS earthquakes. A significant contribution of the CEUS SSC Project is the work conducted to develop an updated and consistent set of conversion relationships between various earthquake size measures (instrumental magnitudes and intensity) and moment magnitude.

The conceptual SSC framework described in Chapter 4 was developed early in the CEUS SSC Project in order to provide a consistent approach and philosophy to SSC by the TI Team. This framework provides the basic underpinnings of the SSC model developed for the project, and it led to the basic structure and elements of the master logic tree developed for the SSC model. In considering the purpose of the CEUS SSC Project, the TI Team identified three attributes that are needed for a conceptual SSC framework:

1. A systematic, documented approach to treating alternatives using logic trees, including alternative conceptual models for future spatial distributions of seismicity (e.g., stationarity); alternative methods for expressing the future temporal distribution of seismicity (e.g., renewal models, Poisson models); and alternative data sets for characterizing seismic sources (e.g., paleoseismic data, historical seismicity data).
2. A systematic approach to identifying applicable data for the source characterization, evaluating the usefulness of the data, and documenting the consideration given to the data by the TI Team.
3. A methodology for identifying seismic sources based on defensible criteria for defining a seismic source, incorporating the lessons learned in SSC over the past two decades, and identifying the range of approaches and models that can be shown to be significant to hazard.

Each of these needs was addressed by the methodology used in the project. For example, the need for a systematic approach to identifying and evaluating the data and information that underlie the source characterization assessments was met by the development of Data Summary

and Data Evaluation tables. These tables were developed for each seismic source to document the information available at the time of the CEUS SSC assessments (the Data Summary tables) and the way those data were used in the characterization process (the Data Evaluation tables). Given the evolution of approaches to identifying seismic sources, it is appropriate to provide a set of criteria and the logic for their application in the CEUS SSC Project. In the project, unique seismic sources are defined to account for distinct differences in the following criteria:

- Earthquake recurrence rate
- Maximum earthquake magnitude (Mmax)
- Expected future earthquake characteristics (e.g., style of faulting, rupture orientation, depth distribution)
- Probability of activity of tectonic feature(s)

Rather than treat these criteria as operating simultaneously or without priority, the CEUS SSC methodology works through them sequentially. Further, because each criterion adds complexity to the seismic source model, it is applied only if its application would lead to hazard-significant changes in the model. In this way, the model becomes only as complex as required by the available data and information.

The CEUS SSC master logic tree is tied to the conceptual SSC framework that establishes the context for the entire seismic source model. The master logic tree depicts the alternative interpretations and conceptual models that represent the range of defensible interpretations, and the relative weights assessed for the alternatives. By laying out the alternatives initially, the subsequent detailed source evaluations were conducted within a framework that ensures consistency across the sources. Important elements of the master logic tree are as follows:

- Representation of the sources defined based on paleoseismic evidence for the occurrence of repeated large-magnitude earthquakes (RLMEs, defined as two or more earthquakes with $M \geq 6.5$).
- Alternatives to the spatial distribution of earthquakes based on differences in maximum magnitudes (Mmax zones approach).
- Representation of uncertainty in spatial stationarity of observed seismicity based on smoothing of recurrence parameters.
- Representation of possible differences in future earthquake characteristics (e.g., style, seismogenic thickness, and orientation of ruptures), which lead to definition of seismotectonic zones in the logic tree (seismotectonic zones approach).

The methodologies used by the project to make the SSC assessments are discussed in Chapter 5. The heart of any SSC model for PSHA is a description of the future spatial and temporal distribution of earthquakes. Continued analysis of the historical seismicity record and network monitoring by regional and local seismic networks has led to acceptance within the community that the general spatial patterns of observed small- to moderate-magnitude earthquakes provide predictive information about the spatial distribution of future large-magnitude earthquakes. The analyses leading to this conclusion have focused on whether the observed patterns of earthquakes

have varied through time; therefore, in effect, this is an assessment of uncertainty in whether small- to moderate-magnitude earthquakes have been relatively stationary through time. However, the available data on larger-magnitude earthquakes and their relationship to the spatial distribution of smaller earthquakes based on the observed record are quite limited. These data are not sufficient to allow confidence in the predictions generated by empirical spatial models. For this reason, geologic and geophysical data are needed to specify the locations of future earthquakes in addition to the observed patterns of seismicity.

Detailed studies in the vicinity of large historical and instrumental earthquakes, and liquefaction phenomena associated with them, coupled with field and laboratory studies of geotechnical properties, are leading to a stronger technical basis for (1) placing limits on the locations of paleoearthquakes interpreted by the distribution of liquefaction phenomena and (2) defining their magnitudes. In some cases, the paleoseismic evidence for RLMEs is compelling, and the TI Team has included the RLME source in the SSC model. The locations of RLME sources notwithstanding, the spatial distribution of distributed seismicity sources has advanced in PSHA largely because of the assumption of spatial stationarity, and the SSC and hazard community uses approaches to “smooth” observed seismicity to provide a map that expresses the future spatial pattern of recurrence rates. The CEUS SSC model is based largely on the assumption, typical in PSHA studies, that spatial stationarity of seismicity is expected to persist for a period of approximately 50 years.

Estimating M_{\max} in SCRs such as the CEUS is highly uncertain despite considerable interest and effort by the scientific community over the past few decades. M_{\max} is defined as the upper truncation point of the earthquake recurrence curve for individual seismic sources, and the typically broad distribution of M_{\max} for any given source reflects considerable epistemic uncertainty. Because the maximum magnitude for any given seismic source in the CEUS occurs rarely relative to the period of observation, the use of the historical seismicity record provides important but limited constraints on the magnitude of the maximum event. Because of the independent constraints on earthquake size, those limited constraints are used to estimate the magnitudes of RLME. For distributed seismicity source zones, two approaches are used to assess M_{\max} : the Bayesian approach and the Kijko approach. In the Bayesian procedure (Johnston et al., 1994), the prior distribution is based on the magnitudes of earthquakes that occurred worldwide within tectonically analogous regions. As part of the CEUS SSC Project, the TI Team pursued the refinement and application of the Bayesian M_{\max} approach because it provides a quantitative and repeatable process for assessing M_{\max} .

The TI Team also explored alternative approaches for the assessment of M_{\max} that provide quantitative and repeatable results, and the team identified the approach developed by Kijko (2004) as a viable alternative. While the Kijko approach requires fewer assumptions than the Bayesian approach in that it uses only the observed earthquake statistics for the source, this is offset by the need for a relatively larger data sample in order to get meaningful results. Both approaches have the positive attribute that they are repeatable given the same data and they can be readily updated given new information. The relative weighting of the two approaches for inclusion in the logic tree is source-specific, a function of the numbers of earthquakes that are present within the source upon which to base the M_{\max} assessment: sources with fewer earthquakes are assessed to have little or no weight for the Kijko approach, while those with

larger numbers of events are assessed higher weight for the Kijko approach. In all cases, because of the stability of the Bayesian approach and the preference for “analogue” approaches within the larger technical community, the Bayesian approach is assessed higher weight than the Kijko approach for all sources.

A major effort was devoted to updating the global set of SCR earthquakes and to assessing statistically significant attributes of those earthquakes following the approach given in Johnston et al. (1994). In doing so, it was found that the only significant attribute defining the prior distribution is the presence or absence of Mesozoic-or-younger extension. The uncertainty in this assessment is reflected in the use of two alternative priors: one that takes into account the presence or absence of crustal domains having this attribute, and another that combines the entire CEUS region as a single SCR crustal domain with a single prior distribution. The use of the Bayesian—and Kijko—approach requires a definition of the largest observed magnitude within each source, and this assessment, along with the associated uncertainty, was incorporated into the Mmax distributions for each seismic source. Consideration of global analogues led to the assessment of an upper truncation to all Mmax distributions at $8\frac{1}{4}$ and a lower truncation at $5\frac{1}{2}$. The broad distributions of Mmax for the various seismic source zones reflect the current epistemic uncertainty in the largest earthquake magnitude within each seismic source.

The CEUS SSC model is based to a large extent on an assessment that spatial stationarity of seismicity will persist for time periods of interest for PSHA (approximately the next 50 years). Stationarity in this sense does not mean that future locations and magnitudes of earthquakes will occur exactly where they have occurred in the historical and instrumental record. Rather, the degree of spatial stationarity varies as a function of the type of data available to define the seismic source. RLME sources are based largely on paleoseismic evidence for repeated large-magnitude ($M \geq 6.5$) earthquakes that occur in approximately the same location over periods of a few thousand years. On the other hand, patterns of seismicity away from the RLME sources within the Mmax and seismotectonic zones are defined from generally small- to moderate-magnitude earthquakes that have occurred during a relatively short (i.e., relative to the repeat times of large events) historical and instrumental record. Thus, the locations of future events are not as tightly constrained by the locations of past events as for RLME sources. The spatial smoothing operation is based on calculations of earthquake recurrence within one-quarter-degree or half-degree cells, with allowance for “communication” between the cells. Both *a*- and *b*-values are allowed to vary, but the degree of variation has been optimized such that *b*-values vary little across the study region.

The approach used to smooth recurrence parameters is a refinement of the penalized-likelihood approach used in EPRI-SOG (EPRI, 1988), but it is designed to include a number of elements that make the formulation more robust, realistic, and flexible. These elements include the reformulation in terms of magnitude bins, the introduction of magnitude-dependent weights, catalog incompleteness, the effect of Mmax, spatial variation of parameters within the source zone, and the prior distributions of *b*. A key assessment made by the TI Team was the weight assigned to various magnitude bins in the assessment of smoothing parameters (Cases A, B, and E). This assessment represents the uncertainty in the interpretation that smaller magnitudes define the future locations and variation in recurrence parameters. Appropriately, the penalized-likelihood approach results in higher spatial variation (less smoothing) when the low-magnitude

bins are included with high weight, and much less variation (higher smoothing) in the case where the lower-magnitude bins are given low or zero weight. The variation resulting from the final set of weights reflects the TI Team's assessment of the epistemic uncertainty in the spatial variation of recurrence parameters throughout the SSC model.

The earthquake recurrence models for the RLME sources are somewhat simpler than those for distributed seismicity sources because the magnitude range for individual RLMEs is relatively narrow and their spatial distribution is limited geographically such that spatial variability is not a concern. This limits the problem to one of estimating the occurrence rate in time of a point process. The data that are used to assess the occurrence rates are derived primarily from paleoseismic studies and consist of two types: data that provide estimated ages of the paleoearthquakes such that the times between earthquakes can be estimated, and data that provide an estimate of the number of earthquakes that have occurred after the age of a particular stratigraphic horizon. These data are used to derive estimates of the RLME occurrence rates and their uncertainty.

The estimation of the RLME occurrence rates is dependent on the probability model assumed for the temporal occurrence of these earthquakes. The standard model applied for most RLME sources in this study is the Poisson model, in which the probability of occurrence of an RLME in a specified time period is completely characterized by a single parameter, λ , the rate of RLME occurrence. The Poisson process is “memoryless”—that is, the probability of occurrence in the next time interval is independent of when the most recent earthquake occurred, and the time between earthquakes is exponentially distributed with a standard deviation equal to the mean time between earthquakes. For two RLME sources (Reelfoot Rift–New Madrid fault system and the Charleston source), the data are sufficient to suggest that the occurrence of RLMEs is more periodic in nature (the standard deviation is less than the mean time between earthquakes). For these RLME sources a simple renewal model can also be used to assess the probability of earthquake occurrence. In making an estimate of the probability of occurrence in the future, this model takes into account the time that has elapsed since the most recent RLME occurrence.

The CEUS SSC model has been developed for use in future PSHAs. To make this future use possible, the SSC model must be combined with a GMC model. At present, the GMPEs in use for SCRs such as the CEUS include limited information regarding the characteristics of future earthquakes. In anticipation of the possible future development of GMPEs for the CEUS that will make it possible to incorporate similar types of information, a number of characteristics of future earthquakes in the CEUS are assessed. In addition to characteristics that might be important for ground motion assessments, there are also assessed characteristics that are potentially important to the modeling conducted for hazard analysis. Future earthquake characteristics assessed include the tectonic stress regime, sense of slip/style of faulting, strike and dip of ruptures, seismogenic crustal thickness, fault rupture area versus magnitude relationship, rupture length-to-width aspect ratio, and relationship of ruptures to source boundaries.

Chapters 6 and 7 include discussions of the seismic sources that are defined by the Mmax zones and the seismotectonic zones branches of the master logic tree. Because of convincing evidence for their existence, both approaches include RLME sources. The rarity of repeated earthquakes relative to the period of historical observation means that evidence for repeated events comes

largely from the paleoseismic record. By identifying the RLMEs and including them in the SSC model, there is no implication that the set of RLMEs included is in fact the total set of RLMEs that might exist throughout the study region. This is because the presently available studies that locate and characterize the RLMEs have been concentrated in certain locations and are not systematic across the entire study region. Therefore, the evidence for the existence of the RLMEs is included in the model where it exists, but the remaining parts of the study region are also assessed to have significant earthquake potential, which is evidenced by the inclusion of moderate-to-large magnitudes in the Mmax distributions for every Mmax zone or seismotectonic zone.

In Chapter 6, each RLME source is described in detail by the following factors: (1) evidence for temporal clustering, (2) geometry and style of faulting, (3) RLME magnitude, and (4) RLME recurrence. The descriptions document how the data have been evaluated and assessed to arrive at the various elements of the final SSC model, including all expressions of uncertainty. The Data Summary and Data Evaluation tables (Appendices C and D) complement the discussions in the text, documenting all the data that were considered in the course of data evaluation and integration process for each particular seismic source.

Alternative models for the distributed seismicity zones that serve as background zones to the RLME sources are either Mmax zones or seismotectonic zones. The Mmax zones are described in Chapter 6 and are defined according to constraints on the prior distributions for the Bayesian approach to estimating Mmax. The seismotectonic zones are described in Chapter 7 and are identified based on potential differences in Mmax as well as future earthquake characteristics. Each seismotectonic zone in the CEUS SSC model is described according to the following attributes: (1) background information from various data sets; (2) bases for defining the seismotectonic zone; (3) basis for the source geometry; (4) basis for the zone Mmax (e.g., largest observed earthquake); and (5) future earthquake characteristics. Uncertainties in the seismotectonic zone characteristics are described and are represented in the logic trees developed for each source.

For purposes of demonstrating the CEUS SSC model, seismic hazard calculations were conducted at seven demonstration sites throughout the study region, as described in Chapter 8. The site locations were selected to span a range of seismic source types and levels of seismicity. The results from the seismic hazard calculations are intended for scientific use to demonstrate the model, and they should not be used for engineering design. Mean hazard results are given for a range of spectral frequencies (PGA, 10 Hz, and 1 Hz) and for a range of site conditions. All calculations were made using the EPRI (2004, 2006) ground-motion models such that results could be compared to understand the SSC effects alone. Sensitivity analyses were conducted to provide insight into the dominant seismic sources and the important characteristics of the dominant seismic source at each site. The calculated mean hazard results are compared with the results using the SSC model from the 2008 U.S. Geological Survey national seismic hazard maps and the SSC model from the Combined Operating License applications for new nuclear power reactors. The hazard results using the CEUS SSC model given in Chapter 8 are reasonable and readily understood relative to the results from other studies, and sensitivities of the calculated hazard results can be readily explained by different aspects of the new model. The TI Team concludes that the SSC model provides reasonable and explainable calculated seismic hazard

results, and the most important aspects of the SSC model to the calculated hazard (e.g., recurrence rates of RLME sources, recurrence parameters for distributed seismicity sources, M_{max}) and their uncertainties have all been appropriately addressed.

Presumably, the GMC model input to the PSHA calculations will be replaced in the future by the results of the ongoing NGA-East project. The calculated hazard at the demonstration sites in Chapter 8 comes from the regional CEUS SSC model and does not include any local refinements that might be necessary to account for local seismic sources. Depending on the regulatory guidance that is applicable for the facility of interest, additional site-specific studies may be required to provide local refinements to the model.

To assist future users of the CEUS SSC model, Chapter 9 presents a discussion on the use of the model for PSHA. The basic elements of the model necessary for hazard calculations are given in the Hazard Input Document (HID). This document provides all necessary parameter values and probability distributions for use in a modern PSHA computer code. The HID does not, however, provide any justification for the values, since that information is given in the text of this report.

Chapter 9 also describes several simplifications to seismic sources that can be made to increase efficiency in seismic hazard calculations. These simplifications are recommended on the basis of sensitivity studies of alternative hazard curves that represent a range of assumptions on a parameter's value. Sensitivities are presented using the test sites in this study. For applications of the seismic sources from this study, similar sensitivity studies should be conducted for the particular site of interest to confirm these results and to identify additional simplifications that might be appropriate. For the seismic sources presented, only those parameters that can be simplified are discussed and presented graphically. The sensitivity studies consisted of determining the sensitivity of hazard to logic tree branches for each node of the logic tree describing that source. The purpose was to determine which nodes of the logic tree could be collapsed to a single branch in order to achieve more efficient hazard calculations without compromising the accuracy of overall hazard results.

Finally, this report provides a discussion of the level of precision that is associated with seismic hazard estimates in the CEUS. This discussion addresses how seismic hazard estimates might change if the analysis were repeated by independent experts having access to the same basic information (geology, tectonics, seismicity, ground-motion equations, site characterization). It also addresses how to determine whether the difference in hazard would be significant if this basic information were to change and that change resulted in a difference in the assessed seismic hazard. This analysis was performed knowing that future data and models will continue to be developed and that a mechanism for evaluating the significance of that information is needed. Based on the precision model evaluated, if an alternative assumption or parameter is used in a seismic hazard study, and it potentially changes the calculated hazard (annual frequency of exceedence) by less than 25 percent for ground motions with hazards in the range 10^{-4} to 10^{-6} , that potential change is within the level of precision at which one can calculate seismic hazard. It should be noted, however, that a certain level of precision does not relieve users from performing site-specific studies to identify potential capable seismic sources within the site region and vicinity as well as to identify newer models and data. Also, this level of precision does not relieve users from fixing any errors that are discovered in the CEUS SSC model as it is

implemented for siting critical facilities. In addition, NRC has not defined a set value for requiring or not requiring siting applicants to revise or update PSHAs.

Included in the report are appendices that summarize key data sets and analyses: the earthquake catalog, the Data Summary and Data Evaluation tables, the paleoliquefaction database, the HID, and documentation important to the SSHAC process. These data and analyses will assist future users of the CEUS SSC model in the implementation of the model for purposes of PSHA. The entire report and database will be provided on a website after the Final Project Report is issued.

The TI Team, Project Manager, and Sponsors determined the approach for quality assurance on the CEUS SSC Project in 2008, taking into account the SSHAC assessment process and national standards. The approach was documented in the CEUS SSC Project Plan dated June 2008 and discussed in more detail in the CEUS SSC Report (Appendix L). Beyond the assurance of quality arising from the external scientific review process, it is the collective, informed judgment of the TI Team (via the process of evaluation and integration) and the concurrence of the PPRP (via the participatory peer review process), as well as adherence to the national standard referred to in Appendix L, that ultimately lead to the assurance of quality in the process followed and in the products that resulted from the SSHAC hazard assessment framework.

October 24, 2011

Cliff Munson
Senior Technical Advisor
Office of New Reactors
U.S. Nuclear Regulatory Commission
Washington, DC 20555

Robert Roche
Project Manager
Office of Nuclear Regulatory Research
U.S. Nuclear Regulatory Commission
Washington, DC 20555

Richard H. Lagdon, Jr.
Chief of Nuclear Safety
Office of the Under Secretary for Nuclear
Security, S-5
U.S. Department of Energy
1000 Independence Avenue SW
Washington, DC 20585

Thomas P. Miller
Senior Technical Advisor
Office of Nuclear Energy, NE-72/GTN
U.S. Department of Energy
1000 Independence Avenue SW
Washington, DC 20585

Jeffrey F. Hamel
Advanced Nuclear Technology Program
Manager
Electric Power Research Institute
3420 Hillview Avenue
Palo Alto, CA 94304

Gentlemen:

Reference: *Central and Eastern United States Seismic Source Characterization for Nuclear Facilities Project: Participatory Peer Review Panel Final Report*

Introduction

This letter constitutes the final report of the PPRP¹ (“the Panel”) for the *Central and Eastern United States Seismic Source Characterization for Nuclear Facilities Project* (the “CEUS SSC Project” or “the Project”). The eight Panel members (Jon P. Ake, Walter J. Arabasz, William J. Hinze, Annie M. Kammerer, Jeffrey K. Kimball, Donald P. Moore, Mark D. Petersen, J. Carl Stepp) participated in the Project in a manner fully consistent with the SSHAC Guidance.² The Panel was actively engaged in all phases and activities of the Project’s implementation, including final development of the Project Plan and planning of the evaluation and integration activities, which are the core of the SSHAC assessment process.

¹ Participatory Peer Review Panel

² Budnitz, R. J., G. Apostolakis, D. M. Boore, L. S. Cluff, K. L. Coppersmith, C. A. Cornell, and P. A. Morris, 1997. *Recommendations for Probabilistic Seismic Hazard Analysis: Guidance on Uncertainty and the Use of Experts* (known as the “Senior Seismic Hazard Analysis Committee Report,” or the “SSHAC Guidance”). NUREG/CR-6372, U. S. Nuclear Regulatory Commission. TIC; 235076. Washington, DC.

The Panel's involvement, described more fully later in this letter, also included review of analyses performed by the Project to support the evaluation and integration processes, review of interim evaluation and integration products, and review of the interim draft project report and the final project report. Additionally, panel members participated in specific analyses as resource experts, and panel members were observers in or participated as resource experts in eight of the eleven Technical Integrator Team (TI Team) working meetings held to implement the integration phase of the assessment process. We want to express our appreciation for the opportunity to participate in the CEUS SSC Project in this way.

In the remainder of this letter we provide our observations and conclusions on key elements of the project implementation process, and we summarize our reviews of the draft and final project reports. As we explain in our comments, assurance that the center, body, and range of the technically-defensible interpretations ("CBR of the TDI")³ have been properly represented in the CEUS SSC Model fundamentally comes from implementing the structure and rigor of the SSHAC Guidance itself. We are aware that the SSHAC Guidance is accepted by the Nuclear Regulatory Commission and the Department of Energy for developing seismic hazard models that provide reasonable assurance, consistent with the seismic safety decision-making practices of these agencies, of compliance with their seismic safety policies and regulatory requirements. For these reasons, we describe aspects of the SSHAC Guidance to provide context for our observations and conclusions.

Project Plan: Conformity to the SSHAC Assessment Process

The SSHAC Guidance recognizes that observed data, available methods, models, and interpretations all contain uncertainties. These uncertainties lead to alternative scientific analyses and interpretations. In other words, experts in the broad technical community do not hold a single interpretation. Accepting this scientific situation, the SSHAC assessment process is designed to engage the scientific community in an orderly assessment of relevant data, methods, models, and interpretations that constitute current scientific knowledge as the basis for development of a seismic hazard model that represents the CBR of the TDI.

The assessment process is carried out by means of two main activities: *evaluation* and *integration*.⁴ In implementation, the evaluation activities are structured to inform the integration activities. The evaluations are carried out by means of workshops in which the TI Team engages proponents of alternative interpretations that represent the range of relevant current community knowledge. Resource experts in the various relevant data sets are also engaged. The workshops have the dual purposes of, first, evaluating the degree to which alternative interpretations are supported by observed data and, second, defining uncertainties in the degree to which the interpretations are defensible, given the observed data. Integration is carried out by individual evaluator experts or evaluator expert teams (Level 4 process) or by a Technical Integrator (TI) Team (Level 3 process) who, informed by the evaluation activities, characterize the range of

³ See Section 2.1 in the CEUS SSC Final Report for discussion of concepts relating to the center, body, and range of the "technically-defensible interpretations" vs. the center, body, and range of the "informed technical community."

⁴ For an excellent discussion of this two-stage process, see *Practical Implementation Guidelines for SSHAC Level 3 and 4 Hazard Studies*, USNRC NUREG-XXXX, Draft for Review, Office of Nuclear Regulatory Research, May 2011.

defensible alternative interpretations in an integrated hazard model and assess the scientific uncertainty distribution. Based on our review of the Project Plan and our subsequent discussions with the Project Team, we concurred that the Plan conformed with the SSHAC Guidance, incorporating lessons learned from fourteen years experience using the Guidance, and that the planned implementation was structured to properly carry out the SSHAC assessment process for development of the CEUS SSC Model.

SSHAC Level 3 Assessment Process

The SSHAC Guidance describes implementation processes for four levels of assessment depending on the scientific complexity of the assessment and the intended use of the assessed hazard model. For an assessment such as the regional SSC model for the Central and Eastern United States, which will be used at many sites for making safety and licensing decisions for nuclear facilities, the SSHAC Guidance recommends using an assessment Level 3 or Level 4.

There are process differences between a Level 3 and Level 4 implementation, but the objective is the same: to obtain from multiple proponent experts information that supports an informed assessment of the range of existent relevant interpretations and associated uncertainties that together represent current community knowledge and to perform an informed assessment of the CBR of the TDI. We understand that within the SSHAC assessment process “technically defensible” means that observed data are sufficient to support evaluation of the interpretation and the corresponding uncertainty.

In a Level 4 assessment process a TI Team facilitates the assessment, identifying and engaging proponent and resource experts, performing supporting analyses, and conducting knowledge evaluation workshops and assessment integration working meetings. Multiple experts or teams of experts perform as evaluators of the range of existent interpretations and as integrators of the hazard model. The individual evaluator experts or evaluator expert teams take ownership of their individual or team assessments. In a Level 3 assessment all of these activities are consolidated under a single TI Team consisting of a TI Lead, multiple evaluator experts representing the scope of required scientific expertise, and experienced data and hazard analysts.

As we noted earlier in this report, assurance that the CBR of the TDI is properly represented in a hazard model comes from rigorously implementing the SSHAC assessment process itself. We note that an important lesson learned from multiple implementations of the SSHAC Guidance over the past fourteen years is that the Level 3 and Level 4 assessment processes provide comparably high assurance that the relevant scientific knowledge and the community uncertainty distribution are properly assessed and represented in the hazard model. The Level 3 assessment is significantly more integrated and cohesive and is more efficient to implement. These considerations led us to endorse use of the Level 3 assessment for implementation of the CEUS SSC Project in our Workshop No. 1 review letter. During the course of the Project we observed that the higher level of cohesiveness inherent in the Level 3 assessment process leads to significantly improved communication, facilitating the experts’ performance of their technical work.

Overall Project Organization

A complex project with multiple sponsors such as the CEUS SSC Project cannot be successful unless it is well organized and energetically managed so that the various participants understand the interconnectedness of their activities and perform their technical work as a cohesive group. In this regard the adopted project management structure allowed the Project Manager to provide integrated overall project leadership, manage the database development activities, and effectively maintain communication with the PPRP and project sponsors while allowing TI Team lead to concentrate on the structural and technical activities of the assessment as the Project unfolded. We conclude that the project organization was effective overall and particularly so with regard to facilitating the TI Team's implementation of the assessment process.

Implementing the SSHAC Level 3 Assessment Process

Irrespective of the level of implementation, evaluation and integration are the main activities of a SSHAC assessment. The evaluation activities aim to identify and evaluate all relevant available data, models, methods, and scientific interpretations as well as uncertainties associated with each of them. The integration activities, informed by the evaluations, aim to represent the CBR of the TDI in a fully integrated SSC model.

Evaluation

Consistent with the SSHAC Guidance the evaluation phase of the CEUS SSC project accomplished a comprehensive evaluation of the data, models, methods, and scientific interpretations existent in the larger technical community that are relevant to the SSC model. In significant part the process was carried out in three structured workshops, each focusing on accomplishing a specific step in the evaluation process.

The first workshop (WS-1) focused on evaluations of relevant geological, geophysical, and seismological datasets (including data quality and uncertainties) and on identification of hazard-significant data and hazard-significant SSC assessment issues. It became clear that a number of issues relating to the earthquake catalog, the paleoliquefaction data set, the potential-field geophysical data, updating procedures for assessing maximum earthquake magnitude, and development of procedures for assessing earthquake recurrence would require focused analyses. These analyses were appropriately carried out within the TI Team working interactively with appropriate resource experts recognized by the larger scientific and technical community.

WS-2 focused on evaluations of the range of alternative scientific interpretations, methods, and models within the larger scientific community and on corresponding uncertainties. WS-3 focused on evaluations of hazard feedback derived at seven representative test locations using a preliminary CEUS SSC model. Specifically, the workshop focused on the identification of the key issues of most significance to completing the SSC model assessment.

Experience has shown that evaluations to gain understanding of the quality of various data sets and uncertainties associated with them are essential for fully informing an SSC assessment. We observed that in WS-1 resource experts for the various data sets did a high-quality job of describing the data sets and giving their perspective about the data quality and associated uncertainties. We conclude that the understanding of data quality and uncertainties gained in WS-1 together with continued interactions between the TI Team and data resource experts

significantly informed the TI Team's evaluations. The TI Team's evaluations of the data quality and uncertainties are well documented in the innovative "Data Summary Tables" and "Data Evaluation Tables" included in the Project Report. Importantly, the TI Team continued to effectively engage data resource experts in productive analyses of potential-field geophysical data, the earthquake catalog, development of the paleoearthquake data set (including an integrated assessment of the paleoliquefaction data in order to extend the earthquake catalog), the development of methods for assessing maximum earthquakes, and the development of earthquake recurrence analyses. All of these focused analyses strongly informed the assessment process. Moreover, documentation of the analyses resulted in stand-alone products of the Project that will serve future users of the CEUS SSC Model.

The compilation and evaluation of potentially relevant methods, models, and alternative scientific interpretations representing the community knowledge and corresponding uncertainties must be considered the core process activity of any SSHAC assessment. This step was largely carried out in WS-2. Success in defining the community knowledge depends on fully engaging proponent experts representing the range of methods, models, and interpretations existent at the time. Full engagement means that the proponent experts completely and clearly describe their interpretations and the data that support them and provide their individual evaluations of corresponding uncertainties. We observed that the actions taken by the Project and TI Team to explain the workshop goals and to guide participants toward meeting those goals was very productive. We conclude that the workshop was highly successful in meeting the stated goals and that it fully met the expectation of the SSHAC Guidance with respect to evaluating the range of alternative scientific interpretations. The discussions during the workshop and between the TI Team and Panel following the workshop evolved the "SSC Framework" concept, which provided transparent criteria that framed the TI Team's systematic identification and assessment of seismic sources throughout the CEUS.

Feedback from hazard calculations and sensitivity analyses is an important step in a SSHAC assessment to understand the importance of elements of the model and inform the final assessments. For development of a regional SSC model to be used for site-specific probabilistic seismic hazard analyses (PSHAs) at many geographically distributed sites, feedback based on the preliminary model is particularly important. Following WS-2 a preliminary SSC model termed "the SSC sensitivity model," was developed and used for hazard sensitivity calculations that were evaluated in WS-3. While the SSC sensitivity model was clearly preliminary, the evaluation of sensitivity results that took place in WS-3 provided important feedback for completing analyses and for supporting the TI Team's development of the preliminary CEUS SSC model. The Panel was able to review the preliminary model and provide feedback in a subsequent project briefing meeting on March 24, 2010.

Together the three workshops provided the TI Team interactions with the appropriate range of resource and proponent experts. These experts were carefully identified to present, discuss, and debate the data, models, and methods that together form the basis for assuring that the CBR of the TDI have been properly represented in the hazard model. Experts representing academia, government, and private industry participated. The TI Team also reached out to a wide range of experts as they developed the database and performed the integration activities to develop the SSC model. The Panel participated throughout this process, and is satisfied that the TI Team fully engaged appropriate experts to accomplish the goals of a SSHAC Guidance.

Integration

Consistent with the SSHAC Guidance, integration is the process of assessing the CBR of the TDI and representing the assessment in the SSC model. Informed by the evaluation process, the integration process includes representation of the range of defensible methods, models, and interpretations of the larger technical community together with new models and methods developed by analyses during the evaluation and integration process.

For the CEUS SSC Project, development of the earthquake catalog, methods for assessing and representing maximum earthquake magnitudes, and methods for earthquake recurrence assessment continued during the integration process. The Panel reviewed all the analyses at various stages of development and provided comments and recommendations. The TI Team performed the integration process by means of eleven working meetings. Members of the Panel participated in most of these working meetings as observers or resource experts. The full Panel participated in the discussions during both feedback meetings and provided formal comments and recommendations following the meetings. We observed that the integration process was thorough and that it acceptably complied with the SSHAC Guidance. Based on our participation and observations we conclude that the integrated CEUS SSC Model appropriately represents the center, body, and range of current methods, models and technically defensible interpretations.

PPRP Engagement

Consistent with the SSHAC Guidance, the Panel was fully engaged in peer-review interactions with the TI Team and the Project Manager of the CEUS SSC Project throughout the entire project period—from development of the Project Plan in early to mid 2008 through production of the Final Project Report in mid to late 2011.⁵ The Panel provided both written and oral peer-review comments on both technical and process aspects at many stages of the Project's evolution. Key PPRP activities, leading up to this final report, have included:

- Review of the Project Plan.
- Formulation of a PPRP implementation plan, specifically for the CEUS SSC Project, to ensure adherence to the general guidance provided by SSHAC and NUREG-1563 for the scope and goals of a PPRP review.
- Involvement in *each* of the three Project workshops, including advising in the planning stage; participating collectively as a review panel during the workshop (and individually as resource experts when requested by the TI Team), providing timely comments on technical and process issues; and submitting a written report of the Panel's observations and recommendations following each workshop.
- Development and implementation of a process, together with the TI Team, to document the resolution of recommendations made in PPRP formal communications.
- Participation as observers (and occasionally as resource experts when requested by the TI Team) in eight of the TI Team's 11 working meetings.
- Peer-review and written comments, including several informal reports, on the TI Team's intermediate work products, particularly early versions of the CEUS SSC Model.

⁵ See CEUS SSC Final Report: Section 2.5, Table 2.2-1, and Appendix I

- Direct interaction with the TI Team and Project Manager in more than 20 teleconferences and four face-to-face briefings—in addition to the three workshops and eight working meetings of the TI Team noted above.
- Extensive, critical peer-review of the Project’s 2010 Draft Report and 2011 Final Report.

The Panel, collectively and individually, fully understood the SSHAC Guidance for a structured participatory peer review and the requirements for a Level 3 assessment process; had full and frequent access to information and interacted extensively with the TI Team and Project Manager throughout the entire project; provided peer-review comments at numerous stages; and, as documented within the Final Project Report, was fully engaged to meet its peer-review obligations in an effective way.

Project Report

The SSHAC Guidance makes clear that adequate documentation of process and results is crucial for their understanding and use by others in the technical community, by later analysis teams, and by the project sponsors. The Panel understood what was needed to conform to the SSHAC requirements, and it was committed to ensuring that the documentation of technical details associated with the CEUS SSC Model in the Project Report was clear and complete. The Panel was equally committed to ensuring the transparency of process aspects of the project, both in implementation and in description in the Project Report.

The Panel provided lengthy compilations of review comments (see Appendix I of the Project Report) for both the 2010 Draft Report and the 2011 Final Report. These included hundreds of comments, categorized as general, specific, relating to clarity and completeness, or editorial. The massive amount of detail provided by the TI Team in the Project Report and the intensiveness of the Panel’s review comments both reflect great diligence and a mutual understanding by the TI Team and the PPRP of the thoroughness and high quality of documentation expected in the Project Report.

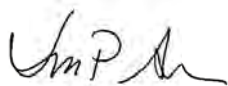
The Project Manager and the TI Lead provided review criteria to the Panel for both the draft and final versions of the Project Report. The criteria for reviewing the Draft Report⁶ covered the range of technical and process issues consistent with requirements of the SSHAC Guidance, including draft implementation guidance (see footnote #4). Key criteria, among others, include sufficiency of explanatory detail; adequate consideration of the full range of data, models, and methods—and the views of the larger technical community; adequate justification of the data evaluation process, logic-tree weights, and other technical decisions; proper treatment of uncertainties; and conformance to a SSHAC Level 3 assessment process. To be clear, the PPRP is charged with judging the adequacy of the documented *justification* for the CEUS SSC Model and its associated logic-tree weights. The TI Team “owns” the Model and logic-tree weights.

Criteria for reviewing the Final Report focused on reaching closure to comments made on the Draft Report and ensuring that no substantive issues remained unresolved. To that end, among its many review comments on the Final Report the Panel identified “mandatory” comments, which the TI Team was required to address in the final version of the Project Report.

⁶ See PPRP report dated October 4, 2010, in Appendix I of CEUS SSC Final Report

The Panel made thorough, extensive efforts in its documented reviews of the 2010 Draft Report and the 2011 Final Report (as well as in many related interactions with the TI Team) to ensure a high-quality Project Report that fully meets SSHAC requirements for clear, complete, and transparent documentation of all aspects of the CEUS SSC Project. We are pleased to confirm that implementation of the CEUS SSC Project fully conformed with the SSHAC Guidance and that the resulting CEUS SSC Model properly meets the SSHAC goal of representing the center, body, and range of technically-defensible interpretations.

This concludes our PPRP Final Report for the CEUS SSC Project.



Jon P. Ake



Walter J. Arabasz



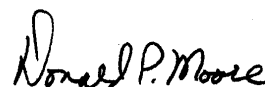
William J. Hinze



Annie M. Kammerer



Jeffrey K. Kimball



Donald P. Moore



Mark D. Petersen



J. Carl Stepp

Copy:

Lawrence A. Salomone

Kevin J. Coppersmith

Brent Gutierrez

PROJECT ACKNOWLEDGMENTS

This study was sponsored by the Electric Power Research Institute (EPRI) Advanced Nuclear Technology Action Plan Committee, the U.S. Department of Energy (DOE) Office of Nuclear Energy and Office of the Chief of Nuclear Safety, and the U.S. Nuclear Regulatory Commission (NRC) Office of Nuclear Regulatory Research. Technical experts from the DOE, NRC, U.S. Geological Survey, Defense Nuclear Facility Safety Board, industry, and academia participated in the study as part of the Technical Integration (TI) Team or as members of the Participatory Peer Review Panel (PPRP). Any statements, opinions, findings, conclusions, or recommendations expressed in this material are those of the authors and do not necessarily reflect those of the participating or sponsoring agencies.

Jeffrey F. Hamel was the EPRI Advanced Nuclear Technology Program Manager. Lawrence A. Salomone of Savannah River Nuclear Solutions, LLC, served as the Project Manager for the study. Kevin J. Coppersmith of Coppersmith Consulting Inc., served as the lead for the TI Team. J. Carl Stepp of Earthquake Hazards Solutions, and Walter J. Arabasz, Research Professor Emeritus of Geology and Geophysics at the University of Utah, served as Co-chairmen for the PPRP. The entire Central and Eastern United States Seismic Source Characterization Project Team and their roles are discussed in Section 2 and are shown on the project organization chart (Figure 2.3-1) of the report.

The authors of the report wish to acknowledge the contributions of the following people: the resource experts who participated in Workshop 1, the proponent experts who participated in Workshop 2, and the technical experts who provided valuable insights, perspective, and references throughout the study. The names of all these contributors are listed in Table 2.2-2.

In addition, the authors of the report appreciate the support of Geraldine Moore-Butler as administrative assistant and Nancy L. Sutherland as technical editor for the project. This report was assembled at AMEC.

Page intentionally left blank

SPONSORS' PERSPECTIVE

This report describes a new seismic source characterization model for the Central and Eastern United States (CEUS) for use in probabilistic seismic hazard analysis (PSHA) for nuclear facilities. PSHA has become a generally accepted procedure for supporting seismic design, seismic safety and decision making for both industry and government. Input to a PSHA consists of seismic source characterization (SSC) and ground motion characterization (GMC); these two components are necessary to calculate probabilistic hazard results (or seismic hazard curves) at a particular geographic location.

The 1986 Electric Power Research Institute and Seismicity Owners Group (EPRI-SOG) study included both an SSC and GMC component. Recent applications for new commercial reactors have followed U.S. Nuclear Regulatory Commission (NRC) regulatory guidance (RG 1.208) by using the EPRI-SOG source model as a starting point and updating it as appropriate on a site-specific basis. This CEUS SSC Project has developed a new SSC model for the CEUS to replace the SSC component of the EPRI-SOG study.

The CEUS SSC Project was conducted using a Senior Seismic Hazard Analysis Committee (SSHAC) Level 3 process, as described in the NRC publication, *Recommendations for Probabilistic Seismic Hazard Analysis: Guidance on Uncertainty and Use of Experts* (NUREG/CR-6372). The goal of the SSHAC process is to represent the center, body, and range of technically defensible interpretations of the available data, models, and methods. The CEUS SSC model is applicable to any site within the CEUS and can be used with the EPRI 2004/2006 GMC model to calculate seismic hazard at any site of interest. Long-term efforts to replace the EPRI 2004/2006 GMC model with the Next Generation Attenuation Relationships for Central and Eastern North America obtained from the NGA-East Project is scheduled for completion in 2014.

The updated CEUS SSC model provides industry and government with the following: a new model for the commercial nuclear industry to perform PSHAs for future reactor license applications; the NRC to support its review of early site permit (ESP) and construction and operating license (COL) applications; and the U.S. Department of Energy (DOE) to support modern PSHAs to meet design and periodic review requirements for its current and future nuclear facilities. Specific benefits of the model are as follows:

- **Consistency:** For many sites, seismic sources at distances up to 300 km (186 mi.) or more significantly contribute to hazard at some spectral frequencies. Consequently, seismic hazard models for many sites have significant geologic overlap. If done separately, there is a likelihood of conflicting assessments for the same regions. A regional source model allows for consistent input into a PSHA. An updated conceptual SSC framework that provides a

consistent basis for identifying and characterizing seismic sources in the CEUS has been developed. The NRC will no longer need to review each time each applicant's regional SSC model when the accepted CEUS SSC model is used. This will avoid lengthy review of the regional SSC model in ESP and COL applications for sites within the CEUS that use the accepted regional CEUS SSC model to develop its site-specific SSC model.

- **Stability:** This CEUS SSC model was developed using the accepted state-of-practice SSHAC methodology that involved the following tasks:
 - Development of a comprehensive database and new tools for documenting the data consideration process.
 - Multiple workshops to identify applicable data, debate alternative hypotheses, and discuss feedback.
 - Multiple working meetings by the Technical Integration (TI) Team to develop the SSC model and fully incorporate uncertainties.
 - Technical advancements in a number of areas, such as developing a uniform earthquake catalog, developing an updated approach for assessing maximum magnitude, compiling data evaluation tables, incorporating paleoseismic data, and using spatial smoothing tools.
 - Participatory peer review, including four panel briefings, multiple interactions, and periodic formal feedback.
 - Proper documentation of all process and technical aspects of the project.

Experience has shown that stability is best achieved through proper and thorough characterization of our knowledge and uncertainties, coupled with the involvement of the technical community, regulators, and oversight groups.

- **Greater Longevity:** An explicit goal of the SSHAC methodology is to represent the center, body, and range of the technically defensible interpretations of the available data, models, and methods. Using the SSHAC process provides reasonable assurance that this goal has been achieved. Representing the center, body, and range of interpretations at the time of the study means that as new information is acquired and various interpretations evolve as a result, the current thinking at any point is more likely to be addressed in the study. As new information becomes available, an existing SSC will require periodic reviews to evaluate the implications of the new findings. The need for updates to a particular study is now better understood as a result of findings of the CEUS SSC Project sensitivity studies to determine the significance of source characteristics.
- **Cost and Schedule Savings:** The CEUS SSC model can be used to perform a PSHA at any geographic location within the CEUS. It is applicable at any point within the CEUS, subject to site-specific refinements required by facility-specific regulations or regulatory guidance. Having stable, consistent input into a regional PSHA will reduce the time and cost required to complete a commercial nuclear site's ESP or COL licensing application, prepare a DOE site's PSHA, and develop design input for new commercial and DOE mission-critical nuclear facilities.

- **Advancement of Science:** The CEUS SSC Project provides new data, models, and methods. This information was shared at three workshops with international observers as a means to provide technology transfer for application in other regions. The CEUS SSC earthquake catalog, which merges and reconciles several catalogs and provides a uniform moment magnitude for all events, and the CEUS SSC paleoliquefaction database provide a new baseline for future research and updates. New approaches used in this project for spatial smoothing of recurrence parameters, assessment of maximum magnitude, and systematical documentation of all data considered and evaluated also benefit future research and PSHA updates.

The sponsors of the CEUS SSC Project are utilities and vendors on the EPRI Advanced Nuclear Technology Action Plan Committee, the DOE Office of Nuclear Energy, the DOE Office of the Chief of Nuclear Safety, and the NRC Office of Nuclear Regulatory Research. Technical experts from the DOE, NRC, U.S. Geological Survey (USGS), and Defense Nuclear Facility Safety Board (DNFSB) participated in the study as part of the TI Team or as members of the Participatory Peer Review Panel (PPRP).

The product of the CEUS SSC Project is a robust peer-reviewed regional CEUS SSC model for use in PSHAs. This model will be applicable to the entire CEUS, providing an important baseline for future research and updates. The CEUS SSC Project demonstrates that a SSHAC Level 3 approach can achieve the goals of considering the knowledge and uncertainties of the larger technical community within a robust and transparent framework. The value of the new CEUS SSC model has been enhanced by the participation of key stakeholders from industry, government, and academia who were part of the CEUS SSC Project Team.

Looking forward, the NRC will publish NUREG-2117 (2012), *Practical Implementation Guidelines for SSHAC Level 3 and 4 Hazard Studies* that provides SSHAC guidance on the need to update a regional model. The guidance covers updating both regional and site-specific assessments. It addresses the “refinement” process of starting with a regional model and refining it for site-specific applications.

Page intentionally left blank

ABBREVIATIONS

AD	anno domini (in the year of the Lord)
AFE	annual frequency of exceedance
AIC	Akaike information criterion
ALM	Alabama-Louisiana-Mississippi (zone of possible paleoseismic features)
AM	Atlantic Margin (seismotectonic zone)
AHEX	Atlantic Highly Extended Crust (seismotectonic zone)
ANSS	U.S. Advanced National Seismic System
ANT	Advanced Nuclear Technology
APC	Action Plan Committee
BA	Blytheville arch
BC	before Christ
BCFZ	Big Creek fault zone
BFZ	Blytheville fault zone
BL	Bootheel lineament
BMA	Brunswick magnetic anomaly
BP	before present
BPT	Brownian passage time
BTP	Branch Technical Position
CAD	computer-aided design

Abbreviations

CBR	center, body, and range
CCFZ	Crittenden County fault zone
CDZ	Commerce deformation zone
CENA	Central and Eastern North America
CERI	Center for Earthquake Research and Information
CEUS	Central and Eastern United States
CFZ	Commerce fault zone
CFR	Code of Federal Regulations
CGL	Commerce geophysical lineament
CGRGC	Cottonwood Grove–Rough Creek graben
CI	confidence interval
CNWRA	Center for Nuclear Waste Regulatory Analysis
COCORP	Consortium for Continental Reflection Profiling
COCRUST	Consortium for Crustal Reconnaissance Using Seismic Techniques
COL	combined construction and operating license
COLA	combined operating license application
COMP	composite prior, composite superdomain
CON	contemporary (with earthquake occurrence)
COV	coefficient of variation
CPT	cone penetration test
CVSZ	Central Virginia seismic zone
D&G	Dewey and Gordon (1984 catalog)
DEM	digital elevation model

DNFSB	Defense Nuclear Facilities Safety Board
DOE	U.S. Department of Energy
DWM	Division of Waste Management
ECC	Extended Continental Crust
ECC-AM	Extended Continental Crust–Atlantic Margin (seismotectonic zone)
ECC-GC	Extended Continental Crust–Gulf Coast (seismotectonic zone)
ECFS	East Coast fault system
ECFS-C	East Coast fault system—central segment
ECFS-N	East Coast fault system—northern segment
ECFS-S	East Coast fault system—southern segment
EC-SFS	East Coast–Stafford fault system
ECMA	East Coast magnetic anomaly
ECRB	East Continent rift basin
ECTM	Eastern Canada Telemetered Network
E[M]	expected moment magnitude listed in the CEUS SSC catalog for an earthquake
ENA	eastern North America
EP	Eau Plain shear zone
EPRI	Electric Power Research Institute
EPRI-SOG	Electric Power Research Institute–Seismicity Owners Group
ERM	Eastern rift margin
ERM-N	Eastern rift margin—north
ERM-RP	Eastern rift margin—river (fault) picks
ERM-S	Eastern rift margin—south

Abbreviations

ERM-SCC	Eastern rift margin—south/Crittenden County
ERM-SRP	Eastern rift margin—south/river (fault) picks
ERRM	Eastern Reelfoot Rift Margin
ESP	early site permit
ESRI	Environmental Systems Research Institute
ETSZ	Eastern Tennessee seismic zone
EUS	Eastern United States
FAFC	Fluorspar Area fault complex
FGDC	Federal Geographic Data Committee
ft	foot or feet
FTP	file transfer protocol
ft/s	feet per second
ft/yr	feet per year
FWLA	Fugro William Lettis & Associates
FWR	Fort Wayne rift
Ga	billion years ago
GC	Gulf Coast
GCVSZ	Giles County, Virginia, seismic zone
GHEX	Gulf Coast Highly Extended Crust (seismotectonic zone)
GIS	geographic information system
GLTZ	Great Lakes tectonic zone
GMC	ground-motion characterization (model)
GMH	Great Meteor Hotspot (seismotectonic zone)

GMPE	ground-motion prediction equation
GMRS	ground-motion response spectra
GPR	ground-penetrating radar
GPS	global positioning system
GSC	Geological Survey of Canada
Gyr	gigayears (10^9 years)
HF	Humboldt fault
HID	hazard input document
I_0	maximum intensity
IAEA	International Atomic Energy Agency
IBEB	Illinois Basin Extended Basement (seismotectonic zone)
IPEEE	Individual Plant Examination for External Events
IRM	Iapetan rifted margin
ISC	International Seismological Centre
ITC	informed technical community
ka	thousand years ago
K-Ar	potassium-argon
km	kilometer(s)
km^2	square kilometer(s)
km/sec	kilometers per second
K-S	Kijko-Sellevoll
K-S-B	Kijko-Sellevoll-Bayes
kyr	thousand years

Abbreviations

LDO	Lamont-Doherty Earth Observatory (catalog)
LHS	Latin hypercube sampling
LLNL	Lawrence Livermore National Laboratory
ln(FA)	logarithm of felt area (with felt area measured in km ²)
LS	least squares
LSA	La Salle anticlinal belt
LWLS	locally weighted least squares
m	meter(s)
M	magnitude
M , M _W	moment magnitudes
Ma	million years ago
MAR	Marianna (RLME source)
m _b	body-wave magnitude (short period)
m _{bLg}	body-wave magnitude determined from higher-mode (L _g) surface waves
M _C	coda magnitude
MCMC	Markov Chain Monte Carlo
M _D	duration magnitude
MESE	Mesozoic and younger extended crust
MESE-N	Mesozoic-and-younger extended crust or Mmax zone that is “narrow”
MESE-W	Mesozoic-and-younger extended crust or Mmax zone that is “wide”
mi.	mile(s)
mi. ²	square mile(s)
MIDC	midcontinent

MidC	Midcontinent-Craton (seismotectonic zone)
Mfa	felt-area magnitude
M _L	local magnitude
M _{max} , Mmax	maximum magnitude
MMI	modified Mercalli intensity
mm/yr	millimeters per year
M _N	Nuttli magnitude
M ₀	Scalar seismic moment
MRS	Midcontinent rift system
m/s	meters per second
M _S	surface-wave magnitude
MSF	Meeman-Shelby fault
M _w	
Myr	million years
NAD83	North American Datum of 1983
NAP	Northern Appalachian (seismotectonic zone)
Nd	neodymium
NEDB	National Earthquake Database
NEI	Nuclear Energy Institute
NEIC	National Earthquake Information Center
NF	Niagara fault zone
NMESE	Non-Mesozoic and younger extended crust
NMESE-N	Mesozoic-and-younger extended crust or Mmax zone that is “narrow”

Abbreviations

NMESE-W	Mesozoic-and-younger extended crust or Mmax zone that is “wide”
NMFS	New Madrid fault system
NMN	New Madrid North fault
NMS	New Madrid South fault
NMSZ	New Madrid seismic zone
NN	New Madrid north (fault segment as designated by Johnston and Schweig, 1996)
NOAA	National Oceanic and Atmospheric Administration
NPP	nuclear power plant(s)
NR	Nemaha Ridge
NRC	U.S. Nuclear Regulatory Commission
NRHF	Nemaha Ridge–Humboldt fault
NSHMP	National Seismic Hazard Mapping Project
NW	New Madrid west (fault segment as designated by Johnston and Schweig, 1996)
OKA	Oklahoma aulacogen (seismotectonic zone)
OKO	Oklahoma Geological Survey Leonard Geophysical Observatory (catalog)
OSL	optically stimulated luminescence
P _a	probability of activity (of being seismogenic)
PEZ	Paleozoic Extended Crust (seismotectonic zone)
PGA	peak ground acceleration
PM	Project Manager
PPRP	Participatory Peer Review Panel
PSHA	probabilistic seismic hazard analysis
PVHA	probabilistic volcanic hazard analysis

RCG	Rough Creek graben
RF	Reelfoot fault
RFT	Reelfoot thrust (fault)
RLME	repeated large-magnitude earthquake (source)
RR	Reelfoot rift zone
RS	Reelfoot South (fault segment)
SA	spectral acceleration
SCL	St. Charles lineament
SCML	south-central magnetic lineament
SCR	stable continental region
SCSN	South Carolina Seismic Network
SEUS	Southeastern United States (catalog)
SEUSSN	Southeastern United States Seismic Network
SGFZ	Ste. Genevieve fault zone
SHmax	maximum horizontal stress, compression, or principal stress
SLR	St. Lawrence rift (seismotectonic zone)
SLTZ	Spirit Lake tectonic zone
SLU	Saint Louis University (catalog)
SNM	Sanford et al. (2002 catalog)
SOG	Seismicity Owners Group
SPT	standard penetration test
SRA	Stover, Reagor, and Algermissen (1984 catalog)
SRTM	Shuttle Radar Topography Mission

Abbreviations

SSC	seismic source characterization
SSE	safe shutdown earthquake
SSHAC	Senior Seismic Hazard Analysis Committee
Str&Tur	Street and Turcotte (1977 catalog)
SUSN	Southeastern United States Network
TC	technical community
TFI	technical facilitator/integrator
TI	technical integration
USGS	U.S. Geological Survey
USNSN	U.S. National Seismograph Network
UTC	Coordinated Universal Time
V_P/V_S	ratio of P-wave velocity to S-wave velocity
WES	Weston Observatory (catalog)
WIPP	Waste Isolation Pilot Project
WQSZ	Western Quebec seismic zone
WRFZ	White River fault zone
WUS	Western United States
WVFS	Wabash Valley fault system
WVSZ	Wabash Valley seismic zone
WWSSN	World-Wide Standardized Seismograph Network

APPENDIX C

Data Evaluation Tables

C

APPENDIX DATA EVALUATION TABLES

Default Source Characteristics for CEUS SSC Project Study Region

Table C-5.4 Future Earthquake Characteristics

RLME Sources

Table C-6.1.1	Charlevoix RLME
Table C-6.1.2	Charleston RLME
Table C-6.1.3	Cheraw Fault RLME
Table C-6.1.4	Oklahoma Aulacogen RLME
Table C-6.1.5	Reelfoot Rift–New Madrid Fault System RLMEs
Table C-6.1.6	Reelfoot Rift–Eastern Margin Fault RLME
Table C-6.1.7	Reelfoot Rift–Marianna RLME
Table C-6.1.8	Reelfoot Rift–Commerce Fault Zone RLME
Table C-6.1.9	Wabash Valley RLME

Seismotectonic Zones

Table C-7.3.1	St. Lawrence Rift Zone (SLR)
Table C-7.3.2	Great Meteor Hotspot Zone (GMH)
Table C-7.3.3	Northern Appalachian Zone (NAP)
Table C-7.3.4	Paleozoic Extended Crust Zone (PEZ; narrow [N] and wide [W])
Table C-7.3.5	Illinois Basin–Extended Basement Zone (IBEB)
Table C-7.3.6	Reelfoot Rift Zone (RR; including Rough Creek Graben [RR-RCG])
Tables C-7.3.7/7.3.8	Extended Continental Crust Zone–Atlantic Margin (ECC-AM) and Atlantic Highly Extended Crust (AHEx)
Tables C-7.3.9/7.3.10	Extended Continental Crust Zone–Gulf Coast (ECC-GC) and Gulf Coast Highly Extended Crust (GHEx)
[No Table C-7.3.11]	[Oklahoma Aulacogen (OKA); see Table C-6.1.4]
Table C-7.3.12	Midcontinent-Craton Zone (MidC)

Mmax Zones

Criteria for defining the MESE/NMESE boundary for the two-zone alternative are discussed in Section 6.2.2. MESE-N includes ECC-AM, ECC-GC, AHEx, GHEx, RR, SLR, NAP, GMH,

and PEZ-N. MESE-W differs from MESE-N in that it adopts the wide alternative geometries (i.e., PEZ-W, RR-RCG, and IBEB). See tables listed above for data pertinent to the definition of the boundaries of the zones and evidence for Mesozoic and younger tectonism. Default future earthquakes rupture parameters (Table 4.1.3-1) are assigned to both the one-zone and two-zone Mmax sources.

Introduction

The Data Evaluation tables were developed to identify the data used, to evaluate the quality of the data, and to specify the degree of reliance on each data set in characterizing seismic sources. Labeling of Data Evaluation tables is keyed to the specific chapter and section where the corresponding source is described. Full citations of references listed in the tables are provided in Chapter 10.

The Data Evaluation tables include the following attributes:

- The first column is a listing of the data, by data type, used in the evaluation for a particular RLME or seismotectonic source. See Appendix A for information regarding the sources for data sets specific to the CEUS SSC Project.
- The second column is an assessment of the quality of the data by the TI Team. This assessment is qualitative and takes into account the resolution, completeness, and distribution of the data relative to the best data of that type currently available. In some cases the assessment of the quality of a particular data set differs somewhat for different seismic sources. This is a reflection of the perceived value of the particular data set toward addressing the SSC characteristics of each seismic source.
- The third column is used for notes about the data quality. This usually includes comments about whether the data have been published in abstract form or full papers and other issues regarding the defensibility of the data.
- The fourth column identifies the particular seismic source to which the data have been applied in the evaluation.
- The fifth and sixth columns provide an assessment of the degree of reliance on the data set for purposes of SSC, and a short description of how the data were relied on. The intent is to assist the reader in understanding how the data set was used and what the evaluation of the degree of reliance was based on.
- The seventh column indicates whether the data exists in GIS format within the project database. If the data are not in GIS format, they will be found in the database in other formats such as a PDF file.

Although many different types of data were considered for the characterization of each seismic source, not all data types were used (e.g., some types of geophysical data or seismological data [such as focal mechanisms] are either not available or have limited usefulness for defining or characterizing a particular seismic source). Therefore, not all of the data types that were considered are listed in the tables. All data that were considered are included in the Data Summary tables (see Appendix D). Additional information on the Data Evaluation tables is provided in Section 4.1.2.2. Finally, please note that magnitudes are reported in the magnitude scale designated in the cited publication.

**Table C-5.4 Data Evaluation
Future Earthquake Characteristics**

**Identified Source
Default for entire CEUS SSC**

Data/References	Quality (1=low, 5=high)	Notes on Quality of Data	Source Considered	Used in SSC and Reliance Level (0=no, 5=high)	Discussion of Data Use	In GIS Database
<i>Instrumental Seismicity</i>						
Atkinson (2004)	4	Compilation of digital seismograms from 186 earthquakes in southeastern Canada and northeastern United States from 1990 to 2003.	All sources	3	Used for focal depth distribution, but range of magnitudes is only 2.5–5.6, so little constraint on larger magnitudes.	N
CEUS SSC earthquake catalog	5	Comprehensive catalog; includes magnitude conversions and uncertainty assessments.	All sources	2	Provides information on focal depth, but quality varies across region.	Y
Chapman et al. (1997)	5	Eastern Tennessee well-constrained focal mechanism solutions derived using a new velocity model and relocated hypocenters.	All sources	4	Used for assessing sense of slip and focal depths.	N
Dineva et al. (2004)	4	Relocated earthquakes in the 1990–2001 period in the southern Great Lakes and three focal mechanisms.	All sources	2	Used for sense of slip but very few events.	N

**Table C-5.4 Data Evaluation
Future Earthquake Characteristics**

**Identified Source
Default for entire CEUS SSC**

Data/References	Quality (1=low, 5=high)	Notes on Quality of Data	Source Considered	Used in SSC and Reliance Level (0=no, 5=high)	Discussion of Data Use	In GIS Database
Horton et al 2005)	4	Compilation of better focal mechanisms in Reelfoot, Rough Creek, and Wabash Valley	All sources	3	Used for assessing sense of slip.	N
Kim (2003)	4	Assessment of the June 18, 2002, Caborn, Indiana, earthquake (MW 4.6) using regional and teleseismic waveform data.	All sources	1	Provides information on focal depth and sense of slip in Wabash Valley area; very localized.	N
Kim and Chapman (2005)	4	Detailed study of 2003 event in central Virginia using regional waveforms.	All sources	2	Provides information on depth and sense of slip, but very few events.	N
Mai (2005)	3	Compilation of data related to hypocenter depths in relation to the normalized downdip width of fault rupture for crustal faults.	All sources	3	Used to assess the expected depth distribution of earthquakes as a function of earthquake magnitude.	N
S. Mazzotti (CEUS SSC WS2 presentation)	3	Compilation of focal mechanisms in the St. Lawrence in the Charlevoix area.	All sources	3	Includes events having range of data quality.	N

**Table C-5.4 Data Evaluation
Future Earthquake Characteristics**

**Identified Source
Default for entire CEUS SSC**

Data/References	Quality (1=low, 5=high)	Notes on Quality of Data	Source Considered	Used in SSC and Reliance Level (0=no, 5=high)	Discussion of Data Use	In GIS Database
Seeber et al. (1998)	3	Local study of Cacoosing Valley earthquakes near Reading, Pennsylvania.	All sources	1	Local study with information on focal depth and sense of slip.	N
Shumway (2008)	5	Special study in New Madrid area with new velocity profile.	All sources	4	High quality focal mechanisms, locations, and focal depths for sense of slip.	N
Sibson (1984)	2	Compilation and physical analysis of earthquake focal depths for larger crustal earthquakes.	All sources	3	Provides a basis for assessing the width of the seismogenic zone using earthquake hypocenters; roughly the 95th percentile cutoff of seismicity.	N
Sibson and Xie (1998)	3	Compilation of fault dips moderate to large ($M > 5.5$) reverse-slip intracontinental earthquakes with the slip-vector raking $90 \pm 30^\circ$ in the fault plane.	All sources	3	Global compilation used to constrain the dips of reverse faults.	N
Somerville et al. (2001)	3	Compilation of modeling-derived rupture areas and seismic moment for eastern North America earthquakes.	All sources	5	Provides preferred rupture area vs magnitude relationship.	N

**Table C-5.4 Data Evaluation
Future Earthquake Characteristics**

**Identified Source
Default for entire CEUS SSC**

Data/References	Quality (1=low, 5=high)	Notes on Quality of Data	Source Considered	Used in SSC and Reliance Level (0=no, 5=high)	Discussion of Data Use	In GIS Database
Sykes et al. (2008)	4	High-quality earthquake locations and focal depths in the New York region.	All sources	3	Good quality focal depths for a local region, limited magnitude range.	N
Talwani (CEUS SSC WS2)	3	Compilation of focal mechanisms and focal depths in the Charleston, South Carolina, area.	All sources	3	Variable data quality but good compilation of data for this region.	N
Tanaka (2004)	5	High quality and large numbers of well-determined focal depths for Japanese earthquakes, as well as extensive compilation of thermal measurements.	All sources	5	Provides strong technical basis for the correlation between the maximum crustal thickness and D_{90} , which is the depth above which 90% of the seismicity lies.	N
van Lanen and Mooney (2007)	3	Compilation of earthquake focal depth in eastern North America as a function of moment magnitude.	All sources	3	Good compilation but variable data quality; used for depth as function of magnitude.	N
Regional Stress						
CEUS SSC stress data set	5	Includes additional data points not shown on World Stress Map.	All sources	3	Provides indications of the expected tectonic stress regime and the sense of slip.	Y

**Table C-5.4 Data Evaluation
Future Earthquake Characteristics**

**Identified Source
Default for entire CEUS SSC**

Data/References	Quality (1=low, 5=high)	Notes on Quality of Data	Source Considered	Used in SSC and Reliance Level (0=no, 5=high)	Discussion of Data Use	In GIS Database
Zoback (1992)	3	Based on focal mechanisms available in late 1980s.	All sources	2	Used to assess the amount of strike-slip versus thrust faulting in the CEUS; also provides indications of orientations of ruptures.	N
<i>Tectonic Strain–Paleoseismicity</i>						
Wesnousky (2008)	4	Compilation of empirical data regarding the seismologic and geologic characteristics of earthquake ruptures.	All sources	3	Used for relationship between fault length-to-width aspect ratio versus magnitude for future ruptures.	N
<i>Geologic Mapping</i>						
Marshak and Paulsen (1997)	3	Maps based on regional-scale extrapolations of local data sets.	All sources	2	Used to confirm the presence of potential northwest-trending future earthquake rupture orientations.	N
<i>Other</i>						
NAGRA (2004)	3	Assessments from expert panel of rupture width as function of magnitude.	All sources	4	Used for characterizing the depth distribution of future earthquake ruptures using the focal depth distribution of observed hypocenters.	N

**Table C-5.4 Data Evaluation
Future Earthquake Characteristics**

**Identified Source
Default for entire CEUS SSC**

Data/References	Quality (1=low, 5=high)	Notes on Quality of Data	Source Considered	Used in SSC and Reliance Level (0=no, 5=high)	Discussion of Data Use	In GIS Database
Sibson (2007)	3	Assessment of base of seismogenic zone based on physical constraints.	All sources	2	Provides physical basis for estimating depth of seismogenic zone from seismicity; confirms magnitude dependence of focal depths.	N

**Table C-6.1.1 Data Evaluation
Charlevoix RLME**

**Identified Source
Charlevoix RLME within the St. Lawrence Rift Zone**

Data/References	Quality (1=low, 5=high)	Notes on Quality of Data	Source Considered	Used in SSC and Reliance Level (0=no, 5=high)	Discussion of Data Use	In GIS Database
<i>Instrumental Seismicity</i>						
CEUS SSC earthquake catalog	5	Comprehensive catalog; includes magnitude conversions and uncertainty assessments.	Charlevoix	5	Used to evaluate recurrence parameters.	Y
Lamontagne and Ranalli (1997)	5	Relocated hypocentral depth.	Charlevoix	5	Used to evaluate thickness of seismogenic crust and style of faulting.	Y
<i>Historical Seismicity</i>						
CEUS SSC earthquake catalog	5	Comprehensive catalog; includes magnitude conversions and uncertainty assessments.	Charlevoix	5	Largest historical earthquake in the CEUS SSC earthquake catalog is the 1663 Charlevoix earthquake	Y
Ebel (1996)	3	Determined magnitude from felt effects.	Charlevoix	5	Used to evaluate maximum magnitude.	Y
Ebel (2006b)	3	Determined magnitude from felt effects.	Charlevoix	5	Used to evaluate maximum magnitude.	N

**Table C-6.1.1 Data Evaluation
Charlevoix RLME**

**Identified Source
Charlevoix RLME within the St. Lawrence Rift Zone**

Data/References	Quality (1=low, 5=high)	Notes on Quality of Data	Source Considered	Used in SSC and Reliance Level (0=no, 5=high)	Discussion of Data Use	In GIS Database
Ebel (2009)	3	Determined magnitude from felt effects and attenuation relationships.	Charlevoix	5	Used to evaluate maximum magnitude.	N
Lamontagne et al. (2008)	4	Earthquake parameters and felt effects for major Canadian earthquakes.	Charlevoix	4	Magnitudes derived from special studies are cited directly in CEUS SSC earthquake catalog.	Y
<i>Magnetic Anomaly</i>						
CEUS SSC magnetic data set	5	High-quality regional data	Charlevoix	1	The Charlevoix zone is not subdivided based on different basement terranes or tectonic features imaged in the magnetic anomaly map.	Y
<i>Gravity Anomaly</i>						
CEUS SSC gravity data set	5	High-quality regional data	Charlevoix	1	The Charlevoix zone is not subdivided based on different basement terranes or tectonic features imaged in the gravity anomaly map.	Y

**Table C-6.1.1 Data Evaluation
Charlevoix RLME**

**Identified Source
Charlevoix RLME within the St. Lawrence Rift Zone**

Data/References	Quality (1=low, 5=high)	Notes on Quality of Data	Source Considered	Used in SSC and Reliance Level (0=no, 5=high)	Discussion of Data Use	In GIS Database
<i>Seismic Reflection</i>						
Tremblay et al. (2003)	3	Relocates offshore SQUIP data	Charlevoix	2	Images a transition from a half graben to a graben of the St. Lawrence fault within the St. Lawrence estuary.	N
<i>Local Geologic and Tectonic Maps</i>						
Lemieux et al. (2003)	4	Delineates spatial relationship between rift faults and impact crater.	Charlevoix	5	Used for source geometry.	N
Tremblay et al. (2003)	4	Delineates relationship between rift faults and impact crater.	Charlevoix	5	Used for source geometry.	N
<i>Geodetic Strain</i>						
Mazzotti and Adams (2005)	3	Seismic moment rate of 0.1–5.0 10 ¹⁷ Nm/yr for Charlevoix.	Charlevoix	3	Provides a model for localizing earthquakes at Charlevoix	N
<i>Regional Stress</i>						
Baird et al., (2009)	4	Performs 2-D stress modeling of the impact crater and rift faults.	Charlevoix	5	Modeling results confirm source geometry.	N

**Table C-6.1.1 Data Evaluation
Charlevoix RLME**

**Identified Source
Charlevoix RLME within the St. Lawrence Rift Zone**

Data/References	Quality (1=low, 5=high)	Notes on Quality of Data	Source Considered	Used in SSC and Reliance Level (0=no, 5=high)	Discussion of Data Use	In GIS Database
CEUS SSC stress data set	4	Provides additional new measurements to World Stress Map.	Charlevoix	1	Data includes thrust mechanisms with minor strike-slip. Orientations vary from E-W to NE-SW.	Y
Heidbach et al. (2008) (World Stress Map)	3	Compilation of worldwide stress data.	Charlevoix	2	Entries for SLR are predominantly thrust mechanisms with some strike-slip. Orientations of maximum horizontal stress vary from E-W to NE-SW.	Y
<i>Focal Mechanisms</i>						
Bent (1992)	3	Analyzed historical waveforms for 1925 earthquake.	Charlevoix	4	Used to characterize future ruptures.	N
Lamontagne (1999)	4	Determined focal mechanisms for Charlevoix earthquakes.	Charlevoix	4	Used to characterize future ruptures.	N
Lamontagne and Ranalli (1997)	4	Well-constrained focal mechanisms within the Charlevoix seismic zone.	Charlevoix	2	Thrust focal mechanisms correspond to larger-magnitude events, whereas smaller-magnitude events display greater variation in nodal planes corresponding to reactivation of fractures.	N
Li et al. (1995)	4	Determined focal mechanisms for two M 4 earthquakes.	Charlevoix	4	Used to characterize future ruptures.	N

**Table C-6.1.1 Data Evaluation
Charlevoix RLME**

**Identified Source
Charlevoix RLME within the St. Lawrence Rift Zone**

Data/References	Quality (1=low, 5=high)	Notes on Quality of Data	Source Considered	Used in SSC and Reliance Level (0=no, 5=high)	Discussion of Data Use	In GIS Database
<i>Paleoseismicity</i>						
Tuttle and Atkinson (2010)	4	Results of regional paleoliquefaction study in Charlevoix.	Charlevoix	4	Mmax assessment—Evidence for prehistoric earthquakes in Charlevoix area. Suggests stationarity of large-magnitude earthquakes in Charlevoix.	Y
CEUS SSC paleoliquefaction database	5	Compilation (with attributions) of paleoliquefaction observations	Charlevoix	4	Contains data presented in Tuttle and Atkinson (2010).	Y
Dionne (2001)	4	Detailed mapping and dating of Holocene deposits.	Charlevoix	5	Evidence of mid-Holocene sea-level lowstand may result in incompleteness interval.	N
Doig (1990)	3	Documents silt layers in cores attributed to earthquake-induced landslides.	Charlevoix	2	Uncertain magnitude estimates difficult to relate specifically to recurrence.	N
Filion et al. (1991)	3	Provides ages for prehistoric landslides attributed to earthquakes.	Charlevoix	2	Uncertain magnitude estimates difficult to relate specifically to recurrence.	N

**Table C-6.1.2 Data Evaluation
Charleston RLME**

Identified Sources

Charleston RLME with alternatives: L: Local; R: Regional; N: Narrow

Data/References	Quality (1=low, 5=high)	Notes on Quality of Data	Source Considered	Used in SSC and Reliance Level (0=no, 5=high)	Discussion of Data Use	In GIS Database
<i>Instrumental Seismicity</i>						
CEUS SSC earthquake catalog	5	Comprehensive catalog; includes magnitude conversions and uncertainty assessments.	L, R, N	5	Highest concentration of seismicity located in local Charleston area. Possible association of seismicity with offshore Helena Banks fault. Locations of Middleton Place–Summerville and Bowman seismic zones. Magnitudes of the earthquakes in the Adams Run seismic zone (coda magnitudes [M_c] < 2.3) are too small to appear in the CEUS SSC earthquake catalog.	Y
Madabhushi and Talwani (1993)	3	Total of 58 instrumentally recorded earthquakes between 1980 and 1991 with M_D 0.8–3.3 in Charleston area.	L	4	Mapped location of Middleton Place–Summerville seismic zone.	Y
Smith and Talwani (1985)	2	Abstract describing location of Bowman seismic zone and gravity surveys conducted in vicinity of Bowman seismic zone.	N	1	Abstract provides brief description of location of Bowman seismic zone.	Y

**Table C-6.1.2 Data Evaluation
Charleston RLME**

Identified Sources

Charleston RLME with alternatives: L: Local; R: Regional; N: Narrow

Data/References	Quality (1=low, 5=high)	Notes on Quality of Data	Source Considered	Used in SSC and Reliance Level (0=no, 5=high)	Discussion of Data Use	In GIS Database
South Carolina Seismic Network (2005)	4	Tabulation of microseismicity in Charleston area, recorded between 1974 and 2002.	L, N	4	Includes local Charleston earthquakes with magnitudes smaller than those listed in the CEUS SSC earthquake catalog. Spatially concentrated in 1886 epicentral area.	Y
Tarr et al. (1981)	2	Instrumentally recorded microseismicity in the Charleston area between 1973 and 1979.	L	2	Mapped locations of the Middleton Place–Summerville, Bowman, and Adams Run seismic zones.	N
Tarr and Rhea (1983)	2	Instrumentally recorded microseismicity in the Charleston area between 1973 and 1979.	L	2	Mapped locations of the Middleton Place–Summerville, Bowman, and Adams Run seismic zones.	N
<i>Historical Seismicity</i>						
Bakun and Hopper (2004b)	5	Preferred 1886 magnitude estimate based on assumed location at Middleton Place–Summerville seismic zone.	L, R, N	5	Magnitude of 1886 Charleston earthquake is estimated between M_w 6.4 and 7.2 (at 95% confidence level), with preferred estimate of M_w 6.9.	Y

**Table C-6.1.2 Data Evaluation
Charleston RLME**

Identified Sources

Charleston RLME with alternatives: L: Local; R: Regional; N: Narrow

Data/References	Quality (1=low, 5=high)	Notes on Quality of Data	Source Considered	Used in SSC and Reliance Level (0=no, 5=high)	Discussion of Data Use	In GIS Database
Bollinger (1977)	5	Isoseismal determinations for 1886 earthquake, based on reinterpretation of Dutton's (1889) basic intensity data.	L	5	Maximum epicentral intensity MMI X, with MMI IX in city of Charleston. Isoseismals define roughly coast-parallel elongation. Magnitude of 1886 earthquake estimated at m_b 6.8 to 7.1.	Y
Bollinger (1983)	3	Poorly constrained estimate of seismogenic crustal thickness at Charleston.	L, R, N	3	Estimates 1886 earthquake at m_b 6.7, with rupture length approximately 25 km, width approximately 12 km, average slip 1 m, based on empirical relations. Notes ongoing microseismicity concentrated in 1886 meizoseismal area.	Y
Bollinger (1992)	4	Estimate of seismogenic crustal thickness at Charleston.	L, R, N	4	Seismic source characterization for the Savannah River Site describes input parameters for PSHA, including seismogenic crustal thickness estimates of 14 and 25 km, respectively, for "Local Charleston" and "SC Piedmont and Coastal Plain" seismic sources.	Y

**Table C-6.1.2 Data Evaluation
Charleston RLME**

Identified Sources

Charleston RLME with alternatives: L: Local; R: Regional; N: Narrow

Data/References	Quality (1=low, 5=high)	Notes on Quality of Data	Source Considered	Used in SSC and Reliance Level (0=no, 5=high)	Discussion of Data Use	In GIS Database
Chapman and Talwani (2002)	4	Estimate of seismogenic crustal thickness at Charleston.	L, R, N	4	Seismic source characterization for South Carolina Department of Transportation describes input parameters for PSHA, including seismogenic crustal thickness estimate of 25 km.	N
Dutton (1889)	4	Intensity data and mapping of liquefaction "craterlets" for the 1886 earthquake.	L	2	Intensity data not explicitly used in source characterization, but these data later reinterpreted by Bollinger (1977), Bakun and Hopper (2004b), and others. Descriptions of largest and most spatially concentrated liquefaction "craterlets" near Charleston used, in part, to define epicentral region of 1886 earthquake.	N
Johnston (1996b)	4	Johnston (1996b) magnitude estimate for 1886 earthquake is significantly lower than Johnston et al. (1994) estimate of 7.56 ± 0.35 .	L, R, N	5	Magnitude estimate for 1886 Charleston earthquake of M_w 7.3 ± 0.26 based on isoseismal area regression accounting for eastern North America anelastic attenuation.	N
Martin and Clough (1994)	4	Magnitude estimate based on critical reassessment of available data.	L, R, N	4	Magnitude estimate for 1886 Charleston earthquake of M_w 7.0 to 7.5 based on geotechnical assessment of 1886 liquefaction data.	N

**Table C-6.1.2 Data Evaluation
Charleston RLME**

Identified Sources

Charleston RLME with alternatives: L: Local; R: Regional; N: Narrow

Data/References	Quality (1=low, 5=high)	Notes on Quality of Data	Source Considered	Used in SSC and Reliance Level (0=no, 5=high)	Discussion of Data Use	In GIS Database
Silva et al. (2003)	4	Estimate of seismogenic crustal thickness at Charleston.	L, R, N	4	Estimates of seismogenic crustal thickness at Charleston of 16 and 20 km, inferred from contemporary seismicity.	N
Talwani (1982)	3	Early depiction of Woodstock fault, refined and superseded by subsequent publications.	N	2	Relocated seismicity in the 1886 meizoseismal area suggests (1) right-lateral strike-slip events on the NE-striking Woodstock fault; and (2) SW-side-up thrust events on the NW-striking Ashley River fault.	N
<i>Magnetic Anomaly</i>						
CEUS SSC magnetic data set	5	High-quality regional data	R	2	Reviewed in defining the regional source configuration.	Y
<i>Gravity Anomaly</i>						
CEUS SSC gravity data set	5	High-quality regional data	R	2	Reviewed in defining the regional source configuration.	Y
<i>Seismic Reflection</i>						

**Table C-6.1.2 Data Evaluation
Charleston RLME**

Identified Sources

Charleston RLME with alternatives: L: Local; R: Regional; N: Narrow

Data/References	Quality (1=low, 5=high)	Notes on Quality of Data	Source Considered	Used in SSC and Reliance Level (0=no, 5=high)	Discussion of Data Use	In GIS Database
Behrendt et al. (1981)	4	Data suggest onshore faulting but do not provide unambiguous constraints on fault geometry and upward terminations within Coastal Plain sediments.	L, R	4	Subsurface fault mapping in 1886 epicentral area, including the proposed Cooke fault.	N
Behrendt et al. (1983)	4	High-resolution, multichannel seismic-reflection data clearly image the Helena Banks fault. Surveys limited to ~50 km SW and NE offshore of Charleston.	R	4	Mapping and age estimate of offshore Helena Banks fault.	N
Behrendt and Yuan (1987)	4	High-resolution, multichannel seismic-reflection data clearly image the Helena Banks fault. Surveys limited to ~50 km SW and NE offshore of Charleston.	R	4	Mapping and age estimate of offshore Helena Banks fault.	Y

**Table C-6.1.2 Data Evaluation
Charleston RLME**

Identified Sources

Charleston RLME with alternatives: L: Local; R: Regional; N: Narrow

Data/References	Quality (1=low, 5=high)	Notes on Quality of Data	Source Considered	Used in SSC and Reliance Level (0=no, 5=high)	Discussion of Data Use	In GIS Database
Chapman and Beale (2008)	5	"Fault C" clearly imaged in reprocessed seismic reflection line. Orientation, length, and upward termination of fault currently unresolved. Strike and length of "fault C" inferred from alignment of possible faults in adjacent seismic lines. Fault at least as young as Miocene or possibly Pliocene.	L, N	5	"Fault C" postulated to be fault that ruptured in 1886 Charleston earthquake. Location used in defining Local source configuration.	Y
Chapman and Beale (2010)	5	Reprocessed seismic reflection data suggest the 1886 epicentral area lies within a zone of extensive upper crustal faulting, but does not constrain geometry/extent of possible faults.	L, N	5	"Fault C" postulated to be fault that ruptured in 1886 Charleston earthquake. Location used in defining Local source configuration.	Y

**Table C-6.1.2 Data Evaluation
Charleston RLME**

Identified Sources

Charleston RLME with alternatives: L: Local; R: Regional; N: Narrow

Data/References	Quality (1=low, 5=high)	Notes on Quality of Data	Source Considered	Used in SSC and Reliance Level (0=no, 5=high)	Discussion of Data Use	In GIS Database
Hamilton et al. (1983)	4	Data suggest onshore faulting but do not provide unambiguous constraints on fault geometry and upward terminations within Coastal Plain sediments.	L, R	4	Postulated Cooke, Gants, and Drayton faults in Charleston 1886 epicentral area. Strikes, lengths, and ages not well constrained.	N
Marple and Miller (2006)	2	Data suggesting the existence of the proposed Berkeley fault are equivocal. Paper includes useful summary of data used by others to constrain previously proposed faults near Charleston.	L, N	2	Marple and Miller (2006) call into question the existence of the Adams Run fault of Weems and Lewis (2002).	N
<i>Regional Geologic and Tectonic Maps</i>						
Nystrom (1996)	4	Simplified seismic hazard map of South Carolina Coastal plain with minimal documentation.	L, R, N	1	Map roughly outlines those areas of coastal South Carolina most susceptible to liquefaction.	N

**Table C-6.1.2 Data Evaluation
Charleston RLME**

Identified Sources

Charleston RLME with alternatives: L: Local; R: Regional; N: Narrow

Data/References	Quality (1=low, 5=high)	Notes on Quality of Data	Source Considered	Used in SSC and Reliance Level (0=no, 5=high)	Discussion of Data Use	In GIS Database
<i>Local Geologic and Tectonic Maps</i>						
Bartholomew and Rich (2007)	2	Authors postulate Dorchester fault in 1886 epicentral area based on indirect evidence.	L	2	Subsurface fault mapping in 1886 epicentral area.	Y
Colquhoun et al. (1983)	3	Data suggesting the existence of proposed Charleston and Garner-Edisto faults are equivocal.	L	3	Early mapping of the proposed Charleston and Garner-Edisto faults based on subsurface stratigraphy and borehole control.	N
Dura-Gomez and Talwani (2009)	4	Article presents minor modifications to previously mapped subsurface faults near Charleston.	L, N	3	Slightly revised mapping of faults in the subsurface near Middleton Place–Summerville seismic zone.	N
Marple and Miller (2006)	4	Data suggesting existence of the proposed Berkeley fault are equivocal. Paper includes useful summary of data used by others to constrain previously proposed faults near Charleston.	L, N	3	Marple and Miller (2006) call into question the existence of the Adams Run fault of Weems and Lewis (2002).	N

**Table C-6.1.2 Data Evaluation
Charleston RLME**

Identified Sources

Charleston RLME with alternatives: L: Local; R: Regional; N: Narrow

Data/References	Quality (1=low, 5=high)	Notes on Quality of Data	Source Considered	Used in SSC and Reliance Level (0=no, 5=high)	Discussion of Data Use	In GIS Database
Marple and Talwani (1993)	4	Early depiction of Zone of River Anomalies and Woodstock fault, refined and superseded by subsequent publications.	L, N	1	Early mapping of Zone of River Anomalies and proposed Woodstock fault. Superseded by subsequent publications.	N
Marple and Talwani (2000)	4	Zone of River Anomalies proposed as tectonic feature, based on equivocal geomorphologic, seismic, and geophysical data. Data suggesting existence of southern segment are more robust than those for central and northern segments.	N	3	Identification of Zone of River Anomalies expands on earlier work (e.g., Marple and Talwani 1993).	Y
McCartan et al. (1984)	4	No faults mapped.	L, R, N	1	Geologic mapping at 1:250,000 scale of greater Charleston area.	N
Talwani and Dura-Gomez (2009)	4	Minor modifications to previously mapped subsurface faults near Charleston.	L, N	3	Subsurface fault mapping in 1886 epicentral area.	Y

**Table C-6.1.2 Data Evaluation
Charleston RLME**

Identified Sources

Charleston RLME with alternatives: L: Local; R: Regional; N: Narrow

Data/References	Quality (1=low, 5=high)	Notes on Quality of Data	Source Considered	Used in SSC and Reliance Level (0=no, 5=high)	Discussion of Data Use	In GIS Database
Talwani and Katuna (2004)	4	Viable alternate explanations (ground-shaking-related) exist for postulated primary surface rupture.	L, N	3	Subsurface fault mapping in 1886 epicentral area. Postulated 1886 coseismic effects and potential surface rupture.	Y
Weems and Lewis (2002)	3	Viable alternate (nontectonic) explanations exist for mapped features, including Adams Run and Charleston faults.	L	4	Subsurface fault mapping in 1886 epicentral area.	Y
Geodetic Strain						
Trenkamp and Talwani (n.d.)	2	Study suffers from admitted monument instability, small number of surveys (three), and short period of GPS measurements (six years).	L, R, N	2	This as-yet-unpublished study presents campaign GPS data from a 20-station grid near Charleston that suggest average shear strain rate ($\sim 10^9$ to 10^7 rad/yr) that is one to two orders of magnitude higher than the surrounding region. Largest interpreted strains located in Middleton Place–Summerville seismic zone and attributed to local fault intersections.	Y

**Table C-6.1.2 Data Evaluation
Charleston RLME**

Identified Sources

Charleston RLME with alternatives: L: Local; R: Regional; N: Narrow

Data/References	Quality (1=low, 5=high)	Notes on Quality of Data	Source Considered	Used in SSC and Reliance Level (0=no, 5=high)	Discussion of Data Use	In GIS Database
<i>Paleoseismicity</i>						
Amick and Gelinas (1991)	3	Short paper published in <i>Science</i> magazine; presents summary of data and interpretations described in more detail in other publications (e.g., Amick, Gelinas, et al., 1990; and Amick, Maurath, and Gelinas, 1990).	L, R, N	5	Largest paleoliquefaction features are at sites near Charleston, suggesting repeated large earthquakes near Charleston. Majority of paleoliquefaction features can be explained by a source near Charleston, but suggest the possibility of a separate (moderate?) source located ~100 km northeast.	N
Amick, Gelinas, et al. (1990)	4	Areas searched in which no features found are identified by 7.5-minute quadrangle only. Detailed reconnaissance maps not available.	L, R, N	5	Paleoliquefaction features found only in coastal Carolinas. Largest paleoliquefaction features are at sites near Charleston, suggesting repeated large earthquakes near Charleston. Return period for large (M ~ 7+) earthquakes near Charleston estimated at 500–600 years.	N

**Table C-6.1.2 Data Evaluation
Charleston RLME**

Identified Sources

Charleston RLME with alternatives: L: Local; R: Regional; N: Narrow

Data/References	Quality (1=low, 5=high)	Notes on Quality of Data	Source Considered	Used in SSC and Reliance Level (0=no, 5=high)	Discussion of Data Use	In GIS Database
Amick, Maurath, and Gelinas (1990)	4	Areas searched in which no features found are identified by 7.5-minute quadrangle only. Detailed reconnaissance maps not available.	L, R, N	5	Paleoliquefaction features found only in coastal Carolinas. Largest paleoliquefaction features are at sites near Charleston, suggesting repeated large earthquakes near Charleston. Return period for large (M ~ 7+) earthquakes near Charleston estimated at 500–600 years.	N
Dutton (1889)	4	Basic intensity data and mapping of liquefaction “craterlets” for the 1886 earthquake.	L, R, N	5	Observed greatest concentration of 1886 liquefaction “craterlets” at and north of Charleston.	N
Hu et al. (2002a)	3	Geotechnical data that form basis of Hu et al.’s (2002b) assessment of paleoearthquake magnitudes.	L, R, N	1	Background geotechnical data used by Hu et al. (2002b) to estimate geotechnical estimates of paleoearthquake magnitudes	N
Hu et al. (2002b)	3	Superseded by Leon et al. (2005) study, which includes two of the same three coauthors.	L, R, N	3	Geotechnical estimates of paleoearthquake magnitudes, based on Talwani and Schaeffer’s (2001) earthquake scenarios.	N

**Table C-6.1.2 Data Evaluation
Charleston RLME**

Identified Sources

Charleston RLME with alternatives: L: Local; R: Regional; N: Narrow

Data/References	Quality (1=low, 5=high)	Notes on Quality of Data	Source Considered	Used in SSC and Reliance Level (0=no, 5=high)	Discussion of Data Use	In GIS Database
Leon (2003)	3	Dissertation, relevant portions of which later published as and superseded by Leon et al. (2005).	L, R, N	3	Geotechnical estimates of paleoearthquake magnitudes. Assumes Talwani and Schaeffer's (2001) earthquake scenarios.	N
Leon et al. (2005)	4	Geotechnical magnitude estimates for Charleston paleoearthquakes generally lower than previously identified (see Hu et al. 2002b).	L, R, N	4	Geotechnical estimates of paleoearthquake magnitudes. Assumes Talwani and Schaeffer's (2001) earthquake scenarios.	N
Noller and Forman (1998)	3	Interpreted two or three paleoliquefaction events at Gapway Ditch site, where Amick, Gelinas, et al. (1990); Amick, Maurath, and Gelinas (1990); and Talwani and Schaeffer (2001) interpreted one paleoliquefaction event. No scale provided with exposure log.	L, R, N	3	Timing of paleoliquefaction events used to help constrain return period for large earthquakes at Charleston.	N

**Table C-6.1.2 Data Evaluation
Charleston RLME**

Identified Sources

Charleston RLME with alternatives: L: Local; R: Regional; N: Narrow

Data/References	Quality (1=low, 5=high)	Notes on Quality of Data	Source Considered	Used in SSC and Reliance Level (0=no, 5=high)	Discussion of Data Use	In GIS Database
Obermeier (1996b)	3	General overview of Charleston liquefaction and paleoliquefaction.	L, R, N	4	Large diameters (3+ m) of some prehistoric craters suggest these likely were caused by earthquakes “much stronger than M5 to 5.5.” (p. 350). Sandblow craters that formed roughly 600 and 1,250 yr BP extend along coast at least as far as 1886 features, suggesting that some prehistoric earthquakes likely may have been at least as large as 1886.	Y
Obermeier et al. (1989)	3	Description of liquefaction and paleoliquefaction feature size and spatial concentration are qualitative and not well documented, but taken as evidence for repeated large earthquakes located at or near Charleston.	L, R, N	4	Size and spatial concentration of both 1886 liquefaction and paleoliquefaction features are greatest near Charleston, and decrease with distance up and down the coast, despite similarities in liquefaction susceptibility throughout region. This indicates repeated large earthquakes located at or near Charleston.	N
Olson et al. (2005b)	5	Magnitude-bound relations calibrated for CEUS.	L, R, N	3	Magnitude-bound relations calibrated for CEUS. Used to help constrain source geometries.	N

**Table C-6.1.2 Data Evaluation
Charleston RLME**

Identified Sources

Charleston RLME with alternatives: L: Local; R: Regional; N: Narrow

Data/References	Quality (1=low, 5=high)	Notes on Quality of Data	Source Considered	Used in SSC and Reliance Level (0=no, 5=high)	Discussion of Data Use	In GIS Database
Talwani and Schaeffer (2001)	4	Paleoearthquake scenarios based on 1-sigma radiocarbon age constraints.	L, R, N	5	Tabulation of available paleoliquefaction data for Charleston region. Talwani and Schaeffer's (2001) 1-sigma radiocarbon age data were recalibrated to 2-sigma for use in CEUS SSC Project. Return period for large (M ~ 7+) earthquakes near Charleston estimated at 500–600 years.	N
Talwani et al. (2008)	2	Single undated paleoliquefaction feature does not provide any reliable constraints on timing, magnitude, or location of paleoearthquakes.	L, R, N	2	Paleoearthquake magnitude estimated at ~6.9 (scale unspecified) based on unspecified geotechnical analyses.	N
Weems and Obermeier (1990)	3	Early assessment of paleoliquefaction-based earthquake recurrence at Charleston, refined and superseded by more recent publications.	L, R, N	2	Describe evidence for three, and possibly four, middle to late Holocene earthquakes preserved in the geologic record as paleoliquefaction features, as well as evidence for events as old as 30,000 years.	N

**Table C-6.1.3 Data Evaluation
Cheraw Fault RLME**

**Identified Source
Cheraw fault**

Data/References	Quality (1=low, 5=high)	Notes on Quality of Data	Source Considered	Used in SSC and Reliance Level (0=no, 5=high)	Discussion of Data Use	In GIS Database
<i>Instrumental Seismicity</i>						
CEUS SSC earthquake catalog	5	Comprehensive catalog; includes magnitude conversions and uncertainty assessments.	Cheraw fault	0	No association of instrumental seismicity with the Cheraw fault.	Y
<i>Historical Seismicity</i>						
CEUS SSC earthquake catalog	5	Comprehensive catalog; includes magnitude conversions and uncertainty assessments.	Cheraw fault	0	No association of historical seismicity with the Cheraw fault.	Y
<i>Magnetic Anomaly</i>						
CEUS SSC magnetic anomaly data set	5	High-quality regional data	Cheraw fault	0	Cheraw fault not expressed as a distinct lineament in the magnetic anomaly map. General NE trend of the fault is subparallel to regional trends to the N and NW of the fault.	Y
<i>Gravity Anomaly</i>						
CEUS SSC gravity anomaly data set	5	High-quality regional data	Cheraw fault	0	Cheraw fault not imaged or apparent in the gravity data.	Y

**Table C-6.1.3 Data Evaluation
Cheraw Fault RLME**

**Identified Source
Cheraw fault**

Data/References	Quality (1=low, 5=high)	Notes on Quality of Data	Source Considered	Used in SSC and Reliance Level (0=no, 5=high)	Discussion of Data Use	In GIS Database
<i>Regional Geologic and Tectonic Maps</i>						
Scott et al. (1978)	4	Scale 1:250,000	Cheraw fault	0	Map source cited by Crone (1997) for bedrock fault. Not used directly for location of Cheraw RLME source geometry.	N
Sharps (1976)	4	Scale 1:250,000 Cited by Crone, Machette, Bradley, et al. (1997) as original map that identified the Sharps (1976) Cheraw fault.	Cheraw fault	0	Original map source cited by Crone (1997) for bedrock fault. Not used directly for location of Cheraw RLME source geometry.	N
<i>Local Geologic and Tectonic Maps</i>						
Petersen et al. (2008)	4	Source characterization parameters went through USGS community review process.	Cheraw fault	4	All parameters for Cheraw fault retained from 2002; fault modeled using a slip rate of 0.15 mm/yr based on data from last two events and a maximum magnitude of 7.0 ± 0.2 determined from the Wells and Coppersmith (1994) fault length relationship based on all slip types together. Fixed recurrence time of 17,400 years is used with truncated Gutenberg-Richter model from M 6.5 to 7.0. This yields a mean recurrence	N

**Table C-6.1.3 Data Evaluation
Cheraw Fault RLME**

**Identified Source
Cheraw fault**

Data/References	Quality (1=low, 5=high)	Notes on Quality of Data	Source Considered	Used in SSC and Reliance Level (0=no, 5=high)	Discussion of Data Use	In GIS Database
					time of 5,000 years for earthquakes with minimum magnitude of 6.5. Fault source parameters (2008 hazard maps) http://gldims.cr.usgs.gov/webapps/cfusion/Sites/c2002_search/search_fault_2002.cfm — Length: 44 km (27.3 mi.) Dip: 60°N Slip rate: 0.15 mm/yr Width: 17 km (10.6 mi.) Characteristic magnitude: 7 (based on Ellsworth (2003) relation. Characteristic rate: 1.15E-04.	
USGS National Hazard Mapping Project	5	Detailed summary of previous mapping and paleoseismic investigations on the Cheraw fault.	Cheraw fault	4	Trace is from 1:24,000-scale mapping (and interpretation of aerial photographs), transferred to a 1:250,000 topographic base (Crone, Machette, Bradley, et al., 1997). Fault source location (total length): 46.24 km (28.73 mi.; measured from Quaternary fault map database).	Y
USGS 10 m DEM	4	Resolution of 10 m data is sufficient to image the Quaternary active trace of the	Cheraw fault	4	Interpretation of 10 m DEM suggests that Cheraw fault may have surface expression beyond the length of fault source as defined in USGS Fault and Fold Database (source length used in	Y

**Table C-6.1.3 Data Evaluation
Cheraw Fault RLME**

**Identified Source
Cheraw fault**

Data/References	Quality (1=low, 5=high)	Notes on Quality of Data	Source Considered	Used in SSC and Reliance Level (0=no, 5=high)	Discussion of Data Use	In GIS Database
		Cheraw fault.			the 2008 National Seismic Hazard Mapping Program). A possible lineament (north-facing scarp) extends approximately 16–20 km (10–12.4 mi.) to NE of mapped end of Cheraw fault. A railroad lies adjacent to and just north of the scarp where it is best expressed, suggesting it may be modified or nontectonic in origin. Assuming lineament is tectonic, total length of fault source inferred from DEM is 62–66 km (38.5–41 mi.).	
<i>Regional Stress</i>						
CEUS SSC stress data set	5	Includes additional data points not shown on World Stress Map.	Cheraw fault	0	No new data points in SE Colorado near Cheraw fault.	Y
Heidbach et al. (2008) (World Stress Map)	3	Worldwide compilation of stress data (updated by CEUS SSC data set).	Cheraw fault	1	No nearby measurements to Cheraw fault. Normal sense of displacement on E-NE-trending fault is consistent with regional stress field.	Y
Zoback and Zoback (1991)	4	Comprehensive regional study that discusses stress data and identifies stress domains for the United	Cheraw fault	3	Regional stress data indicate that Cheraw fault is within the transition region between Cordilleran extension (Basin and Range and Rio Grande rift) and CEUS midplate stress (E-NE-directed maximum horizontal	N

**Table C-6.1.3 Data Evaluation
Cheraw Fault RLME**

**Identified Source
Cheraw fault**

Data/References	Quality (1=low, 5=high)	Notes on Quality of Data	Source Considered	Used in SSC and Reliance Level (0=no, 5=high)	Discussion of Data Use	In GIS Database
		States.			compressive stress). Normal faulting would be consistent with Cordilleran extension.	
<i>Tectonic Strain—Paleoseismicity</i>						
Crone (1997) Crone, Machette, Bradley, et al. (1997)	5	Detailed paleoseismic trenching and mapping investigation.	Cheraw fault	5	Provides detailed source characterization information: Style of faulting—inferred normal based on trench exposures. Length of fault—approximately 44 km (27.3 mi.) based on mapping and interpretation of aerial photograph. Timing of recent events—~8 ka, 12 ka, and 20–25 ka. Older events must have occurred before about 100 ka. Interpretation of amounts of vertical offset on the Cheraw fault— Most recent event: ~0.5–1.1 m (~1.6–3.6 ft.). Penultimate event: ~1.1–1.6 m (~1.6–5.2 ft.). Oldest event: ~1.5 m (4.9 ft.). Fault behavior—temporal clustering (relatively short time intervals of activity [e.g., 15–20 kyr] separated by long intervals of quiescence [e.g., 100 kyr])	N

**Table C-6.1.3 Data Evaluation
Cheraw Fault RLME**

**Identified Source
Cheraw fault**

Data/References	Quality (1=low, 5=high)	Notes on Quality of Data	Source Considered	Used in SSC and Reliance Level (0=no, 5=high)	Discussion of Data Use	In GIS Database
					<p>Avg. recurrence in active period—8 kyr</p> <p>Slip rate—long-term: ≤ 0.007 mm/yr (8 m [26.2 ft.]/1.2 Ma)</p> <p>Late Pleistocene-Holocene rate—0.14–0.18 mm/yr (determined by dividing the amount of offset [3.6 m, or 11.8 ft.] on oldest faulted deposits in trench by age of the deposits [20–25 ka])</p>	
Dr. A. Crone, USGS, electronic comm., April 21, 2010	4	Reconsideration of trenching data to better constrain uncertainties in number of paleoearthquakes.	Cheraw fault	4	Recurrence—Evaluation of number of paleoearthquakes recorded by stratigraphic and structural features in trench. Evidence for the penultimate event as presented by Crone, Machette, et al. (1997) not as definitive as evidence for earliest and latest events.	N

**Table C-6.1.4 Data Evaluation
Oklahoma Aulacogen RLME**

Identified Sources

Meers fault RLME with alternatives—localized and random distribution; Oklahoma Aulacogen Zone (OKA)

Data/References	Quality (1=low, 5=high)	Notes on Quality of Data	Source Considered	Used in SSC and Reliance Level (0=no, 5=high)	Discussion of Data Use	In GIS Database
<i>Instrumental Seismicity</i>						
Luza and Lawson (1993)	4	Data appear robust, but report does not contain comments on how many and which of the reported earthquakes are induced by or related to hydrocarbon exploration.	OKA and Meers fault	3	Reported earthquake depths are used to constrain seismogenic depth and fault depth.	N
<i>Magnetic Anomaly</i>						
CEUS SSC magnetic anomaly data set	4	High-quality regional data	OKA	4	Reviewed in defining geometry of aulacogen source zone. Extent of aulacogen was partially constrained by extent of associated magnetic anomaly.	N
<i>Gravity Anomaly</i>						
CEUS SSC gravity anomaly data set	4	High-quality regional data	OKA	4	Reviewed in defining geometry of aulacogen source zone. Extent of aulacogen was partially constrained by extent of associated gravity anomaly.	N

**Table C-6.1.4 Data Evaluation
Oklahoma Aulacogen RLME**

Identified Sources

Meers fault RLME with alternatives—localized and random distribution; Oklahoma Aulacogen Zone (OKA)

Data/References	Quality (1=low, 5=high)	Notes on Quality of Data	Source Considered	Used in SSC and Reliance Level (0=no, 5=high)	Discussion of Data Use	In GIS Database
<i>Seismic Reflection</i>						
Brewer (1982)	3	Presents only two raw reflection lines, which are poorly reproduced. Maps and interpreted cross section are more useful and considered of moderate quality.	OKA	3	Used to help define geometry of aulacogen source zone based on extent of faults within the Arbuckle-Wichita-Amarillo Uplift.	N
Brewer et al. (1983)	3	Presents only one raw reflection line, which is poorly reproduced. Maps and interpreted cross section are more useful and considered of moderate quality.	OKA	3	Used to help defining geometry of aulacogen source zone based on extent of faults associated with the Arbuckle-Wichita-Amarillo Uplift.	N
Good et al. (1983)	4	Presents interpreted COCORP seismic reflection line across the Meers fault and Oklahoma Aulacogen.	OKA and Meers fault	3	Used to help define N-S extent of the aulacogen and to help constrain dip of Meers fault at depth.	N
McConnell (1989)	3	Data considered of moderate quality for defining the dip of the Meers fault at depth.	Meers fault	4	Used to help constrain dip of fault at depth.	N

**Table C-6.1.4 Data Evaluation
Oklahoma Aulacogen RLME**

Identified Sources

Meers fault RLME with alternatives—localized and random distribution; Oklahoma Aulacogen Zone (OKA)

Data/References	Quality (1=low, 5=high)	Notes on Quality of Data	Source Considered	Used in SSC and Reliance Level (0=no, 5=high)	Discussion of Data Use	In GIS Database
Miller et al. (1990)	4	Presents shallow (<200 m) interpretations of seismic reflection data across the Meers fault.	Meers fault	4	Used to help constrain shallow dip of fault.	N
<i>Regional Geologic and Tectonic Maps</i>						
Ham et al. (1964)	3	Data considered of moderate quality with respect to accuracy and completeness of identifying faults associated with Arbuckle-Wichita-Amarillo Uplift.	OKA	5	Used to help define geometry of aulacogen source zone based on extent of faults associated with the Arbuckle-Wichita-Amarillo Uplift.	N
Keller and Stephenson (2007)	3	Data considered of moderate quality with respect to outlining extent of the aulacogen based on gravity anomaly data.	OKA	3	Used in defining geometry of aulacogen source zone based on the interpreted extent of aulacogen from gravity data.	N
McConnell (1989)	2	Data considered of moderate to poor quality because no details are given with respect to what data constrains the Meers fault dip.	Meers fault	4	Used to help constrain dip of fault.	N

**Table C-6.1.4 Data Evaluation
Oklahoma Aulacogen RLME**

Identified Sources

Meers fault RLME with alternatives—localized and random distribution; Oklahoma Aulacogen Zone (OKA)

Data/References	Quality (1=low, 5=high)	Notes on Quality of Data	Source Considered	Used in SSC and Reliance Level (0=no, 5=high)	Discussion of Data Use	In GIS Database
Texas Bureau of Economic Geology (1997)	3	Data considered of moderate quality with respect to accuracy and completeness of identifying faults associated with Arbuckle-Wichita-Amarillo Uplift.	OKA	5	Used to help define geometry of aulacogen source zone based on extent of faults associated with the Arbuckle-Wichita-Amarillo Uplift.	N
Local Geologic and Tectonic Maps						
Cetin (2003)	2	Proposes a NW extension of Meers fault beyond that previously recognized. Data considered of poor quality because of lack of supporting evidence.	Meers fault	5	Used to define potential NW extension of Meers fault.	N
Ramelli and Slemmons (1986)	5	Data considered of good quality for describing the geomorphic expression of fault trace.	Meers fault	3	Considered in defining extent of the fault and the Quaternary history of the fault.	N
Ramelli and Slemmons (1990)	5	Data considered of good quality with respect to defining extent of fault.	Meers fault	3	Considered in defining extent of fault.	N

**Table C-6.1.4 Data Evaluation
Oklahoma Aulacogen RLME**

Identified Sources

Meers fault RLME with alternatives—localized and random distribution; Oklahoma Aulacogen Zone (OKA)

Data/References	Quality (1=low, 5=high)	Notes on Quality of Data	Source Considered	Used in SSC and Reliance Level (0=no, 5=high)	Discussion of Data Use	In GIS Database
Ramelli et al. (1987)	5	Fault trace is digitized in USGS Quaternary Fault and Fold Database; and this USGS version is used to define fault trace. Data considered of good quality.	Meers fault	5	Used to define trace of Holocene active fault.	N
<i>Paleoseismicity</i>						
Crone and Luza (1990)	4	Data considered of moderate quality with respect to defining characteristics of fault rupture (e.g., surface offset, fault dip, horizontal-to-vertical slip ratio).	Meers fault	2	Considered in defining characteristics of fault rupture.	N
Swan et al. (1993)	4	Data considered of good quality with respect to identifying rupture events on the fault and dates constraining timing of those ruptures. Data considered of moderate quality in defining characteristics of those ruptures (e.g., surface offsets).	Meers fault	5	Used to define recurrence rates and earthquake magnitudes from fault slip estimates.	N

**Table C-6.1.4 Data Evaluation
Oklahoma Aulacogen RLME**

Identified Sources

Meers fault RLME with alternatives—localized and random distribution; Oklahoma Aulacogen Zone (OKA)

Data/References	Quality (1=low, 5=high)	Notes on Quality of Data	Source Considered	Used in SSC and Reliance Level (0=no, 5=high)	Discussion of Data Use	In GIS Database
<i>Other</i>						
Crone (1994)	5	Data considered of good quality with respect to summarizing and evaluating available data on Meers fault.	Meers fault	3	Considered in evaluating robustness and quality of available data on Meers fault.	N
Wheeler and Crone (2001)	5	Data considered of good quality with respect to analyzing available data concerning Meers fault.	Meers fault	3	Considered in evaluating robustness and quality of available data on Meers fault.	Y

Table C-6.1.5 Data Evaluation
Reelfoot Rift–New Madrid Fault System RLMEs

Identified Sources

New Madrid North (NMN); New Madrid South (NMS); Reelfoot Thrust fault (RFT)

Data/References	Quality (1=low, 5=high)	Notes on Quality of Data	Source Considered	Used in SSC and Reliance Level (0=no, 5=high)	Discussion of Data Use	In GIS Database
<i>Instrumental Seismicity</i>						
CEUS SSC earthquake catalog	5	Comprehensive catalog; includes magnitude conversions and uncertainty assessments.	NMN, NMS, and RFT	3	Provides constraints on fault location and geometry.	Y
Chiu et al. (1992)	4	Publication discussing results of Portable Array for Numerical Data Acquisition (PANDA) survey. Provides detailed discussion of seismicity in New Madrid seismic zone (NMSZ).	NMN, NMS, RFT	5	Focal depth—Seismic activity in central NMSZ occurs continuously between ~5 and 14 km (3.1 and 8.7 mi.) depth. Seismicity illuminates fault zones. RFT geometry—Two NE-trending vertical segments are concentrated about a plane that dips at ~31°SW; a separate zone to the SE of axial zone defines a plane that dips at ~48°SW; projects to surface near Reelfoot Lake and Lake County uplift.	N
<i>Historical Seismicity</i>						
Dr. William Bakun (USGS, electronic comm., February 3, 2010)	4	Electronic comm. confirming 2004 magnitude estimates based on intensity for 1811-1812 earthquakes.	NMN, NMS, RFT	5	Magnitude of 1811-1812 earthquakes used to constrain Mmax for NMFS RLMEs (see Table 6.1.5-2).	N

Table C-6.1.5 Data Evaluation
Reelfoot Rift–New Madrid Fault System RLMEs

Identified Sources

New Madrid North (NMN); New Madrid South (NMS); Reelfoot Thrust fault (RFT)

Data/References	Quality (1=low, 5=high)	Notes on Quality of Data	Source Considered	Used in SSC and Reliance Level (0=no, 5=high)	Discussion of Data Use	In GIS Database
Exelon ESP (2004) (includes estimates based on Johnston, 1996b; Hough et al. 2000; Bakun and Hopper, 2004a; pers. comm. from Drs. Johnston, Hough, and Bakun)	3	Compilation and update (2003–2004 time frame) of best estimates of size of 1811-1812 earthquake sequence. NRC reviewed assessment for Early Site Permit Application.	NMN, NMS, and RFT	5	Evaluation of intensity data for the 1811-1812 sequences provides basis for assessing magnitude of these events, which are considered typical of prehistoric events based on similar sizes and distribution of paleoliquefaction features (Tuttle, Schweig, et al., 2002; see Table 6.1.5-2).	N
Hough and Page (2011)	3	Presents magnitude estimates based on assessments by multiple experts.	NMN, NMS, RFT	5	Magnitude of 1811-1812 earthquakes used to constrain Mmax for NMFS RLMEs— Revisions to previous estimates (See Table 6.1.5-2).	N
Dr. Arch Johnston (CERI, pers. comm., February 16, 2010)	2	Telephone conversation—New studies to evaluate size of 1811-1812 earthquakes are being considered but have not yet started.	NMN, NMS, and RFT	4	Estimated sizes of 1811-1812 earthquakes as reported in EGC ESP (2004) study have not been revised.	N
Seismic Reflection						
Interpretation of seismic-reflection data has been integrated with other geologic, geophysical, and seismological data as reported in publications to define the structures within the Reelfoot rift. Specific lines not used directly in this study.						

Table C-6.1.5 Data Evaluation
Reelfoot Rift–New Madrid Fault System RLMEs

Identified Sources

New Madrid North (NMN); New Madrid South (NMS); Reelfoot Thrust fault (RFT)

Data/References	Quality (1=low, 5=high)	Notes on Quality of Data	Source Considered	Used in SSC and Reliance Level (0=no, 5=high)	Discussion of Data Use	In GIS Database
<i>Regional Geologic and Tectonic Maps</i>						
Csontos et al. (2008)	3	Structure-contour map of the top of basement showing subbasins and bounding NE- and SE-striking faults. Due to projection of the map showing interpretations of basement faults, the locations are considered approximate.	NMS and RFT	5	Geometry and style of faulting— Interpretation of basement structures and reactivation of faults (e.g., RFT as inverted basement normal fault).	N
<i>Local Geologic and Tectonic Maps</i>						
Cramer (2001)	4	Publication scale map (Figure 3) with registration for digitization.	NMN, NMS, and RFT	2	Used to help constrain locations of alternative segments of the NMFS.	N
Guccione (2005) and Guccione et al. (2005)	4	Includes detailed maps showing offset geomorphic features.	NMS	4	Used to constrain location of Bootheel fault (previously referred to as the Bootheel lineament).	N
Johnston and Schweig (1996)	3	Small-scale line drawings of faults interpreted to be sources of 1811-1812 events.	NMN, NMS, and RFT	4	Interpretation formed the initial starting basis for the delineation of geometries for the New Madrid fault system sources.	Y

Table C-6.1.5 Data Evaluation
Reelfoot Rift–New Madrid Fault System RLMEs

Identified Sources

New Madrid North (NMN); New Madrid South (NMS); Reelfoot Thrust fault (RFT)

Data/References	Quality (1=low, 5=high)	Notes on Quality of Data	Source Considered	Used in SSC and Reliance Level (0=no, 5=high)	Discussion of Data Use	In GIS Database
Mueller and Pujol (2001)	4	Detailed structure-contour map of fault plane (Figure 3).	RFT	4	Downdip geometry and depth of seismogenic crust—Structure-contour map of Reelfoot blind thrust.	N
Van Arsdale et al. (1999)	4	Publication scale maps—good registration for digitization (Figures 1 and 2).	RFT	5	Used to define the SE segment of the Reelfoot thrust fault.	N
Wheeler et al. (1994)	4	Detailed compilation map, USGS Miscellaneous Investigations Map.	NMS	3	Locations of subsurface faults—Cottonwood Grove fault, Ridgely fault, unnamed fault west of Cottonwood Grove fault.	N
Geodetic Strain						
Calais et al. (2006)	4	Two independent geodetic solutions from close to 300 continuous GPS stations.	NMN, NMS, and RFT	4	Based on observation that there is no detectable residual motion in the NMSZ at the 95% confidence level, some weight is assigned to the model that the NMFS is “out of the cluster.”	N

Table C-6.1.5 Data Evaluation
Reelfoot Rift–New Madrid Fault System RLMEs

Identified Sources

New Madrid North (NMN); New Madrid South (NMS); Reelfoot Thrust fault (RFT)

Data/References	Quality (1=low, 5=high)	Notes on Quality of Data	Source Considered	Used in SSC and Reliance Level (0=no, 5=high)	Discussion of Data Use	In GIS Database
Calais and Stein (2009)	5	Presents current results (through 2008) of GPS measurements.	NMN, NMS, and RFT	4	Temporal clustering—Conclusion of paper suggests that the recurrence rate estimated from seismicity in NMSZ is consistent with rates suggested by geodetic measurements. This supports “out-of-cluster” model.	N
Smalley et al. (2005)	4	Provides discussion of possible mechanisms to explain local but not regional geodetic signal.	NMN, NMS, and RFT	3	Temporal clustering issue—Evidence for ongoing strain across RFT and strike-slip fault zone; no apparent far-field signature. Notes that regardless of geodetic results, the challenge remains to reconcile geodetic observations with the detailed geological evidence available for repeated large earthquakes within Central United States, and that the cause of such earthquakes is not well understood.	N
Regional Stress						
Forte et al. (2007)	3	Regional analysis	NMN, NMS, and RFT	1	Provides rationale for concentrating seismic stress in the vicinity of the Reelfoot rift–NMSZ.	N

Table C-6.1.5 Data Evaluation
Reelfoot Rift–New Madrid Fault System RLMEs

Identified Sources

New Madrid North (NMN); New Madrid South (NMS); Reelfoot Thrust fault (RFT)

Data/References	Quality (1=low, 5=high)	Notes on Quality of Data	Source Considered	Used in SSC and Reliance Level (0=no, 5=high)	Discussion of Data Use	In GIS Database
Grana and Richardson (1996)	4	Regional analysis, models the rift pillow in New Madrid region.	NMN, NMS, and RFT)	3	Temporal clustering—Modeling indicates that stresses from the load of the rift pillow may still be present in the upper crust and may still play a role in present-day deformation. This supports “in-cluster” model.	N
Li et al. (2009)	3	3-D viscoelasto-plastic finite-element model addresses generic issues of spatiotemporal variations in seismicity in intraplate regions.	NMN, NMS, and RFT	2	Temporal clustering—Supports migration of seismicity within NMSZ (out of cluster model). Model replicates some of the spatiotemporal complexity of clustered, episodic, and migrating intraplate earthquakes. Time-scale-dependent spatiotemporal patterns of intraplate seismicity support the suggestions that seismicity patterns observed from short-term seismic records may not reflect the long-term patterns of intraplate seismicity.	N
Tectonic Strain						

Table C-6.1.5 Data Evaluation
Reelfoot Rift–New Madrid Fault System RLMEs

Identified Sources

New Madrid North (NMN); New Madrid South (NMS); Reelfoot Thrust fault (RFT)

Data/References	Quality (1=low, 5=high)	Notes on Quality of Data	Source Considered	Used in SSC and Reliance Level (0=no, 5=high)	Discussion of Data Use	In GIS Database
Hildenbrand and Hendricks (1995)	4	Detailed discussion of interpretations of geopotential data sets.	NMS	2	Temporal clustering—Limit of long-term cumulative deformation—NW-trending features related to South-Central magnetic lineament (SCML) and Paducah gravity lineament (PGL) cross Reelfoot graben with no substantial lateral offsets, thus limiting the amount of lateral movement along axial faults of Reelfoot graben since formation of these features.	N
Van Arsdale (2000)	4	Provides evidence for varying slip rate over time.	RFT	2	Temporal clustering—Geologic observations from interpretation of seismic profiles indicate that cumulative post-Late Eocene slip on structures in the NMSZ is low.	N
<i>Focal Mechanisms</i>						
Herrmann and Ammon (1997)	4	Well-constrained focal mechanisms.	NMFS	3	Seismogenic depth—focal mechanisms show depths of up to 16 km (10 mi.) for earthquakes in Reelfoot rift.	N

Table C-6.1.5 Data Evaluation
Reelfoot Rift–New Madrid Fault System RLMEs

Identified Sources

New Madrid North (NMN); New Madrid South (NMS); Reelfoot Thrust fault (RFT)

Data/References	Quality (1=low, 5=high)	Notes on Quality of Data	Source Considered	Used in SSC and Reliance Level (0=no, 5=high)	Discussion of Data Use	In GIS Database
Shumway (2008)	4	Earthquakes in the NE NMSZ were relocated using a velocity model of Mississippi embayment with appropriate depths to bedrock beneath seismic stations.	NMN	4	NMN long geometry—This shows that this part of the NE NMSZ is influenced by the same fault pattern and stress regime as NMN fault, may be an extension of NMSZ, and therefore may represent alternate locations of January 23, 1812, rupture.	N
Zoback (1992)	4	Well-constrained focal mechanisms.	NMFS	3	Style of faulting in Reelfoot rift—Four focal mechanisms show predominantly strike-slip motion.	N
<i>Paleoseismicity</i>						
CEUS SSC paleoliquefaction database (includes information from Tuttle, 2001; Tuttle, Schweig, et al., 2002, 2006)	5	Comprehensive database, peer-reviewed, includes uncertainties in timing of paleoliquefaction events).	NMN, NMS, and RFT	5	Recurrence—Provides information on “in cluster” recurrence interval for RFT.	Y
Exelon (2004) (includes information from Tuttle, 2001; Tuttle, Schweig, et al., 2002)	4	Comprehensive database; includes published and unpublished data.	NMN, NMS, and RFT	1	Recurrence—Superseded by CEUS SSC paleoliquefaction database.	Y

Table C-6.1.5 Data Evaluation
Reelfoot Rift–New Madrid Fault System RLMEs

Identified Sources

New Madrid North (NMN); New Madrid South (NMS); Reelfoot Thrust fault (RFT)

Data/References	Quality (1=low, 5=high)	Notes on Quality of Data	Source Considered	Used in SSC and Reliance Level (0=no, 5=high)	Discussion of Data Use	In GIS Database
Holbrook et al. (2006)	4	Detailed analysis of geomorphic indicators of Holocene deformation in NMSZ.	RFT	4	Recurrence—Provides information on “out of cluster” recurrence interval for RFT.	N
Kelson et al. (1996)	5	Detailed and well-documented paleoseismic investigation of surface deformation related to paleoearthquakes on RFT.	RFT	3	Recurrence—Basis for estimating timing and recurrence intervals for RFT. Dates of earthquakes in general agreement with paleoliquefaction data.	N

Table C-6.1.6 Data Evaluation
Reelfoot Rift–Eastern Margin Fault(s) RLMEs

Identified Sources

Reelfoot Rift–Eastern Rift Margin (ERM) RLMEs

Eastern Reelfoot Rift Margin fault north (ERM-N)*; Eastern Reelfoot Rift Margin fault south (ERM-S)*; Eastern Rift Margin fault south–river (fault) picks (ERM-RP); and Eastern Rift Margin south–Crittenden County fault zone (ERM-SCC)

Data/References	Quality (1=low, 5=high)	Notes on Quality of Data	Source Considered	Used in SSC and Reliance Level (0=no, 5=high)	Discussion of Data Use	In GIS Database
<i>Instrumental Seismicity</i>						
CEUS SSC earthquake catalog	5	Comprehensive catalog; includes magnitude conversions and uncertainty assessments.	ERM-S	1	Reviewed for alignment of microseismicity.	Y
Chiu et al. (1997)	4	Detailed analysis of seismicity along SE margin of Reelfoot rift.	ERM-S	3	Analysis of seismicity suggests there is an active fault source along the SE flank of the Reelfoot rift.	N
<i>Historical Seismicity</i>						
Hough and Martin (2002)	4	Analysis of sparse intensity data for a large aftershock of the 1811 earthquake.	ERM-S	2	Evidence for active fault along ERM—Aftershock of December 1811 NMSZ earthquake (NM1-B)— M 6.1 ± 0.2, location of event not well constrained, but probably beyond the southern end of the NMSZ, near Memphis, Tennessee (within the SW one-third to one-half of the band of seismicity identified by Chiu et al. [1997]).	N

Table C-6.1.6 Data Evaluation
Reelfoot Rift—Eastern Margin Fault(s) RLMEs

Identified Sources

Reelfoot Rift—Eastern Rift Margin (ERM) RLMEs

Eastern Reelfoot Rift Margin fault north (ERM-N)*; Eastern Reelfoot Rift Margin fault south (ERM-S)*; Eastern Rift Margin fault south—river (fault) picks (ERM-RP); and Eastern rift margin south—Crittenden County fault zone (ERM-SCC)

Data/References	Quality (1=low, 5=high)	Notes on Quality of Data	Source Considered	Used in SSC and Reliance Level (0=no, 5=high)	Discussion of Data Use	In GIS Database
<i>Magnetic Anomaly</i>						
CEUS SSC magnetic anomaly data set	5	High-quality regional data.	ERM zones	2	Geometry—The fault zones coincide with the eastern margin of the rift, which is marked by a change from low values (within the graben) to higher magnetic values. Geopotential anomalies, however, provided less resolution than surface data (i.e., surface expression of faulting, topographic lineament, trench exposures) for locating the zone of recent faulting.	Y
Hildenbrand (1982)	4	Analysis based on closely spaced truck-mounted magnetometer survey.	ERM zones	4	Geometry—Width of zone of faulting associated with the rift margin. Eastern Reelfoot rift margin is interpreted to be a 5.5 km (3.4 mi.) wide zone in which magnetic basement has an average dip of 20°NW into the graben.	N

Table C-6.1.6 Data Evaluation
Reelfoot Rift–Eastern Margin Fault(s) RLMEs

Identified Sources

Reelfoot Rift–Eastern Rift Margin (ERM) RLMEs

Eastern Reelfoot Rift Margin fault north (ERM-N)*; Eastern Reelfoot Rift Margin fault south (ERM-S)*; Eastern Rift Margin fault south–river (fault) picks (ERM-RP); and Eastern Rift Margin south–Crittenden County fault zone (ERM-SCC)

Data/References	Quality (1=low, 5=high)	Notes on Quality of Data	Source Considered	Used in SSC and Reliance Level (0=no, 5=high)	Discussion of Data Use	In GIS Database
<i>Gravity Anomaly</i>						
CEUS SSC gravity anomaly data set	5	High-quality regional data.	ERM RLMEs	0	Gravity anomaly data did not provide good resolution for delimiting the boundaries of the fault zone.	Y
<i>Seismic Reflection</i>						
Cox et al. (2006)	4	Published interpretations of high-resolution S-wave seismic profile (selected portions of uninterpreted profiles provided).	ERM-N and ERM-S	5	Geometry—Seismic profiles (shallow S-wave, electrical profiles) collected at paleoseismic sites are used to identify faults.	N
Luzietti et al. (1992)	4	Interpretation of good-quality high-resolution (Mini-Sosie) seismic data that show stratigraphy down to 1.2 km (0.7 mi.); (selected portions of uninterpreted profiles provided).	ERM-SCC	5	Geometry and activity of fault source—Evidence for reactivation of the Crittenden County fault zone in Pleistocene to possibly Holocene time.	N

Table C-6.1.6 Data Evaluation
Reelfoot Rift—Eastern Margin Fault(s) RLMEs

Identified Sources

Reelfoot Rift—Eastern Rift Margin (ERM) RLMEs

Eastern Reelfoot Rift Margin fault north (ERM-N)*; Eastern Reelfoot Rift Margin fault south (ERM-S)*; Eastern Rift Margin fault south—river (fault) picks (ERM-RP); and Eastern rift margin south—Crittenden County fault zone (ERM-SCC)

Data/References	Quality (1=low, 5=high)	Notes on Quality of Data	Source Considered	Used in SSC and Reliance Level (0=no, 5=high)	Discussion of Data Use	In GIS Database
Beatrice Magnani (CERI) unpublished data Magnani et al. (2009)	3	Preliminary results of location of fault picks provided as PDF.	ERM-RP	4	Geometry and activity—This data provided the basis for the location of the alternative segment defined by seismic data (ERM-RP). Connection of the three localities along the river seismic survey where recent faulting was observed suggest that there may be an alternative, more northerly trending fault along SE margin of rift zone.	N
Odum et al. (2010)	4	Reinterpretation of a seismic-reflection profile across the scarp at Meeman-Shelby Forest State Park 25 km north of Memphis, Tennessee.	ERM-S	2	Figures 1 and 7 show revised orientation of Meeman-Shelby fault (MSF) and relationship to Joiner Ridge. This alternative geometry for the MSF is not modeled directly as part of the RLME due to lack of information regarding timing and recent activity on the MSF. Geometry—Figure 3 is used to define the limits of the zones associated with the eastern Reelfoot rift margin.	N

Table C-6.1.6 Data Evaluation
Reelfoot Rift–Eastern Margin Fault(s) RLMEs

Identified Sources

Reelfoot Rift–Eastern Rift Margin (ERM) RLMEs

Eastern Reelfoot Rift Margin fault north (ERM-N)*; Eastern Reelfoot Rift Margin fault south (ERM-S)*; Eastern Rift Margin fault south–river (fault) picks (ERM-RP); and Eastern Rift Margin south–Crittenden County fault zone (ERM-SCC)

Data/References	Quality (1=low, 5=high)	Notes on Quality of Data	Source Considered	Used in SSC and Reliance Level (0=no, 5=high)	Discussion of Data Use	In GIS Database
Parrish and Van Arsdale (2004)	4	Published interpretations of seismic profile (selected portions of uninterpreted profiles provided).	ERM-S	3	Geometry—Interpretation of major basement faults and Tertiary faults along southeastern margin of Reelfoot rift—used in conjunction with paleoseismic investigations to identify location of fault source.	N
Williams et al. (2001)	4	Published interpretations of a seismic-reflection profile across the scarp at the Meeman-Shelby Forest State Park 25 km north of Memphis, Tennessee. Revised interpretation provided in Odum et al. (2010).	ERM-S	2	Geometry—Meeman-Shelby fault (MSF) pick lies ~5 km (3 mi.) east of the magnetically defined southeastern margin of the Reelfoot rift. Is similar to the Crittenden County fault zone (CCFZ) in seismic profiles (up to the west). Seismic data suggest that the ERM-S may subparallel the CCFZ. Possible continuation of fault on a N33°E trend based on similar structure observed in a proprietary industry seismic line 33 km (20.5 mi.) to the northeast.	N

Table C-6.1.6 Data Evaluation
Reelfoot Rift—Eastern Margin Fault(s) RLMEs

Identified Sources

Reelfoot Rift—Eastern Rift Margin (ERM) RLMEs

Eastern Reelfoot Rift Margin fault north (ERM-N)*; Eastern Reelfoot Rift Margin fault south (ERM-S)*; Eastern Rift Margin fault south—river (fault) picks (ERM-RP); and Eastern rift margin south—Crittenden County fault zone (ERM-SCC)

Data/References	Quality (1=low, 5=high)	Notes on Quality of Data	Source Considered	Used in SSC and Reliance Level (0=no, 5=high)	Discussion of Data Use	In GIS Database
<i>Local Geologic and Tectonic Maps</i>						
Cox et al. (2006)	4	Provides detailed maps of paleoseismic localities.	ERM-S and ERM-N	5	Geometry—Figures 1, 4, and 8 show locations of seismic lines and trenches used to constrain location of fault source. Used to locate detailed paleoseismic investigation sites and ERM-S and ERM-N fault source.	N
Crone (1992)	4	Peer-reviewed publication.	CCFZ	4	Geometry—Figure 2 used to locate the CCFZ.	N
<i>Regional Stress</i>						
CEUS SSC stress data set	5	Most comprehensive data set available for CEUS.	ERM-S and ERM-N	2	Style of faulting—Right-lateral slip on eastern margin fault sources is consistent with stress indicators that show general E-W trend to the maximum horizontal compression axis.	Y

Table C-6.1.6 Data Evaluation
Reelfoot Rift–Eastern Margin Fault(s) RLMEs

Identified Sources

Reelfoot Rift–Eastern Rift Margin (ERM) RLMEs

Eastern Reelfoot Rift Margin fault north (ERM-N)*; Eastern Reelfoot Rift Margin fault south (ERM-S)*; Eastern Rift Margin fault south–river (fault) picks (ERM-RP); and Eastern Rift Margin south–Crittenden County fault zone (ERM-SCC)

Data/References	Quality (1=low, 5=high)	Notes on Quality of Data	Source Considered	Used in SSC and Reliance Level (0=no, 5=high)	Discussion of Data Use	In GIS Database
<i>Tectonic Strain</i>						
Cox et al. (2001a)	3	Summary of paleoseismic investigations and overall structural model for active faults along the SE margin of the Reelfoot rift. Trench log details not sufficient to evaluate postulated offset channel.	ERM-S and ERM-N	4	Geometry—Total length of Eastern Rift Margin faults: 150 km (93.2 mi.). Activity—Topographic expression—Linear topographic scarp.	N
<i>Focal Mechanisms</i>						
Chiu et al. (1997)	4	Provides detailed analysis of focal mechanisms.	ERM-S	4	Style of faulting—The style of faulting along the southeast margin of the Reelfoot rift inferred from analysis of is complex with the dominant pattern being right-lateral strike-slip with reverse movement. Seismogenic crustal thickness—Nine out of 10 well-constrained focal depths are ≤17.3 km. One deeper earthquake is at 22.8 km.	N

Table C-6.1.6 Data Evaluation
Reelfoot Rift—Eastern Margin Fault(s) RLMEs

Identified Sources

Reelfoot Rift—Eastern Rift Margin (ERM) RLMEs

Eastern Reelfoot Rift Margin fault north (ERM-N)*; Eastern Reelfoot Rift Margin fault south (ERM-S)*; Eastern Rift Margin fault south—river (fault) picks (ERM-RP); and Eastern rift margin south—Crittenden County fault zone (ERM-SCC)

Data/References	Quality (1=low, 5=high)	Notes on Quality of Data	Source Considered	Used in SSC and Reliance Level (0=no, 5=high)	Discussion of Data Use	In GIS Database
<i>Paleoseismicity</i>						
CEUS SSC paleoliquefaction database	5	Most comprehensive database of paleolique- faction for CEUS.	ERM-S and ERM-N	4	Constraints on estimated size of prehistoric earthquake— Evaluation of potential 80 km (50 mi.) rupture at ~2,500 yr BP. There are no known paleoliquefaction features of this age observed in rivers in western Tennessee. Location and age of paleoliquefaction in western Kentucky that could possibly be associated with a rupture on the ERM-N: 11,300 yr BP ± 200 yr.	Y

Table C-6.1.6 Data Evaluation
Reelfoot Rift–Eastern Margin Fault(s) RLMEs

Identified Sources

Reelfoot Rift–Eastern Rift Margin (ERM) RLMEs

Eastern Reelfoot Rift Margin fault north (ERM-N)*; Eastern Reelfoot Rift Margin fault south (ERM-S)*; Eastern Rift Margin fault south–river (fault) picks (ERM-RP); and Eastern Rift Margin south–Crittenden County fault zone (ERM-SCC)

Data/References	Quality (1=low, 5=high)	Notes on Quality of Data	Source Considered	Used in SSC and Reliance Level (0=no, 5=high)	Discussion of Data Use	In GIS Database
Cox, Van Arsdale, and Larsen (2002)	3	NEHRP report— Interpretation of trenching and boring data with some constraints on timing from radiocarbon dates. Trench log details not sufficient to evaluate postulated offset channel.	ERM-S and ERM-N	4	<p>Recurrence and style of faulting— Used to evaluate timing of events, recurrence intervals, slip rate, and components of slip (H and V).</p> <p>Confirms that the SE Reelfoot rift margin is a fault zone with multiple high-angle faults and associated folding based on shallow seismic profiles and paleoseismological investigations.</p> <p>Stratigraphic and structural relationships in trench exposure at a site near Porter Gap are interpreted to show 8–15 m (26.2– 49.2 ft.) of right-lateral offset of a late Wisconsinan paleo-channel (~20 ka)., suggesting average slip rate of between 0.85 and 0.37 mm/year.</p> <p>Evidence for an earthquake ca. 2,500–2,000 yr BP on SE Reelfoot rift margin that ruptured ≥ 80 km from Shelby County (15–25 km [9.3–15.5 mi.] north of Memphis metropolitan area) to Porter Gap (just south of intersection with the RF).</p>	N

Table C-6.1.6 Data Evaluation
Reelfoot Rift—Eastern Margin Fault(s) RLMEs

Identified Sources

Reelfoot Rift—Eastern Rift Margin (ERM) RLMEs

Eastern Reelfoot Rift Margin fault north (ERM-N)*; Eastern Reelfoot Rift Margin fault south (ERM-S)*; Eastern Rift Margin fault south—river (fault) picks (ERM-RP); and Eastern rift margin south—Crittenden County fault zone (ERM-SCC)

Data/References	Quality (1=low, 5=high)	Notes on Quality of Data	Source Considered	Used in SSC and Reliance Level (0=no, 5=high)	Discussion of Data Use	In GIS Database
Cox et al. (2006)	3	Interpretation of trenching and boring data with some constraints on timing from radiocarbon dates. Trench log details not sufficient to evaluate postulated offset channel.	ERM-S and ERM-N	5	<p>Recurrence and style of faulting—Used to evaluate timing of events, recurrence intervals, slip rate, and components of slip (H and V).</p> <p>Age constraints from paleoseismic investigations at Shelby County and at Porter Gap site are consistent with an earthquake ca. 2,500–2,000 years ago (most recent event) that ruptured ≥ 80 km (50 mi.).</p> <p>Late Wisconsinan and Holocene faulting along the SE rift margin fault system observed adjacent to hanging wall of Reelfoot thrust, but only Wisconsinan faulting is noted adjacent to footwall of the thrust. It is hypothesized that the NE segment of the SE rift margin turned off in Holocene when Reelfoot stepover thrust turned on.</p>	N

Table C-6.1.6 Data Evaluation
Reelfoot Rift–Eastern Margin Fault(s) RLMEs

Identified Sources

Reelfoot Rift–Eastern Rift Margin (ERM) RLMEs

Eastern Reelfoot Rift Margin fault north (ERM-N)*; Eastern Reelfoot Rift Margin fault south (ERM-S)*; Eastern Rift Margin fault south–river (fault) picks (ERM-RP); and Eastern Rift Margin south–Crittenden County fault zone (ERM-SCC)

Data/References	Quality (1=low, 5=high)	Notes on Quality of Data	Source Considered	Used in SSC and Reliance Level (0=no, 5=high)	Discussion of Data Use	In GIS Database
Tuttle et al. (2006)	4	Detailed discussion of paleoliquefaction features near Marianna, Arkansas.	ERM-S	2	<p>Timing and recurrence of large-magnitude earthquakes—Based on radiocarbon dating liquefaction features at the Daytona Beach and St. Francis sites near Marianna, Arkansas, formed about 3500 BC and 4800 BC (5,000 and 7,000 years ago), respectively. Marianna sand blows are similar in size to NMSZ.</p> <p>Several faults in Marianna area (including eastern Reelfoot rift margin [ERRM], White River fault zone [WRFZ], and Big Creek fault zone [BCFZ]) are thought to be active based on apparent influence on local topography and hydrography. ERRM appears to be most likely source of very large earthquakes during the middle Holocene. (See also Section 6.1.7, Marianna [MAR] RLME.)</p>	Y

* ERM-N and ERM-S are included in the Big Creek fault as defined by Fisk (1944).

**Table C-6.1.7 Data Evaluation
Reelfoot Rift–Marianna RLME**

**Identified Source
Marianna zone (MAR)**

Data/References	Quality (1=low, 5=high)	Notes on Quality of Data	Source Considered	Used in SSC and Reliance Level (0=no, 5=high)	Discussion of Data Use	In GIS Database
<i>Instrumental Seismicity</i>						
CEUS SSC earthquake catalog	5	Comprehensive catalog; includes magnitude conversions and uncertainty assessments.	MAR	1	Reviewed for alignment of microseismicity, seismicity scattered.	Y
<i>Magnetic Anomaly</i>						
CEUS SSC magnetic anomaly data set	5	High-quality regional data.	MAR	0	Location of RLME source is not based on magnetic anomaly map.	Y
<i>Gravity Anomaly</i>						
CEUS SSC gravity anomaly data set	5	High-quality regional data.	MAR	0	Location of RLME source is not based on gravity anomaly map.	Y
<i>Local Geologic and Tectonic Maps</i>						
Csontos et al. (2008)	3	Due to projection of the map showing interpretations of basement faults, the locations are considered approximate.	MAR	2	Potential fault sources for Marianna paleoliquefaction features. Considered in evaluation of the orientation and style of faulting.	N

**Table C-6.1.7 Data Evaluation
Reelfoot Rift–Marianna RLME**

**Identified Source
Marianna zone (MAR)**

Data/References	Quality (1=low, 5=high)	Notes on Quality of Data	Source Considered	Used in SSC and Reliance Level (0=no, 5=high)	Discussion of Data Use	In GIS Database
Fisk (1944)	3	Due to the small scale and methodology used in mapping, the fault locations are considered approximate.	MAR	3	Location of faults with possible geomorphic expression of Quaternary faulting—Potential fault sources for Marianna paleoliquefaction features (e.g., White River fault zone, Big Creek fault zone) considered in evaluation of the orientation and style of faulting.	N
Schumm and Spitz (1996)	4	Detailed analysis and discussion of geomorphic evidence (anomalies in channel morphology) for neotectonic deformation on regional and fault-specific basis.	MAR	3	Location and activity of potential fault sources—White River fault zone, Big Creek fault zone. Considered in evaluation of the orientation and style of faulting.	N
Spitz and Schumm (1997)	4	Detailed analysis and discussion of geomorphic evidence (anomalies in channel morphology) for neotectonic deformation on regional and fault-specific basis.	MAR	3	Location and activity of potential fault sources—White River fault zone, Big Creek fault zone, eastern Reelfoot rift margin. Activity—Geomorphic evidence for Quaternary tectonic deformation in vicinity of Marianna. Style of faulting—White River fault zone is left-lateral strike-slip fault.	N

**Table C-6.1.7 Data Evaluation
Reelfoot Rift–Marianna RLME**

**Identified Source
Marianna zone (MAR)**

Data/References	Quality (1=low, 5=high)	Notes on Quality of Data	Source Considered	Used in SSC and Reliance Level (0=no, 5=high)	Discussion of Data Use	In GIS Database
<i>Regional Stress</i>						
CEUS SSC stress data set	5	Most comprehensive data set available for CEUS.	MAR	2	Right-lateral slip on NE-trending fault and left-lateral slip on NW-trending sources is consistent with stress indicators that show general E-W trend to the maximum horizontal compression axis.	Y
<i>Tectonic Strain</i>						
Al-Qadhi (2010)	2	Unpublished Ph.D. dissertation.	MAR	3	Local source of large-magnitude earthquakes—Provides additional information on total length of the Marianna lineament based on geophysical (GPR) survey data.	Y
Al-Shukri et al. (2009)	4	NEHRP report—Provides good illustrations and discussion of results of high-resolution ground-penetrating radar (GPR) and resistivity profiles and three-dimensional surveys that were conducted to define the morphology and assist in the	MAR	4	Local source of large-magnitude earthquakes—Marianna lineament identified from geophysical surveys, possible fault in trench exhibits similar orientation. Recurrence—Provides constraints on the timing of paleoliquefaction features.	Y

**Table C-6.1.7 Data Evaluation
Reelfoot Rift–Marianna RLME**

**Identified Source
Marianna zone (MAR)**

Data/References	Quality (1=low, 5=high)	Notes on Quality of Data	Source Considered	Used in SSC and Reliance Level (0=no, 5=high)	Discussion of Data Use	In GIS Database
		interpretation of the origin of large earthquake-induced liquefaction features.				
<i>Paleoseismicity</i>						
CEUS SSC paleoliquefaction database (includes results from Al Shukri et al., 2005; Tuttle et al., 2006; Al Shukri et al., 2009)	5	Most comprehensive database of paleoliquefaction for CEUS.	MAR	4	Used to identify locations and ages of paleoliquefaction features in the Marianna region. 4.8 ka, 5.5 ka, 6.8 ka, 9.9 ka, something older (9.9–38 ka?).	Y
Al-Qadhi (2010)	2	Unpublished dissertation.	MAR	3	Local source of large-magnitude earthquakes—Used to constrain total length of the Daytona Beach lineament. GPR surveys used to identify additional paleoliquefaction features along the trend of the lineament.	Y

**Table C-6.1.7 Data Evaluation
Reelfoot Rift–Marianna RLME**

**Identified Source
Marianna zone (MAR)**

Data/References	Quality (1=low, 5=high)	Notes on Quality of Data	Source Considered	Used in SSC and Reliance Level (0=no, 5=high)	Discussion of Data Use	In GIS Database
Tuttle et al. (2006)	4	Provides detailed discussion of studies to evaluate paleoliquefaction features near Marianna, Arkansas.	ERM-S MAR	3	<p>Timing and recurrence of large-magnitude earthquakes—</p> <p>Based on radiocarbon dating liquefaction features at the Daytona Beach and St. Francis sites near Marianna, Arkansas, formed about 3500 BC and 4800 BC (5,000 and 7,000 years ago), respectively. Marianna sand blows are similar in size to NMSZ.</p> <p>Several faults in Marianna area (including the eastern Reelfoot rift margin [ERRM], the White River fault zone [WRFZ], and Big Creek fault zone [BCFZ]) are thought to be active based on apparent influence on local topography and hydrography. ERRM appears to be most likely source of very large earthquakes during the middle Holocene.</p>	N

Table C-6.1.8 Data Evaluation
Reelfoot Rift–Commerce Fault Zone RLME

Identified Source
Commerce fault zone (CFZ)

Data/References	Quality (1=low, 5=high)	Notes on Quality of Data	Source Considered	Used in SSC and Reliance Level (0=no, 5=high)	Discussion of Data Use	In GIS Database
<i>Instrumental Seismicity</i>						
CEUS SSC earthquake catalog	5	Comprehensive catalog; includes magnitude conversions and uncertainty assessments.	CFZ	1	Spatial association of seismicity—Some association of seismicity along Commerce geophysical lineament. Recurrence—Not used to estimate recurrence. Recurrence is based on paleoseismic evidence.	Y
Harrison and Schultz (1994)	2	Publication discussing association of seismicity; includes summary of other publications.	CFZ	1	Support for localized source—Shows 12 earthquakes near proposed trace of Commerce geophysical lineament (CGL) and suggests these earthquakes can be attributed to movement along structures associated with CGL.	N
Langenheim and Hildenbrand (1997)	4	Good maps and tabulated data on $m_b > 3$ earthquakes along or near CGL.	CFZ	2	Evidence for localized source of seismicity—Postulates an association of seismicity with Commerce geophysical lineament (CGL). The diversity of associated focal mechanisms and the variety of surface structural features along length of CGL, however, obscures its relation to release of present-day strain.	N

Table C-6.1.8 Data Evaluation
Reelfoot Rift–Commerce Fault Zone RLME

Identified Source
Commerce fault zone (CFZ)

Data/References	Quality (1=low, 5=high)	Notes on Quality of Data	Source Considered	Used in SSC and Reliance Level (0=no, 5=high)	Discussion of Data Use	In GIS Database
<i>Magnetic Anomaly</i>						
CEUS SSC magnetic anomaly data set	5	High-quality regional data.	CFZ	2	Commerce fault zone source generally coincident with magnetic anomaly. Anomaly extends beyond region where paleoseismic studies document repeated late Pleistocene surface faulting.	Y
Langenheim and Hildenbrand (1997)	4	Detailed evaluation of geopotential anomalies.	CFZ	3	Quaternary active faulting appears to be localized along Commerce geophysical lineament, a magnetic and gravity anomaly. Modeling indicates that source of magnetic and gravity anomalies is probably a mafic dike swarm. However, paleoseismic studies and high-resolution seismic profiles are used to define the location of CFZ.	N
<i>Gravity Anomaly</i>						
CEUS SSC gravity anomaly data set	5	High-quality regional data.	CFZ	1	Commerce geophysical lineament is defined in part by gravity anomaly as described in literature. CFZ RLME zone, however, is not well defined by the regional gravity data.	Y

Table C-6.1.8 Data Evaluation
Reelfoot Rift–Commerce Fault Zone RLME

Identified Source
Commerce fault zone (CFZ)

Data/References	Quality (1=low, 5=high)	Notes on Quality of Data	Source Considered	Used in SSC and Reliance Level (0=no, 5=high)	Discussion of Data Use	In GIS Database
Langenheim and Hildenbrand (1997)	4	Detailed evaluation of geopotential anomalies.	CFZ	2	Quaternary active faulting appears to be localized along Commerce geophysical lineament, a gravity and magnetic anomaly. However, paleoseismic studies and high-resolution seismic profiles are used to define location of active traces of the CFZ.	N
<i>Seismic Reflection</i>						
Palmer, Hoffman, et al. (1997) Palmer, Shoemaker, et al. (1997)	4	Published interpretations of shallow high-resolution seismic-reflection profiles (selected portions of uninterpreted profiles provided).	CFZ	4	Location and style of faulting—The CFZ striking N50°E overlies a major regional basement geophysical lineament and is present on two shallow seismic-reflection lines at southern margin of the escarpment. Fault is favorably oriented to be reactivated as right-lateral strike-slip fault.	N
Stephenson et al. (1999)	4	Published interpretations of high-resolution seismic-reflection profiles (selected portions of uninterpreted profiles provided).	CFZ	4	Location and style of faulting (Quilin site, Idalia Hills, and Benton Hills sites)—Interpretation of post-Cretaceous faulting extending into the Quaternary. Used in conjunction with paleoseismic investigations to identify location of fault source and to evaluate style of faulting and amount of reverse displacement.	N

Table C-6.1.8 Data Evaluation
Reelfoot Rift–Commerce Fault Zone RLME

Identified Source
Commerce fault zone (CFZ)

Data/References	Quality (1=low, 5=high)	Notes on Quality of Data	Source Considered	Used in SSC and Reliance Level (0=no, 5=high)	Discussion of Data Use	In GIS Database
<i>Regional Stress</i>						
CEUS SSC stress database	4	Provides additional new measurements to World Stress Map.	CFZ	2	A and B quality directions of maximum horizontal stress based on focal mechanisms show E-W to WNW trends in vicinity of Commerce fault.	Y
<i>Focal Mechanisms</i>						
Herrmann and Ammon (1997)	4	Presents results based on combination of traditional regional seismic network observations with direct seismogram modeling to improve estimates of small earthquake faulting geometry, depth, and size.	CFZ	3	Style of faulting—Focal mechanism analysis of a M 3.85 earthquake (February 5, 1994) along the northward-projected trend of CFZ shows motion was primarily right-lateral strike-slip along a N-NE azimuth.	N
Langenheim and Hildenbrand (1997)	4	Tabulation of data for $m_b > 3$ earthquakes along CGL.	CFZ	3	Focal mechanism and location of the earthquake near Thebes Gap are consistent with movement along nearly vertical NE-trending Commerce fault in the present regional stress field. However, focal mechanisms of other earthquakes shown by Harrison and Schultz (1994) near CGL are mixed, ranging from thrust to normal fault solutions. Focal mechanisms of two events that predate establishment of a comprehensive seismic network in the	N

Table C-6.1.8 Data Evaluation
Reelfoot Rift–Commerce Fault Zone RLME

Identified Source
Commerce fault zone (CFZ)

Data/References	Quality (1=low, 5=high)	Notes on Quality of Data	Source Considered	Used in SSC and Reliance Level (0=no, 5=high)	Discussion of Data Use	In GIS Database
					Midcontinent may be suspect.	
Shumway (2008)	4	Detailed analysis of seismicity data using recent velocity model.	CFZ	4	Depth of seismogenic crust—well-located earthquakes to depths between 13 and 15 km (8 and 9 mi.). Focal mechanisms—Half of the well-constrained earthquakes have a NE-trending nodal plane with strike-slip component (comparable to previous studies by Chiu et al., 1992).	N
<i>Paleoseismicity</i>						
Baldwin et al. (2006)	4	Detailed discussion of paleoseismic investigations.	CFZ	5	Character of deformation zone—Seismic-reflection data image a 0.5 km (0.3 mi.) wide zone of NE-striking, near-vertical faults that offset Tertiary and Quaternary reflectors and coincide with near-surface deformation. The regional NE strike of fault zone, as well as presence of near-vertical faults and complex flower-like structures, and preferential alignment with contemporary central U.S. stress regime, indicates that the fault zone likely accommodates right-lateral transpressive deformation. Recurrence—Stratigraphic and structural relationships in trenches	N

**Table C-6.1.8 Data Evaluation
Reelfoot Rift–Commerce Fault Zone RLME**

**Identified Source
Commerce fault zone (CFZ)**

Data/References	Quality (1=low, 5=high)	Notes on Quality of Data	Source Considered	Used in SSC and Reliance Level (0=no, 5=high)	Discussion of Data Use	In GIS Database
					<p>provide evidence for at least two late Quaternary faulting events on Idalia Hill fault zone overlying Commerce section of Commerce geophysical lineament. The penultimate event occurred in late Pleistocene (before 23.6–18.9 ka). The most recent event occurred in late Pleistocene to early Holocene (18.5–7.6 ka). Events overlap in age, with two prehistoric events interpreted by Vaughn (1994) that occurred 23–17 ka and 13.4–9 ka, and one event recognized by Harrison et al. (1995) that occurred 35–25 ka.</p> <p>Length of documented Quaternary faulting along CGL: 75 km (45 mi.).</p>	
Baldwin et al. (2008)	4	Well-illustrated NEHRP report; comprehensive discussion of evidence for timing of recent deformation.	CFZ	4	<p>Location and geometry of Penitentiary fault—Evidence for linking observed Pleistocene-Holocene deformation with previously mapped faults overlying the Commerce geophysical lineament. The fault is accommodating dextral transpression.</p> <p>Timing and amount of displacement—Faults project upsection into the latest Pleistocene Henry Formation (older than ~25 ka) and possibly Holocene Cahokia Formation. Vertical offset of</p>	N

Table C-6.1.8 Data Evaluation
Reelfoot Rift–Commerce Fault Zone RLME

Identified Source
Commerce fault zone (CFZ)

Data/References	Quality (1=low, 5=high)	Notes on Quality of Data	Source Considered	Used in SSC and Reliance Level (0=no, 5=high)	Discussion of Data Use	In GIS Database
					reflectors 2–6 m (6.5–20 ft.).	
CEUS SSC paleoliquefaction database	5	Comprehensive database; peer-reviewed; includes uncertainties in timing of paleo-liquefaction events).	CFZ	5	Recurrence—Provides preferred ages for paleoliquefaction features in vicinity of CFZ.	Y
Harrison et al. (1999)	4	Interpretation of high- resolution seismic profile data and paleoseismic trenching investigations (on secondary structures).	CFZ-	5	Style of faulting—The overall style of neotectonic deformation is interpreted as right-lateral strike-slip faulting. Recurrence—Documents evidence for four episodes of Quaternary faulting on secondary structures in hills west of assumed primary fault along range front: one in late- to post-Sangamon, pre- to early Roxana time (~60–50 ka); one in syn- or post-Roxana, pre-Peoria time (~35–25 ka); and two in Holocene time (middle to late Holocene, and possibly during 1811-1812 earthquake sequence).	N
Harrison et al. (2002)	4	USGS Miscellaneous Investigations publication; mapping supplemented by dates.	CFZ	4	Timing of recent earthquakes—At least two events may have occurred in the latest Holocene (just after 2-sigma calibrated calendar ages of 3747–3369 BC and AD 968–639).	N

Table C-6.1.8 Data Evaluation
Reelfoot Rift–Commerce Fault Zone RLME

Identified Source
Commerce fault zone (CFZ)

Data/References	Quality (1=low, 5=high)	Notes on Quality of Data	Source Considered	Used in SSC and Reliance Level (0=no, 5=high)	Discussion of Data Use	In GIS Database
Palmer, Hoffman, et al. (1997) Palmer, Shoemaker, et al. (1997)	4	Publications with high-resolution seismic data images; numerous post-Cretaceous faults and folds; discusses neotectonic significance.	CFZ	4	Style of faulting—English Hills. Evidence for deep-seated tectonic fault. Style of faulting—Faults are interpreted as flower structures with N-NE-striking, vertically dipping, right-lateral oblique-slip faults. Amount of displacement—Near-vertical displacements with maximum offsets on the order of 15 m (50 ft.).	N
Vaughn (1994)	2	NEHRP report—Relatively few liquefaction features studied and dated in area; often significant uncertainties in age estimates.	CFZ	5	Paleoliquefaction results to evaluate timing of events. Preferred ages in CEUS SSC database based on communications between author and Dr. M. Tuttle.	Y

**Table C-6.1.9 Data Evaluation
Wabash Valley RLME**

**Identified Source
Wabash Valley (WV) RLME**

Data/References	Quality (1=low, 5=high)	Notes on Quality of Data	Source Considered	Used in SSC and Reliance Level (0=no, 5=high)	Discussion of Data Use	In GIS Database
<i>Instrumental Seismicity</i>						
CEUS SSC earthquake catalog	5	Comprehensive catalog; includes magnitude conversions and uncertainty assessments.	WV	0	Not used to evaluate recurrence parameters for RLME. Magnitudes smaller than the RLME are included in Illinois Basin Extended Basement or Mmax zone.	Y
Hamburger et al. (2008)	3	Abstract	WV	4	Evidence for reactivation of structures in present stress regime—04:30 CDT, April 18, 2008, M 5.4 earthquake.	Y
Withers et al. (2009)	3	Abstract; preliminary analysis.	WV	4	Evidence for reactivation of structures in the present stress regime—April 18, 2008, M _w 5.2 (M _w 5.4 GCMT [http://www.global.cmt.org]) Mt. Carmel, Illinois, earthquake—Largest event in 20 years in Wabash Valley seismic zone (WVSZ).	Y

**Table C-6.1.9 Data Evaluation
Wabash Valley RLME**

**Identified Source
Wabash Valley (WV) RLME**

Data/References	Quality (1=low, 5=high)	Notes on Quality of Data	Source Considered	Used in SSC and Reliance Level (0=no, 5=high)	Discussion of Data Use	In GIS Database
Yang et al. (2009)	3	Abstract; preliminary analysis.	WV	5	Analysis of aftershocks using sliding-window cross-correlation technique and double-difference relocation algorithm give a best-fit plane having a nearly E-W trend with orientation of 248 and dip angle of 81. Fault is nearly vertical down to ~20 km (12.5 mi.). Provides constraints on seismogenic width.	N
Historical Seismicity						
McBride et al. (2007)	5	Integrated assessment based on seismicity, borehole, geophysical, and industry seismic profile data analysis.	WV	5	Discusses possible association of recent earthquakes (April 3, 1974, $m_b = 4.7$; June 10, 1987, $m_b = 5.2$; and November 9, 1968, $m_b = 5.5$ events) with three distinct upper-crust sources. Provides detailed discussion of parameters (magnitude, depth, focal mechanism) for each event.	Y

**Table C-6.1.9 Data Evaluation
Wabash Valley RLME**

**Identified Source
Wabash Valley (WV) RLME**

Data/References	Quality (1=low, 5=high)	Notes on Quality of Data	Source Considered	Used in SSC and Reliance Level (0=no, 5=high)	Discussion of Data Use	In GIS Database
<i>Magnetic Anomaly</i>						
CEUS SSC magnetic anomaly data set	5	High-quality regional data.	WV	1	Boundaries of WV RLME not uniquely defined by magnetic anomaly map.	Y
<i>Gravity Anomaly</i>						
CEUS SSC gravity anomaly data set	5	High-quality regional data.	WV	1	Boundaries of WV RLME not uniquely defined by gravity anomaly map.	Y
<i>Seismic Reflection</i>						
McBride, Hildenbrand, et al. (2002)	5	Provides simplified line drawings and interpretations of four reprocessed migrated seismic profiles. Also provides excerpts of reprocessed seismic-reflection profiles. Includes detailed geologic discussion based on integrated review of seismic, and geopotential data.	WV	3	Used to define style of faulting and possible source structures within the source zone.	N

**Table C-6.1.9 Data Evaluation
Wabash Valley RLME**

**Identified Source
Wabash Valley (WV) RLME**

Data/References	Quality (1=low, 5=high)	Notes on Quality of Data	Source Considered	Used in SSC and Reliance Level (0=no, 5=high)	Discussion of Data Use	In GIS Database
McBride et al. (2007)	4	Builds on McBride, Hildenbrand, et al. (2002) and provides additional interpretations of seismic-reflection data. Presents both raw (selected excerpts) and interpreted sections.	WV	3	Used to define style of faulting and possible source structures within the source zone.	N
<i>Regional Geologic and Tectonic Maps</i>						
Nelson (1995)	5	Digital file of Illinois structural trends map.	WV	3	Constraint on boundary of source zone—Used to identify major structural trends (Wabash Valley fault system [WVFS], La Salle anticlinal belt).	Y
<i>Local Geologic and Tectonic Maps</i>						
Sexton et al. (1986)	3	Small-scale publication figure.	WV	3	Used to define style of faulting and possible source structures within the source zone—Map of individual faults within the WVFS that extend to basement.	Y
Wheeler et al. (1997)	3	Compilation map (scale 1:250,000).	WV	2	Constraint on boundary of source zone—Identifies areas of possible neotectonic deformation.	N

**Table C-6.1.9 Data Evaluation
Wabash Valley RLME**

**Identified Source
Wabash Valley (WV) RLME**

Data/References	Quality (1=low, 5=high)	Notes on Quality of Data	Source Considered	Used in SSC and Reliance Level (0=no, 5=high)	Discussion of Data Use	In GIS Database
<i>Geodetic Strain</i>						
Hamburger et al. (2002)	1	Only one year of data.	WV	1	Generally consistent with focal mechanism data from historical events.	N
Hamburger et al. (2009)	3	Abstract	WV	1	GPS data for WVSZ indicate systematic northwestward motion of about 0.5–0.7 mm/yr with respect to Stable North American Reference Frame. Results suggest that elevated seismicity and strain in WVSZ could result from aseismic slip triggered by viscous relaxation in the lower crust long after New Madrid earthquake.	N
<i>Regional Stress</i>						
CEUS SSC stress data set	5	Includes two additional new stress measurements based on focal mechanisms.	WV	2	East trend consistent with previous measurements shown on World Stress Map.	Y
Heidbach et al. (2008) (World Stress Map)	3	Worldwide compilation of stress data.	WV	2	Three events used by World Stress Map, while tectonically and spatially distinct, represent	N

**Table C-6.1.9 Data Evaluation
Wabash Valley RLME**

**Identified Source
Wabash Valley (WV) RLME**

Data/References	Quality (1=low, 5=high)	Notes on Quality of Data	Source Considered	Used in SSC and Reliance Level (0=no, 5=high)	Discussion of Data Use	In GIS Database
					contemporary maximum horizontal compressive stress that trends just north of east in southern Illinois and Indiana (McBride et al., 2007).	
<i>Tectonic Strain</i>						
Fraser et al. (1997)	2	Geomorphic analysis. Indirect evidence for neotectonic deformation. Apparent deformation could result from other nontectonic fluvial channel processes.	WV	3	Constraints on boundary of zone—Used as one potential indicator of a more localized region of deformation in vicinity of Vincennes.	Y
Wheeler and Cramer (2002)	4	Systematic evaluation of potential source zone for two largest paleoearthquakes in WVSZ.	WV	4	Constraints on boundary of zone—The Tri-State source zone defined by Wheeler and Cramer and used by USGS to define an Mmax source region for WVSZ is captured by using a leaky boundary for ruptures originating in the WV RLME.	Y
Counts et al. (2008, 2009a, 2009b) Van Arsdale et al.	4	Paleoseismic studies (trenching, paleoliquefaction, and geomorphic analyses) provide good indication of	WV	4	Constraints on boundary of zone—Quaternary activity on faults within WVFS used as an indicator of a more localized region of deformation in vicinity	Y

**Table C-6.1.9 Data Evaluation
Wabash Valley RLME**

**Identified Source
Wabash Valley (WV) RLME**

Data/References	Quality (1=low, 5=high)	Notes on Quality of Data	Source Considered	Used in SSC and Reliance Level (0=no, 5=high)	Discussion of Data Use	In GIS Database
(2009) Woolery (2005)		Quaternary deformation on faults within the WVFS.			of Vincennes.	
<i>Focal Mechanisms</i>						
Hamburger et al. (2002, 2008) Larson (2002) Larson et al. (2009) McBride, Hildenbrand, et al. (2002) McBride et al. (2007) Withers et al. (2009) Yang et al. (2009)	4	Well-constrained focal mechanisms for several recent moderate-sized (M 4–5.4) earthquakes in Wabash Valley region of southern Illinois and Indiana.	WV	5	Style of deformation—Focal mechanisms indicate ongoing deformation along reactivated Precambrian and Paleozoic basement structures. Analyses indicate three seismotectonic environments in upper crust: strike-slip (E-NE and NE trends) and reverse fault.	N
<i>Paleoseismicity</i>						
CEUS SSC paleoliquefaction database	5	Comprehensive database; peer-reviewed; includes uncertainties in timing of paleo-liquefaction events).	WV	4	Recurrence—Provides constraints on timing of Vincennes and Skelton paleoearthquakes	Y

**Table C-6.1.9 Data Evaluation
Wabash Valley RLME**

**Identified Source
Wabash Valley (WV) RLME**

Data/References	Quality (1=low, 5=high)	Notes on Quality of Data	Source Considered	Used in SSC and Reliance Level (0=no, 5=high)	Discussion of Data Use	In GIS Database
[various studies by numerous researchers; see Table 6.1.9-1]	4–5	One of the best paleoliquefaction data sets available for a region in the CEUS. Back-calculations using site-specific field observations and seismological observations have been put into a probabilistic framework.	WV	5	<p>Recurrence and magnitude—Paleoliquefaction data provide a basis for identifying as many as eight prehistoric earthquakes in the region. The proximities of the two largest prehistoric events—the Vincennes (~6,100 yr BP) and the Skelton earthquakes (~12,000 yr BP)—are used to characterize recurrence of RLMEs.</p> <p>Detailed analyses of Vincennes earthquake (~6,100 BP) provide a reasonable constraint on size and location of this event.</p>	Y

Table C-7.3.1 Data Evaluation
St. Lawrence Rift Zone

Identified Source
St. Lawrence Rift (SLR)

Data/References	Quality (1=low, 5=high)	Notes on Quality of Data	Source Considered	Used in SSC and Reliance Level (0=no, 5=high)	Discussion of Data Use	In GIS Database
<i>Instrumental Seismicity</i>						
CEUS SSC earthquake catalog	5	Comprehensive catalog; includes magnitude conversions and uncertainty assessments.	SLR	5	Used to evaluate recurrence parameters.	Y
Lamontagne and Ranalli (1997)	5	Relocated hypocentral depth.	SLR	5	Used to evaluate thickness of seismogenic crust and style of faulting.	Y
<i>Historical Seismicity</i>						
CEUS SSC earthquake catalog	5	Comprehensive catalog; includes magnitude conversions and uncertainty assessments.	SLR	5	The prior distribution for Mmax is modified by the largest observed historical earthquake taken from the CEUS SSC earthquake catalog.	Y
Lamontagne et al. (2008)	4	Earthquake parameters and felt effects for major Canadian earthquakes.	SLR	4	Magnitudes derived from special studies are cited directly in CEUS SSC earthquake catalog.	Y

Table C-7.3.1 Data Evaluation
St. Lawrence Rift Zone

Identified Source
St. Lawrence Rift (SLR)

Data/References	Quality (1=low, 5=high)	Notes on Quality of Data	Source Considered	Used in SSC and Reliance Level (0=no, 5=high)	Discussion of Data Use	In GIS Database
<i>Magnetic Anomaly</i>						
CEUS SSC magnetic anomaly data set	5	High-quality regional data.	SLR	2	<p>St. Lawrence rift zone is not subdivided based on different basement terranes or tectonic features imaged in the magnetic anomaly map.</p> <p>Magnetic anomalies to the west reflect Grenville basement as opposed to rift faulting. Data does not assist in delineating eastern boundary.</p>	Y
<i>Gravity Anomaly</i>						
CEUS SSC gravity data set	5	High-quality regional data.	SLR	0	The St. Lawrence rift zone generally encompasses a region of low-amplitude gravity anomalies. The boundaries were not drawn based on this data set.	Y
<i>Seismic Reflection</i>						
Tremblay et al. (2003)	3	Relocates offshore SQUIP data.	SLR	2	Images a transition from a half graben to a graben of the St. Lawrence fault within the St. Lawrence estuary.	N

Table C-7.3.1 Data Evaluation
St. Lawrence Rift Zone

Identified Source
St. Lawrence Rift (SLR)

Data/References	Quality (1=low, 5=high)	Notes on Quality of Data	Source Considered	Used in SSC and Reliance Level (0=no, 5=high)	Discussion of Data Use	In GIS Database
<i>Geophysical Anomalies</i>						
Li et al. (2003)	3	Determined velocity structure from inversion of Rayleigh waves.	SLR	3	Deep crustal velocity anomalies beneath the Adirondacks are attributed to the Cretaceous Great Meteor hotspot.	N
<i>Local Geologic and Tectonic Maps</i>						
Garritty and Soller (2009) (Database of the Geologic Map of North America)	5	1:5,000,000-scale geologic map in GIS format compiled from various national maps.	SLR	4	Boundary drawn to capture mapped normal faults in the Adirondacks.	N
Higgins and van Breemen (1998)	3	Presents age dates and mapping for the Sept Iles layered mafic intrusion.	SLR	4	Used to define source geometry for Saguenay graben.	N
Hodych and Cox (2007)	3	Presents maps and age dates for the Lac Matapedia and Mt. St.-Anselme basalt flows of Quebec.	SLR	4	Used to define source geometry for eastern boundary.	N
Kamo et al. (1995)	3	Compilation of Iapetan faults, dikes, and other intrusive volcanic rocks.	SLR	5	Defines Ottawa graben and southern limit of rift system.	N

Table C-7.3.1 Data Evaluation
St. Lawrence Rift Zone

Identified Source
St. Lawrence Rift (SLR)

Data/References	Quality (1=low, 5=high)	Notes on Quality of Data	Source Considered	Used in SSC and Reliance Level (0=no, 5=high)	Discussion of Data Use	In GIS Database
Kanter (1994)	3	Data is considered of good quality for defining location of major crustal divisions.	SLR	5	Used to define source geometry.	Y
McCausland and Hodych (1998)	3	Reviews interpretations of the Skinner Cove volcanic of Newfoundland.	SLR	4	Used to define source geometry for Ottawa graben and New York promontory.	N
Wheeler (1995)	3	Compilation of late Neoproterozoic to early Cambrian faults.	SLR	4	Used to define source geometry.	N
Whitmeyer and Karlstrom (2007)	3	Presents regional geologic map of North America documenting the assembly of the continent by successive tectonic events.	SLR	5	Used to define source geometry.	Y
Geodetic Strain						
Mazzotti and Adams (2005)	3	Modeled seismic moment rates from earthquake statistics.	SLR	3	Seismic moment rate varies from $(0.1 \text{ to } 0.5) \times 10^{17} \text{ Nm/yr}$ for entire zone rift system if Charlevoix is confined to its own zone or $(0.1\text{--}5.0) \times 10^{17} \text{ Nm/yr}$ if Charlevoix is combined with the entire rift	N

Table C-7.3.1 Data Evaluation
St. Lawrence Rift Zone

Identified Source
St. Lawrence Rift (SLR)

Data/References	Quality (1=low, 5=high)	Notes on Quality of Data	Source Considered	Used in SSC and Reliance Level (0=no, 5=high)	Discussion of Data Use	In GIS Database
					system.	
<i>Regional Stress</i>						
CEUS SSC stress data set	4	Provides additional new measurements to World Stress Map.	SLR	1	Data includes thrust mechanisms with minor strike-slip. Orientations vary from E-W to NE-SW.	Y
Heidbach et al. (2008) (World Stress Map)	3	Compiled worldwide stress indicators from focal mechanisms, borehole breakouts, etc.	SLR	2	Entries for SLR are predominantly thrust mechanisms with some strike-slip. Orientations of maximum horizontal stress vary from E-W to NE-SW.	Y
<i>Focal Mechanisms</i>						
Bent (1992)	3	Analyzed historical waveforms for 1925 Charlevoix earthquake.	SLR	4	Used to characterize future ruptures.	N
Bent (1996a)	3	Analyzed historical waveforms for 1935 Timiskaming earthquake.	SLR	4	Used to characterize future ruptures.	N
Bent (1996b)	3	Analyzed historical waveforms for 1944 Cornwall-Massena earthquake.	SLR	4	Used to characterize future ruptures.	N

Table C-7.3.1 Data Evaluation
St. Lawrence Rift Zone

Identified Source
St. Lawrence Rift (SLR)

Data/References	Quality (1=low, 5=high)	Notes on Quality of Data	Source Considered	Used in SSC and Reliance Level (0=no, 5=high)	Discussion of Data Use	In GIS Database
Bent and Perry (2002)	4	Determined focal depths for ENA earthquakes.	SLR	4	Used to characterize future ruptures.	N
Bent et al. (2002)	4	Determined earthquake parameters for 2000 Kipawa earthquake.	SLR	4	Used to characterize future ruptures.	N
Bent et al. (2003)	4	Determined focal mechanisms for Western Quebec seismic zone.	SLR	4	Used to characterize future ruptures.	N
Du et al. (2003)	4	Determined focal mechanisms for moderate earthquakes in NE United States and SE Canada.	SLR	4	Used to characterize future ruptures.	N
Lamontagne (1999)	4	Determined focal mechanisms for Charlevoix earthquakes.	SLR	4	Used to characterize future ruptures.	N
Lamontagne and Ranalli (1997)	4	Determined focal mechanisms.	SLR	4	Used to characterize future ruptures.	N

Table C-7.3.1 Data Evaluation
St. Lawrence Rift Zone

Identified Source
St. Lawrence Rift (SLR)

Data/References	Quality (1=low, 5=high)	Notes on Quality of Data	Source Considered	Used in SSC and Reliance Level (0=no, 5=high)	Discussion of Data Use	In GIS Database
Lamontagne et al. (2004)	4	Determined focal mechanism for 1999 Côte-Nord earthquake.	SLR	4	Used to characterize future ruptures.	N
Li et al. (1995)	4	Determined focal mechanisms for two M 4 earthquakes.	SLR	4	Used to characterize future ruptures.	N
Nábělek and Suárez (1989)	3	Determined earthquake parameters for 1983 Goodnow, New York, earthquake.	SLR	4	Used to characterize future ruptures.	N
Seeber et al. (2002)	4	Determined earthquake parameters for 2002 Au Sable Forks, New York, earthquake.	SLR	4	Used to characterize future ruptures.	N
<i>Paleoseismicity</i>						
Aylsworth et al. (2000)	3	Documents disturbed sediment and paleolandslides along Ottawa River.	SLR	4	Provides evidence for persistent prehistoric earthquake activity along the eastern Ottawa-Bonnechere graben.	N
CEUS SSC paleoliquefaction database	5	Compilation (with attributions) of paleoliquefaction	SLR	4	Localization of liquefaction features in Charlevoix support characterization of a RLME	N

Table C-7.3.1 Data Evaluation
St. Lawrence Rift Zone

Identified Source
St. Lawrence Rift (SLR)

Data/References	Quality (1=low, 5=high)	Notes on Quality of Data	Source Considered	Used in SSC and Reliance Level (0=no, 5=high)	Discussion of Data Use	In GIS Database
		observations.			source.	
Doig (1990)	3	Documents silt layers in cores attributed to earthquake-induced landslides near Charlevoix.	SLR	4	Provides evidence for persistent prehistoric earthquake activity near Charlevoix.	N
Doig (1991)	3	Documents silt layers in cores attributed to earthquake-induced landslides near Saguenay.	SLR	4	Provides evidence for persistent prehistoric earthquake activity near Saguenay.	N
Doig (1998)	3	Documents silt layers in cores attributed to earthquake-induced landslides near Timiskaming.	SLR	4	Provides evidence for persistent prehistoric earthquake activity near Timiskaming.	N
Filion et al. (1991)	3	Provides ages for prehistoric landslides attributed to earthquakes.	SLR	4	Provides evidence for persistent prehistoric earthquake activity near Charlevoix.	N
Tuttle et al. (1990)	4	Documents liquefaction features associated with the 1988 Saguenay earthquake.	SLR	4	Provides evidence for at least one older earthquake near Saguenay.	Y

Table C-7.3.1 Data Evaluation
St. Lawrence Rift Zone

Identified Source
St. Lawrence Rift (SLR)

Data/References	Quality (1=low, 5=high)	Notes on Quality of Data	Source Considered	Used in SSC and Reliance Level (0=no, 5=high)	Discussion of Data Use	In GIS Database
Tuttle et al. (1992)	4	Documents liquefaction features associated pre-1988 Saguenay earthquake.	SLR	4	Provides evidence for at least one older earthquake near Saguenay.	Y

**Table C-7.3.2 Data Evaluation
Great Meteor Hotspot Zone**

**Identified Source
Great Meteor Hotspot (GMH)**

Data/References	Quality (1=low, 5=high)	Notes on Quality of Data	Source Considered	Used in SSC and Reliance Level (0=no, 5=high)	Discussion of Data Use	In GIS Database
<i>Instrumental Seismicity</i>						
CEUS SSC earthquake catalog	5	Comprehensive catalog; includes magnitude conversions and uncertainty assessments.	GMH	5	Used to evaluate recurrence parameters.	Y
Ma and Atkinson (2006)	5	Relocated hypocentral depth.	GMH	5	Focal depths cluster at 5, 8, 12, 15, and 22 km and may reflect layering in seismogenic properties within the crust.	N
Ma and Eaton (2007)	5	Relocated hypocentral depth.	GMH	5	Deep earthquakes (greater than 17 km in depth) are localized as clusters at Maniwaki and Mont-Laurier.	N
Ma et al. (2008)	5	Relocated hypocentral depth in Northern Ontario.	GMH	5	Spatial distribution of earthquakes indicates an aseismic area northwest of the GMH seismotectonic zone along the hotspot track.	N
<i>Historical Seismicity</i>						
Adams and Basham (1991)	3	Provides description of earthquakes in northeastern Canada.	GMH	4	Description of Western Quebec seismic zone considered in geometry for GMH seismotectonic zone. NW-trending band of seismicity north of Ottawa River attributed to GMH track.	N

**Table C-7.3.2 Data Evaluation
Great Meteor Hotspot Zone**

**Identified Source
Great Meteor Hotspot (GMH)**

Data/References	Quality (1=low, 5=high)	Notes on Quality of Data	Source Considered	Used in SSC and Reliance Level (0=no, 5=high)	Discussion of Data Use	In GIS Database
CEUS SSC earthquake catalog	5	Comprehensive catalog; includes magnitude conversions and uncertainty assessments.	GMH	5	Prior distribution for Mmax is modified by the largest observed historical earthquake taken from CEUS SSC earthquake catalog.	Y
<i>Magnetic Anomaly</i>						
CEUS SSC magnetic data set	5	High-quality regional data.	GMH	1	GMH zone is not subdivided based on different basement terranes or tectonic features imaged on magnetic anomaly map.	Y
<i>Gravity Anomaly</i>						
CEUS SSC gravity data set	5	High-quality regional data.	GMH	1	GMH zone is not subdivided based on different basement terranes or tectonic features imaged on magnetic anomaly map.	Y
<i>Seismic Reflection</i>						
Ma and Eaton (2007)	4	Compares location of seismicity to published interpretations of Lithoprobe Lines 52 and 53.	GMH	4	Seismicity does not generally correlate with structure in Western Quebec seismic zone (WQSZ); shear zones of Grenville province cut across NW-SE trend of WQSZ at high angle. The Maniwaki cluster exhibits repeating events with deep seismicity localized within footwall of Baskatong crustal ramp, and intermediate and shallow	N

**Table C-7.3.2 Data Evaluation
Great Meteor Hotspot Zone**

**Identified Source
Great Meteor Hotspot (GMH)**

Data/References	Quality (1=low, 5=high)	Notes on Quality of Data	Source Considered	Used in SSC and Reliance Level (0=no, 5=high)	Discussion of Data Use	In GIS Database
					seismicity localized within hanging wall.	
<i>Geophysical Anomalies</i>						
Eaton et al. (2006)	4	Determined crustal thickness from teleseismic results that agree with previous published refraction surveys.	GMH	5	Minima on crustal thickness maps coincides with GMH source zone.	N
Li et al. (2003)	3	Determined velocity structure from inversion of Rayleigh waves.	GMH	3	Southwestern portion of zone includes deep negative crustal velocity anomaly.	N
Rondenay et al. (2000)	3	Modeled velocity of crust from travel time inversion of teleseismic data.	GMH	3	Images a low-velocity corridor oblique to GMH zone.	N
<i>Local Geologic and Tectonic Maps</i>						
Duncan (1984)	4	Determined Ar ages for offshore seamounts.	GMH	2	Source geometry for GMH was not drawn to encompass Cretaceous volcanism in region.	N
Faure et al. (1996b)	5	Paleostress analysis of Cretaceous rocks.	GMH	5	Monteregian plutons intruded along reactivated structures along Ottawa-Bonnechere graben.	N

**Table C-7.3.2 Data Evaluation
Great Meteor Hotspot Zone**

**Identified Source
Great Meteor Hotspot (GMH)**

Data/References	Quality (1=low, 5=high)	Notes on Quality of Data	Source Considered	Used in SSC and Reliance Level (0=no, 5=high)	Discussion of Data Use	In GIS Database
Faure et al. (2006)	5	Jurassic paleostress orientations associated with opening of Atlantic.	GMH	5	Opening of Atlantic resulted in widespread extension hundreds of kilometers into craton. Paleostress orientations from Jurassic rocks differ from those in Cretaceous rocks.	N
Heaman and Kjarvsgaard (2000)	5	Determined U-Pb perovskite ages for kimberlite dikes.	GMH	3	Source geometry for GMH was not drawn to encompass Cretaceous volcanism in the region.	N
Matton and Jebrak (2009)	4	Proposes that Cretaceous alkaline magmas result from periodic reactivation of preexisting zones of weakness combined with coeval asthenospheric upwelling during major stages of Atlantic tectonic evolution.	GMH	5	Provides mechanisms for widespread Cretaceous volcanisms and rationale for not drawing a source zone along proposed hotspot tracks.	N
Poole (1970)	3	Provides descriptions and ages for Cretaceous Monteregian plutons.	GMH	3	Source geometry for GMH incorporates thin crust and deep earthquakes and was not drawn to encompass Cretaceous volcanism in the region.	N

**Table C-7.3.2 Data Evaluation
Great Meteor Hotspot Zone**

**Identified Source
Great Meteor Hotspot (GMH)**

Data/References	Quality (1=low, 5=high)	Notes on Quality of Data	Source Considered	Used in SSC and Reliance Level (0=no, 5=high)	Discussion of Data Use	In GIS Database
Zartman (1977)	2	Compiled ages for plutonic rocks in White Mountains.	GMH	2	Source geometry for GMH incorporates thin crust and deep earthquakes and was not drawn to encompass Cretaceous volcanism in the region.	N
Geodetic Strain						
Mazzotti and Adams (2005)	3	Modeled seismic moment rates from earthquake statistics.	GMH	3	Seismic moment rate of $(0.1\text{--}5.0) \times 10^{17}$ N m/yr (Newton-meter per year) for entire zone, which corresponds to a M_w 7 earthquake every 150 years.	N
Regional Stress						
CEUS SSC stress data set	4	Provides additional new measurements to World Stress Map.	GMH	1	Data includes thrust mechanisms in a variety of orientations.	Y
Heidbach et al. (2008) (World Stress Map)	3	Compiled worldwide stress indicators from focal mechanisms, borehole breakouts, etc.	GMH	2	Limited entries for the GMH—dominantly thrust mechanisms with some strike-slip. Orientations of maximum horizontal stress vary from E-W to NW-SE, N-S, and NNE-SSW.	Y

**Table C-7.3.2 Data Evaluation
Great Meteor Hotspot Zone**

**Identified Source
Great Meteor Hotspot (GMH)**

Data/References	Quality (1=low, 5=high)	Notes on Quality of Data	Source Considered	Used in SSC and Reliance Level (0=no, 5=high)	Discussion of Data Use	In GIS Database
<i>Focal Mechanisms</i>						
Bent (1996b)	3	Compiles existing focal mechanisms with data for the 1944 Cornwall-Massena earthquake.	GMH	3	Mechanisms of GMH are predominantly thrust mechanisms, although interpreting which nodal plane corresponds to the fault plane is ambiguous.	N
Bent et al. (2003)	4	Determines focal mechanisms from earthquakes occurring from 1994 through 2000.	GMH	4	Thrust or oblique-thrust in response to NE compression.	N
Du et al. (2003)	4	Reanalyzes earthquake source parameters from additional stations.	GMH	5	Focal mechanisms have strikes of one of their nodal planes parallel to the general trend of seismicity.	N
Lamontagne et al. (1994)	4	Determines earthquake parameters from several stations in network.	GMH	5	The October 19, 1990, Mont-Laurier earthquake has a reverse mechanism with steeply N-dipping, E-W-oriented nodal plane.	N
Ma and Eaton (2007)	4	Determined focal mechanism for February 25, 2006, M_w 3.7 earthquake and compiled existing focal mechanisms.	GMH	5	Reverse mechanisms have SW-trending P-axes that change to E-W-trending P-axes in southern portion of the zone.	N

**Table C-7.3.2 Data Evaluation
Great Meteor Hotspot Zone**

**Identified Source
Great Meteor Hotspot (GMH)**

Data/References	Quality (1=low, 5=high)	Notes on Quality of Data	Source Considered	Used in SSC and Reliance Level (0=no, 5=high)	Discussion of Data Use	In GIS Database
<i>Paleoseismicity</i>						
Aylsworth et al. (2000)	3	Poor constraints on magnitude or location of paleoearthquakes causing observed deformation.	GMH	1	Study area located outside of GMH within St. Lawrence rift (SLR) seismotectonic zone. Location of paleoearthquakes may lie within SLR or GMH, but no geotechnical analysis of materials has been performed to constrain location and magnitude.	N
CEUS SSC paleoliquefaction database	5	Compilation (with attributions) of paleoliquefaction observations.	GMH	n/a	No data located within zone.	Y

**Table C-7.3.3 Data Evaluation
Northern Appalachian Zone**

**Identified Source
Northern Appalachian (NAP)**

Data/References	Quality (1=low, 5=high)	Notes on Quality of Data	Source Considered	Used in SSC and Reliance Level (0=no, 5=high)	Discussion of Data Use	In GIS Database
<i>Instrumental Seismicity</i>						
CEUS SSC earthquake catalog	5	Comprehensive catalog; includes magnitude conversions and uncertainty assessments.	NAP	5	Used to evaluate recurrence parameters.	Y
<i>Historical Seismicity</i>						
Burke (2004)	4	Identifies historical earthquakes from newspapers.	NAP	4	Defines clusters of seismicity at Moncton, Passamaquoddy Bay, and Central Highlands (Miramichi). Eastern boundary drawn to exclude Passamaquoddy Bay seismicity from NAP to ECC.	N
Burke (2009)	5	Identifies historical earthquakes from newspapers and provides isoseismal maps where available.	NAP	5	Provides estimate of magnitude for historical earthquakes based on felt area.	N
CEUS SSC earthquake catalog	5	Comprehensive catalog; includes magnitude conversions and uncertainty assessments.	NAP	5	The prior distribution for Mmax is modified by the largest observed historical earthquake taken from the CEUS SSC earthquake catalog.	Y

**Table C-7.3.3 Data Evaluation
Northern Appalachian Zone**

**Identified Source
Northern Appalachian (NAP)**

Data/References	Quality (1=low, 5=high)	Notes on Quality of Data	Source Considered	Used in SSC and Reliance Level (0=no, 5=high)	Discussion of Data Use	In GIS Database
Ebel (1996)	3	Estimates magnitude and location of 1638 earthquake.	NAP	5	Considered for maximum observed earthquake.	N
Leblanc and Burke (1985)	4	Estimates magnitude and location of four earthquakes in Maine and New Brunswick.	NAP	3	Provides magnitude estimates for historical earthquakes.	N
<i>Magnetic Anomaly</i>						
CEUS SSC magnetic anomaly data set	5	High-quality regional data.	NAP	2	The NAP is not subdivided based on different basement terranes or tectonic features imaged in the magnetic anomaly map. The eastern boundary follows magnetic highs west of the Fundy basin. Sparse magnetic highs parallel the western boundary.	Y
<i>Gravity Anomaly</i>						
CEUS SSC gravity data set	5	High-quality regional data.	NAP	1	The NAP generally encompasses a region of intermediate gravity anomalies with lower values to the west in the SLR and higher values to the east in ECC.	Y

**Table C-7.3.3 Data Evaluation
Northern Appalachian Zone**

**Identified Source
Northern Appalachian (NAP)**

Data/References	Quality (1=low, 5=high)	Notes on Quality of Data	Source Considered	Used in SSC and Reliance Level (0=no, 5=high)	Discussion of Data Use	In GIS Database
<i>Seismic Reflection</i>						
Hughes and Luetgert (1991)	3	Seismic-refraction results from Adirondacks to Maine.	NAP	4	Delineates crustal thickness within seismotectonic zone.	N
Spencer et al. (1989)	3	Presents results of Quebec-Maine seismic-reflection and seismic-refraction profiles.	NAP	5	Images lapetan growth faults below detachment.	N
Stewart et al. (1993)	3	Integrates results of Quebec-Maine seismic-reflection profiles in tectonostratigraphic units.	NAP	4	Delineates Appalachian terranes.	N
<i>Geophysical Anomalies</i>						
Li et al. (2003)	3	Determined velocity structure from inversion of Rayleigh waves.	NAP	3	SW portion of zone includes deep negative crustal velocity anomaly.	N

**Table C-7.3.3 Data Evaluation
Northern Appalachian Zone**

**Identified Source
Northern Appalachian (NAP)**

Data/References	Quality (1=low, 5=high)	Notes on Quality of Data	Source Considered	Used in SSC and Reliance Level (0=no, 5=high)	Discussion of Data Use	In GIS Database
<i>Local Geologic and Tectonic Maps</i>						
CEUS SSC basins compilation	4	Data is considered of generally good quality; however, quality is likely variable as it represents a compilation from various published maps and various scales/detail.	NAP	5	SW boundary extends to Connecticut River valley in western Massachusetts and Connecticut; eastern boundary extends to Fundy basin.	Y
Klitgord et al. (1988)	3	Review of Mesozoic basins along Atlantic continental margin.	NAP	5	Eastern boundary of NAP drawn to the west of the Bay of Fundy shown on Plate 2C.	N
Moench and Aleinikoff (2003)	3	Presentation of updated tectonic map for northern New England.	NAP	4	Appalachian terrane boundaries from Figure 1 considered in NW boundary.	N
Murphy and Keppie (2005)	3	Compilation of major Paleozoic strike-slip faults.	NAP	4	Eastern boundary in Nova Scotia drawn along strike-slip faults.	N
<i>Geodetic Strain</i>						
Mazzotti and Adams (2005)	3	Modeled seismic moment rates from earthquake statistics.	NAP	3	Seismic moment rate of $(0.1-5.0) \times 10^{17}$ Nm/yr for entire zone.	N

**Table C-7.3.3 Data Evaluation
Northern Appalachian Zone**

**Identified Source
Northern Appalachian (NAP)**

Data/References	Quality (1=low, 5=high)	Notes on Quality of Data	Source Considered	Used in SSC and Reliance Level (0=no, 5=high)	Discussion of Data Use	In GIS Database
<i>Regional Stress</i>						
CEUS SSC stress data set	4	Provides additional new measurements to World Stress Map.	NAP	1	Data includes thrust mechanisms in a variety of orientations.	Y
Heidbach et al. (2008) (World Stress Map)	3	Compiled worldwide stress indicators from focal mechanisms, borehole breakouts, etc.	NAP	2	Limited entries for the NAP—dominantly thrust mechanisms with some strike-slip. Orientations of maximum horizontal stress vary from E-W to NW-SE, N-S and NNE-SSW.	Y
<i>Focal Mechanisms</i>						
Bent et al. (2003)	4	Focal mechanisms for two New Brunswick earthquakes.	NAP	4	Considered in future earthquake characteristics.	N
Brown and Ebel (1985)	3	Source parameters for aftershocks of 1982 Gaza, New Hampshire, earthquake.	NAP	3	Considered in future earthquake characteristics.	N
Ebel and Bouck (1988)	3	Source parameters for earthquakes occurring in NE from 1981 to 1987.	NAP	3	Considered in future earthquake characteristics.	N

**Table C-7.3.3 Data Evaluation
Northern Appalachian Zone**

**Identified Source
Northern Appalachian (NAP)**

Data/References	Quality (1=low, 5=high)	Notes on Quality of Data	Source Considered	Used in SSC and Reliance Level (0=no, 5=high)	Discussion of Data Use	In GIS Database
Ebel et al. (1986)	3	Source parameters for 1940 Ossipee, New Hampshire, earthquakes.	NAP	3	Considered in future earthquake characteristics.	N
<i>Paleoseismicity</i>						
CEUS SSC paleoliquefaction database	4	Compilation (with attributions) of paleoliquefaction observations.	NAP	N	Mmax determined from the largest observed historical earthquake.	Y

**Table C-7.3.4 Data Evaluation
Paleozoic Extended Crust Zone**

Identified Source
Paleozoic Extended Crust Zone (PEZ) with alternatives: W: Wide; N: Narrow

Data/References	Quality (1=low, 5=high)	Notes on Quality of Data	Source Considered	Used in SSC and Reliance Level (0=no, 5=high)	Discussion of Data Use	In GIS Database
<i>Instrumental Seismicity</i>						
CEUS SSC earthquake catalog	5	Comprehensive catalog; includes magnitude conversions and uncertainty assessments.	PEZ-W, PEZ-N	5	Used to evaluate recurrence parameters.	Y
Dineva et al. (2004)	5	Relocated hypocenters near the Great Lakes.	PEZ-W	4	Used to evaluate the spatial relationships of seismicity with structure.	N
<i>Historical Seismicity</i>						
CEUS SSC earthquake catalog	5	Comprehensive catalog; includes magnitude conversions and uncertainty assessments.	PEZ-W, PEZ-N	5	The prior distribution for Mmax is modified by the largest observed historical earthquake taken from the CEUS SSC earthquake catalog.	Y
Seeber and Armbruster (1993)	3	Reviewed historical seismicity in the vicinity of Lakes Ontario and Erie.	PEZ-W	4	Added and removed historical earthquakes from CEUS SSC earthquake catalog.	N

**Table C-7.3.4 Data Evaluation
Paleozoic Extended Crust Zone**

Identified Source
Paleozoic Extended Crust Zone (PEZ) with alternatives: W: Wide; N: Narrow

Data/References	Quality (1=low, 5=high)	Notes on Quality of Data	Source Considered	Used in SSC and Reliance Level (0=no, 5=high)	Discussion of Data Use	In GIS Database
<i>Magnetic Anomaly</i>						
CEUS SSC magnetic anomaly data set	5	High-quality regional data.	PEZ-W, PEZ-N	2	The PEZ zone is not subdivided based on different basement terranes or tectonic features imaged in the magnetic anomaly map. New York–Alabama lineament not used to delineate source zone.	Y
<i>Gravity Anomaly</i>						
CEUS SSC gravity anomaly data set	5	High-quality regional data.	PEZ-W, PEZ-N	4	Eastern boundary defined by gravity gradient.	Y
<i>Seismic Reflection</i>						
Cook and Oliver (1981)	3	Regional synthesis of gravity data and seismic-reflection profiles.	PEZ-W, PEZ-N	4	Gravity gradient used to define the eastern boundary. Provides seismic evidence that gravity gradient is interpreted as an edge effect corresponding to the boundary between continental crust and former oceanic crust.	N
Fakundiny and Pomeroy (2002)	4	Reprocessed seismic data for the Clarendon-Linden fault system.	PEZ-W, PEZ-N	1	Shows evidence of reactivation of Clarendon-Linden fault system in lower Paleozoic units.	N

**Table C-7.3.4 Data Evaluation
Paleozoic Extended Crust Zone**

Identified Source
Paleozoic Extended Crust Zone (PEZ) with alternatives: W: Wide; N: Narrow

Data/References	Quality (1=low, 5=high)	Notes on Quality of Data	Source Considered	Used in SSC and Reliance Level (0=no, 5=high)	Discussion of Data Use	In GIS Database
Forsyth, Milkereit, Davidson, et al. (1994)	4	Reprocessed marine seismic lines from Lakes Erie and Ontario.	PEZ-W		Shows evidence of reactivation in lower Paleozoic units in eastern Lake Erie.	N
O'Dowd et al. (2004)	5	Interprets seismic data from Southern Ontario Seismic Project line 4 with magnetic data.	PEZ-W	5	Defines western boundary along the Central Metasedimentary Belt boundary zone.	N
Ouassaa and Forsyth (2002)	4	Reprocessed seismic data for the Clarendon- Linden fault system.	PEZ-W, PEZ-N	1	Shows evidence of reactivation of the Clarendon-Linden fault system in lower Paleozoic units.	N
<i>Geophysical Anomalies</i>						
Steltenpohl et al. (2010)	5	Reprocesses new magnetic data for Alabama.	PEZ-N	5	Defines the western boundary of PEZ-N.	N

**Table C-7.3.4 Data Evaluation
Paleozoic Extended Crust Zone**

Identified Source
Paleozoic Extended Crust Zone (PEZ) with alternatives: W: Wide; N: Narrow

Data/References	Quality (1=low, 5=high)	Notes on Quality of Data	Source Considered	Used in SSC and Reliance Level (0=no, 5=high)	Discussion of Data Use	In GIS Database
<i>Local Geologic and Tectonic Maps</i>						
CEUS SSC basins compilation	4	Data is considered of generally good quality; however, quality is likely variable as it represents a compilation from various published maps and various scales/detail.	PEZ-W, PEZ-N	5	Western limit of Mesozoic rift basins used to define eastern boundary	Y
Garritty and Soller (2009)	5	Database with 1:5,000,000-scale geologic map in GIS format compiled from various national maps.	SLR	4	Boundary drawn to capture mapped normal faults in the Adirondacks.	N
Kamo et al. (1995)	3	Compilation of Iapetan faults, dikes, and other intrusive volcanic rocks.	PEZ-N	4	Western Boundary includes Grenville dike swarm, which is coeval with Iapetan rifting.	N
Kanter (1994)	4	Data is considered good quality for defining location of major crustal divisions.	PEZ-W, PEZ-N	4	Used to define source geometry.	Y
McKenna et al. (2007)	2	Presents a heat flow map in Figure 2.	PEZ-W, PEZ-N	1	Data not used to define source geometry.	N

**Table C-7.3.4 Data Evaluation
Paleozoic Extended Crust Zone**

Identified Source
Paleozoic Extended Crust Zone (PEZ) with alternatives: W: Wide; N: Narrow

Data/References	Quality (1=low, 5=high)	Notes on Quality of Data	Source Considered	Used in SSC and Reliance Level (0=no, 5=high)	Discussion of Data Use	In GIS Database
Thomas (1991)	2	Locations of transforms and rift faults are approximate—based on palinspastic restorations.	PEZ-W, PEZ-N	3	Provides a conceptual basis for drawing zones; however, location of boundaries is refined by other data sets.	N
Wheeler (1995)	3	Compilation of late Neoproterozoic to early Cambrian faults.	PEZ-W, PEZ-N	4	Used to define source geometry.	N
Whitmeyer and Karlstrom (2007)	4	Presents regional geologic map of North America documenting assembly of the continent by successive tectonic events.	PEZ-W, PEZ-N	3	Used to define source geometry.	Y
<i>Regional Stress</i>						
CEUS SSC stress data set	4	Provides additional new measurements to World Stress Map.	PEZ-W, PEZ-N	1	Data includes strike-slip mechanisms with minor thrust mechanisms. Orientations generally trend NE-SW. Minor normal mechanisms.	Y

**Table C-7.3.4 Data Evaluation
Paleozoic Extended Crust Zone**

Identified Source
Paleozoic Extended Crust Zone (PEZ) with alternatives: W: Wide; N: Narrow

Data/References	Quality (1=low, 5=high)	Notes on Quality of Data	Source Considered	Used in SSC and Reliance Level (0=no, 5=high)	Discussion of Data Use	In GIS Database
Heidbach et al. (2008) (World Stress Map)	3	Compiled worldwide stress indicators from focal mechanisms, borehole breakouts, etc.	PEZ-W, PEZ-N	2	Data includes strike-slip mechanisms with minor thrust mechanisms. Orientations generally trend NE-SW. Minor normal mechanisms.	Y
<i>Focal Mechanisms</i>						
Herrmann (1978)	3	Earthquake parameters.	PEZ-W	4	Considers focal mechanisms and hypocentral depth for 1966 and 1967 Attica earthquakes.	N
Kim et al. (2006)	4	Parameters for an earthquake in Lake Ontario.	PEZ-W	4	Focal mechanism considered in characterization.	N
<i>Paleoseismicity</i>						
CEUS SSC paleoliquefaction database	5	Compilation (with attributions) of paleoliquefaction observations.	PEZ-W; PEZ-N	1	Considered in discussion along with references below; however, largest observed earthquake determined from historical seismicity.	Y
Law et al. (1994)	4	Paleoseismic investigations in New River Valley of Pembroke, Virginia.	PEZ-N; PEZ-W	3	Describes fault and graben structures in alluvial deposits.	N

**Table C-7.3.4 Data Evaluation
Paleozoic Extended Crust Zone**

Identified Source
Paleozoic Extended Crust Zone (PEZ) with alternatives: W: Wide; N: Narrow

Data/References	Quality (1=low, 5=high)	Notes on Quality of Data	Source Considered	Used in SSC and Reliance Level (0=no, 5=high)	Discussion of Data Use	In GIS Database
Law et al. (2000)	4	Paleoseismic investigations in New River Valley of Pembroke, Virginia.	PEZ-N; PEZ-W	3	Describes extensional and reverse faults cutting alluvial surfaces.	N
Tuttle et al. (2002)	5	Paleoliquefaction investigation surrounding the Clarendon-Linden fault system.	PEZ-W	4	Identifies a lack of paleoliquefaction features. Historical seismicity used to evaluate maximum magnitude.	N

Table C-7.3.5 Data Evaluation
Illinois Basin-Extended Basement Zone

Identified Source
Illinois Basin-Extended Basement (IBEB)

Data/References	Quality (1=low, 5=high)	Notes on Quality of Data	Source Considered	Used in SSC and Reliance Level (0=no, 5=high)	Discussion of Data Use	In GIS Database
<i>Instrumental Seismicity</i>						
CEUS SSC earthquake catalog	5	Comprehensive catalog; includes magnitude conversions and uncertainty assessments.	IBEB	5	Used to evaluate recurrence parameters.	Y
Hamburger et al. (2008)	3	Abstract	IBEB	4	Style of faulting and future earthquake characteristics—Reactivation of structures in contemporary stress regime in Illinois basin region—04:30 CDT, April 18, 2008, M 5.4 earthquake, located near New Harmony fault at depth of ~14 km (~9 mi.).	Y
Withers et al. (2009)	3	Abstract—citing preliminary analysis.	IBEB	4	Style of faulting and future earthquake characteristics—Reactivation of structures in contemporary stress regime in Illinois basin region—April 18, 2008, M _w 5.2 (M _w 5.4 GCMT [http://www.globalcmt.org]) Mt. Carmel, Illinois, earthquake. Largest event in 20 years in Wabash Valley seismic zone.	Y

Table C-7.3.5 Data Evaluation
Illinois Basin-Extended Basement Zone

Identified Source
Illinois Basin-Extended Basement (IBEB)

Data/References	Quality (1=low, 5=high)	Notes on Quality of Data	Source Considered	Used in SSC and Reliance Level (0=no, 5=high)	Discussion of Data Use	In GIS Database
Yang et al. (2009)	3	Abstract—citing preliminary analysis.	IBEB	4	Style of faulting and future earthquake characteristics—Reactivation of structures in contemporary stress regime in Illinois basin region. Analysis of aftershocks from 2008 M 5.4 Mt. Carmel earthquake using sliding-window cross-correlation technique and double-difference relocation algorithm gives a best-fit plane having a nearly E-W trend with an orientation of 248 degrees and a dip angle of 81 degrees. Fault is nearly vertical down to ~20 km (~12.5 mi.). Provides constraints on seismogenic width.	N
Historical Seismicity						
Bakun and Hopper (2004a)	5	Analysis of specific historical earthquakes.	IBEB	4	Earthquake catalog and recurrence—Incorporated into earthquake catalog used to evaluate recurrence.	Y

Table C-7.3.5 Data Evaluation
Illinois Basin-Extended Basement Zone

Identified Source
Illinois Basin-Extended Basement (IBEB)

Data/References	Quality (1=low, 5=high)	Notes on Quality of Data	Source Considered	Used in SSC and Reliance Level (0=no, 5=high)	Discussion of Data Use	In GIS Database
McBride et al. (2007)	5	Integrated assessment based on seismicity, borehole, geophysical, and industry seismic profile data analysis.	IBEB	5	Style of faulting and future rupture characteristics—Discusses possible association of recent earthquakes (April 3, 1974, m_b 4.7; June 10, 1987, m_b 5.2; and November 9, 1968, m_b 5.5 events) with three distinct upper-crust sources in Illinois basin region. Provides detailed discussion of parameters (magnitude, depth, focal mechanism) for each event.	Y
<i>Magnetic Anomaly</i>						
CEUS SSC magnetic anomaly data set	5	High-quality regional data.	IBEB	2	Boundaries of proto-Illinois basin (Precambrian rift basin and extended basement terrane) as outlined in publications (based on seismic data, deep boreholes, and geopotential data) are not uniquely defined by magnetic anomaly map. Geopotential field data used by researchers to define published boundaries of basins.	Y

Table C-7.3.5 Data Evaluation
Illinois Basin-Extended Basement Zone

Identified Source
Illinois Basin-Extended Basement (IBEB)

Data/References	Quality (1=low, 5=high)	Notes on Quality of Data	Source Considered	Used in SSC and Reliance Level (0=no, 5=high)	Discussion of Data Use	In GIS Database
McBride et al. (2001)	2	Extended abstract summarizing observations on geopotential field derivative maps.	IBEB	2	<p>Constraints on boundaries to the IBEB—First vertical derivative of the reduced-to-pole magnetic intensity map shows a subdued magnetic intensity character associated with Proterozoic rifting and/or volcanic sequences in the basement as inferred from deep seismic-reflection profiles; pattern continues to the north and east beyond limits of deep-reflection profile data.</p> <p>Outer margins of sequences, especially to the south and west, marked by prominent coincident closed-contour magnetic and gravity anomalies, which indicate mafic igneous source intrusions.</p>	N
Gravity Anomaly						
CEUS SSC gravity anomaly data set	5	High-quality regional data.	IBEB	2	<p>Boundaries of proto-Illinois basin (Precambrian rift basin and extended basement terrane) as outlined in publications (based on seismic data, deep boreholes, and geopotential data) are not uniquely defined by gravity anomaly map.</p> <p>Geopotential field data used by researchers to define published boundaries of basins.</p>	Y

Table C-7.3.5 Data Evaluation
Illinois Basin-Extended Basement Zone

Identified Source
Illinois Basin-Extended Basement (IBEB)

Data/References	Quality (1=low, 5=high)	Notes on Quality of Data	Source Considered	Used in SSC and Reliance Level (0=no, 5=high)	Discussion of Data Use	In GIS Database
<i>Seismic Reflection</i>						
McBride, Hildenbrand, et al. (2002)	5	Simplified line drawings and interpretations of four reprocessed migrated seismic profiles. Excerpts of reprocessed seismic- reflection profiles. Detailed geologic discussion based on integrated review of seismic and geopotential data.	IBEB	4	Used to define style of faulting and possible basement source structures within source zone.	N

Table C-7.3.5 Data Evaluation
Illinois Basin-Extended Basement Zone

Identified Source
Illinois Basin-Extended Basement (IBEB)

Data/References	Quality (1=low, 5=high)	Notes on Quality of Data	Source Considered	Used in SSC and Reliance Level (0=no, 5=high)	Discussion of Data Use	In GIS Database
McBride et al. (2007)	5	Builds on McBride, Hildenbrand, et al. (2002) and provides additional interpretations of seismic-reflection data. Presents both raw (selected excerpts) and interpreted sections.	IBEB	4	<p>Concepts and ideas in paper help inform drawing the zone boundaries.</p> <p>Style of faulting and future earthquake characteristics—Used to define style of faulting and possible reactivated basement structures within source zone.</p> <p>Notes that limitations of available data preclude a precise interpretation of “correspondence” between specific earthquakes and subsurface structures. Notes that geopotential field data display trends that mimic the structural trends interpreted from reflection profiles and earthquake information. This suggests that mapped fault zones correspond in a general way to gross lateral lithologic changes.</p>	N

Table C-7.3.5 Data Evaluation
Illinois Basin-Extended Basement Zone

Identified Source
Illinois Basin-Extended Basement (IBEB)

Data/References	Quality (1=low, 5=high)	Notes on Quality of Data	Source Considered	Used in SSC and Reliance Level (0=no, 5=high)	Discussion of Data Use	In GIS Database
Pratt et al. (1992)	4	Integrated analysis of seismic profile, geopotential anomaly maps, and drilling data to characterize Precambrian basement rocks.	IBEB	2	Describes layered Precambrian rock sequences and internal features (half graben and sequence boundaries that indicate depositional basin) beneath Illinois basin. Shows examples of COCORP lines. Limited constraints on boundary of zone—discusses extent of Centralia sequence (Precambrian layered igneous sequence) and notes presence of half graben and faults within sequence.	N
<i>Regional Geologic and Tectonic Maps</i>						
Baranoski et al. (2009)	3	Interpretation of seismic, boring, and geophysical data sets.	IBEB	4	Concepts and ideas in paper help inform drawing the zone boundaries—Map of the East Continent rift basin used to define limits of IBEB zone.	Y
Drahovzal (2009)	3	Interpretation of seismic, boring, and geophysical data sets.	IBEB	4	Concepts and ideas in paper help inform drawing the zone boundaries—Map of the East Continent rift basin used to define limits of IBEB zone.	Y
McBride, Pugin, et al. (2003)	3	Interpretation of seismic, boring, and geophysical data sets.	IBEB	4	Concepts and ideas in paper help inform drawing the zone boundaries—Map of proto-Illinois basin used to define limits of IBEB zone.	Y

Table C-7.3.5 Data Evaluation
Illinois Basin-Extended Basement Zone

Identified Source
Illinois Basin-Extended Basement (IBEB)

Data/References	Quality (1=low, 5=high)	Notes on Quality of Data	Source Considered	Used in SSC and Reliance Level (0=no, 5=high)	Discussion of Data Use	In GIS Database
Nelson (1995)	5	Comprehensive compilation of structural mapping for entire state of Illinois and adjoining regions. (Digital format)	IBEB	2	Identifies major structural trends (Wabash Valley fault system, La Salle anticlinal belt). Although some historical earthquakes, such as the 1987 m_b 5.2 earthquake, may be associated with a fault-propagation fold (possible reactivation of a basement fault during Laramide orogeny, McBride et al. (2007) suggest that a clear association of seismicity with mapped structural trends is not well documented throughout southern Illinois basin.	Y
<i>Geodetic Strain</i>						
Hamburger et al. (2002)	1	Only one year of data.	IBEB	1	Generally consistent with focal mechanism data from historical events.	N

Table C-7.3.5 Data Evaluation
Illinois Basin-Extended Basement Zone

Identified Source
Illinois Basin-Extended Basement (IBEB)

Data/References	Quality (1=low, 5=high)	Notes on Quality of Data	Source Considered	Used in SSC and Reliance Level (0=no, 5=high)	Discussion of Data Use	In GIS Database
Hamburger et al. (2008)	3	Abstract	IBEB	3	<p>Style of faulting—analysis of GPS data suggests systematic NW motion of about 0.5–0.7 mm/yr with respect to Stable North American Reference Frame.</p> <p>Block models, which assume boundaries along Cottonwood Grove–Rough Creek Graben (CGRCG) and Wabash Valley fault system (WVFS), indicate marginal block velocities, with possible strike-slip motion along the WVFS and E-W motions along the CGRCG.</p>	N
Hamburger et al. (2009)	3	Abstract	IBEB	2	<p>Localization and stationarity of more concentrated seismicity—data from a 56-site-campaign GPS geodetic network in southern Illinois basin indicate systematic NW motion of about 0.5–0.7 mm/yr with respect to Stable North American Reference Frame.</p> <p>Average strains for entire network show marginally significant strains, with an orientation rotated 45 degrees from overall direction of intraplate stress in U.S. midcontinent.</p> <p>Significant changes in strain and seismicity rates in southern Illinois basin can persist for several hundred years following New Madrid earthquakes. The</p>	N

Table C-7.3.5 Data Evaluation
Illinois Basin-Extended Basement Zone

Identified Source
Illinois Basin-Extended Basement (IBEB)

Data/References	Quality (1=low, 5=high)	Notes on Quality of Data	Source Considered	Used in SSC and Reliance Level (0=no, 5=high)	Discussion of Data Use	In GIS Database
					seismicity rate can increase by as much as a factor of seven over background rate in the near field, but by a much smaller amount in the far field.	
<i>Regional Stress</i>						
CEUS SSC stress data set	4	No additional stress measurements from World Stress map except for two events in Wabash Valley RLME.	IBEB	0	Same as World Stress Map—No additional new data.	Y
Heidbach et al. (2008) (World Stress Map)	3	Worldwide compilation of stress data.	IBEB	3	Three events used by the World Stress Map, while tectonically and spatially distinct, represent contemporary maximum horizontal compressive stress that trends just north of east in southern Illinois and Indiana (McBride et al., 2007).	Y

Table C-7.3.5 Data Evaluation
Illinois Basin-Extended Basement Zone

Identified Source
Illinois Basin-Extended Basement (IBEB)

Data/References	Quality (1=low, 5=high)	Notes on Quality of Data	Source Considered	Used in SSC and Reliance Level (0=no, 5=high)	Discussion of Data Use	In GIS Database
<i>Tectonic Strain Focal Mechanisms</i>						
Hamburger et al. (2008) Larson (2002) Larson et al. (2009) McBride, Hildenbrand, et al. (2002) McBride et al. (2007) Withers et al. (2009) Yang et al. (2009)	4	Well-constrained focal mechanisms for several recent moderate-sized (M 4–5.4) earthquakes in Wabash Valley region of southern Illinois and Indiana.	IBEB	4	Focal mechanisms indicate ongoing deformation along reactivated Precambrian and Paleozoic basement structures. Analyses indicate three seismotectonic environments in upper crust: strike-slip (E-NE and NE trends) and reverse fault.	N
Larson et al. (2009)	3	Abstract—citing preliminary analysis	IBEB	4	04:30 CDT, April 18, 2008, M 5.4 earthquake, E-W focal mechanism.	Y

Table C-7.3.5 Data Evaluation
Illinois Basin-Extended Basement Zone

Identified Source
Illinois Basin-Extended Basement (IBEB)

Data/References	Quality (1=low, 5=high)	Notes on Quality of Data	Source Considered	Used in SSC and Reliance Level (0=no, 5=high)	Discussion of Data Use	In GIS Database
<i>Paleoseismicity</i>						
Paleoliquefaction studies by numerous researchers (see Table 6.1.9-1 and Appendix E—CEUS SSC paleoliquefaction database)	4–5	One of best paleoliquefaction data sets available for a region in CEUS.	IBEB	5	<p>Constraint on zone boundary—Evidence for several moderate- to large-magnitude prehistoric earthquakes suggest possible different recurrence rate in southern Illinois/Indiana relative to surrounding regions</p> <p>Mmax—paleoeearthquakes are used to modify likelihood function for Mmax distribution.</p>	Y

Table C-7.3.6 Data Evaluation
Reelfoot Rift Zone

Identified Sources
Reelfoot Rift Zone (RR); Reelfoot Rift–Rough Creek Graben (RR-RCG)

Data/References	Quality (1=low, 5=high)	Notes on Quality of Data	Source Considered	Used in SSC and Reliance Level (0=no, 5=high)	Discussion of Data Use	In GIS Database
<i>Instrumental Seismicity</i>						
CEUS SSC earthquake catalog	5	Comprehensive catalog; includes magnitude conversions and uncertainty assessments.	RR and RR-RCG	5	Used to develop recurrence parameters.	Y
Chiu et al. (1992)	4	Publication discussing results of PANDA survey.	RR	5	Focal depth—Seismic activity in central NMSZ occurs continuously between ~5 and 14 km (~3 and 9 mi.) depth.	N
Chiu et al. (1997)	4	Peer-reviewed publication. Results from three seismic networks (1974–1994).	RR (SE margin)	4	Focal depth—Nine earthquakes with focal mechanisms; 6.3–22.8 km (4–14.2 mi.); five earthquakes between 13.9 and 17.3 km (8.6–10.7 mi.).	N
<i>Magnetic Anomaly</i>						
CEUS SSC magnetic anomaly data set	5	High-quality regional data.	RR and RR-RCG	4	Used to evaluate alternate geometries of RR.	Y
Hildenbrand and Hendricks (1995)	5	Detailed discussion of interpretations of geopotential data sets.	RR and RR-RCG	5	Source boundaries—Used to evaluate locations of plutons of possible Mesozoic or younger age (limits of significant Mesozoic extension).	N

Table C-7.3.6 Data Evaluation
Reelfoot Rift Zone

Identified Sources
Reelfoot Rift Zone (RR); Reelfoot Rift–Rough Creek Graben (RR-RCG)

Data/References	Quality (1=low, 5=high)	Notes on Quality of Data	Source Considered	Used in SSC and Reliance Level (0=no, 5=high)	Discussion of Data Use	In GIS Database
Gravity Anomaly						
CEUS SSC gravity anomaly data set	5	High-quality regional data.	RR and RR-RCG	1	Source boundaries—Used to evaluate alternate geometries of RR.	Y
Seismic Reflection						
(See Table D-6.1.5 Data Summary—Reelfoot Rift–New Madrid Seismic Zone)	n/a	n/a	RR	1	Seismic-reflection data integrated into publications that define structures within RR. Specific lines not used directly in this study.	N
Odum et al. (2010)	3	Provides interpreted high-resolution seismic profile data to support alternative structural model. Discusses evidence for recency.	RR	2	Style of faulting and future rupture characteristics—Potential fault source within RR that is not modeled as an RLME.	N
Pratt (2009)	3	Abstract and poster presentation (pers. comm., October 29, 2010, USGS Memphis meeting).	RR	3	Broad zone of faulting is present in the rift.	N

Table C-7.3.6 Data Evaluation
Reelfoot Rift Zone

Identified Sources

Reelfoot Rift Zone (RR); Reelfoot Rift–Rough Creek Graben (RR-RCG)

Data/References	Quality (1=low, 5=high)	Notes on Quality of Data	Source Considered	Used in SSC and Reliance Level (0=no, 5=high)	Discussion of Data Use	In GIS Database
<i>Regional Geologic and Tectonic Maps</i>						
Csontos et al. (2008)	3	Integrated structure-contour map of top of basement showing subbasins and bounding NE- and SE-striking faults.	RR	5	Source boundaries—Used to constrain boundaries of RR. Geometry and style of faulting—Used to evaluate future rupture characteristics.	N
Bear et al. (1997) Hildenbrand and Hendricks (1995) Hildenbrand and Ravat (1997) Kolata and Hildenbrand (1997) Wheeler (1997)	3	Published articles that provide good documentation of data that can be used to evaluate northern limit of RR.	RR	4	Various publications that provide evidence for northern terminus of RR and lack of continuity with Rough Creek graben (RCG) and structures in Wabash Valley seismic zone region.	N
Hildenbrand et al. (2001)	3	Detailed discussion of structures in the New Madrid seismic zone region of the RR. Good-quality figures showing interpretations.	RR	5	Source boundaries—Used to constrain boundaries of RR.	N

Table C-7.3.6 Data Evaluation
Reelfoot Rift Zone

Identified Sources

Reelfoot Rift Zone (RR); Reelfoot Rift–Rough Creek Graben (RR-RCG)

Data/References	Quality (1=low, 5=high)	Notes on Quality of Data	Source Considered	Used in SSC and Reliance Level (0=no, 5=high)	Discussion of Data Use	In GIS Database
Soderberg and Keller (1981) Kolata and Nelson (1991) Potter and Drahovzal (1994) Nelson (1995)	5	Published articles that provide good documentation of data that can be used to evaluate continuity of RR and RCG.	RR-RCG	4	Possible structural continuity of RR and RCG—The RCG in western Kentucky is structurally connected to northern portion of RR that includes Fluorspar area of southern Illinois.	Y
Local Geologic and Tectonic Maps						
Nelson and Lumm (1987) Kolata and Nelson (1991)	4	Published articles based on integration of subsurface geologic, seismologic, and geophysical data. Published figures are of a quality that can be used to define structures.	RR-RCG	5	Boundaries of RCG—Bounded on north by south-dipping, listric Rough Creek fault, and on NW by Shawneetown fault. Southern boundary approximately follows Pennyryle fault system, which forms southern margin to the Paleozoic syn-rift deposits.	N
Regional Stress						
Forte et al. (2007)	3	Regional analysis of properties of upper mantle and lower crust.	RR and RR-RCG	1	Provides rationale for concentrating seismic stress in the vicinity of RR, but is not specific enough to use to draw source zone boundaries.	N

Table C-7.3.6 Data Evaluation
Reelfoot Rift Zone

Identified Sources
Reelfoot Rift Zone (RR); Reelfoot Rift–Rough Creek Graben (RR-RCG)

Data/References	Quality (1=low, 5=high)	Notes on Quality of Data	Source Considered	Used in SSC and Reliance Level (0=no, 5=high)	Discussion of Data Use	In GIS Database
Grana and Richardson (1996)	3	Detailed discussion of stress data in NMSZ.	RR	1	Modeling indicates that stresses from the load of rift pillow may still be present in upper crust and may still play a role in present-day deformation. Justification for RR.	N
Li et al. (2009)	3	Process-oriented paper based on 3-D viscoelasto-plastic finite-element model.	RR and RR-RCG (out-of-cluster model)	2	Supports migration of seismicity within RR. Model replicates some of the spatiotemporal complexity of clustered, episodic, and migrating intraplate earthquakes. Time-scale-dependent spatio-temporal patterns of intraplate seismicity support suggestions that seismicity patterns observed from short-term seismic records may not reflect long-term patterns of intraplate seismicity.	N

Table C-7.3.6 Data Evaluation
Reelfoot Rift Zone

Identified Sources
Reelfoot Rift Zone (RR); Reelfoot Rift–Rough Creek Graben (RR-RCG)

Data/References	Quality (1=low, 5=high)	Notes on Quality of Data	Source Considered	Used in SSC and Reliance Level (0=no, 5=high)	Discussion of Data Use	In GIS Database
<i>Focal Mechanisms</i>						
Shumway (2008)	4	Detailed analysis of seismicity data using recent velocity model and appropriate depths to bedrock beneath seismic stations.	RR	4	Style of faulting and depth of seismogenic crust based on well-constrained focal mechanism date.	N
Zoback (1992)	4	Well-constrained focal mechanisms.	RR and RR-RCG	3	Style of faulting in RR—Four focal mechanisms show predominantly strike-slip motion.	N
<i>Paleoseismicity</i>						
Database of published and unpublished data provided by Dr. M. Tuttle (included in CEUS SSC paleoliquefaction database)	5	Well-documented database.	RR and RR-RCG	5	No evidence to date for repeated Holocene earthquakes in RCG.	Y
Harrison and Schultz (2002) Wheeler (2005)	3	Published descriptions of Quaternary deformation in Slinkard Quarry, Missouri.	RR	3	Activity and style of faulting—Evidence for possible prehistoric earthquakes in Cape Girardeau, Missouri, area.	N

**Table C-7.3.6 Data Evaluation
Reelfoot Rift Zone**

Identified Sources
Reelfoot Rift Zone (RR); Reelfoot Rift–Rough Creek Graben (RR-RCG)

Data/References	Quality (1=low, 5=high)	Notes on Quality of Data	Source Considered	Used in SSC and Reliance Level (0=no, 5=high)	Discussion of Data Use	In GIS Database
McBride, Nelson, and Stephenson (2002)	4	Integrated analysis of evidence; good-quality maps and figures.	RR	4	Discussion of evidence for timing of earthquakes on Fluorspar Area fault complex; hypothesis of temporal changes and migration of seismicity within rift.	N

**Tables C-7.3.7/7.3.8 Data Evaluation
Extended Continental Crust—Atlantic**

Identified Sources

Extended Continental Crust—Atlantic Margin (ECC-AM); Atlantic Highly Extended Crust (AHEX)

Data Reference	Quality (1=low, 5=high)	Notes on Quality of Data	Source Considered	Used in SSC and Reliance Level (0=no, 5=high)	Discussion of Data Use	In GIS Database
<i>Instrumental Seismicity</i>						
CEUS SSC earthquake catalog	5	Comprehensive catalog; includes magnitude conversions and uncertainty assessments.	ECC-AM, AHEX	5	Used to define recurrence parameters.	Y
<i>Historical Seismicity</i>						
Bakun et al. (2003)	4	Detailed assessment of Cape Ann earthquake and two other historical events using new MMI model and site corrections for eastern North America.	ECC-AM	4	Location of western ECC-AM boundary offshore Massachusetts drawn to include the preferred location of Cape Ann earthquake. The 95% confidence level for location was used in weighting possibility that Cape Ann earthquake should be used to modify Mmax prior distribution for both ECC-AM and NAP.	N
Bollinger et al. (1991)	3	Spatial distribution (including depth) of earthquakes in the CEUS through 1986. Data largely superseded by the CEUS SSC earthquake catalog.	ECC-AM	2	Hypocenters of Coastal Plain shocks are distributed throughout upper 13 km of crust, where focal mechanisms indicate a N-NE maximum compressive stress.	N

**Tables C-7.3.7/7.3.8 Data Evaluation
Extended Continental Crust—Atlantic**

Identified Sources

Extended Continental Crust—Atlantic Margin (ECC-AM); Atlantic Highly Extended Crust (AHEX)

Data Reference	Quality (1=low, 5=high)	Notes on Quality of Data	Source Considered	Used in SSC and Reliance Level (0=no, 5=high)	Discussion of Data Use	In GIS Database
Ebel (2006)	4	Detailed re-examination of 1755 Cape Ann earthquake from firsthand historical accounts.	ECC-AM	4	Location of western ECC-AM boundary offshore Massachusetts drawn to include location of Cape Ann earthquake.	N
<i>Magnetic Anomaly</i>						
CEUS SSC magnetic anomaly database	5	High-quality regional data set	ECC-AM, AHEX	3	Considered for defining boundaries of zone along eastern and southern margins. ECC zone is not subdivided based on different basement terranes or tectonic features imaged in the magnetic anomaly map.	N
Holbrook (1994a, 1994b)	4	Multichannel seismic-reflection and wide-angle ocean-bottom seismic profiles provide seismic velocity model of U.S. Atlantic continental margin	ECC-AM, AHEX	4	Concludes that transitional igneous crust was created by rift-related intrusives, marking eastern boundary of extended continental crust. These studies confirm that the western margin of East Coast magnetic anomaly (ECMA) marks boundary between extended continental crust and transitional crust, and eastern margin of ECMA corresponds approximately to western margin of oceanic crust.	N

**Tables C-7.3.7/7.3.8 Data Evaluation
Extended Continental Crust—Atlantic**

Identified Sources

Extended Continental Crust—Atlantic Margin (ECC-AM); Atlantic Highly Extended Crust (AHEX)

Data Reference	Quality (1=low, 5=high)	Notes on Quality of Data	Source Considered	Used in SSC and Reliance Level (0=no, 5=high)	Discussion of Data Use	In GIS Database
Klitgord et al. (1988)	4	Regional synthesis of structural and geophysical data to develop tectonic framework of U.S. Atlantic continental margin.	ECC-AM, AHEX	4	Eastern boundary follows ECMA presented on Plate 2A.	N
McBride and Nelson (1988)	4	Integration of magnetic anomaly analysis with COCORP deep-reflection data.	ECC-AM	4	Uses seismic data to investigate source of Brunswick magnetic anomaly and concludes that it is a deep structure marking Alleghanian collision. This was used to define southern border of ECC-AM.	N
Gravity Anomaly						
CEUS SSC gravity anomaly database	5	High-quality regional data set	ECC-AM, AHEX	2	The ECC zone is not subdivided based on different basement terranes or tectonic features imaged in the gravity anomaly map.	Y
Klitgord et al. (1988)	4	Regional synthesis of structural and geophysical data to develop tectonic framework of U.S. Atlantic continental margin.	ECC-AM, AHEX	5	Eastern boundary follows landward edge of oceanic crust shown on Plate 2B.	N

**Tables C-7.3.7/7.3.8 Data Evaluation
Extended Continental Crust—Atlantic**

Identified Sources

Extended Continental Crust—Atlantic Margin (ECC-AM); Atlantic Highly Extended Crust (AHEX)

Data Reference	Quality (1=low, 5=high)	Notes on Quality of Data	Source Considered	Used in SSC and Reliance Level (0=no, 5=high)	Discussion of Data Use	In GIS Database
Pratt (1988)	4	Regional seismic reflection line across Virginia Piedmont.	ECC-AM	4	Concludes that Appalachian gravity anomaly gradient marks a fundamental zone of weakness coincident with western extent of thinned continental crust.	N
<i>Seismic Reflection</i>						
[various studies]	3-5	Interpretations from various publications such as Cook and Vasudevan (2006); Glover et al. (1995); Hatcher et al. (1994); and Sheridan et al. (1993). (See ECC Data Summary Table.)	ECC-AM, AHEX	1	Interpretations of deep crustal seismic profiles (COCORP) provide good information for identifying and characterizing structures and major terrane boundaries in basement. No basement structures, however, are identified as specific seismic sources in this study.	N
<i>Geophysical Anomaly</i>						
Li et al. (2003)	4	Determined velocity structure from inversion of Rayleigh waves.	ECC-AM	4	NW-trending prong of ECC in eastern New York, western Massachusetts, and SW Vermont captures the negative crustal velocity anomaly attributed to the Great Meteor hotspot.	N

**Tables C-7.3.7/7.3.8 Data Evaluation
Extended Continental Crust—Atlantic**

Identified Sources

Extended Continental Crust—Atlantic Margin (ECC-AM); Atlantic Highly Extended Crust (AHEX)

Data Reference	Quality (1=low, 5=high)	Notes on Quality of Data	Source Considered	Used in SSC and Reliance Level (0=no, 5=high)	Discussion of Data Use	In GIS Database
<i>Regional Geologic and Tectonic Maps</i>						
CEUS SSC basins compilation	4	Data is considered of generally good quality; however, quality is likely variable as it represents a compilation from various published maps and various scales/detail.	ECC-AM	5	Data set includes digital GIS compilation of Mesozoic basins from a variety of published sources. Used to delineate western margin of ECC zone.	Y
Kanter (1994)	4	Data is considered of good quality for defining location of major crustal divisions (e.g., oceanic crust, extended crust, transitional crust) in the Gulf of Mexico region.	ECC-AM	5	Data on the location of extended crust were used for defining the source geometry.	N

**Tables C-7.3.7/7.3.8 Data Evaluation
Extended Continental Crust—Atlantic**

Identified Sources

Extended Continental Crust—Atlantic Margin (ECC-AM); Atlantic Highly Extended Crust (AHEX)

Data Reference	Quality (1=low, 5=high)	Notes on Quality of Data	Source Considered	Used in SSC and Reliance Level (0=no, 5=high)	Discussion of Data Use	In GIS Database
Klitgord et al. (1988)	4	Regional synthesis of structural and geophysical data to develop tectonic framework of U.S. Atlantic continental margin.	ECC-AM	4	Eastern boundary includes Carolina trough, Baltimore canyon trough, Georgia Banks basin, and Scotia basin inboard of the East Coast magnetic anomaly illustrated on Plate 2C. Western boundary of ECC in New England drawn to the west of Bay of Fundy shown on Plate 2C.	N
Murphy and Keppie (2005)	3	Regional compilation of major Paleozoic strike-slip faults.	ECC-AM	4	Western boundary in Nova Scotia drawn along strike-slip faults separating Avalonia and Meguma terranes.	N
Pe-Piper and Piper (2004)	4	Regional-scale fault mapping in Grand Banks region of Atlantic Canada.	ECC-AM	4	Western boundary in Nova Scotia drawn along strike-slip fault system separating Avalonia and Meguma terranes.	N
<i>Regional Stress</i>						
CEUS SSC stress data set	4	Provides additional new measurements to World Stress Map	ECC-AM	1	Update of World Stress Map data for CEUS shows consistent orientation of maximum horizontal stress in ECC.	Y
Zoback and Zoback (1989)	4	Good-quality data regional set that is outdated but still consistent with updated stress measurements.	ECC-AM	1	Maximum horizontal stress in eastern U.S. roughly NE to ENE.	N

**Tables C-7.3.7/7.3.8 Data Evaluation
Extended Continental Crust—Atlantic**

Identified Sources

Extended Continental Crust—Atlantic Margin (ECC-AM); Atlantic Highly Extended Crust (AHEx)

Data Reference	Quality (1=low, 5=high)	Notes on Quality of Data	Source Considered	Used in SSC and Reliance Level (0=no, 5=high)	Discussion of Data Use	In GIS Database
<i>Paleoseismicity</i>						
CEUS SSC paleoliquefaction database	5	High-quality data set	ECC-AM	2	With the exception of the Charleston RLME, paleoliquefaction data is insufficient for constraining source parameters within ECC-AM.	Y
Obermeier and McNulty (1998)	2	Abstract	ECC-AM	0	The search for paleoliquefaction along 300 km of rivers in Central Virginia seismic zone (CVSZ) documented only two to three features and does not provide evidence for RLME, which, in part, is why CVSZ is not broken out as a separate seismic source in this study. Increased rate of seismicity can be modeled with spatial smoothing.	N

**Tables C-7.3.9/7.3.10 Data Evaluation
Extended Continental Crust–Gulf Coast**

Identified Sources

Extended Continental Crust–Gulf Coast (ECC-GC); Gulf Coast Highly Extended Crust (GHEX)

Data/References	Quality (1=low, 5=high)	Notes on Quality of Data	Source Considered	Used in SSC and Reliance Level (0=no, 5=high)	Discussion of Data Use	In GIS Database
<i>Instrumental Seismicity</i>						
CEUS SSC earthquake catalog	5	Comprehensive catalog; includes magnitude conversions and uncertainty assessments.	ECC-GC, GHEX	5	Used to define recurrence parameters.	Y
<i>Magnetic Anomaly</i>						
CEUS SSC magnetic anomaly database	5	High-quality regional data.	ECC-GC, GHEX	0	Considered for defining boundaries of zone.	Y
<i>Gravity Anomaly</i>						
CEUS SSC gravity anomaly database	5	High-quality regional data.	ECC-GC, GHEX	0	Considered for defining boundaries of zone.	Y
<i>Regional Geologic and Tectonic Maps</i>						
Baksi (1997)	3	Data considered of moderate quality for defining northern extent of Mesozoic extension.	ECC-GC	1	Concepts and ideas in paper helped inform drawing zone boundaries.	N

**Tables C-7.3.9/7.3.10 Data Evaluation
Extended Continental Crust–Gulf Coast**

Identified Sources

Extended Continental Crust–Gulf Coast (ECC-GC); Gulf Coast Highly Extended Crust (GHEX)

Data/References	Quality (1=low, 5=high)	Notes on Quality of Data	Source Considered	Used in SSC and Reliance Level (0=no, 5=high)	Discussion of Data Use	In GIS Database
Bird et al. (2005)	4	Data considered of good quality for defining extent of oceanic crust in Gulf of Mexico.	GHEX	5	Northern boundary of oceanic crust used in defining southern boundary of the zone.	N
Buffler and Sawyer (1985)	3	Data considered of moderate quality for defining extent of transitional and oceanic crust in Gulf of Mexico.	ECC-GC, GHEX	1	Concepts and ideas in paper helped inform drawing the zone boundaries.	N
Byerly (1991)	3	Data considered of moderate quality for defining northern extent of Mesozoic extension.	ECC-GC	1	Concepts and ideas in paper helped inform drawing the zone boundaries.	N
Cook et al. (1979)	3	Data considered of moderate quality for defining extent of Rio Grande rift–related extension.	ECC-GC	2	Used to inform western extent of boundary.	N

**Tables C-7.3.9/7.3.10 Data Evaluation
Extended Continental Crust–Gulf Coast**

Identified Sources

Extended Continental Crust–Gulf Coast (ECC-GC); Gulf Coast Highly Extended Crust (GHEX)

Data/References	Quality (1=low, 5=high)	Notes on Quality of Data	Source Considered	Used in SSC and Reliance Level (0=no, 5=high)	Discussion of Data Use	In GIS Database
Daniels et al. (1983)	4	Data considered of good quality for defining eastern extent of Mesozoic extension.	ECC-GC	4	Eastern extent of Mesozoic extension considered in defining eastern boundary of the zone.	N
Dellinger, Dewey, et al. (2007) Dellinger, Ehlers, and Clarke (2007)	3	Data considered of moderate quality for discussing characteristics of Green Canyon earthquake.	GHEX	3	Used to help inform maximum observed earthquake in the zone.	N
Dewey and Dellinger (2008)	3	Data considered of moderate quality for discussing characteristics of Green Canyon earthquake.	GHEX	3	Used to help inform maximum observed earthquake in the zone.	N
Dickerson and Muehlberger (1994)	3	Data considered of moderate quality for defining extent of Rio Grande rift–related extension.	ECC-GC	2	Used to inform western extent of boundary.	N

**Tables C-7.3.9/7.3.10 Data Evaluation
Extended Continental Crust–Gulf Coast**

Identified Sources

Extended Continental Crust–Gulf Coast (ECC-GC); Gulf Coast Highly Extended Crust (GHEX)

Data/References	Quality (1=low, 5=high)	Notes on Quality of Data	Source Considered	Used in SSC and Reliance Level (0=no, 5=high)	Discussion of Data Use	In GIS Database
Gray et al. (2001)	2	Data considered of moderate quality for defining extent of Rio Grande rift–related extension.	ECC-GC	1	Used to inform western extent of boundary.	N
Hall and Najmuddin (1994)	3	Data considered of moderate quality for defining extent of oceanic crust.	GHEX	1	Concepts and ideas in paper help inform drawing the zone boundaries.	N
Harry and Londono (2004)	3	Data considered of moderate quality for defining extent of Mesozoic extension.	ECC-GC	1	Concepts and ideas in paper help inform drawing the zone boundaries.	N
Hatcher et al. (2007)	3	Data considered of moderate quality for defining northern extent of Mesozoic extension.	ECC-GC	1	Concepts and ideas in paper help inform drawing the zone boundaries.	N
Hendricks (1988)	3	Data considered of moderate quality for defining northern extent of Mesozoic extension.	ECC-GC	1	Concepts and ideas in paper help inform drawing the zone boundaries.	N

**Tables C-7.3.9/7.3.10 Data Evaluation
Extended Continental Crust–Gulf Coast**

Identified Sources

Extended Continental Crust–Gulf Coast (ECC-GC); Gulf Coast Highly Extended Crust (GHEX)

Data/References	Quality (1=low, 5=high)	Notes on Quality of Data	Source Considered	Used in SSC and Reliance Level (0=no, 5=high)	Discussion of Data Use	In GIS Database
Hildenbrand and Hendricks (1995)	4	Data considered of good quality for presenting location of Cretaceous igneous intrusions in southern Arkansas.	ECC-GC	4	Used in defining northern extent of the zone in region of southern Arkansas and eastern Texas.	N
Kanter (1994)	4	Data considered of good quality for defining location of major crustal divisions (e.g., oceanic crust, extended crust, transitional crust) in Gulf of Mexico region.	ECC-GC, GHEX	5	Data on the location of oceanic crust and extent of transitional crust were used in defining source geometries.	Y
Klitgord et al. (1984)	4	Data considered of good quality for defining eastern extent of Mesozoic extension.	ECC-GC	4	Eastern extent of Mesozoic extension considered in defining eastern boundary of the zone.	N
Marton and Buffler (1994)	3	Data considered of moderate quality for defining extent of transitional and oceanic crust in Gulf of Mexico.	ECC-GC, GHEX	1	Concepts and ideas in paper help inform drawing the zone boundaries.	N

**Tables C-7.3.9/7.3.10 Data Evaluation
Extended Continental Crust–Gulf Coast**

Identified Sources

Extended Continental Crust–Gulf Coast (ECC-GC); Gulf Coast Highly Extended Crust (GHEX)

Data/References	Quality (1=low, 5=high)	Notes on Quality of Data	Source Considered	Used in SSC and Reliance Level (0=no, 5=high)	Discussion of Data Use	In GIS Database
McBride and Nelson (1988)	3	Data considered of moderate quality for defining northern extent of Mesozoic extension.	ECC-GC	1	Concepts and ideas in paper help inform drawing the zone boundaries.	N
McBride et al. (2005)	3	Data considered of moderate quality for defining northern extent of Mesozoic extension.	ECC-GC	1	Concepts and ideas in paper help inform drawing the zone boundaries.	N
Murray (1961)	2	Data considered of moderate quality for defining extent of Rio Grande rift–related extension.	ECC-GC	1	Used to inform the western extent of boundary.	N
Nagihara and Jones (2005)	4	Data considered of good quality for defining extent of oceanic crust in Gulf of Mexico.	GHEX	4	Northern boundary of oceanic crust was used in defining southern boundary of the zone.	N

**Tables C-7.3.9/7.3.10 Data Evaluation
Extended Continental Crust–Gulf Coast**

Identified Sources

Extended Continental Crust–Gulf Coast (ECC-GC); Gulf Coast Highly Extended Crust (GHEX)

Data/References	Quality (1=low, 5=high)	Notes on Quality of Data	Source Considered	Used in SSC and Reliance Level (0=no, 5=high)	Discussion of Data Use	In GIS Database
Nettles (2007)	3	Data considered of moderate quality for discussing characteristics of the Green Canyon earthquake.	GHEX	3	Used to help inform the maximum observed earthquake in the zone.	N
Petersen et al. (2008)	4	Data considered of good quality for defining landward limit of Precambrian lapetan rifting.	ECC-GC	5	Limit of Precambrian rifting was used in defining NE boundary of the zone.	N
Pindell and Kennan (2001)	4	Data considered of good quality for defining extent of oceanic crust and transitional crust in Gulf of Mexico.	GHEX	2	Concepts and ideas in paper help inform drawing zone boundaries.	N
Pindell et al. (2000)	4	Data considered of good quality for defining extent of oceanic crust and transitional crust in Gulf of Mexico.	GHEX	4	Northern boundary of the oceanic crust was used in defining southern boundary of the zone.	N

**Tables C-7.3.9/7.3.10 Data Evaluation
Extended Continental Crust–Gulf Coast**

Identified Sources

Extended Continental Crust–Gulf Coast (ECC-GC); Gulf Coast Highly Extended Crust (GHEX)

Data/References	Quality (1=low, 5=high)	Notes on Quality of Data	Source Considered	Used in SSC and Reliance Level (0=no, 5=high)	Discussion of Data Use	In GIS Database
Salvador (1991a)	3	Data considered of moderate quality for defining extent of Mesozoic extension.	ECC-GC	2	Concepts and ideas in paper help inform drawing zone boundaries.	N
Sawyer et al. (1991)	4	Data considered of good quality for defining extent of oceanic crust in Gulf of Mexico.	ECC-GC, GHEX	3	Northern boundary of the oceanic crust was used in defining southern boundary of the zone, and the boundary between the thick and thin transitional crust was used in defining boundaries between the GHEX and ECC-GC zones.	N
Thomas (1988) Thomas (2006)	3	Data considered of moderate quality for defining extent of Mesozoic extension.	ECC-GC	2	Concepts and ideas in paper help inform drawing zone boundaries.	N N
Wheeler and Frankel (2000)	4	Data considered of good quality for defining location of the lapetan margin of the ancestral North American continent.	ECC-GC	4	Used in defining northern extent of the zone in regions where (1) the Mesozoic rifting is thought to be coincident with Paleozoic rifting, or (2) there is considerable uncertainty in the limit of Mesozoic rifting and the various interpretations of rifting encompass the lapetan margin boundary.	N

Table C-7.3.12 Data Evaluation
Midcontinent-Craton Zone

Identified Sources

Alternative Midcontinent-Craton (MidC) source zone configurations (MIDC-A, MIDC-B, MIDC-C, and MIDC-D) are based on different combinations of alternative zone boundaries for the Paleozoic Extended Zone (Table C-7.3.4) and Reelfoot Rift Zone (Table C-7.3.6)

Data Type/References	Quality (1=low, 5=high)	Notes on Quality or Data	Source Considered	Used in SSC and Reliance Level (0=no, 5=high)	Description of Data Use	In GIS Database
<i>Instrumental Seismicity</i>						
CEUS SSC earthquake catalog	5	Comprehensive catalog; includes magnitude conversions and uncertainty assessments.	MIDC-A, MIDC-B, MIDC-C, MIDC-D	5	Used to evaluate recurrence parameters.	Y
<i>Historical Seismicity</i>						
Bakun and Hopper (2004a)	4	Reanalysis of intensity data.	MIDC-A, MIDC-B, MIDC-C, MIDC-D	4	Estimated magnitude for historical earthquake used in recurrence and Mmax assessments—Associates an April 9, 1952, M 4.9 (4.5–5.2) earthquake with the Nemaha fault in Oklahoma.	N
CEUS SSC earthquake catalog	5	Comprehensive catalog includes magnitude conversions and uncertainty assessments.	MIDC-A, MIDC-B, MIDC-C, MIDC-D	5	The prior distribution for Mmax is modified by the largest observed historical earthquake taken from the CEUS SSC earthquake catalog.	Y

Table C-7.3.12 Data Evaluation
Midcontinent-Craton Zone

Identified Sources

Alternative Midcontinent-Craton (Mid-C) source zone configurations (MIDC-A, MIDC-B, MIDC-C, and MIDC-D) are based on different combinations of alternative zone boundaries for the Paleozoic Extended Zone (Table C-7.3.4) and Reelfoot Rift Zone (Table C-7.3.6)

Data Type/References	Quality (1=low, 5=high)	Notes on Quality or Data	Source Considered	Used in SSC and Reliance Level (0=no, 5=high)	Description of Data Use	In GIS Database
Niemi et al. (2004)	1	This paper, which relies on a previous assessment of size of historical earthquake (Seeber and Armbruster, 1991), does not provide any independent analysis of the earthquake catalog.	MIDC-A, MIDC-B, MIDC-C, MIDC-D	2	Considered in evaluating association of a historical earthquake (1867 M 5.2 Wamego earthquake) with basement Nemaha Ridge–Humboldt fault structures.	N
<i>Magnetic Anomaly</i>						
Atekwana (1996) Hinze et al. (1975) Klasner et al. (1982) Bickford et al. (1986) Van Schmus (1992) NICE Working Group (2007)	3	Publications that describe basement terranes that have been mapped and identified in part from interpretation of patterns and characteristics of the magnetic anomalies	MIDC-A, MIDC-B, MIDC-C, MIDC-D	2	Style of faulting and future ruptures—Provides indication of structural trends in basement.	N

**Table C-7.3.12 Data Evaluation
Midcontinent-Craton Zone**

Identified Sources

Alternative Midcontinent-Craton (MidC) source zone configurations (MIDC-A, MIDC-B, MIDC-C, and MIDC-D) are based on different combinations of alternative zone boundaries for the Paleozoic Extended Zone (Table C-7.3.4) and Reelfoot Rift Zone (Table C-7.3.6)

Data Type/References	Quality (1=low, 5=high)	Notes on Quality or Data	Source Considered	Used in SSC and Reliance Level (0=no, 5=high)	Description of Data Use	In GIS Database
CEUS SSC magnetic anomaly data set	5	High-quality regional data.	MIDC-A, MIDC-B, MIDC-C, MIDC-D	2 (except for border with Reelfoot rift where the reliance was 4)	The Mid-C zone is not subdivided based on different basement terranes or tectonic features imaged in the magnetic anomaly map. The border between Reelfoot Rift and Mid-C seismotectonic zones is defined in part by the limit of magnetic anomalies that are interpreted to be Mesozoic plutons associated with Mesozoic rifting in the RR.	Y
Gravity Anomaly						
CEUS SSC gravity anomaly data set	5	High-quality regional data.	MIDC-A, MIDC-B, MIDC-C, MIDC-D	1	The Mid-C zone is not subdivided based on different basement terranes or tectonic features imaged in the gravity anomaly map.	Y

**Table C-7.3.12 Data Evaluation
Midcontinent-Craton Zone**

Identified Sources

Alternative Midcontinent-Craton (Mid-C) source zone configurations (MIDC-A, MIDC-B, MIDC-C, and MIDC-D) are based on different combinations of alternative zone boundaries for the Paleozoic Extended Zone (Table C-7.3.4) and Reelfoot Rift Zone (Table C-7.3.6)

Data Type/References	Quality (1=low, 5=high)	Notes on Quality or Data	Source Considered	Used in SSC and Reliance Level (0=no, 5=high)	Description of Data Use	In GIS Database
Keller (2010)	2	Unpublished report: Provides limited interpretation of area in Oklahoma.	MIDC-A, MIDC-B, MIDC-C, MIDC-D	1	Evaluation of zone of structures associated with a region of elevated seismicity— Midcontinent rift system (MRS)—concludes that MRS may extend south to Wichita uplift and seismicity may be associated with this feature and Nemaha fault zone/ridge. This is accounted for in the variable smoothing of seismicity within the zone.	Y
Seismic Reflection						
(See Table D-7.3.12 Data Summary— Midcontinent-Craton Zone)	3-5	Interpretations from various publications.	MIDC-A, MIDC-B, MIDC-C, MIDC-D	1	Interpretations of deep crustal seismic profiles (COCORP, GLIMPCE) provide best information for identifying and characterizing structures and major terrane boundaries in the basement. No basement structures, however, are identified in this study as specific seismic sources.	N

Table C-7.3.12 Data Evaluation
Midcontinent-Craton Zone

Identified Sources

Alternative Midcontinent-Craton (MidC) source zone configurations (MIDC-A, MIDC-B, MIDC-C, and MIDC-D) are based on different combinations of alternative zone boundaries for the Paleozoic Extended Zone (Table C-7.3.4) and Reelfoot Rift Zone (Table C-7.3.6)

Data Type/References	Quality (1=low, 5=high)	Notes on Quality or Data	Source Considered	Used in SSC and Reliance Level (0=no, 5=high)	Description of Data Use	In GIS Database
<i>Geodetic Strain</i>						
Calais et al. (2006)	3	Provides a combination of two independent geodetic solutions using data from close to 300 continuous GPS stations covering CEUS.	MIDC-A, MIDC-B, MIDC-C, MIDC-D	3	<p>Surface deformation in North American Plate interior is best fit by a model that includes rigid rotation of North America with respect to global reference point and a component of strain related to glacial isostatic adjustment (GIA).</p> <p>No significant deviation from rigidity resolvable at the 0.7 mm/yr level.</p> <p>EW strain < $1.5 \times 10^{-10} \text{ yr}^{-1}$.</p> <p>No areas of localized strain found.</p>	N
<i>Regional Stress</i>						
CEUS SSC stress data set	4	Provides additional new measurements to World Stress Map.	MIDC-A, MIDC-B, MIDC-C, MIDC-D	1	An additional measurement in NE Oklahoma is consistent with previous measurements.	Y

Table C-7.3.12 Data Evaluation
Midcontinent-Craton Zone

Identified Sources

Alternative Midcontinent-Craton (Mid-C) source zone configurations (MIDC-A, MIDC-B, MIDC-C, and MIDC-D) are based on different combinations of alternative zone boundaries for the Paleozoic Extended Zone (Table C-7.3.4) and Reelfoot Rift Zone (Table C-7.3.6)

Data Type/References	Quality (1=low, 5=high)	Notes on Quality or Data	Source Considered	Used in SSC and Reliance Level (0=no, 5=high)	Description of Data Use	In GIS Database
Heidbach et al. (2008) (World Stress Map)	3	Most current published version of map.	MIDC-A, MIDC-B, MIDC-C, MIDC-D	2	Limited entries for the Mid-C— Maximum horizontal compressional stress orientations vary from E-W (NE Kansas) to E-NE (Wisconsin and Ohio) to N-NE (W Minnesota, SW Kansas).	Y
<i>Focal Mechanisms</i>						
Zoback (1992)	4	Well-constrained focal mechanisms.	MIDC-A, MIDC-B, MIDC-C, MIDC-D	3	Limited focal mechanisms for the craton (e.g., W Minnesota; Illinois platform; Sharpsburg, Kentucky) Perry, Ohio; generally indicate strike-slip motion.	N
<i>Paleoseismicity</i>						
CEUS SSC paleoliquefaction database	5	Compilation (with attributions) of paleoliquefaction observations.	MIDC-A, MIDC-B, MIDC-C, MIDC-D	3	Mmax assessment—Evidence for possible prehistoric earthquakes in St. Louis area.	Y

Table C-7.3.12 Data Evaluation
Midcontinent-Craton Zone

Identified Sources

Alternative Midcontinent-Craton (MidC) source zone configurations (MIDC-A, MIDC-B, MIDC-C, and MIDC-D) are based on different combinations of alternative zone boundaries for the Paleozoic Extended Zone (Table C-7.3.4) and Reelfoot Rift Zone (Table C-7.3.6)

Data Type/References	Quality (1=low, 5=high)	Notes on Quality or Data	Source Considered	Used in SSC and Reliance Level (0=no, 5=high)	Description of Data Use	In GIS Database
Niemi et al. (2004)	3	Detailed evaluation of historical seismicity and neotectonic field investigations (including paleoliquefaction studies) in E Kansas.	MIDC-A, MIDC-B, MIDC-C, MIDC-D	3	Nemaha Ridge/Humboldt fault (Kansas)—Initial results suggest that liquefaction features (e.g., clastic dikes), which may be attributed to seismically induced liquefaction, are present, but may not be pervasive in this region. These data suggest that the 1867 M 5.2 Wamego earthquake may characterize the seismic source in this region.	N
Tuttle, Chester, et al. (1999) Tuttle (2005a) Tuttle (2005b)	4	Results of regional paleoliquefaction study in SE Missouri; provides detailed description of features and postulated locations of causative faults (possibly in IBEB).	MIDC-A, MIDC-B, MIDC-C, MIDC-D	3	Mmax assessment—Evidence for possible prehistoric earthquakes in St. Louis area. Location and magnitude of paleoearthquakes is not well constrained by data. There is not sufficient data to support characterization of an RLME source in St. Louis.	N

APPENDIX D

Data Summary Tables

D

APPENDIX DATA SUMMARY TABLES

Default Source Characteristics for CEUS SSC Project Study Region

Table D-5.4 Future Earthquake Characteristics

RLME Sources

Table D-6.1.1	Charlevoix RLME
Table D-6.1.2	Charleston RLME
Table D-6.1.3	Cheraw Fault RLME
Table D-6.1.4	Oklahoma Aulacogen RLME
Table D-6.1.5	Reelfoot Rift–New Madrid Seismic Zone RLMEs
[No Table D-6.1.6]	[Reelfoot Rift–Eastern Rift Margin RLME; see Table D-6.1.5]
[No Table D-6.1.7]	[Reelfoot Rift–Marianna RLME; see Table D-6.1.5]
[No Table D-6.1.8]	[Reelfoot Rift–Commerce Fault Zone RLME; see Table D-6.1.5]
Table D-6.1.9	Wabash Valley RLME

Seismotectonic Zones

Table D-7.3.1	St. Lawrence Rift Zone (SLR)
Table D-7.3.2	Great Meteor Hotspot Zone (GMH)
Table D-7.3.3	Northern Appalachian Zone (NAP)
Table D-7.3.4	Paleozoic Extended Crust Zone (PEZ; narrow [N] and wide [W])
[No Table D-7.3.5]	[Illinois Basin–Extended Basement Zone (IBEB); see Table D-6.1.9]
[No Table D-7.3.6]	[Reelfoot Rift Zone (RR) including Rough Creek Graben (RR-RCG); see Table D-6.1.5]
Table D-7.3.7	Extended Continental Crust Zone–Atlantic Margin (ECC-AM)
[No Table D-7.3.8]	[Atlantic Highly Extended Crust Zone (AHEx); see Table D-7.3.7]
Table D-7.3.9	Extended Continental Crust Zone–Gulf Coast (ECC-GC)
[No Table D-7.3.10]	[Gulf Coast Highly Extended Crust Zone (GHEx); see Table D-7.3.9]
[No Table D-7.3.11]	[Oklahoma Aulacogen (OKA); see Table D-6.1.4]
Table D-7.3.12	Midcontinent–Craton Zone (MidC)

Mmax Zones

Criteria for defining the MESE/NMESE boundary for the two-zone alternative are discussed in Section 6.2.2. MESE-N includes ECC-AM, ECC-GC, AHEx, GHEx, RR, SLR, NAP, GMH, and PEZ-N. MESE-W differs from MESE-N in that it adopts the wide alternative geometries (i.e., PEZ-W, RR-RCG, and IBEB). See the tables listed above for data pertinent to the definition of the boundaries of the zones and evidence for Mesozoic and younger tectonism. Default future earthquakes rupture parameters (Table 4.1.3-1) are assigned to both the one-zone and two-zone Mmax sources.

Introduction

The Data Summary tables were developed to provide information on the various data that were considered during the course of the characterization of seismic sources. The table designation is linked to the chapter and section where the table is first cited. In some cases, information related to multiple seismic sources is included in a single table. The tables provide the citations to the data and a description of the key conclusions and their potential relevance to SSC. Full citations of references listed in the tables are provided in Chapter 10. All data sets included in the tables were reviewed, although not all were ultimately used to characterize a particular seismic source. Additional information on the Data Summary tables is provided in Section 4.1.2.2.

Please note that magnitudes are reported in the magnitude scale designated in the cited publication.

Table D-5.4 Data Summary
Future Earthquake Characteristics

Citation	Title	Description and Relevance to SSC
Atkinson (2004)	Empirical Attenuation of Ground-Motion Spectral Amplitudes in Southeastern Canada and the Northeastern United States	Presents a database of 1,700 digital seismograms from 186 earthquakes of magnitude M_N 2.5–5.6 that occurred in SE Canada and the NE United States from 1990 to 2003. The focus of the paper is the development of ground motion attenuation relationships, but the database represents high-quality instrumental recordings; source parameters are given for all events. This information can be used to examine various future earthquake characteristics such as focal depth.
Chapman et al. (1997)	A Statistical Analysis of Earthquake Focal Mechanisms and Epicenter Locations in the Eastern Tennessee Seismic Zone	This paper reports that 26 well-constrained focal mechanism solutions are derived using a new velocity model and relocated hypocenters. The results suggest that strike-slip motion on steeply dipping planes is the dominant mode of faulting throughout the 300 km (186 mi.) long Eastern Tennessee seismic zone. Most of the mechanisms can be grouped into two populations. The larger population is characterized by steeply dipping N-S- and E-W-striking nodal planes with right-lateral and left-lateral slip, respectively. The second population differs from the first by an approximate 45° eastward rotation about the B-axis. The results suggest a series of NE-trending en echelon basement faults, intersected by several east-trending faults. Most of the larger-magnitude instrumentally located earthquakes in the seismic zone occurred close to the statistically identified potential faults.
Dineva et al. (2004)	Seismicity of the Southern Great Lakes: Revised Earthquake Hypocenters and Possible Tectonic Controls	Using data from 27 seismograph stations for the period 1990–2001, 106 hypocenters with magnitudes of 0.9–5.4 were relocated in the region of the southern Great Lakes. Both the seismicity and magnetic anomalies exhibit statistically significant preferred orientations at N40°E–N45°E, but the correlation of the earthquake clusters with specific magnetic lineaments remains uncertain. Three preliminary focal mechanisms of earthquakes with magnitudes M_N 3.1–3.8 show unusual normal faulting, with nodal planes in almost the same direction as the magnetic trends, N42°E–N52°E.
Heidbach et al. (2008) (World Stress Map)	The World Stress Map Project Database Release 2008	Compilation of stress indicators for the CEUS shows consistent tectonic stress directions in the NE quadrant. No strong evidence for stress subprovinces.

**Table D-5.4 Data Summary
Future Earthquake Characteristics**

Citation	Title	Description and Relevance to SSC
Horton et al. (2005)	The 6 June 2003 Bardwell, Kentucky, earthquake sequence: Evidence for a Locally Perturbed Stress Field in the Mississippi Embayment	Includes a compilation of earthquake focal mechanisms of the earthquakes that occurred in the central U.S. since 1960s, including Reelfoot rift, Rough Creek graben in western Kentucky, and Wabash Valley fault system along SE Illinois/SW Indiana border. Special study of the June 6, 2003, Bardwell, Kentucky, earthquake, including a number of aftershocks, has been done to provide high-quality locations and focal mechanisms. Mechanisms are primarily strike-slip, with a component of reverse faulting. Focal mechanisms of earthquakes in the New Madrid seismic zone with E-W-trending nodal planes have different trending P axes, suggesting a strong perturbation in the stress field over a distance of about 60 km (37 mi.).
Kim (2003)	The 18 June 2002 Caborn, Indiana, Earthquake: Reactivation of Ancient Rift in the Wabash Valley Seismic Zone?	Presents an assessment of the June 18, 2002, Caborn, Indiana, earthquake (M_w 4.6) using regional and teleseismic waveform data, and concludes that the event occurred on a steeply dipping fault at a depth of about 18 km (11 mi.). The source mechanism determined from regional waveform analysis is predominantly strike-slip along near-vertical nodal planes. The June 2002 event at 18 km (11 mi.) depth and the south-central Illinois earthquake on November 9, 1968 (M_w 5.3), which occurred at 25 km (15.5 mi.) depth, suggest that seismogenic depth in the Wabash Valley seismic zone extends to at least 18 km (11 mi.).
Kim and Chapman (2005)	The 9 December 2003 Central Virginia Earthquake Sequence: A Compound Earthquake in the Central Virginia Seismic Zone	The December 9, 2003, central Virginia earthquake sequence was a compound earthquake consisting of two nearly identical events occurring about 12 sec apart. The source mechanism determined from regional waveform inversion indicates predominantly thrust faulting at a depth of approximately 10 ± 2 km (6 ± 1 mi.). A regional stress model for the Central Virginia seismic zone derived from the December 9, 2003, events and 11 previous earthquakes indicates a thrust-faulting stress regime. The December 9, 2003, earthquake sequence occurred among the systems of Paleozoic and Mesozoic faults above the southern Appalachian décollement, which is at 12–19 km (7–12 mi.) depth in the Piedmont geologic province of central Virginia.
Mai et al. (2005)	Hypocenter Locations in Finite-Source Rupture Models	The paper compiles data related to hypocenter depths in relation to the normalized downdip width of fault rupture for crustal faults and subduction zones. The relationships can be used to assess expected depth distribution of earthquakes as a function of earthquake magnitude.

**Table D-5.4 Data Summary
Future Earthquake Characteristics**

Citation	Title	Description and Relevance to SSC
Marshak and Paulsen (1997)	Structural Style, Regional Distribution, and Seismic Implications of Midcontinent Fault-and-Fold Zones, United States	Summarizes steeply dipping faults and associated monoclinally forced folds, which were active in pulses during the Phanerozoic, although it is suggested that they initiated during episodes of Proterozoic extensional tectonism. Based on fault-trace orientation, Midcontinent fault-and-fold zones are divided into two sets—one trending N-NE and the other trending W-NW. Many W-NW-trending fault-and-fold zones link along strike to define semicontinuous NW-trending deformation corridors. One of these, the 200 km (124 mi.) wide Transamerican tectonic zone (TTZ), traces over 2,500 km (1,553 mi.) from Idaho to South Carolina. Seismicity most frequently occurs where N-NE-trending fault-and-fold zones cross the TTZ, suggesting that intracratonic strain in the U.S. currently concentrates at or near intersecting fault zones within this corridor.
Mazzotti (2009 CEUS SSC Workshop 2 presentation)	Strain (and Stress) Constraints on Seismicity in the St. Lawrence Valley	Map showing ~50 focal mechanisms indicates primarily reverse faulting, with a component of strike-slip. Plots of interpreted maximum compressive stress directions show that both σ_1 and σ_2 are horizontal. Also shown are differences in the orientation of σ_1 for events to the north of the axis of the St. Lawrence (in the NE quadrant) versus south (approximately E-W).
NAGRA (2004)	Probabilistic Seismic Hazard Analysis for Swiss Nuclear Power Plant Sites (PEGASOS Project)	This large PSHA was conducted for four nuclear power plant sites in Switzerland, which is characterized by a seismotectonic setting very similar to the CEUS. Presents an approach to characterize the depth distribution of future earthquake ruptures using the focal depth distribution of observed hypocenters. The approach takes advantage of observed seismicity as well as studies of the magnitude dependence of focal depths.
Seeber et al. (1998)	The 1994 Cacoosing Valley Earthquakes near Reading, Pennsylvania: A Shallow Rupture Triggered by Quarry Unloading	The paper discusses the m_{BLg} 4.6 main shock on January 16, 1994, in the Cacoosing Valley, 10 km (6 mi.) west of Reading, SE Pennsylvania. This zone matches the nodal plane with reverse and left-lateral slip (strike 135°, dip 54°SW, and rake 55°) of a focal mechanism obtained from aftershock first motions and from main-shock waveforms.
Shumway (2008)	Focal Mechanisms in the Northeast New Madrid Seismic Zone	Earthquakes in the NE New Madrid seismic zone from June 1995 to June 2006 were relocated using a velocity model of the Mississippi embayment with appropriate depths to bedrock beneath seismic stations. Focal mechanisms were generated for events on the NE-trending alignments. The results show that most of the earthquakes are strike-slip and approximately half the focal mechanisms have a N-NE-striking nodal plane and a right-lateral, strike-slip component consistent with earlier studies of the NMNF to the southwest.

Table D-5.4 Data Summary
Future Earthquake Characteristics

Citation	Title	Description and Relevance to SSC
Sibson (1982)	Fault Zone Models, Heat Flow, and the Depth Distribution of Earthquakes in the Continental Crust of the United States	Models of fault zones in continental crust, based on analysis of rock deformation textures, suggest that depth of seismic activity is controlled by the passage from a pressure-sensitive, dominantly frictional regime to strongly temperature-dependent, quasi-plastic mylonitization at greenschist and higher grades of metamorphism. Based on models of the frictional and rheological properties of quartz-bearing rocks, crude strength-depth curves for different geotherms are developed. In such models, shear resistance peaks sharply at the inferred seismic-aseismic transition. Depth at which 90% of microseismic activity occurs is plotted on the modeled strength-depth curves for various heat flow provinces of the conterminous U.S.
Sibson (1984)	Roughness at the Base of the Seismogenic Zone: Contributing Factors	Observational data such as earthquake focal depths and considerations of the strength profile of continental crust are both used to draw conclusions regarding the controls of the thickness of the seismogenic zone. Implications are drawn regarding the likely depths of large earthquakes and their magnitude dependence.
Sibson (2007)	Au-Quartz Mineralization near the Base of the Continental Seismogenic Zone	The base of the continental seismogenic zone is defined within individual fault zones by the transition with depth from pressure-sensitive frictional (FR) faulting to temperature-sensitive quasi-plastic (QP) ductile shearing. The depth of this FR-QP transition fluctuates principally as a consequence of variations in geothermal gradient and crustal lithology but other factors (e.g., fluid pressure level, strain rate) also play a role. Topographic irregularities in the seismic-aseismic transition determine rupture nucleation sites and probably play a critical role in focusing the discharge of overpressured metamorphic fluids into the seismogenic layer. This information has implications to the depth of larger earthquakes and their nucleation near the base of the seismogenic zone.
Sibson and Xie (1998)	Dip Range for Intracontinental Reverse Fault Ruptures: Truth Not Stranger than Friction?	Histograms of fault dips have been compiled for moderate to large ($M > 5.5$) reverse-slip intracontinental earthquakes with the slip-vector raking $90^\circ \pm 30^\circ$ in the fault plane. The principal data set is restricted to earthquakes where the fault plane in the focal mechanism can be unambiguously distinguished from the auxilliary plane; the reverse fault dips are bracketed within the range of 12° – 60° with a prominent peak in the 25° – 35° interval and a subsidiary peak in the 45° – 55° interval.

**Table D-5.4 Data Summary
Future Earthquake Characteristics**

Citation	Title	Description and Relevance to SSC
Somerville et al. (2001)	Ground Motion Attenuation Relations for the Central and Eastern United States	As part of developing ground-motion attenuation relations, the authors first developed earthquake source scaling relations for use in generating ground motions. The source models have spatially varying slip distributions on the fault plane, and are described by self-similar scaling relations between seismic moment and source parameters such as fault dimensions and rise time derived from the slip models of three recent earthquakes in eastern Canada. Scaling relationships of earthquake rupture models are presented relating fault rupture area and seismic moment that are deemed to be appropriate for eastern North America.
Sykes et al. (2008)	Observations and Tectonic Setting of Historic and Instrumentally Located Earthquakes in the Greater New York City–Philadelphia Area	As part of discussions of seismicity in the New York region, high-quality earthquake locations and focal depths are given. The focal depth distribution provides information on seismogenic crustal thickness for the region.
Talwani (2009 CEUS SSC Workshop 2 presentation)	The Source and Magnitude of the Charleston Earthquake	The presentation summarized the latest instrumental seismicity data for the Charleston region. Included in the talk was a plot of focal depth distribution for instrumental events in the region.
Tanaka (2004)	Geothermal Gradient and Heat Flow Data in and Around Japan (II): Crustal Thermal Structure and Its Relationship to Seismogenic Layer	The high-quality database of seismicity of Japan (Japan Meteorological Agency, or JMA) and an extensive compilation of thermal measurements (Tanaka et al., 2004) are used to quantify the concept of temperature as a fundamental parameter for determining thickness of the seismogenic zone. Qualitative comparisons between each data of heat flow and geothermal gradient, and the lower limit of crustal earthquake hypocentral distributions beneath the Japanese Islands show that, as expected, the lower limit of seismicity is inversely related to heat flow and geothermal gradient. Gridded heat flow or geothermal gradient and D_{90} , the depth above which 90% of earthquakes occur, correlated well with each other. The evaluated temperatures for D_{90} range between 250°C and 450°C except for higher heat flow data. The consistency of temperature for D_{90} over a large depth interval almost all over the Japanese islands support the concept that the temperature is the dominant factor governing the focal depth in the crust.

**Table D-5.4 Data Summary
Future Earthquake Characteristics**

Citation	Title	Description and Relevance to SSC
Tanaka and Ishikawa (2002)	Temperature Distribution and Focal Depth in the Crust of the Northeastern Japan	Comparisons are made between heat flow, thermal gradient and earthquake databases for NE Japan. Temperatures in the crust were calculated using a steady-state one-dimensional heat-conductive transport model with heat generation as a function of heat flow and thermal gradient. The evaluated temperatures for D_{90} , the depth above which 90% of earthquakes occur, range between 200°C and 500°C except for high heat flow and thermal gradient data. The consistency of temperature for D_{90} over a large depth interval supports the theory that temperature is the dominant factor governing the focal depth in the crust.
van Lanen and Mooney (2007)	Integrated Geologic and Geophysical Studies of North American Continental Intraplate Seismicity	The paper provides a histogram of earthquake focal depth in eastern North America (ENA) as a function of moment magnitude. The compilation for ENA is compared to other stable continental regions. The paper concludes that seismicity is correlated with the NE-SW structural grain of the crust of ENA, which in turn reflects the opening and closing of the proto- and modern Atlantic Ocean. This structural grain can be discerned as clear NE-SW lineaments in the Bouguer gravity and aeromagnetic anomaly maps. Stable continental region seismicity either (1) follows the NE-SW lineaments, (2) is aligned at right angles to these lineaments, or (3) forms clusters at what have been termed stress concentrators.
Wesnousky (2008)	Displacement and Geometrical Characteristics of Earthquake Surface Ruptures: Issues and Implications for Seismic-Hazard Analysis and the Process of Earthquake Rupture	This paper includes a compilation of empirical data regarding the seismologic and geologic characteristics of earthquake ruptures. The data set is aimed at establishing rupture characteristics and their uncertainties for use in seismic hazard and fault displacement hazard analyses. A relationship between fault length-to-width aspect ratio versus magnitude is presented.
Zoback (1992)	Stress Field Constraints on Intraplate Seismicity in Eastern North America	Focal mechanisms of 32 North American CEUS earthquakes are evaluated to determine if slip is compatible with a broad-scale regional stress field derived from plate-driving forces and, if so, under what conditions. Independent information on in situ stress orientations from well bore breakout and hydraulic fracturing data is used to assess relative stress magnitudes. The evaluation of the data confirmed a roughly north-to-south contrast in stress regime between the CEUS and SE Canada: most CEUS earthquakes occur in response to a strike-slip stress regime, whereas SE Canada events require a thrust-faulting stress regime.

**Table D-5.4 Data Summary
Future Earthquake Characteristics**

Citation	Title	Description and Relevance to SSC
Zoback (2010)	CEUS SSC stress data set	<p>Database updates the compilation for the CEUS developed originally for the World Stress Map. Uses a variety of indicators (e.g., earthquake focal mechanisms, in situ stress measurements) of the orientation of the maximum compressive stresses. Stress data based on earthquake focal mechanisms and other in situ stress indicators were compiled for the past 10 years and added to the existing world stress map. Orientations of maximum compressive stress directions are consistent with those compiled earlier. There is no longer compelling evidence for a northwesterly directed stress province along the Atlantic margin, as postulated in the 1980s. There is some suggestion of stress rotation within the New Madrid seismic zone, which would suggest a weak zone, but the evidence is not strong.</p>

Table D-6.1.1 Data Summary
Charlevoix RLME

Citation	Title	Description and Relevance to SSC
<i>Geologic Structures Interpreted from Geologic, Gravity, Magnetic, and Seismic Profile Data</i>		
Lemieux et al. (2003)	Structural Analysis of Supracrustal Faults in the Charlevoix Area, Quebec: Relation to Impact Cratering and the St-Laurent Fault System	<p>Two major sets of fault orientations (N290°–N320° and N020°–N040°) are found outside the impact zone, with minor fault sets trending N270–N280 and N000–N020. Within the impact crater, fault orientations are more scattered but are similar to the NW- and NE-trending systems of the external domain. The spread of orientations within the central portion of the crater is attributed to the impact-related polygonal pattern of normal faults, whereas the NW and NE fault sets represent the youngest reactivation.</p> <p>Coarse-grained cataclastic breccias up to 50 m thick are exposed along brittle faults striking NE and NW outside the impact crater. Similar cataclastic breccias are also found within the impact crater but are usually less than a few meters thick. Polymictic clastic matrix breccia is found exclusively within the impact crater. Fragments of cataclastic breccia are present, suggesting recurrent brecciation during incremental faulting events. Pseudotachylyte and foliated gouge are locally related to the cataclastic breccia, indicating that these rocks originate from a post-impact single and progressive tectonic event along the St. Lawrence rift system.</p> <p>The St-Laurent fault influenced the deposition of Ordovician deposits during late stages of the Taconian orogeny by syndepositional faulting preserved as major lateral thickness variations within the section, presence of slump deformation in almost all stratigraphic units, preservation of pseudotachylyte within synsedimentary breccias, and occurrence of fault breccia clasts. However, the geometry and structural characteristics of faulting are consistent with Mesozoic fault reactivation due to rifting of the North Atlantic region.</p>

**Table D-6.1.1 Data Summary
Charlevoix RLME**

Citation	Title	Description and Relevance to SSC
Tremblay and Lemieux (2001)	Supracrustal Faults of the St. Lawrence Rift System Between Cap-Tourmente and Baie-Saint-Paul, Quebec	<p>The Cap-Tourmente and St. Lawrence faults are late Proterozoic–early Paleozoic normal faults attributed to rifting during the opening of the Iapetus Ocean. The St. Lawrence rift system is a NE-trending half graben that links the NW-trending grabens of the Ottawa-Bonnechere and Saguenay aulacogens. The St. Lawrence fault trends N020°–N050° and dips 60°–70° to the southeast. Fault rocks consist of fault breccia, cataclastite, foliated gouge, and pseudotachylyte with a minimum thickness of 20 m near Sault-au-Cochon. Fault rocks exposed at Cap-Tourmente consist of 10–15 m thick zones of protocataclasite, cataclasite, and fault breccia. Within the Charlevoix area, the St. Lawrence fault is characterized by a well-developed and extensive series of cataclastic rock, gouge, and associated pseudotachylyte. The Cap-Tourmente fault trends E-W and dips approximately 80° to the south. Fault rocks consist mostly of fault breccia more than 10 m thick, as well as cataclastic rocks and dark pseudotachylyte veins. The St. Lawrence fault is crosscut by the Cap-Tourmente fault at Cap-Tourmente.</p> <p>West of Cap-Tourmente, the Montmorency Falls fault occupies the same structural position as the St. Lawrence fault, suggesting that they formed from en echelon faults trending parallel to the axis of the St. Lawrence rift. The Cap-Tourmente fault possibly represents a transfer fault, producing an oblique relay between two longitudinal normal faults. The St. Lawrence fault crosses the Charlevoix impact crater without major trend deflection or fault offsets within or at the boundaries of the Devonian impact structure. This observation suggests that impact-related faults did not significantly alter the orientation of preexisting structures and that reactivation is younger than the impact structure, most probably concurrent with the opening of the Atlantic Ocean in the Mesozoic.</p>

Table D-6.1.1 Data Summary
Charlevoix RLME

Citation	Title	Description and Relevance to SSC
Tremblay et al. (2003)	Supracrustal Faults of the St. Lawrence Rift System, Quebec: Kinematics and Geometry as Revealed by Field Mapping and Marine Seismic Reflection Data	<p>Presents strike orientations, dip angles, and pitch angles for faults with evidence for frictional sliding in the St. Lawrence rift system. NE-trending longitudinal faults show three trends (N025, N040, and N070) and generally dip to the SE, although a minor number dip to the NW. Transverse faults show two trends (N290 and N310) and dip to the NE or SW, which is consistent with the horst-and-graben geometry. Both sets of faults are high-angle faults with dip angles averaging 75°–80°. The pitch value of fault lineations is greater than 70°, indicating that most structures are dip-slip faults. Longitudinal and transverse faults show mutual crosscutting relationships, suggesting that they represent conjugate structures related to the same tectonic event.</p> <p>The St-Laurent fault has experienced at least 800 m of vertical throw at Sault-au-Cochon. The Cap-Tourmente fault has a minimum vertical fault throw of 700 m. The Montmorency fault has an 80 m fault scarp near Quebec City, and stratigraphic analysis suggests that fault throw should be less than 150 m, which is considerably less than the other faults. Several offshore faults subparallel to that fault may have vertical downthrow displacements up to 1 km (0.6 mi.).</p> <p>Longitudinal faults likely result from the development of en echelon faults trending parallel to the rift axis, and transfer faults represent transfer faults or accommodation zones. Variations in fault throw are likely a result of propagation of extension along transfer faults.</p> <p>The presence of cataclastic rocks, pseudotachylytes, and fault gouge is consistent with changes of deformation mechanics during progressive and incremental deformation in the upper crust.</p> <p>High-resolution seismic profiles in the St. Lawrence estuary indicate that the Laurentian Channel trough transitions from a half graben to a graben structure from SW to NE.</p> <p>The authors speculate that reactivation of the St. Lawrence rift system is post-Ordovician, younger than the Devonian impact cratering event, and that it experienced additional fault throw and shoulder uplift during the Mesozoic opening of the North Atlantic.</p>

**Table D-6.1.1 Data Summary
Charlevoix RLME**

Citation	Title	Description and Relevance to SSC
<i>Magnitude Estimates</i>		
Bent (1992)	A Re-examination of the 1925 Charlevoix, Québec Earthquake	Analysis of additional waveforms resulted in magnitude estimates of M_w 6.2, M_s 6.2 ± 0.3 , and m_b 6.5 ± 0.4 . Due to insufficient 1-sec period data, m_{bLg} was not determined.
Ebel (1996)	The Seventeenth Century Seismicity of Northeastern North America	Ebel (1996) assigned a $M \geq 7.0 \pm 0.5$ to the 1663 Charlevoix earthquake. This interpretation is based on accounts of landsliding and liquefaction along the St. Lawrence River and several of its tributaries, and on felt effects in Quebec, Acadia (Maine), and eastern Massachusetts. Based on this distribution of felt effects, the magnitude of the 1663 event is somewhat larger than the 1925 Charlevoix earthquake.
Ebel (2006b)	Thoughts Concerning Earthquake Sources in the Northeastern U.S.	Postulated that if the total length of the Charlevoix seismic zone (70 km) produced a single rupture, the 1663 event would be M 7.5, and all modern seismicity can be thought of as aftershocks of this event.
Ebel (2009)	On the Magnitude of the 1663 Charlevoix, Quebec Earthquake	A rupture length of 70 km (43.5 mi.; the length of the seismic zone) could produce a main-shock magnitude of M 7.1–7.5. Interpreted MMI VI reports at Roxbury, Massachusetts, with an intensity-attenuation relationship as an M_{Lg} 7.5 (M 7.8), and with recent ground-motion attenuation relationships as an M 7.5. These lines of evidence suggest a magnitude of M 7.5 ± 0.3 for the 1663 Charlevoix event.
Lamontagne et al. (2008)	Significant Canadian Earthquakes of the Period 1600-2006	Repeated large-magnitude historical earthquakes have occurred in Charlevoix: February 5, 1663, M 7; December 6, 1791, M 5.8; October 17, 1860, M 6; October 20, 1870, M 6.5; and March 1, 1925, M 6.2.
<i>Recurrence</i>		
Doig (1990)	2300 Yr History of Seismicity from Silting Events in Lake Tadoussac, Charlevoix, Quebec	Inferred a variable recurrence rate for the Charlevoix seismic zone from silt layers in lakes due to earthquake-induced landslides. Some silt layers in the section were correlated with historic earthquakes from 1638, 1663, 1791, 1870, and 1925. From 320 BC to AD 800, determined a 120-year recurrence interval, 270 years between AD 800 and 1500, and 75 years from AD 1500 to the present.

Table D-6.1.1 Data Summary
Charlevoix RLME

Citation	Title	Description and Relevance to SSC
Filion et al. (1991)	A Chronology of Landslide Activity in the Valley of Rivière du Gouffre, Charlevoix, Quebec	Sampled tree trunks buried in landslide flow materials from four sectors along the Gouffre River between Saint-Urbain and Baie-Saint-Paul. The age distribution of tree trunks indicates that landslides have occurred at 5,670, 3,170, 2,500, and 1,870 yr BP, with most ages <600 yr BP. Comparison of tree-ring widths throughout the study area suggests that trees died during the latent period between the 1662 and 1663 growing seasons, possibly due to synchronous landslides. The authors interpret these two landslides as having been caused by the February 1663 Charlevoix earthquake. These results provide no evidence for the 1925 earthquake. The authors emphasize the importance of tree-ring techniques to delineate the areal extent of landslides caused by the 1663 earthquake and to caution against exaggerating the geomorphic consequences of earthquakes.
Tuttle and Atkinson (2010)	Localization of Large Earthquakes in the Charlevoix Seismic Zone, Quebec, Canada, During the Past 10,000 Years	Provides evidence for three Holocene paleoearthquakes in Charlevoix with $M \geq 6.2$, including at least two prehistoric episodes at 5 and 10 ka.
Seismicity—Focal Mechanisms and Fault Geometry		
Baird et al. (2009)	Stress Channeling and Partitioning of Seismicity in the Charlevoix Seismic Zone, Quebec, Canada	<p>Seismicity is localized along two elongate bands of seismicity bounded by rift faults extending NE of the Charlevoix impact crater. In a 2-D stress model, faults are represented as frictional discontinuities, and the impact crater as an elastic continuum of reduced modulus. Stress trajectories flow around the weak impact crater, concentrating stress along weak faults into the impact crater, resulting in seismicity in linear bands. The asymmetric placement of the rift faults through the crater results in increased seismicity potential along the rift, north of the crater.</p> <p>Observed seismicity, is therefore interpreted as a result of stress concentration due to the interaction of the crater (local zone of weakness) and rift faults (large-scale weak zone). Small to moderate seismicity occurs within the crater and larger earthquakes are localized along the rift faults.</p> <p>Three-dimensional modeling would be able to accurately model the bowl shape of the crater and may be able to examine why seismicity extends below the crater into Grenville basement. Current observations of reverse reactivation of rift faults associated with glacial rebound could not be assessed with the 2-D model presented in this paper and would require examination with a 3-D model.</p>

**Table D-6.1.1 Data Summary
Charlevoix RLME**

Citation	Title	Description and Relevance to SSC
Bent (1992)	A Re-examination of the 1925 Charlevoix, Québec Earthquake	Analysis of additional waveforms resulted in source parameters of strike $42^\circ \pm 7^\circ$, dip $53^\circ \pm 7^\circ$, rake $105^\circ \pm 10^\circ$, depth 10 km (6.2 mi.), seismic moment $3.1 \pm 2.5 \times 10^{25}$ dyne cm (M_w 6.2), M_s 6.2 ± 0.3 , m_b 6.5 ± 0.4 , source duration 5 sec, and stress drop 35 bars. The dip is shallower than would be expected from observed surface faults but consistent with recent seismicity. The focal mechanism is consistent with horizontal compression in the NW-SE direction, which is orthogonal to the regional stress field, indicating an anomalous stress field in Charlevoix that may be depth dependent.
Lamontagne and Ranalli (1996)	Thermal and Rheological Constraints on the Earthquake Depth Distribution in the Charlevoix, Canada, Intraplate Seismic Zone	Compares the depth distribution of Charlevoix earthquakes to rheological models of the region. The maximum depth of earthquakes can be controlled by either the brittle-ductile transition or the velocity-weakening to velocity-strengthening fault behavior. The rheological change at the brittle-ductile transition was modeled by calculating geotherms assuming a variety of rock compositions in the upper and middle crust. The depth distribution of earthquakes in Charlevoix requires geotherms very close to the upper limit for felsic rocks and a wet lower crust. The temperature-controlled sliding stability transition can occur at 300°C and 450°C for quartz or feldspar plasticity. Hydrolytic weakening of feldspars at 350°C occurs at 25 km (15.5 mi.) for the upper geotherms. The maximum crustal stress difference has an upper limit of about 100–200 MPa, requiring high pore fluid pressure or low coefficient of friction in mid- to lower crust. Thrust reactivation of steeply dipping faults requires a low coefficient of friction. The authors attribute the presence of earthquakes in the Charlevoix region to brittle-ductile transition deeper than 25 km (15.5 mi.), corresponding to higher than average geotherms; onset of ductility for hydrated feldspar at about 350°C; high pore-fluid pressure; and a low friction coefficient, possibly related to unhealed zones of intense fracturing.

Table D-6.1.1 Data Summary
Charlevoix RLME

Citation	Title	Description and Relevance to SSC
Lamontagne and Ranalli (1997)	Faults and Spatial Clustering of Earthquakes near La Malbaie, Charlevoix Seismic Zone, Canada	Focal mechanisms for earthquakes larger than M 3 show reverse faulting, whereas smaller-magnitude earthquakes indicate both normal and strike-slip mechanisms, suggesting that local stress and/or strength conditions control their occurrence. However, focal mechanisms for larger events of the Charlevoix seismic zone suggest reactivation of paleo-rift faults in response to regional stresses. The distribution of spatially clustered events (doublets and triplets) within the Charlevoix seismic zone indicates that very few events have occurred on the same fractures with similar focal mechanisms, implying that these fault zones occur in highly fractured rocks. These observations, indicate that the Charlevoix seismic zone is characterized by highly fractured zones responding to regional stresses and local perturbations in stress or strength, possibly enhanced by pore fluid pressures.
<i>Geodetic and Modeling Studies—Hypotheses for Causes of Intraplate Seismicity</i>		
Mazzotti and Adams (2005)	Rates and Uncertainties on Seismic Moment and Deformation Rates in Eastern Canada	Modeled seismic moment rates from earthquake statistics from the Charlevoix seismic zone can reach up to $2\text{--}10 \times 10^{17} \text{ N m yr}^{-1}$, equivalent to a magnitude $M_w = 7$ earthquake every 35–150 years. Relative motion and strain rates derived from earthquake statistics may reach up to $1\text{--}2 \text{ mm yr}^{-1}$ for the Charlevoix seismic zone. The lack of deformation suggests that the high strain rate might represent a short-term process such as postglacial rebound.
<i>Seismic Source Characterization Models</i>		
Adams and Halchuk (2003)	Fourth Generation Seismic Hazard Maps of Canada: Values for Over 650 Canadian Localities Intended for the 2005 National Building Code of Canada	Charlevoix is separated as a zone in the H model and combined with other St. Lawrence seismicity in the R model. The authors modeled recurrence rates with a beta value of 1.74 ± 0.11 with a maximum magnitude of 7.5.
Tuttle and Atkinson (2010)	Localization of Large Earthquakes in the Charlevoix Seismic Zone, Quebec, Canada, During the Past 10,000 Years	The absence of liquefaction features to the south in the Trois-Rivières seismic zone of the GSC H model (TRR on Figure 3-3) suggests that large-magnitude events in Charlevoix are spatially stationary.

Table D-6.1.2 Data Summary
Charleston RLME

Citation	Title	Description and Relevance to SSC
<i>Geologic Structures Interpreted from Geologic, Geomorphic, Geophysical and Seismic-Profile Data</i>		
Bartholomew and Rich (2007)	The Walls of Colonial Fort Dorchester: A Record of Structures Caused by the August 31, 1886 Charleston, South Carolina, Earthquake and Its Subsequent Earthquake History	The Dorchester fault is proposed as a near-vertical, NW-striking, reverse-oblique (right-lateral) fault. As proposed, the Dorchester fault is a subsurface feature that extends from a depth of about 8 km (5 mi.) below the ground surface downward to a depth between 13 and 25 km (8 and 15.5 mi.). The existence of this proposed fault is not based on direct evidence, but rather is inferred based on the analysis of (1) cracks in the walls of colonial Fort Dorchester; (2) local and regional stress orientations, including borehole breakouts; and (3) fault plane solutions from local microseismicity. There is no direct geologic or geomorphic evidence for the Dorchester fault, thus the existence of this structure is assessed to be questionable.
Behrendt and Yuan (1987)	The Helena Banks Strike-Slip (?) Fault Zone in the Charleston, South Carolina, Earthquake Area; Results from a Marine, High-Resolution, Multichannel, Seismic-Reflection Survey	Data from 24 marine seismic-reflection profiles totaling ~600 km (373 mi.) offshore from Charleston across strands of the Helena Banks fault zone show Miocene strata that are warped in a reverse-faulting sense. Helena Banks fault is described as 110 km (68.4 mi.) long, ~N66°E-striking, and comprising several segments 10–40 km (6.2 to 25 mi.) long. Interpreted as compressional reactivation of an extensional Mesozoic basin-bounding fault.
Behrendt et al. (1981)	Cenozoic Faulting in the Vicinity of the Charleston, South Carolina, 1886 Earthquake	Data from onshore multichannel seismic-reflection profiles in the 1886 meizoseismal area show evidence of Cenozoic faulting, including the NE-striking reverse (?) Cooke fault. Data suggest that most recent slip on the Cooke fault is Eocene or later. Data from offshore multichannel seismic-reflection profiles and single-channel high-resolution data show the Helena Banks fault as a 30+ km (18.5+ mi.) long structure with most recent movement in post-Miocene or Pliocene time.

**Table D-6.1.2 Data Summary
Charleston RLME**

Citation	Title	Description and Relevance to SSC
Behrendt et al. (1983)	Marine Multichannel Seismic-Reflection Evidence for Cenozoic Faulting and Deep Crustal Structure Near Charleston, South Carolina	Seismic-reflection data collected offshore from Charleston show Helena Banks fault as NE-striking, west-dipping reverse fault that extends upward to about 10 km (6.2 mi.) from the sea bottom. Interpreted as a Mesozoic extensional fault reactivated as reverse-oblique fault at least as young as Miocene or Pliocene. Also interpreted a subhorizontal detachment at 11.4 ± 1.5 km (7 ± 1 mi.) depth. Suggested Charleston seismicity is primarily caused by movement along the detachment and that movement on high-angle reverse faults (e.g., the Helena Banks fault and others) may also cause earthquakes.
Chapman et al. (2007)	Attenuation in the Atlantic Coastal Plain of Virginia and Cenozoic Faulting Imaged in the Epicentral Area of the 1886 Charleston, South Carolina Earthquake, Using Data from Seismic Reflection Profiles	Reprocessed seismic-reflection lines near Charleston reveal presence of "fault C," interpreted as reactivated Mesozoic normal fault (reactivated in oblique-reverse sense, up to the east). Fault C is traced upward into Eocene-age deposits in line VT-3b, but cannot be traced higher in section due to poor data resolution in shallow section. Fault C postulated to be the fault that ruptured in 1886 Charleston earthquake. Strike, length, and age of feature unresolved. See also Chapman and Beale (2008).
Chapman and Beale (2008)	Mesozoic and Cenozoic Faulting Imaged at the Epicenter of the 1886 Charleston, South Carolina, Earthquake	Reprocessed seismic-reflection lines near Charleston reveal presence of "fault C," interpreted as reactivated Mesozoic normal fault (reactivated in oblique-reverse sense, up to the east). Fault C is traced upward into Eocene-age deposits in line VT-3b, but cannot be traced higher in section due to poor data resolution in shallow section. Fault C is postulated to be the fault that ruptured in 1886 Charleston earthquake. Strike, length, and age of feature unresolved. See also Chapman et al. (2007).

**Table D-6.1.2 Data Summary
Charleston RLME**

Citation	Title	Description and Relevance to SSC
Chapman and Beale (2009)	Results of Reprocessing Seismic Reflection Data near Summerville, SC	Similar to Chapman and Beale (2008), reprocessed seismic-reflection lines near Summerville reveal Cenozoic compressional reactivation of a Mesozoic extensional basin, suggesting 1886 epicentral area lies within a zone of extensively faulted upper crust. These reflection data essentially reveal point images of fault at widely scattered locations, roughly coincident with the recently proposed Woodstock South, Woodstock North, and Sawmill Branch faults, inferred from a combination of earthquake hypocenters, focal mechanisms, geologic and geomorphic evidence, and intensity reports from 1886 (Dura-Gomez and Talwani, 2009; Talwani and Dura-Gomez, 2009). These faults strike NE and form a right-oblique (thrust) system. Woodstock North fault is a few km SE of the Cenozoic disturbance near Summerville imaged in lines VT4 and VT5, and crosses SC6 near the Cenozoic disturbance imaged in CMP 340. Seismicity attributed to Sawmill Branch fault is coincident with faults imaged in line VT3.
Chapman and Beale (2010)	On the Geologic Structure at the Epicenter of the 1886 Charleston, South Carolina, Earthquake	Reprocessed seismic-reflection lines near Summerville reveal Cenozoic compressional reactivation of a Mesozoic extensional basin, suggesting 1886 epicentral area lies within zone of extensively faulted upper crust. These reflection data essentially reveal point images of fault at widely scattered locations, roughly coincident with recently proposed Woodstock South, Woodstock North, and Sawmill Branch faults, inferred from a combination of earthquake hypocenters, focal mechanisms, geologic and geomorphic evidence, and intensity reports from 1886 (Dura-Gomez and Talwani, 2009; Talwani and Dura-Gomez, 2009). These faults strike NE and form a right-oblique (thrust) system. The Woodstock North fault is a few km SE of the Cenozoic disturbance near Summerville imaged in lines VT4 and VT5, and crosses SC6 near the Cenozoic disturbance imaged in CMP 340. Seismicity attributed to Sawmill Branch fault is coincident with faults imaged in line VT3.
Colquhoun et al. (1983)	Surface and Subsurface Stratigraphy, Structure and Aquifers of the South Carolina Coastal Plain	Early mapping of the proposed Charleston and Garner-Edisto faults based on subsurface stratigraphy and borehole control.

**Table D-6.1.2 Data Summary
Charleston RLME**

Citation	Title	Description and Relevance to SSC
Crone and Wheeler (2000)	Data for Quaternary Faults, Liquefaction Features, and Possible Tectonic Features in the Central and Eastern United States, East of the Rocky Mountain Front	Review of potential Quaternary tectonic features in the CEUS. Includes description of and primary reference citations for Charleston area liquefaction and paleoliquefaction features, Helena Banks fault, Cape Fear arch, and Cooke fault.
Doar and Willoughby (2006)	Revision of the Pleistocene Dorchester and Summerville Scarps, the Inland Limits of the Penholoway Terrace, Central South Carolina	Detailed and updated mapping of geomorphic scarps and terraces in the Coastal Plain of central South Carolina are interpreted as resulting from Pleistocene sea-level high stands, not tectonic activity. These include the Surry, Dorchester, Summerville, Macbeth, Bethera, Suffolk, and Awendaw scarps.
Dura-Gomez and Talwani (2008)	A Revised Seismotectonic Framework for the Charleston, South Carolina Earthquakes	Proposes a slightly revised depiction of faults spatially associated with Middleton Place–Summerville seismic zone and the roughly 6 km (3.7 mi.) wide stepover zone of the Woodstock fault. In this revised depiction, three NW-striking faults accommodate the stepover, the (1) Sawmill Branch; (2) Lincolville; and (3) Charleston faults. This depiction of the Sawmill Branch fault is similar to that proposed by Talwani and Katuna (2004). The Lincolville and Charleston faults newly proposed structures (the latter is not the same as the Charleston fault described by Lennon (1986) and Weems and Lewis (2002)). No figures accompany this abstract. See Dura-Gomez and Talwani (2009) and Talwani and Dura-Gomez (2009) for relevant maps.
Dura-Gomez and Talwani (2009)	Finding Faults in the Charleston Area, South Carolina: 1. Seismological Data	Article describes relocated microseismicity (1974–2004) in the Charleston area. These data are used to (1) refine mapping of and to characterize the proposed Woodstock, Sawmill Branch, and Ashley River faults; and (2) identify two proposed new faults, the Lincolville and Charleston faults. Note: this is not the same Charleston fault described by Lennon (1986) and Weems and Lewis (2002). Each of these structures is located within or near the 1886 meizoseismal area and the Middleton Place–Summerville seismic zone. The Woodstock fault is described as a NE-striking, steeply NW-dipping oblique (right-lateral) reverse fault. The Woodstock fault in the near surface is divided into northern and southern segments by a ~6 km (3.7 mi.) wide left (compressional) step. The Sawmill Branch, Lincolville, and Charleston faults are described as NW-striking faults within or near the stepover zone.

Table D-6.1.2 Data Summary
Charleston RLME

Citation	Title	Description and Relevance to SSC
Gangopadhyay and Talwani (2005)	Fault Intersections and Intraplate Seismicity in Charleston South Carolina: Insights from a 2-D Numerical Model	A simple 2-D numerical model comprising blocks with elastic properties representing simplified geology of the Middleton Place–Summerville seismic zone is used to explain observed seismicity and interpreted fault motions. Model is used to support idea that fault intersections act as stress concentrators and that these intersections may be loci of earthquakes.
Hamilton et al. (1983)	Land Multichannel Seismic-Reflection Evidence for Tectonic Features Near Charleston, South Carolina, Studies Related to the Charleston, South Carolina, Earthquake of 1886—Tectonics and Seismicity	Data from onshore seismic-reflection profiles show evidence for three postulated faults in the Charleston area: the Cooke, Gants, and Drayton faults. The postulated Cooke fault shows ~50 m of vertical displacement (SE-side-down) of a Jurassic basalt layer, with displacement decreasing upward within Cenozoic sediments. The strike of the Cooke fault is not well constrained but estimated at NE. The length of the Cooke fault is not defined. The postulated Gants fault shows similar vertical displacement and orientation as the Cooke fault and likewise shows displacement decreasing upward within Cenozoic sediments. The age of the NE-striking Drayton fault is constrained to the Late Cretaceous.
Hibbard et al. (2006)	Lithotectonic Map of the Appalachian Orogen, Canada–United States of America	Lithotectonic mapping at 1:1,500,000 scale of the Appalachian Mountains in the U.S. and Canada, including faults and shear zones. Mapped area does not cover the Coastal Plain.
Horton and Dicken (2001)	Preliminary Digital Geologic Map of the Appalachian Piedmont and Blue Ridge, South Carolina Segment	Geologic mapping at 1:500,000 scale of the South Carolina, excluding the Coastal Plain.
Lennon (1986)	Identification of a Northwest Trending Seismogenic Graben Near Charleston, South Carolina	Based on shallow (to 85 m) drilling and gamma logging in the 1886 meizoseismal area, inferred a NW-trending graben lying between Charleston and Kiawah Island, South Carolina. The proposed graben is bounded by three postulated faults: the Woodstock, Ashley River, and Charleston faults. Note: this is not the same Charleston fault as described by Dura-Gomez and Talwani (2009) and Talwani and Dura-Gomez (2009).

Table D-6.1.2 Data Summary
Charleston RLME

Citation	Title	Description and Relevance to SSC
Marple and Miller (2006)	Association of the 1886 Charleston, South Carolina, Earthquake and Seismicity Near Summerville with a 12° Bend in the East Coast Fault System and Triple-Fault Junctions	Seismic-reflection data, microseismicity, and other geologic and geophysical data are used to map faults near Charleston, including the newly postulated NW-striking Berkeley fault. These data also are interpreted to show a 12° bend in the southern segment of the East Coast fault system. Ongoing microseismicity in the Middleton Place–Summerville seismic zone and the 1886 Charleston earthquake are interpreted as related to: (1) this fault bend; and (2) fault intersections between the East Coast fault system and the Ashley River, Charleston, Summerville, and Berkeley faults in the Summerville area. Paper includes useful summary of data used to constrain faults near Charleston. As part of this summary, Marple and Miller (2006) call into question the existence of the Adams Run fault of Weems and Lewis (2002).
Marple and Talwani (1990)	Field Investigations of the Woodstock Lineament	Abstract describing preliminary geologic field investigations of the Woodstock lineament. Results and additional work are described in greater detail in subsequent publications (e.g., Marple and Talwani 1993; 2000).
Marple and Talwani (1993)	Evidence for Possible Tectonic Upwarping Along the South Carolina Coastal Plain from an Examination of River Morphology and Elevation Data	Identifies the Zone of River Anomalies as possible geomorphic expression of ongoing slip and surface deformation related to the underlying Woodstock fault. Zone of River Anomalies defined as N-NE-trending alignment of subtle topographic highs and morphologic changes in rivers (including river bends, incised channels, and convex-up longitudinal profiles) in the South Carolina Coastal Plain between the Edisto and Little Pee Dee Rivers. Suggests that the 1886 Charleston earthquake may have occurred on Woodstock fault. Additional studies are described in Marple and Talwani (2000).

Table D-6.1.2 Data Summary
Charleston RLME

Citation	Title	Description and Relevance to SSC
Marple and Talwani (2000)	Evidence for a Buried Fault System in the Coastal Plain of the Carolinas and Virginia—Implications for Neotectonics in the Southeastern United States	Identifies and describes the postulated East Coast fault system as a N-NE-striking, roughly 600 km (373 mi.) long buried fault in the Coastal Plain of the Carolinas and Virginia. This fault system extends from south of Charleston, South Carolina, to east of Richmond, Virginia, as series of three right-stepping en echelon fault segments. Evidence for the existence of these faults segments weakens progressively to the north. Evidence for the southern segment is equivocal and includes the Zone of River Anomalies (see also Marple and Talwani 1993), linear magnetic anomalies, and seismicity and seismic-reflection data in the Middleton Place–Summerville area. Suggests the 1886 Charleston earthquake may have occurred on the southern segment of the East Coast fault system.
Marple and Talwani (2004)	Proposed Shenandoah Fault and East Coast-Stafford Fault System and Their Implications for Eastern U.S. Tectonics	Identifies postulated NW-striking Shenandoah fault in Virginia that coincides with an apparent ~110 km (68 mi.) wide left step separating East Coast fault system from Stafford fault. Implication is that the postulated East Coast fault system and the Stafford fault form a ~1,100 km (684 mi.) long fault system.
McCartan et al. (1984)	Geologic Map of the Area Between Charleston and Orangeburg, South Carolina	Geologic mapping at 1:250,000 scale of greater Charleston area. No faults mapped.
Nystrom (1996)	Earthquake Hazards Map of the South Carolina Coastal Plain	Compilation at 1:400,000 scale showing previously mapped 1886 liquefaction and paleoliquefaction features, and areas susceptible to landsliding and collapse. Map also shows areas of potential liquefaction, which are generally confined to an area within roughly 50 km (31 mi.) of the coast and farther inland along active rivers and streams.
Prowell (1983)	Index of Faults of Cretaceous and Cenozoic Age in the Eastern United States	Map and brief descriptions of postulated Cretaceous and Cenozoic-age faults in eastern U.S.
Seeber and Armbruster (1981)	The 1886 Charleston, South Carolina Earthquake and the Appalachian Detachment	Judging by coseismic and post-seismic strain indicators, back slip over a portion of the Appalachian detachment may have caused 1886 Charleston earthquake, similar to the great Indian detachment earthquakes of 1905 (M ~ 8) and 1934 (M ~ 8.3).

Table D-6.1.2 Data Summary
Charleston RLME

Citation	Title	Description and Relevance to SSC
Talwani and Dura-Gomez (2009)	Finding Faults in the Charleston Area, South Carolina: 2. Complementary Data	This companion paper to Dura-Gomez and Talwani (2009) includes data other than relocated microseismicity used to (1) refine mapping of and to characterize the proposed Woodstock, Sawmill Branch, and Ashley River faults; and (2) identify two proposed new faults, the Lincolnville and Charleston faults. Note: this is not the same Charleston fault described by Lennon (1986) and Weems and Lewis (2002). Each of these structures is located within or near the 1886 meizoseismal area and the Middleton Place–Summerville seismic zone. Woodstock fault is described as a NE-striking, steeply NW-dipping oblique (right-lateral) reverse fault. Woodstock fault in the near-surface is divided into northern and southern segments by a ~6 km (3.7 mi.) wide left (compressional) step. Sawmill Branch, Lincolnville, and Charleston faults are described as NW-striking faults within or near the stepover zone.
Talwani and Katuna (2004)	Macroseismic Effects of the 1886 Charleston Earthquake	Field trip guidebook describes four locations near Charleston where surficial effects of the 1886 earthquake can be seen. Liquefaction features formed during the 1886 earthquake are described at one location near Hollywood. The three remaining locations are described as locations of possible evidence for primary 1886 surface rupture. However, the cracks in Drayton family tomb at Magnolia Gardens, cracks in walls of Colonial Fort Dorchester, and apparent clockwise rotation of St. Paul's Episcopal Church in Summerville likely are result of strong ground shaking and not primary surface rupture.
Trenkamp and Talwani (n.d.)	GPS Derived Strain and Strain Zonation near Charleston, South Carolina	This as-yet-unpublished study presents campaign GPS data from a 20-station grid near Charleston that suggest average shear strain rate ($\sim 10^{-9}$ to 10^{-7} radians/yr) that is one to two orders of magnitude higher than the surrounding region. Measurements were taken in three surveys between 1994 and 2000, and are combined with National Geodetic Survey data that were collected from 1920s to 1990s. Study suffers from admitted monument instability, small number of surveys (three), and short period of GPS measurements (six years). Strain orientations generally consistent with SH max ($\sim N60^{\circ}E$). Largest strains located in the Middleton Place–Summerville seismic zone and attributed to local fault intersections.

Table D-6.1.2 Data Summary
Charleston RLME

Citation	Title	Description and Relevance to SSC
Weems and Lewis (2002)	Structural and Tectonic Setting of the Charleston, South Carolina, Region: Evidence from the Tertiary Stratigraphic Record	Using borehole data and structure contour maps on the Coastal Plain sedimentary units, Weems and Lewis (2002) map the NW-striking Charleston and Adams Run faults. Viable alternate (nontectonic) explanations exist for these features. Marple and Miller (2006) call into question existence of Adams Run fault.
Weems and Obermeier (1990)	The 1886 Charleston Earthquake—An Overview of Geological Studies	Article provides review of geological data describing 1886 Charleston earthquake. Indicates that there is no known surface or near-surface expression of the causative fault. Suggests that the only evidence for geologically recent (upper Pleistocene?) tectonic deformation near Charleston comes from domal features (including the Bonneau, Mt. Holly, and Fort Bull domes) recognized in subsurface Coastal Plain sediments. These domes are not associated with any microseismicity. Describes evidence for three, and possibly four, middle to late Holocene earthquakes preserved in geologic record as paleoliquefaction features, as well as evidence for events as old as 30 ka.
Wentworth and Mergner-Keefer (1983)	Regenerate Faults of the Southeastern United States	Proposes that Mesozoic normal faults in the Piedmont and Coastal Plain have been reactivated as reverse and reverse-oblique faults. Suggests the 1886 Charleston earthquake may have occurred on a NE-striking reactivated Mesozoic normal fault. Also suggests that, based on the existence of Mesozoic normal faults throughout much of the Atlantic Coastal Plain, earthquakes at least as large as 1886 Charleston may occur elsewhere in the domain.
Wheeler (2005)	Known or Suggested Quaternary Tectonic Faulting, Central and Eastern United States—New and Updated Assessments for 2005	Updated review of potential Quaternary tectonic features in the CEUS. Includes description of and primary reference citations for the East Coast fault system.

Table D-6.1.2 Data Summary
Charleston RLME

Citation	Title	Description and Relevance to SSC
Wildermuth and Talwani (2001)	A Detailed Gravity Survey of a Pull-Apart Basin in Northeast South Carolina	Marple and Talwani (2000) propose the East Coast fault system as a right-lateral reverse oblique fault comprising three segments (south, central, and north) configured in a right-stepping en echelon pattern. As such, the right stepover separating the southern and central segments should form an area of extension. Wildermuth and Talwani (2001) test this hypothesis by performing a microgravity survey in the vicinity of the stepover. Their data are consistent with presence of a pull-apart basin, but few details are provided in this abstract.
Willoughby and Nystrom (2005)	Generalized Geologic Map of South Carolina	Generalized geologic mapping at 1:1,000,000 scale of South Carolina, including Coastal Plain wave-cut scarps. No faults mapped in Coastal Plain. Mapping too simplified to be of use in source characterization.
<i>Seismicity and 1886 Earthquake Intensity</i>		
Bakun and Hopper (2004b)	Magnitudes and Locations of the 1811-1812 New Madrid, Missouri, and the 1886 Charleston, South Carolina, Earthquakes	Intensity-based study of 1886 Charleston earthquake. Intensity center computed to be located offshore, but preferred estimate is at Middleton Place–Summerville seismic zone. Magnitude of 1886 Charleston earthquake is estimated to be between M_w 6.4 and 7.2 (at 95% confidence level), with preferred estimate of M_w 6.9.
Bakun and McGarr (2002)	Differences in Attenuation Among the Stable Continental Regions	Systematic differences in the attenuation of large earthquake ground motions exist between different stable continental regions (SCRs) worldwide. Eastern North America attenuation in seismic waves is less than that for other SCRs. As such, some previous studies of 1886 Charleston earthquake that used worldwide average SCR attenuation (e.g., Johnston, 1996c) overestimate the magnitude of this earthquake.
Bollinger (1977)	Reinterpretation of the Intensity Data for the 1886 Charleston, South Carolina, Earthquake	MMI isoseismals for the 1886 Charleston earthquake based primarily on original observations in Dutton (1889). Highest intensities (MMI X) at/near Charleston.
Bollinger (1983)	Speculations on the Nature of Seismicity at Charleston, South Carolina	Estimates 1886 earthquake at m_b 6.7, with rupture length approximately 25 km (15.5 mi.), width approximately 12 km (7.5 mi.), average slip 1 m (3.3 ft.), based on empirical relations. Notes ongoing microseismicity concentrated in 1886 meizoseismal area.

**Table D-6.1.2 Data Summary
Charleston RLME**

Citation	Title	Description and Relevance to SSC
Johnston (1996c)	Seismic Moment Assessment of Earthquakes in Stable Continental Regions—III. New Madrid 1811-1812, Charleston 1886, and Lisbon 1755	Using isoseismal-area-regression methods, the magnitude of the 1886 Charleston earthquake is estimated at $M_w 7.3 \pm 0.26$. Bakun and McGarr (2002) argue that Johnston (1996c) overestimates the magnitude of the 1886 Charleston earthquake.
Madabhushi and Talwani (1990)	Composite Fault Plane Solutions of Recent Charleston, South Carolina, Earthquakes	Reassessment of Middleton Place–Summerville seismic zone seismicity suggests two distinct groups of seismicity: (1) composite focal mechanism with right-lateral strike-slip motion, small dip-slip component, nodal plane oriented N-NE, and hypocentral depths from 3 to 8 km (2 to 5 mi.); and (2) composite focal mechanism with NW-oriented thrust dipping SW and hypocentral depths from 4 to 10 km (2.5 to 6.2 mi.). Data are interpreted as indicating microseismic activity on the postulated intersecting Woodstock and Ashley River faults.
Madabhushi and Talwani (1993)	Fault Plane Solutions and Relocations of Recent Earthquakes in Middleton Place–Summerville Seismic Zone Near Charleston, South Carolina	Single fault-plane solutions obtained for 35 earthquakes in Middleton Place–Summerville seismic zone and grouped into five subsets. Seismicity is attributed to reverse faulting on NW-striking, SW-dipping Ashley River fault and right-lateral strike-slip on the N-NE-striking vertical Woodstock fault. Seismicity is interpreted as concentrated near the intersection of these two faults.
Smith and Talwani (1985)	Preliminary Interpretation of a Detailed Gravity Survey in the Bowman and Charleston, S.C. Seismogenic Zones	Gravity surveys conducted in the vicinity of the Bowman seismic zone suggest presence of NW-trending features, as previously interpreted from magnetic anomaly data.
South Carolina Seismic Network (2005)	List of Earthquakes in Charleston Between 1974 and 2002	Tabulation of microseismicity in the local Charleston area, recorded between 1974 and 2002. Useful to show local Charleston earthquakes with magnitudes smaller than those listed in the CEUS SSC earthquake catalog.
Talwani (1982)	An Internally Consistent Pattern of Seismicity Near Charleston, South Carolina	Relocated seismicity in the 1886 meizoseismal area suggests (1) right-lateral strike-slip events on NE-striking Woodstock fault, and (2) SW-side-up thrust events on NW-striking Ashley River fault.
Talwani (1999)	Fault Geometry and Earthquakes in Continental Interiors	Intersecting faults are proposed as the loci of strain accumulation and seismicity in the upper crust of continental interiors. Postulated Woodstock and Ashley River faults near Charleston are cited as an example of fault intersection model.

Table D-6.1.2 Data Summary
Charleston RLME

Citation	Title	Description and Relevance to SSC
Tarr and Rhea (1983)	Seismicity Near Charleston, South Carolina, March 1973 to December 1979	Description of microseismicity defining the Middleton Place–Summerville, Bowman, and Adams Run seismic zones based on a temporary seismic network installed in 1973 and a permanent network installed in 1974.
Tarr et al. (1981)	Results of Recent South Carolina Seismological Studies	Description of microseismicity defining the Middleton Place–Summerville, Bowman, and Adams Run seismic zones based on a temporary seismic network installed in 1973 and a permanent network installed in 1974. Suggests that 1886 earthquake occurred within the Middleton Place–Summerville seismic zone. Observes that, whereas earthquakes in the Piedmont tend to be scattered, those in the Coastal Plain tend to cluster. This is interpreted as the result of localized stresses on or near intersecting faults or in zones of weakness between crustal blocks.
<i>Liquefaction and Paleoliquefaction</i>		
Ambraseys (1988)	Engineering Seismology	Presents a magnitude-bound relation for liquefaction.
Amick (1990)	Paleoliquefaction Investigations Along the Atlantic Seaboard with Emphasis on the Prehistoric Earthquake Chronology of Coastal South Carolina	Search for paleoliquefaction features along U.S. East Coast at over 1,000 sites from southern Georgia to New Jersey. Features found only in coastal Carolinas. Includes rough maps of areas searched in which no features found, as well as sketches and photographs of selected features. Describes evidence for six M_w 7+ earthquakes near Charleston in the past ~2 kyr. Return period estimated at roughly 500–600 years. Includes discussion of criteria by which seismically induced liquefaction features may be distinguished from “pseudoliquefaction” features.
Amick and Gelinas (1991)	The Search for Evidence of Large Prehistoric Earthquakes Along the Atlantic Seaboard	Search for paleoliquefaction features along U.S. East Coast at over 1,000 sites from southern Georgia to New Jersey. Features found only in coastal Carolinas. Return period estimated at 500–600 years. In general, largest paleoliquefaction features are at sites near Charleston, suggesting repeated large earthquakes near Charleston. Majority of paleoliquefaction features can be explained by a source near Charleston, but the possibility of a separate (moderate?) source located ~100 km (62 mi.) NE is suggested.

Table D-6.1.2 Data Summary
Charleston RLME

Citation	Title	Description and Relevance to SSC
Amick, Gelinas, et al. (1990)	Paleoliquefaction Features Along the Atlantic Seaboard	Search for paleoliquefaction features along U.S. East Coast at over 1,000 sites from southern Georgia to New Jersey. Features found only in coastal Carolinas. In general, largest paleoliquefaction features are at sites near Charleston, suggesting repeated large earthquakes near Charleston. Includes rough maps of areas searched in which no features found, as well as sketches and photographs of selected features. Describes evidence for six M_w 7+ earthquakes near Charleston in the past ~2 kyr. Return period estimated at roughly 500–600 years. Includes discussion of criteria by which seismically induced liquefaction features may be distinguished from “pseudoliquefaction” features.
Amick, Maurath, and Gelinas (1990)	Characteristics of Seismically Induced Liquefaction Sites and Features Located in the Vicinity of the 1886 Charleston, South Carolina Earthquake	Describes evidence for six M_w 7+ earthquakes near Charleston in the past ~2 kyr. Return period estimated at roughly 500–600 years. Includes discussion of criteria by which seismically induced liquefaction features may be distinguished from “pseudoliquefaction” features. Similar to Amick (1990) and Amick, Gelinas, et al. (1990), but with less detail.
Andrus and Heidari (2009) Crone and Wheeler (2000)	Mapping Liquefaction Potential of Soil Deposits near Charleston, SC Data for Quaternary Faults, Liquefaction Features, and Possible Tectonic Features in the Central and Eastern United States, East of the Rocky Mountain Front	Both reports review potential Quaternary tectonic features in the CEUS. These include description of and primary reference citations for Charleston area liquefaction and paleoliquefaction features, Helena Banks fault, Cape Fear arch, and Cooke fault.
Dutton (1889)	The Charleston Earthquake of August 31, 1886	Near-contemporary report of macroseismic effects of 1886 Charleston earthquake, including intensity observations, isoseismal maps (Rossi-Forrel scale), and distribution of sandblow “craterlets.” Highest intensities and greatest number of craterlets found in/near Charleston, decreasing with distance up and down coast. Suggests 1886 epicentral location at Charleston.
Gassman et al. (2009)	Magnitudes of Charleston, South Carolina Earthquakes from In Situ Geotechnical Data	Abstract describing geotechnical analyses of paleoliquefaction in Charleston area. Based on standard penetration test (SPT), cone penetration test (CPT), and shear-wave velocity (V_s) data, Gassman et al. (2009) suggest a preferred magnitude range of M_w 6.7 to 7.0 for prehistoric, historic, and future earthquakes in Charleston seismic zone.

Table D-6.1.2 Data Summary
Charleston RLME

Citation	Title	Description and Relevance to SSC
Gelinas et al. (1998)	Paleoseismic Studies in the Southeastern United States and New England	Search for paleoseismic and paleoliquefaction features along U.S. East Coast, focusing on South Carolina and New England. Numerous features documented in coastal Carolinas. In general, largest paleoliquefaction features are at sites near Charleston, suggesting repeated large earthquakes near Charleston. Inland search for paleoliquefaction features was performed on 3.2 km (2 mi.) stretch of Big Browns Creek in Union County, South Carolina. No features identified.
Hu et al. (2002a)	In-Situ Properties of Soils at Paleoliquefaction Sites in the South Carolina Coastal Plain	Geotechnical estimates of in situ soil properties (including depth and thickness of source layer, normalized shear-wave velocity, percent fines, etc.) at Charleston paleoliquefaction sites. Data not useful for characterizing Charleston paleoearthquake source, but are used by Hu et al. (2002b).
Hu et al. (2002b)	Magnitudes of Prehistoric Earthquakes in the South Carolina Coastal Plain from Geotechnical Data	Magnitude estimates for Charleston paleoearthquakes based on geotechnical estimates of in situ soil properties described in Hu et al. (2002a). Magnitude estimates range from M_w 6.8–7.8 for “large” regional Charleston events to M_w 5.5–7.0 for “moderate” local events at Georgetown. Leon et al.’s (2005) subsequent study, with two of the same three coauthors as Hu et al. (2002a, 2002b), presents lower magnitude estimates for prehistoric Charleston earthquakes.
Leon (2003)	Effect of Aging of Sediments on Paleoliquefaction Evaluation in the South Carolina Coastal Plain	Magnitude estimates for Charleston paleoearthquakes based on geotechnical assessments accounting for the effects of sediment age. Magnitude estimates range from M_w 5.5–7.2 for “large” regional Charleston events to M_w 4.3–6.4 for “moderate” local events at Bluffton and Georgetown. These estimates are lower than those presented in a previous study by Hu et al. (2002b).
Leon et al. (2005)	Effect of Soil Aging on Assessing Magnitudes and Accelerations of Prehistoric Earthquakes	Magnitude estimates for Charleston paleoearthquakes based on geotechnical assessments accounting for effects of sediment age. Magnitude estimates range from M_w 5.5–7.2 for “large” regional Charleston events to M_w 4.3–6.4 for “moderate” local events at Bluffton and Georgetown. These estimates are lower than previous studies, including that of Hu et al. (2002b), which had two of the same three coauthors (Gassman and Talwani).

**Table D-6.1.2 Data Summary
Charleston RLME**

Citation	Title	Description and Relevance to SSC
Martin and Clough (1994)	Seismic Parameters from Liquefaction Evidence	Based on geotechnical analyses and critiques of previous estimates, preferred magnitude estimate for 1886 earthquake is "...no larger than $M = 7.5$, possibly as low as $M = 7...$ " (p. 1360).
Noller and Forman (1998)	Luminescence Geochronology of Liquefaction Features Near Georgetown, South Carolina	Interprets liquefaction evidence for 1886 earthquake and two or three paleoliquefaction events at Gapway Ditch site, where Amick, Gelinas, et al. (1990); Amick, Maurath, and Gelinas (1990); and Talwani and Schaeffer (2001) interpreted one paleoliquefaction event.
Obermeier (1996b)	Using Liquefaction-Induced Features for Paleoseismic Analysis	Describes criteria for recognizing earthquake-induced liquefaction features in the geologic record, with discussion of Charleston paleoliquefaction data. Shows distribution of 1886 liquefaction and paleoliquefaction sites in coastal South Carolina and southernmost coastal North Carolina, and rough outline of area searched. Large diameters (3+ m) of some prehistoric craters suggest that these likely were caused by earthquakes "...much stronger than $M 5$ to $5.5...$ " (p. 350). Also observes that sandblow craters that formed roughly 600 and 1,250 yr BP extend along the coast at least as far as 1886 features, suggesting that some prehistoric earthquakes likely were at least as large as 1886.
Obermeier and Pond (1999)	Issues in Using Liquefaction Features for Paleoseismic Analysis	Summary paper describing issues regarding the use of paleoliquefaction data as evidence of strong ground shaking.
Obermeier et al. (1989)	Liquefaction Evidence for Repeated Holocene Earthquakes in the Coastal Region of South Carolina	Describes distribution of paleoliquefaction features throughout much of coastal South Carolina and southernmost North Carolina. Estimates at least three prehistoric earthquakes in past 7.2 kyr with $m_b > \sim 5.5$. Notes that size and spatial concentration of both 1886 liquefaction and paleoliquefaction features are greatest near Charleston, and decrease with distance up and down the coast, despite similarities in liquefaction susceptibility throughout region. This indicates repeated large earthquakes located at or near Charleston.

Table D-6.1.2 Data Summary
Charleston RLME

Citation	Title	Description and Relevance to SSC
Obermeier et al. (1990)	Earthquake-Induced Liquefaction Features in the Coastal Setting of South Carolina and in the Fluvial Setting of the New Madrid Seismic Zone	Describes criteria for recognizing earthquake-induced liquefaction features in the geologic record, with discussion of Charleston paleoliquefaction data. Describes possible origins other than earthquakes for sand-blow craters and vented sand volcanoes, including compaction-induced dewatering, landslides, artesian springs, and ground disruption by fallen root-wadded trees. Estimates spatial extents of 1886 and prehistoric liquefaction fields. Estimates at least three prehistoric earthquakes in past 7.2 k.y with $m_b > \sim 5.5$. Notes that the abundance and diameters of prehistoric sandblow craters are greatest within the 1886 meizoseismal zone for a given age of craters, indicating repeated large earthquakes located at or near Charleston.
Olson et al. (2005b)	Revised Magnitude Bound Relation for the Wabash Valley Seismic Zone of the Central United States	Presents an updated magnitude-bound relationship for paleoliquefaction in the CEUS.
Talwani (2000)	The Charleston Earthquake Cycle	Radiocarbon dating of paleoliquefaction features in coastal South Carolina suggests return period of $M_w 7+$ earthquakes is approximately 500 years. Campaign GPS survey suggests strain rate of 0.04 μ rad/year (uncertainty unspecified). This is interpreted as consistent with ~ 2 m slip events every 500 years at Charleston.
Talwani and Schaeffer (2001)	Recurrence Rates of Large Earthquakes in the South Carolina Coastal Plain Based on Paleoliquefaction Data	Compilation of paleoliquefaction feature locations and radiocarbon age constraints from sites throughout coastal South Carolina and southernmost coastal North Carolina. Construction of earthquake chronology based on radiocarbon ages with 1-sigma error bounds. Considered scenarios with (1) mix of large ($M_w \sim 7$) regional and moderate ($M_w \sim 6$) local events; and (2) large regional events only. Paleoliquefaction record judged to be complete for past ~ 2 kyr, possibly complete for past ~ 6 kyr. Preferred estimate of 500–600 years for recurrence of large ($M_w \sim 7$) earthquakes.
Talwani et al. (2008)	Studies Related to the Discovery of a Prehistoric Sandblow in the Epicentral Area of the 1886 Charleston SC Earthquake: Trenching and Geotechnical Investigations	Description of newly discovered paleoliquefaction feature near Fort Dorchester, South Carolina. Feature is undated but, based on burial depth and soil formation, estimated to pre-date the 1886 Charleston earthquake. Paleoeearthquake magnitude estimated at ~ 6.9 (scale unspecified) based on unspecified geotechnical analyses.

Table D-6.1.2 Data Summary
Charleston RLME

Citation	Title	Description and Relevance to SSC
Recent Source Characterizations		
Bollinger (1992)	Specification of Source Zones, Recurrence Rates, Focal Depths, and Maximum Magnitudes for Earthquakes Affecting the Savannah River Site in South Carolina	Seismic source characterization for the Savannah River Site describes input parameters for PSHA. Local Zone 1 (LZ1, Charleston) $M_{\max} = m_b$ 6.9. Seismogenic thickness estimated at 14 and 25 km (9 and 15.5 mi.), respectively, for “Local Charleston” and “SC Piedmont and Coastal Plain” seismic sources..
Chapman and Talwani (2002)	Seismic Hazard Mapping for Bridge and Highway Design in South Carolina	Charleston source characteristic earthquakes (M_w 7.0–7.5) modeled as combination of one area source (“coastal”) and two line (“ZRA” and “three parallel faults”) sources. Magnitudes (M_w) [and weights]: 7.1 [0.2]; 7.3 [0.6]; and 7.5 [0.2]. Mean return period: 550 years.
Frankel et al. (1996)	National Seismic-Hazard Maps: Documentation	<p>Charleston source characteristic earthquakes modeled by one areal source zone drawn to encompass (1) a narrow source zone defined by P. Talwani (to represent the Woodstock fault and the Zone of River Anomalies); and (2) a larger zone drawn by S. Obermeier and R. Weems constrained by the areal distribution of paleoliquefaction locations, although the source zone does not encompass all the paleoliquefaction sites.</p> <p>A characteristic rupture model of M_w 7.3 earthquakes is assumed, based on the estimated magnitude of the 1886 event (Johnston, 1996). Assumes recurrence time of 650 years, based on dates of paleoliquefaction events. Assumes vertical faults with random strikes distributed throughout the areal source zone when calculating the hazard. Each of these fictitious faults is centered on a grid cell within the source zone.</p>

Table D-6.1.2 Data Summary
Charleston RLME

Citation	Title	Description and Relevance to SSC
Frankel et al. (2002)	Documentation for the 2002 Update of the National Seismic Hazard Maps	Charleston source characteristic earthquakes (M_w 6.8–7.5) modeled by two areal source zones, weighted at 0.50 each: (1) a narrow zone representing Woodstock lineament and a portion of Zone of River Anomalies; and (2) the same broader zone used in the 1996 model. Assumes a mean recurrence time of 550 years for characteristic earthquakes in the Charleston, South Carolina, region, as presented in the description of paleoseismic evidence by Talwani and Schaeffer (2001). This average recurrence time is derived from the recurrence intervals determined from the 1886 event and three earlier earthquakes of similar size, based on the areal extent of their paleoliquefaction effects. For both areal zones, faults are oriented with strikes parallel to long axis of narrow areal zone. Fault lengths are determined from Wells and Coppersmith (1994). Some of the faults extend outside of source zone boundary. Magnitudes (M_w) [and weights] based on expert opinion and recent work by Bakun and Hopper (2002): 6.8 [0.2], 7.1 [0.2], 7.3 [0.45], 7.5 [0.15].
Petersen et al. (2008)	Documentation for the 2008 Update of the United States National Seismic Hazard Maps	Charleston source characteristic earthquakes (M_w 6.8–7.5) modeled by two areal source zones, weighted 50/50: (1) a geographically narrow zone that follows the Woodstock lineament and an area of river anomalies, and (2) a broader zone that encompasses many of the known liquefaction features resulting from past earthquakes. At the urging of NSHMP Advisory Panel, the SE edge of the larger zone has been extended offshore (relative to 2002 zone) to capture the Helena Banks fault. Assumes a mean recurrence time of 550 years for characteristic earthquakes in the Charleston, South Carolina, region, as presented in description of paleoseismic evidence by Talwani and Schaeffer (2001). Each zone combines a characteristic model with same magnitudes and weights as 2002 model. Additionally, a truncated Gutenberg-Richter model with m_{bLg} from 5.0 to 7.5 accounts for background events in the extended margin, including Charleston zone. The background seismicity has random fault strike.
Silva et al. (2003)	Ground Motion and Liquefaction Simulation of the 1886 Charleston, South Carolina, Earthquake	Simulations of an M_w 7.3 “1886 Charleston-like” earthquake. Rupture plane of 1886 earthquake modeled as (1) 100 km—or 62 mi.—long, 20 km—or 12.5 mi.—wide (static stress drop 27 bars) fault; and (2) 50 km—or 31 mi.—long, 16 km—or 10 mi.—wide (static stress drop 107 bars) fault. Fault assumed coincident with the Woodstock fault.

Table D-6.1.3 Data Summary
Cheraw Fault RLME

Citation	Title	Description and Relevance to SSC
Fault Geometry		
Crone (1997)	Fault Number 2330, Cheraw Fault, in Quaternary Fault and Fold Database of the United States	<p>Cheraw fault was first recognized during regional geologic mapping in late 1960s and 1970s (Sharps, 1976). Structurally, fault is located above W-NW-sloping basement surface between N-trending Las Animas arch to the east and the Denver basin to the NW. Down-to-the-NW sense of motion that occurred during late Quaternary faulting events has same vertical sense as cumulative tectonic relief on Precambrian crystalline rocks. The Las Animas arch is a prominent, but relatively low-relief, 300 km (186.5 mi.) long positive structural element in SE Colorado. Crest of the arch is approximately 20–40 km (12.5–25 mi.) east of the fault. Minor uplift probably occurred along the arch in late Paleozoic time, but most of present relief is Laramide in age.</p> <p>Fault does not appear to have a long history of recurrent movement. Interpretation of structure contours on top of Lower Cretaceous Dakota sandstone shows a similar offset (6–8 m [19.7–26.2 ft.] of down-to-the-NW throw) to that of early Quaternary alluvial deposits along the fault.</p> <p>Length: 44 km (89.5 mi.), avg. strike: N44°E; sense of movement: not well known, inferred to be down-to-the-NW motion on a normal fault based on the attitude of near-surface faults exposed in trench across the fault.</p> <p>The only detailed paleoseismic study of the fault is that by Crone, Machette, Bradley, et al. (1997).</p> <p>Timing of the latest Pleistocene displacements raises possibility that surface-faulting earthquakes have occurred as a temporal cluster. Cumulative vertical offset on the Pleistocene erosional surface cut on Cretaceous shale is 3.2–4.1 m (10.5–13.5 ft.), which represents the total offset from the three post-latest Quaternary (<25 ka) displacements.</p> <p>Lower Pleistocene Rocky Flats Alluvium, which has an estimated age of about 1.2 m.y., is only offset about 7–8 m (23–26 ft.) by the fault. Displacement events older than about 25 ka probably occurred before about 100 ka, based on estimated time needed to incise, widen, and backfill the paleostream channel that is now filled with latest Pleistocene deposits.</p> <p>Temporal clustering of earthquakes, in which relatively short time intervals of activity (e.g., 15–20 k.y.) are separated by long intervals of quiescence (e.g., 100 k.y.) are suggested. A suggested 8 k.y. average recurrence interval is based solely on</p>

**Table D-6.1.3 Data Summary
Cheraw Fault RLME**

Citation	Title	Description and Relevance to SSC
		<p>estimated timing of the latest Pleistocene and Holocene displacement events documented in trenching study. During a quiescent phase, surface-faulting earthquakes may not occur for hundreds of thousands of years. Best estimate of a long-term slip rate is less than or equal to 0.007 mm/yr, based on a cumulative offset of about 8 m (26 ft.) on the 1.2 Ma Rocky Flats Alluvium. Latest Pleistocene-Holocene slip rates are between 0.14 and 0.18 mm/yr (determined by dividing the amount of offset, 3.6 m (11.8 ft.), on oldest faulted deposits by the age of deposits, 20–25 k.y.).</p>
A. Crone (pers. comm., March 3, 2010)		<p>Crone provided a DEM (originally from Dan Clark of Geoscience Australia) showing the Cheraw fault scarp, which may extend farther to the NE than previously thought. He noted that possible NE extension of the Cheraw remains unconfirmed, and its existence was originally suggested based on analysis of SRTM topographic data by Dan Clark (Geoscience Australia). Crone agreed with the TI team's observations that sections of feature are suspiciously parallel and close to cultural features, so SRTM data could easily be capturing cultural effects that fortuitously align with a projection of the fault. Given the highly uncertain nature of possible NE extension, he agrees that it should be assigned low weight in a logic tree evaluation.</p>
A. Crone (pers. comm., April 21, 2010)		<p>After reexamination of Crone et al. (1997) and original trench logs and field photos, Dr. Crone concluded that neither the two-event nor three-event scenario can be ruled out, and that logic tree assessment should reflect this uncertainty. He agreed with TI team's conclusion that "out of cluster" event(s) are mostly unconstrained, and he stated that it seems wise to weight shorter-term history more heavily.</p> <p>In response to a query about age of Rocky Flats Alluvium, Crone stated that "the 1.2 Ma number that we used was the conventional thinking at the time we did our report 15 years ago. Folks have pondered this question for decades, and apparently the latest information is that the age of the deposit varies depending on distance from the mountain front. In a 2006 paper in <i>Geomorphology</i>, Riihimaki et al. use TCN analyses to estimate the age of the Rocky Flats Alluvium between Boulder and Golden. They conclude that the Rocky Flats is as young as 400 ka near the mountains and as old as 2 Ma farther to the east. This is certainly a much wider age range than anyone would have guessed in the past. So, if this conclusion can be extrapolated as far east as the Cheraw area, then our age guesstimate could be too young." Crone concluded that "overall, the logic tree you've constructed is reasonable and captures the options and uncertainties that are associated with the Cheraw fault."</p>

Table D-6.1.3 Data Summary
Cheraw Fault RLME

Citation	Title	Description and Relevance to SSC
Crone et al. (1997)	Late Quaternary Surface Faulting on the Cheraw Fault, Southeastern Colorado	<p>Provides information on a 110 m (361 ft.) long trench excavated across Cheraw fault. Evidence for three episodes of surface faulting was revealed and age dates were obtained. Ages of the surface-rupturing events were estimated to occur at about 8 k, 12, and 20–25 ka (one early Holocene and two latest Pleistocene events). Interpretation of amounts of vertical offset on Cheraw fault is as follows:</p> <p style="padding-left: 40px;">Most recent event: ~0.5–1.1 m (~1.6–3.6 ft.)</p> <p style="padding-left: 40px;">Penultimate event: ~1.1–1.6 m (~3.6–5.2 ft.)</p> <p style="padding-left: 40px;">Oldest event: ~1.5 m (~5 ft.)</p>
Crone and Wheeler (2000)	Data for Quaternary Faults, Liquefaction Features, and Possible Tectonic Features in the Central and Eastern United States, East of the Rocky Mountain Front	<p>This fault is classified as Class A. The fault is located about 140 km (87 mi.) east of the range front of Rocky Mountains and was originally mapped in 1970s as part of a regional mapping program. In 1994, a trench was excavated across the scarp, exposing a record of late Quaternary surface ruptures. Sense of motion on fault is inferred to be down-to-the-NW on a normal fault. Length of fault is about 45 km (28 mi.). Average recurrence interval is about 8 kyr, with 4–12 kyr between individual displacement events, in the past about 25 kyr.</p>
Petersen et al. (2008)	Documentation for the 2008 Update of the United States National Seismic Hazard Maps	<p>Cheraw fault in eastern Colorado shows evidence of Holocene and earlier faulting, based on a study by Crone, Machette, Bradley, et al. (1997). They infer that surface-rupturing earthquakes on fault occurred about 8, 12, and 20–25 ka, which may represent an active earthquake phase. In contrast, displacement events older than about 25 ka must have occurred prior to 100 ka, thus representing a quiescent period of some 75 kyr or more. All parameters for Cheraw fault are retained from 2002; fault was modeled using slip rate of 0.15 mm/yr, based on data from the last two displacement events and maximum magnitude of 7.0 ± 0.2 determined from the Wells and Coppersmith (1994) fault length for all slip types relation. A fixed recurrence time of 17.400 kyr is used with a truncated Gutenberg-Richter model from M 6.5–7.0. This yields mean recurrence time of 5 kyr for earthquakes with minimum magnitude of 6.5.</p>

**Table D-6.1.4 Data Summary
Oklahoma Aulacogen RLME**

Citation	Title	Description and Relevance to SSC
General for Region		
Luza and Lawson (1993)	Oklahoma Seismic Network	Describes local network funded to investigate seismicity in Oklahoma, in particular, seismicity potentially related to Nemaha uplift. Presents earthquakes recorded from 1987 through 1992. Discusses association of seismicity with the Anadarko basin, Arkoma-Ouachita region, and other areas. Loose associations are made between earthquakes and structures, but there is no strong argument for activity on any structure. The depth distributions of earthquakes are likely not well constrained, but they suggest the seismic depth within Oklahoma extends to 15–20 km (9.3–12.4 mi.).
Meers Fault		
Burrell (1997)	Evaluation of Faulting Characteristics and Ground Acceleration Associated with Recent Movement Along the Meers Fault, Southwestern Oklahoma	Investigated the potential for strong earthquakes along Meers fault based on analyses of balanced granite boulders, stream deflections and offsets, and excavation of a fault exposure. Concludes that the presently observable scarp formed in four events with a return period of approximately 2.6–4.3 kyr, with less slip per event than previously suggested, and that magnitudes were significantly less than predicted by other researchers.
Cetin (2003)	Comment on “Known and Suggested Quaternary Faulting in the Midcontinent United States” by Russell L. Wheeler and Anthony Crone”	Summarizes evidence for a 30 km (18.6 mi.) extension of Meers fault to the NW of extent mapped by Ramelli et al. (1987) in an attempt to refute conclusion of Wheeler and Crone (2001) that the Holocene scarp does not extend further to NW.
Crone (1994)	Fault Number 1031b, Meers Fault, Southeastern Section, in Quaternary Fault and Fold Database of the United States	Provides summary of published information on the characteristics of Quaternary activity on Meers fault.
Crone and Wheeler (2000)	Data for Quaternary Faults, Liquefaction Features, and Possible Tectonic Features in the Central and Eastern United States, East of the Rocky Mountain Front	Provides summary of published information on the characteristics of Quaternary activity on Meers fault.

**Table D-6.1.4 Data Summary
Oklahoma Aulacogen RLME**

Citation	Title	Description and Relevance to SSC
Jones-Cecil (1995)	Structural Controls of Holocene Reactivation of the Meers Fault, Southwestern Oklahoma, from Magnetic Studies	Used local magnetic data obtained perpendicular to the Meers fault trace to constrain fault structure. Concludes that magnetic data suggests (1) slip is occurring on the Paleozoic fault, (2) splays along the SW end of the fault are not controlled by Paleozoic structure, and (3) the NW end of the fault appears to be a rupture barrier.
Kelson and Swan (1990) Swan et al. (1993)	Paleoseismic History of the Meers Fault, Southwestern Oklahoma, and Its Implications for Evaluations of Earthquake Hazards in the Central and Eastern United States Draft Report: Investigation of the Quaternary Structural and Tectonic Character of the Meers Fault (Southwestern Oklahoma)	These two publications present the results of the same study, but the report of Swan et al. (1993) is the most detailed. They present the results of an extensive study of Quaternary faulting history of Meers fault based on trenching, soil pits, auger samples, geomorphic analysis, and radiocarbon dating. They identify two Holocene events on the fault (approximately 1,300–1,400 yr BP and 2,100–2,900 yr BP) and a quiescence of approximately 200–500 kyr before the previous events. Swan et al. (1993) also discuss potential evidence for activity along the Criner fault and other portions of the Wichita frontal fault system.
Luza et al. (1987a) Luza et al. (1987b) Crone and Luza (1990)	Investigation of the Meers Fault in Southwestern Oklahoma Investigation of the Meers Fault, Southwestern Oklahoma Style and Timing of Holocene Surface Faulting on the Meers Fault, Southwestern Oklahoma	These three publications report the results of the same trenching and excavation study of Meers fault. They identify one Holocene surface-rupturing event. Their best estimate for the date of the event based on stratigraphic relationships and radiocarbon dating is 1,200–1,300 yr BP.
Madole (1986) Madole (1988)	The Meers Fault: Quaternary Stratigraphy and Evidence for Late Holocene Movement Stratigraphic Evidence of Holocene Faulting in the Mid-Continent: The Meers Fault, Southwestern Oklahoma	These two publications report the results of the same study. They identify one Holocene event on the Meers fault, and constrain the age of the event to approximately 1,280 yr BP (C-14 years), based on stratigraphic relations and radiocarbon dating of deposits distal (tens to hundreds of meters) from the scarp.
Miller et al. (1990)	Shallow Seismic Reflection Survey Across the Meers Fault, Oklahoma	A high-resolution reflection survey was conducted to investigate shallow structure of the fault. Survey elucidated local splay faults off the Meers and demonstrated the presence of high-angle to vertical up-to-the-north displacement along fault.

**Table D-6.1.4 Data Summary
Oklahoma Aulacogen RLME**

Citation	Title	Description and Relevance to SSC
Ramelli and Slemmons (1990)	Implications of the Meers Fault on Seismic Potential in the Central United States	General discussion of the state of knowledge of Meers fault at time of study, including hazard implications. A significant contribution from this study is discussion of surface rupture length and the possibility that the easternmost extension of the fault may not have the same slip history as the better-studied western portion.
Ramelli et al. (1987) Ramelli and Slemmons (1986)	The Meers Fault: Tectonic Activity in Southwestern Oklahoma Neotectonic Activity of the Meers Fault	Provides detailed mapping of Meers fault scarp based on low-sun-angle aerial photography. Based on this mapping, the Holocene scarp of Meers fault was extended further to SE than previously identified. Also documents search for other scarps along northern edge of Wichita Uplift. Digitized trace of fault used for CEUS SSC Project taken from compilation of USGS Quaternary Fault and Fold Database.
Wheeler and Crone (2001)	Known and Suggested Quaternary Faulting in the Midcontinent United States	Summarizes evidence for Quaternary faulting throughout CEUS. With respect to Meers fault, evaluates the suggestion of one researcher that the Holocene scarp associated with Meers fault extends 48 km (30 mi.) to NW of scarp defined by Ramelli et al. (1987), and concludes that there is no strong evidence to support this postulated NW extension of the Holocene scarp.
Wheeler and Crone (2003)	Reply to "Comment on Evaluation of Meers Fault, Oklahoma in 'Known and Suggested Quaternary Faulting in the Midcontinent United States' by Russell L. Wheeler and Anthony Crone"	Provides further justification for decision not to extend to the NW the Holocene Meers fault scarp beyond that mapped by Ramelli et al. (1987), refuting claims of Cetin (2003) that scarp extends further.
<i>Oklahoma Aulacogen Source Zone</i>		
Axtman (1983)	Structural Mechanisms and Oil Accumulation Along the Mountain View-Wayne Fault, South-Central Oklahoma, Part I	Examines structural and stratigraphic relationships of Mountain View fault and discusses the displacement history of fault in relation to structural and tectonic history of Oklahoma aulacogen.
Brewer (1982)	Study of Southern Oklahoma Aulacogen, Using COCORP Deep Seismic-Reflection Profiles	Summarizes how COCORP reflection data constrains timing and structural style of the Oklahoma aulacogen and Wichita uplift. Provides support for interpretation that the aulacogen extends from Hardeman basin (south of Wichita uplift) to Anadarko basin (north of Wichita uplift).

**Table D-6.1.4 Data Summary
Oklahoma Aulacogen RLME**

Citation	Title	Description and Relevance to SSC
Brewer et al. (1981)	Proterozoic Basin in the Southern Midcontinent of the United States Revealed by COCORP Deep Seismic Reflection Profiling	Provides summary of COCORP data from Oklahoma aulacogen showing layered ~1.2 Ga deposits south of Wichita uplift. Makes preliminary conclusions that these deposits suggest the aulacogen is more expansive or older than previously thought. Ideas are refined in later papers by Brewer.
Brewer et al. (1983)	COCORP Profiling Across the Southern Oklahoma Aulacogen: Overthrusting of the Wichita Mountains and Compression Within the Anadarko Basin	Uses COCORP reflection data to detail structure and timing of deformation related to formation of Oklahoma aulacogen and Wichita uplift. Suggests that extent of Oklahoma aulacogen may be more restricted than previously considered.
Coffman et al. (1986)	An Interpretation of the Crustal Structure of the Southern Oklahoma Aulacogen Satisfying Gravity Data	Presents cross section of crustal structure across Oklahoma aulacogen based on gravity data.
Gilbert (1983b)	Timing and Chemistry of Igneous Events Associated with the Southern Oklahoma Aulacogen	Summarizes timing of Oklahoma aulacogen formation as recorded in the record of igneous rocks.
Good et al. (1983)	COCORP Deep Seismic Reflection Traverse Across the Southern Oklahoma Aulacogen	Summarizes initial results of COCORP study of Oklahoma aulacogen. Results and conclusions are similar to papers by Brewer and others (in this table). Main conclusions are the presence of a Proterozoic basin to the south of the Wichita uplift and thrust faults that accommodate overthrusting of the Wichita mountains over the Anadarko basin.
Ham et al. (1964)	Basement Rocks and Structural Evolution of Southern Oklahoma	Provides maps of basement structure and faults of the Amarillo-Wichita-Arbuckle uplift.
Hanson et al. (1997)	Quaternary Deformation Along the Criner Fault, Oklahoma: A Case Study for Evaluating Tectonic Versus Landslide Faulting	Concludes that earlier investigations suggesting Quaternary activity of the Criner fault had misinterpreted landslide deposits and that, in fact, there have been no Holocene events along the Criner.
Keller and Stephenson (2007)	The Southern Oklahoma and Dnieper-Donets Aulacogens: A Comparative Analysis	Summarizes geophysical studies of the Oklahoma aulacogen and provides synthesis velocity and gravity models of the aulacogen and surrounding basins. Interprets base of the Anadarko basin as having rift-fill deposits.

**Table D-6.1.4 Data Summary
Oklahoma Aulacogen RLME**

Citation	Title	Description and Relevance to SSC
Larson et al. (1985)	Petrologic, Paleomagnetic, and Structural Evidence of a Paleozoic Rift System in Oklahoma, New Mexico, Colorado, and Utah	Presents petrologic and paleomagnetic data supporting interpretation that rifting related to the Oklahoma aulacogen extended into New Mexico, Colorado, and Utah.
Liang and Langston (2009)	Three-Dimensional Crustal Structure of Eastern North America Extracted from Ambient Noise	Maps three-dimensional shear-wave velocity throughout the CEUS and discusses presence of rifting episodes apparent in the data.
McConnell (1989)	Determination of Offset Across the Northern Margin of the Wichita Uplift, Southwest Oklahoma	Uses well data to constrain structural relationships of Wichita uplift frontal thrust system. Derives estimates of direction and amount of slip along frontal thrust faults during the Ouachita orogeny.
McConnell and Gilbert (1990)	Cambrian Extensional Tectonics and Magmatism Within the Southern Oklahoma Aulacogen	Uses presence of Cambrian igneous rocks to interpret history of aulacogen formation. Uses gravity and magnetic signature of these rocks to define extent of the Cambrian aulacogen.
Perry (1989)	Tectonic Evolution of the Anadarko Basin Region, Oklahoma	Summarizes tectonic history of Anadarko basin on north side of Oklahoma aulacogen.
Pratt et al. (1992)	Widespread Buried Precambrian Layered Sequences in the U.S. Mid-Continent: Evidence for Large Proterozoic Depositional Basins	Discusses previously published COCORP data for Hardeman basin, south of Wichita uplift. Uses correlation with borings to suggest the basin is potentially filled with 1.3–1.5 Ga felsic igneous rocks interbedded with sedimentary rocks. No real discussion of subsidence history or formation of the aulacogen.
Swan et al. (1993)	Draft Report: Investigation of the Quaternary Structural and Tectonic Character of the Meers Fault (Southwestern Oklahoma)	Assessed the potential for Quaternary activity along Wichita frontal fault system, with emphasis on Meers and Criner faults. Meers fault is discussed in that section of this data summary table. Concludes that only the Meers fault, and potentially the Criner fault, has evidence of Quaternary activity.
Texas BEG (1997)	Tectonic Map of Texas	Provides updated maps of basement structure and faults of the Amarillo-Wichita-Arbuckle uplift.
Viele and Thomas (1989)	Tectonic Synthesis of the Ouachita Orogenic Belt	Presents idea that Oklahoma aulacogen is a “leaky transform” and not a failed rift arm. Cites the existence of extensive volcanism and plutonism and the absence of rift-related sedimentary facies.

**Table D-6.1.4 Data Summary
Oklahoma Aulacogen RLME**

Citation	Title	Description and Relevance to SSC
Walker (2006)	Structural Analysis of the Criner Hills, South-Central Oklahoma	Constructed a detailed subsurface structural model of the Criner fault in the region where Quaternary activity had previously been suggested. Demonstrates that Criner fault is a relatively small secondary fault branching off the major Kirby fault. Based on these structural relationships, concludes that Criner had not slipped since the last activity on the Kirby (early Pennsylvanian).
Williamson (1996)	Observations on the Capability of the Criner Fault, Southern Oklahoma	Conducted a detailed analysis of previously cited evidence of Holocene/Quaternary activity of the Criner fault and determined that there is no evidence of Quaternary activity along the fault.
Zhang et al. (2009b)	Tomographic Pn Velocity and Anisotropy Structure in the Central and Eastern United States	Maps Pn (upper mantle) velocity structure throughout the CEUS and hypothesizes a potential correlation between edges of high-velocity zones and locations of intraplate seismic zones.

Table D-6.1.5 Data Summary
Reelfoot Rift–New Madrid Seismic Zone (NMSZ) Region

<i>Geologic Structures Interpreted from Geologic, Gravity, Magnetic, and Seismic-Profile Data</i>		
Braile et al. (1986)	Tectonic Development of the New Madrid Rift Complex, Mississippi Embayment, North America	Geological and geophysical studies of NMSZ have revealed a buried late Precambrian rift beneath the upper Mississippi embayment area. The rift has influenced tectonics and geologic history of the area since late Precambrian time and is presently associated with contemporary earthquake activity of the NMSZ. The rift formed during late Precambrian to earliest Cambrian time as a result of continental breakup and has been reactivated by compressional or tensional stresses related to plate tectonic interactions. Configuration of the buried rift is interpreted from gravity, magnetic, seismic-refraction, seismic-reflection, and stratigraphic studies. The increased mass of crust in the rift zone, which is reflected by regional positive gravity anomalies over the upper Mississippi embayment area, has resulted in periodic subsidence and control of sedimentation and river drainage in this cratonic region since formation of the rift complex. Correlation of the buried rift with contemporary earthquake activity suggests that earthquakes result from slippage along zones of weakness associated with ancient rift structures. Slippage is due to reactivation of the structure by the contemporary, nearly E-W regional compressive stress, which is the result of plate motions.
Braile et al. (1997)	New Madrid Seismicity, Gravity Anomalies, and Interpreted Ancient Rift Structures	Epicentral patterns, correlative geophysical data, and historical seismic energy release indicate significance of New Madrid area seismicity, both within Reelfoot segment of rift structures and in areas outside of this segment, particularly to the north. Deep structure of the crust, including thickness variations in the upper crust and the presence of a high-density lower-crustal layer, is a controlling factor in New Madrid seismicity.
Clendenin et al. (1989)	Reinterpretation of Faulting in Southeast Missouri	Mine, field, and borehole core observations are reported for late Proterozoic–early Cambrian rift-related faulting in SE Missouri. The principal fault set is composed of NW-striking transfer faults. Initial late Cambrian reactivations extended faults NW across Midcontinent and formed several major lineaments. Transpressive wrench-fault reactivations during late Pennsylvanian–Early Permian time uplifted St. Francois igneous terrane into a positive flower structure. During Cretaceous rifting, the faults acted as transfer faults, and intersections with related extension faults localized associated intrusive activity.

Table D-6.1.5 Data Summary
Reelfoot Rift–New Madrid Seismic Zone (NMSZ) Region

Csontos et al. (2008)	Reelfoot Rift and Its Impact on Quaternary Deformation in the Central Mississippi River Valley	<p>A structure-contour map and 3-D computer model of the top of Precambrian crystalline basement define the NE-trending Reelfoot rift, which is crosscut by SE-trending basement faults. Reelfoot rift consists of two basins separated by intra-rift uplift that are further subdivided into eight subbasins bounded by NE- and SE-striking rift faults. The rift is bounded to the south by White River fault zone and to the north by Reelfoot normal fault. Reelfoot thrust fault is interpreted as an inverted basement normal fault.</p> <p>A structure-contour map of the Pliocene-Pleistocene unconformity (top of Eocene base of Mississippi River alluvium) reveals both river erosion and tectonic deformation. Deformation of the unconformity appears to be controlled by NE- and SE-trending basement faults. NE-trending rift faults have undergone Quaternary dextral transpression that has resulted in displacement of two major rift blocks (uplift in SE half; subsidence in NW half) and formation of the Lake County uplift, Joiner Ridge, and southern half of Crowley's Ridge as compressional stepover zones, which appear to have originated above basement fault intersections. Lake County uplift has been tectonically active over the past ~2,400 years. The aseismic Joiner Ridge and southern portion of Crowley's Ridge may reflect earlier uplift, thus indicating Quaternary strain migration within Reelfoot rift.</p>
Dart and Swolfs (1998)	Contour Mapping of Relic Structures in the Precambrian Basement of the Reelfoot Rift, North American Midcontinent	<p>Presents contour map of the basement of the Reelfoot rift constructed from drillhole and seismic-reflection data and showing the general surface configuration as well as several major and minor structural features. Major features are two asymmetric intrarift basins, bounded by three structural highs, and the rift margins. The basins are oriented normal to NE trend of rift. Two of the highs appear to be ridges of undetermined width that extend across the rift; the third high is an isolated dome or platform located between the basins. Minor features are three linear structures of low relief oriented subparallel to trend of rift. Two of these, located within the rift basins, may divide the rift basins into paired subbasins. These mapped features may be remnants of initial extensional rifting, half graben faulting, and basement subsidence. The rift basins are reinterpreted as having formed as opposing half grabens, and the structural highs are interpreted as having formed associated accommodation zones. Some of these features appear to be reactivated seismogenic structures within the modern Midcontinent compressional</p>

Table D-6.1.5 Data Summary
Reelfoot Rift–New Madrid Seismic Zone (NMSZ) Region

		stress regime.
Hildenbrand (1982)	Model of the Southeastern Margin of the Mississippi Valley Graben near Memphis, Tennessee, from Interpretation of Truck-Magnetometer Data	Modeling of data from detailed magnetic-anomaly profiles suggests (1) that graben margins represent both structural boundaries and conduits for ascending magma and (2) that about 2 km (1.2 mi.) of vertical offset associated with normal faulting occurs within an interpreted 5.5 km (3.4 mi.) wide zone in which magnetic basement has an average dip of 20°NW into the graben. The high apparent susceptibility of magnetic basement associated with this fault zone and with the uplifted block suggests either that ascending magma intruded the upblock or that the two blocks differed lithologically prior to formation of the graben.
Hildenbrand and Hendricks (1995)	Geophysical Setting of the Reelfoot Rift and Relations Between Rift Structures and the New Madrid Seismic Zone	Provides discussion of several potential field features inferred from magnetic and gravity data that may focus earthquake activity in the northern Mississippi embayment and surrounding region. Summarizes complex tectonic and magmatic history of the rift.
Hildenbrand et al. (2001)	Geologic Structures Related to New Madrid Earthquakes near Memphis, Tennessee, Based on Gravity and Magnetic Interpretations	Defines boundaries of regional structures and igneous complexes in the region north of Memphis, Tennessee, and south of latitude 36° that may localize seismicity.
Langenheim and Hildenbrand (1997)	Commerce Geophysical Lineament—Its Source, Geometry, and Relation to the Reelfoot Rift and New Madrid Seismic Zone	The Commerce geophysical lineament (CGL) is a NE-trending magnetic and gravity feature that extends from central Arkansas to southern Illinois over a distance of >400 km (>250 mi.). The CGL is parallel to trend of Reelfoot graben, but offset >40 km (25 mi.) to the NW of the western margin of rift floor. Modeling indicates that the source of the magnetic and gravity anomalies is probably a mafic dike swarm. Age of the source of the CGL is not known, but the linearity and trend of the anomalies suggest a relationship with Reelfoot rift, which has undergone episodic igneous activity. The CGL coincides with several topographic lineaments, movement on associated faults at least as young as Quaternary, and intrusions of various ages. Several earthquakes ($m_b > 3$) coincide with the CGL, but the diversity of associated focal mechanisms and the variety of surface structural features along the length of the CGL obscure its relation to the release of present-day strain. With the available seismicity data, it is difficult to attribute individual earthquakes to a specific structural lineament such as the CGL.

Table D-6.1.5 Data Summary
Reelfoot Rift–New Madrid Seismic Zone (NMSZ) Region

McKeown et al. (1990)	Diapiric Origin of the Blytheville and Pascola Arches in the Reelfoot Rift, East-Central United States: Relation to New Madrid Seismicity	Earthquakes in the NMSZ correlate spatially with the Blytheville arch and part of the Pascola arch, which are interpreted to be the same structure. Both arches were formed by diapirism. Rocks in the arch are more highly deformed, and are therefore weaker, than adjacent rocks. Seismicity is hypothesized to be localized in these weaker rocks.
Mooney et al. (1983)	Crustal Structure of the Northern Mississippi Embayment and a Comparison with Other Continental Rift Zones	Information on the deep structure of the northern Mississippi embayment, gained through an extensive seismic refraction survey, supports a rifting hypothesis. The confirmation and delineation of a 7.3 km/s layer, identified in previous studies, implies that lower crust has been altered by injection of mantle material. Results indicate that this layer reaches a maximum thickness in the north-central embayment and thins gradually to the SE and NW, and more rapidly to the SW along axis of graben. The apparent doming of 7.3 km/s layer in the north-central embayment suggests that rifting may be the result of a triple junction located in the Reelfoot basin area.
Nelson and Zhang (1991)	A COCORP Deep Reflection Profile Across the Buried Reelfoot Rift, South-Central United States	Deep reflection profile line reveals features of the late Precambrian (?)/early Paleozoic Reelfoot rift. The Blytheville arch, an axial antiformal feature, as well as lesser structures indicative of multiple episodes of fault reactivation, is evident on profile.
Odum et al. (1995)	High-Resolution, Shallow, Seismic Reflection Surveys of the Northwest Reelfoot Rift Boundary near Marston, Missouri	<p>Presents and discusses interpretation of six high-resolution seismic-reflection profiles in the epicentral area of the 1811-1812 earthquakes. Three profiles show a master and antithetic fault pair that can be traced for 6 km (3.7 mi.). Geomorphic evidence suggests that the structures are at least 15 km (9 mi.) long. Trend of the fault pair (N50°–55°N) subparallels the magnetically defined Reelfoot rift boundaries and other major structures.</p> <p>Normal and reverse displacement of a Paleozoic surface reflector decreases from 30 m (98 ft.) upward toward the surface. There is evidence for minor amounts of movement into the Eocene. Lack of surface and near-surface deformation may indicate that strike-slip movement became prevalent in the late Tertiary.</p>

Table D-6.1.5 Data Summary
Reelfoot Rift–New Madrid Seismic Zone (NMSZ) Region

Odum et al. (2003)	Variable Near-Surface Deformation Along the Commerce Segment of the Commerce Geophysical Lineament, Southeast Missouri to Southern Illinois, USA	Concludes that there is a plausible link between surface and near-surface tectonic features and the vertical projection of the Commerce geophysical lineament (CGL). The CGL is a 5–10 km (3–6 mi.) wide zone of basement magnetic and gravity anomalies traceable for more than 600 km (373 mi.), extending from Arkansas, through SE Missouri and southern Illinois, and into Indiana. Interprets 12 km (7.5 mi.) of high-resolution seismic-reflection data, collected at four sites along a 175 km (109 mi.) segment of the projection, to show varying amounts of deformation involving Tertiary and some Quaternary sediments. Some of the locally anomalous geomorphic features in the northern Mississippi embayment region (i.e., paleoliquefaction features, anomalous directional changes in stream channels, and areas of linear bluff escarpments) overlying CGL can be correlated with specific faults and/or narrow zones of deformed (faulted and folded) strata that are imaged on high-resolution seismic-reflection data. There is an observable change in near-surface deformation style and complexity progressing from SW to NE along trace of CGL. The seismic-reflection data corroborate mapping evidence that suggests that this region has undergone a complex history of deformation, some of which is documented to be as young as Quaternary, during multiple episodes of reactivation under varying stress fields.
Potter et al. (1995)	Structure of the Reelfoot–Rough Creek Rift System, Fluorspar Area Fault Complex, and Hicks Dome, Southern Illinois and Western Kentucky—New Constraints from Regional Seismic Reflection Data	Interprets an 83 km (51.5 mi.) segment of seismic-reflection data across the northern part of the Reelfoot rift—Fluorspar Area fault complex (FAFC)—in SE Illinois and western Kentucky. Notes that NMSZ appears bounded on the north and south by Cambrian accommodation zones that linked segments with differing rift geometry. A series of grabens and horst in the FAFC document a late Paleozoic reactivation of Cambrian rift. Beneath two of the FAFC grabens, the bounding faults meet within the Knox Group and do not continue to depth. Other normal faults in the FAFC clearly offset the top of Precambrian basement.

Table D-6.1.5 Data Summary
Reelfoot Rift–New Madrid Seismic Zone (NMSZ) Region

Pratt (2009)	Insights into the Structure and Long-Term Deformation in the New Madrid Region from Seismic Reflection Profiles	Summarizes general observations and interprets all available seismic-reflection profiles in the New Madrid region (including Vibroseis profiles acquired by USGS, industry Vibroseis profiles purchased by USGS, COCORP profile across the embayment, and shallow seismic-reflection profiles acquired by USGS). The Blytheville arch is the most prominent feature that can be associated with the NMSZ. The arch is an antiform in Precambrian and early Paleozoic rift strata (as much as 20 km, or 12 mi., wide and 200 km, or 124 mi., long) that coincides with the SE arm of seismicity. The prominent erosional surface that truncates the top of the arch indicates that the arch was largely formed before the erosional surface was cut in the Paleozoic. This erosional surface is slightly folded (Quaternary or Holocene in age). Prominent faults include one coinciding with the Bootheel lineament and one with the SE arm of seismicity; other faults are evident over a wider area of the embayment. The arch appears to coincide with a major crustal boundary. Data are consistent with a rift model in which middle- and lower-crustal reflectivity are associated with rifting, and deformation is distributed across rift zone.
Van Arsdale and TenBrink (2000)	Late Cretaceous and Cenozoic Geology of the New Madrid Seismic Zone	Presents structure-contour maps constructed from well, seismic-reflection, and outcrop data of the tops of the Paleozoic section, Upper Cretaceous section, Paleocene Midway Group, and Eocene section used to illustrate post-Paleozoic structure of the NMSZ region. Maps reveal reactivation of the underlying late Precambrian to Cambrian Reelfoot rift during Midway Group deposition, but no reactivation during Late Cretaceous or Eocene deposition. The maps indicate a subtle, south-plunging depression on the tops of the Paleozoic, Upper Cretaceous, and Midway Group along axis of northern Mississippi embayment that is referred to as a trench. This trench is 50 km (31 mi.) wide, has a maximum depth of 100 m (328 ft.), and appears to have formed during the Eocene. The trench's western boundary coincides with Blytheville arch/Lake County uplift, and its SE margin underlies Memphis. The SE margin, like the NW margin, may be fault-controlled.
Van Arsdale et al. (2007)	Upland Complex of the Central Mississippi River Valley: Its Origin, Denudation, and Possible Role in Reactivation of the New Madrid Seismic Zone	Summarizes information on the distribution of the Upland Complex (Lafayette gravel) in early Pliocene (5.5–4.5 Ma) and what sea level was (+100 m, or 328 ft.) at time of deposition. Subsequent sea-level lowering to –20 m (–65.5 ft.) at 4 Ma resulted in incision that formed the high-level terrace; subsequent denudation of up to 100 m (328 ft.) of sediment may have perturbed the local stress field, possibly reactivating the NMSZ.

Table D-6.1.5 Data Summary
Reelfoot Rift–New Madrid Seismic Zone (NMSZ) Region

Wheeler (1996)	Relative Seismic Hazards of Six Iapetan Rifts and Grabens in Southeastern North America	Ranks six Iapetan rifts and grabens according to their seismic hazard based on seismicity and geologic criteria. Criteria include activity rate (seismicity), indirect evidence that their faults extend to the depths at which earthquakes typically occur in eastern North America, and evidence for Mesozoic extension. From most hazardous to least, the rankings are as follows: Reelfoot rift and Ottawa rift (highest); southern Oklahoma aulacogen and Saguenay rift (intermediate hazard); and Rough Creek and Rome trough (lower relative hazard indistinguishable from that of sparsely seismic cratonic interior regions).
Wheeler et al. (1994)	Map Showing Structure of the Mississippi Valley Graben in the Vicinity of New Madrid, Missouri	Compilation map showing bedrock geology; epicenters; geologic and subcrop contacts; structure contours; radon concentrations; selected wells; selected faults; and arches, troughs, and faulted boundaries of Mississippi Valley graben.
Williams et al. (2009)	Post-Eocene Deformation Observed in Seismic Profiles Across the Southwestern Blytheville Arch, Crowley's Ridge, and Western Reelfoot Rift Margin, Arkansas	Interpretation of three high-resolution minivibe P-wave reflection profiles in NE Arkansas about 70 km (43.5 mi.) NW of Memphis. Profiles are higher resolution than previously acquired in this area. Preliminary results from Crowley's Ridge, an anomalous topographic high, are consistent with previous COCORP and USGS reflection data and strongly suggest that the 50 m (164 ft.) high topography of the ridge is caused by post-Eocene tectonic uplift related to near-vertical ridge-bounding faults. The Lepanto profile images a monocline in Paleozoic and younger reflectors within a seismically active area on eastern margin of buried Blytheville arch (maximum uplift on the Paleozoic through Eocene reflector sequence is 100 m, or 328 ft.). Above the Eocene and possibly into the Quaternary, the sediments thicken east of the monocline, suggesting ongoing growth. Along western Reelfoot rift margin, a 2 km (1.2 mi.) wide zone of deformation is observed, with faulting that displaces Paleozoic and Eocene reflectors about 20–30 m (66–98 ft.) in an up-to-the-west sense. Across the 11 km (7 mi.) length of the profile (that crosses other small faults), the Paleozoic-Cretaceous section gradually rises to the west about 75 m (246 ft.).

Table D-6.1.5 Data Summary
Reelfoot Rift–New Madrid Seismic Zone (NMSZ) Region

Zoback et al. (1980)	Recurrent Intraplate Tectonism in the New Madrid Seismic Zone	Provides information on subsurface structure revealed through a program of seismic-reflection profiling. These data show that New Madrid seismicity can be linked to specific structural features. Major faults are coincident with the main earthquake trends in the area and with structural deformation apparently caused by repeated episodes of igneous activity. Notes that the zones of intense seismicity in the CEUS are associated with ancient rift zones that are favorably oriented for failure relative to the current stress field.
<i>Northern Terminus of Reelfoot Rift</i>		
Bear et al. (1997)	Seismic Interpretation of the Deep Structure of the Wabash Valley Fault System	Interpretation of recently compiled seismic-reflection data suggests that structures associated with the Wabash Valley fault system may not be directly linked to NE-trending structures in New Madrid area. The authors note that a graben may exist within the southern Indiana arm (Braille et al., 1982), but it is limited in geographic extent and is not structurally continuous with the Reelfoot rift–Rough Creek graben.
Heigold and Kolata (1993)	Proterozoic Crustal Boundary in the Southern Part of the Illinois Basin	Concludes that structures associated with the NMSZ may be distinct from structures to the NE (in the Wabash Valley zone), as evidenced by the E-SE-trending geophysical anomaly that separates two areas of distinctly different crust.
Hildenbrand and Hendricks (1995)	Geophysical Setting of the Reelfoot Rift and Relations Between Rift Structures and the New Madrid Seismic Zone	Inspection of regional magnetic and gravity anomaly maps suggests that NW margin does not continue northeastward into southern Indiana. A preferred geometry is that both the NW and SE margins bend to the east and merge with the Rough Creek graben.
Hildenbrand and Ravat (1997)	Geophysical Setting of the Wabash Valley Fault System	Concludes from high-resolution magnetic data and the lack of regional potential-field features extending south from Wabash Valley that the Wabash Valley fault system apparently is not structurally connected to the faults related to the NMSZ.
Kolata and Hildenbrand (1997)	Structural Underpinnings and Neotectonics of the Southern Illinois Basin: An Overview	Summarizes geologic and geophysical information that suggests that cause of earthquakes in the NMSZ is unrelated to that in the region north of Reelfoot rift system.

Table D-6.1.5 Data Summary
Reelfoot Rift–New Madrid Seismic Zone (NMSZ) Region

Pratt et al. (1989)	Major Proterozoic Basement Features of the Eastern Midcontinent of North America Revealed by Recent COCORP Profiling	Interpretation of deep seismic-reflection data from southern Illinois and southern Indiana indicates the absence of a thick section of rift-related sedimentary rocks.
Wheeler (1997)	Boundary Separating the Seismically Active Reelfoot Rift from the Sparsely Seismic Rough Creek Graben	Concludes that the structural boundary between the relatively high hazard of the Reelfoot rift and low hazard of the Rough Creek graben is marked by bends and ends of large faults, a Cambrian transfer zone, and the geographic extent of alkaline igneous rocks.
<i>Seismogenic Faults</i>		
Baldwin et al. (2002)	Preliminary Paleoseismic and Geophysical Investigation of the North Farrenburg Lineament: Primary Tectonic Deformation Associated with the New Madrid North Fault?	Presents geomorphic, geologic, seismic-reflection, trench, and microtextural data that strongly suggest that the North Farrenburg lineament, as well as the South Farrenburg lineament, may be the surface expression of an underlying tectonic fault that ruptured during January 23, 1812, earthquake. NE-trending contemporary microseismicity beneath Sikeston Ridge and previously inferred New Madrid North locations align partly with the lineaments.
Baldwin et al. (2005)	Constraints on the Location of the Late Quaternary Reelfoot and New Madrid North Faults in the New Madrid Seismic Zone, Central United States	Synthesis of existing unpublished and published data with subsurface and geomorphic information to clarify locations of Reelfoot and New Madrid North faults. The Reelfoot fault is interpreted to trend NW across the Kentucky Bend of the Mississippi River as a NW-facing scarp coincident with a slough near New Madrid, Missouri, and anomalous elevated topography on southern Sikeston Ridge NW of New Madrid. Quaternary faulting and folding imaged from seismic-reflection profiles coincide with bedrock structural lineaments, a NE-trending band of contemporary microseismicity, and a distinct NW-trending post-Tertiary change in alluvial thickness. The Reelfoot fault is traced as much as several kilometers NW of the Mississippi River, where it either dies out or steps N-NE to merge with the New Madrid North fault. The New Madrid North fault appears to be expressed geomorphically as left-stepping, en echelon NE-trending fractures preserved in Pleistocene glacial outwash material comprising Sikeston Ridge. The fractures coincide with Quaternary faults and folds, as well as deeper Cretaceous and Paleozoic faults and flexures, imaged in geophysical profiles.

Table D-6.1.5 Data Summary
Reelfoot Rift–New Madrid Seismic Zone (NMSZ) Region

Baldwin et al. (2006)	Geological Characterization of the Idalia Hill Fault Zone and Its Structural Association with the Commerce Geophysical Lineament, Idalia, Missouri	<p>Recent geologic and geophysical studies along faults overlying the Commerce geophysical lineament (CGL) support the notion that the prominent geophysical anomaly may be a source of future large-magnitude earthquakes. Results of geomorphic mapping and acquisition of seismic-reflection and ground-penetrating-radar data, together with paleoseismic trenching and borehole investigations, provide evidence of late Pleistocene to early Holocene deformation on Idalia Hill fault zone.</p> <p>Seismic-reflection data image a 0.5 km (0.3 mi.) wide zone of NE-striking, near-vertical faults that offset Tertiary and Quaternary reflectors and coincide with near-surface deformation. The regional NE strike of the fault zone, coupled with the presence of near-vertical faults and complex flowerlike structures, and preferential alignment with the contemporary central U.S. stress regime, indicate that the fault zone likely accommodates right-lateral transpressive deformation.</p> <p>Stratigraphic and structural relationships in trenches provide evidence for at least two late Quaternary faulting events on the Idalia Hill fault zone overlying Commerce section of the CGL. The penultimate event occurred in the late Pleistocene (prior to 23.6–18.9 ka). The most recent event occurred in the late Pleistocene to early Holocene (18.5–7.6 ka). The events overlap in age with two prehistoric events interpreted by Vaughn (1994) that occurred 23–17 ka and 13.4–9 ka and one event recognized by Harrison et al. (1999) that occurred 35–25 ka. The results of this study and previous studies provide evidence of late Pleistocene to early Holocene deformation along approximately 75 km (46.6 mi.) of the CGL.</p>
Baldwin et al. (2008)	Geophysical and Paleoseismic Evaluation of the Penitentiary Fault and Its Association with the Commerce Geophysical Lineament, Tamms, Southern Illinois	<p>Results of study provide evidence for linking observed Pleistocene-Holocene deformation with previously mapped faults overlying the CGL. The fault is accommodating dextral transpression based on interpretation of seismic data, regional focal mechanisms data, geomorphic data (i.e., deflected streams), regional topography, and previous studies.</p> <p>Data suggest that Penitentiary fault is likely a Paleozoic (?) fault that developed into a fault-line scarp during pre-Quaternary time and has been reactivated in late Quaternary time.</p> <p>Faults project upsection into the latest Pleistocene Henry Formation (older than ~25 kyr) and possibly Holocene Cahokia Formation. Vertical offset of reflectors ranges from 2 to 6 m (6.5 to 20 ft.).</p>

Table D-6.1.5 Data Summary
Reelfoot Rift–New Madrid Seismic Zone (NMSZ) Region

Champion et al. (2001)	Geometry, Numerical Models and Revised Slip Rate for the Reelfoot Fault and Trishear Fault-Propagation Fold, New Madrid Seismic Zone	Analysis of trench excavations, shallow borings, a digital elevation model of topography, and bathymetry shows that Reelfoot monocline is a forelimb on a fault-propagation fold that has accommodated relatively little shortening. Reelfoot fault is a reactivated Paleozoic structure. A late Holocene fault slip rate of 3.9 ± 0.1 mm/year is based on 9 m (29.5 ft.) of structural relief, the $2,290 \pm 60$ yr BP age of folded sediment, and a 75° dip for the fault. The fault tip is 1,016 m (3,333 ft.) beneath the surface. The thrust is flatter at deeper levels (5–14 km, or 3.1–8.7 mi.) based on the location of earthquake hypocenters ($\sim 40^\circ$ SW for northern segment, $\sim 35^\circ$ W for central segment, $\sim 45^\circ$ SW for southern segment).
Chiu et al. (1997)	Seismicity of the Southeastern Margin of Reelfoot Rift, Central United States	Coincidence of seismicity along SE flank of Reelfoot rift suggests that this rift flank is seismically active but at a lower level than main intra-rift NMSZ. Style of faulting as inferred from seismicity is complex, the dominant pattern being right-lateral strike-slip with reverse movement. Authors conclude that seismic data is sufficient to show that SE rift margin contains seismically active faults and has the potential of producing a major ($M \sim 7$) earthquake.
Cox, Van Arsdale, and Harris (2001)	Identification of Possible Quaternary Deformation in the Northeastern Mississippi Embayment Using Quantitative Geomorphic Analysis of Drainage-Basin Asymmetry	The SE Reelfoot rift margin coincides with a 150 km (93 mi.) long linear topographic scarp from near Memphis to the Tennessee-Kentucky line. S-wave reflection profiles, auger data, and a trench excavation reveal late Wisconsinan to early Holocene surface faulting and late Holocene liquefaction associated with this fault-line scarp. Variation in sense of throw along strike and flower-structure geometry suggest that this is a strike-slip fault. Temporal shifts in strain accommodation may give rise to short-term seismicity patterns and/or geodetic velocities that do not reveal long-term tectonic patterns.
Cox, Van Arsdale, et al. (2001)	Neotectonics of the Southeastern Reelfoot Rift Zone Margin, Central United States, and Implications for Regional Strain Accommodation	Suggests that the 150 km (93 mi.) long SE Reelfoot rift margin fault system may be accommodating significant northeastward transport as a right-lateral fault capable of producing earthquakes of $M \geq 7$. Results of paleoseismological investigations show the following: no Holocene movement at the Union City site (north of intersection with Reelfoot fault); ≥ 3 m vertical displacement of \sim Peoria loess (~ 20 ka) at the Porter Gap site (south of intersection with Reelfoot fault); and approximately 9.68 ka deposits postdate main events, while minor liquefaction postdates ~ 4.3 ka.

Table D-6.1.5 Data Summary
Reelfoot Rift–New Madrid Seismic Zone (NMSZ) Region

Cox, Van Arsdale, and Larsen (2002)	Paleoseismology of the Southeastern Margin of the Reelfoot Rift in the Vicinity of Memphis, Tennessee	<p>Confirms that SE Reelfoot rift margin is a fault zone with multiple high-angle faults and associated folding based on shallow seismic profiles and paleoseismological investigations. Documents evidence for 8–15 m (26.2–49.2 ft.) of right-lateral offset of a late Wisconsinan paleochannel (~20 ka) at a site near Porter Gap, suggesting an average slip rate of between 0.85 and 0.37 mm/year.</p> <p>Provides evidence for an earthquake ca. 2,500–2,000 yr BP on SE Reelfoot rift margin that ruptured ≥80 km (50 mi.) from Shelby County (15–25 km, or 9.3–15.5 mi., north of Memphis metropolitan area) to Porter Gap (just south of intersection with Reelfoot fault).</p>
Cox et al. (2006)	Paleoseismology of the Southeastern Reelfoot Rift in Western Tennessee and Implications for Intraplate Fault Zone Evolution	<p>Analysis of shallow S-wave reflection profiles, coring, and trenches show that SE Reelfoot rift is a right-lateral system with high-angle faults showing both up-to-the-NW and down-to-the-NW separations.</p> <p>Offset of a Wisconsinan paleochannel at Porter Gap indicates 8–15 m (26–49 ft.) of right-lateral strike-slip, suggesting that this rift margin may have accommodated much of the regional strain. Age constraints from paleoseismic investigations at Shelby County and at the Porter Gap site are consistent with an earthquake ca. 2,500–2,000 years ago (most recent event) that ruptured ≥80 km (50 mi.).</p> <p>Late Wisconsinan and Holocene faulting along SE rift margin fault system is observed adjacent to the hanging wall of the Reelfoot thrust, but only Wisconsinan faulting is noted adjacent to the footwall of the thrust. It is hypothesized that the NE segment of the SE rift margin turned off in Holocene when the Reelfoot stepover thrust turned on.</p>
Cramer et al. (2006)	The Possibility of Northeastward Unilateral Rupture for the January 23, 1812 New Madrid Earthquake	<p>Suggests that unilateral rupture within New Madrid fault zone led to extraordinary strong motions to the NE. This explanation is compatible with observations of triggered earthquakes in northern Kentucky and liquefaction in the northern New Madrid region and White County, Illinois. This rupture hypothesis cannot be unequivocally established due to lack of intensity data to the SW with which to show an asymmetric pattern of intensities.</p>

Table D-6.1.5 Data Summary
Reelfoot Rift–New Madrid Seismic Zone (NMSZ) Region

Crone (1992)	Structural Relations and Earthquake Hazards of the Crittenden County Fault Zone, Northeastern Arkansas	<p>Interpretation of about 135 km (84 mi.) of seismic-reflection data provides information on the structural relations between the Crittenden County fault zone (CCFZ) and subjacent rift-bounding faults along SE margin of Reelfoot rift in the NMSZ.</p> <p>Rift margin is 4–8 km (2.5–5 mi.) wide and coincides with the margin defined by magnetic data.</p> <p>The CCFZ is a NE-trending zone of high-angle (up-to-the-NW throw) reverse faulting that extends at least 32 km (20 mi.). The fault zone (varying from well-developed reverse faults to 1–3 km [0.6–1.9 mi.] wide zone of warped and disrupted reflectors) is structurally linked to the subjacent rift-bounding faults. Estimated vertical displacement of Cretaceous marker horizon measured across multiple seismic varies from 10 to 49 m (32.8 to 160.8 ft.). Evidence for a history of recurrent reverse slip that began shortly before deposition of the Upper Cretaceous sedimentary rocks and extended into at least the Eocene. The reverse slip may be related to bending-moment faulting in a localized compressional stress field that developed in response to subsidence of the Mississippi embayment.</p> <p>The CCFZ may have the potential for generating major earthquakes, or conversely; however, the possibility that the CCFZ is a bending-moment fault argues against its being an extremely hazardous fault.</p>
Crone (1998a)	Defining the Southwestern End of the Blytheville Arch, Northeastern Arkansas: Delimiting a Seismic Source Zone in the New Madrid Region	Interprets Vibroseis seismic-reflection profiles to document the southwesterly extent of the Blytheville arch and the length (134 km, or 83 mi.) of a fault zone that coincides with the arch.
Crone and Schweig (1994)	Fault Number 1023, Reelfoot Scarp and New Madrid Seismic Zone	<p>The Crittenden County fault zone (feature 1023-6) in NE Arkansas has no known surface expression, but extensive seismic-reflection studies suggest that Quaternary sediments are deformed by movement on the fault (Luzietti et al., 1992). The fault zone, in part, coincides with SE margin of Reelfoot rift and has sense of vertical offset that is opposite to the net structural relief in the underlying rift (Crone, 1992). Drillhole and seismic-reflection data show that the top of Paleozoic rocks is vertically offset about 80 m (262 ft.) across the fault zone and that shallower strata are offset progressively less (Luzietti et al., 1992; Crone, 1992).</p> <p>Deformation associated with the fault zone can be confidently traced through Tertiary rocks that fill the Mississippi embayment (Luzietti et al.,</p>

Table D-6.1.5 Data Summary
Reelfoot Rift–New Madrid Seismic Zone (NMSZ) Region

		1992). Very high-resolution reflection data confirm that late Quaternary deposits are faulted, and a deformed reflector as shallow as 6 or 7 m (20 or 23 ft.) could be resolved with these data (Williams et al., 1995). Lack of nearby stratigraphic control precluded determining if this reflector represented Holocene strata. An exploratory trench coincident with the very high-resolution reflection profile failed to find any unequivocal evidence of Holocene movement on the fault zone (Crone et al., 1995).
Crone et al. (1995)	Paleoseismic Studies of the Bootheel Lineament, Southeastern Missouri, and the Crittenden County Fault Zone, Northeastern Arkansas, New Madrid Seismic Zone, Central United States	<p>Presents results of trenching studies across structures previously identified from interpretation of high-resolution seismic-reflection data: (1) Bootheel lineament and (2) Crittenden County fault zone (CCFZ). The absence of conclusive evidence of faulting associated with the Bootheel lineament was possibly due to young age of sediments (1,000–200 years old) and characteristics of surficial deposits that limit the likelihood of finding evidence of brittle failure (faulting). Liquefaction features in the trench were attributed to the 1811-1812 earthquakes: the site had not been subjected to comparable ground motion for over 1,500 years.</p> <p>Data from the CCFZ trench do not provide absolute evidence for the origin of a monoclinical warp in an unconformity exposed in trench excavations; relief on the unconformity could relate to a paleochannel, or alternatively, could be related to deformation observed in the underlying deeper sediments as imaged in seismic data.</p>
Fischer-Boyd and Schumm (1995)	Geomorphic Evidence of Deformation in the Northern Part of the New Madrid Seismic Zone	Based on geomorphic evaluation, several locations of anomalous surface features within the NMSZ are identified. These include (1) anomalies in the slope, course, sinuosity, and dimensions of the Mississippi River related to the Lake County uplift; (2) anomalous channel behavior near Caruthersville, Missouri, and Barfield, Arkansas, suggestive of structural control; (3) angular course in the Black River suggestive of fracture control; (4) course changes of the Black, St. Francis, and Little rivers that may be tectonically controlled; and (5) topography along Crowley's Ridge that suggests it is composed of at least three structural blocks that are bounded by NE-trending faults. Some can be directly linked to mapped structures in the region, whereas others may result from previously unidentified areas of surface deformation.

Table D-6.1.5 Data Summary
Reelfoot Rift–New Madrid Seismic Zone (NMSZ) Region

Gomberg and Ellis (1994)	Topography and Tectonics of the Central New Madrid Seismic Zone: Results of Numerical Experiments Using a Three-Dimensional Boundary Element Program	Presents results of numerical experiments using seismicity and subtle topographic constraints. Surface displacement fields are calculated for the NMSZ under both far-field (plate tectonic scale) and locally derived driving strains. Results demonstrate that surface displacement fields cannot distinguish between either a far-field simple or pure shear strain field or one that involves a deep shear zone beneath the upper crustal faults. Thus neither geomorphic nor geodetic studies alone are expected to reveal the ultimate driving mechanism behind present-day deformation. Results of testing hypotheses about strain accommodation within the New Madrid contractional stepover by including linking faults, two SW-dipping and one vertical, show that only those models with stepover faults are able to predict the observed topography. These models suggest that the gently dipping central stepover fault is a reverse fault and that the steeper fault, extending to the SE of the stepover, acts as a normal fault over the long term.
Guccione (2005)	Late Pleistocene and Holocene Paleoseismology of an Intraplate Seismic Zone in a Large Alluvial Valley, the New Madrid Seismic Zone, Central USA	Summary paper that provides overview of paleoseismic investigations that have identified and characterized seven fault segments within the NMSZ. Three of the segments (Reelfoot fault, New Madrid North fault, and Bootheel fault) have recognized surface deformation. The Reelfoot fault is a compressive stepover along the strike-slip fault and has up to 11 m (36 ft.) of surface relief (Guccione et al., 2002). The New Madrid North apparently has only strike-slip motion and is recognized by modern microseismicity, geomorphic anomalies, and sand cataclasis (Baldwin et al., 2002). The Bootheel fault, which is not associated with present microseismicity, is associated with extensive liquefaction and offset channels (Guccione et al., 2005); it is dominantly strike-slip but also has a vertical component of slip. Other recognized surface deformation includes relatively low-relief folding at Big Lake/Manila high (Guccione et al., 2000) and Lake St. Francis/Marked Tree high (Guccione and Van Arsdale, 1995), both along the Blytheville arch.

Table D-6.1.5 Data Summary
Reelfoot Rift–New Madrid Seismic Zone (NMSZ) Region

Harris and Street (1997)	Seismic Investigation of Near-Surface Geological Structure in the Paducah, Kentucky Area	In this study, P- and S-wave seismic-refraction and seismic-reflection data were used to characterize shallow geological conditions in Paducah, Kentucky, area for use in earthquake hazard studies. Structure maps of a shallow unconformity and the Paleozoic bedrock surface show subsurface structural variability throughout the area. Ranges of shear-wave velocity for the sediments and bedrock, as well as estimates of the shear-wave velocity contrast at the unconformity and the bedrock, have been determined for the area. These two surfaces are important variables in site response analysis to evaluate ground motion amplification in the Paducah area.
Harrison and Schultz (1994)	Strike-Slip Faulting at Thebes Gap, Missouri and Illinois: Implications for New Madrid Tectonism	Documents evidence for Quaternary faulting in trenches in the Benton Hills of SE Missouri. Shows 12 earthquakes near the proposed trace of the Commerce geophysical lineament (CGL) and suggests that these earthquakes can be related to movement along structures associated with CGL.
Harrison and Schultz (2002)	Tectonic Framework of the Southwestern Margin of the Illinois Basin and Its Influence on Neotectonism and Seismicity	Describes neotectonism along the Commerce geophysical lineament (CGL). The CGL is interpreted to consist of en echelon faults and intrusions in basement related to the Neoproterozoic to early Paleozoic Reelfoot rift, but may have older ancestry. Faults in Thebes Gap and English Hills overlie the CGL; the faults cut Paleozoic, Mesozoic, and Cenozoic deposits and have had a long-lived and episodic tectonic history, including Pleistocene and Holocene activity. In the past 25 years, several dozen m_b 2–4 earthquakes have occurred along or near CGL.
Harrison et al. (1999)	An Example of Neotectonism in a Continental Interior: Thebes Gap, Midcontinent, United States	Documents evidence for four episodes of Quaternary faulting: one in late to post-Sangamon, pre- to early Roxana time (~60–50 ka), one in syn- or post Roxana, pre-Peoria time (~35–25 ka), and two in Holocene time (middle to late Holocene and possibly during 1811-1812 earthquake sequence). The overall style of neotectonic deformation is interpreted as right-lateral strike-slip faulting.
Harrison et al. (2002)	Geologic Map of the Scott City 7.5-Minute Quadrangle, Scott and Cape Girardeau Counties, Missouri	Provides description of geomorphology and surficial geology, general structural geology, and results of trenching investigations at localities within the English Hills. At least two events may have occurred in the latest Holocene (just after 2σ calibrated calendar ages of 3747 to 3369 BC and AD 968 to 639).

Table D-6.1.5 Data Summary
Reelfoot Rift–New Madrid Seismic Zone (NMSZ) Region

Johnston and Schweig (1996)	The Enigma of the New Madrid Earthquakes of 1811-1812	<p>Associated each of three 1811-1812 earthquakes with a specific fault by using historical accounts and geologic evidence:</p> <ul style="list-style-type: none"> • Event D1—BA/CDF or BL • Event J1—East Prairie fault • Event F1—RF
Luzietti et al. (1992)	Shallow Deformation Along the Crittenden County Fault Zone near the Southeastern Boundary of the Reelfoot Rift, Northeast Arkansas	<p>Interpretation of nine Mini-Sosie seismic-reflection profiles (sedimentary strata imaged to a depth of 800 m [2,625 ft.]). Estimates of structural relief across the Crittenden County fault zone (CCFZ) at the Paleocene level range between 14 and 70 m (46 and 230 ft.). Overlying Middle-to-Late Eocene section shows a similar or slightly smaller amount of thinning, indicating that much of the movement on the CCFZ dates from Middle to Late Eocene. Displacement, flexure, and thinning in the geologic section increases as CCFZ converges with Reelfoot rift boundary (SW). Reflections from the Quaternary-Eocene unconformity show warping, dip, or interruptions in places over the CCFZ that suggest at least 16 km (10 mi.) of near-surface deformation; this deformation may represent possible Quaternary or Holocene movement.</p>
B. Magnani (pers. comm. May 29, 2009)	[Preliminary map showing locations of interpreted faults]	<p>Presents map showing preliminary interpretation of near-surface faults observed in high-resolution seismic-reflection profile along the Mississippi River from Caruthersville, Missouri, to Helena, Missouri. Results of the survey suggest that the eastern Reelfoot margin fault may extend south from Memphis along the river (east of the boundary of the Reelfoot rift).</p>
Magnani et al. (2009)	Long-Term Deformation History in the Mississippi Embayment: The Mississippi River Seismic Survey	<p>Seismic survey collected a 300 km (186 mi.) long high-resolution seismic-reflection profile along the Mississippi River from Helena, Arkansas, to Caruthersville, Missouri. Identified three zones of deformation and faulting involving quaternary sediments. Two areas lie outside the NMSZ, suggesting that the long-term seismic activity in this area might extend over a broader region than previously suspected.</p>

Table D-6.1.5 Data Summary
Reelfoot Rift–New Madrid Seismic Zone (NMSZ) Region

McBride et al. (2003)	Variable Post-Paleozoic Deformation Detected by Seismic Reflection Profiling Across the Northwestern Prong of New Madrid Seismic Zone	High-resolution shallow seismic-reflection profiles in the vicinity of the Olmstead fault (which is close to and parallel with the straight segment of the Ohio River) on trend with the westernmost of two groups of NE-aligned prongs of epicenters) show Tertiary reactivations of complex Cretaceous deformations (including normal graben faults). A possible fault-propagation fold associated with one of these faults appears to affect Holocene sediments near the ground surface.
McBride, Nelson, and Stephenson (2002)	Integrated Geological and Geophysical Study of Neogene and Quaternary-Age Deformation in the Northern Mississippi Embayment	<p>Presents results of program of shallow drilling, trenching, outcrop mapping, and seismic-reflection acquisition in southern Illinois just north of NMSZ. Detailed structural cross sections over five NE-trending faults that continue from the Fluorspar Area fault complex (FAFC) southward into the embayment indicate narrow grabens into which latest Cretaceous, Paleocene, and Eocene sediments were dropped and protected from erosion. Bounding faults were active during Neogene through middle Pleistocene time.</p> <p>Definitive faulting of Wisconsinan loess or Holocene alluvium is not observed at any site, which would indicate that the faults have been inactive for at least 55 ka (basal loess ages) to 128 ka (youngest Illinoian age). Seismic profiles indicate that faults in Quaternary sediment penetrate Paleozoic bedrock, and thus are tectonic. Faults exhibit vertical to steeply dipping normal and occasional reverse displacements that outline a variety of structures, including a series of narrow grabens and local folding.</p> <p>Proposes a dynamic structural model that suggests a mechanism by which seismicity and active (Holocene) faulting have shifted within the central Mississippi Valley (away from the FAFC) over the last several ten thousand years.</p>
Mihills and Van Arsdale (1999)	Late Wisconsin to Holocene Deformation in the New Madrid Seismic Zone	Interprets a structure-contour map of the unconformity between the Eocene strata and overlying Quaternary Mississippi River alluvium as representing the late-Wisconsinan-to-present strain field of the NMSZ. Areas of Holocene uplift include the Lake County uplift, Blytheville arch, and Crittenden fault. Areas of Holocene subsidence include Reelfoot Lake, historical Lake Obion, the Sunklands of NE Arkansas, and possibly areas east and west of the Crittenden County fault.

Table D-6.1.5 Data Summary
Reelfoot Rift–New Madrid Seismic Zone (NMSZ) Region

Mueller and Pujol (2001)	Three-Dimensional Geometry of the Reelfoot Blind Thrust: Implications for Moment Release and Earthquake Magnitude in the New Madrid Seismic Zone	<p>According to seismicity data and structural analysis, the Reelfoot blind thrust is a complex fault that changes in geometry along-strike. The thrust is bounded to the north by an east-trending strike-slip fault. The southern end is defined by seismicity; it is not truncated by a known transverse fault. The northern part of the thrust steepens to 75°–80° at shallow depths (within upper 4 km, or 2.5 mi.), forming a listric shape. The center of the central part of the thrust strikes N-S and dips between 31° and 35° west; the north and south segments strike between N10°W and N22°W, respectively. The SE fault segment is oriented N28°W and dips 48°–51° SW. Available data suggest that the thrust flattens to <35° between about 2 and 4 km (1.2 and 2.5 mi.) depth (possibly at the Precambrian basement/Paleozoic cover contact at about 3 km, or 1.9 mi., depth).</p>
Mueller et al. (1999)	Fault Slip Rates in the Modern New Madrid Seismic Zone	<p>Estimates slip rate of 6.1 ± 0.7 mm/year for the past $2,300 \pm 100$ years, based on structural and geomorphic analysis of late Holocene sediments deformed by fault-related folding above the blind Reelfoot thrust fault. Calculates slip rate of 4.8 ± 0.2 mm/year using an alternative method based on the structural relief across the scarp and the estimated dip of the underlying blind thrust. Geometric relations suggest that right-lateral slip rate on the NMSZ is 1.8–2.0 mm/year.</p> <p>The onset of shortening across the Lake County uplift is estimated to be between 9.3 and 16.4 ka, with a preference for the younger age.</p>
Nelson et al. (1997)	Tertiary and Quaternary Tectonic Faulting in Southernmost Illinois	<p>Interprets the Fluorspar Area fault complex (FAFC) as a series of strike-slip pull-apart grabens bounded by N20°E–N40°E striking normal and reverse faults. The faults probably originated as normal faults during an episode of crustal rifting of latest Proterozoic to early Cambrian time that formed the Reelfoot rift (locally, the Lusk Creek fault zone). Evidence exists for episodic reactivation of these faults in post-Pennsylvanian, pre-Cretaceous, and again in late Neogene to Quaternary time.</p> <p>Results of shallow drilling, trenching, outcrop mapping, and seismic-reflection acquisition in southern Illinois just north of New Madrid zone show evidence for Quaternary-age faulting on larger mapped faults in the FAFC in southernmost Illinois. NE-trending faults downdrop Mounds Gravel of Late Miocene to early Pleistocene age (1 Ma to 11 ka) approximately 150 m (490 ft.) in the deepest graben and locally displace</p>

Table D-6.1.5 Data Summary
Reelfoot Rift–New Madrid Seismic Zone (NMSZ) Region

		<p>Metropolis terrace gravel believed to be Illinoian (~185–128 ka) or older.</p> <p>FAFC faults are oriented for reactivation as strike-slip or oblique-slip faults in current stress field: apparent extensional component of slip not a good match for the nearly E-W maximum horizontal stress direction.</p>
Nelson et al. (1999)	Quaternary Grabens in Southernmost Illinois: Deformation near an Active Intraplate Seismic Zone	<p>Grabens are part of the Fluorspar Area fault complex (FAFC), which has been recurrently active throughout Phanerozoic time. The FAFC strikes directly toward the NMSZ, and both the NMSZ and FAFC share origin in a failed Cambrian rift (Reelfoot rift). Every major fault zone of the FAFC in Illinois exhibits Quaternary displacement. The structures appear to be strike-slip pull-apart grabens, but magnitude and direction of horizontal slip and their relationship to the current stress field are unknown. Upper Tertiary strata are vertically displaced more than 100 m (328 ft.); Illinoian and older Pleistocene strata 10–30 m (33–98 ft.); and Wisconsinan deposits 1 m (3.3 ft.) or less. No Holocene deformation has been observed. Average vertical slip rates are estimated at 0.01–0.03 mm/year, and recurrence intervals for earthquakes of M 6–7 are on the order of tens of thousands of years for any given fault.</p>
Odum et al. (1998)	Near-Surface Structural Model for Deformation Associated with the February 7, 1812, New Madrid, Missouri, Earthquake	<p>Integrates geomorphic data and documentation of differential surficial deformation (supplemented by historical accounts) with interpretation of seismic-reflection data to develop a tectonic model of near-surface structures in New Madrid area. Model consists of two primary components: a N-NW-trending thrust fault (Reelfoot fault) and a series of NE-trending strike-slip tear faults. The authors estimate an overall length of at least 30 km (18.6 mi.) and a dip of ~31° for the Reelfoot fault.</p>
Odum et al. (2001)	High-Resolution Seismic-Reflection Imaging of Shallow Deformation Beneath the Northeast Margin of the Manila High at Big Lake, Arkansas	<p>The authors interpret 7 km (4.3 mi.) of high-resolution seismic-reflection data across NE margin of the Manila high to examine its near-surface bedrock structure and possible association with underlying structures such as the Blytheville arch. The Manila high is an elliptical area 19 km (11.8 mi.) long (N-S) by 6 km (3.7 mi.) wide (E-W) located W-SW of Big Lake, Arkansas, that has less than 3 m (10 ft.) of relief. Sense of displacement and character of imaged faults support interpretations for either a NW-trending 1.5 km (0.9 mi.) wide block of uplifted strata or a series of parallel NE-trending faults that bound horst and graben structures. The favored interpretation is that deformation of the Manila high resulted from faulting generated by reactivation of right-lateral strike-slip fault motion along this portion of the Blytheville arch.</p>

Table D-6.1.5 Data Summary
Reelfoot Rift–New Madrid Seismic Zone (NMSZ) Region

Odum et al. (2002)	Near-Surface Faulting and Deformation Overlying the Commerce Geophysical Lineament in Southern Illinois	Seismic-reflection and microgravity data demonstrate post-Devonian displacement associated with the Commerce geophysical lineament in the Tamms area of southern Illinois. Several faults are imaged to the Paleozoic/Quaternary interface, and at one site, deformed Quaternary strata may have been faulted 5–10 m (16.4–32.8 ft.).
Odum et al. (2010)	Multi-Source, High-Resolution Seismic-Reflection Imaging of Meeman-Shelby Fault and Possible Tectonic Model for a Joiner Ridge–Manila High Structure in the Upper Mississippi Embayment Region	Reinterpretation of the Meeman-Shelby fault (MSF) based on high-resolution seismic-reflection profiles, combined with existing industry data and recent structural interpretations. MSF fault trace above the Paleozoic surface is constrained to having an up-to-the-west reverse displacement along a near-vertical (80°) plane that projects to the surface just east of the profiles. Using seismic-reflection data that were both reinterpreted and newly acquired, the authors interpret an orientation of approximately N13°W for the MSF and provide evidence to support an interpretation that the MSF forms the eastern boundary of Joiner Ridge tectonic structure. The authors suggest that Joiner Ridge and Manila high surficial uplift may collectively be considered as segments of a tectonic structure similar to the Reelfoot fault stepover. They concur with Csontos et al. (2008) that Joiner Ridge is a right-lateral compressional stepover between the Eastern Reelfoot Rift margin and the axial fault zone that formed in response to Quaternary N60°E maximum horizontal compressive stress field. Scientific knowledge is not sufficient to speculate about seismic hazard significance of the 50 km (31 mi.) long Joiner Ridge–MSF structure.
Palmer, Hoffman, et al. (1997)	Shallow Seismic Reflection Profiles and Geological Structure in the Benton Hills, Southeast Missouri	Two shallow, high-resolution seismic-reflection surveys (Mini-Sosie method) across southern escarpment of the Benton Hills segment of Crowley's Ridge imaged numerous post-Late Cretaceous faults and folds. The survey did not resolve reflectors within upper 75–100 m (246–328 ft.) of two-way travel time (about 60–100 m, or 197–328 ft.), which would include all of Tertiary and Quaternary and most of Cretaceous. The Paleozoic-Cretaceous unconformity produced an excellent reflection, and locally a shallower reflector within the Cretaceous was resolved. The English Hill fault zone, striking N30°E–N35°E, imaged in one of the seismic lines, has been observed by previous workers to have Pleistocene loess faulted against Eocene sands. The Commerce fault zone, striking N50°E, overlies a major regional basement geophysical lineament and is present on both seismic lines at southern margin of escarpment.

Table D-6.1.5 Data Summary
Reelfoot Rift–New Madrid Seismic Zone (NMSZ) Region

Palmer, Shoemaker, et al. (1997)	Seismic Evidence of Quaternary Faulting in the Benton Hills Area, Southeast Missouri	Seismic profiles show English Hill area to be tectonic in origin. Individual faults have near-vertical displacements with maximum offsets on the order of 15.2 m (50 ft.). Faults are interpreted as flower structures with N-NE-striking, vertically dipping, right-lateral oblique-slip faults. These data suggest that previously mapped faults at English Hill are deep-seated and tectonic in origin.
Parrish and Van Arsdale (2004)	Faulting Along the Southeastern Margin of the Reelfoot Rift in Northwestern Tennessee Revealed in Deep Seismic-Reflection Profiles	Deep seismic-reflection profiles in NW Tennessee reveal structure of SE margin of Reelfoot rift. Rift margin consists of at least two major down-to-the-west late Precambrian to Cambrian normal faults. Dominantly reverse faulting, folding, and positive flower structures in the shallow section indicate Eocene and younger transpression. Numerous faults displace the youngest reflectors, and therefore the age of most recent faulting is not known. SE rift margin is subject to right-lateral movement and transpression within current stress field.
Pujol et al. (1997)	Refinement of Thrust Faulting Models for the Central New Madrid Seismic Zone	Seismicity cross sections define the downdip geometry of the Reelfoot thrust.
Purser and Van Arsdale (1998)	Structure of the Lake County Uplift: New Madrid Seismic Zone	Lake County uplift, which includes the Tiptonville dome and Ridgely Ridge, is interpreted to be a consequence of deformation in the hanging wall above the NW-striking, SW-dipping Reelfoot reverse fault. The Reelfoot fault dips 73° from the surface to the top of the Precambrian at a depth of approximately 4 km (2.5 mi.). From 4 to 12 km (2.5 to 7.5 mi.) depth, the fault dips 32° and is seismically active. Based on a fault-bend fold model, the Reelfoot fault becomes horizontal and aseismic at the top of the quartz brittle-ductile transition zone, at approximately 12 km (7.5 mi.) depth. Western margin of the Tiptonville dome–Ridgely Ridge and western margin of the Lake County uplift are bounded by east-dipping kink bands (backthrusts). The Reelfoot fault, which is postulated to be the source of the February 7, 1812, M 8 earthquake, has less surface area than is necessary for an M 8 earthquake. A possible solution to this discrepancy between magnitude and fault plane area is that the associated backthrusts are seismogenic.

Table D-6.1.5 Data Summary
Reelfoot Rift–New Madrid Seismic Zone (NMSZ) Region

Russ (1979)	Late Holocene Faulting and Earthquake Recurrence in the Reelfoot Lake Area, Northwestern Tennessee	Discusses results of trenching investigations across Reelfoot scarp in NW Tennessee. In excess of 3 m (10 ft.) of vertical displacement believed to be of deep-seated origin occurs across a 0.5 m wide zone of east-dipping normal faults near scarp base. Stratigraphic and geomorphic relationships suggest that little (<0.5 m) or no near-surface fault movement occurred across the zone during 1811-1812 earthquake sequence. Faults, folds, and sand dikes were identified in the trench. Crosscutting geologic features and local geomorphic history suggest that at least two periods of faulting predate sediments deposited before AD 1800. A recurrence interval of approximately 600 years or less is suggested for large earthquakes in the New Madrid area.
Russ (1982)	Style and Significance of Surface Deformation in the Vicinity of New Madrid, Missouri	<p>Lake County uplift is an elongate, composite Quaternary structure associated with faults and modern seismicity. It is subdivided into Tiptonville dome, Ridgely Ridge, and the south end of Sikeston Ridge.</p> <p>The Tiptonville dome is an asymmetrical monocline; the steep eastern flank is bounded by Reelfoot scarp, a complex monoclinical fold that has a zone of normal faults (displacement about 3 m, or 10 ft.) at its base. The zone of faults overlies, and is probably continuous, with Reelfoot fault, a high-angle dip-slip fault that offsets Paleozoic, Mesozoic, and Tertiary rocks. Surface uplift accounts for about 1/5 of the displacement. Most of Tiptonville dome formed between 200 and 2,000 years ago.</p> <p>Ridgely Ridge is a NE-trending symmetrical bulge underlain by a similarly oriented zone of faults. Much of the ridge appears older than Tiptonville dome, but younger than 6,000 yr BP.</p> <p>The southern end of Sikeston Ridge and adjoining areas has undergone broad shallow warping. Deformation probably occurred in late Wisconsinan or early Holocene time.</p> <p>The New Madrid region has been shaken by at least three earthquakes of $m_b \geq 6.2$ in the past 2,000 years.</p>

Table D-6.1.5 Data Summary
Reelfoot Rift–New Madrid Seismic Zone (NMSZ) Region

SAIC (2002)	Seismic Investigation Report for Siting a Potential On-Site CERCLA Waste Disposal Facility at the Paducah Gaseous Diffusion Plant, Paducah, Kentucky	<p>Conclusions from this study are as follows:</p> <ul style="list-style-type: none"> • Field observations made along Ohio River in the vicinity of the Paducah Gaseous Diffusion Plant (PGDP) found no large liquefaction features. • The absence of large paleoliquefaction features within 24 km (15 mi.) of PGDP suggests that local strong ground motion has not occurred within the past few thousand years • The literature does report some small liquefaction features located along the banks of the Ohio River, about 13 km (8 mi.) NE of PGDP, and along the Post Creek Cutoff, about 19 km (12 mi.) NW of PGDP. • The site-specific fault study identified a series of faults beneath Site 3A. For most of the faults beneath Site 3A, relative movement along main fault plane is normal, with the downthrown side to the east. These normal faults, along with their associated splays, either form a series of narrow horst and graben features or divide local sediments into a series of rotated blocks. Several of the faults extend through Porters Creek Clay and into materials underlying the surficial loess of latest Pleistocene age (radiocarbon dated at 13,500–15,600 yr BP). Three of these faults extend to within 6 m (20 ft.) of ground surface. This study did not find Holocene displacement of faults at Site 3A. <p>At the Barnes Creek site located 18 km (11 mi.) NE of PGDP, this study found the following:</p> <ul style="list-style-type: none"> • The relative timing of observed deformations in the geologic structures varies. • Radiocarbon ages confirm that repeated deformation has occurred along some of the observed faults. Deformation began prior to deposition of the lower Metropolis (late Pleistocene), continued during deposition of the upper Metropolis (5,000–7,000 years old) and most recently occurred in the middle Holocene, after deposition of the upper Metropolis (within the last 5,000 years). Therefore, faults observed at Barnes Creek site did extend into Holocene-age deposits. • The maximum displacement observed in a single event is approximately 0.3 m (1 ft.) in the lower Metropolis. • Investigation of the terrace graben area concluded that observed stratigraphy is consistent with a combination of two models: (1) a
-------------	--	--

Table D-6.1.5 Data Summary
Reelfoot Rift–New Madrid Seismic Zone (NMSZ) Region

		graben with up to 15 m (50 ft.) of displacement within the past 12,000 years, and (2) an erosional feature with up to 15 m (50 ft.) of infilling within the past 12,000 years. Radiocarbon ages in the terrace graben area at the Barnes Creek site indicate that deep fine-grained sediments beneath the Metropolis are approximately 11,000 years old, suggesting that overlying Metropolis dates from late Pleistocene or early Holocene.
Schumm and Spitz (1996)	Geological Influences on the Lower Mississippi River and Its Alluvial Valley:	Identifies different reaches of the Mississippi River based on studies of photographs, maps, and channel morphology. The river is not monotonous in appearance, and therefore, it is not completely controlled by hydrology and hydraulics. Results of the study suggest that the Mississippi River has reacted to uplift, faults, clay plugs, outcrops of Tertiary clay, and Pleistocene gravel in its bed and tributaries.
Schweig and Ellis (1992)	Distributed Faulting Along the Bootheel Lineament—Smoothing Over the Rough Spots in the New Madrid Seismic Zone	Shallow seismic-reflection work in the area of the Bootheel lineament shows that the lineament is underlain by a complex zone of deformation consisting of multiple flower structures and fractured rock that show up to 25 m (82 ft.) of vertical relief. Flower structures and lineament occur over a zone at least 5 km (3 mi.) wide. Their discontinuous nature strongly resemble physical models in which flower structures form in less rigid material in response to low finite displacement across a discrete strike-slip shear zone in a rigid basement. The Bootheel lineament links two well-established, seismically active strike-slip zones in the New Madrid region and may be acting to smooth the trace of the NMSZ as displacement increases.
Schweig and Ellis (1994)	Reconciling Short Recurrence Intervals with Minor Deformation in the New Madrid Seismic Zone	Comparison of present-day strain rates to long-term geologic offsets suggests that the NMSZ is a young feature, possibly as young as several tens of thousands of years and no older than a few million years.
Schweig and Marple (1991)	A Possible Coseismic Fault of the Great New Madrid Earthquakes	Identifies the Bootheel lineament from a remote sensing examination of the NMSZ. The lineament may be the surface expression of one of the coseismic faults of the 1811-1812 New Madrid earthquakes. It extends for about 135 km (84 mi.) in a N-NE direction. Morphology suggests that it is a strike-slip fault. The lineament does not coincide with any of the major arms of seismicity. A possible inference is that the arms of seismicity do not precisely reflect the faults that ruptured in 1811-1812.

Table D-6.1.5 Data Summary
Reelfoot Rift–New Madrid Seismic Zone (NMSZ) Region

Schweig and Van Arsdale (1996)	Neotectonics of the Upper Mississippi Embayment	Summarizes geologic and geophysical evidence of neotectonic activity, including faulting in Benton Hills and Thebes Gap, paleoliquefaction in Western Lowlands, subsurface faulting beneath and tilting of Crowley's Ridge, subsurface faulting along the CCFZ, and numerous indicators of historical and prehistoric large earthquakes in NMSZ.
Schweig et al. (1992)	Shallow Seismic Reflection Survey of the Bootheel Lineament Area, Southeastern Missouri	The pattern and character of geomorphic features associated with the Bootheel lineament traces are very similar in geometry to a right-lateral strike-slip fault. Seismic-reflection profiles are interpreted to show a complex zone of deformation consisting of multiple flower structures and fractured rock, with deformation at least as young as the base of the Quaternary.
Sexton and Jones (1986)	Evidence for Recurrent Faulting in the New Madrid Seismic Zone from Mini-Sosie High-Resolution Reflection Data	Interpretation and integration of three seismic-reflection data sets provides evidence for recurrent movement along the Reelfoot fault, the major reverse fault associated with the Reelfoot scarp. Estimated displacements vary from 61 m (200 ft.) for late Paleozoic rocks to 15 m (50 ft.) for Late Eocene sedimentary units. A graben structure is interpreted to be caused by tensional stresses resulting from uplift and folding of the sediments. The location of the graben coincides with normal faults in Holocene sediments observed in trenches. These features are interpreted to be related and caused by reactivation of the Reelfoot fault.
Spitz and Schumm (1997)	Tectonic Geomorphology of the Mississippi Valley Between Osceola, Arkansas, and Friars Point, Mississippi	A geomorphic study of the Mississippi River and its alluvial valley identified anomalous surface features indicative of relatively recent deformation that can be linked to the following known geological structures: Big Creek fault zone, White River fault zone, Bolivar-Mansfield tectonic zone, Blytheville arch, Crittenden County fault zone, and Reelfoot Rift margins. Faults and plutons appear to affect drainage networks, and the morphology of Crowleys Ridge suggests significant fault control. The authors conclude that (1) many anomalies probably reflect a fractured sub-alluvial surface, and (2) although movement along these fractures will most likely occur in seismically active areas, the probability of movement elsewhere is high.

Table D-6.1.5 Data Summary
Reelfoot Rift–New Madrid Seismic Zone (NMSZ) Region

Stephenson et al. (1995)	Characterization of the Cottonwood Grove and Ridgely Faults near Reelfoot Lake, Tennessee, from High-Resolution Seismic Reflection Data	<p>High-resolution seismic-reflection data delineate Cottonwood Grove and Ridgely faults, as well as a new, potentially major fault with approximately 40 m (131 ft.) of apparent vertical displacement east of Ridgely fault. The new fault trends NW—opposite in trend direction to the Cottonwood Grove and Ridgely faults—and dips vertically.</p> <p>The NE-trending Cottonwood Grove fault has as much as 30 m (98.5 ft.) of apparent vertical displacement of all imaged strata, from the Cretaceous/Paleozoic boundary to the Middle Eocene horizon; this suggests faulting began post-Middle Eocene.</p> <p>The NE-trending Ridgely fault appears to be a zone of faults bounding a horst-like feature; apparent vertical displacements across easternmost strand suggest recurrent displacement, with roughly 22–26 m (72.2–85.3 ft.) of apparent offset on Cretaceous/Paleozoic boundary and 18–22 m (59–72.2 ft.) of apparent offset on Middle Eocene deposits. The Quaternary/Eocene boundary was not sufficiently imaged to determine whether faulting has occurred later than post-Middle Eocene.</p>
Stephenson et al. (1999)	Deformation and Quaternary Faulting in Southeast Missouri Across the Commerce Geophysical Lineament	<p>High-resolution seismic-reflection data at three sites along the Commerce geophysical lineament (CGL) reveal post-Cretaceous faulting extending into Quaternary. At Qulin site, ~20 m (65.5 ft.) of apparent Quaternary vertical displacement is observed. At Idalia Hill, a series of reverse and possibly right-lateral strike-slip faults with Quaternary displacement are imaged. At Benton Hills, a complicated series of anticlinal and synclinal fault-bounded blocks occur directly north of CGL.</p>
Van Arsdale (2000)	Displacement History and Slip Rate on the Reelfoot Fault of the New Madrid Seismic Zone	<p>Develops a displacement history and slip rates for the Reelfoot fault in the NMSZ from a seismic-reflection profile and trench data.</p> <p>Average slip rate estimates—seismic profile:</p> <ul style="list-style-type: none"> • 0.0009 mm/year (past 80 Ma) • 0.0007 mm/year (late Cretaceous) • 0.002 mm/year (Paleocene Midway Group) • 0.001 mm/year (Paleocene-Eocene Wilcox Form) • 0.0003 mm/year (post-Wilcox/pre-Holocene) • 1.8 mm/year (Holocene)

Table D-6.1.5 Data Summary
Reelfoot Rift–New Madrid Seismic Zone (NMSZ) Region

		<p>Average slip rate estimates—trench data:</p> <ul style="list-style-type: none"> • 4.4 mm/year (past 2,400 years based on 10 m [33 ft.] of topographic relief and a fault dip of 73°) • 6.2 mm/year (maximum; estimated 5.4 m [17.7 ft.] cumulative displacement for two events between AD 900 and 1812).
Van Arsdale et al. (1999)	Southeastern Extension of the Reelfoot Fault	This evaluation of microseismicity, seismic-reflection profile data, and geomorphic anomalies indicates that prehistoric and 1811-1812 coseismic uplift in the hanging wall of the Reelfoot fault has produced subtle surface warping that extends from Reelfoot Lake to Dyersburg, a total distance of 70 km (43.5 mi.).
Van Arsdale et al. (2002)	Investigation of Faulting Beneath the City of Memphis and Shelby County, Tennessee	Two N-NE-trending faults marked by 20 m (66 ft.) steps, referred to as the Memphis and Ellendale faults, are identified from structure-contour maps on Plio-Pleistocene to Eocene datums. Quaternary activity on both faults is indicated from analysis of the structure-contour maps and from topographic, drainage, and paleodrainage analyses. An anticlinal fold in floodplain sands is observed along the Ellendale fault. Radiocarbon dates indicate that folding occurred between AD 390 and 450 and liquefaction observed in the crest of the anticline occurred after AD 450. Modeling of the fold, which appears to be tectonic, is consistent with 5 m of right-lateral offset.
Velasco et al. (2005)	Quaternary Faulting Beneath Memphis, Tennessee	Structure-contour maps and cross sections of the top of the Pliocene-Pleistocene Upland Complex (Lafayette gravel), Eocene Upper Claiborne Group, and Eocene Lower Claiborne Group reveal two 20 m (66 ft.) down-to-the-NW faults that strike approximately N30°E. Western fault is called the Memphis fault, and eastern fault is the Ellendale fault. Anticlinal folding and liquefaction features are observed coincident with the Ellendale fault. Radiocarbon dates indicated that folding occurred between AD 390 and 450, and that liquefaction occurred after AD 450. Seismic-reflection lines indicate that the fold extends to more than 60 m (197 ft.) depth in the Lower Claiborne Group, has a length of more than 1 km (0.6 mi.), and is therefore judged to be tectonic. It is postulated that the anticline formed during ~5 m (16.5 ft.) of Quaternary right-lateral strike-slip movement on the N25°E-trending fault.

Table D-6.1.5 Data Summary
Reelfoot Rift–New Madrid Seismic Zone (NMSZ) Region

<p>William Lettis & Associates (2006)</p>	<p>Investigation of Holocene Faulting at Proposed C-746-Landfill Expansion</p>	<p>Unpublished report presents findings of a fault hazard investigation for C-746-U landfill's proposed expansion at the Department of Energy's Paducah Gaseous Diffusion Plant (PGDP), in Paducah, Kentucky, within the Fluorspar Area fault complex. The geologic assessment was based on (1) review of relevant geologic and geotechnical data from the site vicinity, (2) analysis of aerial photography, (3) field reconnaissance, (4) collection and stratigraphic analysis of 86 subsurface sediment cores, and (5) laboratory chronological (dating) analyses.</p> <p>Geologic cross sections prepared from the direct-push technology core data identified laterally continuous horizontal strata for assessing possibility of fault displacement, and for evaluating timing of such displacements. Deposits encountered in the cores range in age from about 16 ka to greater than 125 ka. Upper three units (15.4–50.7 ka) generally are flat-lying and they mantle preexisting topography. The lower, older units (53.6–75.5 and ≥ 125–180 ka) exhibit occasional subtle to abrupt undulations of basal contacts, which may reflect fluvial processes and/or tectonic-related deformation.</p> <p>If late Quaternary displacement has occurred beneath the site, the most-recent displacement occurred following deposition of the Unnamed Intermediate Silt between 53.6 and 75.5 ka. Although unlikely, the data do not preclude possibility of displacement of the Roxana Silt beneath the site, which is approximately 34.6–47.2 ka. There is no perceptible displacement of the base of the Upper Peoria Loess, which is approximately 16.6–23.5 ka. If late Pleistocene faulting occurred at the site, age of such deformation would be similar to youngest age of faulting previously interpreted along NE-striking faults in southern Illinois.</p> <p>As part of this study, reconnaissance-level review of exposures where SAIC (2004) reported evidence for Holocene faulting was reviewed with John Nelson. Based on (1) an apparent absence of faulting observed in upper, younger deposits (i.e., presence of only a fracture); (2) uncertain origin of observed fractures (e.g., possibly related to roots); and (3) absence of distinct stratigraphic offset of Holocene deposits, it was concluded that while relatively young geologic deformation is present, the interpretation of Holocene faulting is equivocal.</p>
---	--	--

Table D-6.1.5 Data Summary
Reelfoot Rift–New Madrid Seismic Zone (NMSZ) Region

Williams et al. (1995)	High-Resolution Seismic Imaging of Quaternary Faulting in the Crittenden County Fault Zone, New Madrid Seismic Zone, Northeastern Arkansas	Interpretation of three very high-resolution compressional-wave seismic-reflection profiles across surface projections of faults observed on coincident Mini-Sosie and Vibroseis seismic-reflection profiles. Deformation at and above the Quaternary-Eocene unconformity suggests that Crittenden County fault zone (CCFZ) has been active during the latest Quaternary and may be a possible source of earthquakes. Some evidence supports recurrent events in the Quaternary. There is a lack of clear connection between the faults observed in high-resolution data and the deeper faults imaged in other seismic data. Cites preliminary results of trenching that did not show evidence for faulting in a 2.5–3 m (8.2–9.8 ft.) deep trench excavated across the 7 m (23 ft.) deep fault as imaged in the seismic data. Possible explanation for this is that the shallow, rootless faults are bending-moment faults that relate to monoclinial bulge associated with the CCFZ. Evidence is cited for preference for tectonically driven deformation on the CCFZ. Some aspects of the fault observations fit a strike-slip faulting regime.
Williams et al. (2001)	Seismic-Reflection Imaging of Tertiary Faulting and Post-Eocene Deformation 20 km North of Memphis, Tennessee	Interprets a 4.5 km (2.8 mi.) long Mini-Sosie seismic-reflection profile across eastern bluff along Mississippi River in the Meeman-Shelby Forest State Park north of Memphis. Identifies the Meeman-Shelby fault (MSF), a high-angle (75°) reverse fault that displaces Paleozoic and Cretaceous rocks and upwarps Tertiary deposits. Paleozoic and Cretaceous rocks are vertically faulted about 70 and 40 m (230 and 131 ft.), respectively, in an up-to-west sense of displacement. Overlying Paleocene and Eocene deposits, which are probably the youngest deposits imaged, are upwarped about 50–60 m (164–197 ft.) with the same sense of displacement. Sense of displacement, amplitude, and appearance of the fault in seismic data are very similar to the Crittenden County fault zone (CCFZ), 15 km (9 mi.) west of this profile. Projecting a fault trend of N33°E (same general trend as the CCFZ), a similar fault is observed in a seismic profile 33 km (20.5 mi.) NE of MSF fault pick.

Table D-6.1.5 Data Summary
Reelfoot Rift–New Madrid Seismic Zone (NMSZ) Region

Woolery and Street (2002)	Quaternary Fault Reactivation in the Fluorspar Area Fault Complex of Western Kentucky—Evidence from Shallow SH-Wave Reflection Profiles	Interpreted shallow shear-wave seismic-reflection profiles collected over SW projection of the Fluorspar Area fault complex in the northern Jackson Purchase Region of western Kentucky image clear evidence of fault and apparent fold propagation into the near-surface Quaternary units (less than 10 m [32.8 ft.] below ground surface). Profiles show evidence of various structural styles associated with episodic movement. The exact timing of the latest tectonic episode exhibited on the profiles is not known because of the lack of more accurate stratigraphic detail coincident with the lines. Instrumentally recorded seismic events are located in the immediate vicinity of study area.
Woolery et al. (2009)	Site-Specific Fault Rupture Hazard Assessment—Fluorspar Area Fault Complex, Western Kentucky	Assesses location and recency of faulting at one location along southerly projection of the Fluorspar Area fault complex. Evidence for stratigraphic anomalies associated with five high-angle geophysical anomalies (in a 1 km, or 0.6 mi., long seismic-reflection profile). A total of 86 closely spaced 9.1 m (30 ft.) deep continuous cores were collected above seismic profile anomalies. Interpretation of the resultant geologic cross sections identified stratigraphic anomalies. Stratigraphic anomalies were generally constrained to postdate a 53.6–75.5 ka loess deposit: no perceptible displacement was found at the base of younger loess dated between 16.6 and 23.5 ka.
Magnitude Estimates		
Atkinson and Hanks (1995)	A High-Frequency Magnitude Scale	Based on a high-frequency magnitude scale the 1812 New Madrid event is estimated to be $M 7.7 \pm 0.3$.
Bakun and Hopper (2004b)	Magnitudes and Locations of the 1811-12 New Madrid, Missouri, and the 1886 Charleston, South Carolina, Earthquakes	<p>Estimates M for the three largest events in the 1811-1812 New Madrid sequence. (M_i is intensity magnitude based on inverting observations of intensity.)</p> <ul style="list-style-type: none"> • M_i 7.6 (M 6.8–7.9 at 95% confidence level) for December 16, 1811, event (NM1) that occurred in the NMSZ on the Bootheel lineament or on the Blytheville seismic zone. • M_i 7.5 (M 6.8–7.8 at 95% confidence level) for January 23, 1812, event (NM2) for a location on the New Madrid north zone of the NMSZ. • M_i 7.8 (M 7.0–8.1 at 95% confidence level) for February 7, 1812, event (NM3) that occurred on the Reelfoot blind thrust of the NMSZ.

Table D-6.1.5 Data Summary
Reelfoot Rift–New Madrid Seismic Zone (NMSZ) Region

Hough (2009)	The 1811-1812 New Madrid Sequence: Mainshocks, Aftershocks, and Beyond	<p>Discusses uncertainties associated with intensity assignments, and development of a set of consensus intensities for the four principal New Madrid events, based on independent assignments of four researchers (with experience analyzing historical earthquakes). The consensus values from these assessments are generally lower than those assigned by Hough et al. (2000).</p> <p>Using the Bakun and Wentworth (1997) method with two published attenuation models for the CEUS, intensity magnitude estimates range from M_I 6.5 to 7.0 for the December main shock, “dawn aftershock,” and January main shock, and from M_I 7.3 to 7.6 for the February main shock. Magnitude estimates based on assignments by individual experts for the December 16, 1811, and February 7, 1812, main shocks vary over a range of 0.3 to 0.4 units. Using revised magnitudes, distribution is characterized by a b-value of 1 between roughly M 6 and 7.5.</p> <p>The modern instrumental catalog also reveals that, in low strain-rate regions, moment release will be strongly controlled by the tendency of seismicity to cluster, and an a-value inferred from a short instrumental record will tend to significantly underestimate the long-term rate of small events in the region.</p>
Hough and Martin (2002)	Magnitude Estimates of Two Large Aftershocks of the 16 December 1811 New Madrid Earthquake	<p>Estimates locations and magnitudes for two large aftershocks:</p> <ul style="list-style-type: none"> • NM1-A: $M \sim 7$, thrust mechanism on a SE limb of the Reelfoot fault. • NM1-B: M 6.1 ± 0.2, location of event not well constrained, but probably beyond the southern end of the NMSZ, near Memphis, Tennessee (within the SW third to half of the band of seismicity identified by Chiu et al. [1997]).
Hough et al. (2000)	On the Modified Mercalli Intensities and Magnitudes of the 1811-1812 New Madrid, Central United States, Earthquakes	<p>Reinterprets intensity data, obtaining maximum magnitude estimates from 7.0 to 7.5 for the main three events in the 1811-1812 earthquake sequence:</p> <ul style="list-style-type: none"> • December 16, 1811: M 7.2–7.3 • January 23, 1812: M 7.0 • February 7, 1812: M 7.4–7.5 (thrust event)

Table D-6.1.5 Data Summary
Reelfoot Rift–New Madrid Seismic Zone (NMSZ) Region

Hough et al. (2005)	Wagon Loads of Sand Blows in White County, Illinois	Based on anecdotal accounts of possible liquefaction that occurred at several sites in southern Illinois during the 1811-1812 New Madrid sequence, the authors conclude that (1) either large NMSZ events triggered substantial liquefaction at distances greater than hitherto realized, or (2) at least one large “New Madrid” event occurred significantly north of the NMSZ. Neither can be ruled out, but the following lines of evidence suggest that January 23, 1812, main shock occurred in White County, Illinois, near the location of the 1968 m_b 5.5 southern Illinois earthquake and recent microearthquake activity. Descriptions report substantial liquefaction (sand blows) as well as a 3.2 km (2 mi.) long E-W-trending crack along which 0.6 m (2 ft.) of south-side-down displacement occurred. A modest offset in Paleozoic strata is observed in seismic-reflection survey data at this location. Additional field investigations are needed to further document extent and size of paleoliquefaction features and demonstrate the presence or absence of an E-W fault.
Johnston (1996b)	Seismic Moment Assessment of Earthquakes in Stable Continental Regions—III. New Madrid 1811-1812, Charleston 1886, and Lisbon 1755	Estimates magnitudes for the three largest events of the 1811-1812 earthquake sequence based on intensity data: <ul style="list-style-type: none"> • D1 (December 16, 1811): M 8.1 ± 0.3 • J1 (January 23, 1812): M 7.8 ± 0.3 • F1 (February 7, 1812): M 8.0 ± 0.3
Johnston and Schweig (1996)	The Enigma of the New Madrid Earthquakes of 1811-1812	This review paper focuses on the 1811-1812 earthquakes, their geophysical setting, fault rupture scenarios, and magnitude estimates based on intensity data. Using historical accounts and geologic evidence, the authors associate the three main 1811-1812 earthquakes with specific structures.
Mueller and Pujol (2001)	Three-Dimensional Geometry of the Reelfoot Blind Thrust: Implications for Moment Release and Earthquake Magnitude in the New Madrid Seismic Zone	The area of the blind thrust ($1,301 \text{ km}^2$ [502.3 mi.^2]), coupled with estimates of displacement in the February 7, 1812, earthquake, is used to estimate values of seismic moment from 6.8×10^{26} to 1.4×10^{27} dyne-centimeters, with preferred values between 6.8×10^{26} and 8.7×10^{26} dyne-centimeters. Computed M_w for this event ranges from M_w 7.2 to 7.4, with preferred values between M_w 7.2 and 7.3. The moment magnitude for the AD 1450 event is computed as M_w 7.3.

Table D-6.1.5 Data Summary
Reelfoot Rift–New Madrid Seismic Zone (NMSZ) Region

Mueller et al. (2004)	Analyzing the 1811-1812 New Madrid Earthquakes with Recent Instrumentally Recorded Aftershocks	Instrumentally recorded aftershock locations and models of elastic strain change are used to develop a kinematically consistent rupture scenario for three of the four largest earthquakes of the 1811-1812 earthquake sequence. Three events (NM1, NM1-A, and NM3) likely occurred on two contiguous faults (the strike-slip Cottonwood Grove fault and the Reelfoot thrust fault). The third main shock (NM2), which occurred on January 23, 1812, is inferred to be a more distant triggered event that may have occurred as much as 200 km (124.3 mi.) to the north in the Wabash Valley of southern Illinois-southern Indiana. Magnitudes assigned to each of these events are NM1 (M 7.3); NM1-A (M 7.0); NM2 (M 6.8); and NM3 (M 7.5).
Tuttle (2001)	The Use of Liquefaction Features in Paleoseismology: Lessons Learned in the New Madrid Seismic Zone, Central United States	Uses two approaches to estimate magnitude: <ul style="list-style-type: none"> • Magnitude-bound—estimates minimum magnitude for AD 900 and 1450 events of M 6.9 and M 6.7, respectively, based on Ambraseys's (1988) relationship between M and epicentral distance to surface manifestations of liquefaction. • Energy stress—estimates M 7.5 to 8.3 from in situ geotechnical properties similar to M \geq 7.6 from Ambraseys's relation for largest 1811-1812 earthquakes.
Tuttle et al. (2002)	The Earthquake Potential of the New Madrid Seismic Zone	Size, internal stratigraphy, and spatial distributions of prehistoric sand blows indicate that AD 900 and 1450 earthquakes had source zones and magnitudes similar to those of the three largest shocks in the 1811-1812 sequence.
Recurrence		
Cramer (2001)	A Seismic Hazard Uncertainty Analysis for the New Madrid Seismic Zone	A 498-year mean recurrence interval is obtained based on a Monte Carlo sampling of 1,000 recurrence intervals and using the Tuttle and Schweig (2000) uncertainties as a range of permissible dates (\pm two standard deviations). From these results, 68% confidence limits range from 267 to 725 years; 95% confidence limits range from 162 to 1,196 years (one and two standard deviation ranges, respectively).

Table D-6.1.5 Data Summary
Reelfoot Rift–New Madrid Seismic Zone (NMSZ) Region

Holbrook et al. (2006)	Stratigraphic Evidence for Millennial-Scale Temporal Clustering of Earthquakes on a Continental-Interior Fault: Holocene Mississippi River Floodplain Deposits, New Madrid Seismic Zone, USA	Presents reconstruction of Holocene Mississippi River channels from maps of floodplain strata to identify channel perturbations reflective of major displacement events on Reelfoot thrust fault. Provides evidence of temporal clustering of earthquakes in a compressive Midcontinent intraplate on short-term cycles (months), as well as evidence for longer-term reactivation cycles (10^4 – 10^6). The study makes a case for a ~1,000-year cluster of earthquakes with 10^2 yr spacing on the Reelfoot fault, beginning with a coseismic slip event near end of the middle Holocene at ~2200 to ~1600 BC. This Holocene cluster appears separated from the modern episode of seismicity (beginning ~AD 900) by at least 1,700 years of tectonic quiescence.
Kelson et al. (1996)	Multiple Late Holocene Earthquakes Along the Reelfoot Fault, Central New Madrid Seismic Zone	Based on seismic-reflection data, the authors interpret the scarp as a fault propagation fold over a west-dipping reverse fault. Trench exposures provide evidence for three episodes of deformation in the past 2,400 years: between AD 780 and 1000, between AD 1260 and 1650, and during AD 1812. Each episode had a slightly different style of deformation. The relations suggested that graben development increased through time concomitant with growth of monocline or that the earthquakes are of different magnitude.
Al-Shukri et al. (2005)	Spatial and Temporal Characteristic of Paleoseismic Features in the Southern Terminus of the New Madrid Seismic Zone in Eastern Arkansas	<p>Results of this study show that the 10 km (6.2 mi.) long lineament is associated with sand blows. A fracture that crosscuts the sand blows has a strike similar to that of the lineament and may be related to faulting. Its length and morphology as well as parallelism to the nearby White River fault zone suggest that the lineament is fault controlled. However, additional work, including geophysical and geological investigations, is needed to verify presence of a fault below the layer that liquefied.</p> <p>There appears to be at least a 5–10 kyr long history of strong ground shaking along the Daytona Beach lineament and possibly across the Marianna area. At Daytona Beach SE2 site, trench observations confirm interpretations of geophysical data of at least one major sand dike and a large sand blow at this site. Not imaged by ground-penetrating radar, the trenches revealed additional smaller sand dikes and an older sand blow. Both generations of liquefaction features are very weathered, like the sand blow at the original Daytona Beach site, suggesting they may be as old as 5.5 ka. Radiocarbon dating of buried silt loam soil provides maximum age constraint of 10.1 kyr for the younger of the two sand blows and minimum age constraint for the older sand blow. Optically</p>

Table D-6.1.5 Data Summary
Reelfoot Rift–New Madrid Seismic Zone (NMSZ) Region

		<p>stimulated luminescence dating is under way and should help to further constrain ages of the sand blows.</p> <p>Sand blows in the Marianna area predate those in the NMSZ and are much more weathered. No sand blows have yet been found in the area that are less than 5 ka and could have formed during the AD 900, 1450, and 1811-1812 New Madrid earthquakes. Therefore, the Marianna sand blows do not represent distant effects of earthquakes generated by the NMSZ. Instead, their large size and spatial relations to local faults suggest that the causative earthquakes were centered in Marianna. Furthermore, the compound nature of some of the Marianna sand blows are indicative of sequences of large earthquakes resulting from complex fault interaction similar to the behavior of the New Madrid fault zone.</p>
Al-Shukri et al. (2006)	Three-Dimensional Imaging of Earthquake-Induced Liquefaction Features with Ground Penetrating Radar near Marianna, Arkansas	High-resolution 3-D ground-penetrating radar (GPR) surveys, together with a profiling survey conducted at three sites to study earthquake-related sand blows in east-central Arkansas, were used to site trenches. Trench results confirmed presence of sand dikes at the locations interpreted from GPR results.
Tuttle (2001)	The Use of Liquefaction Features in Paleoseismology: Lessons Learned in the New Madrid Seismic Zone, Central United States	Major earthquakes occurred in New Madrid region in AD 900 \pm 100 years and AD 1450 \pm 150 years. There is evidence for earlier events, but age estimates and areas affected are poorly constrained. Judging by similarities in size and spatial distribution of paleoliquefaction features from these events and close spatial correlation to historical features, NMSZ was the probable source of two of these. This study is consistent with other paleoliquefaction studies in the region and with studies of fault-related deformation along Reelfoot scarp (e.g., Kelson et al., 1996).
Tuttle et al. (2002)	The Earthquake Potential of the New Madrid Seismic Zone	Recurrence intervals are based on studies of hundreds of earthquake-induced paleoliquefaction features at more than 250 sites. The fault system responsible for New Madrid seismicity generated very large earthquakes temporally clustered in AD 900 \pm 100 years and AD 1450 \pm 150 years, as well as 1811-1812. Given uncertainties in dating liquefaction features, the time between the past three events may be as short as 200 years or as long as 800 years, with an average of 500 years. Evidence suggests that prehistoric sand blows probably are either compound structures, resulting from multiple earthquakes closely clustered in time, or earthquake sequences.

Table D-6.1.5 Data Summary
Reelfoot Rift–New Madrid Seismic Zone (NMSZ) Region

Tuttle et al. (2006)	Very Large Earthquakes Centered Southwest of the New Madrid Seismic Zone 5,000–7,000 Years Ago	<p>Large earthquake-induced sand blows and related sand dikes are present at two sites in Marianna area about 180 km (112 mi.) SW of center of the NMSZ (80 km, or 50 mi., SW of the southern limit of NMSZ). Based on radiocarbon dating, liquefaction features at the Daytona Beach and St. Francis sites formed about 3500 and 4800 BC (5 and 7 ka), respectively. These events predate paleoearthquakes attributed to NMSZ faults.</p> <p>The Marianna sand blows are similar in size to NMSZ sand blows, suggesting that they formed as the result of very large earthquakes centered near Marianna and outside NMSZ.</p> <p>Liquefaction features similar in age to, but smaller than, the Daytona Beach sand blow occur near Blytheville (150 km, or 93.2 mi., NE of Marianna) and Montrose, Arkansas (175 km, or 108.7 mi., SE of Marianna). A very large ($M > 7.2$) earthquake centered near Marianna about 3500 BC may account for liquefaction in all three areas.</p> <p>The large sand blows at the St. Francis site are similar to compound sand blows in the NMSZ, suggesting that a NMSZ-type earthquake sequence was centered near Marianna about 4800 BC.</p> <p>Several faults in the Marianna area (including the Eastern Reelfoot rift margin [ERRM], the White River fault zone [WRFZ], and Big Creek fault zone [BCFZ]), are thought to be active, based on apparent influence on local topography and hydrography. ERRM appears to be the most likely source of very large earthquakes during middle Holocene.</p>
Vaughn (1991)	Evidence for Multiple Generations of Seismically Induced Liquefaction Features in the Western Lowlands, Southeast Missouri	<p>Identifies evidence for as many as three to four major ($M \geq 5.5$) earthquakes: the great 1811-1812 New Madrid event and two to three prehistoric events. Preliminary estimates of the ages based on archaeological data and radiocarbon dates on materials associated with buried or truncated liquefaction features suggest the following: (1) event F, 22.75 to 357 ka, and very likely more than 13.4 ka; (2) event L, with maximum timing of 13.43 ka and minimum timing of ca. 5.0 ka; and (3) event R, 12.57 to 0.59 ka, probably closer to 0.59 ka. Potentially, event R could correlate with one of the two major prehistoric earthquakes on the Reelfoot scarp.</p>

Table D-6.1.5 Data Summary
Reelfoot Rift–New Madrid Seismic Zone (NMSZ) Region

<i>Seismicity—Focal Mechanisms and Fault Geometry</i>		
Bakun and Hopper (2004a)	Catalog of Significant Historical Earthquakes in the Central United States	Modified Mercalli intensity assignments are used to estimate source locations and moment magnitude M for 18 nineteenth-century and 20 early twentieth-century earthquakes in the central U.S. for which estimates of M are otherwise not available. The 1811-1812 New Madrid earthquakes apparently dominated CUS seismicity in the first two decades of nineteenth century. M 5–6 earthquakes occurred in the NMSZ in 1843 and 1878, but none have occurred since 1878.
Chiu et al. (1990)	High-Resolution PANDA Experiment in the Central New Madrid Seismic Zone	Accurate earthquake locations from PANDA seismic array deployed in mid-October of 1989 define a narrow and clustered seismic zone. Seismicity is concentrated in upper crust beneath the sedimentary layer and above 15 km (9.3 mi.). Single-event fault plane solutions are well constrained by P-wave first motion and S-wave polarities, which suggest predominantly strike-slip motion with some thrust-component in the region.
Chiu et al. (1992)	Imaging the Active Faults of the Central New Madrid Seismic Zone Using PANDA Array Data	PANDA data clearly delineate planar concentrations of hypocenters that allow for interpretation as active faults. The results corroborate the vertical (strike-slip) faulting of SW (axial), N-NE, and western arms and define two dipping planes in the central segment. Seismicity in the left-step zone between the two NE-trending vertical segments is concentrated around a plane that dips at ~31°SW; a separate zone to the SE of the axial zone defines a plane that dips at ~48°SW. These planes project updip to surface along the eastern boundary of Lake County uplift and the western portion of Reelfoot Lake. Seismic activity in the central NMSZ occurs continuously between ~5 and 14 km (3.1 and 8.7 mi.) depth.
Csontos and VanArsdale (2008)	New Madrid Seismic Zone Fault Geometry	In this study, 1,704 earthquake hypocenters obtained between 1995 and 2006 were analyzed in 3-D space to more accurately map fault geometry in the NMSZ. Most of the earthquakes appear to align along fault planes. Identifies New Madrid North (29°, 72°SE), Risco (92°, 82°N), Axial (46°, 90°), Reelfoot North (167°, 30°SW), and Reelfoot South (150°, 44°SW) faults. A diffuse zone of earthquakes exists where the Axial fault divides the Reelfoot fault into Reelfoot North and Reelfoot South faults. Regional mapping of the top of the Precambrian crystalline basement indicates that the Reelfoot North fault has an average of 500 m (1,640 ft.) and the

Table D-6.1.5 Data Summary
Reelfoot Rift–New Madrid Seismic Zone (NMSZ) Region

		<p>Reelfoot South fault has 1,200 m (3,937 ft.) of down-to-the-SW normal displacement. Since previously published seismic-reflection profiles reveal reverse displacement on top of the Paleozoic and younger strata, the Reelfoot North and South faults are interpreted to be inverted basement normal faults. Reelfoot North and South faults differ in strike, dip, depth, and displacement, and only the Reelfoot North fault has a surface scarp (monocline). Thus the Reelfoot fault is actually composed of two left-stepping restraining bends and two faults that together extend across entire width of Reelfoot rift.</p>
Herrmann and Ammon (1997)	Faulting Parameters of Earthquakes in the New Madrid, Missouri, Region	<p>Combines traditional regional seismic network observations with direct seismogram modeling to improve estimates of small earthquake faulting geometry, depth, and size. Evaluates three earthquakes that occurred within the vicinity of the NMSZ. Comparing new and revised results with existing earthquake mechanisms in the region, this paper concludes that tension axes are generally aligned in a N-S to NW-SE direction, while compression axes are aligned in a NE to E direction. Interesting exceptions to this pattern are the March 3, 1963, earthquake, and two nearby earthquakes that lie within a well-defined 30 km (18 mi.) long left step in seismicity near New Madrid. Depth of well-located events in the Reelfoot rift is ≤ 16 km (10 mi.).</p>
Himes et al. (1988)	Indications of Active Faults in the New Madrid Seismic Zone from Precise Locations of Hypocenters	<p>Based on examination of hypocenters for more than 500 earthquakes in the NMSZ, the relocated earthquakes are separated into three trends: (1) ARK, the SW-trending zone from Caruthersville, Missouri, to Marked Tree, Arkansas; (2) DWM, the NE-trending zone from New Madrid to Charleston, Missouri; and (3) CEN, the central, left-stepping offset zone from Ridgely, Tennessee, to New Madrid, Missouri. Vertical profiles along and across the ARK and DWM trends verify the strike and dip of dominantly strike-slip motion on near-vertical active faults along these trends—in agreement with previously determined composite focal mechanism solutions for these trends. No coherent picture for CEN is obtained. Velocity models from the inversion are found to be reasonably uniform throughout the NMSZ and support the presence of a shallow low-velocity zone in the central part of Mississippi embayment.</p>

Table D-6.1.5 Data Summary
Reelfoot Rift–New Madrid Seismic Zone (NMSZ) Region

Shumway (2008)	Focal Mechanisms in the Northeast New Madrid Seismic Zone	Earthquakes in NE part of the NMSZ from June 1995 to June 2006 were relocated using a velocity model of the Mississippi embayment with appropriate depths to bedrock beneath seismic stations. Focal mechanisms were generated for events on NE-trending alignments. Results show that approximately half the focal mechanisms have a N-NE-striking nodal plane and a right-lateral strike-slip component consistent with earlier studies of the NMNF to the SW. This shows that this part of the NE NMSZ (1) is influenced by the same fault pattern and stress regime as the NMNF, (2) may be an extension of the NMSZ, and (3) therefore may represent alternate locations of January 23, 1812, rupture. Focal depths for 19 earthquakes range from about 3 to 15 km (1.9 to 9.3 mi.).
Stauder (1982)	Present-Day Seismicity and Identification of Active Faults in the New Madrid Seismic Zone	Results of four years of data from a regional seismic network established in 1974 showed the following: <ul style="list-style-type: none"> • a diffuse seismicity over the regional area; • NE-SW trends of faulting within the network varying in length from 25 to 120 km (15.5 to 75 mi.) from Cairo, Illinois, into NW Arkansas; • a major offset in these trends in region between New Madrid, Missouri, and Ridgely, Tennessee; • focal mechanism studies indicate right-lateral, predominantly strike-slip motion on the major NE-trending seismic trend; and • a low-velocity zone extends at least 150 km (93.2 mi.) into upper mantle beneath the region of highest seismicity.
<i>Geodetic and Modeling Studies-Hypotheses for Causes of Intraplate Seismicity</i>		
Calais and Stein (2009)	Time-Variable Deformation in the New Madrid Seismic Zone	This paper speculates that earthquake hazard estimates—assuming that recent seismicity reflects long-term steady-state behavior—may be inadequate for plate interiors and may overestimate hazard near recent earthquakes and underestimate it elsewhere. Recent geodetic results in the NMSZ have shown motions between 0 and 1.4 mm/yr, allowing opposite interpretations. The upper bound is consistent with steady-state behavior, in which strain accumulates at a rate consistent with repeat time for M ~ 7 earthquakes of about 600–1,500 years, as seen in the earthquake record. The lower bound cannot be reconciled with this record, which implies that the recent cluster of

Table D-6.1.5 Data Summary
Reelfoot Rift–New Madrid Seismic Zone (NMSZ) Region

		<p>large-magnitude events does not reflect long-term fault behavior and may be ending. New analysis suggests strain rates lower than 1.3×10^{-9}/yr, less than predicted by a model in which large earthquakes occur because the NMSZ continues to be loaded as a deeper weak zone relaxes (e.g., Kenner and Segall, 2000). At a steady state, a rate of 0.2 mm/yr implies a minimum repeat time of 10,000 years for low $M = 7$ earthquakes with ~2 m (~6.6 ft.) of coseismic slip and one longer than 100,000 years for $M = 8$ events. Strain in the NMSZ over the past several years has accumulated too slowly to account for seismicity over past ~5,000 years; hence steady-state fault behavior is excluded.</p> <p>Elsewhere throughout the plate interior, GPS data also show average deformation less than 0.7 mm/yr, and paleoseismic records show earthquake migration and temporal earthquake clustering. These imply that fault loading, strength, or both vary with time in the plate interior. Time variations in stress could be due to local loading and unloading from ice sheets or sediments or after earthquakes on other faults.</p>
Calais et al. (2006)	Deformation of the North American Plate Interior from a Decade of Continuous GPS Measurements	<p>Two independent geodetic solutions using data from close to 300 continuous GPS stations covering CEUS show that surface deformation in the plate interior is best fit by a model that includes rigid rotation of North America with respect to International Terrestrial Reference Frame (ITRF) 2000 and a component of strain qualitatively consistent with that expected from glacial isostatic adjustment. No detectable residual motion at the 95% confidence level is observed in the NMSZ.</p> <p>On the basis of a 0.7 mm/yr weighted RMS value for the residual velocities of NMSZ sites, random deviations from a rigid plate model in the NMSZ region do not exceed 1.4 mm/yr, the 95% confidence level. This is assumed to represent a conservative upper bound on the magnitude of any long-term slip in the study area. Assuming a simple model where characteristic earthquakes repeat regularly on a given active fault, the results imply a minimum repeat time of about 3,000–8,000 years for future $M 8$ earthquakes with 5–10 m (16–33 ft.) of coseismic slip, and a minimum repeat time of 600–1,500 years for future $M 7$ earthquakes with 1–2 m (3.3–6.6 ft.) of coseismic slip. This is consistent with recent and historical earthquake catalogs, which predict a recurrence interval that exceeds 1,000 years for $M 7$ earthquakes, and 10,000 years for $M 8$ earthquakes, and is consistent with paleoseismic data, which imply recurrence intervals of 400–1,000 years.</p>

Table D-6.1.5 Data Summary
Reelfoot Rift–New Madrid Seismic Zone (NMSZ) Region

Calais et al. (2009)	Time-Variable Deformation in the New Madrid Seismic Zone	<p>New analysis of GPS measurements across the NMSZ shows that deformation accumulates at a rate indistinguishable from zero and less than 0.2 mm/yr. At steady state, a (maximum) rate of 0.2 mm/yr implies a (minimum) repeat time of 10,000 years for low M 7 earthquakes, in contrast with the 500- to 900-year repeat time of paleoearthquakes. This, along with geological observations that large earthquakes and significant motions on Reelfoot fault started in the Holocene, suggests a transient burst of seismic activity rather than steady-state behavior.</p> <p>The authors postulate a model in which stress changes are caused by the Quaternary denudation/sedimentation history of the Mississippi Valley. Flexural stresses are sufficient to trigger earthquakes in a continental crust at failure equilibrium. Resulting viscoelastic relaxation leads to failure again on the main fault (lower strength threshold) and on neighboring faults. In the absence of significant far-field loading, this process can only maintain seismic activity for a few thousand years.</p>
Crone et al. (2003)	Paleoseismicity of Two Historically Quiescent Faults in Australia: Implications for Fault Behavior in Stable Continental Regions	<p>Temporal clustering, in which faults turn on to generate a series of large earthquakes and then turn off for a long time, may reflect the evolution of pore fluid pressure in the fault zone. In this model, low-permeability seals form around the fault zone as stress accumulates, raising pore pressure until an earthquake happens and each of the temporally clustered earthquakes relaxes some of the accumulated strain, and eventually the surrounding crust is sufficiently relaxed to make the fault quiescent.</p>
Forte et al. (2007)	Descent of the Ancient Farallon Slab Drives Localized Mantle Flow Below the New Madrid Seismic Zone	<p>Viscous flow models based on high-resolution seismic tomography show that descent of the ancient Farallon slab into deep mantle beneath central North America induces a highly localized flow directly below the NMSZ. This localization arises because of structural variability in the Farallon slab and low viscosity of the sublithospheric upper mantle, and it represents a heretofore unrecognized and possibly significant driving mechanism for the enigmatic intraplate seismicity in CEUS.</p>
Grana and Richardson (1996)	Tectonic Stress Within the New Madrid Seismic Zone	<p>Refraction data indicate a significant high-density rift pillow beneath the NMSZ. Linear and nonlinear viscoelastic finite-element modeling was conducted to determine whether support of the rift pillow may contribute significantly to the total present-day stress field. Results indicate that the nonlinear viscoelastic model with rheological stratification based on composition and temperature agrees well with observed deformation</p>

Table D-6.1.5 Data Summary
Reelfoot Rift–New Madrid Seismic Zone (NMSZ) Region

		<p>within the zone, and with estimates of regional stress magnitudes.</p> <p>The model predicts maximum compression of 30–40 megapascals above the rift pillow in the center of the rift axis. If the magnitude of local compression predicted by the nonlinear model produces inferred clockwise rotation on the order of 10°–30° in the direction of SHmax (maximum horizontal compression) near the rift axis, the magnitude of regional compression is a factor of one to two times that of local compression and is consistent with an origin due to ridge push forces. Addition of local stress associated with the rift pillow, however, results in an approximately 30% reduction in the resolved maximum horizontal shear stress. Thus, while the stress associated with the rift pillow can rotate the stress field to an orientation favorable for failure, reduction in the resolved shear stress requires a separate mechanism for strength reduction.</p> <p>Results of the modeling indicate that stresses from the load of the rift pillow may still be present in upper crust even after 100 Myr and may still play a role in present-day deformation and seismicity of the NMSZ. Local stress fields of significant tectonic magnitudes may also occur around other ancient rift pillows and help explain the observed correlation between intraplate seismicity and failed rift zones.</p>
Grollimund and Zoback (2001)	Did Deglaciation Trigger Intraplate Seismicity in the New Madrid Seismic Zone?	Modeling of the removal of the Laurentide ice sheet ca. 20 ka changed the stress field in the vicinity of New Madrid and caused seismic strain to increase by about three orders of magnitude. The high rate of seismic energy release observed during late Holocene is likely to remain essentially unchanged for the next few thousand years.
Kenner and Segall (2000)	A Mechanical Model for Intraplate Earthquakes: Application to the New Madrid Seismic Zone	Postulates a time-dependent model for the generation of repeated intraplate earthquakes in which seismic activity is driven by localized transfer of stress from a relaxing lower-crustal weak body. Given transient perturbation to the stress field, the seismicity is also transient, but can have a significantly longer duration. This model suggests that interseismic strain rates computed between damaging slip events would not be geodetically detectable.

Table D-6.1.5 Data Summary
Reelfoot Rift–New Madrid Seismic Zone (NMSZ) Region

Li et al. (2007)	Stress Evolution and Seismicity in the Central-Eastern United States: Insights from Geodynamic Modeling	<p>Explores evolution of stress and strain energy in intraplate seismic zones and contrasts it with interplate seismic zones using simple viscoelastic finite-element models. General observations are as follows:</p> <ul style="list-style-type: none"> • Large intraplate earthquakes can significantly increase Coulomb stress and strain energy in surrounding crust. • Inherited strain energy may dominate the local strain energy budget for thousands of years following main shocks, in contrast to interplate seismic zones, where strain energy is dominated by tectonic loading. • Strain energy buildup from the 1811-1812 large events in NMSZ may explain some of the moderate-sized earthquakes in this region since 1812. • Inherited strain energy is capable of producing some damaging earthquakes ($M > 6$) today in southern Illinois and eastern Arkansas, even in the absence of local loading. • Without local loading, however, the NMSZ would have remained in a stress shadow where stress has not been fully restored from the 1811-1812 events. • Results from compilation of a Pn (upper mantle) velocity map of the CEUS using available seismic data do support the NMSZ's being a zone of thermal weakening. • Predicted high Coulomb stress concentrates near margins of North American tectosphere, correlating spatially with most seismicity in the CEUS.
Li et al. (2009)	Spatiotemporal Complexity of Continental Intraplate Seismicity: Insights from Geodynamic Modeling and Implications for Seismic Hazard Estimation	<p>Explores the complex spatiotemporal patterns of intraplate seismicity using a 3-D viscoelastic-plastic finite-element model. The model simulates tectonic loading, crustal failure in earthquakes, and coseismic and postseismic stress evolution. For a laterally homogeneous lithosphere with randomly pre-specified perturbations of crustal strength, the model predicts various spatiotemporal patterns of seismicity at different time scales, spatial clustering in narrow belts and scattering across large regions over hundreds of years, connected seismic belts over thousands of years, and widely scattered seismicity over tens of thousands of years.</p> <p>The orientation of seismic belts coincides with the optimal failure directions associated with assumed tectonic loading. Stress triggering</p>

Table D-6.1.5 Data Summary
Reelfoot Rift–New Madrid Seismic Zone (NMSZ) Region

		<p>and migration cause spatiotemporal clustering of earthquakes. Fault weakening can lead to repeated earthquakes on intraplate faults. The predicted patterns vary with the weakening history. Clusters of large intraplate earthquakes can result from fault weakening and healing, and these clusters can be separated by long periods of quiescence.</p> <p>The complex spatiotemporal patterns of intraplate seismicity predicted in this simple model suggest that assessment of earthquake hazard based on the limited historical record may be biased toward overestimating the hazard in regions of recent large earthquakes and underestimating the hazard where seismicity has been low during historical time.</p>
Liu and Zoback (1997)	Lithospheric Strength and Intraplate in the New Madrid Seismic Zone	<p>Proposes a simple hypothesis to explain occurrence of localized zones of tectonic deformation and seismicity within intraplate regions subjected to relatively uniform far-field tectonic stresses. The contrast in integrated lithospheric strength between the NMSZ and the surrounding continental region appears to be the principal reason why the New Madrid area is the most active intraplate seismic area in eastern North America. The lower lithosphere's strength in the NMSZ appears to be controlled by a slightly thickened crust and slightly higher heat-flow values compared to surrounding regions. This conclusion is supported by a contrast in Pn (upper mantle) velocity structure, the silica geothermometry, and the rate of Cenozoic subsidence and recurrence of late Mesozoic and possible Cenozoic magmatic activity. Because of localized deformation in the lower crust of the NMSZ, repeated earthquakes occur with recurrence times that are relatively short for intraplate areas.</p>
McKenna et al. (2007)	Is the New Madrid Seismic Zone Hotter and Weaker Than Its Surroundings?	<p>Evaluates sparse heat-flow data in the New Madrid area and concludes that there is no compelling case for assuming that the NMSZ is significantly hotter and weaker than its surroundings, and that this result is consistent with the migrating seismicity model and the further possibility that the NMSZ is shutting down, which is suggested by the small or zero motion observed geodetically. In this model, the present seismicity is aftershocks of the large earthquakes of 1811-1812, and such large earthquakes will not recur there for a very long time.</p>

Table D-6.1.5 Data Summary
Reelfoot Rift–New Madrid Seismic Zone (NMSZ) Region

Newman et al. (1999)	Slow Deformation and Lower Seismic Hazard at the New Madrid Seismic Zone	<p>Recent geodetic measurements indicate that the rate of strain accumulation is less than the current detection threshold. Global positioning system (GPS) data show no significant differences in velocities on either side of southern arm of NMSZ. Near-field and intermediate-field (primarily hard-rock) sites yield measurements of 0.6 ± 3.2 and -0.9 ± 2.2 mm/year, respectively. They are consistent with both 0 and 2 mm/year at 2-sigma.</p> <p>GPS data for upper Mississippi embayment show that interior of the Reelfoot rift is moving NE relative to the North American Plate. Modeling stable North America as a single rigid plate fits the site velocities, with a mean residual of 1.0 mm/year.</p> <p>The authors conclude that the present GPS data imply that 1811-1812-sized earthquakes are either much smaller or far less frequent than previously assumed (i.e., smaller than M 8 [5–10 m, or 16.4–32.8 ft., slip/event], or longer than a recurrence interval of 400–600 years).</p>
Smalley et al. (2005)	Space Geodetic Evidence for Rapid Strain Rates in the New Madrid Seismic Zone of Central USA	<p>Recent analysis of geodetic measurements from a permanent GPS array in mid-America installed in the mid- to late 1990s provides evidence for rapid strain rates in the NMSZ. Rates of strain are on the order of 10^{-7} per year, comparable in magnitude to those across active plate boundaries. The rates are consistent with known active faults in the region. Relative convergence across the Reelfoot fault is $\sim 2.7 \pm 1.6$ mm/year. Relative fault-parallel, right-lateral motion of ~ 1 mm/year is measured across southern right-lateral strike-slip fault zone, which is highlighted by a prominent NE-trending and vertical zone of microseismicity and right-lateral focal mechanisms. Surface velocities at distances beyond a few fault dimensions (far-field) from active faults do not differ significantly from zero. It is not certain whether the driving force behind current surface velocities is related to post-1811-1812 postseismic processes or to accumulation of a locally sourced strain. Data indicate, however, that aseismic slip is almost certainly required across faults (or shear zones) within upper few kilometers of the surface.</p>

Table D-6.1.5 Data Summary
Reelfoot Rift–New Madrid Seismic Zone (NMSZ) Region

Stuart et al. (1997)	Stressing of the New Madrid Seismic Zone by a Lower Crust Detachment Fault	The authors suggest that the cause of stress concentration onto the NMSZ is slip on a weak subhorizontal detachment fault or equivalent shear zone in the lower crust where high temperatures reduce rock strength. The proposed detachment fault is placed at or just above the top surface of a layer of lower crust with anomalous high-density and seismic velocity called the “rift pillow” or “rift cushion.” Regional horizontal compression induces slip on the fault, and the slip creates a stress concentration in upper crust above rift pillow dome. The model implies that rift pillow geometry is a significant influence on the maximum possible earthquake magnitude.
Zhang et al. (2009a)	Lithospheric Velocity of the New Madrid Seismic Zone: A Joint Teleseismic and Local P Tomographic Study	Inversion of teleseismic P and local P first-arrival times from a nine-year data set are used to infer the lithospheric velocity structure beneath the NMSZ. Results show that the seismically active zone is associated with a local NE-SW-trending low-velocity anomaly in the lower crust and upper mantle, instead of high-velocity intrusive bodies proposed in previous studies. The low-velocity anomaly is on the edge of a high-velocity lithospheric block, consistent with notion of stress concentration near rheological boundaries. This lithospheric weak zone may shift stress to upper crust when loaded, thus leading to repeated shallow earthquakes.
Seismic Source Characterization Models		
Cramer (2001)	A Seismic Hazard Uncertainty Analysis for the New Madrid Seismic Zone	Develops a logic tree of possible alternative parameters to characterize earthquake sources in the NMSZ. Source model alternatives include fictional faults from Frankel et al. (1996) and actual faults (Bootheel lineament, eastern rift boundary, NE arm, SW arm, Reelfoot fault, west arm, and western rift boundary).
Frankel et al. (2002)	Documentation for the 2002 Update of the National Seismic Hazard Maps	Identifies three alternative fault sources: a fault trace matching recent microearthquake activity, and two adjacent sources situated near borders of the Reelfoot rift. The center fault is given twice the weight of the other two. Mean recurrence interval = 500 years: M 7.3: (0.15 wt) M 7.5: (0.20 wt) M 7.7: (0.50 wt) M 7.9: (0.15 wt)

Table D-6.1.5 Data Summary
Reelfoot Rift–New Madrid Seismic Zone (NMSZ) Region

Petersen et al. (2008)	Documentation for the 2008 Update of the United States National Seismic Hazard Maps	<p>Revisions to the characterization of the NMSZ include the following:</p> <ul style="list-style-type: none"> • Reduced magnitudes in northern NMSZ by 0.2 unit and added logic-tree branch for recurrence rate of 1/750 years. • Added logic-tree branch for 1/1,000-year recurrence rate of earthquakes in New Madrid (recommended by advisory panel). • Implemented temporal cluster model for New Madrid earthquakes. • Modified fault geometry for New Madrid to include five hypothetical strands and increased weight on central strand to 0.7. • Revised dip of Reelfoot fault to 38°.
Toro and Silva (2001)	Scenario Earthquakes for Saint Louis, MO, and Memphis, TN, and Seismic Hazard Maps for the Central United States Region Including the Effect of Site Conditions	<p>Develops alternative geometries for NMSZ. Uses fault sources identified by Johnston and Schweig (1996), augmented by alternative fault source model to the north (East Prairie extension), to represent more diffuse patterns of seismicity. Assumes that a large seismic-moment release in the region involves events on all three NMSZ faults occurring within a short interval. Occurrences of large earthquakes in the NMSZ are not independent in time. Uses mean recurrence intervals of 500 to 1,000 years.</p>

Table D-6.1.9 Data Summary
Wabash Valley RLME

Citation	Title	Description and Relevance to SSC
General for Region		
Basement Structure		
Drahovzal et al. (1992)	The East Continent Rift Basin: A New Discovery	<p>Integration of lithologic, stratigraphic, geochemical, gravity, magnetic, structural, and seismic data resulted in recognition of an eastern arm of the Midcontinent rift system named the East Continent rift basin (ECRB). An elongate N-S-trending Precambrian rift basin is present from SE Michigan through Ohio and Indiana, into central Kentucky. The ECRB is filled with red continental lithic arenites, minor red siltstones and shales, and volcanics. Gravity, magnetic, and seismic data indicate that the basin is composed of several subbasins.</p> <p>The basin is bounded by the Grenville Front to the east and by normal block faults to the west. The basin narrows to the north; the southern boundary is not well constrained. The basin is interpreted to be Keweenawan in age and associated with the middle Proterozoic Midcontinent rift system. The ECRB predates the Grenville orogeny, which resulted in folding and faulting of the rift-fill sequence. Post-Grenville erosion, Paleozoic inversion, and wrench faulting resulted in the present configuration of the basin.</p>
Drahovzal (1994)	Basin-Floor Fan Complexes: A New Exploration Strategy for the Rough Creek Graben	Extent of possible extended basement crust below the southern Illinois basin is inferred from seismic-reflection data.
Harrison and Schultz (2002)	Tectonic Framework of the Southwestern Margin of the Illinois Basin and Its Influence on Neotectonism and Seismicity	The authors propose that along the SW margin of the Illinois basin, the Commerce geophysical lineament (CGL) to the south and the St. Charles lineament (SCL) to the north divide the region into three distinct tectonic domains. The authors suggest that these lineaments represent ancient shear zones, or accommodation zones, that juxtapose different-aged Proterozoic crustal blocks, and that these accommodation zones have partitioned strain throughout the Phanerozoic, which is reflected in the northward decrease of seismic activity in the region. The authors report that structural features within each of the three tectonic domains vary in deformational styles and orientations, reflecting decoupling of deformation across the two lineaments. (See also Midcontinent Data Summary Table for description of CGL and SCL.)

Table D-6.1.9 Data Summary
Wabash Valley RLME

Citation	Title	Description and Relevance to SSC
Harrison and Schultz (2008)	A Tectonic Model for the Midcontinent U.S. Lithosphere Based on Structural Analyses of Mesoproterozoic Through Cenozoic Deformation	<p>The general conclusion from this abstract is that in the midcontinent U.S., some seismicity can be attributed to reactivation of vertical strike-slip fault zones that are not associated with any rift. Furthermore, some seismically active, old rift structures in the Midcontinent may be inherently related to an even older strike-slip fault system.</p> <p>Mesoproterozoic basement rocks of the St. Francois terrane possess an orthogonal pattern of vertical NW- and NE-trending strike-slip fault zones. The NW trend dominates Mesoproterozoic deformation and is inherent from an older fabric that controlled the location of Mesoproterozoic igneous activity.</p> <p>The assembly and breakup of Rodinia is recorded by accumulative left slip of 60–75 km (37.3–46.6 mi.) and 30–75 km (19–47 mi.) on NW-trending structures, pre-Late Cambrian vertical, right-lateral, strike-slip faulting on NW-trending in the St. Francois terrane, emplacement of dominantly NE-trending, 1.33 Ga mafic dikes, and uplift and erosion of ~2–4 km (~1.2–2.5 mi.) of rocks. Reactivation of NE-trending structures in the Late Cambrian resulted in formation of the Reelfoot rift and was accompanied by reactivation of vertical NW-trending structures with left-lateral displacement. Faulting in the Paleozoic, Mesozoic, and Cenozoic cover sequences documents reactivation of both vertical trends as far-field strike-slip faults during the Acadian, Taconic, Ouachita, Alleghany, and Laramide orogenies. Stepovers within the strike-slip fault system produced local uplift along restraining bends and subsidence in pull-apart grabens and basins. A tectonic model of the Midcontinent lithosphere is best portrayed as consisting of an orthogonal mosaic of vertical zones of shear that presumably penetrate the crust and upper mantle and are long-lived and prone to reactivation under lithospheric stresses.</p>

Table D-6.1.9 Data Summary
Wabash Valley RLME

Citation	Title	Description and Relevance to SSC
Hildenbrand and Ravat (1997)	Geophysical Setting of the Wabash Valley Fault System	<p>Analyses of gravity and magnetic data have been used to evaluate the geologic framework of the northern Mississippi embayment and Illinois basin regions. Inversion of high-resolution aeromagnetic data shows that interpreted ultramafic dikes closely follow mapped faults; their abundance suggests that the Wabash Valley fault system (WVFS) contains more faults than those mapped. Both dike pattern and mapped WVFS terminate near the Reelfoot–Rough Creek–Rome rift system. The Grayville graben (~20 km [~12.5 mi.] wide, ~700 m [~2,297 ft.] maximum basement relief, and <40 km [~25 mi.] long) underlying the Wabash Valley developed during rifting, perhaps in response to stress concentrations generated by a bend in the rift system.</p> <p>The Wabash Valley faults are interpreted to be minor tectonic structures (relative to the Reelfoot rift and Rough Creek graben) and probably do not represent a failed rift arm. There is a lack of any obvious relation between the WVFS and the epicenters of historical and prehistoric earthquakes. Five prehistoric earthquakes lie near structures associated with the Commerce geophysical lineament.</p>
Hildenbrand et al. (2002)	The Commerce Geophysical Lineament and Its Possible Relation to Mesoproterozoic Igneous Complexes and Large Earthquakes in the Central Illinois Basin	<p>Inversions of magnetic and gravity data provide insights on upper-crustal structures in the central Illinois basin. The results of 2-D and 3-D inversion techniques suggest that the source of the Commerce geophysical lineament (CGL) follows the SE boundary of a dense, magnetic, NE-trending igneous center named the Vincennes igneous center. The CGL, defining the 5–10 km (3–6 mi.) wide Commerce deformation zone (CDZ), appears to have influenced the structural development of the Vincennes igneous center. Overlying the igneous center is the Centralia seismic-reflection sequence, expressed as highly coherent reflectors.</p> <p>It is hypothesized that (1) the Vincennes igneous center is the source of inferred volcanic units of the Centralia sequence and is related to a rifted margin or a Proterozoic plate boundary; (2) the CDZ evolved in the Mesoproterozoic (1.1–1.5 Ga) as a major cratonic rheological boundary (possible rifted margin, suture, or accreted belt) and was the focus of episodic reactivation related to varying stress regimes throughout its history; and (3) spatial relations of the CDZ with large Pleistocene and Holocene earthquakes suggest that this major rheological boundary is intimately related to both surface and deep structures and to the seismic hazard of the Illinois basin region. Assuming recent right-lateral slip along the CDZ, a jog or left step in the Vincennes area leads to thrusting or a restraining bend, where associated stress accumulations may have resulted in nearby large prehistoric earthquakes.</p>

Table D-6.1.9 Data Summary
Wabash Valley RLME

Citation	Title	Description and Relevance to SSC
Kolata and Hildenbrand (1997)	Structural Underpinnings and Neotectonics of the Southern Illinois Basin: An Overview	<p>The southern end of the Illinois basin is one of the most structurally complex regions in the midcontinent U.S. Two major structural elements exist: (1) a broad SW-plunging cratonic depression across central Illinois and SW Indiana is characterized by moderate to high earthquake potential and enigmatic earthquake sources; and (2) the southernmost part is underlain by the Reelfoot rift and Rough Creek graben, a rift system that formed during late Precambrian to middle Cambrian time. Geological and geophysical information suggests that the cause of earthquakes in the New Madrid seismic zone is unrelated to that of the region north of the rift system.</p>
Kolata and Nelson (1991)	Tectonic History of the Illinois Basin	<p>The Illinois basin is a polyhistory basin that formed primarily during the Paleozoic era. The basin began as a failed rift concurrent with the breakup of a supercontinent during latest Precambrian or early Cambrian time. Following the rift basin phase, which lasted from early to middle Cambrian, the tectonic setting changed to a broad cratonic basin centered over the rift. Plate tectonic interactions along the eastern and southern margins of North America have repeatedly reactivated the rift and have influenced basin subsidence, sedimentation, formation of geologic structures, migration of subsurface fluids, and contemporary earthquake activity.</p>
McBride and Kolata (1999)	Upper Crust Beneath the Central Illinois Basin, United States	<p>Interpretation of industry seismic-reflection data provides information for understanding the structure and origin of the upper crust (0–12 km [0–7.5 mi.] depth) beneath the central Illinois basin. Highly coherent basement reflectivity is expressed as a synformal wedge of dipping and subhorizontal reflections situated beneath the center of the Illinois basin that thickens and deepens to the northeast (e.g., 0–5.3 km—or 0–3.3 mi.—thickness along a 123 km—76.5 mi.—N-S line). The boundaries of an anomalous subsequence of disrupted reflections located along the southern margin of this wedge are marked by distinct steeply dipping reflections (possible thrust faults) that continue or project up to antiformal disruptions of lower Paleozoic marker reflectors, suggesting Paleozoic or possibly later tectonic reactivation of Precambrian structures. There are multiple hypotheses for the origin of the Precambrian reflectivity, including basaltic flows or sills interlayered with clastic sediments and/or emplaced within felsic igneous rocks.</p>

Table D-6.1.9 Data Summary
Wabash Valley RLME

Citation	Title	Description and Relevance to SSC
McBride et al. (2001)	Refining the Target for EarthScope in the Central Midcontinent	<p>Overview summary stating that new images (industry data) of deep structure, extending at least as deep as about 65 km (40.5 mi.), represent the largest concentration of deep seismic-reflection profiles between the Appalachians and the Rockies. Interpretation of these data shows the presence of three highly coherent Precambrian “stratigraphic” sequences beneath the Paleozoic Illinois basin that continue down to 15–20 km (9–12.5 mi.) depth. Review of 3-D mapping of these sequences reveals broad “basinal” packages that may be related to a Proterozoic rift and/or volcanic episode.</p> <p>Normal-fault reflector offsets that progressively disrupt the sequences with depth are possibly related to a Proterozoic rift and/or volcanic episode related to the original thermal event that produced the Granite-Rhyolite province. These sequences may be analogous to younger Keweenawan-type rift-related volcanism and sedimentation that affected the central Midcontinent during the Proterozoic. The circular-to-oval shape of the sequences in plan view seems to argue against a linear rift origin and is more suggestive of a large rhyolitic collapsed caldera complex that could have developed in association with the Granite-Rhyolite province.</p> <p>The deeper parts of the seismic sequences correspond to subdued geopotential field values and spatial wavelengths, meaning that the seismic sequences are lacking in widespread high-density, high-magnetization rocks relative to the surrounding region. The outer margins, especially to the west and south, are marked by prominent coincident closed-contour magnetic and gravity anomalies, which do indicate mafic igneous source intrusions (expressed as highly diffractive zones on the deep-reflection profiles. The continuation of the subdued magnetic intensity character (as expressed in the first vertical derivative) to the north and east may point to the extension of the upper-crustal layering in those directions, beyond where regional seismic data are available. The geopotential field data preclude a large mafic igneous component to the crust, except for isolated igneous centers, suggesting that the rifting or volcanic episode must not have tapped deeply or significantly into the lower crust or upper mantle.</p> <p>The presence of newly observed mantle reflectivity beneath the Illinois basin indicates significant upper-mantle heterogeneity relative to other parts of the U.S. studied using reflection methods. The mantle reflectors do not obviously correlate to any particular geologic feature.</p> <p>The reprocessed profiles suggest that the seismogenic source beneath the seismically active southern Illinois basin may be closely associated with (1)</p>

**Table D-6.1.9 Data Summary
Wabash Valley RLME**

Citation	Title	Description and Relevance to SSC
		midcrustal dipping reflectors associated with thrust-mechanism earthquakes and (2) seismically imaged steep faults in basement associated with strike-slip-mechanism earthquakes.
McBride et al. (2007)	Deep Faulting and Structural Reactivation Beneath the Southern Illinois Basin	<p>Integrates seismicity, borehole, geophysical, and seismic profile data to create a 2.5-dimensional picture down to local seismogenic depth (0–15 km, or 0–9.3 mi.) along western flanks of two of the major structures within the Illinois basin: Wabash Valley fault system (WVFS), and La Salle anticlinal belt (LSA). The results of reprocessing seismic-reflection profiles, combined with earthquake hypocenter parameters, suggest three distinct seismotectonic environments in the upper crust.</p> <ol style="list-style-type: none"> 1. A fault pattern that appears to correspond to the steep nodal plane of a strike-slip mechanism is delineated for the April 3, 1974, $m_b = 4.7$ earthquake. The focal mechanism is consistent with a dominant stress system of NE-striking dextral strike-slip. The fault pattern is interpreted to be a deeply buried rift zone or zone of intense normal faulting underpinning a major Paleozoic depocenter of the Illinois basin (Fairfield basin). 2. A similar earthquake (June 10, 1987, $m_b = 5.2$) and its well-located aftershocks define a narrow zone of deformation that occurs along and parallel to the frontal thrust of the LSA. The strike and dip of the NW-trending nodal plane were reported by Langer and Bollinger (1991) to be 312° and 80°SW, respectively. This frontal thrust is associated with an asymmetric Laramide-style fold in the Paleozoic section. The NW trend of local epicenters and the steep rupture plane are both consistent with the basement fault, defined from seismic-reflection profiles that core the monocline flexure within the basin sediments. 3. The hypocenter of largest earthquake (November 9, 1968; $m_b = 5.5$) may be spatially associated with a prominent zone of dipping middle-crustal reflections, just west of WVFS, which have been interpreted as a deeply buried blind thrust (McBride, Hildenbrand, et al., 2002). This may indicate that shallow Paleozoic structures are effectively decoupled from deeper seismogenic structure in this case. The earthquake was originally interpreted to have occurred on a $N15^\circ\text{E}$-trending reverse fault dipping about 45°W; interpretation of seismic data indicates it may have occurred on a more NE-trending blind reverse fault in the basement (fault F). <p>The geopotential field data display trends that mimic structural trends interpreted from reflection profiles and earthquake information. The proposed correlation of preexisting structures with earthquakes having consistently oriented structural</p>

Table D-6.1.9 Data Summary
Wabash Valley RLME

Citation	Title	Description and Relevance to SSC
		parameters supports the reactivation of old deformation zones by contemporary stresses. The degree to which deformation has propagated upward from Precambrian basement into Paleozoic rocks varied significantly even over a small study area.
Pratt et al. (1992)	Widespread Buried Precambrian Layered Sequences in the U.S. Mid-Continent: Evidence for Large Proterozoic Depositional Basins	Seismic-reflection data in the Illinois region show a Precambrian layered assemblage extending 320 km (199 mi.) in an E-W direction and 200 km (124.3 mi.) in an N-S direction. The assemblage is approximately 12 km (7.5 mi.) thick. Apparent sequence boundaries (onlap, downlap) within the assemblage suggest they are part of a large depositional basin with diffractions and dipping strata due to faulting. The layered sequence correlates with regions of relatively long-wavelength and low-amplitude magnetic anomalies; the extent of this magnetic signature suggests that about 200,000 km ² (77,220 sq. mi.) of Illinois, Indiana, and western Ohio may be underlain by similar Precambrian strata.
Sparlin and Lewis (1994)	Interpretation of the Magnetic Anomaly over the Omaha Oil Field, Gallatin County, Illinois	A magnetic anomaly identified in an aeromagnetic survey over southern Illinois is expressed in contours as a localized magnetic high on the west flank of a regional magnetic low. An industry well drilled near the apex of the Omaha structural dome, which is coincident with the anomaly, encountered two zones of ultramafic intrusive rock identified as mantle-derived ultramafic rock that can be associated with incipient stages of crustal rifting. The anomaly is modeled using two ultramafic sills with an igneous feeder plug.
PALEOZOIC STRUCTURES (Evidence for Reactivation)		
La Salle Anticlinorium		
Marshak and Paulsen (1997)	Structural Style, Regional Distribution, and Seismic Implications of Midcontinent Fault-and-Fold Zones, United States	This paper interprets the La Salle deformation belt as consisting of three segments composed of north-trending fault arrays. Each segment terminates at a NW-trending discontinuity. The authors note that this geometry resembles the pattern of rift segments linked at accommodation zones, typical of low-strain rifts.
McBride and Nelson (1999)	Style and Origin of Mid-Carboniferous Deformation in the Illinois Basin, USA—Ancestral Rockies Deformation?	Interprets the La Salle anticlinorium as the product of Late Paleozoic displacements on high-angle reverse faults in crystalline basement that propagated upward to monoclines and asymmetrical anticlines in Paleozoic sedimentary cover. This paper presents reflection profiles in the Fairfield basin that do not support the hypothesis presented by Marshak and Paulsen (1997).

Table D-6.1.9 Data Summary
Wabash Valley RLME

Citation	Title	Description and Relevance to SSC
Nelson (1995)	Structural Features in Illinois	<p>Introduces the name La Salle anticlinorium for the feature that previously had been referred to as the La Salle anticlinal belt. The feature trends N-NW and extends for more than 320 km (200 mi.) from Lee County in the northwest to Lawrence County in the southeast. It comprises numerous subparallel anticlines, domes, monoclines, and synclines, several dozen of which are individually named. The pattern of the individual structures comprising the feature has previously been described as an echelon. The author, however, states that this term is misleading, that in a true echelon fold belt the structures are aligned at an angle to the overall trend of the system, reflecting strike-slip deformation. The author reports that in the La Salle anticlinorium, individual folds are oriented predominantly parallel to the trend of the larger system. He also describes the individual folds as being offset from one another and partially overlap; toward the north, individual folds generally step to the west. The La Salle anticlinorium is described as locally exhibiting a branching pattern.</p> <p>The author reports that the primary uplift of the La Salle anticlinorium occurred in the Late Paleozoic. An angular unconformity at the base of Pennsylvanian-age strata is observed along the entire length of the structure. Seismic-reflection profiles across the Charleston monocline indicate that the entire Paleozoic sedimentary column (pre-Pennsylvanian) is folded and that the amount of structural relief does not change significantly with depth.</p> <p>High-angle reverse faults are documented at depth in several places along the southern part of the La Salle anticlinorium. The author's proprietary seismic-reflection profiles reveal faults on the west flank of the Lawrenceville dome, the east flank of the Bridgeport anticline, and the SW flank of the Hardinville anticline. These faults displace the top of Precambrian basement and overlying Cambrian strata, dying out at or below the Ordovician Knox Group. About 152 m (500 ft.) of displacement occurs on the basement surface of the Bridgeport anticline, and the largest fault on the Hardinville anticline has about 91–122 m (300–400 ft.) of throw.</p> <p>Based on borehole data in Cambrian sandstone at the northern part of the anticlinorium, several E-W-trending faults defining a graben are shown on the west side of the dome east of the Peru monocline. Borehole data in Coles County also indicate faulting in Mississippian strata near the west flank of Ashmore dome (a small dome near the southern end of the Murdock syncline). No orientations of these faults are reported.</p> <p>The author interprets the La Salle anticlinorium as the product of Late Paleozoic</p>

Table D-6.1.9 Data Summary
Wabash Valley RLME

Citation	Title	Description and Relevance to SSC
		displacements on high-angle reverse faults in crystalline basement that propagated upward to monoclines and asymmetrical anticlines in Paleozoic sedimentary cover. The faults could be classified as drape folds or fault-propagation folds. The complex arrangement of folds in the La Salle anticlinorium suggests a mosaic of faults in the basement of eastern Illinois.
Peru Monocline		
Heigold (1972)	Notes on the Earthquake of September 15, 1972, in Northern Illinois	Based on the proximity of this earthquake to the Peru monocline, this paper suggests that the earthquake was the result of faulting related to a zone of weakness near the region where the monocline merges with the Ashton anticline.
Herrmann (1979)	Surface Wave Focal Mechanisms for Eastern North American Earthquakes with Tectonic Implications	The 1972 earthquake occurred about 16 km (10 mi.) SE of the 1999 earthquake. A focal mechanism solution from the 1972 earthquake indicates movement on a high-angle strike-slip fault, either right-lateral to the N-NW or left-lateral to the E-NE.
Larson (2001) Larson (2002)	The Earthquake of September 2, 1999, in Northern Illinois: Big Lessons from a Small Earthquake The Earthquake of 2 September 1999 in Northern Illinois: Intensities and Possible Neotectonism	Descriptions of two recent earthquakes that have been associated with the Peru monocline: a September 1972 magnitude m_b 4.6 earthquake and a September 1999 magnitude m_b 3.5 earthquake. Within the precision of the seismographic data, the 1999 and 1972 earthquakes were located 5 and 13 km (3 and 8 mi.), respectively, below the Peru monocline. A third earthquake, which occurred May 27, 1881, also might be related to the Peru monocline, based on damage reports from La Salle, which sits directly on the structure, but an exact location for this earthquake is not known. The 2002 paper concludes that the spatial association of recent seismicity may suggest that Peru monocline is a reactivated Paleozoic structure.
Nelson (1995)	Structural Features in Illinois	Describes the Peru monocline, which lies within the northern La Salle deformation belt, as a 105 km (65 mi.) long NW-SE-trending fold belt in which the rocks dip steeply to the southwest into the Illinois basin. The structure is most prominent in La Salle County, where the relief on the SW limb is as much as 396 m (1,300 ft.). In some area coal mines, the coal beds dip 45° on the steep flank of the monocline. The Peru monocline is less pronounced to the northwest, where the relief decreases and the dip becomes very gentle as the structure merges with the Ashton anticline.

Table D-6.1.9 Data Summary
Wabash Valley RLME

Citation	Title	Description and Relevance to SSC
Du Quoin Monocline		
Marshak and Paulsen (1997)	Structural Style, Regional Distribution, and Seismic Implications of Midcontinent Fault-and-Fold Zones, United States	This paper includes the Du Quoin monocline within the broad southern La Salle deformation belt.
Nelson (1995)	Structural Features in Illinois	<p>The Du Quoin monocline of southern Illinois trends N-S and warps Paleozoic strata down to the east. Normal faults of the Dowell and Centralia fault zones are coincident with the dipping flank of the fold, and displace strata down to the west.</p> <p>The paper reports that several high-resolution seismic lines across the Centralia fault zone indicate a normal fault dipping 70°–75° toward the west, affecting all reflectors down to Ordovician strata. Infers that the fault has undergone two episodes of movement. The greatest displacements on the structures took place during early to middle Pennsylvanian, with intermittent and lesser movements continuing into late Pennsylvanian and possibly Permian time. Post-Pennsylvanian extension and normal faulting occurred along the Centralia fault.</p>
Su and McBride (1999)	Final Technical Report—Study of a Potential Seismic Source Zone in South-Central Illinois	This paper reports that low-resolution seismic-reflection data reveal a west-dipping reverse fault in the Precambrian basement beneath the monocline that cuts the top of the basement-cover contact. Faulting affects the upper Mississippian to Ordovician strata. The Centralia fault zone probably represents extensional reactivation of the basement structure beneath the Du Quoin monocline, and these structures likely connect at depth. The authors consider the Du Quoin monocline—and related Centralia fault—as a potential source for an earthquake that could have produced middle Holocene paleoliquefaction features in SW Illinois and possibly SE Missouri.
Tuttle, Chester, et al. (1999)	Paleoseismology Study Northwest of the New Madrid Seismic Zone	This paper, like Su and McBride (1999), considers the Du Quoin monocline, and related Centralia fault, as a potential source for an earthquake that could have produced middle Holocene paleoliquefaction features in SW Illinois and possibly SE Missouri. The conclusions are based on paleoliquefaction studies in southern Missouri and southern Illinois.

Table D-6.1.9 Data Summary
Wabash Valley RLME

Citation	Title	Description and Relevance to SSC
Louden Anticline		
Su and McBride (1999)	Final Technical Report—Study of a Potential Seismic Source Zone in South-Central Illinois	Reports that recent digital Vibroseis data over this feature, which is located directly NE of the Du Quoin monocline, reveals a major deep basement fault that projects to a depth of about 12 km (7.5 mi.) from the forward hinge point of the east-facing flexure of the dipping limb. A surface area of 252 km ² (97 sq. mi.) for the fault is estimated based on the axial length of the anticline, 29 km (18 mi.), and the vertical length of the basement fault, 8.7 km (5.4 mi.). This associated basement fault may be a source structure for paleoliquefaction events.
Waterloo-Dupo Anticline		
Harrison and Schultz (2002)	Tectonic Framework of the Southwestern Margin of the Illinois Basin and Its Influence on Neotectonism and Seismicity	The Waterloo-Dupo anticline is a N-NW-trending asymmetrical anticline that has been interpreted to be a southern continuation of the Cap au Gres structures. Similar to the Cap au Gres structure, it experienced at least two periods of deformation: moderate folding in the Late Devonian and a major episode of folding during late Mississippian to early Pennsylvanian. Apparent offset of the Waterloo-Dupo anticline suggests right-lateral slip on the St. Louis fault. The authors conclude that this offset of the Waterloo-Dupo anticline is consistent with late Mississippian to early Pennsylvanian NE-SW compression.
Nelson (1995)	Structural Features in Illinois	The Waterloo-Dupo anticline has a steep western limb, >45° in places, and a gentle east limb. Slight post-Pennsylvanian folding may have occurred on the structure.
Tuttle, Chester, et al. (1999)	Paleoseismology Study Northwest of the New Madrid Seismic Zone	Based on the spatial distribution of prehistoric liquefaction features, the paper indicates that the Waterloo-Dupo anticline, Valmeyer anticline, and St. Louis fault are possible sources for paleoearthquake features observed in eastern Missouri, but also emphasizes that other scenarios relying on sources farther east are equally possible (i.e., on the Du Quoin monocline—Centralia fault).

Table D-6.1.9 Data Summary
Wabash Valley RLME

Citation	Title	Description and Relevance to SSC
Farmington Anticline		
Harrison and Schultz (2002)	Tectonic Framework of the Southwestern Margin of the Illinois Basin and Its Influence on Neotectonism and Seismicity	The Farmington anticline/Avon block is a broad (up to 19.3 km [12 mi.] wide) NW-trending low-relief structural feature that lies between Ste. Genevieve and Simms Mountain faults. Weak to moderate seismicity is clustered around this structure, which has been interpreted to occur above buried faults cutting middle Proterozoic basement rock. A zone of NW-trending horsts and grabens with subsidiary and contemporaneous NE-striking oblique-slip faults coincides with axis of the fold.
Peoria Folds		
Nelson (1995)	Structural Features in Illinois	Designates a series of subtle anticlines and synclines, originally identified in 1957, as the Peoria folds. Individual folds named are the Astoria, Farmington, Littleton, Bardolph, Brereton, St. David, Sciota, Seville, and Versailles anticlines and the Bryant, Bushnell, Canton, Elmwood, Fairview, Ripley, and Table Grove synclines; they were mapped from surface and subsurface data on various Pennsylvanian and Mississippian horizons. Nearly all strike slightly north of east. They are linear to slightly arcuate, with the convex side to the north. The folds plunge eastward, as does the regional dip. Most have less than 30 m (100 ft.) of structural relief. This paper notes the correspondence of these minor folds with topography, in particular the E-NE alignment of small streams. This is the only region in Illinois where topography appears to be so strongly influenced by bedrock structure through glacial drift. The source of the horizontal compression that may have formed these folds is unknown.
Sandwich Fault		
Kolata et al. (1978)	The Sandwich Fault Zone of Northern Illinois	The NW-trending Sandwich fault zone, which also lies within the northern La Salle deformation belt in NE Illinois, has a maximum vertical displacement of about 244 m (800 ft.).
Larson (2002)	The Earthquake of 2 September 1999 in Northern Illinois: Intensities and Possible Neotectonism	Notes that two historical earthquakes (in 1909 and 1912) may be associated with the Sandwich fault zone, and that these two earthquakes may indicate reactivation of a fault within the Precambrian basement associated with the Sandwich fault zone.

Table D-6.1.9 Data Summary
Wabash Valley RLME

Citation	Title	Description and Relevance to SSC
Nelson (1995)	Structural Features in Illinois	Movement along Sandwich fault zone may have been contemporaneous with formation of Peru monocline.
Plum River Fault Zone		
Bunker et al. (1985)	The Plum River Fault Zone and the Structural and Stratigraphic Framework of Eastern Iowa	Describes northward dips of late Quaternary loess-covered terraces along an ancient, south-flowing channel of Mississippi River where terraces cross Plum River fault zone. Although the northward dips could be interpreted as evidence of Quaternary slip on the fault zone, they could also be explained by terrace erosion and subsequent burial beneath a blanket of loess.
Crone and Wheeler (2000)	Data for Quaternary Faults, Liquefaction Features, and Possible Tectonic Features in the Central and Eastern United States, East of the Rocky Mountain Front	Geologic evidence is insufficient to demonstrate Quaternary slip or deformation associated with the feature; therefore, the fault is characterized as non-Quaternary.
Wheeler and Crone (2001)	Known and Suggested Quaternary Faulting in the Midcontinent United States	
Nelson (1995)	Structural Features in Illinois	Plum River fault zone strikes E-W across NW Illinois and into NE Iowa. The author reports that primary movements on Plum River faults were post-Devonian and pre-Pennsylvanian. Structural relationships between Pennsylvanian strata and the fault zone preclude more than about 10 m (30 ft.) of post-Pennsylvanian movement.
Centralia Fault Zone		
Nelson (1995)	Structural Features in Illinois	Normal faults of Centralia fault zone are coincident with dipping flank of Du Quoin monocline and displace Paleozoic strata down to the west. The author reports that several high-resolution seismic lines across Centralia fault zone indicate a normal fault dipping 70°–75° toward the west, affecting all reflectors down to Ordovician strata. The author and Su and McBride (1999) infer that the zone has undergone two episodes of movement: reverse (west side up) during the Pennsylvanian to form Du Quoin monocline, and normal (west side down) after the Pennsylvanian.

Table D-6.1.9 Data Summary
Wabash Valley RLME

Citation	Title	Description and Relevance to SSC
Su and McBride (1999)	Final Technical Report—Study of a Potential Seismic Source Zone in South-Central Illinois	Observes similar displacement of 30–49 m (100–160 ft.) for all levels imaged (upper Mississippian to Ordovician). The authors suggest that the Centralia fault zone represents extensional reactivation of the basement structure beneath the Du Quoin monocline, and that these structures likely connect at depth. Possible association of earthquakes located near the structural axis of the Centralia fault and Du Quoin monocline with focal mechanisms is consistent with strike-slip along north-trending structures. The Centralia fault zone may be the source of earthquakes that produced paleoliquefaction features in the region. Like Nelson (1995), this paper infers that the fault has undergone two episodes of movement: reverse (west side up) during the Pennsylvanian to form the Du Quoin monocline, and normal (west side down) after the Pennsylvanian.
Tuttle, Chester, et al. (1999)	Paleoseismology Study Northwest of the New Madrid Seismic Zone	In agreement with Su and McBride (1999), this paper suggests that the Centralia fault may be the source of earthquakes that produced paleoliquefaction features in the region.
Rend Lake Fault		
Nelson (1995)	Structural Features in Illinois	The Rend Lake fault zone parallels the west flank of the Benton anticline, which is located directly east of the Du Quoin monocline.
Su and McBride (1999)	Final Technical Report—Study of a Potential Seismic Source Zone in South-Central Illinois	Reports that seismic-reflection data indicate a pattern of basement-penetrating faulting in and near the Rend Lake fault zone that probably is a product of the same post-Pennsylvanian, E-W extensional stress regime that created the Centralia fault zone.
Cap au Gres Structure		
Harrison and Shultz (2002)	Tectonic Framework of the Southwestern Margin of the Illinois Basin and Its Influence on Neotectonism and Seismicity	<p>Strikes of the axial surface of the fold and related faults range from N5°W to N85°W. The Cap au Gres structure, the north-striking Florissant dome, the Waterloo-Dupo anticline, and the Lincoln fold are all parts of the same deformational system.</p> <p>Although the feature has undergone recurrent movement, initial uplift occurred in Devonian and early Mississippian time. This paper summarizes studies related to the early deformational events on this structure. Based on kinematic indicators on faults and layer-parallel shortening associated with folding, the authors conclude that two episodes of deformation occurred along the Cap au Gres structure during</p>

Table D-6.1.9 Data Summary
Wabash Valley RLME

Citation	Title	Description and Relevance to SSC
		<p>the late Mississippian and earliest Pennsylvanian. The initial episode, which was relatively minor, resulted from N-S compression and produced extension along N-S segments of the structure. The next phase was a major episode of NE-SW compression that produced most of the deformational features along the structure. Following this period of deformation, some NW-striking segments of the structure were reactivated as high-angle normal faults. This deformation, which probably was of early Pennsylvanian age, appears to be the product of NW-SE maximum horizontal stress.</p> <p>The authors note that interpretation of possible deformation of Quaternary gravels (see Nelson, 1995, below) is tentative because of uncertainties in correlating individual erosional surfaces that may not represent contiguous or equivalent contacts, and the fact that the Grover Gravel occurs at various elevations.</p>
Mateker and Segar (1965)	Gravity Investigation Along the Eastern Flank of the Ozark Uplift	Geophysical surveys (gravity) along the structure indicate that the faults are nearly vertical and extend at least several kilometers into the crust.
Nelson (1995)	Structural Features in Illinois	<p>The Cap au Gres structure is a faulted monocline that exhibits an overall W-NW trend in Missouri and an E-W trend in Illinois. The north side has been raised as much as 366 m (1,200 ft.) relative to the south side. Various workers have concluded that this structure corresponds to a high-angle, north-dipping reverse fault in Precambrian basement rocks and the associated locally fractured fold near the surface. Apparent displacement of the Plio-Pleistocene Grover Gravel and its underlying peneplain indicates possible Tertiary tectonic activity on this structure. The gravel and underlying erosional surface on the south side of the flexure lie about 45.7 m (150 ft.) lower than on the north.</p>
Eureka–House Springs Structure		
Clendenin et al. (1993)	Sequencing Reelfoot Extension Based on Relations from Southeast Missouri and Interpretations of the Interplay Between Offset Preexisting Zones of Weakness	Interprets Middle and Late Ordovician, Middle Devonian, and post-Mississippian episodes of deformation on the Eureka–House Springs structure, suggesting that it experienced a minimum of 10 km (6 mi.) of left-lateral strike-slip motion.

Table D-6.1.9 Data Summary
Wabash Valley RLME

Citation	Title	Description and Relevance to SSC
Harrison and Schultz (2002)	Tectonic Framework of the Southwestern Margin of the Illinois Basin and Its Influence on Neotectonism and Seismicity	This paper summarizes the various interpretations of the complex NW-striking Eureka–House Springs structure in eastern Missouri. The structure has been described as a doubly plunging anticline and associated faults or, alternatively, as three right-stepping en echelon fault segments. In addition, the Valmeyer anticline in Illinois may be an en echelon segment of the Eureka–House Springs structure. The general conclusion of this paper is that the zone may have originated as a Proterozoic structure and may extend north of the St. Charles lineament, although only those segments south of this lineament were reactivated at various times in the Phanerozoic.
Tuttle, Chester, et al. (1999)	Paleoseismology Study Northwest of the New Madrid Seismic Zone	Estimates of significant lateral strike-slip motion are considered tentative given the lack of piercing points and insufficient strike length for that displacement. The authors observe no clear evidence of recent fault activity associated with the Eureka fault system, but note that proximity to their Meramec River liquefaction site and the uncertainties regarding the exact nature of this structure may warrant additional study.
Ste. Genevieve Fault Zone		
Harrison and Schultz (2002)	Tectonic Framework of the Southwestern Margin of the Illinois Basin and Its Influence on Neotectonism and Seismicity	<p>Detailed studies of this fault zone document contractional, extensional, and strike-slip movement along high-angle faults, as well as multiple periods of movement. The zone dies out near both the St. Charles and Commerce lineaments (see Midcontinent-Craton Data Summary Table), suggesting a genetic link and demonstrating the influence of these structural features on tectonism in the region.</p> <p>Deformation along this structure is correlative to the late Mississippian to middle Pennsylvanian tectonic episode identified elsewhere in the Midcontinent. The paper provides evidence for a period of extension probably of Late Pennsylvanian to Permian age.</p> <p>Detailed and reconnaissance mapping along the SGFZ for more than 75 years has revealed no evidence for Tertiary or Quaternary faulting.</p>
Heigold and Kolata (1993)	Proterozoic Crustal Boundary in the Southern Part of the Illinois Basin	The fault may have originated as a crustal plate boundary or suture zone during the Proterozoic.

Table D-6.1.9 Data Summary
Wabash Valley RLME

Citation	Title	Description and Relevance to SSC
<p>Nelson (1995)</p> <p>Nelson et al. (1997)</p>	<p>Structural Features in Illinois</p> <p>Tertiary and Quaternary Tectonic Faulting in Southernmost Illinois</p>	<p>The Ste. Genevieve fault zone (SGFZ) is mapped for approximately 193 km (120 mi.) along strike from SE Missouri into SW Illinois. It consists of numerous en echelon strands and braided segments having variable deformation styles and a complex history of reactivation. Displacement across the zone ranges from less than 198 m (650 ft.) to as much as 1,189 m (3,900 ft.). Detailed studies of this fault zone document contractional, extensional, and strike-slip movement along high-angle faults, as well as multiple periods of movement.</p> <p>In Illinois, compressional deformation is documented along the Ste. Genevieve fault in early Pennsylvanian rocks (Nelson, 1995). The later report, Nelson et al. (1997), however, indicates that some faults along the SE part of the SGFZ in Illinois displace Cretaceous and Tertiary sediments, but Quaternary deposits are not faulted.</p>
<p>Tuttle, Chester, et al. (1999)</p>	<p>Paleoseismology Study Northwest of the New Madrid Seismic Zone</p>	<p>Identifies soft-sediment deformation that could be related to low levels of ground shaking at one location along a strand of the fault. Diffuse seismicity occurs in the block between the SGFZ and Simms Mountain fault system. However, no evidence has been documented of any tectonic deformation of Quaternary deposits, nor has convincing evidence for paleoliquefaction been observed in this area.</p>
<p>Simms Mountain Fault System</p>		
<p>Clendenin et al. (1993)</p>	<p>Sequencing Reelfoot Extension Based on Relations from Southeast Missouri and Interpretations of the Interplay Between Offset Preexisting Zones of Weakness</p>	<p>Faults along the entire system were active in the late Cambrian as transfer faults related to Reelfoot rift extension.</p>
<p>Harrison and Schultz (2002)</p>	<p>Tectonic Framework of the Southwestern Margin of the Illinois Basin and Its Influence on Neotectonism and Seismicity</p>	<p>The Simms Mountain fault system in SE Missouri consists of numerous braided and en echelon fault strands that are continuous southward into the Cape Girardeau fault system. Together these fault systems extend more than 106 km (66 mi.), and in places reach as wide as 79 km (24 mi.). Left-lateral strike-slip movement occurred on the fault system, primarily before formation of Mississippi Valley-type ore deposits of Permian age, although some are later or of unknown age.</p>

Table D-6.1.9 Data Summary
Wabash Valley RLME

Citation	Title	Description and Relevance to SSC
Bodenschatz-Lick Fault System		
Clendenin et al. (1993)	Sequencing Reelfoot Extension Based on Relations from Southeast Missouri and Interpretations of the Interplay Between Offset Preexisting Zones of Weakness	Similarities in strike, dip, and early Paleozoic history suggest that this fault system may be related to the Greenville fault, which has been interpreted as a major early Paleozoic extensional fault associated with the Reelfoot rift.
Harrison and Schultz (2002)	Tectonic Framework of the Southwestern Margin of the Illinois Basin and Its Influence on Neotectonism and Seismicity	The Bodenschatz-Lick fault system is a complex NE-striking zone that has been mapped for approximately 40 km (25 mi.) in SE Missouri and southern Illinois.
Tuttle, Chester, et al. (1999)	Paleoseismology Study Northwest of the New Madrid Seismic Zone	Two clusters of low-magnitude seismicity have been recorded by the New Madrid network near the SW part of the Bodenschatz-Lick fault system near its intersection with the Simms Mountain–Cape Girardeau fault systems. Field investigations in the areas of seismicity found no evidence of earthquake-induced paleoliquefaction in Holocene deposits.
Cape Girardeau Fault System		
Harrison and Schultz (2002)	Tectonic Framework of the Southwestern Margin of the Illinois Basin and Its Influence on Neotectonism and Seismicity	<p>The Cape Girardeau fault system, which is a continuation of the Simms Mountain fault system, consists of numerous branching and anastomosing, dominantly NW-striking near-vertical faults. Although NE and N-NW-striking faults are less common, they appear to show evidence for the most recent deformation. There are rhomb-shaped pull-apart grabens related to strike-slip faulting that can be divided into three groups: (1) those that contain only Paleozoic rocks, (2) those that contain Upper Cretaceous and lower Tertiary formations, and (3) those that contain Quaternary strata.</p> <p>Unequivocal evidence of faulting of Quaternary gravel has been observed in a quarry and roadcut at the SE end of the fault system near its intersection with the Commerce geophysical lineament. Results of recent trenching show evidence for Quaternary faulting, possibly post-Sangamon in age. Unfaulted Peoria Loess (late Wisconsinan in age) and possibly Roxana Silt overlie the fault and graben fill. The authors interpret the Quaternary deformation to have formed under E-NE horizontal maximum principal stress. They favor erosion and fill as an alternative to the finding</p>

**Table D-6.1.9 Data Summary
Wabash Valley RLME**

Citation	Title	Description and Relevance to SSC
		by Tuttle, Chester, et al. (1999) of a source of possible faulting in Quaternary gravel discovered on part of the Cape Girardeau fault system approximately 14.5 km (9 mi.) to the NW.
Wabash Valley Fault System		
Bear et al. (1997)	Seismic Interpretation of the Deep Structure of the Wabash Valley Fault System	This paper concludes that the fault system is not a northward continuation of the Reelfoot rift, because fault displacements of the WVFS decrease southward in the direction of the rift complex. Analysis of industry reflection data across the fault system indicates Cambrian fault movements as well as early Paleozoic dextral strike-slip along some of the faults.
Bristol and Treworgy (1979)	The Wabash Valley Fault System in Southeastern Illinois	Major structures within the Illinois portion of the Wabash Valley fault system are identified from interpretation of drillhole and downhole geophysical logs. The WVFS is about 90–100 km (55–60 mi.) long and as much as 48 km (30 mi.) wide. The faults of the WVFS outline elongate, gently tilted or arched horsts and grabens, with the axial part of the system down-faulted relative to the margins. Drillhole data indicate predominantly normal movement with vertical offset of as much as 146 m (480 ft.) along the faults that is post-late Pennsylvanian. The faults die out downward; some may reach basement but do not necessarily penetrate it.
Counts, Durbin, and Obermeier (2008)	Seismic Ground-Failure Features in the Vicinity of the Lower Wabash and Ohio River Valleys	Field trip guidebook that describes tectonically induced ground failures of Tertiary and Quaternary age in the lower Wabash River and Ohio River valleys of southern Illinois, SW Indiana, and western Kentucky.
Counts et al. (2009a)	Investigation of Quaternary Displacement on the Uniontown Fault, Western Kentucky	Paleoseismic investigations (trenching and boreholes) of a prominent north-trending scarp on the floodplain of the Ohio River suggest that the scarp is tectonic rather than erosional. The trench across the scarp exposed flat-lying floodplain strata east of the scarp and a 3 m (9.8 ft.) down-to-the-west monoclinial flexure at the scarp. The scarp displaces Quaternary sediment and thus represents Quaternary folding. Shallow seismic-reflection lines reveal faulting that extends from the Paleozoic bedrock, up into the Quaternary alluvium, to near the base of the scarp. The monoclinial flexure is interpreted to have formed as a consequence of underlying Quaternary reverse faulting. The fault, referred to as the Uniontown fault, is part of the Wabash Valley fault system. Movement on the Uniontown fault appears to have controlled the course of the Ohio River in a fashion similar to the New Madrid bend of the Mississippi River around the north-trending Reelfoot fault in SW Kentucky.

Table D-6.1.9 Data Summary
Wabash Valley RLME

Citation	Title	Description and Relevance to SSC
Counts et al. (2009b)	Paleoseismic Features Within the Wabash Valley Seismic Zones in Western Kentucky	<p>Identifies several large clastic dikes in the banks of the Green River in Davies County. The largest was a weakly cemented gravel dike, 4–7 cm (1.6–2.8 in.) wide and 3.3 m (10.8 ft.) high, that was injected upward into silty floodplain deposits. The base of this dike penetrated clay bed containing $9,850 \pm 70$ yr BP wood, indicating that the earthquake occurred during the early to middle Holocene.</p> <p>A fault scarp 5 km (3 mi.) long was mapped in the Ohio River floodplain. The scarp trends north, faces west, and is 2.5 m (8.2 ft.) high at its southern end. Seismic-reflection profiles across the scarp show that faulting in the Paleozoic bedrock extends upward and offsets Quaternary sediments just below the base of the scarp. A monoclinial flexure 3 m (9.8 ft.) down to the west was exposed at the base of the scarp in a trench. Radiocarbon dates indicate that the strata were folded between 3,500 and 295 yr BP, so the scarp represents Holocene folding.</p>
Fraser et al. (1997)	Geomorphic Response to Tectonically-Induced Ground Deformation in the Wabash Valley	In the restraining bend region along the western edge of the Commerce deformation zone, morphometric analysis of the land surface, detailed geologic mapping, and structural analysis of bedrock indicate west-dipping surfaces in the Wabash Valley.
Heigold and Larson (1994)	Geophysical Investigations of Possible Recent Ground Deformation and Neotectonism in White County, Illinois	At a locality in the lower Wabash Valley, the authors investigated two sites where suspected neotectonism and ground deformation were associated with historical seismicity. One of the sites experienced liquefaction during the 1811 New Madrid earthquake. The other was an escarpment (referred to as the Meadow Bank) along a projection of the Herald-Phillipstown fault zone. Vertical electrical soundings, seismic refraction profiling, resistivity profiling, and boreholes were used to evaluate the depth to Pennsylvanian bedrock across the escarpment. It was concluded that the escarpment probably formed as a result of erosion, possibly along the fault zone. The study found no evidence to support recent movement along preexisting or newly formed faults.
<p>Nelson and Lumm (1987)</p> <p>Nelson (1995)</p>	<p>Structural Geology of Southeastern Illinois and Vicinity</p> <p>Structural Features in Illinois</p>	The Wabash Valley fault system (WVFS) is a major zone of NE-trending, high-angle normal and strike-slip faulting along the border area of Illinois, Kentucky, and Indiana. These faults lie within and form the borders of the NE-trending Grayville graben. The WVFS includes the following faults: Albion-Ridgeway, Cottonwood, Herald-Phillipstown, Inman, Inman West, Inman East, Junction, Maunie, Mt. Carmel–New Harmony, North Fork, Pitcher Lake, and Ribeyre Island. The Grayville graben and WVFS are bounded to the south by the Rough Creek–Shawneetown fault system.

**Table D-6.1.9 Data Summary
Wabash Valley RLME**

Citation	Title	Description and Relevance to SSC
		<p>The authors suggest that the WVFS most likely developed in the Early Permian and is therefore the same age as the Cottage Grove fault system. They note that individual faults within the zone are characterized by slightly arcuate segments that overlap. They also conclude that the WVFS does not cross the Rough Creek–Shawneetown fault zone.</p> <p>Based on previous interpretations of WVFS structures as primarily normal faults (Bristol and Treworgy, 1979), the conclusion of Nelson and Lumm (1987) is that the WVFS developed in response to W-NW and E-SE extension. Nelson (1995) proposes that the faults originated from a deformation episode that initially produced doming along a N-NE-trending axis.</p>
Sexton et al. (1986)	Seismic Reflection Profiling Studies of a Buried Precambrian Rift Beneath the Wabash Valley Fault Zone	<p>Based on interpretation of seismic-reflection profiles, this paper argues that the faults of the WVFS developed by reactivation of a Precambrian rift zone (Grayville graben) that was the northern extension of the Reelfoot–Rough Creek system. The paper also discusses regional and detailed gravity and magnetic anomaly data. Regional data sets had previously been used to infer the existence of a NE-trending rift beneath the Wabash Valley in SW Indiana and SE Illinois. Detailed gravity and magnetic profile data collected along the Wabash Valley seismic-reflection lines were also examined. Calculations of theoretical gravity anomalies associated with the locations of the Wabash Valley faults suggest that due to the small amplitude of the offsets, no identifiable anomalies would be expected in the detailed gravity anomaly data. Large, observed regional gravity and magnetic anomalies over the Wabash Valley fault area are almost certainly caused by density contrasts associated with the pre-Mt. Simon rocks and intrabasement sources.</p>
Van Arsdale et al. (2009)	Quaternary Displacement Along the Hovey Lake Fault of Southern Indiana and Western Kentucky	<p>A shallow S-wave seismic-reflection line acquired across the Hovey Lake fault in southern Indiana and western Kentucky reveals Paleozoic bedrock that is folded and normal faulted 10.5 m (34.4 ft.). The overlying Quaternary alluvium has 2 m (6.6 ft.) of reverse displacement at a depth of 5 m (16.4 ft.), thus revealing structural inversion. Although there is no surface scarp, a line of shallow borings, acquired across the seismically identified fault, indicates that the faulting may come to the surface. Trenching was not permitted at this site.</p> <p>Folding and faulting in Paleozoic bedrock and overlying Quaternary alluvium also was observed in a shallow S-wave seismic-reflection line that was acquired across a down-to-the-west scarp within the Hovey Lake fault system in western Kentucky. A trench exposed folded 3,500 yr BP Ohio River alluvium. The down-to-the-west fold, which has an amplitude of 3 m (9.8 ft.), is believed to have formed in response</p>

**Table D-6.1.9 Data Summary
Wabash Valley RLME**

Citation	Title	Description and Relevance to SSC
		to underlying down-to-the-west Holocene fault displacement. Fractures within an undeformed unit that laps onto the scarp indicate that minor fault reactivation may have occurred within the last 295 years.
Wheeler et al. (1997)	Seismotectonic Map Showing Faults, Igneous Rocks, and Geophysical and Neotectonic Features in the Vicinity of the Lower Wabash Valley, Illinois, Indiana, and Kentucky	Describes possible neotectonic points in the lower Wabash Valley based on Heigold and Larson (1994).
Woolery (2005)	Geophysical and Geological Evidence of Neotectonic Deformation Along the Hovey Lake Fault, Lower Wabash Valley Fault System, Central United States	High-resolution seismic (shear-wave) reflection profiles collected along the Hovey Lake fault, a known Paleozoic fault within a system of faults in the southernmost Wabash Valley fault system in an area of recognized prehistoric and contemporary seismicity, show high-angle deformation extending above the Paleozoic bedrock and into Upper Quaternary sediment. Time-displacement calculations from the data show approximately 10.5 m (34.4 ft.) of offset on the top-of-bedrock horizon, located 7.7 m (25.3 ft.) below ground surface, suggesting fault movement at this site as late as ~37 ka.
<i>Paleoliquefaction Studies (See also Table 6.1.9-1)</i>		
Chester and Tuttle (2000)	Paleoseismology Study in the Cach River Valley, Southern Illinois	Six sand dikes were observed at four locations. The sand dikes range from 1 to 9 cm (0.4 to 3.5 in.) wide and pinch upward, extending to 1.1 m (3.6 ft.) above the water table or 2.4 m (7.9 ft.) below the top of the cutbank. Differences in weathering characteristics may indicate two generations of sand dikes. A radiocarbon date of AD 1020–1250 represents a maximum age for the younger generation, and possibly the older generation as well. The results are consistent with ground shaking of modified Mercalli intensity VIII-IX.
Counts et al. (2009b)	Paleoseismic Features Within the Wabash Valley Seismic Zones in Western Kentucky	Identifies several large clastic dikes in the banks of the Green River in Davies County. The largest was a weakly cemented gravel dike, 4–7-cm (1.6–2.8 in.) wide and 3.3 m (10.8 ft.) high, that was injected upward into silty floodplain deposits. The base of this dike penetrated clay bed containing $9,850 \pm 70$ yr BP wood, indicating that the earthquake occurred during the early to middle Holocene.

Table D-6.1.9 Data Summary
Wabash Valley RLME

Citation	Title	Description and Relevance to SSC
Green et al. (2005)	Engineering Geologic and Geotechnical Analysis of Paleoseismic Shaking Using Liquefaction Effects: Field Examples	<p>This paper cites the assessment of the Vincennes paleoearthquake as a case study for implementing the methods outlined in Olson et al. (2005a) for assessing uncertainties in (1) the significance of changes in the geotechnical properties of post-liquefied sediments (e.g., aging and density changes); (2) the selection of appropriate geotechnical soil indices from individual paleoliquefaction sites; and (3) the methodology for integration of back-calculated results of strength of shaking from individual paleoliquefaction sites into a regional assessment of paleoseismic strength of shaking.</p> <p>Twelve sites that are at scattered locations in the Wabash Valley and that exhibit paleoliquefaction features are analyzed. The features are first provisionally attributed to the Vincennes earthquake, which occurred around 6,100 yr BP, and are used to illustrate the proposed approach for selecting representative soil indices of the liquefied sediments. These indices are used in back-calculating the strength of shaking at the individual sites, the results from which are then incorporated into a regional assessment of the moment magnitude, M, of the Vincennes earthquake. The regional assessment validated the provisional assumption that the paleoliquefaction features at the scattered sites were induced by the Vincennes earthquake, in the main, which was determined to have a magnitude of M ~ 7.5.</p>
Hajic et al. (1995)	Distribution and Dating of Prehistoric Earthquake Liquefaction in Southeastern Illinois, Central U.S.	<p>Presents results of a paleoliquefaction survey along streams in SE and central Illinois. A total of 127 paleoliquefaction sites are identified. Relatively wide dikes in the Sangamon and Kaskaskia river valleys at distances of 200 and 175 km (124.3 and 108.7 mi.) from Vincennes suggest either shaking from multiple sources or a noncircular distribution of features associated with the Vincennes earthquake.</p> <p>Stratigraphic, geomorphic, pedologic, archaeological, and preliminary radiocarbon evidence indicates that SE Illinois was shaken by substantial earthquakes at a minimum two, and possibly six, times in the past: possibly around 18,500 yr BP, around 6,100 yr BP, possibly around 3,750 yr BP, and during the 1811-1812 New Madrid earthquakes. Two additional Holocene earthquakes are possibly represented by liquefaction features along the Sangamon River (<9,200 yr BP) and lower Kaskaskia River.</p>

Table D-6.1.9 Data Summary
Wabash Valley RLME

Citation	Title	Description and Relevance to SSC
Hajic and Wiant (1997)	Dating of Prehistoric Earthquake Liquefaction in Southeastern and Central Illinois	<p>Presents results of an additional stream bank survey along reaches of Big Muddy, Miller, Mill, and Big creeks and an unnamed ditch in the Little Wabash Valley, all in SE Illinois. An additional stream bank survey along reaches of rivers and creeks in central and west-central Illinois and east-central Missouri resulted in negative evidence for any paleoliquefaction features, suggesting that the part of west-central Illinois north of St. Louis covered by these surveys was not struck by an earthquake of sufficient magnitude to cause liquefaction during the Holocene.</p> <p>The majority of paleoliquefaction observed in SE Illinois is attributable to the Vincennes earthquake. An earthquake near Mt. Auburn (subsequently referred to by McNulty and Obermeier (1999) as the Springfield earthquake) occurred after around 7,400 yr BP and before around 4,500 yr BP. Two other sites in Illinois are possibly attributable to the Skelton–Mt. Carmel earthquakes. Dikes at two SE Illinois sites most likely were emplaced about $19,800 \pm 1,100$ yr BP; these may be related to features observed in SW Indiana or they may be glaciotectonic.</p>
McNulty and Obermeier (1999)	Liquefaction Evidence for At Least Two Strong Holocene Paleoeearthquakes in Central and Southwestern Illinois	<p>Discusses evidence for the timing and magnitude of two middle Holocene earthquakes in Illinois: the Springfield and Shoal Creek earthquakes. The Springfield earthquake occurred between 5,900 and 7,400 yr BP; dikes are as much as 0.4 m (1.3 ft.) in width near the presumed energy center about 35 km (21.7 mi.) NE of Springfield, Illinois; the magnitude is estimated to be at least M 6.2 and less than M 6.8. The Shoal Creek earthquake occurred around 5,700 yr BP; dikes probably extend approximately 35 km (22 mi.) from the energy center (assumed to be approximately 65 km, or 40.5 mi., E-SE of St. Louis, Missouri; dikes as wide as 0.5 m (1.6 ft.) are observed; the magnitude is estimated to be M 6.0 or greater.</p>
Munson et al. (1997)	Liquefaction Evidence for Holocene and Latest Pleistocene in the Southern Halves of Indiana and Illinois—A Preliminary Overview	<p>Identifies evidence for at least eight paleoeearthquakes having magnitudes stronger than any in the historical era in southern Illinois and southern Indiana. At least six prehistoric earthquakes occurred during the Holocene and at least two others occurred during the latest Pleistocene. The two largest paleoeearthquakes were centered in the lower Wabash Valley. The estimated magnitude of the largest earthquake, which occurred $6,100 \pm 200$ yr BP, is M 7.5–7.8. The next largest earthquake, an estimated M 7.1–7.3 earthquake, occurred $12,000 \pm 1,000$ yr BP. Two other paleoeearthquakes likely had magnitudes of M ≥ 6.8.</p> <p>It is likely that liquefaction evidence has been discovered for all Holocene and latest Pleistocene paleoeearthquakes with M ≥ 7 (radius of liquefaction effects > 50 km [31 mi.]) in southern Illinois and Indiana. However, in addition to the six or more M 6.0–7.0 earthquakes that have been discovered, numerous other earthquakes</p>

Table D-6.1.9 Data Summary
Wabash Valley RLME

Citation	Title	Description and Relevance to SSC
		strong enough to potentially induce limited liquefaction could have struck other areas but, based on the lack of liquefiable deposits, left no evidence. In some parts of the southern halves of Indiana and Illinois, an earthquake with a potential radius of liquefaction effects of 30–40 km (18.6–25 mi.) could have struck without leaving liquefaction evidence.
Obermeier et al. (1993)	Liquefaction Evidence for One or More Strong Holocene Earthquakes in the Wabash Valley of Southern Indiana and Illinois, with a Preliminary Estimate of Magnitude	Provides criteria for interpreting an earthquake origin for dikes observed in the Wabash Valley. Concludes that virtually all of the dikes were formed by a single large earthquake that took place between 1.500 and 7.5 ka. The epicenter of the strongest earthquake(s) was near Vincennes, Indiana. The strength of the earthquake far exceeds the level of shaking and magnitude of the 1895 M 6.8 Charleston, Missouri, earthquake; the magnitude of the Vincennes earthquake appears to have been similar to that of the 1886 Charleston, South Carolina, earthquake (M ~ 7.5).
Obermeier (1998)	Liquefaction Evidence for Strong Earthquakes of Holocene and Latest Pleistocene Ages in the States of Indiana and Illinois, USA	<p>Major conclusions outlined in this summary paper are as follows:</p> <ul style="list-style-type: none"> • Virtually all dikes observed are from seismic liquefaction. Dikes were induced by prehistoric earthquakes whose energy centers (and epicenters) were almost exclusively in Indiana and Illinois (with the exception of some features in Cache Valley related to 1811-1812 New Madrid earthquakes). • Probably nine paleoearthquakes larger than historical earthquakes are identified, at least seven and probably eight Holocene earthquakes of which have a magnitude of M 6 or higher. • The largest, which occurred ~6,100 ± 100 yr BP, was on the order of M 7.5; the next largest (M ~ 7.1) occurred ~12,000 ± 1,000 yr BP. Three more had magnitudes of M > 6.5. • The two strongest were in proximity to each other and took place in the general vicinity of the most numerous and strongest historical earthquakes (M 4–5.5) in the lower Wabash Valley of Indiana and Illinois. Paleoeearthquakes of lower magnitudes are more randomly distributed and have struck in regions having no significant historical seismicity. • Probably all earthquakes of M > 7 have been identified in Illinois and Indiana. • A significant number (10 or more) of moderate to strong paleoearthquakes (M 6–7) likely occurred during Holocene and latest Pleistocene time but are not recorded in paleoliquefaction record because of a lack of liquefiable deposits.

**Table D-6.1.9 Data Summary
Wabash Valley RLME**

Citation	Title	Description and Relevance to SSC
Olson et al. (2005a)	Geotechnical Analysis of Paleoseismic Shaking Using Liquefaction Effects: A Major Updating	Describes a new methodology proposed for the geotechnical analysis of strength of paleoseismic shaking using liquefaction effects. The proposed method provides recommendations for the selection of both individual and regionally located test sites, provides techniques for the validation of field data for use in back-analysis, and presents a recently developed energy-based solution to back-calculate paleo-earthquake magnitude and strength of shaking. The proposed method allows investigators to qualitatively assess the influence of post-earthquake density change and aging. The proposed method also describes how the back-calculations from individual sites should be integrated into a regional assessment of paleoseismic parameters.
Olson et al. (2005b)	Revised Magnitude Bound Relation for the Wabash Valley Seismic Zone of the Central United States	Provides a revised regional magnitude-bound curve for the central U.S. using a consistent site-to-source distance measure, a detailed review of liquefaction accounts resulting from historical earthquakes, and magnitude estimates for those historical earthquakes that have factored in data from recent seismological studies. Reassessed magnitudes for four paleoearthquakes in the Wabash Valley are approximately 0.5–0.7 magnitude units smaller than previously suggested. The revised magnitude estimates are M 7.3 (Vincennes earthquake), M 6.7 (Skelton earthquake), M 6.3 (Vallonia earthquake), and M 6.2 (Waverly earthquake).
Olson et al. (2007)	Quantifying Uncertainties in Paleoliquefaction Studies	A preliminary M 7.99 ± 0.27 is estimated for the Vincennes paleoearthquake (around 6,100 yr BP) using simplified and rigorous statistical and probabilistic methods to quantify uncertainties in liquefaction susceptibility (aging and density change, liquefaction severity, fines content adjustment, and overburden stress correction); field data quality (field observations and in situ test measurement, ground failure mechanism, and field setting); seismicity and seismic demand (attenuation relationships, magnitude scaling factor, depth reduction factor, and local site response); and a Bayesian updating framework that uses the magnitude bound method to estimate a prior distribution,.
Pond and Martin (1997)	Estimated Magnitudes and Accelerations Associated with Prehistoric Earthquakes in the Wabash Valley Region of the Central United States	Presents results of a geotechnical study of soil conditions at paleoliquefaction sites to estimate both the magnitude and accelerations of four prehistoric earthquakes. Using an energy-stress approach, the geotechnical and seismological estimates of surface accelerations suggest M 6.9 (Waverly earthquake), M 7.1 (Vallonia earthquake), M 7.3 (Skelton earthquake), and M 7.8 (Vincennes earthquake).

Table D-6.1.9 Data Summary
Wabash Valley RLME

Citation	Title	Description and Relevance to SSC
Su and McBride (1999)	Final Technical Report—Study of a Potential Seismic Source Zone in South-Central Illinois	Discusses interpretation of reprocessed seismic-reflection profiles across the Du Quoin monocline–Louden anticline region and paleoliquefaction reconnaissance along 90 km (56 mi.) of the Big Muddy River and its tributaries in the vicinity of these structures. No new paleoliquefaction features were observed, but this may be due to lack of liquefiable sediments. The report concludes that all previously recognized paleoliquefaction features in the study region could be induced by earthquakes on the Du Quoin monocline–Louden anticline structures.
Tuttle, Chester, et al. (1999)	Paleoseismology Study Northwest of the New Madrid Seismic Zone	The results of this study are summarized and updated in Tuttle (2005b); see below.
Tuttle (2005b)	Paleoseismological Study in the St. Louis Region: Collaborative Research	This paper summarizes and updates observations reported by Tuttle, Chester, et al. (1999). At least two generations of Holocene earthquake-induced liquefaction features, including sand and silt dikes and sills, and only two sand blows, are identified in the St. Louis region. Some features probably formed during the 1811-1812 or earlier New Madrid earthquakes, and others formed during a middle Holocene earthquake in 4520 BC \pm 160 years. Late Holocene sand dikes, up to 26 cm (10.2 in.) in width, occur along the Kaskaskia River and its tributaries, Crooked, Shoal, and Silver creeks, as well as along Cahokia and Piasa creeks and the Cache, Castor, Marys, and Meramec rivers. The 4250 BC earthquake may or may not have been responsible for all of the middle Holocene features. The relatively large size of features identified near Germantown, Illinois, suggests that the earthquake source may be located east of St. Louis. Alternative sizes and locations are suggested. The Meramec River features could have formed as a result of a moderate-to-large earthquake centered in the St. Louis area or a very large earthquake centered 80–100 km (50–62 mi.) east of St. Louis.
Seismicity		
Bakun and Hopper (2004a)	Catalog of Significant Historical Earthquakes in the Central United States	Modified Mercalli intensity assignments are used to estimate source locations and moment magnitude M for 18 nineteenth-century and 20 early twentieth-century earthquakes in the central U.S. for which estimates of M are otherwise not available. There has been persistent seismic activity in the Illinois basin in southern Illinois and Indiana, with M > 5.0 earthquakes in 1895, 1909, 1917, 1968, and 1987. Historical earthquakes (pre-1952) in the Illinois basin have been associated with the Wabash Valley fault zone, the Cottage Grove fault zone, the Du Quoin monocline, the Ste. Genevieve fault zone, and the La Salle anticlinorium.

Table D-6.1.9 Data Summary
Wabash Valley RLME

Citation	Title	Description and Relevance to SSC
Hamburger et al. (2008)	Geodetic Observations from the Region Surrounding the M 5.2 Mt. Carmel, Illinois Earthquake	The April 18, 2008, M 5.2 earthquake was located close to the New Harmony fault at ~14 km (~8.7 mi.) depth. Analysis of GPS data suggests systematic NW motion of about 0.5–0.7 mm/yr with respect to the Stable North American Reference Frame. Block models, which assume boundaries along the Cottonwood Grove–Rough Creek Graben (CGRCG) and the WVFS, indicate marginal block velocities with possible strike-slip motion along the WVFS, and E-W motions along the CGRCG.
Hamburger et al. (2009)	Is There a Connection Between Seismicity and Deformation in the New Madrid and Wabash Valley Seismic Zones?	Comparison of geodetic and geophysical data between WVSZ and NMSZ. In both cases, regional seismic and potential field data provide evidence for high-angle, basement-penetrating faults that define narrow, elongate Precambrian grabens that lie beneath relatively undeformed Paleozoic or Mesozoic rocks. Data from a 56-site-campaign GPS geodetic network in the southern Illinois basin indicate systematic NW motion of about 0.5–0.7 mm/yr with respect to the Stable North American Reference Frame. Average results for the entire network show marginally significant strains, with an orientation rotated 45° from the overall direction of intraplate stress in the U.S. Midcontinent.
Kim (2003)	The 18 June 2002 Caborn, Indiana, Earthquake: Reactivation of Ancient Rift in the Wabash Valley Seismic Zone?	The June 18, 2002, M_w 4.6 earthquake occurred on a steeply dipping fault at a depth of about 18 km (11.2 mi.; better than ± 2 km—or ± 1.2 mi.—horizontal and vertical location accuracy). The source mechanism determined from regional waveform analysis is predominantly strike-slip along near-vertical nodal planes (dips 82° and 84°) striking 28° and 297°. The close proximity of the epicenter to the trace of the Caborn fault, and good agreement between the strike and dip of that fault and source mechanism for the June 18, 2002, earthquake suggest that the earthquake occurred on that fault. This earthquake may suggest that buried faults associated with a possible Precambrian rift system are being reactivated by the contemporary E–E-NE-trending regional horizontal compressive stress.
Larson et al. (2009)	Analysis of Effects from the April 18, 2008 Illinois Earthquake	Analyzes the April 18, 2008, M 5.4 earthquake that occurred in the Wabash Valley seismic zone at depth of 11.6 km (7.2 mi.). The earthquake was located in a mature oil and coal production region; E-W elongation of the Intensity IV and higher regions. Some of the E-W elongation may be attributed to the E-W focal mechanism of the earthquake, whereas other patterns coincide with major river channels (soil amplification) and a geologic structure.

Table D-6.1.9 Data Summary
Wabash Valley RLME

Citation	Title	Description and Relevance to SSC
McBride et al. (2007)	Deep Faulting and Structural Reactivation Beneath the Southern Illinois Basin	Seismotectonic implications described above (Basement Structure section). McBride, Hildenbrand, et al. (2002) provide a table summarizing depths and magnitudes for instrumentally recorded earthquakes of the Wabash Valley seismic zone (m_{bLg} 3.1–5.2) that range from 4.9 ± 14.1 km (3 ± 8.8 mi.) to 23.4 ± 2.1 km (14.5 ± 1.3 mi.).
McBride, Hildenbrand, et al. (2002)	Interpreting the Earthquake Source of the Wabash Valley Seismic Zone (Illinois, Indiana, and Kentucky) from Seismic Reflection, Gravity, and Magnetic Intensity	
Withers et al. (2009)	Introduction and Background for the April 18, 2008 Illinois Earthquake	Discusses the April 18, 2008, Mt. Carmel, Illinois, earthquake, the largest earthquake in the Wabash Valley seismic zone in the past 20 years. The earthquake took place near Mt. Carmel, Illinois; the magnitude was M_w 5.2 (M_w 5.4 according to GCMT [http://www.globalcmt.org]); a relatively long-lasting aftershock sequence included 37 earthquakes located by the network, with 3 earthquakes greater than magnitude 4).
Yang et al. (2009)	Determination of the Fault Plane for the April 18, 2008 Illinois Earthquake by Detecting and Relocating Aftershocks	Analysis of aftershocks using the sliding-window cross-correlation technique and the double-difference relocation algorithm gives a best-fit plane having a nearly E-W trend with an orientation of 248 and a dip angle of 81. The fault is nearly vertical down to ~20 km (~12.4 mi.).
Seismic Hazard Models		
Petersen et al. (2008)	Documentation for the 2008 Update of the United States National Seismic Hazard Maps	Although the Wabash Valley region in southern Indiana and Illinois is part of the craton, M 7.5 is used for M_{max} there, based on the distribution of paleoliquefaction features resulting from past large earthquakes.
Wheeler and Cramer (2002)	Updated Seismic Hazard in the Southern Illinois Basin: Geological and Geophysical Foundations for Use in the 2002 USGS National Seismic-Hazard Maps	Based on estimates of the magnitudes (M 7.1 and M 7.5) of prehistoric earthquakes in the southern Illinois basin, this paper outlines three alternative source configurations that can be combined in a logic tree: the oval tri-state seismicity source zone that is centered on the two energy centers; a narrow source zone that follows the Vincennes bend in the Commerce geophysical lineament; and the Grayville graben. M_{max} is set at 7.5 inside each alternative source.

Table D-7.3.1 Data Summary
St. Lawrence Rift Zone

Citation	Title	Description and Relevance to SSC
<i>Initiation of Iapetan Rifting</i>		
Abdel-Rahman and Kumarapeli (1998)	Geochemistry of Mantle-Related Intermediate Rocks from the Tibbit Hill Volcanic Suite, Quebec Appalachians	Major and trace-element geochemistry of intermediate volcanic rocks of the Tibbit Hill volcanic suite provide evidence for anorogenic A1 type suites, consistent with the earlier interpretation of an Iapetan triple junction. Trace-element modeling suggests that these intermediate magmas were produced by up to 20% fractional crystallization of alkaline to transitional basaltic melts, representing differentiates of basalts related to hotspot plumes or continental rift zones. The authors also suggest that the intermediate rocks of the Tibbit Hill volcanic suite are comagmatic and coeval with the Adirondack dike swarm and formed shortly before the onset of seafloor spreading.
Abdel-Rahman and Kumarapeli (1999)	Geochemistry and Petrogenesis of the Tibbit Hill Metavolcanic Suite of the Appalachian Fold Belt, Quebec–Vermont: A Plume-Related and Fractionated Assemblage	<p>Presents the geochemistry of the Tibbit Hill mafic to felsic volcanic assemblage based on data presented in previous studies. The study concludes that the mafic basalts from the Tibbit Hill volcanic suite crystallized from basaltic magma produced by approximately 2.5% batch partial melting of garnet lherzolite with a final basaltic melt segregation depth of 80–100 km (50–62 mi.), which is consistent with melting within a rising mantle plume below the Sutton Mountains triple junction. Twenty-five percent fractionation of these basaltic magmas produced the intermediate melts.</p> <p>The Adirondack dike swarm is geochemically similar to the Tibbit Hill basalt and both differ from the geochemically depleted Grenville dike swarm, suggesting that Tibbit Hill (and therefore the Adirondack dike swarm) represent the youngest, pre-breakup, extension-related volcanism prior to the initiation of seafloor spreading.</p> <p>This paper does not consider the results of other Iapetan volcanics in the region—specifically, the work of McCausland and Hodych (1998).</p>
Bédard and Stevenson (1999)	The Caldwell Group Lavas of Southern Quebec: MORB-Like Tholeiites Associated with the Opening of Iapetus Ocean	Trace-element and Nd isotopic data were obtained for the Caldwell Group lavas of southern Quebec. These undated rocks, which belong to the internal nappe domain of the Humber zone, were deformed during the Taconic orogeny. These rocks initially formed at an advanced stage in the transition from rift to drift along the Iapetan margin. Despite exhibiting clear evidence of hydrothermal alteration, several conclusions were inferred from the geochemistry of these basalts. These basalts crystallized from melts derived from normal mid-ocean ridge basalt (MORB) at low to medium pressure.

Table D-7.3.1 Data Summary
St. Lawrence Rift Zone

Citation	Title	Description and Relevance to SSC
		fractional crystalization. Most lavas represent about 20% melting from a source slightly less depleted than fertile MORB mantle (asthenospheric mantle), whereas subpopulations of the Caldwell lavas are characterized by 6%–15% melting of the same source mantle. These data are substantiated by Nd-isotope data that indicate derivation from a light rare-earth-element-depleted mantle that is more radiogenic than other lapetus basalts, implying that other basalts in the region were derived from a more enriched source. Sedimentary samples reflect a mixture of old (Archean) and juvenile (Iapetan) crustal sources for the basin.
Cawood et al. (2001)	Opening Iapetus: Constraints from the Laurentian Margin in Newfoundland	<p>Evaluates the age relationships of the Skinner Cove Formation (550.5 \pm 3/–2 Ma), the Lady Slipper pluton (555 \pm 3/–5 Ma), and the youngest marine carbonate sediments (540–535 Ma) interpreted as the rift drift transition from within the Humber zone of the Appalachian orogen in Newfoundland. Compares these age relationships with the paleomagnetic data of McCausland and Hodych (1998) and data for other igneous activity on the eastern margin of Laurentia. Attributes these data to a two-stage rifting process along the eastern margin of Laurentia.</p> <p>Igneous activity 760–700 Ma in the Appalachian Blue Ridge corresponds with the opening of the proto-Pacific between East Australia/West Antarctic conjugate margins. The younger set of igneous activity observed in eastern Laurentia between 620 and 550 Ma involves rifting and separation of Laurentia from the West Gondwana cratons corresponding to the closure of the Mozambique Ocean and assembly of East and West Gondwana; initiation of subduction of the proto-Pacific beneath East Gondwana; and rifting of Baltica and Siberia from Laurentia and Gondwana. The Iapetus Ocean was initiated between Laurentia and Gondwana by 570 Ma, while Baltica had already separated from Laurentia. A proto-Pacific spreading center may have also propagated at that time.</p>
Faill (1997a)	A Geologic History of the North-Central Appalachians. Part 1. Orogenesis from the Mesoproterozoic Through the Taconic Orogeny	Crustal extension and rifting late in the Neoproterozoic and into the earliest Cambrian separated the Neoproterozoic supercontinent Rodinia into East Gondwana, West Gondwana, and Laurentia. This rifting event resulted in the development of the St. Lawrence rift system. The breakup of Rodinia spanned approximately 200 Myr, with separation of East Gondwana from western Laurentia approximately 750 million years ago and rifting of eastern Laurentia from West Gondwana resulting in the opening of several intervening oceans.

Table D-7.3.1 Data Summary
St. Lawrence Rift Zone

Citation	Title	Description and Relevance to SSC
		<p>The Iapetus Ocean was initially defined as the early Paleozoic ocean between Baltica and Laurentia (Greenland); the Theic Ocean was defined as the ocean between Laurentia and Gondwana; and the Rheic Ocean between Baltica and Gondwana.</p> <p>Emphasizes that the subsequent usage of the name “Iapetus” to refer to the Paleozoic ocean off the Laurentia east margin became nearly universal, and that <i>sensu stricto</i> the Iapetus Ocean was closed in the Late Silurian Caledonia orogeny during the docking of Avalonia microcontinents with Laurentia. The remaining ocean that lay east of Avalonia is generally called Theic, leading the author to recognize the Paleozoic ocean east of Laurentia as Theia. This discussion uses the name Iapetus as given by various authors cited by Faill (1997a), recognizing the distinction between these three Paleozoic oceans.</p>
Higgins and van Breemen (1998)	The Age of the Sept Îles Layered Mafic Intrusion, Canada: Implications for the Late Neoproterozoic/Cambrian History of Southeastern Canada	<p>Authors obtained U-Pb ages of 565 ± 4 Ma for the Sept Îles layered mafic pluton located on islands and peninsulas of the Gulf of St. Lawrence. Combining these results with other published ages for Neoproterozoic to Cambrian igneous rocks from the Laurentian margin suggests three phases of magmatism:</p> <ol style="list-style-type: none"> 1. Tholeiitic dike emplacement was diachronous along the Laurentian margin: the Long Range dike swarm in Newfoundland was dated at 615 ± 2 Ma over a distance of 400 km (249 mi.; Kamo et al., 1989); Grenville dike swarm formed synchronously with the Ottawa graben at $590 \pm 2/-1$ Ma over a distance of 400 km (249 mi.; Kumarapeli, 1993; Kamo et al., 1995). These dike swarms may have been produced by one or two mantle plumes between 615 and 590 Ma, possibly one at Sept Îles. 2. Following dike emplacement, alkaline plutons intruded into a relatively large region spanning Quebec, Ontario, Greenland, and Scandinavia as early as 578 Ma and as late as the Sept Îles intrusion (565 Ma). The authors attribute these plutons to a major plume and triple junction located at Sept Îles instead of the location below the Sutton Mountains proposed by Kumarapeli (1993), but acknowledge that the two dike swarms could be the result of two mantle plumes separated by 25 Myr. The authors also observe that the alkaline plutons were intruded along rift faults that developed after the emplacement of dikes. 3. Undated diabase dikes and metabasaltic flows occur throughout the

Table D-7.3.1 Data Summary
St. Lawrence Rift Zone

Citation	Title	Description and Relevance to SSC
		<p>Northern Appalachians, indicating the earliest stages of the formation of the Iapetus Ocean. Tholeiitic lavas of the Tibbit Hill Formation have U-Pb zircon ages of 554 ± 4–2 Ma (Kumarapeli et al., 1989), and alkaline volcanic rocks at Skinners Cove, Newfoundland, have U-Pb ages of 550 ± 3–2 Ma (McCausland et al., 1997).</p>
Hodych and Cox (2007)	Ediacaran U-Pb Zircon Dates for the Lac Matapédia and Mt. St.-Anselme Basalts of the Quebec Appalachians: Support for a Long-Lived Mantle Plume During the Rifting Phase of Iapetus Opening	<p>U-Pb zircon ages for the Lac Matapédia basalt (565 ± 6 Ma and 556 ± 5 Ma) and the Mt. St.-Anselme basalt (550 ± 7 Ma) support the interpretation of a long-lived Sutton Mountains mantle plume. These data close the gap between the end of flood basalt and the beginning of plume magmatism and support a rift-drift transition at 540 Ma as opposed to 570 Ma (McCausland and Hodych, 1998). This hypothesis implies that Laurentia drifted northward more slowly than was suggested by McCausland and Hodych (1998).</p>
Kamo et al. (1995)	Age of the Grenville Dyke Swarm, Ontario–Quebec: Implications for the Timing of Iapetan Rifting	<p>Improves the geochronology of the Grenville dike swarm by obtaining U-Pb baddeleyite ages from the widest dikes throughout the Ottawa graben. These results give an age of 590 Ma, implying that the Grenville dike swarm was emplaced within a relatively short time span. These dikes are thought to have formed at the onset of rifting within the Ottawa graben, the Sutton Mountains triple junction, and the related segment of the Iapetan margin. Comparison with ages of similar rift-related igneous rocks along the Iapetan margin of Laurentia, including the Bakersville dike swarm of the Blue Ridge (570 Ma), Franklin swarm of northern Canadian Shield (723 Ma), and Long Range dikes of SE Labrador and Newfoundland (615 Ma), indicate that Iapetan rifting occurred along vast distances of the northern and eastern margins of Laurentia.</p> <p>The timing of initial rifting within the Ottawa graben is somewhat earlier than other parts of North America, suggesting that rift initiation progressed from the northern Laurentia margin at 723 Ma to Labrador and Newfoundland at 615 Ma, followed by the Grenville dike swarm at 590 Ma.</p>

Table D-7.3.1 Data Summary
St. Lawrence Rift Zone

Citation	Title	Description and Relevance to SSC
Kumarapeli (1985)	Vestiges of lapetan Rifting in the Craton West of the Northern Appalachians	Proposes that a mantle plume produced the initial ruptures of lapetan rifting along a triple junction that led to continental fragmentation and the development of an aulacogen in the Ottawa graben. Carbonatite complexes of the Ottawa and Saguenay grabens with ages of 565 and 564 Ma, respectively, support the view that these two rifts formed as parts of a single event. Alkaline to transitional bimodal volcanic rocks of the Tibbit Hill volcanics are deposited within the Sutton Mountains salient, east of the Ottawa graben, and are thought to be coeval with the Grenville dike swarm within the Ottawa graben. Interprets the Sutton Mountains as the triple junction that initiated lapetan rifting.
Kumarapeli (1993)	A Plume-Generated Segment of the Rifted Margin of Laurentia, Southern Canadian Appalachians, Seen Through a Completed Wilson Cycle	Improves upon the model presented by the author in 1983 with the addition of geochronology of dike swarms and volcanic rocks. Proposes that initiation of rifting was accompanied by the emplacement of the 590 Ma Grenville mafic dike swarm of tholeiitic composition. Rifting continued for 35 million years until 554 Ma when alkaline to transitional basalts erupted at the Sutton Mountains triple junction. This was quickly followed by a short period of rift-facies clastic sedimentation consisting of conglomerates attributed to a large river delta. The rift-drift transition is indicated by the deposition of open marine sedimentation, thought to have occurred 550 Ma because of the presence of early Cambrian fauna above this transition.
Kumarapeli et al. (1988)	Volcanism on the Passive Margin of Laurentia: An Early Paleozoic Analogue of Cretaceous Volcanism on the Northeastern American Margin	Transitional to alkaline basalts and mid-ocean ridge basalts (MORBs) found within the Granby nappe of SE Quebec provide evidence for late Cambrian to Early Ordovician volcanism within transverse fracture zones analogous to Early Cretaceous volcanism in the Atlantic. The authors acknowledge that this data set is not sufficient to determine whether the volcanism took place during the drifting phase of the continental margin, because the precise age of these rocks is not known. These allochthonous blocks are thought to represent slabs dislodged from the ancient shelf-margin sequence, possibly by faults of the Ottawa graben in addition to NE-trending faults.

Table D-7.3.1 Data Summary
St. Lawrence Rift Zone

Citation	Title	Description and Relevance to SSC
McCausland and Hodych (1998)	Paleomagnetism of the 550 Ma Skinner Cove Volcanics of Western Newfoundland and the Opening of the Iapetus Ocean	Authors obtained paleomagnetic data for volcanic flows and volcanoclastic sediments of the Skinner Cove Formation in western Newfoundland dated at 550 Ma that point to a paleolatitude of $19^{\circ}\text{S} \pm 9^{\circ}$. This result represents the paleolatitude of the Iapetus margin at that time. Comparison of these results to the 577 Ma Callander Complex of Ontario indicates rapid northward drift of Laurentia at approximately 570 Ma resulting from the opening of the Iapetus Ocean, which continued to the rift drift transition at approximately 550 Ma.
Puffer (2002)	A Late Neoproterozoic Eastern Laurentian Superplume: Location, Size, Chemical Composition, and Environmental Impact	Compiles a database of high field-strength elements for late Neoproterozoic to early Paleozoic flood basalts and dike swarms in eastern North America. Displaying these results on spider diagrams normalized to the bulk composition of the earth confirms that these rocks are derived from a mantle plume. The spatial distribution of these data reveals a peak concentration at the inferred Sutton Mountains triple junction, indicating that superplume magmatic activity peaked at 550 Ma. A second, earlier population of less geochemically enriched melts was derived from a subcontinental lithospheric mantle source mixed with mantle from a plume source. These older rocks (615–564 Ma) represent early lavas extruded from rifts, consistent with the early stages of mantle plume upwelling. The author favors the interpretation that these rocks are the result of one superplume as opposed to two plumes.
Ratcliffe (1987)	Basaltic Rocks in the Rensselaer Plateau and Chatham Slices of the Taconic Allochthon: Chemistry and Tectonic Setting	<p>Tholeiitic to transitional alkaline basalts flows, sills, and metasedimentary rocks represent a restricted period of basaltic volcanic activity associated with Iapetus rifting. These volcanic rocks are interbedded with greywacke interpreted as turbidite fan complexes extending into deeper water. These assemblages are thought to form as short-lived rift-stage volcanics on a structurally evolving cratonic margin.</p> <p>The author proposes that these rocks formed in a fault-controlled continental margin with high relief and a narrow shoreline. Continental flood basalts capped the basement rocks, with flows erupting through local fissures into the water, and flowed onto greywacke fans.</p>
St. Seymour and Kumarapeli (1995)	Geochemistry of the Grenville Dyke Swarm: Role of Plume-Source Mantle in Magma Genesis	Confirms a mantle source for the synrift Grenville dike swarm, suggesting that the triple junction formed over a mantle plume, with dikes crystallizing from melts derived from the cooler plume head.

Table D-7.3.1 Data Summary
St. Lawrence Rift Zone

Citation	Title	Description and Relevance to SSC
Walsh and Aleinikoff (1999)	U-Pb Zircon Age of Metafelsite from the Pinney Hollow Formation: Implications for the Development of the Vermont Appalachians	U-Pb zircon age of 571 ± 5 Ma for metafelsite from the Pinney Hollow Formation of Vermont records the age of rhyolitic volcanism and deposition in a largely pelitic sequence interpreted as a pre-shelf rift-clastic sequence. This age agrees with other ages from rift-clastic volcanic rocks in the Appalachians. The relative distribution and thickness of metavolcanic and metafelsic sections throughout the Appalachians suggest that the basin that the Pinney Hollow Formation was deposited into was already well developed when the 571 Ma metafelsite was deposited. Therefore, the 554 Ma age for the Tibbit Hill volcanic suite at the Sutton Mountains triple junction does not represent the first pulse of volcanic activity during the initial opening of the Iapetan basin in the Vermont and Quebec Appalachians. This age also validates that the Wood Peak fault is a significant thrust fault separating the autochthonous and para-autochthonous cover sequence rocks, which supports the interpretation that the Taconic root zone is located in the hinterland of the Vermont Appalachians on the eastern side of the Green Mountain massif.
Faulting in St. Lawrence		
Faure et al. (1996b)	State of Intraplate Stress and Tectonism of Northeastern America Since Cretaceous Times, with Particular Emphasis on the New England–Quebec Igneous Province	Along the Ottawa-Bonnechere graben, E-W-trending Cretaceous normal faults mark the contact between Paleozoic rocks to the south and Grenvillian basement to the north. The NE-SW-directed extension associated with NW-SE-trending normal faults is more widespread and older than the N-S-directed extension associated with E-W-trending normal faults. The Ottawa-Bonnechere graben and associated basement faults acted as localized zones of weakness in the early stage of Cretaceous extension, resulting in reorientation of the regional stress field and formation of the localized zone of N-S-directed extension.

Table D-7.3.1 Data Summary
St. Lawrence Rift Zone

Citation	Title	Description and Relevance to SSC
Kumarapeli and Saul (1966)	The St. Lawrence Valley System: A North American Equivalent of the East African Rift Valley System	<p>Proposes a rift origin for the St. Lawrence valley system, including the Ottawa-Bonnechere and Saguenay grabens. Evidence supporting this conclusion includes the following:</p> <ul style="list-style-type: none"> • Escarpments on the NW side of the St. Lawrence valley, north side of the Ottawa Bonnechere graben, and western margin of the Champlain valley. • South of the Ottawa-Bonnechere graben, tilting of the Madawaska Highlands to the south, NW tilting of the Adirondack massif, north tilting of a Laurentian block south of the Saguenay graben, and south block tilting of the Gaspé Peninsula. • En echelon normal faults along the NW boundary with vertical displacements between 450 and 1,200 m. • St. Barnabe fault is a 55 km (34 mi.) normal fault on the SE margin with 600 m of downthrow to the west. • Concentrations of historical seismicity along the St. Lawrence and Ottawa valleys and the St. Lawrence trough. • Presence of a negative Bouguer anomaly in the rift valley. • Connection of the St. Lawrence valley with the Mississippi embayment. • Westward continuation of the Ottawa-Bonnechere graben with the Midcontinent rift system. <p>Because the publication pre-dated plate tectonics, many aspects of the authors' ideas are not consistent with current tectonic models of the region. After comparing St. Lawrence rift system to East African rift system, the authors suggest the Great Lakes may be analogous to Lakes Victoria and Kyoga. The authors also associate Montereian alkaline intrusives with St. Lawrence valley. Recent work associates this with Cretaceous intrusion associated with reactivation of the Ottawa-Bonnechere graben. .</p>

Table D-7.3.1 Data Summary
St. Lawrence Rift Zone

Citation	Title	Description and Relevance to SSC
Lamontagne et al. (2003)	Seismotectonic Characteristics of the Lower St. Lawrence Seismic Zone, Quebec: Insights from the Geology, Magnetism, Gravity, and Seismics	Reviewed the seismotectonic model of the lower St. Lawrence seismic zone from focal depths, focal mechanisms, gravity and magnetic data, offshore seismic lines, and mapped onshore geology. Concluded that seismicity is generally located where regional Iapetan and later faults change orientation from SW-NE to mostly E-W. Based on the correlation of seismicity with faults and geopotential lineaments, small earthquakes are thought to have occurred in fractured rock as opposed to large normal faults. Localized seismicity of the lower St. Lawrence seismic zone may be the result of enhanced stress due to a number of factors, including change in regional fault strike, mafic rocks of the Sept Îles layered igneous complex, presence of fluids at depth, and low coefficient of friction where fault gouge exists.
Lemieux et al. (2003)	Structural Analysis of Supracrustal Faults in the Charlevoix Area, Quebec: Relation to Impact Cratering and the St-Laurent Fault System	<p>Two major sets of fault orientations (N290–N320 and N020–N040) are found outside the impact zone with minor fault sets trending N270–N280 and N000–N020. Within the impact crater, fault orientations are more scattered but are similar to the NW- and NE-trending systems of the external domain. The spread of orientations within the central portion of the crater is attributed to the impact-related polygonal pattern of normal faults, whereas the NW and NE fault sets represent the youngest reactivation.</p> <p>Coarse-grained cataclastic breccias up to 50 m thick are exposed along brittle faults striking NE and NW outside the impact crater. Similar cataclastic breccias are also found within the impact crater but are usually less than a few meters thick. Polymictic clastic matrix breccia is found exclusively within the impact crater. Fragments of cataclastic breccia are present, suggesting recurrent brecciation during incremental faulting events. Pseudotachylyte and foliated gouge are locally related to the cataclastic breccia, indicating that these rocks originate from a post-impact, single, and progressive tectonic event along the St. Lawrence rift system.</p> <p>The St-Laurent fault influenced the deposition of Ordovician deposits during late stages of the Taconian orogeny by syndepositional faulting preserved as major lateral thickness variations within the section, presence of slump deformation in almost all stratigraphic units, preservation of pseudotachylyte within synsedimentary breccias, and occurrence of fault breccia clasts. However, the geometry and structural characteristics of faulting are consistent with Mesozoic fault reactivation due to rifting of the North Atlantic region.</p>

Table D-7.3.1 Data Summary
St. Lawrence Rift Zone

Citation	Title	Description and Relevance to SSC
Rocher et al. (2003)	Brittle Fault Evolution of the Montréal Area (St. Lawrence Lowlands, Canada): Rift-Related Structural Inheritance and Tectonism Approached by Palaeostress Analysis	<p>NW-SE extension associated with the opening of the Iapetus Ocean resulted in the formation of N040-trending faults along the north shore of the St. Lawrence lowlands, the development of three major N090-trending faults that define a succession of horsts and grabens on Montreal and Jesus islands, and N120-trending faults in the Montreal area. The three N090-trending faults have the following geometries:</p> <ol style="list-style-type: none"> 1. The Bas-Sainte-Rose fault zone, the northernmost series of N090-trending faults in the Montreal area, is a steeply north-dipping fault with approximately 200 m of vertical displacement and nearly 3 km (2 mi.) of apparent left-lateral offset. Offsets on the Bas-Sainte-Rose fault zone decrease as the fault zone extends westward, where it apparently crosscuts the N020-trending Rivière-aux-Mille-Iles fault zone. 2. Rapide-du-Cheval-Blanc consists of a series of steeply south-dipping normal faults (the Ile-Bizard, the Rapide-du-Cheval-Blanc, and Outremont faults) with a total vertical offset of approximately 100 m. 3. The Sainte-Anne-de-Bellevue fault zone is a north-dipping normal fault with a left-lateral strike-slip component in the southern part of Montreal Island. Its vertical offset has not been precisely determined. <p>All three faults clearly crosscut NNE-SSW-trending folds from the Appalachian Chambly-Fortierville syncline system in the Trois-Rivières seismic zone.</p> <p>WNW-ESE compressions followed by minor NNW compressional events are associated with Appalachian thrusting. WNW compression reactivated N090-trending faults into strike-slip right-lateral faults, and N040–070 and N120 faults as reverse to strike-slip faults. Subsequent NNW compression is responsible for strike-slip conjugate faults trending NW-SE and NNE.</p> <p>NE-SW and NNW-SSE extension is associated with the opening of the North Atlantic–Labrador Sea and reactivated faults with normal to strike-slip motions. NNW extension is responsible for the horst-and-graben geometry of the major N090 normal faults described above. Late NE-SW compression is recorded in Montereian plutons.</p> <p>NE-SW compression postdating these events is associated with the formation of strike-slip faults that crosscut the Montereian intrusions and is consistent with the current stress regime.</p>

Table D-7.3.1 Data Summary
St. Lawrence Rift Zone

Citation	Title	Description and Relevance to SSC
Roden-Tice, Brandt, and Tremblay (2009)	Apatite Fission-Track Evidence for Late Paleozoic to Early Mesozoic Unroofing and Potential Fault Reactivation Along the Saguenay River Graben, Quebec	Apatite fission-track age discontinuities across the Montmorency and Saint-Laurent faults are consistent with Late Jurassic to Early Cretaceous fault reactivation and uplift.
Spencer et al. (1989)	The Extension of Grenville Basement Beneath the Northern Appalachians: Results from the Quebec-Maine Seismic Reflection and Refraction Surveys	A master decollement separating autochthonous Grenville basement from overlying allochthonous rocks of the Appalachian orogen extends over a distance of 200 km (125 mi.) and can be traced from shallow depths beneath the St. Lawrence lowlands SE to about 25 km (15.5 mi.) depth beneath the SE edge of the Chain Lakes massif. Basement is offset by closely spaced en echelon normal faults with displacements between 200 and 1,000 m interpreted as lapetan growth faults. The Baie Verte–Brompton line, separating Cambrian and Ordovician continental slope and rise deposits from oceanic arc and magmatic assemblages to the south, including the Chain Lakes massif, is imaged as a shallow, thin-skinned structure. The Chain Lakes terrane is thought to underlie much of the Connecticut Valley–Gaspé Synclinorium. The Acadian Guadeloupe fault disrupts the master decollement of the Taconian orogeny and thrust the Connecticut Valley–Gaspé Synclinorium over the Chain Lakes massif.
St. Julien and Hubert (1975)	Evolution of the Taconian Orogen in the Quebec Appalachians	Describes 11 lithostratigraphic assemblages distributed among the autochthonous, external, and internal domains of Quebec Appalachians. The autochthonous domain contains Cambrian and Ordovician sandstones and carbonates representing transgressive shelf deposits, Middle and Upper Ordovician flysch deposits, and Upper Ordovician shale and sandstone representing the post-tectonic regressive sequence. This domain contains E-W- and N30E-trending normal faults active between late Precambrian and Late Ordovician.

Table D-7.3.1 Data Summary
St. Lawrence Rift Zone

Citation	Title	Description and Relevance to SSC
Tremblay and Lemieux (2001)	Supracrustal Faults of the St. Lawrence Rift System Between Cap-Tourmente and Baie-Saint-Paul, Quebec	<p>The Cap-Tourmente and St. Lawrence faults are late Proterozoic–early Paleozoic normal faults attributed to rifting during the opening of the Iapetus Ocean.</p> <p>The St. Lawrence fault trends N020–N050 and dips 60°–70° to the SE. Fault rocks consist of fault breccia, cataclastite, foliated gouge, and pseudotachylyte with a minimum thickness of 20 m near Sault-au-Cochon. Fault rocks exposed at Cap-Tourmente consist of 10–15 m thick zones of protocataclasite, cataclasite, and fault breccia. Within the Charlevoix area, the St. Lawrence fault is characterized by a well-developed and extensive series of cataclastic rock, gouge, and associated pseudotachylyte.</p> <p>The Cap-Tourmente fault trends E-W and dips approximately 80° to the south. Fault rocks consist mostly of fault breccia more than 10 m thick, as well as cataclastic rocks and dark pseudotachylyte veins. The St. Lawrence fault is crosscut by the Cap-Tourmente fault at Cap-Tourmente.</p> <p>West of Cap-Tourmente, the Montmorency Falls fault occupies the same structural position as the St. Lawrence fault, suggesting that they formed from an echelon fault trending parallel to the axis of the St. Lawrence rift.</p> <p>The Cap-Tourmente fault possibly represents a transfer fault, producing an oblique relay between two longitudinal normal faults.</p> <p>The St. Lawrence fault crosses the Charlevoix impact crater without major trend deflection or fault offsets within or at the boundaries of the Devonian impact structure. This observation suggests that impact-related faults did not significantly alter the orientation of preexisting structures and that reactivation is younger than the impact structure, most probably concurrent with the opening of the Atlantic Ocean in the Mesozoic.</p>
Tremblay et al. (2003)	Supracrustal Faults of the St. Lawrence Rift System, Quebec: Kinematics and Geometry Revealed by Field Mapping and Marine Seismic Reflection Data	<p>This paper builds on work presented by Tremblay and Lemieux (2001) and presents strike orientations, dip angles, and pitch angles for faults with evidence for frictional sliding in the St. Lawrence rift system.</p> <p>NE-trending longitudinal faults show three trends (N025, N040, and N070) and generally dip to the SE, although a minor number dip to the NW. Transverse faults show two trends (N290 and N310) and dip to the NE or SW, which is consistent with the horst-and-graben geometry. Both sets of faults are high-angle faults with dip angles averaging 75°–80°. The pitch value of fault</p>

Table D-7.3.1 Data Summary
St. Lawrence Rift Zone

Citation	Title	Description and Relevance to SSC
		<p>lineations is greater than 70°, indicating that most structures are dip-slip faults. Longitudinal and transverse faults show mutual crosscutting relationships, suggesting that they represent conjugate structures related to the same tectonic event.</p> <p>The St-Laurent fault has experienced at least 800 m of vertical throw at Sault-au-Cochon. The Cap-Tourmente fault has a minimum vertical fault throw of 700 m. The Montmorency fault has an 80 m fault scarp near Quebec City; stratigraphic analysis suggests that fault throw should be less than 150 m, which is considerably less than the other faults. Several offshore faults subparallel to that fault may have vertical downthrow displacements up to 1 km (0.6 mi.).</p> <p>Longitudinal faults likely result from the development of en echelon faults trending parallel to the rift axis, and transfer faults represent transfer faults or accommodation zones. Variations in fault throw are likely a result of propagation of extension along transfer faults.</p> <p>The presence of cataclastic rocks, pseudotachylytes, and fault gouge is consistent with changes of deformation mechanics during progressive and incremental deformation in the upper crust.</p> <p>High-resolution seismic profiles in the St. Lawrence estuary indicate that the Laurentian Channel trough transitions from a half graben to a graben structure from SW to NE.</p> <p>Tremblay et al. (2003) speculate that reactivation of the St. Lawrence rift system is post-Ordovician, younger than the Devonian impact cratering event, and experienced additional fault throw and shoulder uplift during the Mesozoic opening of the North Atlantic.</p>
<i>Faulting in the Ottawa-Bonnechere Graben</i>		
Mereu et al. (1986)	The 1982 COCRUST Seismic Experiment Across the Ottawa-Bonnechere Graben and Grenville Front in Ontario and Quebec	Results of the 1982 Canadian Consortium for Crustal Reconnaissance Using Seismic Techniques (COCRUST) long-range seismic refraction experiment show a sharp, step-like displacement of the Moho beneath the south shoulder of the Ottawa graben, confirming the deep-seated nature of its faults and penetration of mantle melts into the crust. Furthermore, the COCRUST surveys show a poorly defined Moho at unusually shallow depths beneath the graben.

Table D-7.3.1 Data Summary
St. Lawrence Rift Zone

Citation	Title	Description and Relevance to SSC
Rimando and Benn (2005)	Evolution of Faulting and Paleo-Stress Field Within the Ottawa graben, Canada	Authors observe three periods of faulting in Cambro-Ordovician sedimentary rocks within the eastern end of the Ottawa graben, near Ottawa. The oldest generation of faults formed in a stress field with a horizontal maximum compressive stress (σ_1) oriented NW. These structures are kinematically congruent with the compression direction associated with the closing of the Iapetus Ocean. The second generation of faults indicates a WNW-oriented σ_1 and coincides with the emplacement of Cretaceous carbonatite dikes. The third generation of faults has a σ_1 oriented SW, which is consistent with the post-Cretaceous stress field in eastern North America.
<i>Faulting in the Saguenay Graben</i>		
Du Berger et al. (1991)	The Saguenay (Quebec) Earthquake of November 25, 1988: Seismologic Data and Geologic Setting	The Saguenay graben is defined by the Lac Tchitogama and Ste-Marguerite River normal faults on the north wall and the Lac Kénogami normal fault on the south wall. Ordovician limestones show downthrow of 500 m along the north wall. Subvertical brittle faults are found within and outside the graben. Lineaments in the regional cluster at 000°, 015°, 030°, 050°, 105°, and 160°. The 015 and 030 lineaments correspond to NNE late Grenvillian ductile belts and some post-Ordovician brittle faults. The St. Lawrence rift reactivated the 030° trend and produced the 050° trend. The 160 trend is parallel to glacial strike. The 105° trend is prominent only in the rosette of the Saguenay graben. The 000° trend corresponds to a complex array of en echelon oblique short breaks near the St. Maurice lineament, suggesting that the St. Maurice marks the transition between two structural domains.
Roden-Tice, Brandt, and Tremblay (2009)	Apatite Fission-Track Evidence for Late Paleozoic to Early Mesozoic Unroofing and Potential Fault Reactivation Along the Saguenay River Graben, Quebec	Apatite fission-track age discontinuities across the Sainte-Marguerite fault suggest Late Triassic to Early Jurassic reactivation, whereas age discontinuities across the Lac Kénogami fault to the south indicate Middle Jurassic reactivation.

Table D-7.3.1 Data Summary
St. Lawrence Rift Zone

Citation	Title	Description and Relevance to SSC
<i>Stratigraphic Evidence for Fault Activity</i>		
Hersi et al. (2003)	Reappraisal of the Beekmantown Group Sedimentology and Stratigraphy, Montreal Area, Southwestern Quebec: Implications for Understanding the Depositional Evolution of the Lower-Middle Ordovician Laurentian Passive Margin of Eastern Canada	Detailed lithostratigraphic mapping and conodont biostratigraphy of the Beekmantown Group of SE Quebec indicates that the platform evolved as a distally steepened ramp during deposition of the Lower Ordovician Theresa Formation and the Ogdensburg Member of the Beauharnois Formation.
Lavoie et al. (2003)	Stratigraphic Framework for the Cambrian-Ordovician Rift and Passive Margin Successions from Southern Quebec to Western Newfoundland	In the Quebec Reentrant, platform rocks were only marginally involved in the tectonic stacking of the Taconic orogeny and form a spatially restricted frontal Taconian deformation zone known as the para-autochthonous or imbricate fault domain and therefore not considered part of the Humber Zone. The Quebec Reentrant is rooted in the autochthonous St. Lawrence platform. These structural relationships allow for stratigraphic and paleogeographic scenarios for the early evolution of the Quebec-Newfoundland segment of the continental margin slope of Laurentia. Neoproterozoic to latest early Cambrian rift volcanics are overlain by rift-drift transition successions of the early Cambrian Sauk I sequence. A global sea-level lowstand resulted in an unconformity that separates these rocks from shallow marine middle Cambrian to Middle Ordovician rocks of the Sauk II and Sauk III subsequences. An extensive debris flow unit resedimented the middle Cambrian slope succession and is attributed to tectonic instability during the middle to late Cambrian. The authors suggest that reactivation of the Saguenay graben could be responsible for the anomalous upper Cambrian succession. Similar syndepositional tectonic activity is observed in the younger St. Lawrence platform succession in the Charlevoix area during the Middle to Late Ordovician. The authors present locations of reentrants and promontories for the eastern margin of Laurentia farther north than those of Thomas (1991).

Table D-7.3.1 Data Summary
St. Lawrence Rift Zone

Citation	Title	Description and Relevance to SSC
Longuépée and Cousineau (2005)	Reappraisal of the Cambrian Glauconite-Bearing Anse Maranda Formation, Quebec Appalachians: from Deep-Sea Turbidites to Clastic Shelf Deposits	Paleogeographic reconstruction led to a significant reinterpretation of the sedimentary environment of the Anse Maranda Formation, originally explained as proximal turbidites of a deep-sea fan and now explained as shelf sediments deposited in storm-influenced deep subbasins seaward of a headland (Montmorency promontory). These sediments were deposited along a narrow shelf with irregular topography south of the Saguenay graben.
Seismicity and Focal Mechanism Data		
Adams and Basham (1991)	The Seismicity and Seismotectonics of Eastern Canada	The western Quebec seismic zone consists of two bands of seismicity. The western band trends slightly west of northwest and lies along the Ottawa River between Lake Timiskaming and Montreal. This portion of the western Quebec seismic zone is attributed to rift faults of the Ottawa graben. Focal mechanisms for earthquakes within this zone are consistent with thrust faulting on NW-striking faults. The authors dispute the hypothesis that Mesozoic extension in the St. Lawrence rift extends SE into the Great Lakes.
Baird et al. (2009)	Stress Channeling and Partitioning of Seismicity in the Charlevoix Seismic Zone, Quebec, Canada	<p>Seismicity is localized along two elongate bands of seismicity bounded by rift faults extending NE of the Charlevoix impact crater. In a 2-D stress model, faults are represented as frictional discontinuities, and the impact crater as an elastic continuum of reduced modulus. Stress trajectories flow around the weak impact crater, concentrating stress along weak faults into the impact crater, resulting in seismicity localized in linear bands. The asymmetric placement of the rift faults through the crater results in increased seismicity potential along the rift, north of the crater.</p> <p>Observed seismicity is therefore interpreted as a result of stress concentration due to the interaction of the crater (local zone of weakness) and rift faults (large-scale weak zone). Small to moderate seismicity occurs within the crater, and larger earthquakes are localized along the rift faults.</p> <p>Modeling in 3-D would be able to accurately represent the bowl shape of the crater but may not be able to explain why seismicity extends below the crater into Grenville basement. Current observations of reverse reactivation of rift faults associated with glacial rebound could not be assessed with the 2-D model presented in this paper and would need to be examined with a 3-D model.</p>

Table D-7.3.1 Data Summary
St. Lawrence Rift Zone

Citation	Title	Description and Relevance to SSC
Bent (1992)	A Re-examination of the 1925 Charlevoix, Québec, Earthquake	<p>Analysis of additional waveforms resulted in source parameters of strike $42^\circ \pm 7^\circ$, dip $53^\circ \pm 7^\circ$, rake $105^\circ \pm 10^\circ$, depth 10 km (6.2 mi.), seismic moment $3.1 \pm 2.5 \times 10^{25}$ dyne cm (M_w 6.2), M_s 6.2 ± 0.3, m_b 6.5 ± 0.4, source duration 5 sec, and stress drop 35 bars. Due to insufficient 1-sec period data, m_{bLg} was not determined; however, Street and Turcotte (1977) obtained a m_{bLg} 6.6, and Atkinson and Boore (1987) obtained a m_{bLg} 6.8. Felt area estimates range from 3.3×10^6 km² (Street and Lacroix, 1979) to 5.2×10^6 km² (Smith, 1962). Drysdale and Cajka (1989) obtained a m_{bLg} 6.1 using Nuttli et al. (1979) and m_{bLg} 6.2 using Toro and McGuire (1987). The dip is shallower than would be expected from observed surface faults but consistent with recent seismicity. The focal mechanism is consistent with horizontal compression in the NW-SE direction that is orthogonal to the regional stress field, indicating an anomalous stress field in Charlevoix that may be depth dependent.</p>
Bent (1996a)	An Improved Source Mechanism for the 1935 Timiskaming, Quebec Earthquake from Regional Waveforms	<p>Analysis of seismograms from 11 stations for the November 1, 1935, Timiskaming earthquake led to the determination of seismic moment of $2.3 \pm 1.3 \times 10^{25}$ dyne cm, corresponding to M_w of 6.1 ± 0.2.</p>
Lamontagne and Ranalli (1996)	Thermal and Rheological Constraints on the Earthquake Depth Distribution in the Charlevoix, Canada, Intraplate Seismic Zone	<p>Compares the depth distribution of Charlevoix earthquakes to rheological models of the region. The maximum depth of earthquakes can be controlled by either the brittle-ductile transition or the velocity-weakening to velocity-strengthening fault behavior. The rheological change at the brittle-ductile transition was modeled by calculating geotherms assuming a variety of rock compositions in the upper and middle crust. The depth distribution of earthquakes in Charlevoix requires geotherms very close to the upper limit for felsic rocks and a wet lower crust. The temperature-controlled sliding stability transition can occur at 300°C and 450°C for quartz or feldspar plasticity. Hydrolytic weakening of feldspars at 350°C occurs at 25 km (15.5 mi.) for the upper geotherms. The maximum crustal stress difference has an upper limit of about 100–200 MPa, requiring high pore fluid pressure or low coefficient of friction in mid- to lower crust. Thrust reactivation of steeply dipping faults requires a low coefficient of friction. The authors attribute the presence of earthquakes in the Charlevoix region to brittle-ductile transition deeper than 25 km (15.5 mi.), corresponding to higher than average geotherms, onset of ductility for hydrated feldspar at about 350°C, high pore-fluid pressure and a low friction coefficient, possibly related to unhealed zones of intense fracturing.</p>

Table D-7.3.1 Data Summary
St. Lawrence Rift Zone

Citation	Title	Description and Relevance to SSC
Lamontagne and Ranalli (1997)	Faults and Spatial Clustering of Earthquakes near La Malbaie, Charlevoix Seismic Zone, Canada	Focal mechanisms for earthquakes larger than M 3 show reverse faulting, whereas smaller-magnitude earthquakes indicate both normal and strike-slip mechanisms, suggesting that local stress and/or strength conditions control their occurrence. Focal mechanisms for larger events of the Charlevoix seismic zone, however, suggest reactivation of paleo-rift faults in response to regional stresses. The distribution of spatially clustered events (doublets and triplets) within the Charlevoix seismic zone indicates that very few events have occurred on the same fractures with similar focal mechanisms, implying that these fault zones occur in highly fractured rocks. These observations indicate that the Charlevoix seismic zone is characterized by highly fractured zones responding to regional stresses and local perturbations in stress or strength, possibly enhanced by pore fluid pressures.
Ma and Atkinson (2006)	Focal Depths for Small to Moderate Earthquakes ($M_N \geq 2.8$) in Western Quebec, Southern Ontario, and Northern New York	Performs regional depth-phase modeling of earthquakes occurring in southern Ontario, western Quebec, and northern New York between 1980 and 2004. Events with depths greater than 15 km (9.3 mi.) are restricted to the Ottawa graben and western Quebec seismic zone. The wide depth distribution could indicate faults of throughgoing crustal extent or different faults that occur at different depths in the crust. In the entire study region, focal depths cluster at 5, 8, 12, 15, and 22 km (3, 5, 7.5, 9.3, and 13.7 mi.) and may reflect layering in seismogenic properties within the crust.
Ma and Eaton (2007)	Western Quebec Seismic Zone (Canada): Clustered, Midcrustal Seismicity Along a Mesozoic Hotspot Track	Deep earthquakes (greater than 17 km, or 10.6 mi., in depth) are localized as clusters at Timiskaming, Maniwaki, Mont Laurier, and Adirondack. The Timiskaming cluster is located near the 1935 Timiskaming earthquake, has a lower <i>b</i> -value than the other clusters and the regional average, and is spatially associated with faults of the Ottawa-Bonnechere graben. The authors speculate that heat from the hotspot track weakened faults of the Ottawa-Bonnechere graben, which explains the lack of historical seismicity along most of the extent of the graben system.

Table D-7.3.1 Data Summary
St. Lawrence Rift Zone

Citation	Title	Description and Relevance to SSC
<i>Paleoseismic Investigations</i>		
Aylsworth et al. (2000)	Did Two Massive Earthquakes in the Holocene Induce Widespread Landsliding and Near-Surface Deformation in Part of the Ottawa Valley, Canada?	Examines large prehistoric landslides in abandoned channels of the Ottawa River and disturbed sediment of the erosional plane adjacent to the Ottawa River. Radiocarbon ages for buried wood and plant material from landslide debris cluster at 4,550 yr BP, which are thousands of years younger than the age of paleochannel abandonment. This observation cannot be attributed to either fluvial erosion or wet-weather-induced landslides. East of the landslides, disturbed sediment and possible sand boils dated at 7,060 yr BP are preserved within the flat erosional plane adjacent to the Ottawa River. These two age distributions are attributed to paleoearthquakes of uncertain magnitude and source.
Doig (1990)	2300 Yr History of Seismicity from Silting Events in Lake Tadoussac, Charlevoix, Quebec	Inferred a variable recurrence rate for the Charlevoix seismic zone from silt layers in lakes due to earthquake-induced landslides. Some silt layers in the section were correlated with historical earthquakes from 1638, 1663, 1791, 1870, and 1925. From 320 BC to AD 800, determined a 120-year recurrence interval, 270 years from AD 800 to 1500, and 75 years from AD 1500 to the present.
Doig (1991)	Effects of Strong Seismic Shaking in Lake Sediments, and Earthquake Recurrence Interval, Témiscaming, Quebec	Sampled lake sediments from Lac Tee, located within 15 km (9.3 mi.) of the epicenter of the 1935 magnitude 6.3 Timiskaming earthquake. Observed three silt layers in six sediment cores attributed to earthquake-induced landslides. A 15–22 cm thick chaotic mixture of black to brown organic material and large, partly tabular fragments of previously formed silt layers is interpreted as sediment redeposit during the 1935 Timiskaming earthquake. The basal silt layer may imply a two-stage event, such as a small foreshock or a major aftershock. A second 6 cm thick silt layer in core 4 and a 1–2 mm thick silt layer in cores 2 and 6 are interpreted as the result of a distant or smaller earthquake. A third silt layer at 100 cm overlain by gyttja containing lumps of silt is interpreted as a similar-sized event as the 1935 Timiskaming earthquake. The upper 2–3 cm from cores 2, 4, and 6 contain brown, homogeneous flocculent gyttja interpreted as normal accumulation of sediment since 1935. This sedimentation rate was used to infer ages of 400 and 1,500 years for the second and third silt layers, respectively. Doig (1991) does not explicitly correlate the second silt layer to the 1663 Charlevoix earthquake. This data set suggests two magnitude 6–6.5 events in 1,500 years.

Table D-7.3.1 Data Summary
St. Lawrence Rift Zone

Citation	Title	Description and Relevance to SSC
Doig (1998)	3000-Year Paleoseismological Record from the Region of the 1988 Saguenay, Quebec, Earthquake	Author has determined a recurrence interval ranging from 350 to 1,000 years for the Saguenay graben based on evidence of earthquake-induced landslide deposits within lakes near the epicenter of the 1988 earthquake.
Filion et al. (1991)	A Chronology of Landslide Activity in the Valley of Rivière du Gouffre, Charlevoix, Quebec	Samples of tree trunks buried in landslide flow materials were collected from four sectors along the Gouffre River between Saint-Urbain and Baie-Saint-Paul. The age distribution of tree trunks indicates that landslides have occurred at 5,670, 3,170, 2,500, 1,870 yr BP, with most occurring less than 600 yr BP. Comparison of tree-ring widths throughout the study area suggests that trees died during the latent period between the 1662 and 1663 growing seasons, possibly due to synchronous landslides. The authors interpret these two landslides as having been caused by the February 1663 Charlevoix earthquake. These results provide no evidence for the 1925 earthquake. The authors emphasize the importance of tree-ring techniques to delineate the areal extent of landslides caused by the 1663 earthquake and to caution against exaggerating the geomorphic consequences of earthquakes.
Tuttle and Atkinson (2010)	Localization of Large Earthquakes in the Charlevoix Seismic Zone, Quebec, Canada, During the Past 10,000 Years	Provides evidence for three Holocene paleoearthquakes in Charlevoix with $M \geq 6.2$, including at least two prehistoric episodes at 5,000 and 10,000 years ago.
Tuttle et al. (1990)	Liquefaction and Ground Failure Induced by the 1988 Saguenay, Quebec, Earthquake	Sand boil deposits and ground fissures were documented immediately following the November 25, 1988, $M 5.9$ Saguenay earthquake. Lateral spreading was the principal mode of ground failure during the 1988 earthquake and in the past, with displacements on the order of centimeters.
Tuttle et al. (1992)	Liquefaction Induced by Modern Earthquakes as a Key to Paleoseismicity: A Case Study of the 1988 Saguenay Earthquake	One, possibly two, earthquakes caused pre-1988 liquefaction features identified in Tuttle et al. (1990). One has a well-constrained age of 340 ± 70 radiocarbon yr BP, possibly corresponding to the 1663 Charlevoix earthquake.

Table D-7.3.2 Data Summary
Great Meteor Hotspot Zone

Citation	Title	Description and Relevance to SSC
<i>Geologic Evidence for Hotspot Track</i>		
Adams and Basham (1991)	The Seismicity and Seismotectonics of Eastern Canada	Postulated that differential uplift of the shield may have thermally stressed and fractured Precambrian crust during passage of the hotspot. Attributed localized release of seismic energy to this weakened crust. Speculated that New England may not exhibit same rates of seismicity because plutonism may have healed deep crustal fractures.
Crough (1981)	Mesozoic Hotspot Epeirogeny in Eastern North America	This study attributes a 600 km (373 mi.) wide zone of epeirogeny in SE Canada and New England during the Cretaceous and early Tertiary to the Great Meteor hotspot as evidenced by apatite fission-track dating.
Duncan (1984)	Age Progressive Volcanism in the New England Seamounts and the Opening of the Central Atlantic Ocean	Duncan (1984) obtained radiometric ages for dredged volcanic rocks from seven of the New England seamounts and concluded that the seamounts increase in age from SE (82 Ma for the Nashville seamount) to NW (103 Ma for the Bear seamount). Linear rate of migration of volcanisms of 4.7 cm/yr determined from these ages is in agreement with age of the Corner seamounts (70–75 Ma) and the youngest phase of igneous activity in White Mountains (100–124 Ma).
Faure et al. (1996b)	State of Intraplate Stress and Tectonism of Northeastern America Since Cretaceous Times, with Particular Emphasis on the New England–Quebec Igneous Province	<p>Performed a paleostress analysis of Cretaceous dyke trends and regional- and mesoscopic-scale faults from the Montereian plutons. Dykes display ESE-WNW and ENE-WSW trends and are spatially distributed in three E-W-trending dyke swarms 75 by 300 km (47 by 186 mi.) in area. Most dykes surrounding Cretaceous plutons are radially distributed and perpendicular to contacts with hosting sedimentary rocks. Leucocratic dykes occur closer to plutons and disappear within 3–4 km (2–2.5 mi.), likely recording local stress effects due to pluton emplacement. Crosscutting dykes clearly show a dominant E-W-trending orientation. Lamprophyre dykes occur independently of plutons and strike parallel to regional dyke swarms, recording regional far-field stresses.</p> <p>Southwest of Mont Brome and around Mont Megantic, N-S- to NE-SW-trending dykes found in slates strike parallel to the regional foliation of Taconic or Acadian metamorphic rocks. Their emplacement is controlled by preexisting anisotropy and, therefore, poorly records the paleostress. NW-SE-trending dykes indicate NE-SW-striking extension with a slight clockwise rotation near Montreal. E-W-trending dykes indicate a N-S-striking extension. In some</p>

Table D-7.3.2 Data Summary
Great Meteor Hotspot Zone

Citation	Title	Description and Relevance to SSC
		<p>plutons, these E-W-trending dykes crosscut radially distributed dykes.</p> <p>Normal faults in the region display two orientations:</p> <ol style="list-style-type: none"> 1. E-W-trending normal faults are found predominantly in the Montreal area parallel to graben boundaries and the axis of the Monteregian hills. These faults have vertical offsets ranging between 100 and 430 m (328 and 1,411 ft.) and record homogeneous N-S-trending extension. 2. NW-SE to WNW-ESE-trending normal faults record NE-SW-trending extension and are found everywhere in Quebec. These faults trend obliquely to graben boundaries with less than 100 m (328 ft.) of vertical offset. The stress orientation varies between NNE-SSW near Ottawa and Montreal and ENE-WSW in southern Quebec. <p>The NW-SE to WNW-ESE faults are older than the E-W-trending faults but exhibit crosscutting relationships, suggesting that some were reactivated during the formation of the E-W-trending faults. Some E-W-trending brittle faults and joints are observed in several Cretaceous plutons with similar orientations to dykes that are locally crosscut by these normal faults, suggesting that dyke emplacement and faulting are contemporaneous. The NE-SW-directed extension is more widespread and older than the N-S-directed extension, suggesting that the Ottawa-Bonnechere graben and associated basement faults acted as localized zones of weakness in the early stage of Cretaceous extension, resulting in reorientation of the regional stress field and formation of the localized zone of N-S-directed extension.</p> <p>These orientations are attributed to to an initial NE-SW extension event associated with rifting between Labrador and Greenland at 140 Ma, opening of the South Atlantic at 130 Ma, and related reactivation of the Temiskaming graben. Subsequent N-S-oriented extension associated with the emplacement of the Monteregian Hills corresponds to global fragmentation of Pangaea when Iberia separated from Newfoundland when dominant tensional stress propagated along the Labrador rift.</p> <p>Conjugate sets of NE-SW dextral and ESE-WNW sinistral strike-slip faults and WNW-SSW reverse faults provide evidence for a compressional stress regime postdating emplacement of Cretaceous plutons. Stress regime shifted to ENE-WSW-directed compressional in early Tertiary when oceanic spreading rate decreased due to an increasing number of convergent boundaries in Pacific.</p>

Table D-7.3.2 Data Summary
Great Meteor Hotspot Zone

Citation	Title	Description and Relevance to SSC
Faure et al. (2006)	Paleostress Analysis of Atlantic Crustal Extension in the Quebec Appalachians	Fault stress tensors indicate that most E-W- to ESE-WNW-oriented stress is found in Montreal and Gaspé area, whereas SE-NW stress is found in SE Quebec. Late Triassic–Jurassic dikes in New England and southern Quebec indicate SE-NW-oriented extension consistent with fault slip stress. The N-S-trending portion of a Jurassic dike in southern Quebec is consistent with regional E-W extensional stress axis, whereas the NE-SW branch of this dike is more compatible with a local and adjacent NW-SE extension. Stress axes exhibit clockwise rotation in White Mountain magma series, possibly due to local deviatoric stresses or a NE-SW-oriented basement fault. The authors attribute these two extensional paleostress trends to either (1) contemporaneous regional partitioning of ESE-WNW-oriented extension influenced by N-S-trending structures in Champlain Lake Valley and NE-SW-trending structures of St. Lawrence rift, or (2) an initial Late Triassic E-W extension related to formation of Bay of Fundy and South Georgia rift basins and Early Jurassic ESE-WNW extension related to central Atlantic rift system.
Heaman and Kjarsgaard (2000)	Timing of Eastern North American Kimberlite Magmatism: Continental Extension of the Great Meteor Hotspot Track?	Extends Great Meteor hotspot track NW to Rankin Inlet on west side of James Bay by identifying four periods of kimberlite magmatism (at 196, 180–176, 148–146, and 142–134 Ma) from U-Pb perovskite ages that extend from NW to SE from Rankin Inlet through to the Attawapiskat, Kirkland Lake, and Timiskaming fields. These results are not consistent with Morgan's (1983) study, which identified two Mesozoic hotspot tracks in New England separated by 40 Myr. Heaman and Kjarsgaard (2000) suggest that this age progression and the change from kimberlitic to basaltic magmatism correspond to change from thick lithosphere to thinner lithosphere east of Monteregeian Hills.
Matton and Jebrak (2009)	The Cretaceous Peri-Atlantic Alkaline Pulse (PAAP): Deep Mantle Plume Origin or Shallow Lithospheric Break-Up?	Cretaceous magmatism occurred along widely separated peri-Atlantic continental margins as widespread alkaline igneous activity. This volcanism, along with the Central Atlantic magmatic province associated with Jurassic rifting, has been attributed to either deep mantle plumes or a combination of tensional forces, lithospheric rifting, and structural controls. Matton and Jebrak (2009) propose that periodic reactivation of deep-seated preexisting zones of weakness during major stages of Atlantic tectonic evolution, combined with coeval asthenospheric upwelling due to edge-driven convection and continental insulation flow, enhanced the ascent of alkaline magmas. The authors prefer shallow, small-scale upwelling during periodic structural reactivation to a mantle plume as a mechanism for alkaline magmas.

Table D-7.3.2 Data Summary
Great Meteor Hotspot Zone

Citation	Title	Description and Relevance to SSC
McHone (1996)	Constraints on the Mantle Plume Model for Mesozoic Alkaline Intrusions in Northeastern North America	<p>The author proposes that one or more deep-mantle plumes do not provide a satisfactory mechanism for distribution of Cretaceous alkaline rocks of NE New England. Observed that previous studies oversimplify evidence for a hotspot track across New England by ignoring important petrological data, including the following:</p> <ul style="list-style-type: none"> • Jurassic syenite-monzonite-alkali granite of the White Mountain magma series has been described as separate province from Cretaceous intrusions, although many Early Jurassic dikes and several mafic to felsic plutons in the province are petrographically and chemically similar to Early Cretaceous intrusions that overlap. • Early Cretaceous dikes and plutons of the New England–Quebec igneous province have statistically similar paleomagnetic poles between 122 and 124 Ma and show no consistent trend for published ages in any direction across region. • Seamount volcanism is not limited to ages defined by a linear hotspot track, nor is it in line with the New England–Quebec province. • Cretaceous alkaline rocks do not exhibit a consistent chemical signature indicative of a mantle source. <p>These observations indicate that lithospheric processes were necessary to start and stop generation of magmas from the same source in the mantle, and petrological studies should emphasize local and regional tectonic features.</p>
McHone (2000)	Non-plume Magmatism and Rifting During the Opening of the Central Atlantic Ocean	<p>Presents a model for Mesozoic rifting in the Atlantic based on several convection cells beneath the rift zone as opposed to a mantle plume. The presence of dikes with lengths up to 700 km (435 mi.) displaying uniform composition can be explained by either (1) flow of magma away from a single, local magma source for each large dike or dike swarm, or (2) vertically moving magmas from compositionally different subhorizontal layers that are homogeneous across large mantle source regions. Cretaceous intraplate hotspots postdate Jurassic tholeiitic magmatism and Atlantic Ocean rifting by 80 Myr or more.</p> <p>McHone (2000) proposes that rifting of Pangaea progressed through a series of linear zones of mantle upwelling that gradually coalesced into the modern segments of the mid-ocean ridges. The lithosphere promoted an increase in</p>

Table D-7.3.2 Data Summary
Great Meteor Hotspot Zone

Citation	Title	Description and Relevance to SSC
		upper mantle temperatures beneath the incipient rift zone, culminating in the great Early Jurassic magmatic event. Subsequent cooling resulted in evolution of the rift into a zone of shallow linear upwelling and convection by which the mantle ejects ridge basalts and accretes new oceanic crust. This is supported by the presence of Cretaceous and Cenozoic alkaline igneous volcanoes in eastern North America, the northern North Atlantic, western Africa, South America, and as seamounts and islands throughout the central North Atlantic Ocean.
Morgan (1983)	Hotspot Tracks and the Early Rifting of the Atlantic	Study tested the hypothesis that hotspots are fixed in space by generating plate reconstructions for the Atlantic Ocean from the last 180 Myr using ages of known hotspot tracks. Morgan (1983) recognized two hotspot tracks passing through New England at different times: the Verde hotspot track at about 160 Ma and the Meteor hotspot at about 120 Ma. The Verde hotspot traveled from south of Hudson Bay to the New England seamounts from 180 to 130 Ma, and the Meteor track parallels the Verde track through Ontario, New England, and the New England seamounts approximately 40 Myr after the Verde track. The predicted track for the Great Meteor hotspot closely follows known ages for the White Mountain magma series in New Hampshire, the Cretaceous seamounts of offshore New England, the Corner Rise (recording when the mid-Atlantic Ridge crossed over the hotspot), and the Great Meteor seamount (11–17 Ma) in the Central Atlantic.
Poole et al. (1970)	Geology of Southeastern Canada	Alkaline rocks of the Monteregian Hills consist of nepheline, syenite, essexite, nordmarkite, pulaskite, yamaskite, and rougemontite forming circular plugs with steep walls and laccoliths within a 241 km (150 mi.) long west-trending line between Montreal and Lake Megantic in Quebec. These intrusions range in age from 84 to 123 Ma, with many falling between 100 and 115 Ma. Rocks may be related to a NW-striking kimberlite dike at Kirkland Lake (151 ± 8 Ma).
Roden-Tice and Tice (2005)	Regional-Scale Mid-Jurassic to Late Cretaceous Unroofing from the Adirondack Mountains Through Central New England Based on Apatite Fission-Track and (U-Th)/He Thermochronology	Apatite fission-track ages and (U-Th)/He ages from the Adirondack Mountains and eastern New York State, Vermont, western Massachusetts and Connecticut, and western New Hampshire indicate that widespread unroofing during the Middle Jurassic to Late Cretaceous occurred at a rate of 0.07 to 0.08 km/Myr. This regional uplift is attributed to remnant heating from the Great Meteor hotspot. Differential unroofing was accommodated by extensional fault reactivation.

Table D-7.3.2 Data Summary
Great Meteor Hotspot Zone

Citation	Title	Description and Relevance to SSC
Roden-Tice and Wintsch (2002)	Early Cretaceous Normal Faulting in Southern New England: Evidence from Apatite and Zircon Fission-Track Ages	Apatite and zircon fission-track age transects across Hartford-Deerfield basin in Connecticut and Massachusetts increase to the east, indicating that unroofing occurred during the Late Jurassic through Early Cretaceous. Age of graben structure of Hartford Basin is Cretaceous and may not be an early Mesozoic “rift” basin.
Roden-Tice, West, et al. (2009)	Presence of a Long-Term Lithospheric Thermal Anomaly: Evidence from Apatite Fission-Track Analysis in Northern New England	Apatite fission-track ages across New Hampshire, NE Vermont, and western Maine range from 70 to 140 Ma and reflect widespread Early to Late Cretaceous cooling. This regional cooling and unroofing is attributed to passage of North America Plate over the Great Meteor hotspot, emplacement of White Mountain magma series in the Early Jurassic, and associated E-W and NW-SE extension. Regional uplift on the order of 5–7 km (3–4 mi.) may explain lack of rift basins in central New England and Quebec.
Sleep (1990)	Monteregian Hotspot Track: A Long-Lived Mantle Plume	From modeling the buoyancy flux of the Great Meteor hotspot, the author observed that the trace of the hotspot changes orientation, concluding that the plume was weak beneath Ontario and strong beneath Montreal where the track changed orientation through the White Mountains, and became weakened at the Nashville seamount where the track changed orientation to the Corner seamounts. Sleep (1990) also suggested that the lack of tracks west of the Monteregian Hills may be the result of the Canadian Shield’s being less vulnerable to the hotspot than the Paleozoic sediments of the Montreal area were.
Zartman (1977)	Geochronology of Some Alkaline Rock Provinces in Eastern and Central United States	Provides ages for the White Mountain plutonic suite, consisting of mildly alkaline rocks with compositions of granite, quartz syenite, syenite, and lesser amounts of intermediate and mafic units occupying a batholith, several stocks, and related ring dikes. The mapped relationships of these rocks indicate post-tectonic character from host rocks and a relatively slow intrusion of complexly evolved magma chambers into shallow crust. These rocks were emplaced over three rather broad pulses of magmatism at 220–235 Ma, 155–200 Ma, and 95–125 Ma but lack any regular time-transgressive pattern of ages. Alignment of these rocks with the Monteregian Hills of Quebec and Cretaceous seamounts of offshore New England can be attributed to the trace of a mantle hotspot between the Early Triassic to Early Cretaceous or to emplacement along fractures, indicative of intraplate stresses.

Table D-7.3.2 Data Summary
Great Meteor Hotspot Zone

Citation	Title	Description and Relevance to SSC
Geophysical Characteristics		
Eaton et al. (2006)	Crustal Thickness and V_p/V_s Variations in the Central Grenville Orogen (Ontario, Canada) from Analysis of Teleseismic Receiver Functions	Crustal thickness maps derived from teleseismic analysis and results of regional seismic-refraction surveys image the hotspot track NE of the Ottawa-Bonnechere graben as minima on these maps. Thinnest crust (34.5–37.0 km) coincides with the elevated seismicity rates of Western Quebec seismic zone, NE of Ottawa-Bonnechere graben.
Li et al. (2003)	Shear Velocity Structure and Azimuthal Anisotropy Beneath Eastern North America from Rayleigh Wave Inversion	Determined velocity structure and anisotropic variations in velocity structure from inversion of Rayleigh waves in order to detect asthenospheric flow beneath the thick continental lithosphere beneath NE United States and SE Canada. Rayleigh wave-phase velocity anomaly with a period of 33 s, corresponding to sensitivity to structure down to 40 km (25 mi.) in depth, indicates a low-velocity band oriented NE-SW. North American continental keel beneath Grenville province is imaged in the upper mantle down to roughly 200 km (124 mi.) in depth. The North American keel has an irregular shape and a low-velocity zone beneath eastern New York and central New England to 200 km (124 mi.), with particularly high amplitudes at depths of 60–140 km (37–87 mi.). This velocity anomaly is interpreted as the lateral contrast between relatively thick lithosphere beneath western New York and Pennsylvania and the warm asthenosphere beneath the thinned New England lithosphere caused by thermal erosion associated with the Cretaceous hotspot. Additionally, weak anisotropy observed from shear-wave splitting indicates that source must be at least 200 km (124 mi.) deep, suggesting that a sublithospheric shear zone may decouple motions of lithosphere and deeper mantle.
Rondenay et al. (2000)	Teleseismic Studies of the Lithosphere Below the Abitibi-Grenville Lithoprobe Transect	Travel-time inversions of teleseismic results from southern Ontario image a low-velocity corridor between 50 and 300 km (31 and 373 mi.) that crosscuts regional structures of the Grenville province and Ottawa-Bonnechere graben. This low-velocity corridor is coincident with northwestward continuation intrusions of Monteregean Hills. These results are attributed to a zone of contrasting thermal-compositional-anisotropic properties interpreted to have been formed by the same process responsible for emplacement of the Monteregean Hills (either a fixed mantle plume of the Great Meteor hotspot or rifting associated with opening of Atlantic Ocean). This anomaly is flanked on both sides by high seismic velocity, possibly representing zones of depleted residuum or transitions in mantle fabric.

Table D-7.3.2 Data Summary
Great Meteor Hotspot Zone

Citation	Title	Description and Relevance to SSC
Seismicity		
Adams and Basham (1991)	The Seismicity and Seismotectonics of Eastern Canada	The Western Quebec seismic zone contains two distinct bands of seismicity: a W-NW-trending band of seismicity along the Ottawa River between Ottawa and Lake Timiskaming associated with rift faults of the Ottawa River valley, and a N-NW-trending band extending from Montreal to the Baskatong Reservoir attributed to crustal fracturing associated with passage of a Cretaceous hotspot track. Recent seismicity of this second band includes the 1975 M 4.2 Maniwaki and 1978 M 4.1 St. Donat earthquakes. These two bands of seismicity converge near the St. Lawrence River.
Ma and Atkinson (2006)	Focal Depths for Small to Moderate Earthquakes ($M_N \geq 2.8$) in Western Quebec, Southern Ontario, and Northern New York	Performed regional-depth-phase modeling of earthquakes occurring in southern Ontario, western Quebec, and northern New York between 1980 and 2004. Events with depths greater than 15 km (9.3 mi.) are restricted to Ottawa graben and Western Quebec seismic zone (WQSZ). Hypocentral depths for events in WQSZ range from 2 to 25 km (1.2 to 15.5 mi.). The wide depth distribution could indicate faults of throughgoing crustal extent or different faults that occur at different depths in the crust. In entire study region, focal depths cluster at 5, 8, 12, 15, and 22 km (3, 5, 7.5, 9.3, and 13.7 mi.) and may reflect layering in seismogenic properties within the crust.
Ma and Eaton (2007)	Western Quebec Seismic Zone (Canada): Clustered, Midcrustal Seismicity Along a Mesozoic Hot Spot Track	<p>The authors determined focal depths for 73 earthquakes, combined these data with those computed by Ma and Atkinson (2006), and compared the spatial distribution of earthquakes with focal mechanisms to evaluate tectonic controls of the Western Quebec seismic zone (WQSZ), a 160 km (100 mi.) wide band of intraplate seismicity extending 500 km (311 mi.) from Adirondack Highlands to James Bay.</p> <p>Shallow events with depths less than 8 km (5 mi.) are randomly distributed with reverse mechanisms attributed to glacial isostatic adjustment. Earthquakes with intermediate depths define a linear band of earthquakes. Deep earthquakes (greater than 17 km, or 10.6 mi., in depth) are localized as clusters at Timiskaming, Maniwaki, Mont-Laurier, and Adirondack. Timiskaming cluster is located near the 1935 Timiskaming earthquake, has a lower <i>b</i>-value than the other clusters and the regional average, and is associated with faults of the Ottawa-Bonnechere graben. Adirondack cluster is located near the 1944 Cornwall-Massena earthquake, and two events within the cluster have focal mechanisms with an E-W-oriented P axis. The Mont-Laurier cluster is adjacent</p>

Table D-7.3.2 Data Summary
Great Meteor Hotspot Zone

Citation	Title	Description and Relevance to SSC
		<p>to paleoseismic evidence near Ottawa River studied by Aylsworth et al. (2000).</p> <p>Seismicity does not generally correlate with structure in WQSZ; shear zones of Grenville province cut across the NW-SE trend of WQSZ at a high angle. The Maniwaki cluster exhibits repeating events, with deep seismicity localized within the footwall of the Baskatong crustal ramp, and intermediate and shallow seismicity localized within the hanging wall. Clustered seismicity, with the exception of the Timiskaming clusters, has little spatial overlap with Ottawa-Bonnechere and Timiskaming graben structures.</p> <p>The authors speculate that localized seismicity in the WQSZ is attributed to either weakened faults and shear zones caused by reheating of crust by hotspot track, or to stress concentrations associated with the emplacement of major bodies in more felsic crust. Near-surface expression of the hotspot track progressively changes from kimberlitic melts in interior of craton to more voluminous crustal magmatism as the hotspot interacted with a progressively thinner lithosphere. The authors propose that the WQSZ represents an area of blind intrusions associated with entrapment of mantle-derived melt in the crust that is located between kimberlitic dikes to the NW and Montereian intrusions to the SE.</p>
Ma et al. (2008)	Intraplate Seismicity of a Recently Deglaciated Shield Terrane: A Case Study from Northern Ontario, Canada	<p>Determined depth phases of 537 earthquakes occurring in Northern Ontario between 1980 and 2006. Identified two active clusters south of James Bay and near Kapuskasing where focal depths range from a few km to more than 20 km (12.4 mi.). James Bay cluster was not recognized until regional monitoring began in 2002. Cluster is centered around 53N, 80.7W with focal depths varying from 4 to 20 km (2.5 to 12.4 mi.), indicating that earthquakes occur along deep-rooted geologic structures. Largest magnitude observed in cluster is M_N 3.6. Kapuskasing cluster is located 100 km (62 mi.) NW of Western Quebec seismic zone (WQSZ), separated by an aseismic zone. Kapuskasing cluster contains the December 1, 1928, M_L 5.0; April 13, 1980, M_N 4.1; and December 7, 2007, M_N 4.2 earthquakes. Focal mechanisms from both clusters indicate thrust mechanisms with NW-striking nodal planes. Focal depths increase successively in time, consistent with progressive rupture migration down a fault. The authors attribute the Kapuskasing cluster to extension of WQSZ, and this seismicity to a combination of thermal rejuvenation of the crust and/or rheological contrast between igneous rocks and older crust resulting from passage of North America over the Great Meteor hotspot.</p>

Table D-7.3.2 Data Summary
Great Meteor Hotspot Zone

Citation	Title	Description and Relevance to SSC
<i>Paleoseismic Investigations</i>		
Aylsworth et al. (2000)	Did Two Massive Earthquakes in the Holocene Induce Widespread Landsliding and Near-Surface Deformation in Part of the Ottawa Valley, Canada?	Examines large prehistoric landslides in abandoned channels of Ottawa River and disturbed sediment of the erosional plane adjacent to Ottawa River, south of Great Meteor Hotspot seismotectonic zone. Radiocarbon dates from buried wood and plant material that collected in landslide debris cluster at 4,550 yr BP, which is thousands of years younger than the age of paleochannel abandonment. This observation cannot be attributed to either fluvial erosion or wet-weather-induced landslides. East of the landslides, disturbed sediment and possible sand boils dated at 7,060 yr BP are preserved within flat erosional plane adjacent to Ottawa River. These two age distributions are attributed to paleoearthquakes of uncertain magnitude and source.

**Table D-7.3.3 Data Summary
Northern Appalachian Zone**

Citation	Title	Description and Relevance to SSC
General for Region		
Adams et al. (1995)	Northeastern North American Earthquake Potential—New Challenges for Seismic Hazard Mapping	Presents rationale for source characterization used in the seismic hazard maps of Canada. The Northern Appalachian zone consists of crust of the northern Appalachians that overrode the Iapetan passive margin. The geometry extends from the landward limit of Mesozoic extensional faulting to the seaward limit of thinned Grenville crust of the Iapetan passive margin. The Miramichi earthquake is considered the paradigm earthquake.
Tremblay and Castonguay (2002)	Structural Evolution of the Laurentian Margin Revisited (Southern Quebec Appalachians): Implications for the Salinian Orogeny and Successor Basins	The northern Appalachians consist of several tectonostratigraphic zones: Humber, Dunnage, Gander, Avalon, and Meguma. The external Humber zone consists of sedimentary rocks and mafic volcanic rocks deformed into a series of imbricate NW-directed thrust nappes of prehnite-pumpellyite to sub-greenschist facies. The internal Humber zone consists of distal facies of external Humber zone units of greenschist to amphibolite metamorphic grade. The Dunnage zone consists of ophiolites, melanges, volcanic arc sequences, and flysch deposits. The surface boundary between the Humber and Dunnage zones defines the Baie Verte–Brompton line. In southern Quebec, the Dunnage zone is overlain by the Connecticut Valley–Gaspé trough.
Taconic Orogeny		
Fail (1997a)	A Geologic History of the North-Central Appalachians, Part 1: Orogenesis from the Mesoproterozoic Through the Taconic Orogen	The Middle to Late Ordovician Taconic orogeny extended from Labrador to Alabama and is currently exposed in the southern Appalachians in the Piedmont and Great Valley allochthons and western New England. Assemblages in the southern Appalachians contain complexes formed in the Theic Ocean, whereas assemblages of western New England consist of two magmatic arcs: the Halway arc of the Brompton-Cameron terrane and the Ammonoosuc arc of the Central Maine terrane.
Fail (1997b)	A Geologic History of the North-Central Appalachians, Part 2: The Appalachian Basin from the Silurian Through the Carboniferous	Several Theic components, including microcontinents, magmatic arcs, and accretionary prisms were obducted along the broad carbonate shelf that existed on the eastern edge of Laurentia. These Taconic terranes formed a topographic barrier creating the Appalachian basin from Alabama to at least Quebec.

Table D-7.3.3 Data Summary
Northern Appalachian Zone

Citation	Title	Description and Relevance to SSC
Faure et al. (2004)	Reconstruction of Taconian and Acadian Paleostress Regimes in the Quebec and Northern New Brunswick Appalachians	Paleostress analysis of brittle faults in Quebec and New Brunswick indicate that Taconic deformation produced N-S- to NE-SW-trending reverse conjugated brittle faults under a pure compressional stress regime late in the development of the orogeny. This Taconic compressional event also resulted in reactivation of lapetan faults in the St. Lawrence Lowlands as E-NE/W-SW dextral and NW-SE sinistral faults.
Moench and Aleinikoff (2003)	Stratigraphy, Geochronology, and Accretionary Terrane Settings of Two Bronson Hill Arc Sequences, Northern New England	Volcanic arcs of the Bronson Hill anticlinorium developed in the late Cambrian within the Theic Ocean during the Penobscot orogeny. They were obducted to the Laurentian margin during the Middle to Late Ordovician Taconic orogeny. These arcs developed from multiple accretionary events with changing polarity shortly before the closing of the lapetus Ocean at 460 Ma.
Spencer et al. (1989)	The Extension of Grenville Basement Beneath the Northern Appalachians: Results from the Quebec-Maine Seismic Reflection and Refraction Surveys	A master decollement separating autochthonous Grenville basement from overlying allochthonous rocks of the Appalachian orogen extends over a distance of 200 km (124 mi.) and can be traced from shallow depths beneath the St. Lawrence Lowlands SE to about 25 km (15.5 mi.) depth beneath the SE edge of the Chain Lakes massif. Basement is offset by closely spaced en echelon normal faults, with displacements between 200 and 1,000 m interpreted as lapetan growth faults. The Baie Verte–Brompton line, separating Cambrian and Ordovician continental slope and rise deposits from oceanic arc and magmatic assemblages to the south, including the Chain Lakes massif, is imaged as a shallow, thin-skinned structure. The Chain Lakes terrane is thought to underlie much of the Connecticut Valley–Gaspé synclinorium. The Acadian Guadeloupe fault disrupts the master decollement of the Taconian orogeny and thrust the Connecticut Valley–Gaspé synclinorium over the Chain Lakes massif.
St. Julien and Hubert (1975)	Evolution of the Taconian Orogen in the Quebec Appalachians	<p>Describes 11 lithostratigraphic assemblages distributed between the autochthonous, external, and internal domains of the Quebec Appalachians. The autochthonous domain contains Cambrian and Ordovician sandstones and carbonates representing transgressive shelf deposits, Middle and Upper Ordovician flysch deposits, and Upper Ordovician shale and sandstone representing the post-tectonic regressive sequence. This domain contains E-W- and N30E-trending normal faults active between late Precambrian and Late Ordovician.</p> <p>The external domain is divided into an outer belt containing imbricated thrusts and an inner belt composed of nappes separated by Logan's Line. Assemblages</p>

Table D-7.3.3 Data Summary
Northern Appalachian Zone

Citation	Title	Description and Relevance to SSC
		<p>of the autochthonous domain can be found within the thrust-imbricated belt. lower Cambrian clastic-carbonate, Cambrian shale-feldspathic sandstone, and upper Cambrian/Lower Ordovician shale-limestone conglomerate assemblages constitute nappes of the inner belt of the external domain. East-dipping reverse faults of the external belt repeat through successive imbricated structures on a decollement surface that cuts southeastward into progressively older rocks. Polarity of the nappes indicates that right-side-up nappes with the oldest rock assemblages always rest on nappes containing the youngest. Emplacement of the nappes is constrained by elevation and denudation of the nappes beginning in early Middle Ordovician and progressing westward until late Middle Ordovician and prior to dynamothermal metamorphism, as evidenced by a regional penetrative cleavage associated with a late fold system.</p> <p>The internal domain contains assemblages from the inner belt, and ophiolite, shale-melange, slate-sandstone tuff, and calc-alkaline volcanic assemblages. The internal domain is deformed by late recumbent folds genetically related to dynamothermal metamorphism in the latest Ordovician or earliest Silurian. Imbrication along major thrust faults likely occurred in the Upper Ordovician.</p> <p>These assemblages were accumulated on a Grenville-like basement to the west and newly formed oceanic crust to the east. The Taconian orogeny coincides with obduction of newly formed ocean crust in late Early Ordovician and subduction of oceanic crust during early and late Middle Ordovician. Rocks within the internal and external domains exhibit Devonian deformation associated with Acadian orogeny.</p>
Stewart et al. (1993)	Global Geoscience Transect 8: Quebec-Maine-Gulf of Maine Transect, Southeastern Canada, Northeastern United States of America	Integrates interpretations from the Maine-Quebec seismic lines and provides descriptions of major tectonostratigraphic terranes, including the Laurentian craton, the Brompton-Cameron, Central Maine, Nashoba-Casco-Miramichi, and Atlantica composite terranes, and the Meguma terrane.
Salinian Orogeny		
Murphy and Keppie (2005)	The Acadian Orogeny in the Northern Appalachians	Late Cambrian–Middle Ordovician Penobscottian orogeny amalgamated composite terranes within arcs of the Iapetus Ocean, and therefore did not result in deformation within Laurentia. Late Ordovician–Silurian Salinic orogeny accreted the Gander, Avalon, Nashoba, and Carolina terranes to Laurentia during closing of the Iapetus Ocean during the Laurentia-Avalonia collision.

Table D-7.3.3 Data Summary
Northern Appalachian Zone

Citation	Title	Description and Relevance to SSC
Tremblay and Castonguay (2002)	Structural Evolution of the Laurentian Margin Revisited (Southern Quebec Appalachians): Implications for the Salinian Orogeny and Successor Basins	Silurian metamorphism (430–410 Ma) in the northern Appalachians is attributed to retrograde metamorphism following the main compression event. The event involved SE-directed transport of Taconian crustal wedge followed by normal faulting (Saint-Joseph and Baie Verte–Brompton faults) and development of the fault-bounded sedimentary basins of the Connecticut Valley–Gaspé trough. This extension is inconsistent with coeval compression in Newfoundland, suggesting that the Salinian orogeny is geographically restricted or the entire Laurentian margin is characterized by crustal extension that induced the formation of major sedimentary basins during the Silurian and Devonian.
Tremblay and Pinet (2005)	Diachronous Supracrustal Extension in an Intraplate Setting and the Origin of the Connecticut Valley–Gaspé and Merrimack Troughs, Northern Appalachians	Attributes the late-stage extension to supracrustal extensional collapse due to late-stage delamination of the lithospheric mantle in a SE-dipping subduction zone.
Acadian Orogeny		
Faill (1997b)	A Geologic History of the North-Central Appalachians, Part 2: The Appalachian Basin from the Silurian Through the Carboniferous	The Acadian orogeny is expressed in the Appalachian basin as siliclastic sedimentation from the Middle to Late Devonian, with additional pulses of uplift occurring in the early and late Carboniferous. The principle tectonic activity occurred in New England.
Faure et al. (2004)	Reconstruction of Taconian and Acadian Paleostress Regimes in the Quebec and Northern New Brunswick Appalachians	Deformation from the Acadian orogeny is expressed as E-SE/W-NW compression in a transpressional regime, producing E-NE/W-NW dextral and NW-SE sinistral strike-slip faults that crosscut Taconian thrust faults in the Appalachians of Quebec and New Brunswick. This deformation also resulted in reactivation of Iapetan structures in the St. Lawrence Lowlands.
Murphy and Keppie (2005)	The Acadian Orogeny in the Northern Appalachians	The Devonian Acadian orogeny has been attributed to either the collision of Avalonia with Laurentia or the accretion of the Meguma terrane; however, recent work indicates that the Meguma terrane is the passive margin on the southern margin of Avalonia. The authors interpret the Acadian orogeny as forming along an Andean-type margin that possibly overrides a plume and swell.

Table D-7.3.3 Data Summary
Northern Appalachian Zone

Citation	Title	Description and Relevance to SSC
Tremblay et al. (2000)	Acadian Metamorphism in the Dunnage Zone of Southern Québec, Northern Appalachians: 40Ar/39Ar Evidence for Collision Diachronism	Acadian metamorphism is well dated as 385–375 Ma in the southern part of the Dunnage zone.
<i>Alleghanian Orogeny</i>		
Faill (1998)	A Geologic History of the North-Central Appalachians, Part 3: The Alleghany Orogeny	The Alleghanian orogeny produced decollement tectonism in the central and southern Appalachians, along with early penetrative shortening, late low-angle thrusts, low-grade metamorphism, and transpressional shear zones. NE of the Pennsylvania salient, the Alleghany orogeny is confined to Carboniferous basins and rocks previously affected by the Taconic and Acadian orogenies. In New England, Alleghany tectonism was driven by docking of the Avalon terrane. The northern Appalachians exhibit high-pressure metamorphism of Taconic and Acadian crust in east-central Connecticut and Massachusetts and deformation of Appalachian deposits near the Hudson Valley.
Faure et al. (1996a)	Alleghanian Paleostress Reconstruction in the Northern Appalachians: Intraplate Deformation Between Laurentia and Gondwana	Brittle faults of the northern Appalachians exhibit three phases of compression during the Alleghanian orogeny: an early NNW-SSE compression, a NNE-SSW compression, and a late WNW-ESE compression.
Murphy and Keppie (2005)	The Acadian Orogeny in the Northern Appalachians	There is general consensus that the late Carboniferous–Permian Alleghany orogeny was due to terminal collision between Gondwana and Laurentia-Baltica that closed the Rheic Ocean and resulted in the formation of Pangaea.
<i>Opening of the Atlantic</i>		
Faure et al. (1996b)	State of Intraplate Stress and Tectonism of Northeastern America Since Cretaceous Times, with Particular Emphasis on the New England–Quebec Igneous Province	Results of a paleostress analysis of brittle faults in the Quebec Appalachians provide evidence for two distinct phases of Cretaceous extension: an initial geographically widespread NE-SW phase of extension and a later N-S phase of extension confined to southern Quebec. The authors attributed this Cretaceous volcanism to continued fragmentation of Pangaea. Early NE- to E-NE-oriented extension and associated magmatism between 140 and 90 Ma are correlated to rifting between Labrador and Greenland at ~140 Ma, early breakup stages of South Atlantic Ocean at 130 Ma, and N-S-oriented extension and emplacement of dikes at 125 Ma, corresponding to separation of Iberia from Newfoundland.

Table D-7.3.3 Data Summary
Northern Appalachian Zone

Citation	Title	Description and Relevance to SSC
Faure et al. (2006)	Paleostress Analysis of Atlantic Crustal Extension in the Quebec Appalachians	<p>Fault stress tensors indicate that most E-W- to ESE-WNW-oriented stress is found in the Montreal and Gaspé area, whereas SE-NW stress is found in SE Quebec. Late Triassic–Jurassic dikes in New England and southern Quebec indicate SE-NW-oriented extension consistent with fault slip stress. The N-S-trending portion of a Jurassic dike in southern Quebec is consistent with the regional E-W extensional stress axis, whereas the NE-SW branch of this dike is more compatible with a local and adjacent NW-SE extension. Stress axes exhibit clockwise rotation in the White Mountain magma series, possibly due to local deviatoric stresses or a NE-SW-oriented basement fault.</p> <p>The authors attribute these two extensional paleostress trends to either (1) contemporaneous regional partitioning of ESE-WNW-oriented extension that was influenced by N-S-trending structures in the Champlain Lake Valley and the NE-SW-trending structures of the St. Lawrence rift, or (2) an initial Late Triassic E-W extension related to the formation of the Bay of Fundy and South Georgia rift basins and Early Jurassic ESE-WNW extension related to the central Atlantic rift system.</p>
<i>Cretaceous Great Meteor Hotspot</i>		
Crough (1981)	Mesozoic Hotspot Epeirogeny in Eastern North America	Attributes a 600 km (373 mi.) wide zone of epeirogeny in SE Canada and New England during the Cretaceous and early Tertiary to the Great Meteor hotspot, as evidenced by apatite fission-track dating.
Duncan (1984)	Age Progressive Volcanism in the New England Seamounts and the Opening of the Central Atlantic Ocean	The author obtained radiometric ages for dredged volcanic rocks from seven of the New England seamounts and concluded that the seamounts increase in age from the SE (82 Ma for the Nashville seamount) to the NW (103 Ma for the Bear seamount).
Faure et al. (1996b)	State of Intraplate Stress and Tectonism of Northeastern America Since Cretaceous Times, with Particular Emphasis on the New England–Quebec Igneous Province	Performed a paleostress analysis of the New England–Quebec igneous province that provided an alternative interpretation for the distribution of Cretaceous plutons. Dikes display ESE-WNW and ENE-WSW trends and are spatially distributed in three E-W-trending dike swarms 75 by 300 km (47 by 186 mi.) in area. Leucocratic dikes occur closer to plutons and disappear within 3–4 km (2–2.5 mi.), likely recording local stress affects due to pluton emplacement. Lamprophyre dikes occur independently of plutons and strike parallel to regional dike swarms, recording regional far-field stresses.

Table D-7.3.3 Data Summary
Northern Appalachian Zone

Citation	Title	Description and Relevance to SSC
		<p>Normal faults in the regions display two orientations: (1) E-W-trending normal faults found predominantly in the Montreal area are parallel to graben boundaries and the axis of the Monteregian hills, with vertical offsets ranging between 100 and 430 m; and (2) NW-SE to WNW-ESE-trending normal faults oblique to graben boundaries with less than 100 m of vertical offset. The NW-SE to WNW-ESE faults are older than the E-W-trending faults but exhibit crosscutting relationships, suggesting that some were reactivated during the formation of the E-W-trending faults. Some E-W-trending brittle faults and joints are observed in several Cretaceous plutons with similar orientations to dikes that are locally crosscut by these normal faults, suggesting that dike emplacement and faulting are contemporaneous. Conjugate sets of NE-SW dextral and ESE-WNW sinistral strike-slip faults and NNW-SSE reverse faults provide evidence for a compressional stress regime postdating the emplacement of the Cretaceous plutons.</p> <p>The authors attribute these data to an initial NE-SW extension event associated with rifting between Labrador and Greenland at 140 Ma, opening of the South Atlantic at 130 Ma, and related reactivation of the Timiskaming graben. Subsequent N-S-oriented extension associated with the emplacement of the Monteregian Hills corresponds to global fragmentation of Pangaea when Iberia separated from Newfoundland when dominant tensional stress propagated along the Labrador rift. The stress regime shifted to ENE-ESE-directed compressional in the early Tertiary when the oceanic spreading rate decreased due to an increasing number of convergent boundaries in the Pacific. The authors conclude that the emplacement of Cretaceous intrusions is consistent with a lithospheric fracture model as opposed to a hotspot model, emphasizing the role of preexisting structure in the Ottawa-Bonnechere graben.</p>
McHone (1996)	Constraints on the Mantle Plume Model for Mesozoic Alkaline Intrusions in Northeastern North America	<p>The author proposes that one or more deep-mantle plumes do not provide a satisfactory mechanism for the distribution of Cretaceous alkaline rocks of NE New England, and observes that previous studies oversimplify the evidence for a hotspot track across New England by ignoring important petrological data, including the following:</p> <ul style="list-style-type: none"> • Jurassic syenite-monzonite-alkali granite of the White Mountain magma series has been described as a separate province from Cretaceous intrusions, although many Early Jurassic dikes and several mafic to felsic plutons in the province are petrographically and chemically similar to Early

**Table D-7.3.3 Data Summary
Northern Appalachian Zone**

Citation	Title	Description and Relevance to SSC
		<p>Cretaceous intrusions that overlap.</p> <ul style="list-style-type: none"> • Early Cretaceous dikes and plutons of the New England–Quebec igneous province have statistically similar paleomagnetic poles between 122 and 124 Ma and show no consistent trend for published ages in any direction across the region. • Seamount volcanism is not limited to ages defined by a linear hotspot track, nor is it in line with the New England–Quebec province. • Cretaceous alkaline rocks do not exhibit a consistent chemical signature indicative of a mantle source. <p>These observations indicate that lithospheric processes were necessary to start and stop the generation of magmas from the same source in the mantle, and petrological studies should emphasize local and regional tectonic features.</p>
Morgan (1983)	Hotspot Tracks and the Early Rifting of the Atlantic	Attributes this age distribution to two hotspot tracks passing through New England at different times: the Verde hotspot track at about 160 Ma and the Meteor hotspot about 120 Ma
Roden-Tice and Tice (2005)	Regional-Scale Mid-Jurassic to Late Cretaceous Unroofing from the Adirondack Mountains Through Central New England Based on Apatite Fission-Track and (U-Th)/He Thermochronology	Apatite fission-track ages and (U-Th)/He ages from the Adirondack Mountains and eastern New York state, Vermont, western Massachusetts and Connecticut, and western New Hampshire indicate that widespread unroofing during the Middle Jurassic to Late Cretaceous occurred at a rate of 0.07 to 0.08 km/Myr. This regional uplift is attributed to remnant heating from the Great Meteor hotspot. Differential unroofing was accommodated by extensional fault reactivation.
Roden-Tice, West, et al. (2009)	Presence of a Long-Term Lithospheric Thermal Anomaly: Evidence from Apatite Fission-Track Analysis in Northern New England	Apatite fission-track ages across New Hampshire, NE Vermont, and western Maine range from 70 to 140 Ma and reflect widespread Early to Late Cretaceous cooling. This regional cooling and unroofing is attributed to passage of the North American Plate over the Great Meteor hotspot, emplacement of the White Mountain magma series in the Early Jurassic, and associated E-W and NW-SE extension. Regional uplift on the order of 5–7 km (3–4 mi.) may explain lack of rift basins in central New England and Quebec.

**Table D-7.3.3 Data Summary
Northern Appalachian Zone**

Citation	Title	Description and Relevance to SSC
Sleep (1990)	Monteregian Hotspot Track: A Long-Lived Mantle Plume	From modeling the buoyancy flux of the Great Meteor hotspot, the author observed that the trace of the hotspot changes orientation, concluding that the plume was weak beneath Ontario and strong beneath Montreal where the track changed orientation through the White Mountains, and became weakened at the Nashville seamount where the track changed orientation to the Corner seamounts. The author suggests that the lack of tracks west of the Monteregian Hills may be the result of the Canadian Shield's being less vulnerable to the hotspot than the Paleozoic sediments of the Montreal area were.
Zartman (1977)	Geochronology of Some Alkalic Rock Provinces in Eastern and Central United States	The author observed that although the mapped relationships of alkalic intrusive rocks of New Hampshire indicate post-tectonic character from their host rocks, relatively shallow emplacement depths, and alignments with the Monteregian Hills of Quebec and Cretaceous seamounts of offshore New England, radiometric ages of the New Hampshire plutons range from Early Triassic to Early Cretaceous but lack any regular time-transgressive pattern of ages.
<i>Geophysical Anomalies</i>		
Hughes and Luetgert (1991)	Crustal Structure of the Western New England Appalachians and the Adirondack Mountains	Interpreted seismic refraction data from the eastern Adirondack Mountains, northern Vermont, northern New Hampshire, and SE Maine. The lower crust has indistinct reflectors and was modeled with a velocity of 6.7 km/s. The depth to Moho thickens from 36 km (22 mi.) in western Maine to 40 km (25 mi.) in Vermont. Crust thins to the east along the transect. Coherent large-amplitude Moho reflections beneath Vermont and New Hampshire suggest compositional lamination at the base of the crust. Locally, the apparent velocity of the upper mantle exceeds 8.1 km/s (5 m/s).
Li et al. (2003)	Shear Velocity Structure and Azimuthal Anisotropy Beneath Eastern North America from Rayleigh Wave Inversion	Determined the velocity structure beneath NE United States and SE Canada using Rayleigh wave inversion. The North American continental keel beneath Grenville Province is imaged in the upper mantle down to roughly 200 km (124 mi.) in depth. The North American keel has an irregular shape and a low velocity zone beneath eastern New York and central New England to 200 km (124 mi.), with particularly high amplitudes at depths of 60–140 km (37–87 mi.). Thin lithosphere beneath west-central New England and easternmost New York may be caused by thermal erosion associated with the Cretaceous hotspot.

**Table D-7.3.3 Data Summary
Northern Appalachian Zone**

Citation	Title	Description and Relevance to SSC
Seismicity		
Brown and Ebel (1985)	An Investigation of the January 1982 Gaza, New Hampshire Aftershock Sequence	Presents source parameters for aftershocks of the January 19, 1982, Gaza, New Hampshire, earthquake. Arrival time data for these aftershocks indicate a northwestward progression of epicentral location with time, suggesting the potential for NW-trending basement structures in the region along with the presence of shallow, multidirectional fracture patterns.
Burke (2004)	Historical Seismicity in the Central Highlands, Passamaquoddy Bay, and Moncton Regions of New Brunswick, Canada, 1817-1961	The author revised magnitudes and locations for historical earthquakes within the Central Highlands subzone (October 22, 1869, M_N 5.7; May 16, 1896, m_{bLg} 4.0; August 8, 1908, m_{bLg} 4.4; July 22, 1922, m_{bLg} 4.9; January 4, 1930, m_{bLg} 4.2; and September 30, 1937, m_{bLg} 4.8) and identified additional historical earthquakes (March 16, 1863, m_{bLg} 4.0; December 18, 1903, m_{bLg} 4.2; March 20, 1911, m_{bLg} 4.5; June 27, 1915, m_{bLg} 3.8; and March 30, 1925, m_{bLg} 4.1). Identified the August 12, 1867, m_{bLg} 3.7 Moncton earthquake and revised the time for the February 8, 1824, M_N 5.2 Moncton earthquake. Also identified the February 25, 1935, m_{bLg} 3.2 earthquake and revised times and locations for the January 1, 1883, m_{bLg} 5.3; March 23, 1896, m_{bLg} 4.2; and December 11, 1912, m_{bLg} 4.7 Passamaquoddy Bay earthquakes.
Burke (2009)	Historical Earthquakes Felt in New Brunswick (1764, 1811-1960)	Presents a compilation of historical earthquakes in New Brunswick that updates findings in Burke (2004) and Leblanc and Burke (1985). The text contains a discussion of felt report, felt area for all events, and isoseismal area of intensity IV reports for selected earthquakes.
Ebel (1996)	The Seventeenth Century Seismicity of Northeastern North America	Places the epicenter for the June 11, 1638, earthquake in the seismically active part of central New Hampshire and estimates a magnitude of 6.5 ± 0.5 to account for felt effects in Trois Rivières, Quebec, and Boston, Massachusetts.
Ebel and Bouck (1988)	New Focal Mechanisms for the New England Region: Constraints on the Regional Stress Regime	Presents focal mechanisms for small to moderate events occurring in New England between 1981 and 1987. These mechanisms are predominantly reverse with a component of strike-slip. These mechanisms have variable strike directions, including NE-SW, NW-SW, N-S, and E-W.

**Table D-7.3.3 Data Summary
Northern Appalachian Zone**

Citation	Title	Description and Relevance to SSC
Ebel et al. (1986)	A Study of the Source Parameters of Some Large Earthquakes of Northeastern North America	Examines source parameters for the two earthquakes occurring in December 1940 near Ossipee, New Hampshire: the December 20 M_L 5.3 and the December 24 M_L 5.4 earthquakes. Synthetic seismograms for the December 20, 1940, Ossipee earthquake provide evidence for a predominantly thrust mechanism with either a N-S- or E-W-striking nodal plane.
Leblanc and Burke (1985)	Re-evaluation of the 1817, 1855, 1869, and 1904 Maine–New Brunswick Area Earthquakes	Compiled felt reports and determined magnitudes for the March 21, 1904, m_{bLg} 5.9; October 22, 1869, m_{bLg} 5.7; February 8, 1855, m_{bLg} 5.2–5.5; and May 22, 1817, m_{bLg} 4.5–5 historical earthquakes in Maine and New Brunswick.
Structures		
Moench and Aleinikoff (2003)	Stratigraphy, Geochronology, and Accretionary Terrane Settings of Two Bronson Hill Arc Sequences, Northern New England	The Ammonoosuc fault is a major Triassic normal fault extending 200 km (124 mi.) from northern New Hampshire SW to Springfield, Vermont, with about 4 km (2.5 mi.) of vertical displacement. Although Triassic displacement is assumed, several earlier displacements may have occurred.
Roden-Tice, West, et al. (2009)	Presence of a Long-Term Lithospheric Thermal Anomaly: Evidence from Apatite Fission-Track Analysis in Northern New England	Apatite fission-track ages across the Ammonoosuc fault in the Connecticut River valley do not display age discontinuities that would imply significant displacement; however, in NW New Hampshire, age discontinuities suggest normal displacement during the Late Cretaceous. Similar age discontinuities are observed between the Bill Little fault and west-dipping normal Northey Hill fault. Samples collected from the area between these two faults display modeled time-temperature histories representing higher structural levels that were downdropped in a grabenlike structure during the Late Cretaceous.
Tremblay and Castonguay (2002)	Structural Evolution of the Laurentian Margin Revisited (Southern Quebec Appalachians): Implications for the Salinian Orogeny and Successor Basins	<p>The following faults have regional significance:</p> <ul style="list-style-type: none"> • Logan's Line marks the end of the Appalachian front. • The Richardson fault forms the boundary between the external and internal Humber zones. • The Bennett-Brome fault forms a composite structure along the NW limbs of the Notre Dame and Sutton Mountains anticlinoria. • Saint-Joseph fault defines the SE limb of the Notre Dame Mountains anticlinorium. Exhibited normal faulting during the Late Silurian to Early Devonian.

Table D-7.3.3 Data Summary
Northern Appalachian Zone

Citation	Title	Description and Relevance to SSC
		<ul style="list-style-type: none"> • The Baie Verte–Brompton line forms the SE limb of the Sutton Mountains anticlinorium. Exhibited normal faulting during the Late Silurian to Early Devonian. • The La Guadeloupe fault is an Acadian reverse fault. The unusual thrust geometry is attributed to tectonic inversion of normal faults during Acadian compression.
West and Roden-Tice (2003)	Late Cretaceous Reactivation of the Norumbega Fault Zone, Maine: Evidence from Apatite Fission-Track Ages	Apatite fission-track ages across the Norumbega fault zone in southern Maine range from 113 to 89 Ma west of the fault and 159 to 140 Ma east of the fault. This age distribution is attributed to 2 km (1.2 mi.) east-side-down vertical displacement during the Late Cretaceous.

Table D-7.3.4 Data Summary
Paleozoic Extended Crust Zone

Citation	Title	Description and Relevance to SSC
General for Region		
Adams et al. (1995)	Northeastern North American Earthquake Potential—New Challenges for Seismic Hazard Mapping	The authors developed seismic source zones based on hypothesis that stable continental earthquakes occur through reactivation of rift faults that break the integrity of continental crust, including Atlantic and Iapetus margins. Characterized faulted edge of Grenville continental crust that rifted during opening of Iapetus Ocean. Normal faults are currently reactivated as thrust faults within Canada and strike-slip faults in the U.S. The authors distinguish between Iapetus rift basins and failed Iapetus rifts.
Aleinikoff et al. (1995)	U-Pb Ages of Metarhyolites of the Catoclin and Mount Rogers Formations, Central and Southern Appalachians: Evidence for Two Pulses of Iapetus Rifting	<p>The authors determined U-Pb ages for zircons sampled from Catoclin (564 ± 9 Ma) and Mount Rogers (758 ± 12 Ma) formations. Tholeiitic flood metabasalt of Catoclin Formation crops out on both flanks of Blue Ridge anticlinorium from SE Pennsylvania to central Virginia and is overlain by Lower Cambrian rocks of Chilhowee Group. Catoclin Formation is underlain by rhyolite and arkose of Mechum River Formation, which contains clasts of Mesoproterozoic basement and Neoproterozoic Robertson River Igneous Suite. These rhyolites are thought to be the extrusive equivalent of the Battle Mountain Alkali Feldspar Granite of the Robertson River Igneous Suite.</p> <p>Bimodal volcanic rocks and interlayered sedimentary rocks of 760 Ma Mount Rogers Formation crop out in SW Virginia, North Carolina, and Tennessee. The Mount Rogers Formation nonconformably overlies Mesoproterozoic Cranberry Gneiss and is overlain by glaciogenic Konnarock Formation, which is overlain by the Chilhowee Group. The authors attribute these ages to two rifting events between 760 and 700 Ma and 570 and 560 Ma and correlate rifting in Sutton Mountains region with younger event. Study suggests that thick sediments of Ocoee Supergroup represent a long, slow episode of crustal extension and that Mount Rogers embayment is older than South Mountain and Sutton Mountains embayments.</p>

Table D-7.3.4 Data Summary
Paleozoic Extended Crust Zone

Citation	Title	Description and Relevance to SSC
Bédard and Stevenson (1999)	The Caldwell Group Lavas of Southern Quebec: MORB-Like Tholeiites Associated with the Opening of Iapetus Ocean	The authors obtained trace element and Nd isotopic data for Caldwell Group lavas of southern Quebec. These undated rocks, within Internal Nappe domain of Humber zone, were deformed during the Taconic orogeny. The rocks initially formed at an advanced stage in transition from rift to drift along Iapetus margin. Despite exhibiting clear evidence of hydrothermal alteration, several conclusions were inferred from the geochemistry of these basalts. These basalts crystallized from melts derived from normal mid-ocean ridge basalt (MORB) at low- to medium-pressure fractional crystallization. Most lavas represent about 20% melting from a source slightly less depleted than fertile MORB mantle (asthenospheric mantle), whereas subpopulations of Caldwell lavas represent only 6%–15% melting of the same source mantle. These data are substantiated by Nd-isotope data that indicate derivation from a mantle depleted of light rare earth elements that is more radiogenic than other Iapetus basalts, implying other basalts in the region were derived from a more enriched source. Sedimentary samples reflect mixture of old (Archean) and juvenile (Iapetus) crustal sources for the basin.
Du Berger et al. (1991)	The Saguenay (Quebec) Earthquake of November 25, 1988: Seismologic Data and Geologic Setting	Saguenay graben is defined by Lac Tchitogama and Ste-Marguerite River normal faults on north wall and Lac Kénogami normal fault on south wall. Ordovician limestones show downthrow of 500 m (1,640 ft.) along north wall. Subvertical brittle faults are found within and outside the graben. Lineaments in the region cluster at 000°, 015°, 030°, 050°, 105°, and 160°. The 015° and 030° lineaments correspond to NNE late Grenvillian ductile belts and some post-Ordovician brittle faults. The St. Lawrence rift reactivated 030° trend and produced 050° trend. The 160° trend is parallel to glacial strike. The 105° trend is prominent only in the Saguenay graben rosette. The 000° trend corresponds to a complex array of en echelon oblique short breaks near St. Maurice lineament, suggesting that St. Maurice marks transition between two structural domains.

Table D-7.3.4 Data Summary
Paleozoic Extended Crust Zone

Citation	Title	Description and Relevance to SSC
Faill (1997a)	A Geologic History of the North-Central Appalachians. Part 1. Orogenesis from the Mesoproterozoic Through the Taconic Orogeny	<p>Crustal extension and rifting late in the Neoproterozoic and into the earliest Cambrian separated Neoproterozoic supercontinent Rodinia into East Gondwana, West Gondwana, and Laurentia. Breakup of Rodinia spanned approximately 200 Myr, with separation of East Gondwana from western Laurentia approximately 750 Ma, and rifting of eastern Laurentia from West Gondwana resulting in the opening of several intervening oceans. Iapetus Ocean initially defined as early Paleozoic ocean between Baltica and Laurentia (Greenland); Theic Ocean defined as ocean between Laurentia and Gondwana, and Rheic Ocean as ocean between Baltica and Gondwana. This study emphasizes that subsequent universal usage of Iapetus refers to the Paleozoic ocean off Laurentia east margin and that sensu stricto the Iapetus Ocean was closed in Late Silurian Caledonia orogeny during docking of Avalonia microcontinents with Laurentia. The remaining ocean that lay east of Avalonia is generally called Theic, leading the author to recognize Paleozoic ocean east of Laurentia as Theia.</p> <p>Evidence of initial breakup of Rodinia along western margin of Laurentia exists in southern Appalachian Virginia/North Carolina Blue Ridge as 760 Ma continental rift-facies volcanic Mount Rogers Formation and as largely nonvolcanic Ocoee rift deposits farther to the SW. The events may have been related to opening of Pacific Ocean.</p> <p>Rocks of Catoclin rift of Virginia, Maryland, and Pennsylvania comprise volcanic rocks of Catoclin Formation and sedimentary clastics of Chilhowee Group. These rocks, along with rocks of the St. Lawrence rift, suggest a fairly uniform-composition magma generation along eastern margin of Laurentia during the second phase of rifting.</p>

Table D-7.3.4 Data Summary
Paleozoic Extended Crust Zone

Citation	Title	Description and Relevance to SSC
Faure et al. (2006)	Paleostress Analysis of Atlantic Crustal Extension in the Quebec Appalachians	<p>Fault stress tensors indicate that most E-W to ESE-WNW-oriented stress is found in Montreal and Gaspé area, whereas SE-NW stress is found in SE Quebec. Late Triassic–Jurassic dikes in New England and southern Quebec indicate SE-NW-oriented extension consistent with fault slip stress. The N-S-trending portion of a Jurassic dike in southern Quebec is consistent with regional E-W extensional stress axis, whereas the NE-SW branch of this dike is more compatible with a local and adjacent NW-SE extension. Stress axes exhibit clockwise rotation in the White Mountain magma series, possibly due to local deviatoric stresses or a NE-SW-oriented basement fault.</p> <p>Faure et al. (2006) attribute these two extensional paleostress trends to either (1) contemporaneous regional partitioning of ESE-WNW-oriented extension influenced by N-S-trending structures in the Champlain Lake Valley and by NE-SW-trending structures of the St. Lawrence rift, or (2) an initial Late Triassic E-W extension related to formation of Bay of Fundy and South Georgia rift basins and Early Jurassic ESE-WNW extension related to central Atlantic rift system.</p>
Gates and Volkert (2004)	Vestiges of an Iapetan Rift Basin in the New Jersey Highlands: Implications for the Neoproterozoic Laurentian Margin	<p>Neoproterozoic rift basin deposits of Chestnut Hill Formation allow correlation between Iapetan rift basins in both northern and southern Appalachians. Immature, locally derived sediments of Chestnut Hill Formation were deposited into early alluvial, and later fluvial, lacustrine, and deltaic environments. Outcrops of Chestnut Hill Formation are associated with Morgan Hill and Chestnut Hill fault systems, which display transition in normal faulting from ductile to brittle moving upward in the geologic section. The authors recognize that Chestnut Hill basin may not be the most inboard Neoproterozoic basin, and may in fact open the possibility that Iapetan margin contains other basins beneath Valley and Ridge cover.</p>

Table D-7.3.4 Data Summary
Paleozoic Extended Crust Zone

Citation	Title	Description and Relevance to SSC
Higgins and van Breemen (1998)	The Age of the Sept Iles Layered Mafic Intrusion, Canada: Implications for the Late Neoproterozoic/Cambrian History of Southeastern Canada	<p>The authors obtained U-Pb ages of 565 ± 4 Ma for Sept Iles layered mafic pluton located on Gulf of St. Lawrence islands and peninsulas. Combining these results with other published ages for Neoproterozoic to Cambrian igneous rocks from Laurentian margin suggests three phases of magmatism:</p> <ol style="list-style-type: none"> 1. Tholeiitic dike emplacement was diachronous along Laurentian margin: Long Range dike swarm in Newfoundland was dated at 615 ± 2 Ma over a distance of 400 km (250 mi.) (Kamo et al., 1989); Grenville dike swarm formed synchronously with the Ottawa graben at $590 +2/-1$ Ma over a distance of 400 km (250 mi.) (Kumarapeli, 1993; Kamo et al., 1995). These dike swarms may have been produced by one or two mantle plumes between 615 and 590 Ma, possibly one at Sept Iles. 2. Following dike emplacement, alkali plutons intruded into a relatively large region spanning Quebec, Ontario, Greenland, and Scandinavia as early as 578 Ma and as late as Sept Iles intrusion (565 Ma). The authors attribute these plutons to a major plume located at Sept Iles instead of the location below the Sutton Mountains proposed by Kumarapeli (1993), but acknowledge that the two dike swarms could be result of two mantle plumes separated by 25 Myr. The authors also observe that alkalic plutons were intruded along rift faults that developed after emplacement of dikes. 3. Undated diabase dikes and metabasaltic flows occur throughout northern Appalachians, indicating earliest stages of formation of Iapetus Ocean. Tholeiitic lavas of Tibbit Hill Formation have U-Pb zircon ages of $554 +4/-2$ Ma (Kumarapeli et al., 1989); and alkali volcanic rocks at Skinners Cove, Newfoundland, have U-Pb ages of $550 +3/-2$ Ma (McCausland et al., 1997).
Hodych and Cox (2007)	Ediacaran U-Pb Zircon Dates for the Lac Matapédia and Mt. St.-Anselme Basalts of the Quebec Appalachians: Support for a Long-Lived Mantle Plume During the Rifting Phase of Iapetus Opening	<p>U-Pb zircon ages for Lac Matapédia basalt (565 ± 6 Ma and 556 ± 5 Ma) and Mt. St.-Anselme basalt (550 ± 7 Ma) support interpretation of a long-lived Sutton Mountains mantle plume. These data close the gap between end of flood basalt and beginning of plume magmatism, and support a rift-drift transition at 540 Ma, as opposed to 570 Ma (McCausland and Hodych, 1998). This hypothesis implies that Laurentia drifted northward more slowly than was suggested by McCausland and Hodych (1998).</p>

Table D-7.3.4 Data Summary
Paleozoic Extended Crust Zone

Citation	Title	Description and Relevance to SSC
Howell and van der Pluijm (1999)	Structural Sequences and Styles of Subsidence in the Michigan Basin	Subsidence of Michigan basin began in late Cambrian to Early Ordovician. Subsequent episodes of subsidence responded to Appalachian tectonic events, resulting in evolution of the style and geometry of subsidence. These observations do not indicate that lapetan rifting affected the Michigan basin.
Kanter (1994)	Tectonic Interpretation of Stable Continental Crust	<p>Northern and central portions of North America are an amalgamation of various Archean and Proterozoic domains assembled during the Mesoproterozoic. During the very late Neoproterozoic and continuing into the earliest Paleozoic, rifting occurred along eastern and southern margins, resulting in a passive margin.</p> <p>The author classified St. Lawrence–Ottawa domain (#227) as a Paleozoic rift, remnant of an east-facing continental margin of an ocean basin that closed during formation of Appalachian Mountains, as evidenced by Appalachian thrust sheets overlapping eastern edge. Domain is defined on basis of fractures and normal faults in basement, alkalic intrusions, and Paleozoic sedimentary rocks that overlie basement. The presence of coarse clastics presumed to be of late Proterozoic age in eastern end of Ottawa graben implies that initiation of this rift system may have occurred in late Neoproterozoic.</p> <p>The author did not classify as extended any other Paleozoic domains south of St. Lawrence–Ottawa domain along eastern margin. The Newfoundland (#220) and Acadia (#222) domains consist of large clastic wedges formed as a result of Taconic accretionary events. Portions of Piedmont domain (#223) were deformed during Taconic orogeny, were accreted during Acadian strike-slip deformation (which affected the entire Appalachians), and experienced intense deformation during the widespread Alleghanian orogeny. Valley and Ridge province (domain #224) consists of miogeoclinal sediments overlying Grenville-age basement deformed as a thin-skinned fold and thrust belt west of Piedmont domain.</p> <p>Outboard of these domains, the Eastern Seaboard domain (#218) records Mesozoic extension resulting from breakup of Pangaea.</p> <p>Study determined that the distinction between extended and non-extended domains was the only statistically significant variable on basis of maximum magnitude.</p>

Table D-7.3.4 Data Summary
Paleozoic Extended Crust Zone

Citation	Title	Description and Relevance to SSC
Kamo et al. (1995)	Age of the Grenville Dyke Swarm, Ontario, Quebec: Implications for the Timing of Iapetan Rifting	<p>Updates geochronology of Grenville dike swarm by obtaining U-Pb baddeleyite ages from widest dikes throughout Ottawa graben. Revised age of 590 Ma suggests Grenville dike swarm was emplaced within a relatively short time span. These dikes are thought to have formed at onset of rifting within Ottawa graben, Sutton Mountains triple junction, and the related segment of Iapetan margin. Comparison with ages of similar rift-related igneous rocks along Iapetan margin of Laurentia, including Bakersville dike swarm of the Blue Ridge (570 Ma), Franklin swarm of northern Canadian Shield (723 Ma), and Long Range dikes of SE Labrador and Newfoundland (615 Ma), indicate that Iapetan rifting occurred along vast distances of northern and eastern margins of Laurentia. The timing of initial rifting within Ottawa graben is somewhat earlier than other parts of North America, suggesting that rift initiation progressed from northern Laurentia margin at 723 Ma to Labrador and Newfoundland at 615 Ma, followed by Grenville dike swarm at 590 Ma.</p>
Kumarapeli and Saul (1966)	The St. Lawrence Valley System: A North American Equivalent of the East African Rift Valley System	<p>Proposes rift origin for St. Lawrence valley system, including Ottawa-Bonnechere and Saguenay grabens. Discusses the evidence supporting this conclusion, including the following:</p> <ul style="list-style-type: none"> • Escarpments on NW side of St. Lawrence valley, north side of Ottawa Bonnechere graben, and western margin of Champlain Lake Valley. • South of Ottawa-Bonnechere graben, tilting of Madawaska Highlands to the south, NW tilting of Adirondack massif, north tilting of a Laurentian block south of Saguenay graben, and south block tilting of Gaspé Peninsula. • En echelon normal faults along NW boundary with vertical displacements between 450 and 1,200 m (1,476 and 3,937 ft.). • St. Barnabe fault, a 55 km (34 mi.) normal fault on SE margin with 600 m (1,969 ft.) of downthrow to the west. • Concentrations of historical seismicity along St. Lawrence and Ottawa valleys and St. Lawrence trough. • Presence of a negative Bouguer anomaly in rift valley. • Connection of St. Lawrence valley with Mississippi embayment. • Westward continuation of Ottawa-Bonnechere graben with Midcontinent rift system.

**Table D-7.3.4 Data Summary
Paleozoic Extended Crust Zone**

Citation	Title	Description and Relevance to SSC
		Because the publication pre-dated plate tectonics, many aspects of the authors' ideas are not consistent with current tectonic models of the region. After comparing St. Lawrence rift system to East African rift system, the authors suggest that the Great Lakes may be analogous to Lakes Victoria and Kyoga. The authors also associate Monteregian alkaline intrusives with St. Lawrence valley. Recent work associates them with Cretaceous intrusion that formed during reactivation of Ottawa-Bonnechere graben.
Kumarapareli (1985)	Vestiges of Iapetan Rifting in the Craton West of the Northern Appalachians	Proposes that a mantle plume produced initial ruptures of Iapetan rifting along a triple junction that led to continental fragmentation and development of an aulacogen in Ottawa graben. Alkaline to transitional bimodal volcanic rocks of the Tibbit Hill volcanics are deposited within Sutton Mountains salient, east of Ottawa graben, and are thought to be coeval with Grenville dike swarm within Ottawa graben. Interprets Sutton Mountains as the triple junction that initiated Iapetan rifting.
Kumarapeli et al. (1988)	Volcanism on the Passive Margin of Laurentia: An Early Paleozoic Analogue of Cretaceous Volcanism on the Northeastern American Margin	Transitional to alkaline basalts and mid-ocean ridge basalts (MORBs) found within Granby nappe of SE Quebec provide evidence for late Cambrian to Early Ordovician volcanism within transverse fracture zones analogous to Early Cretaceous volcanism in the Atlantic. The authors acknowledge that this data set is not sufficient to determine whether volcanism took place during drifting phase of continental margin because precise age of these rocks is not known. These allochthonous blocks are thought to represent slabs dislodged from the ancient shelf-margin sequence, possibly by Ottawa graben faults and NE-trending faults.
Kumarapeli (1993)	A Plume-Generated Segment of the Rifted Margin of Laurentia, Southern Canadian Appalachians, Seen Through a Completed Wilson Cycle	Updates mantle plume model presented by Kumarapeli (1985) with geochronology of dike swarms and volcanic rocks. Proposes that initiation of rifting was accompanied by emplacement of 590 Ma Grenville mafic dike swarm of tholeiitic composition. Rifting continued for 35 Myr until an outburst of alkaline to transitional basalts at Sutton Mountains triple junction dated at 554 Ma. This was quickly followed by a short period of rift-facies clastic sedimentation consisting of conglomerates attributed to a large river delta. Rift-drift transition is indicated by deposition of open-marine sedimentation, thought to have occurred 550 Ma based on presence of rocks with early Cambrian fauna above this transition.

Table D-7.3.4 Data Summary
Paleozoic Extended Crust Zone

Citation	Title	Description and Relevance to SSC
Lavoie et al. (2003)	Stratigraphic Framework for the Cambrian-Ordovician Rift and Passive Margin Successions from Southern Quebec to Western Newfoundland	<p>In the Quebec Reentrant, platform rocks were only marginally involved in tectonic stacking of Taconic orogeny, and form a spatially restricted frontal Taconian deformation zone that is known as the para-autochthonous or imbricate fault domain, and is therefore not considered part of Humber zone. The Quebec Reentrant is rooted in the autochthonous St. Lawrence platform. These structural relationships allow for stratigraphic and paleogeographic scenarios for early evolution of Quebec-Newfoundland segment of continental margin slope of Laurentia.</p> <p>Neoproterozoic to latest early Cambrian rift volcanics are overlain by rift-drift transition successions of early Cambrian Sauk I sequence. A global sea-level lowstand resulted in an unconformity that separates these rocks from shallow marine middle Cambrian to Middle Ordovician rocks of Sauk II and Sauk III subsequences. An extensive debris flow unit resedimented the middle Cambrian slope succession and is attributed to tectonic instability during middle to late Cambrian. The authors suggest that reactivation of Saguenay graben could be responsible for the anomalous upper Cambrian succession. Similar syndepositional tectonic activity is observed in the younger St. Lawrence platform succession in Charlevoix area during Middle to Late Ordovician. The authors present locations of reentrants and promontories for eastern margin of Laurentia farther north than those of Thomas (1991).</p>
Lemieux et al. (2003)	Structural Analysis of Supracrustal Faults in the Charlevoix Area, Quebec: Relation to Impact Cratering and the St-Laurent Fault System	<p>Two major sets of fault orientations (N290°–N320° and N020°–N040°) are found outside impact zone, with minor fault sets trending N270°–N280° and N000°–N020°. Within the impact crater, fault orientations are more scattered but are similar to NW- and NE-trending systems of external domain. Spread of orientations within central portion of crater is attributed to the impact-related polygonal pattern of normal faults, whereas NW and NE fault sets represent youngest reactivation.</p> <p>Coarse-grained cataclastic breccias up to 50 m (164 ft.) thick are exposed along brittle faults striking NE and NW outside impact crater. Similar cataclastic breccias are also found within the impact crater but are usually less than a few meters thick. Polymictic clastic matrix breccia are found exclusively within impact crater. Fragments of cataclastic breccia are present, suggesting recurrent brecciation during incremental faulting events. Pseudotachylyte and foliated gouge are locally related to cataclastic breccia, indicating that these rocks originate from a post-impact, single, and progressive tectonic event along</p>

**Table D-7.3.4 Data Summary
Paleozoic Extended Crust Zone**

Citation	Title	Description and Relevance to SSC
		<p>St. Lawrence rift system.</p> <p>The St-Laurent fault influenced deposition of Ordovician deposits during late stages of Taconian orogeny as indicated by syndepositional faulting preserved as major lateral thickness variations within the section, presence of slump deformation in almost all stratigraphic units, preservation of pseudotachylyte within synsedimentary breccias, and occurrence of fault breccia clasts. However, the geometry and structural characteristics of faulting are consistent with Mesozoic fault reactivation due to rifting of North Atlantic region.</p>
McBride et al. (2005)	Integrating Seismic Reflection and Geological Data and Interpretations Across an Internal Basement Massif: The Southern Appalachian Pine Mountain Window, USA	The authors trace the master Appalachian decollement from Inner Piedmont to Coastal Plain. They find that beneath the Carolina terrane, the decollement roots to the Moho, indicating the location of Acadian-Alleghanian suture.
McCausland and Hodych (1998)	Paleomagnetism of the 550 Ma Skinner Cove Volcanics of Western Newfoundland and the Opening of the Iapetus Ocean	The authors obtained paleomagnetic data for volcanic flows and volcanoclastic sediments of Skinner Cove Formation in western Newfoundland dated at 550 Ma that point to paleolatitude of $19^{\circ}\text{S} \pm 9^{\circ}$. This result represents paleolatitude of Iapetus margin at that time. Comparison of these results to those of 577 Ma Callander Complex of Ontario indicates rapid northward drift of Laurentia at approximately 570 Ma resulting from opening of Iapetus Ocean, which continued to the rift-drift transition at approximately 550 Ma.
Mereu et al. (1986)	The 1982 COCRUST Seismic Experiment Across the Ottawa-Bonnechere Graben and Grenville Front in Ontario and Quebec	Results of 1982 Canadian Consortium for Crustal Reconnaissance Using Seismic Techniques (COCRUST) long-range seismic refraction experiment show a sharp, step-like displacement of the Moho beneath south shoulder of Ottawa graben, confirming deep-seated nature of its faults and penetration of mantle melts into crust. Furthermore, COCRUST surveys show poorly defined Moho at unusually shallow depths beneath graben.
Petersen et al. (2008)	Documentation for the 2008 Update of the United States National Seismic Hazard Maps	The most recent model for the national seismic hazard maps for CEUS incorporates maximum magnitude distributions that are considered separately for the craton and the Iapetus rifted margin as determined by Wheeler (1995). Model selects values based on analogy with other stable continental regions: four values of moment magnitude between M 6.6 and M 7.2 (Charleston areal zone) for the craton, and four values of moment magnitude between M 7.1 (Charleston main shock) and M 7.7 (Bhuj, India) for the extended margin.

Table D-7.3.4 Data Summary
Paleozoic Extended Crust Zone

Citation	Title	Description and Relevance to SSC
Pratt et al. (1988)	A Geophysical Study of the Earth's Crust in the Central Virginia: Implications for Appalachian Crustal Structure	The authors conclude that crustal thinning (at Taconic suture) in the Piedmont is responsible for Appalachian gravity gradient.
Rimando and Benn (2005)	Evolution of Faulting and Paleo-Stress Field Within the Ottawa Graben, Canada	The authors observe three periods of faulting in Cambro-Ordovician sedimentary rocks within eastern end of Ottawa graben, near Ottawa. The oldest generation of faults formed in stress field with a horizontal maximum compressive stress (σ_1) oriented NW. These structures are kinematically congruent with the compression direction associated with closing of Iapetus Ocean. Second generation of faults indicates a WNW-oriented σ_1 and coincides with emplacement of Cretaceous carbonatite dikes. Third generation of faults has a σ_1 oriented SW, which is consistent with post-Cretaceous stress field in eastern North America.
Rocher et al. (2003)	Brittle Fault Evolution of the Montréal Area (St. Lawrence Lowlands, Canada): Rift-Related Structural Inheritance and Tectonism Approached by Palaeostress Analysis	<p>NW-SE extension associated with opening of Iapetus Ocean resulted in formation of N040-trending faults along north shore of St. Lawrence Lowlands and development of three major N090-trending faults that define a succession of horsts and grabens on Montréal and Jésus islands and N120-trending faults in Montreal area. The N090-trending faults have the following geometries:</p> <ol style="list-style-type: none"> 1. Bas-Sainte-Rose fault zone, the northernmost series of N090-trending faults in Montreal area, is a steeply north-dipping fault with approximately 200 m (656 ft.) of vertical displacement and nearly 3 km (2 mi.) of apparent left-lateral offset. Offsets on Bas-Sainte-Rose fault zone decrease as fault zone extends westward, where it apparently crosscuts the N020-trending Rivière-aux-Mille-Iles fault zone. 2. Rapide-du-Cheval-Blanc consists of a series of steeply south-dipping normal faults (Ile-Bizard, Rapide-du-Cheval-Blanc, and Outremont) with a total vertical offset of approximately 100 m (326 ft.). 3. Sainte-Anne-de-Bellevue fault zone is a north-dipping normal fault with a left-lateral strike-slip component in southern part of Montréal Island. Its vertical offset has not been precisely determined. <p>All three faults clearly crosscut NNE-SSW-trending folds from Appalachian Chambly-Fortierville syncline system in Trois-Rivières seismic zone.</p> <p>WNW-ESE compressions followed by minor NNW compressional events are</p>

**Table D-7.3.4 Data Summary
Paleozoic Extended Crust Zone**

Citation	Title	Description and Relevance to SSC
		<p>associated with Appalachian thrusting. WNW compression reactivated N090-trending faults as strike-slip right-lateral faults, and reactivated N040-070 and N120 faults as reverse to strike-slip faults. Subsequent NNW compression is responsible for strike-slip conjugate faults trending NW-SE and NNE.</p> <p>NE-SW and NNW-SSE extension is associated with opening of North Atlantic–Labrador Sea and reactivated faults with normal to strike-slip motions. NNW extension is responsible for horst-and-graben geometry of major N090 normal faults described above. Late NE-SW compression is recorded in Montereian plutons. NE-SW compression postdating these events is associated with formation of strike-slip faults that crosscut Montereian intrusions and is consistent with current stress regime.</p>
Spencer et al. (1989)	The Extension of Grenville Basement Beneath the Northern Appalachians: Results from the Quebec-Maine Seismic Reflection and Refraction Surveys	<p>A master decollement separating autochthonous Grenville basement from overlying allochthonous rocks of Appalachian orogen extends over a distance of 200 km (124 mi.) and can be traced from shallow depths beneath St. Lawrence Lowlands SE to about 25 km (15.5 mi.) depth beneath SE edge of Chain Lakes massif. Basement is offset by closely spaced en echelon normal faults, with displacements between 200 and 1,000 m (656 and 3,281 ft.) interpreted as lapetan growth faults.</p> <p>The Baie Verte–Brompton line, separating Cambrian and Ordovician continental slope and rise deposits from oceanic arc and magmatic assemblages to south, including Chain Lakes massif, is imaged as shallow, thin-skinned structure. Chain Lakes terrane is thought to underlie much of Connecticut Valley–Gaspé synclinorium. Acadian Guadeloupe fault disrupts master decollement of Taconian orogeny and thrusts Connecticut Valley–Gaspé synclinorium over Chain Lakes massif.</p>
St. Julien and Hubert (1975)	Evolution of the Taconian Orogen in the Quebec Appalachians	<p>Describes 11 lithostratigraphic assemblages distributed among autochthonous, external, and internal domains of Quebec Appalachians.</p> <p>The autochthonous domain contains Cambrian and Ordovician sandstones and carbonates representing transgressive shelf deposits, Middle and Upper Ordovician flysch deposits, and Upper Ordovician shale and sandstone representing the post-tectonic regressive sequence. This domain contains E-W- and N30E-trending normal faults active between late Precambrian and Late Ordovician.</p>

Table D-7.3.4 Data Summary
Paleozoic Extended Crust Zone

Citation	Title	Description and Relevance to SSC
Swanson (1986)	Preexisting Fault Control for Mesozoic Basin Formation in Eastern North America	Correlates Mesozoic basin formation with reactivation of specific Paleozoic reverse and strike-slip faults along Appalachians.
Thomas (1991)	The Appalachian-Ouachita Rifted Margin of Southeastern North America	<p>Synthesizes available data into an interpretation of mechanisms controlling shape and timing of lapetan rifted margin. NW-SE extension along entire rift system resulted in NE-trending rift (normal) faults and NW-trending transform faults. Rifting began in late Precambrian along Blue Ridge rift. By beginning of Cambrian, Blue Ridge progressed to a passive margin flanked by lapetus Ocean, extension occurred along Mississippi Valley, Rough Creek, Rome, and Birmingham fault systems, and mafic magmas were emplaced along Southern Oklahoma fault system, suggesting the spreading center moved from Blue Ridge rift to Ouachita rift in early Cambrian. This was accompanied by initiation of Alabama-Oakland transform and Southern Oklahoma fault system. Some extension was propagated into Mississippi Valley, Rough Creek, Rome, and Birmingham fault systems, but this did not result in opening of an ocean. By early late Cambrian, the entire rift and transform margin evolved into passive margin.</p>
Thomas (2006)	Tectonic Inheritance at a Continental Margin	<p>Explores tectonic inheritance of crustal structure through two Wilson cycles. The pre-Rodinia continental margin is unknown; however, possible inheritance from a dextral offset in older continental margin may result in the dextral bend of Grenville front beneath Gulf Coastal Plain. The New York–Alabama lineament, possibly an intra-Grenville suture, may represent either accretion along a straight segment of rifted margin or orogen-parallel slip across the shape of the margin. The palinspastically restored lapetan margin consists of NE-striking rift segments offset by NW-striking transform faults, which in turn frame promontories and embayments of rifted continental margin.</p> <p>The trace of Alabama-Oklahoma transform corresponds to probable location of a large-scale dextral bend in Grenville front. Rift-parallel graben systems, including Rome trough and Birmingham graben, indicate late synrift extension inboard from the rifted margin; their relationship to older tectonic fabrics is obscure and presently unrecognized. A pervasive lithospheric fabric may result in successive reoccupation of traces of transform faults at continental margin and differential crustal subsidence along transform faults at rift offsets in continental embayments. The shape of lapetan margin controlled orientation of Appalachian-Ouchita foreland structures and subsequent continental margin of</p>

Table D-7.3.4 Data Summary
Paleozoic Extended Crust Zone

Citation	Title	Description and Relevance to SSC
		Atlantic and Gulf Coastal Plain.
Tremblay and Lemieux (2001)	Supracrustal Faults of the St. Lawrence Rift System Between Cap-Tourmente and Baie-Saint-Paul, Quebec	<p>The Cap-Tourmente and St. Lawrence faults are late Proterozoic–early Paleozoic normal faults attributed to rifting during opening of the Iapetus Ocean.</p> <p>The St. Lawrence fault trends N020°–N050° and dips 60°–70° to SE. Fault rocks consist of fault breccia, cataclastite, foliated gouge, and pseudotachylyte with a minimum thickness of 20 m near Sault-au-Cochon. Fault rocks exposed at Cap-Tourmente consist of 10–15 m thick zones of protocataclasite, cataclasite, and fault breccia. Within Charlevoix area, the St. Lawrence fault is characterized by a well-developed and extensive series of cataclastic rock, gouge, and associated pseudotachylyte.</p> <p>The Cap-Tourmente fault trends E-W and dips approximately 80° to the south. Fault rocks consist mostly of fault breccia more than 10 m thick, as well as cataclastic rocks and dark pseudotachylyte veins. The St. Lawrence fault is crosscut by Cap-Tourmente fault at Cap-Tourmente.</p> <p>West of Cap-Tourmente, the Montmorency Falls fault occupies the same structural position as the St. Lawrence fault, suggesting that they formed from an echelon faults trending parallel to axis of St. Lawrence rift.</p> <p>The Cap-Tourmente fault possibly represents a transfer fault, producing an oblique relay between two longitudinal normal faults.</p> <p>The St. Lawrence fault crosses the Charlevoix impact crater without major trend deflection or fault offsets within or at the boundaries of the Devonian impact structure. This observation suggests that impact-related faults did not significantly alter the orientation of preexisting structures and that reactivation is younger than the impact structure, most probably concurrent with opening of the Atlantic Ocean in the Mesozoic.</p>
Tremblay et al. (2003)	Supracrustal Faults of the St. Lawrence Rift System, Quebec: Kinematics and Geometry Revealed by Field Mapping and Marine Seismic Reflection Data	Presents strike orientations, dip angles, and pitch angles for faults with evidence of frictional sliding in the St. Lawrence rift system. NE-trending longitudinal faults show three trends (N025, N040, and N070) and generally dip to SE, although a minor number dip to NW. Transverse faults show two trends (N290 and N310) and dip to NE or SW, which is consistent with horst-and-graben geometry. Both sets of faults are high-angle faults with dip angles averaging 75°–80°. The pitch value of fault lineations is greater than 70°, indicating that most structures are dip-slip faults. Longitudinal and transverse

Table D-7.3.4 Data Summary
Paleozoic Extended Crust Zone

Citation	Title	Description and Relevance to SSC
		<p>faults show mutual crosscutting relationships, suggesting that they represent conjugate structures related to same tectonic event.</p> <p>St-Laurent fault has experienced at least 800 m (2,625 ft.) of vertical throw at Sault-au-Cochon. Cap-Tourmente fault has a minimum vertical fault throw of 700 m (2,297 ft.). Montmorency fault has an 80 m (262 ft.) fault scarp near Quebec City; stratigraphic analysis suggests that fault throw should be less than 150 m (492 mi.), which is considerably less than the other faults. Several offshore faults subparallel to that fault may have vertical downthrow displacements up to 1 km (0.6 mi.).</p> <p>Longitudinal faults likely result from development of en echelon faults trending parallel to the rift axis, and transfer faults represent transfer faults or accommodation zones. Variations in fault throw are likely a result of propagation of extension along transfer faults.</p> <p>Presence of cataclastic rocks, pseudotachylytes, and fault gouge is consistent with changes of deformation mechanics during progressive and incremental deformation in upper crust.</p> <p>High-resolution seismic profiles in St. Lawrence estuary indicate that Laurentian Channel trough transitions from a half graben to a graben structure from SW to NE.</p> <p>The authors speculate that reactivation of St. Lawrence rift system is post-Ordovician, younger than the Devonian impact cratering event, and that the rift system experienced additional fault throw and shoulder uplift during Mesozoic opening of North Atlantic.</p>
Valentino and Gates (1995)	Iapetan Rift-Related Turbidite-Fan Deposits from the Central Appalachian Piedmont	<p>Peters Creek Formation of SE Pennsylvania and northern Maryland consists of two submarine turbidite-fan systems. Metaclastic strata of Peters Creek Formation preserve primary detrital and bedding features indicative of deposition in turbidite-fan systems. Presence of greenstone interlayered with feldspathic metasandstone suggests rift-related deposition. Granitic lithic fragments indicate unroofing of continental crust. Peters Creek Formation may represent deposits transported along an Iapetan rift-related transform fault linking southern Lynchburg rift basin with a comparable rift basin in southern New England.</p>

Table D-7.3.4 Data Summary
Paleozoic Extended Crust Zone

Citation	Title	Description and Relevance to SSC
Walsh and Aleinikoff (1999)	U-Pb Zircon Age of Metafelsite from the Pinney Hollow Formation: Implications for the Development of the Vermont Appalachians	U-Pb zircon age of 571 ± 5 Ma for metafelsite from Pinney Hollow Formation of Vermont records age of rhyolitic volcanism and deposition in a largely pelitic sequence interpreted as pre-shelf rift-clastic sequence. This age agrees with other ages from rift-clastic volcanic rocks in the Appalachians. Relative distribution and thickness of metavolcanic and metafelsic sections throughout Appalachians suggest the basin that Pinney Hollow Formation was deposited into was already well developed when the 571 Ma metafelsite was deposited. Therefore, the 554 Ma age for Tibbit Hill Formation at Sutton Mountains triple junction does not represent first pulse of volcanic activity during initial opening of Iapetan basin in Vermont and Quebec Appalachians. This age also validates theory that Wood Peak fault is a significant thrust fault separating autochthonous and para-autochthonous cover sequence rocks, which in turn supports interpretation that the Taconic root zone is located in hinterland of Vermont Appalachians on eastern side of Green Mountain massif.
Wheeler (1995)	Earthquakes and the Cratonward Limit of Iapetan Faulting in Eastern North America	Recognizes that seismic activity within the Charlevoix, Quebec; Giles County, Virginia; Eastern Tennessee; and, possibly, Clarendon-Linden seismic zones is attributed to compressional reactivation of NE-trending Iapetan normal faults. Defines NW limit of potentially seismogenic Iapetan normal faults from a variety of data sets available at the time. This boundary, with an uncertainty of 21 km (13 mi.), separates lower rates of seismicity to the NW from higher rates to the SE and suggests that seismic zones to the SE of the line can produce large earthquakes such as those at Charlevoix.
Whitmeyer and Karlstrom (2007)	Tectonic Model for the Proterozoic Growth of North America	Breakup of Rodinia consists of diachronous disassembly. Early stages of rifting resulted in opening of a paleo-Pacific Ocean along western margin of Laurentia between 780 and 680 Ma, corresponding to separation of Australia, Antarctica, south China, and Siberia, and failed rifting along eastern margin of Laurentia. Complete breakup along eastern margin of Laurentia initiated by 620 Ma from Newfoundland to southern Appalachians. This final stage of breakup involved rifting of Argentina Precordillera terrane from Ouachita embayment. Transfer of Precordillera terrane across Iapetus Ocean requires relocating Iapetus spreading ridge from present-day Alabama to central Texas. This change in spreading may have occurred because of at least two incipient triple junctions that combined in SE United States in early Cambrian to initiate a new spreading ridge-transform system.

Table D-7.3.4 Data Summary
Paleozoic Extended Crust Zone

Citation	Title	Description and Relevance to SSC
<i>Geophysical Anomalies</i>		
New York–Alabama (NY-AL) Lineament		
King and Zietz (1978)	The New York–Alabama Lineament: Geophysical Evidence for a Major Crustal Break in the Basement Beneath the Appalachian Basin	NY-AL lineament consists of series of linear magnetic gradients that correspond with west side of regional Appalachian gravity low. This lineament extends more than 1,600 km (994 mi.) from Mississippi embayment to Green Mountains of Vermont. It separates north-trending gravity anomalies on the NW from NE-trending anomalies to the SE. Magnetic gradient of NY-AL lineament faces SE for some sections and NE for others. Given that regions of high magnetic values are cut off by the lineament, it likely represents a strike-slip fault as opposed to a vertical displacement. The lineament constitutes a major break in crystalline basement rocks of Appalachian basement separating stable craton of continental interior from more mobile Appalachian block of continental margin.
Steltenpohl et al. (2010)	New York–Alabama Lineament: A Buried Right-Slip Fault Bordering the Appalachians and Mid-continent North America	<p>NY-AL lineament is a N40E-trending magnetic lineament extending 1,600 km (994 mi.) from Vermont to southern Tennessee. From southern West Virginia to Tennessee, it separates a mottled pattern of magnetic highs and lows of the granite-rhyolite province and Neoproterozoic mafic rocks to the NW, from NE-trending magnetic lineaments of Appalachian orogen to the SE. NY-AL lineament is a fundamental tectonic boundary that may represent either an escape strike-slip fault related to Grenvillian contractual orogenesis, an axis of anatexis melting following continental collision, or an intra-Grenvillian suture.</p> <p>In Eastern Tennessee seismic zone (ETSZ), the Ocoee block is bounded by NY-AL lineament on the north and Clingman lineament on the south. NY-AL lineament is interpreted as strike-slip fault zone, based on truncation of Amish anomaly in West Virginia and on documentation of ~220 km (~137 mi.) of right-slip displacement and a trending magnetic high-low pair in SE block in Tennessee, Georgia, and Alabama. Linear fault segments that border Rome trough are parallel to and locally coincide with NY-AL lineament. SE border fault parallels lineament for nearly 250 km (155 mi.) from eastern KY to SW Pennsylvania. This segment of lineament was reactivated as a normal fault that underwent west-side-down dip-slip displacement during formation of Rome trough. Crust NW of NY-AL lineament behaved as a coherent block.</p> <p>Seismicity of ETSZ may be localized along the N15E-trending magnetic low</p>

Table D-7.3.4 Data Summary
Paleozoic Extended Crust Zone

Citation	Title	Description and Relevance to SSC
		anomaly in the Ocoee block, which coincides with metasedimentary gneiss correlative with the Amish anomaly. Modern stress field is compatible with the one that initiated dextral motion along NY-AL lineament.
Structures		
Rome Trough		
Drahovzal (1997)	Proterozoic Sequences and Their Implications for Precambrian and Cambrian Geologic Evolution of Western Kentucky: Evidence from Seismic Reflection Data	Rough Creek graben and Rome trough exhibit Cambrian fan complexes deposited in a subsiding basin to the north. This subsidence likely occurred in late Precambrian and may represent inboard extension of Iapetan rifting along the Mesoproterozoic East Continent rift basin.
Fail (1997a)	A Geologic History of the North-Central Appalachians. Part 1. Orogenesis from the Mesoproterozoic Through the Taconic Orogeny	Rome trough consists of steep normal faults that become listric at depth, recording intracontinental extension during middle and late Cambrian. It acted as middle Cambrian sediment trap, with quartzose facies accumulating to the west during late Cambrian. Siliclastic deposition along eastern margin of Laurentia was replaced by carbonate deposition during early Cambrian.
Stark (1997)	The East Continent Rift Complex: Evidence and Conclusions	Attributes development of Rome trough and reactivation of Kentucky River fault system to late Neoproterozoic extension associated with opening of Iapetus Ocean within East Continent rift complex.
Steltenpohl et al. (2010)	New York–Alabama Lineament: A Buried Right-Slip Fault Bordering the Appalachians and Mid-continent North America	Linear fault segments that border Rome trough parallel and locally coincide with the NY-AL lineament. The SE border fault is parallel to lineament for nearly 250 km (155 mi.) from eastern Kentucky to SW Pennsylvania. This segment of lineament was reactivated as a normal fault that underwent west-side-down dip-slip displacement during formation of Rome trough.
Van Arsdale and Sergeant (1992)	Post-Pliocene Displacement on Faults Within the Kentucky River Fault System of East-Central Kentucky	Kentucky River fault system forms northern boundary of Rome trough, a Paleozoic aulacogen. The absence of post-Paleozoic deposits prevents determination of Mesozoic and early Tertiary displacements. Trenches in terrace materials indicate folding and faulting within last five million years, and probably within last million years.

**Table D-7.3.4 Data Summary
Paleozoic Extended Crust Zone**

Citation	Title	Description and Relevance to SSC
Central Metasedimentary Belt Boundary Zone		
Forsyth, Milkereit, Davidson, et al. (1994)	Seismic Images of a Tectonic Subdivision of the Grenville Orogen Beneath Lakes Ontario and Erie	The authors observed extensional reactivation in Paleozoic section above Central Metasedimentary Belt boundary zone in eastern Lake Erie.
O'Dowd et al. (2004)	Structural Fabric of the Central Metasedimentary Belt of Southern Ontario, Canada, from Deep Seismic Profiling	Using results of Southern Ontario Seismic Project and analysis of regional magnetic data, the authors conclude that Central Metasedimentary Belt boundary zone must be located on west side of Mississauga domain, thereby placing it farther west.
Zones of Elevated Seismicity		
Clarendon-Linden Fault System		
Crone and Wheeler (2000)	Data for Quaternary Faults, Liquefaction Features, and Possible Tectonic Features in the Central and Eastern United States, East of the Rocky Mountain Front	Crone and Wheeler (2000) identify Clarendon-Linden fault zone in New York as Class C tectonic feature. Assessment is based on absence of paleoseismological evidence that fault zone has slipped during the Quaternary.
Dineva et al. (2004)	Seismicity of the Southern Great Lakes: Revised Earthquake Hypocenters and Possible Tectonic Controls	Hypocenters from earthquakes occurring between 1990 and 2001 were relocated; the redefined zones of seismicity delineate several clusters of events beneath Lake Ontario. The authors identified a cluster C that is parallel to Clarendon-Linden fault system but shifted slightly to SE by about 4 km (2.5 mi.). They note that during the 1990–2001 recording period for this analysis, little seismic activity occurred along Clarendon-Linden fault system, with only two events near southern end.
Fakundiny and Pomeroy (2002)	Seismic-Reflection Profiles of the Central Part of the Clarendon-Linden Fault System of Western New York in Relation to Regional Seismicity	Describes Clarendon-Linden fault system as broad zone of small faults with small displacements in lower Paleozoic bedrock. Fault system is at least 77 km (48 mi.) long and 7–17 km (4.5–10.5 mi.) wide; total vertical displacement across the zone is small (>91 m). Fault system is spatially coincident with a north-trending geophysical (combined magnetic and gravity) lineament within basement rock. Most earthquakes in the region cannot be unequivocally associated spatially with individual tectonic structures and lineaments.

Table D-7.3.4 Data Summary
Paleozoic Extended Crust Zone

Citation	Title	Description and Relevance to SSC
Forsyth, Milkereit, Zelt, et al. (1994)	Deep Structure Beneath Lake Ontario: Crustal-Scale Grenville Subdivisions	Using deep crustal seismic images, at least three major shear zones are interpreted to underlie Lake Ontario. Elzevir-Frontenac boundary zone defined based on a shear zone transition exposed to north of Lake Ontario between these two terranes and linked to a seismically defined shear zone extending beneath Lake Ontario to south shore. Iroquoian high is defined on basis of gradual thinning of Paleozoic section over a crestal area of Elzevir-Frontenac boundary zone. Iroquoian high is interpreted to help explain Paleozoic fractures that formed Clarendon-Linden structure in New York.
Jacobi (2002)	Basement Faults and Seismicity in the Appalachian Basin of New York State	Evaluates regional sets of lineaments identified on Landsat images and their relationship to faults and earthquake epicenter locations. Identifies Clarendon-Linden fault system as the most prominent of western New York State fault sources. A seismicity swarm is located along western flank of the gravity high associated with this fault system. The swarm terminates on north where gravity high diminishes in amplitude.
Jacobi and Fountain (2002)	The Character and Reactivation History of the Southern Extension of the Seismically Active Clarendon-Linden Fault System, Western New York State	By integrating a variety of surface and subsurface data, the authors determined that Clarendon-Linden fault system in SW New York State consists of as many as 10 parallel, segmented faults. Fault segments are truncated by cross-strike discontinuities. The rock record indicates that fault blocks formed by the fault segments and that cross-strike discontinuities were active in Precambrian and subsequently reactivated multiple times until Late Devonian.
Ouassaa and Forsyth (2002)	Interpretation of Seismic and Potential Field Data from Western New York State and Lake Ontario	Lithoprobe and seismic data provide evidence of major zones of east-dipping Grenville deformed crust extending from north of Lake Ontario toward SW. In the vicinity of Clarendon-Linden fault, N-NE-trending magnetic and gravity anomalies are parallel to, but are not restricted to, the principal trend of this fault system. Surface continuity of inferred faults constituting Clarendon-Linden fault system is not strongly supported by reprocessed seismic data.
<i>Paleoseismic Investigations</i>		
Seeber and Armbruster (1993)	Natural and Induced Seismicity in the Lake Erie–Lake Ontario Region: Reactivation of Ancient Faults with Little Neotectonic Displacement	Historical and recent earthquake activity is interpreted to form a prominent seismic zone associated with Clarendon-Linden fault. Location of 1929 m _b 5.2 Attica earthquake suggests this event could have been associated with Clarendon-Linden fault. Also, earthquakes induced from injection of brine into wells in the Dale area could be associated with Clarendon-Linden fault.

Table D-7.3.4 Data Summary
Paleozoic Extended Crust Zone

Citation	Title	Description and Relevance to SSC
Tuttle, Dyer-Williams, and Barstow (2002)	Paleoliquefaction Study of the Clarendon-Linden Fault System, Western New York State	Investigations indicated a lack of earthquake-induced liquefaction features in geologic units, which suggests the fault system did not generate large $M > 6$ earthquakes in past 12,000 years. It was concluded that the fault system could have produced small and moderate earthquakes, but probably not large ones, during late Wisconsinan and Holocene.
White et al. (2000)	A Seismic-Based Cross-Section of the Grenville Orogen in Southern Ontario and Western Quebec	Describes Elzevir-Frontenac boundary zone as major structural boundary zone based on prominent geophysical signatures. These make up a broad zone of SE-dipping reflections and midcrustal velocity contours that shallow at depths of 12–15 km (7.5–9.5 mi.).
Giles County (Virginia) Seismic Zone (GCVSZ)		
<i>Seismicity and Fault Geometry Data</i>		
Bollinger and Wheeler (1988)	The Giles County, Virginia, Seismic Zone—Seismological Results and Geological Interpretations	Defines 40 km (25 mi.) long seismic zone based on instrumental seismicity. A damaging earthquake that occurred in 1897 in Giles County is believed to have occurred within this seismic zone. Compressional reactivation of an Iapetan normal fault is likely responsible for formation of seismic zone.
Bollinger et al. (1991)	Seismicity of the Southeastern United States; 1698 to 1986	Provides an overview of historical and instrumental seismicity in SE United States. Describes dimensions of GCVSZ and notes that zone of seismicity is beneath rocks detached by thrusting, thus demonstrating the lack of association with fault structures observed at the surface. Release of seismic energy in GCVSZ most likely related to reactivation of Precambrian faults.
Gresko (1985)	Analysis and Interpretation of Compressional (P Wave) and Shear (SH Wave) Reflection Seismic and Geologic Data over the Bane Dome, Giles County, Virginia	Seismic-reflection data acquired in Giles County were analyzed. Interpreted thickening of basement rock beneath the Bane Dome is postulated to represent late Precambrian–early Cambrian rifting. Faults generated at that time may now be reactivated in the present stress regime.

Table D-7.3.4 Data Summary
Paleozoic Extended Crust Zone

Citation	Title	Description and Relevance to SSC
<i>Paleoseismic Investigations</i>		
Anderson and Spotila (2001)	The Relationship of Geologic Structure to the Giles County Seismic Zone in Southwest Virginia, Based on Fracture Mapping in Allochthonous Paleozoic Strata	Describes study to characterize brittle fractures that occur along 7 km (4.5 mi.) of discontinuous outcrops in Giles County. Fractures range from diffuse hairline cracks to through-going, clay-filled faults. Fracture orientations have no apparent relationship to local topography or karst-related subsidence. Earthquakes in region could have ruptured entire upper crust; however, without age control on the fractures, a strong conclusion cannot yet be made.
Bollinger et al. (1992)	Geologically Recent Near-Surface Faulting in the Valley and Ridge Province: New Exposures of Extensional Faults in Alluvial Deposits, Giles County, SW Virginia	Describes characteristics of two extensional faults that cut a series of alluvial terrace deposits along north side of New River Valley near Pembroke in Giles County. The age of neither the faults nor the sediments is known, but both appear to be relatively recent (Tertiary or Quaternary). The faults are important because they indicate at least local occurrence of geologically recent near-surface faulting. Seismic monitoring in area indicates earthquake hypocenters occur at depths greater than 5 km (3 mi.).
Chapman and Krimgold (1994)	Seismic Hazard Assessment for Virginia	Attributes earthquakes in GCVSZ to a 40 km (25 mi.) long NNE-trending, steeply dipping structure oriented approximately 20° counterclockwise to detached sedimentary structures mapped at surface. Earthquakes occur below Valley and Ridge thrust sheets at depths of 5–25 km (3–15.5 mi.). Focal mechanisms exhibit strike-slip motions on steeply dipping northerly and easterly planes with a maximum compressive stress direction that is northeasterly and nearly horizontal. This pattern of seismicity attributed to reactivation of one or more Eocambrian extensional faults. On basis of this information, Chapman and Krimgold delineated a separate seismic zone for Giles County region.
Crone and Wheeler (2000)	Data for Quaternary Faults, Liquefaction Features, and Possible Tectonic Features in the Central and Eastern United States, East of the Rocky Mountain Front	Describes Pembroke faults in terrace deposits of probable Quaternary age at a locality along north side of New River Valley near Pembroke, Virginia. These faults were reported but not named by others (e.g., Law et al., 1992). The faults overlie a steeply dipping tabular zone of hypocenters; however, it has not been determined whether they are tectonic or the result of solution collapse. Characteristics of the faults are described. Based on uncertainty in fault origin, Pembroke faults are assigned to Class B,

Table D-7.3.4 Data Summary
Paleozoic Extended Crust Zone

Citation	Title	Description and Relevance to SSC
Granger et al. (1997)	Quaternary Dncutting Rate of the New River, Virginia, Measured from Differential Decay of Cosmogenic ^{26}Al and ^{10}Be in Cave-Deposited Alluvium	Describes how cosmogenic radionuclides ^{26}Al and ^{10}Be in quartz can be used to infer time of emplacement of cave-deposited river sediment. Analyses of these radionuclides from caves high above New River indicate a dncutting rate of $27.3 \pm 4.5 \text{ m/Myr}$. A tectonic tilt rate over the late Quaternary of $1.05 \pm 0.35 \text{ m km}^{-1} \text{ Myr}^{-1}$ is estimated near GCVSZ.
Law et al. (1994)	Geologically Recent Near-Surface Faulting and Folding in Giles County, Southwest Virginia: New Exposures of Extensional and Apparent Reverse Faults in Alluvial Sediments Between Pembroke and Pearisburg	Describes faults and graben structures investigated in alluvial deposits at Pembroke excavation site on the New River. The ages of faults and sediments are unknown; however, unlithified nature of the deposits suggests relatively young ages (Tertiary or Quaternary). Excavation site is within defined area of GCVSZ. Authors use three models to explain formation of exposed fold and fault structures: landsliding, solution collapse, and basement faulting of tectonic origin.
Law et al. (2000)	Folding and Faulting of Plio-Pleistocene Sediments in Giles County, SW Virginia: (1) Surface Data and Interpretation	Describes excavations along New River Valley that have revealed series of extensional and reverse faults cutting alluvial terrace deposits. Terrace sediments are arched into broad, gently plunging antiform. Features are consistent with continued sedimentation in a depression formed by progressive solution of limestone, followed by inversion to form the anticlinal structure. The fine structure preserved in some terrace deposits precludes sudden slip on the faults and indicates slow slip rates.
Mills (1985)	Descriptions of Backhoe Trenches Dug on New River Terraces Between Radford and Pearisburg, Virginia, June 1981	Provides information on 20 backhoe trenches dug on terraces of the New River in and near Giles County. No evidence of seismic shaking, faulting, or surface rupture was found in the 2 trenches within GCVSZ or in 18 trenches near the zone.
Mills (1986)	Possible Differential Uplift of New River Terraces in Southwestern Virginia	Describes studies of terrace elevations along New River in SW Virginia. Differences in elevation between two areas can be explained by differential uplift between 30 and 200 mm/ka. Uplift is consistent with probable movements on faults associated with GCVSZ.

**Table D-7.3.4 Data Summary
Paleozoic Extended Crust Zone**

Citation	Title	Description and Relevance to SSC
Wheeler (2005)	Known or Suggested Quaternary Tectonic Faulting, Central and Eastern United States—New and Updated Assessments for 2005	Reviews information about GCVSZ. This seismic zone has no recognized geomorphic expression, and no geologic evidence has yet demonstrated Quaternary surface deformation caused by tectonic faulting within the zone. Accordingly, it is assigned to Class C. Nonetheless, occurrence of a significant historical earthquake in 1897 (M 5.9) and of continuing smaller earthquakes demonstrates that a notable level of seismic hazard exists for zone.
<i>Geophysical Investigations</i>		
Robinson et al. (1993)	A Seismic Refraction and Electrical Resistivity Survey of Faulted Alluvial Deposits in Giles County, VA	Imaged high-angle faults and a broad antiformal fold in young, unconsolidated sediment in Giles County, Virginia, were imaged with seismic refraction and electrical resistivity. Results from seismic refraction indicate the faults extend through sediments more than 40 m (131 ft.) thick and local topography exists at bedrock surface, which can be attributed to faulting, karst, or inherited topography. Results from resistivity survey indicate that high-angle anomalies are high-angle faults.
Robinson et al. (2000)	Folding and Faulting of Plio-Pleistocene Sediments in Giles County, SW Virginia: (3) Seismic Refraction, Potential Fields, and Borehole Data	Describes excavations along New River Valley that have revealed series of faults cutting alluvial terrace deposits. Terrace sediments are arched into broad, gently plunging antiform, with a graben in hinge zone of antiform. Subsurface investigations indicate that terrace deposits reach maximum of 40 m (131 ft.) thick and contain possible voids. Geophysical measurements in limestone basement do not reveal any features that might be related to fold and graben structures in overlying terrace deposits.
Williams et al. (2000)	Folding and Faulting of Plio-Pleistocene Sediments in Giles County, SW Virginia: (2) Ground-Penetrating Radar and Seismic Reflection Data	Describes excavations along New River Valley that have revealed series of faults cutting alluvial terrace deposits. Terrace sediments are arched into broad, gently plunging antiform, with a graben in hinge zone of antiform. Seismic-reflection and ground-penetrating radar were used to image faults below excavation level. This information indicates that exposed faults are contained within a larger system of SSE- and NNW-dipping normal faults and that there is a linear depression in limestone bedrock that corresponds to the graben in terrace deposits. The authors note that it is unlikely that the faults were caused by collapse of an isolated subcircular sinkhole.

Table D-7.3.4 Data Summary
Paleozoic Extended Crust Zone

Citation	Title	Description and Relevance to SSC
Eastern Tennessee Seismic Zone (ETSZ)		
<i>Seismicity and Fault Geometry Data</i>		
Bollinger et al. (1991)	Seismicity of the Southeastern United States; 1698 to 1986	Describes seismicity in eastern Tennessee. This area is the most seismically active in Southeast. Largest recorded earthquake reported at time of publication was 1973 M _s 4.6 Maryville-Alcoa event. Active faulting is reported as occurring on steeply dipping fault planes, the majority of which are located beneath the master Appalachian decollement.
Chapman (1996)	Focal Mechanisms and the Geometry of Basement Faults in the Eastern Tennessee Seismic Zone	Compares relocated hypocenters for 474 earthquakes with more than 40 focal mechanisms for earthquakes monitored between 1982 and 1993. Results indicate that earthquakes exhibit predominantly strike-slip motion that occur either on left-stepping en echelon basement faults striking SW-NE or on a conjugate system of E-W-striking faults.
Chapman et al. (1997)	A Statistical Analysis of Earthquake Focal Mechanisms and Epicenter Locations in the Eastern Tennessee Seismic Zone	Describes location and orientation of possible seismogenic basement faults based on information provided by focal mechanisms and earthquake epicenters. Spatial aspects of the seismicity are examined. Strike-slip motion on steeply dipping planes is dominant mode of faulting in the 300 km (186 mi.) long seismic zone. A series of NE-trending en echelon basement faults are intersected by several east-trending faults.
Chapman et al. (2002)	The Eastern Tennessee Seismic Zone: Summary after 20 Years of Network Monitoring	Provides information on focal depths and mechanisms of earthquakes in ETSZ. Focal mechanism solutions indicate strike-slip faulting on steeply dipping planes. Epicenters form linear segments that may reflect basement fault structure being reactivated in the modern stress regime. Largest historical earthquake in ETSZ was magnitude 4.6. Although no evidence for larger shocks has been found, microearthquakes suggest coherent stress accumulation within a large volume. The authors propose that a hydrologic element may link seismicity, uniform regional stress, and basement structure.
Dunn and Chapman (2006)	Fault Orientation in the Eastern Tennessee Seismic Zone: A Study Using the Double-Difference Earthquake Location Algorithm	Uses double-difference earthquake location algorithm to examine earthquake hypocenter relocations and resolve fault orientations. Relocations in the most seismically active portion of ETSZ indicate diffuse west-striking, north-dipping zone of hypocenters. Zone is consistent with a structure imaged on a seismic-reflection profile that appears to be a seismogenic basement fault.

Table D-7.3.4 Data Summary
Paleozoic Extended Crust Zone

Citation	Title	Description and Relevance to SSC
Johnston et al. (1985)	Seismotectonics of the Southern Appalachians	Describes majority of southern Appalachian seismicity as occurring in a concentrated zone beneath Valley and Ridge province of eastern Tennessee. Zone is bounded on NW by NY-AL lineament and on SE by Clingman/Ocoee lineaments. Analyses indicate that seismic activity occurs beneath the decollement, thus supporting hypothesis that Appalachian seismicity is unrelated to surficial geologic or tectonic features.
Kaufmann and Long (1996)	Velocity Structure and Seismicity of Southeastern Tennessee	Describes SE Tennessee seismic zone as located at confluence of major crustal features. Using a velocity model, the authors demonstrate that seismicity is concentrated in areas of average to below average velocity and does not appear to be associated with a major crustal feature. Instead, seismicity is characterized by distribution of hypocenters and their association with low-velocity regions at midcrustal depths.
Keller et al. (1982)	Evidence for a Major Late Precambrian Tectonic Event (Rifting?) in the Eastern Midcontinent Region	Describes large linear gravity anomaly that extends through eastern Kentucky and Tennessee and coincides with a zone of complex, high-amplitude magnetic anomalies. This area appears to have been location of an ancient rift that formed about 1,100 Ma and has been locally reactivated. Basement lithologies in area appear to be metamorphosed volcanics that are relatively strong.
King and Zietz (1978)	The New York–Alabama Lineament: Geophysical Evidence for a Major Crustal Break in the Basement beneath the Appalachian Basin	Defines NY-AL lineament that extends for more than 1,600 km (994 mi.), marked by series of magnetic gradients that trend NE. Seismic activity is correlated to location of lineament, with an active area to SE and an inactive area along NW side of lineament.
Long and Kaufmann (1994)	The Velocity Structure and Seismotectonics of Southeastern Tennessee	Evaluates relationship of midcrustal structures and seismicity from a velocity model derived from inversion of travel-time residuals and gravity data. The authors observed that spatial patterns of historical seismicity correlate with low velocity regions at midcrustal depths, which suggests that intraplate earthquakes occur in weakened crust. Velocity data does not support NY-AL lineament as a linear feature parallel to a deep sedimentary basin.

**Table D-7.3.4 Data Summary
Paleozoic Extended Crust Zone**

Citation	Title	Description and Relevance to SSC
Powell et al. (1994)	A Seismotectonic Model for the 300-Kilometer-Long Eastern Tennessee Seismic Zone	Describes characteristics of seismicity in ETSZ, including the association of earthquakes with major potential field anomalies; greatest density of epicenters is near NY-AL magnetic lineament. The authors propose that ETSZ is evolving, with earthquakes coalescing into NE-trending zone near juncture between relatively weak and strong basement crustal blocks. The authors suggest that deformation in ETSZ may evolve eventually into a longer through-going strike-slip fault.
Powell (2002)	Three-Dimensional Velocity Structure in the New Madrid and Other SCR Seismic Zones	Velocity images obtained for SCR areas reveal strong velocity contrasts that appear to control distribution of seismicity. Earthquakes tend to concentrate where strain energy is concentrated, which is in areas of low velocity or along edges of high-velocity zones. A prominent low-velocity zone was detected in ETSZ; most earthquakes occur in rocks that surround the lowest-velocity regions of this zone.
Tavernier and Williams (2002)	The Basement Faults in the East Tennessee Seismic Zone: Observations from the Swan Creek Gas Field	Seismic-reflection and well data from Swan Creek gas field in eastern Tennessee have been used to study basement structure and its relationship to NY-AL lineament in ETSZ. A system of normal faults is apparent in Precambrian basement NW of the field; the faults are locally coincident with NY-AL lineament. A left-lateral strike-slip fault is also recognized in Paleozoic basement rock. The two directions of basement faults are consistent with those of faults interpreted in ETSZ from earthquake focal mechanisms.
Teague et al. (1986)	Focal Mechanism Analyses for Eastern Tennessee Earthquakes (1981-1983)	The authors determined 10 single-event and 6 composite focal mechanisms from 37 events in eastern Tennessee occurring between September 1981 and July 1983. Focal mechanisms are predominantly strike-slip along nearly vertical N-S- (right-lateral) or E-W- (left-lateral) oriented nodal planes, consistent with compressional reactivated lapetan normal faults. The P axes systematically converge from N40°E to N50°E with depth. Distribution of P axes from this data set restricts the maximum compressive stress (σ_1) between N30°E and N76°E with plunge angles from 15° to -40°. Result is similar to that determined for GCVSZ and is consistent with values derived for the Midcontinent.
USGS (2003)	Poster of the Fort Payne, Alabama Earthquake of 29 April 2003—Magnitude 4.6	Provides information on April 29, 2003, Fort Payne earthquake of M 4.6 and summarizes seismic hazard in SE United States.

Table D-7.3.4 Data Summary
Paleozoic Extended Crust Zone

Citation	Title	Description and Relevance to SSC
Vlahovic et al. (1996)	P and S Wave Velocity Structure and Hypocenter Locations in the Eastern Tennessee Seismic Zone	The authors developed 3-D crustal velocity model from inversion of arrival time data and observed that higher velocities are associated with more seismogenic crust SE of NY-AL lineament, whereas lower-velocity anomalies are NW of lineament. Relocation of events with this model places most seismicity in a 30 km (19 mi.) wide block between 4 and 22 km (2.5 and 14 mi.) along entire length of seismic zone (300 km, or 186 mi.).
Vlahovic et al. (1998)	Joint Velocity Hypocenter-Velocity Inversion for the Eastern Tennessee Seismic Zone	Describes velocity structure model used to update focal mechanisms and hypocenters for earthquakes in ETSZ. Relocated hypocenters define a seismogenic volume consistent with a tectonic model of faulting along NY-AL lineament, which is characterized by sharp contrasts in strength of adjoining crustal blocks. Earthquakes tend to concentrate along steepest velocity gradients, suggesting they occur on ancient faults separating rocks of different compositions.
Wheeler (2005)	Known or Suggested Quaternary Tectonic Faulting, Central and Eastern United States—New and Updated Assessments for 2005	Summarizes characteristics of ETSZ. Small to moderate earthquakes in zone demonstrate active subsurface faulting; however, zone has had no historical earthquakes of M 5 or larger, and there is no surficial geologic evidence for occurrence of large earthquakes. Accordingly, ETSZ is assigned to Class C for lack of geologic evidence of large earthquakes.
<i>Paleoseismic Investigations</i>		
Whisner et al. (2003)	Disturbed Sediments in the East Tennessee Seismic Zone: Evidence of Large Prehistoric Earthquakes in East Tennessee?	Summarizes detailed geologic studies in ETSZ focused on trying to locate paleoseismic features. Geologic mapping in a 300 km ² (186 mi. ²) area within most active part of ETSZ did not reveal concrete evidence of large prehistoric earthquakes. Information was provided from two localities in Tennessee where anomalously deformed sediments occur. The two localities include folded and faulted pebble layers at Tellico Plains site and clastic dikes in a small fault at Gray site (outside recognized ETSZ). Deformed sediments could indicate late Pleistocene or early Holocene earthquake activity.

Table D-7.3.7 Data Summary
Extended Continental Crust Zone—Atlantic Margin

Citation	Title	Description and Relevance to SSC
General for Region		
Austin et al. (1990)	Crustal Structure of the Southeast Georgia Embayment-Carolina Trough: Preliminary Results of a Composite Seismic Image of a Continental Suture(?) and a Volcanic Passive Margin	The authors use multichannel seismic-reflection data to image the Carolina platform and conclude that observed magnetic anomaly in this region is the product of Mesozoic rifting processes, not Paleozoic collision.
Bird et al. (2005)	Gulf of Mexico Tectonic History: Hotspot Tracks, Crustal Boundaries, and Early Salt Distribution	The authors interpret deep basement structural highs in Gulf of Mexico as hotspot tracks. In this interpretation, the basin began to form as the Yucatan experienced continental crustal extension and 22° of counterclockwise rotation (160–150 Ma). This was followed by a further 20° of counterclockwise rotation and seafloor spreading in the gulf.
Cook (1984)	Geophysical Anomalies Along Strike of the Southern Appalachian Piedmont	Documents trends in both Bouguer gravity and magnetic anomalies associated with the Appalachians in Georgia and Virginia.
Crough (1981)	Mesozoic Hotspot Epeirogeny in Eastern North America	Attributes a 600 km (373 mi.) wide zone of epeirogeny in SE Canada and New England during the Cretaceous and early Tertiary to the Great Meteor hotspot, as evidenced by apatite fission-track dating.
Daniels et al. (1983)	Distribution of Subsurface Lower Mesozoic Rocks in the Southeastern United States, as Interpreted from Regional Aeromagnetic and Gravity Maps	<p>Concludes that Brunswick magnetic anomaly must be older than the Mesozoic features that it can be traced over, and is therefore not sourced by South Georgia rift.</p> <p>The authors performed a paleostress analysis of the New England–Quebec igneous province, which provides an alternative interpretation for the distribution of Cretaceous plutons. Dikes display ESE-WNW and ENE-WSW trends and are spatially distributed in three E-W-striking dike swarms 75 by 300 km (47 by 186 mi.) in area. Leucocratic dikes occur closer to plutons and disappear within 3–4 km (2–2.5 mi.), likely recording local stress effects due to pluton emplacement. Lamprophyre dikes occur independently of plutons and strike parallel to regional dike swarms, recording regional far-field stresses. Normal faults in the regions display two orientations:</p> <ol style="list-style-type: none"> 1. E-W-striking normal faults found predominantly in Montreal area are parallel to graben boundaries and axis of the Monteregian Hills, with vertical offsets ranging between 100 and 430 m (328 and 1,411 ft.). 2. NW-SE to WNW-ESE-striking normal faults are oblique to graben boundaries, with less than 100 m (328 ft.) of vertical offset.

Table D-7.3.7 Data Summary
Extended Continental Crust Zone—Atlantic Margin

Citation	Title	Description and Relevance to SSC
		<p>NW-SE to WNW-ESE faults are older than E-W-striking faults but exhibit crosscutting relationships, suggesting that some were reactivated during formation of the E-W-striking faults. Some E-W-striking brittle faults and joints are observed in several Cretaceous plutons with similar orientations to dikes that are locally crosscut by these normal faults, suggesting that dike emplacement and faulting are contemporaneous. Conjugate sets of NE-WS dextral and ESE-WNW sinistral strike-slip faults and WNW-SSW reverse faults provide evidence for a compressional stress regime postdating emplacement of the Cretaceous plutons.</p>
Faure et al. (1996)	State of Intraplate Stress and Tectonism of Northeastern America Since Cretaceous Times, with Particular Emphasis on the New England–Quebec Igneous Province	<p>Faure et al. (1996) attribute intraplate stress and tectonism in NE America to an initial NE-SW extension event associated with rifting between Labrador and Greenland at 140 Ma, opening of South Atlantic at 130 Ma, and related reactivation of Timiskaming graben. Subsequent N-S-oriented extension associated with emplacement of the Monteregian Hills corresponds to global fragmentation of Pangaea when Iberia separated from Newfoundland when dominant tensional stress propagated along Labrador rift. The stress regime shifted to ENE-ESE-directed compressional stress in early Tertiary when the oceanic spreading rate decreased because of an increasing number of convergent boundaries in the Pacific. Faure et al. (1996) conclude that emplacement of Cretaceous intrusions is consistent with a lithospheric fracture model as opposed to a hotspot model, emphasizing role of preexisting structure in Ottawa-Bonnechere graben.</p>
Faure et al. (2006)	Paleostress Analysis of Atlantic Crustal Extension in the Quebec Appalachians	<p>Identifies two phases of extension: (1) an initial Late Triassic E-W extension related to formation of rift basins in Bay of Fundy and southern Georgia, and (2) Early Jurassic ESE-WNW extension related to central Atlantic rift system.</p>
Funck et al. (2004)	Crustal Structure of the Northern Nova Scotia Rifted Continental Margin (Eastern Canada)	<p>The authors used seismic refraction to image along-strike variation in crustal structure where Atlantic margin transitions from volcanic to nonvolcanic rifting (Nova Scotia). They find that continental crust thins from 36 to 3 km (22 to 2 mi.) over a distance of 180 km (112 mi.). Further seaward, they find a 150 km (93 mi.) long section of serpentinized mantle overlain by a 3 km (2 mi.) thick section of continental crust. Beyond this transition zone, they find oceanic crust with average thickness of 4 km (2.5 mi.). These data support idea that Atlantic margin becomes progressively more nonvolcanic to the NE, and place the continent-ocean boundary 60 km (37 mi.) farther SE than did Keen and Potter (1995b).</p>

Table D-7.3.7 Data Summary
Extended Continental Crust Zone—Atlantic Margin

Citation	Title	Description and Relevance to SSC
Hatcher et al. (1994)	E-5 Cumberland Plateau to Blake Plateau, Centennial Continent/Ocean Transect #18	Geologic cross section is based on surface geology, drillholes, shipboard and aeromagnetic anomaly data, and gravity and seismic-reflection data.
Hatcher et al. (2007)	Tectonic Map of the Southern and Central Appalachians: A Tale of Three Orogens and a Complete Wilson Cycle	Provides comprehensive review of formation and geologic history of Appalachian orogen.
Hibbard et al. (2004)	The Appalachian Orogen	Reviews structural geology, tectonics, and history of Appalachian orogen.
Hibbard et al. (2006)	Lithotectonic Map of the Appalachian Orogen, Canada–United States of America	Lithotectonic mapping at 1:1,500,000 scale of the Appalachians in the U.S. and Canada, including faults and shear zones. Mapped area includes western portion of ECC, namely Piedmont.
Hibbard et al. (2007)	A Comparative Analysis of Pre-Silurian Crustal Building Blocks of the Northern and the Southern Appalachian Orogen	The authors investigate each phase of orogeny in Appalachians and determine that pre-Silurian Appalachians were uniform from north to south. Heterogeneities must postdate Late Ordovician events.
Holbrook, Purdy, et al. (1994)	Seismic Structure of the U.S. Mid-Atlantic Continental Margin	Uses multichannel and wide-angle seismic data to investigate the nature of continent-ocean boundary of the Atlantic margin (Virginia). The authors find that continent-ocean boundary is not sharp, but is instead a 100 km (62 mi.) wide transition zone characterized by rift-related mafic igneous material, up to 25 km (15.5 mi.) thick. Location of these igneous rocks also coincides with East Coast magnetic anomaly (ECMA), and the authors therefore conclude the ECMA does not mark an Appalachian suture zone, but rather is sourced by igneous rocks emplaced during rifting. Supports the idea that Atlantic margin is strongly volcanic and not consistent with plume models.
Holbrook, Reiter, et al. (1994)	Deep Structure of the U.S. Atlantic Continental Margin, Offshore South Carolina, from Coincident Ocean Bottom and Multichannel Seismic Data	Combined seismic-reflection study and wide-angle ocean-bottom seismic profile of Carolina Trough. Finds rifted continental crust for the first 80 km (50 mi.) along transect, characterized by 1–4 km (0.6–2.5 mi.) of post-rift sediment overlying 30–34 km (19–21 mi.) thick crust. Further seaward, transitional crust is a 70–80 km (43–50 mi.) wide zone containing up to 12 km (7.5 mi.) of post-rift sediment overlying 10–24 km (6–15 mi.) thick crust. Beyond this, 8 km (5 mi.) thick oceanic crust is overlain by 8 km (5 mi.) of sediments. Transitional crust, which is the product of rifting-induced magmatism, produces the Brunswick and East Coast magnetic anomalies.

Table D-7.3.7 Data Summary
Extended Continental Crust Zone—Atlantic Margin

Citation	Title	Description and Relevance to SSC
Hutchinson et al. (1983)	Crustal Structure Beneath the Southern Appalachians: Nonuniqueness of Gravity Modeling	The authors modeled Appalachian gravity gradient and favor the interpretation that it marks a suture zone.
Johnston (1994)	Seismotectonic Interpretations and Conclusions from the Stable Continental Region Seismicity Database	Defines nine major and several minor stable continental regions (SCRs), finding that annual seismic moment released in rifted SCR exceeds that in nonrifted SCR by a factor of 15.
Kanter (1994)	Tectonic Interpretation of Stable Continental Crust	Subdivides stable continental regions in North America (and world) into tectonic domains based on geologic and geophysical characteristics, such as age and whether domain is extended or non-extended. The characterization of the ECC-AM seismotectonic zone is influenced by Eastern Seaboard domain (#218) of extended Paleozoic continental crust.
Karner and Watts (1983)	Gravity Anomalies and Flexure of the Lithosphere at Mountain Ranges	Documents phenomenon of gravity gradients along Himalayas, Alps, and Appalachians and concludes that this gradient generally marks subsurface loads, which for Appalachians is attributed to foreland basin development.
Keen and Potter (1995a)	The Transition from a Volcanic to a Nonvolcanic Rifted Margin off Eastern Canada	The authors use seismic-reflection data SE of Nova Scotia to show presence of seaward-dipping reflectors (SDRs), also commonly found farther south along Atlantic margin. They interpret the SDRs to be derived by igneous and sedimentary material accreted into a widening, subsiding rift zone. Presence of both SDRs and strong East Coast magnetic anomaly (ECMA), combined with the disappearance of both these features farther north, suggests that ECMA is created by igneous rocks forming the SDRs. The relative abruptness with which both features disappear to north also argues for small-scale convection to be the volcanic source along this rift zone.
Keen and Potter (1995b)	Formation and Evolution of the Nova Scotia Rifted Margin: Evidence from Deep Seismic Reflection Data	The authors use seismic-reflection data to document a 100–200 km (62–124 mi.) wide zone of thinned continental crust (factor of 3) off coast of Nova Scotia, which is much wider than typical width of crustal extension along Atlantic margin farther south (~20 km, or 12 mi.). They propose that this may be related to the shift from volcanic rifting (to south) to nonvolcanic rifting (Nova Scotia). Thinning in this study is accommodated by simple shear in crust and pure shear in mantle lithosphere. The authors propose that continent-ocean boundary lies just seaward of the limit of synrift sediments, adjacent to a 100 km (62 mi.) wide zone of thinned (<9 km, or 6 mi.) continental crust that underlies the continental slope/rise.

Table D-7.3.7 Data Summary
Extended Continental Crust Zone—Atlantic Margin

Citation	Title	Description and Relevance to SSC
Keller and Hatcher (1999)	Some Comparisons of the Structure and Evolution of the Southern Appalachian-Ouachita Orogen and Portions of the Trans-European Suture Zone Region	Interprets Appalachian gravity gradient as marking a suture zone of the Alleghanian orogeny.
Klitgord et al. (1988)	U.S. Atlantic Continental Margin; Structural and Tectonic Framework	Mesozoic rifting resulted in breakup of Pangaea. This rifting is associated with separation of the North American and African plates, producing rift basins along Atlantic seaboard that are situated landward of hinge zone of continental margin. This landward region experienced considerably less crustal thinning than did the region seaward of hinge zone that includes the deeper marginal sedimentary basins. Basement hinge zone consists of series of parallel half graben structures that deepen seaward. At hinge zone, basement deepens steeply to east by a series of downdropped fault blocks from about 2–4 km (1–2.5 mi.) depth to over 8 km (5 mi.) depth. The character of block faulting at hinge zone varies along the margin and may reflect influence of older crustal structure on Mesozoic rifting. Half graben structures with seaward-dipping border faults are observed at Georges Bank hinge zone, whereas faulted blocks with landward-dipping faults form hinge zone in Baltimore Canyon trough.
LASE Study Group (1986)	Deep Structure of the U.S. East Coast Passive Margin from Large Aperture Seismic Experiments (LASE)	The authors use large-aperture seismic reflection to image Baltimore Canyon trough, revealing a continuous high-velocity deep-crustal layer that extends from beneath continental crust to oceanic crust. They interpret this layer as having formed either late in continental rifting process or early in seafloor spreading process.
Li et al. (2003)	Shear Velocity Structure and Azimuthal Anisotropy Beneath Eastern North America from Rayleigh Wave Inversion	The authors determined the velocity structure and anisotropic variations in velocity structure from inversion of Rayleigh waves in order to detect asthenospheric flow beneath the thick continental lithosphere beneath NE United States and SE Canada. Rayleigh wave–phase velocity anomaly with a period of 33 sec, corresponding to sensitivity to structure down to 40 km (25 mi.) in depth, indicates a low-velocity band oriented NE-SW. The North American continental keel beneath Grenville Province is imaged in upper mantle down to roughly 200 km (124 mi.) in depth. North American keel has an irregular shape and a low-velocity zone beneath eastern New York and central New England to 200 km (124 mi.), with particularly high amplitudes at depths of 60–140 km (37–87 mi.). This velocity anomaly is interpreted as lateral contrast between relatively thick lithosphere beneath western New York and Pennsylvania and warm asthenosphere beneath thinned New

Table D-7.3.7 Data Summary
Extended Continental Crust Zone—Atlantic Margin

Citation	Title	Description and Relevance to SSC
		England lithosphere caused by thermal erosion associated with the Cretaceous hotspot. Additionally, weak anisotropy that is observed from shear-wave splitting indicates that the source must be at least 200 km (124 mi.) deep, suggesting that a sublithospheric shear zone may decouple motions of the lithosphere and deeper mantle.
Manspeizer et al. (1989)	Post-Paleozoic Activity	Reviews rifting and igneous activity in the post-Paleozoic period.
McBride and Nelson (1988)	Integration of COCORP Deep Reflection and Magnetic Anomaly Analysis in the Southeastern United States: Implications for Origin of the Brunswick and East Coast Magnetic Anomalies	The authors suggest three possible sources for Brunswick magnetic anomaly: subducted root nappes of the Inner Piedmont, obducted upper mantle, or Mesozoic rifting. The authors do not strongly support a particular solution, but do suggest that the Brunswick and East Coast magnetic anomalies may have a continuous, related source.
McBride et al. (2005)	Integrating Seismic Reflection and Geological Data and Interpretations Across an Internal Basement Massif: The Southern Appalachian Pine Mountain Window, USA	The authors trace the master Appalachian decollement from Inner Piedmont to Coastal Plain. They find that beneath the Carolina terrane, the decollement roots to Moho, indicating the location of Acadian-Alleghanian suture.
McHone (1996)	Constraints on the Mantle Plume Model for Mesozoic Alkaline Intrusions in Northeastern North America	<p>Proposes that one or more deep-mantle plumes do not provide a satisfactory mechanism for distribution of Cretaceous alkaline rocks of New England, and observes that previous studies oversimplify evidence for a hotspot track across New England by ignoring important petrological data, including the following:</p> <ul style="list-style-type: none"> • Jurassic syenite-monzonite-alkali granite of the White Mountain magma series (WMMS) has been described as separate province from Cretaceous intrusions, although many Early Jurassic dikes and several mafic to felsic plutons in the province are petrographically and chemically similar to Early Cretaceous intrusions that overlap. • Early Cretaceous dikes and plutons of New England–Quebec igneous province have statistically similar paleomagnetic poles between 122 and 124 Ma and show no consistent trend for published ages in any direction across region. • Seamount volcanism is not limited to ages defined by linear hotspot track nor is it on trend with New England–Quebec province. • Cretaceous alkaline rocks do not exhibit a consistent chemical signature

Table D-7.3.7 Data Summary
Extended Continental Crust Zone—Atlantic Margin

Citation	Title	Description and Relevance to SSC
		<p>indicative of a mantle source.</p> <p>These observations indicate that lithospheric processes were necessary to start and stop generation of magmas from the same source in mantle, and that petrological studies should emphasize local and regional tectonic features.</p>
Murphy and Keppie (2005)	The Acadian Orogeny in the Northern Appalachians	Avalonia and Meguma terranes in Nova Scotia are separated by strike-slip system of faults.
Pe-Piper and Piper (2004)	The Effects of Strike-Slip Motion Along the Cobequid-Chedabucto-SW Grand Banks Fault System on the Cretaceous-Tertiary Evolution of Atlantic Canada	Proposes that reactivation of Cobequid–Chedabucto–SW Grand Banks fault system could explain several features related to Canadian Atlantic margin, including rapid subsidence on Scotian margin and deep-water margin off the SW Grand Banks.
Pratt et al. (1988)	A Geophysical Study of the Earth's Crust in Central Virginia: Implications for Appalachian Crustal Structure	Concludes that crustal thinning (at Taconic suture) in the Piedmont is responsible for Appalachian gravity gradient.
Shillington et al. (2006)	Evidence for Asymmetric Nonvolcanic Rifting and Slow Incipient Oceanic Accretion from Seismic Reflection Data on the Newfoundland Margin	<p>The authors use seismic-reflection data to image Newfoundland nonvolcanic margin. They observe a region of extended continental crust (ECC) successively bordered by transitional basement and slow-spreading oceanic basement. They compare this structure to that of Iberian margin, the well-studied conjugate to Newfoundland. Two important differences are noted, however:</p> <ol style="list-style-type: none"> 1. The ECC of Newfoundland has few if any normal faults accommodating extension. 2. The transitional basement is not exhumed peridotite. The authors infer instead that the transition is thinned continental crust denuded by late-stage rifting (via rolling-hinge or detachment faulting) and possibly altered by magmatic intrusions/oceanic accretion.
Spencer et al. (1989)	The Extension of Grenville Basement Beneath the Northern Appalachians: Results from the Quebec-Maine Seismic Reflection and Refraction Surveys	The authors image the contact between Grenville basement and overlying allochthonous rocks of the Appalachians.

Table D-7.3.7 Data Summary
Extended Continental Crust Zone—Atlantic Margin

Citation	Title	Description and Relevance to SSC
Trehu et al. (1989)	Structure of the Lower Crust Beneath the Carolina Trough, U.S. Atlantic Continental Margin	The authors image Carolina trough along three seismic profiles and find a lens of high-velocity lower-crustal material spatially correlated with East Coast magnetic anomaly. They conclude that this layer was caused during either rifting or seafloor spreading.
Van Avendonk et al. (2009)	Extension of Continental Crust at the Margin of the Eastern Grand Banks, Newfoundland	The authors confirm previous reports of rapidly thinning crust beneath continental slope of offshore Newfoundland (from about 30 to 6 km, or 19 to 4 mi., producing a Moho dip of 50°). The thinned continental crust extends seaward for 80 km (50 mi.); this is interpreted as the result of strong (possibly gabbroic) lower crust that rotated upward during extension, localizing thinning to distal margin. The authors also observe high mantle seismic velocities at continent-ocean transition, a fairly unique observation that they interpret as evidence for nonserpentinized mantle. The lack of seaward-dipping normal faults in this region is explained by models that allow for large-scale detachment faults to be active during rifting.
Williams (1978)	Tectonic Lithofacies Map of the Appalachian Orogen	Maps location of both Paleozoic thrusts and later Mesozoic basins along the length of Appalachians.
Williams and Hatcher (1983)	Appalachian Suspect Terranes	Defines major suspect terranes of eastern North America and relates these to various orogenies responsible for uplift of Appalachians.
Zoback and Zoback (1989)	Tectonic Stress Field of the Continental United States	The authors conclude that direction of maximum horizontal compression in the eastern U.S. is oriented roughly NE-ESE, consistent with far-field ridge-push motion in the Atlantic.
Mesozoic Extension		
Benson (1992)	Map of Exposed and Buried Early Mesozoic Rift Basins/Synrift Rocks of the U.S. Middle Atlantic Continental Margin	Compilation of buried rift basins reveals high degree of parallelism with exposed basins and Paleozoic structural grain of Appalachians.
Cumbest et al. (1992)	Gravity and Magnetic Modeling of the Dunbarton Basin, South Carolina	Presents a model of Dunbarton extensional basin in South Carolina and Georgia in which gravity and magnetic anomalies are modeled simultaneously.
Hutchinson et al. (1986)	Rift Basins of the Long Island Platform	The authors map rift basins of Long Island platform using seismic-reflection, magnetic, and gravity data. They conclude that basin formation was controlled by Paleozoic structural trends.

Table D-7.3.7 Data Summary
Extended Continental Crust Zone—Atlantic Margin

Citation	Title	Description and Relevance to SSC
Nelson et al. (1985)	Profiling in the Southeastern United States. Part I: Late Paleozoic Suture and Mesozoic Rift Basin	COCORP profile in western Georgia is interpreted as imaging the Paleozoic suture between North America and Africa.
Oh et al. (1995)	Seaward-Dipping Reflectors Offshore the Southeastern United States: Seismic Evidence for Extensive Volcanism Accompanying Sequential Formation of the Carolina Trough and Blake Plateau Basin	Presents evidence to suggest that seaward-dipping reflectors represent voluminous volcanism beneath Carolina trough and Blake Plateau basin and that breakup of NW Africa and North America was time-transgressive from north to south during early Middle Jurassic.
Olsen et al. (1991)	Rift Basins of Early Mesozoic Age	Presents summary and mapping of Mesozoic extensional basins in eastern U.S.
Roden-Tice and Tice (2005)	Regional-Scale Mid-Jurassic to Late Cretaceous Unroofing from the Adirondack Mountains Through Central New England Based on Apatite Fission-Track and (U-Th)/He Thermochronology	Apatite fission-track ages across Adirondack Mountains, eastern New York, Vermont, western Massachusetts and Connecticut, and western New Hampshire provide evidence for differential unroofing that may have been accommodated by fault reactivation during Late Cretaceous. The authors attribute this regional unroofing to a change from extension to horizontal compression to the Great Meteor hotspot.
Roden-Tice and Wintsch (2002)	Early Cretaceous Normal Faulting in Southern New England: Evidence from Apatite and Zircon Fission-Track Ages	Apatite and zircon fission-track age transects across Hartford-Deerfield basin in Connecticut and Massachusetts increase to the east, indicating that unroofing took place during Late Jurassic through Early Cretaceous. Age of graben structure of Hartford Basin is Cretaceous and may not be an early Mesozoic "rift basin."
Roden-Tice, West, et al. (2009)	Presence of a Long-Term Lithospheric Thermal Anomaly: Evidence from Apatite Fission-Track Analysis in Northern New England	Apatite fission-track ages across New Hampshire, NE Vermont, and western Maine range from 70 to 140 Ma and reflect widespread Early to Late Cretaceous cooling. This regional cooling and unroofing is attributed to passage of North America Plate over Great Meteor hotspot, emplacement of White Mountain magma series in Early Jurassic, and associated E-W and NW-SE extension. Regional uplift on the order of 5–7 km (3–4 mi.) may explain lack of rift basins in central New England and Quebec.
Schlische (1993)	Anatomy and Evolution of the Triassic-Jurassic Continental Rift System, Eastern North America	Maps and details evolution of Mesozoic basins along Atlantic margin.

Table D-7.3.7 Data Summary
Extended Continental Crust Zone—Atlantic Margin

Citation	Title	Description and Relevance to SSC
Schlische (2003)	Progress in Understanding the Structural Geology, Basin Evolution, and Tectonic History of the Eastern North America Rift System	Presents summary and mapping of Mesozoic extensional basins in eastern U.S.
Schlische and Olsen (1990)	Quantitative Filling Model for Continental Extensional Basins with Application to the Early Mesozoic Rifts of Eastern North America	Presents quantitative model for stratigraphic evolution of extensional basins with the simplifying assumptions of constant volume input of sediments and water per unit time, as well as uniform subsidence rate and fixed outlet level. The model makes it possible to extract from sedimentary record those events in the history of an extensional basin that are due solely to the filling of a basin growing in size through time, and those events that are due to changes in tectonics, climate, or sediment and water budgets.
Schlische et al. (1996)	Geometry and Scaling Relations of a Population of Very Small Rift-Related Normal Faults	The authors studied geometry and scaling relationships on normal faults within Solite Quarry of Dan River rift basin. The data indicate that there is no significant change in displacement geometry and linear length–displacement scaling relation between small and large faults.
Sheridan et al. (1993)	Deep Seismic Reflection Data of EDGE U.S. Mid-Atlantic Continental-Margin Experiment: Implications for Appalachian Sutures and Mesozoic Rifting and Magmatic Underplating	A seismic-reflection study across Virginia continental margin that outlines a Paleozoic suture, buried Appalachian terranes, and Mesozoic rifting and magmatic events.
Smoot (1985)	The Closed-Basin Hypothesis and Its Use in Facies Analysis of the Newark Supergroup	A sedimentological analysis of the Newark Supergroup using various basin models to decide which basins are open or closed and used to help reconstruct facies.
Swanson (1986)	Preexisting Fault Control for Mesozoic Basin Formation in Eastern North America	Correlates Mesozoic basin formation with reactivation of specific Paleozoic reverse and strike-slip faults along Appalachians.
Talwani and Abreau (2000)	Inferences Regarding Initiation of Oceanic Crust Formation from the U.S. East Coast Margin and Conjugate South Atlantic Margins	East Coast magnetic anomaly is associated with seaward-dipping reflectors that represent volcanic rocks. These reflectors and underlying intrusive rocks are interpreted as constituting earliest crust and upper mantle generated at the time of initial opening of Atlantic Ocean.

Table D-7.3.7 Data Summary
Extended Continental Crust Zone—Atlantic Margin

Citation	Title	Description and Relevance to SSC
Withjack et al. (1998)	Diachronous Rifting, Drifting, and Inversion on the Passive Margin of Central Eastern North America: An Analog for Other Passive Margins	Uses new data to analyze and outline timeline of rifting along eastern North America (ENA). Features map of early Mesozoic rift basins of ENA.
Withjack et al. (2002)	Rift-Basin Structure and Its Influence on Sedimentary Systems	Describes four types of rift basins based on structure and their influence on processes within sedimentary systems.
Central Virginia Seismic Zone (CVSZ)		
Bollinger (1973)	Seismicity and Crustal Uplift in the Southeastern United States	Defines and names CVSZ as area of persistent, low-level seismicity in central Virginia.
Bollinger and Hopper (1971)	Virginia's Two Largest Earthquakes—December 22, 1875 and May 31, 1897	Largest earthquake in CVSZ occurred near center of zone on December 22, 1875, with m_b 5.0 and MMI VII.
Bollinger and Sibol (1985)	Seismicity, Seismic Reflection Studies, Gravity, and Geology of the Central Virginia Seismic Zone: Part I. Seismicity	Defines CVSZ as area of persistent, low-level seismicity that extends about 120 km (75 mi.) in N-S direction and about 150 km (93 mi.) in an E-W direction from Richmond to Lynchburg, Virginia. The largest historical earthquake in CVSZ is the December 22, 1875, m_b 5.0 (MMI VII) Goochland County event. Roughly three-quarters of the observed seismicity is located in upper 11 km (7 mi.) of crust.
Coruh et al. (1988)	Seismogenic Structures in the Central Virginia Seismic Zone	Interprets structures from I-64 seismic-reflection line. Suggests that seismicity in central and western parts of zone may be associated with west-dipping reflectors that form roof of a detached antiform; seismicity in eastern part of zone near Richmond may be related to near-vertical diabase dike swarm of Mesozoic age.
de Witt and Bayer (1986)	Seismicity, Seismic Reflection, Gravity, and Geology of the Central Virginia Seismic Zone: Part 3. Gravity	Provides clarification of figures in Keller et al. (1985).
Glover et al. (1995)	Tectonics of the Central Appalachian Orogen in the Vicinity of Corridor E-3; With Implications for Tectonics of the Southern Appalachians	Provides maps, cross sections, and discussion of major structures in vicinity of CVSZ and beyond. The authors thoroughly review paleogeography and associated pre-Mesozoic tectonics of central Appalachians; however, they provide little discussion of post-Paleozoic paleogeography or tectonics.

Table D-7.3.7 Data Summary
Extended Continental Crust Zone—Atlantic Margin

Citation	Title	Description and Relevance to SSC
Keller et al. (1985)	Seismicity, Seismic Reflection, Gravity, and Geology of the Central Virginia Seismic Zone: Part 3. Gravity	The authors use a variety of techniques to model position of thrust fault separating Greenville basement from overlying units in Virginia.
Kim and Chapman (2005)	The 9 December 2003 Central Virginia Earthquake Sequence: A Compound Earthquake in the Central Virginia Seismic Zone	Describes December 9, 2003, earthquake as M_w 4.3 ($\approx m_b$ 4.5) and Max MMI = VI, largest event recorded by seismograph in CVSZ. Predominantly thrust faulting with depth 10 ± 2 km (6 ± 1 mi.). Compound earthquake comprising two nearly identical events separated by 12 sec and 300 m (984 ft.) along an azimuth of $\sim 195^\circ$. Focal mechanisms from December 9, 2003, event and 11 other events in CSVZ inverted to obtain local stress tensor: maximum principal stress trends 133° and plunges 14° ; least principal stress trends 25° and plunges 52° . Indicates a broad-scale thrust-faulting stress regime in CSVZ. Maximum principal stress direction is rotated 68° clockwise relative to the average orientation of 65° for ENA.
Klose and Seeber (2007)	Shallow Seismicity in Stable Continental Regions	The authors investigate seismicity of stable continental regions (SCRs) and determine that while it has a bimodal depth distribution, $\sim 80\%$ of SCR earthquakes are shallow (< 7 km, or 4 mi.).
Marple and Talwani (2000)	Evidence for a Buried Fault System in the Coastal Plain of the Carolinas and Virginia—Implications for Neotectonics in the Southeastern United States	Proposes the East Coast fault system (ECFS) in Coastal Plain of Carolinas and Virginia. ECFS comprises three segments: southern, central, and northern. Northern segment located in vicinity of CVSZ. The authors provide data suggesting existence is strongest for southern segment, weakens northward.
Marple and Talwani (2004)	Proposed Shenandoah Fault and East Coast-Stafford Fault System and Their Implications for Eastern U.S. Tectonics	Proposes that Shenandoah fault is a deep, NW-striking ~ 300 km (186 mi.) long basement fault that accommodates an apparent ~ 110 km (68 mi.) offset between the NE-striking Stafford and East Coast fault systems (restraining bend). Fault was formed by late Alleghanian indentation in Salisbury embayment by NW Africa. CVSZ seismicity may be related to compression at restraining bend.
Munsey and Bollinger (1985)	Focal Mechanism Analyses for Virginia Earthquakes (1978-1984)	Focal mechanisms from single earthquakes located in CVSZ show no consistent orientation and show both reverse and strike-slip faulting. Hypocentral locations are scattered geographically and no surface ruptures are known, so no systematic sense of movement is indicated for CVSZ.

Table D-7.3.7 Data Summary
Extended Continental Crust Zone—Atlantic Margin

Citation	Title	Description and Relevance to SSC
Obermeier and McNulty (1998)	Paleoliquefaction Evidence for Seismic Quiescence in Central Virginia During Late and Middle Holocene Time	<p>Survey of 300 km (186 mi.) of river banks for liquefaction and paleoliquefaction features along portions of Rapidan, Mataponi, North Anna (during high-water conditions with poor exposures), South Anna, Appomattox, and James rivers, including Rivanna, Hardware, Rockfish, Slate, and Willis tributaries. Moderately susceptible deposits of 2–3 ka are common; only three small prehistoric liquefaction features are identified.</p> <p>“Near total lack of widespread liquefaction features in large search area strongly suggests that very strong seismic shaking cannot have occurred often in 2–3 ka and for past 5 ka west and north of Richmond...Paucity of liquefaction features in central Virginia makes it seem unlikely that any earthquakes in excess of ~M 7 have struck there...even if M 6–7 earthquakes had been relatively abundant, then many more liquefaction effects would have been expected.”</p>
Seeber and Armbruster (1988)	Seismicity Along the Atlantic Seaboard of the U.S.: Intraplate Neotectonics and Earthquake Hazard	The authors investigate intraplate seismicity in the eastern U.S. and compare it to other intraplate regions, as well as to the western U.S. They determine that the Appalachian front spatially controls seismicity on a large scale and may be boundary of a stress province for the eastern U.S.
Weems and Edwards (2007)	Post-Middle Miocene Origin of Modern Landforms in the Eastern Piedmont of Virginia	Recognizes intermittent Cenozoic fault motion in the NE-striking Stafford fault system and north-striking Dutch Gap fault. Indicates a fault-bounded trough filled with Coastal Plain marine sediments of late Middle Miocene age.
Recent Source Characterizations of CVSZ		
Bollinger (1992)	Specification of Source Zones, Recurrence Rates, Focal Depths, and Maximum Magnitudes for Earthquakes Affecting the Savannah River Site in South Carolina	Estimates the following parameter values for areal source zone representing CVSZ: $a = 1.18$, $b = 0.64$, $M_{\max} = m_b 6.4$.
Chapman and Krimgold (1994)	Seismic Hazard Assessment for Virginia	Estimates the following parameter values for areal source zone representing CVSZ: $a = 1.18$, $b = 0.64$, $M_{\max} = m_b 7.25$.
Frankel et al. (1996)	National Seismic-Hazard Maps: Documentation	Does not designate a finite source or zone for CVSZ; modeled using a gridded seismicity cell network within extended margin region: $M_{\max} = M_w 7.5$. No source- or zone-specific b -value. Background b -value for extended margin region = 0.96.

Table D-7.3.7 Data Summary
Extended Continental Crust Zone—Atlantic Margin

Citation	Title	Description and Relevance to SSC
Frankel et al. (2002)	Documentation for the 2002 Update of the National Seismic Hazard Maps	Does not designate a finite source or zone for CVSZ; modeled using a gridded seismicity cell network within extended margin region: $M_{\max} = M_w$ 7.50. Assumes same b -value as Frankel et al. (1996), i.e., 0.96.
Petersen et al. (2008)	Documentation for the 2008 Update of the United States National Seismic Hazard Maps	Does not designate a finite source or zone for CVSZ; modeled using a gridded seismicity cell network within extended margin region: $M_{\max} = M_w$ 7.50. Assumes same b -value as Frankel et al. (1996), i.e., 0.96.
Seismicity		
Ammon et al. (1998)	Faulting Parameters of the January 16, 1994 Wyomissing Hills, Pennsylvania Earthquakes	The January 1994 Wyomissing Hills, Pennsylvania, earthquake sequence was dominated by M 4.0 foreshock and M 4.6 main shock. The sequence was well recorded by U.S. and Canadian national seismic networks, which provided data for waveform modeling. Both events exhibit thrust-fault geometry with a nearly horizontal compression axis oriented NE-SW, consistent with regional stress patterns. A preferred depth of 3–5 km (2–3 mi.) is estimated for these two events, which are located in the region of historical seismicity termed the Lancaster seismic zone by Armbruster and Seeber (1987).
Armbruster et al. (1994)	The Jan. 1994 Wyomissing Hills Earthquakes ($m_b L_g = 4.0$ & 4.6) in Southeastern Pennsylvania: A 2-km-Long Northwest-Striking Fault Illuminated by Aftershocks	Abstract describes locations and magnitudes of the instrumentally observed January 1994 Wyomissing Hills earthquakes in SE Pennsylvania.
Bakun et al. (2003)	Estimating Locations and Magnitudes of Earthquakes in Eastern North America from Modified Mercalli Intensities	The authors create modified Mercalli intensity model for eastern North America, and use that model to determine the epicenter and magnitude of several historical earthquakes, including 1755 Cape Ann, Massachusetts, earthquake.
Bent (1995)	A Complex Double-Couple Source Mechanism for the M_s 7.2 1929 Grand Banks Earthquake	Analysis of additional seismographs indicates that M_s 7.2 1929 Grand Banks earthquake is in fact an earthquake with a complex source mechanism as opposed to a landslide. The first and largest sub-event was a strike-slip double-couple event occurring on a NW-striking plane. Two later sub-events were probably strike-slip double couples on NE-striking planes. All appear to have occurred at a depth of 20 km (12 mi.). The sum of sub-event moments corresponds to M_w of 7.2 ± 0.3 .

Table D-7.3.7 Data Summary
Extended Continental Crust Zone—Atlantic Margin

Citation	Title	Description and Relevance to SSC
Bollinger et al. (1991)	Seismicity of the Southeastern United States: 1698 to 1986	<p>Seismicity within ECC is not randomly distributed, but tends to be clustered with intervening areas exhibiting low seismicity. Hypocenters of events in Coastal Plain regions are distributed throughout upper crust (~13 km, or 8 mi., deep), and focal-mechanism solutions indicate N-NE maximum compressive stress.</p> <p>The authors review the seismicity of SE United States as documented by the studies to date of historical and network databases. The reasons for that division are the differences in levels of completeness and accuracy with respect to earthquake size and location. A regional summary synthesizes historical, instrumental, and network seismicity results with respect to the regional host geologic/physiographic provinces. The authors note that the feature of Coastal Plain seismicity is the apparent NW trend, perpendicular to northeasterly tectonic fabric of adjoining Piedmont and Appalachian Highlands and their associated seismicity. Although various interpretations have been put forth, the faults associated with Coastal Plain earthquakes have not been unambiguously identified. In Georgia and Alabama, the Coastal Plain earthquakes are spatially and temporally sparse. The earthquakes of Georgia Piedmont have been interpreted to represent failure on planes of weakness or joints within 4 km (2.5 mi.) of surface.</p> <p>The largest earthquake in the SE United States during historical times occurred in this province in 1886 (m_b 6.7, M_S = 7.7, MMI = X). Epicenter was probably about 20–30 km (12–19 mi.) NW of Charleston in Middleton Place–Summerville seismic zone (see Charleston Table). The hypocenters of Coastal Plain shocks are distributed throughout upper 13 km (8 mi.) of crust where focal mechanisms indicate N-NE maximum compressive stress.</p>
Bollinger and Wheeler (1988)	The Giles County, Virginia, Seismic Zone—Seismological Results and Geological Interpretations	The authors define Giles County seismic zone from a three-year study of microseismicity and interpret results in the context of the greater tectonic forces that formed Appalachians.

Table D-7.3.7 Data Summary
Extended Continental Crust Zone—Atlantic Margin

Citation	Title	Description and Relevance to SSC
Dawers and Seeber (1991)	Intraplate Faults Revealed in Crystalline Bedrock in the 1983 Goodnow and 1985 Ardsley Epicentral Areas, New York	<p>Presents argument that bedrock geologic studies in epicentral areas of 1983 Goodnow ($M_w = 5.1$) and 1985 Ardsley ($m_L = 4.0$) earthquakes in New York State suggest that seismogenic intraplate faults have subtle, but recognizable, expressions in crystalline bedrock along surface extrapolations of these well-defined earthquake ruptures. The 1983 Goodnow and 1985 Ardsley ruptures are correlated with Caitlin Lake fault zone (CLFZ) and Dobbs Ferry fault zone (DFFZ), respectively. The authors base these correlations on (1) spatial correlation of rupture plane, as defined by aftershock hypocenters, with a prominent fracture-controlled topographic lineament, and (2) observations of mesoscopic brittle structures along the lineaments that reflect larger-scale structures and, more importantly, that are consistent with both rupture orientation and sense of slip determined from seismic data.</p> <p>The authors point out that there is considerable uncertainty as to age of formation of both CLFZ and DFFZ, and some fault surfaces along DFFZ record evidence of reactivation in the form of superimposed slickensides. It is difficult to argue that the fault zones formed entirely in intraplate environment, instead; some of deformation could be Mesozoic in age. The authors speculate that the fault zones were activated as extensional structures during the Mesozoic and, being weaker than surrounding rock, remained active in the present intraplate regime. The authors state that the issue of small displacements on active structures that are relatively large and possibly old remains problematic.</p>
Ebel (2000)	A Reanalysis of the 1727 Earthquake at Newbury, Massachusetts	Uses analysis of felt reports, aftershocks, and recent instrumental seismicity near Amesbury, Massachusetts, to infer main-shock source parameters for the 1727 Newburyport, Massachusetts, earthquake. Data suggest that 1727 earthquake was shallow, located NW of Newbury, Massachusetts, and had m_b about 5.6.
Ebel and Hart (2001)	Observational Evidence for Amplification of Earthquake Ground Motions in Boston and Vicinity	Uses analysis of felt reports, aftershocks, and recent instrumental seismicity near Amesbury, Massachusetts, to infer main-shock source parameters for the 1727 Newburyport, Massachusetts, earthquake. Data suggest that 1727 earthquake was shallow, located NW of Newbury, Massachusetts, and had m_b about 5.6.
Ebel (2006a)	The Cape Ann, Massachusetts Earthquake of 1755: A 250th Anniversary Perspective	The earthquake of November 18, 1755, is likely located about 40 km (25 mi.) ENE of Cape Ann, Massachusetts. Based on attenuation of MMI with epicentral distance, the magnitude was estimated as m_{bLg} 6.2 or M 5.9.

Table D-7.3.7 Data Summary
Extended Continental Crust Zone—Atlantic Margin

Citation	Title	Description and Relevance to SSC
Hough and Seeber (1991)	Seismological Constraints on Source Properties of the $m_b = 4.0$, 1985 Ardsley, New York, Earthquake: A Characteristic Rupture?	Analyzes October 19, 1985, magnitude 4.0 earthquake that occurred in southern Westchester County, New York, approximately 30 km (19 mi.) north of central Manhattan. The earthquake was part of sequence of six events (m_b 1.8 to 4.0) that occurred along NW-trending Dobbs Ferry fault zone that cuts across Manhattan Prong. Hypocenters fall within 1 km (0.6 mi.) of each other, indicating rupture on a relatively small segment of Dobbs Ferry fault, which is at least 10 km (6 mi.) long. Aftershocks delineate a subvertical plane striking roughly 300° and define a rupture area roughly 700 m (2,300 ft.) across and between 4.5 and 5.5 km (3–3.5 mi.) deep. First-motion data indicate that left-lateral strike-slip motion predominates. The 500–1,000 m (1,640–3,281 ft.) wide rupture inferred from the hypocenter distribution corresponds to 1 km (0.6 mi.) long structurally defined segment of Dobbs Ferry fault zone.
Kafka et al. (1985)	Earthquake Activity in the Greater New York City Area: Magnitudes, Seismicity, and Geologic Structures	Describes locations and magnitudes of instrumentally observed seismicity in greater New York City area. Roughly half the earthquakes are located near Ramapo fault system, and many other earthquakes located near Newark basin. Despite these spatial associations, the cause of earthquakes in this area remains unknown.
Klose and Seeber (2007)	Shallow Seismicity in Stable Continental Regions	<p>Presents a worldwide compilation of well-constrained fault ruptures and focal depths of earthquakes for stable continental regions (SCRs). Depth distributions of fault ruptures and earthquakes in well-monitored SCRs worldwide indicate the following features:</p> <ul style="list-style-type: none"> • Many earthquakes and fault ruptures are bimodally distributed with depth modes in upper third of crust (<10 km, or 6 mi.) and lower third of crust (>20 km, or 12 mi.). • Depth and strength of contrasting modes vary regionally and indicate less stable intracrustal boundaries that may be located by seismic profiling. • Many medium-to-large earthquakes ($4.5 < M < 8.0$) tend to nucleate at very shallow depths (<7 km, or 4 mi.) and ruptures often reach surface. • Almost 80% of seismic moment density for shallow ruptures is released in uppermost 7 km (4 mi.) of crust. • Hypocentral depths of earthquakes are on average overestimated by $88\% \pm 30\%$ (standard mean \pm standard mean error).

Table D-7.3.7 Data Summary
Extended Continental Crust Zone—Atlantic Margin

Citation	Title	Description and Relevance to SSC
Seborowski et al. (1982)	Tectonic Implications of Recent Earthquakes near Annsville, New York	<p>The authors analyze a sequence of microearthquakes that occurred in January 1980 near Annsville, New York. The events yielded a composite focal mechanism solution indicating E-NE compression, resulting in thrust motion on N-NW-striking fault plane, with main shock having strike of N34°W and dip of 26°NE. A major structural feature of epicentral area is Annsville fault, a fault of Paleozoic age that strikes to NE and dips SE. The authors indicate that epicentral alignments and focal mechanism solutions for earthquakes near Annsville do not permit interpretation that movement occurred on this or other subparallel structures. Instead, the fault structure inferred to be associated with these earthquakes is transverse to Annsville fault. The active structure has no apparent surface expression and is possibly limited in spatial extent. Focal mechanisms reported for Annsville events suggest that major geologic structures may not be involved directly in current seismic activity of region. But the authors note that the structures may serve as zones of weakness that focus strain along less significant or less apparent structures within crust.</p>
Seeber and Armbruster (1988)	Seismicity Along the Atlantic Seaboard of the U.S.: Intraplate Neotectonics and Earthquake Hazard	<p>The authors discuss the potential for damaging earthquakes along Atlantic Seaboard and observe the following:</p> <ul style="list-style-type: none"> • Seismicity along Atlantic Seaboard moderately high for an intraplate region and includes large, damaging earthquakes. These tend to be distributed among many faults with small ruptures about 1–2 km (0.6–1.2 mi.) across for ~M 5 earthquakes and may be characterized by high stress drops. • Damaging earthquakes in east can be generated by small faults that do not reach surface and that may not be detected by geological and geophysical investigations. • The Appalachian Front, defined as NW limit of allochthonous crystalline slab above the master detachment, appears to control spatial distribution of seismicity on a large scale. Further, stress indicators are ambiguous about a distinct stress province along Appalachians/Atlantic Seaboard. • At an intermediate scale, seismicity is also often controlled by preexisting structure. Newark basin is an example in that it is aseismic but is bounded by concentrations of seismicity. • The apparent lack of one-to-one correlation between seismicity and preexisting structural features may be the result of changes in patterns of seismicity that occur over periods longer than the available historical record.

Table D-7.3.7 Data Summary
Extended Continental Crust Zone—Atlantic Margin

Citation	Title	Description and Relevance to SSC
Seeber and Armbruster (1989)	Low-Displacement Seismogenic Faults and Nonstationary Seismicity in the Eastern United States	Historical seismicity record shows that distribution of seismicity is nonrandom and that generally the pattern of seismicity derived from short-term instrumental data resembles that derived from long-term samples of historical data. The authors note that earthquake data associated with 1886 Charleston, South Carolina, earthquake suggests that hazard analysis based on assumption of stationarity may be appropriate for small- and intermediate-magnitude events, but may be misleading for large events.
Seeber and Dawers (1989)	Characterization of an Intraplate Seismogenic Fault in the Manhattan Prong, Westchester Co., N.Y.	The authors argue that there is close correlation in location, orientation, and sense of slip between Dobbs Ferry fault zone (DFFZ) and 1985 Ardsley earthquake rupture ($m_b = 4.0$) in southern Westchester County, New York. The DFFZ is a tabular zone of discontinuous faults and fractures rather than a single through-going fault, and cumulative offset across it is very small, considering size and Paleozoic age of structure. Mesoscopic structural data argue for predominantly left-lateral motion on DFFZ, while accumulated displacement on the fault zone shown by offset Paleozoic-age markers is right-lateral (20–30 m, or 66–98 ft.). While DFFZ is at least 8 km (5 mi.) long (later found to be at least 10 km, or 6 mi., long by Hough and Seeber [1991]), there is little evidence in surface outcrops of a single through-going fault; in addition, there is no evidence for Quaternary surface displacement. The authors consider that, given the small total accumulated displacement, Quaternary surface offset seems unlikely. They argue that segmented geometry of DFFZ suggests that structural data may provide criteria to constrain the largest possible ruptures on intraplate faults, as opposed to analyzing length of entire fault. Therefore, the concept of characteristic earthquake and characteristic rupture may be applicable to intraplate regions.
Wise and Fail (1998)	Lancaster County Seismic Zone (Penna.): Reactivation of a Taconic Structural Feature?	Abstract describes instrumentally observed seismicity in Lancaster County seismic zone of Pennsylvania. Suggests that if short, shallow faults of Lancaster seismic zone do not slip seismically, faults and earthquakes together might reflect some other, deeper geologic control on seismicity.
Zoback (1992)	Stress Field Constraints on Intraplate Seismicity in Eastern North America	Uses focal mechanisms from 32 midplate earthquakes in North America to determine how maximum horizontal compressive stress changes from the central eastern United States (strike-slip faulting stress regime) to SE Canada (thrust faulting stress regime).

Table D-7.3.7 Data Summary
Extended Continental Crust Zone—Atlantic Margin

Citation	Title	Description and Relevance to SSC
<i>Geologic Structures Interpreted from Geologic, Geomorphic, Geophysical, and Seismic-Profile Data</i>		
Cook and Oliver (1981)	The Late Precambrian–Early Paleozoic Continental Edge in the Appalachian Orogen	Integration of geological and geophysical data indicates that eastern edge of the late Precambrian–early Paleozoic North American continent is buried beneath crystalline rocks of southern Appalachian orogen. The transition appears to be essentially coincident with strong gravity gradient that is continuous throughout much of the length of the orogen. COCORP seismic-reflection data in southern Appalachians indicate that most of near-surface crystalline rocks of Blue Ridge and Inner Piedmont are allochthonous and that reflection character in the crust changes near Inner Piedmont–Charlotte belt boundary. Layered reflectors beneath Kings Mountain belt, Charlotte belt, and Carolina slate belt in Georgia are interpreted as sedimentary (or metasedimentary) strata, and associated gravity change is interpreted as an edge effect corresponding to boundary between continental and former oceanic or attenuated continental crust.
Cook and Vasudevan (2003)	Are There Relict Crustal Fragments Beneath the Moho?	Images of upper mantle structure from lithoprobe seismic-reflection profile suggests that a relict Mesoproterozoic subduction zone lies beneath Moho in NW Canada.
Cook and Vasudevan (2006)	Reprocessing and Enhanced Interpretation of the Initial COCORP Southern Appalachians Traverse	<p>The authors present results of reprocessed 1978–1980 COCORP Southern Appalachian seismic-reflection data that has produced improved images of structures related to emplacement of Blue Ridge–Inner Piedmont allochthon. Results enhance and extend the interpretation presented previously (Cook et al., 1979) that Blue Ridge and Inner Piedmont are allochthonous above a shallow and shallow-dipping detachment that can be followed from outcrop at the Blue Ridge/Valley and Ridge transition to at least beneath Carolina terrane. Continuity of reflections in the new images supports interpretation that southern Appalachian detachment is not rooted on east side of Inner Piedmont, but rather projects as a low-angle detachment (or zone of decoupling) to beneath Coastal Plain. An implication of this geometry is that terranes, such as Carolina terrane, between autochthonous North America and the Alleghanian suture beneath Coastal Plain are detached, thin flakes.</p> <p>Some key structures, such as layered supracrustal rocks beneath Appalachian detachment, were visible previously but are considerably improved. Other features (e.g., continuity of subhorizontal reflections beneath Carolina terrane and the shallowing of the Moho) that either were only marginally visible or were surmised based on ancillary information (e.g.,</p>

Table D-7.3.7 Data Summary
Extended Continental Crust Zone—Atlantic Margin

Citation	Title	Description and Relevance to SSC
		<p>palinspastic reconstructions) are now apparent. Still others, such as a prominent west-dipping midcrustal reflection beneath the Inner Piedmont ramp are visible for first time. These new results, combined with interpretations of regional reflection data recorded during 1980s south and west of the initial survey, have been incorporated into a schematic three-dimensional interpretation of crustal structure of the region. According to this interpretation, terranes (e.g., Carolina terrane) that were caught between ancient North American (Laurentian) lithosphere and African lithosphere are represented today as thin flakes that were juxtaposed with and emplaced above SE margin of Grenvillian basement.</p>
Cook et al. (1979)	Thin-Skinned Tectonics in the Crystalline Southern Appalachians: COCORP Seismic Reflection Profiling of the Blue Ridge and Piedmont	<p>COCORP seismic-reflection profiling in Georgia, North Carolina, and Tennessee and related geological data indicate that crystalline Precambrian and Paleozoic rocks of Blue Ridge, Inner Piedmont, Charlotte belt, and Carolina slate belt constitute an allochthonous sheet, generally 6–15 km (4–9 mi.) thick, which overlies relatively flat-lying autochthonous lower Paleozoic sedimentary rocks, 1–5 km (0.6–3 mi.) thick, of proto-Atlantic continental margin. Thus crystalline rocks of southern Appalachians appear to have been thrust at least 260 km (162 mi.) to west, and they overlie sedimentary rocks that cover an extensive area of central and southern Appalachians. The data show that Brevard fault is surface expression of an eastward-dipping splay of the main sole thrust, and the authors indicate that other major faults of this region have similar origins. The data support view that large-scale, thin crystalline thrust sheets may be significant features of orogenic zones.</p>
Cook et al. (1980)	The Brevard Fault: A Subsidiary Thrust Fault to the Southern Appalachian Sole Thrust	<p>COCORP seismic-reflection profiling data suggest that Brevard fault is a subsidiary thrust fault related to southern Appalachian detachment.</p>
Cook et al. (1981)	COCORP Seismic Profiling of the Appalachian Orogen Beneath the Coastal Plain of Georgia	<p>A southeastward extension onto Coastal Plain of an earlier COCORP traverse yielded the following results:</p> <ul style="list-style-type: none"> • Confirmation of east-dipping layers beneath Charlotte belt and subhorizontal layers east of these. Such midcrustal layers are apparently extensive beneath Eastern Piedmont and are most easily interpreted as late Precambrian–early Paleozoic metasediments and metavolcanics. Lateral correlation of these reflectors implies that a major detachment extends eastward beneath crystalline rocks of Eastern Piedmont and Coastal Plain.

Table D-7.3.7 Data Summary
Extended Continental Crust Zone—Atlantic Margin

Citation	Title	Description and Relevance to SSC
		<ul style="list-style-type: none"> • Recognition of a major SE-dipping reflector in crystalline basement that projects to surface location of Augusta fault and is thus interpreted as its subsurface extension. This feature extends 80 km (50 mi.) or more SE of surface trace of Augusta fault and is apparently a major lithologic and tectonic boundary in this area. • Recognition of upwardly concave reflectors that are listric into Augusta fault. These may be late Paleozoic thrust faults, Mesozoic listric normal faults, or both. • Observation of a significant thickness (up to 6.0 sec) of layered reflections beneath Augusta fault. One interpretation of these events is that they are late Precambrian–early Paleozoic basinal strata that have been thickened by repeated thrusting. • Discovery of an anticlinal feature in crystalline rocks beneath eastern Coastal Plain. Tectonic evolutionary models must now incorporate compressional deformation in North America at least as far east as eastern limit of Augusta fault (about 80 km, or 50 mi., east of its surface trace).
Gates and Costa (1998)	Multiple Reactivations of Rigid Basement Block Margins: Examples in the Northern Reading Prong, USA	Suggests that zones of crustal weakness in northern Reading Prong that formed during Grenville orogenesis were reactivated during subsequent tectonic events. As many as seven phases of reactivation are identified within Morgan Hill, Ramapo, and Reservoir faults.
Kean and Long (1981)	A Seismic Refraction Line Along the Axis of the Southern Piedmont and Crustal Thicknesses in the Southeastern United States	Describes COCORP seismic-reflection profiling data from southern Piedmont and estimates of crustal thickness.
Nelson et al. (1987)	Results of Recent COCORP Profiling in the Southeastern United States	The authors describe COCORP seismic-reflection profiling data from SE United States. They interpret reflections associated with Appalachian detachment, Alleghanian suture, South Georgia rift basin, and other features.
Talwani et al. (1995)	The Edge Experiment and the U.S. East Coast Magnetic Anomaly	The East Coast magnetic anomaly is spatially correlated with a zone of transitional igneous crust that extends along entire Atlantic margin. The authors suggest that basalts and underlying intrusives source the anomaly.

Table D-7.3.7 Data Summary
Extended Continental Crust Zone—Atlantic Margin

Citation	Title	Description and Relevance to SSC
<i>Faults with Cenozoic Activity</i>		
Behrendt et al. (1981)	Cenozoic Faulting in the Vicinity of the Charleston, South Carolina, 1886 Earthquake	Data from onshore multichannel seismic-reflection profiles in 1886 meizoseismal area show evidence of Cenozoic faulting, including the reverse (?) Cooke fault. Data suggest that most recent slip on the Cooke fault is Eocene or later. Data from offshore multichannel seismic-reflection profiles and single-channel high-resolution data show Helena Banks fault as a 30+ km (19 mi.) long structure with most recent movement in post-Miocene or Pliocene time.
Behrendt et al. (1983)	Marine Multichannel Seismic-Reflection Evidence for Cenozoic Faulting and Deep Crustal Structure near Charleston, South Carolina	Seismic-reflection data collected offshore from Charleston show Helena Banks fault as NE-striking, west-dipping reverse fault that extends upward to about 10 km (6 mi.) from sea bottom. The authors interpret it as Mesozoic extensional fault reactivated as reverse-oblique fault at least as young as Miocene or Pliocene. They also interpret it as a subhorizontal detachment at 11.4 ± 1.5 km (7 ± 1 mi.) depth. They suggest that Charleston seismicity is primarily caused by movement along the detachment, and that movement on high-angle reverse faults (e.g., the Helena Banks fault and others) may also cause earthquakes.
Bramlett et al. (1982)	The Belair Fault: A Cenozoic Reactivation Structure in the Eastern Piedmont	The authors determined that Belair fault zone (near Augusta, Georgia) represents a tear fault in upper plate of Augusta fault and that most of the ~23 km (14 mi.) of lateral displacement estimated by Prowell and O'Connor (1978) occurred during Paleozoic Alleghanian orogeny and not post-Cretaceous time. During Late Cretaceous and Cenozoic, the Belair fault was reactivated as an oblique-slip reverse fault displacing Middendorf and Barnwell formations of Atlantic Coastal Plain. Prowell et al. (1975) and Prowell and O'Connor (1978) document Cenozoic brittle reverse slip on Belair fault. Quaternary slip on Belair fault is allowed but not demonstrated by the available data (i.e., Crone and Wheeler, 2000).
Darton (1950)	Configuration of the Bedrock Surface of the District of Columbia and Vicinity	Geologic mapping of extension of Stafford fault system at Fredricksburg, Virginia, suggests possible faulted fluvial terraces that may indicate post-Pliocene movement.
Faye and Prowell (1982)	Effects of Late Cretaceous and Cenozoic Faulting on the Geology and Hydrology of the Coastal Plain near the Savannah River, Georgia and South Carolina	Geologic and hydrologic studies in Coastal Plain of Georgia and South Carolina suggest faulted upper Cretaceous to lower Tertiary rocks near Millet, South Carolina. The postulated Statesboro fault strikes NE and shows apparent down-to-the-NW motion.

Table D-7.3.7 Data Summary
Extended Continental Crust Zone—Atlantic Margin

Citation	Title	Description and Relevance to SSC
Jacobeen (1972)	Seismic Evidence for High Angle Reverse Faulting in the Coastal Plain of Prince Georges and Charles County, Maryland	Recognizes subsurface high-angle reverse Brandywine fault system in Cenozoic sediments of SW Maryland, based on seismic-reflection profiling.
Mayer and Wentworth (1983)	Geomorphic Differences East and West of the Stafford Fault System, Northeastern Virginia	Geomorphic relationships of fluvial terraces near Stafford fault system. Where faults are found to displace Cenozoic sediments of Coastal Plain, inferred cumulative rates tend to be less than 1 m (3 ft.) per million years (from Seeber and Armbruster, 1988).
Mixon and Newell (1978)	The Faulted Coastal Plain Margin at Fredericksburg, Virginia	The authors identify four en echelon NE-trending structures, including SE-dipping monoclines and NW-dipping high-angle reverse faults, along inner edge of Coastal Plain in NE Virginia termed the Stafford fault system. The structures affect the present distribution of Coastal Plain sediments with estimated displacements of 15–60 m (49–197 ft.). The fault system extends at least 56 km (35 mi.) parallel to Fall Line and NE-trending reach of the Potomac estuary where the authors hypothesize that the Fall Line and major river deflections along it have been tectonically influenced. The authors suggest possible relationship between Coastal Plain deformational belts and zones of weakness in crystalline basement rocks characterized by normal faulting in Triassic. The speculative relationship of Stafford fault system to Triassic or older basement structures is based on alignment of Stafford fault with Farmville basin Triassic fault trend and Brandywine fault system that could potentially mark a major zone of deformation in basement rocks that records recurrent movement in pre-Mesozoic, Mesozoic, and Cenozoic time.
Newell (1985)	Architecture of the Rappahannock Estuary—Neotectonics in Virginia	The authors describe Stafford fault system as zone of NW-dipping, en echelon reverse faults near the Fall Line in NE Virginia.
Pavich et al. (1989)	Investigations of the Characteristics, Origin, and Residence Time of the Upland Residual Mantle of the Piedmont of Fairfax County, VA	This study suggests that regolith of Piedmont most likely represents Pliocene and Quaternary weathering system that is product of interaction of bedrock and ground water in an actively eroding landscape. Variation in saprolite thickness, and therefore regolith thickness, is a function of distribution of minerals in the rock, grain contact relations, and structural fabric.
Pavrides (1994)	Continental Margin Deposits and the Mountain Run Fault Zone of Virginia—Stratigraphy and Tectonics	Provides descriptions and geologic mapping of NE-striking reverse Everona–Mountain Run fault zone in Virginia. From offset late Cenozoic gravels and rugged topography of scarps along Everona fault, the author infers possible Quaternary reactivation of Everona fault or some part of Mountain Run fault zone.

Table D-7.3.7 Data Summary
Extended Continental Crust Zone—Atlantic Margin

Citation	Title	Description and Relevance to SSC
Pavlides et al. (1983)	Late Cenozoic Faulting Along the Mountain Run Fault Zone, Central Virginia Piedmont	The authors investigate faulting along Everona–Mountain Run fault zone near Everona, Virginia, including late Cenozoic stream gravels apparently offset vertically ~1.5 m (5 ft.).
Prowell (1983)	Index of Faults of Cretaceous and Cenozoic Age in the Eastern United States	Many investigators have recognized and documented post-rift faulting of Cretaceous and Cenozoic ages in Atlantic Coastal Plain. The author compiled information and describes evidence for possible Cretaceous and Cenozoic faults in the eastern U.S. Faults, fractures, and joints in eastern New York State generally trend N-NE, but none of these structures have been shown to displace Holocene deposits. Within the ECC, the geometry of the Coharie unconformity on adjacent sides of the Hares Crossroads fault plane suggests that significant lateral offset may have occurred on fault. It is considered to be a reverse fault that has a strike of N7°E and a dip of 63° to the SE. Basement rock affected by faulting includes Paleozoic Piedmont schist, slate, and phyllite. Sedimentary rocks (or sediments) affected by faulting include unconsolidated clayey sand of Coharie Formation (Pliocene-Pleistocene). Greatest vertical displacement is 2.8 m (9 ft.) and greatest horizontal displacement is 2 m (>6 ft.).
Prowell (1988)	Cretaceous and Cenozoic Tectonism on the Atlantic Coastal Margin	The author indicates that the predominant orientation of mapped Cretaceous and younger faults within ECC is N-S to NE-SW. Further, post-Cretaceous movement on these faults is reverse slip, with limited evidence for strike-slip movement. Within the ECC source zone, several NE-trending reverse fault zones in fault systems up to 100 km (62 mi.) long have experienced Cenozoic activity. These faults typically strike N-NE, dip steeply, and displace sedimentary rocks of Late Cretaceous to Miocene (100–5.3 Ma) age. Observed displacements are dip-slip, but some strike-slip may have occurred. Individual fault zone displacements are generally tens of meters, with a maximum cumulative offset of as much as 80 m (262 ft.). The available stratigraphic data generally show greater displacement on older units, indicating progressive displacement through time. The author describes vertical slip rates as ranging from 0.0003 to 0.00015 meters per thousand years (m/kyr) during the past 110 Ma, averaging 0.0005 m/kyr.

Table D-7.3.7 Data Summary
Extended Continental Crust Zone—Atlantic Margin

Citation	Title	Description and Relevance to SSC
Prowell and O'Connor (1978)	Belair Fault Zone: Evidence of Tertiary Fault Displacement in Eastern Georgia	The authors describe Belair fault zone as comprising NE-striking oblique-slip reverse faults with as much as 30 m (98 ft.) of apparent vertical offset since deposition of Late Cretaceous–middle Tertiary Coastal Plain sediments. In contrast with Prowell et al. (1975), the authors indicate that no fault movement has occurred in past 2,000 years, but that movement may have occurred in late Tertiary time.
Prowell et al. (1975)	Preliminary Evidence for Holocene Movement Along the Belair Fault Zone near Augusta, Georgia	Describes results of paleoseismic trenching across Belair fault near Augusta, Georgia. Lenses of organic material are interpreted as faulted and deformed. A composite sample of this material yielded mid- to late Holocene ages.
Sykes et al. (2008)	Observations and Tectonic Setting of Historic and Instrumentally Located Earthquakes in the Greater New York City–Philadelphia Area	<p>The authors compiled a catalog of 383 earthquakes (from historical and instrumental data) in SE New York, SW Connecticut, northern New Jersey, and eastern Pennsylvania. Observations from this study are as follows:</p> <ul style="list-style-type: none"> • Most hypocenters are concentrated in older terranes bordering Mesozoic Newark basin in Reading, Manhattan, and Trenton prongs and in similar rocks found at shallow depth beneath Coastal Plain from south of New York City across central New Jersey. Historical shocks of m_{bLg} 3 and larger were more numerous in latter zone. • Most earthquakes are shallow (94% are ≤ 10 km, or 6 mi., deep). • Many earthquakes have occurred beneath 12 km (7.5 mi.) wide Ramapo seismic zone (RSZ) in eastern part of Reading Prong, where station coverage has been the most extensive since 1974. • The SE boundary of the RSZ, which is nearly vertical, extends from near the surface trace of Mesozoic Ramapo fault to depths of 12–15 km (7.5–9 mi.). Mesozoic border fault dips about 50°–60°SE; therefore, earthquakes are occurring within middle Proterozoic through early Paleozoic rocks. • Causative faults and their orientations within RSZ in eastern part of Reading Prong are uncertain. • Seismicity is nearly absent in Mesozoic sedimentary rocks of Newark basin and in Cambro-Ordovician rocks inferred beneath them. This is attributed to either those rocks being relatively weak, in the velocity-strengthening rheological regime, being decoupled from the basement beneath them by thrust and/or detachment faults along weak layers, or a lack of preexisting brittle faults that are suitably oriented with respect to contemporary stresses.

Table D-7.3.7 Data Summary
Extended Continental Crust Zone—Atlantic Margin

Citation	Title	Description and Relevance to SSC
		<ul style="list-style-type: none"> • A newly identified feature—NW-trending Peekskill-Stamford seismic boundary—is nearly vertical, extends from near surface to depths of about 12–15 km (7.5–9 mi.), and is subparallel to brittle faults farther south in Manhattan Prong. • These brittle faults may have formed between Mesozoic basins to accommodate Mesozoic extension. • The Great Valley in NW part of study region is nearly devoid of known earthquakes. • Maximum compressive stress is nearly horizontal and is oriented about N64°E. • Extrapolation of the frequency-magnitude relationship indicates that an event of $m_{bLg} - 6.0$ is expected about once every 670 years. • Which faults are active in this intraplate region has been a subject of ongoing debate. Several faults displace Mesozoic sedimentary and igneous rocks, but evidence of faulting in younger sediments of Coastal Plain and in postglacial sediments is either missing or debatable.
Wentworth and Mergner-Keefer (1983)	Regenerate Faults of Small Cenozoic Offset—Probable Earthquake Sources of the Southeastern United States	Proposes that Mesozoic normal faults in Piedmont and Coastal Plain have been reactivated as reverse and reverse-oblique faults.
Postulated Faults		
Crone and Wheeler (2000)	Data for Quaternary Faults, Liquefaction Features, and Possible Tectonic Features in the Central and Eastern United States, East of the Rocky Mountain Front	<p>The authors provide a compilation and evaluation of Quaternary faults, liquefaction features, and possible tectonic features in CEUS. They assigned faults to three classes, which they define by features as follows. Class A features are those for which geologic evidence demonstrates existence of a Quaternary fault of tectonic origin. Class B features are those for which the fault may not extend deeply enough to be a potential source of significant earthquakes, or for which currently available geologic evidence is not definitive enough to assign the feature to either Class C or Class A. Class C features are those for which geologic evidence is insufficient to demonstrate existence of a tectonic fault, Quaternary slip, or deformation associated with the feature.</p> <p>Class A structures or seismic zones within the ECC include the following:</p> <ul style="list-style-type: none"> • Central Virginia seismic zone, Virginia—Zone of elevated seismicity.

Table D-7.3.7 Data Summary
Extended Continental Crust Zone—Atlantic Margin

Citation	Title	Description and Relevance to SSC
		<ul style="list-style-type: none"> • Charleston-Bluffton-Georgetown liquefaction features (see Charleston Data Summary Table D-6.1.2) • Newbury, Massachusetts, liquefaction features. <p>Class B—<i>There are no Class B faults in the ECC.</i></p> <p>Class C structures and features within the ECC and explanation of Class C assignment are as follows:</p> <ul style="list-style-type: none"> • Belair fault zone, Georgia—Two trenches record pre-Quaternary age. • Cacoosing Valley earthquake, Pennsylvania—No surface rupture from earthquake correlated to this fault. • Cape Fear arch, North Carolina—South Carolina—Lack of evidence for Quaternary faulting. • Catlin Lake—Goodnow Pond lineament, New York—No evidence of continuous fault zone and lacks paleoseismological evidence of Quaternary motion. • Champlain lowlands normal faults, New York—Vermont—No evidence for Quaternary motion. • Clarendon-Linden fault zone, New York—No paleoseismological evidence for Quaternary motion. • Cooke fault, South Carolina—Lack of evidence of faulting younger than Eocene. • Cornwall-Massena earthquake, New York—Ontario—No paleoseismological evidence for Quaternary motion. • Dobbs Ferry fault zone, New York—Earthquakes were too deep to produce any recognized surface cracking along trace of fault zone; no paleoseismologic evidence for Quaternary motion. • Everona fault—Mountain Run fault zone, Virginia—No detailed paleoseismologic or other investigations. • Hares Crossroads fault, North Carolina—Faulting is not demonstrably of Quaternary age. • Helena Banks fault zone, offshore South Carolina—No reported evidence for slip younger than Miocene. • Kingston fault, New Jersey—Faulting is not demonstrably of Quaternary

Table D-7.3.7 Data Summary
Extended Continental Crust Zone—Atlantic Margin

Citation	Title	Description and Relevance to SSC
		<p>age.</p> <ul style="list-style-type: none"> • Lancaster seismic zone, Pennsylvania—No structural, stratigraphic, or paleoseismological evidence for Quaternary faulting. • Lebanon Church fault, Virginia—Faulting is not demonstrably of Quaternary age. • Moodus seismic zone, Connecticut—Causes and causative faults of the earthquakes remain enigmatic. • Mosholu fault, New York—Faulting is not demonstrably of Quaternary age. • New York Bight fault, offshore New York—Fault lacks documented Quaternary offset. • Offset glaciated surfaces, Maine–Massachusetts–New Hampshire–New York–Vermont—Their most likely origin is in frost heaving, not tectonics. • Old Hickory faults, Virginia—Faulting was probably of Pliocene age. • Pen Branch fault, South Carolina—Lack of evidence for post-Eocene slip. • Ramapo fault system, New Jersey–New York—Lack of evidence for Quaternary slip on fault. • Upper Marlboro faults, Maryland—Surficial structures do not extend to hypocentral depths.
<p>Dominion Nuclear North Anna LLC (2004)</p>	<p>North Anna Early Site Permit Application Response to Request for Additional Information No.3.</p>	<p>The key observations and conclusions from the Dominion assessment regarding the East Coast fault system (ECFS-N segment) are summarized as follows:</p> <ul style="list-style-type: none"> • No consistent co-occurrence of two or more anomalies along each of the drainages was observed, as may be expected if they have developed in response to uplift of northern zone of river anomalies (ZRA-N). • There is no consistent pattern of anomalies along trend of ZRA-N, as expected if structure was active along its entire length. • It was not possible to verify or duplicate geomorphic observations, such as channel incision. • The “upward displaced fluvial surfaces” are inferred only from qualitative analysis of convexities of river profiles, and therefore, this type of “anomaly” does not provide evidence for tectonic uplift and is inconsistent with other geomorphic observations. These features in most cases are

Table D-7.3.7 Data Summary
Extended Continental Crust Zone—Atlantic Margin

Citation	Title	Description and Relevance to SSC
		<p>more objectively characterized as convexities, or local increases in gradient of longitudinal profiles of floodplains due to intersection of concave profiles at river confluences.</p> <ul style="list-style-type: none"> • Direct stratigraphic evidence for no Quaternary deformation was documented in vicinity of a large meander of Nottoway River that Marple and Talwani (2000) interpreted to have formed in response to systematic folding and northeastward tilting. • The fluvial geomorphic features cited by Marple and Talwani (2000) are likely produced by nontectonic fluvial processes and are not anomalous, which does not support Marple and Talwani's interpretation of the presence and activity of ZRA-N (ECFS-N).
Marple and Talwani (2000)	Evidence for a Buried Fault System in the Coastal Plain of the Carolinas and Virginia—Implications for Neotectonics in the Southeastern United States	<p>The authors postulate a N-NE-/S-SW-striking buried fault system in Coastal Plain of Carolinas and Virginia, named East Coast fault system (ECFS). Geomorphic analyses of Coastal Plain rivers led to differentiation of three nearly collinear, approximately 200 km (125 mi.) long segments (ECFS-S, ECFS-C, and ECFS-N) that were initially referred to as southern, central, and northern zones of river anomalies (ZRA-S, ZRA-C, and ZRA-N). Southern segment is located primarily in South Carolina; central segment is located primarily in North Carolina; and northern segment extends from NE North Carolina through Virginia. Identification of postulated fault system is based on alignment of geomorphic changes along streams, areas of uplift, and local evidence of faulting. The authors concluded that (1) ZRAs were produced by gentle late Quaternary uplift along an approximately 600 km (370 mi.) long buried fault system, and (2) because most of the river anomalies occur in unconsolidated floodplain sediments of upper Pleistocene (<130 ka) or younger age, deformation occurred during this period and may be ongoing.</p>
Marple and Talwani (2004)	Proposed Shenandoah Fault and East Coast–Stafford Fault System and Their Implications for Eastern U.S. Tectonics	<p>Comparison of Shenandoah igneous province, Central Virginia seismic zone, a NW-trending linear magnetic anomaly offshore Virginia, and other tectonic features in Virginia suggests presence of a deep crustal NW-striking basement fault, named Shenandoah fault. Along Shenandoah fault, the Central Virginia seismic zone coincides with an apparent –110 km (–68 mi.) offset between NE-striking Stafford fault zone and East Coast fault system (ECFS). The authors postulate that the following series of events likely occurred in the formation of the fault system:</p> <ul style="list-style-type: none"> • Stafford fault zone and ECFS formed a continuous ~1,100 km (684 mi.)

Table D-7.3.7 Data Summary
Extended Continental Crust Zone—Atlantic Margin

Citation	Title	Description and Relevance to SSC
		<p>long East Coast–Stafford fault system (EC-SFS) extending from South Carolina to New Jersey before the Alleghanian orogeny.</p> <ul style="list-style-type: none"> • During Alleghanian or an earlier orogeny, EC-SFS was beheaded by NW-vergent thrusting of allochthonous terranes, concealing it beneath those terranes. • Late Alleghanian indentation in Salisbury embayment by Reguibat uplift of NW Africa produced Shenandoah fault and offset EC-SFS left-laterally—110 km (–68 mi.) beneath allochthonous terranes in central Virginia. • Late Jurassic to Cenozoic dextral reactivation of ECFS and Stafford fault at depth fractured overlying terranes and may have produced N-NE-oriented linking faults that reconnected EC-SFS along a large left-step restraining bend. • The cause of seismicity in central Virginia may be from compression at the bend, which is causing displacements on a variety of faults in the area, including linking faults, Shenandoah fault, and older Paleozoic faults. • Late Jurassic and Middle Eocene dextral deformation along the large restraining bend along EC-SFS in central Virginia produced tension across Shenandoah fault to the NW. This tension caused normal sense reactivation of the fault beneath the allochthonous terranes of Blue Ridge and Valley and Ridge provinces. • Consequently, magma migrated up Shenandoah fault and then along bedding planes and NW joints within Valley and Ridge strata to form Shenandoah igneous province.
Progress Energy Carolinas, Inc. (2008)	Shearon Harris Nuclear Power Plants Units 2 and 3, Docket Nos. 52-022 and 52-023, Supplement 1 to Response to Requests for Additional Information Letter 030 Related to Basic Geologic and Seismic Information	<p>The key observations and conclusions from the Progress Energy assessment of East Coast fault system (ECFS) are summarized as follows:</p> <ul style="list-style-type: none"> • There is supporting geological, geophysical, and seismological information to suggest that geomorphic anomalies identified along southern half of ECFS-S segment may be associated with Quaternary displacement on Woodstock fault and that this fault may be source of Charleston earthquake (see Charleston Data Summary Table D-6.1.2). • There is no similar evidence to suggest that northern part of ECFS-S, ECFS-C, and ECFS-N segments are capable tectonic structures as defined by the U.S. Nuclear Regulatory Commission (Regulatory Guide 1.208).

Table D-7.3.7 Data Summary
Extended Continental Crust Zone—Atlantic Margin

Citation	Title	Description and Relevance to SSC
		<ul style="list-style-type: none"> • Observations and lines of evidence presented by Marple and Talwani (2000) do not provide convincing arguments in support of a buried N-NE-striking strike-slip fault (postulated ECFS-C) through North Carolina Coastal Plain region. • Evidence of neotectonic deformation (i.e., differential uplift of the Piedmont relative to the Coastal Plain regions, regional tilting, and broad zones of tilting or flexure) can be explained by lithospheric flexure (i.e., long-wavelength bending or warping of lithosphere) related to regional patterns of erosion and Cenozoic deposition. • Localized Cenozoic faulting observed near Piedmont–Coastal Plain boundary may be related to stresses in the region of greatest flexure (Pazzaglia, 1999). • The possibility cannot be precluded given the available data that some local structures along general trend of ECFS may be present and may be favorably oriented for reactivation in the present tectonic setting. • There are no geological data, however, to demonstrate Quaternary surface faulting. • There is no associated seismicity or reported evidence of paleoliquefaction to indicate activity along ECFS-C segment. • The implication that the postulated central and northern segments of ECFS if they exist may produce earthquakes of a similar size to the 1886 Charleston earthquake, as inferred by Marple and Talwani, is not demonstrated.
Wheeler (2005)	Known or Suggested Quaternary Tectonic Faulting, Central and Eastern United States-New and Updated Assessments for 2005	<p>Provides 13 assessments, 12 of which are new; the 13th incorporates significant new information. The new assessments describe faults, fields of paleoliquefaction features, seismic zones, and geomorphic features for which too little geologic information was available to write an assessment before now. The following features are located within ECC and are all assigned to Class C for their respective reasons.</p> <p>Class C updated structures:</p> <ul style="list-style-type: none"> • Eastern Border fault, Connecticut—No faulting demonstrated in Quaternary sediments. • East Coast fault system, North Carolina–South Carolina–Virginia—The 1886 and prehistoric liquefying earthquakes in coastal South Carolina

Table D-7.3.7 Data Summary
Extended Continental Crust Zone—Atlantic Margin

Citation	Title	Description and Relevance to SSC
		<p>demonstrates occurrence of repeated Quaternary tectonic faulting, but the link between these earthquakes and East Coast fault system or Woodstock fault remains speculative.</p> <ul style="list-style-type: none"> • Fall Lines of Weems, North Carolina, Virginia, and Tennessee—Fall zones are not demonstrably reproducible. Tectonic faulting is not yet demonstrated. • Hopewell fault, Virginia—No observed offsets of Pleistocene terrace deposits. • New Castle County faults, Delaware—Subsurface studies showed no evidence of Quaternary faulting. • Stafford fault system, Virginia—None of the strands of Stafford fault system are known to have moved during Quaternary.
<i>Paleoseismic Investigations</i>		
Amick (1990)	Paleoliquefaction Investigations Along the Atlantic Seaboard with Emphasis on the Prehistoric Earthquake Chronology of Coastal South Carolina	Search for paleoliquefaction features along U.S. East Coast at over 1,000 sites from southern Georgia to New Jersey. Features found only in coastal Carolinas. Includes rough maps of areas searched in which no features found, as well as sketches and photographs of selected features. Includes discussion of criteria by which to distinguish seismically induced liquefaction features from “pseudoliquefaction” features.
Amick, Gelinas, et al. (1990)	Paleoliquefaction Features Along the Atlantic Seaboard	Search for paleoliquefaction features along U.S. East Coast at over 1,000 sites from southern Georgia to New Jersey. Features found only in coastal Carolinas. Includes discussion of criteria by which to distinguish seismically induced liquefaction features from “pseudoliquefaction” features.
Amick and Gelinas (1991)	The Search for Evidence of Large Prehistoric Earthquakes Along the Atlantic Seaboard	Search for paleoliquefaction features along U.S. East Coast at over 1,000 sites from southern Georgia to New Jersey. Features found only in coastal Carolinas.
Obermeier and McNulty (1998)	Paleoliquefaction Evidence for Seismic Quiescence in Central Virginia During Late and Middle Holocene Time	<p>Survey of 300 km (186 mi.) of river banks for liquefaction and paleoliquefaction features along portions of Rapidan, Mataponi, North Anna (high water with poor exposures), South Anna, Appomattox, and James rivers, including Rivanna, Hardware, Rockfish, Slate, and Willis tributaries. Moderately susceptible deposits of 2–3 ka common; only three small prehistoric liquefaction features identified.</p> <p>“Near total lack of widespread liquefaction features in large search area</p>

Table D-7.3.7 Data Summary
Extended Continental Crust Zone—Atlantic Margin

Citation	Title	Description and Relevance to SSC
		strongly suggests that very strong seismic shaking cannot have occurred often in 2–3 ka and for past 5 ka west and north of Richmond...Paucity of liquefaction features in central Virginia makes it seem unlikely that any earthquakes in excess of ~M 7 have struck there...even if M 6–7 earthquakes had been relatively abundant, then many more liquefaction effects would have been expected.”
Tuttle (2007)	Re-evaluation of Earthquake Potential and Source in the Vicinity of Newburyport, Massachusetts	Recent searches for earthquake-induced liquefaction features in Newburyport, Massachusetts, area yielded only one small sand dike.
Tuttle (2009)	Re-evaluation of Earthquake Potential and Source in the Vicinity of Newburyport, Massachusetts	Searches for earthquake-induced liquefaction features along several rivers south of Newburyport, in vicinity of Hampton Falls, and west of Hampton Falls in New Hampshire yielded only one liquefaction feature: a small sand dike along Hampton Falls River in New Hampshire.
Tuttle and Seeber (1991)	Historic and Prehistoric Earthquake-Induced Ground Liquefaction in Newbury, Massachusetts	The authors found both historical and prehistoric liquefaction features (sand dikes). The historical features were attributed to 1727 earthquake, and the prehistoric features were estimated to have formed during past 4,000 years.

Table D-7.3.9 Data Summary
Extended Continental Crust Zone—Gulf Coast

Citation	Title	Description and Relevance to SSC
Seismicity		
Angell and Hitchcock (2007)	A Geohazard Perspective of Recent Seismic Activity in the Northern Gulf of Mexico	Describes seismotectonic setting of northern Gulf of Mexico with specific reference to the 2006 earthquakes. Presents detailed information regarding seismic source characteristics of the 2006 earthquakes. Also addresses seismogenic capability of growth faults. Discusses implications to seismic hazard assessment in Gulf of Mexico. Presents a possible two-layer source model for Gulf of Mexico.
Davis et al. (1989)	A Compendium of Earthquake Activity in Texas	Comprehensive review and database of historical earthquake activity in Texas 1847–1986. Largest earthquakes have occurred in W Texas and are interpreted as resulting from either tectonic stresses or oil and gas field operations. Helps to constrain estimates of the minimum maximum earthquake magnitude for Gulf of Mexico coastal plain.
Dellinger and Nettles (2006) Dellinger, Dewey et al. (2007) Dellinger, Ehlers et al. (2007)	The 10 February 2006, Magnitude 5.2 Gulf of Mexico Earthquake: Insights and Implications Relocating and Characterizing the 10 Feb 2006 “Green Canyon” Gulf of Mexico Earthquake Using Oil-Industry Data The Green Canyon Event as Recorded by the Atlantis OBS Node Survey	Detailed analysis of the earthquake with focus on the relative amount and timing energy release during the event. Focuses on determining a location and magnitude for the event, and hypothesizes that the event is most consistent with a slow, nontectonic event (e.g., large-scale slump, landslide).
Dewey and Dellinger (2008)	Location of the Green Canyon (Offshore Southern Louisiana) Seismic Event of February 10, 2006	Presents analysis constraining location and depth of February 10, 2006, earthquake. Provides information on the seismotectonic setting of the earthquake, and minor discussion of potential causes of the event (i.e., nontectonic event).
Frohlich (1982)	Seismicity in the Central Gulf of Mexico	Provides general overview of the sparse seismicity in Gulf of Mexico and a more detailed discussion of July 24, 1978, M 5.0 earthquake. Interprets the location and reverse mechanism for the event to possibly indicate that the event is related to crustal subsidence and downwarping of Gulf of Mexico basin.

Table D-7.3.9 Data Summary
Extended Continental Crust Zone—Gulf Coast

Citation	Title	Description and Relevance to SSC
Frohlich and Davis (2002)	Texas Earthquakes	Provides catalog of earthquakes in Texas 1847–2001. Helps constrain minimum maximum magnitude estimate for the Gulf of Mexico coastal plain region. Provides only minor discussions of potential earthquake mechanisms for the region.
Gangopadhyay and Sen (2008)	A Possible Mechanism for the Spatial Distribution of Seismicity in Northern Gulf of Mexico	Modeling of regional stress concentrations and the mechanical properties of salt and surrounding sediments to investigate the possible mechanism for the 2006 Gulf of Mexico earthquakes. Results show that locations of high shear stress in the Gulf of Mexico correlate well with the spatial distribution of seismicity in the northern Gulf of Mexico, suggesting a possible causal association between mechanical differences between salt and surrounding sediment and regional shear stresses.
Gomberg and Wolf (1999)	Possible Cause for an Improbable Earthquake: The 1997 Mw 4.9 Southern Alabama Earthquake and Hydrocarbon Recovery	An investigation into possible causes of 1997 Alabama earthquake. Concludes that hydrocarbon recovery is likely cause, but that tectonic mechanisms or influence cannot be ruled out.
Nettles (2006)	Two Unusual Seismic Events in the Gulf of Mexico	Seismological analysis of the February 10, 2006, m_b 5.2 and April 18, 2006, M_s 4.8 earthquakes in the northern Gulf of Mexico. Concludes from waveforms and energy release that the two events are best modeled as gravity-driven “landslide” mechanisms.
Nettles (2007)	Analysis of the 10 February 2006 Gulf of Mexico Earthquake from Global and Regional Seismic Data	Describes analysis of February 10, 2006, m_b 5.2 earthquake and the conclusion that earthquake was gravity-driven and did not have a tectonic source.
Nunn (1985)	State of Stress in the Northern Gulf Coast	Addresses state of stress in Gulf of Mexico coastal plain region as related to Quaternary fault activity. Concludes that activity is consistent with lithospheric flexure caused by sediment loading in Gulf of Mexico. Also concludes that lack of seismicity may be due to relaxation of these stresses over time.
Peel (2007)	The Setting and Possible Mechanism of the 2006 Green Canyon Seismic Event	Describes geologic setting of February 10, 2006, m_b 5.2 earthquake. Presents an interpretation of the ocean-continent boundary as interpreted from industry seismic and nonseismic potential field geophysical data. Concludes that earthquake was restricted to growth sedimentary section in shallow upper crust.

Table D-7.3.9 Data Summary
Extended Continental Crust Zone—Gulf Coast

Citation	Title	Description and Relevance to SSC
Stevenson and McCulloh (2001)	Earthquakes in Louisiana	General description of earthquakes and fault activity in Louisiana with earthquake database. Concludes that most active faulting is associated with creeping growth faults.
Todd and Ammon (2007)	Characteristics of Recent Seismic Activity in the Gulf of Mexico	Presents information on depth and source characteristics of September 10 and February 10, 2006, earthquakes in Gulf of Mexico. Concludes that they occur within a “stable cratonic region” of North America and there are no well-known fault systems in the vicinity of the earthquakes, and therefore earthquakes of similar size may occur elsewhere in Gulf of Mexico. Provides constraints on the estimate of a minimum maximum earthquake magnitude for northern Gulf of Mexico.
Crustal Structure		
Anderson and Schmidt (1983)	The Evolution of Middle America and the Gulf of Mexico-Caribbean Sea Region During Mesozoic Time	Provides plate reconstruction model for the Gulf of Mexico and Caribbean region. Focuses on structures accommodating microplate motions in Mexico (e.g., Mojave-Sonora megashear).
Baksi (1997)	The Timing of Late Cretaceous Alkalic Igneous Activity in the Northern Gulf of Mexico Basin, Southeastern USA	Discusses distribution and age of Cretaceous igneous rocks in northern Gulf of Mexico. In particular, discusses Magnet Cove rocks of southern Arkansas that provide evidence of Mesozoic igneous activity in southern Arkansas.
Bird (2001)	Shear Margins: Continent-Ocean Transform and Fracture Zone Boundaries	Presents compilation of interpretations of plate tectonic continental shear margins worldwide. Compares plate tectonic models of Pindell (2000) to those of Buffler and Thomas (1994), and the implications of a Gulf Coast–parallel shear margin (Buffler and Thomas, 1994) to a shear margin along eastern coast of Mexico (Pindell, 2000).
Bird et al. (2005)	Gulf of Mexico Tectonic History: Hotspot tracks, Crustal Boundaries, and Early Salt Distribution	Provides constraints on location of ocean-continent crust boundary in northern Gulf of Mexico based on seismic-reflection and potential field geophysical data. Includes a comparison of the ocean-continent boundary as interpreted by multiple authors.
Buffler and Sawyer (1985)	Distribution of Crust and Early History, Gulf of Mexico Basin	Provides general overview of geologic and tectonic evolution of Gulf of Mexico. The tectonic reconstruction model is compared with previous models. Provides constraints on the locations of continental and oceanic crust in Gulf of Mexico.

Table D-7.3.9 Data Summary
Extended Continental Crust Zone—Gulf Coast

Citation	Title	Description and Relevance to SSC
Buffler and Thomas (1994)	Crustal Structure and Evolution of the Southwestern Margin of North America and the Gulf of Mexico Basin	Presents interpretations of E-W-trending tectonic elements in south-central U.S. (Alabama-Arkansas fault system and Suwanee-Wiggins suture) as major structural features associated with development of Gulf of Mexico. These E-W structures are important with respect to crosscutting relationships with NW-trending fracture zones in eastern Gulf of Mexico.
Byerly (1991)	Igneous Activity	Presents a synthesis of the igneous activity throughout Gulf of Mexico during the Mesozoic and Cenozoic.
Christenson (1990)	The Florida Lineament	Provides interpretations of location and geometry of a major NW-trending fracture zone (the Florida lineament) based on borehole, regional gravity, and regional magnetic data. Describes a major structure in eastern Gulf of Mexico located near September 10, 2006, M 5.8 earthquake.
Collins (2004)	Summary of the Balcones Fault Zone, Central Texas: A Prominent Zone of Tertiary Normal Faults Marking the Western Margin of the Texas Coastal Plain	Discusses tectonic history of Balcones fault zone.
Cook et al. (1979)	Crustal Structure and Evolution of the Southern Rio Grande Rift	Discusses southern extent of Rio Grande rift in New Mexico using geophysical data (gravity, heat flow, seismic reflection).
Cox et al. (2000)	Quaternary Faulting in the Southern Mississippi Embayment and Implications for Tectonics and Seismicity in an Intraplate Setting	Proposes existence of a Quaternary active Saline River fault zone in southern Arkansas based on equivocal observations of deformed Eocene and potentially Pliocene to Pleistocene deposits in natural exposures and shallow trenches.
Daniels et al. (1983)	Distribution of Subsurface Lower Mesozoic Rocks in the Southeastern United States, as Interpreted from Regional Aeromagnetic and Gravity Maps	Discusses extent of Mesozoic rocks in northwestern Gulf of Mexico, in particular, in Florida and Georgia. Presents figures showing extent of Bahamas fracture zone and South Georgia rift.
Dickerson and Muehlberger (1994)	Basins of the Big Bend Segment of the Rio Grande Rift, Trans-Pecos Texas	Discusses southern extent of Rio Grande rift in western Texas and northern Mexico. Presents maps of faults in Big Bend region of Texas and neighboring Mexico.

Table D-7.3.9 Data Summary
Extended Continental Crust Zone—Gulf Coast

Citation	Title	Description and Relevance to SSC
Dunbar and Sawyer (1987)	Implications of Continental Crust Extension for Plate Reconstruction: An Example from the Gulf of Mexico	Presents kinematic model for the opening of Gulf of Mexico.
Ewing and Lopez (1991)	Principal Structural Features of the Gulf of Mexico Basin	Map of geologic and structural features of Gulf of Mexico region.
Gordon et al. (1997)	Cenozoic Tectonic History of the North America-Caribbean Plate Boundary Zone in Western Cuba	Summarizes tectonic history of Cuba.
Gray et al. (2001)	Thermal and Chronological Record of Syn- to Post-Laramide Burial and Exhumation, Sierra Madre Oriental, Mexico	Presents thermo-chronological data constraining development of the Sierra Madre Oriental in western Gulf of Mexico.
Hall et al. (1982)	The Rotational Origin of the Gulf of Mexico Based on Regional Gravity Data	Presents interpretations of regional gravity data to constrain first-order tectonic elements in northern Gulf of Mexico. Provides review of previous interpretations of location and extent of oceanic crust.
Hall and Najmuddin (1994)	Constraints on the Tectonic Development of the Eastern Gulf of Mexico Provided by Magnetic Anomaly Data	Provides constraints on location of ocean-continent crust boundary in northern Gulf of Mexico. Also provides constraints on depth of oceanic crust.
Hatcher et al. (2007)	Tectonic Map of the Southern and Central Appalachians: A Tale of Three Orogens and a Complete Wilson Cycle	Comprehensive review of formation of Appalachians.
Hendricks (1988)	Bouguer Gravity Anomaly of Arkansas	Presents map of Arkansas. Discusses gravity anomalies of Arkansas and evidence of Cretaceous igneous activity.

Table D-7.3.9 Data Summary
Extended Continental Crust Zone—Gulf Coast

Citation	Title	Description and Relevance to SSC
Hildenbrand and Hendricks (1995)	Geophysical Setting of the Reelfoot Rift and Relations Between Rift Structures and the New Madrid Seismic Zone	Discusses geophysical signature of Reelfoot rift. Presents summary of Cretaceous igneous intrusions in southern Arkansas thought to indicate southernmost extent of rift.
Jacques et al. (2004)	Digital Integration of Potential Fields and Geologic Datasets for Plate Tectonic and Basin Dynamic Modeling—The First Step Towards Identifying New Play Concepts in the Gulf of Mexico Basin	Presents plate tectonic reconstructions of Gulf of Mexico showing major tectonic elements. Principal features are the location and extent of oceanic crust, major transform faults within oceanic crust, major NW-trending fracture zones in eastern Gulf of Mexico—related Atlantic rifting, and N- and NW-trending deep structural trends within transitional and thinned continental crust.
Kanter (1994)	Tectonic Interpretation of Stable Continental Crust	Presents locations of continental crust, extended crust, and oceanic crust in Gulf of Mexico region.
Klitgord et al. (1984)	Florida: A Jurassic Transform Plate Boundary	Discusses existence of Bahamas fracture zone that was active in the Jurassic during the opening of Gulf of Mexico. Presents maps of Florida delineating extent of Mesozoic rift basins and pre-Mesozoic crust.
Marton and Buffler (1994)	Jurassic Reconstruction of the Gulf of Mexico Basin	Presents detailed discussion of Gulf of Mexico structure and a model for the opening of Gulf of Mexico. Includes interpretation of extent of oceanic crust in Gulf of Mexico.
McBride and Nelson (1988)	Integration of COCORP Deep Reflection and Magnetic Anomaly Analysis in the Southeastern United States: Implications for Origin of the Brunswick and East Coast Magnetic Anomalies	Suggests three possible sources for the Brunswick magnetic anomaly (BMA): subducted root nappes of the Inner Piedmont, obducted upper mantle, or Mesozoic rifting. Authors do not strongly support a particular solution, but go on to suggest that the BMA and East Coast magnetic anomaly may have a continuous, related source.
McBride et al. (2005)	Integrating Seismic Reflection and Geological Data and Interpretations Across an Internal Basement Massif: The Southern Appalachian Pine Mountain Window, USA	Traces master Appalachian decollement from the Inner Piedmont to Coastal Plain. Authors find that beneath the Carolina terrane, the decollement roots to the Moho, indicating location of Acadian-Alleghanian suture.

Table D-7.3.9 Data Summary
Extended Continental Crust Zone—Gulf Coast

Citation	Title	Description and Relevance to SSC
McHuron and Rice (1974)	Tectonic Evolution of the Gulf Coast: Relation to Nuclear Power Plant Site Selection and Design Criteria	Delineates different crustal types in Gulf of Mexico and describes characteristics such as crustal type, relative stability, and history of stress application represented by tectonic fabrics. Directly addresses application of crustal characterization to seismic hazard and the siting of nuclear power plants in Gulf of Mexico coastal plain region.
Nagihara and Jones (2005)	Geothermal Heat Flow in the Northeast Margin of the Gulf of Mexico	Presents heat flow data for NE Gulf of Mexico and uses the data to revise estimates of location of oceanic crust within Gulf of Mexico.
Pindell and Dewey (1982)	Permo-Triassic Reconstruction of Western Pangea and the Evolution of the Gulf of Mexico/Caribbean Region	Presents a detailed reconstruction of Gulf of Mexico and Caribbean region. Outlines extent of oceanic crust within Gulf of Mexico.
Pindell and Kennan (2001)	Kinematic Evolution of the Gulf of Mexico and Caribbean	Presents plate tectonic reconstructions of Gulf of Mexico and Caribbean region. Helps to constrain location of oceanic crust in Gulf of Mexico.
Pindell et al. (2000)	Putting It All Together Again	Presents interpretations of location and geometry of oceanic crust beneath Gulf of Mexico basin. Northern margin agrees well with Peel (2007).
Russo (2006)	Earthquakes in the Gulf of Mexico	Presents possible mechanism for producing the September 10, 2006, M 5.8 earthquake. Influx of sediment into deep portions of Gulf of Mexico basin loads the underlying Mesozoic oceanic crust, causing flexure and buckling. Reverse earthquakes are produced by bending moment faults caused by buckling.
Salvador (1991)	Origin and Development of the Gulf of Mexico Basin	Presents comprehensive overview of geologic development of Gulf of Mexico. Provides information regarding distribution of crustal types and relationship to overlying growth-fault systems.
Sarwar (2002)	Northern Gulf of Mexico: A Passive or Passive Active Margin?	Presents alternative model for the modern tectonic setting of northern Gulf of Mexico that includes the region in a right-lateral mega-shear extending eastward from the Pacific–North America Plate margin.
Sawyer et al. (1991)	The Crust Under the Gulf of Mexico Basin	Presents interpretations of the deep crustal structure of Gulf of Mexico based on compilation of regional seismic-reflection, seismic-refraction, gravity, magnetic, and subsidence techniques. Presents a map and cross sections constraining the depth to basement and locations of different types of crust.

Table D-7.3.9 Data Summary
Extended Continental Crust Zone—Gulf Coast

Citation	Title	Description and Relevance to SSC
Thomas (1988)	Early Mesozoic Faults of the Northern Gulf Coastal Plain in the Context of Opening of the Atlantic Ocean	Discusses role of Mesozoic faults in the opening of Gulf of Mexico and the coincidence of some of those faults (e.g., Alabama-Arkansas transform) to transform faults associated with the Paleozoic rifting that opened the Iapetus ocean.
Thomas (2006)	Tectonic Inheritance at a Continental Margin	Presents interpretations of NW-trending transform faults in eastern Gulf of Mexico. Provides information on possible crustal source of September 10, 2006, M 5.8 earthquake.
Wheeler and Frankel (2000)	Geology in the 1996 USGS Seismic-Hazard Maps, Central and Eastern United States	Discusses the geologic data used in development of USGS National Seismic Hazard Map source model (e.g., source geometries).
White (1980)	Permian–Triassic Continental Reconstruction of the Gulf of Mexico–Caribbean Area	Presents kinematic model for the opening of Gulf of Mexico.
<i>Growth Faults</i>		
Bradshaw and Watkins (1994)	Growth-Fault Evolution in Offshore Texas	Presents line drawing of seismic data across major growth-fault systems in northern Gulf of Mexico. Presents conceptual model for evolution of the growth-fault systems. Provides important constraints on the depth distribution, kinematic style, and origin. These characteristics contribute to the understanding of seismic potential of growth faults.
Dokka et al. (2006)	Tectonic Control of Subsidence and Southward Displacement of Louisiana with Respect to Stable North America	Description of southern coastal Louisiana as part of a 7–10 km (4.3–6.2 mi.) thick allochthonous region detached from cratonic North America based on GPS data collected between 1995 and 2006. Describes a spatial association of post-1978 earthquakes with the allochthonous region. Concludes that earthquakes result from internal deformation of the allochthon. Cites subsidence rate of ~7 mm/yr relative to mean sea level.
DuBar et al. (1991)	Quaternary Geology of the Gulf of Mexico Coastal Plain	Provides description of Quaternary geology of Gulf of Mexico coastal plain of the U.S. Includes general discussion of fault activity due to movement on growth faults and man-induced seismicity associated with subsurface mineral withdrawal (oil, gas, and water).

Table D-7.3.9 Data Summary
Extended Continental Crust Zone—Gulf Coast

Citation	Title	Description and Relevance to SSC
Gagliano (2005)	Effects of Earthquakes, Fault Movements, and Subsidence on the South Louisiana Landscape	Describes growth faulting on Louisiana coast and its possible relationship to earthquake activity. No firm conclusions regarding source of earthquakes in the region, but suggests that movement on growth faults is the causative mechanism. Does not include a discussion of creep vs. strike-slip behavior, and the implications to earthquake generation potential of growth faults.
Jackson (1982)	Fault Tectonics of the East Texas Basin	Discussion of distribution, geometry, displacement history, and origin of Quaternary faulting in the East Texas basin, and implications to the siting of hypothetical high-level nuclear waste repositories. Concludes that none of the faults pose a seismic threat.
Karlo and Shoup (2000)	Classifications of Syndepositional Systems and Tectonic Provinces of the Northern Gulf of Mexico	Presents detailed overview of growth-fault systems in northern Gulf of Mexico, showing the style and relative ages of deformation. Provides important constraints on geometry and evolution of growth-fault systems.
Morton et al. (2001)	Shallow Stratigraphic Evidence of Subsidence and Faulting Induced by Hydrocarbon Production in Coastal Southeast Texas	Describes effects of growth faulting in coastal Texas and its relationship to hydrocarbon production. Concludes that fault activity is related to hydrocarbon withdrawal.
Peel et al. (1995)	Genetic Structural Provinces and Salt Tectonics of the Cenozoic Offshore U.S. Gulf of Mexico: A Preliminary Analysis	Provides overview of Gulf of Mexico growth-fault domain and provinces. Emphasizes the linked structural system of updip extension and downdip compression, and illustrates the development of the Sigsbee salt nappe.
Rowan et al. (1999)	Salt-Related Fault Families and Fault Welds in the Northern Gulf of Mexico	Presents a classification of different types of salt-related growth faults in northern Gulf of Mexico. Provides information on kinematics and origin of growth faults.
Watkins and Buffler (1996)	Gulf of Mexico Deepwater Frontier Exploration Potential	Describes deepwater environments of entire Gulf of Mexico that may contain significant hydrocarbon reserves. Shows cross section across Florida escarpment in the vicinity of September 10, 2006, M 5.8 earthquake. Provides information on the geologic environment of the earthquake.
Watkins et al. (1996)	Bipolar Simple-Shear Rifting Responsible for Distribution of Mega-salt Basins in Gulf of Mexico?	Describes relationship between basement structure (basins and fracture zones) and the setting of Louann “mother” salt in Gulf of Mexico. Shows a diagram emphasizing importance of NW-trending fracture zones in compartmentalizing salt accumulation and the development of salt basins.

Table D-7.3.9 Data Summary
Extended Continental Crust Zone—Gulf Coast

Citation	Title	Description and Relevance to SSC
Watkins et al. (1996)	Structure and Distribution of Growth Faults in the Northern Gulf of Mexico OCS	Overall description with seismic data examples of growth-fault systems of the Gulf of Mexico and Gulf coastal plain. Provides constraints on the map and cross-sectional geometry and location of growth faults, their depth extent and their relationship to underlying salt.
Wheeler (1999b)	Fault Number 924, Gulf-Margin Normal Faults, Texas, Quaternary Fault and Fold Database of the United States	Provides description of evidence and characteristics of Quaternary faulting in the coastal plain region of Texas, Louisiana, and Alabama. Concludes that fault activity is due to three driving forces: movement over mobile salt and shale, mineral extraction, and flexure of continental margin due to sediment loading in Gulf of Mexico.
Wu et al. (1990)	Allochthonous Salt, Structure and Stratigraphy of the North-Eastern Gulf of Mexico. Part II: Structure	Presents line drawing of seismic data across major growth-fault systems in northern Gulf of Mexico. Presents a conceptual model for evolution of growth-fault systems. Provides important constraints on depth distribution, kinematic style, and origin. These characteristics contribute to the understanding of the seismic potential of growth faults.
Seismic Source Models		
American Petroleum Institute (2000)	Recommended Practice for Planning, Designing and Constructing Fixed Offshore Platforms—Working Stress Design (API RP 2A-WSD)	Provides guidance for seismic engineering design criteria for fixed structures in northern offshore Gulf of Mexico. Places the region in “Zone 0,” reflecting a design acceleration of 0.2 g.
Frankel et al. (2002)	Documentation for the 2002 Update of the National Seismic Hazard Maps	Presents seismic hazard model and seismic source characterization for the U.S. The northern Gulf of Mexico background source is assigned a maximum earthquake magnitude of M 7.5.
Johnston and Nava (1990)	Seismic-Hazard Assessment in the Central United States	Presents a seismic source zonation for Central U.S., including northern Gulf of Mexico coastal region. Characterizes Gulf coastal plain and northern offshore Gulf of Mexico as aseismic.
Johnston et al. (1994)	The Earthquakes of Stable Continental Regions	Presents maps and information constraining ages and types of crustal domains (e.g., extended vs. non-extended continental crust, oceanic vs. continental crust, etc.) in northern Gulf of Mexico and in Gulf coastal plain. These domains and seismotectonic characteristics provide some precedence for characteristics of an updated seismic source model for the region.

Table D-7.3.9 Data Summary
Extended Continental Crust Zone—Gulf Coast

Citation	Title	Description and Relevance to SSC
Petersen et al. (2008)	Documentation for the 2008 Update of the United States National Seismic Hazard Maps	Presents boundary of Mesozoic/Paleozoic crust in southern CEUS.
Potential ALM Source Zone		
Ambraseys (1988)	Engineering Seismology	Presents magnitude-bound relation for liquefaction.
Calais et al. (2006)	Deformation of the North American Plate Interior from a Decade of Continuous GPS Measurements	Uses regionally extensive continuous GPS stations throughout CEUS to determine the deformation field within the CEUS. No anomalies are present within the project study region, but it should be noted that there are very few stations within this region.
Cox (1994)	Analysis of Drainage-Basin Symmetry as a Rapid Technique to Identify Areas of Possible Quaternary Tilt-Block Tectonics: An Example from the Mississippi Embayment	Uses spatial distribution of drainage basin asymmetry to hypothesize existence of active faults and block tilting in Saline, Ouachita, and Arkansas River area.
Cox (2002)	Investigation of Seismically-Induced Liquefaction in the Southern Mississippi Embayment	NEHRP final report presenting results of paleoliquefaction trenching in Ashley and Desha Counties, Arkansas.
Cox (2009)	Investigations of Seismically-Induced Liquefaction in Northeast Louisiana	NEHRP technical report documenting preliminary results for the Louisiana liquefaction fields investigated by Cox. Identifies two sand blows in one field and one sand blow in another. Radiocarbon dating can only loosely constrain minimum ages, essentially providing no constraints on timing of sand blows. Cox notes that some of the blow-like features observed in aerial photos in Louisiana are eolian deposits.
Cox and Gordon (2008)	Sand Blows on Late Quaternary Surfaces in Northeast Louisiana	Abstract presenting preliminary results of paleoliquefaction investigations identifying sand blows in NE Louisiana.
Cox and Larsen (2004)	Investigation of Seismically-Induced Liquefaction in the Southern Mississippi Embayment	NEHRP final report presenting results of paleoliquefaction trenching in Ashley and Desha Counties, Arkansas.

Table D-7.3.9 Data Summary
Extended Continental Crust Zone—Gulf Coast

Citation	Title	Description and Relevance to SSC
Cox and Van Arsdale (1997)	Hotspot Origin of the Mississippi Embayment and Its Possible Impact on Contemporary Seismicity	Hypothesizes role of the Bermuda hotspot in the formation of Mississippi embayment and suggests that the hotspot may have significantly weakened the lithosphere. Also notes correlation between hotspot tracks and the Charleston, South Carolina and the St. Lawrence rift system, regions of moderate to large earthquakes.
Cox et al. (2000)	Quaternary Faulting in the Southern Mississippi Embayment and Implications for Tectonics and Seismicity in an Intraplate Setting	Hypothesizes existence of a Quaternary-active Saline River fault zone based on a concentration of historical seismicity and the apparent deformation of Pliocene-Pleistocene deposits in road cuts.
Cox, Forman, et al. (2002)	New Data of Holocene Tectonism in the Southern Mississippi Embayment	Abstract presenting preliminary results of paleoliquefaction trenching in Ashley County, Arkansas.
Cox, Harris, et al. (2004)	More Evidence for Young Tectonism Along the Saline River Fault Zone, Southern Mississippi Embayment	Abstract presenting preliminary results and interpretation of S-wave reflection profiles of Saline River fault zone and the relation of these structures to preliminary sand-blow dates.
Cox, Larsen, and Hill (2004)	More Paleoliquefaction Data from Southeastern Arkansas: Implications for Seismic Hazards	Abstract presenting preliminary results of paleoliquefaction trenching in Ashley and Desha Counties, Arkansas.
Cox, Larsen, Forman, et al. (2004)	Preliminary Assessment of Sand Blows in the Southern Mississippi Embayment	Presents compilation of all paleoliquefaction trenching and dating done through 2004 within the Saline River area. Hypothesizes a correlation between source of liquefaction and Cox's proposed Quaternary deformation features within Saline River area.
Cox et al. (2007)	Seismotectonic Implications of Sand Blows in the Southern Mississippi Embayment	Presents compilation of paleoliquefaction trenching and dating done from 2004 through 2007 within Saline River area. Also presents results of geotechnical studies of sand-blow host deposits and the implications for that data with respect to the amount of ground shaking required to cause liquefaction. Hypothesizes a correlation between source of liquefaction and Cox's proposed Quaternary deformation features within Saline River area.
Cushing et al. (1964)	General Geology of the Mississippi Embayment	Provides general discussion of geology and structure of Mississippi embayment.

Table D-7.3.9 Data Summary
Extended Continental Crust Zone—Gulf Coast

Citation	Title	Description and Relevance to SSC
Ewing (1991)	Structural Framework	Provides general discussion of tectonic and geologic structures of Gulf of Mexico region.
Garrote et al. (2006)	Tectonic Geomorphology of the Southeastern Mississippi Embayment in Northern Mississippi, USA	Uses the spatial distribution of drainage basin asymmetry to hypothesize the existence of active faults.
Gordon and Cox (2008)	Recurrent Mesozoic and Cenozoic Faulting along the Southern Margin of the North American Craton	Abstract hypothesizing that the Alabama-Oklahoma transform and related structures may be the tectonic feature that is source of strong ground shaking that caused the Arkansas liquefaction features and the deformed Saline River fault zone deposits.
Green et al. (2005)	Engineering Geologic and Geotechnical Analysis of Paleoseismic Shaking Using Liquefaction Effects: Field Examples	Presents examples of how to back-calculate ground motions (e.g., earthquake magnitudes) from paleoliquefaction data.
Harry and Londono (2004)	Structure and Evolution of the Central Gulf of Mexico Continental Margin and Coastal Plain, Southeast United States	Identifies location of the potential Precambrian, passive-margin, transform plate boundary that trends from Alabama to Oklahoma. Uses gravity modeling, industry seismic data, and well data to construct transects across the transform.
Hosman (1996)	Regional Stratigraphy and Subsurface Geology of Cenozoic Deposits, Gulf Coastal Plain, South-Central United States	Provides general discussion of structure and geology of Gulf coastal plain and Mississippi embayment from the perspective of an aquifer analysis.
Liang and Langston (2009)	Three-Dimensional Crustal Structure of Eastern North America Extracted from Ambient Noise	Maps three-dimensional shear-wave velocity throughout CEUS and discusses presence of rifting episodes apparent in the data.
Mickus and Keller (1992)	Lithospheric Structure of the South-Central United States	Constructs a N-S cross section from Gulf of Mexico to Missouri along the Texas-Louisiana border using primarily gravity data but qualitatively including seismic-reflection, well log, and geologic data.

Table D-7.3.9 Data Summary
Extended Continental Crust Zone—Gulf Coast

Citation	Title	Description and Relevance to SSC
Murray (1961)	Geology of the Atlantic and Gulf Coastal Province of North America	Provides general discussion of structure and geology of Gulf of Mexico region.
Obermeier and Pond (1999)	Issues in Using Liquefaction Features for Paleoseismic Analysis	Summary paper describes concerns about the use of paleoliquefaction data as evidence of strong ground shaking.
Olson et al. (2005a)	Geotechnical Analysis of Paleoseismic Shaking Using Liquefaction Features: A Major Updating	Presents methodology for how to back-calculate ground motions (e.g., earthquake magnitudes) from paleoliquefaction data.
Olson et al. (2005b)	Revised Magnitude Bound Relation for the Wabash Valley Seismic Zone of the Central United States	Presents an updated magnitude-bound relationship for paleoliquefaction in CEUS.
Salvador (1991)	Origin and Development of the Gulf of Mexico Basin	Provides general discussion of the structure of Gulf of Mexico region, as well as the tectonic history of the Gulf. Identifies location of Alabama-Oklahoma transform.
Saucier and Smith (1986)	Geomorphic Mapping and Landscape Classification of the Ouachita and Saline River Valleys, Arkansas	Presents detailed mapping of terraces within the Ouachita and Saline River valleys. Dating and terrace classification presented in this report was used by others (e.g., Cox, 1994) to correlate terraces in the basins.
Al-Shukri et al. (2005)	Spatial and Temporal Characteristics of Paleoseismic Features in the Southern Terminus of the New Madrid Seismic Zone in Eastern Arkansas	Presents preliminary results of investigation of liquefaction features further discussed by Tuttle et al. (2006).
Tuttle (2001)	The Use of Liquefaction Features in Paleoseismology: Lessons Learned in the New Madrid Seismic Zone, Central United States	Summary paper describing use of paleoliquefaction data within New Madrid seismic zone to constrain paleo-earthquakes within the zone.

Table D-7.3.9 Data Summary
Extended Continental Crust Zone—Gulf Coast

Citation	Title	Description and Relevance to SSC
Tuttle, Schweig, et al. (2002)	The Earthquake Potential of the New Madrid Seismic Zone	Presents summary of paleoseismic history of New Madrid seismic zone and the areas of liquefaction associated with New Madrid earthquakes.
Tuttle et al. (2006)	Very Large Earthquakes Centered Southwest of the New Madrid Seismic Zone 5,000–7,000 Years Ago	Presents results of paleoliquefaction trenching and dating in central-eastern Arkansas. Identifies at least two different sets of sand blows at ~5,500 and 6,800 yr BP.
Wheeler (2005)	Known or Suggested Quaternary Tectonic Faulting, Central and Eastern United States—New and Updated Assessments for 2005	Presents summary discussion of the Arkansas paleoliquefaction features discovered by Cox, and Cox's hypothesized Saline River fault zone.
Zhang et al. (2009b)	Tomographic Pn Velocity and Anisotropy Structure in the Central and Eastern United States	Maps Pn (upper mantle) velocity structure throughout CEUS and hypothesizes at a potential correlation between edges of high-velocity zones and the locations of intraplate seismic zones.

Table D-7.3.12 Data Summary
MidContinent-Craton Zone

Citation	Title	Description and Relevance to SSC
General for Region		
Atekwana (1996)	Precambrian Basement Beneath the Central Midcontinent United States as Interpreted from Potential Field Data	References previous geologic and geophysical investigations (Hinze et al., 1975; Klasner et al., 1982; Bickford et al., 1986; Van Schmus, 1992) that reveal that Precambrian basement within the Midcontinent region consists of several provinces that formed before 900 million years ago (Ma), including the Superior province (2.7 billion years ago [Ga]); Penokean province (1.83–1.88 Ga); Central Plains province (1.63–1.7 Ga); Eastern Granite-Rhyolite province (1.42–1.5 Ga); Midcontinent rift system (1.1–1.0 Ga); and Grenville province (0.8–1.1 Ga).
Li et al. (2009)	Spatiotemporal Complexity of Continental Intraplate Seismicity: Insights from Geodynamic Modeling and Implications for Seismic Hazard Estimation	<p>This paper explores the complex spatiotemporal patterns of intraplate seismicity using a 3-D viscoelasto-plastic finite-element model. The model simulates tectonic loading, crustal failure in earthquakes, and coseismic and postseismic stress evolution. For a laterally homogeneous lithosphere with randomly prespecified perturbations of crustal strength, the model predicts various spatiotemporal patterns of seismicity at different time scales: spatial clustering in narrow belts and scattering across large regions over hundreds of years, connected seismic belts over thousands of years, and widely scattered seismicity over tens of thousands of years.</p> <p>The orientation of seismic belts coincides with the optimal failure directions associated with the assumed tectonic loading. Stress triggering and migration cause spatiotemporal clustering of earthquakes. Fault weakening can lead to repeated earthquakes on intraplate faults. The predicted patterns vary with the weakening history. Clusters of large intraplate earthquakes can result from fault weakening and healing, and the clusters can be separated by long periods of quiescence. The complex spatiotemporal patterns of intraplate seismicity predicted in this simple model suggest that assessment of earthquake hazard based on the limited historical record may be biased toward overestimating the hazard in regions of recent large earthquakes and underestimating the hazard where seismicity has been low during the historical record.</p>

Table D-7.3.12 Data Summary
MidContinent-Craton Zone

Citation	Title	Description and Relevance to SSC
Liang and Langstrom (2009)	Three-Dimensional Crustal Structure of Eastern North America Extracted from Ambient Noise	<p>Group velocity dispersion curves of surface waves extracted from ambient seismic noise are inverted to find 3-D shear-wave structure of the crust beneath eastern North America. The 3-D model consists of one sediment layer and another six layers with fixed depths of 5, 7.5, 10, 15, 25, and 43 km (3, 4.7, 6.2, 9.3, 15.5, and 26.7 mi.). Almost all failed ancient rifting earthquakes (e.g., the Reelfoot rift, Ouachita triple junction, and Midcontinent rift) and rifting-related earthquakes (e.g., the Ozark uplift and Nashville dome) are associated with high-velocity bodies in the middle and lower crust.</p> <p>Results suggest the existence of a triple-junction-like high-velocity body centered around the New Madrid and Wabash Valley seismic zones (NMSZ and WVSZ), with the Reelfoot rift, the Ozark uplift, and the Nashville dome being on its SW, NW, and SE arms, respectively. The Appalachian Mountains are characterized by high-velocity upper crust underlain with relatively low-velocity middle and lower crust. All major seismic zones are associated with either divergent or convergent events. The NMSZ and WVSZ are clearly associated with the failed Reelfoot rift. Both the eastern Tennessee seismic zone and the Ouachita orogen are located along convergent boundaries.</p>
Marshak and Paulsen (1997)	Structural Style, Regional Distribution, and Seismic Implications of Midcontinent Fault-and-Fold Zones, United States	<p>Paleozoic/Mesozoic strata of the U.S. continental interior contain arrays of steeply dipping faults and associated monoclinally forced folds. This paper hypothesizes that these structures were initiated during episodes of Proterozoic extensional tectonism. Two sets identified: one trending N-NE and the other trending W-NW. These sets break upper crust into blocks that cause slight movements in response to changes in stress state. Many W-NW-trending fault and fold zones link along strike to define semicontinuous NW-trending deformation corridors. One of these, the 200 km (124 mi.) wide Transamerican tectonic zone, traces over 2,500 km (1,553 mi.) from Idaho to South Carolina. Seismicity most frequently occurs where N-NE-trending fault and fold zones cross the Transamerican tectonic zone, suggesting that intracratonic strain in the U.S. currently concentrates at or near intersecting fault zones within this corridor.</p>

Table D-7.3.12 Data Summary
MidContinent-Craton Zone

Citation	Title	Description and Relevance to SSC
NICE Working Group (2007)	Reinterpretation of Paleoproterozoic Accretionary Boundaries of the North-Central United States Based on a New Aeromagnetic-Geologic Compilation	Presents a new tectonic province map, based on interpretation of a new aeromagnetic compilation, published geologic maps, and geochronologic data. The map shows a progressive accretion of juvenile arc terranes from ca. 1,900–1,600 Ma. The Spirit Lake tectonic zone, characterized by a sharp magnetic discontinuity that marks the southern limit of Archean and Penokean-interval rocks, is interpreted to represent an eastern analog of the Cheyenne belt suture zone in southern Wyoming. The data reveal a progressive tectonic younging to the south as the Laurentian craton grew southward and stabilized during the Proterozoic. Late Mesoproterozoic rift magmatism produced pronounced geophysical anomalies, indicating strong but localized crustal modification. Little tectonism has occurred here in the last billion years, providing a preserved record of the Precambrian evolution of the continental U.S. lithosphere.
Sims et al. (2005)	Preliminary Precambrian Basement Structure Map of the Continental United States—An Interpretation of Geologic and Aeromagnetic Data	<p>The systematics of major regional post-assembly Precambrian basement structures throughout the continental U.S. point to a common causal mechanism for their development. The model presented accords with geodynamic models for North and South American Plate motions, based on seismic anisotropy beneath the continents that invoke mechanical coupling and subsequent shear between the lithosphere and asthenosphere such that a major driving force for plate movement is deep-mantle flow.</p> <p>Two orthogonal sets of shear zones and faults are predominant in the continent: (1) NE-striking, partitioned ductile shear zones, and (2) NW-trending strike-slip ductile-brittle faults. The NE-striking shear zones are interpreted as resulting from NW-SE shortening, apparently formed during the interval 1.76–1.70 Ga. The NW-trending (1.7–1.5 Ga) transcurrent fault system consists of W-NW to NW synthetic faults and northerly trending antithetic transfer faults; it is attributed to transpressional-transensional deformation, i.e., strike-slip deformation that deviates from simple shear because of a component of shortening or extension orthogonal to the deformation zone. The NE- and NW-oriented shears and faults mimic orthogonal teleseismic images of the upper mantle. These structures were reactivated during the Mesoproterozoic and later times.</p> <p>The kinematics of regional basement structures within the continental U.S. suggest that deformation since at least early Proterozoic time has been predominantly transpressional. Transcurrent lithospheric structures formed</p>

Table D-7.3.12 Data Summary
MidContinent-Craton Zone

Citation	Title	Description and Relevance to SSC
		<p>during Proterozoic mantle deformation are oriented obliquely to the SW (absolute) motion of the North American Plate. Stress caused by traction between the asthenosphere and lithosphere during the SW drift focused on preexisting block boundaries repeatedly have reactivated basement zones of weakness, thus localizing sedimentation, magmatism, and generation of ore deposits.</p>
Whitmeyer and Karlstrom (2007)	Tectonic Model for the Proterozoic Growth of North America	<p>Presents a plate-scale model for the Precambrian growth and evolution of the North American continent. The core of the North American continent (Canadian shield) came together in the Paleoproterozoic (2.0–1.8 Ga) by plate collisions. The thick, buoyant, and compositionally depleted mantle lithosphere that now underlies North America, although dominantly of Archean age, took its present shape by processes of collisional orogenesis and likely has a scale of mantle heterogeneity similar to that exhibited in the overlying crust.</p> <p>In marked contrast, lithosphere of southern North America (much of the continental U.S.) was built by progressive addition of a series of dominantly juvenile volcanic arcs and oceanic terranes accreted along a long-lived southern (present coordinates) plate margin. The lithospheric collage that formed from dominantly juvenile terrane accretion and stabilization (1.8–1.0 Ga) makes up about half of the present-day North American continent. Throughout (and as a result of) this long-lived convergent cycle, mantle lithosphere below the accretionary provinces was more hydrous, fertile, and relatively weak compared to mantle lithosphere under the Archean core.</p>
Zhang et al. (2009b)	Tomographic Pn Velocity and Anisotropy Structure in the Central and Eastern United States	<p>Inversion of tomographic data to map the velocity and anisotropy structure of the lithospheric mantle in the CEUS. The Pn tomographic model shows a broad region of very fast velocity under the North American craton (northern CEUS) and significant lateral variation within the rest of the CEUS. The surface locations of the major intraplate seismic zones are near the edges of high-velocity anomalies, which is consistent with the notion that stress accumulation—and hence focused deformation—is likely to occur at the rheological boundaries around the rigid lithospheric root. Ancient rifts show no clear correlation to the low-velocity anomalies in the lithospheric mantle.</p>

Table D-7.3.12 Data Summary
MidContinent-Craton Zone

Citation	Title	Description and Relevance to SSC
<i>Geophysical Anomalies</i>		
Commerce Geophysical Lineament (CGL)		
Hildenbrand and Hendricks (1995)	Geophysical Setting of the Reelfoot Rift and Relations Between Rift Structures and the New Madrid Seismic Zone	The Commerce geophysical lineament (CGL) is a NE-trending feature that extends from NE Arkansas to at least Vincennes, Indiana. This lineament comprises a series of linear, NE-trending magnetic and gravity anomalies traceable for more than 384 km (239 mi.). This feature has been interpreted to consist of en echelon faults and igneous intrusions in the basement that are related to the Neoproterozoic to early Paleozoic Reelfoot rift; however, it is postulated to have an even older ancestry.
Langenheim and Hildenbrand (1997)	Commerce Geophysical Lineament—Its Source, Geometry, and Relation to the Reelfoot Rift and New Madrid Seismic Zone	
Hildenbrand et al. (2002)	The Commerce Geophysical Lineament and Its Possible Relation to Mesoproterozoic Igneous Complexes and Large Earthquakes in the Central Illinois Basin	<p>New inversions of existing magnetic and gravity data provide information on upper-crustal structures in the central Illinois basin. Results of 2-D and 3-D inversion techniques suggest that the source of the CGL follows the SE boundary of a dense and magnetic NE-trending igneous center named the Vincennes igneous center. The buried Vincennes igneous center is suggested to be the source of inferred volcanic units of the Centralia sequence and is related to a rifted margin or a Proterozoic plate boundary.</p> <p>Comparing gravity and magnetic fields of the Vincennes igneous center with those of the St. Francois Mountains igneous center in SE Missouri suggests that the associated sources in each region are similar in composition and perhaps origin. The CGL that is defined in this region by a 5–10 km (3–6 mi.) wide deformation zone appears to have influenced the structural development of the Vincennes igneous center. The Commerce deformation zone evolved in the Mesoproterozoic (1.1–1.5 Ga) as a major cratonic rheological boundary and has been the focus of episodic reactivation related to varying stress regimes throughout its history.</p>

Table D-7.3.12 Data Summary
MidContinent-Craton Zone

Citation	Title	Description and Relevance to SSC
South-Central Magnetic Lineament (SCML)		
Hildenbrand et al. (1983)	Digital Magnetic-Anomaly Map of Central United States: Description of Major Features	Describes a regional W-NW-trending lineament characterized by a band of steep magnetic gradients that coincides with a prominent Bouguer anomaly and the general position of the Cottage Grove fault system, Ste. Genevieve fault zone, and Hicks dome.
Kolata and Hildenbrand (1997)	Structural Underpinnings and Neotectonics of the Southern Illinois Basin: An Overview	Seismic-reflection profiles show that a layered Precambrian sequence in the upper crust in the southern Illinois basin terminates abruptly at this boundary.
St. Charles Lineament (SCL)		
Harrison and Schultz (2002)	Tectonic Framework of the Southwestern Margin of the Illinois Basin and Its Influence on Neotectonism and Seismicity	<p>The St. Charles lineament (SCL) is the informal name given to an alignment of geochemical and geophysical features that extends from SW Ontario to SE Oklahoma. A paleotectonic history of the SCL is difficult to decipher because many structural features related to the lineament lie beneath the alluvial plain of the Missouri River. There is no apparent stratigraphic offset of Paleozoic strata across the SCL, but a zone of conjugate strike-slip faults of probable late Mississippian to early Pennsylvanian age is exposed along the SCL near Acton, Illinois. These faults do not displace overlying Pleistocene loess.</p> <p>Harrison and Schultz postulate two lines of weak and nondefinitive evidence for neotectonic activity along the SCL: (1) the Missouri River bends to a NE course upon encountering the SCL, suggesting a tectonic control on the river, which alternatively could reflect the influence of an older deformational fabric; and (2) the postdepositional tilting of Miocene (?) Grover Gravel may be due to faulting along the SCL.</p>
Hildenbrand and Kucks (1992)	Filtered Magnetic Anomaly Maps of Missouri	This lineament is defined by a regional neodymium (Nd) isotopic boundary that coincides with linear geophysical trends along most of its length.
Hildenbrand and Hendricks (1995)	Geophysical Setting of the Reelfoot Rift and Relations Between Rift Structures and the New Madrid Seismic Zone	

Table D-7.3.12 Data Summary
MidContinent-Craton Zone

Citation	Title	Description and Relevance to SSC
Mateker et al. (1966)	Geophysical Evidence for a Northeast Crustal Lineament near St. Louis	Notes that the SCL is parallel to the Reelfoot rift and the New Madrid seismic zone as well as to a trend of minor earthquake activity in the St. Louis–St. Charles area.
Sims (1990) Sims and Peterman (1986)	Precambrian Basement Map of the Northern Midcontinent, U.S.A. Early Proterozoic Central Plains Orogen: A Major Buried Structure in the North-Central United States	These publications map the boundary between Paleoproterozoic metamorphic/granitoid rocks and Mesoproterozoic rhyolitic/granitoid rocks along the SCL, which they interpret as the margin of a Paleoproterozoic Central Plains orogen.
Sims et al. (1987)	Geology and Metallogeny of Archean and Proterozoic Basement Terranes in the Northern Midcontinent, U.S.A.—An Overview	Suggests that the margin coincident with the SCL is an ancient suture zone.
Van Schmus et al. (1996)	Proterozoic Geology of the East-Central Midcontinent Basement	Interprets the Nd isotopic boundary as a Paleoproterozoic crustal margin that separates late Paleoproterozoic lower-crustal rocks to the NW from early Mesoproterozoic lower-crustal rocks to the SE.
Seismicity <i>(Note: The Anna, Ohio, and Northeast Ohio seismicity zones are both discussed in the section on Paleoliquefaction Studies.)</i>		
Bakun and Hopper (2004a)	Catalog of Significant Historical Earthquakes in the Central United States	Modified Mercalli intensity assignments are used to estimate source locations and moment magnitude, M , for 18 nineteenth-century and 20 early twentieth-century earthquakes in the central U.S. for which estimates of M are otherwise not available. Four $M > 5.0$ central U.S. historical earthquakes have occurred: in Kansas in 1867, Nebraska in 1877, Oklahoma in 1882, and Kentucky in 1980.
Hinze and Hildenbrand (1988)	The Utility of Geopotential Field Data in Seismotectonic Studies in the Eastern United States	The Sharpsburg earthquake of July 27, 1980 ($m_b = 5.1$) originated at a depth of 15 km (9.3 mi.), in the vicinity of a prominent gravity gradient and complex magnetic anomalies caused by mafic Grenvillian (Precambrian) basement rocks, suggesting that this moderate-sized earthquake originated in the reactivation of a Precambrian zone of weakness.

Table D-7.3.12 Data Summary
MidContinent-Craton Zone

Citation	Title	Description and Relevance to SSC
Joeckel et al. (2003)	Earthquake History, Seismicity, and Related Tectonics in Nebraska	Nebraska experienced two significant earthquakes in 2002: a June 20, M 3.5 earthquake and a November 3, M 4.3 earthquake. About 50 earlier earthquakes, almost all M < 4, have occurred in Nebraska since 1867. A cluster of microearthquakes reported in 1979 in Red Willow County in SW Nebraska may have been related to petroleum production. Other earthquakes occurred at about the same time in SE Nebraska along the Nemaha uplift, a major N-S structure extending into basement rocks. Larger earthquakes seem to be related to the periodic release of accumulated regional stresses in major structures (Nemaha uplift, Midcontinent rift) and around proposed sutures resulting from the Proterozoic (1.8–1.6 Ga) accretion of island arcs across the region.
Structures		
Anton Escarpment, Colorado		
Wheeler (2005)	Known or Suggested Quaternary Tectonic Faulting, Central and Eastern United States—New and Updated Assessments for 2005	Classifies the Anton escarpment as a Class C feature. The NE-facing topographic escarpment is 20–30 m high. A trench excavated across the escarpment in 2004 did not expose any faults associated with the topographic feature; no significant vertical offset exists across the escarpment, as indicated by stratigraphy correlated between the trench and nearby boreholes. If the feature is a fault-line scarp, displacement has not occurred for a long time. The lack of a demonstrated fault-related origin for the escarpment justifies the Class C classification.
Brockton-Froid Fault Zone, Montana		
Crone and Wheeler (2000)	Data for Quaternary Faults, Liquefaction Features, and Possible Tectonic Features in the Central and Eastern United States, East of the Rocky Mountain Front	Classifies the Brockton-Froid fault zone as Class B.

Table D-7.3.12 Data Summary
MidContinent-Craton Zone

Citation	Title	Description and Relevance to SSC
Wheeler (1999a)	Fault Number 707, Brockton-Froid Fault Zone, Quaternary Fault and Fold Database of the United States	Classified as a Class B fault, this feature is located in the glaciated plains of NE Montana. The fault zone contains Quaternary deformation; the deformation may not have occurred by faulting, but it also may indicate a basement fault that was reactivated during glacial or postglacial time. The linear fault zone is about 54 km (33.5 mi.) long and does not have an obvious fluvial, glacial, or glaciotectionic origin. The origin of the feature is enigmatic.
Wheeler and Crone (2001)	Known and Suggested Quaternary Faulting in the Midcontinent United States	The Brockton-Froid fault needs further study to determine whether it is a Quaternary tectonic fault. Late Wisconsinan outwash and Quaternary sheetwash alluvium and colluvium occupy a straight zone a few hundred meters wide and at least 53 km (33 mi.) long along the trace of the inferred fault zone. The narrow zone is bounded by till on both sides. Data from lines of auger holes show that the Quaternary deposits inside the zone are thicker than the adjacent deposits. The 1:24,000-scale topographic maps along the zone show its geomorphic expression as alignments of straight stream segments and valleys, elongated hills and ridges, and large, closed depressions; the zone descends to cross streams and rises to cross interfluvies without obvious deflection. The authors reference Colton (1963a, 1963b), who interpreted the zone as a fault-bounded feature—yet nowhere are faults exposed that juxtapose outwash and till. Structure-contour and isopach maps of Paleocene lignites at depths of 240 m and less do not show detectable offset across the zone (Hardie and Arndt, 1988; Biewick et al., 1990). If the straight zone is bounded by faults, it is unclear whether the faults penetrate deeply enough into bedrock to pose a seismic threat.
Wong et al. (2005)	Probabilistic Earthquake Hazard Maps for the State of Montana	The Brockton-Froid fault zone was characterized as a possible fault source (probability of activity of 0.5) in a statewide seismic hazard study conducted for the State of Montana. The map data and length were from M. Stickney of the Montana Bureau of Mines and Geology (digital shape-files, May 1, 2002, to S. Olig, URS) after recent mapping by Bergantino and Wilde (1998a, 1998b), which includes a possible NE extension near Medicine Lake. Subsurface data is ambiguous with regard to the depth extent of this enigmatic structure and its sense of slip (Crone and Wheeler, 2000). Additionally, slip may have been related to postglacial relaxation and, if so, it may no longer be as active; thus the authors assigned a lower probability of activity. Slip rates are based on one or two possible post-late Wisconsinan (<40 ka) earthquakes (Crone and Wheeler, 2000).

Table D-7.3.12 Data Summary
MidContinent-Craton Zone

Citation	Title	Description and Relevance to SSC
Cape Girardeau Fault System, Missouri		
Harrison and Schultz (2002)	Tectonic Framework of the Southwestern Margin of the Illinois Basin and Its Influence on Neotectonism and Seismicity	<p>The Cape Girardeau fault system, which is a continuation of the Simms Mountain fault system, consists of numerous branching and anastomosing, dominantly NW-striking, near-vertical faults. Although NE- and N-NW-striking faults are less common, they appear to show evidence for the most recent deformation. There are rhomb-shaped pull-apart graben related to strike-slip faulting that can be divided into three groups: (1) those that contain only Paleozoic rocks, (2) those that contain upper Cretaceous and lower Tertiary formations, and (3) those that contain Quaternary strata.</p> <p>Unequivocal evidence of faulting of Quaternary gravel has been observed in a quarry and roadcut at the SE end of the fault system near its intersection with the Commerce geophysical lineament. Results of recent trenching show evidence of Quaternary faulting, possibly post-Sangamon in age. Unfaulted Peoria Loess (late Wisconsinan in age) and possibly Roxana Silt overlie the fault and graben fill. The authors interpret the Quaternary deformation to have formed under E-NE horizontal maximum principal stress. They favor erosion and fill as an alternative to the finding by Tuttle, Chester, et al. (1999) of a source of possible faulting in Quaternary gravel discovered on part of the Cape Girardeau fault system approximately 14.5 km (9 mi.) to the NW.</p>
Wheeler (2005)	Known or Suggested Quaternary Tectonic Faulting, Central and Eastern United States—New and Updated Assessments for 2005	<p>Classifies the Slinkard quarry graben in Missouri as a Class A feature, noting that faults that bound the graben or are near it have undergone multiple periods of movement, including pre-Cenozoic, Paleocene, and at least two periods in the Quaternary, with the youngest being post-Sangamon Geosol (< 130 ka) and pre-Wisconsinan loess. The NW margin of the graben juxtaposes Quaternary gravel against late Tertiary Mounds Gravel. The fault on the NW margin strikes N35°–40°E and dips approximately 74°SE. Mounds Gravel in the footwall has been rotated to dip 54°–85°E, with strike parallel to the fault. The faults are assigned to a slip-rate category of less than 0.2 mm/yr. The sense of movement is normal dextral; the graben is interpreted to be a pull-apart graben in a dextral strike-slip system. The length of the Slinkard quarry graben is unknown, but the NW margin fault is at least 180 m long.</p>

Table D-7.3.12 Data Summary
MidContinent-Craton Zone

Citation	Title	Description and Relevance to SSC
Criner Fault, Oklahoma		
Hanson et al. (1997)	Quaternary Deformation Along the Criner Fault, Oklahoma: A Case Study for Evaluating Tectonic Versus Landslide Faulting	This study summarizes field investigations at a locality (a natural stream exposure) along the Criner fault where deformation of late Pleistocene alluvium had been suggested as evidence for Quaternary faulting on the Criner fault, which is part of the 310 km (193 mi.) long Meers-Duncan-Criner fault system. Excavation and detailed mapping of the exposure, in which a steep shear zone juxtaposes Quaternary alluvium against bedrock, provided evidence to indicate that the deformation was due to landsliding.
Wheeler and Crone (2001)	Known and Suggested Quaternary Faulting in the Midcontinent United States	Summarizes studies that evaluated possible evidence for Quaternary deformation on the Criner fault. A topographic and vegetation lineament, a linear hill, and scarps 0.3–1.0 m high along the hill front and across gullies suggested possible Quaternary movement. This study cites the results of Hanson et al. (1997) that the preferred interpretation of the only locality where Quaternary deformation was clearly documented is that the faulting is due to landsliding rather than tectonic faulting.
Crooked Creek Fault		
Crone (1998b)	Fault Number 1032, Crooked Creek Fault, in Quaternary Fault and Fold Database of the United States	<p>Classified in the USGS Quaternary Fault and Fold Database as a Class B feature because of the uncertainty concerning the cause of subsurface deformation. Deformation may be solely the result of dissolution of soluble subsurface strata or deep-seated tectonic movements. The postulated fault is defined largely on the basis of drillhole data and anomalous geomorphic features above the subsurface structure. No exposures of the fault are known. Deformation associated with the feature has resulted in a structural depression in the subsurface and an elongate topographic trough.</p> <p>Due to the absence of any clear surface expression, the postulated structure is poorly located and defined; the length is unknown. The sense of movement and dip are not well known; data suggest significant vertical movement, but no information exists to determine if the offset would be reverse or normal.</p> <p>Pleistocene and Holocene (sinkholes) deformation is associated with the postulated structure. Due to uncertainty related to the origin of this postulated structure, it is not possible to assign a time of the most recent paleo-earthquake or recurrence interval.</p>

Table D-7.3.12 Data Summary
MidContinent-Craton Zone

Citation	Title	Description and Relevance to SSC
East Continent Rift Basin (ECRB)		
Drahovzal et al. (1992)	The East Continent Rift Basin: A New Discovery	Integration of lithologic, stratigraphic, geochemical, gravity, magnetic, structural, and seismic data resulted in recognition of an eastern arm of the Midcontinent rift system named the East Continent rift basin (ECRB). An elongate N-S-trending Precambrian rift basin is present from SE Michigan through Ohio and Indiana, into central Kentucky. The ECRB is filled with red continental lithic arenites, minor red siltstones and shales, and volcanics. Gravity, magnetic, and seismic data indicate that the basin is composed of several subbasins. The basin is bounded by the Grenville Front to the east and by normal block faults to the west. The basin narrows to the north; the southern boundary is not well constrained. The basin is interpreted to be Keweenawan in age and associated with the middle Proterozoic Midcontinent rift system. The ECRB predates the Grenville orogeny, which resulted in folding and faulting of the rift-fill sequence. Post-Grenville erosion, Paleozoic inversion, and wrench faulting resulted in the present configuration of the basin.
Farmington Anticline, Missouri		
Harrison and Schultz (2002)	Tectonic Framework of the Southwestern Margin of the Illinois Basin and Its Influence on Neotectonism and Seismicity	The Farmington anticline–Avon block is a broad (as much as 19.3 km, or 12 mi., wide) NW-trending low-relief structural feature that lies between the Ste. Genevieve and Simms Mountain faults. Weak to moderate seismicity is clustered around this structure, which has been interpreted to occur above buried faults cutting middle Proterozoic basement rock. A zone of NW-trending horsts and graben with subsidiary and contemporaneous NE-striking oblique-slip faults coincides with the axis of the fold.
Goodpasture Fault, Colorado		
Widmann (1997c)	Complete Report for Goodpasture Fault (Class A) No. 2329	The Goodpasture fault forms a fairly prominent escarpment and vegetation lineation that trends NW to the east of Hogback Mountain in the Wet Mountains in Colorado. The most recent fault displacement may have occurred in the early to middle Quaternary. Geomorphic features on Quaternary deposits indicative of youthful faulting have not been observed in aerial reconnaissance. The fault is 5 km (3 mi.) long.

Table D-7.3.12 Data Summary
MidContinent-Craton Zone

Citation	Title	Description and Relevance to SSC
Great Lakes Tectonic Zone (GLTZ), Minnesota		
Atekwana (1996)	Precambrian Basement Beneath the Central Midcontinent United States as Interpreted from Potential Field Data	Major E-NE Archean crustal boundary, which is observed on gravity and magnetic anomaly maps, separates greenstone-granite terranes (~2,700 Ma) on the north from gneiss terrane (3,600 Ma) on the south. The feature is a locus of repeated reactivation.
Sims et al. (1980)	The Great Lakes Tectonic Zone—A Major Crustal Structure in Central North America	<p>The Great Lakes tectonic zone is a major Precambrian crustal feature more than 1,200 km (746 mi.) long extending eastward from Minnesota into Ontario, Canada. It is a zone of distinctive tectonism, affecting both Archean and early Proterozoic rocks along the northern margin of the early Proterozoic Penokean fold belt adjacent to the Archean Superior province. The zone coincides with the boundary between two Archean crustal segments recognized in the region: a greenstone-granite terrane (~2,700 Ma) to the north (Superior province) and an older (in part 3,500 Ma) gneiss terrane to the south. Tectonism along the zone began in the late Archean, during the joining together of the two terranes into a single continental mass, and culminated in the early Proterozoic, when steep or northward-facing overturned folds were formed in the supracrustal rocks, and intense cataclasis and a penetrative cleavage developed in subjacent basement rocks of the greenstone-granite terrane. The Proterozoic deformation took place under low to intermediate pressures.</p> <p>In the early Proterozoic, crustal foundering, which was parallel to the zone and was diachronous, initiated the structural basins in which the early Proterozoic sequences of the Lake Superior and Lake Huron regions were deposited. Later, during the Penokean orogeny (~1,850–1,900 Ma), compression deformed the sequences in both regions. Still later (~1,850–1,100 Ma), intermittent crustal extension provided sites for emplacement of abundant mafic igneous rocks. There is no definite evidence that any of the extensional events progressed to the stage of development of oceanic crust; probably the zone has been wholly intracratonal since its inception in late Archean time.</p> <p>During the Phanerozoic, minor differential movements occurred locally in the Great Lakes tectonic zone, as recorded by the thinning of Cretaceous strata and their subsequent tilting and by historical earthquakes in Minnesota.</p>

Table D-7.3.12 Data Summary
MidContinent-Craton Zone

Citation	Title	Description and Relevance to SSC
Kentucky River Fault System, Kentucky		
Van Arsdale (1986)	Quaternary Displacement on Faults Within the Kentucky River Fault System of East-Central Kentucky	The Kentucky River fault system (KRFS) is the north-bounding fault system of the Rome Trough (a Paleozoic aulacogen). Recurrent Paleozoic movement is documented, but recognition of Mesozoic and lower Tertiary displacement is complicated by the absence of preserved post-Paleozoic stratigraphy. Numerous faults of the KRFS are partially overlain by Pliocene-Pleistocene terrace sediments. Preliminary drilling and electrical-resistivity surveys suggest that a number of the faults have been active since deposition of the terraces. The folding and faulting is interpreted to be tectonic in origin, indicating that the KRFS has been active within the past five million years and probably within the past million years.
Wheeler and Crone (2001)	Known and Suggested Quaternary Faulting in the Midcontinent United States	Notes that the seismic hazard associated with the Lexington and Kentucky River fault systems remains uncertain. A personal communication from R. Van Arsdale to the authors in 2000 indicates that although Van Arsdale favored the deformation as tectonic faulting, solution collapse cannot be ruled out as a cause of Quaternary deformation.
Midcontinent Rift Basin–Midcontinent Rift System (MRS)		
Behrendt et al. (1988)	Crustal Structure of the Midcontinent Rift System: Results from GLIMPCE Deep Seismic Reflection Profiles	Interpretation of Great Lakes International Multidisciplinary Program on Crustal Evolution (GLIMPCE) seismic-reflection profiles indicates that the 1,100 Ma Midcontinent rift system (MRS), or Keweenawan rift, of volcanic rocks and postvolcanic and interbedded sedimentary rocks extends to depths as great as 32 km (20 mi.; about 10.5 s reflection time) along profiles crossing western, central, and eastern Lake Superior and the northern end of Lake Michigan. The area may overlie the greatest thickness of intracratonic rift deposits on earth. Times to Moho reflections vary along strike from about 37–46 km (23–29 mi.) depth in the western portion, 55 km (34 mi.) in the central portion, and 42–49 km (26–29 mi.) depth in the eastern portion of Lake Superior. The prerift crust, however, was thinned 25–30 km (15.5–18.5 mi.) beneath the central rift (compared with its flanks), providing evidence for crustal extension by factors of about 3–4. The MRS differs from Phanerozoic rifts in having total crustal thicknesses equal to or greater than the surrounding (presumably unextended) regions.

Table D-7.3.12 Data Summary
MidContinent-Craton Zone

Citation	Title	Description and Relevance to SSC
Cannon (1994)	Closing of the Midcontinent Rift—A Far-Field Effect of Grenvillian Compression	<p>The Midcontinent rift formed in the Laurentian supercontinent between 1,109 and 1,094 Ma. Soon after rifting, stresses changed from extensional to compressional, and the central graben of the rift was partly inverted by thrusting on original extensional faults. Thrusting culminated at about 1,060 Ma but may have begun as early as 1,080 Ma. On the SW-trending arm of the rift, the crust was shortened about 30 km (18.5 mi.); on the SE-trending arm, strike-slip motion was dominant. The rapid evolution from an extensional to a compressional feature was coincident with renewal of NW-directed thrusting in the Grenville, probably caused by continent-continent collision. Stresses transmitted from the Grenville province utilized the zone of weak lithosphere to close and invert the rift.</p>
Cannon et al. (1989)	The North American Midcontinent Rift Beneath Lake Superior from GLIMPCE Seismic Reflection Profiling	<p>The Midcontinent rift is a 1.1 Ga structure, generally buried beneath Paleozoic rocks but traceable by its strong gravity and magnetic anomalies. Seismic-reflection surveys by GLIMPCE imaged the deep structure of the rift beneath Lake Superior. Major observations are as follows:</p> <ul style="list-style-type: none"> • Presence of a deep, asymmetrical central graben. • In addition to crustal sagging, normal faulting played a major role in subsidence of the axial region of the rift. • A sequence of volcanic and sedimentary rocks, in places >30 km (18.5 mi.) thick, fills the graben. • Thinner volcanic and sedimentary units lie on broad flanks of the rift outside of the graben. • Near the axis, the prerift crust is thinned to about one-fourth of its original thickness, by a combination of low-angle extensional faulting and ductile stretching or distributed shear. • The sense of asymmetry of the central graben changes along the trend of the rift, documenting the segmented nature of the structure and suggesting the existence of accommodation zones between the segments. • The location of the accommodation zones is inferred from abrupt disruptions in the Bouguer gravity signature. • Uplift of the central graben occurred when the original graben-bounding normal faults were reactivated as high-angle reverse faults with throws of 5 km (3 mi.) or more in places.

Table D-7.3.12 Data Summary
MidContinent-Craton Zone

Citation	Title	Description and Relevance to SSC
Cannon et al. (1991)	Deep Crustal Structure of the Precambrian Basement Beneath Northern Lake Michigan, Midcontinent North America	<p>The Midcontinent rift is expressed by a northward-thickening wedge of strong, continuous reflections as deep as 7 s (921 km) that are interpreted as basalt flows. The very high gravity values in this region cannot be accounted for solely by the thick basalt section, but also require an unusually high density for the lower crust, which may be due to large volumes of rift-related mafic rocks intruded into the lower crust or upper mantle. The unusual thickness of the crust in this region may be caused, in part, by underplating of mafic rocks, as is suggested for comparably thick crust beneath Lake Superior.</p>
Keller (2010)	An Integrated Geophysical Analysis of the Mid-Continent Rift System	<p>Discusses the possible extension of the MRS through Oklahoma to at least the Wichita uplift. The structural grain of the Precambrian basement provides a basis to differentiate between features related to the MRS and older ones. It is noted that a major zone of seismicity in Oklahoma and Kansas follows the Nemaha fault zone/ridge and gravity and magnetic anomalies that are likely related to the MRS.</p> <p>Rose diagrams from processed potential maps delineate basement features that are parallel to the NW and NE-strike direction of lineaments identified from the seismic-reflection data. Basement structure lineaments were found to be parallel in orientation with the trend of lineaments seen within the Mississippian and Arbuckle Group. NW-striking lineaments are interpreted to be related to the late-Paleozoic tectonism that affected both the Precambrian and Paleozoic section in Osage County to the south. The NE lineaments are interpreted to be primarily related to features associated with the MRS/Nemaha fault zone.</p> <p>Based on the gravity maps, the MRS is interpreted to likely extend across Oklahoma, abutting against the Southern Oklahoma aulacogen. This cannot be substantiated at this time given available geochronologic ages. It is suggested that the relatively young MRS structures are the ones most likely to be tectonically reactivated, and that this assertion is supported by trends in historical seismicity.</p>

Table D-7.3.12 Data Summary
MidContinent-Craton Zone

Citation	Title	Description and Relevance to SSC
Nyquist and Wang (1988)	Flexural Modeling of the Midcontinent Rift	<p>A 2-D flexural model of basin formation for the Midcontinent rift at a latitude of 45°25'N is constrained from a seismic-reflection profile. Based on seismic refraction data and comparison with other rifts, this paper hypothesizes that a magmatic "rift pillow" intruded into the lower crust. The basaltic pillow subsequently solidified to produce a large, high-velocity region in the lower crust, centered under the rift axis, as determined from deep seismic refraction. This crystallization and cooling may be responsible for the "sag" phase of rift evolution, as evidenced by laterally widespread occurrence of postvolcanic sediments.</p>
Trehu et al. (1991)	Imaging the Midcontinent Rift Beneath Lake Superior Using Large Aperture Seismic Data	<p>Presents a detailed velocity model across the Midcontinent rift system (MRS) in central Lake Superior derived primarily from onshore-offshore large-aperture seismic and gravity data. Total crustal thickness decreases rapidly from 55 to 60 km (34 to 37 mi.) beneath the axis of the rift to about 40 km (25 mi.) beneath the south shore of the lake, and decreases more gradually to the north. Above the Moho is a high-velocity lower crust interpreted to result from syn-rift basaltic intrusion into and/or underplating beneath the Archean lower crust. Lower crust is thickest beneath the axis of the main rift half graben. A second region of thick lower crust is found ~100 km (62 mi.) north of the axis of the rift beneath a smaller half graben that is interpreted to reflect an earlier stage of rifting.</p> <p>The model resembles recent models of some passive continental margins and is in marked contrast to many models of both active and extinct Phanerozoic continental rift zones. In the absence of major tectonic activity, the Moho is very stable, since the large, abrupt variations in crustal thickness beneath the MRS have been preserved for at least a billion years.</p>

Table D-7.3.12 Data Summary
MidContinent-Craton Zone

Citation	Title	Description and Relevance to SSC
Nemaha Ridge and Humboldt Fault Zone (NRHF)		
Bakun and Hopper (2004a)	Catalog of Significant Historical Earthquakes in the Central United States See below	Associates a 4.9 (4.5–5.2) magnitude earthquake on April 9, 1952, with the Nemaha fault in Oklahoma.
Gay (2003a, 2003b)	The Nemaha Trend—A System of Compressional Thrust-Fold, Strike-Slip Structural Features in Kansas and Oklahoma, Part 1; and Part 2 (Conclusion)	<p>Association with seismicity:</p> <ul style="list-style-type: none"> References Koff (1978, unpublished MS thesis, University of Oklahoma), which shows possible association of seismicity with Oklahoma City fault. <p>Crustal extent/bedrock deformation:</p> <ul style="list-style-type: none"> The Nemaha ridge/uplift was generated by thrusting in three regional compressional events that were contemporaneous with Appalachian (and probably Rocky Mountain) orogenic events. The main bounding thrust (generally on the east side) is steeply dipping or vertical (frequently mistaken for a normal fault). Based on well data, the fault has reverse displacement and dips steeply west. It appears to decrease in dip with depth in basement (becoming listric). Considerable left-lateral (6 km) strike-slip movement occurred on the Nemaha system during later phases of thrusting. “Relaxation” normal faulting occurred in response to isostatic adjustments after the compressive phase ceased in Late Permian or post-Permian time. An apparent misconception regarding the origin of the Nemaha system is that it is somehow related to the 1.1 Ga Proterozoic Midcontinent rift system (MRS). The MRS lies 40–60 km (25–40 mi.) to the west and is not parallel to the Nemaha trend, and it is more than 600 Myr older and was formed under a distinctly different structural regime. These may be relict weakness zones that were later reactivated, but author is not aware of them and has not seen this on magnetic data.
Niemi et al. (2004)	Investigation of Microearthquakes, Macroseismic Data, and Liquefaction Associated with the 1867 Wamego Earthquake in Eastern Kansas	<p>Association with seismicity:</p> <ul style="list-style-type: none"> Historical felt earthquakes and instrumentally recorded microseismicity loosely associated with basement structures (Humboldt fault and subparallel Nemaha uplift). Seismicity is somewhat dispersed and does not follow a single, well-defined fault feature. Joint inversion with 3-D seismic velocity

Table D-7.3.12 Data Summary
MidContinent-Craton Zone

Citation	Title	Description and Relevance to SSC
		<p>variations.</p> <p>Crustal extent/bedrock deformation:</p> <ul style="list-style-type: none"> • Possible association with 1867 M 5.2 Wamego earthquake basement Nemaha Ridge–Humboldt fault (NRHF) structures. The NRHF lies to the east and is roughly parallel to the Proterozoic MRS, which extends from Kansas NE to Lake Superior. • Nemaha Ridge (NR) is a N-NE-trending anticlinal structure of folded Paleozoic rocks overlying an uplifted Precambrian granitic rock core. Tectonic motion has been accommodated along the steeply dipping Humboldt fault that lies along the eastern boundary of the NR. The Abilene anticline structure overlies basement faults along the western boundary of the NR uplift. NR is complexly broken into a series of horsts and graben by cross faults and folds. The Humboldt fault (HF) is buried along most of its length, but is at the surface in NE Kansas where both right-lateral strike-slip and reverse motion are observed on surface faults offsetting late Paleozoic rocks. • Major uplift of the Nemaha structure occurred during the Pennsylvanian but the structure has been reactivated by post-Permian deformation. Precambrian offset as much as 1,000 m across the HF. Post-Permian throw of 75 m on high-angle faults (down to the east). <p>Quaternary deformation-paleoseismicity:</p> <ul style="list-style-type: none"> • Quaternary-age sediments overlie the HF. Field investigations confirm that sedimentary deposits with moderate liquefaction susceptibility are present in the vicinity of Wamego and Wabaunsee, Kansas, the preferred source location of the 1867 Wamego earthquake. Soft-sediment deformation features, including flame and dish structures, are present in late Holocene floodplain deposits of the Kansas River and appear to be concentrated in the horseshoe bend region of the Kansas River near Wamego and Wabaunsee, Kansas. • Initial results suggest that liquefaction features (e.g., clastic dikes), which may be attributed to seismically induced liquefaction, are present but may not be pervasive in this region. These data suggest that the 1867 M 5.2 Wamego earthquake may characterize the seismic source in this region.

Table D-7.3.12 Data Summary
MidContinent-Craton Zone

Citation	Title	Description and Relevance to SSC
Serpa et al. (1984)	Structure of the Southern Keweenawan Rift from COCORP Surveys Across the Midcontinent Geophysical Anomaly in Northeastern Kansas	<p>Crustal extent/bedrock deformation observations:</p> <ul style="list-style-type: none"> • COCORP profiling reveals structural basins and other features of the Precambrian Keweenawan rift buried beneath the Phanerozoic cover. • The main basin, which is asymmetric, is 40 km (25 mi.) wide and has a maximum depth of 3 km (2 mi.) on the east and 8 km (5 mi.) on the west. • Basin fill is characterized by a lower layered sequence of strong, west-dipping reflectors interpreted to be middle Keweenawan interbedded volcanic and clastic rocks exposed along the MGA in the Lake Superior region. Upper fill is correlated to upper Keweenawan sequence. • A shallower, tilted basin lies to the east of the main rift basin. • Mafic intrusions are interpreted to lie beneath the main rift basin. • Normal faults that are associated with the rift dip at moderate angles to the east. • The data for reactivation of preexisting structures is inconclusive.
Wheeler and Crone (2001)	Known and Suggested Quaternary Faulting in the Midcontinent United States	<p>Summarizes the following observations from previous studies, concluding that the potential for large-magnitude earthquakes in the area remains uncertain:</p> <ul style="list-style-type: none"> • Two damaging earthquakes occurred in the vicinity of the Humboldt fault zone on the Nemaha uplift: a M 5.5 in eastern Kansas in 1867 and a M 5.7 in central Oklahoma in 1952. • Felt historical earthquakes and microearthquakes located by a regional seismograph network tend to concentrate near the fault zone and uplift. • Historical accounts report possible liquefaction during the 1867 Kansas earthquake, but a search for these liquefaction features and for prehistoric liquefaction features was unsuccessful (see Niemi et al., 2004, results above).

Table D-7.3.12 Data Summary
MidContinent-Craton Zone

Citation	Title	Description and Relevance to SSC
Niagara Fault Zone		
Atekwana (1996)	Precambrian Basement Beneath the Central Midcontinent United States as Interpreted from Potential Field Data	Interpreted suture between a northern and southern zone: the northern consisting of early Proterozoic epicratonic rocks and associated Archean basement gneiss, and the southern consisting of volcanic and granitoid rocks (the Wisconsinan magmatic terrane).
Cannon et al. (1991)	Deep Crustal Structure of the Precambrian Basement Beneath Northern Lake Michigan, Midcontinent North America	Deep seismic-reflection profile in northern Lake Michigan provides a cross section of the crust across the 1,850 Ma Penokean orogen, in which an early Proterozoic island arc complex was deformed between two converging Archean continental masses. The Niagara fault zone is interpreted as a sharp inflection in the gravity profile; no strong reflectors can be ascribed to the fault surface, which is interpreted to dip steeply (80° to south), similar to an exposed section to the west.
Plum River Fault, Illinois		
Wheeler and Crone (2001)	Known and Suggested Quaternary Faulting in the Midcontinent United States	Summarizes previous studies that suggested there might be Quaternary deformation along the Plum River fault, an E-W-trending fault that offsets Paleozoic rocks in Iowa and Illinois. Late Quaternary loess-covered terraces along an ancient south-flowing channel of the Mississippi River have northward dips where the terraces cross the Plum River fault, but they could also be explained by terrace erosion and subsequent burial beneath a blanket of loess. No paleoseismic work has been done to evaluate the hypothesis of Quaternary tectonic faulting.
Potter County Fault, Texas		
Wheeler and Crone (2001)	Known and Suggested Quaternary Faulting in the Midcontinent United States	An apparent offset of a lithologic escarpment by the Potter Creek fault in the Texas panhandle that was considered possible evidence of Quaternary faulting was investigated through interpretation of aerial photographs and aerial and field reconnaissance studies. This paper summarizes the conclusions from studies by other researchers that showed no evidence of Quaternary faulting along the fault trace. Field studies showed that at two localities, the base of Miocene rocks is unfaulted at both sides of the fault.

Table D-7.3.12 Data Summary
MidContinent-Craton Zone

Citation	Title	Description and Relevance to SSC
Rampart Range Fault, Colorado		
Widmann (1997b)	Complete Report for Rampart Range Fault (Class A) No. 2328	This fault trends N-S along the eastern margin of the Front Range, north of Colorado Springs, for about 46 km (29 mi.). The fault is marked by topographic breaks and vegetation lineaments. It is a range-front fault that had reverse movement during the Laramide, but normal movement during the late Cenozoic. Approximately 8 m (26 ft.) of down-to-the-west Quaternary displacement has been reported. Trenching investigations indicated that the most recent displacement occurred between 600 ka and 30–50 ka.
Ste. Genevieve Fault Zone (SGFZ), Missouri and Illinois		
Harrison and Schultz (2002)	Tectonic Framework of the Southwestern Margin of the Illinois Basin and Its Influence on Neotectonism and Seismicity	<p>Detailed studies of this fault zone document contractional, extensional, and strike-slip movement along high-angle faults, as well as multiple periods of movement.</p> <p>The zone dies out near both the St. Charles and Commerce lineaments (see the Geophysical Anomalies section of this table), suggesting a genetic link and demonstrating the influence of these structural features on tectonism in the region.</p> <p>Deformation along this structure is correlative to the late Mississippian to middle Pennsylvanian tectonic episode identified elsewhere in the Midcontinent. The paper provides evidence for a period of extension probably of late Pennsylvanian to Permian age.</p> <p>Detailed and reconnaissance mapping along the Ste. Genevieve fault zone for more than 75 years has revealed no evidence of Tertiary or Quaternary faulting.</p>
Heigold and Kolata (1993)	Proterozoic Crustal Boundary in the Southern Part of the Illinois Basin	The fault may have originated as a crustal plate boundary or suture zone during the Proterozoic.

Table D-7.3.12 Data Summary
MidContinent-Craton Zone

Citation	Title	Description and Relevance to SSC
<p>Nelson (1995)</p> <p>Nelson et al. (1997)</p>	<p>Structural Features in Illinois</p> <p>Tertiary and Quaternary Tectonic Faulting in Southernmost Illinois</p>	<p>The SGFZ is mapped for approximately 193 km (120 mi.) along strike from SE Missouri into SW Illinois. It consists of numerous en echelon strands and braided segments having variable deformation styles and a complex history of reactivation. Displacement across the zone ranges from less than 198 m (650 ft.) to as much as 1,189 m (3,900 ft.). Detailed studies of this fault zone document contractional, extensional, and strike-slip movement along high-angle faults, as well as multiple periods of movement.</p> <p>In Illinois, compressional deformation is documented along the Ste. Genevieve fault in early Pennsylvanian rocks (Nelson, 1995). The later report, Nelson et al. (1997), however, indicates that some faults along the SE part of the SGFZ in Illinois displace Cretaceous and Tertiary sediments, but Quaternary deposits are not faulted.</p>
<p>Tuttle, Chester, et al. (1999)</p>	<p>Paleoseismology Study Northwest of the New Madrid Seismic Zone</p>	<p>Identifies soft-sediment deformation that could be related to low levels of ground shaking at one location along a strand of the fault. Diffuse seismicity occurs in the block between the SGFZ and Simms Mountain fault system. However, no evidence has been documented of any tectonic deformation of Quaternary deposits, nor has convincing evidence for paleoliquefaction been observed in this area.</p>
<p>Simms Mountain Fault System, Missouri</p>		
<p>Harrison and Schultz (2002)</p>	<p>Tectonic Framework of the Southwestern Margin of the Illinois Basin and Its Influence on Neotectonism and Seismicity</p>	<p>The Simms Mountain fault system in SE Missouri consists of numerous braided and en echelon fault strands that are continuous southward into the Cape Girardeau fault system. Together these fault systems extend more than 106 km (66 mi.), and in places reach as wide as 79 km (24 mi.). Left-lateral strike-slip movement occurred on the fault system, primarily before formation of Mississippi Valley–type ore deposits of Permian age, although some are later or of unknown age (Harrison and Schultz, 2002).</p>

Table D-7.3.12 Data Summary
MidContinent-Craton Zone

Citation	Title	Description and Relevance to SSC
Ute Pass Fault Zone		
Widmann (1997a)	Complete Report for Ute Pass Fault Zone (Class A) No. 2327	This fault zone consists of five generally NW-trending faults that define the west and SW margins of the Rampart Range west of Colorado Springs. There is evidence of late Cenozoic movement along most of the fault. Quaternary deposits do not appear to be offset across the north end of the fault zone; on the south end of the fault zone, scarps developed on Quaternary rockfall deposits may indicate Quaternary fault activity. No evidence of offset in late Pleistocene to Holocene deposits has been found. The length of the fault zone is about 71 km (44 mi.).
Vaughn Fault, New Mexico		
Wheeler and Crone (2001)	Known and Suggested Quaternary Faulting in the Midcontinent United States	Summarizes information regarding an escarpment along the north-striking Vaughn fault that impounds Quaternary sediments on its west side and blocks most local streams. Based on geologic mapping, an inferred 150–300 m of west-side-down subsurface offset is present along the fault. Although the evidence is suggestive of Quaternary faulting, such faulting has not been demonstrated, and the fault might be a near-surface effect of subsurface solution.
Valmont Fault, Colorado		
Wheeler and Crone (2001)	Known and Suggested Quaternary Faulting in the Midcontinent United States	Summarizes reported information on the Valmont fault that was inferred from a single road cut that exposes a 13 m wide zone of disrupted and shingled stones in Quaternary alluvium. The alluvium is offset 1.5 m across the zone. The fault lacks geomorphic expression. The faulting has been explained by both tectonic faulting and intrusion of a nearby dike.
Washita Valley Fault, Oklahoma		
Van Arsdale et al. (1989)	Post-Pennsylvanian Reactivation Along the Washita Valley Fault, Southern Oklahoma	This study searched for geomorphic, structural, and other geologic evidence of young faulting at sites along the Washita Valley fault. Two trenches at site A exposed unfaulted Holocene alluvium dated at $1,910 \pm 80$ yr BP. One trench and a natural exposure at site B contained unfaulted 12–15 ka terrace alluvium. Seven trenches and two natural exposures at site E revealed faulted Cretaceous strata overlain by unfaulted Wisconsinan terrace alluvium.

Table D-7.3.12 Data Summary
MidContinent-Craton Zone

Citation	Title	Description and Relevance to SSC
Wheeler and Crone (2001)	Known and Suggested Quaternary Faulting in the Midcontinent United States	This paper summarizes work by Van Arsdale et al. (1989) that found no evidence of Quaternary faulting along the Washita Valley fault.
<i>Nontectonic Faults</i>		
Wheeler and Crone (2001)	Known and Suggested Quaternary Faulting in the Midcontinent United States	Summarizes field studies that have shown that six previously inferred Quaternary faults have nontectonic origins: Barrera and Carlsbad faults, New Mexico; Fowler fault, Colorado; Harlan County fault, Nebraska; Ord escarpment, Nebraska; and two small faults west of Pierre, South Dakota.
<i>Paleoliquefaction Studies</i>		
Tuttle, Chester, et al. (1999)	Paleoseismology Study Northwest of the New Madrid Seismic Zone	Based on the spatial distribution of prehistoric liquefaction features, the paper indicates that the Waterloo-Dupo anticline, Valmeyer anticline, and St. Louis fault are possible sources for paleoearthquake features observed in eastern Missouri, but also emphasizes that other scenarios relying on sources farther east are equally possible (i.e., on the DuQuoin monocline–Centralia fault). (For further discussion of these structures, see the Illinois Basin-Wabash Valley Data Summary Table [Appendix Table D-6.1.9])
Tuttle (2005b)	Paleoseismological Study in the St. Louis Region: Collaborative Research	This paper summarizes and updates observations reported by Tuttle, Chester, et al. (1999). At least two generations of Holocene earthquake-induced liquefaction features, including sand and silt dikes and sills, and only two sand blows, are identified in the St. Louis region. Some features probably formed during the 1811-1812 or earlier New Madrid earthquakes, and others formed during a middle Holocene earthquake in 4520 BC \pm 160 yr. Late Holocene sand dikes, up to 26 cm in width, occur along the Kaskaskia River and its tributaries, Crooked, Shoal, and Silver creeks, as well as along Cahokia and Piassa creeks and the Cache, Castor, Marys, and Meramec rivers. The 4250 BC earthquake may or may not have been responsible for all of the middle Holocene features. The relatively large size of features identified near Germantown, Illinois, suggests that the earthquake source may be located east of St. Louis. Alternative sizes and locations are suggested. The Meramec River features could have formed as a result of a moderate-to-large earthquake centered in the St. Louis area or a very large earthquake centered 80–100 km (50–62 mi.) east of St. Louis.

Table D-7.3.12 Data Summary
MidContinent-Craton Zone

Citation	Title	Description and Relevance to SSC
Anna Seismic Zone		
Atekwana (1996)	Precambrian Basement Beneath the Central Midcontinent United States as Interpreted from Potential Field Data	<p>Portions of the NW-trending anomalies of the East Continent gravity high have been called the Fort Wayne rift (FWR) and are interpreted to be older than N-S-trending anomalies in central Ohio to Kentucky and the Grenville Front, further suggesting that the Grenville Front truncates the FWR. The author attributes the formation of the FWR to processes occurring in the formation of the Granite-Rhyolite province or later reactivation of preexisting basement structures. A whole-rock rubidium-strontium date of 1.325 Ga is older than dates reported for the Midcontinent rift system, suggesting that Fort Wayne rifting formed during an earlier rifting event.</p>
Baranoski et al. (2009)	Unconformity-Bounded Seismic Reflection Sequences Define Grenville-Age Rift System and Foreland Basins Beneath the Phanerozoic in Ohio	<p>Interprets four sequences of layered reflectors (A, B, C, and D) below the Phanerozoic deposits and above basement of the Granite-Rhyolite and Grenville provinces from reprocessed data of COCORP Line OH-1. Episodic deposition of these sequences records rifting and a westward shift of the major axis of depositional thickening that began as a series of half graben and culminated in a highly deformed foreland basin at the end of the Grenville orogeny. The unconformities at the top of sequences A, B, and C represent the end of an episode of crustal extension in the west and rejuvenation of crustal shortening in the east, recording a westward progression of thrusting and crustal loading during the Grenville orogeny. Sequences A and B are more localized and may contain volcanoclastic and alluvial sediments deposited above a NW-trending gravity low in a rapidly subsiding fault bounding the FWR.</p> <p>Each sequence becomes more widespread due to continued subsidence. The more widespread sequences C and D are correlated with the Middle Run Formation of the East Continent rift basin. The deposition of discontinuous, intertonguing clastic sediments of sequence D marks the end of subsiding rift basins in response to late Grenville collision, culminating in a widespread regional foreland basin marking the end of the Grenville orogeny. Without datable drill core samples, the authors are unable to establish, on the basis of sequence stratigraphy, structural relationships, and geopotential field data, whether the FWR is coeval with the SE arm of the Midcontinent rift in Michigan.</p>

Table D-7.3.12 Data Summary
MidContinent-Craton Zone

Citation	Title	Description and Relevance to SSC
Crone and Wheeler (2000)	Data for Quaternary Faults, Liquefaction Features, and Possible Tectonic Features in the Central and Eastern United States, East of the Rocky Mountain Front	<p>Assigns the Anna seismic zone to Class C. (Geologic evidence is insufficient to demonstrate Quaternary fault displacement for features assigned to Class C.) Earthquakes associated with the seismic zone span approximately 80 km (50 mi.), with most of the seismicity concentrated within an area 30–35 km (18.6–21.7 mi.) across. Most epicenters cluster along the NW-striking Anna-Champaign fault, which has been mapped in the basement beneath Paleozoic platform strata. The largest earthquakes recorded in the zone were two that occurred in March 1937 and had intensities of VII and VIII and M 4.9 and 5.1. Focal mechanisms indicate strike-slip faulting.</p> <p>Selected stream banks and sand and gravel pits in the Anna area were examined by Obermeier (1995) for evidence of prehistoric liquefaction features; none were found. Based on the spacing of potentially liquefiable materials, he concluded that an earthquake larger than M 7 has not occurred in the past several thousand years, although smaller ones cannot be excluded.</p>
Drahovzal et al. (1992)	The East Continent Rift Basin: A New Discovery	<p>Identified the East Continent rift basin (ECRB) based on the following evidence:</p> <ul style="list-style-type: none"> • presence of Middle Run Formation (a pre-Mt. Simon lithic arenite interbedded with basalt representative of continental flood basalts); • association with the East Continent gravity high, a NW-trending positive gravity anomaly from NE Indiana, SW Michigan, and central-western Ohio, crossing the Grenville Front tectonic zone into Kentucky and coincident with the Fort Wayne rift (FWR) in Indiana and Ohio; and • magnetic anomalies coincident with gravity anomalies, suggesting deep-rooted bodies of mafic composition, possibly emplaced during rifting. <p>The ECRB and FWR have uncertain Proterozoic ages based on a few age dates from drill core. Less distinct magnetic anomalies east of the Grenville Front and east-dipping thrust sheets overlying Middle Run Formation in Kentucky indicate that the ECRB cannot be as young as Cambrian. The overthrust relationship between the Grenville and ECRB is not clear on data from COCORP line OH-1. Rifting associated with the ECRB may be contemporaneous with Keweenawan rifting in Michigan. The thickness of the basin-fill sequence exceeds 20,000 feet at several locations along the Grenville Front tectonic zone in central Kentucky and central Ohio and</p>

Table D-7.3.12 Data Summary
MidContinent-Craton Zone

Citation	Title	Description and Relevance to SSC
		northern Ohio. The basin-fill sequence thins on an uplifted block in SE Indiana and along the trend of the FWR in the vicinity of COCORP line OH-1. The trend of the FWR defines a NW-trending basement high that separates deeper portions of the basin.
Hansen (1987)	July 1986 Auglaize County Earthquake	<p>The July 12, 1986, M_L 4.5 earthquake in western Auglaize County, near St. Marys township, occurred on the Anna-Champaign fault, a NW-SE-trending structure that extends into Shelby, Auglaize, and Mercer counties. The ancient Teays River followed the trace of the Anna-Champaign fault before Pleistocene glaciations. The deep alluvial valley was thought to amplify ground motions during earthquakes, which was not observed during the July 12, 1986, earthquake.</p> <p>This observation suggests that relocating the March 2 and March 9, 1937, earthquakes to the vicinity of the July 12, 1986, earthquake and adjusting their magnitudes downward is not warranted. Review of a seismic record made of these 1937 earthquakes by a Jesuit priest suggests they occurred at or SE of Anna, Ohio. Such a location would be more consistent with the felt reports of the 1937 earthquakes and the isoseismal map of the 1986 earthquake. The July 12, 1986, earthquake had no associated foreshocks or aftershocks and produced MMI VI shaking confined to a small area surrounding the epicenter.</p>
Hansen (1993)	Earthquakes and Seismic Risk in Ohio	The Anna seismic zone, also called the Western Ohio seismic zone, coincides with NW-SE-trending basement faults associated with the FWR in Shelby, Auglaize, and nearby counties. This zone has produced at least 40 felt earthquakes since 1875, including earthquakes in 1875, 1930, 1931, 1937, 1977, and 1986 that caused minor to moderate damage. The July 12, 1986, earthquake near the town of St. Marys in Auglaize County was the largest earthquake to occur in the zone since 1937. The author concludes that the historical record indicates a maximum magnitude of 5, but suggests that this zone was capable of producing a magnitude 6.0–7.0 earthquake.
Hauser (1993)	Grenville Foreland Thrust Belt Hidden Beneath the Eastern U.S. Midcontinent	Interprets the Middle Run Formation as forming in a Grenville foreland basin or, alternatively, as a constituent of the Granite-Rhyolite province. Does not recognize a rift origin.

Table D-7.3.12 Data Summary
MidContinent-Craton Zone

Citation	Title	Description and Relevance to SSC
McPhee (1983)	Regional Gravity Analysis of the Anna, Ohio, Seismogenic Region	Generated regional and local gravity and magnetic models to evaluate the relationship of seismicity and basement geology in the Anna seismic zone. The models require a large source of positive density contrast extending upward from the Moho into the lower crust beneath the FWR, interpreted as a deep crustal mafic source. Seismicity appears to be concentrated at the boundary between the rift-type mafic volcanic rocks of the FWR and the granitic body to the NE. This pattern of seismicity can be attributed to either reactivation of graben-type faults, activation of a zone of weakness at the contrasting lithologies, or extension of the Bowling Green fault in the basement.
Obermeier (1995)	Paleoseismic Liquefaction Studies—Central U.S. and Pacific Northwestern U.S.	Investigated stream banks in the vicinity of Anna, Ohio, and portions of the Auglaize, Great Miami, Stillwater, and St. Marys rivers and found no evidence of paleoliquefaction features indicative of a M 7 earthquake in the past several thousand years.
Ruff et al. (1994)	Geophysical Investigations of the Western Ohio–Indiana Region: Final Report 1986–September 1992	Describes earthquake activity in the western Ohio–Indiana region that was monitored with a regional seismograph network between 1977 and 1992. A total of 78 local and regional earthquakes were recorded by the network during this time period. The largest earthquake recorded was the July 12, 1986, St. Marys earthquake (m_b 4.5) within the Anna seismic zone. The focal mechanism indicated a strike-slip earthquake with an E-NE-striking compressional axis. The history of felt earthquakes in the Anna zone dates back to the late 1700s and includes several earthquakes of about magnitude 5. Attributes seismicity to the Anna-Champaign, Logan, and Auglaize faults.
Schwartz and Christensen (1988)	The 12 July 1986 St. Marys, Ohio Earthquake and Recent Seismicity in the Anna, Ohio Seismogenic Zone	Determined hypocenter of 3 mi. (5 km) for the magnitude (m_b) 4.5 earthquake and a focal mechanism (strike = 25°, dip = 90°, rake = 175°) representing mostly strike-slip, with a small oblique component approximately parallel to Anna-Champaign fault and a nearly horizontal P axis oriented E-NE.

Table D-7.3.12 Data Summary
MidContinent-Craton Zone

Citation	Title	Description and Relevance to SSC
Stark (1997)	The East Continent Rift Complex: Evidence and Conclusions	<p>Informed with the work of Drahovzal et al. (1992), Stark extends the concept of the East Continent rift basin (ECRB) to a major multiphase rift complex in the eastern Midcontinent: the East Continent rift complex. This interpretation involves four phases:</p> <ol style="list-style-type: none"> 1. Keweenawan extension (1.05–1.3 Ga) rifted the Granite-Rhyolite province along the ECRB/FWR, the English Graben/Flatrock subbasin, and the Southern Indiana graben into an internally complex half graben along rift margins containing considerable thickness of rift fill sediments and volcanic rocks. 2. Grenvillian contraction (880–990 Ma) resulted in overthrusting the eastern margin of the East Continent rift complex, emplacement of an allochthon of metamorphic strata above and adjacent to the rift strata, remobilization of NW-SE-trending transtensive wrench systems as transpressive detachment zones, and formation of a foreland basin with concomitant fold systems. 3. Pre-Eocambrian uplift and erosion (650–550 Ma) resulted in substantial syn- and/or postdepositional deformation before the Sauk unconformity, which may have removed most or all of the Grenvillian foreland basin. 4. Eocambrian extension (650–560 Ma) associated with the opening of the Iapetus Ocean initiated rifting of Reelfoot rift, Rough Creek graben, and Rome trough; and reactivation of Rough Creek graben/Shawneetown fault system, Kentucky River fault system, Lexington fault system, Bowling Green fault zone, and Warfield fault system. Middle Cambrian thermal subsidence downwarped these rifts, leading to widespread deposition of the Sauk Sequence carbonates. <p>Deep wells along the FWR at the Anna seismic zone encountered mafic basalt fill sequence, whereas wells to the north and south encountered Middle Run Formation. This observation implies that structures associated with the Anna seismic zone were uplifted before the late Proterozoic erosion and therefore must have remobilized through geologic time, further suggesting that the Anna seismic zone is associated with an accommodation structure within the ECRB/FWR.</p>

Table D-7.3.12 Data Summary
MidContinent-Craton Zone

Citation	Title	Description and Relevance to SSC
<i>Northeast Ohio Seismic Zone</i>		
Crone and Wheeler (2000)	Data for Quaternary Faults, Liquefaction Features, and Possible Tectonic Features in the Central and Eastern United States, East of the Rocky Mountain Front	Assigns Northeast Ohio seismic zone to Class C. (Geologic evidence is insufficient to demonstrate Quaternary fault displacement for features assigned to Class C.) Earthquakes associated with this zone form a diffuse cluster aligned NE-SW and about 80 km (50 mi.) long and 40 km (25 mi.) wide. The 11 largest epicenters lie along and NW of Akron magnetic lineament. Obermeier (1995) examined selected stream banks in this area for evidence of prehistoric liquefaction, but found none. Exposures that could provide definitive evidence of prehistoric earthquakes are scarce in region; still, the zone lacks paleoseismological evidence of Quaternary faulting.
Dineva et al. (2004)	Seismicity of the Southern Great Lakes: Revised Earthquake Hypocenters and Possible Tectonic Controls	Describes results of analyses to establish better constraints on epicenter locations and focal depth estimations for 106 earthquakes that occurred from 1990 to 2001 in southern Great Lakes region. Earthquakes within Northeast Ohio seismic zone, also referred to as a cluster of earthquakes south of Lake Erie on the Ohio-Pennsylvania border, were relocated. Earthquakes in this zone form a cluster that trends NE-SW and follows Lake Erie shoreline for about 60 km (37 mi.). Hypocenter locations are confined to the crust above 30 km (18.6 mi.); most occur above 20 km (12.4 mi.). Seismicity appears to be localized where preexisting tectonic structures (e.g., the Akron magnetic boundary) are favorably oriented with respect to present-day stress field, and where water is present at surface.
Hansen et al. (2001)	Seismic Spotlight Shines on Ashtabula	Describes the series of earthquakes in 1987 and 2001 that occurred in the vicinity of Ashtabula in NE Ohio. Before the 1987 earthquake, earthquakes had not been felt in this area since it was settled in the early 1800s. Portable seismographs deployed in the region and the Ohio Seismic Network implemented in 1999 provide detailed information on these earthquakes. An isoseismal map for areas of approximately equal MM intensity for the January 25, 2001, main shock at Ashtabula shows a N-S elongation for this shoreline earthquake; the cause of this phenomenon is reported as unknown.

Table D-7.3.12 Data Summary
MidContinent-Craton Zone

Citation	Title	Description and Relevance to SSC
Hartline (1995)	Deep Structural Analysis Related to the Akron Magnetic Boundary Using Geophysical Well Logs and Potential Field Data, East-Central Ohio	Reviews geophysical well logs, gravity data, magnetic data, and COCORP seismic data in Knox, Coshocton, Muskingum, and Licking counties, Ohio, and presents structure-contour and isopach maps on 16 key horizons in the Paleozoic cover to evaluate basement-controlled faulting associated with the Akron magnetic boundary. Finds no evidence of basement-controlled faulting along the Akron magnetic boundary; however, the study area is in central Ohio, not along the Northeast Ohio seismic zone.
Hoehn (1991)	An Integrated Geophysical Study of the Grenville Province in the Greater Lake Erie Region	Reprocesses Vibroseis seismic-reflection data from line LE-01 in Lake Erie and compares the results to potential field data. The reprocessed data can resolve reflections to a depth of 18 km (11.2 mi.). Decrease in the gravity profile across Akron magnetic boundary is attributed to an east-dipping low-density body in the upper crust. Interprets the Eastern Midcontinent magnetic belt as relic structures associated with a reversal of subduction polarity within the Proterozoic bound to the east by NW-directed thrusts of Akron magnetic boundary. Sedimentary units east of the Akron magnetic boundary exhibit extension within the Elzevir terrane. Multiple reflections within the first two seconds of the data obscure Akron magnetic boundary in the upper crust.
Lidiak and Hinze (1993)	Grenville Province in the Subsurface of Eastern United States	Interprets Akron magnetic boundary as a major Grenville suture separating contrasting magnetic anomalies and seismic reflectors. To the east of the Akron magnetic boundary, basement is characterized by lower-amplitude anomalies and west-dipping reflectors that exhibit ductile deformation. Crust to the west exhibits high-amplitude magnetic anomalies and east-dipping reflectors indicative of the Grenville front and related structures. The authors present a mapped location trending NE through eastern Lake Erie; they postulate that Akron magnetic boundary separates Elzevir terrane in the east from their proposed Eastern Midcontinent magnetic belt to the west.

Table D-7.3.12 Data Summary
MidContinent-Craton Zone

Citation	Title	Description and Relevance to SSC
Nicholson et al. (1988)	The Northeastern Ohio Earthquake of 31 January 1986: Was It Induced?	Describes the January 31, 1986, earthquake that occurred about 40 km (25 mi.) east of Cleveland, Ohio, with m_b 5.0 and intensity VI–VII at distances of 15 km (9.3 mi.). Focal depths for this earthquake and the aftershocks ranged from 2 to 6 km (1.2 to 3.7 mi.). The aftershocks occurred in a tight cluster about 1 km (0.6 mi.) wide and oriented to the N-NE, and focal mechanisms of the aftershocks represent predominantly oblique right-slip motion on nearly vertical planes oriented N15°–45°E, with a nearly horizontal P (maximum compressive stress) axis, consistent with the modern stress regime. Factors that suggest a natural origin for the earthquake include a history of small and moderate earthquakes in the region prior to the initiation of injection, and the lack of large numbers of small earthquakes typical of many induced sequences. The 1986 cluster is coincident with a N40°E-trending gravity and magnetic anomaly (Akron magnetic boundary).
Nicholson and Wesson (1990)	Earthquake Hazard Associated with Deep Well Injection—A Report to the U.S. Environmental Protection Agency	Includes descriptions of earthquakes that occurred about 40 km (25 mi.) apart in NE Ohio in January 1986 and July 1987 and reviews evidence for possible triggering of these earthquakes. Reviews the state of knowledge about earthquakes related to injection of fluid into deep wells. Describes the probable physical mechanism for the triggering and the criteria for predicting whether earthquakes will be triggered that depend on the local state of stress in the earth's crust, the injection pressure, and the physical and hydrologic properties of rocks into which the fluid is being injected. Concludes that the January 1986 earthquake had a natural origin, although triggering by well activities of at least a few small aftershock earthquakes could not be precluded, and that the July 1987 earthquakes were most likely induced.
Obermeier (1996a)	Summary of 1995 Paleoliquefaction Field Search in the Vicinity of Perry, Ohio	<p>Letter report summarizing a paleoliquefaction investigation performed in the vicinity of the Perry Nuclear Power Plant along the Grand River, Trumbull Creek, and Cuyahoga River and near a tributary to Phelps Creek of NE Ohio. Based on observations along these streams, Obermeier made the following conclusions:</p> <ul style="list-style-type: none"> • The lack of suitable exposures within 20 km (12.5 mi.) of the nuclear power plant at Perry, Ohio, precludes definitive statements as to whether there has been strong seismic shaking for most of Holocene time. • The lack of exposures with liquefiable sediment more than a few thousand years old and within 20–25 km (12.5–25 mi.) of the plant precludes any

Table D-7.3.12 Data Summary
MidContinent-Craton Zone

Citation	Title	Description and Relevance to SSC
		<p>statement concerning whether there could have been strong shaking at the plant locale from even moderate-sized earthquakes ($M \sim 6$) occurring more than a few thousand years ago.</p> <ul style="list-style-type: none"> • The lack of liquefaction features in latest Pleistocene sediment (moderate to high liquefaction susceptibility through time) in the locality of a large sand and gravel pit ("Pit-CL") does not provide sufficient data to make a statement on seismic shaking at a distance of 32 km (20 mi.) from the Perry Nuclear Power Plant. <p>Obermeier noted in the letter report that perennial streams flowing subparallel and through a beach ridge/sand dune complex within 2–6 km (1.2–3.7 mi.) inland from the shore (identified from examination of the Soil Survey Report of Lake County) might offer the possibility of a field setting where liquefaction features could have developed for much of Holocene time.</p>
Seeber and Armbruster (1993)	Natural and Induced Seismicity in the Lake Erie-Lake Ontario Region: Reactivation of Ancient Faults with Little Neotectonic Displacement	<p>Defines the Northeast Ohio seismic zone on the basis of a 50+ km (31+ mi.) long belt of seismicity striking NE near the shoreline of Lake Erie. Proposes that the belt of seismicity may be associated with a major fault and related secondary faults. The Northeast Ohio seismic zone correlates spatially with the Akron magnetic lineament and a portion of the Akron magnetic boundary. The authors speculate that the Akron magnetic boundary may be associated with the Niagara-Pickering magnetic lineament/Central Metasedimentary Belt boundary zone as a continental scale Grenville-age structure.</p> <p>Evaluates the hypothesis that the July 13, 1987, m_{bLg} 3.8 Ashtabula earthquake and sequence of 36 aftershocks were triggered by fluid injection into a deep waste disposal well penetrating the basal Mt. Simon sandstone. The well had been in operation since July 1986. Well-located earthquakes of the Ashtabula sequence cluster in a narrow, east-trending vertical zone about 1.5 km (1 mi.) long and between 1.7 and 3.5 km (1.1 and 2.2 mi.) deep, located as close as 0.7 km (0.4 mi.) to the injection well. The depth to basement in this area is approximately 1.8 km (1.1 mi.), indicating that this cluster of seismicity is concentrated below the Mt. Simon–Grenville unconformity.</p> <p>The authors interpret this narrow zone as an active fault, referred to as the Ashtabula fault. Subsequent seismicity from 1987 to 1992 suggests a westward migration by 5–10 km (3.1–6.2 mi.), possibly along the proposed</p>

Table D-7.3.12 Data Summary
MidContinent-Craton Zone

Citation	Title	Description and Relevance to SSC
		<p>fault. However, because the temporary seismic network used to locate the aftershocks of the 1987 main shock was no longer in operation, the locations of the 1992 earthquakes are not as well constrained as the aftershocks of the main 1987 earthquake.</p> <p>Based on the assumption that the 1992 seismicity and the 1987 earthquakes defined a single rupture plane, the authors estimate that the postulated Ashtabula fault could produce a magnitude 5–6 earthquake.</p>
Seeber et al. (2004)	A Fluid-Injection-Triggered Earthquake Sequence in Ashtabula, Ohio: Implications for Seismogenesis in Stable Continental Regions	<p>Describes an earthquake sequence near Ashtabula in NE Ohio that is believed to have been triggered by fluid injection. The sequence began in 1987 with a m_{blg} 3.8 main shock; the largest earthquake recorded was a m_{blg} 4.3 earthquake in 2001. Well-located aftershocks of the June 3, 2001, m_{blg} 3.0 and the July 17, 2003, m_{blg} 2.5 earthquakes define a 7 km (4.3 mi.) long plane striking 96° and dipping 65° south. The authors interpret this plane as the source fault for the 2001 seismicity, which resembles the postulated E-W-striking fault with left-lateral slip defined by the 1987 seismicity (Seeber and Armbruster, 1993). These subparallel faults are 4.5 and 0.7 km (2.9 and 0.4 mi.) south of the injection well, respectively.</p> <p>Seeber et al. revise the previous interpretation of Seeber and Armbruster (1993) regarding the tectonic implications of the 1987 earthquake sequence and subsequent earthquakes in 1992 to conclude that the linear patch of 1987 earthquakes is a portion of a basement fault activated by high pore pressure rather than evidence of a single rupture. This conclusion was based in part on the observation that these earthquakes are scattered over the patch as opposed to clustering at the edges.</p> <p>Seeber et al. attribute the quiescence from 1995 to 2000 to a lack of favorably oriented structures between these two fault planes. They speculate that seismicity initiates when and where a significant pore-pressure rise intersects preexisting faults close to failure, and is turned off when pressure starts dropping back. They conclude that these faults are preexisting faults located in the uppermost portion of the Grenville basement reactivated by a high pore-pressure anomaly spreading from the injection site.</p>

Table D-7.3.12 Data Summary
MidContinent-Craton Zone

Citation	Title	Description and Relevance to SSC
Wesson and Nicholson (eds.) (1986)	Studies of the January 31, 1986, Northeastern Ohio Earthquake—A Report to the U.S. Nuclear Regulatory Commission	This earthquake occurred about 17 km (10.5 mi.) south of the Perry Nuclear Power Plant and generated accelerations of 0.18 g of short duration at the plant. Analysis of the main shock and aftershocks indicated no obvious structure or fault with which the earthquakes could be associated. The earthquakes were located within 15 km (9.3 mi.) of three deep waste-disposal injection wells and could have been due to fluid injection that reactivated favorably oriented, preexisting fractures. Available information indicated that although triggering was a possibility, the probability that injection played a significant role should be regarded as low. It was reported that there was nothing to suggest the occurrence of an earthquake larger than expected for the region, or the activation of a major structure close to the wells or near the power plant.

APPENDIX E

**CEUS Paleoliquefaction Database, Uncertainties Associated with
Paleoliquefaction Data, and Guidance for Seismic Source Characterization**

E

APPENDIX

**CEUS Paleoliquefaction Database, Uncertainties Associated with
Paleoliquefaction Data, and Guidance for Seismic Source Characterization**

DISCLAIMER OF WARRANTIES AND LIMITATION OF LIABILITIES

THIS DOCUMENT WAS PREPARED BY THE ORGANIZATION(S) NAMED BELOW AS AN ACCOUNT OF WORK SPONSORED OR COSPONSORED BY THE ELECTRIC POWER RESEARCH INSTITUTE, INC. (EPRI). NEITHER EPRI, ANY MEMBER OF EPRI, ANY COSPONSOR, THE ORGANIZATION(S) BELOW, NOR ANY PERSON ACTING ON BEHALF OF ANY OF THEM:

(A) MAKES ANY WARRANTY OR REPRESENTATION WHATSOEVER, EXPRESS OR IMPLIED, (I) WITH RESPECT TO THE USE OF ANY INFORMATION, APPARATUS, METHOD, PROCESS, OR SIMILAR ITEM DISCLOSED IN THIS DOCUMENT, INCLUDING MERCHANTABILITY AND FITNESS FOR A PARTICULAR PURPOSE, OR (II) THAT SUCH USE DOES NOT INFRINGE ON OR INTERFERE WITH PRIVATELY OWNED RIGHTS, INCLUDING ANY PARTY'S INTELLECTUAL PROPERTY, OR (III) THAT THIS DOCUMENT IS SUITABLE TO ANY PARTICULAR USER'S CIRCUMSTANCE; OR

(B) ASSUMES RESPONSIBILITY FOR ANY DAMAGES OR OTHER LIABILITY WHATSOEVER (INCLUDING ANY CONSEQUENTIAL DAMAGES, EVEN IF EPRI OR ANY EPRI REPRESENTATIVE HAS BEEN ADVISED OF THE POSSIBILITY OF SUCH DAMAGES) RESULTING FROM YOUR SELECTION OR USE OF THIS DOCUMENT OR ANY INFORMATION, APPARATUS, METHOD, PROCESS, OR SIMILAR ITEM DISCLOSED IN THIS DOCUMENT.

ORGANIZATIONS THAT PREPARED THIS DOCUMENT

M. Tuttle & Associates

Fugro William Lettis & Associates

CITATIONS

This report was prepared by

M. Tuttle & Associates

128 Tibbetts Lane

Georgetown, ME 04548

Principal Investigator

M.P. Tuttle

Fugro William Lettis & Associates

27220 Turnberry Lane Suite 110

Valencia, CA 91355

Principal Investigator

R.D. Hartleb

This report describes research sponsored by the U.S. Nuclear Regulatory Commission, U.S. Department of Energy (DOE), and Electric Power Research Institute (EPRI).

Acknowledgments

Drs. Martin Chapman, Russell Green, and Scott Olson, specialists in seismology and geotechnical engineering, reviewed an outline of this document and provided comments and suggestions that were incorporated into the report. Laurel Bauer, Randal Cox, Hanan Mahdi, Stephen Obermeier, Okba Al-Qahdi, Haydar Al-Shukri, Pradeep Talwani, Martitia Tuttle, Roy Van Arsdale, and James Vaughn contributed data to the CEUS paleoliquefaction database. Scott Lindvall assisted with database design and provided overall guidance for the contents of this document. Tanya Broadbent, Jason Finley, Caroline Moseley, David Slayter, and Kathy Tucker assisted with data entry and verification, database management, map development, graphics, and copyright research. Lawrence Salomone, Project Manager for the CEUS SSC Project, conveyed the importance of this study to industry and government stakeholders, helped to coordinate our efforts, and facilitated communications among the Participatory Peer Review Panel (PPRP), CEUS SSC Project Team and Sponsors. Thanks to the reviewers whose comments and suggestions enhanced the depth and breadth of this report: TI Team member Stephen McDuffie, members of the PPRP and U.S. NRC staff, and Russell Wheeler of the U.S. Geological Survey.

CONTENTS

1 Development of the Paleoliquefaction Database	1
1.1 Database Structure	1
1.2 Regional Data Sets	4
1.2.1 New Madrid Seismic Zone and Surrounding Region	8
1.2.1.1 Overview	8
1.2.1.2 Data Description	9
1.2.1.3 Recommendations	9
1.2.2 Marianna, Arkansas, Area	10
1.2.2.1 Overview	10
1.2.2.2 Data Description	12
1.2.2.3 Recommendations	12
1.2.3 St. Louis Region	13
1.2.3.1 Overview	13
1.2.3.2 Data Description	14
1.2.3.3 Recommendations	14
1.2.4 Wabash Valley Seismic Zone and Surrounding Region	15
1.2.4.1 Overview	15
1.2.4.2 Data Description	16
1.2.4.3 Recommendations	16
1.2.5 Arkansas-Louisiana-Mississippi Region	17
1.2.5.1 Overview	17
1.2.5.2 Data Description	17
1.2.5.3 Recommendations	18
1.2.6 Charleston Seismic Zone	18
1.2.6.1 Overview	18
1.2.6.2 Data Description	18
1.2.6.3 Recommendations	19

1.2.7 Atlantic Coast Region and the Central Virginia Seismic Zone	20
1.2.8 Newburyport, Massachusetts, and Surrounding Region	20
1.2.8.1 Overview	20
1.2.8.2 Data Description	21
1.2.8.3 Recommendations	21
1.2.9 Charlevoix Seismic Zone and Surrounding Region	22
1.2.9.1 Overview	22
1.2.9.2 Data Description	23
1.2.9.3 Recommendations	23
2 Uncertainties Associated with Paleoliquefaction Data	24
2.1 Collection of Paleoliquefaction Data	24
2.1.1 Identification of Earthquake-Induced Liquefaction Features	25
2.1.2 Dating Liquefaction Features	27
2.1.3 Dating Techniques	28
2.1.3.1 Dendrochronology	29
2.1.3.2 Radiocarbon Dating	29
2.1.3.3 Optically Stimulated Luminescence	31
2.1.3.4 Archeological Context	32
2.1.3.5 Stratigraphic Context	33
2.1.3.6 Soil Development	34
2.2 Uncertainties Related to Interpretation of Paleoliquefaction Data	34
2.2.1 Timing of Paleoeearthquakes	35
2.2.2 Correlation of Liquefaction Features	36
2.2.3 Location of Paleoeearthquakes	37
2.2.4 Magnitude of Paleoeearthquakes	38
2.2.4.1 Comparative Studies	38
2.2.4.2 Empirical Relations	39
2.2.4.3 Geotechnical Analysis	40
2.2.5 Recurrence of Paleoeearthquakes	41
2.2.5.1 Age Estimates of Liquefaction Features and Paleoeearthquakes	41
2.2.5.2 Length and Completeness of the Paleoliquefaction Record	42

2.3 Recommendations for Future Research	42
3 Guidance for the Use of Paleoliquefaction Data in Seismic Source Characterization	44
4 Glossary	45
5 References	48
5.1 References Cited in Paleoliquefaction Database	48
5.2 References Cited in Appendix E	53

LIST OF FIGURES

Figure E-1. Map of CEUS showing locations of regional data sets included in the CEUS SSC Project paleoliquefaction database, including New Madrid seismic zone and surrounding region; Marianna, Arkansas, area; St. Louis region; Wabash Valley seismic zone and surrounding region; Arkansas-Louisiana-Mississippi region; Charleston seismic zone; Atlantic Coastal region and the Central Virginia seismic zone; Newburyport, Massachusetts, and surrounding region; and Charlevoix seismic zone and surrounding region.

Figure E-2. Diagram illustrating size parameters of liquefaction features, including sand blow thickness, width, and length; dike width; and sill thickness, as well as some of the diagnostic characteristics of these features.

Figure E-3. Diagram illustrating sampling strategy for dating of liquefaction features as well as age data, such as ^{14}C maximum and ^{14}C minimum, used to calculate preferred age estimates and related uncertainties of liquefaction features.

Figure E-4. GIS map of New Madrid seismic zone and surrounding region showing portions of rivers searched for earthquake-induced liquefaction features by M. Tuttle, R. Van Arsdale, and J. Vaughn and collaborators (see explanation); information contributed for this report. Map projection is USA Contiguous Albers Equal Area Conic, North America Datum 1983.

Figure E-5. GIS map of New Madrid seismic zone and surrounding region showing locations of liquefaction features for which there are and are not radiocarbon data. Map projection is USA Contiguous Albers Equal Area Conic, North America Datum 1983.

Figure E-6. GIS map of New Madrid seismic zone and surrounding region showing locations of liquefaction features that are thought to be historical or prehistoric in age or whose ages are poorly constrained. Map projection is USA Contiguous Albers Equal Area Conic, North America Datum 1983.

Figure E-7. GIS map of New Madrid seismic zone and surrounding region showing preferred age estimates of liquefaction features; features whose ages are poorly constrained are excluded. Map projection is USA Contiguous Albers Equal Area Conic, North America Datum 1983.

Figure E-8. GIS map of New Madrid seismic zone and surrounding region showing measured thicknesses of sand blows. Map projection is USA Contiguous Albers Equal Area Conic, North America Datum 1983.

Figure E-9. GIS map of New Madrid seismic zone and surrounding region showing preferred age estimates and measured thicknesses of sand blows. Map projection is USA Contiguous Albers Equal Area Conic, North America Datum 1983.

Figure E-10. GIS map of New Madrid seismic zone and surrounding region showing measured widths of sand dikes. Map projection is USA Contiguous Albers Equal Area Conic, North America Datum 1983.

Figure E-11. GIS map of New Madrid seismic zone and surrounding region showing preferred age estimates and measured widths of sand dikes. Map projection is USA Contiguous Albers Equal Area Conic, North America Datum 1983.

Figure E-12. GIS map of New Madrid seismic zone and surrounding region illustrating preferred age estimates and measured thicknesses of sand blows as well as preferred age estimates and measured widths of sand dikes for sites where sand blows do not occur. Map projection is USA Contiguous Albers Equal Area Conic, North America Datum 1983.

Figure E-13. GIS map of Marianna, Arkansas, area showing seismicity and locations of paleoliquefaction features relative to mapped traces of Eastern Reelfoot rift margin fault, White River fault zone, Big Creek fault zone, Marianna escarpment, and Daytona Beach lineament. Map projection is USA Contiguous Albers Equal Area Conic, North America Datum 1983.

Figure E-14. (A) Trench log and (B) ground-penetrating radar profile, showing vertical sections of sand blows and sand dikes at Daytona Beach SE2 site along the Daytona Beach lineament southwest of Marianna, Arkansas. Vertical scale of GPR profile is exaggerated (modified from Al-Shukri et al., 2009).

Figure E-15. GIS map of Marianna, Arkansas, area showing locations of liquefaction features for which there are and are not radiocarbon data. Map projection is USA Contiguous Albers Equal Area Conic, North America Datum 1983.

Figure E-16. GIS map of Marianna, Arkansas, area showing locations of liquefaction features that are thought to be historical or prehistoric in age or whose ages are poorly constrained. To date, no liquefaction features thought to have formed during 1811-1812 earthquakes have been found in area. Map projection is USA Contiguous Albers Equal Area Conic, North America Datum 1983.

Figure E-17. GIS map of Marianna, Arkansas, area showing preferred age estimates of liquefaction features; features whose ages are poorly constrained are excluded. Map projection is USA Contiguous Albers Equal Area Conic, North America Datum 1983.

Figure E-18. GIS map of Marianna, Arkansas, area showing measured thicknesses of sand blows. Map projection is USA Contiguous Albers Equal Area Conic, North America Datum 1983.

Figure E-19. GIS map of Marianna, Arkansas, area showing preferred age estimates and measured thicknesses of sand blows. Map projection is USA Contiguous Albers Equal Area Conic, North America Datum 1983.

Figure E-20. GIS map of Marianna, Arkansas, area showing measured widths of sand dikes. Map projection is USA Contiguous Albers Equal Area Conic, North America Datum 1983.

Figure E-21. GIS map of Marianna, Arkansas, area showing preferred age estimates and measured widths of sand dikes. Map projection is USA Contiguous Albers Equal Area Conic, North America Datum 1983.

Figure E-22. GIS map of St. Louis, Missouri, region showing seismicity and portions of rivers searched for earthquake-induced liquefaction features by Tuttle and collaborators; information contributed for this report. Map projection is USA Contiguous Albers Equal Area Conic, North America Datum 1983.

Figure E-23. GIS map of St. Louis, Missouri, region showing locations of liquefaction features, including several soft-sediment deformation structures, for which there are and are not radiocarbon data. Map projection is USA Contiguous Albers Equal Area Conic, North America Datum 1983.

Figure E-24. GIS map of St. Louis, Missouri, region showing locations of liquefaction features that are thought to be historical or prehistoric in age or whose ages are poorly constrained. Map projection is USA Contiguous Albers Equal Area Conic, North America Datum 1983.

Figure E-25. GIS map of St. Louis, Missouri, region showing preferred age estimates of liquefaction features; features whose ages are poorly constrained, including several that are prehistoric in age, are not shown. Map projection is USA Contiguous Albers Equal Area Conic, North America Datum 1983.

Figure E-26. GIS map of St. Louis, Missouri, region showing measured thicknesses of sand blows at similar scale as used in Figure E-8 of sand blows in New Madrid seismic zone. Note that few sand blows have been found in St. Louis region. Map projection is USA Contiguous Albers Equal Area Conic, North America Datum 1983.

Figure E-27. GIS map of St. Louis, Missouri, region showing preferred age estimates and measured thicknesses of sand blows. Map projection is USA Contiguous Albers Equal Area Conic, North America Datum 1983.

Figure E-28. GIS map of St. Louis, Missouri, region showing measured widths of sand dikes at similar scale as that used in Figure E-10 for sand dikes in New Madrid seismic zone. Map projection is USA Contiguous Albers Equal Area Conic, North America Datum 1983.

Figure E-29. GIS map of St. Louis, Missouri, region showing measured widths of sand dikes at similar scale as that used in Figures E-42 and E-48 for sand dikes in the Newburyport and Charlevoix regions, respectively. Map projection is USA Contiguous Albers Equal Area Conic, North America Datum 1983.

Figure E-30. GIS map of St. Louis, Missouri, region showing preferred age estimates and measured widths of sand dikes. Map projection is USA Contiguous Albers Equal Area Conic, North America Datum 1983.

Figure E-31. GIS map of Wabash Valley seismic zone and surrounding region showing portions of rivers searched for earthquake-induced liquefaction features (digitized from McNulty and Obermeier, 1999). Map projection is USA Contiguous Albers Equal Area Conic, North America Datum 1983.

Figure E-32. GIS map of Wabash Valley seismic zone and surrounding region showing measured widths of sand dikes at similar scale as that used in Figures E-10 and E-11 for sand dikes in New Madrid seismic zone. Map projection is USA Contiguous Albers Equal Area Conic, North America Datum 1983.

Figure E-33. GIS map of Wabash Valley region of Indiana and Illinois showing preferred age estimates and paleoearthquake interpretation. Map projection is USA Contiguous Albers Equal Area Conic, North America Datum 1983.

Figure E-34. GIS map of Arkansas-Louisiana-Mississippi (ALM) region showing paleoliquefaction study locations. Map projection is USA Contiguous Albers Equal Area Conic, North America Datum 1983.

Figure E-35. GIS map of Charleston, South Carolina, region showing locations of paleoliquefaction features for which there are and are not radiocarbon dates. Map projection is USA Contiguous Albers Equal Area Conic, North America Datum 1983.

Figure E-36. GIS map of Charleston, South Carolina, region showing locations of historical and prehistoric liquefaction features. Map projection is USA Contiguous Albers Equal Area Conic, North America Datum 1983.

Figure E-37. Map of Atlantic coast region showing areas searched for paleoliquefaction features by Gelinas et al. (1998) and Amick, Gelinas, et al. (1990). Rectangles indicate 7.5-minute quadrangles in which sites were investigated for presence of paleoliquefaction features. The number of sites investigated is shown within that quadrangle, if known. Orange and yellow indicate quadrangles in which paleoliquefaction features were recognized.

Figure E-38. Map of Central Virginia seismic zone region showing portions of rivers searched for earthquake-induced liquefaction features by Obermeier and McNulty (1998).

Figure E-39. GIS map of Newburyport, Massachusetts, and surrounding region showing seismicity and portions of rivers searched for earthquake-induced liquefaction features (Gelinas et al., 1998; Tuttle, 2007, 2009). Solid black line crossing map represents Massachusetts–New Hampshire border. Map projection is USA Contiguous Albers Equal Area Conic, North America Datum 1983.

Figure E-40. GIS map of Newburyport, Massachusetts, and surrounding region showing locations of liquefaction features for which there are and are not radiocarbon dates. Map projection is USA Contiguous Albers Equal Area Conic, North America Datum 1983.

Figure E-41. GIS map of Newburyport, Massachusetts, and surrounding region showing locations of liquefaction features that are thought to be historical or prehistoric in age or whose ages are poorly constrained. Map projection is USA Contiguous Albers Equal Area Conic, North America Datum 1983.

Figure E-42. GIS map of Newburyport, Massachusetts, and surrounding region showing measured widths of sand dikes. Map projection is USA Contiguous Albers Equal Area Conic, North America Datum 1983.

Figure E-43. GIS map of Newburyport, Massachusetts, and surrounding region showing preferred age estimates and measured widths of sand dikes. Map projection is USA Contiguous Albers Equal Area Conic, North America Datum 1983.

Figure E-44. Map of Charlevoix seismic zone and adjacent St. Lawrence Lowlands showing mapped faults and portions of rivers along which reconnaissance and searches for earthquake-induced liquefaction features were performed. Charlevoix seismic zone is defined by concentration of earthquakes and locations of historical earthquakes northeast of Quebec City.

Devonian impact structure in vicinity of Charlevoix seismic zone is outlined by black dashed line. Taconic thrust faults are indicated by solid black lines with sawteeth on upper plate; Iapetan rift faults are shown by solid black lines with hachure marks on downthrown side (modified from Tuttle and Atkinson, 2010).

Figure E-45. GIS map of Charlevoix seismic zone and surrounding region showing locations of liquefaction features, including several soft-sediment deformation structures, for which there are and are not radiocarbon data. Note the location of 1988 **M** 5.9 Saguenay earthquake northwest of the Charlevoix seismic zone. Map projection is USA Contiguous Albers Equal Area Conic, North America Datum 1983.

Figure E-46. GIS map of Charlevoix seismic zone and surrounding region showing locations of liquefaction features that are modern, historical, or prehistoric in age, or whose ages are poorly constrained. Map projection is USA Contiguous Albers Equal Area Conic, North America Datum 1983.

Figure E-47. GIS map of Charlevoix seismic zone and surrounding region showing preferred age estimates of liquefaction features; features whose ages are poorly constrained are excluded. Map projection is USA Contiguous Albers Equal Area Conic, North America Datum 1983.

Figure E-48. GIS map of Charlevoix seismic zone and surrounding region showing measured widths of sand dikes. Map projection is USA Contiguous Albers Equal Area Conic, North America Datum 1983.

Figure E-49. GIS map of Charlevoix seismic zone and surrounding region showing preferred age estimates and measured widths of sand dikes. Map projection is USA Contiguous Albers Equal Area Conic, North America Datum 1983.

Figure E-50. Photograph of moderate-sized sand blow (12 m long, 7 m wide, and 14 cm thick) that formed about 40 km from epicenter of 2001 **M** 7.7 Bhuj, India, earthquake (from Tuttle, Hengesh, et al., 2002), combined with schematic vertical section illustrating structural and stratigraphic relations of sand blow, sand dike, and source layer (modified from Sims and Garvin, 1995).

Figure E-51. Tree trunks buried and killed by sand blows, vented during 1811-1812 New Madrid earthquakes (from Fuller, 1912).

Figure E-52. Large sand-blow crater that formed during 2002 **M** 7.7 Bhuj, India, earthquake. Backpack for scale. Photograph: M. Tuttle (2001).

Figure E-53. Sand-blow crater that formed during 1886 Charleston, South Carolina, earthquake. Photograph: J.K. Hillers (from USGS Photograph Library).

Figure E-54. Photograph of sand blow and related sand dikes exposed in trench wall and floor in New Madrid seismic zone. Buried soil horizon is displaced downward approximately 1 m across two dikes. Clasts of soil horizon occur within dikes and overlying sand blow. Degree of soil development above and within sand blow suggests that it is at least several hundred years old and formed prior to 1811-1812 New Madrid earthquakes. Organic sample (location marked by red flag) from crater fill will provide close minimum age constraint for formation of sand blow. For scale, each colored intervals on shovel handle represents 10 cm. Photograph: M. Tuttle.

Figure E-55. Sand dikes, ranging up to 35 cm wide, originate in pebbly sand layer and intrude overlying diamicton. These features were exposed in cutbank along Cahokia Creek about 25 km northeast of downtown St. Louis (from Tuttle, 2000).

Figure E-56. Photograph of small diapirs of medium sand intruding base of overlying deposit of interbedded clayey silt and very fine sand, and clasts of clayey silt in underlying medium sand, observed along Ouelle River in Charlevoix seismic zone. Sand diapirs and clasts probably formed during basal erosion and foundering of clayey silt due to liquefaction of the underlying sandy deposit. Red portion of shovel handle represents 10 cm (modified from Tuttle and Atkinson, 2010).

Figures E-57. (A) Load cast formed in laminated sediments of Van Norman Lake during 1952 Kern County, California, earthquake. Photograph: J. Sims (from Sims, 1975). (B) Load cast, pseudonodules, and related folds formed in laminated sediment exposed along Malbaie River in Charlevoix seismic zone. Sand dikes crosscutting these same laminated sediments occur at a nearby site. For scale, each painted interval of the shovel handle represents 10 cm (modified from Tuttle and Atkinson, 2010).

Figure E-58. Log of sand blow and uppermost portions of related sand dikes exposed in trench wall at Dodd site in New Madrid seismic zone. Sand dikes were also observed in opposite wall and trench floor. Sand blow buries pre-event A horizon, and a subsequent A horizon has developed in top of sand blow. Radiocarbon dating of samples collected above and below sand blow brackets its age between 490 and 660 yr BP. Artifact assemblage indicates that sand blow formed during late Mississippian (300–550 yr BP or AD 1400–1670) (modified from Tuttle, Collier, et al., 1999).

Figures E-59. (A) Photograph of earthquake-induced liquefaction features found in association with cultural horizon and pit exposed in trench wall near Blytheville, Arkansas, in New Madrid seismic zone. Photograph: M. Tuttle. (B) Trench log of features shown in (A). Sand dike formed in thick Native American occupation horizon containing artifacts of early Mississippian cultural period (950–1,150 yr BP). Cultural pit dug into top of sand dike contains artifacts and charcoal used to constrain minimum age of liquefaction features (modified from Tuttle and Schweig, 1995).

Figure E-60. In situ tree trunks such as this one buried and killed by sand blow in New Madrid seismic zone offer opportunity to date paleoearthquakes to the year and season of occurrence. Photograph: M. Tuttle.

Figure E-61. Portion of dendrocalibration curve illustrating conversion of radiocarbon age to calibrated date in calendar years. In example, 2-sigma radiocarbon age of 2,280–2,520 BP is converted to calibrated date of 770–380 BC (from Tuttle, 1999).

Figure E-62. Empirical relation developed between A horizon thickness of sand blows and years of soil development in New Madrid region. Horizontal bars reflect uncertainties in age estimates of liquefaction features; diamonds mark midpoints of possible age ranges (from Tuttle et al., 2000)

Figure E-63. Diagram illustrating earthquake chronology for New Madrid seismic zone for past 5,500 years based on dating and correlation of liquefaction features at sites (listed at top) across region from north to south. Vertical bars represent age estimates of individual sand blows, and

horizontal bars represent event times of 138 yr BP (AD 1811-1812); 500 yr BP \pm 150 yr; 1,050 yr BP \pm 100 yr; and 4,300 yr BP \pm 200 yr (modified from Tuttle, Schweig, et al., 2002; Tuttle et al., 2005).

Figure E-64. Diagram illustrating earthquake chronology for New Madrid seismic zone for past 2,000 years, similar to upper portion of diagram shown in Figure E-63. As in Figure E-63, vertical bars represent age estimates of individual sand blows, and horizontal bars represent event times. Analysis performed during CEUS SSC Project derived two possible uncertainty ranges for timing of paleoearthquakes, illustrated by the darker and lighter portions of the colored horizontal bars, respectively: 503 yr BP \pm 8 yr or 465 yr BP \pm 65 yr, and 1,110 yr BP \pm 40 yr or 1055 \pm 95 yr (modified from Tuttle, Schweig, et al., 2002).

Figure E-65. Maps showing spatial distributions and sizes of sand blows and sand dikes attributed to 500 and 1,050 yr BP events. Locations and sizes of liquefaction features that formed during AD 1811-1812 (138 yr BP) New Madrid earthquake sequence shown for comparison (modified from Tuttle, Schweig, et al., 2002).

Figure E-66. Liquefaction fields for 138 yr BP (AD 1811-1812); 500 yr BP (AD 1450); and 1,050 yr BP (AD 900) events as interpreted from spatial distribution and stratigraphy of sand blows (modified from Tuttle, Schweig, et al., 2002). Ellipses define areas where similar-age sand blows have been mapped. Overlapping ellipses indicate areas where sand blows are composed of multiple units that formed during sequence of earthquakes. Dashed ellipse outlines area where historical sand blows are composed of four depositional units. Magnitudes of earthquakes in 500 yr BP and 1,050 yr BP are inferred from comparison with 1811-1812 liquefaction fields. Magnitude estimates of December (D), January (J), and February (F) main shocks and large aftershocks taken from several sources; rupture scenario from Johnston and Schweig (1996; modified from Tuttle, Schweig, et al., 2002).

Figure E-67. Empirical relation between earthquake magnitude and epicentral distance to farthest known sand blows induced by instrumentally recorded earthquakes (modified from Castilla and Audemard, 2007).

Figure E-68. Distances to farthest known liquefaction features indicate that 500 and 1,050 yr BP New Madrid events were at least of **M** 6.7 and 6.9, respectively, when plotted on Ambraseys (1988) relation between earthquake magnitude and epicentral distance to farthest surface expression of liquefaction. Similarity in size distribution of historical and prehistoric sand blows, however, suggests that paleoearthquakes were comparable in magnitude to 1811-1812 events or **M** \sim 7.6 (modified from Tuttle, 2001).

LIST OF TABLES

Table E-1.2-1. Summary of Information on Liquefaction Features in Regional Data Sets

Table E-1.2-2. Summary of Type and Prevalence of Paleoliquefaction Features

Table E-2.1.3. Summary of Dating Techniques Used in Paleoliquefaction Studies

Table E-2.2. Uncertainties Related to Interpretation of Paleoearthquake Parameters

E

APPENDIX

Over the past 30 years, paleoliquefaction studies have contributed to the understanding of the earthquake hazards of various regions in the Central and Eastern United States (CEUS) and southeastern Canada. Paleoliquefaction studies have provided estimates of ages, source areas, magnitudes, and recurrence times of large paleoearthquakes and uncertainties associated with these estimates. Given the need for this information in probabilistic seismic hazard assessment (PSHA), the paleoliquefaction task was undertaken to aid in the development of the seismic source model for the CEUS SSC Project. Under this task, a new paleoliquefaction database, including regional data sets, was created and this report was prepared, documenting and illustrating the database, discussing uncertainties associated with paleoliquefaction data, and providing guidance on the use of paleoliquefaction data in seismic source characterization.

All large data sets of paleoliquefaction features are included in the CEUS paleoliquefaction database, including those collected in the vicinity of the Charleston seismic zone in eastern South Carolina, the New Madrid seismic zone in southeastern Missouri, northeastern Arkansas, western Tennessee, and western Kentucky, the Wabash Valley seismic zone in southern Illinois and southern Indiana, and the Charlevoix seismic zone in southeastern Quebec (Figure E-1). The paleoliquefaction data compiled for this task are used to estimate recurrence rates and magnitudes of paleoearthquakes, critical seismic source parameters in PSHA and in characterization of seismic source zones for the CEUS SSC Project.

E.1 Development of the Paleoliquefaction Database

Building on a regional paleoliquefaction database for the New Madrid seismic zone and surrounding region previously developed by M. Tuttle & Associates, the Center for Earthquake Research and Information, and the U.S. Geological Survey, the new CEUS database includes readily available paleoliquefaction data gathered by a diverse group of investigators. The structure of the new database was designed to capture pertinent information for source characterization, as explained below. There are some significant differences between regional data sets in the types of features that have been used to identify paleoearthquakes in the geologic record and in the approaches used to estimate the ages and related uncertainties of paleoliquefaction features. These differences are discussed below for each regional data set.

E.1.1 Database Structure

This section describes the database structure, including definitions of column headings, units of measure, and other relevant information for all data entries. The database itself is available in digital format on the CEUS SSC Project website. For fields where no data are available or that do not apply, that database entry field is left blank. The following paragraphs describe each data field and provide information on how data was and was not tabulated. Each data field is

described individually and in the order in which they appear in the database. Discussions of earthquake-induced liquefaction features as well as various approaches and dating techniques used to estimate the ages of liquefaction features can be found in Sections E.2.1.1, E.2.1.2, and E.2.1.3. Figures E-2 and E-3 are provided to illustrate size parameters of liquefaction features and age data used to estimate preferred ages and related uncertainties of liquefaction features.

KEY: Unique numeric designator of study region for each entry in database. The following ranges are used for the specified priority study areas:

- 1000–1999: Alabama-Louisiana-Mississippi region (ALM)
- 2000–2999: Charleston seismic zone
- 3000–3999: Wabash Valley seismic zone and surrounding region
- 4000–4999: St. Louis, Missouri, region
- 5000–5999: New Madrid seismic zone and surrounding region
- 6000–6999: Marianna, Arkansas, area
- 7000–7999: Newburyport, Massachusetts, and surrounding region
- 8000–8999: Charlevoix seismic zone and surrounding region
- 9000–9999: Atlantic Coast Region and the Central Virginia Seismic Zone

SITE_NAME: Alphabetic designator of study site within study region.

FEAT_ID: Unique alphabetic paleoliquefaction feature identifier that includes shortened version of site name (example: “Bluf-2” indicates paleoliquefaction feature 2 from the Bluffton, South Carolina site).

XCOORD: Numeric value of longitude, in decimal degrees. All values should be negative (“-”). Coordinates of archeological sites rounded to 0.1 decimal degree to protect locations of sites.

YCOORD: Numeric value of latitude, in decimal degrees. All values should be positive. Coordinates of archeological sites rounded to 0.1 decimal degree to protect locations of sites.

COORD_ORIG: Alphabetic description (≤ 254 characters) of positional data for paleoliquefaction feature, including reference shorthand (examples: “digitized from Talwani and Schaeffer (2001) Figure 1” or “unpublished hand-held GPS coordinates from Tuttle”).

OBS_TYPE: Alphabetic description of observation type. Includes: trench, cutbank, aerial photograph, quarry, field mapping, and test pit / auger.

FEAT_TYPE: Alphabetic description of feature type. Includes: sand blow, crater fill, dike, sill, and SSD (for soft sediment deformation structures that are likely earthquake-related).

SSD_DESCR: Alphabetic description (≤ 254 characters) of SSD. This field is used only where “SSD” is entered in the FEAT_TYPE column. Includes description of SSD and assessment of likelihood that it is/is not earthquake-related. Features that are clearly non-earthquake-related are not included in the database.

FEAT_REF: Alphabetic description of citation shorthand for source of FEAT_TYPE information and, where applicable, SSD_DESCR.

SB_THICK, SB_WIDTH, SB_LENGTH, DK_WIDTH, and SILL_THICK: Numeric values of dimensions of sand blow thickness, sand blow width, sand blow length, dike width, and sill thickness, respectively (see Figure E-2). All dimensions are in cm. Because these dimensions typically are from limited trench exposures, values typically are minimum values (with a few exceptions). Additional descriptive information is entered into the COMMENT field(s), as needed.

DIM_REF: Alphabetic description of reference shorthand for dimensional values listed in previous five columns.

C14_MAX: Numeric value of lower bracketing 2-sigma radiocarbon age on feature, in yr BP relative to AD 1950.

C14_MIN: Numeric value of upper bracketing 2-sigma radiocarbon age on feature, in yr BP relative to AD 1950.

C14_REF: Alphabetic description of reference shorthand for radiocarbon data listed in previous two columns.

OSL_MAX: Numeric value of lower bracketing 2-sigma optically stimulated luminescence (OSL) age on feature, in yr BP relative to AD 1950.

OSL_MIN: Numeric value of upper bracketing 2-sigma OSL age on feature, in yr BP relative to AD 1950.

OSL_REF: Alphabetic description of reference shorthand for OSL data listed in previous two columns.

PREFAGEEST: Numeric value of preferred age estimate. In most cases, this will simply be the average or value midway between either: (1) C14_MAX and C14_MIN; and/or (2) OSL_MAX and OSL_MIN, in yr BP (see Figure E-3). However, in special circumstances, this value may represent a researcher's preferred age estimate, taking into account specific archeological, stratigraphic, or other criteria. Additional descriptive information is entered into the COMMENT field(s), as needed.

PREFAGEUNP: Numeric value of the upper bound of the preferred age estimate. This value represents the "+" portion of the 2-sigma "±" uncertainty value associated with the PREFAGEEST value.

- In most cases this value will be symmetric about the PREFAGEEST value. In other words, a preferred age estimate of 600 ± 200 yr BP is entered into the database as follows: "600" in PREFAGEEST field, "200" in the PREFAGEUNP field, and "200" in the PREFAGEUNM field.
- In some cases, the uncertainty will be asymmetric about the PREFAGEEST (e.g., $600 +200/-150$ yr BP). If so, "600" will appear in the PREFAGEEST field, "200" in the PREFAGEUNP field, and "150" in the PREFAGEUNM field (described below).

PREFAGEUNM: Numeric value of the lower bound of the preferred age estimate. This value represents the "-" portion of the 2-sigma "±" uncertainty value associated with the PREFAGEEST value. See above.

PREFAGEREF: Alphabetic description of reference shorthand for preferred age and preferred age uncertainty data listed in previous three columns.

STRAT: Alphabetic description of qualitative age data from stratigraphic relationships, if any. Also includes reference shorthand information.

ARCHEO: Alphabetic description of archaeological age data, if any. Also includes reference shorthand information.

WEATHERING: Alphabetic description of degree of weathering of feature (not weathering of surrounding sediments), if available. Also includes reference shorthand information.

GEOTEC: Alphabetic description of availability of geotechnical information describing paleoliquefaction feature. “Local” or “regional” indicate the type of geotechnical data available for the feature or site.

GEOTEC_REF: Alphabetic description of reference shorthand for geotechnical data listed in previous column.

COMMENT: Alphabetic description of other relevant data not captured in other fields. Note: if > 254 characters required, comments continued in COMMENT2 and COMMENT3 fields, as needed.

E.1.2 Regional Data Sets

All large data sets of paleoliquefaction features in the CEUS and southeastern Canada that have been described in published articles are included in the project paleoliquefaction database (Figure E-1). Summaries of regional data sets are provided below, including overviews of paleoliquefaction studies, descriptions of date types and age estimates, and recommendations for future research. In addition, maps were generated with the geographical information system (GIS) ArcGIS to illustrate the regional data sets and to show geographical and geological features mentioned in the text.

There are some significant differences between data sets, including the types of liquefaction features used to identify paleoearthquakes, information gathered about those features (e.g., their dimensions), basis of age estimates of the features, and overall quality of the data. A summary of the differences in the regional data sets is presented in Table E-1.2.-1. Additional information about the specific types of liquefaction features and their prevalence in the various regions is summarized in Table E-1.2.-2. To try to maintain consistency between data sets, we adopted well-established criteria that features must meet to be accepted as earthquake-induced liquefaction features and to be used in seismic source characterization. These criteria include the following (Obermeier, 1996; Tuttle, 2001):

- sedimentary characteristics consistent with case histories of earthquake-induced liquefaction;
- sedimentary characteristics indicative of sudden, strong, upwardly directed hydraulic force of short duration;
- occurrence of more than one type of liquefaction feature and of similar features at multiple locations;
- occurrence in geomorphic settings where hydraulic conditions described in (2) would not develop under nonseismic conditions; and
- age data to support both contemporaneous and episodic formation of features over a large area.

Table E-1.2-1. Summary of Information on Liquefaction Features in Regional Data Sets

Regional Data Set ¹	Type ²			Size ³	Age Estimate ⁴		Arch Data ⁵	Soils Data ⁶	Geotech Data ⁷	Quality ⁸
	SB	SD	SS		Num	Infer				
NMSZ	+	+	–	+	+	–	√	+	√	1
Marianna	+	+	–	+	+			+	√	2
St. Louis	–	+	√	+	√	–	–	+	√	2
WVSZ		+		–	–	+	–	–	√	3
ALM		–		√						4
CSZ	+		–		+	–			√	2
AC-CVA		–				√				3
NEWBURY		–		+	√	–		–		3
CxSZ	√	+	–	+	√	–		+	√	2

1. NMSZ = New Madrid seismic zone and surrounding region; WVSZ = Wabash Valley seismic zone and surrounding region; ALM = Arkansas-Louisiana-Mississippi region; CSZ = Charleston seismic zone; AC-CVA = Atlantic Coast and Central Virginia reconnaissance; NEWBURY = Newburyport, Massachusetts, and surrounding region; CxSZ = Charlevoix seismic zone and surrounding region (includes information of features that formed during 1988 Saguenay earthquake).
2. SB = sand blow; SD = sand dike; SS = other soft-sediment deformation structures (see Section E.2.1.1 and Glossary); + = many features; √ = some features; – = few features; blank = no features.
3. Size = measured dimension of liquefaction features provided; + = many features; √ = some features; – = few features; blank = no features.
4. Num = numerical, based on radiocarbon and or OSL dating; Infer = inferred, based on weathering characteristics and/or stratigraphic position.
5. Arch Data= archeological data helps to estimate age of liquefaction features.
6. Soils Data = information on soil and/or weathering characteristics of liquefaction features.
7. Geotech Data = geotechnical data used to assess liquefaction susceptibility of sediments and/or to estimate magnitude of paleoearthquake.
8. Quality = overall quality of data set based on feature type meeting identification criteria, availability of information on feature size, and age estimates based primarily on numerical minimum and maximum constraints; 1 = high quality; 2 = good quality; 3 = fair quality; 4 = low quality.

In addition, we identified sedimentary characteristics consistent with these criteria to facilitate the evaluation of regional data sets. These characteristics are based on studies of modern and historical earthquake-induced liquefaction features and are discussed in more detail in Section E.2 of this appendix (see Figure E-2). Sedimentary characteristics of earthquake-induced liquefaction features include the following:

- Sand blows or sand-blow craters (with feeder dikes)
 - Typically elliptical or linear, sometimes circular, in plan view
 - Connected to feeder dikes below
 - Often characterized by “cut-and-fill” structure and flow structures, and/or lineations, above the feeder dike

- Vented sediment typically fine to coarse sand, may include some silt and clay
- Often becomes finer-grained upsection and laterally away from feeder dike/vent
- Usually thins laterally away from feeder dike/vent
- May comprise multiple fining-up depositional units related to a sequence of earthquakes; seismites may be separated by layers of fines such as silty clay or clay that accumulated between earthquakes
- May contain clasts of host deposit, especially near feeder dike, clast size generally decreases with distance from vent
- Volume of vented deposit should “make sense” relative to size and number of sand dikes
- Subsidence structures may be seen near vent, including localized downwarping of surface soil and host strata and possible vertical displacement across feeder dikes
- Sand-blow craters often form in organic-rich soils or clay-rich host deposits
- Sand-blow craters contain vented sand deposits and clasts of host material; overlain by crater fill deposits and/or reworked material
- Sand dikes
 - Dike sidewalls typically subparallel, usually widen downward; also may broaden upward into vent structure at the ground surface (event horizon)
 - Typically a few meters to tens of meters long (in plan view); therefore, often, but not always, exposed in both walls of a trench
 - Sand within dikes often fines upward
 - Often characterized by flow structure or lineations
 - Often contain clasts of host deposit(s)
 - Near-vertical dikes may exhibit grading, with finer material along dike margins; inclined dikes may exhibit bedding
 - May be characterized by subsidiary dikes and/or sills
 - Source layer often lacks original sedimentary structure where fluidized, may exhibit flow structure or lineations as well as soft-sediment deformation structures such as ball-and-pillow structures and dish structures (see Glossary and Section E.2.1.1)

There also are significant differences between data sets in the approaches used to estimate the ages of paleoliquefaction features, and in the uncertainty associated with those age estimates. To minimize these differences, preferred age estimates and their associated uncertainty have been calculated for this project from 2-sigma minimum and maximum constraining ages for individual liquefaction features. The preferred age estimate is the average of the minimum and maximum values of the constraining age ranges (see Figure E-3). The uncertainty is the difference between the average and the minimum and maximum values of the constraining age ranges. Since they more closely reflect the ages of the liquefaction features, close minimum and close maximum constraining ages, as well as contemporary ages, are preferred over minimum and maximum constraining ages in calculating age estimates. In some cases, additional information provided by

archeological or stratigraphic context or by soil development in the liquefaction feature itself is used to help to estimate feature age. Differences in feature types and approaches used to estimate ages of paleoliquefaction features are discussed below in the summaries for each regional data set.

Table E-1.2-2
Summary of Type and Prevalence of Paleoliquefaction Features

Feature Type ¹	Prevalence ² of Paleoliquefaction Features in Regions ³									Selected References ⁴
	NMSZ	MAR	STL	WVSZ	ALM	CSZ	AC-CVA	NBY	CxSZ	
Sand blow	+	+	-	√		-			√	(a) (b) (c) (d) (e) (f) (g) (h) (i) (j) (k) (l) (m)
Sand-blow crater	√					+			-	(a) (n) (o) (p) (q)
Sand dike	+	+	+	+	-	√	-	√	+	(b) (e) (g) (n) (p) (r) (s) (t) (u) (v) (w) (x) (y) (z)
Sand sill	√	-	√	-				-		(d) (e) (f) (g) (j) (r)
Ball-and-pillow structure			-							(f) (g)
Basal erosion and sand diapirs	-	-	-						-	(f) (g) (z)
Dish structure	-	-								(f) (g)
Load casts			-						-	(f) (g) (z)
Pseudo-nodules	-		-						-	(f) (g) (z)

1. See Section E.2.1.1 and Glossary.
2. Prevalence of liquefaction features: + = many features; √ = some features; - = few features; blank = no features.
3. NMSZ = New Madrid seismic zone and surrounding region; MAR = Marianna Area; STL = St. Louis and surrounding region; WVSZ = Wabash Valley seismic zone and surrounding region; ALM = Arkansas-Louisiana-Mississippi region; CSZ = Charleston seismic zone; AC-CVA = Atlantic Coast and Central Virginia reconnaissance; NBY = Newburyport, Massachusetts, and surrounding region; CxSZ = Charlevoix seismic zone and surrounding region.
4. Selected references shown here (also see paleoliquefaction database and reference lists at the end of this report). (a) Amick, 1990; (b) Tuttle et al., 1990; (c) Saucier, 1991; (d) Hajic et al., 1995; (e) Munson and Munson, 1996; (f) Tuttle, 1999; (g) Tuttle, Chester, et al., 1999; (h) Tuttle, Schweig, et al., 2002; (i) Tuttle et al., 2005; (j) Al-Shukri et al., 2005; (k) Tuttle et al., 2006; (l) Wolf et al., 2006; (m) Talwani et al., 2008; (n) Tuttle et al., 1992; (o) Talwani et al., 1993; (p) Noller and Forman, 1998; (q) Talwani and Schaeffer, 2001; (r) Tuttle and Seeber, 1991; (s) Obermeier et al., 1991; (t) Obermeier et al., 1993; (u) Munson et al., 1995; (v) McNulty and Obermeier, 1999; (w) Broughton et al., 2001; (x) Cox, Larsen, et al., 2004; (y) Exelon, 2003, 2004; (z) Tuttle and Atkinson, 2010.

E.1.2.1 New Madrid Seismic Zone and Surrounding Region

E.1.2.1.1 Overview

In 1811-1812, a major earthquake sequence including three main shocks with moment magnitudes, **M** 7 to 8, and several large aftershocks, struck the central United States (Figures E-4 through E-12; e.g., Johnston, 1996c; Hough et al., 2000; Bakun and Hooper, 2004). These earthquakes are inferred to have been centered in the New Madrid seismic zone (NMSZ) and to include some of the largest known intraplate earthquakes in the world (Johnston and Kanter, 1990). The large liquefaction field produced by the 1811-1812 main shocks, including liquefaction more than 240 km from their inferred epicenters, supports the interpretation that they were very large-magnitude earthquakes (Fuller, 1912; Ambraseys, 1988; Johnston and Schweig, 1996; Tuttle, Schweig, et al., 2002; Castilla and Audemard, 2007).

During the past 20 years, various investigators have searched for and studied earthquake-induced liquefaction features in the NMSZ and surrounding region (Figures E-4 through E-12). Initially, most liquefaction features were assumed to have formed in 1811-1812; but attention to soil development and relations with cultural horizons and features at archeological sites led to the discovery of pre-1811 sand blows and related sand dikes (Saucier, 1991; Tuttle and Schweig, 1995; Tuttle, Lafferty, Guccione, et al., 1996). Since then, paleoseismic studies have focused on finding and dating paleoliquefaction features, constraining their ages, comparing their internal stratigraphy, size, and spatial distribution to features that formed during the 1811-1812 earthquakes, and estimating the locations, magnitudes, and recurrence times of their causative paleoearthquakes (e.g., Saucier, 1989; Tuttle, Schweig, et al., 2002; Figures E-5 through E-12). Some studies involved investigations of sand blows at archeological sites in the New Madrid seismic zone (e.g., Craven, 1995b; Tuttle et al., 1998, 2000, and 2005), whereas others involved searching for liquefaction features along drainage ditches and river cutbanks across the Mississippi River floodplain and along tributary valleys (Figure E-4; e.g., Vaughn, 1994; Li et al., 1998; Tuttle, 1999; Broughton et al., 2001).

The age estimates of liquefaction features across the region cluster around AD 1810 \pm 130 years, AD 900 \pm 100 years, AD 1450 \pm 150 years, and 2350 BC \pm 200 yr and were interpreted to be the dates of causative earthquakes (Figure E-7; Tuttle, Schweig, et al., 2002; Tuttle et al., 2005; Guccione, 2005). Other Holocene paleoliquefaction features have been documented across the region, suggesting additional paleoearthquakes, but the ages of these features are poorly constrained or do not correlate temporally with one another making interpretation difficult. One of these sand blows is similar in age to a “channel straightening” event of the Mississippi River attributed to reverse faulting on the Reelfoot thrust between 2,750 and 3,250 yr BP (Holbrook et al., 2006). In addition, several Late Wisconsin sand blows and dikes have been found in the Western Lowlands (Vaughn, 1994) and in western Kentucky (Tuttle, 2005a; see Figure E-7).

The size, compound nature, and spatial distributions of sand blows that formed circa AD 900 \pm 100 years and AD 1450 \pm 150 years were found to be strikingly similar to those that formed in 1811-1812 (Figures E-9 and E-12; Tuttle, 1999; Tuttle, Schweig, et al., 2002). The similarity between the historical and prehistoric liquefaction fields suggested that the paleoearthquakes were generated by the same source and had similar magnitudes, **M** 7 to 8, to the main shocks of the 1811-1812 sequence. These magnitude estimates were supported by several studies that conducted liquefaction potential analysis of geotechnical data collected in different parts of the region (e.g., Schneider and Mayne, 2000; Schneider et al., 2001; Liao et al., 2002; Stark, 2002;

Tuttle and Schweig, 2004). Taken together, the paleoliquefaction findings suggested that the NMSZ generated earthquake sequences including very large, **M** 7 to 8, main shocks every 500 years on average during the past 1,200 years (Tuttle, 1999; Tuttle, Schweig, et al., 2002).

E.1.2.1.2 Data Description

Paleoliquefaction data sets were contributed by the foremost researchers in the New Madrid region including M. Tuttle, J. Vaughn, R. Van Arsdale, R. Cox, and their collaborators and compiled in the CEUS SSC Project paleoliquefaction database. Additional paleoliquefaction data are drawn from journal articles, technical reports, and graduate student theses. All the data were previously published as indicated in the paleoliquefaction database. For this project, Tuttle, Vaughn, and Van Arsdale identified river sections searched by them and their collaborators, which allowed us to produce Figure E-4. All data were reviewed, 2-sigma minimum and maximum constraining ages entered, and preferred age estimates reassessed. Most of the radiocarbon ages were determined by Beta Analytic Radiocarbon Laboratory and calibrated using the Pretoria procedure (Talma and Vogel, 1993; Vogel et al., 1993). High precision radiocarbon ages were determined for several subsamples by the University of Washington Quaternary Isotope Laboratory. The results compared favorably to those of Beta Analytic. In addition, several calibrated dates provided by Beta Analytic were checked with the calibration program CALIB (Stuiver and Reimer, 1993; Stuiver et al., 2005). This exercise also produced similar results.

For most liquefaction features, preferred age estimates and related uncertainties are calculated from minimum and maximum constraining ages (Figure E-3). The constraining ages are usually 2-sigma calibrated radiocarbon dates, but in a few cases they are optically simulated luminescence (OSL) dates. For a few liquefaction features with only minimum or maximum age constraints and with other information that can help assess the feature's age (e.g., archeological horizons and features, soil development, and stratigraphic position), preferred age estimates have been assigned. In a few other cases, preferred age estimates and uncertainties have been calculated from close maximum radiocarbon dates. In these instances, the preferred age estimate is the average of the range of the 2-sigma calibrated date and the uncertainty is the difference between the average and the maximum and minimum values of the range. For features with neither minimum nor maximum constraining ages, no preferred age estimate is assigned, unless there are constraining ages for a similar feature in the same stratigraphic position at a nearby site. The paleoliquefaction data in this data set form the basis of the CEUS SSC Project analyses of the timing, location, and magnitude of paleoearthquakes that induced liquefaction in the NMSZ.

E.1.2.1.3 Recommendations

Although a great effort was made between 1995 and 2005 to understand paleoseismicity in the NMSZ and surrounding region, several important issues remain to be resolved that would improve understanding of the earthquake potential of the most hazardous region on the North American continent east of the Rocky Mountains. These issues include the uncertainty in recurrence times of large earthquakes, sources other than the NMSZ that may be capable of large earthquakes such as the Commerce and Eastern Reelfoot Rift Margin faults (e.g., Baldwin et al., 2006; Cox et al., 2006; Magnani and McIntosh, 2009), and migration of seismicity from one part of the Reelfoot Rift fault system to another (e.g., McBride et al., 2002; Tuttle et al., 2006; Al-

Shukri et al., 2009). Therefore, we recommend the following research to help resolve these issues:

- Additional paleoseismic studies in the NMSZ and surrounding region to improve completeness of the paleoearthquake record for the period 1–4 ka and to extend the earthquake chronology back to 10–20 ka. It would be advantageous to investigate sand blows at archeological sites where there would be a high probability of finding suitable organic material for narrowly constraining the ages of the sand blows and thus their causative earthquakes. At sites where in situ tree stumps are found buried beneath sand blows, dendrochronology may help to precisely date paleoearthquakes with uncertainty of a few months to a few years. In addition, it would be advisable to search for sand blows in Late Wisconsin deposits where there may be a longer and older record of paleoearthquakes. It may be advantageous to use OSL dating of sediments at sites of older liquefaction features where organic samples may not be available for radiocarbon dating. Information gained through these efforts would help to reduce uncertainties related to recurrence of large earthquakes.
- Additional paleoseismic studies in the vicinity and along other proposed active faults such as the Eastern rift margin and Commerce faults. Evaluate whether or not the ages and sizes of liquefaction features in close proximity to these faults support the hypothesis that the Eastern rift margin and Commerce faults generated repeated large earthquakes during the Late Wisconsin and Holocene. Additional information is needed to constrain the sizes and recurrence of paleoearthquakes produced by these seismic sources.
- Study of the spatial and temporal characteristics of paleoearthquakes across the region to determine if seismicity migrates from one part of the Reelfoot Rift fault system to another, and if so, if it migrates in a systematic way or with a certain periodicity. The results could help to characterize long-term deformation in the Reelfoot Rift region and may have implications for other aulacogens in intraplate settings.

E.1.2.2 Marianna, Arkansas, Area

E.1.2.2.1 Overview

The Marianna area is located at the southwestern end of the Reelfoot Rift and characterized by little to no seismic activity during the instrumental period (Al-Shukri et al., 2005; Figures E-12 and E-13). In the early 2000s, light-colored patches that appeared to represent large sand blows were identified on satellite images and aerial photographs of the Marianna area about 80 km southwest of the southern end of the NMSZ (Al-Shukri et al., 2005; Figure E-12). Several of these features southwest of Marianna were located on the ground, surveyed with ground-penetrating radar (GPR), and excavated (Figures E-13 and E-14). Trench exposures revealed large sand blows and related feeder dikes. No suitable organic samples were collected for radiocarbon dating, but their high degree of weathering suggested that the sand blows were prehistoric in age.

Subsequently, several other sand blows were excavated, including an exceptionally large (approximately 2.45 m thick, 70 m wide, and 230 m long) sand blow that occurred along a northwest-oriented lineament, referred to as the Daytona Beach lineament (Figures E-13 and E-15 through E-21; Al-Shukri et al., 2006; Tuttle et al., 2006). Radiocarbon and OSL dating of

the buried soil immediately below the sand blow provided a close maximum age constraint of about 5,500 years for the formation of the sand blow (Figures E-17 and E-19; Tuttle et al., 2006). The sand blow's large feeder dike had a strike similar to the lineament. Noting that other large sand blows and sand dikes occurred along the Daytona Beach lineament, the researchers proposed that the lineament is the surface expression of an active fault (Figure E-13; Al-Shukri et al., 2006; Tuttle et al., 2006). In addition, a compound sand blow with the uppermost sand blow interbedded with the basal layers of a backswamp deposit was discovered northeast of Marianna during reconnaissance of the St. Francis Ditch. Radiocarbon and OSL dating of the backswamp deposit immediately above the sand blow provided close minimum age constraint of about 6,800 years (Figures E-17 and E-19; Tuttle et al., 2006).

During the past 5 years, numerous sand blows identified on satellite images and aerial photographs of the Marianna area were confirmed in soil pits, trenches, and with GPR surveys that imaged sand dikes below the sand blows (Figures E-14 through E-21; Al-Shukri et al., 2009; Al-Qadhi, 2010). Many of these sand blows occur along the Daytona Beach lineament that was traced for a total of 17 km by conducting GPR surveys (Figure E-13). One of the trenched sand blows along the lineament is composed of two stratigraphically stacked sand blows and several large feeder dikes. A possible fault, similar in strike to the Daytona Beach lineament, crosscuts one of the large feeder dikes and extends into the upper sand blow (Figure E-14, sand blow 2 on trench log). Layering and layer thickness within the upper sand blow varies across the possible fault suggesting lateral displacement. Both sand blows exposed in the trench were weathered, but the lower, smaller sand blow was especially so (Figure E-14, sand blow 1 on trench log). Radiocarbon and OSL dating of the buried soil immediately below the upper sand blow provided close maximum age constraints of about 10 ka and 12 ka, respectively (Al-Shukri et al., 2009). OSL dating of a sample collected from the soil immediately below the smaller lower sand blow indicates that it formed less than 38 ka. The researchers have concluded that there is a 12 k.y., and possibly 38 k.y., long history of strong ground shaking in the vicinity of the Daytona Beach lineament. The length and linear morphology of the Daytona Beach lineament, as well as the observation of a possible fault crosscutting a large sand blow that formed along the lineament, support the interpretation that the lineament is the surface expression of an active fault.

The sand blows in the Marianna area have been attributed to large paleoearthquakes generated by a source in the Marianna area, possibly the southwestern extension of the Eastern rift margin fault, or the northwest-oriented White River fault zone (WRFZ), or both (Figure E-13; Tuttle et al., 2006; Al-Shukri et al., 2009). As observed in the NMSZ, compound sand blows are indicative of sequences of large earthquakes resulting from complex fault interaction (Saucier, 1989; Tuttle, 1999). As discussed above, the Daytona Beach lineament, subparallel to the nearby WRFZ, may be the surface expression of an active fault (Tuttle et al., 2006; Al-Shukri et al., 2009). The large size of the Marianna sand blows and their spatial association with local faults suggest that the causative earthquakes were centered near Marianna (Figures E-13 and E-18 through E-21). The sand blows are thought not to be distant liquefaction features produced by a large New Madrid earthquake. The ages of the Marianna sand blows do not correlate with events in the New Madrid paleoearthquake chronology and no sand blow has yet been found in the Marianna area that is less than 5,000 years old and could have formed during the historical or prehistoric New Madrid earthquakes.

The investigators noted that a few liquefaction features have been found elsewhere in the Mississippi embayment that are similar in age (approximately 5,500 years) but smaller in size

than some of the Marianna sand blows (Tuttle et al., 2006; Tuttle, 2010). These include a sand blow and related feeder dikes near Marked Tree, Arkansas, about 80 km northeast of Marianna (Figure E-12). According to empirical relations between earthquake magnitude and distance to surface manifestation of liquefaction (i.e., sand blows; Ambraseys, 1988; Castilla and Audemard, 2007), a $M \sim 6.6$ earthquake could produce sand blows up to 80 km from its epicenter. Therefore, a large earthquake centered near Marianna might be responsible for the 5,500-year-old liquefaction features near Marked Tree (Tuttle, 2010).

E.1.2.2.2 Data Description

Paleoliquefaction data were contributed by H. Mahdi, O. Al-Qahdi, H. Al-Shukri, and M. Tuttle for the Marianna, Arkansas, area and compiled in the CEUS SSC Project paleoliquefaction database. Most of the data were previously published in journal articles, technical reports, and graduate student theses as indicated in the paleoliquefaction database. For this project, all the data were reviewed, 2-sigma minimum and maximum constraining ages entered, and preferred age estimates calculated. All of the radiocarbon ages were determined by Beta Analytic Radiocarbon Laboratory and calibrated using the Pretoria procedure (Talma and Vogel, 1993; Vogel et al., 1993).

In the Marianna area, most of the samples used in radiocarbon and OSL dating were collected from buried soil immediately below sand blows and provide close maximum age constraint (see Figure E-3). A few samples were collected above sand blows and provide close minimum age constraint. Constraining ages are derived from 2-sigma calibrated radiocarbon dates and from a few OSL dates. In calculating preferred age estimates, radiocarbon dates are given preference over OSL dates since the radiocarbon dates have smaller uncertainties. In most cases, preferred age estimates and related uncertainties of liquefaction features have been calculated from either close maximum or close minimum radiocarbon dates, not both. The preferred age estimate is the average of the range of the 2-sigma calibrated date and the uncertainty is the difference between the average and the end members of the range. No preferred age estimate is assigned to features that have neither close minimum nor close maximum constraining ages. The paleoliquefaction data in this data set form the basis of the CEUS SSC Project analyses of the timing, location, and magnitude of paleoearthquakes that induced liquefaction in the Marianna area.

E.1.2.2.3 Recommendations

Paleoseismic studies have been conducted in the Marianna area over the past 10 years but have been limited in scope. Most of the work has been concentrated along the northwest-oriented Daytona Beach lineament (Figure E-13). The compound nature of some of the sand blows suggests that multiple faults may rupture in a short period of time to produce earthquake sequences much like the NMSZ. Clearly, there is still much more to be learned in the Marianna area regarding the timing, location, and magnitude of paleoearthquakes that would help to improve the earthquake source model at the southern end of the Reelfoot Rift. To these ends, we recommend the following research:

- Additional paleoseismic investigations of sand blows in the Marianna area including those spatially associated with the northwest-oriented lineament and the northeast-oriented extension of the Eastern Rift fault and other sand blows not associated with any lineament or fault trend. It may be necessary to use OSL dating of sediments buried by sand blows at sites of older liquefaction features where organic samples are not available for radiocarbon dating.

- Additional reconnaissance for and investigation of liquefaction features in the region surrounding Marianna. More information on the ages, size, and spatial distribution of sand blows will help to constrain the timing, locations, and magnitudes of the paleoearthquakes in the region.
- Liquefaction potential analysis of geotechnical data already collected by the USGS and the Arkansas State Highway and Transportation Department to help assess the magnitudes of the paleoearthquakes in the Marianna area.
- Further development of an earthquake chronology for the Marianna area and comparison of the chronology with that for the NMSZ and with the fault displacement history of the Eastern rift margin fault in western Tennessee.
- Geophysical investigations to determine if the Daytona Beach lineament is underlain by a fault and to help assess its long-term displacement history.

E.1.2.3 St. Louis Region

E.1.2.3.1 Overview

In contrast to the NMSZ about 200 km to the south-southeast, the St. Louis region is characterized by low to moderate seismic activity (Figures E-4 and E-22; Nuttli and Brill, 1981; Johnston and Schweig, 1996). A diffuse concentration of seismicity extends northwest from the NMSZ to St. Louis. Seismicity in this region often is attributed to reactivation of old basement faults and earthquake epicenters are spatially associated with the St. Louis fault (Harrison, 1997) and the Centralia fault zone (Mitchell et al., 1991). Over the last 20 years, however, seismicity has not been directly related to any mapped basement structures.

Since the initial discovery of sand dikes along the Kaskaskia River east of St. Louis, paleoseismology studies have documented scores of liquefaction features along rivers in southwestern Illinois and southeastern Missouri (Figures E-22 through E-30; Hajic et al., 1995; McNulty and Obermeier, 1997, 1999; Tuttle, Lafferty, Chester, et al., 1996; Tuttle, Chester, et al., 1999; Tuttle et al., 2004; see also Figures E-31 through 33 and Section E.1.2.4). There are at least two generations of liquefaction features that are Holocene in age. Some of the features are young and probably formed during the 1811-1812 New Madrid earthquakes, known to have induced liquefaction near Cahokia, Illinois. Other features are middle Holocene in age and probably formed during an earthquake about 6,470 yr BP \pm 160 yr (Figures E-24, E-25, E-27, and E-30; Tuttle, Lafferty, Chester, et al., 1999).

McNulty and Obermeier (1997, 1999) attributed the middle Holocene liquefaction features in the Shoal Creek-Kaskaskia River area to a $M > 6$ earthquake located near the lower portion of Shoal Creek (Figure E-33). The earthquake source area was inferred from the distribution and widths of sand dikes. The magnitude of the earthquake was derived from the relation between earthquake magnitude and maximum epicentral distance to surface evidence of liquefaction (e.g., Ambraseys, 1988). Tuttle et al. (Tuttle, Lafferty, Chester, et al., 1996; Tuttle, Chester, et al., 1999; Tuttle et al., 2004) found liquefaction features, mostly sand dikes and one sand blow, in the St. Louis region along the Big Muddy, Kaskaskia, and Marys rivers and Cahokia, Crooked, Mud, Piasa, Shoal, and Silver creeks in Illinois and along the Big and Meramec rivers and Saline Creek in Missouri (Figures E-23 through E-30). The largest dikes occur along Shoal Creek, but

fairly large dikes also occur along Cahokia Creek and the Meramec River (Figures E-26 through E-29). The age estimates of many of the sand dikes are poorly constrained and regional correlation problematic (Figure E-30). Various locations and magnitudes of scenario earthquakes were evaluated using liquefaction potential analysis that could explain the observed distribution of liquefaction features (Tuttle, Lafferty, Chester, et al., 1999).

E.1.2.3.2 Data Description

Paleoliquefaction data were contributed by M. Tuttle and collaborators in the St. Louis region and compiled in the CEUS SSC Project paleoliquefaction database. Most of the data were published in technical reports to the U.S. NRC and U.S. Geological Survey as indicated in the database. Tuttle identified river sections searched by her and collaborators that allowed us to produce Figure E-22. All the data were reviewed, 2-sigma minimum and maximum constraining ages entered, and preferred age estimates calculated. All of the radiocarbon ages were determined by Beta Analytic Radiocarbon Laboratory and calibrated using the Pretoria procedure (Talma and Vogel, 1993; Vogel et al., 1993). Paleoliquefaction data gathered in this region by E. Hajic, S. Obermeier, and collaborators are included in the data set for the Wabash Valley seismic zone (see discussion below).

Paleoseismic data in the St. Louis regional data set are from reconnaissance-level studies. Most of the liquefaction features found in the area are sand dikes (Tables E-1.2-1 and E-1.2-2). The ages of the liquefaction features are poorly constrained, except for a few features that formed during the historic period and about 6,470 yr BP (Figure E-25). Some of the sand dikes are greater than 30 cm in width, suggesting that the paleoearthquake responsible for their formation was located in the St. Louis region (Figures E-19 and E-30). However, given that the 1811-1812 New Madrid earthquakes induced liquefaction near St. Louis and several historical sand dikes have been found in the region, it raises the question whether some of the paleoliquefaction features could have formed during paleoearthquakes generated by the NMSZ. To date, no known New Madrid paleoearthquake occurred circa 6,470 yr BP (Figure E-12). The paleoliquefaction data in this data set contributed to the CEUS SSC Project analyses of the timing, location, and magnitude of paleoearthquakes that induced liquefaction in the St. Louis region.

E.1.2.3.3 Recommendations

Additional study and dating of liquefaction features in the St. Louis region is needed to better constrain the number and timing of paleoearthquakes and to make regional correlations of similar-age liquefaction features. A more complete picture of the size and spatial distributions of liquefaction features would help to reduce the uncertainty of the location and magnitudes of paleoearthquakes, including the 6,470 yr BP event. Therefore, the following research is recommended:

- Add overlapping portion of Wabash Valley data set to St. Louis data set, reviewing each site to avoid duplication.
- Resurvey portions of the Meramec and Kaskaskia rivers and Shoal and Cahokia creeks, where the largest have been found (Figures E-26, E-28, and E-29), in the hopes of finding additional sand blows and collecting samples above and below the sand blows for radiocarbon and OSL dating. At the same time, try to relocate documented liquefaction sites and collect samples for radiocarbon and OSL dating that would improve age estimates of

liquefaction features. These efforts would likely improve estimates of the timing, locations, and magnitudes of paleoearthquakes.

- Study whether the liquefaction features in the Shoal Creek–Kaskaskia River area (Figures E-26, E-28, and E-29) could be due to earthquake characteristics such as directivity of ground motions, Moho bounce, or site amplification of ground motions generated by large New Madrid earthquakes. This effort would likely reduce uncertainties related to the locations and magnitudes of paleoearthquakes.

E.1.2.4 Wabash Valley Seismic Zone and Surrounding Region

E.1.2.4.1 Overview

Numerous small- to moderate-magnitude earthquakes have occurred in the Wabash Valley region of southeastern Illinois and southwestern Indiana in historical time. Paleoliquefaction features identified in the region provide evidence for multiple older, moderate- to large-magnitude earthquakes (e.g., Obermeier et al., 1991, 1993; Hajic et al., 1995; Munson et al., 1995, 1997; Munson and Munson, 1996; Obermeier, 1996, 1998, 2009; and McNulty and Obermeier, 1999; Figures E-31 through E-33). The causative fault or faults for the Wabash Valley paleoearthquakes are not known. The great majority of the paleoliquefaction features in the Wabash Valley region are sand dikes found along actively eroding stream banks, but researchers also have identified sand blows and sand sills. Figure E-31 shows river sections searched for liquefaction features and was produced by digitizing published maps from Munson et al. (1997) and McNulty and Obermeier (1999).

The identification of paleoearthquakes in the Wabash Valley region primarily is based on age estimates of paleoliquefaction features, the regional pattern of paleoliquefaction features (especially dike widths), and geotechnical analyses of liquefaction potential. Researchers interpret from six (Munson and Munson, 1996) to eight (McNulty and Obermeier, 1999) Holocene earthquakes, with at least one more during latest Pleistocene time. Based on overlapping radiocarbon ages and the spatial distribution and widths of dikes, McNulty and Obermeier (1999) correlate paleoliquefaction features between sites to estimate the timing, location, and magnitude of paleoearthquakes in the Wabash Valley region (Figure E-33). Magnitude estimates for the paleoearthquakes range from **M** 6 to ~7.8 (Pond and Martin, 1997; Obermeier, 1998; McNulty and Obermeier, 1999; Green et al., 2005; Olson et al., 2005b).

Section 6.1.9 of the main report provides detailed discussion of magnitude estimates for the interpreted paleoearthquakes in the Wabash Valley region. The two largest earthquakes inferred from paleoliquefaction data are the Vincennes-Bridgeport and Skelton–Mt. Carmel paleoearthquakes. The **M** ~7 to 7.8 Vincennes paleoearthquake occurred at approximately 6,100 ± 200 yr BP (Hajic et al., 1995; Munson and Munson, 1996; Munson et al., 1997). The **M** ~6.3 to 7.3 Skelton paleoearthquake occurred at approximately 12 k.y. ± 1,000 yr BP (Munson and Munson, 1996; Munson et al., 1997). The energy centers for these two earthquakes are inferred to be located within 25–40 km (15.5–25 mi.) of Vincennes, Indiana (Munson et al., 1997; McNulty and Obermeier, 1999).

E.1.2.4.2 Data Description

Paleoliquefaction data are drawn from published journal articles and reports by the foremost researchers in the Wabash Valley region, including S. Obermeier, P. Munson, and E. Hajic (Hajic et al., 1995; Munson et al., 1995; Munson and Munson, 1996; Obermeier, 1998; McNulty and Obermeier, 1999), as well as from a technical report to the Exelon Generation Company's Clinton site in central Illinois (Exelon, 2003, 2004). Most of the liquefaction features found in the Wabash Valley area are planar, sand-filled dikes (Tables E-1.2-1 and E-1.2-2) that are vertically to steeply dipping and that widen downward and connect to a sediment source at depth (Obermeier et al., 1991). Apparent widths of these sand dikes were measured in the field, the largest of which is 2.5 m wide (Munson and Munson, 1996). Ages of some of these dikes are estimated from radiocarbon dating of organic-rich materials collected from the sediment crosscut by the sand dikes, with supporting evidence from archeological and stratigraphic context, and the relative degree of soil profile development (Hajic et al., 1995; Munson et al., 1995; Munson and Munson, 1996; Obermeier, 1998; McNulty and Obermeier, 1999). For this regional data set, we did not estimate preferred age estimates of liquefaction features because we did not have the necessary information to do so (e.g., C14 or OSL sample location relative to sand dikes and sand blows). Instead, we entered the investigators' assigned ages into the database.

E.1.2.4.3 Recommendations

Numerous researchers have studied paleoliquefaction in the Wabash Valley region during the past 20 years, and this research is ongoing. As a result, the Wabash Valley data set is relatively mature. However, we recommend the following as useful topics for future paleoliquefaction research in the Wabash Valley region:

- Re-evaluation of previously collected age data and estimation of preferred age estimates of liquefaction features.
- Additional sampling and age analyses to further refine and reduce uncertainties of age estimates and correlation of paleoliquefaction features between sites, if possible.
- Additional geotechnical testing to provide better estimates for the locations and magnitudes of paleoearthquakes, as recommended by McNulty and Obermeier (1999).
- Additional reconnaissance in the northern part of the Illinois basin where moderate-sized earthquakes are recorded in the instrumental record. Documenting the presence or absence of paleoearthquakes in the northern part of the basin in an area with similar susceptible deposits would help to better evaluate the apparent spatial stationarity of earthquakes in the southern part of the Illinois basin.

E.1.2.5 Arkansas-Louisiana-Mississippi Region

E.1.2.5.1 Overview

Cox and collaborators have conducted studies in southeastern Arkansas, northeastern Louisiana, and western Mississippi areas (ALM) investigating what they interpret to be paleoliquefaction features related to moderate- to large-magnitude earthquakes possibly produced by the Saline River fault zone in southeastern Arkansas (Cox, 2002, 2009; Cox, Harris, et al., 2004; Cox, Larsen, et al., 2004; Cox, Larsen, and Hill, 2004; Cox and Larsen, 2004; Cox and Gordon, 2008;

Figure E-34). Many of the features interpreted as earthquake-induced liquefaction features were not reviewed in the field by other geologists with prior experience with such features. The ALM observations and interpretations can be summarized as follows:

- On aerial photographs, Cox and collaborators observed roughly circular light-colored patches throughout the Arkansas and Mississippi River valleys between southeastern Arkansas and northeastern Louisiana and interpreted the patches to be seismically induced sand blows.
- In trenches excavated at seven locations, sandy deposits and crosscutting features were observed and interpreted as sand blows and sand dikes, respectively, and attributed to several episodes of earthquake-induced liquefaction.
- On the basis of similar sedimentary stratigraphy as well as radiocarbon and OSL dating of deposits, Cox and collaborators attributed the features they interpreted as sand blows and sand dikes to several moderate- to large-magnitude earthquakes centered near the Saline River fault zone.

As part of the CEUS SSC Project, the results of the investigations by Cox and collaborators in the ALM were evaluated to determine if there is either (1) paleoseismic evidence of repeated large-magnitude earthquakes; or (2) evidence for a single large-magnitude Quaternary event that might affect seismic source characterization. As described in Section 7.3.9 (Extended Continental Crust-Gulf Coast, or ECC-GC) of the main CEUS SCC Project report, no evidence was found for repeated large-magnitude earthquakes and little to no evidence was found for large ($M > 6$) earthquakes during a review of published papers as well as original photographs and logs.

In general, the ALM features did not exhibit sedimentary characteristics typical of earthquake-induced liquefaction features and therefore did not meet the criteria adopted for this project and described above in Section E.1.2. More specifically, the sandy deposits interpreted as sand blows often lacked a clear connection to sand dikes below and rarely appeared to thin and fine laterally away from the main feeder dike. Many of the features interpreted as sand dikes lacked clear margins and lateral continuity and rarely broadened downward. The best candidate for a paleoliquefaction feature comes from the west wall of the Portland, Arkansas, trench, where a possible small (<6 cm wide) dike is shown in logs and photographs at approximately meter 4.5 (Cox, Larsen, et al., 2004). It remains unclear whether this relatively small dike is the result of (1) a moderate-magnitude local earthquake; (2) a larger, more distant earthquake; or (3) non-earthquake processes. Other small sand dikes may occur in other trenches. Please see Section 7.3.9 of the main CEUS SCC Project report for a thorough discussion of the evaluation of the ALM features.

E.1.2.5.2 Data Description

Paleoliquefaction data for the ALM region were contributed by R. Cox and drawn from journal articles and technical reports by Cox and his collaborators. We reviewed the paleoliquefaction data from the ALM region and consider them highly uncertain and the data set relatively immature. These data do not provide evidence for a source of repeated large-magnitude earthquakes in the ALM region. The CEUS paleoliquefaction database includes the locations of seven paleoseismic trenches in the ALM region (Cox, Harris, et al., 2004; Cox, Larsen, et al.,

2004; Cox et al., 2007; Figure E-34), with a brief description of the researchers' interpreted results provided in the COMMENT data field.

E.1.2.5.3 Recommendations

As determined for the CEUS SSC Project (see Section 7.3.9 of the main report), the paleoliquefaction data from the ALM region are considered highly uncertain and do not provide evidence for a source of repeated large-magnitude earthquakes in the ALM area. We recommend the following as topics for future paleoliquefaction research in the ALM region:

- Additional field work and trenching to evaluate the interpretation that the roughly circular sandy deposits observed in aerial photographs are earthquake-induced sand blows (e.g., Cox, Harris, et al., 2004; Cox, Larsen, et al., 2004; Cox et al., 2007; Cox, 2009) or if they formed by some other means.
- Additional sampling and age analyses to further refine the timing and correlation of any paleoliquefaction features between trench sites and with other areas of paleoliquefaction such as the Marianna area, if possible.

E.1.2.6 Charleston Seismic Zone

E.1.2.6.1 Overview

Strong ground shaking during the 1886 Charleston, South Carolina, earthquake produced extensive liquefaction expressed primarily as sand-blow craters at the ground surface (Dutton, 1889). Liquefaction features from the 1886 event are preserved in geologic deposits at numerous locations in the South Carolina coastal region (e.g., Talwani and Cox, 1985; Amick, 1990; Amick, Gelinas, et al., 1990; Amick, Maurath, and Gelinas, 1990; Amick and Gelinas, 1991; Obermeier et al., 1989, 1990; and Talwani and Schaeffer, 2001; Figures E-35 and E-36). Documentation of sand-blow craters and other paleoliquefaction features throughout coastal South Carolina provides evidence for prior strong ground motions during prehistoric large earthquakes (e.g., Obermeier et al., 1989, 1990; Weems and Obermeier, 1990; Amick, Gelinas, et al., 1990; Amick, Maurath, and Gelinas, 1990; Talwani and Schaeffer, 2001; Talwani et al., 2008; Figures E-35 and E-36). Talwani and Schaeffer (2001) interpret between three and four large-magnitude earthquakes in the past approximately 2,000 years, and between five and seven large-magnitude earthquakes in the past approximately 5,800 years.

As described in more detail in Section E.1.2.7, reconnaissance-level searches for paleoliquefaction features have been conducted along the eastern seaboard (e.g., Amick, Gelinas, et al., 1990; Gelinas et al., 1998; Figure E-37). These studies did not find paleoliquefaction features beyond the Charleston region and suggest a stationary source of repeated, large-magnitude earthquakes located near Charleston.

E.1.2.6.2 Data Description

Data for the Charleston region in the CEUS SSC study paleoliquefaction database primarily are taken from Talwani and Schaeffer's (2001) compilation, with additional data from other studies (e.g., Noller and Forman, 1998; Talwani et al., 2008). Most of the age estimates of paleoliquefaction features in coastal South Carolina are based on radiocarbon dating. Noller and Forman (1998) present luminescence age estimates for five samples collected from sand-blow

craters exposed at Gapway, South Carolina. However, they emphasize that their reported age estimates are preliminary and “should be used with caution” (Noller and Forman, 1998, pp. 4-56). Therefore, the age estimates of paleoliquefaction features used by the CEUS SSC Project to constrain the timing of prehistoric earthquakes in the Charleston region are based on radiocarbon analyses. Talwani and Schaeffer (2001) combine radiocarbon ages from previously published sources with their own studies of paleoliquefaction features in the South Carolina coastal region. Their compilation forms the basis of the CEUS SSC Project analyses of Charleston paleoliquefaction. These data include ages that provide contemporary, minimum, and maximum limiting ages for the formation of paleoliquefaction features.

Talwani and Schaeffer (2001) identify individual earthquake episodes based on samples with a “contemporary” age constraint that have overlapping calibrated radiocarbon ages at approximately 1-sigma confidence interval. The standard in paleoseismology, however, is to use calibrated ages with 2-sigma (95.4 percent confidence interval) error bands (Grant and Sieh, 1994). Likewise, in paleoliquefaction studies, to more accurately reflect the uncertainties in radiocarbon dating and age estimates of paleoliquefaction features, Tuttle (2001) advises the use of calibrated radiocarbon dates with 2-sigma error bands (as opposed to narrower 1-sigma error bands). In recognition of this, the conventional radiocarbon ages presented in Talwani and Schaeffer (2001) are recalibrated and reported with 2-sigma error bands for use in the CEUS SSC Project. This recalibration was performed with the radiocarbon calibration program OxCal version 4.1 (Bronk Ramsey, 2009) using the calibration curve of Stuiver et al. (1998). The recalibrated 2-sigma radiocarbon ages form the basis of the CEUS SSC Project analyses of the timing, location, and magnitude of paleoearthquakes that induced liquefaction in the vicinity of Charleston, South Carolina. Section 6.1.2 of the main report provides additional discussion of the earthquake chronology for the Charleston seismic zone, including space-time diagrams and tabulated results.

E.1.2.6.3 Recommendations

Numerous researchers have studied paleoliquefaction in the Charleston region during the past 30+ years, and this research is ongoing. As such, the Charleston data set is relatively mature. However, we recommend the following as useful topics for future paleoliquefaction research in the Charleston region:

- Additional and more detailed documentation of feature size (e.g., dike width, sand-blow deposit thickness). This additional information could be used to further refine locations and magnitude estimates of paleoearthquakes.
- More detailed documentation of areas searched. This additional information could be used to assess the uncertainties associated with paleoearthquake locations and design future studies to improve those locations.
- Additional site-specific and regional geotechnical characterizations, including liquefaction susceptibility and liquefaction potential. This additional information could be used to further refine locations and magnitude estimates of paleoearthquakes.

E.1.2.7 Atlantic Coast Region and the Central Virginia Seismic Zone

Reconnaissance-level searches for paleoliquefaction features were conducted along the eastern seaboard from southernmost Georgia to New Jersey (Amick, Gelinas, et al., 1990) and as far north as New England (e.g., Gelinas et al., 1998; Figure E-37). These studies did not find paleoliquefaction features beyond the Charleston region and suggest a stationary source of repeated, large-magnitude earthquakes located near Charleston.

The Central Virginia seismic zone is an area of persistent, low-level earthquake activity that extends about 120 km in a north-south direction and about 145 km in an east-west direction from Richmond to Lynchburg, Virginia (Bollinger and Sibol, 1985). Seismicity in the Central Virginia seismic zone ranges in depth from about 3 to 13 km (Wheeler and Johnston, 1992). The largest historical earthquake that has occurred in the Central Virginia seismic zone is the December 23, 1875, m_b 5.0 Goochland County earthquake (Bollinger and Sibol, 1985). It is difficult to attribute the seismicity to any known geologic structure, and it appears that the seismicity extends both above and below the Appalachian detachment.

Searches for paleoliquefaction features were conducted along several rivers in the vicinity of the Central Virginia seismic zone (Obermeier and McNulty, 1998; Dominion, 2004) (Figure E-38). They identified possible small sand dikes at three sites and interpreted them as paleoliquefaction features resulting from at least one, and possibly as many as three, moderate-magnitude earthquakes during the Holocene. Obermeier and McNulty (1998) conclude that “the paucity of liquefaction features in central Virginia makes it seem unlikely that any earthquake in excess of $M \sim 7$ has struck there.”

We recommend that any additional searches for liquefaction features in the Atlantic Coast region and Central Virginia seismic zone include documentation of rivers searched, of the liquefaction features including their sedimentological characteristics and stratigraphic context, and field conditions such as quality of exposures and water levels at the time of reconnaissance.

E.1.2.8 Newburyport, Massachusetts, and the Surrounding Region

E.1.2.8.1 Overview

Northeastern Massachusetts, southeastern New Hampshire, and southernmost Maine have experienced many small, and several moderate to large, earthquakes during the past 400 years (Figure E-39). The two most notable earthquakes, the 1727 felt-area magnitude (M_{fa}) 5.5 Newburyport and 1755 M_{fa} 6 Cape Ann events, induced liquefaction and caused damage to buildings (Ebel, 2000, 2001). During a paleoseismology study in the late 1980s, both historical and prehistoric liquefaction features were found in the Newburyport area (Tuttle et al., 1987; Tuttle and Seeber, 1991; Figures E-40 through E-43). This initial study involved interpreting aerial photographs, excavating trenches at locations described in historical accounts of liquefaction, and searching for liquefaction features in exposures provided by sand and gravel pits and excavations for new building foundations.

The historical features were attributed to the 1727 earthquake and the prehistoric features were estimated to have formed during the past 4,000 years. Because the ages of the prehistoric liquefaction features were poorly constrained, the number and timing of paleoearthquakes were not estimated. In addition, the area over which the prehistoric earthquake(s) induced liquefaction

was not determined, limiting interpretations of earthquake source area and magnitude. During a subsequent paleoseismic study, searches for earthquake-induced liquefaction features were conducted in marshes, rivers, and bays in northeastern Massachusetts and southeastern New Hampshire (Gelinas et al., 1998; Figure E-39). No additional liquefaction features were found, but sedimentary conditions suitable for the formation of liquefaction features were notably sparse in many of the areas searched. The failure to find additional liquefaction features was interpreted as a lack of evidence for a $M \geq 6$ earthquake in the region during the late Holocene (Gelinas et al., 1998).

More recently, searches for earthquake-induced liquefaction features have been conducted along several rivers south of Newburyport, Massachusetts, as well as in the vicinity of Hampton Falls and west of Hampton Falls in New Hampshire (Figure E-39; Tuttle, 2007, 2009).

Reconnaissance was performed in areas where ground failure indicative of liquefaction was reported for the 1727 earthquake (Brown, 1990; Coffin, 1845). Surveys were conducted when river levels and tides were low and cutbank exposures were at a maximum. During the surveys, only one liquefaction feature, a small sand dike, was found along the Hampton Falls River in New Hampshire (Figures E-42 and E-43). The upper portion of the sand dike had been eroded and any relation to an overlying sand lens (possibly a sand blow or sand sill) could not be determined. Radiocarbon dating of organics collected adjacent to the uppermost intact portion of the dike provides a maximum constraining age of 2,750 yr BP. In addition, a distinctive 2,200-year-old sand layer, that exhibits some characteristics of tsunami deposits, was observed in several marshes along the Massachusetts–New Hampshire coast (Tuttle, 2007, 2009).

E.1.2.8.2 Data Description

Paleoliquefaction data were contributed by M. Tuttle and collaborators for the Newburyport, Massachusetts, region and compiled in the CEUS SSC Project paleoliquefaction database. Most of the data were published previously in journal articles and technical reports. Sections of rivers searched by Tuttle and collaborators as well as by Gelinas et al. (1998) are shown in Figure E-39. The Newburyport paleoliquefaction data were reviewed, 2-sigma minimum and maximum constraining ages entered, and preferred age estimates calculated. All of the radiocarbon ages were determined by Beta Analytic Radiocarbon Laboratory and calibrated using the Pretoria procedure (Talma and Vogel, 1993; Vogel et al., 1993). All of the liquefaction features dated in the Newburyport region are sand dikes (Tables E-1.2-1 and E-1.2-2). Relations with possible sand blows could not be confirmed. Only maximum constraining ages are available for some of the dikes. Crosscutting relations and weathering characteristics suggest two generations of features, one of which is historical in age. The paleoliquefaction data in this data set contributed to the CEUS SSC Project analyses of the timing, location, and magnitude of paleoearthquakes in this part of New England.

E.1.2.8.3 Recommendations

Newburyport, Massachusetts, and the surrounding region is a seismically active area relative to the rest of New England. Historically, the largest earthquake to have occurred in the region was the 1775 $M_f \sim 6$ earthquake. Paleoseismic studies have found several liquefaction features in the Newburyport-Hampton Falls area attributed to the 1727 $M_f \sim 5.5$ earthquake and to a paleoearthquake sometime during the past 4,000 years (Figure E-43). The scarcity of liquefaction features may be due to the limited distribution of sandy sediments susceptible to liquefaction at

relatively low levels of ground shaking. Also, the lateral and vertical variability of Late Wisconsin deposits in the region makes searching for liquefaction features especially challenging (Tuttle and Seeber, 1991). Significant uncertainties remain regarding the maximum magnitude earthquake and the recurrence rates of earthquakes in this region. Therefore, despite the challenges of working in this region, the following research is recommended to help reduce these uncertainties:

- Broader search for liquefaction features targeting areas where sediments susceptible to liquefaction are present and where exposures are available along river cutbanks.
- Re-excavation of some of the paleoliquefaction sites in Newburyport to better constrain their ages and to re-evaluate their relationships to possible sand blows.

E.1.2.9 Charlevoix Seismic Zone and the Surrounding Region

E.1.2.9.1 Overview

The Charlevoix seismic zone in Quebec Province of southeastern Canada is one of the most seismically active areas in eastern North America and is spatially associated with Iapetan faults and the Charlevoix impact crater (Figure E-44; e.g., Adams and Basham, 1989; Lamontagne et al., 2000). Charlevoix was the source of three historical earthquakes of $M > 6$ dating back to the 1660s (e.g., Bent, 1992; Lamontagne et al., 2007; Lamontagne, 2009). Accounts of ground failure during the 1870 and 1925 Charlevoix earthquakes are indicative of liquefaction in the Gouffre River valley (Smith, 1966).

Recently, a paleoseismic study was conducted in the Charlevoix seismic zone and the St. Lawrence Lowlands to the southwest in the Quebec City–Trois Rivières region (Figure E-44; Tuttle and Atkinson, 2010). During the study, river cutbanks were searched for earthquake-induced liquefaction features, including 40 km in the Charlevoix region and 100 km in the Quebec City–Trois Rivières region. In the Charlevoix region, three generations of earthquake-induced liquefaction features that formed during the past 10.2 k.y. were found in Late Wisconsin and Holocene deposits, whereas no liquefaction features were found in the Quebec City–Trois Rivières region despite searching more than twice the river length in similar deposits (Figures E-44 through E-49).

The Charlevoix liquefaction features included sand dikes and soft-sediment deformation structures such as basal erosion and sand diapirs, load casts, pseudonodules, and related folds (Tables E-1.2-1 and E-1.2-2; see Section E.2.1.1). The authors suggested that the liquefaction record of paleoearthquakes is likely to be incomplete for the Holocene due to fluctuating hydrologic conditions related to changes in relative sea level in the St. Lawrence estuary (Tuttle and Atkinson, 2010). Thus three earthquakes large enough to induce liquefaction during the past 10.2 k.y. should be viewed as a minimum. During the study, various magnitudes and locations of earthquakes were evaluated using liquefaction potential analysis. The results indicated that the distribution of liquefaction features could be explained by $M > 6.2$ earthquake located in the Charlevoix seismic zone (Tuttle and Atkinson, 2010).

In 1988, the M 5.9 Saguenay earthquake occurred north of the Charlevoix seismic zone in the Laurentide Mountains, an area that had been thought to have a low seismic hazard. The 1988 Saguenay earthquake (Somerville et al., 1990; Du Berger et al., 1991) triggered rock falls and

landslides and induced liquefaction in Holocene fluvial and Late Wisconsin glaciofluvial and glaciolacustrine deposits (Tuttle et al., 1989, 1990). Liquefaction occurred in the epicentral area and up to 30 km from its epicenter in the Ferland-Boilleau valley (Figures E-45 through E-49). During excavation and documentation of modern sand blows in Ferland, the researchers found evidence for a prior earthquake (Tuttle et al., 1992; Tuttle, 1994). Radiocarbon dating of the paleoliquefaction features indicated that a large earthquake occurred in the region in AD 1420 \pm 200 yr. Given the relative size of the two generations of features, the previous event may have been larger or located closer to the Ferland-Boilleau valley than the 1988 earthquake.

E.1.2.9.2 Data Description

Paleoliquefaction data from the Charlevoix seismic zone and the Saguenay region, as well as liquefaction data related to the 1988 Saguenay earthquake, were contributed by M. Tuttle and collaborators to the CEUS SSC Project paleoliquefaction database. The paleoliquefaction data and information about river sections searched in the Charlevoix seismic zone and the Quebec City–Trois Rivières region were previously published in journal articles and/or technical reports. For this project, a new map was created of the Charlevoix seismic zone and the Quebec City–Trois Rivières region showing mapped structures and river sections along which reconnaissance and systematic searched for liquefaction features were performed (Figure E-44). All Quebec paleoliquefaction data were reviewed, 2-sigma minimum and maximum constraining ages entered, and preferred age estimates calculated. All age estimates of liquefaction features are based on radiocarbon dating, and all radiocarbon ages were determined by Beta Analytic Radiocarbon Laboratory and calibrated using the Pretoria procedure (Talma and Vogel, 1993; Vogel et al., 1993).

In the Charlevoix region, most of the samples used in radiocarbon dating were collected from deposits cut by sand dikes, from animal burrows or root casts that crosscut sand dikes, or from deposits in which soft-sediment deformation structures had formed (Tables E-1.2-1 and E-1.2-2). In the Saguenay region, there was no need to date the sand blows that formed during the 1988 Saguenay earthquake, but paleoliquefaction features, including sand-blow craters, sand blows, and sand dikes were dated with samples that pre- and post-dated them. Constraining ages were derived from 2-sigma calibrated radiocarbon dates, and preferred age estimates and uncertainties were calculated from minimum and maximum constraining ages. In one case, a preferred age estimate and related uncertainty is calculated from a close minimum constraining age. In this case, the preferred age estimate is the mean of the 2-sigma calibrated age range and the uncertainty is the difference between the average and the end values of the range. The paleoliquefaction data in this data set contributed to the CEUS SSC Project analyses of the timing, location, and magnitude of paleoearthquakes in the Charlevoix seismic zone and surrounding region.

E.1.2.9.3 Recommendations

The Charlevoix paleoseismic study suggests that seismicity may be stationary and localized in the Charlevoix seismic zone. However, the search for paleoliquefaction features outside the Charlevoix seismic zone only extended toward the southwest (Figure E-44). The largest historical earthquake in the region, the 1663 $M \sim 7$ earthquake, has been thought to have occurred in the Charlevoix seismic zone but there are new results from studies of terrestrial and subaqueous mass movements that suggest that the 1663 event may have been centered in the

Saguenay region instead (e.g., Levesque et al., 2006; Locat, 2008). The Saguenay liquefaction study found evidence for a paleoearthquake about AD 1420 that was larger or located closer to the Ferland-Boilleau valley than the 1988 **M** 5.9 earthquake, suggesting that an earthquake source capable of large earthquakes may occur in the Saguenay region (Figure E-49). There are large uncertainties regarding the maximum magnitude and recurrence rates of earthquakes in the Charlevoix seismic zone and the Saguenay region. Both may be capable of future large earthquakes that could affect southeastern Canada and northeastern United States. To help address these issues, the following research topics are recommended:

- Additional searches for paleoliquefaction features in the Charlevoix region that might help to improve age estimates and recurrence times of paleoearthquakes. Employ OSL dating to help date liquefaction features at sites where organic material is not available for radiocarbon dating.
- Additional searches for paleoliquefaction features along tributaries of the St. Lawrence River both southwest of Trois Rivières and northeast of the Charlevoix seismic zone to further test the hypothesis that seismicity in the Charlevoix seismic zone is stationary and that its rate of seismicity is higher than other locations along the Iapetan rift margin.
- Additional searches for paleoliquefaction features in the Saguenay region to determine the timing, location, and magnitude of the paleoearthquake about AD 1420 and to test the hypothesis that the 1663 **M** ~7 earthquake was located in the Saguenay region.

E.2 Uncertainties Associated with Paleoliquefaction Data

E.2.1 Collection of Paleoliquefaction Data

It is advisable that experienced, qualified investigators be involved in planning and execution of paleoliquefaction studies. Lacking familiarity with earthquake-induced liquefaction features and the conditions under which they form, inexperienced investigators can squander time and resources searching for features in the wrong settings, misidentify features in the geologic record, and misinterpret the presence and absence of features.

For the results of a paleoliquefaction study to be most useful in assessing seismic hazards, search areas must be selected where sedimentological and hydrological conditions are conducive for the formation and preservation of liquefaction features. These conditions include (1) the presence of loose to moderately dense sandy sediments that occur below the water table or are otherwise saturated at the time of an earthquake; (2) an overlying layer of less permeable clay or clayey silt to promote the increase in pore-water pressure in and liquefaction of saturated sandy sediment during ground shaking; and (3) an environment of sediment accumulation or relative stability that is not undergoing denudation (Sims, 1975; Obermeier, 1996; Tuttle, 2001).

Utmost care must be taken to correctly identify earthquake-induced liquefaction features and not to confuse them with features that formed as the result of other processes. Deposits and features that have been misidentified as earthquake-induced liquefaction feature include fluvial deposits, chemical weathering, tree-throw, and cultural features. Liquefaction features have certain characteristics, described below and summarized in Section E.1.2, that help to distinguish them from other deposits and features (Figure E-50). For example, the presence of feeder dikes helps to distinguish earthquake-related sand blows from fluvial deposits and deformation related to tree

throw. With close examination of deposits and features by an experienced eye, earthquake-induced liquefaction features can be identified with confidence.

Exposure of sediments must be adequate to reveal liquefaction features, if they are present. Dense forests and other vegetation can obscure surficial sand blows, making it difficult to identify them on aerial photographs and satellite images. Agricultural practices such as plowing and grading can disturb and destroy them. Exposures can be created to verify interpretations from aerial photographs and satellite images by excavating trenches in sand blows. Geophysical techniques such as electrical resistivity and ground-penetrating radar can be used to map sand blows and locate sand dikes (Figure E-14; Wolf et al., 1998, 2006; Al-Shukri et al., 2006; Al-Qadhi, 2010). Fieldwork should be conducted at times of the year, and even the time of day in coastal areas, when exposure is optimal in order to minimize chances that liquefaction features are missed due to high water, heavy vegetation, or snow cover. Exposures along actively eroding river cutbanks and recently excavated drainage ditches can be used to search for liquefaction features and to examine their sedimentary characteristics and structural relations.

Field studies should be designed to try to fully characterize the size and spatial distribution of paleoliquefaction features. As the size and frequency of liquefaction features decrease, the more cutbank exposure must be examined to find and characterize them. If liquefaction features are not found, it is important to verify that the search areas are underlain by sediments that are susceptible to liquefaction.

E.2.1.1 Identification of Earthquake-Induced Liquefaction Features

Liquefaction is the phenomenon by which saturated sandy sediments, when subjected to strong ground shaking, lose shear strength as pore-water pressure in the sediments increases, leading to ground failure, injection of sand dikes and sills, ejection of sand volcanoes or sand blows, and formation of sand-blow craters (Figures E-2 and E-50; Seed and Idriss, 1982; Youd, 1984). Sand dikes, sand blows, and sand-blow craters are considered diagnostic of earthquake-induced liquefaction, and their characteristics have been documented following historical (e.g., Dutton, 1889; Fuller, 1912) and modern earthquakes (e.g., Tuttle et al., 1990; Tuttle, Schweig, et al., 2002; Sims and Garvin, 1995). Several notable studies in the Charleston seismic zone (e.g., Amick, Gelinas, et al., 1990; Amick, Maurath, and Gelinas, 1990; Obermeier et al., 1989; and Talwani and Schaeffer, 2001); the New Madrid seismic zone (e.g., Russ, 1982; Saucier, 1991; Tuttle, Schweig, et al., 2002; and Tuttle et al., 2005); and the Wabash Valley seismic zone (e.g., Obermeier et al., 1993; Munson et al., 1997; and Obermeier, 1998) have used paleoliquefaction features to reconstruct the earthquake history from the geologic record (Table E-1.2-2).

The following general criteria have been advanced for identifying earthquake-induced liquefaction features: (1) sedimentary characteristics consistent with case histories of earthquake-induced liquefaction; (2) sedimentary characteristics indicative of sudden, strong, upwardly directed hydraulic force of short duration; (3) occurrence of more than one type of liquefaction feature and of similar features at multiple locations; (4) occurrence in geomorphic settings where hydraulic conditions described in (2) would not develop under nonseismic conditions; and (5) age data to support both contemporaneous and episodic formation of features over a large area (Obermeier, 1996; Tuttle, 2001).

Sand blows are sand deposits that result from liquefaction of loose, saturated, sandy sediment, usually within 15–20 m of the ground surface, and venting of the slurry of pressurized pore-

water and entrained sediment through fissures, cracks, and other voids to the surface (Figures E-2, E-50, and E-51). In the case of sand-blow craters, a crater forms at the ground surface and the sand blow is deposited around the rim of the crater (Figures E-51 through E-53). In plan view, the shape of the sand blows and sand-blow craters is related to the void through which the slurry vented. Most sand blows and sand-blow craters are elliptical in shape because the slurry vented through fissures (Tuttle and Barstow, 1996). Sand blows and sand-blow craters that are circular in shape result from venting through tubular-shaped voids such as decomposed tree roots and trunks and animal burrows (Audemard and de Santis, 1991; Tuttle, 1999).

In cross section, sand blows usually bury soil horizons and are connected at their bases to one or more feeder dikes or tubular conduits, which are the sand-filled voids through which the fluidized sediment vented (Figures E-2, E-50, and E-54). Sand blows are thickest and coarsest-grained immediately above the feeder dikes or tubular conduits and thin and fine away from the vent. Sand blows often contain clasts of the underlying deposits through which water and sand vented. The clasts tend to be larger and more concentrated above the vent. In cases of ground subsidence related to venting of subsurface sediment or to lateral spreading, the buried soil may dip toward or be displaced across the sand-filled vent structures such as sand dikes. Sand blows and sand-blow craters should exhibit most if not all of these characteristics including a structural connection with feeder dikes (Section E.1.2) and should not be confused with fluvial deposits such as overbank sediments or crevasse splays that bury soils and may be limited in extent.

As mentioned above, sand dikes and tubes are the sand-filled voids resulting from liquefaction of sediment at depth and intrusion of overlying deposits by the pressurized slurry of water and entrained sediment (Figures E-50, E-54, and E-55). Sand dikes usually have well-defined margins and can be differentiated from the host deposit by differences in grain-size and weathering characteristics. Sand dikes originate in a layer of sandy sediment, often referred to as the source bed, that has undergone liquefaction and fluidization. The source beds of sand dikes may lack original sedimentary structure and may exhibit soft-sediment deformation structures such as ball-and-pillow structures and dish structures as well as flow structure or lineations (see Glossary). The sand dikes intrude overlying deposits and crosscut bedding. They often narrow, branch, and become finer-grained upward, are characterized by flow structure, and contain clasts of the deposits that they intrude (Section E.1.2; Obermeier, 1996; Tuttle, 2001). In cases where the slurry of water and sand did not make it to the surface, sand dikes pinch out or terminate within the stratigraphic section (Figure E-2). Extensions of sand dikes, sand sills sometimes form along the base of less permeable layers. Sand-filled root casts and dessication cracks that branch and pinch downward should not be confused with sand dikes resulting from earthquake-induced liquefaction.

Soft-sediment deformation structures, including sand diapirs, basal erosion, convolute bedding, pseudonodules, load casts and related folds, have been attributed to earthquake-induced liquefaction on the basis of laboratory experiments (Kuenen, 1958) and field studies (Sims, 1973 and 1975; Obermeier, 1996; Tuttle, 1999). During field studies of earthquake-induced liquefaction features, sand diapirs and basal erosion have been found to form where fine-grained deposits overlie coarse-grained deposits (Figures E-2 and E-56). Pieces of the overlying fine-grained sediment founder into the coarse-grained sediment due to loss of its bearing strength during liquefaction. Simultaneously, coarse-grained sediment moves upward to replace the founded material forming sand diapirs. Sand diapirs and basal erosion may form when ground

motions are capable of inducing liquefaction in susceptible sediments but not capable of generating the pore-water pressures required for hydraulic fracturing of the overlying deposits.

Load casts, pseudonodules, and related folds typically form in interbedded fine- and coarse-grained deposits when fine-grained sediment sinks into coarse-grained sediment due to loss of bearing strength (Figure E-57). In cases where layer integrity is maintained, the resulting features are called load casts. In cases where layer integrity is not maintained and coarse-grained sediment separates into domains or irregular masses, the features are called pseudonodules. Pseudonodules, load casts, and related folds typically form close to the sediment-water interface at the time of deposition. It is important to note that the soft-sediment deformation structures mentioned above also can form by non-earthquake processes (e.g., Lowe and LoPiccolo, 1974; Lowe, 1975; Allen, 1982; and Owen, 1987). Criteria have been proposed for distinguishing seismic from nonseismic soft-sediment deformation structures. These criteria are similar to those advanced for identifying earthquake-induced sand blows and sand dikes and include the following (Wheeler, 2002):

- evidence for sudden formation,
- synchronicity and zoned map distribution over many exposures,
- size of the structures, and
- tectonic and depositional settings.

Soft-sediment deformation structures that meet these criteria and are used with caution in combination with sand blows and sand dikes may aid in mapping areas of liquefaction and defining the limits of liquefaction fields (e.g., Tuttle and Atkinson, 2010).

E.2.1.2 Dating Liquefaction Features

By dating liquefaction features, it is possible to estimate the ages of the paleoearthquakes that were responsible for their formation. It is important to constrain the ages of liquefaction features as narrowly as possible to help correlate similar-age features across a region and differentiate closely timed events. The dating strategy depends on the type of liquefaction features encountered, as does the likelihood of narrowly constraining their ages. Because it is often possible to determine both maximum and minimum age constraints and thus bracket their ages, sand blows usually provide the best opportunity for estimating the ages of paleoearthquakes with relatively small uncertainties (Figure E-3; Tuttle, 2001). Close maximum age constraint can be determined by dating plant material, such as twigs and leaves, and sediments that were at or near the ground surface and buried by the sand blows at the time of the event (Figure E-58). Similarly, plant material derived from surface soils and incorporated in the vented deposits of sand blows and sand-blow craters also provides close maximum age constraint. For those cases in which samples are reworked, there is more uncertainty regarding their origin and thus their age relation to the liquefaction features.

In addition, minimum age constraint, and sometimes, close minimum age constraint, can be determined for sand blows and sand-blow craters. For example, close minimum age constraint can be achieved by dating plant material and sediment that accumulated in craterlets in the upper surface of sand blows soon after they formed. More commonly, minimum age constraints come

from dating plant material in soils that developed in the sand blows over time and from tree roots and cultural pits that extend down into sand blows from above (Figure E-59).

Estimating the age of sand dikes and sand sills usually involves greater uncertainty than for sand blows and sand-blow craters (Tuttle, 2001). This is because dikes and sills may terminate several meters below the ground surface at the time of the paleoearthquake (Figure E-2). Maximum age constraints can be determined by dating the uppermost stratigraphic units that they crosscut or overlie, but these ages may be hundreds to thousands of years older than the liquefaction feature (Figure E-3; Tuttle, Chester, et al., 1999). Minimum age constraints of dikes and sills can be determined by dating roots, animal burrows, and cultural pits that clearly intrude and postdate the liquefaction features or by dating deposits that overlie unconformities that truncate the liquefaction features. However, it is fairly uncommon to find circumstances such as these that help to constrain the minimum age of dikes and sills (Tuttle, 2001). Therefore, age estimates of sand dikes and sills often have large uncertainties. Some investigators will make educated guesses as to the ages of these types of liquefaction features based on weathering characteristics of the features themselves or the approximate age of the deposits in which they occur. There can be large uncertainties in these estimates on the order of thousands of years.

Pseudonodules, load casts, and related folds typically form close to the sediment-water interface at the time of sediment deposition (Figure E-57; Sims, 1973, 1975). Age estimates and related uncertainties for causative earthquakes can be derived by dating the deformed sediments themselves or by dating plant material above and below the deformed sediment. There often are much larger uncertainties in estimating the ages of sand diapirs and basal erosion. This type of soft-sediment deformation may have formed anytime following deposition of the stratigraphic units involved. Maximum age constraint can be established by dating the deformed deposits but the deformation may be hundreds or thousands of years younger than the deposits.

E.2.1.3 Dating Techniques

This section provides discussion of dating techniques used in paleoliquefaction studies, including dendrochronology, radiocarbon dating, optically stimulated luminescence, archaeological and stratigraphic context, and soil development. Table E-2.1.3 provides a summary of these dating techniques.

E.2.1.3.1 *Dendrochronology*

Dendrochronology is the dating of past events through the study of the tree ring record and has the potential to date events to the year and even the season (Table E-2.1.3; Pierce, 1986; Stahle et al., 2004). For example, trees killed by coseismic subsidence along the coast of Washington State helped to provide exact dates of megathrust earthquakes along the Cascadia subduction zone (Atwater et al., 2004). Abrupt changes in soil-moisture conditions due to liquefaction-related subsidence of the ground surface and/or burial by thick sand blows as well as disruption of tree root systems by lateral spreading, may affect tree ring growth and even lead to tree death (Figures E-51 and E-60; Tuttle, 1999). Therefore, trees buried and preserved below sand blows may provide precise dates of paleoearthquakes. Before dendrochronology can be used, however, regional chronologies for affected tree species must be developed. Long-lived tree species provide the best dendrochronology records. In the New Madrid region, a regional chronology has been developed only for baldcypress and only for the past 1,000 years (Stahle et al., 1985). So

far, dendrochronology has been used very little in paleoliquefaction studies but has the potential to better constrain age estimates of paleoearthquakes, especially in regions where liquefaction-related ground failures were severe (Table E-2.1.3).

Table E-2.1.3. Summary of Dating Techniques Used in Paleoliquefaction Studies

Dating Technique	Applicable Time Period (Years BP)	Dating Precision (Years)	Applied in CEUS Regions¹	Selected References²
Dendro-chronology	1–1,000's	Annual, possibly seasonal	(1) NMSZ	(1) Stahle et al., 1985; Tuttle, 1999
Radiocarbon	1–50,000	10's–100's	(1) NMSZ (2) MAR (3) STL (4) WVSZ (5) ALM (6) CSZ (7) AC-CVA (8) NEWBURY (9) CxSZ	(1) Tuttle et al., 2005 (2) Tuttle et al., 2006 (3) Tuttle, Chester, et al., 1999 (4) Munson and Munson, 1996 (5) Cox, Larsen, et al., 2004 (6) Talwani and Schaeffer, 2001 (7) Obermeier and McNulty, 1998 (8) Tuttle and Seeber, 1991 (9) Tuttle and Atkinson, 2010
Optically stimulated luminescence	100–100,000	10's–1,000's	(1) NMSZ (2) MAR (3) WVSZ (4) ALM	(1) Mahan et al., 2009 (2) Tuttle et al., 2006 (3) Mahan and Crone, 2006 (4) Cox, Larsen, et al., 2004
Archeological context	1–12,000	10's–1,000's	(1) NMSZ (2) STL (3) WVSZ	(1) Tuttle et al., 1998, 2000 (2) Tuttle, Chester, et al., 1999 (3) Munson and Munson, 1996
Stratigraphic context	1–100,000+	100's–1,000's	(1) NMSZ (2) WVSZ	(1) Tuttle, 1999 (2) Hajic et al., 1995; Munson and Munson, 1996
Soil development	1–100,000+	Varies with soil property	(1) NMSZ	(1) Tuttle et al., 2000

1. NMSZ = New Madrid seismic zone and surrounding region; MAR = Marianna Area; STL = St. Louis and surrounding region; WVSZ = Wabash Valley seismic zone and surrounding region; ALM = Arkansas-Louisiana-Mississippi region; CSZ = Charleston seismic zone; AC-CVA = Atlantic Coast and Central Virginia reconnaissance; NEWBURY = Newburyport, Massachusetts, and surrounding region; CxSZ = Charlevoix seismic zone and surrounding region.

2. Selected references shown here. Also see paleoliquefaction database and reference lists at the end of this report.

E.2.1.3.2 Radiocarbon Dating

Radiocarbon dating or ¹⁴C dating is the most common dating technique used in paleoliquefaction studies (Table E-2.1.3). Although reliable for only the past 50,000 years, radiocarbon dating is useful for the time period of interest for most paleoseismic studies. Uncertainties in the results are related to the dating techniques, to conversion of radiocarbon ages to calibrated ages, and to sampling of materials that are used in dating liquefaction features.

Two different radiocarbon dating techniques are used, depending on the size of the sample (Aiken, 1990). The radiometric technique is used for larger samples (e.g., charcoal ≥ 15 grams, wood ≥ 25 grams, and soil ≥ 200 grams). The accelerator mass spectrometry (AMS) technique is used for smaller samples (charcoal ≥ 20 milligrams, wood ≥ 20 milligrams, and soil ≥ 2 grams).

The radiometric technique involves converting carbon to benzene, measuring the sample's beta activity in a liquid scintillator, and calculating the radiocarbon age (Aiken, 1990). A precision of better than $\pm 1\%$, corresponding to ± 80 radiocarbon years, can usually be achieved for samples that are less than 10 k.y. High-precision measurements can be made on wood samples of ≥ 1 kilogram by measuring the beta activity of the sample in a proportional gas counter (Stuiver et al., 1998). For these very large samples, a precision $\pm 0.25\%$, corresponding to ± 20 radiocarbon years, can be obtained.

The AMS technique involves reducing the sample to graphite and then measuring carbon ions in an accelerator mass spectrometer (Aiken, 1990). A precision of about $\pm 0.5\%$, corresponding to ± 40 radiocarbon years, can be achieved with the AMS technique. Isotopic fractionation may occur during sample preparation and can affect the radiocarbon age. This effect can be taken into account by measuring the $^{13}\text{C}/^{12}\text{C}$ ratio for each sample and making the appropriate correction. Other experimental uncertainties are related to contamination during sample preparation, lack of constancy of counter background and counter efficiency, residual ^{14}C within the accelerator, and human error (Aiken, 1990). These uncertainties are taken into account by applying a laboratory error multiplier (1.3 to 2). The error multiplier is a measure of the laboratory reproducibility and is usually derived from repeated dating of a standard of known or consensus age (Stuiver and Pearson, 1993). Because of its higher precision, the AMS technique is now preferred by many investigators despite its greater cost.

Radiocarbon dating results are reported as both measured and conventional ^{14}C ages. Conventional ages are derived from measured ages by normalizing them to the modern standard through the use of $^{13}\text{C}/^{12}\text{C}$ ratios. Because ^{14}C in the atmosphere has fluctuated over time due to variations in cosmic radiation and, recently, to burning of fossil fuels and testing of nuclear devices (Stuiver et al., 1993), it is desirable to convert conventional ages to actual or calendar years by using the radiocarbon calibration curve (Figure E-61; Tuttle, 1999). Although the recent part of the curve (12 k.y.) based on tree-ring records is the most secure and reliable, the calibration curve now extends to 50 k.y. BP (Walker, 2005; Reimer et al., 2009). Several calibration procedures have been developed that are commonly used and yield similar results. These procedures include CALIB (Stuiver and Reimer, 1993; Stuiver et al., 2005), OxCal (Bronk Ramsey, 1995, 2001), and Pretoria (Talma and Vogel, 1993; Vogel et al., 1993). It is preferable to use 2-sigma calibrated dates to either bracket or approximate the ages of the liquefaction features. This assures with a high probability that the actual ages of the liquefaction features fall within the estimated age range. Calibrated ages rarely have 2-sigma ranges of less than 100 years, more often have 2-sigma ranges of about 200–300 years, and sometimes have two or three ranges depending on the number of intercepts of the conventional radiocarbon age with the calibration curve (Table E-2.1.3).

The type and location of samples collected for radiocarbon dating affect the uncertainty of the age estimate of the liquefaction features. Plant remains that occur in close stratigraphic position to a sand blow will fairly closely reflect its age. For example, leaves or burned wood that occur at the contact of a buried soil horizon and an overlying sand blow would provide close maximum age constraint for the sand blow (Figures E-3 and E-58). Similarly, maize kernels, leaves, or burned wood incorporated into the top of a sand blow would provide close minimum age constraint. In contrast, a piece of charcoal within the buried soil or underlying sediment would provide maximum age constraint, but could be hundreds or even thousands of years older than the sand blow. Unless associated with in situ cultural or biological features such as fire pits and

tree trunks, a charcoal sample could be reworked, in which case its age relation to the sand blow would be even more uncertain. Bulk samples of soils buried by or developed in sand blows can also be dated. However, radiocarbon dates of soils reflect the mean residence time of carbon in those samples (Trumbore, 1989; Walker, 2005). Also, contamination by young (e.g., modern humic acids) and old (e.g., lignite and calcium carbonate) carbon can be a significant problem in soils. Therefore, dating soils is usually a last resort and requires a sampling strategy to help minimize the uncertainties (Tuttle, 1999).

E.2.1.3.3 Optically Stimulated Luminescence

Luminescence techniques, including optically stimulated luminescence (OSL), provide an estimate of the time since quartz and feldspar grains were last exposed to light (which zeros the luminescence signal). After burial, the luminescence signal grows with exposure to radiation in the surrounding sediments (K, U, Th, Rb). The luminescence signal can be measured in the laboratory and related to the duration of burial and in situ and cosmic radiation environment (Murray and Olley, 2002). In other words, OSL is a numerical method used to determine the amount of time that has passed since sediment was last exposed to light (e.g., Wintle and Murray, 1997; Aitken, 1998; Forman et al., 2000; McKeever, 2001) and therefore holds promise for estimating the ages of paleoearthquakes by dating sediment buried by sand blows and that buries sand blows (Mahan and Crone, 2006; Tuttle et al., 2006; Mahan et al., 2009). The preponderance of age estimates in the CEUS SSC Project paleoliquefaction database are based on radiocarbon dating conducted over the past 20 years. However, OSL dating of sand blows is being increasingly used and results for several features in the New Madrid (e.g., Clarke River site) and Marianna (e.g., Daytona Beach and St. Francis 500 sites) regions are included in the database.

OSL geochronology is a useful tool that can be used in a variety of terrestrial stratigraphic settings, particularly for sediments that receive brief exposure to sunlight prior to deposition. In general, the technique is most useful for sediments approximately 100 years to more than 100 k.y. old (Forman et al., 2000; Lepper, 2007; LDRL, 2010). As such, OSL dating is useful even further back in time than radiocarbon techniques. The primary difference between radiocarbon dating and OSL dating is that the former is used to date organic materials, whereas the latter is used to date the timing of exposure of certain minerals to light.

The preferred sediment for OSL dating is coarse silt to medium sand (quartz or feldspar) that has had at least one hour of sunlight exposure. Feldspar is both structurally and chemically more variable than quartz and requires longer exposure to sunlight to zero the luminescence signal (i.e., bleach). Accordingly, quartz often results in more reliable dates than feldspar. It is preferred if samples come from a relatively homogeneous stratigraphic unit that is at least 30 cm thick, and has not undergone significant water-content variations or diagenetic changes during burial (LDRL, 2010). OSL analysis of a sample collected from, for example, the sediment immediately below the base of a sand-blow deposit can yield an estimate of the time of the causative earthquake.

Studies have compared the results of OSL and radiocarbon dating of sand blows in the central United States. This was done by dating co-located samples collected above and below sand blows (Mahan and Crone, 2006; Tuttle et al., 2006; Mahan et al., 2009). Correlation of OSL and radiocarbon dates was best for samples collected immediately below sand blows and for samples collected in association with sand blows buried several meters beneath fluvial deposits.

Correlation was poor for samples collected in soils developed in surface sand blows and in sediment buried beneath sand blows that had been subjected to bioturbation.

There are a number of possible uncertainties and errors that can limit the precision and accuracy of OSL dating. The most common complication is that the sediment has not received enough sunlight exposure prior to burial in order to rid the sample of previously acquired luminescence (i.e., “partial” vs. “full” bleaching; Forman et al., 2000). Partial bleaching is very unlikely in eolian and coastal marine sands, but is more likely in Holocene fluvial deposits. This is because light attenuates significantly in water. Additionally, silt and sand grains that are coated with clay may be shielded from the bleaching effects of sunlight.

The accuracy of OSL dating may also be limited in pure quartz deposits because the naturally occurring background radiation in surrounding sediments often is low. As a result, cosmic radiation becomes the main source of ionizing radiation that ejects electrons from atoms in the crystal lattice (which are ultimately the source of the luminescence signal). Because cosmic radiation often fluctuates and attenuates quickly with depth below grade, uncertainty in depositional history has a bigger influence on the overall uncertainty of the resulting OSL age estimates.

Water content of the soil also influences the rate of attenuation of ionizing radiation in situ. As a result, uncertainties in the average water content of the sediment since deposition influences the overall uncertainty of the resulting OSL age estimates. Additional complications include bioturbation, diagenesis and postdepositional weathering, and accumulation of secondary minerals (silica, calcium carbonate, and clay). Therefore, careful selection and sampling of sediment is crucial. Uncertainties in OSL dates increase with sediment age from a few tens to a few hundreds of years for the past 1–10 k.y. and to several thousands of years for the past 10–100 k.y. (Table E-2.1.3).

E.2.1.3.4 Archeological Context

Archeological chronologies have been developed for many regions. These chronologies are developed primarily on the basis of the following: (1) seriation, or the sequence of artifact and ceramic types particularly within cultural horizons; and (2) radiocarbon dating of organic material associated with artifacts and cultural horizons (Aiken, 1990; O’Brien and Lyman, 1999). Referring to the regional archeological chronologies, artifacts found at liquefaction sites can help to estimate the ages of the liquefaction features (Saucier, 1991; Tuttle, Lafferty, Guccione, et al., 1996; Munson et al., 1997). Some artifact types are well-constrained to specific cultural periods while others are not. Age estimates of liquefaction features based on their archeological context will have uncertainties at least as great as those based on radiocarbon dating (Table E-2.1.3).

Cultural artifacts found in, or associated with, liquefaction features during reconnaissance can provide a preliminary estimate of the ages of the features. The stratigraphic relations of liquefaction features and cultural horizons and features as well as the assemblage of artifacts, especially if diagnostic artifact types are present, can help to further constrain the ages of the liquefaction features (e.g., Tuttle, 2001; Tuttle et al., 2005). For example, the assemblage of artifacts within an A horizon buried by a sand blow can provide an estimate of the maximum age of the liquefaction feature. The assemblage of artifacts within an occupation horizon developed in a sand blow or cultural features such as a storage pit or wall trench dug into a sand blow can

provide an estimate of its minimum age (Figures E-58 and E-59). It is important to study assemblages of artifacts since there are still many uncertainties regarding the temporal and geographical ranges of artifact types.

Due to their abundance of organic-rich material, archeological sites often provide good opportunities for finding samples suitable for radiocarbon dating and constraining the age(s) of any liquefaction feature that is present (Tuttle and Schweig, 1995). In these cases, it is desirable to conduct both archeological analyses and radiocarbon dating of organic samples because they provide a means of cross-checking results and add confidence to the age estimates of liquefaction features.

E.2.1.3.5 Stratigraphic Context

Stratigraphic context and relationships can be used as a means to estimate the relative ages of buried sand blows and sand dikes, and to correlate paleoliquefaction features between exposures. The law of superposition, crosscutting relationships, and identification of paleosurface indicators preserved in the stratigraphic record can be used to help determine the relative ages of paleoliquefaction features. Moreover, in an area with laterally continuous stratigraphy or prominent marker beds, age equivalence can be established between different exposures or sites. If the ages of some or all of these strata are determined by numerical or other means at one site, these ages can be extrapolated to other nearby sites. However, correlation of paleoliquefaction features identified in similar-age sediments is potentially problematic. For example, most of the mid- to late-Holocene sand-blow craters identified in the Charleston, South Carolina region are found in beach ridge deposits that are 100 ka and older (McCartan et al., 1984). If only the host deposits had been used to correlate and date paleoliquefaction features, the timing of the events may have been overestimated and the number of paleoearthquakes underestimated. Ages derived through other methods reveal earthquakes separated by significant periods have caused paleoliquefaction features within correlative stratigraphic units.

In addition, stratigraphic context and relationships can be used to place maximum ages on, for example, sand dikes that terminate upward at a stratigraphic level that may be lower than the paleo-ground surface at the time of the causative earthquake (Figure E-2). Sand dikes that terminate below the event horizon commonly are encountered outside of the most active seismic zones and at greater distances from the seismic source than sand blows. By numerical or relative dating of the host deposits, it is possible to place at least a maximum age constraint on the timing of dike formation (Figure E-3).

As described above, stratigraphic context can be used to estimate the relative ages of paleoliquefaction features. However, these methods typically are less precise and less accurate than numerical dating techniques and therefore should be calibrated using, for example, radiocarbon or OSL numerical dating methods where possible. Even so, uncertainties in age estimates of paleoliquefaction features based on their stratigraphic context are likely to be on the order of several hundreds to several thousands of years at best (Table E-2.1.3).

E.2.1.3.6 Soil Development

The state of a soil system is defined as a function of five soil-forming factors: climate, biological activity, topography, parent material, and time (Jenny, 1941, 1961; Birkeland, 1999). In genetically related suites of soils in which all soil forming factors except for time are about

equal, soil profiles, as well as certain soil properties, develop systematically with age (Harden, 1982; Harden and Taylor, 1983). These soil properties include rubification (reddening and brightening of soil colors), clay accumulation, soil structure, consistence, and pH. Therefore, soil profiles and properties can be used to estimate the age of a soil if they are calibrated with numerical techniques, such as radiocarbon dating and OSL dating (Table E-2.1.3).

In most paleoliquefaction studies, soil development is used as a relative dating technique to distinguish young, unweathered features from significantly older, more weathered features. In the New Madrid seismic zone, the thickness of A horizons developed in sand blows has been used to derive preliminary age estimates of sand blows and to aid in the selection of sand blows for detailed investigations (Tuttle et al., 2000). The estimates were based on a rate of A horizon development derived by studying soil characteristics of sand blows of known ages. The age estimates had uncertainties on the order of 100 years, similar to the uncertainties of radiocarbon dating on which the rate of A horizon development was based (Figure E-62).

In a few regions where sand dikes have terminated within the stratigraphic section and organic material and cultural artifacts have not been available for constraining the ages of the features, soil characteristics such as iron staining and accumulation of fine-grained sediment have been used to correlate features over large distances. This practice is not recommended unless the soil characteristics have been calibrated and the uncertainties associated with their rates of development quantified. Otherwise, the spatial correlation of features and the interpretations related to the spatial distribution of those features may be erroneous (Tuttle, 2001).

E.2.2 Uncertainties Related to Interpretation of Paleoliquefaction Data

This section provides discussion of uncertainties related to the interpretation of paleoearthquake parameters from paleoliquefaction data, including the timing, magnitude, and location of paleoearthquakes. Table E-2.2 provides a summary of these uncertainties.

E.2.2.1 Timing of Paleoearthquakes

Uncertainty in the timing of paleoearthquakes is largely a function of age constraints of multiple liquefaction features correlated across a region (Table E-2.2). If ages of liquefaction features cannot be constrained within a few hundred years, it may not be possible to correlate features chronologically, to resolve the timing of paleoearthquakes with confidence, or to estimate recurrence rates for sources with earthquake cycles of less than 1,000 years. Preferably, 2-sigma calibrated radiocarbon dates are used to either bracket or approximate the ages of the liquefaction features. Clustering of age estimates of liquefaction features reflects the timing of paleoearthquakes (Figure E-63). For a particular cluster, the union of well-constrained age estimates of liquefaction features represents the time period during which the paleoearthquake is likely to have occurred. It is not uncommon for this time period to have a range of 100 to 1,000 years. The timing of the event can be expressed as the average of the range plus and minus the difference between the average and the endpoints of the range. A few well-constrained age estimates of liquefaction features can lead to a more narrowly defined range of tens to hundreds of years and thus smaller uncertainties in the timing of the paleoearthquakes (Table E-2.2). For the CEUS SSC Project, uncertainty ranges of tens to hundreds of years were derived for the timing of paleoearthquakes in the New Madrid and Charleston seismic zones by using subsets of

the better-constrained age estimates of liquefaction features (Figure E-64; see Section 6.1.5.4 of the main report).

Table E-2.2. Uncertainties Related to Interpretation of Paleoseismicity Parameters

Earthquake Parameter	Range in Uncertainty	Factors that Contribute to Uncertainty	Observations and Analyses that Reduce Uncertainty
Timing	10's–1,000's of years	(1) Dating of liquefaction features (2) Use of sand dikes in absence of sand blows	(1) Well-constrained age estimates of liquefaction features (2) Space-time diagrams (3) Statistical analysis of uncertainty range of age estimates of multiple liquefaction features
Location	Few–100's of km	(1) above (2) Correlation of features across region (3) Size and spatial distribution of contemporaneous features a. Style of faulting b. Earthquake source characteristics c. Directivity of seismic energy d. Attenuation and amplification of ground motion e. Relative density of sediment f. Distribution of liquefiable sediments g. Water table depth (4) Field sampling and exposure	(1) through (3) above (4) Size distribution of features (5) Information regarding uncertainty factors (3a) through (3g). (6) Field studies conducted where sedimentary and hydrologic conditions suitable for formation and preservation of liquefaction features, and when adequate exposure available to find features, if present (7) Comparative study with calibration event in same region (8) Relationship to active fault
Magnitude	0.25–1 unit	(1) through (4) above (5) Epicentral distance to farthest sand blow unlikely to be known (6) Changes in source sediments due to liquefaction or to postliquefaction effects such as cementation and compaction	(1) through (8) above (9) Empirical relations based on global database of earthquakes that induced liquefaction (10) Evaluation of scenario earthquakes using liquefaction potential analysis
Recurrence time	10's–1,000's of years	(1) Uncertainty in timing of paleoseismicity (2) Completeness of paleoseismicity record in space and time	(1) Well-constrained age estimates of paleoseismicity (2) Space-time diagrams (3) Consideration of history of sedimentation and erosion as well as of changes in water table

E.2.2.2 Correlation of Liquefaction Features

The correlation of liquefaction features between sites is necessary for interpretation of the timing, location, and magnitude of paleoseismicity. This correlation is based on available information, including one or more of the following:

- Chronological control: Paleoearthquakes are distinguished based on grouping paleoliquefaction features that have overlapping age estimates. As described above, sand blows typically are best to use due to more straightforward identification of the event horizon and their typically better-constrained age estimates, whereas the event horizon and age estimates associated with sand dikes often are relatively poorly constrained.
- Size distribution: Paleoearthquakes are distinguished based on the assumption that feature size diminishes with ground shaking and therefore with magnitude of, and distance from, the causative earthquake. The size distribution of liquefaction features is important for interpreting whether similar-age features formed during single large earthquake or multiple smaller earthquakes.
- Stratigraphic control: Paleoearthquakes are distinguished based on grouping paleoliquefaction features found in similar-age sediments (see caveats described in Section E.2.1.3.5 of this appendix).
- Pedologic or weathering characteristics: Paleoearthquakes are distinguished based on grouping paleoliquefaction features with similar soil or weathering characteristics (see caveats described in E. 2.1.3.6 of this appendix).

If the information described above provides conflicting correlations for a specific field study, it is incumbent upon the researcher to assess the relative qualities of the different sources of information, and to thereby define a preferred interpretation of the available data.

Earthquake ages are defined by selecting the age range common to multiple sand blows in a region. For example, an earthquake age can be defined by the union or the intersection of overlapping 2-sigma radiocarbon age estimates of sand blows. Using the union of overlapping age estimates may be overly conservative since they may include poorly constrained age estimates. Using the intersection of overlapping age estimates may provide the best estimate of the earthquake age, so long as there is a high degree of confidence in the accuracy of the age estimates.

E.2.2.3 Location of Paleoearthquakes

Once they have been correlated across a region on the basis of one or more of the criteria described above (e.g., chronological or stratigraphic control), liquefaction features, particularly sand blows and sand dikes, can be used to infer the approximate locations of paleoearthquakes. The regional distribution of contemporaneous liquefaction features, sometimes referred to as the liquefaction field, is thought to reflect the meizoseismal (strong shaking) area or source area of a particular paleoearthquake, and the area with the concentration of the largest liquefaction features is interpreted as the epicentral area (Tuttle, 2001; Castilla and Audemard, 2007) or energy center (Obermeier et al., 2001). As mentioned above in Section E.2.1.1, soft-sediment deformation structures such as basal erosion and related sand diapirs may be useful in delineating the outer limits of liquefaction fields so long as they meet certain criteria and are used in combination with sand blows and sand dikes. Lone occurrences of liquefaction features may be indicators of unique site conditions and should be interpreted with care.

As demonstrated by modern earthquakes, sand blows generally decrease in size and frequency with increasing distance from the epicenter (e.g., Ambraseys, 1988; Castilla and Audemard, 2007). Nevertheless, the size and spatial distribution of sand blows can be influenced by a

variety of factors including style of faulting, earthquake characteristics, directivity of seismic energy, attenuation and amplification of ground motion, relative density of sediments, distribution of liquefiable sediments, and water table depth as demonstrated by recent earthquakes such as the 1988 **M** 5.9 Saguenay, Quebec; 1989 **M** 6.9 Loma Prieta, California; and 2001 **M** 7.7 Bhuj, India, earthquakes. The complexity of processes and conditions influencing sand-blow formation contribute to uncertainties in interpreting paleoliquefaction data. Accounting for various seismological, geological, and hydrological factors may help to reduce uncertainties to some degree. In addition, the sampling strategy and sediment exposure will affect uncertainties related to the spatial distribution of paleoliquefaction features. If sampling, or searching, for liquefaction features is not performed where conditions are suitable for the formation and preservation of liquefaction features and at times when exposure is adequate to find features, information gained during paleoliquefaction studies may be skewed spatially and/or temporally, which can lead to erroneous interpretations.

Taking together the possible factors affecting the occurrence and observation of paleoliquefaction features, uncertainty in interpreting the locations of paleoearthquakes from paleoliquefaction data is probably on the order of tens to hundreds of kilometers (Table E-2.2). Modern earthquakes that induced liquefaction, such as the 1988 **M** 5.9 Saguenay, Quebec, and 2001 **M** 7.7 Bhuj, India, earthquakes, whose locations and magnitudes are fairly well known, can be used to demonstrate the uncertainty in interpreting locations of earthquakes from liquefaction data. If the concentration of liquefaction features that formed near Ferland, Quebec, in 1988 was interpreted as the earthquake's epicentral area, the inferred location would be off by 25–30 km (Figure E-46). Similarly, if large sand-blow craters that formed along the Allah Bund during the 2001 Bhuj earthquake were interpreted as the epicentral area, the inferred earthquake location would be in error by 100–130 km.

Modern and historical earthquakes that induced liquefaction can serve as calibration events for interpreting paleoliquefaction features. If the size and spatial distribution of liquefaction features generated by a paleoearthquake are similar to those for a modern or historical earthquake in the same region, the paleoearthquake can be inferred to have a similar source area to that of the modern or historical earthquake. For example, the source area of the 1886 Charleston, South Carolina, earthquake is thought to have produced several large paleoearthquakes in the past 5,500 years, judging from similar spatial distributions of historical and prehistoric sand-blow craters (Talwani and Schaeffer, 2001).

Similarly, the New Madrid seismic zone is thought to be the source of several sequences of large paleoearthquakes like the 1811-1812 earthquake sequence, judging from the size, internal stratigraphy, and spatial distributions of historical and prehistoric sand blows (Figures E-65 and E-66; Tuttle, Schweig, et al., 2002; Tuttle et al., 2005). In comparative studies, however, the accuracy of the inferred locations of the paleoearthquakes is less than that for the modern or historical earthquakes, usually a few kilometers to a few tens of kilometers, respectively. For example, the location of the 1886 Charleston, South Carolina, earthquake has an uncertainty of about ± 25 km (e.g., Johnston, 1996c). Therefore, an estimated location of a paleoearthquake based on a comparison of its liquefaction field with that of the 1886 earthquakes will have an uncertainty of at least 25 km. If paleoliquefaction features can be directly related to a fault, such as has been done with the Reelfoot fault in the New Madrid seismic zone, uncertainty in the location of the paleoearthquake may be reduced to just a few kilometers (e.g., Kelson et al., 1996; Tuttle, Schweig, et al., 2002; Table E-2.2).

E.2.2.4 Magnitude of Paleoearthquakes

As demonstrated by case studies of instrumentally recorded earthquakes that induced liquefaction, the size of sand blows, as well as the epicentral distance of sand blows, increases with earthquake magnitude (e.g., Ambraseys, 1988; Castilla and Audemard, 2007). Therefore, the size and spatial distribution of paleoliquefaction features can help to estimate the magnitudes of paleoearthquakes (e.g., Obermeier, 1996; Tuttle, 2001). Due to the many factors affecting the occurrence, distribution, and observation of liquefaction features as described above in Section E.2.2.3, however, uncertainty in magnitudes of paleoearthquakes estimated from paleoliquefaction data can be fairly large, perhaps ranging up to 1 magnitude unit. The uncertainty can be reduced by conducting comparative studies, using empirical relations, and performing geotechnical analysis to better constrain the magnitudes of paleoearthquakes (Table E-2.2; Tuttle, 2001).

E.2.2.4.1 *Comparative Studies*

In comparative studies, the size and spatial distribution of sand blows generated by a paleoearthquake are compared to those induced by a local modern or historical earthquake, whose magnitude is fairly well known. For example, paleoearthquakes centered in the New Madrid seismic zone about AD 1450 (500 yr BP) and AD 900 (1,050 yr BP) are thought to be on the order of **M** 7 to 8 based on the similarity in the size and spatial distribution of sand blows with those that formed during the 1811-1812 New Madrid earthquakes (Figures E-65 and E-66; Tuttle, Schweig, et al., 2002). A similar approach was used in the southeastern U.S. comparing the spatial distribution of paleoliquefaction features to those that formed during the 1886 **M** ~7 Charleston, South Carolina, earthquake (Talwani and Schaeffer, 2001). In studies such as these, the uncertainty related to the inferred magnitudes of the paleoearthquakes is greater than that for the modern and historical earthquakes, usually 0.25 to 0.75 of a magnitude unit, respectively. For example, magnitude estimates of the main shocks of the 1811-1812 New Madrid earthquake sequence have uncertainties of 0.5 to 0.7 of a magnitude unit (see Figure E-66).

E.2.2.4.2 *Empirical Relations*

Empirical relations have been developed between earthquake magnitude and epicentral distance of sand blows as well as distance of sand blows from the seismic energy source or fault rupture (e.g., Kuribayashi and Tatsuoka, 1975; Ambraseys, 1988). These relations were derived using regional and worldwide databases of instrumentally recorded earthquakes that induced liquefaction. The worldwide database included earthquakes in areas of low as well as high ground motion attenuation and differentiated between shallow- and intermediate-depth events. Subsequently, the worldwide database of earthquakes that induced liquefaction and the empirical relation between earthquake magnitude and epicentral distance of sand blows were updated (Figure E-67; Castilla and Audemard, 2007). In addition, the effects of various earthquake characteristics on liquefaction were studied. The style of faulting was found to influence both size and epicentral distance of liquefaction features, with thrust or reverse faulting causing the largest and farthest sand blows. Directivity of seismic energy along fault planes also appears to be an important factor (Tuttle, Hengesh, et al., 2002; Castilla and Audemard, 2007). Despite these effects, the relation between earthquake magnitude and epicentral distance of sand blows was found to be a useful estimator of approximate magnitudes of pre-instrumental earthquakes (Castilla and Audemard, 2007).

The earthquake magnitude-liquefaction distance relations have been used in paleoliquefaction studies to estimate magnitudes of paleoearthquakes from their farthest observed sand blows. This method is sometimes referred to as the magnitude-bound procedure (Obermeier, 1996).

Magnitude estimates derived from these relations are considered minimum values since the actual epicentral distance to farthest sand blow is unlikely to be known (Tuttle, 2001; Castilla and Audemard, 2007). A great deal of reconnaissance by an experienced investigator is often required to find and recognize distal sand blows since they become smaller, less frequent, and may occur in areas underlain by sediments that are especially susceptible to liquefaction. The distance to the farthest observed sand dikes should not be used to estimate magnitudes of paleoearthquakes. To do so could lead to overestimation of paleoearthquake magnitudes since sand dikes can form at greater distances than sand blows, and the magnitude-distance relations were based on “surface manifestations” of liquefaction.

The magnitude-distance relations have been used to estimate magnitudes of paleoearthquakes in the New Madrid and Wabash Valley seismic zones. For New Madrid, minimum magnitudes of **M** 6.7 and 6.9 were estimated for the paleoearthquakes of AD 1450 (500 yr BP) and AD 900 (1,050 yr BP), respectively, from the distance of observed sand blows (Figure E-68; Tuttle, 2001). Even though more than 1,000 km of river cutbanks have been searched, the limits of liquefaction have not yet been defined for these earthquakes. To improve the magnitude estimates of paleoearthquakes centered in the Wabash Valley seismic zone, the magnitude-bound relation was calibrated using one modern and several historical cases of earthquake-induced liquefaction in the Central and Eastern United States and southeastern Canada (Olson et al., 2005b). This was done in an attempt to account for regional differences in earthquake source characteristics, ground motion attenuation, local site effects, and liquefaction susceptibility of sediments. The magnitude estimates based on the calibrated relation differed little (0 to 0.1 magnitude unit) from those using the worldwide relation developed by Ambraseys (1988), suggesting that historical earthquakes, with poorly constrained locations and magnitudes, are unlikely to significantly improve the worldwide relation based on instrumental earthquakes. Calibration of the magnitude-bound relation may be most fruitful for regions that have experienced instrumental earthquakes that induced liquefaction.

There are several obvious factors that contribute to uncertainties in magnitude estimates for paleoearthquakes based on the magnitude-bound method. The epicentral location may be poorly defined and the farthest sand blow is unlikely to be known. In addition, the magnitude-distance relation itself has some inherent uncertainties since the epicentral distance to the farthest sand blow may not be known even for instrumental earthquakes. The relation is poorly constrained for earthquakes greater than magnitude 7.2 (Figure E-67).

Given the various unknowns, uncertainties associated with magnitude estimates determined with the magnitude-bound method are likely to range from 0.25 to 0.6 magnitude unit (Table E-2.2). The 2001 **M** 7.7 Bhuj, India, earthquakes can be used to demonstrate the uncertainty in magnitude estimates derived using the magnitude-bound method. If the small sand blows that formed near Ahmedabad (approximately 240 km from the epicenter of the Bhuj earthquake) were not found and those along the Allah Bund (about 130 km from the epicenter of the Bhuj earthquake) were thought to be the farthest sand blows induced by a paleoearthquake centered near Bhuj, a magnitude estimate of 7.1 would be derived using the method (Figure E-46). In this example, the magnitude-bound method would have underestimated the magnitudes of the hypothetical paleoearthquakes by 0.6 magnitude unit.

E.2.2.4.3 *Geotechnical Analysis*

In addition to the methods described above, the magnitudes of liquefaction-inducing paleoearthquakes also can be estimated using geotechnical characterizations of in situ soil properties and liquefaction potential analysis (e.g., Olson et al., 2001, 2005b; Green et al., 2005). The cyclic-stress (e.g., Seed and Idriss, 1982; Youd, 2001; Cetin et al., 2004) and seismic energy (e.g., Pond, 1996) methods of liquefaction potential analysis have been applied in paleoearthquake studies. Typically, these back-calculations are based on the identification of the soil layers that may have liquefied during paleoearthquakes, the measurement of geotechnical properties of these layers (penetration resistance, soil density, effective confining or overburden stress, etc.), and the relation between the geotechnical properties and the ground motions necessary to trigger liquefaction. The geotechnical approach to back-calculating magnitudes of paleoearthquakes has been used widely in the Charleston seismic zone (e.g., Hu et al., 2002a, 2002b; Leon, 2003; Leon et al., 2005; Gassman et al., 2009) and the Wabash Valley seismic zones (e.g., Obermeier et al., 1993; Olson et al., 2001). It has also been used to a more limited extent in the New Madrid seismic zone (e.g., Schneider and Mayne, 2000; Schneider et al., 2001; Liao et al., 2002; Stark, 2002; Tuttle and Schweig, 2004) and the Charlevoix seismic zone (e.g., Tuttle and Atkinson, 2010; Table 1.2-1).

Green et al. (2005) identify three main sources of uncertainty associated with the back-calculation of ground motion characteristics from paleoliquefaction data:

- Uncertainty due to changes in the geotechnical properties of the source sediments of liquefaction features, including but not limited to density changes due to liquefaction and to postliquefaction effects related to aging and groundwater conditions.
- The selection of appropriate geotechnical soil indices to be measured at paleoliquefaction sites.
- The selection of appropriate methodology for integration of back-calculated results of ground shaking from individual paleoliquefaction sites into a regional assessment of paleoseismic strength of shaking. An appropriate methodology must account for uncertainty in seismic parameters (e.g., amplitude, duration, frequency, and directivity), regional ground motion attenuation, local site effects, and site-to-source distance.
- The understanding of these sources of uncertainty remains the focus of ongoing research. At present, the geotechnical approach may yield a broad range of possible magnitudes for a given paleoearthquake, and these ranges may provide only a minimum constraint on magnitude. For example, Leon et al. (2005) calculate magnitude estimates for each of the Charleston paleoearthquakes and, for each paleoearthquake, their estimates vary by 0.8 to 1.4 magnitude units. For the CEUS SSC Project, estimates of paleoearthquake magnitude based on geotechnical analysis were used where available to help characterize M_{max} , in conjunction with other indicators of magnitude such as magnitude-bound and magnitude-feature size relations (e.g., Ambraseys, 1988; Castilla and Audemard, 2007).

E.2.2.5 Recurrence of Paleoearthquakes

E.2.2.5.1 *Age Estimates of Liquefaction Features and Paleoearthquakes*

As described above, the goal of dating seismically induced paleoliquefaction features is to bracket the time of the causative earthquake as tightly as possible. Typically, numerical constraining ages are obtained that predate and postdate paleoliquefaction features. The timing of paleoearthquakes is defined by selecting the age range common to multiple paleoliquefaction features in a region. Therefore, the precision with which recurrence can be calculated depends on the precision of the estimated timing of the paleoearthquakes. Once a paleoearthquake chronology (or alternative paleoearthquake scenarios) has been developed using methodologies outlined above, estimates of earthquake recurrence can be calculated for that region. Well-constrained age estimates of paleoearthquakes contribute to well-constrained estimates of recurrence times (Table E-2.2). For the CEUS SSC Project, paleoliquefaction data were used to estimate uncertainty ranges for the timing of paleoearthquakes and to calculate rates of repeated large-magnitude earthquakes (see Section 6.1.5.4 of the main report). For example, well-constrained age estimates of sand blows in the New Madrid seismic zone contributed to well-constrained ages estimates of paleoearthquakes (10–100 years) during the past 1,200 years (Figure E-64). However, incompleteness of the paleoearthquake record prior to 1,200 yr BP and questions regarding sources outside the New Madrid seismic zone led to significant uncertainty in recurrence time (tens to thousands of years) of repeated large-magnitude earthquake (RLME) sources in the greater New Madrid region.

E.2.2.5.2 *Length and Completeness of the Paleoliquefaction Record*

The completeness of the paleoearthquake record should be considered in estimating earthquake recurrence. The completeness of the record will vary depending on the location of the study area and its geologic and hydrologic history. The longer and more continuous the history of sedimentation, the more complete the earthquake record is likely to be (Table E-2.2). Also, loose sandy sediments must be saturated in order to liquefy during earthquakes. Therefore, significant changes in land level and sea (or lake) level related to glacio-eustatic processes can affect the liquefaction susceptibility of sediments and thus the completeness of the earthquake record. These changes may be especially important in glaciated and coastal regions.

Many paleoearthquake chronologies are limited by the age range, distribution, and exposure of the deposits that were susceptible to liquefaction during the period of interest. In the New Madrid region, for example, liquefiable fluvial deposits are widespread, but the deposits, in general, increase in age from east to west across the Lower Mississippi River valley. A large percentage of the liquefiable fluvial deposits in the immediate vicinity of the New Madrid seismic zone are only five thousand years old, so the record of paleoearthquakes is relatively short. In addition, older sand blows may be buried too deep in the section to be exposed in river and ditch cutbanks. Like many depositional environments where paleoliquefaction features form, exposure in the Lower Mississippi River valley is limited to times of year when the water table is low.

Liquefaction features identified along the South Carolina coast range in age from mid-Holocene to historical, but it remains unclear whether the older portions of the Charleston paleoearthquakes record is complete. Talwani and Schaeffer (2001) suggest that the record is complete only for the most recent approximately 2,000 years and that it is possible that liquefaction events are missing from the older portions of the record, especially between about

2,000 and 5,000 yr BP. Talwani and Schaeffer (2001) suggest that past fluctuations in sea level have produced time intervals of low water table conditions, and thus low liquefaction susceptibility, during which large earthquakes may not have induced liquefaction. Similarly, the Late Wisconsin–Holocene record of paleoearthquakes in the Charlevoix seismic zone and St. Lawrence Lowlands is thought to be incomplete due to fluctuations in sea level, especially during the period between 6 and 7 ka (Tuttle and Atkinson, 2010).

By evaluating the completeness of the paleoearthquake record, informed decisions can be made regarding which data sets or portions of data sets to use to estimate realistic recurrence times. Incomplete data sets can provide a minimum numbers of earthquakes for a certain time period and help to constrain recurrence rates.

E.2.3 Recommendations for Future Research

Liquefaction studies have contributed to the characterization of seismic sources by providing information about the timing, locations, magnitudes, and recurrence rates of paleoearthquakes. However, there are often large uncertainties associated with these earthquake parameters. In addition, there are few trained professionals to carry out this type of study. With additional development of the field of study and of trained personnel, it may be possible to reduce uncertainties associated with earthquake parameters and advance the usefulness and application of paleoliquefaction studies. To this end, recommendations for future research are given below.

Development of a manual of best practice would provide guidance in conducting paleoliquefaction studies and would promote accuracy and completeness of paleoliquefaction data. The manual could be complemented by training workshops with experts in the field. During these workshops, professional earth scientists and the next generation of paleoseismologists would gain experience searching for, documenting, and interpreting liquefaction features.

Case studies of liquefaction induced by modern earthquakes, with well-constrained locations, magnitudes, and other earthquake parameters, are encouraged and would help to further characterize the size and spatial distributions of liquefaction features. Such case studies should be regional in scope and include detailed descriptions of liquefaction features such as size and sedimentary characteristics of sand blows, dikes, sills and other soft-sediment deformation structures (see Section E.2.1.1 and Figure E-2). These case studies would be helpful in providing analogue events for direct comparison as well as information that could be used to further improve empirical relations of earthquake and liquefaction parameters.

To gain a better understanding of both the processes of liquefaction and the effects on the source beds that liquefied, instrumentation of liquefaction-prone sites is encouraged, as is pre- and post-event measurement of geotechnical properties. This information may help to reduce uncertainties related to back-calculating magnitudes using post-event measurements. Field experiments of earthquake-induced liquefaction are more likely to be conducted in interplate settings where large earthquakes occur more frequently. Therefore, if results of these field experiments are to be applied in the CEUS, it would be beneficial to better understand differences between characteristics of intraplate and interplate earthquakes, such as frequency content and attenuation of ground motion, that influence liquefaction.

In regions where paleoearthquake records exist but have not been fully developed, paleoseismic studies could be designed that would improve the completeness and extend the length of the

paleoearthquake chronologies in order to improve recurrence estimates of large earthquakes and to improve understanding of earthquake sources. It is also recommended that paleoliquefaction studies be conducted in regions of low seismicity that share geologic and tectonic characteristics with known seismogenic zones to better understand the earthquake potential of these regions and to test the hypothesis that inherited structure, particularly faults that were active during the Mesozoic, controls seismicity in the CEUS.

Radiocarbon and OSL are the two most common dating techniques used in paleoliquefaction studies. Because they are often collected stratigraphically above and below sand blows, samples provide minimum and maximum constraining dates for liquefaction features and thus the earthquakes that caused them. Although the individual dates may have precisions of ± 20 –80 years, the age estimates of liquefaction features based on the combination of the minimum and maximum constraining dates will have uncertainties of about 100 years in the best of circumstances (see Figure E-3). Dating techniques that provide more precise results and dating strategies that provide more accurate results would help to improve age estimates of liquefaction features and thus their causative earthquakes. Dendrochronology is one technique that could improve precision of age estimates of liquefaction features. Therefore, we recommend that efforts be made to use dendrochronology to date paleoliquefaction features in regions where chronologies of long-lived tree species already have been developed. If those efforts are successful, it would be worthwhile to extend the chronologies of long-lived tree species further back in time and to help constrain the ages of older liquefaction features.

E.3 Guidance for the Use of Paleoliquefaction Data in Seismic Source Characterization

The following is a summary of guidance for the use of paleoliquefaction data:

- Ensure liquefaction features have an earthquake origin and are not the result of other processes. Potential uncertainties regarding feature identification and interpretation are described in Section E.2 of this appendix.
- Use liquefaction features with well-constrained calibrated (2-sigma) ages to determine timing of paleoearthquakes (Figure E-3). Space-time diagrams illustrating age constraints and estimated ages of features can help to estimate timing of paleoearthquakes.
- Correlate features that are similar in age and/or occur in similar stratigraphic context within the same exposure or where strata are laterally continuous.
- Compare size and distribution of paleoliquefaction features with those that formed during modern or historical earthquakes in the same or similar geologic and tectonic settings to help interpret the source areas and magnitudes of causative earthquakes.
- Use information on surficial geology, geologic and groundwater history, and geotechnical data and analysis, to help interpret the source areas and magnitudes of paleoearthquakes. Time-slice maps and animations may help to interpret earthquake source areas, and ground motion simulations may help to interpret earthquake magnitudes.
- Use empirical relations developed from case studies of modern earthquakes in similar geologic and tectonic settings to estimate magnitudes of paleoearthquakes on the basis of maximum distance of sand blows from the inferred epicenters.

- If sufficient data are available, incorporate the effect of ground motion parameters (e.g., attenuation and site response) on the size and distribution of liquefaction features when interpreting source areas and magnitudes of paleoearthquakes.
- Consider the completeness of the paleoearthquake record in both space and time when estimating source areas, magnitudes, and recurrence times of paleoearthquakes.
- If sufficient data are available, estimate recurrence times of paleoearthquakes with well-defined timing, source areas, and magnitudes of paleoearthquakes.

E.4 Glossary

Ball-and-pillow structures. Deformation structures that form when lobes of sediment sink into underlying sediment forming isolated masses that resemble balls and pillows.

Basal erosion. Foundering of the base on a sedimentary unit due to liquefaction and loss of strength of the underlying sediment.

Bearing capacity. The ability of soil or sediment to carry a load without failing.

Close maximum constraining age. Maximum possible age derived by dating material collected immediately below a feature of interest that nearly approximates its age.

Close minimum constraining age. Minimum possible age derived by dating material collected immediately above a feature of interest that nearly approximates its age.

Consistence. Term describing a soil's ability to resist crushing and to be molded.

Contemporary age. An age that reflects the formation of the deposit from which the dated sample was collected.

Convolute bedding. Contorted bedding usually confined to a single sedimentary unit.

Dendrocalibration curve. Relation used to convert radiocarbon ages to calendar ages based on radiocarbon dating of tree rings of known ages.

Dessication crack. Crack in clayey sediment that forms by shrinkage as the result of drying.

Dish structures. Deformation structures consisting of flat to concave upward laminations caused by liquefaction and fluidization of sediment and commonly associated with pillars.

Earthquake recurrence. The repetition of a similar magnitude earthquake generated by the same fault or source zone.

Effective stress or overburden pressure. The portion of the load or force from overlying material that is supported by the soil or sediment grains.

Eustacy. Of, or pertaining to, worldwide sea level.

Flow lineation. Lineation in sediment related to liquefaction and fluidization of sediment.

Fluidization. Process by which vertical fluid flow through sediment exerts sufficient drag force on the grains to lift or suspend them against the force of gravity.

Glacio-isostasy. Lithospheric adjustment in response to the weight or melting of glaciers.

Holocene. The most recent geologic epoch, following the last glaciation, known as the Wisconsin in North America and beginning about 12,000 years BP.

Liquefaction. A process by which saturated, granular sediment temporarily loses its strength and behaves as a viscous liquid due to earthquake ground shaking

Liquefaction field. The area over which liquefaction features form during a particular earthquake.

Load structure. A deformation structure that forms when sediment sinks into underlying sediment that has lost its strength in some cases due to liquefaction.

Magnitude-bound. Relation defining the lowest magnitude at which liquefaction is likely to occur at any given epicentral distance.

Maximum constraining age. Maximum possible age derived by dating material collected stratigraphically below a feature of interest.

Minimum constraining age. Minimum possible age derived by dating material collected stratigraphically above a feature of interest.

Optically simulated luminescence (OSL). Dating technique used to determine the amount of time that has passed since sediment was last exposed to light (see Section E.2.1.3.3).

Penetration resistance. Measure of soil or sediment density expressed as N or the number of hammer blows it takes to drive a split-tube sampler 12 inches.

pH. Measure of acidity of an aqueous solution and is related to the negative logarithm of the concentration of hydrogen ions and their tendency to interact with other components of the solution.

Pillars. Deformation structures including tubular to sheet-like zones of structureless to swirled sediment that form during forceful and explosive water escape.

Pleistocene. The earlier of the two geologic epochs comprising the Quaternary; characterized by multiple glaciations.

Pore-water pressure. The water pressure within the voids or spaces between soil or sediment grains.

Pseudonodule. A deformation structure similar to a load structure except that the sediment that sinks into underlying sediment becomes detached to form separate bodies or domains.

Quaternary. The youngest geologic period beginning about 2.6 million years ago; subdivided into Pleistocene and Holocene epochs.

Relative density. The relation between the actual void ratio and the maximum and minimum void ratios of a soil or sediment.

Sand blow. Deposit resulting from liquefaction and fluidization of subsurface sandy sediment and expulsion of liquefied sediment onto the ground surface.

Sand dike. Intrusive sand body, often tabular in shape, resulting from liquefaction and fluidization of subsurface sandy sediment and injection of liquefied sediment into overlying deposits.

Sand diapir. A small, sandy intrusion into overlying, usually fine-grained, sediment.

Soft-sediment deformation structures. A variety of structures, including sand diapirs, basal erosion, convolute bedding, pseudonodules, and load casts, that form in unconsolidated sediments as the result of deformation ranging from bulk transport of the sediment mass to in situ relative grain displacement.

Soil structure. The arrangement of primary soil particles into secondary units known as pedons.

Space-time diagram. Diagram showing variations in some parameter over space and time.

Void ratio. The ratio of the volume of voids, or space between grains, to the volume of solids in a soil or sediment.

Wisconsin. The last glacial age of the Pleistocene epoch of North America.

E.5 References

E.5.1 References Cited in Paleoliquefaction Database

- Amick, D., Gelinas, R., Maurath, G., Cannon, R., Moore, D., Billington, E., and Kemppinen, H., 1990, Paleoliquefaction features along the Atlantic Seaboard: U.S. Nuclear Regulatory Commission Report, NUREG/CR-5613.
- Amick, D., Maurath, G., and Gelinas, R., 1990, Characteristics of Seismically Induced Liquefaction Sites and Features Located in the Vicinity of the 1886 Charleston, South Carolina Earthquake: *Seismological Research Letters*, v. 61, no. 2, pp. 117-130.
- Barnes, A. A., 2000, An interdisciplinary study of earthquake-induced liquefaction features in the New Madrid seismic zone, central United States: M.S. thesis, Auburn University, Alabama, 266 p.
- Bauer, L. M., 2006, Studies of Historic and Prehistoric Earthquake-induced Liquefaction Features in the Meizoseismal Area of the 1811-1812 New Madrid Earthquakes, Central United States: M.S. thesis, University of Memphis, Memphis, Tennessee, p. 135.
- Broughton, A. T., Van Arsdale, R. B., and Broughton, J. H., 2001, Liquefaction susceptibility mapping in the city of Memphis and Shelby County, Tennessee (in Earthquake hazard evaluation in the central United States): *Engineering Geology*, v. 62 (1-3), pp. 207-222.
- Browning, S. E., 2003, Paleoseismic studies in the New Madrid Seismic Zone, Central United States: M.S. thesis, Auburn University, Auburn, Alabama, 134 p.
- Buchner, C. A., Cox, R., Skinner, C. T., Kaplan, C., and Albertson, E. S., 2010, Data recovery excavations at the Laplant I Site (23NM51), New Madrid County, Missouri: Report to U.S. Army Corps of Engineers, Memphis District.
- Collier, J. W., 1998, Geophysical investigations of liquefaction features in the New Madrid seismic zone: Northeastern Arkansas and southeastern Missouri: M.S. thesis, Auburn University, Auburn, Alabama, 163 p.
- Cox, R. T., Van Arsdale, R. B., Harris, J. B., and Larsen, D., 2001, Neotectonics of the southeastern Reelfoot rift zone margin, central United States, and implications for regional strain accommodation: *Geology*, v. 29, pp. 419-422.
- Cox, R.T., Larsen, D., Forman, S.L., Woods, J., Morat, J., Galluzzi, J., 2004, Preliminary assessment of sand blows in the southern Mississippi Embayment: *Bulletin of the Seismological Society of America*, v. 94, no. 3, pp. 1125-1142.
- Cox, R. T., Cherryhomes, J., Harris, J. B., Larsen, D., Van Arsdale, R. B., and Forman, S. L., 2006, Paleoseismology of the southeastern Reelfoot rift in western Tennessee, U.S.A. and implications for intraplate fault zone evolution: *Tectonics*, v. 25, TC3019, doi:10.1029/2005TC001829, 17 p.
- Cox, R. T., Hill, A. A., Larsen, D., Holzer, T., Forman, S. L., Noce, T., Gardner, C., and Morat, J., 2007, Seismotectonic implications of sand blows in the southern Mississippi Embayment, *Engineering Geology*, v. 89, pp. 278-299.

- Craven, J. A., 1995a, Paleoseismological Study in the New Madrid Seismic Zone Using Geological and Archeological Features to Constrain Ages of Liquefaction Deposits: M.S. thesis, University of Memphis, 51 pp.
- Craven, J. A., 1995b, Evidence of paleoseismicity within the New Madrid seismic zone at a late Mississippian Indian occupation site in the Missouri Bootheel: *Geological Society of America, Abstracts with Programs, 1995 Annual Meeting*, p. A-394.
- Dominion Nuclear North Anna, LLC (Dominion), 2004, North Anna Early Site Permit Application, Response to Request for Additional Information No. 3, Nuclear Regulatory Commission Accession Number ML042800292, July 8.
- Exelon Generation Company, 2004, Clinton Early Site Permit Application, Response to Request for Additional Information Letter No. 7, October 11.
- Gassman, S., Talwani, P., and Hasek, M., 2009, Maximum Magnitudes of Charleston, South Carolina Earthquakes from In-Situ Geotechnical Data: Abstracts Volume from Meeting of Central and Eastern U.S. Earthquake Hazards Program, University of Memphis, Memphis, TN, October 28-29, p. 19.
- Green, R. A., Obermeier, S. F., and Olson, S. M., 2005, Engineering geologic and geotechnical analysis of paleoseismic shaking using liquefaction effects: Field examples: *Engineering Geology*, v. 76, pp. 263-293.
- Hajic, E. R., Wiant, M. D., and Oliver, J. J., 1995, Distribution and dating of prehistoric earthquake liquefaction in southeastern Illinois, central U.S.: National Earthquake Hazards Reduction Program, Final Technical Report, Agreement No. 1434-93-G-2359, 34 pp.
- Hu, K., Gassman, S. L., and Talwani, P., 2002a, In-situ properties of soils at paleoliquefaction sites in the South Carolina coastal plain: *Seismological Research Letters*, v. 73, no. 6, pp. 964-978.
- Hu, K., Gassman, S. L., and Talwani, P., 2002b, Magnitudes of prehistoric earthquakes in the South Carolina coastal plain from geotechnical data: *Seismological Research Letters*, v. 73, no. 6, pp. 979-991.
- Law, K.T., 1990, Analysis of soil liquefaction during the 1988 Saguenay earthquake: *Proceedings of the 43rd Canadian Geotechnical Conference, Quebec*, v. 1, pp. 189-196.
- Leon, E., 2003, Effect of Aging of Sediments on Paleoliquefaction Evaluation in the South Carolina Coastal Plain: unpublished Ph.D. dissertation, University of South Carolina, 181 pp.
- Leon, E., Gassman, S. L., and Talwani, P., 2005, Effect of soil aging on assessing magnitudes and accelerations of prehistoric earthquakes: *Earthquake Spectra*, v. 21, no. 3, pp. 737-759.
- Li, Y., Schweig, E. S., Tuttle, M. P., and Ellis, M. A., 1998, Evidence for large prehistoric earthquakes in the northern New Madrid seismic zone, central United States: *Seismological Research Letters*, v. 69, no. 3, pp. 270-276.
- Liao, T., Mayne, P. W., Tuttle, M. P., Schweig, E. S., and Van Arsdale, R. B., 2002, CPT site characterization for seismic hazards in the New Madrid seismic zone: *Soil Dynamics and Earthquake Engineering*, v. 22, pp. 943-950.

- Mayne, P. W., 2001, Cone penetration testing for seismic hazards evaluation in Memphis and Shelby County, Tennessee, U.S. Geological Survey, Earthquake Hazards Program, Final Report (00HQGR0025), 21 pp.
- McNulty, W. E. and Obermeier, S. F., 1999, Liquefaction Evidence for at Least Two Strong Holocene Paleo-Earthquakes in Central and Southwestern Illinois, USA: *Environmental and Engineering Geoscience*, v. V, no. 2, pp. 133-146.
- Munson, P. J. and Munson, C. A., 1996, Paleoliquefaction Evidence for Recurrent Strong Earthquakes Since 20,000 Years BP in the Wabash Valley Area of Indiana, report submitted to the U.S. Geological Survey in fulfillment of National Earthquake Hazards Reduction Program Grant No. 14-08-0001-G2117, 137 pp.
- Munson, P. J., Obermeier, S. F., Munson, C. A., and Hajic, E. R., 1997, Liquefaction evidence for Holocene and latest Pleistocene seismicity in the southern halves of Indiana and Illinois: A preliminary overview: *Seismological Research Letters*, v. 68, pp. 521-536.
- Noller, J. S. and Forman, S. L., 1998, Luminescence Geochronology of Liquefaction Features Near Georgetown, South Carolina: in J.M. Sowers, J.S. Noller, and W.R. Lettis (eds.) *Dating and Earthquakes: Review of Quaternary Geochronology and Its Application to Paleoseismology*: U.S. Nuclear Regulatory Commission Report, NUREG/CR-5562, pp. 4.49-4.57.
- Obermeier, S. F., 1998, Liquefaction evidence for strong earthquakes of Holocene and latest Pleistocene ages in the states of Indiana and Illinois, USA: *Engineering Geology*, v. 50, pp. 227-254.
- Olson, S. M., Green, R. A., and Obermeier, S. F., 2005b, Revised magnitude bound relation for the Wabash Valley seismic zone of the central United States: *Seismological Research Letters*, v. 76, no. 6, pp. 756-771.
- Pond, E. C., and Martin, J. R., 1997, Estimated magnitudes and accelerations associated with prehistoric earthquakes in the Wabash Valley region of the central United States: in Kolata, D. R., and Hildenbrand, T. G. (editors), *Investigations of the Illinois Basin Earthquake Region*: *Seismological Research Letters*, v. 68, pp. 611-623.
- Al-Qadhi, O., 2010, Geophysical investigation of paleoseismological features in eastern Arkansas, USA: Ph.D. Dissertation, University of Arkansas at Little Rock, p. 277.
- Saucier, R. T., 1991, Geoarchaeological evidence of strong prehistoric earthquakes in the New Madrid (Missouri) seismic zone: *Geology*, v. 19, pp. 296-298.
- Al-Shukri, H., Lemmer, R. E., Mahdi, H. H., and Connelly, J. B., 2005, Spatial and temporal characteristics of paleoseismic features in the southern terminus of the New Madrid seismic zone in eastern Arkansas: *Seismological Research Letters*, v. 76, no. 4, pp. 502-511.
- Al-Shukri, H., Mahdi, H., Al Kadi, O., and Tuttle, M. P., 2009, *Spatial and Temporal Characteristics of Paleoseismic Features in the Southern Terminus of the New Madrid Seismic Zone in Eastern Arkansas*: Final Technical Report to U.S. Geological Survey, 24 pp.
- Talwani, P., Amick, D. C., and Schaeffer, W. T., 1999, *Paleoliquefaction Studies in the South Carolina Coastal Plain*: U.S. Nuclear Regulatory Commission Report NUREG/CR 6619, 109 pp.

- Talwani, P., and Cox, J., 1985, Paleoseismic evidence for recurrence of earthquakes Near Charleston, South Carolina: *Science*, v. 228, pp. 379-381.
- Talwani, P., Dura-Gomez, I., Gassman, S., Hasek, M., and Chapman, A., 2008, Studies related to the discovery of a prehistoric sandblow in the epicentral area of the 1886 Charleston SC earthquake: Trenching and geotechnical investigations: *Program and Abstracts, Eastern Section of the Seismological Society of America*, p. 50.
- Talwani, P., Rajendran, C. P., Rajendran, K., and Madabhushi, S., 1993, *Assessment of Seismic Hazard Associated with Earthquake Source in the Bluffton-Hilton Head Area*: Technical Report SCUREF Task Order 41, University of South Carolina at Columbia, 85 pp.
- Talwani, P., and Schaeffer, W. T., 2001, Recurrence rates of large earthquakes in the South Carolina coastal plain based on paleoliquefaction data: *Journal of Geophysical Research*, v. 106, no. B4, pp. 6621-6642.
- Tuttle, M.P., 1994, *The Liquefaction Method for Assessing Paleoseismicity*, U.S. Nuclear Regulatory Commission, NUREG/CR-6258, 38 pp.
- Tuttle, M. P., 1999, Late Holocene Earthquakes and Their Implications for Earthquake Potential of the New Madrid Seismic Zone, Central United States: Ph.D. dissertation, University of Maryland, College Park, Maryland, 250 pp.
- Tuttle, M. P., 2000, *Paleoseismological Study in the St. Louis Region*: U.S. Geological Survey, Earthquake Hazards Program, Final Technical Report (99HQGR0032), 29 pp.
- Tuttle, M. P., 2005, *Improving the Earthquake Chronology for the St. Louis Region*: U.S. Geological Survey, Earthquake Hazards Program, Annual Project Summary (05HQGR0045), 6 pp.
- Tuttle, M. P., 2007, *Re-evaluation of Earthquake Potential and Source in the Vicinity of Newburyport, Massachusetts*: U.S. Geological Survey, Earthquake Hazards Program, Final Technical Report (01HQGR0163).
- Tuttle, M. P., 2008, Paleoseismological investigations at the East Site, The Gilmore/Tyronza Mitigation Project, v. 4, Data Recovery at the Tyronza Sites, Poinsett County, Arkansas, The East Site (3P0610): in *Technical Report to Arkansas State Highway and Transportation Department*, pp. 259-277.
- Tuttle, M. P., 2009, *Re-evaluation of Earthquake Potential and Source in the Vicinity of Newburyport, Massachusetts*: U.S. Geological Survey, Earthquake Hazards Program, Final Technical Report (03HQGR0031).
- Tuttle, M. P., 2010, *Search for and Study of Sand Blows at Distant Sites Resulting from Prehistoric and Historic New Madrid earthquakes*: Collaborative Research, M. Tuttle & Associates and Central Region Hazards Team, U.S. Geological Survey, Final Technical Report (02HQGR0097), 48 pp.
- Tuttle, M.P., Such, R., and Seeber, L., 1989, Ground failure associated with the November 25th, 1988 Saguenay earthquake in Quebec Province, Canada: in Jacob, K., ed., *The 1988 Saguenay Earthquake of November 25, 1988, Quebec, Canada: Strong Motion Data, Ground Failure Observations, and Preliminary Interpretations*, Buffalo, New York, National Center for Earthquake Engineering Research, pp. 1-23.

- Tuttle, M., Law, T., Seeber, L., and Jacob, K., 1990, Liquefaction and ground failure in Ferland, Quebec, triggered by the 1988 Saguenay Earthquake: *Canadian Geotechnical Journal*, v. 27, pp. 580-589.
- Tuttle, M., and Seeber, L., 1991, Historic and prehistoric earthquake-induced liquefaction in Newbury, Massachusetts: *Geology*, v. 19, pp. 594-597.
- Tuttle, M. P., Cowie, P., and Wolf, L., 1992, Liquefaction induced by modern earthquakes as a key to paleoseismicity: A case study of the 1988 Saguenay earthquake: in Weiss, A., ed., *Proceedings of the Nineteenth International Water Reactor Safety Information Meeting*, NUREG/CP-0119, v. 3, pp. 437-462.
- Tuttle, M. P., and Schweig, E. S., 1995, Archeological and pedological evidence for large earthquakes in the New Madrid seismic zone, central United States: *Geology*, v. 23, pp. 253-256.
- Tuttle, M. P., Lafferty, R. H., III, and Schweig, E. S., III, 1998, *Dating of Liquefaction Features in the New Madrid Seismic Zone and Implications for Earthquake Hazard*: U.S. Nuclear Regulatory Commission, NUREG/GR-0017, 77 pp.
- Tuttle, M., Chester, J., Lafferty, R., Dyer-Williams, K., and Cande, B., 1999, *Paleoseismology Study Northwest of the New Madrid Seismic Zone*: U.S. Nuclear Regulatory Commission, NUREG/CR-5730, 98 pp.
- Tuttle, M. P., Sims, J. D., Dyer-Williams, K., Lafferty, R. H., III, and Schweig, E. S., III, 2000, *Dating of Liquefaction Features in the New Madrid Seismic Zone*: U.S. Nuclear Regulatory Commission, NUREG/GR-0018, 42 pp.
- Tuttle, M. P., and Wolf, L. W., 2003, *Towards a Paleoearthquake Chronology of the New Madrid Seismic Zone*: U.S. Geological Survey, Earthquake Hazards Program, Progress Report (01HQGR0164), 38 pp.
- Tuttle, M. P., and Schweig, E. S., 2004, *Search for and Study of Sand Blows at Distant Sites Resulting from Prehistoric and Historic New Madrid Earthquakes*: U.S. Geological Survey, Earthquake Hazards Program, Annual Project Summary (02HQGR0097), 18 pp.
- Tuttle, M., and Chester, J. S., 2005, *Paleoseismology Study in the Cache River Valley, Southern Illinois*: U.S. Geological Survey, Earthquake Hazards Program, Final Technical Report (HQ98GR00015), 14 pp.
- Tuttle, M. P., Schweig, E., III, Campbell, J., Thomas, P. M., Sims, J. D., and Lafferty, R. H., III, 2005, Evidence for New Madrid earthquakes in AD 300 and 2350 B.C.: *Seismological Research Letters*, v. 76, no. 4, pp. 489-501.
- Tuttle, M. P., Al-Shukri, H., and Mahdi, H., 2006, Very large earthquakes centered southwest of the New Madrid seismic zone 5,000-7,000 years ago: *Seismological Research Letters*, v. 77, no. 6, pp. 664-678.
- Tuttle, M. P., and Atkinson, G. M., 2010, Localization of large earthquakes in the Charlevoix seismic zone, Quebec, Canada during the past 10,000 years: *Seismological Research Letters*, v. 81, no. 1, pp. 18-25.
- Vaughn, J. D., 1994, *Paleoseismology Studies in the Western Lowlands of Southeast Missouri*: U.S. Geological Survey, Final Report (14-08-0001-G1931), 27 pp.

- Weems, R. E., and Obermeier, S. F., 1990, The 1886 Charleston earthquake—An overview of geological studies: in *Proceedings of the U.S. Nuclear Regulatory Commission Seventeenth Water Reactor Safety Information Meeting*, NUREG/CP-0105, volume 2, pp. 289-313.
- Weems, R.E., Obermeier, S.F., Pavich, M.J., Gohn, G.S., and Rubin, M., 1986, Evidence for three moderate to large prehistoric Holocene earthquakes near Charleston, South Carolina: in *Proceedings of the 3rd U.S. National Conference on Earthquake Engineering, Charleston, South Carolina*, v. 1, pp. 3-13.
- Wesnowsky, S. G., and Johnson, D. L., 1996, Stratigraphic, paleosol, and C-14 evidence for a large pre-1811 magnitude earthquake in the New Madrid seismic zone: *Seismological Research Letters*, v. 67, no. 2, p. 60.
- Wolf, L.W., 2004, *Geophysical Investigations of Earthquake-Induced Liquefaction Features in the New Madrid Seismic Zone*: Earthquake Hazards Program, Final Technical Report (01HQGR0003), 36 pp.

E.5.2 References Cited in Appendix E

- Aiken, M. J., 1990, *Science-Based Dating in Archaeology*: Longman Group, London and New York, 274 pp.
- Aitken, M. J., 1998, *An Introduction to Optical Dating: The Dating of Quaternary Sediments by the Use of Photon-Stimulated Luminescence*: Oxford University Press, 280 pp.
- Adams, J., and Basham, P., 1989, The seismicity and seismotectonics of Canada east of the Cordillera: *Geoscience Canada*, v. 16, pp. 3-16.
- Allen, J. R. L., 1982, *Sedimentary Structures: Their Character and Physical Basis*, Elsevier, Amsterdam.
- Ambraseys, N. N., 1988, Engineering seismology: earthquake engineering and structural dynamics: *Journal of the International Association of Earthquake Engineering*, v. 17, pp. 1-105.
- Amick, D. C., 1990, Paleoliquefaction Investigations Along the Atlantic Seaboard with Emphasis on the Prehistoric Earthquake Chronology of Coastal South Carolina: unpublished Ph.D. dissertation, University of South Carolina.
- Amick, D., Gelinas, R., Maurath, G., Cannon, R., Moore, D., Billington, E., and Kempainen, H., 1990, *Paleoliquefaction Features Along the Atlantic Seaboard*: U.S. Nuclear Regulatory Commission Report, NUREG/CR-5613.
- Amick, D., Maurath, G., and Gelinas, R., 1990, Characteristics of seismically induced liquefaction sites and features located in the vicinity of the 1886 Charleston, South Carolina earthquake: *Seismological Research Letters*, v. 61, no. 2, pp. 117-130.
- Amick, D. and Gelinas, R., 1991, The search for evidence of large prehistoric earthquakes along the Atlantic seaboard: *Science*, v. 251, pp. 655-658.
- Atwater, B. F., Tuttle, M. P., Schweig, E. S., Rubin, C. M., Yamaguchi, D. K., and Hemphill-Haley, E., 2004, Earthquake recurrence inferred from paleoseismology: in Gillespie, A. R., Porter, S. C., and Atwater, B. F., eds., *The Quaternary Period in the United States*, Developments in Quaternary Science 1, Elsevier, Amsterdam and New York, pp. 331-350.

- Audemard, F., and de Santis, F., 1991, Survey of liquefaction structures induced by recent moderate earthquakes: *Bulletin of the International Association of Engineering Geology*, v. 44, pp. 5-16.
- Bakun, W. H., and Hopper, M., 2004, Magnitudes and locations of the 1811-1812 New Madrid, Missouri and the 1886 Charleston, South Carolina earthquakes: *Bulletin of the Seismological Society of America*, v. 94, pp. 64-75.
- Baldwin, J. N., Witter, R. C., Vaughn, J. D., Harris, J. B., Sexton, J. L., Lake, M., Forman, S. L., and Barron, AD, 2006, Geological characterization of the Idalia Hill fault zone and its structural association with the Commerce Geophysical Lineament, Idalia, Missouri: *Bulletin of the Seismological Society of America*, v. 96, pp. 2281-2303.
- Bent, A., 1992, A re-examination of the 1925 Charlevoix, Quebec earthquake: *Bulletin of the Seismological Society of America*, v. 82, pp. 2097-2113.
- Birkeland, P. W., 1999, *Soils and Geomorphology, 3rd Edition*: Oxford University Press, New York and Oxford, 448 pp.
- Bollinger, G. A., and Sibol, M. S., 1985, Seismicity, seismic reflection studies, gravity and geology of the Central Virginia seismic zone: Part I. Seismicity: *Geological Society of America Bulletin*, v. 96, pp. 49-57.
- Bronk Ramsey, C., 1995, Radiocarbon calibration and analysis of stratigraphy: The OxCal program: *Radiocarbon*, v. 37, no. 2, pp. 425-430.
- Bronk Ramsey, C., 2001, Development of the radiocarbon calibration program OxCal: *Radiocarbon*, v. 43, no. 2A, pp. 355-363.
- Bronk Ramsey, C., 2009, Bayesian analysis of radiocarbon dates: *Radiocarbon*, v. 51, no. 1, pp. 337-360.
- Brown, W., 1900, *History of the Town of Hampton Falls, New Hampshire: From the Time of the First Settlement Within Its Borders, 1640 Until 1900*: John F. Clark, Manchester, N.H., 637 pp.
- Broughton, A. T., Van Arsdale, R. B., and Broughton, J. H., 2001, Liquefaction susceptibility mapping in the city of Memphis and Shelby County, Tennessee (in earthquake hazard evaluation in the central United States): *Engineering Geology*, v. 62, no. 1-3, pp. 207-222.
- Castilla, R. A., and Audemard, F. A., 2007, Sand blows as a potential tool for magnitude estimation of pre-instrumental earthquakes: *Journal of Seismology*, v. 11, pp. 473-487.
- Cetin, K. O., Seed, R. B., Kiureghian, A. D., Tokimatsu, K., Harder, Jr., L. F., Kayen, R. E., and Moss, R. E. S., 2004, Standard penetration test-based probabilistic and deterministic assessment of seismic soil liquefaction potential: *Journal of Geotechnical and Geoenvironmental Engineering*, ASCE, pp. 1314-1340.
- Coffin, J., 1845, *A Sketch of the History of Newbury, Newburyport, and West Newbury, from 1635-1845*: S.G. Drake, Boston, Mass., 416 pp.
- Cox, R. T., 2002, *Investigation of Seismically-Induced Liquefaction in the Southern Mississippi Embayment*: U.S. Geological Survey National Earthquake Hazards Reduction Program, Final Technical Report, Award #01-HQGR-0052, 15 pp.

- Cox, R. T., 2009, Investigations of Seismically-Induced Liquefaction in Northeast Louisiana, U.S. Geological Survey National Earthquake Hazards Reduction Program, Final Technical Report, Award #08-HQR-0008.
- Cox, R. T., and Larsen, D., 2004, *Investigation of Seismically-Induced Liquefaction in the Southern Mississippi Embayment*: National Earthquake Hazards Reduction Program, Final Technical Report No. 03HQGR0011, 19 pp.
- Cox, R. T., Harris, J. B., Hill, A. A., Forman, S. L., Gardner, C., and Csontos, R., 2004, More evidence for young tectonism along the Saline River fault zone, southern Mississippi embayment: *Eos, Transactions of the American Geophysical Union*, v. 85, no. 47, Fall Meeting Supplement, Abstract T41F-1289.
- Cox, R. T., Larsen, D., Forman, S. L., Woods, J., Morat, J., and Galluzzi, J., 2004, Preliminary assessment of sand blows in the southern Mississippi embayment: *Bulletin of the Seismological Society of America*, v. 94, pp. 1125-1142.
- Cox, R. T., Larsen, D., and Hill, A. A., 2004c, More paleoliquefaction data from southeastern Arkansas: Implications for seismic hazards (abstract): GSA Joint Northeastern and Southeastern Section Meeting, Washington, D.C.
- Cox, R. T., Cherryhomes, J., Harris, J. B., Larsen, D., Van Arsdale, R. B., and Forman, S. L., 2006, Paleoseismology of the southeastern Reelfoot rift in western Tennessee, U.S.A. and implications for intraplate fault zone evolution: *Tectonics*, v. 25, TC3019, doi:10.1029/2005TC001829, 17 pp.
- Cox, R. T., Hill, A. A., Larsen, D., Holzer, T., Forman, S. L., Noce, T., Gardner, C., and Morat, J., 2007, Seismotectonic implications of sand blows in the southern Mississippi embayment: *Engineering Geology*, v. 89, pp. 278-299.
- Cox, R. T., and Gordon, J., 2008, Sand blows on late Quaternary surfaces in northeast Louisiana: *Geological Society of America Abstracts with Programs*, v. 40, no. 6, p. 151.
- Craven, J. A., 1995, Paleoseismological Study in the New Madrid Seismic Zone Using Geological and Archeological Features to Constrain Ages of Liquefaction Deposits: M.S. thesis, University of Memphis, 51 pp.
- Dominion Nuclear North Anna, LLC (Dominion), 2004, North Anna Early Site Permit Application, Response to Request for Additional Information No. 3, Nuclear Regulatory Commission Accession Number ML042800292, July 8.
- Du Berger, R., Roy, D. W., Lamontagne, M., Woussen, G., North, R. G., and Wetmiller, R. J., 1991, The Saguenay (Quebec) earthquake of November 25, 1988: Seismologic data and geologic setting: *Tectonophysics*, v. 186, pp. 59-74.
- Dutton, C. E., 1889, The Charleston earthquake of August 31, 1886: *U.S. Geological Survey 9th Annual Report 1887-1888*, pp. 203-528.
- Ebel, J. E., 2000, A reanalysis of the 1727 Earthquake at Newbury, Massachusetts: *Seismological Research Letters*, v. 71, pp. 364-374.
- Ebel, J. E., 2001, A new look at the 1755 Cape Ann, Massachusetts earthquake: *EOS, Transactions of the American Geophysical Union*, v. 82, S271.

- Exelon Generation Company, 2003, Clinton Early Site Permit Application, Docket No. 05200007, September 25.
- Exelon Generation Company, 2004, Clinton Early Site Permit Application, Response to Request for Additional Information Letter No. 7, October 11.
- Forman, S. L., Pierson, J., and Lepper, K., 2000, Luminescence geochronology: in Noller, J. S., Sowers, J. M., and Lettis, W. R., *Quaternary Geochronology: Methods and Applications*, AGU Reference Shelf, v. 4, pp. 157-176.
- Fuller, M. L., 1912, *The New Madrid Earthquake*: U.S. Geological Survey Bulletin 494, 115 pp.
- Gassman, S., Talwani, P., and Hasek, M., 2009, Maximum magnitudes of Charleston, South Carolina earthquakes from in-situ geotechnical data: abstracts volume from meeting of Central and Eastern U.S. Earthquake Hazards Program, University of Memphis, Memphis, Tenn., October 28-29, p. 19.
- Gelinas, R., Cato, K., Amick, D., and Kemppinen, H., 1998, *Paleoseismic Studies in the Southeastern United States and New England*: U.S. Nuclear Regulatory Commission Report, NUREG/CR-6274.
- Globensky, Y., 1987, Geologie des Basses-Terres du Saint-Laurent, Ministère des Richesses Naturelles, MM 85-02, 63 pp. and carte (1:250000) no. 1999.
- Grant, L. B. and Sieh, K., 1994, Paleoseismic evidence of clustered earthquakes on the San Andreas fault in the Carrizo Plain, California: *Journal of Geophysical Research*, v. 99, no. B4, pp. 6819-6841.
- Green, R. A., Obermeier, S. F., and Olson, S. M., 2005, Engineering geologic and geotechnical analysis of paleoseismic shaking using liquefaction effects: Field examples: *Engineering Geology*, v. 76, pp. 263-293.
- Guccione, M. J., 2005, Late Pleistocene and Holocene paleoseismology of an intraplate seismic zone in a large alluvial valley, the New Madrid seismic zone, central USA: *Tectonophysics*, v. 408, pp. 237-264.
- Hajic, E. R., Wiant, M. D., and Oliver, J. J., 1995, *Distribution and Dating of Prehistoric Earthquake Liquefaction in Southeastern Illinois, Central U.S.*: National Earthquake Hazards Reduction Program, Final Technical Report to U.S. Geological Survey under agreement no. 1434-93-G-2359, 34 pp.
- Harden, J. W., 1982, A quantitative index of soil development from field descriptions: Examples from a chronosequence in central California: *Geoderma*, v. 28, pp. 1-28.
- Harden, J. W., and Taylor, E. M., 1983, A quantitative comparison of soil development in four climatic regions: *Quaternary Research*, v. 20, pp. 342-359.
- Harrison, R. W., 1997, Bedrock geologic map of the St. Louis 30' x 60' quadrangle, Missouri and Illinois: U.S. Geological Survey Miscellaneous Investigations Series Map I-2533, scale 1:100,000.
- Holbrook, J., Autin, W. J., Rittenour, T. M., Marshak, S., and Goble, R. J., 2006, Stratigraphic evidence for millennial-scale temporal clustering of earthquakes on a continental-interior

- fault: Holocene Mississippi River floodplain deposits, New Madrid seismic zone, USA: *Tectonophysics*, v. 420, pp. 431-454.
- Hough, S. E., Armbruster, J. G., Seeber, L., and Hough, J. F., 2000, On the modified Mercalli intensities and magnitudes of the 1811-1812 New Madrid: *Journal of Geophysical Research*, v. 105, pp. 23,839-23,864.
- Hough, S. E., and Martin, S., 2002, Magnitude estimates of two large aftershocks of the 16 December 1811 New Madrid earthquake: *Bulletin of the Seismological Society of America*, v. 92, no. 8, pp. 3259-3268.
- Hough, S. E., and Page, M., 2011, Toward a consistent model for strain accrual and release for the New Madrid seismic zone, Central U.S.: *Journal of Geophysical Research*, v. 116, B03311, doi:10.1029/2010JB007783.
- Hu, K., Gassman, S. L., and Talwani, P., 2002a, In-situ properties of soils at paleoliquefaction sites in the South Carolina coastal plain: *Seismological Research Letters*, v. 73, no. 6, pp. 964-978.
- Hu, K., Gassman, S. L., and Talwani, P., 2002b, Magnitudes of prehistoric earthquakes in the South Carolina coastal plain from geotechnical data: *Seismological Research Letters*, v. 73, no. 6, pp. 979-991.
- Jenny, H., 1941, *Factors of Soil Formation*: McGraw-Hill, New York, 281 pp.
- Jenny, H., 1961, Derivation of state factor equations of soils and ecosystems, *Soil Science Society of America, Proceedings*, v. 25, pp. 385-388.
- Johnston, A. C., 1996c, Seismic moment assessment of stable continental earthquakes, Part III: 1811-1812 New Madrid, 1886 Charleston and 1755 Lisbon: *Geophysical Journal International*, v. 126, pp. 314-344.
- Johnston, A. C., and Kanter, L. R., 1990, Earthquakes in stable continental crust: *Scientific American*, v. 262, pp. 68-75.
- Johnston, A. C., and Schweig, E. S., 1996, The enigma of the New Madrid earthquakes of 1811-1812: *Annual Review of Earth and Planetary Sciences*, v. 24, pp. 339-384.
- Kelson, K. I., Simpson, G. D., Van Arsdale, R. B., Harris, J. B., Haradan, C. C., and Lettis, W. R., 1996, Multiple Holocene earthquakes along the Reelfoot fault, central New Madrid seismic zone: *Journal of Geophysical Research*, v. 101, pp. 6151-6170.
- Kuenen, P. H., 1958, Experiments in geology: *Transactions of the Geological Society of Glasgow*, v. 23, pp. 1-28.
- Kumarapeli, P. S., and Saull, V., 1966, The St. Lawrence valley system: North American equivalent of the East African rift valley system: *Canadian Journal of Earth Sciences*, v. 3, pp. 639-658.
- Kuribayashi, E., and Tatsuoka, F., 1975, Brief review of liquefaction during earthquakes in Japan: *Soils and Foundations*, v. 15, pp. 81-92.
- Lamontagne, M., 2009, Description and analysis of the earthquake damage in the Quebec city region between 1608 and 2008: *Seismological Research Letters*, v. 80, no. 3, pp. 514-424.

- Lamontagne, M., Halchuk, S., Cassidy, J. F., and Rogers, G. C., 2007, *Significant Canadian Earthquakes, 1600-2006*: Geological Survey of Canada Open File 5539, 32 pp.
- Lamontagne, M., Keating, P., and Toutin, T., 2000, Complex faulting confounds earthquake research in the Charlevoix seismic zone, Québec: *Eos, Transactions of the American Geophysical Union*, v. 81, pp. 26, 289, 292, 293.
- LDRL (Luminescence Dating Research Laboratory, University of Illinois at Chicago), 2010, Luminescence Tutorial—Optically Stimulated Luminescence (OSL), website accessed June 10, 2010, <http://www.uic.edu/labs/ldrl/osl.html>.
- Leon, E., 2003, Effect of Aging of Sediments on Paleoliquefaction Evaluation in the South Carolina Coastal Plain: unpublished Ph.D. dissertation, University of South Carolina, 181 pp.
- Leon, E., Gassman, S. L., and Talwani, P., 2005, Effect of soil aging on assessing magnitudes and accelerations of prehistoric earthquakes: *Earthquake Spectra*, v. 21, no. 3, pp. 737-759.
- Lepper, K., 2007, Optically stimulated luminescence dating—An introduction: *New Mexico Geology*, v. 29, no. 4, p. 111.
- Levesque, C., Locat, J., and Leroueil, S., 2006, Dating submarine mass movements triggered by earthquakes in the Upper Saguenay Fjord, Quebec, Canada: *Norwegian Journal of Geology*, v. 86, pp. 231-242.
- Liao, T., Mayne, P. W., Tuttle, M. P., Schweig, E. S., Van Arsdale, R. B., 2002, CPT site characterization for seismic hazards in the New Madrid seismic zone: *Soil Dynamics and Earthquake Engineering*, v. 22, pp. 943-950.
- Locat, J., 2008, Localization et magnitude du séisme du 5 Février 1663 (Quebec) revues à l'aide des mouvements de terrain: in Locat, J., Perret, D., Turmel, D., Demers, D., and Leroueil, S., eds., *Proceedings of the 4th Canadian Conference on Geohazards: From Causes to Management*, University of Laval Press, Quebec, 594 pp.
- Lowe, D. R., 1975, Water escape structures in coarse-grained sediment: *Sedimentology*, v. 22, pp. 157-204.
- Lowe, D. R., and LoPiccolo, R. D., 1974, The characteristics and origins of dish and pillar structures: *Journal of Sedimentary Petrology*, v. 44, pp. 484-501.
- Magnani, B., and McIntosh, K., 2009, *Towards an Understanding of the Long-Term Deformation of the Mississippi Embayment*: U.S. Geological Survey, Final Technical Report (08HQGR0089), 19 pp.
- Mahan, S., Counts, R., Tuttle, M., and Obermeier, S., 2009, Can OSL be used to date paleoliquefaction events? Abstracts volume from meeting of Central and Eastern U.S. Earthquake Hazards Program, University of Memphis, Memphis, Tenn., October 28-29, pp. 24-25.
- Mahan, S. A., and Crone, A. J., 2006, Luminescence dating of paleoliquefaction features in the Wabash River Valley of Indiana: in Wide, R. A., ed., *Proceedings of the 4th New World Luminescence Dating and Dosimetry Workshop, Denver, Colorado*: U.S. Geological Survey Open-File Report 2006-1351, 22 pp.

- McBride, J. H., Nelson, W. J., and Stephenson, W. J., 2002, Integrated geological and geophysical study of Neogene and Quaternary-age deformation in the northern Mississippi embayment: *Seismological Research Letters*, v. 73, pp. 597-627.
- McCartan, L., Lemon, E. M., Jr., and Weems, R. E., 1984, Geologic Map of the Area Between Charleston and Orangeburg, South Carolina: U.S. Geological Series Miscellaneous Investigations Series Map I-1472, 1: 250,000-scale.
- McKeever, S. W. S., 2001, Optically stimulated luminescence dosimetry: *Nuclear Instruments and Methods in Physics Research B—Beam Interactions with Materials & Atoms*, v. 184, no. 1-2, pp. 29-54.
- McNulty, W. E., and Obermeier, S. F., 1997, *Liquefaction Evidence for Two Holocene Paleo-earthquakes in Central and Southwestern Illinois*: U.S. Geological Survey Open-File Report 97-435, 14 pp.
- McNulty, W. E., and Obermeier, S. F., 1999, Liquefaction evidence for at least two strong Holocene paleo-earthquakes in central and southwestern Illinois, USA: *Environmental and Engineering Geoscience*, v. 5, no. 2, pp. 133-146.
- Mitchell, B. J., Nuttli, O. W., Herrmann, R. B., and Stauder, W., 1991, Seismotectonics of the central United States: in Slemmons, D.B., Engdahl, E.R., Zoback, M.D., and Blackwell, D.D., eds., *Neotectonics of North America*: Decade Map Volume 1, Geological Society of America, pp. 245-260.
- Munson, P. J., and Munson, C. A., 1996, *Paleoliquefaction Evidence for Recurrent Strong Earthquakes Since 20,000 Years BP in the Wabash Valley Area of Indiana*: report submitted to the U.S. Geological Survey in fulfillment of National Earthquake Hazards Reduction Program Grant No. 14-08-0001-G2117, 137 pp.
- Munson, P. J., Munson, C. A., and Pond, E. C., 1995, Paleoliquefaction evidence for a strong Holocene earthquake in south-central Indiana: *Geology*, v. 23, pp. 325-328.
- Munson, P. J., Obermeier, S. F., Munson, C. A., and Hajic, E. R., 1997, Liquefaction evidence for Holocene and latest Pleistocene seismicity in the southern halves of Indiana and Illinois: A preliminary overview: *Seismological Research Letters*, v. 68, pp. 521-536.
- Murray, A. S., and Olley, J. M., 2002, Precision and accuracy in the optically stimulated luminescence dating of sedimentary quartz—An overview: *Geochronometria*, v. 21, pp. 1-16.
- Noller, J. S., and Forman, S. L., 1998, Luminescence geochronology of liquefaction features near Georgetown, South Carolina: in Sowers, J. M., Noller, J. S., and Lettis, W. R., eds., *Dating and Earthquakes: Review of Quaternary Geochronology and Its Application to Paleoseismology*, U.S. Nuclear Regulatory Commission Report, NUREG/CR-5562, pp. 4.49-4.57.
- Nuttli, O., and Brill, K., 1981, Earthquake source zones in the central United States determined from historical seismicity: in Barstow, N.L., Brill, K.G., Nuttli, O.W., and Pomeroy, P.W., eds., *Approach to Seismic Zonation for Siting Nuclear Electric Power Generating Facilities in the Eastern United States*, U.S. Nuclear Regulatory Commission Report NUREG/CR-1577, pp. 98-143.

- Obermeier, S. F., 1989, *The New Madrid Earthquakes: An Engineering-Geologic Interpretation of Relict Liquefaction Features*: U.S. Geological Survey Professional Paper 1336-B, p. 114.
- Obermeier, S. F., 1996, Using liquefaction-induced features for paleoseismic analysis: in McCalpin, J. P., ed., *Paleoseismology*, Academic Press, San Diego, CA, pp. 331-396.
- Obermeier, S. F., 1998, Liquefaction evidence for strong earthquakes of Holocene and latest Pleistocene ages in the states of Indiana and Illinois, USA: *Engineering Geology*, v. 50, pp. 227-254.
- Obermeier, S. F., 2009, Using liquefaction-induced and other soft-sediment features for paleoseismic analysis: *International Geophysics*, v. 95, pp. 499-566.
- Obermeier, S. F., Weems, R. E., Jacobson, R. B., and Gohn, G. S., 1989, Liquefaction evidence for repeated Holocene earthquakes in the coastal region of South Carolina: *Annals of the New York Academy of Sciences*, v. 558, pp. 183-195.
- Obermeier, S. F., Jacobson, R. B., Smoot, J. P., Weems, R. E., Gohn, G. S., Monroe, J. E., and Powars, D. S., 1990, *Earthquake-Induced Liquefaction Features in the Coastal Setting of South Carolina and in the Fluvial Setting of the New Madrid Seismic Zone*: U.S. Geological Survey Professional Paper 1504, pp. 44.
- Obermeier, S. F., Bleuer, N. R., Munson, C. A., Munson, P. J., Martin, W. S., McWilliams, K. M., Tabaczynski, D. A., Odum, J. K., Rubin, M., and Eggert, D. L., 1991, Evidence of strong earthquake shaking in the lower Wabash Valley from prehistoric liquefaction features: *Science*, v. 251, pp. 1061-1062.
- Obermeier, S. F., Martin, J. R., Frankel, A. D., Youd, T. L., Munson, P. J., Munson, C. A., and Pond, E. C., 1993, *Liquefaction Evidence for One or More Strong Holocene Earthquakes in the Wabash Valley of Southern Indiana and Illinois, with a Preliminary Estimate of Magnitude*: U.S. Geological Survey Professional Paper 1536, 27 pp.
- Obermeier, S. F., and McNulty, W. E., 1998, Paleoliquefaction evidence for seismic quiescence in central Virginia during late and middle Holocene time: *Eos, Transactions of the American Geophysical Union*, v. 79, no. 17, Spring Meeting Supplement, Abstract T41A-9.
- Obermeier, S. F., Pond, E. C., Olson, S. M., Green, R. A., Stark, T. D., and Mitchell, J. K., 2001, *Paleoseismic Studies in Continental Settings—Geologic and Geotechnical Factors in Interpretations and Back-Analysis*: U.S. Geological Survey Open-File Report 01-29, 53 pp.
- O'Brien, M. J., and Lyman, R. L., 1999, *Seriation, Stratigraphy, and Index Fossils: The Backbone of Archaeological Dating*: Plenum Press, New York, 261 pp.
- Olson, S. M., Green, R. A., and Obermeier, S. F., 2005b, Revised magnitude bound relation for the Wabash Valley seismic zone of the central United States: *Seismological Research Letters*, v. 76, no. 6, pp. 756-771.
- Olson, S. M., Obermeier, S. F., and Stark, T. D., 2001, Interpretation of penetration resistance for back-analysis at sites of previous liquefaction: *Seismological Research Letters*, v. 72, no. 1, pp. 46-59.
- Owen, H. G., 1987, Deformation processes in unconsolidated sands: *Geological Society of London Special Publications 1987*, v. 29, pp. 11-24.

- Pierce, K., 1986, Dating methods: in Geophysics Study Committee, Geophysics Research Forum, National Research Council, authors, *Active Tectonics: Impact on Society*, The National Academies Press, Washington, D.C., pp. 195-214.
- Pond, E.C., 1996, Seismic Parameters from the Central United States Based on Paleoliquefaction Evidence in the Wabash Valley: Ph.D. Dissertation, Virginia Polytechnic Institute, Blacksburg, Virginia, 583 pp.
- Pond, E. C., and Martin, J. R., 1997, Estimated magnitudes and accelerations associated with prehistoric earthquakes in the Wabash Valley region of the central United States: in Kolata, D. R., and Hildenbrand, T. G. (editors), *Investigations of the Illinois Basin Earthquake Region: Seismological Research Letters*, v. 68, pp. 611-623.
- Al-Qadhi, O., 2010, Geophysical Investigation of Paleoseismological Features in Eastern Arkansas, USA: Ph.D. Dissertation, University of Arkansas at Little Rock, p. 277.
- Reimer, P. J., Baillie, M. G. L., Bard, E., Bayliss, A., Beck, J. W., Blackwell, P. G., Bronk Ramsey, C., Buck, C. E., Burr, G., Edwards, R. L., Friedrich, M., Grootes, P. M., Guilderson, T. P., Hajdas, I., Heaton, T. J., Hogg, A. G., Hughen, K. A., Kaiser, K. F., Kromer, B., McCormac, F. G., Manning, S. W., Reimer, R. W., Richards, D. A., Southon, J., Turney, C. S. M., van der Plicht, J., and Weyhenmeyer, C., 2009, IntCal09 and Marine09 radiocarbon age calibration curves, 0–50,000 years cal BP: *Radiocarbon*, v. 51, no. 4, pp. 1111–1150.
- Rondot, J., 1979, *Reconnaissances Géologiques dans Charlevoix-Saguenay*: Ministère des Richesses Naturelles du Québec, Rapport DPV-682, 44 pp.
- Russ, D. P., 1982, Style and significance of surface deformation in the vicinity of New Madrid, Missouri: in McKeown, F. A. and Pakiser, L. C., eds., *Investigations of the New Madrid, Missouri, Earthquake Region*, U.S. Geological Survey Professional Paper 1236, pp. 94-114.
- Saucier, R. T., 1977, *Effects of the New Madrid Earthquake Series in the Mississippi Alluvial Valley*: U.S. Army Corps of Engineers Waterways Experiment Station Misc. Paper S-77-5.
- Saucier, R. T., 1989, Evidence for episodic sand-blow activity during the 1811-12 New Madrid (Missouri) earthquake series: *Geology*, v. 17, p. 103-106.
- Saucier, R. T., 1991, Geoarchaeological evidence of strong prehistoric earthquakes in the New Madrid (Missouri) seismic zone: *Geology*, v. 19, p. 296-298.
- Saucier, R. T., 1994, *Geomorphology and Quaternary Geologic History of the Lower Mississippi*: U.S. Army Corps of Engineers Waterways Experiment Station, vols. 1 and 2, 364 pp., 28 plates.
- Schneider, J.A., and Mayne, P.W., 2000, *Liquefaction Response of Soils in Mid-America Evaluated by Seismic Cones Test*: Mid-America Earthquake Center Report MAE-GT-3A, 292 pp.
- Schneider, J.A., Mayne, P.W., and Rix, G.J., 2001, Geotechnical site characterization in the greater Memphis area using CPT: *Engineering Geology*, v. 62, no. 1-3, pp. 169-184.
- Seed, H. B., and Idriss, I. M., 1982, *Ground Motions and Soil Liquefaction During Earthquakes*, Earthquake Engineering Research Institute, Berkeley, Calif., 134 pp.

- Al-Shukri, H., Lemmer, R. E., Mahdi, H. H., and Connelly, J. B., 2005, Spatial and temporal characteristics of paleoseismic features in the southern terminus of the New Madrid seismic zone in eastern Arkansas: *Seismological Research Letters*, v. 76, no. 4, pp. 502-511.
- Al-Shukri, H., Mahdi, H., Al Kadi, O., and Tuttle, M. P., 2009, *Spatial and Temporal Characteristics of Paleoseismic Features in the Southern Terminus of the New Madrid Seismic Zone in Eastern Arkansas*: Final Technical Report to U.S. Geological Survey, 24 pp.
- Al-Shukri, H., Mahdi, H., and Tuttle, M., 2006, Three-dimensional imaging of earthquake-induced liquefaction features with ground penetrating radar near Marianna, Arkansas: *Seismological Research Letters*, v. 77, pp. 505-513.
- Sims, J. D., 1973, Earthquake-induced structures in sediments of Van Norman Lake, San Fernando California: *Science*, v. 182, pp. 161-163.
- Sims, J. D., 1975, Determining earthquake recurrence intervals from deformational structures in young lacustrine sediments: *Tectonophysics*, v. 29, pp. 141-153.
- Sims, J. D., and Garvin, C. D., 1995, Recurrent liquefaction at Soda Lake, California, induced by the 1989 Loma Prieta earthquake, and 1990 and 1991 aftershocks: Implications for paleoseismicity studies: *Bulletin of the Seismological Society of America*, v. 85, pp. 51-65.
- Smith, W. E. T., 1966, Earthquakes of eastern Canada and adjacent areas 1928-1959, Publication of the Dominion Observatory v. 32, pp. 87-121.
- Somerville, P. G., McLaren, J. P., Saikia, C. K., and Helmberger, D. V., 1990, The 25 November 1988 Saguenay, Quebec, earthquake source parameters and the attenuation of strong ground motion: *Bulletin of the Seismological Society of America*, v. 80, pp. 1118-1143.
- Stahle, D. W., Cook, E. R., and White, J. W. C., 1985, Tree-ring dating of baldcypress and the potential for millennia-long chronologies in the Southeast: *American Antiquity*, v. 50, pp. 796-802.
- Stahle, D. W., Fye, F. K., and Therrell, M. D., 2004, Interannual to decadal climate and streamflow variability estimates from tree rings: in Gillespie, A. R., Porter, S. C., and Atwater, B. F., eds., *The Quaternary Period in the United States: Developments in Quaternary Science 1*, Elsevier, Amsterdam and New York, pp. 491-504.
- Stark, T. D., 2002, Interpretation of Ground Shaking from Paleoliquefaction Features: U.S. Geological Survey, Annual Technical Report.
- Stuiver, M., Long A., Kra, R. S., and Devine, J. M., 1993, Calibration—1993: *Radiocarbon*, v. 35, no. 1, pp. 35-65.
- Stuiver, M., and Pearson, G. W., 1993, High-precision bidecadal calibration of the radiocarbon time scale, AD 1950-500 BC and 2500-6000 BC: *Radiocarbon*, v. 35, no. 1, pp. 1-25.
- Stuiver, M., and Reimer, P. J., 1993, Extended ^{14}C data base and revised CALIB 3.0 ^{14}C age calibration program: *Radiocarbon*, v. 35, pp. 215-230.
- Stuiver, M., Reimer, P. J., and Braziunas, T. F., 1998, High-precision radiocarbon age calibration for terrestrial and marine samples: *Radiocarbon*, v. 40, no. 3, pp. 1127-1151.
- Stuiver, M., Reimer, P. J., and Reimer, R. W., 2005, CALIB 6.0, [WWW program and documentation - <http://intcal.qub.ac.uk/calib/>].

- Talma, A. S., and Vogel, J. C., 1993, A simplified approach to calibrating C14 dates: *Radiocarbon*, v. 35, pp. 317-322.
- Talwani, P. and Cox, J., 1985, Paleoseismic evidence for recurrence of earthquakes near Charleston, South Carolina: *Science*, v. 228, pp. 379-381.
- Talwani, P., Dura-Gomez, I., Gassman, S., Hasek, M., and Chapman, A., 2008, Studies related to the discovery of a prehistoric sandblow in the epicentral area of the 1886 Charleston SC earthquake: Trenching and geotechnical investigations: *Program and Abstracts, Eastern Section of the Seismological Society of America*, p. 50.
- Talwani, P., and Schaeffer, W. T., 2001, Recurrence rates of large earthquakes in the South Carolina Coastal Plain based on paleoliquefaction data: *Journal of Geophysical Research*, v. 106, no. B4, pp. 6621-6642.
- Trumbore, S. E., 1989, AMS ^{14}C measurements of fractionated soil organic matter: an approach to deciphering the soil carbon cycle: *Radiocarbon*, v. 31, no. 3, pp. 644-654.
- Tuttle, M. P., 1994, *The Liquefaction Method For Assessing Paleoseismicity*: U.S. Nuclear Regulatory Commission, NUREG/CR-6258, 38 pp.
- Tuttle, M. P., 1999, Late Holocene Earthquakes and Their Implications for Earthquake Potential of the New Madrid Seismic Zone, Central United States: Ph.D. dissertation, University of Maryland, 250 pp.
- Tuttle, M. P., 2000, *Paleoseismological Study in the St. Louis Region*: U.S. Geological Survey, Earthquake Hazards Program, Final Technical Report (99HQGR0032), 29 pp.
- Tuttle, M. P., 2001, The use of liquefaction features in paleoseismology: Lessons learned in the New Madrid seismic zone, central United States: *Journal of Seismology*, v. 5, pp. 361-380.
- Tuttle, M. P., 2005a, *Improving the Earthquake Chronology for the St. Louis Region*: U.S. Geological Survey, Earthquake Hazards Program, Annual Project Summary (05HQGR0045), 6 pp.
- Tuttle, M. P., 2007, *Re-evaluation of Earthquake Potential and Source in the Vicinity of Newburyport, Massachusetts*: U.S. Geological Survey, Earthquake Hazards Program, Final Technical Report (01HQGR0163).
- Tuttle, M. P., 2009, *Re-evaluation of Earthquake Potential and Source in the Vicinity of Newburyport, Massachusetts*: U.S. Geological Survey, Earthquake Hazards Program, Final Technical Report (03HQGR0031).
- Tuttle, M. P., 2010, Search for and Study of Sand Blows at Distant Sites Resulting from Prehistoric and Historic New Madrid Earthquakes: Collaborative Research, M. Tuttle & Associates and Central Region Hazards Team, U.S. Geological Survey, Final Technical Report (02HQGR0097), 48 pp.
- Tuttle, M. P., Seeber, L., and Bradley, L., 1987, Liquefaction of glaciomarine sediments during the 1727 earthquake in Newburyport, Massachusetts: in Jacob, K. H., ed., *Proceedings from the Symposium on Seismic Hazards, Ground Motions, Soil-Liquefaction and Engineering Practice in Eastern North America*, NCEER Technical Report NCEER-87-0025, pp. 467-479.

- Tuttle, M. P., Such, R., and Seeber, L., 1989, Ground failure associated with the November 25th, 1988 Saguenay earthquake in Quebec Province, Canada: in Jacob, K., ed., *The 1988 Saguenay Earthquake of November 25, 1988, Quebec, Canada: Strong Motion Data, Ground Failure Observations, and Preliminary Interpretations*, National Center for Earthquake Engineering Research, Buffalo, New York, pp. 1-23.
- Tuttle, M., Law, T., Seeber, L., and Jacob, K., 1990, Liquefaction and ground failure in Ferland, Quebec, triggered by the 1988 Saguenay earthquake: *Canadian Geotechnical Journal*, v. 27, pp. 580-589.
- Tuttle, M., and Seeber, L., 1991, Historic and prehistoric earthquake-induced liquefaction in Newbury, Massachusetts: *Geology*, v. 19, pp. 594-597.
- Tuttle, M. P., Cowie, P., and Wolf, L., 1992, Liquefaction induced by modern earthquakes as a key to paleoseismicity: A case study of the 1988 Saguenay earthquake: in Weiss, A., ed., *Proceedings of the Nineteenth International Water Reactor Safety Information Meeting*, NUREG/CP-0119, v. 3, pp. 437-462.
- Tuttle, M. P., and Schweig, E. S., 1995, Archeological and pedological evidence for large earthquakes in the New Madrid seismic zone, central United States: *Geology*, v. 23, no. 3, pp. 253-256.
- Tuttle, M., and Barstow, N., 1996, Liquefaction-related ground failure: A case study in the New Madrid seismic zone, Central United States: *Bulletin of the Seismological Society of America*, v. 86, pp. 636-645.
- Tuttle, M. P., Lafferty, R. H., Chester, J. S., and Haynes, M., 1996, Evidence of earthquake-induced liquefaction north of the New Madrid seismic zone, central United States: *Seismological Research Letters*, v. 67, no. 2, p. 58.
- Tuttle, M. P., Lafferty, R. H., Guccione, M. J., Schweig, E. S., Lopinot, N., Cande, R. F., Dyer-Williams, K., and Haynes, M., 1996, Use of archaeology to date liquefaction features and seismic events in the New Madrid seismic zone, central United States: *Geoarchaeology: An International Journal*, v. 11, no. 6, pp. 451-480.
- Tuttle, M. P., Lafferty, R. H., III, and Schweig, E. S., III, 1998, *Dating of Liquefaction Features in the New Madrid Seismic Zone and Implications for Earthquake Hazard*: U.S. Nuclear Regulatory Commission, NUREG/GR-0017, 77 pp.
- Tuttle, M., Chester, J., Lafferty, R., Dyer-Williams, K., and Cande, B., 1999, *Paleoseismology Study Northwest of the New Madrid Seismic Zone*: U.S. Nuclear Regulatory Commission, NUREG/CR-5730, 98 pp.
- Tuttle, M. P., Collier, J., Wolf, L. W., and Lafferty, R. H., 1999, New evidence for a large earthquake in the New Madrid seismic zone between AD 1400 and 1670: *Geology*, v. 27, no. 9, pp. 771-774.
- Tuttle, M. P., Sims, J. D., Dyer-Williams, K., Lafferty, R. H., III, and Schweig, E. S., III, 2000, *Dating of Liquefaction Features in the New Madrid Seismic Zone*: U.S. Nuclear Regulatory Commission, NUREG/GR-0018, 42 pp.

- Tuttle, M. P., Schweig, E. S., Sims, J. D., Lafferty, R. H., Wolf, L. W., Haynes, M. L., 2002, The earthquake potential of the New Madrid seismic zone: *Bulletin of the Seismological Society of America*, v. 92, no. 6, pp. 2080-2089.
- Tuttle, M. P., Hengesh, J., Tucker, K. B., Lettis, W., Deaton, S. L., and Frost, J. D., 2002, Observations and comparisons of liquefaction features and related effects induced by the Bhuj earthquake: *Earthquake Spectra*, v. 18, Supplement A, pp. 79-100.
- Tuttle, M. P., and Schweig, E., 2004, *Search for and Study of Sand Blows at Distant Sites Resulting from Prehistoric and Historic New Madrid Earthquakes*: U.S. Geological Survey, Annual Technical Report.
- Tuttle, M. P., Schweig, E. S., and Dyer-Williams, K., 2004, *Paleoseismology Study in the St. Louis Region*: USGS Final Technical Report.
- Tuttle, M. P., Schweig, E., III, Campbell, J., Thomas, P. M., Sims, J. D., and Lafferty, R. H., III, 2005, Evidence for New Madrid earthquakes in AD 300 and 2350 B.C: *Seismological Research Letters*, v. 76, no. 4, pp. 489-501.
- Tuttle, M. P., Al-Shukri, H., and Mahdi, H., 2006, Very large earthquakes centered southwest of the New Madrid seismic zone 5,000-7,000 years ago: *Seismological Research Letters*, v. 77, no. 6, pp. 664-678.
- Tuttle, M. P., and Atkinson, G. M., 2010, Localization of large earthquakes in the Charlevoix zone, Quebec, Canada, during the past 10,000 years: *Seismological Research Letters*, v. 81, no. 1, pp. 140-147.
- Vaughn, J. D., 1994, *Paleoseismology Studies in the Western Lowlands of Southeast Missouri*: U.S. Geological Survey, Final Report (14-08-0001-G1931), 27 pp.
- Vogel, J. C., Fuls, A., Visser, E., and Becker, B., 1993, Pretoria calibration curve for short lived samples: *Radiocarbon*, v. 33, pp. 73-86.
- Walker, M., 2005, *Quaternary Dating Methods*: John Wiley and Sons, Ltd, West Sussex, England, 286 pp.
- Weems, R. E. and Obermeier, S. F., 1990, The 1886 Charleston Earthquake—An Overview of Geological Studies: in Proceedings of the U.S. Nuclear Regulatory Commission Seventeenth Water Reactor Safety Information Meeting, NUREG/CP-0105, volume 2, pp. 289-313.
- Wheeler, R.L., 2002, Distinguishing seismic from non-seismic soft-sediment structures: Criteria from seismic hazard analysis: in Ettensohn, F.R., Rast, N., and Brett, C.E., eds., *Ancient Seismites*, Geological Society of America Special Paper 359, Boulder, Colorado, pp. 1-11.
- Wheeler, R. L., and Johnston, A. C., 1992, Geologic implications of earthquake source parameters in central and eastern North America: *Seismological Research Letters*, v. 63, no. 4, pp. 491-505.
- Wintle, A. G., and Murray, A. S., 1997, The relationship between quartz thermoluminescence, photo-transferred luminescence, and optically stimulated luminescence: *Radiation Measurements*, v. 27, no. 4, pp. 611-624.

- Wolf, L. W., Collier, J., Tuttle, M., and Bodin, P., 1998, Geophysical reconnaissance of earthquake-induced liquefaction features in the New Madrid seismic zone: *Journal of Applied Geophysics*, v. 39, pp. 121-129.
- Wolf, L. W., Tuttle, M. P., Browning, S., and Park, S., 2006, Geophysical surveys of earthquake-induced liquefaction deposits in the New Madrid seismic zone: *Geophysics*, v. 71, no. 6, pp. B223-230.
- Youd, T. L., 1984, *Geologic Effects—Liquefaction and Associated Ground Failure*: U.S. Geological Survey Open-File Report 84-760, pp. 210-232.
- Youd, T. L., Idriss, I. M., Andrus, R. D., Arango, I., Castro, G., Christian, J. T., Dobry, R., Finn, W. D. L., Harder, Jr., L. F., Hynes, M. E., Ishihara, K., Koester, J. P., Liao, S. S. C., Marcuson, III, W. F., Martin, G. R., Mitchell, J. K., Yoshiharu, M., Power, M. S., Robertson, P. K., Seed, R. B., and Stokoe, II, K. H., 2001, Liquefaction resistance of soils: Summary report from the 1996 NCEER and 1998 NCEER/NSF workshops on evaluation of liquefaction resistance of soils: *Journal of Geotechnical and Geoenvironmental Engineering*, ASCE, v. 127, pp. 817-833.

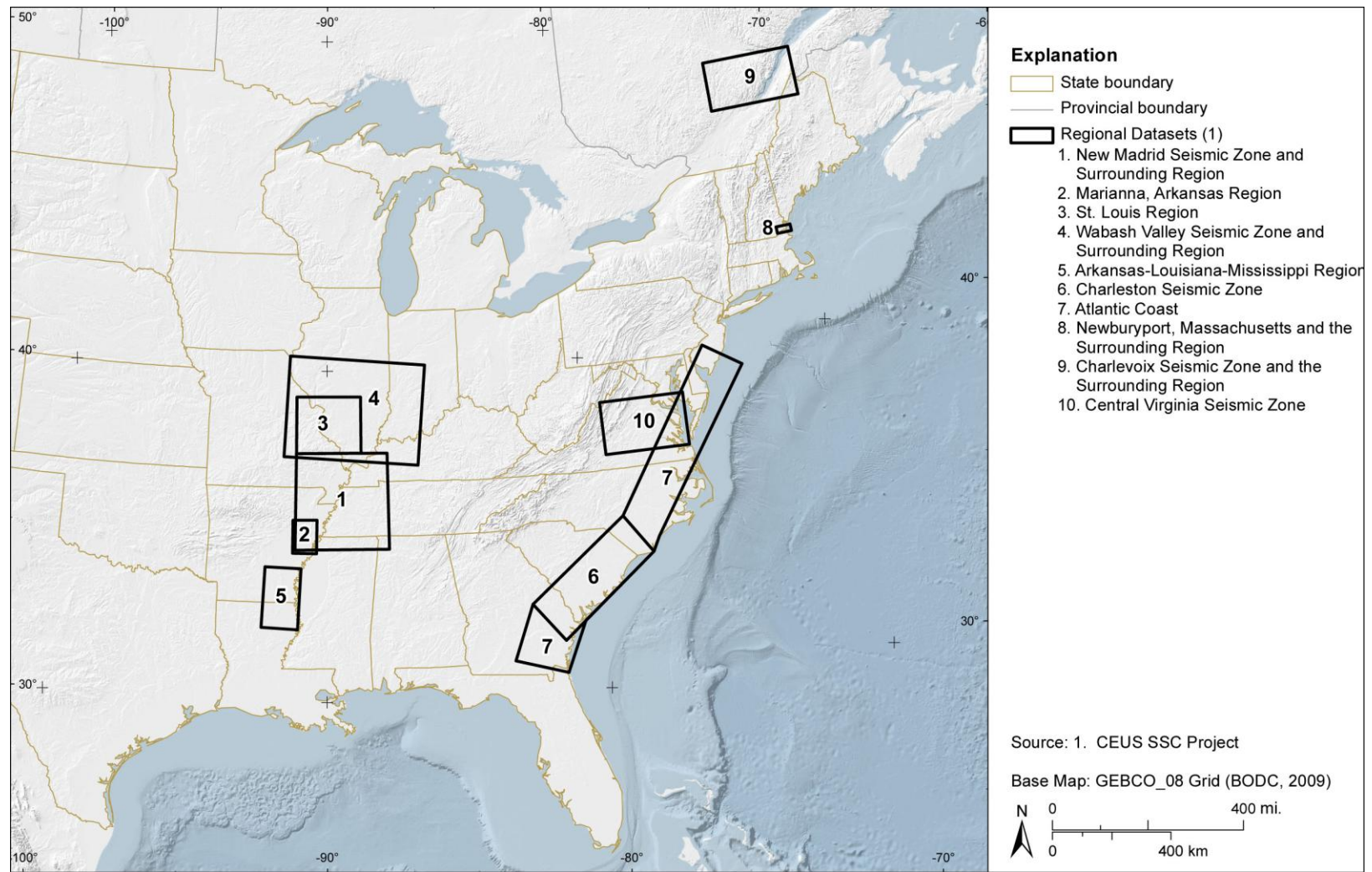


Figure E-1

Map of CEUS showing locations of regional data sets in the CEUS SSC Project paleoliquefaction database, including New Madrid seismic zone and surrounding region; Marianna, Arkansas, area; St. Louis region; Wabash Valley seismic zone and surrounding region; Arkansas-Louisiana-Mississippi region; Charleston seismic zone; Atlantic Coastal region and the Central Virginia seismic zone; Newburyport, Massachusetts, and surrounding region; and Charlevoix seismic zone and surrounding region.

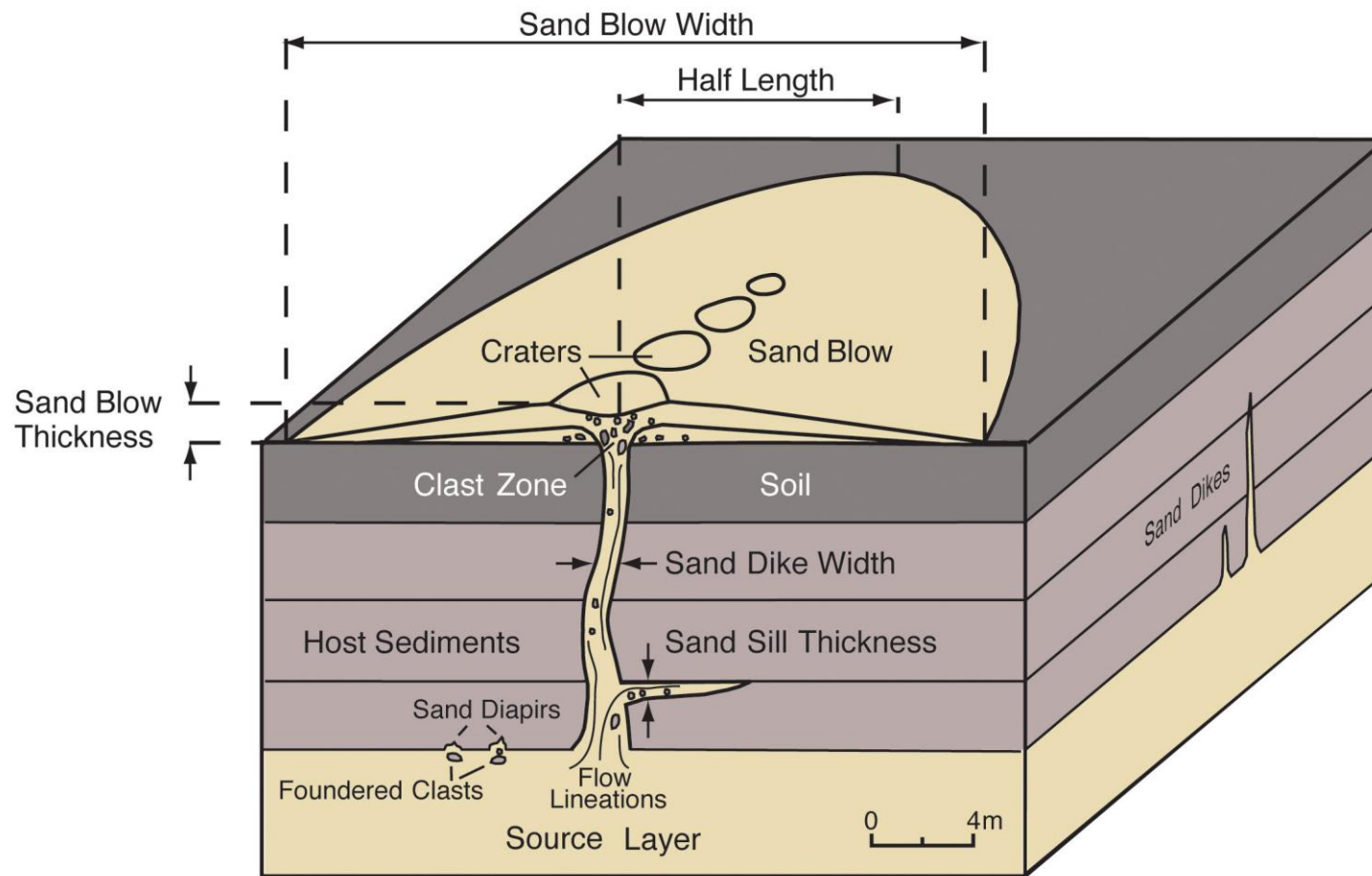


Figure E-2

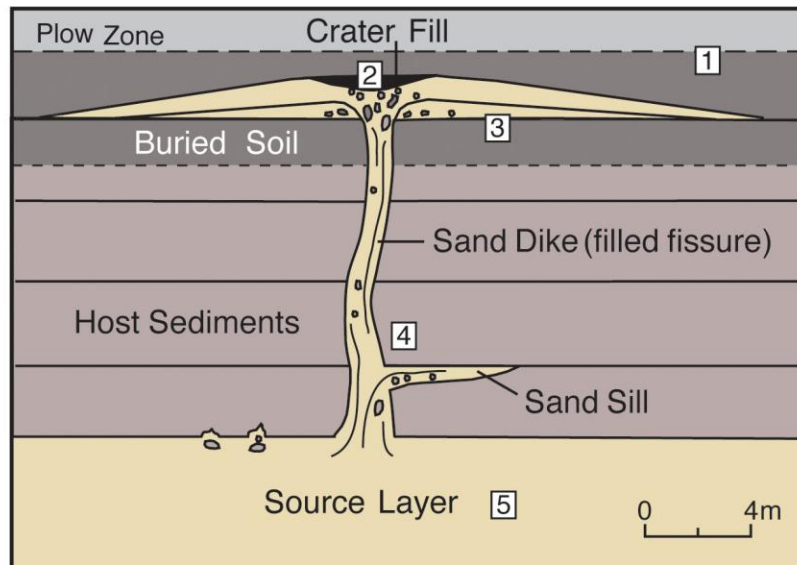
Diagram illustrating size parameters of liquefaction features including sand blow thickness, width, and length, dike width, and sill thickness, as well as some of the diagnostic characteristics of these features.

Age Estimate of Sand Blow = Average of Minimum Minimum and Maximum Maximum Constraining Ages \pm Uncertainty

Example:

Age Estimate of Sand Blow = $\frac{950 + 1150}{2}$ = 1050 Yr BP \pm 100 yr (800 to 1000 C.E.)

Soil Developed in Sand Blow



Sample	Description	Age Yr BP	Constraint
[1]	Charcoal within soil above sand blow	650 - 740	Minimum
[2]	Leaves accumulated in crater	950 - 1050	Close minimum
[3]	Twigs in buried soil immediately below sand blow	1050 - 1150	Close maximum
[4]	Charcoal within host sediments	2750 - 2680	Maximum
[5]	Tree trunk bedded within sand layer	4530 - 4720	Maximum; source layer age

Figure E-3

Diagram illustrating sampling strategy for dating of liquefaction features as well as age data, such as ^{14}C maximum and ^{14}C minimum, used to calculate preferred age estimates and related uncertainties of liquefaction features.

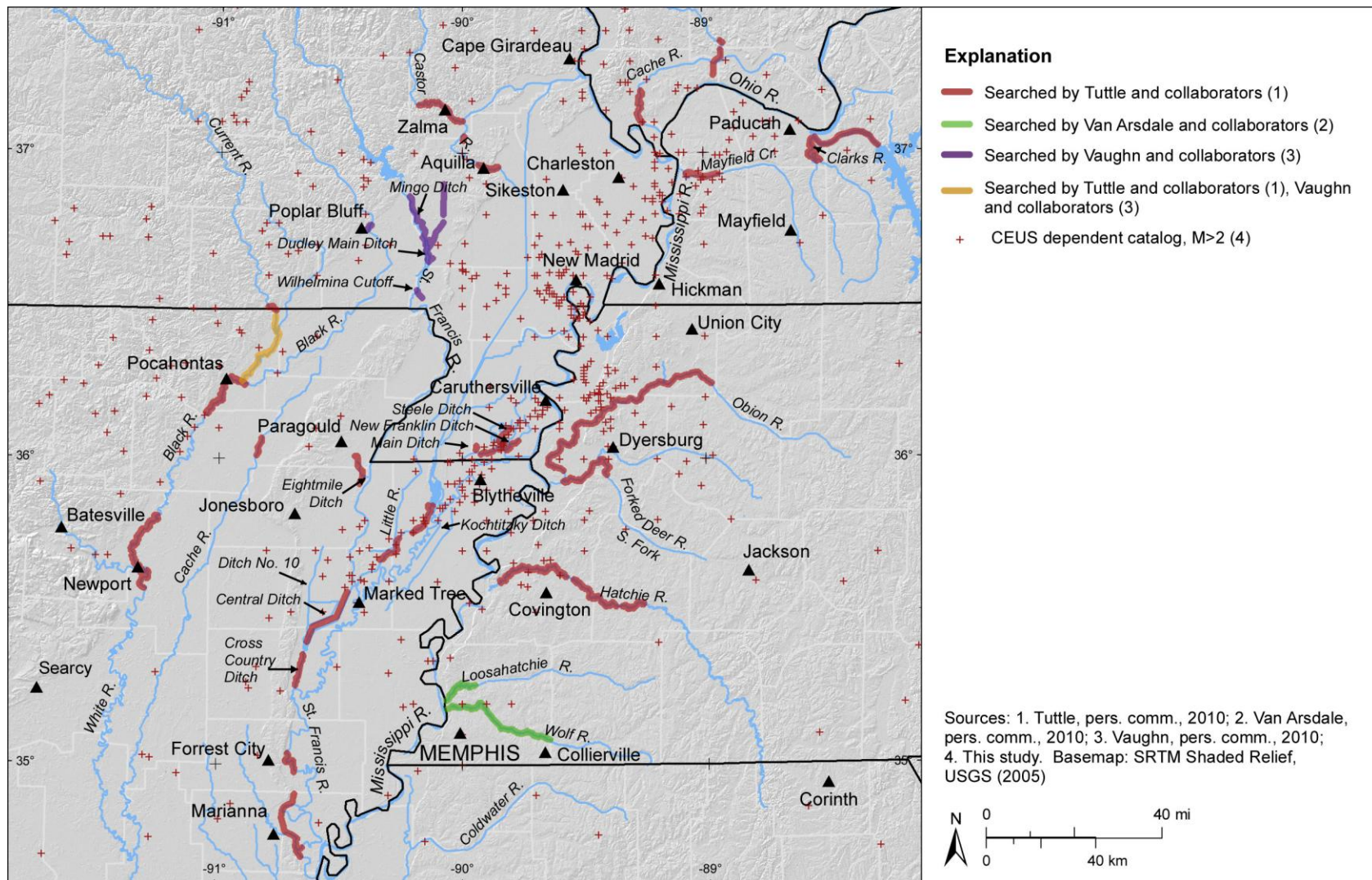


Figure E-4

GIS map of New Madrid seismic zone and surrounding region showing portions of rivers searched for earthquake-induced liquefaction features by M. Tuttle, R. Van Arsdale, and J. Vaughn and collaborators (see explanation); information contributed for this report. Map projection is USA Contiguous Albers Equal Area Conic, North America Datum 1983.

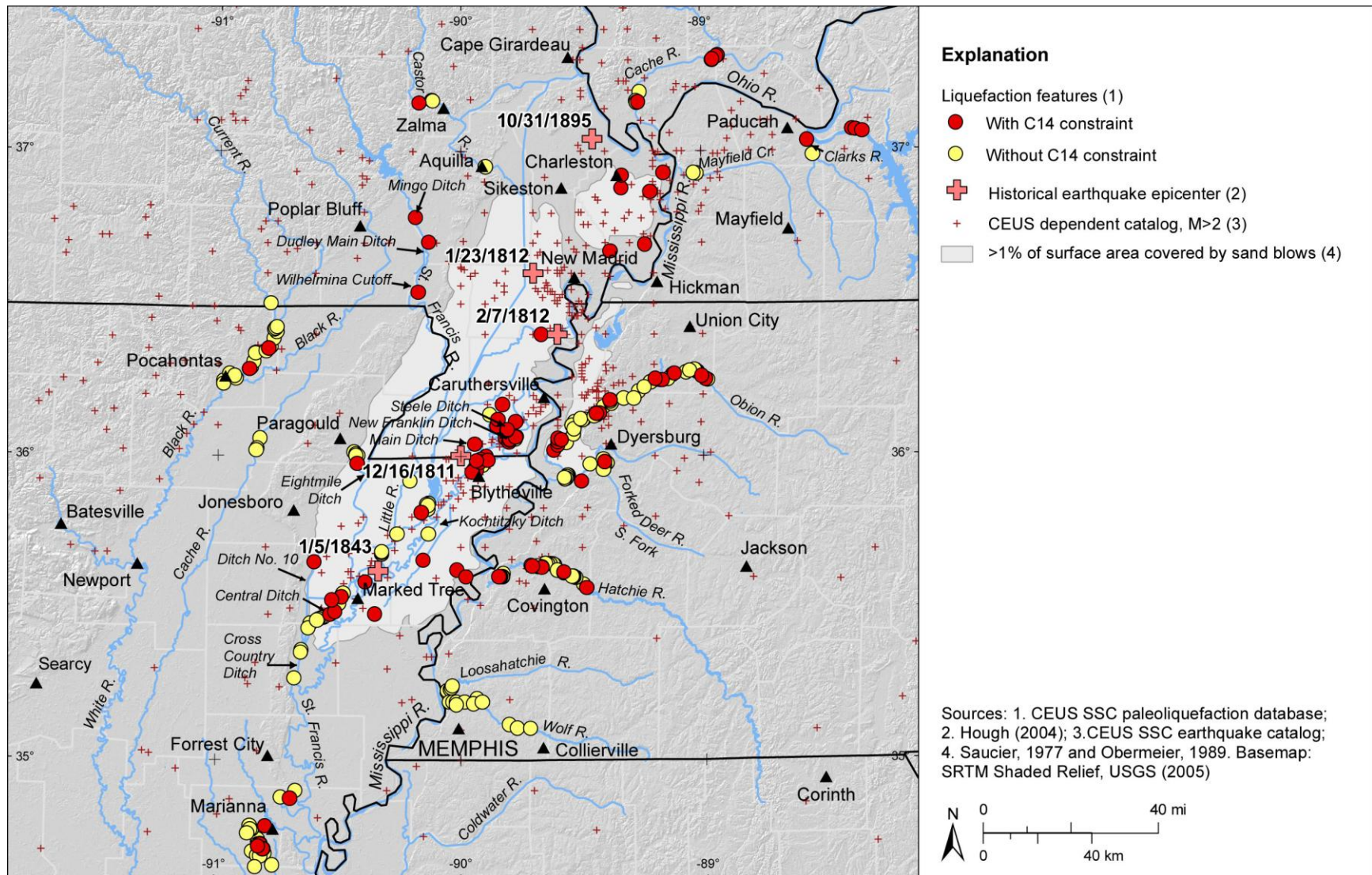


Figure E-5

GIS map of New Madrid seismic zone and surrounding region showing locations of liquefaction features for which there are and are not radiocarbon data. Map projection is USA Contiguous Albers Equal Area Conic, North America Datum 1983.

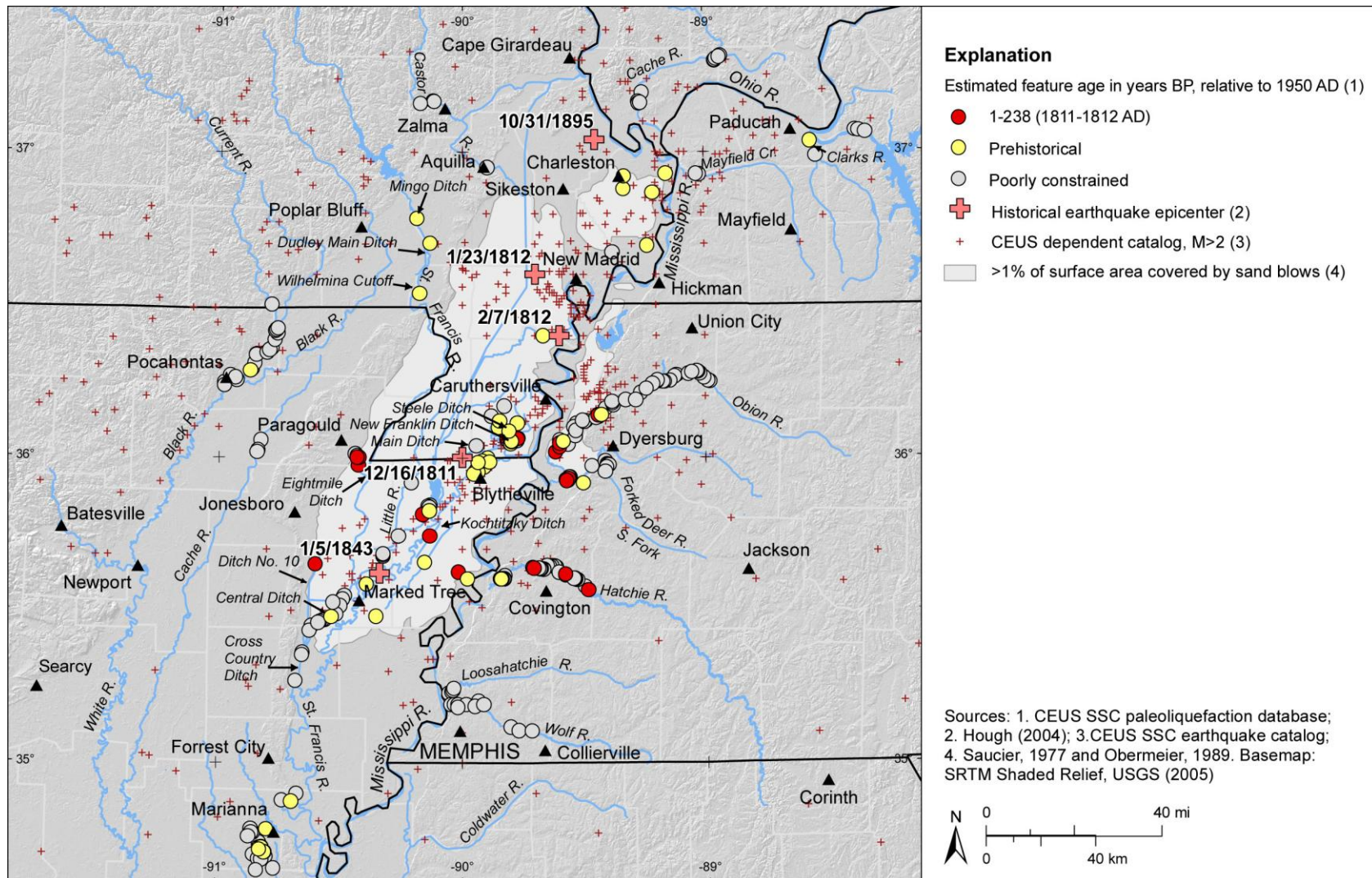


Figure E-6

GIS map of New Madrid seismic zone and surrounding region showing locations of liquefaction features that are thought to be historical or prehistoric in age or whose ages are poorly constrained. Map projection is USA Contiguous Albers Equal Area Conic, North America Datum 1983.

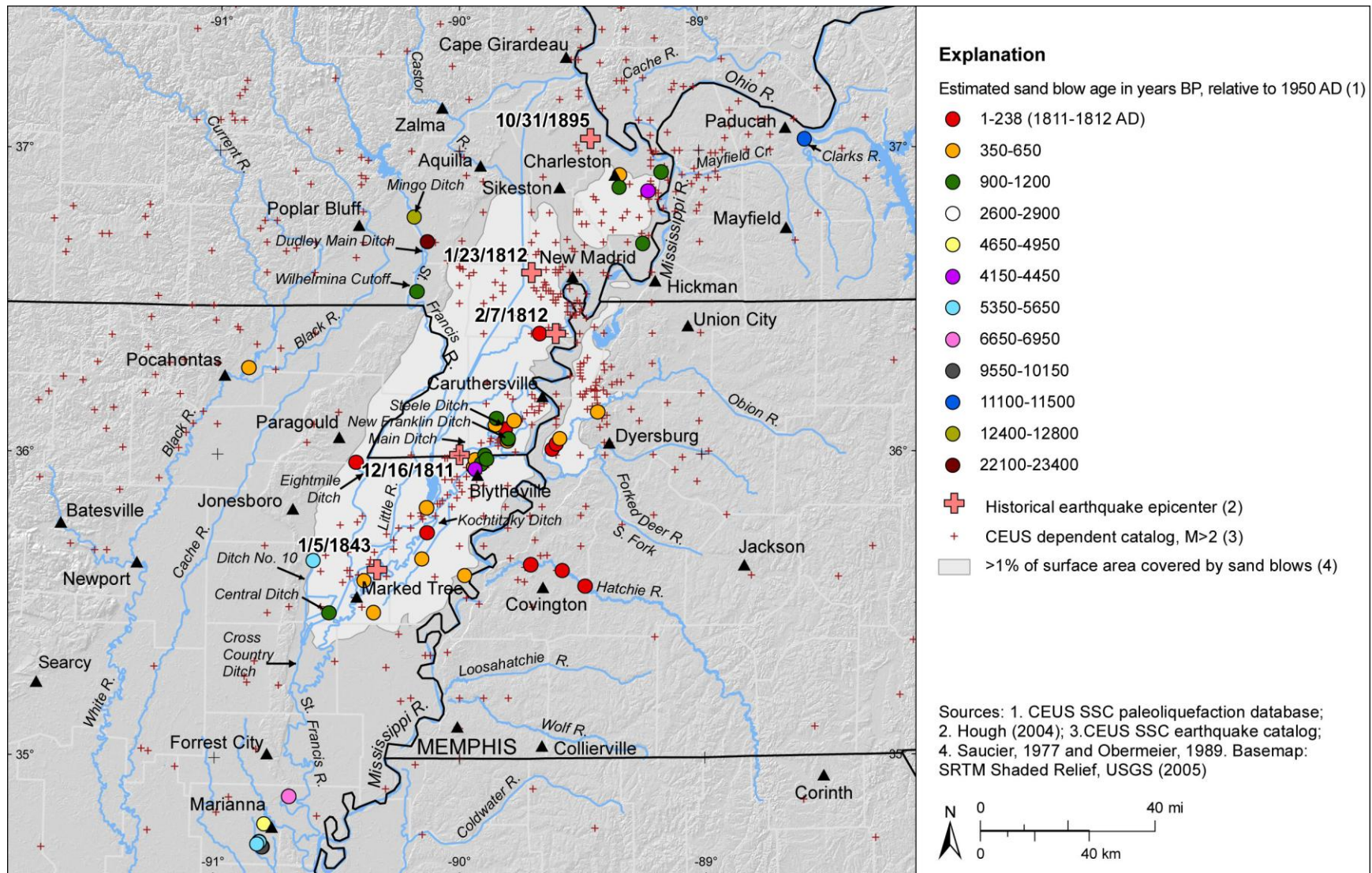


Figure E-7

GIS map of New Madrid seismic zone and surrounding region showing preferred age estimates of liquefaction features; features whose ages are poorly constrained are excluded. Map projection is USA Contiguous Albers Equal Area Conic, North America Datum 1983.

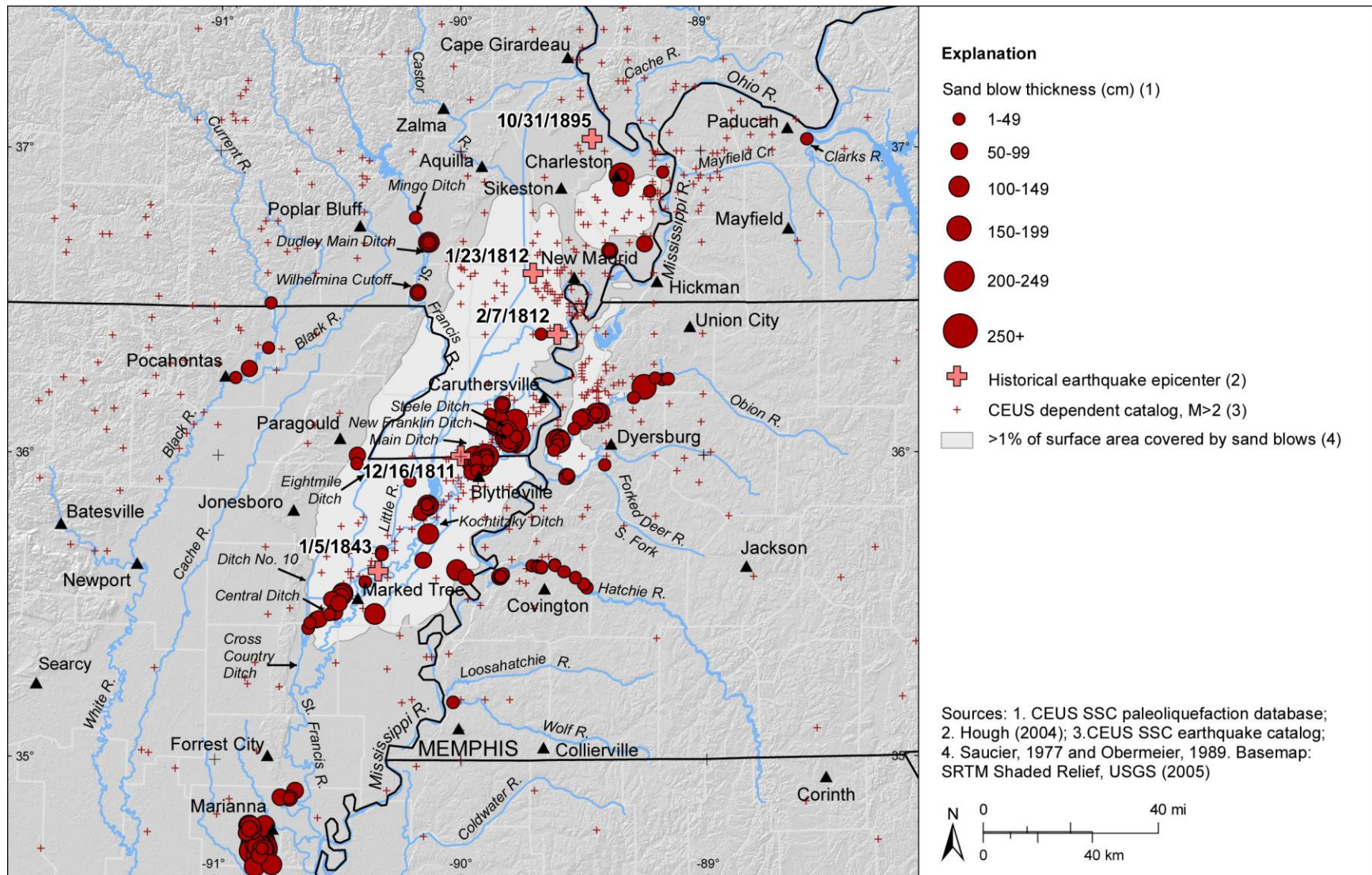


Figure E-8

GIS map of New Madrid seismic zone and surrounding region showing measured thicknesses of sand blows. Map projection is USA Contiguous Albers Equal Area Conic, North America Datum 1983.

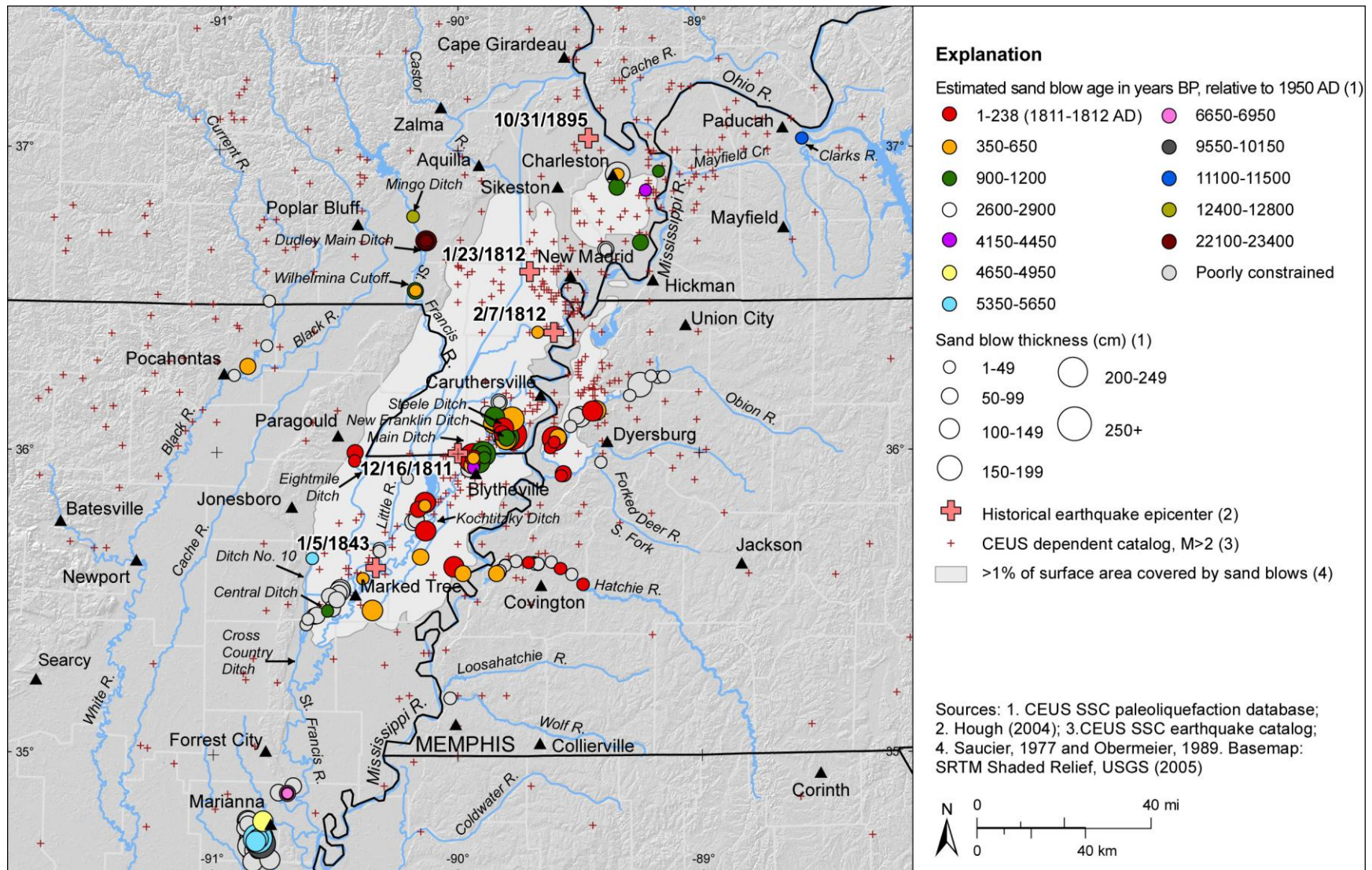


Figure E-9

GIS map of New Madrid seismic zone and surrounding region showing preferred age estimates and measured thicknesses of sand blows. Map projection is USA Contiguous Albers Equal Area Conic, North America Datum 1983.

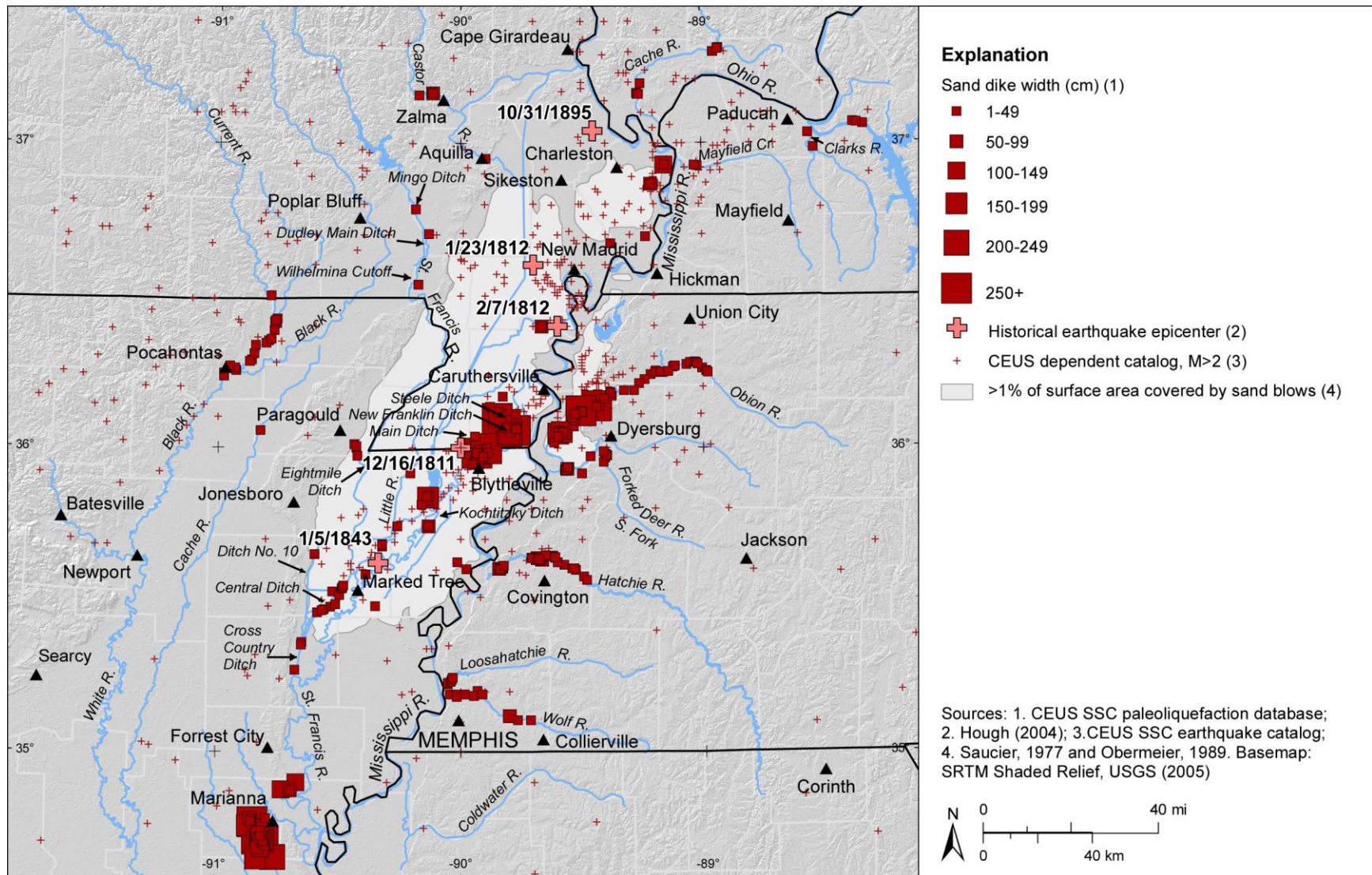


Figure E-10

GIS map of New Madrid seismic zone and surrounding region showing measured widths of sand dikes. Map projection is USA Contiguous Albers Equal Area Conic, North America Datum 1983.

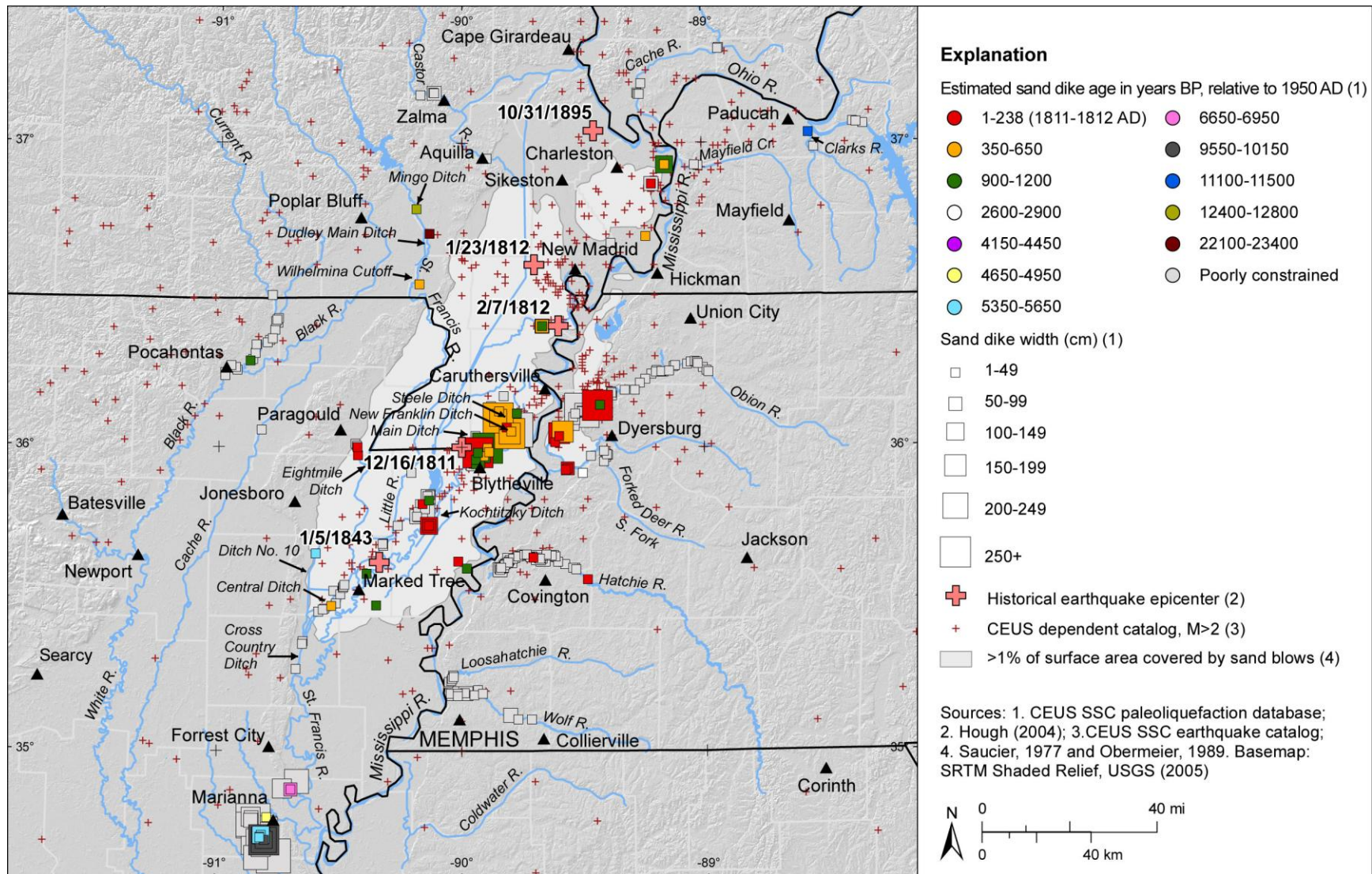


Figure E-11

GIS map of New Madrid seismic zone and surrounding region showing preferred age estimates and measured widths of sand dikes. Map projection is USA Contiguous Albers Equal Area Conic, North America Datum 1983.

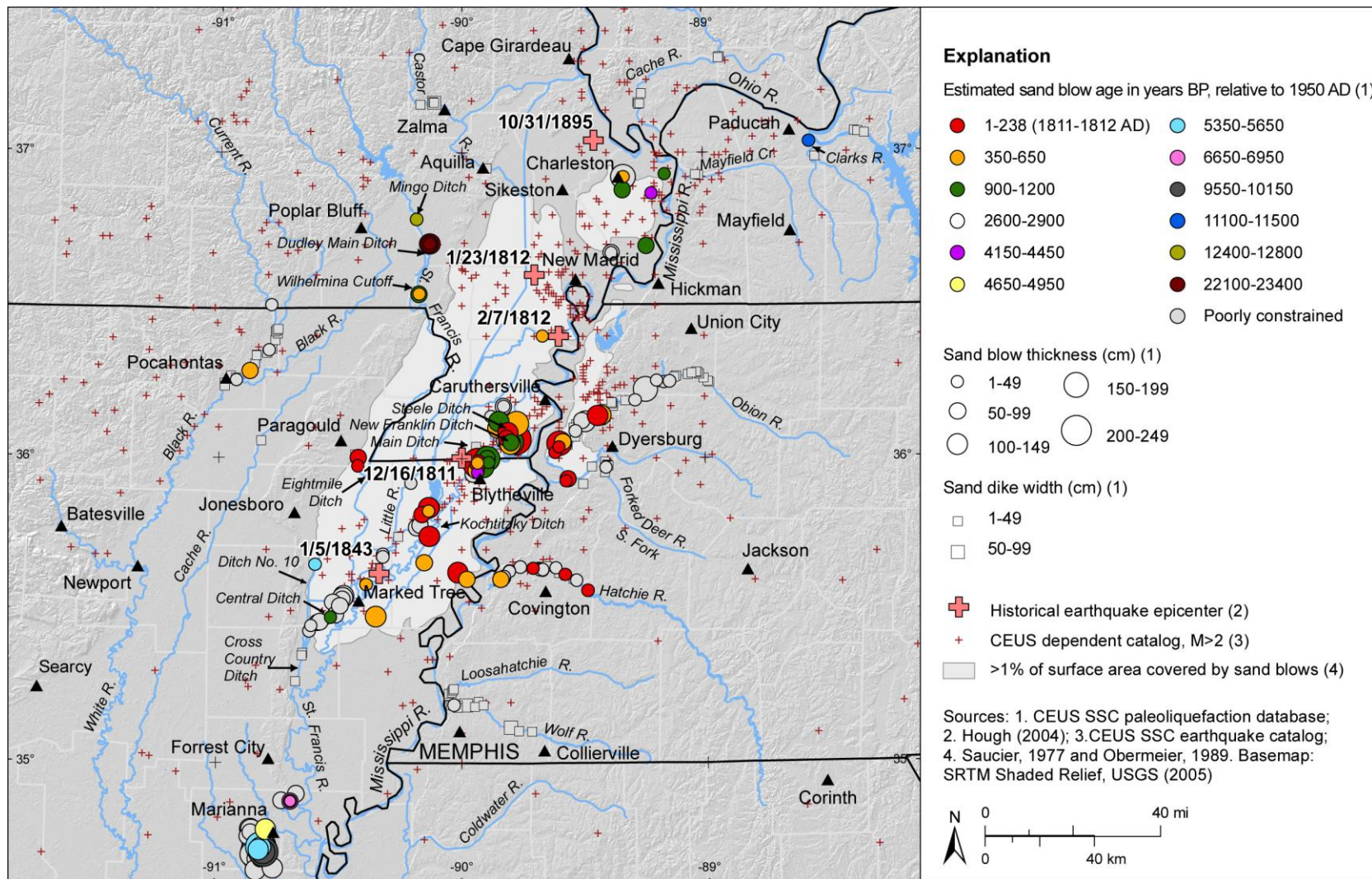


Figure E-12

GIS map of New Madrid seismic zone and surrounding region illustrating preferred age estimates and measured thicknesses of sand blows as well as preferred age estimates and measured widths of sand dikes for sites where sand blows do not occur. Map projection is USA Contiguous Albers Equal Area Conic, North America Datum 1983.

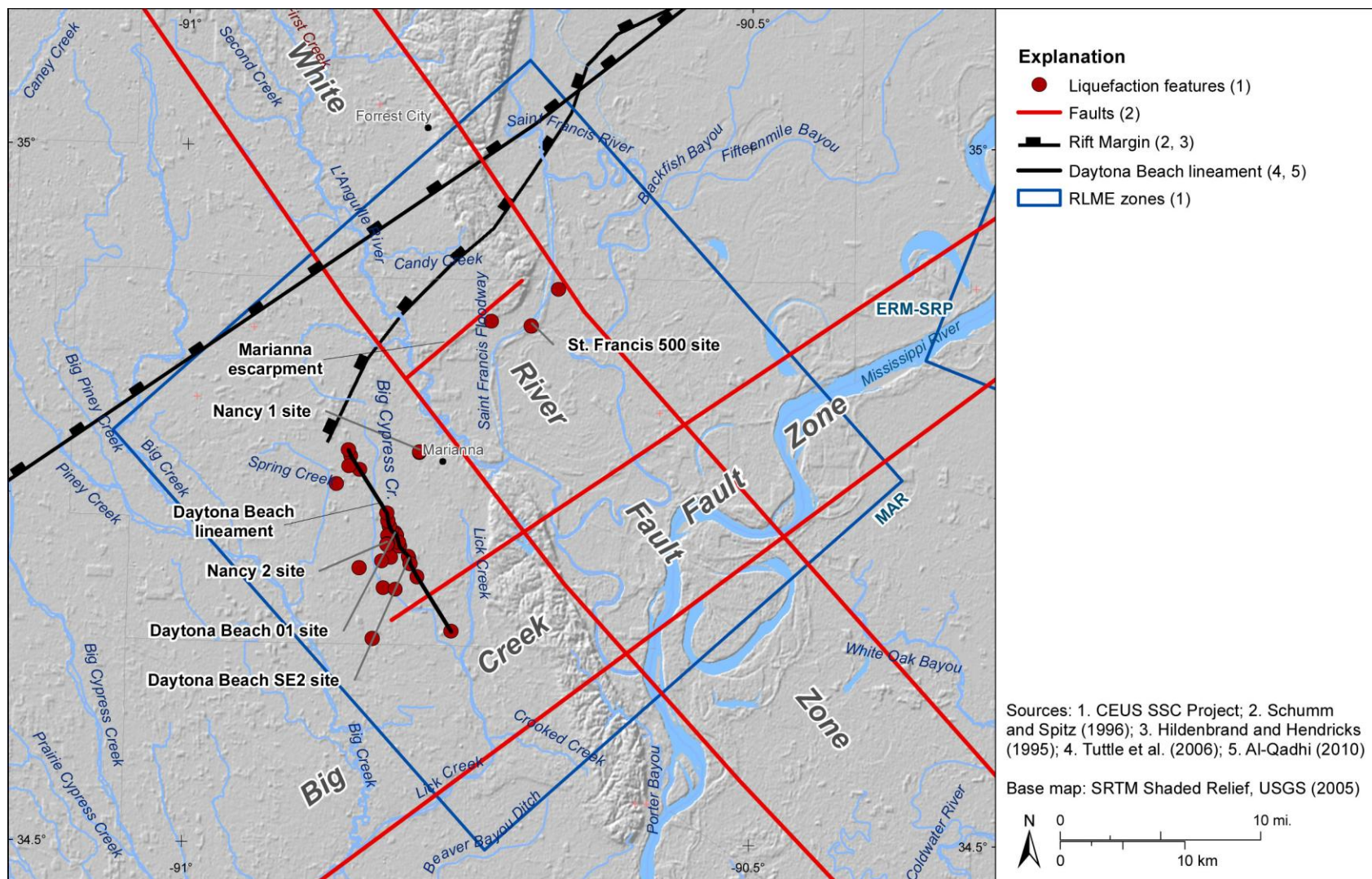


Figure E-13

GIS map of Marianna, Arkansas, area showing seismicity and locations of paleoliquefaction features relative to mapped traces of Eastern Reelfoot rift margin fault, White River fault zone, Big Creek fault zone, Marianna escarpment, and Daytona Beach lineament. Map projection is USA Contiguous Albers Equal Area Conic, North America Datum 1983.

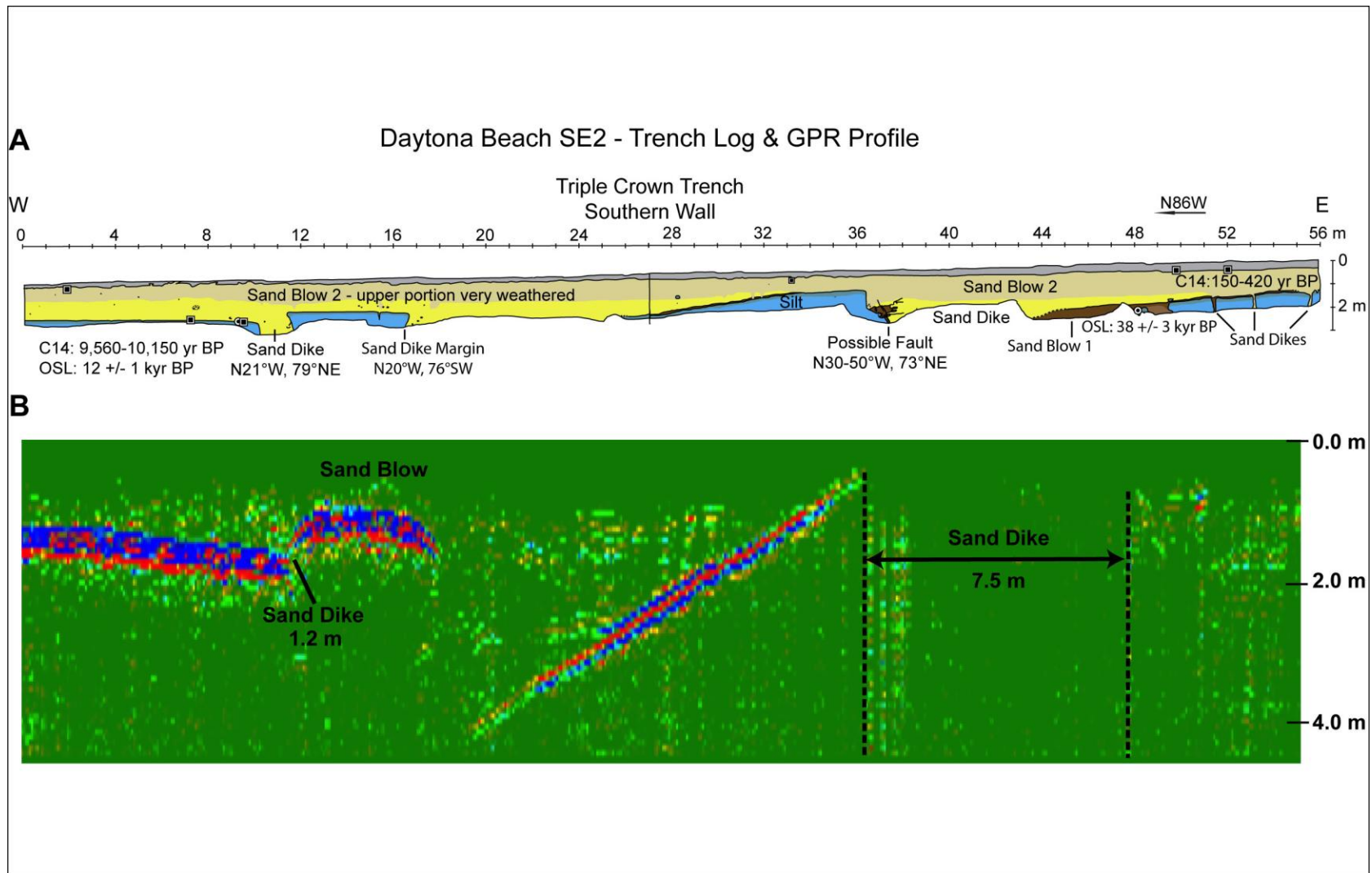


Figure E-14

(A) Trench log and (B) ground-penetrating radar profile, showing vertical sections of sand blows and sand dikes at Daytona Beach SE2 site along the Daytona Beach lineament southwest of Marianna, Arkansas. Vertical scale of GPR profile is exaggerated (modified from Al-Shukri et al., 2009).

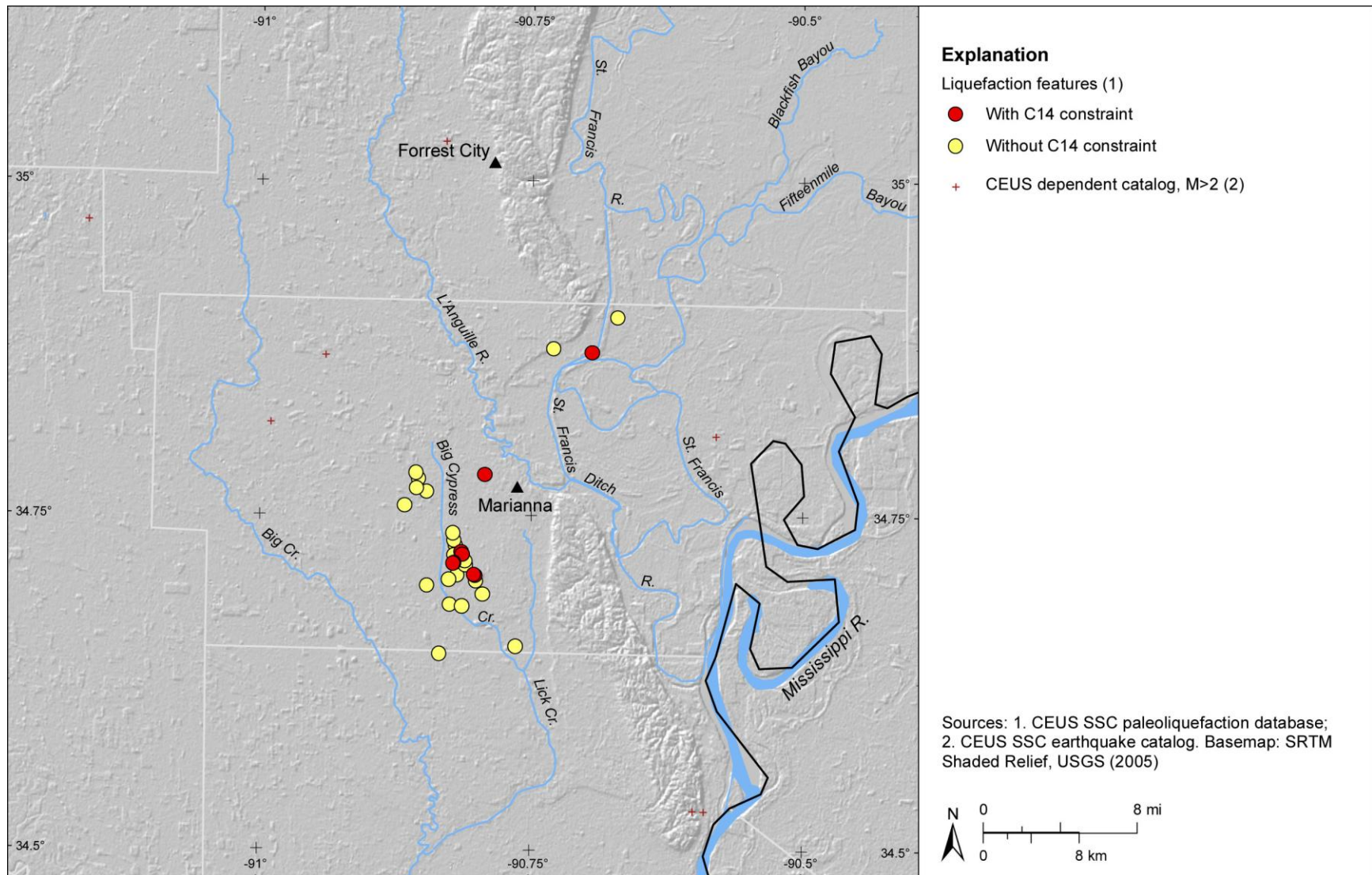


Figure E-15

GIS map of Marianna, Arkansas, area showing locations of liquefaction features for which there are and are not radiocarbon data. Map projection is USA Contiguous Albers Equal Area Conic, North America Datum 1983.

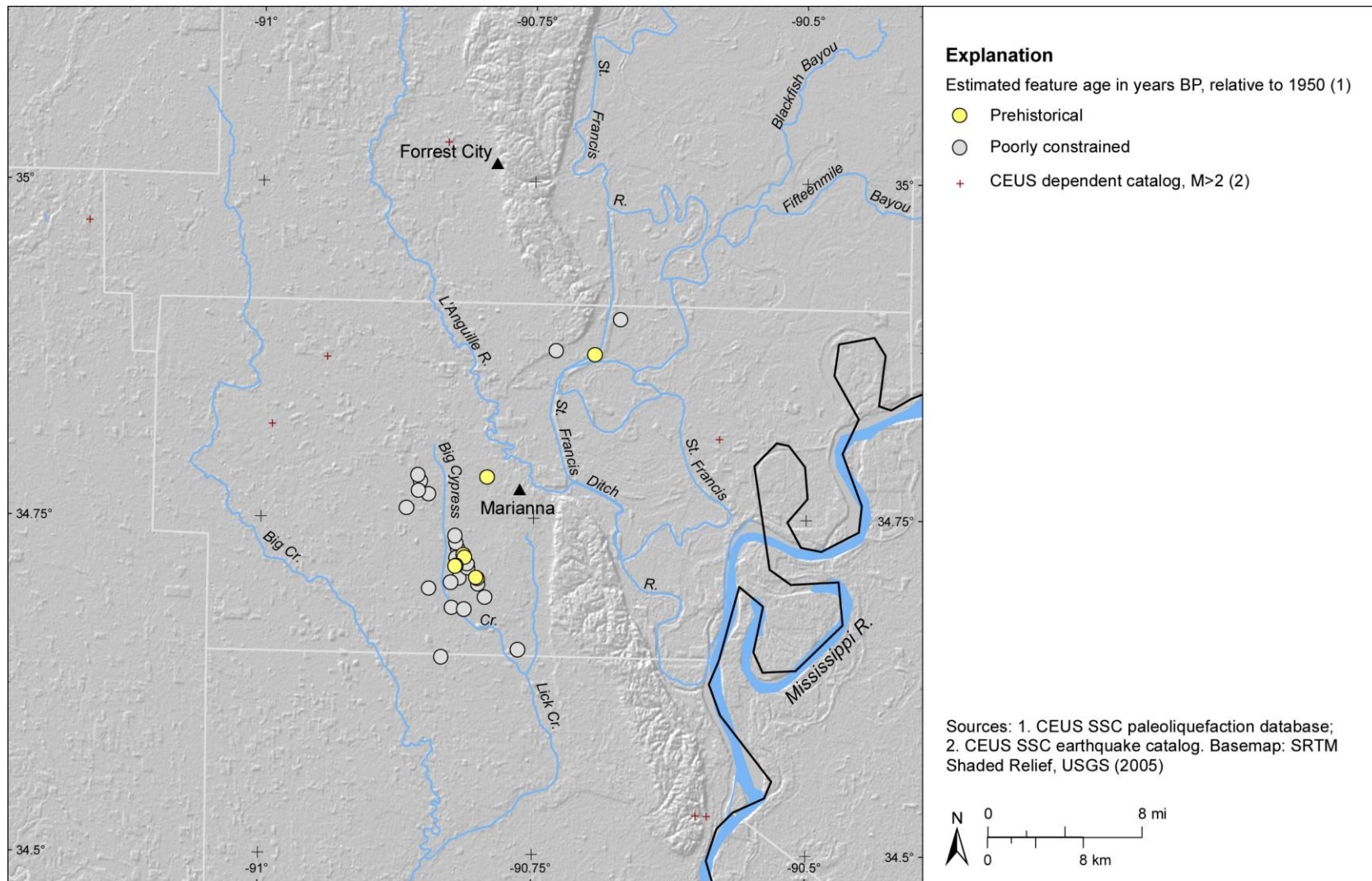


Figure E-16

GIS map of Marianna, Arkansas, area showing locations of liquefaction features that are thought to be historical or prehistoric in age or whose ages are poorly constrained. To date, no liquefaction features thought to have formed during 1811-1812 earthquakes have been found in area. Map projection is USA Contiguous Albers Equal Area Conic, North America Datum 1983.

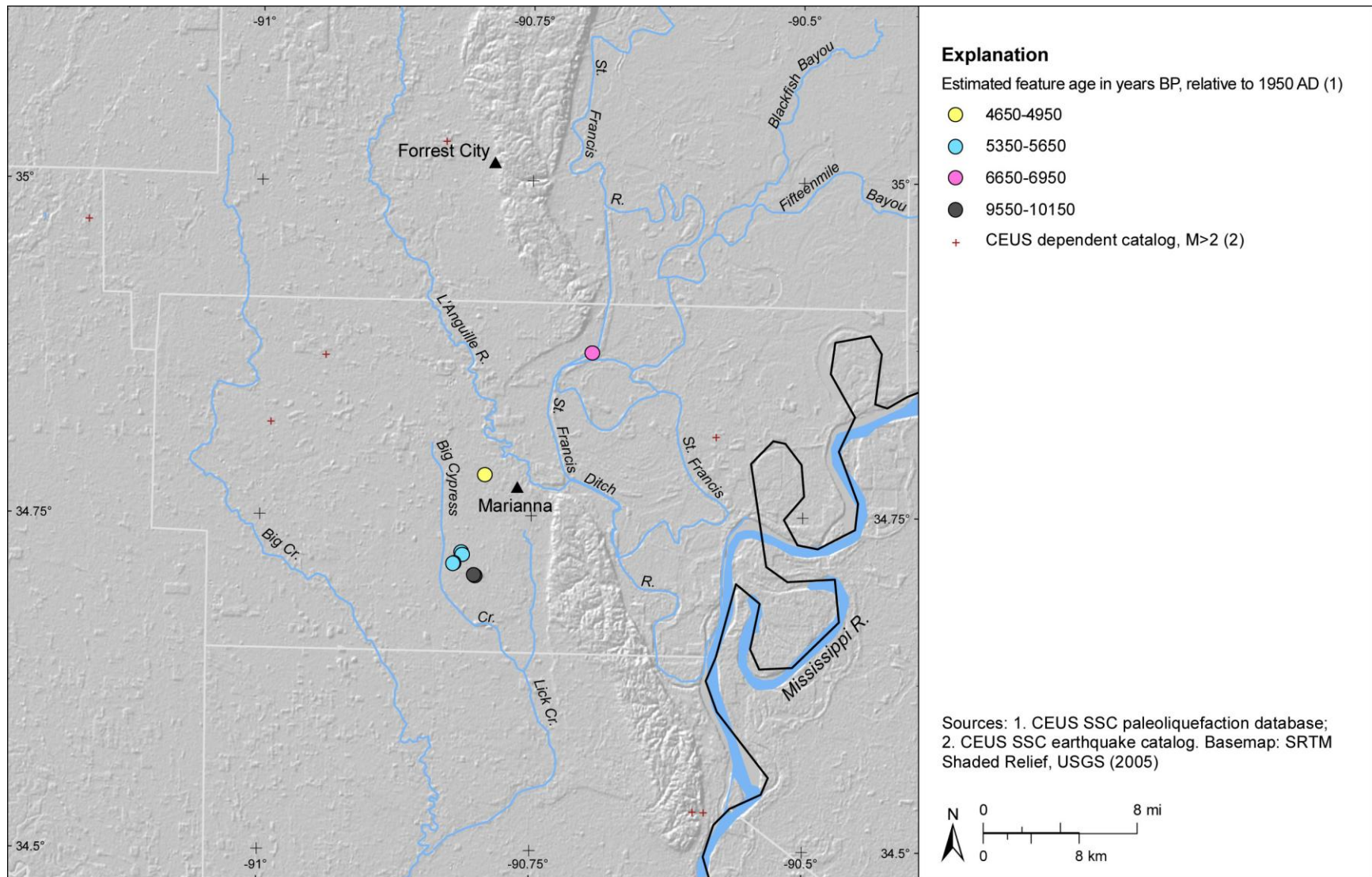


Figure E-17

GIS map of Marianna, Arkansas, area showing preferred age estimates of liquefaction features; features whose ages are poorly constrained are excluded. Map projection is USA Contiguous Albers Equal Area Conic, North America Datum 1983.

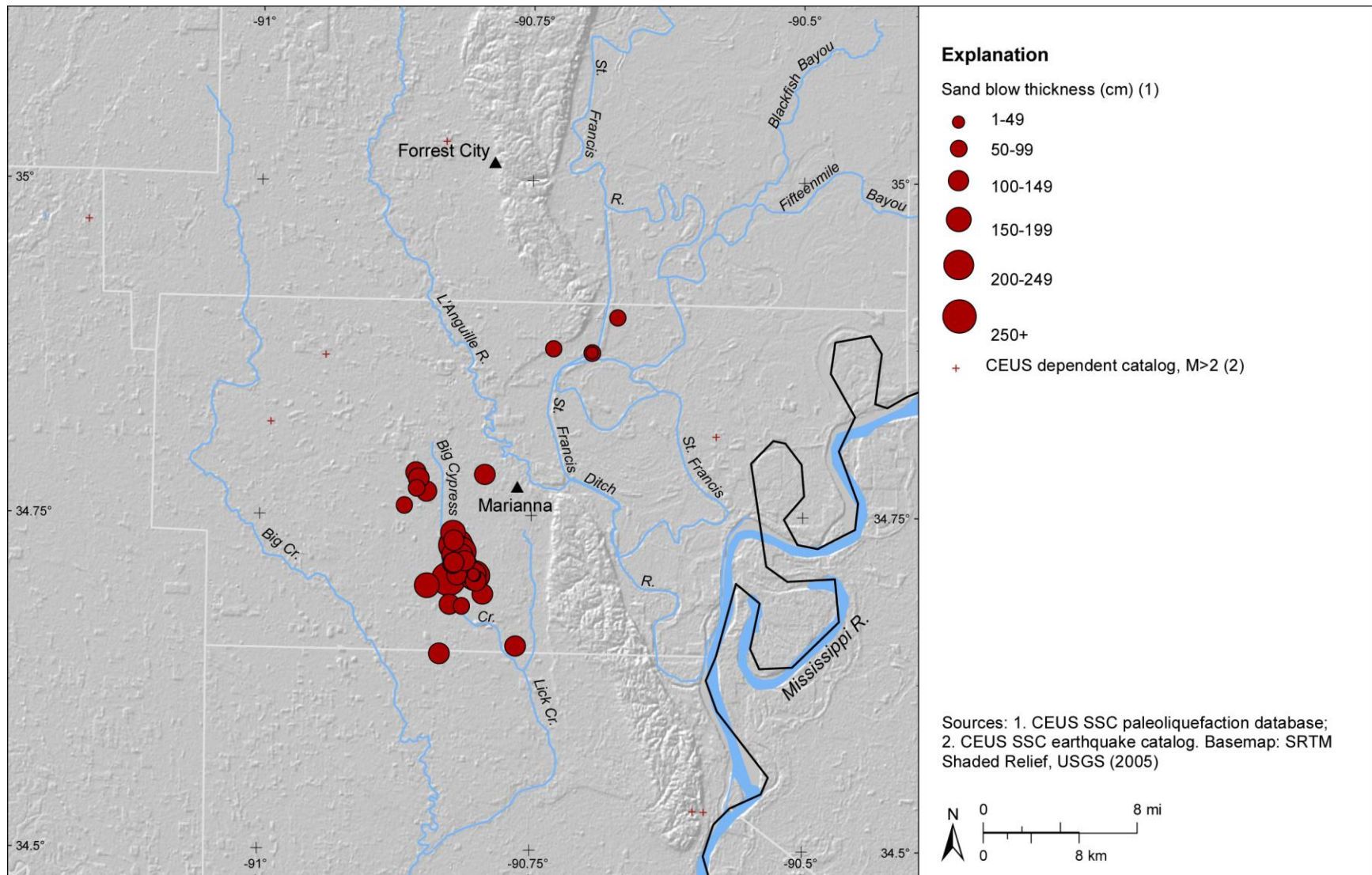


Figure E-18

GIS map of Marianna, Arkansas, area showing measured thicknesses of sand blows. Map projection is USA Contiguous Albers Equal Area Conic, North America Datum 1983.

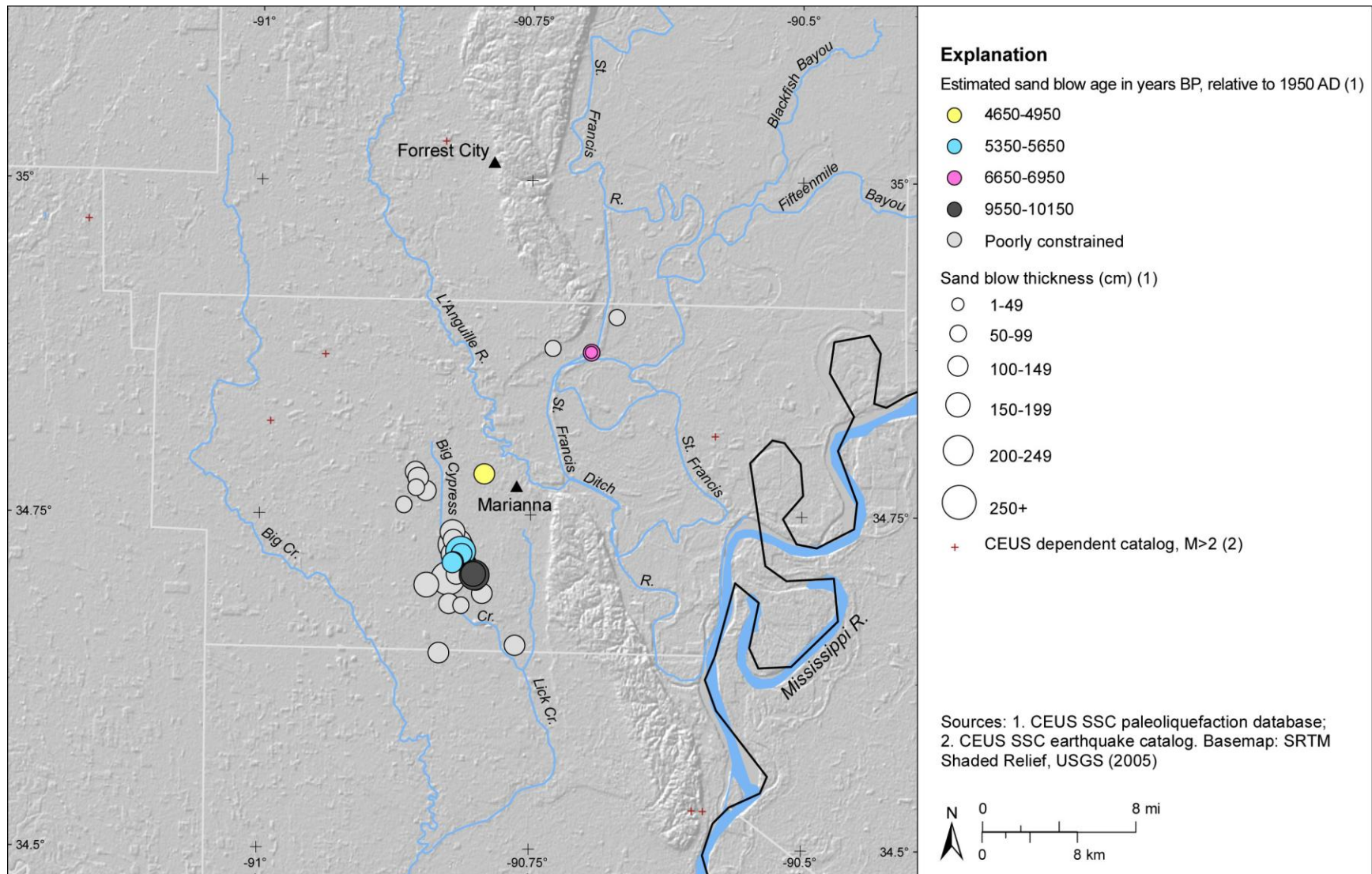


Figure E-19

GIS map of Marianna, Arkansas, area showing preferred age estimates and measured thicknesses of sand blows. Map projection is USA Contiguous Albers Equal Area Conic, North America Datum 1983.

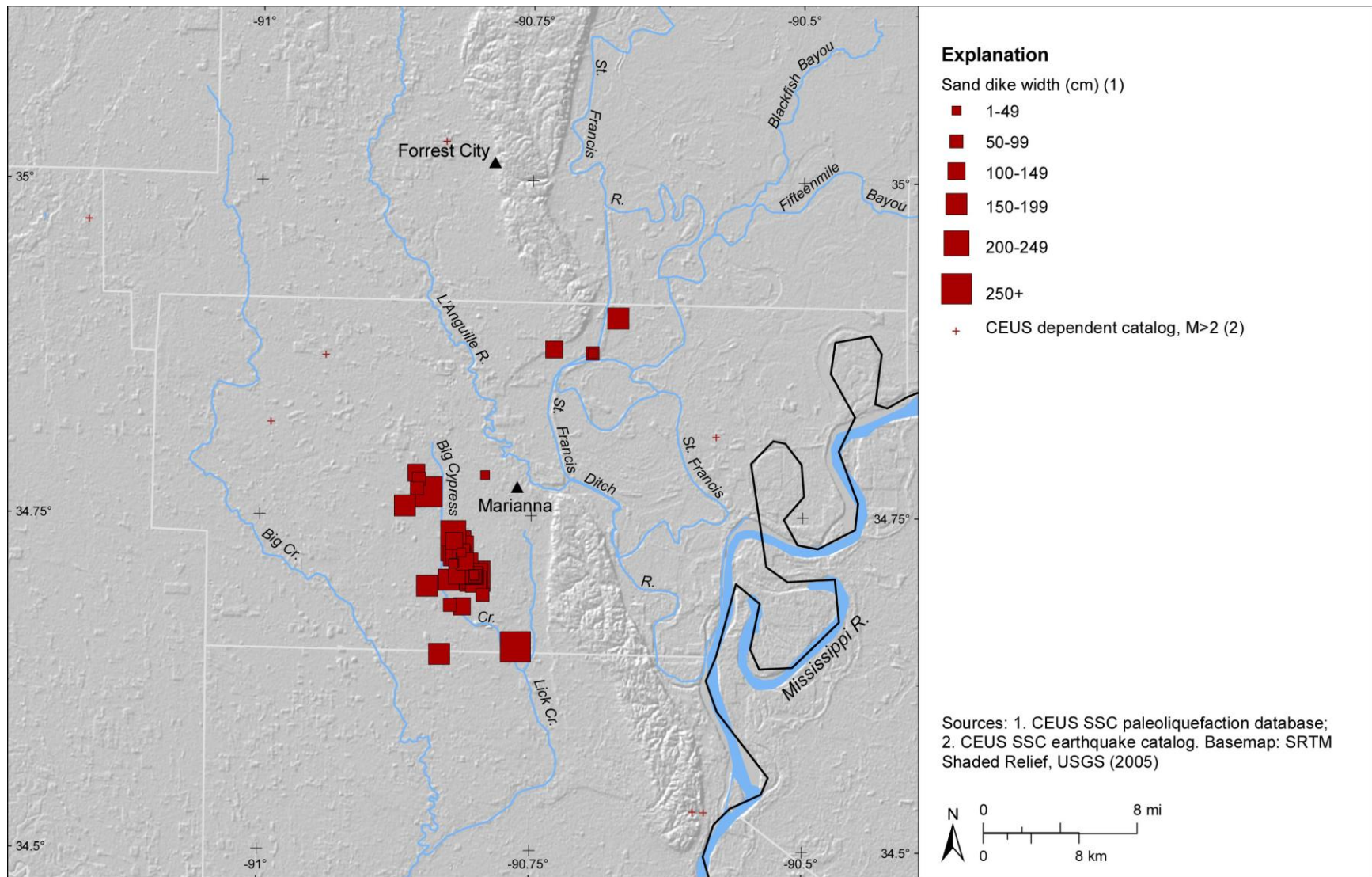


Figure E-20

GIS map of Marianna, Arkansas, area showing measured widths of sand dikes. Map projection is USA Contiguous Albers Equal Area Conic, North America Datum 1983.

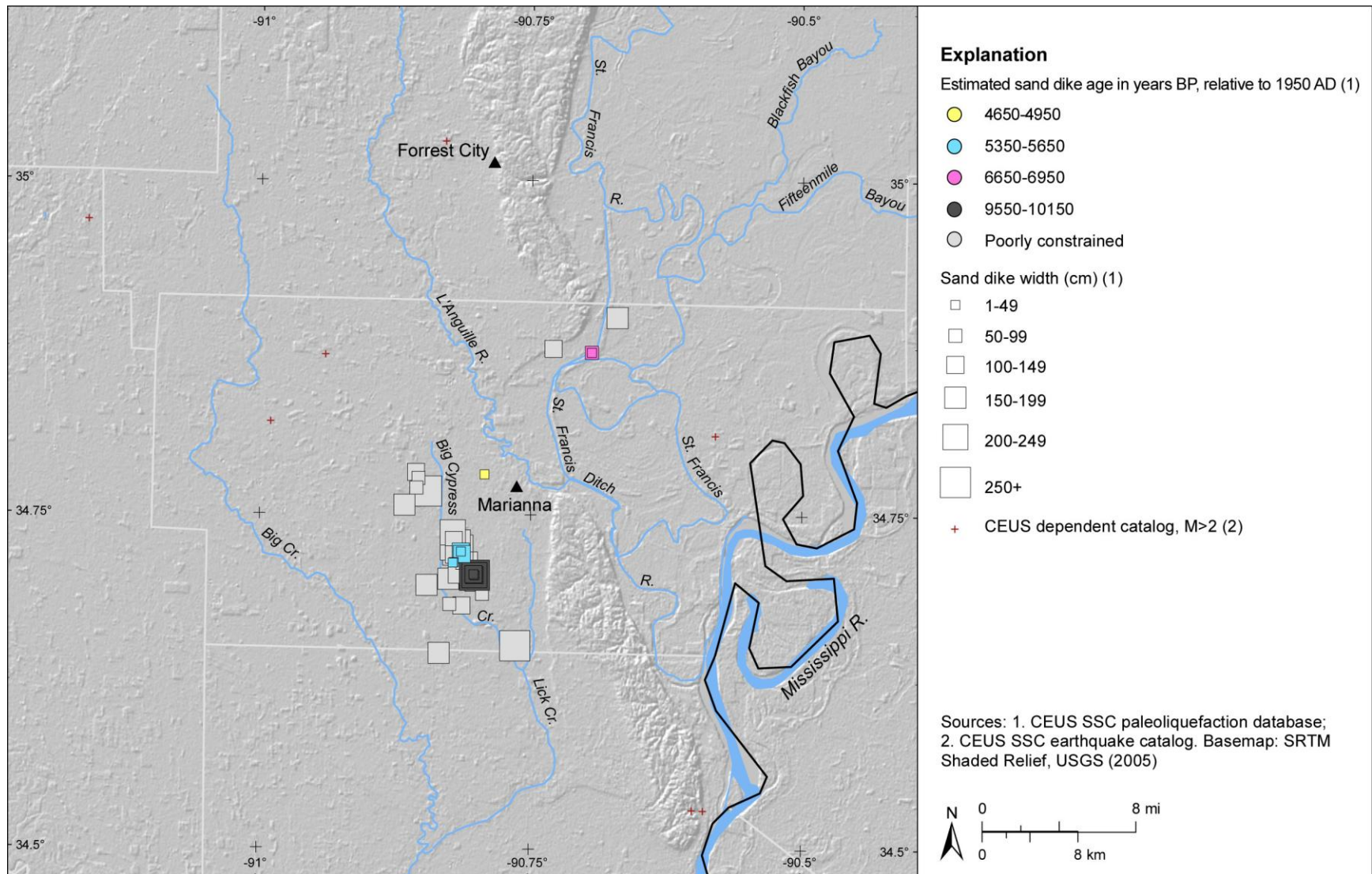


Figure E-21

GIS map of Marianna, Arkansas, area showing preferred age estimates and measured widths of sand dikes. Map projection is USA Contiguous Albers Equal Area Conic, North America Datum 1983.

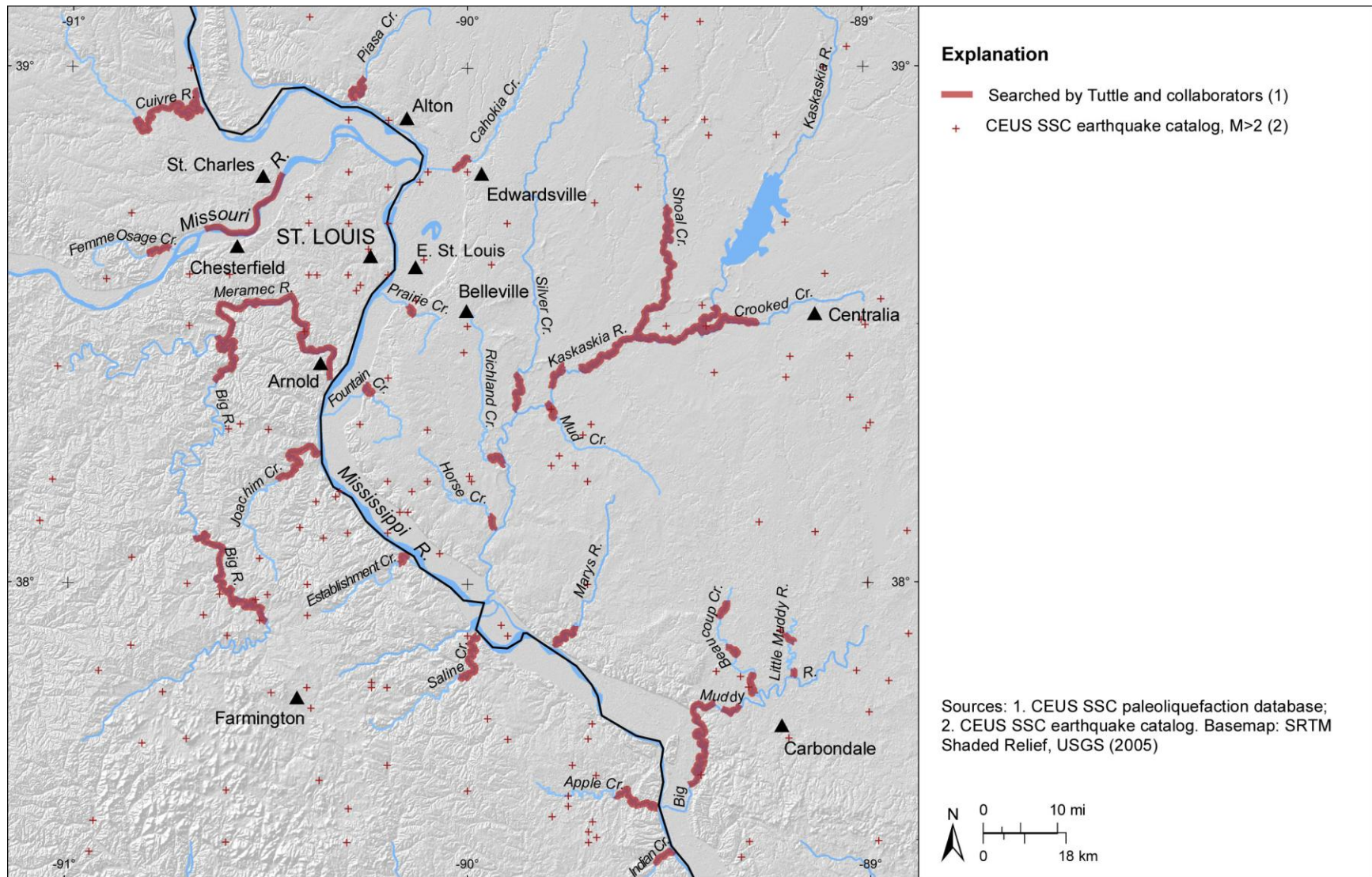


Figure E-22

GIS map of St. Louis, Missouri, region showing seismicity and portions of rivers searched for earthquake-induced liquefaction features by Tuttle and collaborators; information contributed for this report. Map projection is USA Contiguous Albers Equal Area Conic, North America Datum 1983.

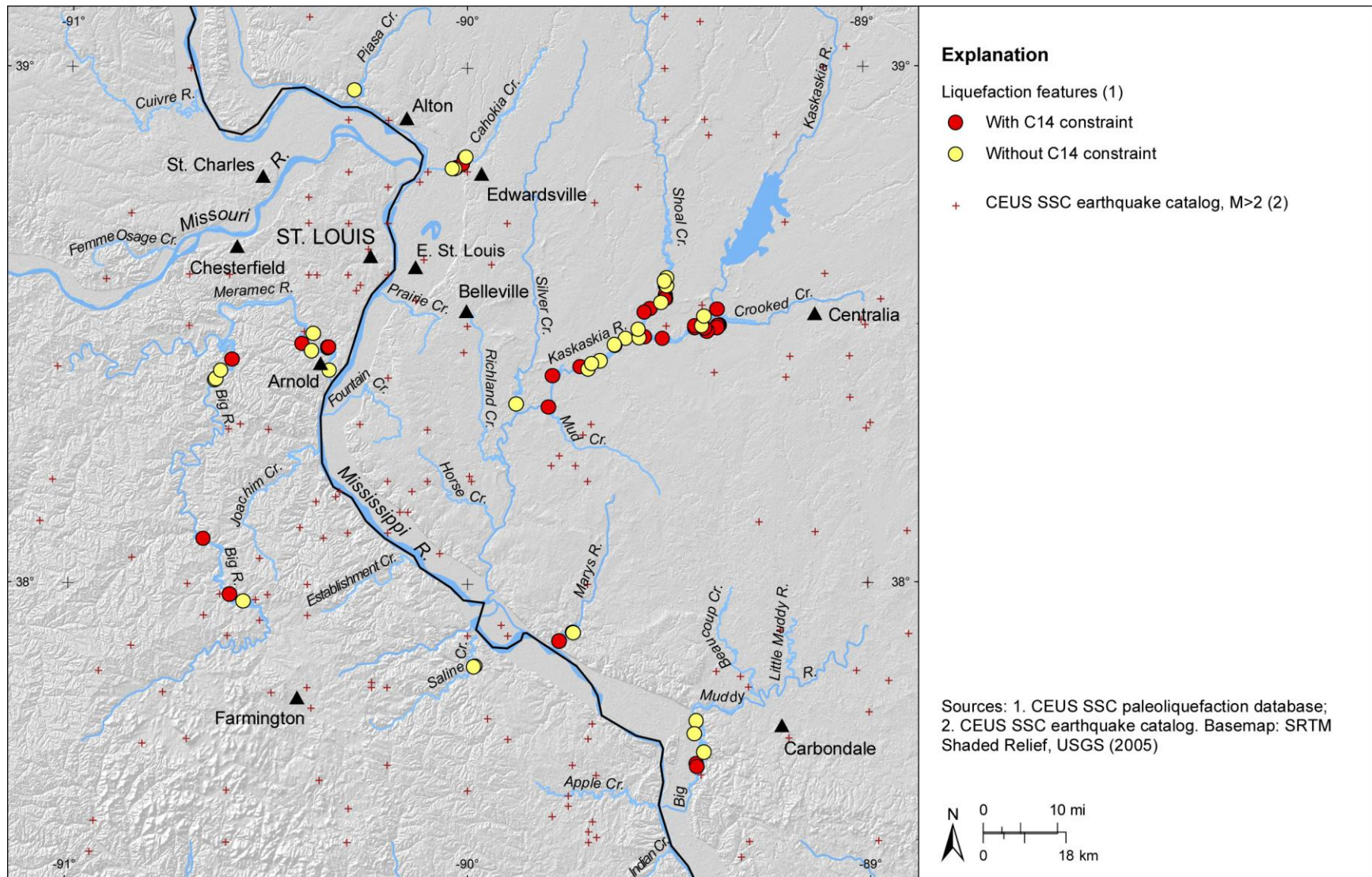


Figure E-23

GIS map of St. Louis, Missouri, region showing locations of liquefaction features, including several soft-sediment deformation structures, for which there are and are not radiocarbon data. Map projection is USA Contiguous Albers Equal Area Conic, North America Datum 1983.

E-90

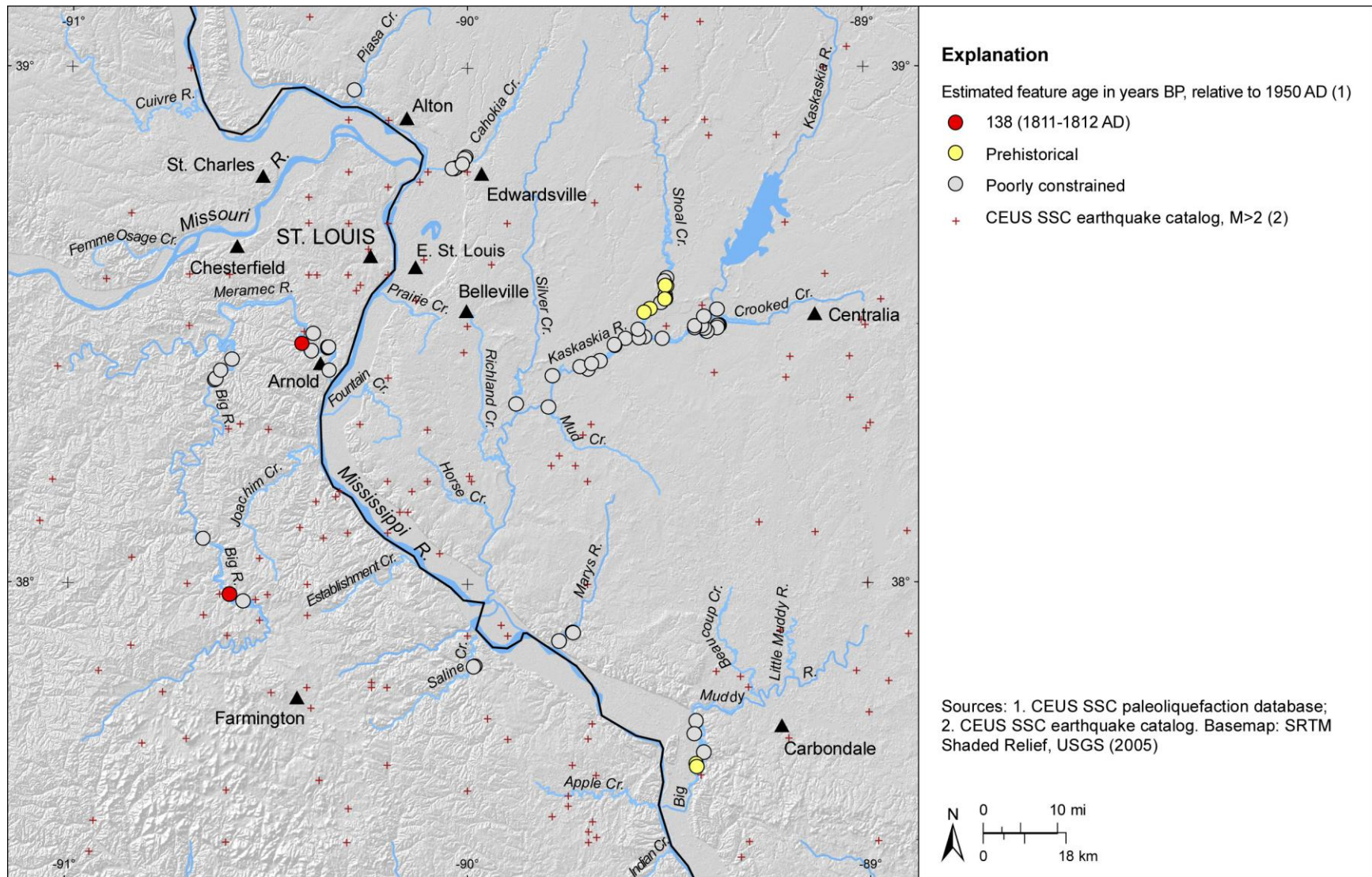


Figure E-24

GIS map of St. Louis, Missouri, region showing locations of liquefaction features that are thought to be historical or prehistoric in age or whose ages are poorly constrained. Map projection is USA Contiguous Albers Equal Area Conic, North America Datum 1983.

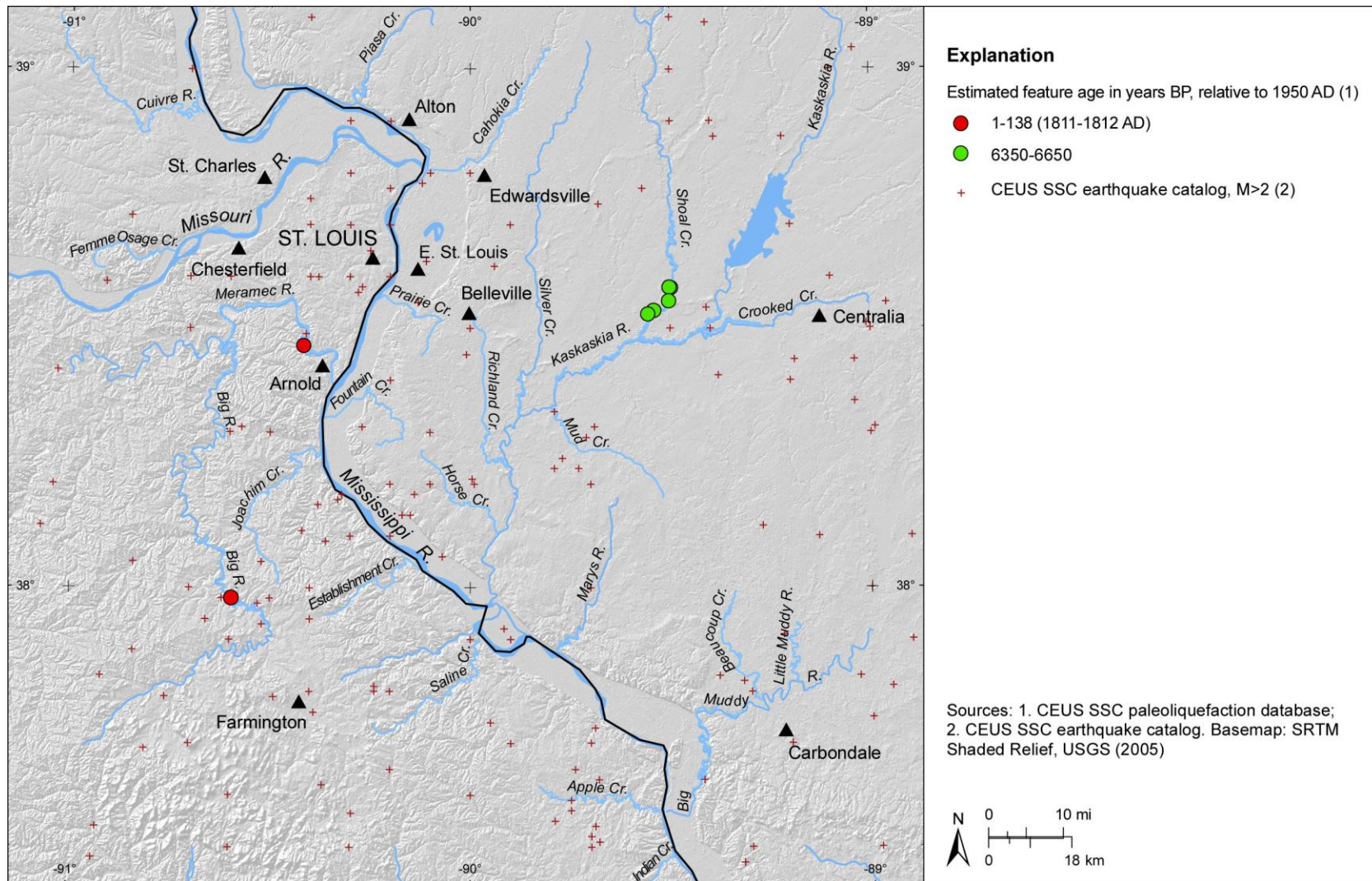


Figure E-25

GIS map of St. Louis, Missouri, region showing preferred age estimates of liquefaction features; features whose ages are poorly constrained, including several that are prehistoric in age, are not shown. Map projection is USA Contiguous Albers Equal Area Conic, North America Datum 1983.

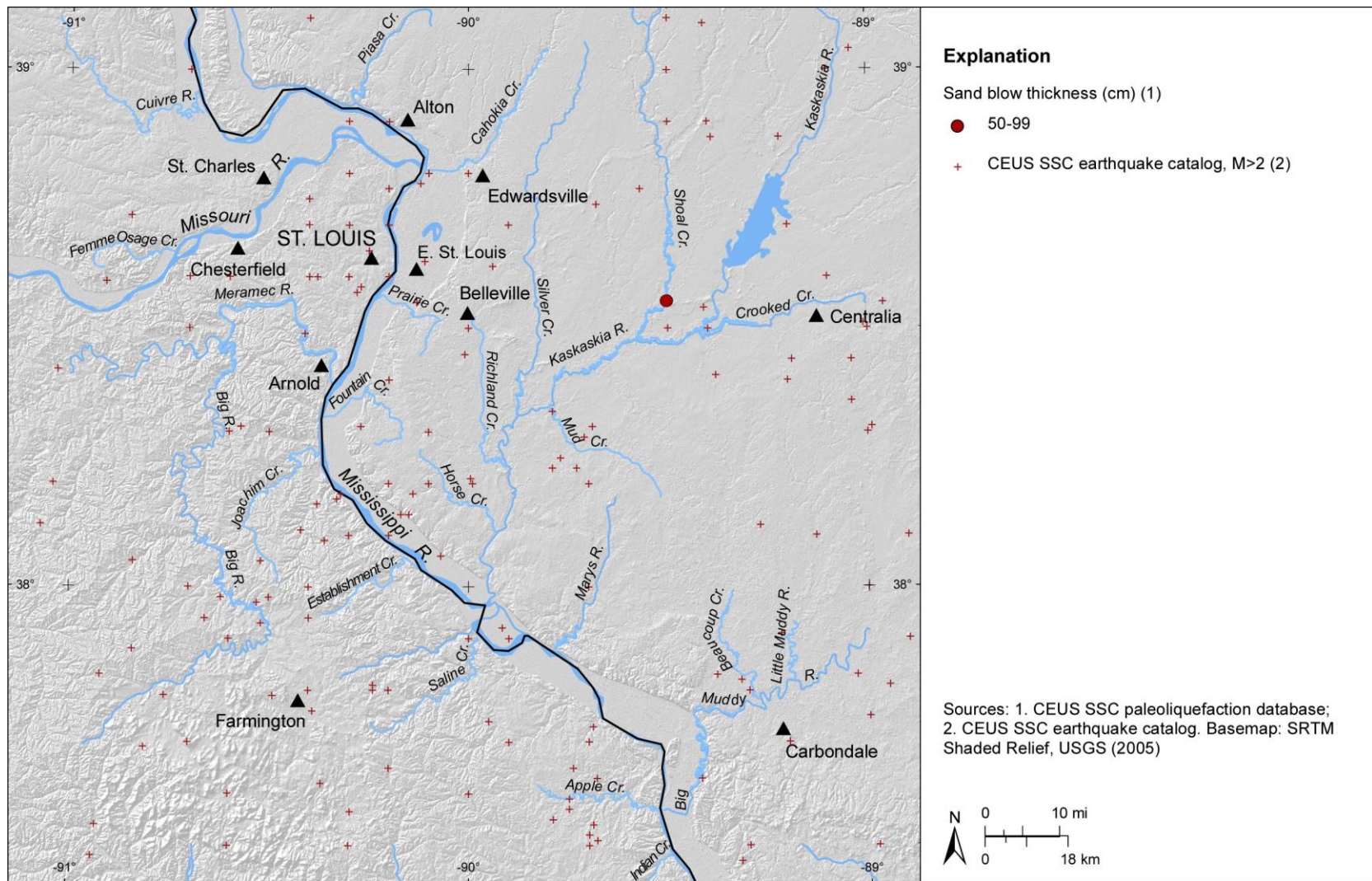


Figure E-26

GIS map of St. Louis, Missouri, region showing measured thicknesses of sand blows at similar scale as used in Figure E-8 of sand blows in New Madrid seismic zone. Note that few sand blows have been found in St. Louis region. Map projection is USA Contiguous Albers Equal Area Conic, North America Datum 1983.

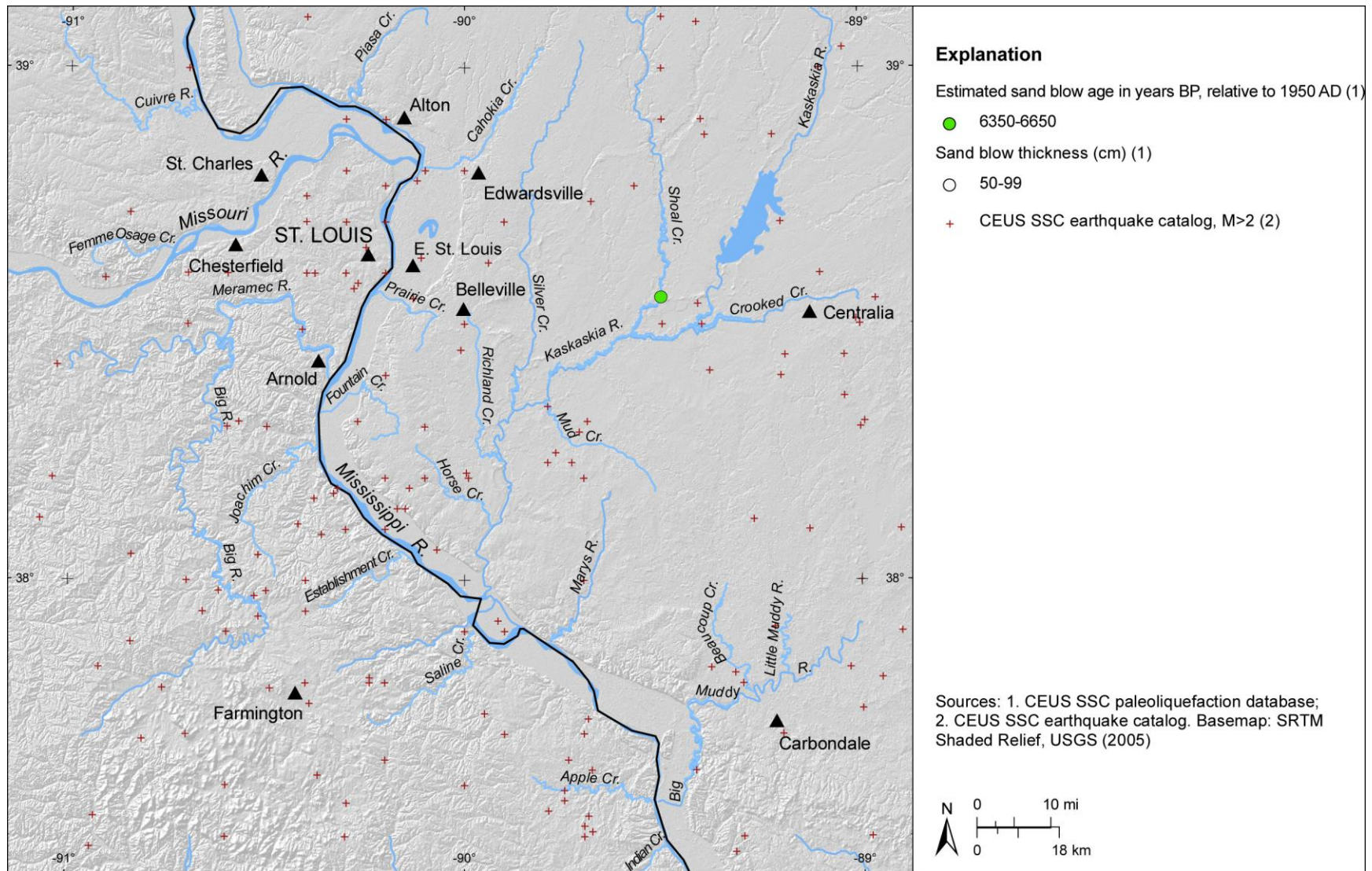


Figure E-27

GIS map of St. Louis, Missouri, region showing preferred age estimates and measured thicknesses of sand blows. Map projection is USA Contiguous Albers Equal Area Conic, North America Datum 1983.

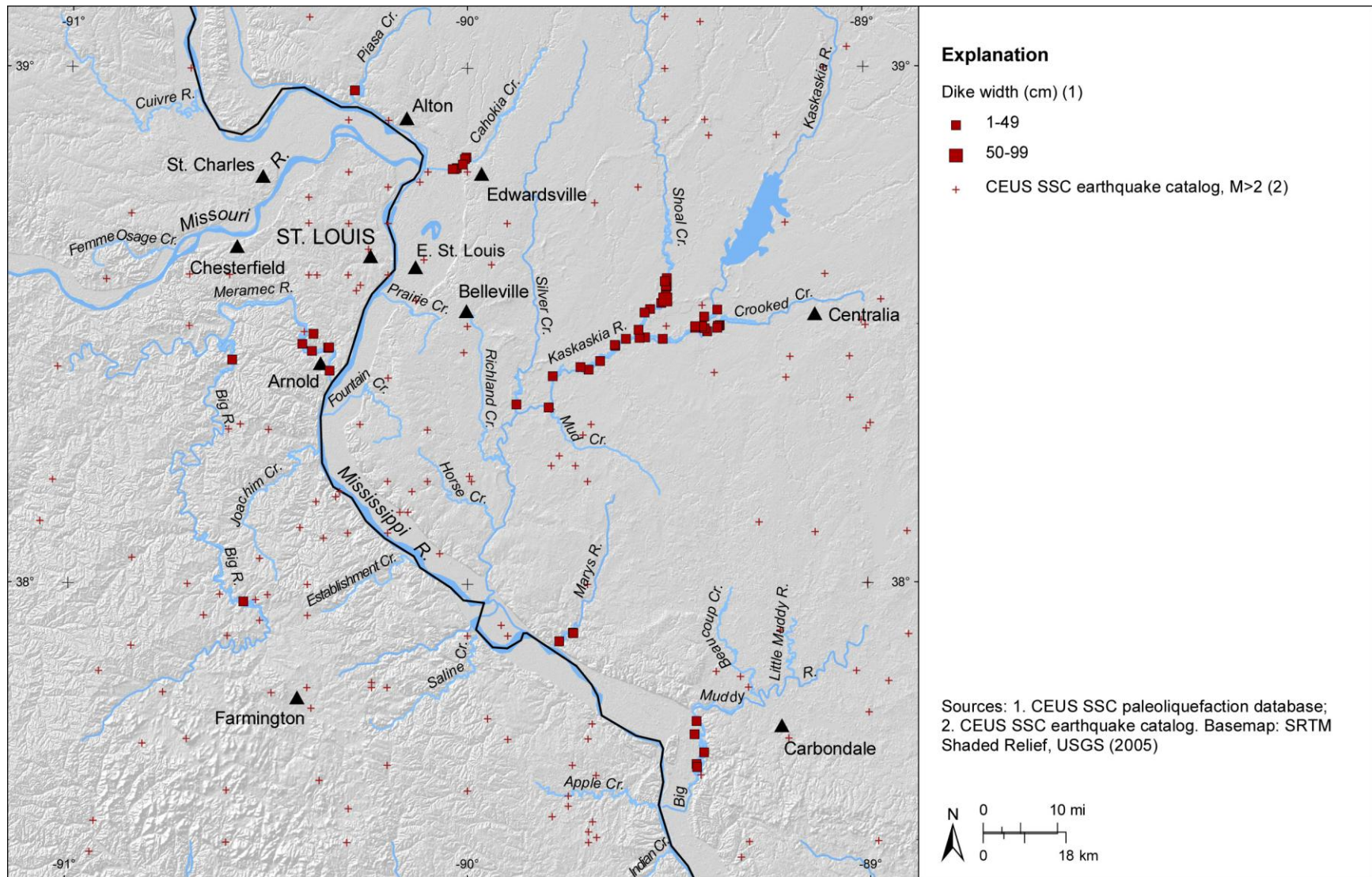


Figure E-28

GIS map of St. Louis, Missouri, region showing measured widths of sand dikes at similar scale as that used in Figure E-10 for sand dikes in New Madrid seismic zone. Map projection is USA Contiguous Albers Equal Area Conic, North America Datum 1983.

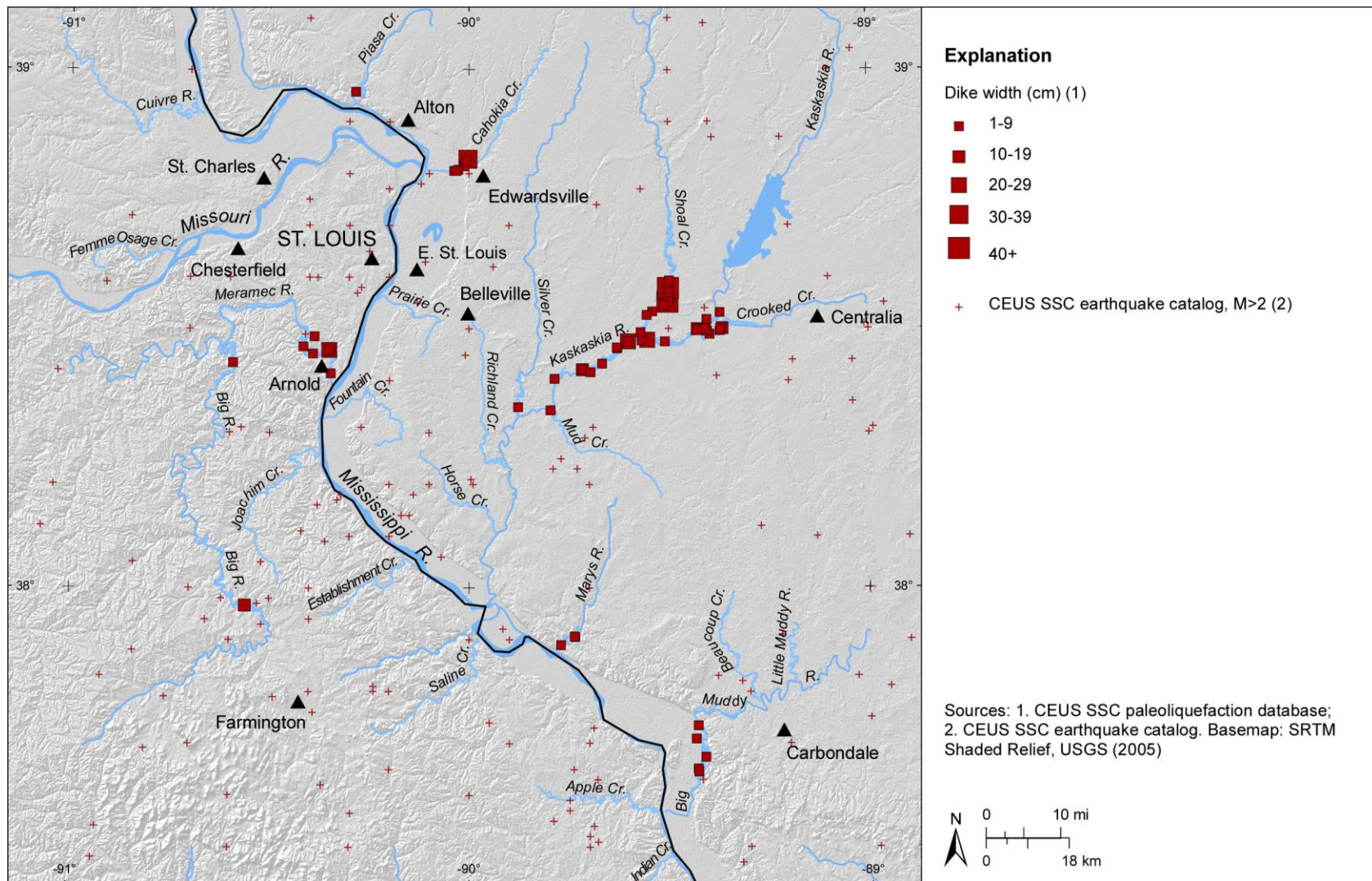


Figure E-29

GIS map of St. Louis, Missouri, region showing measured widths of sand dikes at similar scale as that used in Figures E-42 and E-48 for sand dikes in the Newburyport and Charlevoix regions, respectively. Map projection is USA Contiguous Albers Equal Area Conic, North America Datum 1983.

E-96

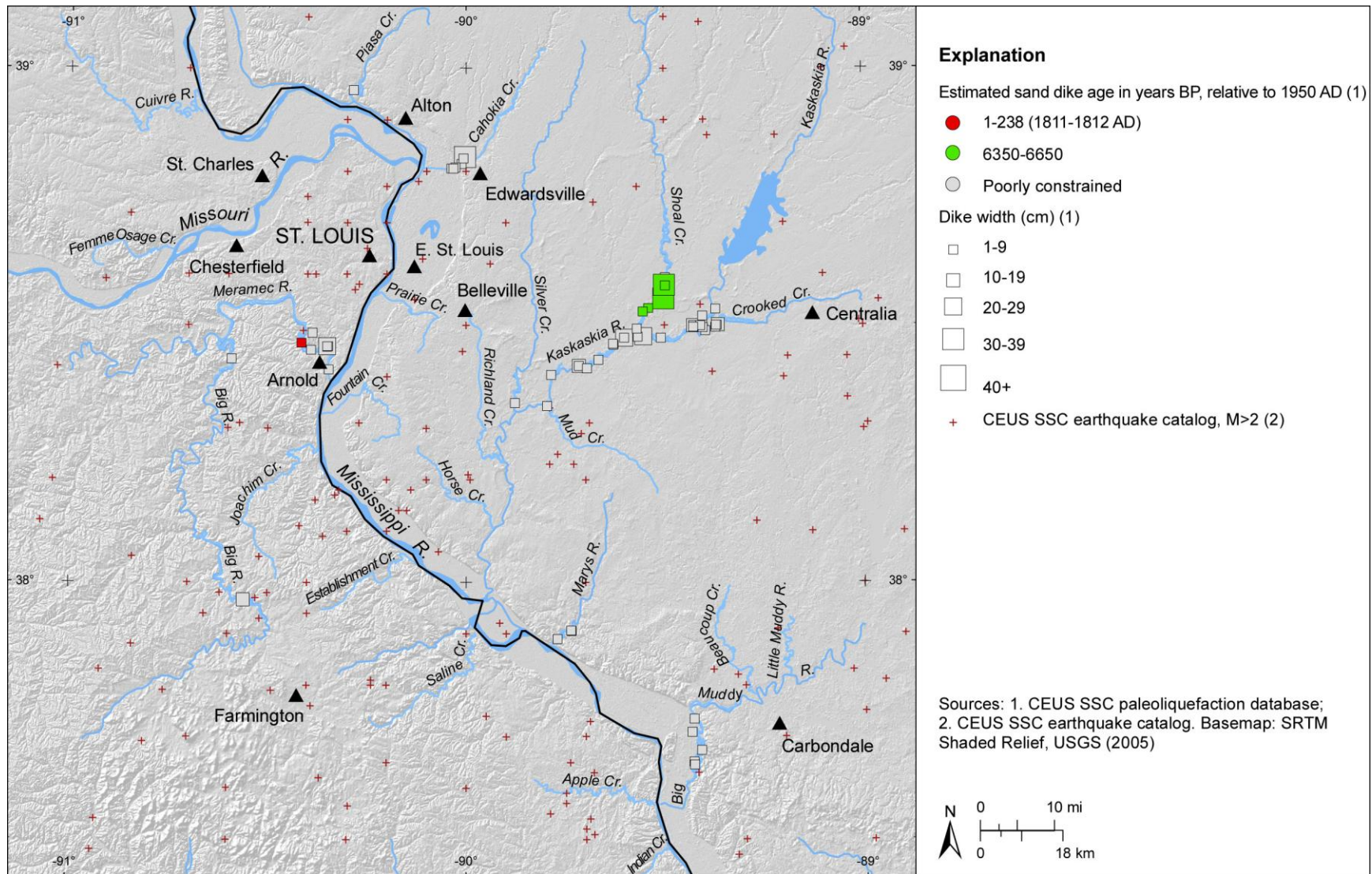


Figure E-30

GIS map of St. Louis, Missouri, region showing preferred age estimates and measured widths of sand dikes. Map projection is USA Contiguous Albers Equal Area Conic, North America Datum 1983.

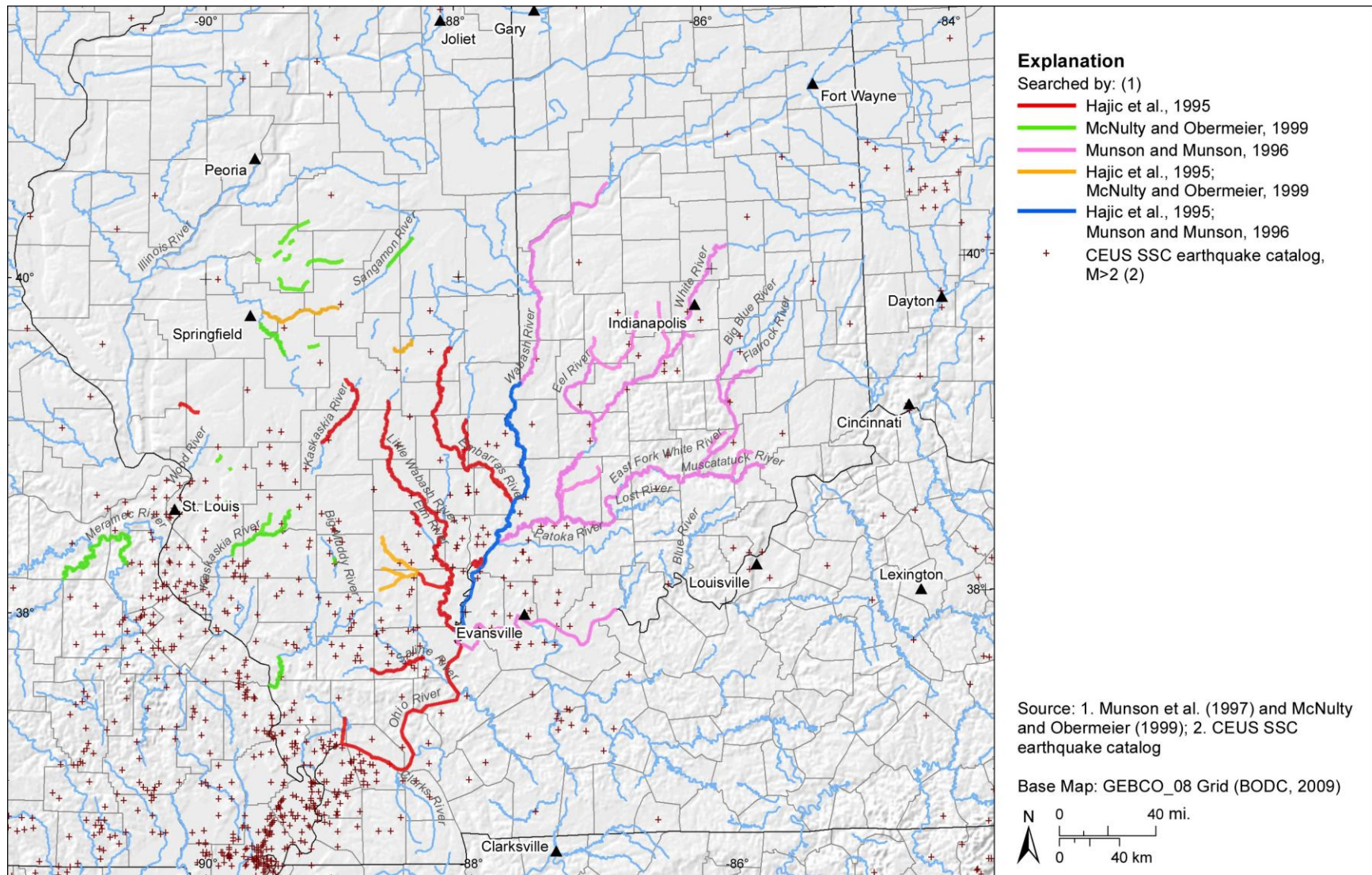


Figure E-31

GIS map of Wabash Valley seismic zone and surrounding region showing portions of rivers searched for earthquake-induced liquefaction features (digitized from McNulty and Obermeier, 1999). Map projection is USA Contiguous Albers Equal Area Conic, North America Datum 1983.

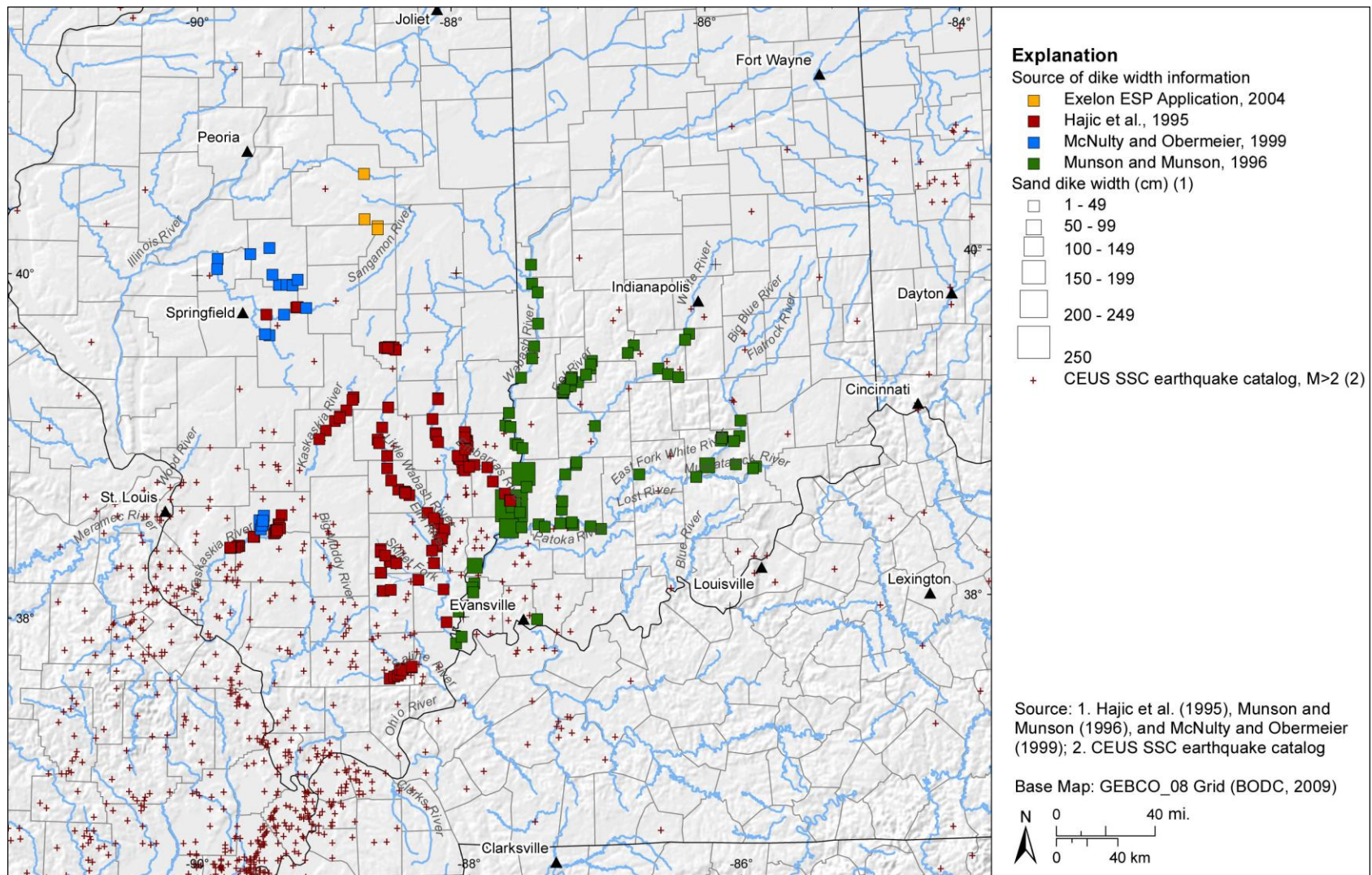


Figure E-32

GIS map of Wabash Valley seismic zone and surrounding region showing measured widths of sand dikes at similar scale as that used in Figures E-10 and E-11 for sand dikes in New Madrid seismic zone. Map projection is USA Contiguous Albers Equal Area Conic, North America Datum 1983.

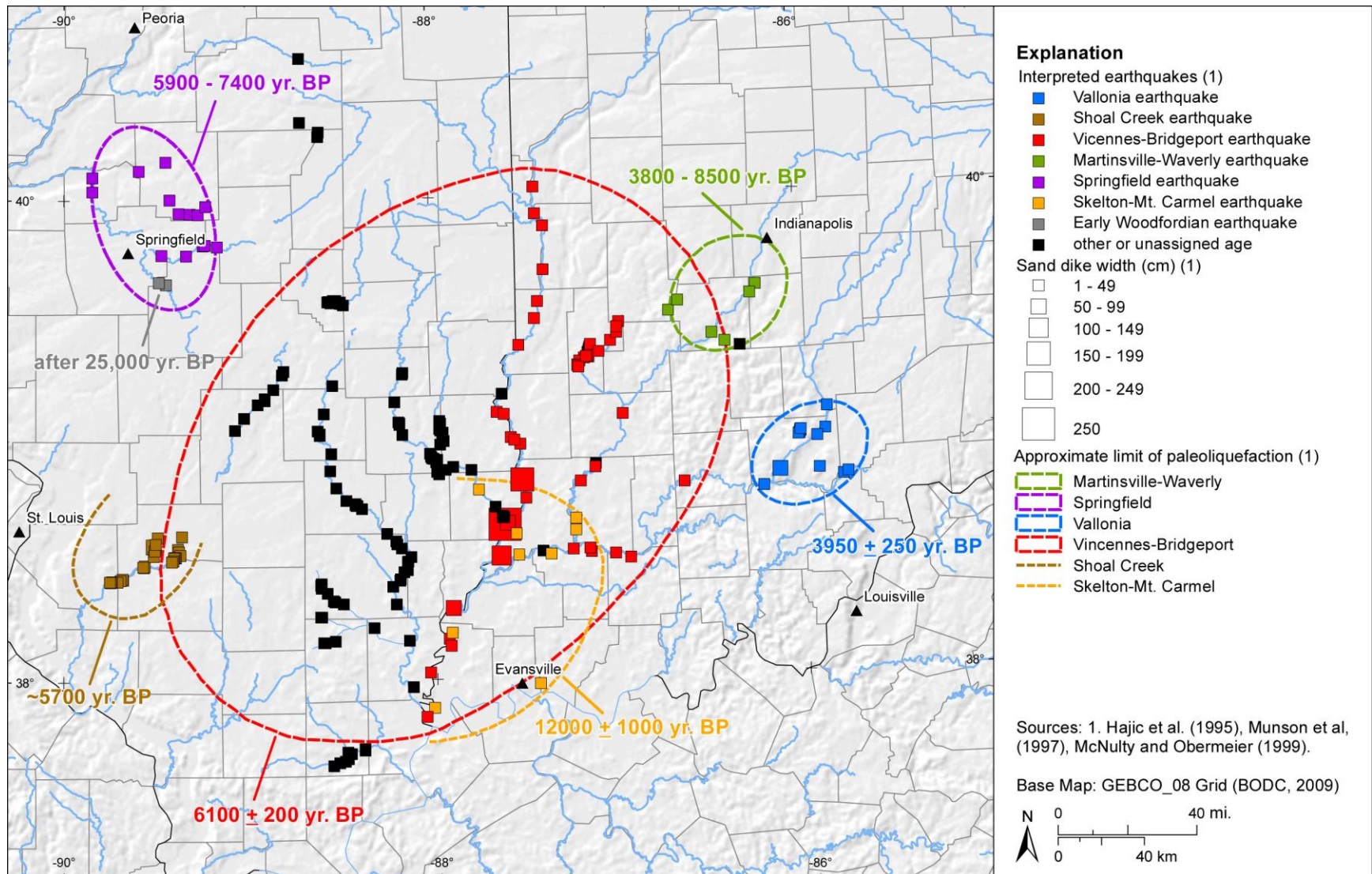


Figure E-33

GIS map of Wabash Valley region of Indiana and Illinois showing preferred age estimates and paleoearthquake interpretation. Map projection is USA Contiguous Albers Equal Area Conic, North America Datum 1983.

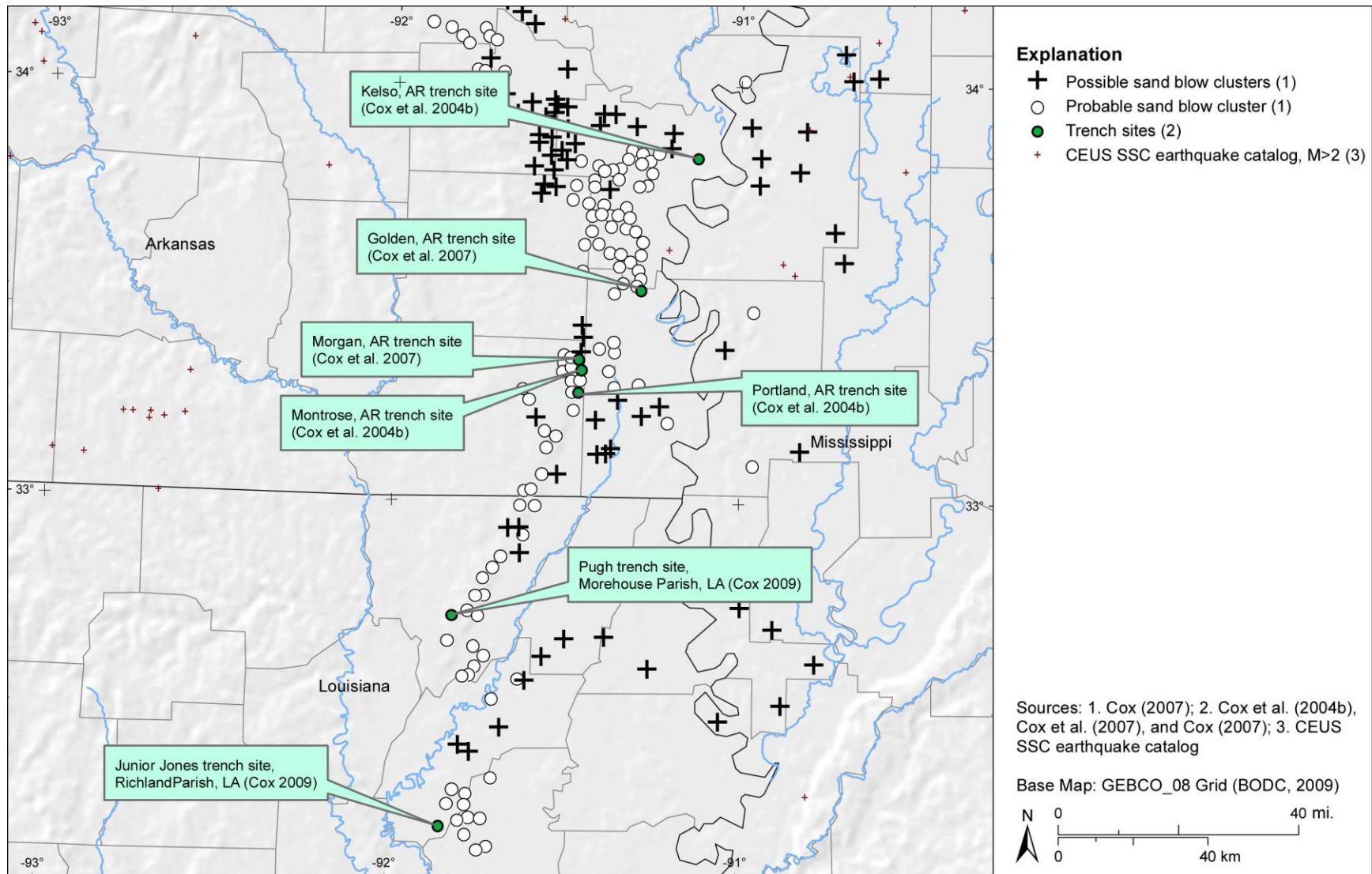


Figure E-34

GIS map of Arkansas-Louisiana-Mississippi (ALM) region showing paleoliquefaction study locations. Map projection is USA Contiguous Albers Equal Area Conic, North America Datum 1983.

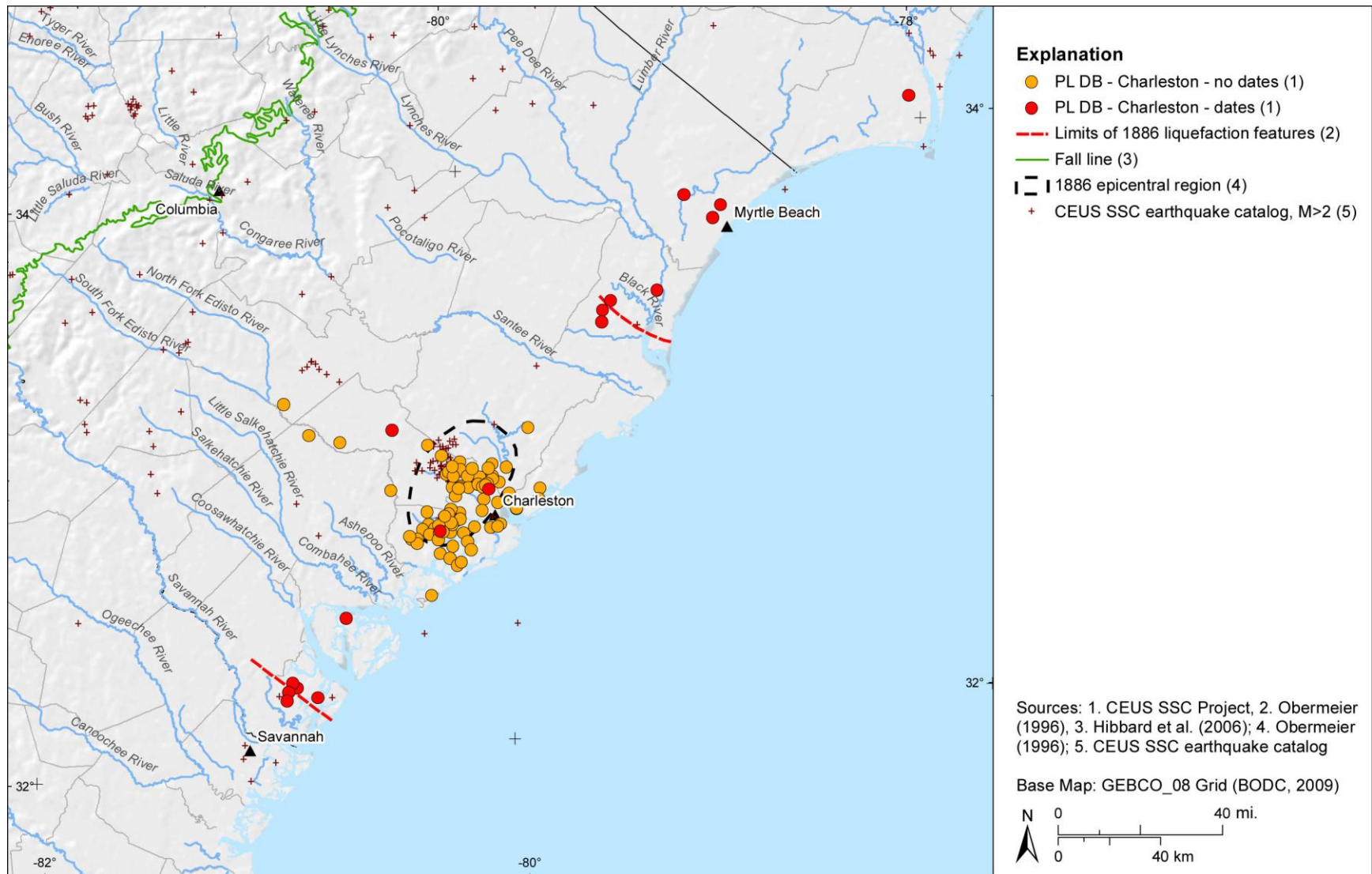


Figure E-35

GIS map of Charleston, South Carolina, region showing locations of paleoliquefaction features for which there are and are not radiocarbon dates. Map projection is USA Contiguous Albers Equal Area Conic, North America Datum 1983.

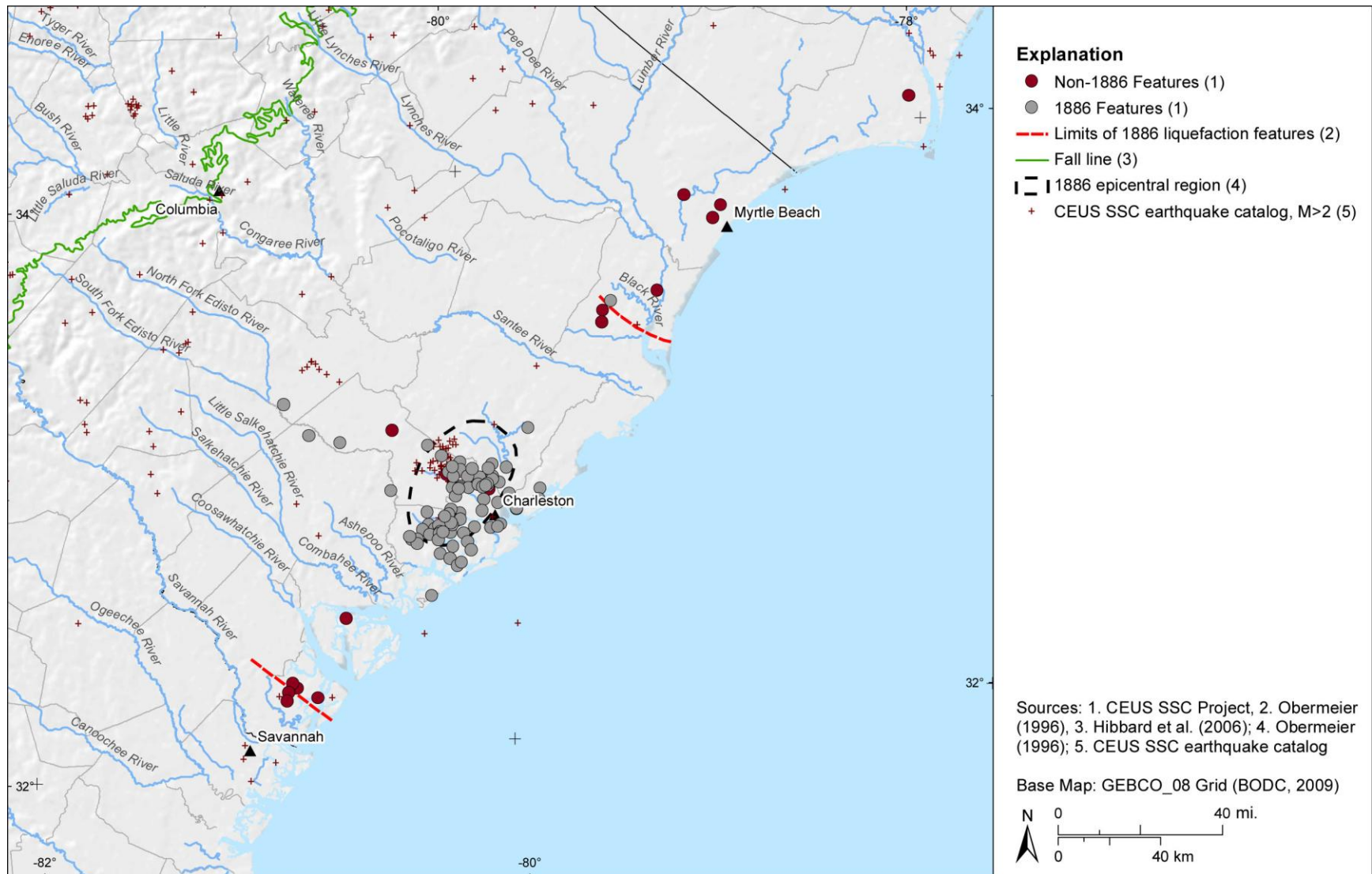


Figure E-36

GIS map of Charleston, South Carolina, region showing locations of historical and prehistoric liquefaction features. Map projection is USA Contiguous Albers Equal Area Conic, North America Datum 1983.

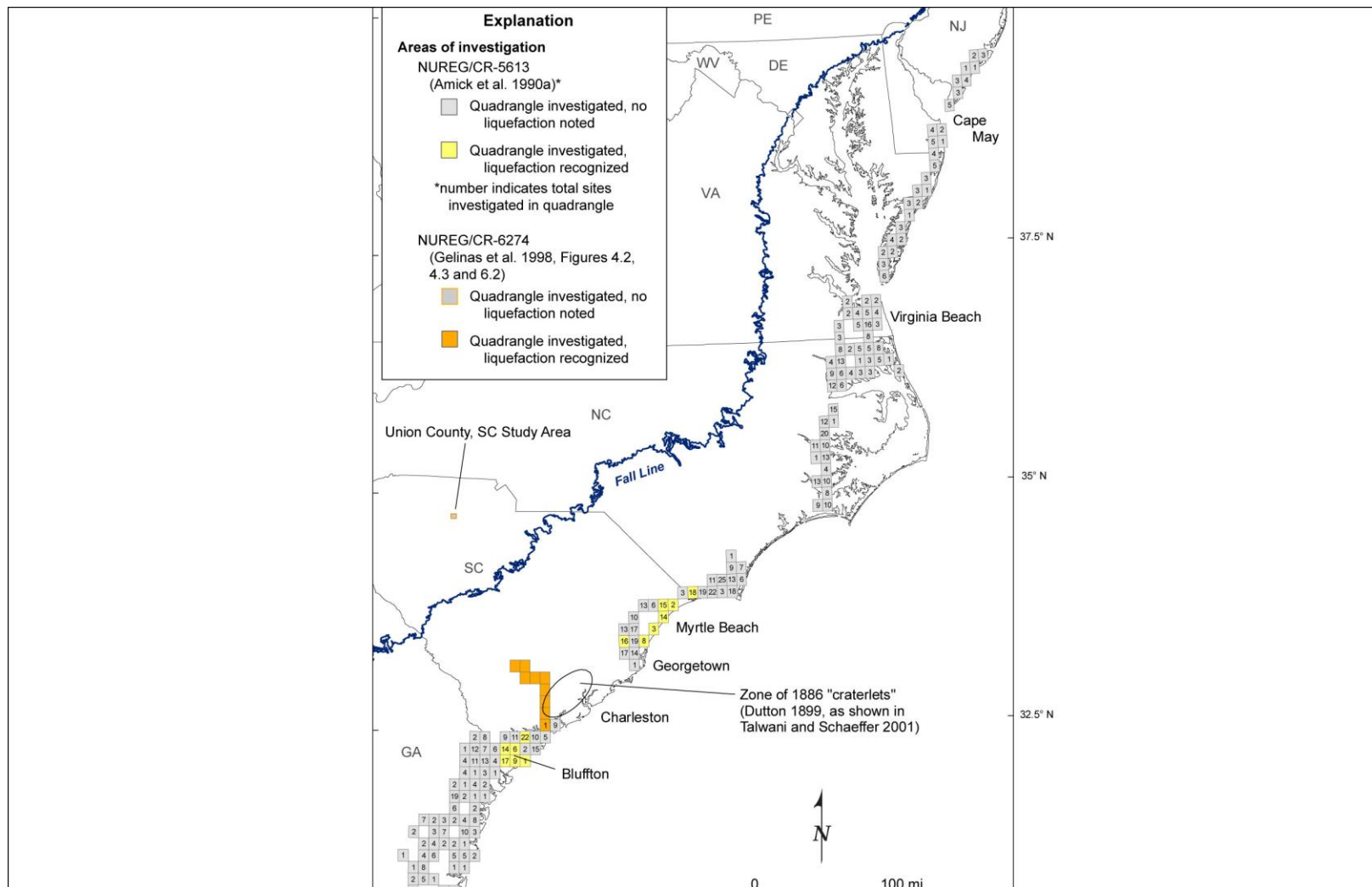


Figure E-37

Map of Atlantic coast region showing areas searched for paleoliquefaction features by Gelinas et al. (1998) and Amick, Gelanis, et al. (1990). Rectangles indicate 7.5-minute quadrangles in which sites were investigated for presence of paleoliquefaction features. The number of sites investigated is shown within that quadrangle, if known. Orange and yellow indicate quadrangles in which paleoliquefaction features were recognized.

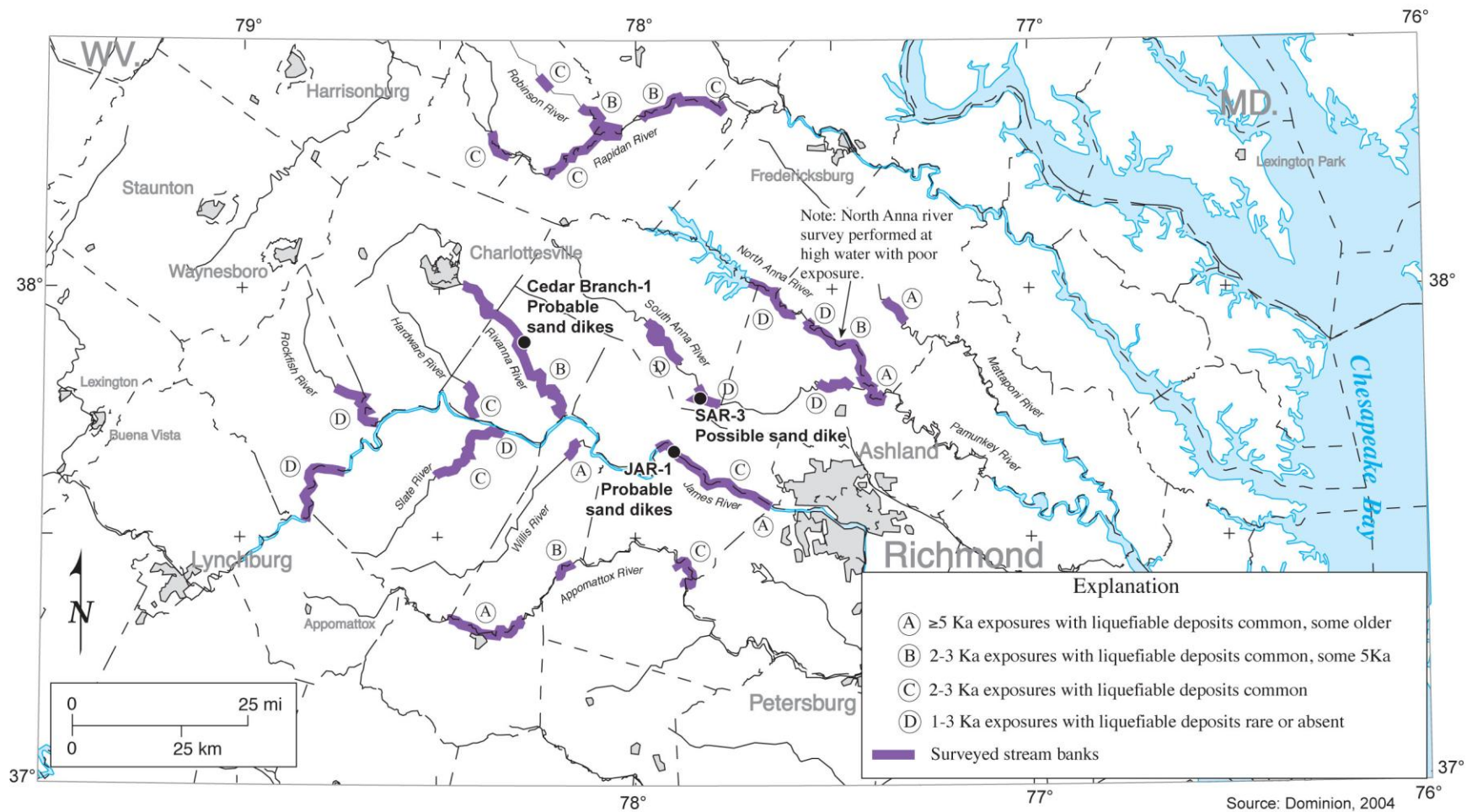


Figure E-38

Map of Central Virginia seismic zone region showing portions of rivers searched for earthquake-induced liquefaction features by Obermeier and McNulty (1998).

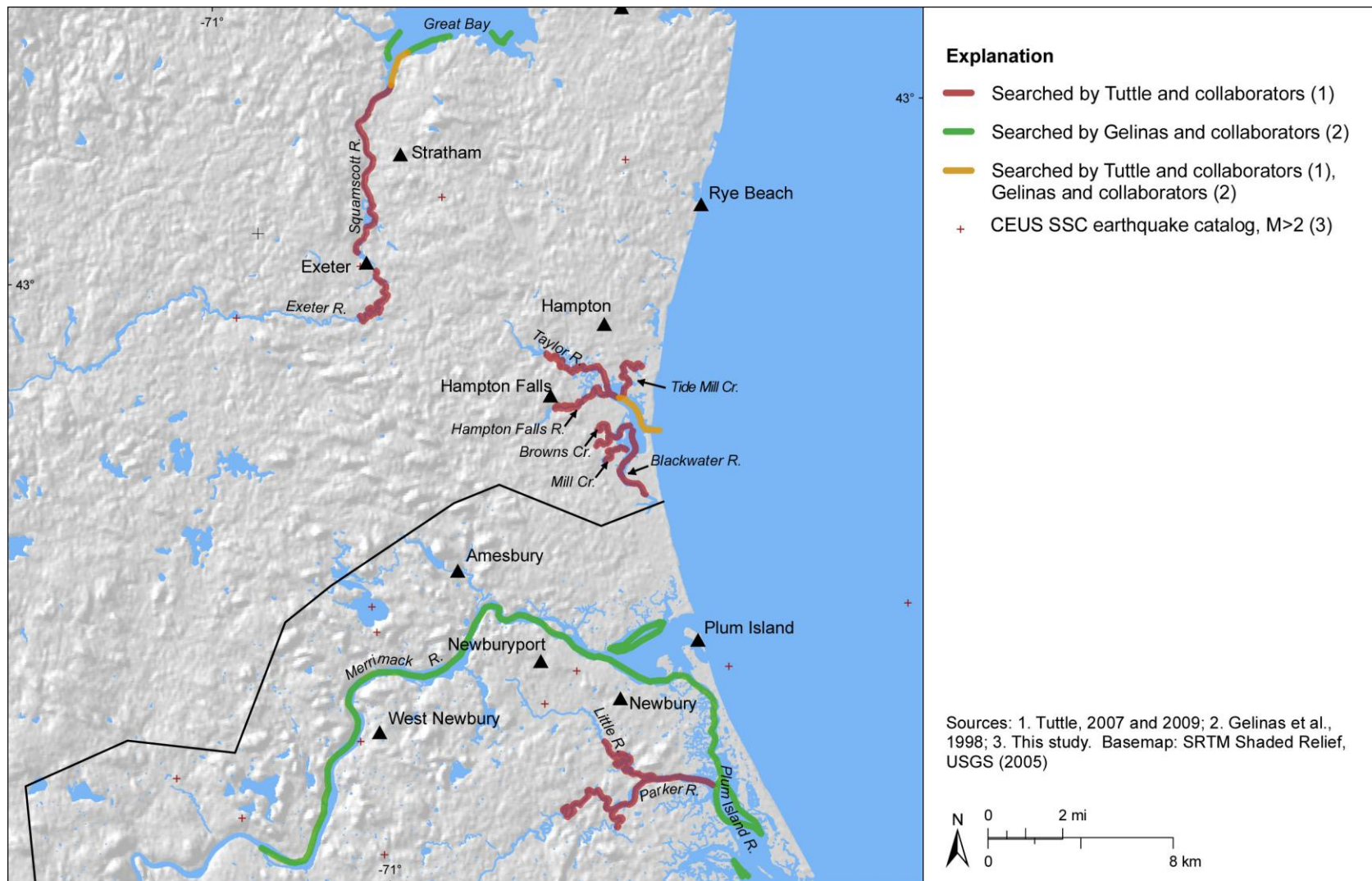


Figure E-39

GIS map of Newburyport, Massachusetts, and surrounding region showing seismicity and portions of rivers searched for earthquake-induced liquefaction features (Gelinas et al., 1998; Tuttle, 2007, 2009). Solid black line crossing map represents Massachusetts–New Hampshire border. Map projection is USA Contiguous Albers Equal Area Conic, North America Datum 1983.

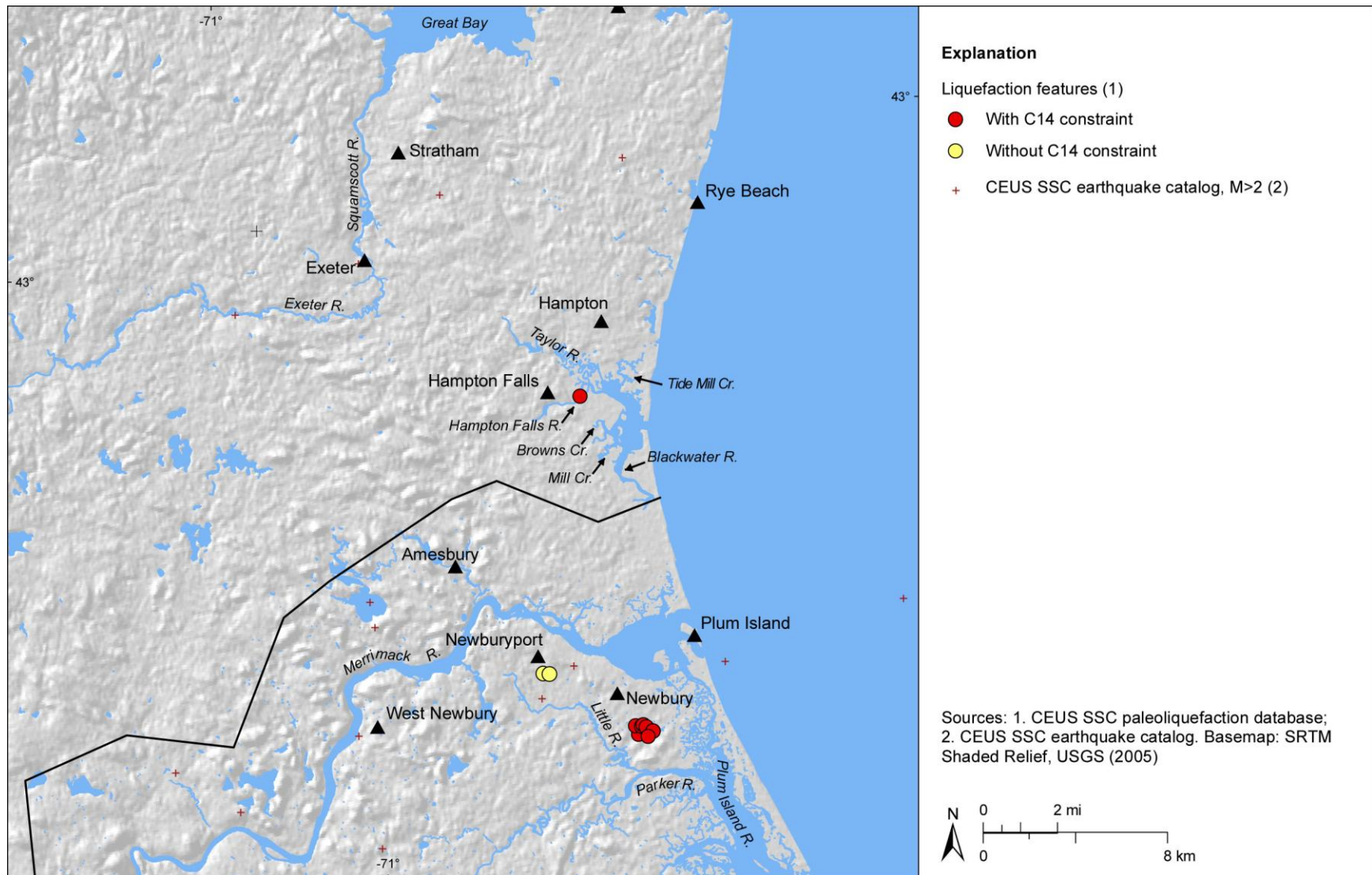


Figure E-40

GIS map of Newburyport, Massachusetts, and surrounding region showing locations of liquefaction features for which there are and are not radiocarbon dates. Map projection is USA Contiguous Albers Equal Area Conic, North America Datum 1983.

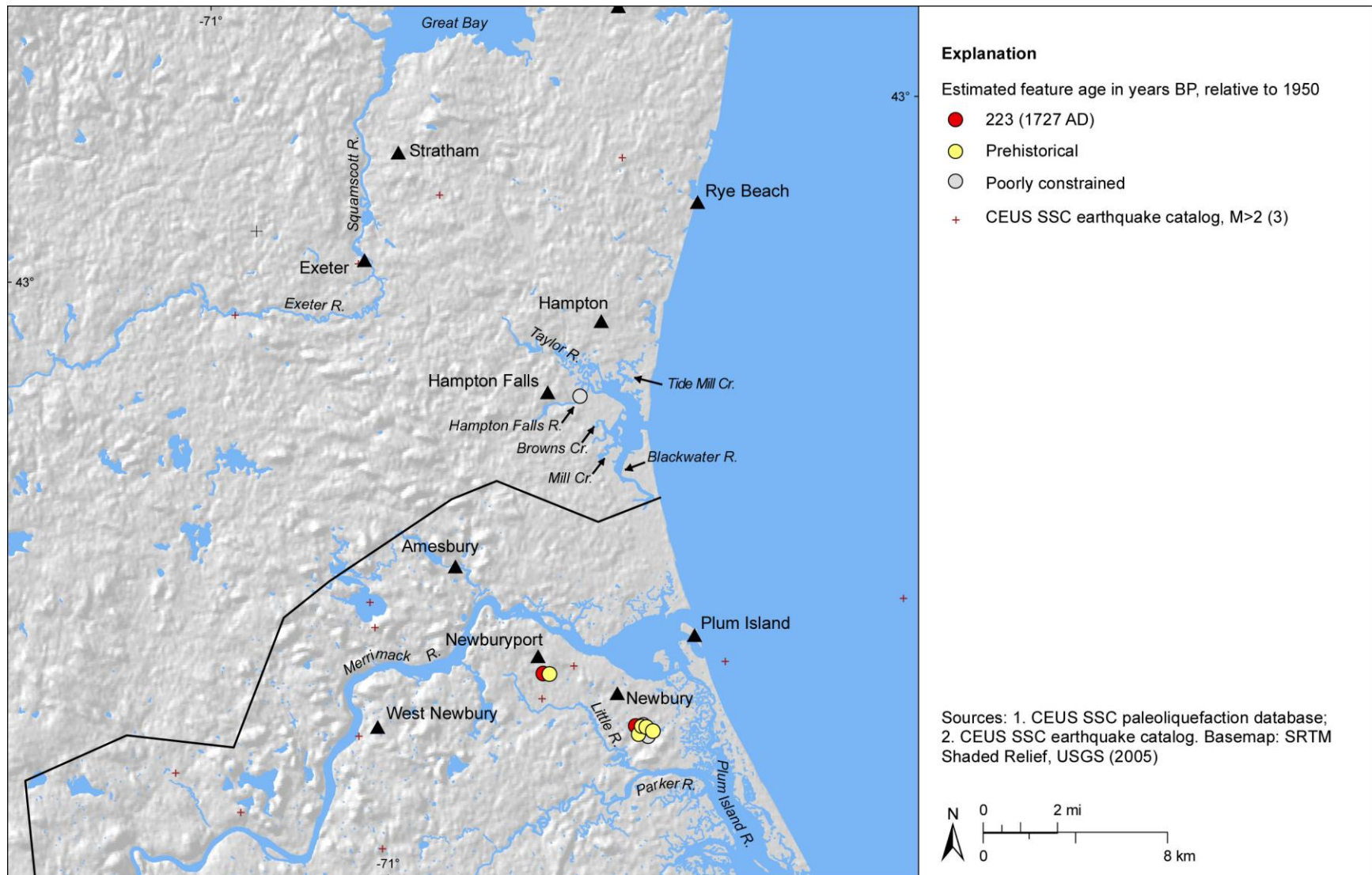


Figure E-41

GIS map of Newburyport, Massachusetts, and surrounding region showing locations of liquefaction features that are thought to be historical or prehistoric in age or whose ages are poorly constrained. Map projection is USA Contiguous Albers Equal Area Conic, North America Datum 1983.

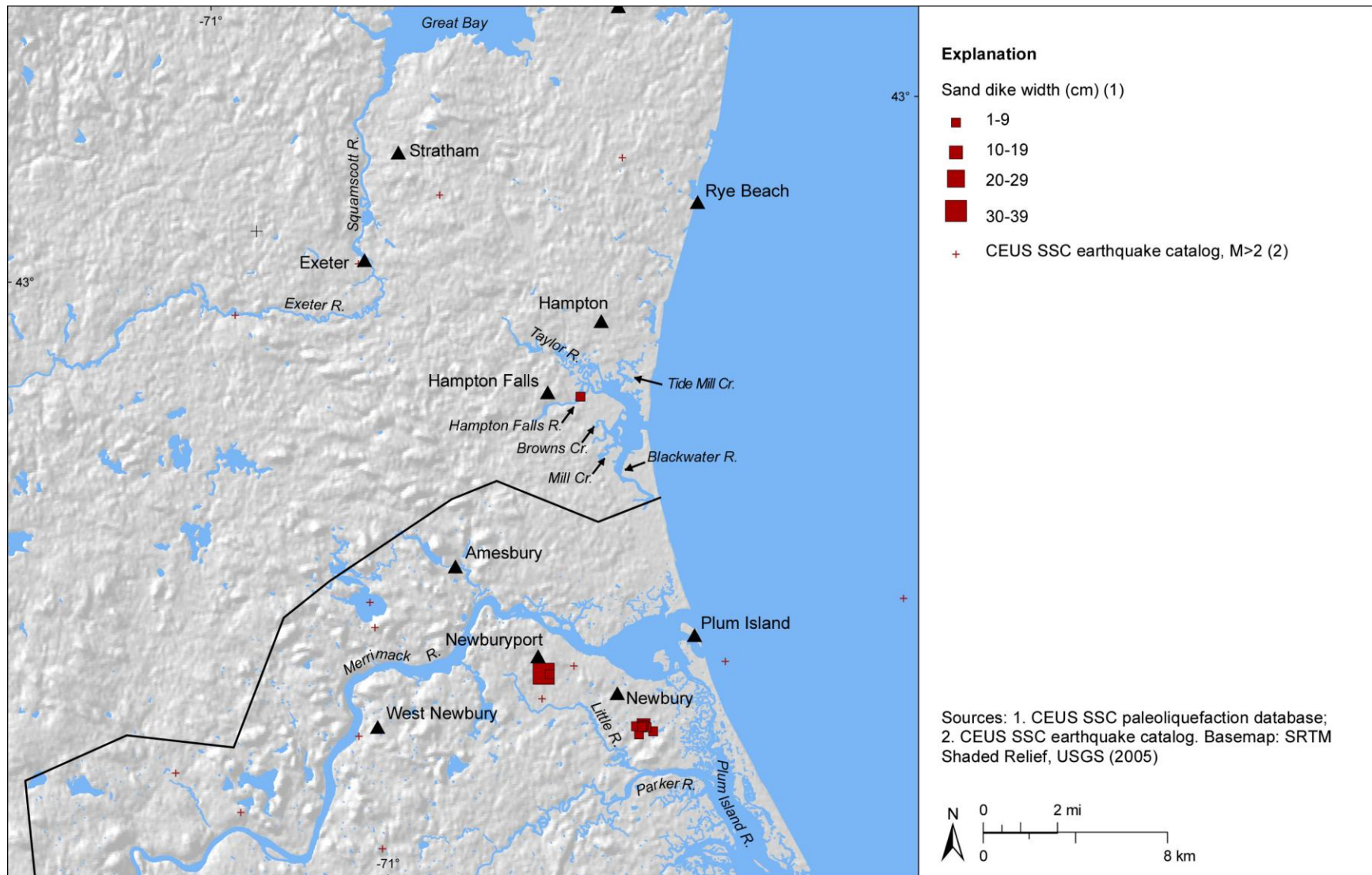


Figure E-42

GIS map of Newburyport, Massachusetts, and surrounding region showing measured widths of sand dikes. Map projection is USA Contiguous Albers Equal Area Conic, North America Datum 1983.

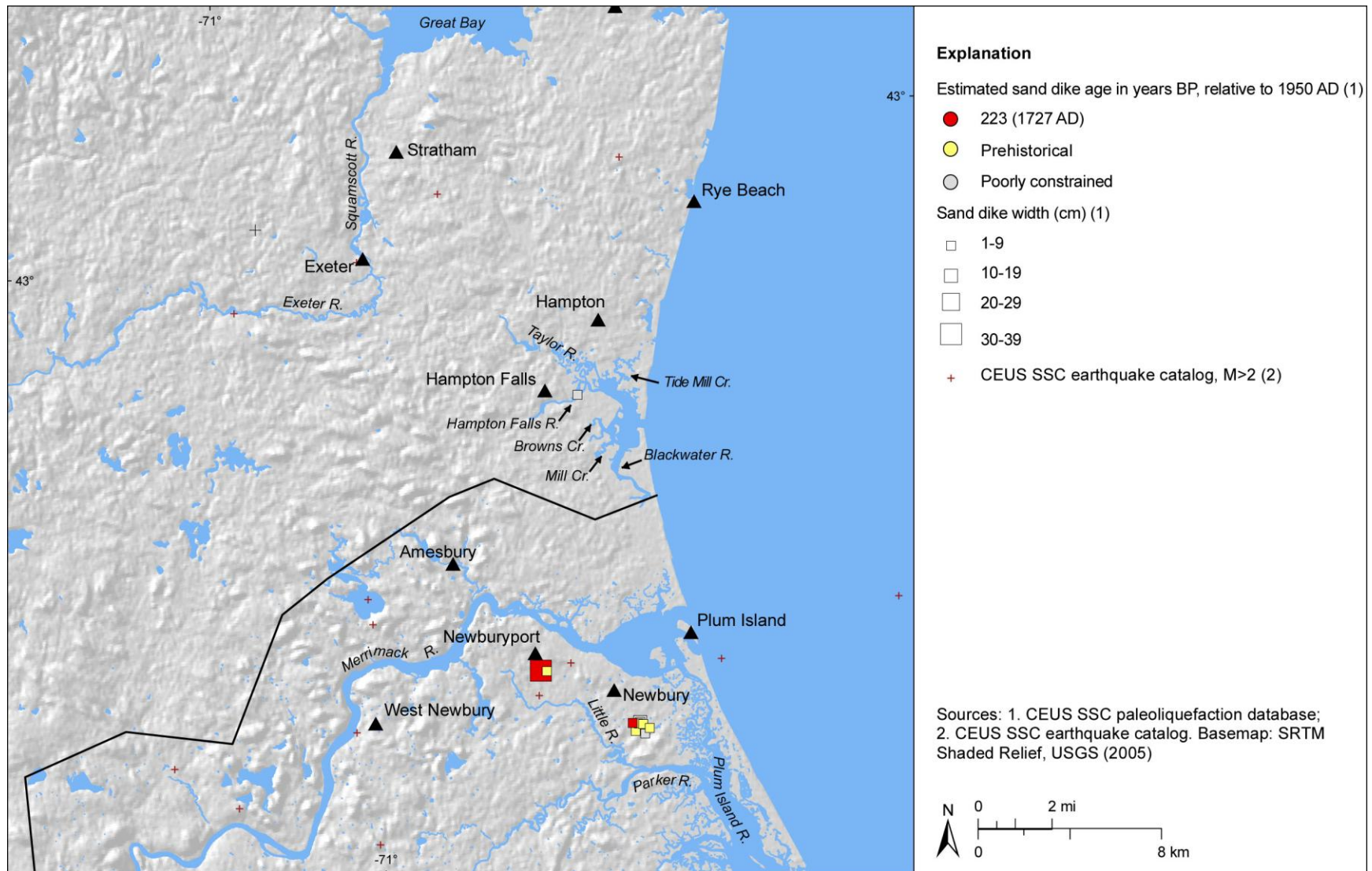


Figure E-43

GIS map of Newburyport, Massachusetts, and surrounding region showing preferred age estimates and measured widths of sand dikes. Map projection is USA Contiguous Albers Equal Area Conic, North America Datum 1983.

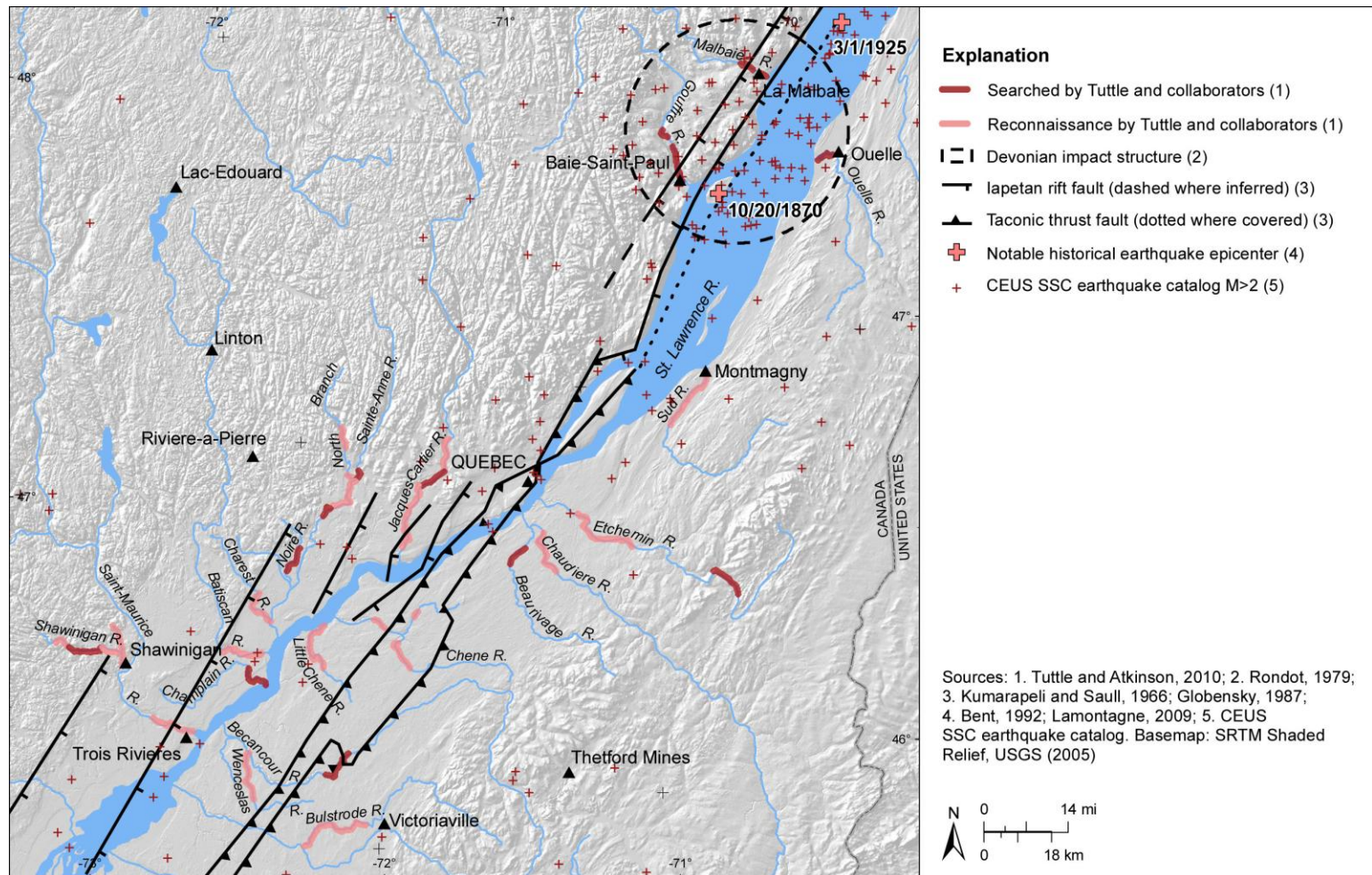


Figure E-44

Map of Charlevoix seismic zone and adjacent St. Lawrence Lowlands showing mapped faults and portions of rivers along which reconnaissance and searches for earthquake-induced liquefaction features were performed. Charlevoix seismic zone is defined by concentration of earthquakes and locations of historical earthquakes northeast of Quebec City. Devonian impact structure in vicinity of Charlevoix seismic zone is outlined by black dashed line. Taconic thrust faults are indicated by solid black lines with sawteeth on upper plate; lapetan rift faults are shown by solid black lines with hachure marks on downthrown side (modified from Tuttle and Atkinson, 2010).

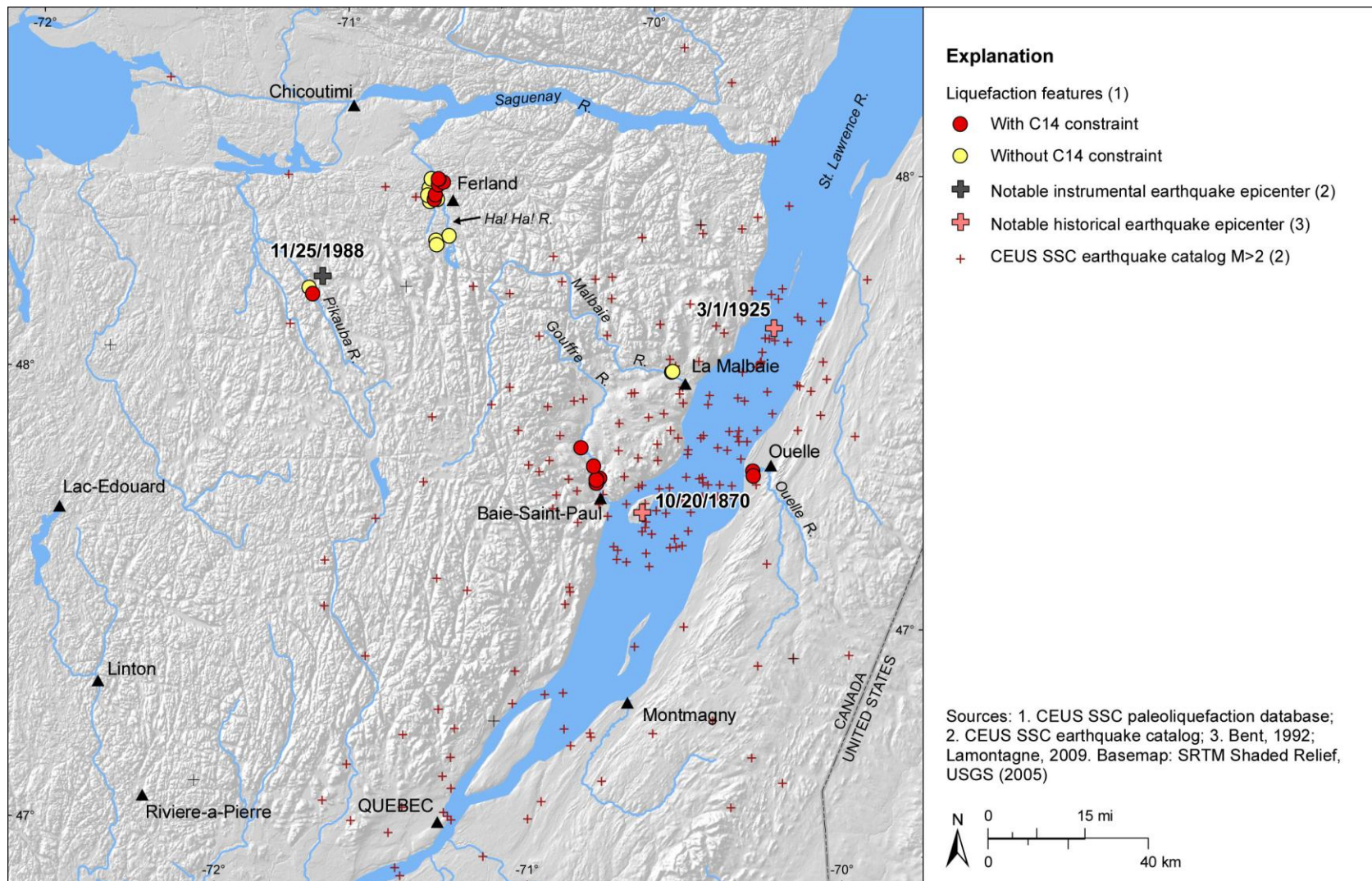


Figure E-45

GIS map of Charlevoix seismic zone and surrounding region showing locations of liquefaction features, including several soft-sediment deformation structures, for which there are and are not radiocarbon data. Note the location of the 1988 **M** 5.9 Saguenay earthquake northwest of the Charlevoix seismic zone. Map projection is USA Contiguous Albers Equal Area Conic, North America Datum 1983.

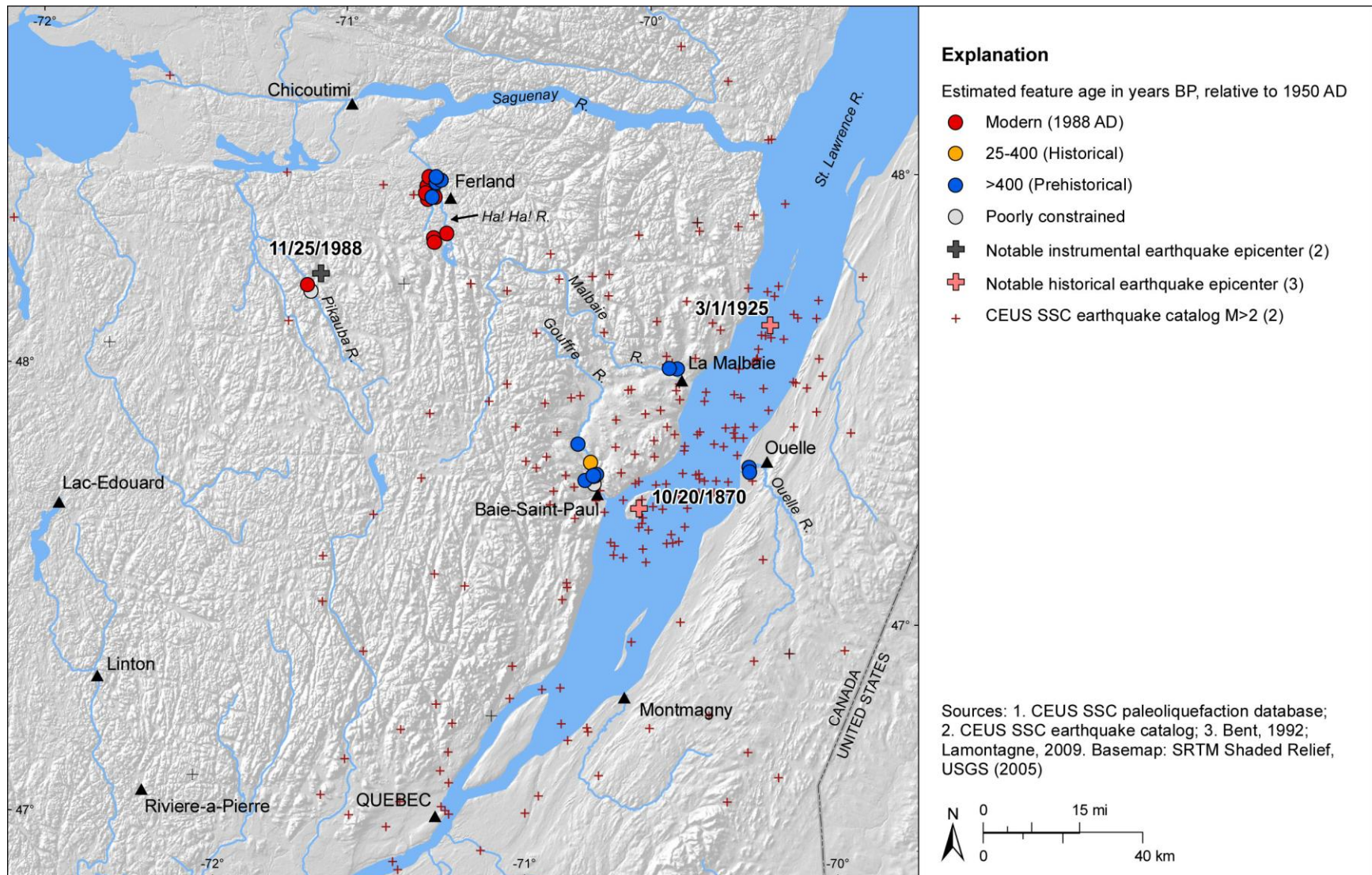


Figure E-46

GIS map of Charlevoix seismic zone and surrounding region showing locations of liquefaction features that are modern, historical, or prehistoric in age, or whose ages are poorly constrained. Map projection is USA Contiguous Albers Equal Area Conic, North America Datum 1983.

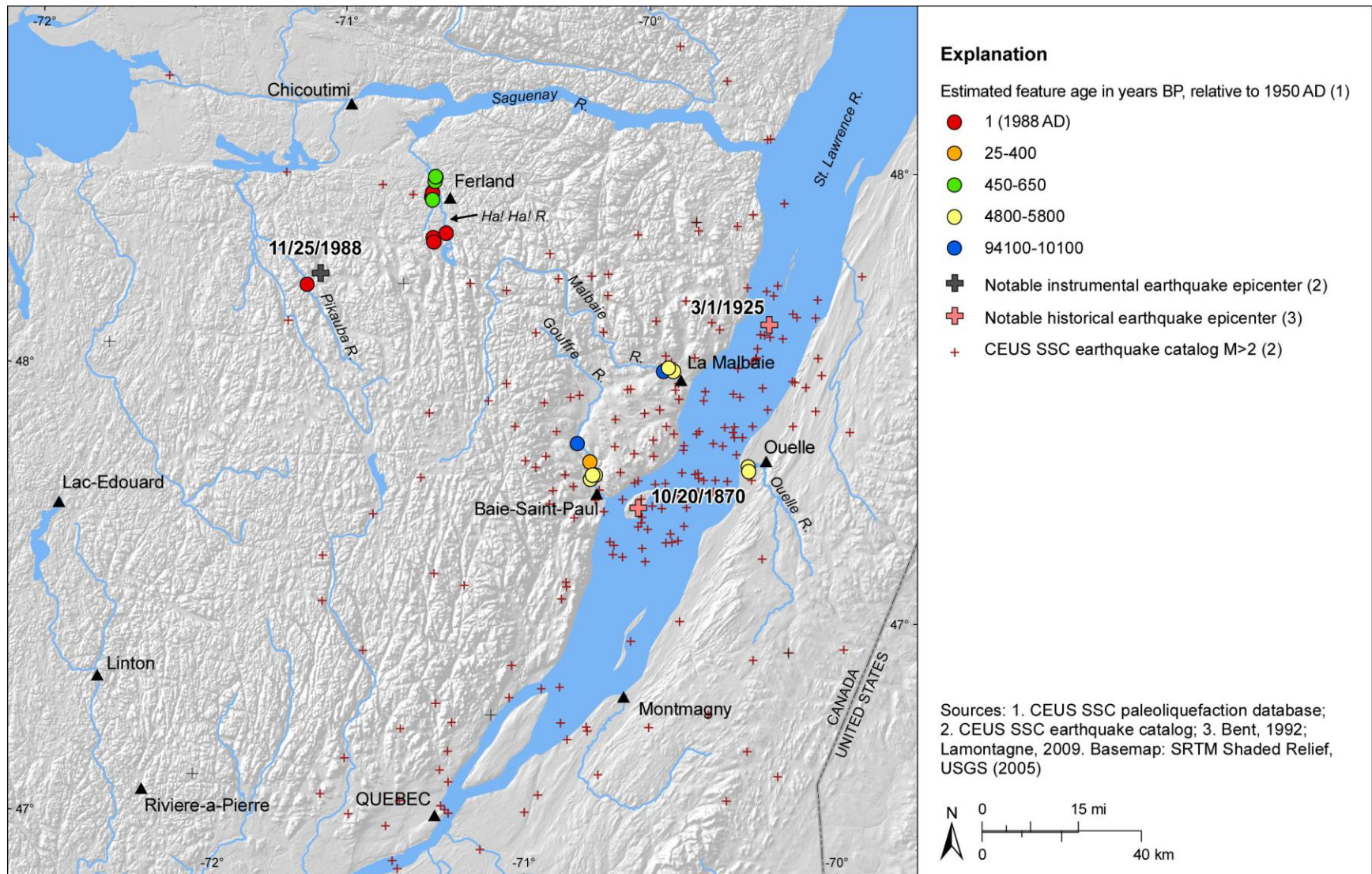


Figure E-47

GIS map of Charlevoix seismic zone and surrounding region showing preferred age estimates of liquefaction features; features whose ages are poorly constrained are excluded. Map projection is USA Contiguous Albers Equal Area Conic, North America Datum 1983.

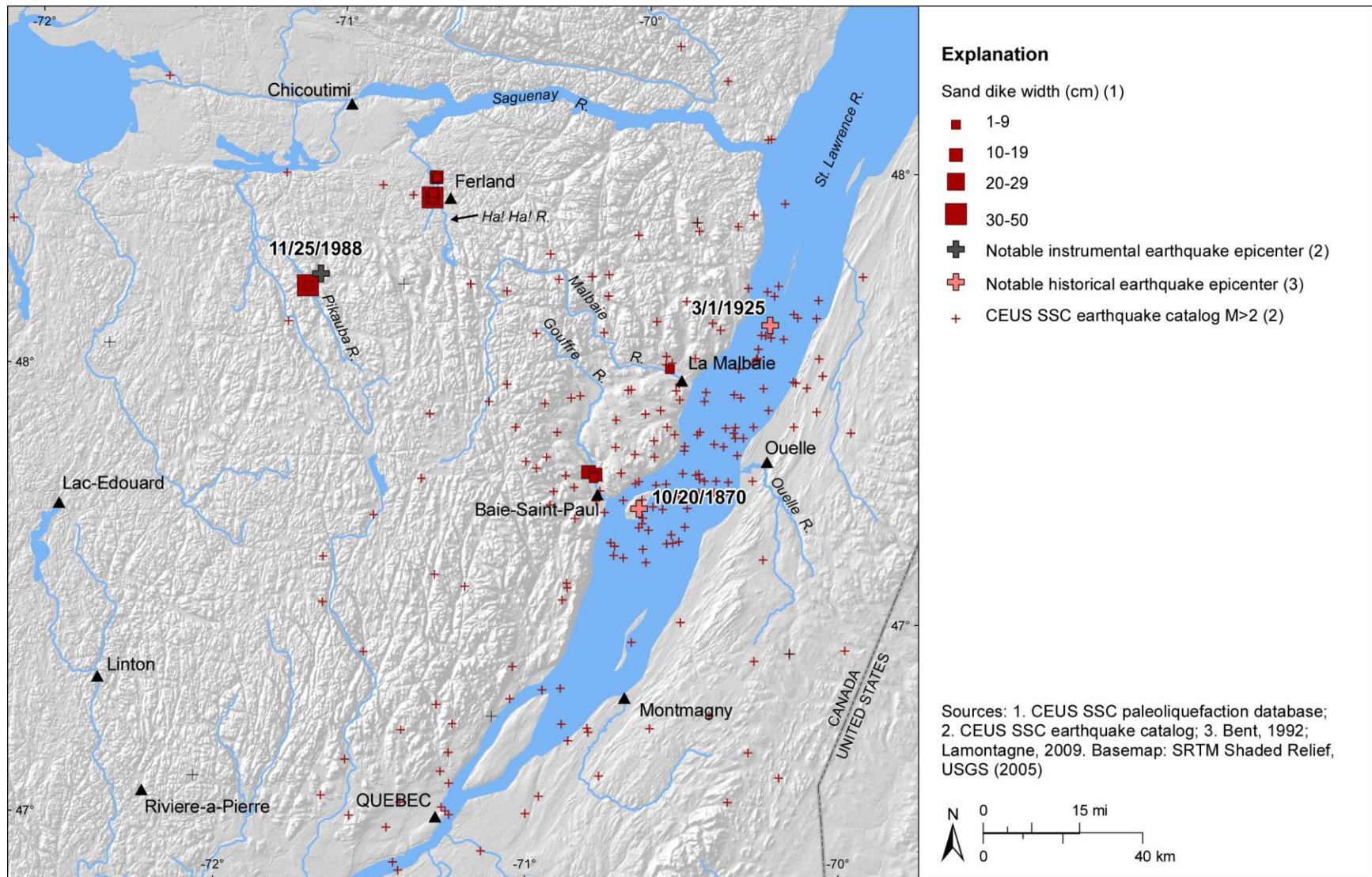


Figure E-48

GIS map of Charlevoix seismic zone and surrounding region showing measured widths of sand dikes. Map projection is USA Contiguous Albers Equal Area Conic, North America Datum 1983.

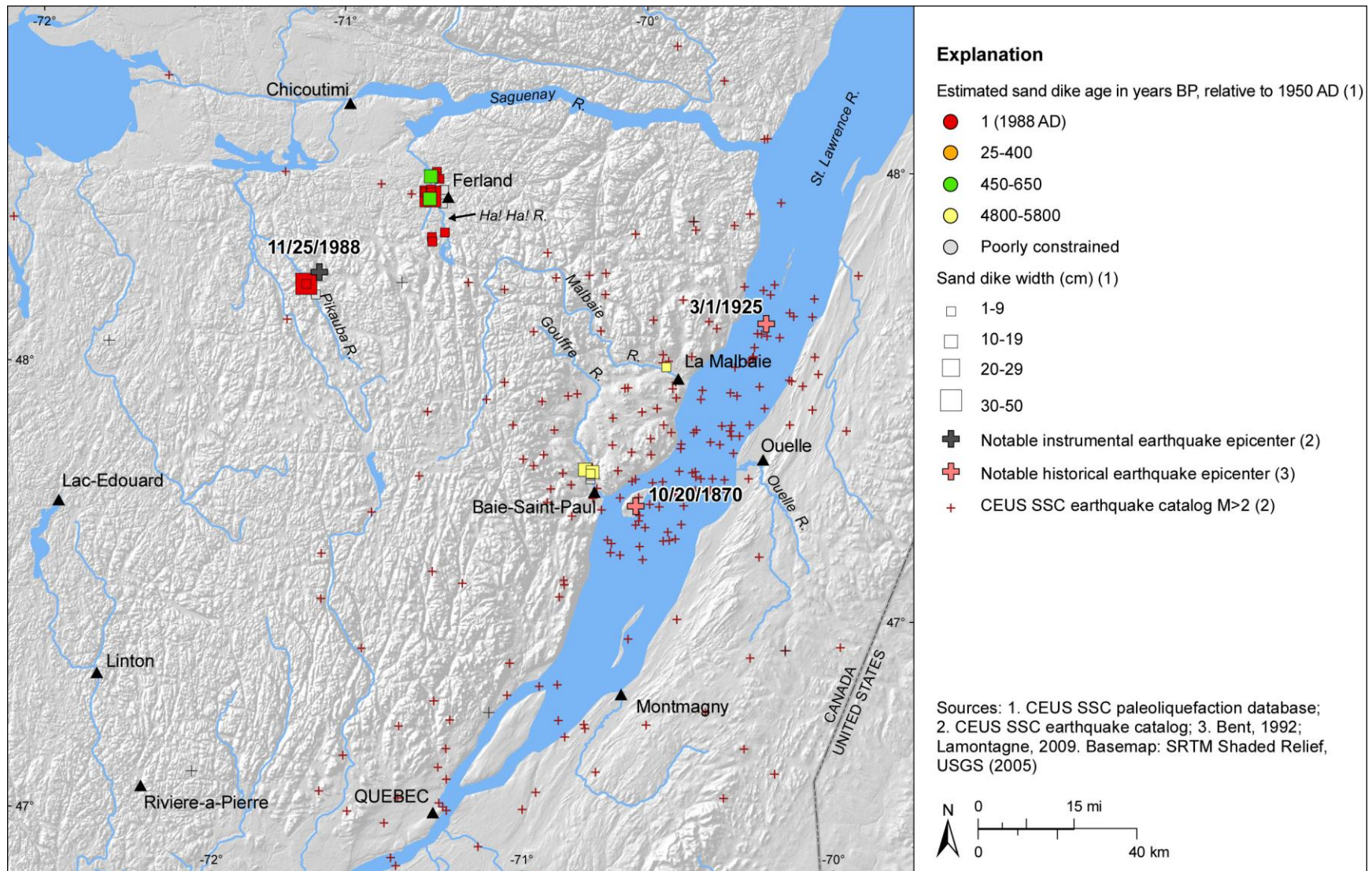


Figure E-49

GIS map of Charlevoix seismic zone and surrounding region showing preferred age estimates and measured widths of sand dikes. Map projection is USA Contiguous Albers Equal Area Conic, North America Datum 1983.

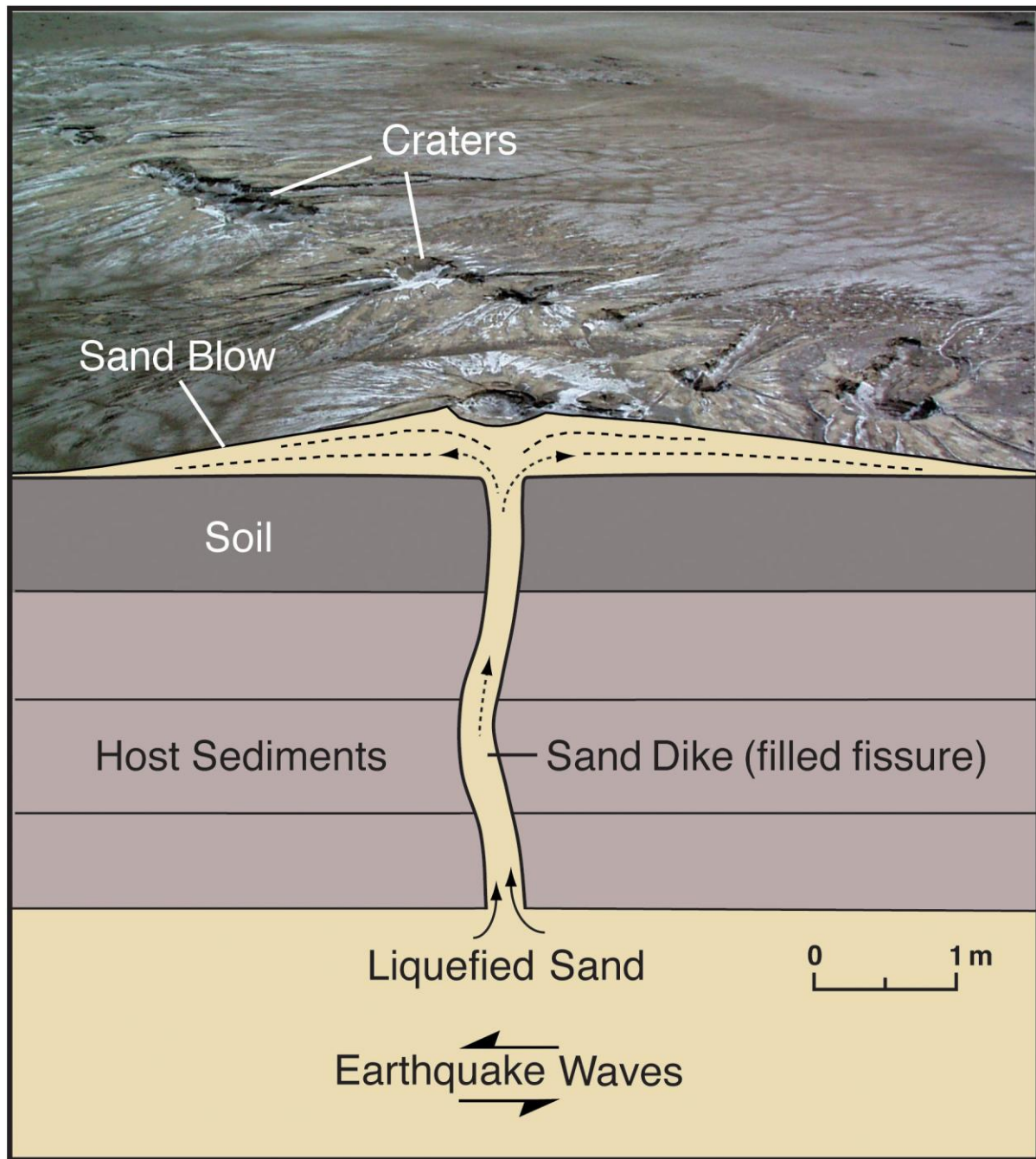


Figure E-50

Photograph of moderate-sized sand blow (12 m long, 7 m wide, and 14 cm thick) that formed about 40 km from epicenter of 2001 **M** 7.7 Bhuj, India, earthquake (from Tuttle, Hengesh, et al., 2002), combined with schematic vertical section illustrating structural and stratigraphic relations of sand blow, sand dike, and source layer (modified from Sims and Garvin, 1995).

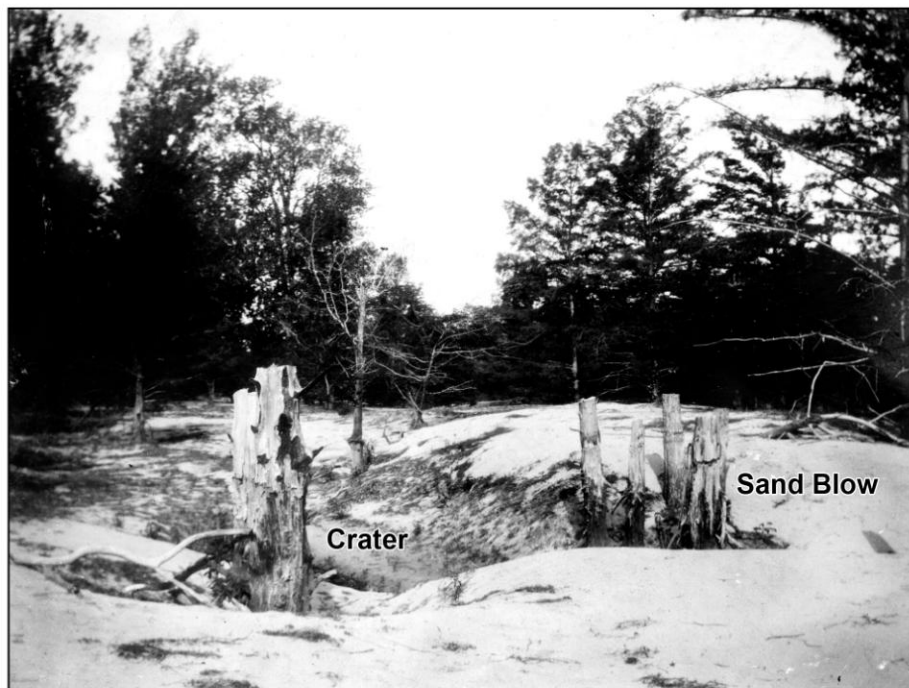


Figure E-51

Tree trunks buried and killed by sand blows, vented during 1811-1812 New Madrid earthquakes (from Fuller, 1912).



Figure E-52

Large sand-blow crater that formed during 2001 **M** 7.7 Bhuj, India, earthquake. Backpack for scale. Photograph: M. Tuttle (2001).



Figure E-53

Sand-blow crater that formed during 1886 Charleston, South Carolina, earthquake. Photograph: J.K. Hillers (from USGS Photograph Library).

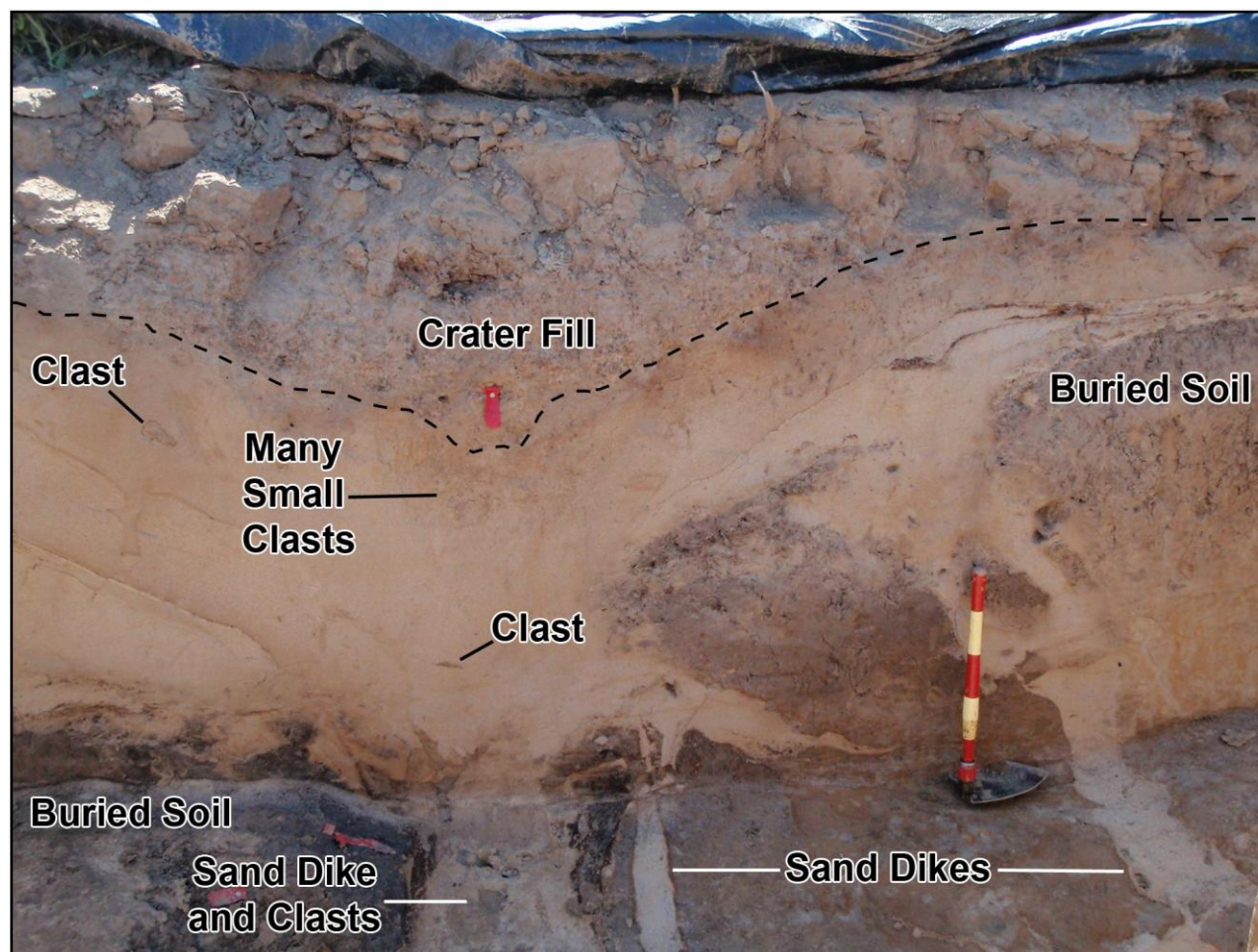


Figure E-54

Photograph of sand blow and related sand dikes exposed in trench wall and floor in New Madrid seismic zone. Buried soil horizon is displaced downward ~1 m across two dikes. Clasts of soil horizon occur within dikes and overlying sand blow. Degree of soil development above and within sand blow suggests that it is at least several hundred years old and formed prior to 1811-1812 New Madrid earthquakes. Organic sample (location marked by red flag) from crater fill will provide close minimum age constraint for formation of sand blow. For scale, each colored intervals on shovel handle represents 10 cm. Photograph: M. Tuttle.

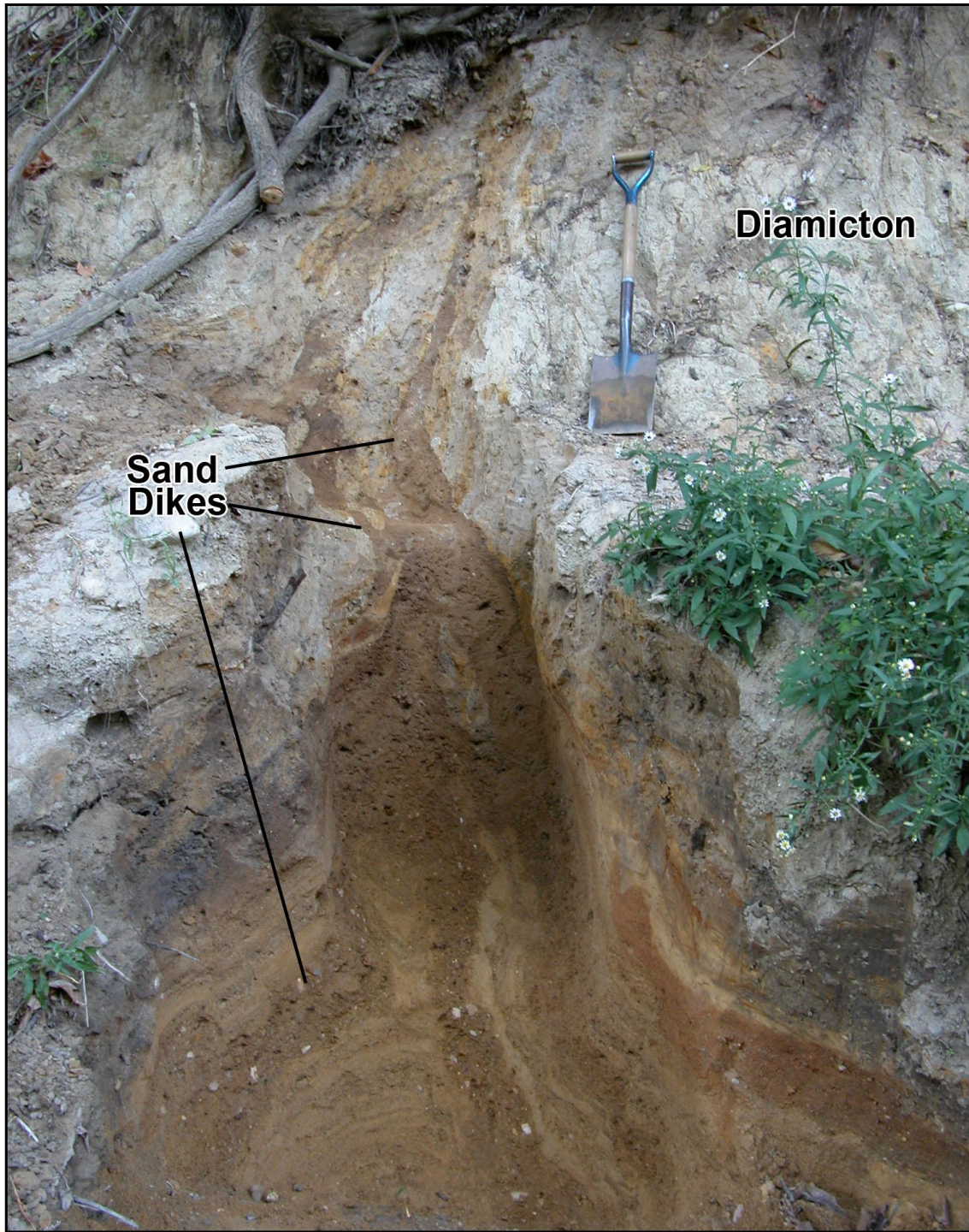


Figure E-55

Sand dikes, ranging up to 35 cm wide, originate in pebbly sand layer and intrude overlying diamicton, These features were exposed in cutbank along Cahokia Creek about 25 km northeast of downtown St. Louis, Missouri (from Tuttle, 2000).

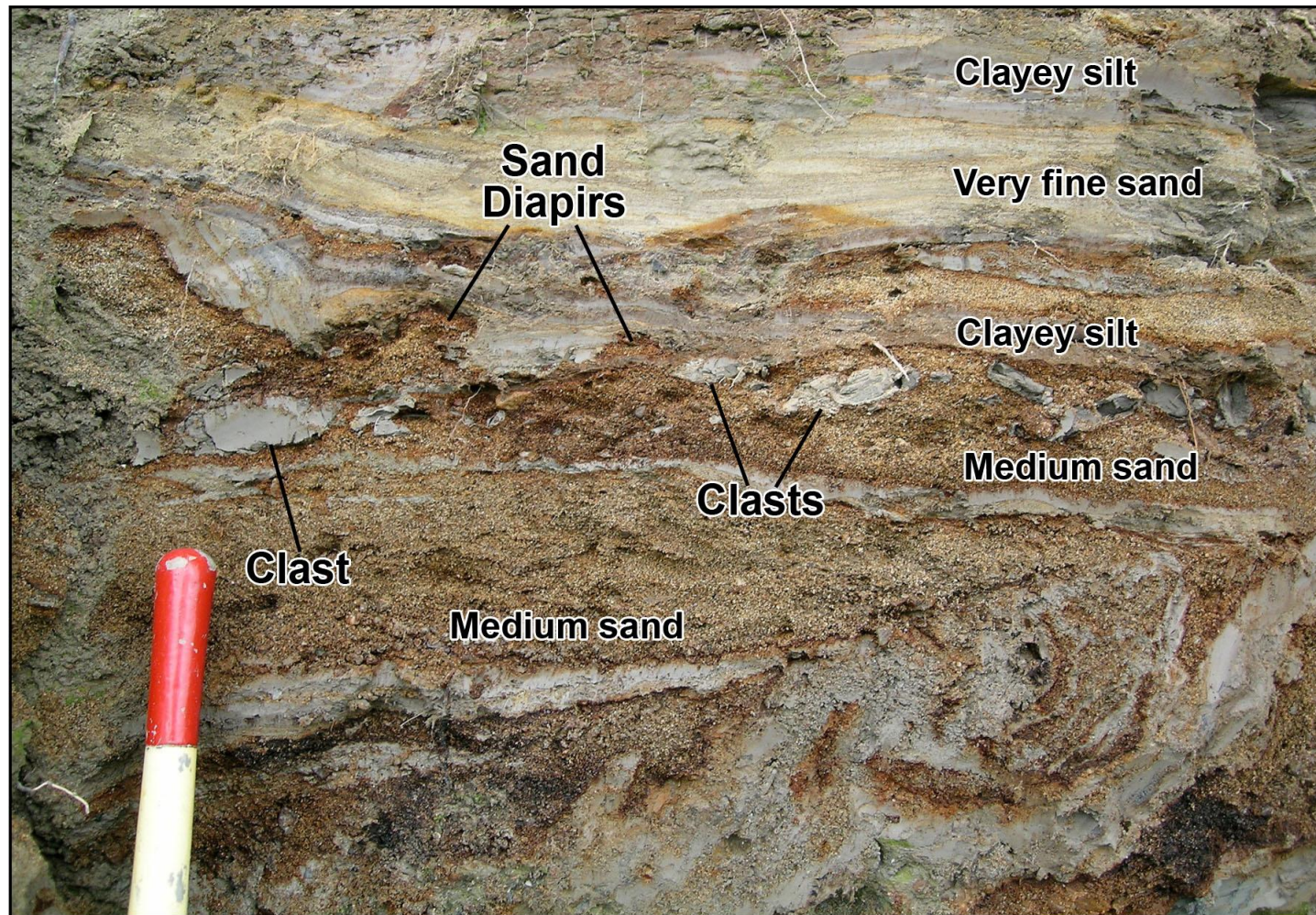
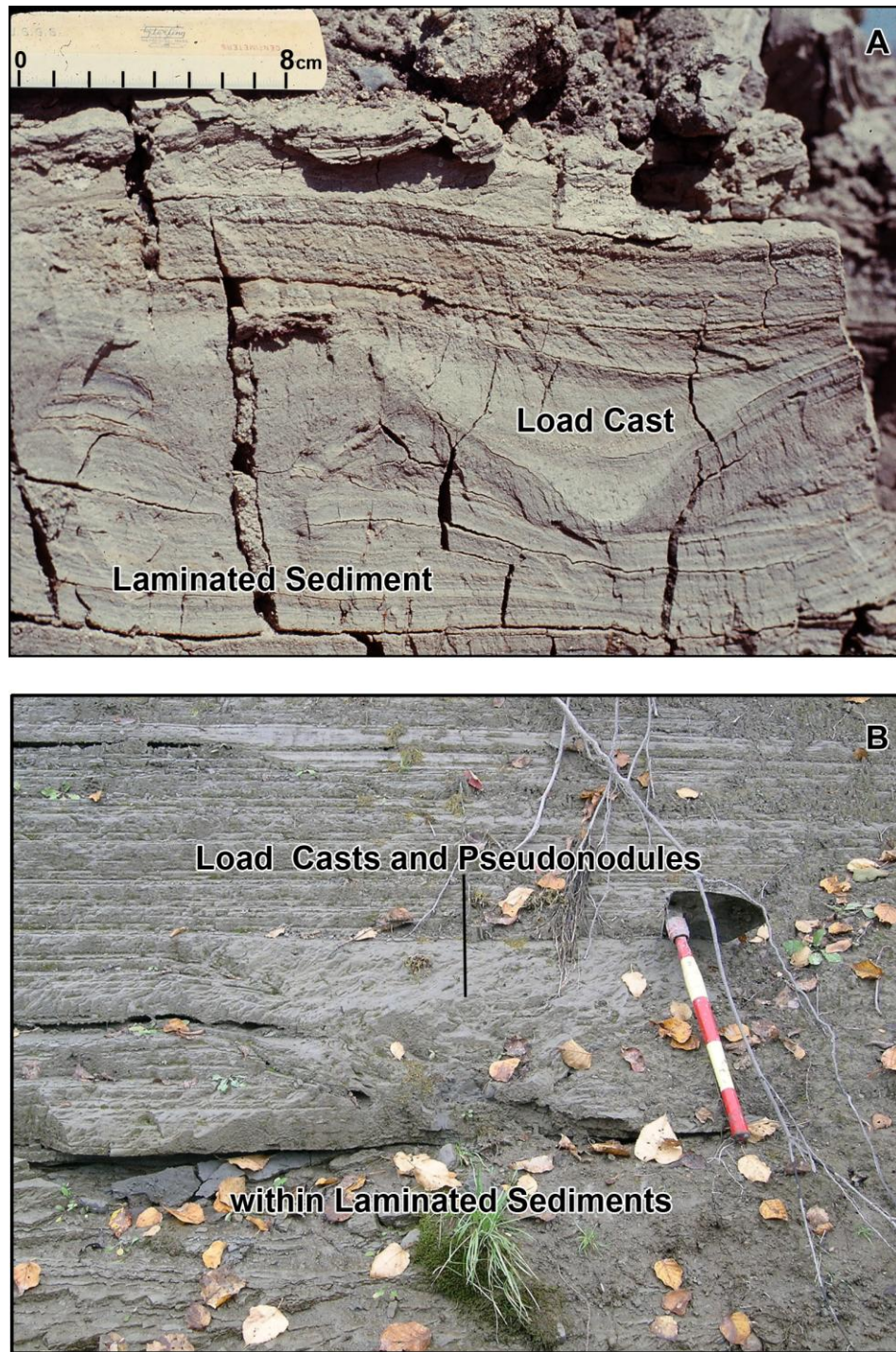


Figure E-56

Photograph of small diapirs of medium sand intruding base of overlying deposit of interbedded clayey silt and very fine sand, and clasts of clayey silt in underlying medium sand, observed along Ouelle River in Charlevoix seismic zone. Sand diapirs and clasts probably formed during basal erosion and foundering of clayey silt due to liquefaction of the underlying sandy deposit. Red portion of shovel handle represents 10 cm (modified from Tuttle and Atkinson, 2010).



Figures E-57

(A) Load cast formed in laminated sediments of Van Norman Lake during 1952 Kern County, California, earthquake. Photograph: J. Sims (from Sims, 1975). (B) Load cast, pseudonodules, and related folds formed in laminated sediment exposed along Malbaie River in Charlevoix seismic zone. Sand dikes crosscutting these same laminated sediments occur at a nearby site. For scale, each painted interval of the shovel handle represents 10 cm (modified from Tuttle and Atkinson, 2010).

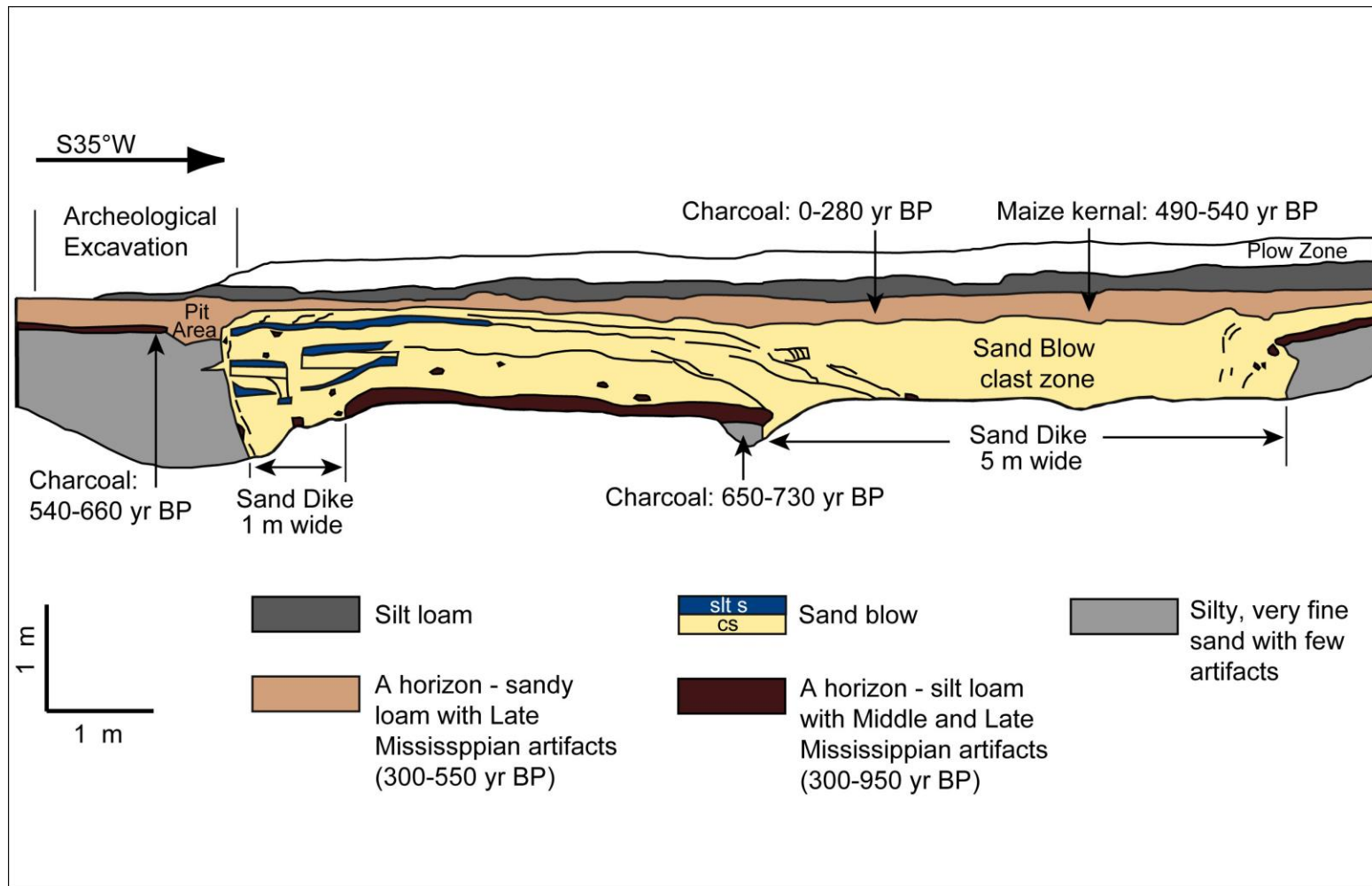
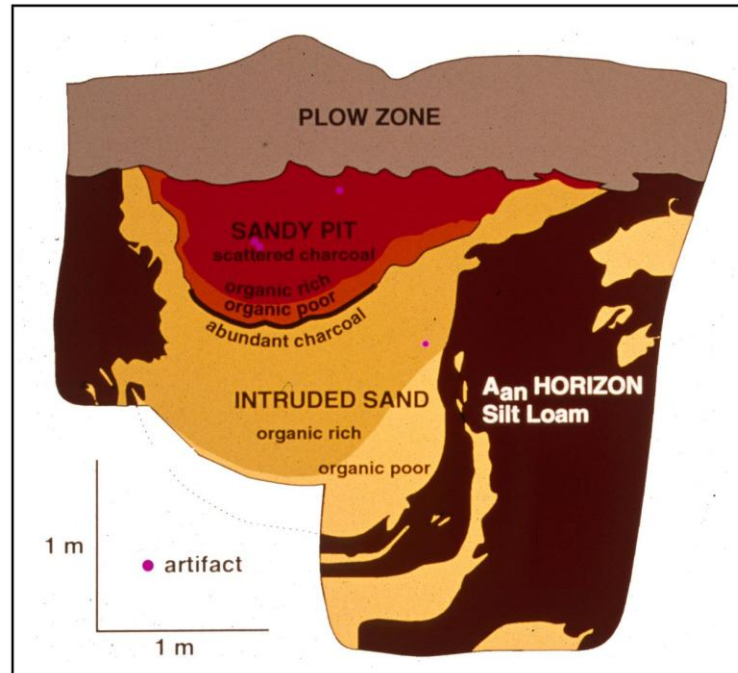


Figure E-58

Log of sand blow and uppermost portions of related sand dikes exposed in trench wall at Dodd site in New Madrid seismic zone. Sand dikes also were observed in opposite wall and trench floor. Sand blow buries pre-event A horizon, and a subsequent A horizon has developed in top of sand blow. Radiocarbon dating of samples collected above and below sand blow brackets its age between 490 and 660 yr BP. Artifact assemblage indicates that sand blow formed during late Mississippian (300–550 yr BP or AD 1400–1670) (modified from Tuttle, Collier, et al., 1999).

A**B****Figures E-59**

(A) Photograph of earthquake-induced liquefaction features found in association with cultural horizon and pit exposed in trench wall near Blytheville, Arkansas, in New Madrid seismic zone. Photograph: M. Tuttle. (B) Trench log of features shown in (A). Sand dike formed in thick Native American occupation horizon containing artifacts of early Mississippian cultural period (950–1,150 yr BP). Cultural pit dug into top of sand dike contains artifacts and charcoal used to constrain minimum age of liquefaction features (modified from Tuttle and Schweig, 1995).

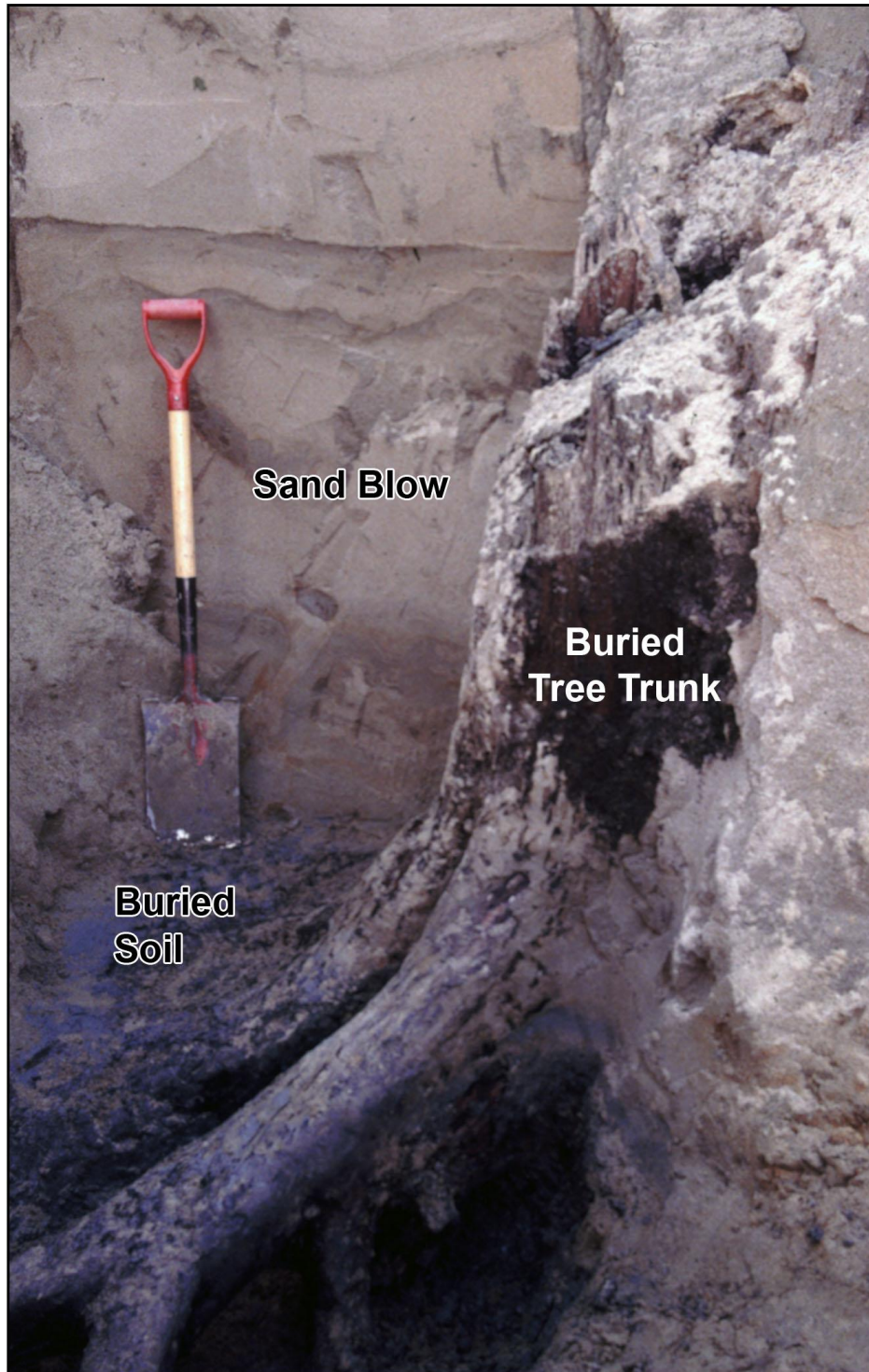


Figure E-60

In situ tree trunks such as this one buried and killed by sand blow in New Madrid seismic zone offer opportunity to date paleoearthquakes to the year and season of occurrence. Photograph: M. Tuttle.

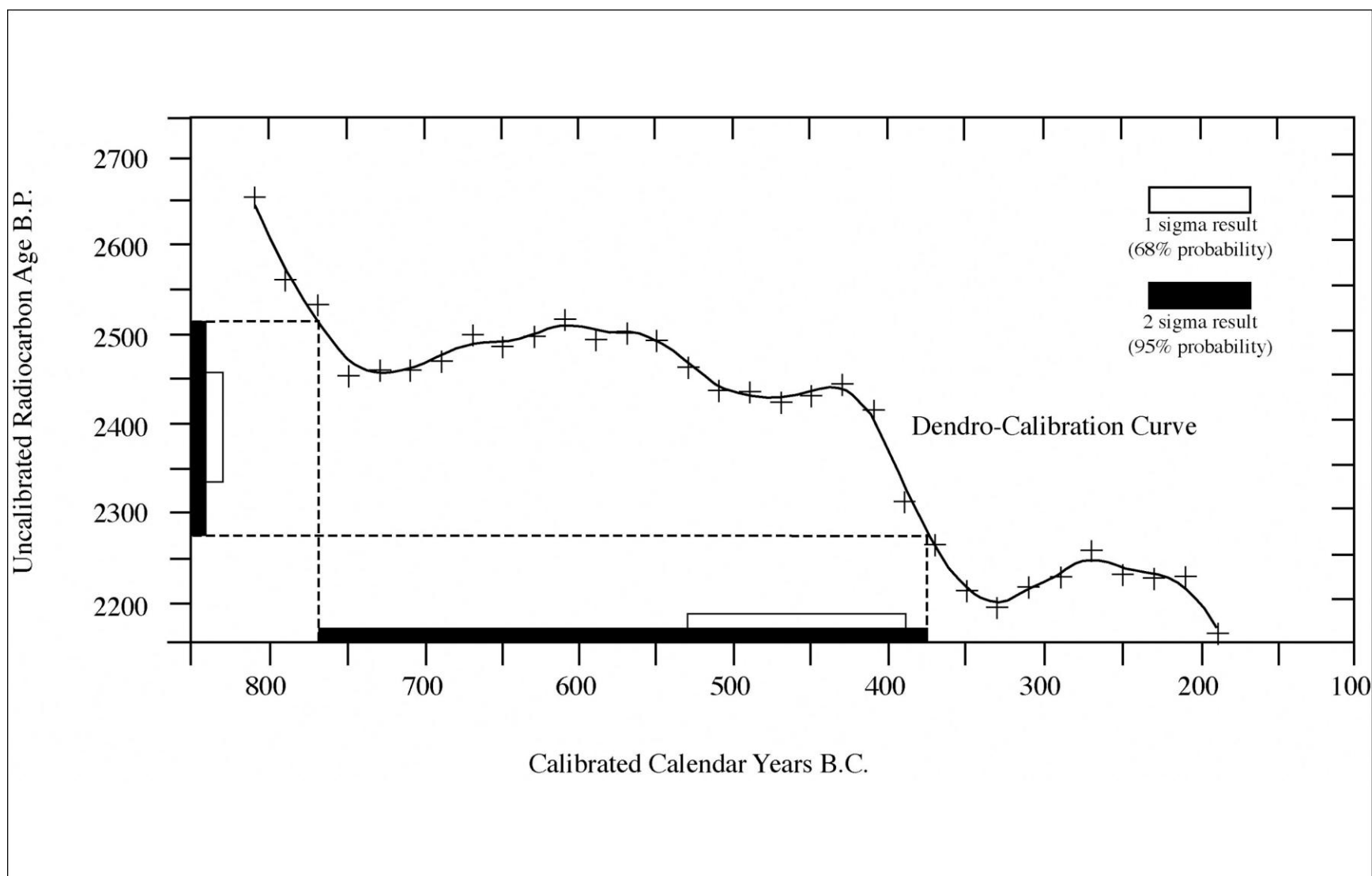


Figure E-61

Portion of dendrocalibration curve illustrating conversion of radiocarbon age to calibrated date in calendar years. In example, 2-sigma radiocarbon age of 2,280–2,520 BP is converted to calibrated date of 770–380 BC (from Tuttle, 1999).

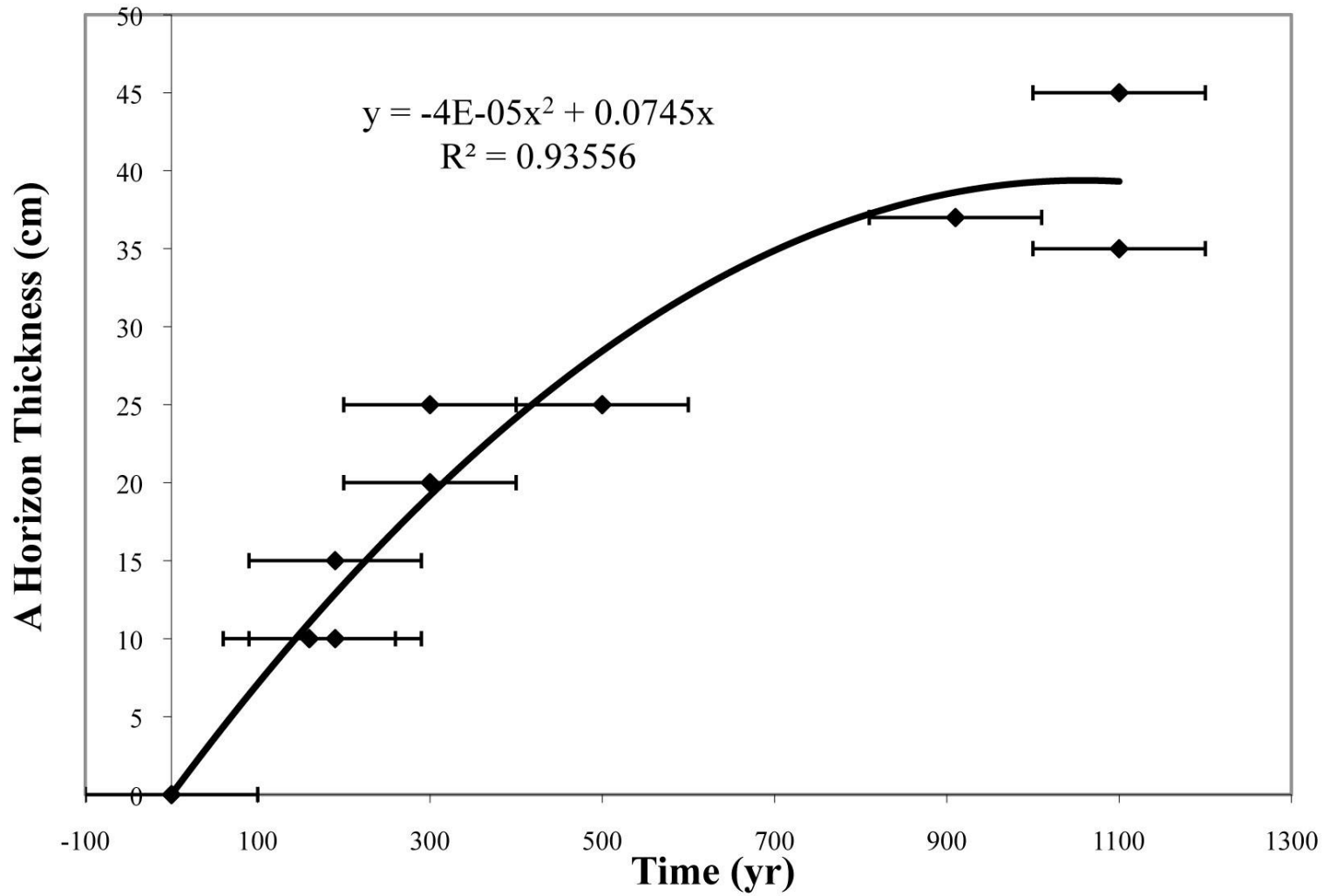


Figure E-62

Empirical relation developed between A horizon thickness of sand blows and years of soil development in New Madrid region. Horizontal bars reflect uncertainties in age estimates of liquefaction features; diamonds mark midpoints of possible age ranges (from Tuttle et al., 2000).

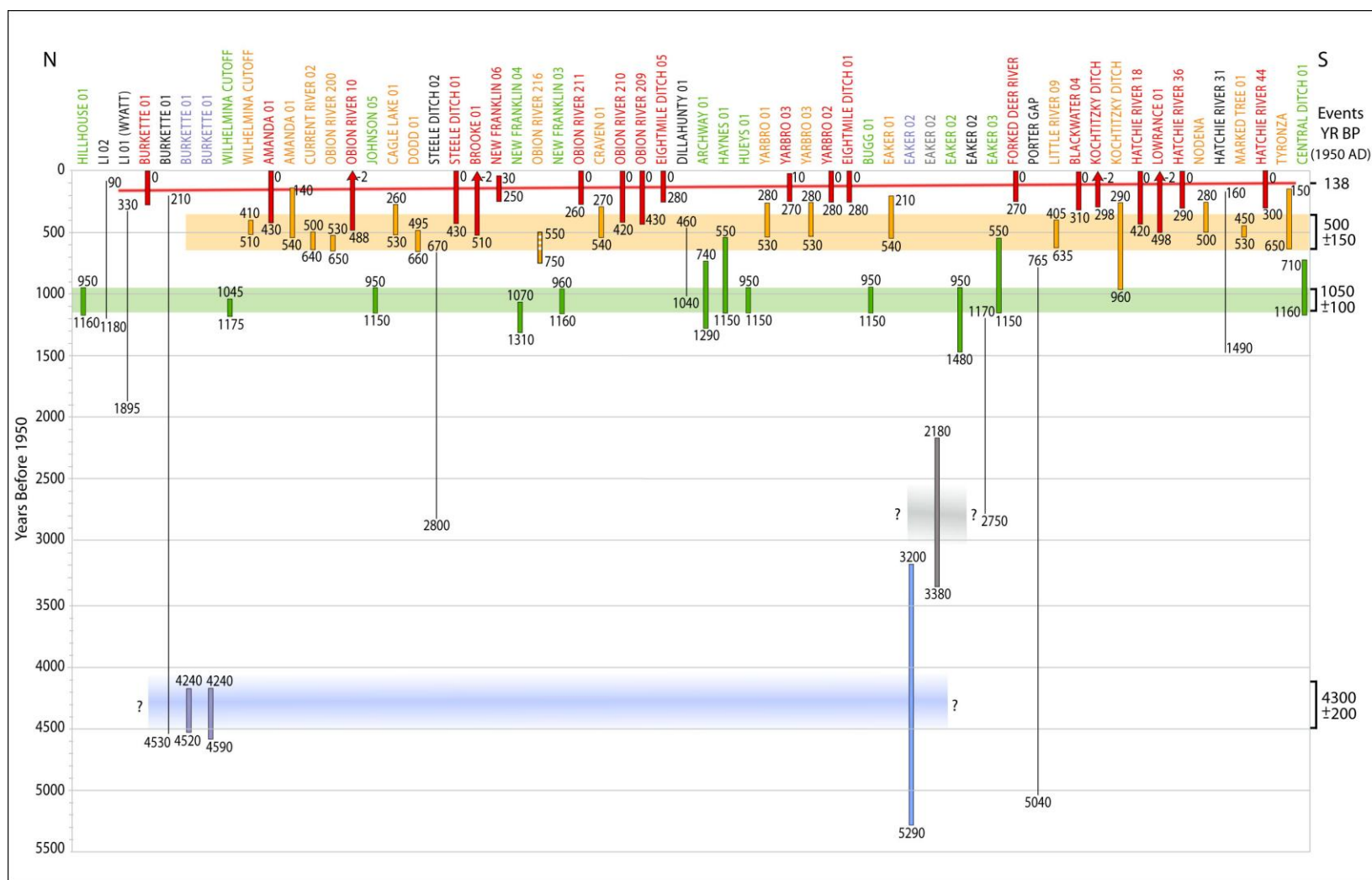


Figure E-63

Diagram illustrating earthquake chronology for New Madrid seismic zone for past 5,500 years based on dating and correlation of liquefaction features at sites (listed at top) across region from north to south. Vertical bars represent age estimates of individual sand blows, and horizontal bars represent event times of 138 yr BP (AD 1811-1812); 500 yr BP \pm 150 yr; 1,050 yr BP \pm 100 yr; and 4,300 yr BP \pm 200 yr (modified from Tuttle, Schweig, et al., 2002; Tuttle et al., 2005).

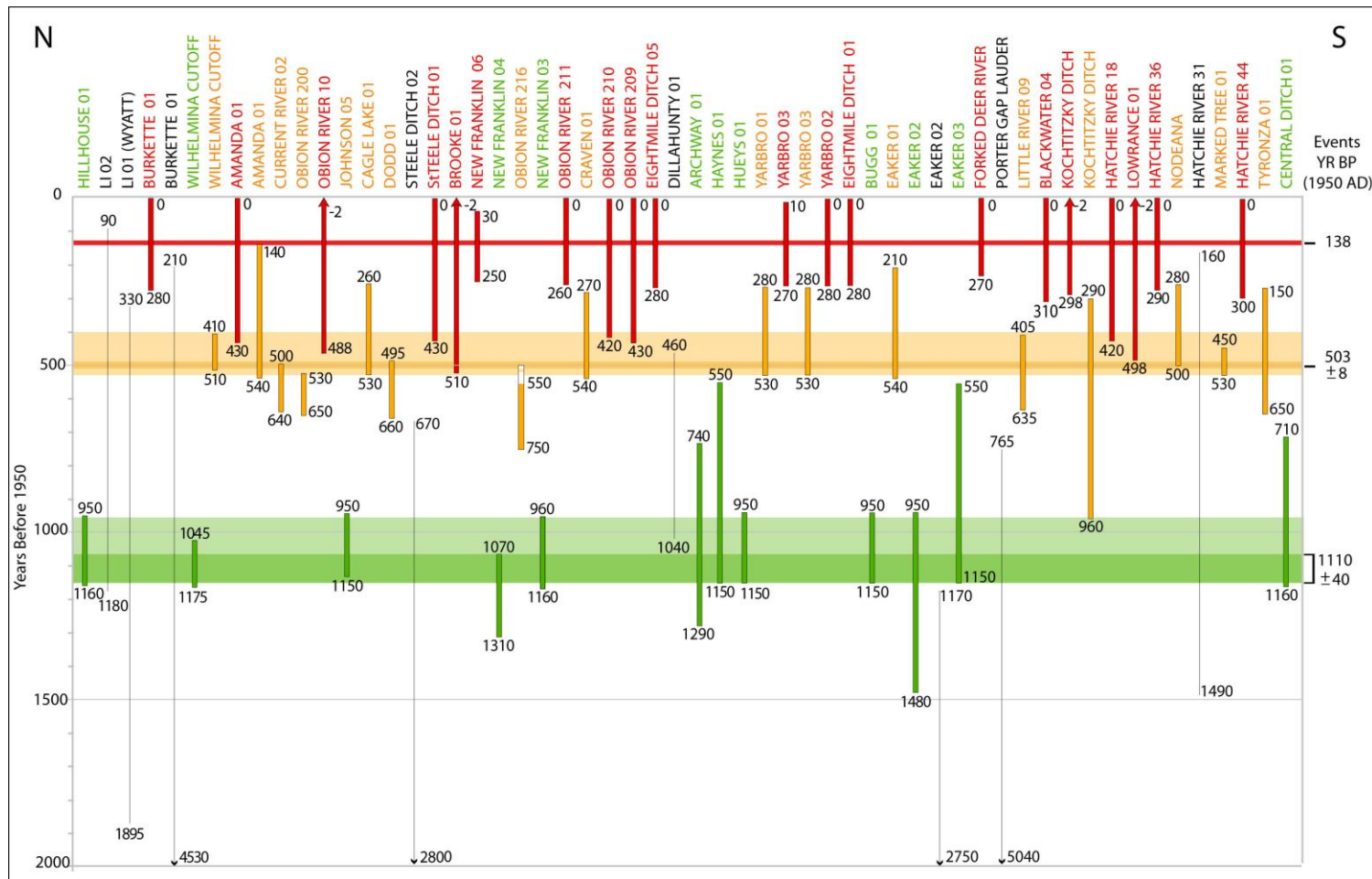


Figure E-64

Diagram illustrating earthquake chronology for New Madrid seismic zone for past 2,000 years, similar to upper portion of diagram shown in Figure E-63. As in Figure E-63, vertical bars represent age estimates of individual sand blows, and horizontal bars represent event times. Analysis performed during CEUS SSC Project derived two possible uncertainty ranges for timing of paleoearthquakes, illustrated by the darker and lighter portions of the colored horizontal bars: 503 yr BP \pm 8 yr or 465 yr BP \pm 65 yr, and 1,110 yr BP \pm 40 yr or 1055 \pm 95 yr, respectively (modified from Tuttle, Schweig, et al., 2002).

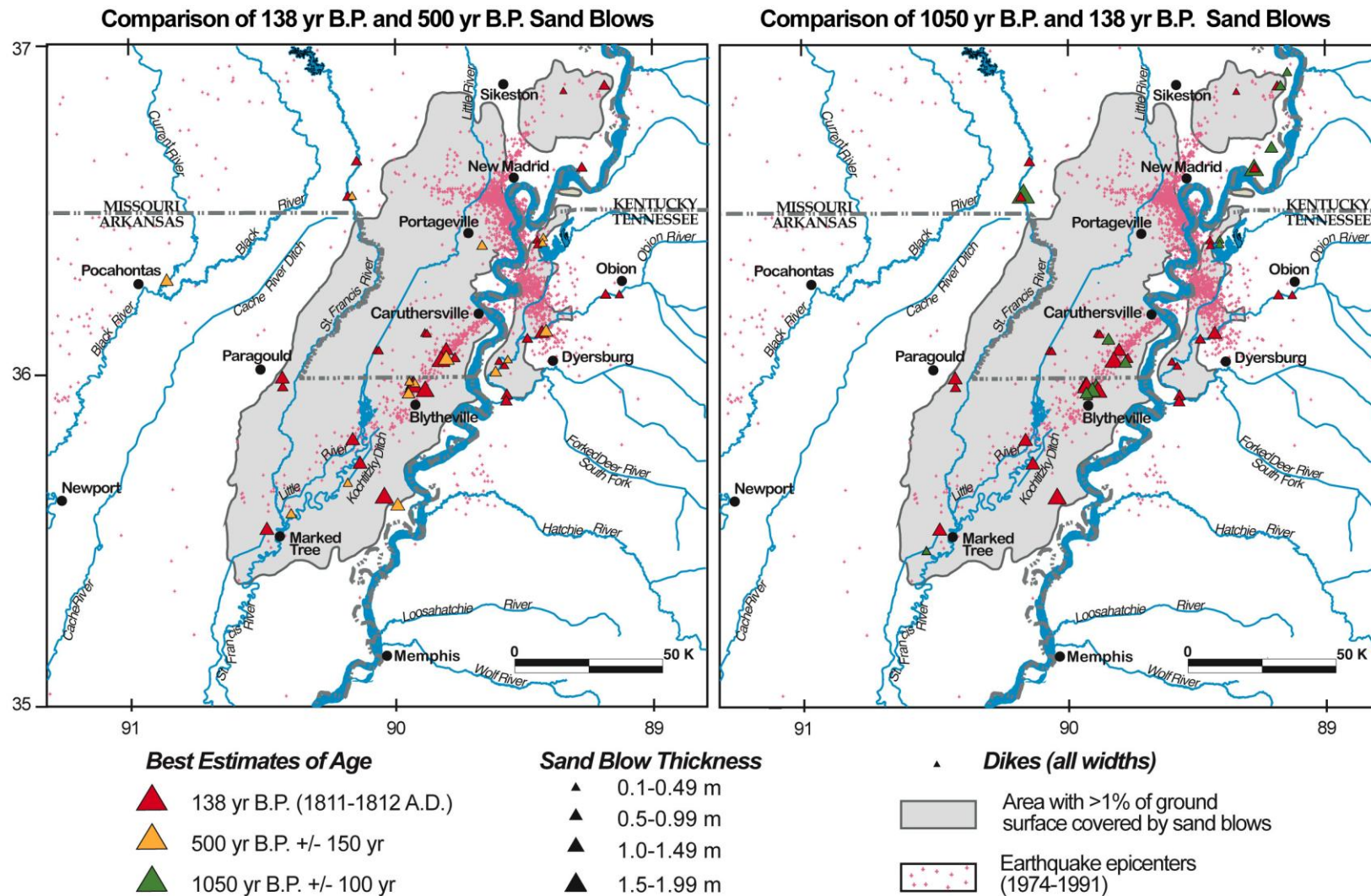


Figure E-65

Maps showing spatial distributions and sizes of sand blows and sand dikes attributed to 500 and 1,050 yr BP events. Locations and sizes of liquefaction features that formed during AD 1811-1812 (138 yr BP) New Madrid earthquake sequence are shown for comparison (modified from Tuttle, Schweig, et al., 2002).

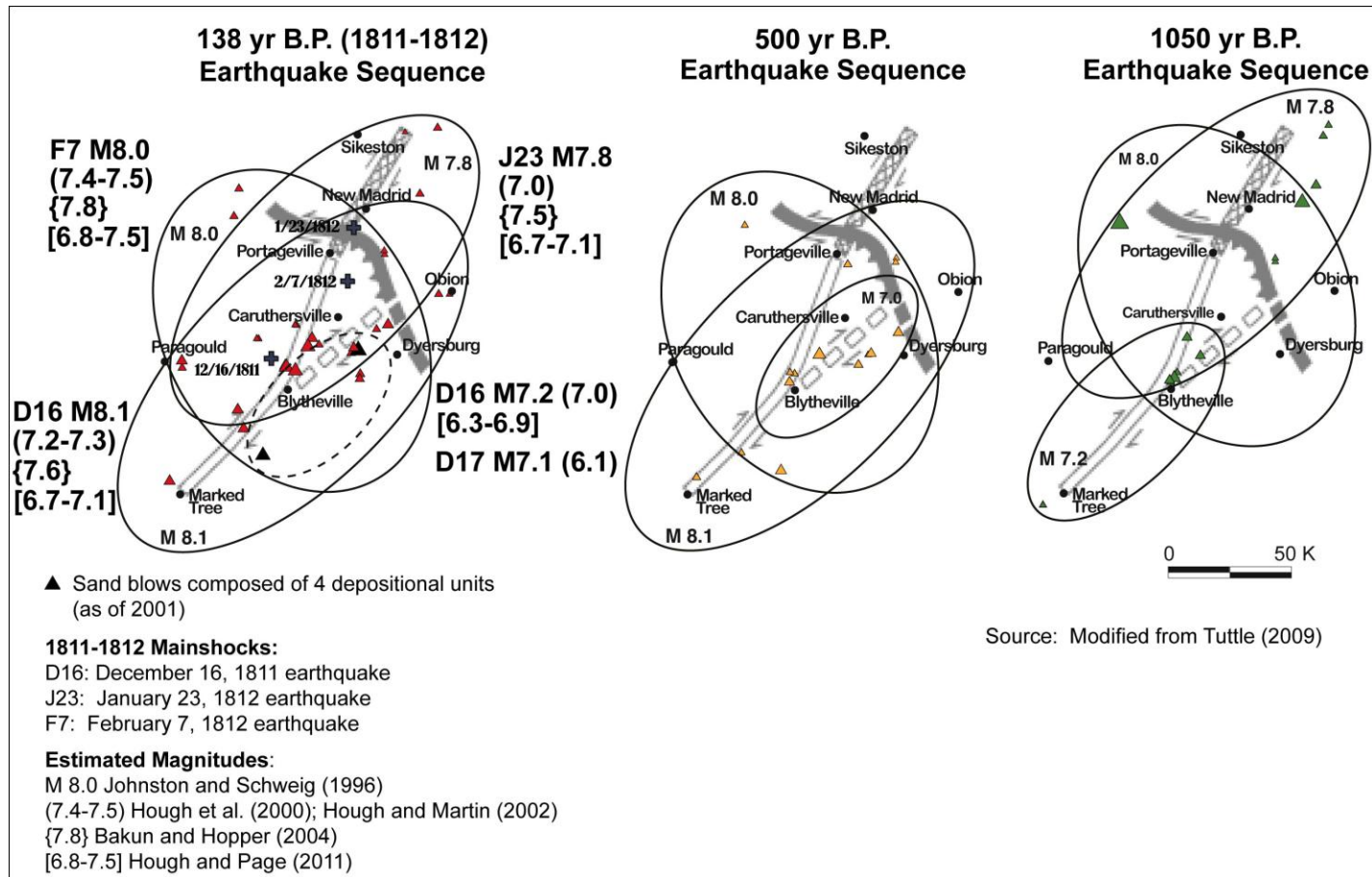


Figure E-66

Liquefaction fields for 138 yr BP (AD 1811-1812); 500 yr BP (AD 1450); and 1,050 yr BP (AD 900) events as interpreted from spatial distribution and stratigraphy of sand blows (modified from Tuttle, Schweig, et al., 2002). Ellipses define areas where similar-age sand blows have been mapped. Overlapping ellipses indicate areas where sand blows are composed of multiple units that formed during sequence of earthquakes. Dashed ellipse outlines area where historical sand blows are composed of four depositional units. Magnitudes of earthquakes in 500 yr BP and 1,050 yr BP are inferred from comparison with 1811-1812 liquefaction fields. Magnitude estimates of December (D), January (J), and February (F) main shocks and large aftershocks taken from several sources; rupture scenario from Johnston and Schweig (1996; modified from Tuttle, Schweig, et al., 2002)

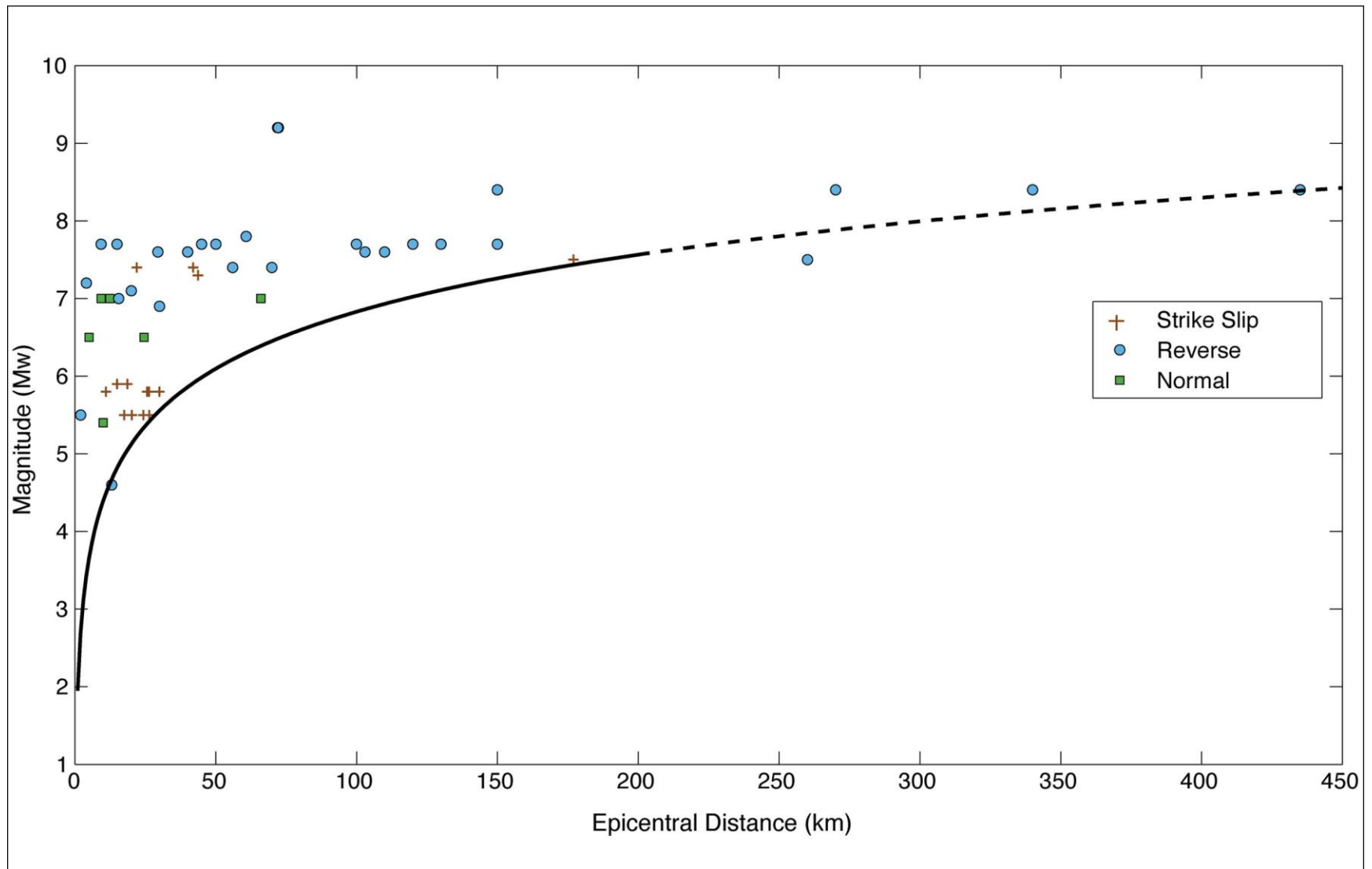


Figure E-67

Empirical relation between earthquake magnitude and epicentral distance to farthest known sand blows induced by instrumentally recorded earthquakes (modified from Castilla and Audemard, 2007).

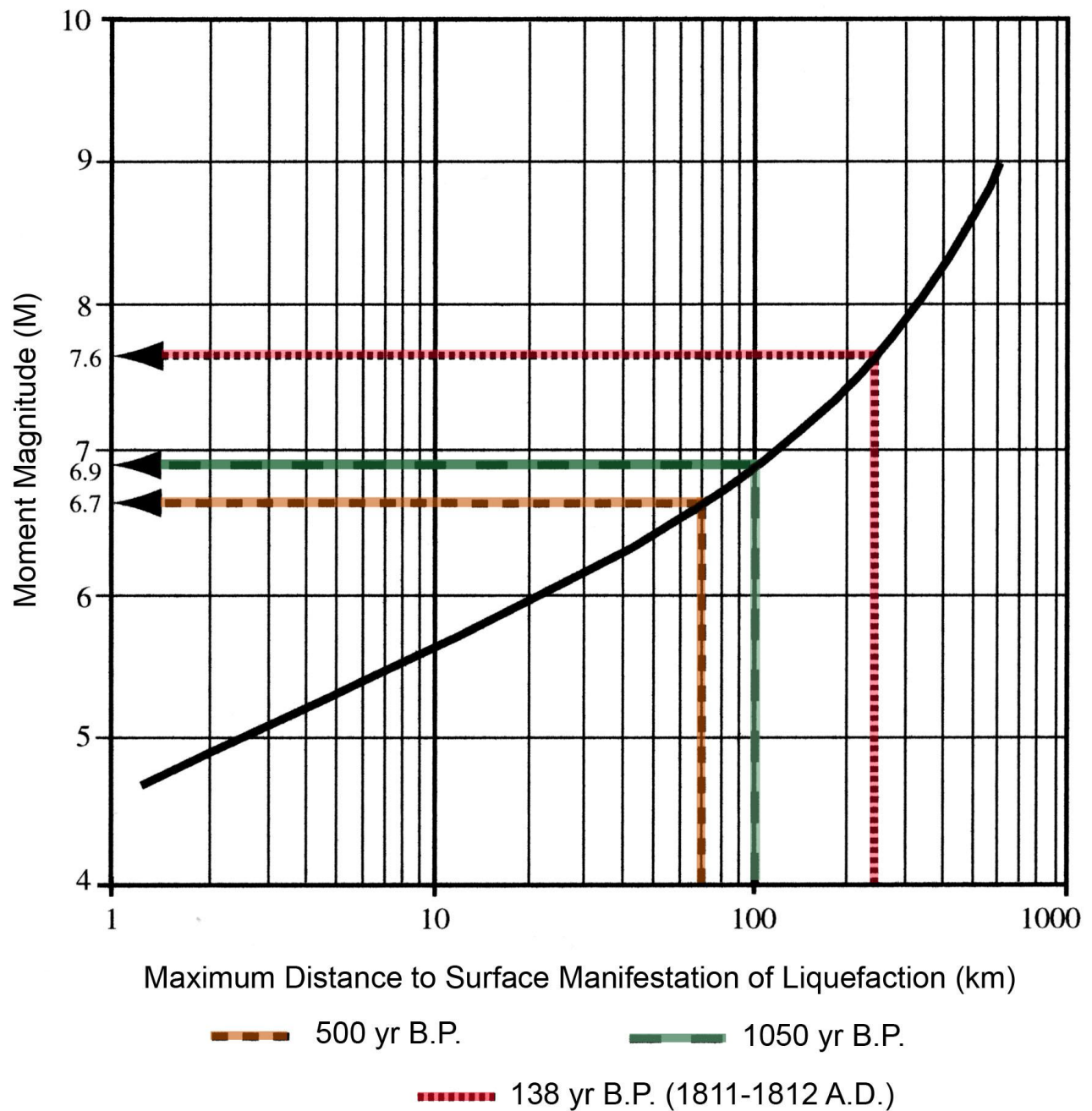


Figure E-68

Distances to farthest known liquefaction features indicate that 500 and 1,050 yr BP New Madrid events were at least of M 6.7 and 6.9, respectively, when plotted on Ambraseys (1988) relation between earthquake magnitude and epicentral distance to farthest surface expression of liquefaction. Similarity in size distribution of historical and prehistoric sand blows, however, suggests that paleoearthquakes were comparable in magnitude to 1811-1812 events or $M \sim 7.6$ (modified from Tuttle, 2001).

APPENDIX F

Workshop Summaries

F

APPENDIX WORKSHOP SUMMARIES

WORKSHOP 1: KEY ISSUES AND AVAILABLE DATA July 22–23, 2008

Electric Power Research Institute
3420 Hillview Ave.
Palo Alto, California 94304

The Workshop on Key Issues and Available Data was the first in a series of workshops jointly sponsored by the Electric Power Research Institute (EPRI) Advanced Nuclear Technology (ANT) Program and the U.S. Department of Energy (DOE) in support of the Central and Eastern U.S. Seismic Source Characterization for Nuclear Facilities (CEUS SSC) Project. The objective of the CEUS SSC is to develop a comprehensive and up-to-date SSC for a probabilistic seismic hazard analysis (PSHA) that is appropriate for use at any site in the CEUS. The goals of this workshop were to (1) introduce the various participants in the project to the goals, expectations, and schedule for the CEUS SSC project; (2) review the SSHAC Level 3 methodology (Budnitz et al., 1997) to be used for the project; (3) identify the key issues that need to be addressed in the course of the seismic source characterization; (4) review the available data, including data quality; and (5) identify the path forward for the project.

DAY 1–TUESDAY, JULY 22

Workshop participants were welcomed by Mr. Jeffrey Hamel, the EPRI Project Manager for the CEUS SSC project. He stated the importance of this project to the nuclear industry and noted that applications for 15 nuclear power plant units are currently pending and that 9 additional applications are planned to be submitted in 2009. He showed a “prism” slide that indicated the potential roles of electric sector technologies, including the role of nuclear power, in lowering CO₂ emissions by the year 2030. He reviewed the status of the current fleet of nuclear power plants in the United States and cited EPRI projections of a total of ~24 GWe by 2020 and ~64 GWe by 2030 from the new fleet that will be deployed.

The EPRI program for supporting new nuclear power plants, the Advanced Nuclear Technology (ANT) program, was described briefly. The program efforts are focused around facilitating standardization across the new fleet, transferring technology to new plant designs, and ensuring top plant performance from the start of operations. ANT program activities characterized as emerging, growth (including the CEUS SSC project), mature and declining activities were described. The program is funded by more than 25 utilities, vendors, and government agencies

interested in promoting light water reactors. In addition, there is substantial interest from utilities based in Europe, which reflects the growth of this technology outside the United States as well.

Next, Mr. Lawrence Salomone, Project Manager for the CEUS SSC project, welcomed everyone and expressed his appreciation for their participation in the project. He asked all workshop participants to introduce themselves and identify their affiliations. He began his talk by emphasizing that nuclear capabilities are essential as clean, safe options to achieve base load capacity increases, noting that 50 new units will provide 25 percent of the projected increased demand. To expedite the licensing of next-generation nuclear power plants, Mr. Salomone emphasized that we can do “more for less to achieve stability, with reduced risk through standardization and partnering.” He described the industry and government plan to advance the science for nuclear technology, which includes using the CEUS SSC project to replace the previous EPRI-Seismicity Owners Group (EPRI-SOG, 1988) and Lawrence Livermore National Laboratory (LLNL; Bernreuter et al. 1989) seismic hazard studies that were conducted in the 1980s.

Next, Mr. Salomone described the goals for the CEUS SSC project, which include developing a “commercially viable” approach for SSC model development with respect to cost and schedule that meets the expectations of sponsors, regulators, and oversight groups. He reviewed the Workshop 1 objectives, noting that a documentation package would be prepared for the workshop to be consistent with the objective of having a transparent project process. Next he reviewed the CEUS SSC project history to date and outlined industry and U.S. Department of Energy (DOE) expectations for the project. The primary expectations are to advance the science and obtain a PSHA update that is based on a stable and consistent SSC model, thereby expediting the licensing of the next generation of nuclear power plants.

Mr. Salomone then noted that the number of proposed sites for next-generation plants in the CEUS is increasing and that existing plants in the DOE complex require an updated PSHA. Such studies are time-consuming and costly if each utility prepares a PSHA independently; at the same time, regulators want to streamline the review process and be capable of moving forward quickly. In addition, the EPRI-SOG (1988) and LLNL (1989) seismic hazard studies need to be updated using new data and interpretations; also, a void exists for an SSC model that postdates 10CFR 100.23. Accordingly, assembling a single team of experts to develop a new and stable CEUS SSC model that incorporates a full range of uncertainty provides many benefits, thus industry and government agencies have been brought together to sponsor this project.

Next, the organization chart for the CEUS SSC project was described. The Program Managers have overall responsibility for the project. The Technical Integration (TI) team, which includes the TI staff, has responsibility for the technical assessments made during the project. The Participatory Peer Review Panel (PPRP) is responsible for reviewing the process and technical aspects of the project. Specialty contractors are involved in database, hazard input and calculation, and documentation support. Participants in each of the project workshops are important because they have databases and alternative interpretations that are valuable to the project. Project milestones were described for the next two years; the final milestone will be an EPRI Technical Report to be published in 2010. Mr. Salomone concluded his talk by summarizing the benefits of the project, which include (1) supporting a research and development program to advance the state of practice for seismic hazard assessment; (2) obtaining PSHA input based on a stable and consistent SSC model vetted by a wide range of

experts; (3) avoiding unnecessary conservatism and reduction in design margins; (4) expediting approvals of the seismic design basis for nuclear facilities; and (5) yielding significant economic benefits by reducing PSHA update costs for individual sites.

Mr. Salomone then introduced Dr. Kevin Coppersmith (Coppersmith Consulting, Inc.), the lead of the TI team, to speak in more detail about the CEUS SSC project and the goals of the workshop. Dr. Coppersmith began by stating that 20 years have passed since the previous seismic hazard assessments for the CEUS were conducted (e.g., EPRI-SOG, 1988, and LLNL, 1989). The current project will provide an unbiased seismic hazard assessment that captures uncertainty by following the process specifically designed to achieve this objective by the Senior Seismic Hazard Analysis Committee (SSHAC) (Budnitz et al., 1997).

Dr. Coppersmith described SSC as fundamentally a scientific issue involving three questions: where will future earthquakes occur, how large will they be, and how frequently will they happen? He described some of the scientific assessments needed for SSC and stated that locations of observed events are based on historical and instrumental earthquakes, yet for a hazard analysis there is a need to assess the future pattern of seismicity. Spatial stationarity, seismogenic potential of geologic structures, the nature of boundaries between seismic zones, and other assessments needed for SSC were mentioned as he showed examples that included San Francisco Bay Area seismicity, the active Meers fault in Oklahoma, the New Madrid seismic zone, seismicity in Switzerland, and an isoseismal map of the 1356 Basel, Switzerland, earthquake. Scientific assessments of earthquake size, especially maximum magnitude (M_{\max}), and recurrence, were also illustrated using examples. He described how uncertainties in seismic hazard assessments need to be captured through the use of logic tree structures and noted that these were new at the time the EPRI-SOG work was conducted.

Next, Dr. Coppersmith described the SSHAC methodology that provides a framework for incorporation of scientific assessments. In this methodology the views of the larger scientific community are captured as a “snapshot in time” of our knowledge and uncertainties. He described elements of the SSHAC methodology, including the goal of all probabilistic hazard analyses to represent the center, body, and range of technical interpretations that the larger, informed technical community could provide. To achieve this goal, expert roles and responsibilities have been defined. Experts must be “evaluators” who need to understand and evaluate information provided by “proponents.” Stability and longevity are the larger goals of all PSHA methodologies, which are achieved in part from identifying and incorporating uncertainties. With these attributes a PSHA will have public and regulatory confidence that all hypotheses have been considered and the conclusions are not subject to significant change with each new scientific finding; new information can also be considered and incorporated into a PSHA.

Dr. Coppersmith then reviewed the SSHAC study levels 1 thru 4, which are designed to address increasingly difficult and contentious problems by processes that increase complexity. The CEUS SSC project is a Level 3 study and includes both a TI team and the active involvement of a participatory peer review team, led by Drs. J. Carl Stepp and Walter Arabasz as co-chairmen.

The CEUS SSC task schedule was reviewed next. Dr. Coppersmith emphasized that a ground motion assessment was not part of the current project, as new alternative models were recently developed for the CEUS (EPRI, 2004, 2006). He then described the goals of Workshop 1, which include identifying key hazard-significant SSC issues and the data sets available to address these

issues. He reviewed the ground rules for workshops, which are designed primarily for the TI team to exchange data, present interpretations, challenge and defend technical hypotheses, gain information on the project, interact, and ask questions. Observers will be provided with opportunities for questions/comments. Finally, he reviewed the roles of workshop participants, including expert roles of proponents and evaluators, and concluded his talk by reviewing the agenda for Workshop 1.

After a short break, the workshop session titled “Key Hazard-Significant CEUS SSC Issues” commenced. The purpose of this session was to review and discuss the technical issues of importance to the CEUS SSC study in the context of preparation of a PSHA. Dr. Robin McGuire (Risk Engineering, Inc.) gave a talk titled “Perspectives on Seismic Hazard Sensitivity to Input Assumptions.” He noted that the purpose of his comments was to illustrate the sensitivity of seismic hazard to input parameter choices, and he emphasized the importance of keeping aleatory and epistemic uncertainties separate. He reviewed the definitions of these types of uncertainties and gave an example of how they are used in characteristic magnitude distribution (i.e., the aleatory uncertainty is that successive characteristic earthquakes have different magnitudes [e.g., M 7.2-7.7] and the epistemic uncertainty is in the range of these magnitudes [e.g., M 7.2-7.7 or M 7.0-8.0]). He explained also that these represent a “snapshot in time” and that uncertainty tends to migrate from aleatory to epistemic as better models are developed.

Next Dr. McGuire showed some examples for a set of sites affected by faults that represented the New Madrid event by showing example parameters and uncertainties for these hypothetical sources from the SSHAC report (Budnitz et al., 1997). He discussed the relationships between earthquake magnitude and hazard, such that if beta goes down, hazard increases, especially at larger distances; at close distances smaller events may dominate the hazard. Also, he mentioned that seismic hazard may be more sensitive to changes in distance if M_{\max} is low. For purposes of sensitivity analysis, he defined a significant change as a hazard result change of more than 20 percent, as a result of alternative parameter inputs. He illustrated this with examples from Group A sites and Group B sites. Most changes result in a change in hazard of less than 20 percent, and some have no sensitivity. The integration of hazard over many events with various parameters is not inconsistent with the finding that the occurrence of a particular rare event could cause lots of damage. Multiple interpretations of seismic sources are important; this is especially critical for specific sites, as hazard results could be very sensitive to the boundaries defined for a particular seismic source.

Dr. McGuire showed examples of the contribution of high- and low-frequency hazard to the magnitudes and distances of the earthquakes that contribute to hazard at a site within the area of influence of the 1886 Charleston event. He showed a series of plots with increasingly larger ground motions, which progressively showed an increased contribution from close-by, smaller events. Then he showed a set of plots for low-frequency hazard and the associated events that contribute to hazard. He provided an example in the Eastern Tennessee seismic zone (ETSZ), showing M_{\max} distributions for the ETSZ from recently completed studies as well as a series of slides showing the source zones for this region defined by the six EPRI-SOG teams. These give multiple alternative source zone interpretations and a resulting range of a factor of 5 in hazard from curves produced at 10 hertz (HZ) (the individual team results were ultimately weighted equally to produce a single hazard curve). Some of the differences are related to different seismicity rates within the alternative zones, which are influenced by the approach used to

smooth the historical seismicity. At low structural frequencies, the New Madrid seismic zone is a major contributor and there is a tighter hazard range across the teams. He also showed that at high frequencies there is low sensitivity to M_{\max} , whereas at low frequencies there is increased sensitivity to M_{\max} . Therefore, if M_{\max} is low, it can be more important to hazard than if it is high.

Dr. McGuire then showed geometries of New Madrid seismic sources from a recent study, the earthquake magnitudes for the sources used in a cluster model, and the associated sensitivity of 1 Hz and 10 Hz spectral acceleration hazard. He showed plots of New Madrid seismic sources from the EPRI-SOG teams and the resulting differences in hazard at specific locations (e.g., moving a site 20 km could result in a 30 percent reduction in hazard). Next he showed examples of updated Charleston seismic source geometry alternatives and how these were merged with the EPRI-SOG team Charleston sources as revised (“doughnut hole”) sources containing the updated Charleston source information. As with the examples shown previously, the sensitivity of the mean hazard varies as a function of ground-motion structural frequency. From a distribution of seismic hazard curves for the 85th, mean, 50th, and 15th fractile hazard, the hazard (15th to 85th) is known within a factor of 20; the mean of the hazard is known more precisely. There is a high level of sensitivity to the characteristic earthquake (M_{char}).

Seismicity parameters used in the EPRI-SOG project were the next topic discussed by Dr. McGuire. The EPRI-SOG seismicity parameters were determined by statistical analysis of historical seismicity and the parameters were calculated for each source per degree cell using smoothing options specified by each team. Alternative sets of seismicity parameters were weighted by each team. Dr. McGuire showed examples from the Bechtel team’s source BZ5. He showed a visual representation of different smoothing assumptions used within the zone and plots of the sensitivity of hazard curves to smoothing. Next, he showed examples of the central Virginia seismic zone using alternative zone geometries selected by the EPRI-SOG teams and the range of related seismicity parameters. He looked at the effect of seismic hazard at three sites, and found that site location is extremely sensitive to these zones: a difference in hazard of more than a factor of two for two sites located about 30 km apart, which is a huge difference. His conclusion is that alternative zone boundaries or boundary treatments are essential, as defining only a single source could significantly affect the hazard results for sites located either just inside or outside the zone boundaries.

Next Dr. McGuire showed a CEUS region and the geometries of faults in the New Madrid seismic zone as modeled in a recently conducted PSHA. The hazard results for sites at three different locations in the region show that at a low frequency (1 Hz), there is a large contribution to hazard from New Madrid sources, but at 10 Hz, there is a greater contribution (two to three times) from local sources at each of the sites.

In a last set of examples, Dr. McGuire showed seismic sources defined in the Gulf of Mexico region by each of the EPRI-SOG teams. He stated that it will be important for the CEUS SSC study to consider earthquakes outside the United States. Seismicity maps for Central America and the Caribbean were shown; both areas have seismicity that may need to be included in models for sites in the southeastern United States. Also shown were EPRI-SOG seismic sources and hazard curves for Houston, Texas. The hazard curve for 1 Hz shows strange behavior, having a huge range of almost two orders of magnitude difference between the 15th and 85th

fractiles. Dr. McGuire postulated that one particular ground motion equation that was used may be affecting the mean hazard curve.

Following a break for lunch, Dr. McGuire concluded his presentation. He described the Cumulative Absolute Velocity (CAV) model developed to calculate cumulative ground motions at a site. This model indicates a short-duration, high-frequency earthquake will have less effect on a site than a large, distant earthquake. Sites where small magnitude earthquakes contribute the most to the overall hazard have lower hazard as a result of application of a CAV filter.

Dr. McGuire closed by listing his recommendations regarding the relative significance of SSC issues in order of priority. Assessments of seismic sources having potentially large earthquake magnitudes (e.g., New Madrid and Charleston regions) are the most important in terms of characteristic magnitude distributions and source zone locations because so many sites are potentially affected by these sources. These sources should be given highest priority, and the details of the characterization will be important to many sites. Next in importance are seismic sources having moderate magnitudes; and the remaining zones are background sources away from the more active sources. At this point, Dr. McGuire turned the session over to Dr. Gabriel Toro (Risk Engineering, Inc.).

Dr. Toro began by describing the equations that allow comparisons between sensitivity products. These comparisons are important for focusing on situations with an important seismic source where high sensitivity is combined with high uncertainty. He showed an example from the PEGASOS study in Switzerland, in which hazard in the 10^{-4} to 10^{-5} range is important. Input parameters used by the four PEGASOS SSC teams were all approximately equal in importance (exclusive of ground motion issues). For some sites, a specific parameter dominated over other parameters, but in general all parameters were equally important.

Dr. Coppersmith opened the group discussion at the end of the session by noting that the TI team will interact with Risk Engineering to define and properly consider sensitivities. The group discussed seismic source zones with large magnitudes, especially the need to define the characteristics of zone boundaries (e.g., uncertainties in location, “fuzzy” boundaries) and develop alternatives to assess the hazard for a site located near a source boundary. It may be useful to define generalized zones for most sources but have alternative boundaries for use with close-in sites. Source zone definitions and logic tree complexity were discussed. Differences between the PSHA approaches used for the EPRI-SOG project and what is available now for the CEUS SSC project were discussed, including significantly increased information on tectonic environments, modeling approaches such as spatial smoothing, computing power, GIS tools, and alternative methods for incorporating uncertainties. The TI team will review alternative interpretations of data at Workshop 2, planned for February 2009.

The next session of the workshop focused on data that are available to conduct the CEUS SSC and that may be useful in addressing the key issues discussed in the previous session. Dr. William Lettis of William Lettis and Associates (WLA) began with a presentation titled “Database Development.” He stated that the group was brought together for Workshop 1 to identify what we do and (most importantly) do not know about seismic hazard in the CEUS, especially for capturing uncertainty. What data sets do we have that are needed, and can some be targeted for additional analysis that would be useful for this project? He noted that Dr. McGuire had described the parameters that are most sensitive for source zone characterization, and this information will help the TI team focus on what is most important. Dr. Lettis described the data

compilation objectives, which include identifying critical data sets of geologic and geophysical coverage, and compiling COLA and ESP data as well as DOE PSHA and other data as available and relevant. A data compilation and documentation process is being established. This effort will include constructing a GIS platform to support TI alternative interpretations and establishing a data server to facilitate share of data and information. Dr. Lettis reviewed the presentation outline and indicated the speakers who would discuss the different aspects of database development.

Dr. Frank Syms (WLA) discussed the administrative issues for the data documentation process. He noted that it will be important to document exactly how data are evaluated and transcribed into GIS. He noted that there will be some sharing restrictions, as some data have to be purchased. Data quality will be assessed with help from the data experts. An FTP site will be established to store and share data, which will include all data sets plus the metadata summary sheet, ArcGIS shape files, and a PDF of ArcGIS coverage, as appropriate. The earthquake catalog for the project will be available. COLA and ESP data from relevant sites will be assembled and made available, as will relevant U.S. Nuclear Regulatory Commission (NRC) Request for Additional Information (RAI) data. He described the status of COLA and ESP data; nine COLAs for sites in the CEUS are currently under review by the NRC and six additional COLA's have been identified as in preparation. Additionally, relevant information is available for the DOE Savannah River Site, as well as for the Los Alamos National Laboratory, where information on the seismic source characteristics of the Rio Grande Rift will be important to the CEUS SSC project.

Dr. Randy Cumbest (WLA) spoke next. He showed text from the project plan about the database scope and coverage. The western boundary of the study region will be the foothills of the Rocky Mountains (about longitude 105° W), except that it will include the Rio Grande Rift system; coverage will extend a minimum of 200 miles beyond the coastline and 200 miles from the U.S. borders with Canada and Mexico. Next he showed a series of slides with the database contents, which will include regional geophysics, including potential field, tectonic stress, and seismic reflection and refraction data; regional geology, including crystalline basement, tectonic features, crustal thickness, Quaternary faults, paleoliquefaction sites and dates; and the earthquake catalog for the project. Dr. Cumbest has already determined the availability of data sets by contacting many of the principal investigators. For the remainder of the talk he reviewed specific data sources from the list and noted for many items where coverage was currently complete or incomplete.

The group considered possible gaps in the list of available data sets. Items discussed included GPS data, mantle velocity information, Paleozoic and Mesozoic structural information, earthquake intensity and focal mechanism data, and shallow seismic reflection data. It was noted that many of the additional data sets mentioned by workshop participants would be discussed by presenters during the second day of Workshop 1.

Mr. Scott Lindvall (WLA) followed up with a list of logistical questions and issues. These included focus on the western boundary of the study region, defined at 105° W longitude, but which also includes the Rio Grande Rift, although the 200-mile buffer zone also includes the rift zone. It was noted that seismic sources throughout the buffer zone could affect sites within the study region boundaries; this is particularly the case along the western boundary. However, the major focus of the CEUS SSC study needs to be seismic sources within the defined boundary

region. Using source models from other studies, especially the U.S. Bureau of Reclamation studies for dams in some of the western states (e.g., Colorado and Wyoming) was mentioned as a possible source of information for the WUS buffer zone areas. Offshore there are earthquakes with epicenters on the continental slope that need to be included in the analyses. Earthquakes in Cuba could be important for a site located in southern Florida. The appropriate way to deal with study area boundary questions will continue to evolve. Mr. Lindvall also discussed the USGS Quaternary faults and folds database that needs to be updated by adding available Wheeler (2005) and Crone and Wheeler (2007) information, specifically, the Class C and D features. Finally, data sharing and copyright limitations were discussed for both GIS data and published papers.

After a break, Dr. Randy Keller (University of Oklahoma) described the on-land gravity database being developed by the scientific community. The initial compilation of gravity data for the conterminous United States is currently being expanded by merging data from many organizations for all of North America and including data from Canada and Mexico. The organizations contributing to the effort include the USGS, NASA, NSF, NOAA, and others. A number of corrections have been made to the database to remove duplicate points, bad points, and to terrain-correct the data. Dr. Keller showed maps of data available from 900,000 stations in 1999 and from 1,282,787 station locations in December of 2003. He described the processes used to remove duplicate points. Data sets of this type incorporate thousands of different data sets and he described methods used to remove bad points. He mentioned that a significant part of the database development effort is the creation of new standards for gravity data reduction; these standards are published in a Hinze et al. (2005) article in *Geophysics*. Next he showed a map that indicates the complexity of the upper crustal structure in the CUS. Basement structures are far from homogeneous and thus difficult to correlate with other geologic information. Dr. Keller showed a series of maps and identified the location of the Meers fault in Oklahoma, as well as other geologic features, that have clear gravity signatures. He noted that different filters can be used to display the data in different ways. Magnetic data are an obvious complement to the gravity database. GIS-type approaches allow for many types of data to be overlain and examined. He closed with an example of a desalinization plant in El Paso, Texas, and the search for a brine disposal site, ultimately found in a basin identified as a gravity low. Following his comments the group discussed the use of isostatic adjustments (i.e., the effect of topography removal), the association of lineaments with gravity data, and terrain corrections that can be made.

Magnetic data were discussed next by Dr. Dhananajay Ravat (University of Kentucky). He began by showing maps of North America displaying the magnetic anomaly databases in 1987 and 2002, developed from hundreds of different aeromagnetic data sets. The variations between the different data sets resulted in significant problems when they were compiled, so he has undertaken the process of compiling improved data products. The National Uranium Reconnaissance Evaluation (NURE) data obtained in the 1970s are an important source of data. Dr. Ravat has used CM (the Comprehensive Model of the Near-Earth Magnetic Field) to improve the NURE data products. Some gaps remain where data have been lost, but his colleagues in Egypt inserted North American Magnetic Anomaly Group (NAMAG) data segments to fill gaps. To identify problems, second vertical derivatives (filters) are used; short wavelength data integrity problems result, which are correctable but require a time-consuming effort. To obtain the best full-spectrum magnetic anomaly product possible in the short term for his presentation, he combined NURE and NAMAG data for the conterminous United States.

Next Dr. Ravat described interpretations of the data set using reduction-to-pole of NAMAG data, which is important for some applications. Most modern source interpretation techniques require high-quality first and second derivatives. He also briefly described methods for structural mapping, source edge complexity, and determining continuity of sources (e.g., the use of interpretive products).

Workshop participants discussed combining geologic maps with the magnetic data maps, although it was noted that for some regions, geologic maps have been directly derived from magnetic data. The major limitations for use of the new map developed for this study were also discussed. Dr. Ravat knows the resolution could be improved by fixing some NURE problems, and he described some of the corrections that can be made using second vertical derivatives. Data for many areas have been collected but are not available for use at this time (e.g., U.S. Navy and industry data).

Dr. Walter Mooney (USGS) gave the final presentation of the day, titled “Global Seismic Refraction Catalog (GSC).” The USGS is interested in building a global seismic refraction catalog containing the most up-to-date information available about the Earth’s crust. The Global Seismic Refraction Catalog (GSC) is a Digital Earth crustal model derived from seismic refraction and other geophysical data. It is an important product for seismic hazard assessments, earthquake studies, and petroleum research. Dr. Mooney described key features of the GSC, which provides global coverage using a comprehensive set of data collected from 1939 through the present. Using these data, 10,200 data points have been digitized at 50 km intervals; recently, additional high-resolution data have become available and will be added to the database. The database consists of seismic refraction and other data captured from open-file and published scientific literature sources. Dr. Mooney’s study began with comparisons of refraction data and laboratory experiments; velocity data have also been compiled. Dr. Mooney showed current coverage of the GSC database; there is a strong correlation of survey areas with areas where there is interest in oil and gas resources. He described what is included in data records (location, structure of crust, tectonic environment and experimental details, etc.) and he showed a sample data record. For North America there are more than 1,400 data points, containing varying amounts of information. North America data have not been added consistently to the database since 2002; many thousands of additional points have been identified and need to be added to the model.

Turning to products that can be developed using GSC data, Dr. Mooney showed various maps of North America that displayed sediment thickness, depth to the Moho, and shear-wave velocity maps. The data currently being collected by the Earthscope project will eventually provide additional valuable information for the catalog. Dr. Mooney gave examples of how the database can be queried to filter information such as maps and cross sections that indicate different layers of the crust and the structure of the crust-mantle contact. For the workshop, a cross section showing variations in crustal thickness and the location of the Moho was created across the United States from the Pacific to Atlantic oceans at 35° N. Next Dr. Mooney showed some average statistics for North American crust: average thickness of continental crust of 36.72 km and oceanic crust of 8.39 km; average P and S velocities, and other information. He then showed a histogram of crustal thickness for North America (the thinnest crust is in northern California; the thickest in the Great Basin) and stated that thickness values are much higher in the Alps, Andes, and Himalayas. Heat flow data were also discussed, and he noted that assumptions need to be made about radioactive element contributions to heat flow. There is about a 500-degree C

range in temperatures within the crust; in colder areas there are fewer earthquakes. Heat flow data can also be used to estimate thickness of the lithospheric root: as the root thickens, fewer earthquakes are observed, as deformation tends to be concentrated in areas of thinner lithosphere.

Next, Dr. Mooney showed the “Bigfoot” array of broadband instrument stations that is being moved east across the United States; these data will not be available in time for use in the CEUS study area. He concluded his talk with examples of maps of the upper mantle from surveys in southern Africa.

Mr. Salomone opened the workshop to comments and questions from observers. Several workshop participants commented on the data sets that had been described or were on the agenda to be described the following day. The workshop was then adjourned for the day.

DAY 2–WEDNESDAY, JULY 23

Dr. Coppersmith welcomed the group to the second day of the workshop and reminded everyone that the time period of interest for the CEUS SSC study is the ~50-year period of operation typical for conventional nuclear power plants and that the annual hazard probabilities of interest will be in the 10^{-4} to 10^{-7} range. Dr. Randy Cumbest (WLA) then resumed leading the presentations and discussions in the “Available Data” session that began the previous day.

The first talk of the morning was given by Dr. Robert Hatcher (University of Tennessee, Knoxville). Dr. Hatcher’s talk was titled “Available Data: Geologic Domains, Tectonic Features, Rifts,” and he addressed the difficulties of understanding the origin of earthquakes within continental plates. He began by showing a series of geologic maps, tectonic maps, and maps of the assembly and dispersal of the supercontinent of Rodinia. He spoke in more detail about the series of geologic maps of the United States and the improvements made in the level of detail through time. Next he showed magnetic and residual isostatic gravity anomaly maps of North America and pointed out structural trends and features of interest, including accreted terrains and suture zones. He noted that integrating geophysical data with geologic data was essential for understanding the geologic domains and tectonic features of the CEUS. Interpretations of geologic features based on a variety of geophysical data sets, including residual isostatic gravity anomaly data, magnetic data, and seismic reflection data, were discussed.

Next Dr. Hatcher discussed rifting processes. He described how Africa collided with North America at the end of the Paleozoic, and then showed geologic maps that provide the evidence for the collision sequence. He also described the New Madrid area and indicated the boundaries of the Reelfoot Rift; instrumentally recorded seismicity is not completely within the rift and therefore is not clearly associated with it. The crust-forming processes and features that began to form in the late Proterozoic and into the Mesozoic were described.

Dr. Hatcher then described EUS earthquake frequency and magnitude patterns. He discussed the eastern Tennessee seismic zone, in which earthquakes are occurring at depths of 7 to 25 km, and stated that there is no apparent structure in the lower crust or apparent offset of the basement that could be associated with this seismicity. He postulated that the Farallon Plate may extend below the EUS and is a possible cause of earthquakes such as the New Madrid events. In his concluding remarks he stated that old structural boundaries may concentrate stress and produce earthquakes, but they do not provide answers about why they occur where they do. Incomplete data sets,

especially for information about the mantle, are a major handicap in understanding the seismic setting of the CEUS.

The next talk was given by Dr. W.R. Van Schmus (University of Kansas), titled “Major Tectonic Features of the Precambrian Basement in the Midcontinent Region, USA.” Dr. Van Schmus reviewed available data sources, including outcrop, drillhole (core and cuttings), magnetic, and gravity maps, that allow interpretation of the geology of the midcontinent. He commented that outcrop availability is quite limited and drill cores can be useful when extended into granitic basement. Geologic maps can be developed from all available data. Next Dr. Van Schmus reviewed Archean-Proterozoic continental growth in the CEUS and showed maps of the accretionary belts and rock provinces that were emplaced progressively towards the south and southeast over a time span of about three billion years. Major boundaries between various terrains, the timing of their formation, and fundamental differences in the crust in various areas were described. Dr. Van Schmus traced the boundaries of some of the terranes and noted the difficulties in interpreting the associated histories, as some boundaries may be erosional and not tectonic in origin. Next he described the Eastern Granite-Rhyolite Province and Southern Granite-Rhyolite Province, both of which contain isolated plutons, juvenile basement, and stratified rock in older basement. He also described aspects of the Midcontinent Rift system, a large gravity feature that contains many faults.

Dr. Mark Zoback (Stanford University) was the next speaker, and he presented results of work conducted with Dr. Mary Lou Zoback (Risk Management Solutions). His talk was titled “In Situ Stress and Earthquake Focal Mechanisms in the Central and Eastern U.S.—An Update.” First he reviewed the state of stress in the CEUS as it was understood in the early 1980s. At that time, regional ENE-WSW compression over a large area was recognized, and detailed information about the New Madrid zone was starting to become available. Next he compared the state of understanding in the late 1980s with that of the early 1980s and noted that dramatic changes occurred in interpretations as a result of a great increase in data on the state of stress in the United States. Most significantly, data were becoming available from wellbore breakouts, which are the best indicators available of stress orientation because they are uniform and consistent. The improved database also included earthquake focal mechanisms, which indicate that faulting in the northern part of the EUS ranges from strike-slip to strike-slip-reverse to reverse faulting along a NE-trending gradient. Subsequently, structural information on faults became available and these data are consistent with the regional stress field. Dr. Zoback noted that the current view of the state of stress in the CEUS is essentially the same as that presented in 1989.

Next Dr. Zoback noted that there are relatively uniform stress orientations across many complex geologic boundaries. He emphasized that intraplate earthquakes resulting from the contemporary stress field are acting on pre-existing faults. No evidence has been found for localized sources of stress in intraplate seismic zones such as New Madrid and Charleston. Dr. Zoback continued his talk by stating that several hypotheses considered in the mid-1980s for identifying seismic source zones are no longer valid. These hypotheses include reactivation of Triassic basin bounding faults and low-angle normal faulting in the Appalachian decollement, which appears unlikely because of the depths of earthquakes beneath the decollement and other factors. Faults slip in response to regional stress, thus the greatly improved stress orientation and relative magnitude databases improve the geologic bases for zonation. Dr. Zoback noted that where good data are available (e.g., in Japan), a remarkable correlation is apparent between maximum horizontal stress and strain, indicating that intraplate deformation is occurring in a coherent way. A key

question about the New Madrid region is how to reconcile the fast Holocene rate of deformation with the extremely slow Cenozoic rate. Also, he stated that we now understand some of the real physical bounds on rates of deformation and other processes, and these data are helpful for defining source zone boundaries.

Following Dr. Zoback's talk the group discussed some of the data from studies in various regions of the EUS and how to explain the indicated stresses. Aspects of the data sets, including data quality, were discussed. The availability of industry data was discussed. The discussion continued about the degree to which rocks are close to being in a breaking state. Dr. Zoback noted that in general, rocks in the EUS are close to breaking and will respond to driving stress; what distinguishes an active area from a craton is not the state of stress in the brittle crust (even when rocks are near failure) but the strain rate. He stated that cratons are characterized by cold temperatures and low strain; in areas of higher heat flow, earthquakes occur more frequently. He also noted that when rocks in the upper crust creep, they are not at the state of brittle failure; the crystalline basement below, however, will likely be brittle.

Dr. Andrew Newman (Georgia Institute of Technology) spoke next with a talk titled "The State of Strain in the Eastern US: Can We See It?" His talk focused on strain fields in the EUS and he stated that GPS data is the best way to obtain strain information. He noted that because a significant amount of time is involved in processing GPS databases, differences can arise; recently, however, more stable results are being obtained. Since GPS data are derivative, he prefers to use the term "velocity field" when discussing strain. He noted that high strain rates do not necessarily equal high seismic hazard, as strain may be a result of discontinuity or poor data. He discussed rigid body motion of a plate on a sphere, the residual GPS velocity field for North America when plate motions are removed, and a model for glacial unloading of North America. No significant strain fields are recognized in the EUS except for glacial rebound areas.

To provide contrast Dr. Newman showed a map of the Chinese GPS field and stated that China has a large range of velocities and transitions across structural boundaries. He compared the strain rates between China and North America. He noted the strain localization indicated around the New Madrid seismic zone. He also stated, however, that geologic maps indicate the Eastern coastal plain has poor bedrock coupling, thus GPS instruments may not be firmly attached to bedrock and may not reflect tectonic motion. Since the New Madrid zone is very close to the Eastern coastal plain boundary, there could be some inaccuracies in the strain measurements. He noted that results of GPS campaigns in 1991, 1993, and 1997 showed no discernable motion (<2.4 mm/yr) in the New Madrid area. He compared velocity information with what is known from paleoseismic data and found that these data sets are consistent. Recently collected GPS data indicate rapid convergence is occurring at two sites near Reelfoot Lake. Dr. Newman checked and replotted these data. He believes that some New Madrid aftershocks are still occurring, and he identified different strain results from instruments at varying distances from the linear trend of seismicity. The apparent differences, however, may also be a result of instruments that are not all located on a homogenous medium. In his concluding remarks he stated that it is better to discuss bulk velocity fields rather than strain rates and that no large-scale tectonic deformation is yet observable in the EUS. Then he asked a final question of the workshop group: will we ever observe Chinese-style tectonic deformation in the EUS?

The group discussed this question and strain information for the EUS. Plate movement in China was discussed; it is not clear if some blocks are rigid. The extremely low strain rates in the EUS

(10^{-7} /yr) were also considered. It was noted that Holocene strain rates have been very high, but the Cenozoic rate overall is low. It is possible that we are currently in an earthquake cluster, but GPS data are not adequate to resolve this question. The limited amount of information available on the pre-1811/1812 earthquakes in the New Madrid area was discussed. Limitations inherent in available data sets, including the short time period in which GPS measurements have been made in the New Madrid area and gathering paleoliquefaction data in the soft sediment of the Mississippi Basin embayment, were discussed.

After a short break, two speakers gave presentations on paleoliquefaction in the CEUS. Before these speakers began, Dr. Ross Hartleb (WLA) gave a brief introduction about paleoliquefaction data sets, which are fundamentally important for assessing seismic hazards in the CEUS. Past large or moderate earthquakes can be identified by paleoliquefaction information, but we also need to answer questions about where, when, how often, and how large these events are. Paleoliquefaction data are difficult to correlate across space and time. Also, it is difficult to identify if these features were associated with one large event or multiple moderate events, and whether or not they were seismically induced. He noted that a comprehensive database of paleoliquefaction information is currently not available but developing such a database is a goal of this project.

Mr. Steve Obermeier (USGS, retired) gave the first talk, beginning by briefly describing his background, which includes significant geotechnical engineering experience. He gave a short overview of paleoliquefaction studies, noting that it is not known what controls the abundance of features so it is necessary to look at many miles of exposures. When he begins a study in a new area, he identifies localities where the water table is shallow and susceptible deposits are present, then he concentrates on examining exposures. He described why paleoliquefaction studies are useful and gave an overview of factors involved in conducting studies. He always begins with an air photo study to identify the features to be field-checked. Many streams are ideal for study, as extensive exposures are needed because features can be 1,000 feet or more apart. Mr. Obermeier stated that the New Madrid area is in an optimal setting for observing paleoliquefaction because of the high water table and a continuous Holocene sedimentary record. The Wabash Valley is a close second, but conditions there are more problematic. The principal questions to be answered in making interpretations include liquefaction susceptibility (based on factors such as grain size, packing, cementation, and thickness of units), density of sands as reflected by blow counts, depth to water table, age of sediments, and an assessment as to whether or not deformation is of seismic liquefaction origin. The experience level of the investigator is also important. Mr. Obermeier noted the optimal conditions for liquefaction, including a water table depth of 0 to a few meters, and then described techniques for assessing ages of sediments. Finally, he noted that artesian conditions, thrown trees, and chemical weathering can all result in features that look similar to paleoliquefaction.

Mr. Obermeier continued by discussing assessments of magnitude and showed a map with the extent of liquefaction features associated with large prehistoric earthquakes in the Wabash Valley region. Based on the severity and areal extent of liquefaction associated with the New Madrid earthquakes, he believes they had magnitudes in the high 7 range. He concluded his talk by describing five regions in the CEUS where he has worked and suggesting areas where additional information could be collected.

A second talk on paleoliquefaction was given by Dr. Martitia (Tish) Tuttle (M. Tuttle and Associates), who focused on data and databases. She acknowledged Dr. Kathy Tucker (CERI) and Dr. Buddy Schweig (USGS), who contributed to the work described in her presentation. She began by showing a map of locations in the CEUS where liquefaction studies have been conducted, identifying whether or not features were found and which sites had features that were equivocal. She described how she began developing a paleoliquefaction database with very limited experience and that the lessons learned will be of benefit to the CEUS SSC project. A database must be designed after considering how data will be used, queried, and displayed, both currently and in the future. She showed the process of converting data in an Excel spreadsheet to ArcGIS data and ArcMap plots. She also described work done in the New Madrid area, showing a map with estimates of sediment ages and the thickness of sandblows.

Next Dr. Tuttle described an archaeological site with an associated sand blow for which a well-constrained age could be determined using radiocarbon dating and artifact analysis. She described another area in which well-constrained ages of numerous large and broadly distributed sand blows allowed recognition of two events in 1,200 years. Next she showed example map queries by location, attribute, thickness, and age. She provided a list of data fields recommended to be included in a database. She concluded her talk with a list of lessons learned. She emphasized that it is important to carefully consider how to query and use data and that a uniform identification convention should be used for locality names. Her concluding statement was that paleoseismology can provide ground truth for seismic hazard assessments.

The group discussed preservation patterns of paleoliquefaction features in the geologic record and uncertainties associated with interpretations. Dr. Tuttle stated that for some features, geologic evidence including weathering patterns and fining upwards sedimentary sequences can clearly indicate a hiatus in deposition and allow separate events to be resolved within a few months.

Following a lunch break, Mr. Salomone asked the resource experts to send their lists of references to lawrence.salomone@srs.gov and syms@lettis.com. After this announcement the final session of the workshop, whose topic was the seismicity catalog, commenced; presentations and discussions in the session were led by Dr. Robert Youngs (AMEC Geomatrix). Dr. Youngs gave the first presentation, titled "Development of Earthquake Catalog for Seismic Source Characterization." He began by stating that the catalog would contain events compiled for the period 1600 to 2008 and that event sizes would be defined in terms of moment magnitude. Uncertainties in size and location will be defined for incorporation into a hazard model. The primary sources from which the catalog will be compiled include the EPRI-SOG (1988) catalog; the NCEER-91 revision of EPRI-SOG; the USGS seismic hazards mapping catalog, and the Canadian seismic hazard mapping catalog. Studies for ESP and COL applications in the CEUS will provide useful information, as will special studies of individual earthquake events or regions. Dr. Youngs described the catalog development process in which data from all sources will be summarized for earthquakes larger than magnitude ~3. The compiled information will be reviewed with a team of experts to select preferred values, assign uncertainties, and classify nontectonic events. Dr. Youngs explained the data needs for development of moment magnitude estimates for each event; these include moment magnitude estimates from other catalogs and special studies for instrumentally recorded earthquakes, plus intensity/felt area data for both instrumentally recorded as well as historical earthquakes.

Next, Dr. Youngs presented a series of slides on macroseismic data for the CEUS prepared by Ms. Margaret Hopper (USGS), who was unable to attend the workshop and be a presenter. Her slides provided information on a database of over 150 earthquakes in the CEUS for which intensity data are available. This database will be useful for the CEUS SSC project.

Dr. Youngs concluded his talk by describing the processes planned to identify dependent events within the catalog and to assess catalog completeness. The workshop group then discussed the possible compilation of earthquake focal mechanisms for the project, as these are important for mapping stress. The TI team will discuss how to proceed with this effort.

The next speaker was Dr. Charles Mueller (USGS), who described the approach used to develop the USGS catalog. He stated that a mix of published and well-documented, national-scale source catalogs was used, and he listed many of these catalogs. Objectives for the catalog are to have it be dominated by events from the well-researched NCEER-91 catalog as well as to have the catalog be appropriate for use for PSHA. He described the procedure followed to compile the catalog, including selecting a single record for each earthquake, selecting a preferred magnitude if more than one is reported, and declustering and removing man-made events if they pose no hazard (e.g., mining-related seismicity in Colorado and Utah). Next he displayed various aspects of the data for the portion of the catalog in the CEUS. In his concluding statements he mentioned that improvements were being made in the USGS catalog as a result of better source catalogs, a more reliable update process, and incorporation of uncertainty estimates for magnitude and location of some events. He stated that the catalog prepared as part of the CEUS SSC study will be incorporated into the USGS catalog. Mr. Mueller commented that with additional resources he would like to focus efforts on the incorporation of uncertainty in the catalog.

The next talk, titled “Revising the Earthquake History of the CEUS: Identification of New Events and New Sources of Information,” was given by Mr. Jeff Munsey (Tennessee Valley Authority). In his first slide, Mr. Munsey listed impacts and benefits of updating an earthquake catalog, including providing additional information to define seismic source boundaries; refining activity rates, especially at local scales; increasing temporal and spatial completeness; and improving location and magnitude estimates. He reviewed sources of catalog information for the region surrounding the Tennessee Valley that had become available since the EPRI-SOG catalog was completed, including his own work that resulted in identification of more than 400 events from 1724 to 1927, primarily using historical newspapers available online. He listed the primary online data sources he uses and then briefly described some of the newly identified earthquakes. He also described how he has tracked down felt information and made estimates about earthquake magnitude. He concluded his talk by listing challenges and tasks ahead. These include establishing and recording the basis for existing events, reconciling multiple accounts of dramatic events, and evaluating clues to assess event depths and distances.

The final talk of the session, titled “Earthquake Data for Seismic Hazard Determinations in the Northeastern U.S.,” was given by Professor John E. Ebel (Boston College). He began by listing seismic issues and items to be addressed to update a catalog. He has studied early historic earthquake events (1600s) based on journal entries and accounts of city funds appropriated to repair earthquake-induced damage. He described updates of the Northeastern United States (NEUS) catalog over the past decades, noting that when the NRC eliminated regional seismic network funding in the early 1990s, most seismic stations in the NEUS were lost. Only in the past few years have significant improvements been made, in part due to equipment changes that

have improved both detection capabilities and magnitude determinations. Dr. Ebel discussed the problems of overlap between U.S. and Canadian seismicity catalogs, which result in multiple reports as well as possibly different decisions about whether a particular event has a seismic or nonseismic origin. Epicenter accuracy is better with a denser network, so the NEUS catalog reflects data of varying quality.

Next Dr. Ebel described regional earthquakes in the EUS in the recent past, as this pattern is expected to continue in the future. On average, about six small earthquakes (magnitude ≤ 3.5) are felt in New England each year and this regular, persistent earthquake activity has been observed for more than 25 years. Temporally clustered earthquake activity can also be observed. Dr. Ebel showed a plot of the variations of earthquake activity with time in New England since 1979. He described the 2006-2007 Bar Harbor earthquake sequence that resulted in M 3.4 and M 4.2 events.

Turning to the historical catalog, Dr. Ebel described issues concerning historical NEUS earthquake data, including the need to identify additional events and adequately assess event sizes from detailed historical research. He noted that small aftershocks can help pinpoint the location of a stronger earthquake in the historical record. Following a 1727 earthquake, over 150 aftershocks were felt in two different areas (17 were magnitude ≥ 4) and this information could be used to more accurately locate the epicenter of the main shock. Clusters of small earthquakes may be aftershocks from strong events that occurred hundreds or even thousands of years ago. Unlike the situation in California, there is no baseline level of earthquakes in the NEUS, so it is easier to identify earthquake clusters as aftershocks. Dr. Ebel has developed estimated ages and magnitudes for many events extending back more than 1,000 yrs.

Dr. Ebel concluded his talk with several recommendations. These include extending the catalog to the northeast by acquiring additional available databases and cross-checking duplicate event data; conducting a research program to study magnitudes of instrumental earthquakes in the NEUS; and targeting selected historical events for additional research to better constrain event size and location. In response to discussions with the group, Dr. Ebel noted that the focal mechanisms for most events are consistent with a tectonic origin, although glacial unloading is a possible cause for some. He also stated he believes a Charleston-type earthquake is possible anywhere in the NEUS region, although others question whether the crust could support an event of this magnitude.

Dr. Coppersmith asked for comments and questions from the workshop participants, including the international observers. Participants discussed different areas of seismicity and earthquake events in the CEUS and their relevance in defining source zones.

Dr. Coppersmith then made final remarks about the path forward for the CEUS SSC project. He mentioned the SSHAC implementation project that is under way and how lessons learned from that effort will be implemented in the current project (several participants in the CEUS SSC project are also participants in the SSHAC workshops). He noted the point of contact for the CEUS SSC project: lawrence.salomone@srs.gov, and he showed the task schedule for the project, noting the February 2009 timing for Workshop 2 on Alternative Interpretations. In the months before Workshop 2, many of the activities discussed in Workshop 1 will be under way, including database development and seismicity catalog development. A preliminary SSC model will be developed and used to identify the key alternatives for discussion at Workshop 2. Hazard and sensitivity analyses will be used to evaluate the preliminary SSC model.

Mr. Salomone thanked the international observers for taking the time to attend the workshop, and then he offered his parting comments. He noted that the high level of expertise of the presenters was clearly indicated by the content of their presentations. He expressed his appreciation to all who have made the project and first workshop a success, and who will continue to do so as the project continues. He believes that the CEUS SSC project will ultimately be viewed as a landmark study. He then adjourned the workshop.

REFERENCES

Bernreuter, D.L., J.B. Savy, R.W. Mensing, and J.C. Chen. 1989. "Seismic Hazard Characterization of 69 Nuclear Plant Sites East of the Rocky Mountains," Report NUREG/CR-5250, Vols. 1–8, prepared by Lawrence Livermore National Laboratory for the U.S. Nuclear Regulatory Commission.

Budnitz, R.J.; G. Apostolakis, D.M. Boore, L.S. Cluff, K.J. Coppersmith, C.A. Cornell, and P.A. Morris. 1997. Recommendations for Probabilistic Seismic Hazard Analysis: Guidance on the Uncertainty and Use of Experts, NUREG/CR-6372. Two volumes. U.S. Nuclear Regulatory Commission, Washington, D.C.

Electric Power Research Institute and Seismicity Owners Group (EPRI-SOG), 1988. Seismic Hazard Methodology for the Central and Eastern United States, Technical Report NP-4726-A, Vols. 1–10.

Electric Power Research Institute (EPRI). 2004. CEUS Ground Motion Project Final Report, EPRI Report 1009684, December 2004.

Electric Power Research Institute (EPRI). 2006. Program on Technology Innovation: Truncation of the Lognormal Distribution and Value of the Standard Deviation for Ground Motion Models in the central and Eastern United States, EPRI Report 1013105, Technical Update, February.

WORKSHOP 2: ALTERNATIVE INTERPRETATIONS

February 18–20, 2009

Electric Power Research Institute
3420 Hillview Ave.
Palo Alto, California 94304

The Workshop on Alternative Interpretations was the second in a series of workshops jointly sponsored by the Electric Power Research Institute (EPRI) Advanced Nuclear Technology (ANT) Program, U.S. Nuclear Regulatory Commission, and the U.S. Department of Energy (DOE) in support of the Central and Eastern U.S. Seismic Source Characterization (CEUS SSC) for Nuclear Facilities Project. The objective of the CEUS SSC is to develop a comprehensive and up-to-date SSC for a probabilistic seismic hazard analysis (PSHA) that is appropriate for use at any site in the CEUS. The Technical Integration (TI) team and TI Staff are charged with developing a seismic source model that captures the knowledge and uncertainties within the larger informed technical community. The goals of this workshop were to (1) review the project Senior Seismic Hazard Analysis Committee (SSHAC) Level 3 methodology, ground rules, expert roles, and peer review processes; (2) provide an opportunity for the TI team and TI Staff to understand proponent views regarding important technical issues; (3) discuss the range of alternative views and uncertainties within the larger technical community; and (4) discuss the path forward for the CEUS SSC project. The goals were accomplished by a series of presentations and discussions designed to provide the TI team and TI Staff with the information it needs to develop a preliminary seismic source characterization model.

DAY 1–WEDNESDAY, FEBRUARY 18

Workshop participants were welcomed by Mr. Jeffrey Hamel, the EPRI ANT Project Manager for the CEUS SSC project, who also reviewed some workshop logistics. Mr. Lawrence Salomone, Project Manager for the CEUS SSC project, then welcomed workshop participants and thanked them for attending. He reviewed some of the project logistics. Next Mr. Salomone reviewed the project goals: (1) replace the previous EPRI Seismicity Owners Group (EPRI-SOG, 1988) and Lawrence Livermore National Laboratory (LLNL; Bernreuter et al., 1989) seismic hazard studies that were conducted in the 1980s; (2) capture the knowledge and uncertainties of the informed scientific community using the SSHAC process, and (3) present a new CEUS SSC model to the Nuclear Regulatory Commission, DOE, and others for review. Transparency of the project process is a key goal. He reviewed the management chart for the project and showed samples of the data sets available for the study region. Mr. Salomone summarized the project milestones, including the preliminary SSC model feedback to be reviewed at Workshop 3, which is scheduled to be held August 25–26, 2009. In his concluding remarks he noted that the project is on track to meet the target completion date in 2010.

Dr. Kevin Coppersmith, the lead of the TI team, then welcomed the workshop participants. His talk focused on the goals of the workshop and the ground rules. Dr. Coppersmith began by reviewing aspects of the SSHAC project, which is documented in NUREG/CR-6372 (Budnitz et al., 1997) and will be implemented in the CEUS project. He reviewed the SSHAC basic principles for a PSHA, key attributes of the process, and expert roles, with their application to the current workshop. He indicated that the focus of the workshop would be on providing information that the TI team can use in developing the preliminary SSC model, which will be

completed prior to the third workshop. As such, the workshop would be structured to allow the TI team maximum opportunity to have their questions answered by the resource experts making the presentation. He reviewed the CEUS SSC task schedule and the process to be followed for Workshop 2. Prior to the workshop, key questions and issues were posed to the presenters to address in their talks (see Table 1); the knowledge and uncertainties of these members of the larger informed technical community are what the TI team is charged with capturing.

The first of the talks was given by Dr. Stephane Mazzotti of the Geological Survey of Canada. His talk was titled “Strain (and Stress) Constraints on Seismicity in the St. Lawrence Valley.” Dr. Mazzotti began by discussing the distribution of earthquakes and the definition of seismic zones based on concentrations of earthquakes in regional “hot spots,” in this case, the Charlevoix and lower St. Lawrence Seaway regions. He noted that earthquakes are concentrated along Iapetus rifted margins and grabens that formed about 600 million years ago (Ma). He also noted that seismic moment and deformation rates for eastern Canada can be based on two alternative models for earthquake distribution: (1) earthquake statistics in historical source zones, which indicate a few high-strain zones and relative motion of 0.0 to 2.5 millimeters per year (mm/yr); and (2) geological source zones, which have no high-strain zone and motion of only 0.0 to 0.5 mm/yr. Dr. Mazzotti reviewed GPS (global positioning systems) observations from regional networks and showed the vertical and horizontal velocities obtained from this data, noting that there is very good agreement between continuous data (3 to 6 years) and campaign data (7 to 12 years). Next he discussed preliminary results of GPS measurements in the Charlevoix and lower St. Lawrence seismic zones. This data shows very low strain rates overall, as expected, but east-west horizontal strain rates appear to be higher in high-seismicity zones. Within these zones, the recurrence rates derived from the observed seismicity are in good agreement with rates derived from geodetic data translated into seismic moment rates. Current strain rates and seismicity are not steady-state on a million-year time scale, inasmuch as the rates imply cumulative deformation over million-year time scales that are not observed. Within a resolution of approximately 1 mm/yr at 95 percent, it is not possible to discriminate between alternative models.

Next Dr. Mazzotti described the potential role of glacial isostatic adjustment (GIA) processes and models. GIA is very small and it is debatable as to whether or not it is associated with earthquakes. Dr. Mazzotti’s work shows there may be a significant role of GIA and local weak rheology in seismicity for some seismic zones, as indicated in the Charlevoix and lower St. Lawrence regions. In his conclusions, Dr. Mazzotti mentioned that the observed seismic strain signal (<1 mm/yr) is at the limit of GPS precision and that GPS data cannot yet represent earthquake hazard over the next 500 to 5,000 years. He believes GPS strain rates should be used in combination with other data sets, including rheology, geology, and historical seismicity, to define seismic source zones and rates, but only once a robust integrative geodynamic model has been developed.

The following talk was given by Dr. John Ebel of Boston College, who addressed “ M_{\max} for Eastern North America: An Examination of the 1663 Charlevoix Earthquake.” Dr. Ebel began by stating that many of the small earthquakes in the northeastern part of North America may be aftershocks of strong earthquakes that took place hundreds or even thousands of years ago. To provide a frame of reference, he first showed examples of seismicity in California, which indicate that aftershock zones can be active for decades after a main shock. Next he described the methods he used to estimate the magnitude of the 1663 Charlevoix earthquake. This event was

felt strongly in Canada, with major ground deformations in what is today recognized as the Charlevoix seismic zone. Dr. Ebel obtained data from damage reports in Boston and Roxbury in Massachusetts that were possibly associated with this earthquake, and he used the data to estimate the intensity and magnitude of the 1663 event. (The Charlevoix seismic zone is between 560 and 640 kilometers [km] from Boston.) He also compared the reported earthquake effects with isoseismal maps from the 1811–1812 New Madrid earthquakes and estimated the earthquake magnitude from the length of the “aftershock” zone that is currently active in the Charlevoix region. The best estimate of the moment magnitude (M_w) of the 1663 Charlevoix earthquake from his study is $M_w \sim 7.3\text{--}7.5$.

Next, Dr. Ebel began speculation on the characteristics of large earthquake events in stable continental regions. He believes that larger aftershocks concentrate at the edges of an earlier earthquake rupture due to stress concentration at the crack tip. This appears to be the pattern at Charlevoix, where recently occurring $M 4$ events have been located at the edges of the 1663 event. Dr. Ebel also speculated on recurrence rates of $M > \sim 7$ for the CEUS and eastern North America. The observed rate of $M > \sim 7$ earthquakes is greater than expected from extrapolations from the smaller earthquakes recorded in these regions. If small events reflect aftershocks of larger events, then the rate of $M > \sim 7$ earthquakes during the past few thousand years may be approximately two to three times greater than predicted by recurrence relationships that extrapolate the number of large events from small events.

The next presenter was Dr. Alan Kafka of Boston College, who spoke on “Use of Seismicity to Define Seismic Sources: Application to Eastern North America.” Dr. Kafka discussed how “cellular seismology” can be used to delineate future seismicity based on what is known about past seismicity. Empirical analysis of earthquakes is based on historical and instrumental earthquake history, but this information does not address causes of earthquakes and whether analysis of what is currently observed will show persistence over long time scales. Is the “tendency for future earthquakes to occur near past earthquakes” a real, measurable, physical phenomenon? Dr. Kafka has investigated this question and uses a simple method of analysis based on separating observed seismicity data into two parts before and after some point in time. He then looks at the percentage of events after that time (future events) that fall within zones defined by various radii from earthquakes prior to that time (past events). As the radii increase, of course, the probability that a future event will fall within the zone for past events increases even for a random process. However, Dr. Kafka has found that the probability increases more rapidly than a random process, suggesting that future events are more likely to occur near past events. He has looked at many regions in the United States and worldwide for these patterns. He has found that future large earthquakes in the CEUS have about 86 percent probability of occurring within 36 km of past earthquakes. He has compared the accuracy of cellular seismicity to other methods, including rate-based forecasts (percentage of hits vs. percentage of defined mapped areas). In general, he finds that for his method, greater than 60 percent hits are obtained (whereas a random process would be about 30 percent). In his conclusions, Dr. Kafka noted that he has not found any other method of forecasting locations of future earthquakes that performs better than cellular seismology.

Following a lunch break, Dr. John Adams of Natural Resources Canada discussed the Canadian seismic hazard models in a talk titled “Eastern Canadian Experience with Geological Source Zones and M_{\max} .” He briefly reviewed aspects of the third- and fourth-generation seismic hazard models developed for Canada. He believes that smoothed seismicity is interesting but not

sufficient for assessing future hazard levels. As an example, he cited the 1988 M 5.9 Saguenay earthquake in an area that had no prior earthquake activity of $M_N > 3$ for more than 50 years prior. He believes geological sources provide essential information, and noted that geological sources were proposed in Canada as early as 1983 for the passive continental margin. For the United States, he noted that Russell Wheeler did good work on geological sources in the early 1990s, but these were not explicitly incorporated in USGS hazard maps. Dr. Adams described the association of large earthquakes ($M \geq 7$) with rifted margins, noting the 1933 Baffin Bay and 1929 Grand Banks events, which occurred on large through-going faults that were reactivated in the Mesozoic. He then showed a map of seismic source zones in eastern Canada and into the eastern United States and described how various zones were modeled, based on both geologic history (ancient rifted margins and failed rift arms) and seismicity. He noted geological structures/source zones form a way of “filling in” between historical earthquake clusters.

The eastern Canadian experience with maximum magnitude (M_{\max}) was described in the next part of Dr. Adams’s talk. He described how the M_{\max} estimates in previous generations of seismic hazard maps had been exceeded by significant earthquakes that occurred in Canada between 1982 and 2001. Accordingly, M_{\max} estimates chosen for the fourth-generation studies were larger and based on continent-scale and global analogs, using methods similar to the EPRI Stable Continental Region (Johnston et al., 1994) study. A study of M_{\max} in Australia was described as an analog for the CEUS and Canada. M_{\max} choices for eastern Canada were also described, including weights assigned to a range of observed M_{\max} for different tectonic environments; these included Mesozoic rifted margins, Paleozoic rifted margins, and plate interiors. In his concluding remarks, Dr. Adams stated that earthquakes of $M_{\max} \sim M_w 7.0$ could not be ruled out anywhere, although probabilities will be very low in many stable continental regions. Phanerozoic rifted crust typically contains enough long and deep faults (or fault systems) that $M_{\max} \sim 8.0 M_w$ seems plausible. In his final slides, Dr. Adams showed how Canadian seismic source zones can be extended into the CEUS. Extensions of Canadian source zones could be postulated to extend into the US, such as the Atlantic Rifted Zone extended to Charleston, South Carolina; the Iapetan Rifted Margin extending to Giles County Virginia and the Eastern Tennessee seismic zone.

Dr. Coppersmith announced that the next scheduled speaker, Dr. Leonardo (Nano) Seeber (Lamont-Doherty Earth Observatory) was unable to attend the workshop. A talk originally scheduled for Day 3 of the workshop was substituted.

Dr. Frank Pazzaglia of Lehigh University presented a talk titled “Approaches Used to Identify and Evaluate Neotectonic Features in Appalachian Piedmont/Coastal Plain Setting.” The focus of the talk was the geology and geomorphology of the passive margin in the Atlantic states. Dr. Pazzaglia addressed the influence of broad regional flexure of the Atlantic margin on current patterns of seismicity, noting that there is spatial overlap in topography, active river incision, and seismicity. He described how topography and rivers respond to rock uplift, rock hardness, and erosion. He showed maps of many of the rivers along the Atlantic coast and described different geographic areas and their association with seismic activity. He discussed the Fall Zone and its location on the classic passive margin, emphasizing that the Coastal Plain is narrow and no waterways are navigable, which doesn’t make logical sense for that type of setting. Coastal margin topography suggest that this area has been undergoing uplift, thus leading to convex upward longitudinal profiles for the rivers. He suggested that the Appalachians might be more tectonically active than previously thought. For example, New England has been uplifted since

the Miocene, and over time, the Hudson River has moved the sediments of the former Coastal Plain to the south. Dr. Pazzaglia described the stratigraphy along the edges of Chesapeake Bay. He provided evidence for faults up and down the coastal margin that are concentrated around the Fall Zone.

Dr. Pazzaglia believes that future earthquakes could occur in areas with low seismicity that also have apparent fault structures. He showed nick points along the Fall Zone, noting that it is clear that a base-level fall has occurred since the Miocene, although within this 10-million-year (m.y.) period we cannot tell if this occurred early or late. It is now known that the Miocene sea level was about the same as at present, so the Piedmont is clearly rising. Faults located coincident with the Fall Zone would be useful targets for detailed studies to see if river anomalies are related to tectonics. Dr. Pazzaglia continued by discussing flexural effects from glaciations and ice unloading during the Quaternary. Finally, he described the Chesapeake Bay impact structure emplaced approximately 35.4 Ma. Rivers drained into the low area created by the impact, and pulses of subsidence are apparent. Dr. Pazzaglia believes that this impact structure could be a causative structure for some of the seismicity in the eastern United States.

Dr. William Thomas of the University of Kentucky gave the next talk, titled “Ouachita Sub-Detachment Structures.” He described the geology of the CEUS at 250 Ma, showing major structural features based on data from wells and seismic reflection lines. He indicated the leading edge of aulacogen (tectonic trough) locations for the Alabama-Oklahoma transform and Ouachita thrust sheets. He discussed the stratigraphy and timing of activity of faults at about 308 Ma, showing the Mississippi embayment and other major structural features in palinspastic restorations. He also noted that episodes of movement were coincident with Iapetan rifting and then thrusting. He showed several seismic reflection profiles and cross sections that indicated stratigraphy and structure. The Ouachita thrust belt was compared with the Appalachian thrust belt, and different styles of deformation were described. The Ouachita accretionary prism was emplaced about 310 to 307 Ma, and to the east, the Suwannee terrane was emplaced about 306 to 300 Ma. Reconstructions give information about the timing of faulting. Dr. Thomas next discussed the Southern Oklahoma fault system, including the Wichita uplift, which is located above a leaky transform fault. In his conclusion, he noted that major structures were formed in the CEUS about 550 to 530 Ma and 310 to 300 Ma (late Paleozoic); some structures were reactivated in 245 Ma.

After a short break, Dr. James Drahovzal of the University of Kentucky gave a talk titled “Rifts in the Midcontinent: East Continent Rift Basin, Rough Creek Graben and the Rome Trough.” In his talk he discussed these structures and the associated Grenville and Hoosier thrust belts, along with the Fort Wayne rift, which is coincident with the Anna seismic zone. Dr. Drahovzal began by showing the classic CEUS “basement” bedrock geology and then noted that more complex stratigraphy and structure have been constructed from well data. Sedimentary and volcanic rocks underlie many areas of granite and other igneous rocks in the midcontinent. Dr. Drahovzal described drillhole and seismic data for portions of Ohio, Kentucky, and Indiana; seismic data indicates layered reflectors within sequences of as much as 20,000 to 25,000 feet of Mesoproterozoic rocks that are folded and faulted. He provided a preliminary Proterozoic chronology that indicates alternating episodes of extension and compression in the midcontinent. Next he described the sequence of geologic events that formed structures within the East Continent rift basin, including the aseismic Rough Creek graben and Rome trough. Both of the latter structures are likely to have experienced Mesozoic reactivation but are currently aseismic.

The Rome trough is a symmetrical Cambrian rift basin that contains three major fault zone boundaries. Several reactivations since the Paleozoic are recognized for this structure. The Rough Creek graben in western Kentucky also shows evidence of Mesozoic reactivation, with Precambrian rock offsets of up to 17,000 feet. Dr. Drahovzal described the east continent gravity high and the relationship of this structure to the Rome trough and East Tennessee seismic zone. The 1980 M 5.2 Sharpsburg earthquake was located close to the East Continent gravity high.

The next talk was by Dr. John McBride of Brigham Young University, who discussed “Geophysical Characterization of Faulting and Folding in the Illinois Basin and Relation to Seismicity.” Seismic reflection data is used to understand fault deformation and seismicity in an area of the midcontinent centered on the Illinois Basin and the New Madrid seismic zone (NMSZ). Dr. McBride noted that reactivation of faults is not always clear, even in a well-constrained area like California, so fault reactivation is even more difficult to recognize in the Midwest. However, a large amount of geophysical data is available for the Illinois basin, particularly seismic profile data, because of oil production in the state that peaked in 1937. Dr. McBride showed a map displaying a CEUS earthquake catalog and questioned if an area showing little seismicity is real or an artifact of limited instrumental coverage. Next he showed a map of major structures in the southern Illinois basin and described some of these, including the La Salle deformation belt. He reviewed information for recent earthquakes in the region and showed a seismic reflection profile of the La Salle anticline. A 1987 earthquake and aftershocks associated with a frontal thrust, plus evidence of paleoliquefaction in the region, provide evidence of this anticline as a possible seismic source zone.

Next Dr. McBride described several possibly seismogenic structural features in the Illinois basin. The Fairfield subbasin (a deep part of the Illinois basin) includes a zone of locally more intense faulting, in which three fault zones can be mapped from seismic reflection profiles. Earthquakes that occurred in 1974 and 1987 were within the interpreted zone of rifting beneath the Fairfield subbasin. Dr. McBride showed the Wabash Valley fault system as imaged on a seismic profile. A 1968 earthquake event occurred in this region and may possibly have originated on a blind thrust fault. The Commerce geophysical lineament corresponds locally to disrupted geologic structures that may be seismogenic. The Du Quoin monocline complex was described. This monocline and the overlying Centralia fault zone may be an overlooked possible seismic source. Folds in this area provide some evidence for reactivation along an older reverse fault. The Cottage Grove fault system corresponds to a major crustal boundary, although the seismicity rate in the area appears to be low. The Fluorspar Area fault complex trends towards the New Madrid seismic zone; there is complexity in Fluorspar Area structures and evidence for Tertiary displacements. In his conclusions, Dr. McBride noted that the area where the La Salle anticline and Wabash Valley fault systems meet may have a high potential for fault reactivation.

After this talk, Dr. Coppersmith invited comments from observers. The participants discussed improvements in data available for smaller earthquakes, including better-constrained focal mechanisms. The group listed Paleozoic rifts that have not been reactivated. These include the Birmingham graben and the southern part of the Mississippi graben; the Ouachita graben also may not have been reactivated, but the underlying rocks are too old to indicate this history. At the conclusion of the discussions, the meeting was adjourned for the day.

DAY 2—THURSDAY, FEBRUARY 19

Dr. Coppersmith welcomed the group to the second day of the workshop. The first talk was given by Dr. Roy Van Arsdale (University of Memphis) on “Quaternary Deformation within the Reelfoot Rift, Rome Trough, and Wabash Valley Fault System.” Dr. Van Arsdale began by showing the location of the Mississippi embayment and its relationship to the New Madrid seismic zone (NMSZ); earthquakes in the NMSZ define faults in the region. He showed a cross section of the Reelfoot fault with “kink bands” or back thrusts, as well as photos of trenches on the Reelfoot scarp trench. The recurrence interval for earthquakes is estimated to be approximately 500 years. He noted that the trench data is in good agreement with the regional earthquake chronology developed from paleoliquefaction features.

Dr. Van Arsdale described displacement history and slip rate on the Reelfoot fault from the late Cretaceous to the present. The slip rate increased dramatically in the Holocene, indicating an active period of fault history, but the end of this period may be near. Seismic reflection lines indicate deep basement faults with as much as 3 km displacement. Trenches opened above the seismic reflection lines show faults with transpressive right-lateral strike-slip movement. Right-lateral shear across the Reelfoot rift is responsible for the NMSZ earthquakes at the northern end of the rift. Rift margin faults are “big players” in the picture. Dr. Van Arsdale described features in the Shelby County and Memphis region, where liquefaction deposits (sand blows) and a broad fold forming an anticline are present. The anticline appears to be a tectonic feature formed about 400 a.d.

Dr. Van Arsdale then described work he did many years ago in the Rome trough near the area of the 1980 Sharpsburg earthquake, where he focused on the Kentucky River fault system. He showed the log of a trench excavated in a terrace that exhibited folding and an apparent shear zone. He estimated the timing of fault movement as within the past 5 m.y. Next he described the Hovey Lake fault in the Wabash Valley fault system and the Stull trench site in Union County, Kentucky. He concluded his talk by showing a schematic of fault scarp evolution based on the information obtained from the trench.

Mr. Robert Givler of William Lettis & Associates, Inc., gave the next talk, which was co-authored with Mr. John Baldwin. The title of the talk was “Commerce Geophysical Lineament and Northwestern Margin of the New Madrid Seismic Zone.” The Commerce geophysical lineament (CGL) is a 400- to 600-km-long feature that exhibits Quaternary strike-slip and normal faulting along a 75 to 120 km portion of its length in the New Madrid region. Mr. Givler described the regional geologic setting for the CGL and the detailed studies conducted at Qulin Ridge. This locality contains Late Wisconsin glacial outwash deposits; seismic profiles show Quaternary offset along a fault, and four paleoliquefaction events have been identified. Next Mr. Givler described the Holly Ridge locality associated with the Idalia Hills fault. Seismic reflection profiles show displacement of Quaternary deposits that project upwards and correlate with surface geomorphic features. Trench data from the Bloomfield Hills locality on the Idalia Hills fault indicate two poorly constrained faulting events. Mr. Givler described trench studies for localities on the Commerce fault and the Penitentiary fault. The Benton Hills locality is on the Commerce fault, where strike-slip faulting is recognized for four late Quaternary events. The Quaternary-active Penitentiary fault is located in the Cache River valley. The Penitentiary fault is a step-over from the Commerce fault and has a prominent east-facing scarp. Seismic lines in the area were used to further test the hypothesis that the Penitentiary fault is a seismic source; these

data indicate multiple faults disrupting Pleistocene and possible early Holocene deposits. A fault segment 75 to 120 km in length is recognized in southeast Missouri and southern Illinois along the Commerce fault. A weak alignment of microseismicity is associated with this fault. Based on all of this data, the CGL appears to have been active into the early Holocene. The fault has long earthquake recurrence intervals of 5 to 10 thousand years and possibly episodic activity.

Next, Dr. Randy Cox of the University of Memphis gave a talk titled "Some Mississippi Valley Holocene Faulting and Liquefaction beyond the New Madrid Seismic Zone." He began by discussing southeast Reelfoot rift margin surface faulting. He showed a map of the topographic lineament of the southeast rift margin and the locations of trenches excavated to study this feature. He described the Porter Gap trench site where a late Holocene earthquake was recognized, showing the trench logs and a shallow seismic reflection line. Structural relief and topographic relief are consistent with faulting. Evidence of faulting in the trenches indicated an event with >4 meters (m) vertical displacement and horizontal (strike-slip event) displacement of about 8 to 15 m. Earlier events of approximately equal magnitude were also observed in early Holocene deposits. Next Dr. Cox described a newly recognized sand blow field in the southern Mississippi embayment area of northeastern Louisiana, south of the New Madrid area, which was identified from an aerial photo survey. He has delineated five separate fields containing clusters of sand blows. A trench log across an area of sand blows, and photographs of sand blows were shown. The earthquakes that caused the liquefaction are estimated to be $M > 6$ on the basis of the minimum radii of the fields and on cone penetration tests in the region. Multiple events are indicated, and based on limited data, the earthquake recurrence rate is roughly 1,000 to 2,000 years. The earthquake events that Dr. Cox recognizes can be correlated with multiple regional events that affected more than one of his five zones, or they could be related to local earthquakes that are separate for each zone.

He concluded his talk by describing his studies of the Saline River fault system in the craton margin area of the Alabama-Oklahoma transform. Seismicity data is sparse in this region but he has examined many exposures containing features that suggest deformation. Seismic lines show Triassic grabens and flower structures that extend upward into Cenozoic deposits. The trenches that have been excavated show faulting in mid-Pleistocene deposits; overlying Holocene deposits may be warped. Paleoliquefaction features of dense sand blows have been recognized in the area, indicating multiple earthquake events in the late Pleistocene through the late Holocene. Dr. Cox believes the paleoliquefaction features were caused by local earthquakes and are not related to far-field events such as those in the New Madrid area to the north.

After a break, Dr. Russell Green of Virginia Polytechnic Institute gave a talk titled "Paleoliquefaction Interpretation of the Vincennes Earthquake, Wabash Valley Seismic Zone." Dr. Green began his talk by reviewing liquefaction phenomena. He showed photographs of classic liquefaction phenomena as well as video footage of liquefaction phenomena resulting from the 1964 Niigata, Japan, earthquake. He described a "simplified" liquefaction evaluation procedure to assess cyclic resistance or the capacity of a soil to resist liquefaction. He described combinations of conditions that can be used to assess when liquefaction will or will not occur, related to peak ground acceleration and other factors. His work has been focused on the Wabash Valley seismic zone and specifically, the effects of the Vincennes earthquake that occurred approximately 6,100 years BP. Dr. Green has estimated the probable M_{max} of this earthquake by using plots of the severity of liquefaction with distance from the epicenter. The method he has

developed to assess magnitude from data at various field sites incorporates an assessment of overall uncertainty.

Dr. Green discussed constraints on seismic sources, noting that the dimensions of a source can be estimated by contouring maximum dike width. Distinguishing between a small local earthquake event vs. a large distant earthquake event is difficult. Next he discussed sources of uncertainty, including ground-motion predictive relationships and field interpretations. To properly assess the uncertainties and their influence on a back-calculated M_{max} , input is needed from geologists, geotechnical engineers, and seismologists, depending on the information to be evaluated. Dr. Green then reviewed ground-motion attenuation relationship information for the CEUS and described alternative presentations of site amplification data. Based on his analyses, the Vincennes earthquake may have been an M 7.3–7.5 event, with the epicenter located within an area having a defined radius of about 160 km.

In a related talk, Dr. Scott Olson of the University of Illinois at Urbana-Champaign described a geotechnical approach to evaluate the strength of shaking associated with liquefaction phenomenon. His talk was titled “Quantifying Uncertainties in Paleoliquefaction Studies.” Dr. Olson began by reviewing existing methods for paleoliquefaction back-analysis, including the cyclic stress method, the magnitude bound method, and several other approaches. The cyclic stress method is suitable for evaluating a lower bound for a best estimate of an earthquake magnitude. Dr. Olson noted the variety in worldwide estimates of different magnitude bounds, which are a function of source characteristics, transmission characteristics (attenuation and site effects), and regional soil liquefaction susceptibility. To develop a magnitude bound for the CEUS, he examined historical earthquakes having $M > \sim 5$ and the liquefaction features associated with these events. He compiled the best estimates of magnitudes made by seismologists and then looked for the farthest-distance liquefaction features that could be associated with a specific earthquake. From this data he developed a CEUS magnitude bound, in which M 5.5 is the minimum magnitude for liquefaction at close-in locations; increasingly larger-magnitude events can trigger liquefaction at greater distances.

Sources of uncertainties in liquefaction susceptibility, field observations, seismicity, in situ testing techniques, and the magnitude bound approach were described. Then, Dr. Olson discussed aging, the process by which soils develop a structure that results in improved soil properties (e.g., shear strength); he noted that there may not be a need to make any correction for aging in many cases. He described characteristics of liquefaction severity (based on size of liquefaction features), and the factors of safety for different levels of liquefaction severity. A better tool than factor of safety, however, is a liquefaction potential index that incorporates stratigraphy, especially the depth and thickness of potentially liquefiable layers. Dr. Olson went on to discuss failure mechanisms and their relationship to liquefaction resistance. He listed a number of sources of uncertainty in field data, including depth of groundwater at the time of an earthquake, and variability of geologic settings. He then illustrated his approach by using data on the Vincennes earthquake. For this event he has calculated M_w 7.5 \pm 0.3. He noted that the Wabash Valley work was based on the availability of abundant geotechnical field data; by contrast, few sites in the New Madrid seismic zone have sufficient geotechnical data for conducting a good back-analysis of magnitude.

Following a lunch break, the first talk of the afternoon session was given by Dr. Eric Calais of Purdue University, who talked about geodetic interpretations of New Madrid rates. Dr. Calais

began by describing the notion of a steady-state “elastic rebound” model, in which geodesy and paleoseismology should agree. This model works particularly well for plate boundary faults, as present-day strain has predictive power. Current GPS measurements indicate an upper-bound movement of 0.02 mm/yr at New Madrid. Dr. Calais also showed velocities measured at about 500 sites in North America with respect to a constant reference frame. Velocity analyses on deformation east of the Rocky Mountains have indicated that most measured velocities are not significant at a 95 percent confidence level. However, patterns in velocities, especially radial patterns, are apparent. Residual velocities of 0.6 mm/yr have been measured in the CEUS.

Next, Dr. Calais showed residual velocities for areas worldwide, including Europe and Australia, where these velocities are about 0.4 mm/yr. Velocity results have been stable over the past 5 years, so there can be high confidence in the measured rates. Available information indicates that velocities of 0.2 to 0.4 mm/yr are typical of stable continental areas as an upper bound. GPS detects with confidence only velocities of higher than 0.5 mm/yr and strain rates of approximately 10–9. The New Madrid region may contain the only “active” intraplate system in the world where a local, continuous GPS network is available. Dr. Calais discussed the varying levels of precision and accuracy generally obtained from the 500 GPS stations in North America, and specific results for the New Madrid region. In the past few years, velocity uncertainties have decreased by at least a factor of two at all sites; residual velocities have decreased as well. In the same region, there are no significant strain rates at 95 percent confidence level.

Dr. Calais then addressed recurrence of earthquakes indicated by paleoliquefaction. Assuming steady-state strain accumulation and release, there is a 500-year average repeat time over 12,000 years. Dr. Calais concluded that the current strain accumulation rate in the New Madrid region cannot be sustained and is not in steady state. As a counterexample, he referred to the Wasatch fault in Utah, where GPS and paleoseismology are in good agreement. His hypothesis is that some slow faults are in steady state at the 10,000-year time scale but some are not. The New Madrid region is not in steady state because the loading (equal to stressing) rate varies with time, and/or fault strength varies with time. Dr. Calais remarked that it is time to think outside the “rebound model box,” noting that the more we measure, the closer to zero we get, but the more we look, the more potential active faults we seem to find. Local strain accumulation may not be a prerequisite for large earthquakes, as perhaps earthquakes can “tap into” larger-scale reservoirs of strain.

Dr. Seth Stein of Northwestern University gave the next talk, titled “Rethinking Midcontinental Seismicity and Hazards”. He explained the evolution of his thinking about seismicity patterns. Previously he believed that focused, quasi-periodic long-term seismicity occurred in weak zones, but lately he has been moving toward the concept of episodic, clustered, and migrating patterns of seismicity. The latter suggests that the past is an extremely poor predictor of the future and that seismicity migrates between zones of rocks of similar strength. Dr. Stein noted that GPS campaigns were started in the NMSZ in 1991. Initially, fairly high rates of movement were expected but by 1999 the GPS results indicated essentially no motion. In 1999 he postulated that we could be near the end of a seismic sequence; this idea has held up over time. Maximum motion steadily converges to zero, as rate precision improves with longer observations. Dr. Stein now believes that the past 2,000 years are not representative of long-term NMSZ behavior and that the recent large earthquake cluster in this zone may be ending. He noted that geology implies NMSZ earthquakes are episodic and clustered through the Holocene; similar episodic patterns are seen in other continental plate regions. He stated that the NMSZ is not hot, weak, or

special relative to surrounding regions of the CEUS. He also discussed differences between time-independent hazard and time-dependent hazard; the latter approach generally predicts lower hazard levels in the CEUS.

Dr. Stein then asked: how we can make better progress in understanding seismic hazard? He believes more and better data are needed, and that the dynamics of forces, faulting, and fault interactions in the plate interior need to be incorporated in a model and explored in detail. He noted that GPS is giving constraints on effects like postglacial rebound. In his conclusions he noted that geodetic deformation is probably required for large earthquakes, so its absence argues against large earthquakes any time soon.

Continuing on the topic of using geodetic data, Dr. Bob Smalley of the University of Memphis gave a talk titled “Geodetic Interpretations of New Madrid Rates.” Dr. Smalley noted that his work was based on the same data set that was described by the previous two speakers. He began by noting that maps of worldwide strain rates indicate that plate boundaries have the highest rates, which is in good agreement with plate tectonics. Multiple occurrences of large earthquakes in a few areas, like the NMSZ, are not explained by either plate tectonic or rebound paradigms. Dr. Smalley discussed theories of how plates might deform, and the extent to which deformation can be recognized using GPS. He noted that in concentrated zones of deformation within inactive regions, it is “challenging” to see this deformation with GPS. From examination of plate tectonic dynamics, it is clear that strain rates in stable plate interiors are bound at very low rates. The challenge is to detect a small signal buried in a larger signal. Dr. Smalley believes that GPS is on the verge of not being significant for the NMSZ, thus it is difficult to see how this zone is different from the rest of North America. However, just because we see nothing there now, we cannot say this information is significant. Within the next 10 years, better data may be obtained for the New Madrid region.

Dr. Smalley went on to discuss a number of explanations for stable continental region earthquakes, including reactivation of zones of weakness, crustal weakening by fluids, and stress changes due to deglaciation or sediment loading. For the design of a continuous GPS network for the NMSZ, local, crustal, and regional scales were considered in the placement of monuments. Questions about monument stability were acknowledged and are related to factors that include water level changes in the Mississippi River, and the rise and fall of groundwater levels due to pumping. A longer time period and a larger number of stations providing higher density and redundancy are needed to collect data. Dr. Smalley then gave GPS results for other stable continental regions in the United States, Europe, and India: rates are low, but in general there are few stations in these stable areas. He believes that short-term geodetic signals should be integrated with long-term geologic deformation rates. In his conclusion he noted that GPS will continue to improve, but both denser sampling at the scale of seismic structures and longer observation times are needed.

Following a short break, Dr. Mark Zoback of Stanford University gave a talk titled “Intraplate Stress and Strain in the Central and Eastern United States and Their Relation to Intraplate Seismicity.” The work he has conducted indicates relatively uniform stress orientations across complex geologic boundaries. He noted that during the past several years (since the last World Stress Map effort) there has been little progress on mapping intraplate stress in the CEUS, but for the CEUS SSC project he has gathered the new stress information available and plotted it. He showed a series of Google Earth photographs with the stress data plotted, and discussed the new

data, including 38 earthquake focal mechanism data points. In the New Madrid area the new stress data indicates strong east-to-west trends, whereas the surrounding craton and eastern margin shows dominantly northeasterly stress directions. This area may have an anomalous crust and upper mantle structure in which the viscosity of the upper mantle may be lower than that of the surrounding mantle, thus leading to stress rotation.

Next, Dr. Zoback reviewed focal mechanism data for recent earthquakes, including the 2002 Mw Caborn earthquake in the Wabash area, which had slip on a west-northwest plane consistent with east-to-west stress. He noted that with uncertainties incorporated, significantly different results could be obtained, and additional well-constrained data are needed. The characteristics of New Madrid seismicity were then reviewed. Dr. Zoback discussed the hypothesis that the retreat of the glacial ice sheets triggered Holocene earthquakes. The use of a localized weak-mantle model indicates there will be concentrated deformation locally for tens of thousands of years, as that is the amount of time needed for the mantle to recover. Dr. Zoback concluded by asserting that the New Madrid region is unique and that he believes earthquake recurrence rates are not likely to change in the near future.

Dr. Coppersmith opened the workshop to questions from all participants. After further discussion about New Madrid seismicity, the association of earthquakes with glacial unloading, stress accumulation in the crust vs. the mantle, and other topics, Dr. Coppersmith commented that these topics could be discussed again on Day 3 of the workshop. He thanked all the presenters and noted that the meeting would reconvene the following morning.

DAY 3—FRIDAY, FEBRUARY 20, 2009

Dr. Coppersmith welcomed the workshop participants to the third and final day of the workshop. The first talk of the day was by Dr. Martitia (Tish) Tuttle of USGS and was titled “Clustered Model for New Madrid Earthquakes.” Dr. Tuttle began with a review of the timing, location, magnitude, and recurrence times estimated for New Madrid region paleoearthquakes. She described evidence for paleoliquefaction, noting that sand blows usually provide the best opportunities to provide minimum and maximum age estimates for paleoearthquakes because they may contain in situ materials (e.g., charcoal, sticks) that can be dated. Dating methods include radiocarbon and OSL (optically stimulated luminescence) dating, artifact analysis, and dendrochronology; age date uncertainties can range from ± 1 to 1,000 years. The New Madrid earthquake chronology based on paleoliquefaction has age estimate clusters at 1450 a.d., 900 a.d., and 2350 b.c. Independent paleoseismic studies have provided data that support these event ages. Dr. Tuttle believes the clusters formed during very large New Madrid-type events. In addition to the 1811–1812 New Madrid earthquakes, possible analog events include the 2001 M 7.6–7.7 Bhuj, India, earthquake. Available information suggests the New Madrid region earthquakes have an approximately 500-year repeat time. Clustered earthquakes (i.e., separated by days or months) are indicated by stratigraphic information associated with sand blows.

Dr. Tuttle reviewed all the paleoseismology information available for the Reelfoot Rift. Faults in the rift region were active at different times during the past 5,000 to 15,000 years; the most recent earthquake activity in the migration pattern is focused on the New Madrid region. She went on to discuss negative evidence for paleoearthquakes. Certain conditions need to be present (e.g., loose and sandy sediments, water-saturated conditions, and good exposures of older deposits) to conclude that liquefaction could have occurred; however, even if these conditions

are met and no liquefaction features are found, the occurrence of earthquakes cannot be ruled out. Next, Dr. Tuttle discussed studies in the Charlevoix seismic zone. Three generations of liquefaction features within the past 10,000 years were identified along rivers in this region. These features were likely produced by earthquakes of $M \geq 6.2$. In the Quebec City–Trois Rivières region, which is located in a historically seismically quiet part of the St. Lawrence Valley, similar river exposures were examined but no paleoliquefaction features were found; however, the occurrence of paleoearthquakes cannot be ruled out.

The following talk by Dr. Shelley Kenner was titled “New Madrid Model for Repeated Events: Geodetic Signature along the Southeast Margin and Elsewhere.” Dr. Kenner began by reviewing intraplate seismicity, noting that the majority of knowledge of earthquake physics has been developed from plate boundary regions. She then noted key differences between intraplate and plate boundary regions with respect to the (1) kinematics and temporal characteristics of seismicity; (2) reason for stress localization; and (3) source of stress that drives seismicity. She reviewed reasons for stress accumulation along faults and described the crustal stress cycle that consists of localized loading, coseismic rupture, postseismic relaxation, and associated localized loading that induces clusters of earthquakes. She also reviewed aspects of the NMSZ, emphasizing the location above a failed rift that has been reactivated repeatedly, and the increase in seismicity during the Holocene.

Dr. Kenner discussed aspects of weak zone model behavior and the question of whether such a zone could be present in regions of concentrated intraplate seismicity. Triggers for seismicity may include glaciation and sedimentation in the Mississippian embayment. Dr. Kenner then spoke about weak zone relaxation and described aspects of associated seismicity over time, including earthquake recurrence intervals. Analyses have indicated that the total duration of transient relaxation processes is very long and may last more than 20 times longer than the characteristic relaxation time of weak zone material even though surface deformation rates are low. To examine the temporal evolution of where shear zones take place, three-dimensional (3-D) weak zone models were developed and their behavior assessed. Total plastic strain plots show that with increasing time, shear zones move toward weak zone boundaries. In summary, stress loading from an underlying weak zone is a physically plausible mechanism for earthquake generation. Sequences of earthquakes due to weak zone relaxation may be triggered by temporally variable localized stress transients

Dr. Coppersmith asked Dr. Stein and Dr. Zoback for their thoughts about Dr. Kenner’s model. Dr. Stein commented that if the New Madrid region is special or representative of a large number of faults everywhere, then does that indicate a weak zone is present under each of the many places where large intraplate earthquakes have occurred? Many crustal faults are known and he dislikes the concept of having to associate a weak zone with each of these faults. Dr. Zoback indicated that he agreed with Dr. Stein in terms of the global implications of Dr. Kenner’s model. He noted that conceptually, Dr. Kenner’s model is similar to other models proposed to explain the Holocene record of earthquakes in the New Madrid region, and it would satisfy the other criteria that are unique to New Madrid, such as the absence of a geodetic signature and the small amount of cumulative deformation. He suggested exercising caution in applying models too broadly.

Dr. Alessandro Forte of the University of Quebec at Montreal gave the next talk, titled “Physical Processes Occurring in the Mantle under the EUS and Their Implications for Surface Stress and

Deformation.” He noted that plate tectonics is a 3-D process, in which deep-seated forces that drive horizontal motions also drive substantial vertical displacements that contribute to crustal stress. Vertical motions, however, are below the current level of resolution of GPS. Dr. Forte reviewed several previously proposed dynamic models of the origin of stress and seismicity in the NMSZ. He then showed his work on tomographic imaging of the shallow mantle structure below North America. In the past five years he has been working on modeling present-day mantle flow dynamics in fully global calculations of mantle flow. His tomography-based mantle convection model successfully predicts plate velocities and observations of surface gravity and topography on the North American Plate.

With viscosity structure and driving forces available, the differences in direction of subcontinental mantle flow at various depths can be evaluated. Dr. Forte showed a cross section of mantle flow below the CEUS that indicates downward movement (flow foundering) beneath the New Madrid and Mississippi region at depths below approximately 400 km. He showed a map of mantle-flow-induced horizontal tractions on the crust in the region of NMSZ. He noted that the Mississippi Valley region is being pulled down dynamically because of drag from the descending Kula-Farallon slab below. Descent of the slab into the lower mantle induces a region of maximum horizontal flow convergence and maximum compressive surface stresses directly below the CEUS oriented in a northeasterly direction. Stress directions are modeled as the same along the eastern margin of the continent, but their amplitude is lower. These stresses are generated on mantle-convection time scales, which are on the order of millions of years and can therefore support long-lived seismicity. Dr. Forte showed a video of time-dependent mantle dynamics and surface flexure (topography) over the past 30 million years. He noted that mantle-flow-induced surface depression and associated bending stress may be an important and long-lived contributor to the clustered and migrating seismic activity in the Mississippi Basin, extending from the Great Lakes to the Gulf of Mexico.

Following a short break, Dr. Martin Chapman of Virginia Polytechnic Institute spoke about seismicity in the southeastern United States in a talk about the Eastern Tennessee and Charleston fault models. The Eastern Tennessee seismic zone (ETSZ) is the most seismically active area in the Southern Appalachians. Seismicity in the zone is associated with a major potential field anomaly known as the New York–Alabama lineament. Dr. Chapman reviewed key findings of previous studies of Eastern Tennessee seismicity. He showed maps that indicated correlation of NOAA magnetic data and Bouguer gravity data with earthquake epicenters in the southern Appalachian region. From focal mechanism data, earthquake epicenters are northeast trending and many appear to be aligned along a north-dipping plane. Studies indicate that earthquakes are occurring in response to a highly uniform regional stress, with strike-slip motion predominant. The New York–Alabama lineament marks an abrupt boundary between zones of different seismicity; however, the geologic nature of this feature remains a mystery.

Dr. Chapman then talked about seismicity in the Charleston area, noting liquefaction features and the identified earthquake epicenters. Gregg's Landing on the Ashley River is the focus of current seismicity and is also the location of strong shaking in the 1886 Charleston event. A seismic reflection profile in this area provides clear evidence of Cenozoic reactivation of Mesozoic extensional faulting. In the Summerville area, seismic profiles show possible faulting of Cenozoic sediments to shallow depths in close proximity to a strong magnetic gradient. Dr. Chapman also showed COCORP lines that indicate a faulted Mesozoic section underlying the Summerville and Charleston region. The imaged faulting in these areas is within the zone of

modern earthquake activity. Dr. Chapman concluded his talk by saying that progress in understanding the seismicity of this area requires a long-term commitment to secure precision hypocenter locations and focal mechanism determinations.

Following a lunch break, Dr. Pradeep Talwani of the University of South Carolina gave a talk titled “The Source and Magnitude of the Charleston Earthquakes.” He began by describing the revised tectonic framework for the region that he and his colleagues have developed. He showed a map of seismicity from 1974 to 2004 and the varied focal mechanisms associated with these events. Earthquakes were relocated to develop the revised tectonic framework that shows a series of faults, which he showed projected onto a series of cross sections. Dr. Talwani described structural features in the region, including the uplifted zone of river anomalies (ZRA) and the East Coast fault system (ECFS). Results of the new seismotectonic framework indicate that seismicity is occurring primarily at the compressional left step within the southernmost segment of the ECFS. Dr. Talwani discussed paleoliquefaction studies that indicate seven separate earthquake events. Using his new work, he can link these events to faults. He described offset in the thick walls of Fort Dorchester during the 1886 earthquake event. A trench was excavated on the projection of the fault that offset the fort walls. Although the fault was not seen in the trench, a sand blow was revealed. Age dating indicated the sand blow formed in a pre-1886 event. Geotechnical data, including piezometer tests and cores, were collected in the area. Using these data, the magnitude of the earthquake was back-calculated to be $\sim M 6.2$.

Next Dr. Talwani reviewed results of GPS studies in the Charleston region. Delaunay triangle modeling indicates that the strain rate in the vicinity of Charleston is high. Dr. Talwani showed magnitude estimates for the 1886 Charleston earthquake from intensity data; the latest value is $M 6.9$. He also provided a list of magnitudes of prehistoric regional earthquakes associated with liquefaction from in situ SPT (Standard Penetration Test) data. In his conclusions, Dr. Talwani noted that the 1886 Charleston earthquake and seismicity that is currently being recorded are related to the Woodstock fault and associated faults at a compressional left step in the Middleton Place–Summerville seismic zone. He believes that only this southernmost segment of the ECFS is seismically active and poses a seismic hazard.

The next talk, titled “Seismotectonic Setting and Seismic Sources of the Northern Gulf of Mexico,” was given by Mr. Michael Angell of William Lettis & Associates. Mr. Angell began by stating that although the Gulf of Mexico region has generally low seismicity, three earthquakes having $M_b > 4.5$ ($M_w 5.8$ was the largest) occurred in the northern Gulf in 2006. Causative mechanisms for these earthquakes were a topic of his talk, and he proceeded to describe the historical seismicity, bathymetry, and stress indicators in the Gulf region. He noted that numerous growth faults (faults driven by gravitational forces) are located above salt diapirs (mobile salt beds). Then he reviewed the information available on the 2006 earthquakes. Two of these events occurred within an area containing growth faults.

Next Mr. Angell reviewed the tectonic setting of this region. Interpretations of the tectonic history indicate that a block of oceanic crust was emplaced in the late Jurassic. Oceanic crust can be delineated on seismic lines and with gravity and magnetic data. Mr. Angell described different models that show the distribution of the oceanic crust in the Gulf of Mexico. Some of the largest recorded earthquakes occurred within this crust. Large, northwest-southeast-trending fracture zones are located to the east of the earthquakes. Turning to a discussion of seismic source models for the Gulf, Mr. Angell reviewed existing alternative models for seismic hazard. Apparent

alignments of seismicity suggest a possible underlying source and association with deep structure.

Mr. Angell went on to describe growth fault settings and the associated seismicity. He discussed aspects of the February and April 2006 earthquakes, which have been modeled as gravity-driven on a shallow-dipping plane. He noted that the most appropriate model for the Gulf may be two-layered, having shallow seismic sources in growth fault areas and deeper seismotectonic sources in the basement. He discussed the possibility of a link between upper and lower faulting, mentioning that a trigger could originate from an event in either the upper or lower zone. He concluded by stating that earthquakes associated with growth faults have limited depth extent (to about 5 km), are “slow” (i.e., they do not radiate high-frequency energy), and have low magnitudes ($M < 5$); therefore they may not be significant in seismic hazard assessments.

The next talk was given in two parts by Dr. Mark Petersen and Dr. Chuck Mueller, both of the U.S. Geological Survey. Dr. Petersen spoke first in a talk titled “2008 USGS Seismic Source Model for the Central and Eastern U.S.” The national hazard maps released in April 2008 were based on the 2002 and 2006 USGS models. Dr. Petersen briefly described some of the changes made for the 2008 CEUS model, including development of maximum magnitude distributions for seismicity. He reviewed New Madrid and Charleston area site-characterization details. Branches of a logic tree were used to evaluate fault rupture models (clustered and unclustered), location uncertainty, recurrence intervals, and M_{\max} alternatives. To obtain alternative M_{\max} , the recorded M 7.1 to 7.7 magnitudes of earthquakes in stable continental regions worldwide were considered.

During the second part of the talk, Dr. Mueller focused on how seismicity was used in the USGS seismic hazard model. His talk was titled “Hazard from Seismicity: the USGS Approach.” He listed organizing principles for the hazard model: specific fault sources considered, historical seismicity gridded and smoothed, and large background zones defined based on geologic criteria. He described the various zones delineated on the hazard map and what earthquake catalogs were used, and he addressed regional completeness levels and b values. He reviewed how historical seismicity was gridded based on analyses from four different models, and he showed example results of smoothed seismicity for the different models used. He noted that gridded seismicity models are essentially a localized, variable b -value model. Dr. Mueller concluded his talk by describing seismic hazard studies previously conducted for the CEUS and associated hazard assessed for selected nuclear power plant sites.

With the workshop’s technical talks completed, Dr. Coppersmith commented on the path forward for the project. He showed the task schedule and described the work to be completed in the next few months. The tasks include constructing the preliminary SSC model, compiling the seismicity catalog, and completing preliminary hazard calculations and sensitivity analyses that will be presented at Workshop 3. Dr. Coppersmith then thanked the presenters and complimented them on the high professional level of their interactions.

Mr. Salomone closed the meeting with several remarks. First he described the role of the Participatory Peer Review Panel (PPRP) and their review relationship with the TI team. He acknowledged the members of the PPRP, beginning with the co-chairs, Drs. Carl Stepp and Walter Arabasz. Then he acknowledged the participation at the workshop of the international observers as well as the younger professionals, who will ultimately take over the process of hazard assessment. He thanked EPRI for its support of the workshop. Finally, he observed that

the original vision of what the workshop organizers had hoped would occur had, indeed, happened.

REFERENCES

Bernreuter, D.L., J.B. Savy, R.W. Mensing, and J C. Chen. 1989. "Seismic Hazard Characterization of 69 Nuclear Plant Sites East of the Rocky Mountains," Report NUREG/CR-5250, Vols. 1–8, prepared by Lawrence Livermore National Laboratory for the U.S. Nuclear Regulatory Commission.

Budnitz, R.J.; G. Apostolakis, D.M. Boore, L.S. Cluff, K.J. Coppersmith, C.A. Cornell, and P.A. Morris. 1997. *Recommendations for Probabilistic Seismic Hazard Analysis: Guidance on the Uncertainty and Use of Experts*, NUREG/CR-6372. Two volumes. U.S. Nuclear Regulatory Commission, Washington, D.C.

Electric Power Research Institute and Seismicity Owners Group (EPRI-SOG), 1988. *Seismic Hazard Methodology for the Central and Eastern United States*, Technical Report NP-4726-A, Vols. 1–10.

Johnston, A.C., Coppersmith, K.J., Kanter, L.R. & Cornell, C.A. 1994: The Earthquakes of Stable Continental Regions. Volume 1, Assessment of Large Earthquake Potential.

Electric Power Research Institute (EPRI) TR-102261-VI, v. 1.

Table 1:
Key Questions and Topics That Workshop 2 Presenters Were Asked to Address

Topic	Presenter	Questions/Topics to Address at WS2
Geodetic observations in St. Lawrence and implications to Mmax; big picture tectonic framework; limits of glacial rebound	Mazzotti, Stephane	<p>What criteria should be used to define seismic sources?</p> <p>Do glacial rebound processes influence seismicity (rates-focal mechanisms) and should this be considered in defining seismic source zones?</p> <p>What are rates and uncertainties on geodetic observations? What is geographic area of coverage for geodetic observations?</p> <p>What is your confidence that observed geodetic rates reflect long-term tectonic deformation rates or short term seismicity pattern and rates?</p> <p>What weight would you give geodetic vs seismicity in establishing rate of EQ occurrence?</p>
Size of 1663 Charlevoix earthquake; treating St. Lawrence seismicity zones as aftershocks	Ebel, John	<p>What is your confidence that current patterns of seismicity represent aftershocks from large historic or prehistoric events? What maximum magnitude range and source zone geometry would you assign to sources in the St Lawrence-Charlevoix area?</p>
Use of seismicity to define seismic sources, application in the eastern North America region.	Kafka, Alan	<p>What approaches should be used to capture uncertainty in stationarity of seismicity with regard to defining seismic sources?</p>
Use of geological structures and assessing Mmax for Canadian national hazard maps	Adams, John	<p>What methodology is being used to define Mmax distributions for source zones?</p> <p>What is the Canadian perspective on the limitations of the Johnston et al. (EPRI) approach and prior distributions?</p> <p>What are reasonable worldwide analogs for stable continental regions appropriate for CEUS and Canada?</p>

Topic	Presenter	Questions/Topics to Address at WS2
Seismicity and potential faults in NYC, Pennsylvania, Ohio, New England	Seeber, Leonardo (Nano)	<p>What are reasonable criteria for defining seismic source zones in NE US?</p> <p>Previous models have used hotspot tracks, onshore extensions of older transforms, evidence for reactivated structures along the Fall Zone and Mesozoic rift basins—are these still valid concepts?</p> <p>What is your preferred causative mechanism for seismicity in the region?</p> <p>What is your preferred seismic source model (geometry, Mmax) for the NY region?</p>
Ouachita, sub-detachment structures	Thomas, Bill	<p>What is the influence of any of older structures (e.g., Iapetan transforms) on present seismicity?</p> <p>What is the evidence for reactivation of these structures in the Mesozoic?</p> <p>What is your confidence that the Ouachita basement structure represents a seismogenic source?</p>
Rift structures in the mid-continent (Rough Creek Graben, Rome Trough, East Continent rifts)	Drahovzal, James	<p>Is there evidence to suggest that the Rough Creek and Rome Trough may be continuous features?</p> <p>Is there any evidence of Mesozoic reactivation of either structure?</p> <p>What is the relationship of the East Continent gravity high to the Rome Trough and to regions of elevated seismicity in Eastern Tennessee?</p>

Topic	Presenter	Questions/Topics to Address at WS2
Integration of seismic reflection, geopotential field, and subsurface information in southern Illinois Basin	McBride, John	<p>Previous publications suggest that moderate earthquakes (like the 1968 event may have occurred on thrust faults in the basement?</p> <p>What if any structural relationship is there between these structures and the Commerce Geophysical lineament?</p> <p>Is there sufficient evidence to model other structures such as the DuQuoin monocline as potential fault sources?</p> <p>What are your thoughts on the distributed paleoliquefaction 'energy centers'—is there other geologic information to suggest local sources of moderate events or are these features more likely due to more distant larger magnitude events?</p> <p>Should the faults in the Flurospar Area complex region be modeled as independent active faults in the current tectonic environment and if so, what are your thoughts on the timing, maximum magnitude, and recurrence of events on these structures?</p>
Margins of Reelfoot and update on Kentucky River fault zone	Van Arsdale, Roy	<p>What are the constraints on the continuity and length of possible fault sources along the margins of the Reelfoot rift? Are there paleoseismic data that can be used to estimate Mmax?</p> <p>Is there evidence of paleoliquefaction associated with events on the margin fault sources?</p> <p>Please comment on the southern continuation on potential continuity of the NM and Saline River source zones.</p>
Commerce lineament and northwest boundary of New Madrid	Baldwin, John	<p>What data is available to constrain or estimate Mmax for fault-specific sources along the northwestern margin of the Reelfoot rift?</p> <p>What is the extent, origin, and seismogenic potential of the Commerce Geophysical lineament?</p>
Saline River and Reelfoot Rift	Cox, Randy	<p>What are the uncertainties in the timing and relationships of paleoliquefaction events in the Saline River area relative to the central part of the NMSZ?</p> <p>Please comment on the southern continuation or potential continuity of the NM and Saline River source zones.</p> <p>Have you identified a tectonic feature as a potential seismic source responsible for observed liquefaction in the Saline River area?</p>

Topic	Presenter	Questions/Topics to Address at WS2
Geotechnical evaluation of the Vincennes event in southern Illinois	Green, Russell	How can this analysis be used to constrain the dimensions of the Vincennes earthquake seismic source? Can you use similar approaches to evaluate smaller energy centers that have been identified elsewhere in southern IL and IN—i.e., what methods can be used to assess the issue of local small events versus larger more distant earthquakes? What is your uncertainty in using liquefaction to assess Mmax?
Magnitude bound relation for the Wabash Valley seismic zone; Geotechnical analysis of paleoseismic shaking using liquefaction effects	Olson, Scott	What are limitations of the magnitude bound approach? What is your uncertainty in using liquefaction to assess Mmax? What Mmax would you assign to NM, Charleston, Wabash, based on paleoliquefaction observations? Please comment on the minimum magnitude required to generate liquefaction?
Geodetic interpretations of New Madrid rates	Calais, Eric	What is your confidence that observed geodetic rates reflect long-term tectonic deformation rates or short term seismicity pattern and rates? What weight would you give geodetic vs seismicity in establishing rate of EQ occurrence? Do current data allow one to discern tectonic rates from measurement uncertainties?
Rates and recurrence in New Madrid	Stein, Seth	What is the relationship between geodetic deformation and earthquake occurrence? Have you compared the geodetic signature of other zones of seismicity in stable continental regions? Is the absence of evidence for geodetic deformation a definitive indicator of future earthquake potential?
Geodetic interpretations of New Madrid rates	Smalley, Bob	What is the relationship between geodetic deformation and earthquake occurrence? How do you relate relatively short-term geodetic deformation rates to longer-term geologic deformation rates? Have you compared the geodetic signature of other zones of seismicity in stable continental regions?

Topic	Presenter	Questions/Topics to Address at WS2
Update of stress map, strain localization, New Madrid rates	Zoback, Mark	<p>Do available stress and strain data provide sufficient resolution to aid in defining local source zones?</p> <p>What is the cause of stress of intraplate stress?</p> <p>What are mechanisms to localize stress?</p> <p>Are observed rates of historic and prehistoric seismicity consistent with observed stress and strain rates?</p>
Clustered model for New Madrid events	Tuttle, Tish	<p>What are the resolution issues for identifying individual events and estimating the size of such events?</p> <p>What is your confidence that the regional absence of liquefaction in susceptible deposits reflects an absence of large magnitude (>6) earthquakes?</p>
New Madrid model for repeated events; geodetic signature along the southeast margin and elsewhere	Kenner, Shelley	<p>What are likely triggering events?</p> <p>Is the absence of a significant geodetic signal across the NMSZ consistent with this model?</p> <p>What are implications of the model for future large magnitude earthquakes (location, timing)?</p>
Physical processes occurring in the mantle under the Eastern US and their implications for surface stress and deformation	Forte, Alessandro	<p>Do mantle processes influence current seismicity?</p> <p>Can these patterns be used as criteria for defining seismic source zones?</p> <p>Do mantle processes occur at rates that should influence short term (10-1) or long-term (10-3) seismicity?</p> <p>What is your confidence that available heat flow data can be used to detect mantle anomalies?</p>

Topic	Presenter	Questions/Topics to Address at WS2
Update on eastern TN and Charleston; fault model for these sources	Chapman, Martin	<p>Please comment on your interpretation of the causative mechanism for the events in ETSZ?</p> <p>Do current seismicity analyses support previous models of alignments of seismicity as potential fault sources?</p> <p>What is the influence of the NYAL lineaments on patterns of seismicity?</p> <p>Are there unique conditions (fluid pressures, basement rocks, etc.) that distinguish ESTZ from other seismically active regions of the Appalachians, (i.e., Giles Co.)?</p> <p>Is there any current new information that can be used to assess Mmax?</p> <p>Please comment on your interpretation of the causative mechanism for the Charleston earthquake?</p>
The source and magnitude of the Charleston earthquakes	Talwani, Pradeep	<p>Please comment on your interpretation of the causative mechanism for the Charleston earthquake?</p> <p>Is there evidence to suggest that the tectonic features (i.e., Woodstock fault, and related thrust faults in the step over regions) that appear to be likely candidates for the source of the repeated large magnitude Charleston events extend along the full length of the postulated ECFS-S?</p>
Approaches Used to Identify and Evaluate Neotectonic Features in Appalachian Piedmont/Coastal Plain Setting	Pazzaglia, Frank	<p>What influence if any do the broad regional flexures have on current patterns of seismicity?</p> <p>Should these features be explicitly considered in defining seismic sources?</p> <p>Please comment on your interpretation of the causative mechanism for earthquakes in the northeastern US?</p>
Gulf coast faulting and seismicity	Angell, Mike	<p>Please comment on your interpretation of the causative mechanism(s) for earthquakes in the Gulf?</p>

Topic	Presenter	Questions/Topics to Address at WS2
Seismic source model for the US National Hazard maps	Peterson, Mark	<p>Current modeling tools (smoothed seismicity) reduce the need for using discrete seismic source zones to capture areas of elevated seismicity.</p> <p>Please comment on what characteristics (i.e., Mmax) would warrant defining a separate source zone?</p>

WORKSHOP 3: FEEDBACK

August 25-26, 2009

Electric Power Research Institute
3420 Hillview Ave.
Palo Alto, California 94304

The Workshop on Feedback was the third in a series of workshops jointly sponsored by the Electric Power Research Institute (EPRI) Advanced Nuclear Technology (ANT) Program, U.S. Nuclear Regulatory Commission (NRC), and U.S. Department of Energy (DOE) in support of the Central and Eastern United States (CEUS) Seismic Source Characterization (SSC) for Nuclear Facilities Project. The objective of the CEUS SSC is to develop a comprehensive and up-to-date SSC for a probabilistic seismic hazard analysis (PSHA) that is appropriate for use at any site in the CEUS. The technical integration (TI) team and TI staff are charged with developing a seismic source model that captures the knowledge and uncertainties within the larger informed technical community.

The goals of this workshop were as follows:

- Review the progress of the project in terms of meeting key milestones, such as the database development and earthquake catalog.
- Review the processes being followed to attain the SSHAC goal of capturing the informed technical community.
- Discuss the seismicity catalog developed for the CEUS SSC project.
- Discuss the seismic source characteristics of the SSC sensitivity model.
- Present feedback to the TI team and staff in the form of SSC sensitivity analyses and hazard sensitivity analyses.
- Identify the key issues of most significance to the SSC models.
- Discuss the analyses being conducted related to hazard significance.
- Discuss the path forward for the CEUS SSC project.

These goals were accomplished by a series of presentations and discussions.

DAY 1–TUESDAY, AUGUST 25

Workshop participants were welcomed by **Mr. Frank Rahn** (EPRI), who reviewed workshop logistics. **Mr. Lawrence Salomone**, project manager for the CEUS SSC project, then welcomed workshop participants and thanked them for attending. He reviewed the project goals:

- Replace the previous EPRI Seismicity Owners Group (EPRI-SOG) and Lawrence Livermore National Laboratory (LLNL) seismic hazard studies that were conducted in the 1980s (EPRI-SOG, 1988; Bernreuter et al., 1989).
- Capture the knowledge and uncertainties of the informed scientific community using the SSHAC process (documented in NUREG/CR-6372; Budnitz et al., 1997).

- Present a new CEUS SSC model to the NRC, DOE, and others for review.

Next Mr. Salomone showed a map of the study area and the demonstration sites used for sensitivity analyses for the project. He reviewed the topics of the previous two workshops, noting the contributions of numerous resource experts, and went over the goals of Workshop 3. He also described communications with the Participatory Peer Review Panel (PPRP) and project and tracking milestones. The project appears to be on track to meet the target completion date in December 2010.

Dr. Kevin Coppersmith (Coppersmith Consulting, Inc.), the lead of the TI team, then welcomed the workshop participants. He began by reviewing aspects of the SSHAC project, including basic principles for a PSHA, key attributes of the process, and expert roles. He reviewed the purpose and goals of Workshop 3. The TI team has developed a sensitivity SSC model that is complete in that it captures the range of views in the technical community, but the TI team has not devoted a lot of effort to weighting the alternative branches of the model until they see the results of the sensitivity analyses. Sensitivity analyses to be presented in the workshop will allow understanding of the importance of key assessments of most significance to the SSC models. Dr. Coppersmith clarified that a draft data summary package—consisting of the Data Summary and Data Evaluation Tables—completed prior to the workshop and distributed to PPRP members is a “work in progress” (i.e., it is incomplete and subject to revision). Nonetheless, he noted that the data evaluation process was conducted with a focus on identifying and evaluating the data, models, and methods that have credibility. By understanding the potentially important elements of the SSC model, subsequent work for the CEUS SSC can be prioritized.

Dr. Coppersmith went on to give a talk titled “SSHAC Goal of Capturing the Informed Technical Community.” He explained that the talk is based on his experience both from being a SSHAC member and from subsequently implementing SSHAC processes during the years since the 1997 SSHAC study was completed. After giving a brief historical context to probabilistic risk studies and the use of expert assessments, he noted that there has been increasing recognition of the importance of uncertainties. Probabilistic hazard is important to risk analysis, and uncertainties are important to hazard, thus quantifying uncertainties is an important aspect of the analysis. Dr. Coppersmith stated that more stable estimates of hazard are obtained by incorporating the range of views within the expert community. Based on this knowledge, there has been increased attention to concerns about expert issues, including representativeness, independence, consensus, and aggregation. Of particular importance have been strategies to deal with potential outlier judgments that may have a disproportionately large influence on results.

Dr. Coppersmith described the SSHAC concept of integration as capturing the view of the informed technical community (ITC). (Being “informed” in this case refers to being familiar with site-specific databases as well as participating in the SSHAC interactive process.) He stated that integration is not just an aggregation process for parameter values across a panel of experts, as very few parameters can be directly assessed in PSHA. Instead it is necessary to evaluate data, develop models, and quantify uncertainties. Obtaining a composite, or community, distribution is the most important objective of consensus in the SSHAC process.

Dr. Coppersmith described the steps taken in the CEUS SSC project to ensure that the views of the ITC have been captured. All participants understood their roles and agreed to abide by them within the framework of the SSHAC process. The TI team and staff, as well as members of the PPRP, have first-hand knowledge of data sets, reflecting their extensive experience in SSC for

the CEUS. They have developed and are using explicit data evaluation processes to demonstrate a thorough awareness of all applicable data. Dr. Coppersmith noted that the interactive workshop processes used have proven to be a highly effective mechanism for identifying all available data and models that presently exist or are under development. In addition, he noted that the TI team and staff have expertise with the integration process. He said steps are in place that will ensure that the views of the ITC are reflected in the final results of the CEUS SSC project.

Dr. Coppersmith then gave a case history for the CEUS SSC project and traced the documentation in place to date. The case history was about the work of Drs. Eric Calais and Seth Stein, both of whom made presentations at Workshop 2, who suggested a lack of deformation in the New Madrid seismic zone and the potential that the zone will not be seismically active in the future. Dr. Coppersmith showed the questions they were asked to address in their talks, as well as a photograph of them as workshop participants, slides from their presentations, text included in the Workshop 2 summary and in a letter from the PPRP, text in a data summary table, and the logic tree used to model the hazard associated with the New Madrid fault source. He noted that the full documentation of the evaluations made by the TI team and the justification for all elements of the final SSC model will be part of the project final report. Dr. Coppersmith concluded his talk by stating that the SSHAC study will provide approaches that are instrumental in achieving the goal of capturing the views of the ITC. These approaches have been followed in the CEUS SSC project and they provide reasonable assurance that the ITC has been captured.

Workshop participants then discussed such concepts as “range of the technical opinions that the informed technical community would have,” outlier judgments, and reasonable assurance. Regarding range of opinions, sensitivity studies are useful for showing when an analysis input has little or no hazard significance. There has been a gradual move away from a when-in-doubt-put-it-into-the-analysis approach and toward more careful consideration of whether or not an input is credible (e.g., tails on distributions that extend to infinity), as these approaches affect computational efforts and analysis results differently.

Workshop participants also discussed the possible subjectivity inherent in efforts to limit outlier views by promoting evaluator roles instead of proponent roles for expert inputs. A representation of the distribution of community judgments, as represented by the ITC, is the goal of the SSHAC process and underlies the importance of the evaluator role. Finally, the group addressed the concept of reasonable assurance as an accepted standard for safety decision making, based on meeting standards of practice. A member of PPRP and others at the workshop believe that the SSHAC process, if properly implemented, goes beyond the standard of preponderance of evidence in assuring that the views of the ITC have been considered and represented.

Following a short break, Dr. Robert Youngs (AMEC Geomatrix, Inc.) gave a talk on development of the CEUS SSC earthquake catalog. A preliminary earthquake catalog was completed for use in preparing the sensitivity analyses. Dr. Youngs reviewed the catalog development beginning with compilation of earthquakes from available existing catalogs, through the process of declustering, noting that the approaches used for several of these steps were initially used for the EPRI-SOG study. The primary earthquake catalogs used for the compilation were from the U.S. Geological Survey (USGS) and the Geological Survey of Canada (GSC), but several other national, regional, and historical catalogs were also used. Information on relocated events was obtained from studies described in published literature. Nontectonic events (particularly blasts) were identified. Moment magnitudes were assessed for

all events, and Dr. Youngs showed plots of the alternative relationships used to convert different magnitude scales into moment magnitude. He described the process used to combine estimates from multiple magnitude measurements, when available, into a uniform magnitude scale. After conversions were completed, additional corrections were made to account for the bias in recurrence parameters due to magnitude uncertainty.

Next, Dr. Youngs explained how declustering was performed and how of the 26,426 total events in the catalog, 14,674 dependent events were identified. The final step in the catalog development process was to assess catalog completeness for events of various magnitudes. He showed the plots of catalog completeness regions within the study region for 15 different regions identified based on instrumentation and population history. He has sent the catalog to PPRP, USGS, GSC, and TVA colleagues to review selected preferential catalog entries, identify any additional data sources, evaluate conversions to moment magnitude, and garner any other suggestions. Response is needed by the end of 2009. At the conclusion of Dr. Youngs's talk, the workshop participants discussed the declustering approach and the identification of earthquakes related to blasts and located in offshore regions.

Dr. Youngs then gave a talk titled "The "EPRI" Bayesian M_{\max} Approach for Stable Continental Regions (SCR)—Updated Priors." In the EPRI (1994) study, SCRs were divided into domains based on crustal type, geologic age, stress regime, and stress angle with structures. For the CEUS SSC project source zones, observed M_{\max} distributions were developed based on the SCR domains identified for the 1994 study. In the project update, revised magnitude estimates were added for the New Madrid ($M7.8$) and Charleston ($M6.9$) events, and additional worldwide earthquakes were added from recent catalogs. The number of $M \geq 4.5$ events in the SCR increased from 940 to 1,550 earthquakes. Dr. Youngs described an interesting case of a large 1917 earthquake in China and the differences in the size and location of this event as reported in various catalogs. Next he discussed bias adjustment, which is used to move from the relatively small number of observed maximum earthquakes toward what could be expected if more data were available. He described domain "pooling," in which estimates of bias adjustment can be obtained by pooling similar domains to increase sample sizes (essentially, trading space for time). He concluded the talk by describing work that needs to be completed, including the criteria used to distinguish and combine domains and to examine bias correction techniques.

Following a lunch break, Dr. Youngs briefly described the talks planned for the afternoon; these consisted of feedback on various parameters and their effects on hazard, calculated for the seven demonstration sites examined in the study. Dr. Youngs gave the first talk, titled "Logic Tree Structure for Seismic Source Sensitivity Model." He began by describing the master logic tree developed for the CEUS SSC sensitivity model. Two types of seismic sources are recognized: (1) distributed seismicity within regional source zones, characterized using historical and instrumental seismicity, and (2) repeated large-magnitude earthquake (RLME) sources characterized using the paleoearthquake record. For each of these sources, zoneless and seismotectonic structure approaches are used for characterizations and assessment of M_{\max} . Distributed seismicity sources have two alternative geometries based on different extended and non-extended crust delineations.

Next, Dr. Youngs discussed the two alternative methods used to address spatially varying seismicity rates. These are the kernel model approach, based on a constant b -value and a cell-by-cell model approach that uses a variable b -value. The uncertainties and advantages and

disadvantages of using each of these approaches were discussed. Dr. Youngs then described the use of a zoneless treatment of RLMEs based on use of an earthquake catalog that includes paleoearthquakes, noting that an important issue is completeness with respect to spatial and temporal earthquake coverage. What to do in areas that have not been examined in detail is problematic; hence this model is not yet ready to be used. Dr. Youngs also described the logic tree structure used for the structure-specific approach to assessing RLMEs.

Dr. Youngs moved on to a talk titled “One Approach for Spatially Varying Seismicity,” in which he discussed the kernel model smoothing approach in detail. This approach assumes a constant b -value within a zone and a variable “ a .” Uncertainty in overall seismicity parameters is largely decoupled from estimation of spatial density. Dr. Youngs discussed testing for spatial non-uniformity to assess if seismicity is occurring in clusters. He showed kernel density estimation in one dimension, depicting a “classical” uniform density graph and Gaussian kernels approach. When combined, these approaches give information important for assessing the size of the kernel, which is an important parameter.

Next, Dr. Youngs described alternative kernel forms and how they affect data density. Kernel size can be adjusted as a function of data density using an adaptive kernel. Dr. Youngs showed examples of fixed kernel estimates and adaptive kernel estimates and how they affect display of data using a normalized density. He described the issue of varying completeness and how to account for this using a single catalog; possibilities include using minimum completeness for the lowest magnitude used (minimum data) and assigning a weight to each earthquake interval based on specific measures of relative completeness. He reviewed the approaches of high smoothing using uniform spatial density and low smoothing using adaptive kernel density estimation. He concluded by describing estimation of uncertainty distributions for earthquake rate and b -value.

The next talk, given by Dr. Gabriel Toro (Risk Engineering, Inc.), was titled “Characterization of Variable Seismicity: Penalty Approach with Variable a and b .” Dr. Toro stated that the variable seismicity approach is essentially a modification of the 1988 EPRI study approach developed by Veneziano and Van Dyke (1988). He began with an overview of the 1988 EPRI study approach and described the key elements and equations. Next he discussed the new features included in the updated approach, including smaller (0.25 degree) cell size and a new solution algorithm that estimates uncertainty in certain parameters and objectively estimates penalty terms to use in the calculation (i.e., downweighting is applied if there is a large difference in value between a cell and the adjoining cells).

He then described the solution algorithm and the results that can be obtained. The approach has been used for two cases: (1) a low smoothing case using objectively determined smoothness penalty terms and a low prior of $b = 1$, and (2) a high smoothing case with fixed smoothness penalty terms and no prior on b . Dr. Toro displayed the results of the CEUS SSC earthquake catalog using these approaches; with low smoothing there are more local peaks depicted than with high smoothing. He compared these results with results of the approaches used by Dr. Youngs and noted that they are similar.

Dr. Toro moved on to a discussion of uncertainty characterization for the variable seismicity approach, which represents a significant improvement over the EPRI 1988 model. He described the objective and approach, which includes randomization, and showed sample results obtained for low smoothing and high smoothing examples. His conclusions included the observation that the variable b approach is particularly well suited for large source zones, and that the approach

allows both objective (data-driven) and subjective specification of the smoothing parameter (i.e., penalty terms). Finally, Dr. Toro described additional work that could be conducted in the future to make improvements in the application of the updated approach.

Dr. Youngs presented maps of the historical seismicity of the CEUS that depicted the alternative spatial density models, plotted as frequency of occurrence (i.e., events per year per 0.25 degree). These maps provided feedback for the project team on the results produced by different smoothing approaches. Dr. Youngs showed three sets of maps displaying $M \geq 5$, $M \geq 6$, and $M \geq 7$ events for each of the alternative models. He described and compared the results of different models for selected regions. The number and magnitude of earthquakes within a particular region can have a strong effect on the nature of the boundary between adjoining zones. Workshop participants discussed some of the results of the various models, as well as the basis for defining the boundary between extended and non-extended crust.

After a break, Dr. Youngs announced that talks for the remainder of the afternoon would provide a whirlwind tour of seismic hazard in the CEUS. He began by showing a map of locations of the regional sources, RMLE sources, and the seven demonstration sites that are being analyzed for the CEUS SSC project. He described the master logic tree used to assess all the seismic sources and discussed various parameter estimation approaches. He showed results of M_{\max} assessments for the regional sources. Next he described in detail the analyses for the Cheraw fault and Wabash area RLME sources. He showed the logic trees used for these sources and discussed results of analyses of event frequency and magnitude distributions for each source. He then went on to describe the New Madrid RLME. The analysis is based on two groups of sources (a central zone of faults and a set of faults on the boundary of the rift) and three models of characterization (one with all structures in active mode; one with all structures turned off and a default to background seismicity; and one with only the Reelfoot thrust active). Dr. Youngs concluded his talk by showing the results of analyses of event frequency and magnitude distributions for the various structures associated with the New Madrid RLME.

Dr. Robin McGuire (Risk Engineering, Inc.) gave the next talk, titled “Seismic Hazard Sensitivity in the CEUS,” noting that he would be giving his opinions of what is or is not important for hazard analyses. He began by discussing general sources of imprecision, including random and systematic errors, variability and unpredictability, expert disagreement, and approximations. Next he reviewed the hazard from the New Madrid RLME source at two demonstration sites (Central Illinois and Jackson, Mississippi). For each site he first showed PGA hazard fractiles and the mean for hard rock. He then showed the sensitivity to the ground motion model used, the cluster frequency, the characteristic magnitude, and rupture length scenarios. For the dependence on cluster frequency he noted that we are less than halfway into the recurrence interval following the 1811-1812 earthquakes; thus the renewal recurrence model gives higher hazard than the Poisson model. After showing the sensitivity results, Dr. McGuire showed the mean and fractile hazard results at 1 and 10 Hz spectral acceleration.

Next, Dr. McGuire showed PGA hazard curves from three New Madrid seismic zone models (2008 USGS, 2003 Geomatrix, and 2009 CEUS SSC) that had been computed by different analysts at Risk Engineering, and he noted that all give near-identical results. The hazard curve for additional faults (e.g., Commerce and Fluorspar) and the hazard curves for 1 and 10 Hz are also all virtually identical. Dr. McGuire also showed hazard results at the Topeka, Kansas, demonstration site. Again, at 1 and 10 Hz, the newly calculated hazard results are virtually the

same as those obtained in the 2008 USGS and 2003 Geomatrix studies. Dr. McGuire emphasized that this comparison was not done using total hazard, but with the hazard contributions from the New Madrid seismic sources only. Workshop participants discussed the agreement between the different models, which is based in part on the long source-to-site distances. Also, it was noted that results from pre-2000 models would have varied, in part because these were based only on observed seismicity (i.e., no paleoearthquakes).

The next speaker was Ms. Allison Shumway (William Lettis & Associates, Inc.), who described hazard results from the Cheraw fault and Wabash Valley seismic sources at the Topeka demonstration site. The recurrence rate parameter for the Cheraw fault has the greatest effect on hazard at the Topeka site. For the Wabash Valley source, two alternative source geometry interpretations were used: narrow and wide (circular shape, consistent with the 2008 USGS source zone); the geometry has a moderate effect on hazard. The source recurrence rates used in the analysis give a factor-of-10 range, however, so this parameter is the most sensitive. The paleoseismic record appears to indicate a higher recurrence rate than the historical seismicity. To clarify the basis for the source logic trees, Ms. Kathryn Hanson (AMEC Geomatrix, Inc.) briefly described the paleoseismic record of the Cheraw fault, which includes three events in the past 20,000 years. For the Wabash source, she described the basis for rates from the paleoearthquakes near Vincennes, Indiana.

Dr. Youngs spoke next about the Oklahoma Aulacogen (OKA)/Meers fault RLME; the Meers fault is located within the OKA, so the two sources are always linked. He showed the logic tree and reviewed the branches for an in- or out-of-earthquake cluster, source geometry, earthquake model, rupture size relation, magnitude approach, and recurrence approach. A separate logic tree has been developed for OKA with broad and narrow source geometry and with the Meers fault in or out of a cluster. Additionally, given the alternative that the Meers fault is “turned off,” there is a probability that seismic activity will move to another location within the OKA but have the same source characteristics as the Meers fault. This alternative was added because numerous structures have been identified within the OKA that parallel the Meers fault.

The Alabama-Louisiana-Mississippi source (ALM; this source includes the Saline River region) located on the southern edge of the Reelfoot rift system was described next by Dr. Youngs. Four alternative source geometries were evaluated and Dr. Youngs described the data used to develop each alternative. Logic tree branches included consideration of event correlation or no correlation for paleoliquefaction interpretations, plus alternative numbers of paleoearthquakes related to these interpretations. This region does not have elevated seismicity, but paleoliquefaction evidence is present and possibly represents multiple earthquakes.

Ms. Shumway showed sensitivity results for the OKA/Meers fault RLME source. Alternative geometries may be sensitive, but this interpretation needs to be checked. The background M_{\max} earthquake within the aulacogen only (i.e., without the influence of the Meers fault) is also potentially important. Next she discussed the ALM source. Four alternative geometries are considered and hazard was calculated for the highest weighted source (the Cox/Quaternary alternative) at the Jackson, Mississippi, and Houston, Texas, sites. Randomly oriented structures that are or are not allowed to extend beyond the boundary of the source zone were tested (“leaky” or “strict” source cases) and shown to have low sensitivity. Recurrence rate has a high sensitivity, and Ms. Shumway noted that with more small events, higher hazard is indicated at

higher probabilities. Workshop participants discussed the paleoliquefaction data and hazard sensitivity results for the ALM source.

Dr. Coppersmith adjourned the meeting for the day.

DAY 2–WEDNESDAY, AUGUST 26

Mr. Salomone welcomed the group to the second day of the workshop. He announced that in October there would be a workshop on earthquake hazards sponsored by the USGS; this workshop is one of several synergistic projects currently under way that overlap the work being conducted as part of the CEUS SSC project. He introduced Mr. Oliver Boyd (of the USGS), who is an organizer of the upcoming earthquake hazards workshop. Mr. Boyd said that the workshop will be held October 27-28, 2009, in Memphis, Tennessee. It will provide an opportunity for researchers to present and discuss their recent investigations, discuss upcoming New Madrid bicentennial activities, and identify topics for future research priorities.

Dr. Coppersmith gave a summary of the model sensitivity information presented on Day 1 of the workshop. He noted the apparently large impact locally on predicted rate density of alternative interpretations of the position of the extended/non-extended crust boundary and seismotectonic zone boundaries. Some of the smoothing results show a distinct rate change (step function) at the boundary, which could be important for sites very near the boundary. This also highlights the potential importance of evaluating the need for source boundaries or boundaries for purposes of M_{\max} assessment (i.e., the extended/non-extended boundary). For the repeated large-magnitude earthquake (RLME) sources, he noted that comparisons made the previous day showing similarity in hazard for post-2000 PSHAs near New Madrid indicate that these studies are comparable in their treatment of the New Madrid seismic zone.

Given that the RLME sources are within a cluster, there is strong sensitivity to the recurrence rate. Sensitivity analyses have not yet been conducted to demonstrate the differences between within-cluster and out-of-cluster hazard at nearby sites, but it is expected that there will be strong sensitivity to in- or out-of-earthquake-cluster recurrence rates, as well as to characteristic magnitude distributions at all RLME sources. A renewal model was developed and exercised for some of the RLME sources; the short elapsed time at New Madrid relative to the mean RLME repeat time results in somewhat lower hazard estimates than the Poisson model. The results illustrate the importance of the parameters of the renewal model, including the coefficient of variation (COV) of the mean repeat time. Sensitivity studies for the Central Illinois site (which is not immediately adjacent to the New Madrid source) indicate little sensitivity to alternative models for the rupture of the northernmost segment and to rupture length models. With increasing distances to an RLME source, the background or regional seismotectonic zones are increasingly important and contribute more than the RLME sources.

Dr. Coppersmith also reviewed the particular sensitivities associated with the RLME sources at the test sites. He listed additional feedback information that will be needed, including the hazard significance of all logic tree branches at all logic tree nodes at all seven demonstration sites. He noted that he would be adding to this list as the day progressed and would review it with the TI team at the end of the day.

Dr. Youngs continued the presentations on sensitivity models by discussing the Charleston, South Carolina, RLME source. He described the weights on various logic tree branches,

including alternative interpretations for in- or out-of-earthquake-cluster recurrence rates; four source geometry configurations; various paleoliquefaction scenarios, including length of paleoliquefaction record (2,000 versus 5,000 years); the range of maximum magnitude (M_{\max}) values (M 6.7 to 7.5); and the possible overlap in the earthquake magnitudes included within this RLME and those that are accounted for within the surrounding regional source zone.

Next, Ms. Shumway described the geometry, rate, and M_{\max} sensitivity studies for the Charleston RLME and the resulting hazard at the Savannah, Georgia, and Chattanooga, Tennessee, demonstration sites. The hazard results reflect the wide range of input parameters. There is high sensitivity to earthquake recurrence models. The renewal (time-dependent) model results in lower recurrence rates for the next 50 years because the elapsed time since the large 1886 earthquake is relatively short compared to the mean repeat time for RLME events. Workshop participants discussed the relative merits of using renewal versus Poisson recurrence models. Weights on these model branches may need to reflect the maturity of the structures involved; additional feedback on sensitivity is needed.

Dr. Youngs recounted early discussions about placing an RLME source around the Charlevoix region. The project team decided this was unnecessary as the recurrence rate from the observed seismicity is comparable to or even exceeds the rates identified using paleoliquefaction data. Neither the cell-by-cell nor kernel-smoothing methods provide a close fit, in part because of uncertainty in the record of paleoliquefaction events. Checking the relative fit of the two smoothing methods using an RLME-equivalent source in the St. Lawrence and Charlevoix region may provide useful information.

Dr. Coppersmith asked PPRP members for their opinions about the use of the renewal versus Poisson smoothing approaches. Dr. Stepp remarked that if the in-cluster alternative is selected for the Charleston RLME, then a tectonic interpretation is being made and therefore the renewal model needs to be highly weighted. Dr. Coppersmith observed that the renewal model is sensitive to knowledge of COV and time since the last event; when the uncertainties in both of these factors are added, the problem is moved toward a Poissonian approach. Workshop participants discussed the use of the renewal approach for known seismic sources (e.g., structures in the New Madrid region). There was agreement that more work on COVs is needed, as there is extreme uncertainty in this parameter for many areas and thus the use of the renewal model may not be reasonable. Workshop participants also discussed how to structure a logic tree given that an in-cluster state is assumed. Dr. Coppersmith noted that the influence of the in-cluster versus out-of-cluster models on hazard still needs to be examined.

Following a break, Dr. Coppersmith announced that the next talks would address regional seismic source zones. Dr. Toro gave the first talk, titled "Sensitivity Results for CEUS Source Zones." He began by comparing the CEUS SSC project hazard results (for the source zones only; no RLME sources) with hazard results using the zones defined by the USGS. In general, the hazard levels calculated for the CEUS project are lower than those for the USGS study, but this is likely due to not including the RLME events in the comparison. At the Savannah site the difference in hazard levels is about 50 percent; for the Chattanooga and Manchester, New Hampshire, sites the difference is closer to 20 percent. For the Central Illinois, Houston, Jackson, and Topeka sites, the hazard curves are closer together.

Dr. Toro then discussed hazard sensitivity results for seismic source zones for each of the seven demonstration sites. He noted that he would concentrate on the results from the CEUS SSC

study, which incorporates SSC uncertainty but does not address ground motion uncertainty. For each demonstration site, he showed hazard results at PGA and 1 Hz and discussed the contributions to hazard for the dominant seismic sources. He also showed the mean and fractile hazard curves and described sensitivity to branches of the master logic tree, focusing on M_{\max} and recurrence for the dominant sources.

Dr. Toro stated that for all sites there is moderate sensitivity to choice of smoothing approach (i.e., kernel or variable a and b) and to selection of M_{\max} values. He believes that in areas having higher levels of seismicity (e.g., many low-magnitude events), the two smoothing approaches are in better agreement; however, this observation needs to be tested further. Dr. Coppersmith noted that areas having higher levels of seismicity tend to have lower uncertainty in the recurrence parameters and, hence lower sensitivity to most alternative input parameters. These observations apply to the Savannah, Manchester, Central Illinois, Topeka, and Chattanooga sites. The hazard results for the two sites in regions of lower seismicity, Houston and Jackson, have more pronounced differences in sensitivity between PGA and 1 Hz hazard curves. For both sites there is a moderately high sensitivity to the M_{\max} of the Gulf of Mexico source zone and to choice of smoothing parameter. Dr. Toro noted that these differences can be at least partially attributed to the low seismicity (fewer data points) in these regions. Another potential contributor to these differences is the use of the Gulf of Mexico attenuation equations for local zones and the Midcontinent attenuation equations for distant zones.

Workshop participants discussed whether or not to keep all of the branches of the logic tree used for the initial hazard calculations, given the apparent low sensitivity of many branches. Advantages include the relative ease of making future changes to update the models; disadvantages include longer computational time. Several individuals noted that results will vary by site. The general preference of the group was to keep all of the branches as the study moves forward, since this will serve to demonstrate that all alternative hypotheses have been considered. Although the CEUS SSC project is applicable to the entire CEUS, its future applications will be for individual sites and it will be possible to simplify (e.g., by pruning the logic tree) for individual sites by showing that there is no sensitivity to more distant sources in the model.

Following a lunch break, Dr. Coppersmith showed a slide with a list of additional feedback items needed, based on the discussions at the workshop, as follows:

- the hazard significance of all logic tree branches, at all logic tree nodes, at all seven demonstration sites;
- additional evaluation of predicted versus observed seismicity for the entire CEUS and all seismotectonic zones;
- differences in earthquake recurrence related to smoothing approach and alternative zone boundaries; and
- the issue of a migrating RLME (e.g., the Meers fault versus another structure within the OKA source region).

Dr. Coppersmith indicated that these items would be addressed by the TI team during an upcoming telephone conference call. Workshop participants discussed these and related topics, including the zoneless model concept (smoothing of seismicity used in place of defined zone

boundaries); separating large-magnitude events within the RLME sources from events in the surrounding host zones; offshore earthquakes in the Gulf region; and appropriate truncation of M_{\max} distributions.

Dr. McGuire gave the next talk, titled “Quantifying the Precision of Seismic Hazard Results in the CEUS.” The purpose of the analysis described in the talk was to derive quantitative estimates of how seismic hazard results might change if studies were repeated by different researchers using the same basic information. Dr. McGuire began by listing many general sources of imprecision, which include random error and statistical variation, overconfidence in estimating uncertainties, unpredictability, expert disagreement, and the use of approximations. Then he listed the hazard studies that provided data used to quantify levels of precision of seismic hazard results. Data on SSC was obtained from the 1989 EPRI-SOG study, the PEGASOS project that evaluated seismic hazard for nuclear power plant sites in Switzerland, and recent characterizations of the Charleston and New Madrid seismic sources.

Dr. McGuire explained the formula he used for combining sources of imprecision. He showed hazard results obtained from the PEGASOS project, including COV of mean hazard from SSC expert teams. Turning to the 1989 EPRI-SOG project, he showed COV of hazard at various levels for each of the seven demonstration sites used for the CEUS SSC project. He then provided a summary of uncertainties for the Charleston source by showing logic tree alternatives and weights. He also described the mean and variance of hazard when weights on models are variable (depending on who is making the interpretation) and how COV can be calculated for various weighted alternatives. Similar analyses were shown for the New Madrid source.

Turning to the ground motion and site response components of seismic hazard analysis, Dr. McGuire showed the relevant hazard results from the PEGASOS and 2004 EPRI Ground Motion studies. Next he used the data from the 2004 EPRI study to assess the COV of hazard versus hazard results at each of the seven demonstration sites. He noted that there is a tendency to get much lower COV from seismic source and ground motion models, relative to site response. He then listed several conclusions:

- There is less uncertainty in site response than other components of hazard.
- The source parameter contribution is smaller for area sources than RLME sources.
- For ground motion equations, area sources have a higher COV than RLME sources.

Dr. McGuire showed a plot of these results, which indicate that a minimum estimate of uncertainty in mean hazard varies between a COV of mean hazard of 0.2 to a COV of mean hazard of 0.4 for an annual frequency of exceedance of 1×10^{-4} to 1×10^{-6} , respectively. Dr. McGuire stated that an overall level of precision in mean hazard estimates would be a COV of 0.25 in annual frequency, which corresponds to a precision in ground motion of $\pm 8\%$. He said that to apply this knowledge going forward, this method of quantification would give confidence in levels of mean hazard and how much they could change with additional analyses, which reflects on how well the hazard is understood.

Dr. Coppersmith followed this presentation with the final talk of the workshop. In this talk, titled “Path Forward,” he identified short-term activities to occur within the following few weeks, including meetings between the TI team and staff and preparation and distribution of documentation for Workshop 3. He then showed key dates and activities for the remainder of the

calendar year, including delivery of new data sets of reprocessed gravity and magnetic field data and an updated world stress map. The preliminary SSC model will be completed by the end of February 2010, and discussed in a briefing with the PPRP in mid-March. The final SSC model is to be completed at the end of April 2010 and the draft report by the end of July 2010. The final project report will be delivered at the end of December 2010. The group discussed the schedules for the review of CEUS SSC project components by the NRC and USGS staff. Mr. Salomone will work with the NRC and the USGS to ensure the process goes smoothly.

Concluding remarks were made by Mr. Salomone, who noted that Workshop 3 was the last formal workshop for the project. For this reason he wanted to provide an engineering perspective and review the larger project context by looking at industry and government use of what will be developed for this project. He reviewed the following general guiding principles on which the project is based:

- Managing the seismic issue is critical to control cost and delays for critical mission nuclear facilities.
- Having a stable, consistent, and defensible seismic design spectrum throughout the design phase of critical mission nuclear facilities is essential.
- Accomplishing more for less with reduced risk through standardization and partnering is important to advance science and the state of practice.

Mr. Salomone showed a flow chart titled “Disciplined, Systematic Approach to Seismic Safety.” Key steps in the disciplined, systematic approach to seismic safety included:

1. Define scope of work as per regulatory and owner guidance documents.
2. Analyze seismic hazards by performing PSHAs using the CEUS SSC model and available attenuation models from studies such as the EPRI 2004/2006 CEUS Ground Motion and the Next Generation of Ground Motion Attenuation Models—East (in development). .
3. Develop controls through installation of strong motion seismic monitoring instrumentation and settlement monitoring instrumentation.
4. Perform work by designing, building, and operating facilities.
5. Obtain feedback from regulatory oversight and technical exchanges using qualified consultants and expert panel members; modify surface spectrum as required.

Mr. Salomone stated that the CEUS SSC project is part of an initial step to analyze hazards and will ultimately be used for facility design. He cautioned that factors used for increased conservatism should be applied to the design spectrum used by structural engineers and not the geologically, seismologically derived spectrum used by geotechnical engineers when performing soil response analyses.

Mr. Salomone finished by thanking Mr. Rahn for the hospitality of EPRI, and the workshop participants for their contributions to the CEUS SSC project.

NRC FORM 335 (12-2010) NRCMD 3.7		U.S. NUCLEAR REGULATORY COMMISSION		1. REPORT NUMBER (Assigned by NRC, Add Vol., Supp., Rev., and Addendum Numbers, if any.) NUREG-2115 Vol. 5					
BIBLIOGRAPHIC DATA SHEET (See instructions on the reverse)									
2. TITLE AND SUBTITLE Central and Eastern United States Seismic Source Characterization for Nuclear Facilities Volume 5: Appendices C to F				3. DATE REPORT PUBLISHED <table border="1"> <tr> <td>MONTH</td> <td>YEAR</td> </tr> <tr> <td>January</td> <td>2012</td> </tr> </table>		MONTH	YEAR	January	2012
				MONTH	YEAR				
				January	2012				
4. FIN OR GRANT NUMBER K6877									
5. AUTHOR(S) G. Stirewalt (NRC), L. Salomone (Savannah River Nuclear Solutions, LLC), S. McDuffie (DOE), K. Coppersmith (Coppersmith Consulting, Inc), Fugro William Lettis & Associates, Inc.: C. Fuller, R. Hartleb, W. Lettis, S. Lindvall, R. McGuire, G. Toro, D. Slayter, R. Cumbest, A. Shumway, F. Syms, AMEC Geomatrix, Inc: L. Glaser, K. Hanson, R. Youngs, S. Bozkurt, V. Montaldo Falero, R. Perman, R. McGuire (Risk Engineering), M. Tuttle (M. Tuttle & Associates)				6. TYPE OF REPORT Technical					
7. PERIOD COVERED (Inclusive Dates)									
8. PERFORMING ORGANIZATION - NAME AND ADDRESS (If NRC, provide Division, Office or Region, U.S. Nuclear Regulatory Commission, and mailing address; if contractor, provide name and mailing address.) U.S. Nuclear Regulatory Commission, Office of Nuclear Regulatory Research, Washington DC 20555 U.S. Department of Energy, 1000 Independence Avenue SW, Washington DC 20585 Electric Power Research Institute, 3420 Hillview Avenue, Palo Alto, CA 94304									
9. SPONSORING ORGANIZATION - NAME AND ADDRESS (If NRC, type "Same as above"; if contractor, provide NRC Division, Office or Region, U.S. Nuclear Regulatory Commission, and mailing address.) U.S. Nuclear Regulatory Commission, Office of Nuclear Regulatory Research, Washington DC 20555 U.S. Department of Energy, 1000 Independence Avenue SW, Washington DC 20585 Electric Power Research Institute, 3420 Hillview Avenue, Palo Alto, CA 94304									
10. SUPPLEMENTARY NOTES									
11. ABSTRACT (200 words or less) This report describes a new seismic source characterization (SSC) model for the Central and Eastern United States (CEUS). It will replace the Seismic Hazard Methodology for the Central and Eastern United States, EPRI Report NP-4726 (July 1986) and the Seismic Hazard Characterization of 69 Nuclear Plant Sites East of the Rocky Mountains, Lawrence Livermore National Laboratory Model, (Bernreuter et al., 1989). The objective of the CEUS SSC Project is to develop a new seismic source model for the CEUS using a Senior Seismic Hazard Analysis Committee (SSHAC) Level 3 assessment process. The goal of the SSHAC process is to represent the center, body, and range of technically defensible interpretations of the available data, models, and methods. Input to a probabilistic seismic hazard analysis (PSHA) consists of both seismic source characterization and ground motion characterization. These two components are used to calculate probabilistic hazard results (or seismic hazard curves) at a particular site. This report provides a new seismic source model.									
12. KEY WORDS/DESCRIPTORS (List words or phrases that will assist researchers in locating the report.) Probabilistic seismic hazard analysis (PSHA) Seismic source characterization (SSC) Seismic source characterization model Central and Eastern United States (CEUS)				13. AVAILABILITY STATEMENT unlimited					
				14. SECURITY CLASSIFICATION (This Page) unclassified					
				(This Report) unclassified					
				15. NUMBER OF PAGES					
				16. PRICE					

